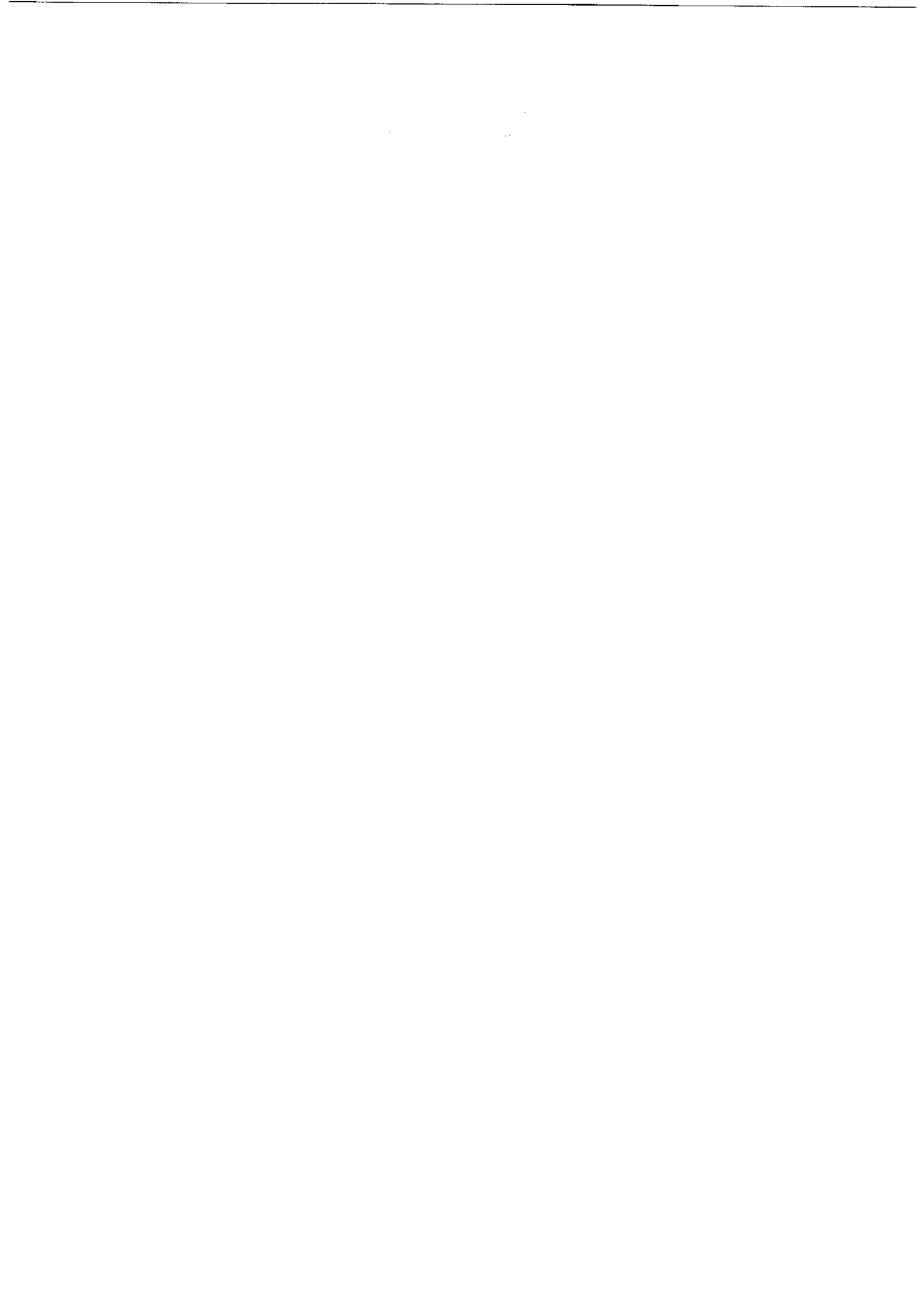

PRINCIPLES OF COMBUSTION

SECOND EDITION

Kenneth K. Kuo



JOHN WILEY & SONS, INC.



This book is printed on acid-free paper.[∞]

Copyright © 2005 by John Wiley & Sons, Inc. All rights reserved.

Published by John Wiley & Sons, Inc., Hoboken, New Jersey
Published simultaneously in Canada

No part of this publication may be reproduced, stored in a retrieval system, or transmitted in any form or by any means, electronic, mechanical, photocopying, recording, scanning, or otherwise, except as permitted under Section 107 or 108 of the 1976 United States Copyright Act, without either the prior written permission of the Publisher, or authorization through payment of the appropriate per-copy fee to the Copyright Clearance Center, Inc., 222 Rosewood Drive, Danvers, MA 01923, (978) 750-8400, fax (978) 750-4470, or on the web at www.copyright.com. Requests to the Publisher for permission should be addressed to the Permissions Department, John Wiley & Sons, Inc., 111 River Street, Hoboken, NJ 07030, (201) 748-6011, fax (201) 748-6008, e-mail: permcoordinator@wiley.com.

Limit of Liability/Disclaimer of Warranty: While the publisher and author have used their best efforts in preparing this book, they make no representations or warranties with respect to the accuracy or completeness of the contents of this book and specifically disclaim any implied warranties of merchantability or fitness for a particular purpose. No warranty may be created or extended by sales representatives or written sales materials. The advice and strategies contained herein may not be suitable for your situation. You should consult with a professional where appropriate. Neither the publisher nor author shall be liable for any loss of profit or any other commercial damages, including but not limited to special, incidental, consequential, or other damages.

For general information on our other products and services please contact our Customer Care Department within the United States at (800) 762-2974, outside the U.S. at (317) 572-3993 or fax (317) 572-4002.

Wiley also publishes its books in a variety of electronic formats. Some content that appears in print, however, may not be available in electronic books. For more information about Wiley products, visit our web site at www.wiley.com

Library of Congress Cataloging-in-Publication Data

Kuo, Kenneth K.

Principles of combustion / Kenneth K. Kuo.—2nd ed.

p. cm.

Includes bibliographical references and index.

ISBN 0-471-04689-2 (alk. paper)

1. Combustion engineering. I. Title.

TJ254.5.K85 2005

621.402'3—dc22

2004007136

Printed in the United States of America.

10 9 8 7 6 5 4 3 2

To my wife — Olivia (Jeon-lin)
and daughters Phyllis and Angela
for their love, understanding, patience, and support



CONTENTS

Preface	xxi
Preface to the First Edition	xxv
Introduction	1
Importance of Combustion in Various Applications / 1	
Related Constituent Disciplines for Combustion Studies / 3	
General Method of Approach to Combustion Problems / 4	
General Objectives of Combustion Modeling / 4	
Classification of Combustion Problems / 4	
General Structure of a Theoretical Model / 6	
Governing Equations for Combustion Modeling (Conservation and Transport Equations) / 6	
Some Common Assumptions Made in Combustion Models (Especially for Classical Models) / 6	
Several Basic Definitions / 8	
1 Review of Chemical Thermodynamics	11
Nomenclature / 11	
1 Brief Statement of Thermodynamic Laws / 15	
2 Equation of State / 17	
3 Conservation of Mass / 18	
4 The First Law of Thermodynamics; Conservation of Energy / 20	
5 The Second Law of Thermodynamics / 24	
5.1 Equilibrium Thermodynamics / 24	
5.2 Nonequilibrium Thermodynamics / 26	
6 Criteria for Equilibrium / 34	
7 Conservation of Atomic Species / 36	

8	Various Methods for Reactant-Fraction Specification / 38
8.1	Mole Fraction X and Mass Fraction Y / 38
8.2	Fuel–Oxidant Ratio F/O and Fuel–Air Ratio F/A / 39
8.3	Equivalence Ratio ϕ / 39
8.4	Mixture Fraction f / 40
9	Standard Enthalpies of Formation / 43
10	Thermochemical Laws / 47
11	Relationship Between Bond Energies and Heats of Formation / 48
12	Heats of Reaction for Constant-Pressure and Constant-Volume Combustion / 52
12.1	Constant-Pressure Combustion / 53
12.2	Constant-Volume Combustion / 66
13	Energy Balance Considerations for Flame Temperature Calculations / 68
14	Equilibrium Constants / 73
15	Real-Gas Equations of State and Fugacity Calculation / 90
16	More-Complicated Dissociation in the Combustion of Hydrocarbons / 93
17	The Clausius–Clapeyron Equation for Phase Equilibrium / 96
18	Calculation of Equilibrium Compositions with NASA’s CEA Computer Program / 98
18.1	Assumptions and Capabilities / 101
18.2	Equations Describing Chemical Equilibrium / 103
18.2.1	Thermodynamic Equations / 103
18.2.2	Minimization of Gibbs Free Energy / 104
19	Other Well-Established Chemical Equilibrium Codes / 107
References / 109	
Homework / 110	
Projects / 114	

2 Chemical Kinetics and Reaction Mechanisms

116

Nomenclature / 116	
1	Rates of Reaction and Their Functional Dependence / 118
1.1	Total Collision Frequency / 119
1.2	Equation of Arrhenius / 122
1.3	Apparent Activation Energy / 125
1.4	Rates of Reaction / 126
1.5	Methods for Measurement of Gas-Phase Reaction Rates / 131
1.5.1	Static Methods / 132
1.5.1.1	Flash Photolysis Resonance Fluorescence Technique / 133
1.5.1.2	Relative Rate-Constant Photolysis Technique / 134

1.5.1.3 Laser Photolysis/Laser Induced Fluorescence Technique / 135
1.5.2 Dynamic Methods for Reactions in Flow Systems / 136
1.5.3 Several Methods for Measuring Rapid Reaction Rates / 137
2 One-Step Chemical Reactions of Various Orders / 141
2.1 First-Order Reactions / 141
2.2 Second-Order Reactions / 144
2.3 Third-Order Reactions / 147
3 Consecutive Reactions / 148
4 Competitive Reactions / 150
5 Opposing Reactions / 150
5.1 First-Order Reaction Opposed by a First-Order Reaction / 151
5.2 First-Order Reaction Opposed by a Second-Order Reaction / 153
5.3 Second-Order Reaction Opposed by a Second-Order Reaction / 153
6 Chain Reactions / 154
6.1 Free Radicals / 154
6.2 Lindemann's Theory for First-Order Reaction / 156
6.3 Complex Reactions / 159
6.3.1 Hydrogen–Bromine Reaction / 159
7 Chain-Branching Explosions / 162
8 Chemkin Analysis and Code Application for Gas-Phase Kinetics / 164
8.1 Thermodynamic Properties / 165
8.2 Reaction Rate Expressions / 166
8.3 Brief Description of Procedures in Using Chemkin Code / 169
9 Surface Reactions / 173
9.1 Surface Adsorption Processes / 174
9.1.1 The Langmuir Adsorption Isotherm / 176
9.1.2 Adsorption with Dissociation / 177
9.1.3 Competitive Adsorption / 178
9.2 Surface Reaction Processes / 178
9.2.1 Reaction Mechanism / 178
9.2.2 Unimolecular Surface Reactions / 180
9.2.3 Bimolecular Surface Reactions / 181
9.2.4 Desorption / 182
9.3 Kinetic Model of Hydrogen–Oxygen Reaction on Platinum Surface / 183
9.3.1 Simple Kinetic Model of H ₂ /O ₂ Reaction on Platinum Surface / 184

9.3.2 Kinetic Rates of H ₂ /O ₂ Reaction on Platinum Surface / 186
9.4 Experimental Methods to Study Surface Reactions / 187
9.4.1 Spectroscopic Methods / 187
9.4.1.1 Auger Electron Spectroscopy / 187
9.4.2 Temperature-Controlled Methods / 189
9.4.3 Combination of Spectroscopic and Temperature-Controlled Methods / 190
9.5 Surface Reaction Rate Determination / 190
9.5.1 An Example of Application of LIF Technique in Surface Reaction Rate Determination / 191
9.5.1.1 The Elementary Steps / 192
9.5.1.2 Experimental Setup / 193
9.5.1.3 Experimental Results / 193
10 Rate Laws for Isothermal Reactions Utilizing Dimensionless Parameters / 195
10.1 Equilibrium Constants / 197
10.2 Net Rate of Production of Chemical Species / 199
11 Procedure and Applications of Sensitivity Analysis / 199
11.1 Introduction to Sensitivity Analysis / 200
11.2 The Procedure for Local Sensitivity Analysis / 205
11.2.1 Time-Dependent Zero-Dimensional Problems / 205
11.2.2 The Procedure for Steady-State One-Dimensional Problems / 208
11.2.3 The Procedure for Time-Dependent Spatial Problems / 209
11.3 The Example of Sensitivity Analysis of Aliphatic Hydrocarbon Combustion / 210
11.3.1 Local Sensitivity Analysis in One-Dimensional Flame Fronts / 210
11.3.2 Sensitivity Analysis for Zero-Dimensional Problems / 210
12 Reaction Flow Analysis / 211
13 Reaction Mechanisms of H ₂ /O ₂ Systems / 215
13.1 Background Information about H ₂ /O ₂ Reaction Systems / 216
13.2 Explosion Limits of H ₂ /O ₂ Systems / 220
14 Gas-Phase Reaction Mechanisms of Aliphatic Hydrocarbon and Oxygen System / 223
14.1 Specific Mechanisms / 224
14.1.1 Gas-Phase Kinetics of H ₂ Oxidation / 225
14.1.2 O ₃ Decomposition Mechanism / 232
14.1.3 CO Oxidation Mechanism / 233
14.1.4 CH ₂ O Reaction / 233

14.1.5 CH ₄ Oxidation / 234
14.1.6 C ₂ H ₆ (Ethane) Oxidation / 236
14.1.7 C ₂ H ₄ (Ethylene) Oxidation / 237
14.1.8 C ₂ H ₂ (Acetylene) Oxidation / 238
14.1.9 CH ₂ CO (Ketene) Oxidation / 240
14.1.10 CH ₃ OH (Methanol) Reactions / 241
14.1.11 C ₂ H ₅ OH (Ethanol) Reactions / 242
14.1.12 CH ₃ CHO (Acetaldehyde) Reaction / 243
14.2 Discussion of More Complex Cases / 244
15 Reduction of Highly Complex Reaction System to Simpler Reaction Mechanisms / 245
15.1 Quasi-Steady-State Assumption (QSSA) and Partial Equilibrium Assumption / 246
15.2 Computational Singular Perturbation Methods for Stiff Equations / 247
15.2.1 Stiff Equations / 248
15.2.2 Chemical Kinetic Systems as Stiff Equations / 248
15.2.3 Formulation of the Problem / 249
15.2.3.1 The Fast Subspace / 249
15.2.3.2 The Equations for f^I / 250
15.2.3.3 Determination of m , the Choice of \mathbf{a}_I and \mathbf{b}^J / 251
15.2.4 Procedures for Solving the Chain Reaction Problems / 252
15.3 Some Observations of the CSP Method / 252
16 Formation Mechanism of Nitrogen Oxides / 255
16.1 Thermal NO Mechanism (Zel'dovich Mechanism) / 255
16.2 Prompt NO Mechanism (Fenimore Mechanism) / 258
16.3 NO Production from Fuel-Bound Nitrogen / 262
16.3.1 The Oxidation of HCN / 262
16.3.2 The NO → HCN → N ₂ Mechanism / 264
16.3.3 The Oxidation of NH ₃ / 265
16.4 NO ₂ Mechanism / 267
16.5 N ₂ O Mechanism / 267
16.6 Overall Remarks on NO _x Formation / 269
17 Formation and Control of CO and Particulates / 270
17.1 Carbon Monoxide / 270
17.2 Particulate Matter / 271
17.2.1 Major Types of Particulates / 272
17.2.2 Harmful Effects / 272
17.2.3 Particulate Matter Control Methods / 272
References / 274
Homework / 281

3 The Conservation Equations for Multicomponent Reacting Systems	285
Nomenclature / 285	
1 Definitions of Concentrations, Velocities, and Mass Fluxes / 287	
2 Fick's Law of Diffusion / 289	
3 Theory of Ordinary Diffusion in Gases at Low Density / 290	
4 Continuity Equation and Species Mass Conservation Equations / 293	
5 Conservation of Momentum / 297	
5.1 Momentum Equation in Terms of Stress / 297	
5.1.1 Momentum Equation Derivation by Infinitesimal Particle Approach / 298	
5.1.2 Momentum Equation Derivation by Infinitesimal Control Volume Approach / 302	
5.1.3 Finite Control Volume / 303	
5.2 Stress–Strain Rate Relationship (Constitutive Relationship) / 304	
5.2.1 Strain Rate / 305	
5.2.2 Stress Tensor / 307	
5.3 Navier–Stokes Equations / 310	
6 Conservation of Energy / 320	
7 Physical Derivation of the Multicomponent Diffusion Equation / 328	
8 Other Necessary Equations in Multicomponent Systems / 331	
9 Solution of a Multicomponent-Species System / 331	
10 Shvab–Zel'dovich Formulation / 332	
11 Dimensionless Ratios of Transport Coefficients / 336	
12 Boundary Conditions at an Interface / 337	
References / 350	
Homework / 350	
Projects / 353	
4 Detonation and Deflagration Waves of Premixed Gases	354
Nomenclature / 354	
1 Qualitative Differences Between Detonation and Deflagration / 356	
2 The Hugoniot Curve / 357	
3 Properties of the Hugoniot Curve / 361	
3.1 Entropy Distribution along the Hugoniot Curve / 365	

3.2 Comparison of the Burned-Gas Velocity Behind a Detonation Wave with the Local Speed of Sound /	367
4 Determination of Chapman–Jouguet Detonation Wave Velocity /	373
4.1 Trial-and-Error Method /	373
4.2 The Newton–Raphson Iteration Method /	375
4.3 Comparison of Calculated Detonation-Wave Velocities with Experimental Data /	379
5 Detonation-Wave Structure /	381
5.1 Zel'dovich–von Neumann–Döring (ZND) One-Dimensional Wave Structure /	381
5.2 Multidimensional Detonation-Wave Structure /	384
5.3 Numerical Simulation of Detonations /	386
6 The Mechanism of Deflagration-to-Detonation Transition (DDT) in Gaseous Mixtures /	388
7 Detonability and Chemical Kinetics: Limits of Detonability /	395
7.1 Classical Model of Belles /	395
7.2 Detonability Limits of Confined Fuel Mixtures /	401
7.2.1 Initial Condition Dependence /	402
7.2.2 Boundary Condition Dependence /	402
7.2.3 Single-Head Spin Detonation /	403
7.3 Detonability Criteria and Detonation Cell Size /	405
7.4 Chemical Kinetics of Detonation in H ₂ –Air–Diluent Mixtures /	410
8 Nonideal Detonations /	413
8.1 Definition of Nonideal Detonation and Zel'dovich and Shchelkin's Detonation Mechanisms in Rough Tubes /	414
8.2 Theoretical Considerations of Energy and Momentum Losses /	415
8.3 Critical Pipe Diameter Consideration /	416
8.4 Effect of Several Physical and Chemical Parameters on Detonability /	419
8.5 Possible Measures for Reducing Potential of Detonation Wave Generation /	420
9 Consideration of Spontaneous Detonation Initiation /	422
9.1 Functional Form of Distribution of Ignition Delay /	424
9.2 Experimental Verification of Processes of Nonexplosive Detonation Initiation /	425
9.2.1 Photochemical Initiation of Detonation in Mixtures with Nonuniform Concentration /	425
9.2.2 Gasdynamic Jet as a Method of Creating Temperature-Concentration Nonuniformity /	426
9.3 General Observation and Status of Understanding /	428

References / 428

Homework / 434

Project / 435

5 Premixed Laminar Flames

437

Nomenclature / 437

- 1 Introduction and Flame Speed Measurement Methods / 438
 - 1.1 Bunsen Burner Method / 438
 - 1.2 Constant-Volume Spherical Bomb Method / 442
 - 1.3 Soap-Bubble (Constant-Pressure Bomb) Method / 443
 - 1.4 Particle-Track Method / 445
 - 1.5 Flat-Flame Burner Method / 445
 - 1.6 Diagnostic Method for Flame Structure Measurements / 447
 - 1.6.1 Velocity Measurements / 448
 - 1.6.2 Density Measurements / 448
 - 1.6.3 Concentration Measurements / 448
 - 1.6.4 Temperature Measurements / 448
- 2 Classical Laminar-Flame Theories / 449
 - 2.1 Thermal Theory: Mallard and LeChatelier's Development (1883) / 449
 - 2.2 Comprehensive Theory: The Theory of Zel'dovich, Frank-Kamenetsky, and Semenov / 451
 - 2.3 Diffusion Theory: The Theory of Tanford and Pease / 458
- 3 Contemporary Method for Solving Laminar-Flame Problems / 461
 - 3.1 Premixed O₃/O₂ Laminar Flames / 461
 - 3.2 Chemkin Code for Solving Premixed Laminar-Flame Structures / 468
- 4 Dynamic Analysis of Stretched Laminar Premix Flames / 471
 - 4.1 Definition of Flame Stretch Factor and Karlovitz Number / 471
 - 4.2 Balance Equation for Premixed Laminar-Flame Area / 476
 - 4.3 The Use of Expanding Spherical Flames to Determine Burning Velocities and Stretch Effects in Hydrogen/Air Mixtures / 477
 - 4.4 Laminar Burning Velocities and Markstein Numbers of Hydrocarbon/Air Flames / 484
 - 4.5 Burning Rates of Ultra-Lean to Moderately Rich H₂/O₂/N₂ Laminar Flames with Pressure Variations / 490
- 5 Effect of Chemical and Physical Variables on Flame Speed / 496
 - 5.1 Chemical Variables / 496
 - 5.1.1 Effect of Mixture Ratio / 496
 - 5.1.2 Effect of Fuel Molecular Structure / 497
 - 5.1.3 Effects of Additives / 499
 - 5.2 Physical Variables / 500
 - 5.2.1 Effect of Pressure / 500

5.2.2 Effect of Initial Temperature / 501	
5.2.3 Effect of Flame Temperature / 502	
5.2.4 Effect of Thermal Diffusivity and Specific Heat / 502	
6 Principle of Stabilization of Combustion Waves in Laminar Streams / 503	
7 Flame Quenching / 507	
8 Flammability Limits of Premixed Laminar Flames / 510	
8.1 Flammability Limits Determined from a Standard Glass Tube / 510	
8.2 Effect of Pressure and Temperature on Flammability Limits / 512	
8.3 Spalding's Theory of Flammability Limits and Flame Quenching / 513	
8.4 Flame Structure near the Flammability Limits of Premixed Hydrogen–Oxygen Flames / 523	
References / 528	
Homework / 533	
Project / 535	

6 Gaseous Diffusion Flames and Combustion of a Single Liquid Fuel Droplet 537

Nomenclature / 537	
1 Burke and Schumann's Theory of Laminar Diffusion Flames / 539	
1.1 Basic Assumptions and Solution Method / 544	
1.2 Flame Shape and Flame Height / 546	
2 Phenomenological Analysis of Fuel Jets / 548	
3 Laminar Diffusion Flame Jets / 551	
3.1 Laminar Jet Mixing / 551	
3.2 Laminar Jet with Chemical Reactions / 557	
3.3 Numerical Solution of Two-Dimensional Axisymmetric Laminar Diffusion Flames / 561	
3.4 Effect of Preferential Diffusion of Species and Heat in Laminar Diffusion Flames / 566	
4 Evaporation and Burning of a Single Droplet in a Quiescent Atmosphere / 569	
4.1 Evaporation of a Single Fuel Droplet / 572	
4.2 Mass Burning Rate of a Single Fuel Droplet / 578	
5 Fuel Droplet in a Convective Stream / 581	
5.1 Correlation Development for Nearly Spherical Droplets in Convective Streams / 581	
5.2 Simulation of Deformed Droplet Dynamics / 583	
5.3 Effect of Internal Circulation on Droplet Vaporization Rate / 585	

6 Supercritical Burning of Liquid Droplets in a Stagnant Environment / 590	
6.1 Thermodynamic and Transport Properties / 593	
6.1.1 Extended Corresponding-State Principle / 594	
6.1.2 Equation of State / 595	
6.1.3 Thermodynamic Properties / 596	
6.1.4 Transport Properties / 597	
6.2 Vapor–Liquid Phase Equilibrium / 598	
6.3 Droplet Vaporization in Quiescent Environments / 603	
6.4 Droplet Combustion in Quiescent Environments / 606	
6.5 Droplet Vaporization in Supercritical Convective Environments / 610	
6.6 Droplet Response to Ambient Flow Oscillation / 613	
References / 614	
Homework / 618	
Projects / 620	

Appendix A Evaluation of Thermal and Transport Properties of Gases and Liquids

623

Nomenclature / 623	
Introduction / 625	
1 Gas Density / 625	
1.1 Baseline Method / 627	
Ideal-Gas Equation of State / 627	
1.2 High-Pressure Correction / 628	
Van der Waals Equation of State / 628	
Redlich–Kwong Equation of State / 628	
Soave (SRK) and Peng–Robinson Equations of State / 628	
Virial Equation of State / 629	
Beattie–Bridgeman Equation of State / 630	
Benedict–Webb–Rubin (BWR) Equation of State / 630	
1.3 Mixing Rules / 631	
Ideal-Gas Mixing Rules / 631	
Mixing Rules for Redlich–Kwong Type of Equation of State / 631	
Benedict–Webb–Rubin Mixing Rules / 632	
Virial Equation Mixing Parameters / 632	
2 Liquid Density / 633	
2.1 Baseline Method / 633	
Spencer–Danner Correlation and Other Modifications / 633	
COSTALD (Hankinson–Thomson Correlation) / 634	

2.2 High-Pressure Correction / 635	
	Hankinson–Brobst–Thomson (HBT) Model / 635
	Generalized COSTALD / 636
	Chang–Zhao Equation / 636
	Model of Aalto et al. / 637
2.3 Mixing Rules / 638	
	Mixing Rules for Critical Temperature of Liquid Mixtures / 638
	Mixing Rules for Critical Volume $V_{c,m}$ and Characteristic Volume V_m^* / 639
	Mixing Rule for Acentric Factor / 639
	Estimation of the Critical Pressure for a Mixture / 640
3 Gas Specific Heat / 641	
3.1 Baseline Method / 641	
	Evaluation of Ideal-Gas Heat Capacity at Constant Pressure, J/(mol · K) / 642
	Joback Method ¹ / 642
	Method of Thinh et al. ²⁶ / 644
3.2 High-Pressure Correction / 645	
3.3 Mixing Rules / 650	
4 Liquid Specific Heat / 651	
4.1 Baseline Method / 651	
	Group Contribution Method / 651
	Corresponding States Method / 654
4.2 High-Pressure Correction / 654	
4.3 Mixing Rule for Liquid Mixtures / 654	
5 Gas Viscosity / 654	
5.1 Baseline Method / 655	
	Chapman–Enskog Approach / 655
	Method of Corresponding States / 657
5.2 High-Pressure Correction / 658	
	Reichenberg Method / 658
	Lucas Method / 659
5.3 Mixing Rules / 660	
6 Liquid Viscosity / 661	
6.1 Baseline Method / 661	
	Correlating Equations / 662
	Low-Temperature Viscosity Estimation Methods / 664
	Van Velzen, Cardozo, and Langenkamp's Group Contribution Method ⁶² / 665
	Orrick and Erbar's Group Contribution Method ¹ / 665

Przezdziecki and Sridhar's Corresponding States Method ⁶³ / 666
High-Temperature Liquid Viscosity Estimation Methods / 667
Letsou and Stiel's Method for Saturated Liquids ⁶⁷ / 667
Brule and Starling's ⁶⁸ and Chung et al.'s ⁶⁹ Method / 667
6.2 High-Pressure Correction / 668
Lucas's Estimation Method ⁴⁸ / 668
6.3 Mixing Rules / 669
Grunberg and Nissan's Method ⁷¹ / 669
Teja and Rice's Method ⁷⁴ / 670
7 Gas Thermal Conductivity / 671
7.1 Baseline Method / 671
7.2 High-Pressure Correction / 672
7.3 Mixing Rules / 673
Gas Mixture at Low to Moderate Pressures / 673
Gas Mixture at High Pressures / 673
8 Liquid Thermal Conductivity / 674
8.1 Baseline Method / 674
Miller et al.'s Empirical Correlation ⁸⁶ / 674
Baroncini et al.'s Method / 675
8.2 High-Pressure Correction / 677
8.3 Mixing Rules / 677
9 Gas Diffusivity / 678
9.1 Baseline Method / 678
Chapman and Enskog's Method ⁴³ / 678
Wilke and Lee's Method ⁹¹ / 680
9.2 High-Pressure Correction / 680
9.3 Mixing Rules / 683
10 Liquid Diffusivity / 684
10.1 Baseline Method / 684
Wilke–Chang Correlation ⁹⁴ / 684
Tyn and Calus's Method ⁹⁵ / 685
Hayduk and Minhas's Method ⁹⁶ / 686
Tyn's Method for Higher Temperatures ⁹⁷ / 686
10.2 High-Pressure Correction / 687
10.3 Mixing Rules / 687
Perkins and Geankoplis's Method ⁹⁹ / 687
References / 688

Appendix B Constants and Conversion Factors Often Used in Combustion	693
Appendix C Naming of Hydrocarbons and Properties of Hydrocarbon Fuels	697
Appendix D Melting, Boiling, and Critical Temperatures of Elements	705
Appendix E Periodic Table and Electronic Configurations of Neutral Atoms in Ground States	707
Reference / 711	
Author Index	713
Subject Index	718



PREFACE

The field of combustion has advanced substantially in the past few decades. Major advancements have been made in experimental, theoretical, and computational areas. Newly developed nonintrusive diagnostic techniques allow researchers to explore detailed phenomena associated with ignition and combustion processes. At the same time, increased computational power allows engineers and scientists to simulate detailed reaction mechanisms and transport processes. Highly comprehensive model simulations can also be conducted with in-depth consideration of many complex physicochemical processes. For example, the thermal and transport properties can be treated as functions of local state variables (like temperature and pressure) in the reacting flow field. Multidimensional time-dependent combustion problems can also be solved with intricate details. Furthermore, new combustible materials have been synthesized and developed. Some of these materials include nano-sized energetic ingredients. It is also feasible to study combustion of materials with complex composition and geometry.

In view of rapid expansion of knowledge and capability in the exciting field of combustion, it is impossible to present the basic principles and representative studies of various topics in a single book. Therefore, I have decided to expand the original edition into two books. The added space allows me to include relevant information in many subject areas. For example, in Chapter 2, much more chemical kinetic information and reaction mechanisms are now covered in the new edition. Reaction mechanisms of H_2/O_2 system, hydrocarbon/ O_2 and hydrocarbon/air systems are especially covered. NO_x formation mechanisms are discussed in detail. Results of many sensitivity analyses are presented. A description of the manage of a very powerful Chemkin code is also included.

This book is intended to touch upon many works and include a substantial amount of up-to-date information on basic principles associated with combustion processes. However, it is still impossible to include every aspect of combustion science and engineering development. This book emphasizes the fundamentals of combustion, as follows:

- An Introduction shows a global picture of combustion and its applications;
- Chapters 1–3 give background information for beginners in chemical thermodynamics, chemical kinetic and reaction mechanisms, and conservation

equations and boundary conditions for multicomponent chemically reacting systems;

- Chapter 4 addresses the differences between gas-phase deflagration and detonation waves and contains more up-to-date-studies in multidimensional detonation of premixed gases;
- Chapter 5 discusses laminar premixed flames with many new approaches and solutions;
- Chapter 6 discusses laminar diffusion flames and single liquid droplet combustion with significant coverage of supercritical combustion;
- Appendix A contains a brand new section describing the fundamental relationships of transport and thermal properties with state variables, high-pressure correction methods, and mixing rules for gaseous and liquid mixtures. This information can be used to facilitate the evaluation of transport and thermal properties;
- Appendixes B, C, D, and E contain useful information for research purposes.

A future book, addressing more advanced combustion problems, will be finalized at a later date and will concentrate on the combustion of condensed-phase material in two-phase flows (such as spray combustion of liquid droplets and combustion of an aggregate of solid particles), fundamentals of turbulent flows, turbulent premixed flames, turbulent diffusion flames of single-phase systems, ignition processes of homogeneous gas mixtures and condensed-phase materials, reacting boundary-layer flows, and combustion of nano-sized energetic materials.

The second edition of *Principles of Combustion* is aimed towards graduate (or advanced undergraduate) students who have an interest in combustion. It is also designed for combustion engineers and scientists to be used as a reference book in their research, development, and design work.

Based upon my teaching experience at the Pennsylvania State University, the content of this book can be covered in one graduate course if key portions of the first six chapters and Appendix A are selected. Certain portions of the first four chapters can also be used for undergraduate combustion course material. The material covered in the future book is usually taught in a subsequent combustion course, called “Turbulent and Two-Phase Combustion.”

I would like to thank the many graduate students who took my combustion courses and conducted numerous projects based upon recent published articles in their term papers. Certain portions of selected term papers were modified and expanded to form a part of the new text in the second edition.

I would like to acknowledge the contribution of many of my colleagues at The Pennsylvania State University (Prof. Daniel Haworth, Prof. Richard A. Yetter, Prof. Matthew Mench, Prof. Robert J. Santoro, Prof. Michael M. Micci and Prof. Vigor Yang), who have spent their valuable time in reading parts of my manuscripts and providing extremely valuable comments and suggestions for clarifications and modifications. Ragini Acharya, one of my Ph.D. students, has helped in organizing and assembling many technical papers for Chapter 2 and

has assisted me in making the manuscript more readable for beginners. Thanks to Debbie Kimble and Fred Coppersmith for their help in typing different chapters and putting the manuscript into the format required by the publisher. Without their help, the publication of this new edition would have been impossible.

I had planned to develop the second edition for some time. However, my research, teaching, and professional society activities have occupied an enormous amount of time. I was unable to complete the modifications of this second edition until now. I would like to thank Wiley for its patience. I would also like to take this opportunity to apologize to those individuals who have been waiting to read the second edition of this book.

I want to also thank my family for their encouragement and support, including my wife, Olivia J. Kuo, my daughters, Phyllis and Angela, my parents, Wen-li and Wen-chen, and my sister, Katherine K. Lu. This book is dedicated to my beloved wife, Olivia, and two daughters, whose understanding, patience, and support have greatly enhanced my professional career and facilitated the opportunity for the completion of this book.

KENNETH K. KUO

University Park, Pennsylvania

June 16, 2004



PREFACE TO THE FIRST EDITION

Today's combustion engineers and scientists are often confronted with complex phenomena which depend upon interrelated processes of fluid mechanics, heat and mass transfer, chemical kinetics, thermodynamics, and turbulence. Understanding of the fundamental concepts of these coupled processes will provide engineers and scientists with the technical background and training required to solve various combustion problems. This book is devoted to the fundamentals of chemically reacting flow systems with application to power production, jet and rocket propulsion, fire prevention and safety, pollution control, material processing industries, and so on.

As is evident from the above applications, the subject of combustion is wide-ranging and important. Although many idealized problems of combustion have been attacked and solved in simplified forms in the past, there are still many practical problems that defy exact solution today. Real life is indeed much more complicated than the idealized situations considered in the past. The investigation of real-life problems in the combustion field has really just begun. The techniques for formulating and solving coupled problems certainly will and should receive increasingly greater attention in the years ahead. The need for instructional material which stresses interrelations of heat, mass, and momentum transfer in chemical reacting systems is therefore quite obvious and indeed crucial.

Only a few books have been published on combustion, and of them, many do not include recent major developments. Other books are specialized and often too advanced for a general combustion course. Having taught a graduate level combustion course for the last several years, I am actually aware of the need for a book which gives a comprehensive and modern treatment of combustion. To do justice to the subject, I had to collect material from many sources to form my lecture notes. This book has been developed through a continuous updating and modification of these lecture notes.

Another problem with existing textbooks on combustion is the paucity of examples to demonstrate the application of theory. In this book—especially in the first few chapters, which deal with the fundamental aspects of combustion—many examples have been presented to help readers assimilate the important concepts of combustion.

In keeping with recent practice, metric units have been employed throughout the book.

The level of this book is suitable for either senior or graduate courses in combustion. Full coverage of the material will generally require six semester credits of course work. It is suggested that Chapters 1 through 6 be covered in the first semester and Chapters 7 through 10 in the second.

The emphasis of this book is on the theoretical modeling of combustion, though experimental techniques are described wherever relevant. Particular attention has been paid to theoretical formulations of combustion problems for solution with the aid of digital computers. It should be noted that rapid progress in the combustion field precludes any possibility of including all theoretical models for exhaustive treatment.

The book has been organized into 10 chapters with exercises and/or projects at the end of each chapter. Many chapters are provided with a list of the new symbols introduced in them. A short, perspicuous introduction to combustion modeling is provided at the beginning of this book to give the reader an overview of the need, basic procedures, and application of combustion modeling. Chapters 1, 2, and 3 are essential background material for the study of combustion, dealing with chemical thermodynamics, chemical kinetics, and conservation equations for multicomponent reacting flows. Chapter 4 deals with deflagration and detonation waves in premixed gases as well as the deflagration-to-detonation transition. The next chapter deals with premixed laminar flames. Chapter 6 is a treatment of laminar diffusion flame jets and the combustion of a single liquid droplet. Turbulent flames and their modeling techniques are discussed in Chapter 7. Spray combustion of fuel droplets and burning of solid particles in convective streams are treated in Chapter 8. Chapter 9 deals with various types of chemically reacting boundary-layer flows. The final chapter covers the topic of ignition, which is intimately related to combustion.

Those who are familiar with my research in the field of solid propellant combustion may be surprised to see a limited coverage of it in this book. I must mention that the recent developments in this field were summarized by many specialists in the AIAA Progress Series, Volume 90, entitled *Fundamentals of Solid Propellant Combustion*, edited by Professor Martin Summerfield and me, published in December 1984 by the AIAA.

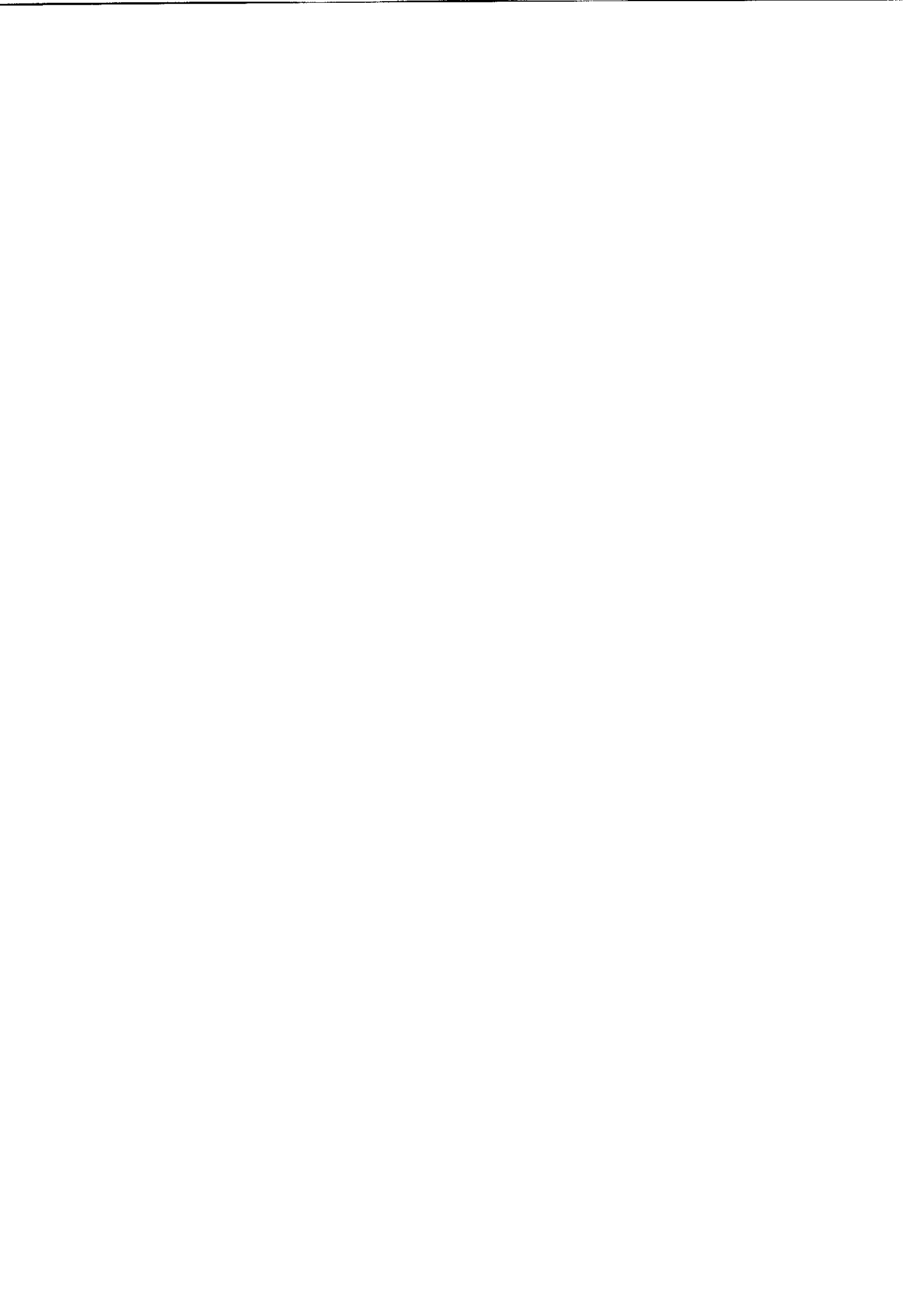
I would like to give special thanks to my colleague Professor Gerard M. Faeth, not only for his encouragement for writing this book, but also for his valuable suggestions for improving this book. He generously provided much useful information on spray combustion, which forms a major portion of Chapter 8; to the field of spray combustion, he and his coworkers have made many significant contributions. I must also thank Dr. Kevin White and Mr. Leland A. Watermeier of the U.S. Army Ballistic Research Laboratory (BRL) for organizing a combustion course at BRL during my sabbatical leave. Through the teaching of that course, I have obtained valuable feedback from many combustion scientists and engineers. I would also like to thank Dr. Joseph M. Heimerl of BRL for his

valuable suggestions and comments. All the graduate students in my combustion course have contributed immensely toward the improvement of my class notes. Through their term papers and project assignments, I have been able to incorporate many up-to-date theoretical models and techniques. The painstaking efforts of Dr. Louis K. Chang in drawing most of the illustrations deserve special thanks. The help of Mrs. Mary Jane Coleman in typing the manuscript is also highly appreciated. Last, but by no means least, I would like to thank my wife, Olivia, for her understanding, love, and patience. I would also like to thank my daughters, Phyllis and Angela, who gave me love and happiness during my undertaking of this time-consuming but enjoyable task.

KENNETH K. KUO

University Park, Pennsylvania

March 1986



INTRODUCTION

The field of combustion is extremely broad, covering theoretical, experimental, and numerical areas. The emphasis of this book is on theoretical modeling so that combustion processes can be formulated properly for analytical or numerical solution. Model validation by experimental data is also included for many combustion problems.

IMPORTANCE OF COMBUSTION IN VARIOUS APPLICATIONS

Now let us address the question “Why is combustion important?” As we know, a very high percentage ($\sim 80\%$) of energy comes from combustion of liquids (such as gasoline and hydrocarbon fuels), solids (such as coal and wood), and gases (such as natural gas composed of largely methane and other hydrocarbons like ethane, propane, butanes, and pentanes). There are broad applications of combustion in the following areas:

Power Generation

- Coal particles are burned in furnaces of power stations to produce steam for driving turbines in order to generate electricity.
- Liquid fuels are used as the source of energy for transportation purposes with automobiles, aircrafts, ships, etc.
- Natural gases are used for gas turbines, reciprocating engines, etc.

2 INTRODUCTION

- Solid propellants and fuels are burned in rocket motors for space and missile propulsion.
- Fuel cells are used for direct electricity production (strictly speaking, not a combustion process but involving chemical reactions).
- Waste materials are incinerated.

It is anticipated that combustion will remain a predominant source of power for many generations. The coal storage on earth can still be used for another thousand years.

Process Industry for Production of Engineering Materials

- Production of iron, steel, glass, ceramics, cement, carbon black, refined fuels, etc., through thermal heating processes
- Direct fabrication of ceramic materials by self-propagating high-temperature synthesis (SHS) processes
- Combustion synthesis of nanosized powders

Household and Industrial Heating

- Heating of residence homes, industrial factories, offices, hospitals, schools, and various types of buildings
- Heating of sky labs and many special facilities

Safety Protections for Unwanted Combustion

- Fire prevention for forest fires
- Fire prevention for building fires
- Reduction of industrial explosions
- Reduction of susceptibility for deflagration-to-detonation transitions leading to catastrophic hazards

Ignition of Various Combustible Materials for Safety Enhancement under Emergency Situations

- Inflation of airbags during collision of automobiles
- Actuation of ejection pilot seats and other emergency escape systems
- Fire extinguishment by strong-flow gas generators

Pollutant Emission Control of Combustion Products

- Reduction of formation of NO_x , SO_x , CO, etc.
- Reduction of formation of particulates such as soot, coke, etc.
- Control of the temperature and chemical compositions of combustion products
- Control of the production rate of greenhouse gases such as CO_2 by using nonhydrocarbon fuels

Active Control of Combustion Processes

- Control of combustion instabilities in various propulsion systems
- Enhancement of combustion efficiencies of reactors by external energy sources, such as acoustic emission
- Enhancement of combustion efficiencies of certain systems with injection of nano-sized energetic particles

As one example, it may be useful at this stage to ask the question “Why is it necessary to burn in chemical rockets?” As we know, chemical rockets are designed to produce high thrust forces during their takeoff and flight. In order to gain high thrust force for propulsion, we have to convert the chemical energy of propellants to thermal energy by combustion and then expand the flow through an exit nozzle so that a good portion of the thermal energy is converted to kinetic energy of the discharging jet from a convergent-divergent nozzle to produce thrust. The thrust of the propulsion system is proportional to the momentum of the exhaust jet. The specific impulse (I_{sp}), defined as the thrust per unit propellant weight flow rate, is known to be proportional to the square root of flame temperature divided by the average molecular weight of the combustion products, i.e., $I_{sp} \sim [T_f/M_w]^{1/2}$. Therefore, the higher the T_f from combustion, the higher the I_{sp} .

RELATED CONSTITUENT DISCIPLINES FOR COMBUSTION STUDIES

Besides the broad applications previously mentioned, another major reason for the importance of combustion is the fact that many combustion problems are yet to be solved. Our society indeed needs many well-trained combustion engineers and scientists to tackle numerous challenging combustion problems. The science of combustion often involves complex interactions between many constituent disciplines. Background in the following areas would be very helpful for combustion studies:

- Thermodynamics
- Chemical kinetics
- Fluid mechanics
- Heat and mass transfer
- Turbulence
- Transport phenomena
- Statistical mechanics
- Quantum physics
- Instrumentation and diagnostic techniques
- Materials' structure and behavior
- Mathematical and statistical theories
- Numerical methods

4 INTRODUCTION

- Design of combustion test apparatus
- Data analysis and correlation methods
- Safety and hazard analysis

GENERAL METHOD OF APPROACH TO COMBUSTION PROBLEMS

In terms of the method of approach for solving combustion problems, one can consider the following methods:

- Theoretical methods
- Numerical methods
- Experimental methods
- Any combination of the above methods

Whenever possible, it is best to be able to tackle combustion problems both theoretically and experimentally. To be economic and efficient, it is essential to apply the basic principles in our combustion studies.

GENERAL OBJECTIVES OF COMBUSTION MODELING

The objectives of combustion modeling are given below:

- To simulate certain combustion processes
- To develop predictive capability for combustion systems under various operating conditions
- To help in interpreting and understanding observed combustion phenomena
- To substitute for difficult or expensive experiments
- To guide the design of combustion experiments
- To determine the effect of individual parameters in combustion processes by conducting parametric studies

In general, any theoretical model should be validated by comparison with reliable experimental data before it is used for prediction and evaluation of the influence of any parameters. Thus the combustion test rig design, diagnostic measurements, and data analysis are very useful for model validation purpose.

CLASSIFICATION OF COMBUSTION PROBLEMS

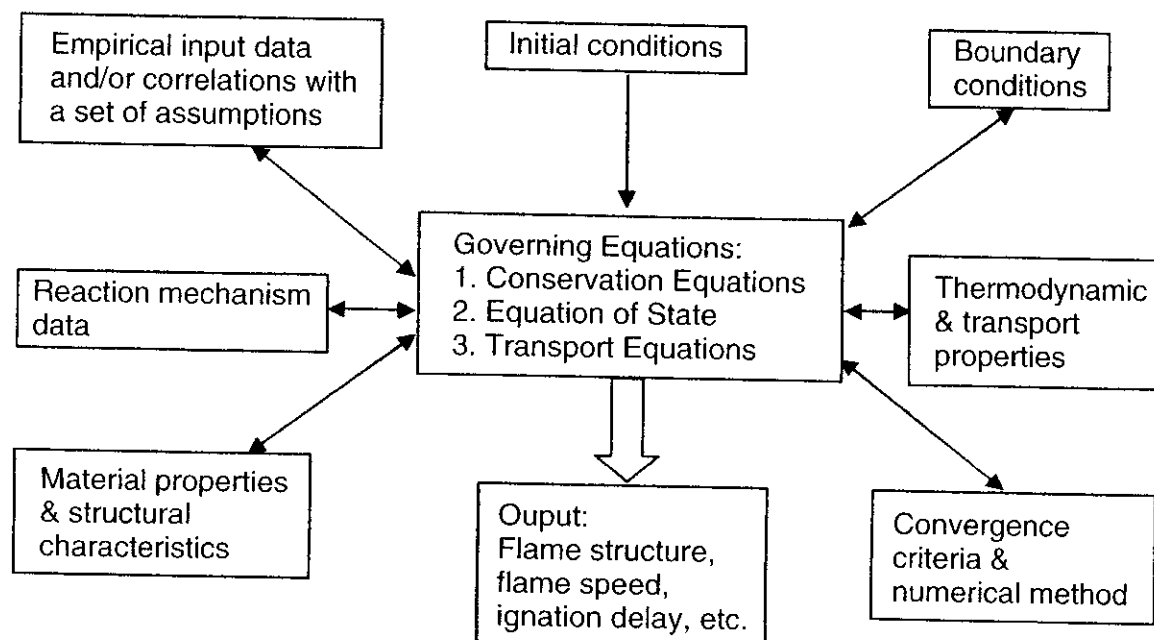
Now, let us make some classifications of combustion problems. Usually, the classification is based on several factors, including the time and spatial dependence, the mixing condition of the initial reactants, flow conditions, initial phases of reactants, sites of reactions, rate of reaction, type of convection, degree of compressibility of the flow, and speed of the combustion wave. Table I.1 summarizes the various classifications of combustion problems. This table is particularly

Table I.1 Classification of Combustion Problems

Condition of Combustion	Classification Adjectives
Time dependence	Steady or unsteady
Spatial dependence	1D, 2D planar, 2D axisymmetric, or 3D
Mixing condition of initial reactants	Premixed or nonpremixed (diffusion)
Flow conditions	Laminar or turbulent
Initial phases of reactants	Single-phase, two-phase, or multiphase
Sites of reactions	Homogeneous or heterogeneous
Rate of reaction	Chemical equilibrium (infinite rate) or finite rate
Type of convection	Natural convection or forced convection
Degree of compressibility of flow	Incompressible or compressible
Speed of the combustion wave	Deflagration (subsonic combustion wave) or Detonation (supersonic combustion wave)

useful to beginners in becoming familiar with the terminology used in chemically reacting flows.

Figure I.1 illustrates the essential elements required to form a theoretical model. It also describes the relationships between various components of the model. It is evident that the governing equations are coupled to all other branches of the model. Depending on the complexity of the specific problem, some coupling relationships may exist between various branches of the model. Based on the difference in simplification of some detailed processes, some models require more empirical input data/correlations than others. Quite often these required empirical input data/correlations must be determined separately from some experiments if they are not readily available.

**Figure I.1** General structure of a theoretical model.

GENERAL STRUCTURE OF A THEORETICAL MODEL

Governing Equations for Combustion Modeling (Conservation and Transport Equations)

Conservation equations consist of

- Conservation of mass (continuity equation)
- Conservation of molecular species (or conservation of atomic species)
- Conservation of momentum (for each independent spatial direction)
- Conservation of energy
- Conservation of angular momentum

Usually the conservation equations are used together with the equations of state (both thermal and caloric) to solve for flow property distributions, including temperature, density, pressure, velocity, and concentrations of chemical species. The angular momentum components in different directions are solved when the conservation equations of angular momentum are considered in the model.

Transport equations are additional equations that are usually required for turbulent combustion problems; typical examples are

- Transport of turbulence kinetic energy
- Transport of turbulence dissipation rate
- Transport of turbulent Reynolds stresses
- Transport of probability density function
- Transport of moments such as $\widetilde{u''Y_i''}$, $\widetilde{T''^2}$, $\widetilde{Y_i''^2}$, $\overline{u'v'}$, $\overline{u'Y_i'}$...

Figure I.2 shows the general procedure in the development of a theoretical model for simulating combustion processes. This chart is self-explanatory.

Some Common Assumptions Made in Combustion Models (Especially for Classical Models)

- Reacting fluid can be treated as a continuum.
- Infinitely fast chemistry (chemical equilibrium).
- Simple, one-step, forward irreversible reaction.
- Ideal gas law.
- Lewis, Schmidt, and Prandtl numbers equal to one.
- Equal mass diffusivities of all species.
- Fick's law of diffusion is valid.
- Constant specific heats of the gas phase.
- Reacting solid surfaces are energetically homogeneous.
- Uniform pressure for low-speed combustion situations.
- Dufour and Soret effects are negligible.

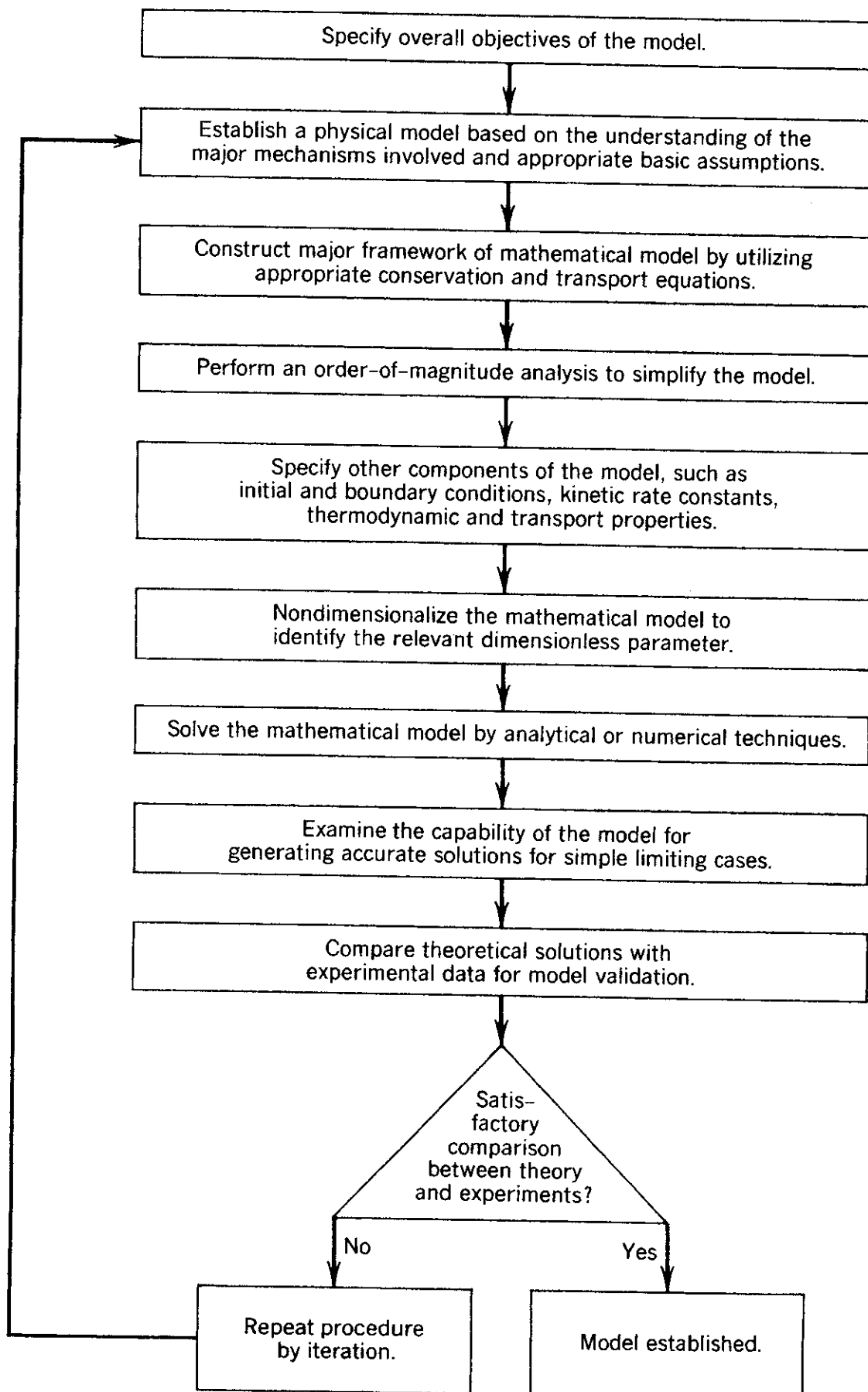


Figure I.2 General procedure in the theoretical model development.

- Bulk viscosity is negligibly small.
- Negligible combustion-generated turbulence.

With the advancement of computer and numerical techniques, many of these assumptions can now be avoided.

SEVERAL BASIC DEFINITIONS

Mole Numbers Gaseous molecules and atoms are conveniently counted in terms of amount of substances or mole numbers. One mole (1 mol or 1 g-mol) of compound corresponds to 6.02252×10^{23} molecules (or atoms).

Avogadro's Number

$$N_A = 6.02252 \times 10^{23} \text{ molecules/mol}$$

Mole Fraction

$$X_i = \frac{n_i}{\sum_{i=1}^N n_i} = \frac{n_i}{n} \quad (\text{I-1})$$

where n_i represents the number of moles of the i th species in the mixture

Mass Fraction

$$Y_i = \frac{m_i}{\sum_{i=1}^N m_i} = \frac{m_i}{m} \quad (\text{I-2})$$

Molecular Weight

Mw_i (unit: g/mol or kg/kmol)

e.g., $Mw_{H_2} = 2.016 \text{ g/mol}$, $Mw_C = 12 \text{ g/mol}$,

$Mw_{O_2} = 32 \text{ g/mol} = 32 \text{ kg/kmol}$, $Mw_{CH_4} = 16 \text{ g/mol}$

Average Molecular Weight of a Mixture

$$\overline{Mw} = \sum_{i=1}^N X_i Mw_i \quad (\text{I-3})$$

The relationship between Y_i and n_i or Y_i and X_i are given below.

$$Y_i = \frac{Mw_i n_i}{\sum_{j=1}^N Mw_j n_j} = \frac{Mw_i X_i}{\sum_{j=1}^N Mw_j X_j} = \frac{Mw_i X_i}{\overline{Mw}} \quad (\text{I-4})$$

This implies

$$X_i = \frac{Y_i}{Mw_i} \overline{Mw} = \frac{Y_i / Mw_i}{\sum_{j=1}^N (Y_j / Mw_j)} \quad (\text{I-5})$$

Mass Density (Density)

$$\rho = \frac{m}{V} \quad (\rho \text{ in kg/m}^3) \quad (\text{I-6})$$

Molar Density (Concentration)

$$C = \frac{n}{V} \quad (C \text{ in mol/m}^3) \quad (\text{I-7})$$

$$\frac{\rho}{C} = \frac{m}{n} = \overline{M_w} \quad (\text{I-8})$$

Equation of State For an ideal gas, we can use the following equation of state:

$$PV = nR_uT = mRT \quad (\text{I-9})$$

where R_u is the universal gas constant [$= 8.314 \text{ J/(mol K)}$]. The values of R_u in other units are listed in Appendix B.

$$c = \frac{n}{V} = \frac{P}{R_u T} = \frac{P}{R \overline{M_w} T} \quad (\text{I-10})$$

$$\rho = \frac{m}{V} = \frac{P}{RT} = \frac{P \overline{M_w}}{R_u T} = \frac{P}{R_u T \sum_{i=1}^N (Y_i / M_{w,i})} \quad (\text{I-11})$$

Fuel–Oxidant Ratio, F/O

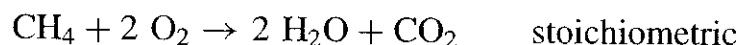
$$F/O \equiv \frac{F}{O} = \frac{\text{mass of fuel}}{\text{mass of oxidant}} \quad (\text{I-12})$$

Equivalence Ratio, ϕ

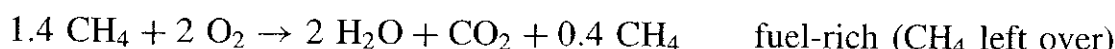
$$\phi = \frac{(F/O)}{(F/O)_{\text{st}}} \quad (\text{I-13})$$

- $0 < \phi < 1$ fuel-lean
- $\phi = 1$ stoichiometric condition
- $1 < \phi < \infty$ fuel-rich

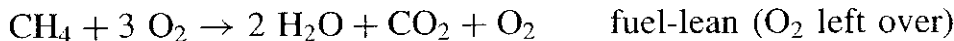
A premixed gas mixture is said to be *stoichiometric* if the fuel (e.g., CH₄) and oxidizer (e.g., O₂) consume each other completely, forming only carbon dioxide (CO₂) and water (H₂O); i.e.,



If there is an excess of fuel, the system is called fuel-rich; e.g.,



If there is an excess of oxidizer, the system is called fuel-lean; e.g.,



If the chemical reaction equation is written in the form to describe exactly the reaction of 1 mol of fuel, the mole fraction of the fuel in a stoichiometric mixture with oxygen can be calculated as

$$X_{\text{fuel,st}} = \frac{1}{1 + n_{\text{O}_2,\text{st}}} \quad (\text{I-14})$$

If dry air is used as the oxidizer to react with 1 mole of fuel, then the mole fraction of the fuel in a stoichiometric mixture with dry air can be calculated as

$$X_{\text{fuel,st}} = \frac{1}{1 + n_{\text{O}_2,\text{st}} + n_{\text{N}_2,\text{st}}} = \frac{1}{1 + 4.762 \cdot n_{\text{O}_2,\text{st}}} \quad (\text{I-15a})$$

The factor of 4.762 comes from $(1 + \frac{79}{21})$, since air contains 21% oxygen and 79% N₂ (with the noble gas portion lumped into nitrogen). Therefore, the $X_{\text{N}_2,\text{st}}$ is related to $X_{\text{O}_2,\text{st}}$ by

$$X_{\text{N}_2,\text{st}} = 3.762 X_{\text{O}_2,\text{st}} \quad (\text{I-15b})$$

The mole fraction of O₂ in the stoichiometric mixture, $X_{\text{O}_2,\text{st}}$ is related to $X_{\text{fuel,st}}$ by

$$X_{\text{O}_2,\text{st}} = n_{\text{O}_2,\text{st}} X_{\text{fuel,st}} \quad (\text{I-15c})$$

For a more general situation, other than stoichiometric condition, the mole fractions of different chemical components in a combustible mixture with air having an equivalence ratio ϕ are related by the following set of equations:

$$X_{\text{fuel}} = \frac{1}{1 + (4.762 \cdot n_{\text{O}_2,\text{st}})/\phi} \quad (\text{I-16a})$$

$$X_{\text{air}} = 1 - X_{\text{fuel}} \quad (\text{I-16b})$$

$$X_{\text{O}_2} = X_{\text{air}}/4.762 \quad (\text{I-16c})$$

$$X_{\text{N}_2} = 3.762 X_{\text{O}_2} \quad (\text{I-16d})$$

Stoichiometry, Ψ A parameter called *stoichiometry* (Ψ) has been used in the combustion field. This parameter is defined as the ratio of the mole percent of the fuel in the combustible mixture to the mole percent of the fuel under stoichiometric condition, i.e.,

$$\Psi \equiv X_{\text{fuel}} / X_{\text{fuel,st}} \quad (\text{I-17})$$

Note that Ψ is closely related to the equivalence ratio (ϕ) but they are not identical to each other.

1

REVIEW OF CHEMICAL THERMODYNAMICS

Symbol	Description	Dimension
a	Affinity	
C	Molar concentration	N/L^3
C_P	Constant-pressure specific heat	$Q/(MT)$
C_v	Constant-volume specific heat	$Q/(MT)$
e	Specific internal energy	Q/M
e_t	Total stored energy per unit mass	Q/M
E	Stored energy	Q
f	Fugacity	F/L^2
f	Mixture fraction	
F/O	Fuel–oxidant ratio	
G	Gibbs free energy	Q
g	Gravitational acceleration	L/t^2
g_c	Factor of proportionality	ML/Ft^2
g_i	Molar specific Gibbs free energy for i th species	Q/N
H	Enthalpy	Q
\mathcal{H}	Molar specific enthalpy	Q/N
K_C	Equilibrium constant based on species concentration	$(N/L^3)^{\sum(v''_{i,e} - v'_{i,e})}$
K_n	Equilibrium constant based on moles of species	$N^{\sum(v''_{i,e} - v'_{i,e})}$

(continued overleaf)

Symbol	Description	Dimension
K_P	Partial-pressure equilibrium constant	
K_X	Mole-fraction equilibrium constant	
K_Y	Mass-fraction equilibrium constant	
KE	Kinetic energy	Q
m	Order of chemical reaction	
M	Total mass	M
M_i	Chemical symbol for species i	
m_i	Mass of species i	M
$M_{w,i}$	Molecular weight of species i	M/N
n_i	Number of moles of species i	N
n_t	Total number of moles of chemical species	N
p	Total system pressure	F/L^2
p_i	Partial pressure of species i	F/L^2
PE	Potential energy	Q
\hat{Q}	Heat	Q
R	Gas constant of gas mixture	$Q/(MT)$
R_u	Universal gas constant	$Q/(NT)$
S	Entropy	Q/T
s	Molar specific entropy	$Q/(NT)$
T	Temperature	T
t	Time	t
u_i	Velocity in the x_i -direction	L/t
U	Internal energy	Q
v	Specific volume	L^3/M
\mathbf{v}	Resultant velocity	L/t
V	Volume	L^3
\hat{W}	Work	Q
x_i	Space coordinate in the i th direction	L
X	Mole fraction	
Y	Mass fraction	
z	Elevation	L
Z	Compressibility factor, $pv = ZRT$	
$\Delta\mathcal{H}_{f,i}^\circ$	Standard heat of formation of species i	Q/N
ΔH_r	Heat of reaction	Q
$\Delta\mathcal{H}_v$	Heat of vaporization	Q/N
Γ	Proportionality constant f_i/p_i	
ε	Reaction progress variable	
μ	Chemical potential	Q/N
v'_i	Stoichiometric coefficient for species i appearing as a reactant	N
v''_i	Stoichiometric coefficient for species i appearing as a product	N
ρ	Density	M/L^3
ϕ	Equivalence ratio	

Symbol	Description	Dimension
<i>Superscript</i>		
^o	Standard-state condition (298.15 K and 1 bar)	
<i>Subscripts</i>		
<i>g</i>	Gas phase	
<i>i</i>	Index for <i>i</i> th species, or initial condition	
<i>l</i>	Liquid phase	
<i>p</i>	Constant-pressure process	
<i>s</i>	Solid phase	
<i>v</i>	Constant-volume process	
<i>Dimension Symbols</i>		
<i>F</i>	Force	
<i>L</i>	Length	
<i>M</i>	Mass	
<i>N</i>	Mole	
<i>Q</i>	Heat	
<i>t</i>	Time	
<i>T</i>	Temperature	

In this chapter, we briefly introduce and discuss some of the fundamental concepts of chemical thermodynamics and their application in solving those types of combustion problems in which only the initial and final thermodynamic states of a system are concerned. The application of a well-established chemical equilibrium calculation program (CEA), developed by Gordon and McBride^{1,2} to solve for the final equilibrium product composition and adiabatic flame temperature of a chemical system, is also discussed. Although many examples are given in this chapter to illustrate the use of chemical thermodynamic principles, the scope is too limited to provide an extensive discussion of every aspect of chemical thermodynamics. The reader is referred to the bibliography at the end of this chapter³⁻¹⁵ for broader coverage on chemical thermodynamics.

To set the scope of the chemical thermodynamics, let us first make a distinction between heat-transfer theory and thermodynamics. While heat-transfer theory deals with energy-transfer processes within a system or between a system and its surroundings due to a temperature gradient, thermodynamics deals with systems in equilibrium and therefore is applicable to phenomena involving flow and irreversible chemical reactions only when departures from equilibrium are small.

It is also important to note that the approach used in chemical thermodynamics is not a microscopic approach. Chemical thermodynamics treats matter in bulk, that is, with no regard for detailed molecular structures and microscopic events. Unlike kinetic theory, which can provide a certain amount of information about the rates of chemical processes, chemical thermodynamics can give only the final equilibrium conditions.

It is useful to define *thermodynamic equilibrium* by considering the following three distinct kinds of equilibrium:

- *Mechanical equilibrium* exists when there are no unbalanced forces in the interior of a system or between a system and its surroundings.
- *Thermal equilibrium* exists when all parts of a system are at the same temperature, which is the same as that of the surroundings.
- *Chemical equilibrium* exists when a system has no tendency to undergo a spontaneous change in chemical composition, no matter how slow.

When all three kinds of equilibrium are satisfied, the system is said to be in a state of *thermodynamic equilibrium*. Under such condition, the analysis becomes simpler, since the state variables do not change with respect to time. The state of complete equilibrium can then be described in terms of macroscopic coordinates. It is found that the thermodynamic coordinates that are independent and appropriate for combustion studies are the pressure in the system p , the volume V , and n_i , which represents the moles of all chemical species in different phases present in the system. Therefore, the symbol n_i stands for $n_{1g}, n_{2g}, \dots, n_{Ng}$ of all gas-phase species plus $n_{1l}, n_{2l}, \dots, n_{Nl}$ of all liquid-phase species and $n_{1s}, n_{2s}, \dots, n_{Ns}$ of all solid-phase species in the system.

The approach to be taken here will be that of irreversible (nonequilibrium) thermodynamics rather than classical. It is useful to understand the major difference between the two and the reason for using the nonequilibrium approach in combustion studies. First of all, classical thermodynamics can make predictions only about states of thermodynamic equilibrium; it can tell us nothing about the rates at which processes take place. When a process is followed by means of classical thermodynamics, it must be regarded as consisting of a succession of states of thermodynamic equilibrium, that is, as taking place infinitely slowly. Such processes are necessarily reversible. A *reversible* process is one that is performed in such a way that the system and its surroundings can both return to their initial states. Such a process must be carried out very slowly so that the system remains in equilibrium throughout. In the real world, we must deal with irreversible processes that are a succession of nonequilibrium states. To do this in any detail, the notions of classical thermodynamics must be supplemented.

For systems in mechanical or thermal nonequilibrium, the usual procedure is to divide the system into a large number of subsystems that are of infinitesimal size relative to the original system, but still of macroscopic size relative to the molecular structure of the medium. By assuming that each subsystem is in local equilibrium internally (but not necessarily in equilibrium with its surrounding subsystems), we can apply equilibrium thermodynamics and the concept of state variables to the subsystems. We can thus construct, by integration, a picture of the behavior of the entire nonequilibrium system. This is normally done with such success in fluid dynamics and heat transfer that it is scarcely given a second thought.

When we come to the description of a system in chemical nonequilibrium, the procedure is somewhat different. We shall assume that the system is in mechanical and thermal equilibrium and that it is homogeneous in space. We assume the system to have a definite volume V ; since it is in mechanical and thermal equilibrium, we can assign to it a definite pressure p . Furthermore, since the system is homogeneous, its composition can be specified by giving the number of moles,[†] n_i , of each of the constituent chemical species, M_i . Thus, the thermodynamic state of a system of N chemical species can be completely stated by specifying the values of p , V , n_1, n_2, \dots, n_N ; the pressure, p , is an intensive property, while V and n_i ($i = 1, 2, \dots, N$) are extensive properties. Intensive and extensive properties are defined as follows:

An *intensive* property is one that is unchanged when the size of the system is increased by adding to it any number of systems that are identical to the original system. Some intensive properties are density, pressure, temperature, specific internal energy u , specific entropy s , chemical potential of j th species μ_j , mass fraction of k th species Y_k , and so on.

An *extensive* property is one that increases in proportion to the size of the system in such a process. Some extensive properties are volume V , mass m , total stored energy E , enthalpy H , Gibbs free energy G , kinetic energy KE, potential energy PE, and so on.

An intensive property can be formed by dividing an extensive property by another extensive property.

1 BRIEF STATEMENT OF THERMODYNAMIC LAWS

When discussing the laws of thermodynamics, it is useful to classify systems according to the exchanges of energy (heat and work) and mass that can take place across the system boundary:

- *Isolated* systems exchange neither energy nor mass with their surroundings; i.e., $\delta\hat{Q} = 0$ and $\Delta m = 0$.
- *Closed* systems exchange energy but no mass with their surroundings.
- *Open* systems exchange both energy and mass with their surroundings.

A. The Zeroth Law of Thermodynamics This states that there exists an intensive variable, the temperature

$$T = T(p, V, n_i) \quad (1-1)$$

[†] The unit g-mole is commonly used for n_i ; one g-mole designates the quantity of substance M_i whose mass in grams is equal to the molecular weight of the substance. One mole of any substance contains 6.02252×10^{23} molecules; these molecules could be in the form of atoms, ions, radicals, or undissociated molecules. This number is called Avogadro's number in honor of the Italian physicist Amedeo Avogadro. Avogadro's number can also be considered as 6.02252×10^{26} molecules/kmole.

When two bodies have the same temperature as a third body, they have the same temperature as each other and therefore will be in equilibrium if placed in thermal contact. In other words, two systems are in thermal equilibrium with each other if they have the same temperature. This seems very obvious to us because we are so familiar with the experimental result. Though formulated after the other laws, it precedes them logically, and for this reason it has been called the zeroth law. This law suggests the need for a standard scale for temperature measurements. Equation (1-1) is called the equation of state.

B. The First Law of Thermodynamics (Conservation of Energy) This states that there exists an extensive function called the stored energy E , composed of (1) internal energy U , (2) kinetic energy KE, and (3) potential energy PE:

$$E = U + \text{KE} + \text{PE} \quad (1-2)$$

where

$$E = E(p, V, n_i) \quad (1-3)$$

The function E has the property that, for a closed system (no mass exchange with its surroundings), the heat added to the system in an infinitesimal process is related to the change of E and the work done by the system ($\delta\hat{W}$), according to

$$\delta\hat{Q} = dE + \delta\hat{W} \quad (1-4)$$

where the caret (\wedge) over a variable indicates that the variable is not a thermodynamic property, and δ indicates an inexact differential, since \hat{Q} and \hat{W} are path-dependent functions. Note that the work done by the system in chemical equilibrium can be written as $p dV$.

The first law under no change of KE and PE can be written as

$$dU = \delta\hat{Q} - p dV \quad (1-4a)$$

For a constant-volume condition, we have

$$du = \delta\hat{Q} \quad (1-4b)$$

Since the enthalpy H is defined as $H \equiv U + pV$ or $dH = dU + p dV + V dp$, the first law in the form of Eq. (1-4a) becomes

$$dH = \delta\hat{Q} + V dp \quad (1-4c)$$

For $p = \text{constant}$,

$$dH = \delta\hat{Q} \quad (1-4d)$$

The work terms in the energy conservation equation in a flow system are derived in Chapter 3. The conversion between heat and work for systems undergoing cyclic variations is discussed in the next section.

C. The Second Law of Thermodynamics This states that there exists an absolute scale for the temperature and an extensive function called the entropy:

$$S = S(p, V, n_i) \quad (1-5)$$

Thus, for an infinitesimal process in a closed system,

$$TdS \geq \delta\hat{Q} \quad (1-6)$$

where the equality is valid for reversible processes and the inequality valid for natural (irreversible) processes.

D. The Third Law of Thermodynamics According to W. H. Nernst and M. Planck, this states that the entropy of a perfect crystal is zero at the absolute zero of temperature. This is used as the base or the reference value for evaluating entropies of various substances. As stated clearly by Van Wylen and Sonntag,³ from a statistical point of view this means that the crystal structure is such that it has the maximum degree of order. It also follows that a substance that does not have a perfect crystalline structure at absolute zero but instead has a degree of randomness (such as a solid solution or a glassy solid) has a finite value of entropy at absolute zero. The experimental evidence on which the third law rests is primarily data on chemical reactions at low temperatures and measurements of the heat capacity at temperatures approaching absolute zero. The molar entropy of the substance at temperature T and 1 bar can be calculated from

$$S_T^o = S_{T_o}^o + \int_{T_o}^T \frac{\bar{C}_P}{T} dT$$

where T_o is the reference temperature, at which $S_{T_o}^o$ is known. At temperature T and pressure p , the molar entropy can be calculated from

$$S_{T,P} = S_T^o - R_u \ln \frac{p}{p_o}$$

if the assumption of ideal gas behavior along the isotherm at T yields an insignificant amount of error.

2 EQUATION OF STATE

In general, for a closed system of known material at a volume V and temperature T , there will be one set of values of n_i for which the system is in chemical equilibrium. Then,

$$n_i^* = n_i^*(V, T) \quad (1-7)$$

where the values of n_i^* are the equilibrium values. The equation of state for a system in equilibrium becomes

$$p = p(V, T, n_1^*, n_2^*, \dots, n_N^*) \quad (1-8)$$

From Dalton's law of partial pressures, we know that for a mixture of thermally perfect gases in thermodynamic equilibrium,

$$p = \frac{1}{V} \sum_{i=1}^N n_i^* R_u T \quad (1-9)$$

The pressure of the system in chemical nonequilibrium can be represented by the following equation, which has the same form as Eq. (1-9) except the asterisk has been removed from n_i :

$$p = \frac{1}{V} \sum_{i=1}^N n_i R_u T \quad (1-10)$$

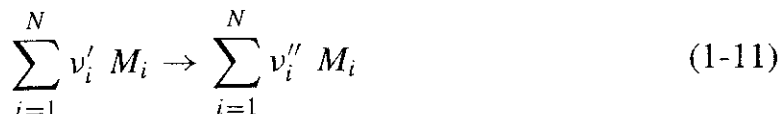
or expressed as

$$p = \frac{n_t R_u T}{V} = \frac{mRT}{V} = \frac{RT}{v} \quad (1-10a)$$

where n_t is the total number of moles of all chemical species in the system.

3 CONSERVATION OF MASS

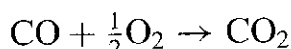
In a closed system, the total mass of the contents cannot change. If the system is under a chemical nonequilibrium situation, the amounts of the individual species will vary. A single arbitrary chemical reaction can be written as



where v'_i is the coefficient for species i appearing as a reactant, v''_i is the coefficient for species i appearing as a product, and M_i represents the chemical symbol for species i . Species that are not reactants have $v'_i = 0$, while those that do not appear as products have $v''_i = 0$.

Equation (1-11) implies that when $(v''_i - v'_i)$ moles of M_i are formed, $(v'_j - v''_j)$ moles of M_j disappear due to the chemical reaction (note that $j \neq i$). This reaction equation indicates a relationship between the changes in the number of moles of each species.

Example 1.1. Let us consider the oxidation of CO to form CO₂, according to



Let

$$M_1 = \text{CO}$$

$$M_2 = \text{O}_2$$

$$M_3 = \text{CO}_2$$

Then,

$$v'_1 = 1 \quad v''_1 = 0$$

$$v'_2 = \frac{1}{2} \quad v''_2 = 0$$

$$v'_3 = 0 \quad v''_3 = 1$$

When

$$v_3'' - v_3' = 1 \text{ mole of CO}_2 \text{ is formed, } \Delta n_3 = 1$$

$$v_1' - v_1'' = 1 \text{ mole of CO disappears, } \Delta n_1 = -1$$

$$v_2' - v_2'' = \frac{1}{2} \text{ mole of O}_2 \text{ disappears, } \Delta n_2 = -\frac{1}{2}$$

#

This example shows that we obtained the following relationship between the changes of moles of reactants and the product species:

$$\frac{\Delta n_1}{v_1'' - v_1'} = \frac{\Delta n_2}{v_2'' - v_2'} = \frac{\Delta n_3}{v_3'' - v_3'}$$

Now let us generalize it to any elementary reaction involving an infinitesimal change. It is convenient to introduce a dimensionless single-reaction progress variable ε , so that

$$dn_i = (v_i'' - v_i') d\varepsilon \quad i = 1, 2, \dots, N \quad (1-12)$$

If $n_{i,r}$ denotes the number of moles of the various species at the same initial or reference condition at which ε is zero, the above equation can be integrated to obtain

$$n_i - n_{i,r} = (v_i'' - v_i')\varepsilon \quad i = 1, 2, \dots, N \quad (1-13)$$

It follows from Eq. (1-13) that for a closed system in which a single reaction occurs, the n_i 's in the thermodynamic state relations can be replaced by the quantities $n_{i,r}$ and the degree of reaction ε . For a system in which the composition at some reference condition is known, the thermochemical state of the system can be specified by

$$p = p(V, T, \varepsilon) \quad (1-14)$$

where the quantity ε can itself be regarded as a state variable. Chemical equilibrium for a given V and T will correspond to certain equilibrium values of n_i^* , and hence to a specific value ε^* of ε .

If m_i is the mass of the i th species and Mw_i the molecular weight of that species, then from Eq. (1-12)

$$dm_i = (v_i'' - v_i') Mw_i d\varepsilon \quad i = 1, 2, \dots, N \quad (1-15)$$

Since the total mass of a closed system is constant,

$$m = \sum_{i=1}^N m_i = \text{constant} \quad (1-16)$$

We therefore have

$$\sum_{i=1}^N dm_i = 0 \quad (1-17)$$

Substituting Eq. (1-15) into Eq. (1-17), we have

$$\sum_{i=1}^N [(v''_i - v'_i) Mw_i] d\varepsilon = 0 \quad (1-18)$$

If the degree of the reaction is not zero (i.e., $d\varepsilon \neq 0$), then

$$\sum_{i=1}^N [(v''_i - v'_i)] Mw_i = 0 \quad (1-19)$$

which is known as the *stoichiometric equation*. If Eq. (1-12) is differentiated with respect to time, we obtain

$$\frac{dn_i}{dt} = (v''_i - v'_i) \frac{d\varepsilon}{dt} \quad (1-20)$$

which is the rate equation.

4 THE FIRST LAW OF THERMODYNAMICS; CONSERVATION OF ENERGY

The first law of thermodynamics states that during any cycle a system undergoes, the cyclic integral of the heat is equal to the cyclic integral of work, i.e.,

$$\oint \delta \hat{Q} = \oint \delta \hat{W} \quad (1-21)$$

where $\oint \delta \hat{Q}$ is the cyclic integral of the energy transfer or the net heat transferred during the cycle, and $\oint \delta \hat{W}$ is the cyclic integral of the work or the net work done during the cycle. The first law also implies the existence of a function of state called the stored energy E of the system and relates the change of this function to the flow of energy from the surroundings.

The existence of the thermodynamic property E can be demonstrated as follows: By Eq. (1-21), we can write the cyclic integral of heat and work by taking paths a and b (Fig. 1.1). Then, we have

$$\int_{1a}^{2a} \delta \hat{Q} + \int_{2b}^{1b} \delta \hat{Q} = \int_{1a}^{2a} \delta \hat{W} + \int_{2b}^{1b} \delta \hat{W} \quad (1-22a)$$

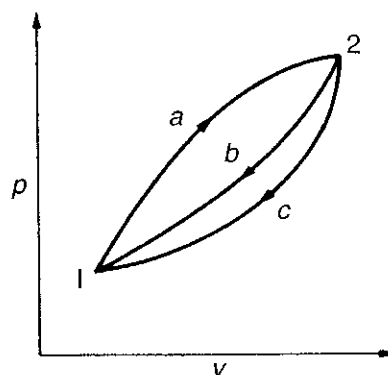


Figure 1.1 Demonstration of the existence of the thermodynamic property E .

We now consider another cycle, the system changing from state 1 to state 2 by process a , as before, and returning to state 1 by process c . Then,

$$\int_{1a}^{2a} \delta \hat{Q} + \int_{2c}^{1c} \delta \hat{Q} = \int_{1a}^{2a} \delta \hat{W} + \int_{2c}^{1c} \delta \hat{W} \quad (1-22b)$$

After subtracting the second of these equations from the first and rearranging them, we have

$$\int_{2b}^{1b} (\delta \hat{Q} - \delta \hat{W}) = \int_{2c}^{1c} (\delta \hat{Q} - \delta \hat{W}) \quad (1-23)$$

Since b and c represent arbitrary processes between states 1 and 2, $(\delta \hat{Q} - \delta \hat{W})$ is the same for all processes between 1 and 2. Therefore, $(\delta \hat{Q} - \delta \hat{W})$ depends only on the initial and final state and not on the path followed between the two states. We may conclude that $(\delta \hat{Q} - \delta \hat{W})$ is a point function and therefore is the exact differential of the system. This property is the energy of the system and is represented by the symbol E . We have

$$dE \equiv \delta \hat{Q} - \delta \hat{W} \quad (1-24)$$

where the sign preceding $\delta \hat{W}$ is negative because $\delta \hat{W}$ is the work done *by* the system.

The physical significance of the property E is that it represents all the energy of the system in the given state. This energy can be present in many forms, including thermal energy, kinetic energy, potential energy (with respect to the chosen coordinate frame), energy associated with the motion and position of molecules, energy associated with atomic structure, chemical energy (e.g., in a storage battery), electrostatic energy (e.g., in a charged capacitor), and so on.

In the study of thermodynamics, it is convenient to consider the bulk kinetic energy and potential energy separately and then to lump all other forms of energy of the system in a single property, which we shall call *internal energy* and give the symbol U . Therefore,

$$E = \text{internal energy} + \text{kinetic energy} + \text{potential energy} = U + \text{KE} + \text{PE}$$

where

$$\text{KE} = \frac{1}{2}m|\mathbf{v}|^2 \quad \text{and} \quad \text{PE} = mgz \quad (1-25)$$

In differential form, this is $dE = dU + d(\text{KE}) + d(\text{PE})$, which from Eqs. (1-24) and (1-25) may be written

$$\delta\hat{Q} = dU + d(\frac{1}{2}m|\mathbf{v}|^2) + d(mgz) + \delta\hat{W} \quad (1-26)$$

Assuming g is a constant, the above equation may be integrated between states 1 and 2 to give

$$_1\hat{Q}_2 = (U_2 - U_1) + m \left[\frac{|\mathbf{v}_2|^2 - |\mathbf{v}_1|^2}{2} \right] + mg(z_2 - z_1) + _1\hat{W}_2 \quad (1-27)$$

Here, the internal energy U is an extensive property like the kinetic and potential energies, since all depend on the mass of the system.

The work term includes three forms of work. *Shaft work* (\hat{W}_s) is work done to produce an effect external to the system, that is, work that can be made to turn a shaft or raise a weight. *Flow work* is work performed to overcome pressure effects at any point on the boundary where mass flow occurs. The flow work rate can be written as

$$p \frac{dV}{dt} = \frac{p}{\rho} \left(\frac{\rho dV}{dt} \right) = \frac{p}{\rho} \dot{m} \quad (1-28)$$

Viscous work (\hat{W}_μ) is work done to overcome fluid friction effects on the boundary where mass flow occurs. The work rate can be written as

$$\frac{\delta\hat{W}}{\delta t} = \frac{\delta\hat{W}_s}{\delta t} + \frac{\delta\hat{W}_\mu}{\delta t} + \int \frac{p}{\rho} d\dot{m}_{\text{out}} - \int \frac{p}{\rho} d\dot{m}_{\text{in}} \quad (1-29)$$

For a closed system undergoing an infinitesimal reversible process, the law is usually expressed in classical (i.e., equilibrium) thermodynamics by the equation

$$dU = \delta\hat{Q} - p dV \quad (1-30)$$

where we have assumed no viscous or shaft work and no kinetic or potential energy change. $\delta\hat{Q}$ represents the amount of heat the system receives from its surroundings, and $p dV$ represents the flow work done by the system. Here, p and U are state functions related to the other variables V and T by state equations of the form

$$p = p(V, T), \quad U = U(V, T) \quad (1-31)$$

For studying chemical nonequilibrium problems, the law of conservation of energy can be applied. It is necessary, however, to redefine the state functions p and U as

$$p = p(V, T, n_1, n_2, \dots, n_N), \quad U = U(V, T, n_1, n_2, \dots, n_N) \quad (1-32)$$

When the system is in equilibrium, the n_i reduce to $n_i^*(T, V)$ and the state equations (1-32) reduce to the equilibrium relations (1-31). We can thus consider complete thermodynamic equilibrium as a special, limiting case of chemical nonequilibrium. In nonequilibrium thermodynamics, as in equilibrium thermodynamics, it is useful to define the enthalpy by the equation

$$H \equiv U + pV \quad (1-33)$$

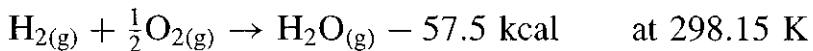
For chemical nonequilibrium cases, H is also given by a state relation of the form

$$H = H(V, T, n_1, n_2, \dots, n_N) \quad (1-34)$$

or

$$H = H(V, T, \varepsilon) \quad (1-35)$$

Example 1.2. Consider the following reaction occurring at a constant volume without any product dissociation:



For a constant-volume process, the first law becomes

$$dU = \delta \hat{Q} \quad (1-36)$$

Since the internal energy is a point function and independent of the path, the energy change equals the heat change for the chemical process, and

$$\Delta U = (\Delta \hat{Q})_v = -57.5 \text{ kcal}$$

Consider the same reaction occurring under constant pressure. The first law for this case is

$$dU = \delta \hat{Q} - p dV \quad (1-37)$$

this integrates to

$$\Delta U = (\Delta \hat{Q})_p - p(\Delta V)_p \quad (1-38)$$

If the reaction is carried out isothermally at T and a constant pressure p , then per mole of H_2O we have

$$\Delta U = (\Delta \hat{Q})_p - R_u T \Delta n$$

where $\Delta n = (n_{\text{products}} - n_{\text{reactants}})_{\text{ideal gas}} = -\frac{1}{2}$. Therefore,

$$(\Delta \hat{Q})_p = \Delta U - \frac{1}{2}R_u T = -57.796 \text{ kcal}$$

Note that this value is different from that of $(\Delta \hat{Q})_v$, since \hat{Q} is a path-dependent variable. This example further demonstrates that 0.296 kcal more heat is evolved

when the reaction is carried out at a constant pressure than at a constant volume. The additional heat, $R_u T \Delta n$, is a result of the work of the surroundings on the gas in maintaining it at a constant pressure p during the reaction, while its volume is decreasing. This shows that the heat evolved in a chemical reaction depends on the physical conditions (path-dependent) under which the reaction occurs.

#

It is useful to note that the first law places no restrictions on the direction of flow of heat and work. We know from our experience that a proposed cycle that does not violate the first law does not ensure that the cycle will actually occur. It is this kind of experimental evidence that has led to the formulation of the second law of thermodynamics. Thus, a cycle³ (such as Rankine cycle, Brayton cycle, Diesel cycle, Otto cycle) will occur only if both the first and second laws of thermodynamics are satisfied.

5 THE SECOND LAW OF THERMODYNAMICS

Before we talk about the second law of thermodynamics, let us recall that a *reversible process* for a system is defined as a process that, once having taken place, can be reversed and, in so doing, leaves no change in either the system or surroundings. In general, factors that render processes irreversible include friction, heat transfer, mixing of different gases, combustion, unrestrained expansion, $i^2 R$ loss, etc.

5.1 Equilibrium Thermodynamics

The second law of thermodynamics postulates the existence of a state function called the entropy S and defines the basic properties of this function. For a closed system that undergoes a change from one state of thermodynamic equilibrium 1 to another state 2, the change in entropy is given by

$$S_2 - S_1 = \int_1^2 \left(\frac{\delta \hat{Q}}{T} \right)_{\text{rev}} \quad (1-39)$$

where *rev* implies any reversible path between 1 and 2, $\delta \hat{Q}$ is the heat received from or added to the system, and T is the corresponding absolute temperature of the reservoir or the system. The important point to note here is that since the change in the entropy of a substance is path-independent, it is also the same for all processes. The equation given here enables us to find the change in entropy only along a reversible path, but once evaluated, the magnitude of change is the same for all processes between these two states. We may also note here that T takes the role of an integrating factor in that it has converted the inexact differential $\delta \hat{Q}$ to the exact differential $(\delta \hat{Q}/T)_{\text{rev}}$.

If the same system undergoes an irreversible or real process between the same two equilibrium end states 1 and 2, we have

$$(S_2 - S_1)_{\text{irrev}} > \int_1^2 \left(\frac{\delta \hat{Q}}{T} \right)_{\text{irrev}} \quad (1-40)$$

where $\delta \hat{Q}$ is the heat added to the system in the particular process.

The above result is arrived at by the following considerations. Consider a system that undergoes two cycles between states 1 and 2; one cycle consists of two reversible processes *a* and *b*, and the other cycle consists of path *a* and an irreversible process *c*. (See Fig. 1.2.) For the reversible cycle,

$$\oint \frac{\delta \hat{Q}}{T} = \int_{1a}^{2a} \frac{\delta \hat{Q}}{T} + \int_{2b}^{1b} \frac{\delta \hat{Q}}{T} = 0 \quad (1-41)$$

For the cycle consisting of the reversible process *a* and the irreversible process *c*, we have

$$\oint \frac{\delta \hat{Q}}{T} = \int_{1a}^{2a} \frac{\delta \hat{Q}}{T} + \int_{2c}^{1c} \frac{\delta \hat{Q}}{T} < 0 \quad (1-42)$$

which is a statement of the inequality of Clausius.³ (The inequality of Clausius is a corollary of the second law of thermodynamics. It has been demonstrated to be valid for all possible cycles.) Subtracting Eq. (1-42) from Eq. (1-41) gives

$$\int_{2b}^{1b} \frac{\delta \hat{Q}}{T} > \int_{2c}^{1c} \frac{\delta \hat{Q}}{T} \quad (1-43)$$

Since entropy is a thermodynamic property and *b* is a reversible process,

$$\int_{2b}^{1b} \frac{\delta \hat{Q}}{T} = \int_{2b}^{1b} dS = \int_{2c}^{1c} dS \quad (1-44)$$

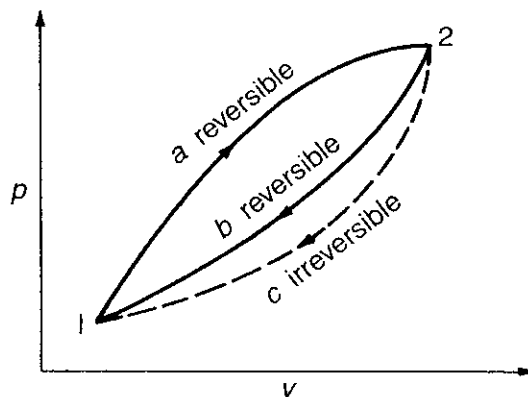


Figure 1.2 Two different cycles to demonstrate the fact that entropy is a property of a substance.

Therefore,

$$\int_{2b}^{1b} dS > \int_{2c}^{1c} \frac{\delta \hat{Q}}{T} \quad (1-45)$$

or, in general,

$$dS \geq \frac{\delta \hat{Q}}{T} \quad (1-46)$$

which when integrated between states 1 and 2 gives the desired result

$$(S_2 - S_1)_{\text{irrev}} > \int_1^2 \left(\frac{\delta \hat{Q}}{T} \right)_{\text{irrev}} \quad (1-47)$$

In both cases considered, the temperature T is the absolute temperature of the reservoir that supplies the heat $\delta \hat{Q}$. Since the temperature of the reservoir and the temperature of the system are equal in a reversible process, T in Eq. (1-39) is also the temperature of the system. For irreversible processes, however, the temperature of the system is undefined within the context of classical thermodynamics. Therefore, we have to consider the nonequilibrium thermodynamics.

5.2 Nonequilibrium Thermodynamics

Given the existence of a variable of state called the entropy S , the change in entropy, dS , in any closed system undergoing any process can be split into two parts:

$$dS = d_e S + d_i S \quad (1-48)$$

where $d_e S$ is the change in entropy resulting from interaction between the system and its surroundings (i.e., heat transfer to or from the system), and $d_i S$ is the change in entropy resulting from a process taking place within the system (e.g., chemical reaction, constant-pressure mixing of different gases). These differential quantities may also be thought of respectively as the flow of entropy into the system from the surroundings and the production of entropy by irreversible processes within the system.

The entropy change $d_i S$ is never negative:

$d_i S = 0$	(reversible process)	(1-49)
-------------	----------------------	--------

$d_i S > 0$	(irreversible process)	(1-50)
-------------	------------------------	--------

For a *closed* system undergoing any process, reversible or irreversible, $d_e S$ is given by

$$d_e S = \frac{\delta Q}{T} \quad (1-51)$$

For a closed system undergoing an irreversible process, Eq. (1-48) becomes, after integration,

$$S_2 - S_1 = \int_1^2 dS = \int_1^2 \left(\frac{\delta \hat{Q}}{T} \right) + \int_1^2 d_i S \quad (1-52)$$

For an irreversible process, $d_i S > 0$, and thus Eq. (1-52) includes the inequality of the classical statement. The latter relationship [Eq. (1-52)] is much more useful than the former [Eq. (1-47)] in that it replaces an inequality by an equality, and thus implies an ability to actually calculate $d_i S$.

For an *isolated* system, $\delta \hat{Q} = 0$; hence $d_e S = 0$ and Eq. (1-48) reduces to

$$dS = d_i S \geq 0 \quad (1-53)$$

This is equivalent to the familiar classical statement that the entropy of an isolated system can never decrease.

If mass is added to an *inert open reversible* system, the entropy associated with the additional mass can be considered to be a part of the entropy flow into the system from the surroundings. We then have

$$dS = d_e S = \frac{\delta \hat{Q}}{T} + \sum_{j=1}^N s_j d_e n_j \quad (1-54)$$

where s_j is the entropy per mole of the j th species added, and $d_e n_j$ is the change in number of moles of the j th species flowing into the system. With mass addition, the first law becomes

$$dU = \delta \hat{Q} - pdV + \sum_{j=1}^N h_j d_e n_j \quad (1-55)$$

where h_j is the enthalpy per mole associated with the j th species flowing into the system.

Let us define a new parameter μ_j in which

$$\mu_j \equiv h_j - Ts_j \quad (1-56)$$

where μ_j represents the chemical potential, which will later be shown to equal the change of Gibbs free energy per mole of the i th species. [The more fundamental definition of μ_j is given by Eq. (1-80), to be discussed later in detail.] Dividing Eq. (1-55) by T , we obtain

$$\frac{\delta \hat{Q}}{T} = \frac{dU}{T} + \frac{pdV}{T} - \frac{1}{T} \sum_{j=1}^N h_j d_e n_j \quad (1-57)$$

Substituting Eqs. (1-57) and (1-56) into Eq. (1-54) gives

$$dS = d_e S = \frac{1}{T} dU + \frac{p}{T} dV - \frac{1}{T} \sum_{j=1}^N \mu_j d_e n_j \quad (1-58)$$

for an *inert open reversible* system.

Equation (1-58) is based on the assumption that all the species involved were chemically inert; hence there exist no irreversible processes resulting from chemical reactions within the system. When chemical reactions occur, the mole number of j th species may change both by mass addition from outside the system and by chemical reaction inside. Then, an infinitesimal process involving change in p , T , and n_j will, in general, be irreversible, since the system will not be in chemical equilibrium. Therefore,

$$dn_j = d_i n_j + d_e n_j \quad (1-59)$$

where $d_i n_j$ represents internal differential change of the moles of the j th species due to chemical reaction occurring inside the system, while $d_e n_j$ represents differential change of the moles of the j th species due to the exchange of j th material with its surrounding. If we further consider each species j to occupy a separate subsystem of the total system, then each subsystem can be regarded as an inert open system. This means that for each species

$$dS_j = \frac{1}{T} dU_j + \frac{p_j}{T} dV - \frac{1}{T} \mu_j dn_j \quad (1-60)$$

where p_j is the partial pressure due to species j , and U_j is the internal energy associated with species j . Summing the preceding equation over all species (i.e., over all subsystems) and noting that

$$p = \sum_{j=1}^N p_j \quad (1-61)$$

$$U = \sum_{j=1}^N U_j \quad (1-62)$$

$$S = \sum_{j=1}^N S_j \quad (1-63)$$

we obtain for the total system

$$dS = \frac{1}{T} dU + \frac{p}{T} dV - \frac{1}{T} \sum_{j=1}^N \mu_j dn_j \quad (1-64)$$

which is the fundamental equation of chemical thermodynamics for *open irreversible chemical processes*. This is identical to Eq. (1-58) with the subscript *e* dropped from the *d*. Equation (1-64) is the result obtained by combining the first and second laws to describe an open system with chemical reactions.

From the equation of state, we have

$$S = S(U, V, n_1, n_2, \dots, n_N) \quad (1-65)$$

or in differential form

$$dS = \left(\frac{\partial S}{\partial U} \right)_{V, n_j} dU + \left(\frac{\partial S}{\partial V} \right)_{U, n_j} dV + \sum_{j=1}^N \left(\frac{\partial S}{\partial n_j} \right)_{U, V, n'_j} dn_j \quad (1-66)$$

where the symbol n'_j in the last term indicates that all mole numbers except n_j itself are held constant when the derivative is taken. By comparing Eqs. (1-64) and (1-66) we have

$$\left(\frac{\partial S}{\partial U} \right)_{V, n_j} = \frac{1}{T} \quad (1-67)$$

$$\left(\frac{\partial S}{\partial V} \right)_{U, n_j} = \frac{p}{T} \quad (1-68)$$

and

$$-T \left(\frac{\partial S}{\partial n_j} \right)_{U, V, n'_j} = \mu_j \quad (1-69)$$

The enthalpy is defined as

$$H \equiv U + pV \quad (1-70)$$

or, in the differential form, as

$$dU = dH - p dV - V dp \quad (1-71)$$

Substituting Eq. (1-71) into Eq. (1-64), we obtain

$$dS = \frac{1}{T} dH - \frac{V}{T} dp - \frac{1}{T} \sum_{j=1}^N \mu_j dn_j \quad (1-72)$$

Similarly we can obtain

$$\mu_j = -T \left(\frac{\partial S}{\partial n_j} \right)_{H, p, n'_j} \quad (1-73)$$

Combining Eq. (1-69) with Eq. (1-73) gives

$$\left(\frac{\partial S}{\partial n_j}\right)_{H,p,n'_j} = \left(\frac{\partial S}{\partial n_j}\right)_{U,V,n'_j} \quad (1-74)$$

In the following, we shall develop the relationship between μ_j and the change of Gibbs free energy. The *Gibbs free energy* G , an extensive property, is defined by the relation

$$G \equiv H - TS = U + pV - TS \quad (1-75)$$

where G , like H , may be considered as a secondary state variable.

In differential form

$$dG = dH - T dS - S dT \quad (1-76)$$

which upon substitution into Eq. (1-72) gives

$$dG = V dp - S dT + \sum_{j=1}^N \mu_j dn_j \quad (1-77)$$

Since

$$dG = \left(\frac{\partial G}{\partial p}\right)_{T,n_j} dp + \left(\frac{\partial G}{\partial T}\right)_{p,n_j} dT + \sum_{j=1}^N \left(\frac{\partial G}{\partial n_j}\right)_{P,T,n'_j} dn_j$$

by comparing the coefficients of the above two equations, we can therefore write

$$V = \left(\frac{\partial G}{\partial p}\right)_{T,n_j} \quad (1-78)$$

$$S = - \left(\frac{\partial G}{\partial T}\right)_{p,n_j} \quad (1-79)$$

$$\mu_j \equiv \left(\frac{\partial G}{\partial n_j}\right)_{p,T,n'_j} = -T \left(\frac{\partial S}{\partial n_j}\right)_{H,p,n'_j} \quad (1-80)$$

where Eq. (1-80) can be taken as the definition of μ_j , which is known as the chemical potential and plays an important role in chemical thermodynamics. The chemical potential, an intensive variable, is in general a function of the state of the system, as given by p , T , and all n_j . Even though a species is not present in a system, its chemical potential need not be zero. There is always the possibility of introducing it into the system, in which case the value of G will be altered, and the value of the corresponding μ_j must therefore be different from zero.

The first law of thermodynamics for an open system can be expressed as

$$dU = \delta \hat{Q} - p dV + d_e U \quad (1-81)$$

where $d_e U$ is the internal energy carried in by mass addition. Substituting this into Eq. (1-64), we obtain

$$dS = d_e S + d_i S = \frac{1}{T} \overbrace{(\delta \hat{Q} - p dV + d_e U)}^{dU} + \frac{p}{T} dV - \underbrace{\frac{1}{T} \sum_{j=1}^N \mu_j d_e n_j}_{-\frac{1}{T} \sum_{j=1}^N \mu_j dn_j} - \frac{1}{T} \sum_{j=1}^N \mu_j d_i n_j$$

Thus,

$$dS = \frac{1}{T} \left(\delta \hat{Q} + d_e U - \sum_{j=1}^N \mu_j d_e n_j \right) - \frac{1}{T} \sum_{j=1}^N \mu_j d_i n_j \quad (1-82)$$

where the two terms on the right-hand side correspond to the terms $d_e S$ and $d_i S$, respectively. Therefore,

$$d_i S = -\frac{1}{T} \sum_{j=1}^N \mu_j d_i n_j \quad (1-83)$$

which upon substitution of Eq. (1-73) becomes

$$d_i S = \sum_{j=1}^N \left(\frac{\partial S}{\partial n_j} \right)_{H, p, n'_j} d_i n_j \quad (1-84)$$

If we consider a single-step forward reaction in a closed system, then $d_i n_j$ can be given in terms of the change of the reaction progress variable, $d\varepsilon$, i.e.,

$$d_i n_j = (v''_j - v'_j) d\varepsilon \quad (1-85)$$

Substitution into Eq. (1-83) gives

$$d_i S = -\frac{1}{T} \left(\sum_{j=1}^N (v''_j - v'_j) \mu_j \right) d\varepsilon \geq 0 \quad (1-86)$$

This expression is required by the second law to be either positive, corresponding to an irreversible process, or zero, corresponding to a reversible process. Saying that a process is reversible in the present context is, however, equivalent to saying that the system is in chemical equilibrium at all times, or that the process is one of an infinitely slow succession of states of chemical equilibrium. The condition for chemical equilibrium is therefore that $d_i S$ be zero at all times, which requires

$$\sum_{j=1}^N (v''_j - v'_j) \mu_j^* = 0 \quad (1-87)$$

where μ_j^* is the value of the chemical potential at the equilibrium state. Therefore, this is the equation of reaction equilibrium. It may be regarded as a universally valid formulation of the law of mass action, since it is not restricted to gases. The quantity $-\sum_{j=1}^N (\nu_j'' - \nu_j') \mu_j$ is known in chemical literature as the *affinity* of the chemical reaction and is commonly denoted by the symbol a :

$$a \equiv -\sum_{j=1}^N (\nu_j'' - \nu_j') \mu_j \quad (1-88)$$

The chemical affinity can play a central role in chemical thermodynamics as elaborated by De Donder and his school¹⁷. In the late 1800s, van't Hoff used affinity to describe the maximum work obtainable from a chemical process in a quantitative expression. In a way, it is equivalent to interpreting the Gibbs free energy of reaction (ΔG)_{T,p} as the driving force of a reaction. Essentially, the word *affinity* is used in connection with reaction tendency. For a reaction at equilibrium, the affinity is zero.

Let us now summarize several important points and physical interpretations about the chemical potential μ_j as follows:

- A. μ_j is often referred to as the partial molar Gibbs function $\mu_j \equiv \left(\frac{\partial G}{\partial n_j} \right)_{p,T,n_j'}$; it represents the change in Gibbs free energy as an infinitesimal amount of species j is added to the system while holding pressure, temperature, and the amount of other species constant.
- B. It is an intensive property and has units of energy/mole.
- C. Equation (1-77) can be integrated in a “process” in which the size of the system is increased by adding systems with the same intensive properties, all intensive properties remain constant, and all extensive properties increase proportionally. Hence, $dT = 0$, $dP = 0$, and $d\mu_j = 0$ in such a process, showing that Eq. (1-77) can readily be integrated from $(G = 0, n_j = 0)$ to (G, n_j) , yielding

$$G = \sum_{j=1}^N \mu_j n_j \quad (1-89)$$

since

$$dG = \sum_{j=1}^N \mu_j dn_j + \sum_{j=1}^N n_j d\mu_j = \sum_{j=1}^N d(\mu_j n_j) = d \left[\sum_{j=1}^N \mu_j n_j \right] \quad (1-90)$$

Therefore, μ_j may be regarded as the contribution of 1 mole of that constituent to the total G value of the system. It might be imagined, in view of the above interpretation, that μ_j was equal to the value of G_j for 1 mole of the constituent j in the pure state. However, this is only true in certain limited circumstances.⁹

In general, μ_j in a solution is not equal to G_j for the pure substance, and further, the value of μ_j varies as the composition of the system changes.

D. For a closed system at constant temperature and constant pressure, it can be shown from Eqs. (1-77) and (1-90) that

$$\sum_{j=1}^N n_j d\mu_j = -S dT + V dp = 0 \quad \text{for constant } T \text{ and } p \quad (1-91)$$

This relation is called the Gibbs-Duhem equation and has many applications, especially in connection with the study of liquid-vapor equilibria.

E. For a system in chemical equilibrium at constant temperature and pressure, we have

$$\sum \mu_j dn_j = 0 \quad (1-92)$$

where the summation includes all the μdn terms for *all the phases* constituting the system. This relation forms the basis of the well-known *phase rule*.

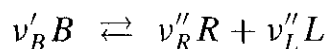
F. When a system consists of a number of components having several phases in complete equilibrium under a given temperature and pressure condition, the chemical potential of each component is the same in all the phases, i.e.,

$$\mu_{j(g)} = \mu_{j(l)} = \mu_{j(s)} \quad \text{for all } j \quad (1-93)$$

This is shown in Ref. 9 and Example 1.3b.

G. If different phases of a given species in a system are not in equilibrium, the chemical potentials of this component will not be the same for different phases. There will then be a tendency for component j to pass spontaneously from a phase in which its chemical potential μ_j is higher than that with lower μ_j . In other words, matter tends to change from a state of higher chemical potential to a state of lower chemical potential. This is the reason why μ_j is given the name of chemical potential. It is a measure of the driving force tending to cause a chemical reaction to take place.

Example 1.3a. Consider the following chemical equilibrium reaction established in any homogeneous mixture in a closed system:



Show that

$$v'_B \mu_B^* = v''_R \mu_R^* + v''_L \mu_L^*$$

Solution: According to Eq. (1-92), the equilibrium condition is

$$\mu_B^* dn_B + \mu_R^* dn_R + \mu_L^* dn_L = 0$$

Note that the variations in the numbers of molecules are not arbitrary, but are governed by the equations

$$dn_R = \frac{v''_R}{v'_B}(-dn_B) \quad \text{and} \quad dn_L = \frac{v''_L}{v'_B}(-dn_B)$$

relating the number of product molecules formed to the number of reactant molecules consumed through appropriate coefficients. Upon substituting these equations into the first one and eliminating the common term dn_B , we have

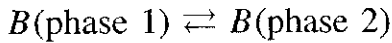
$$v'_B \mu_B^* = v''_R \mu_R^* + v''_L \mu_L^*$$

In general, the condition of homogeneous equilibrium is that the sum of chemical potentials of the reactants equals the sum of the chemical potentials of the products:

$$\sum v'_i \mu_i^* \text{ (reactants)} = \sum v''_j \mu_j^* \text{ (products)}$$

#

Example 1.3b. Consider the following phase equilibrium established between two different phases of a chemically identical substance:



Show that $\mu_1^* = \mu_2^*$.

Solution: The condition of phase equilibrium requires that

$$\mu_1^* dn_1 + \mu_2^* dn_2 = 0$$

Since the total mass is constant, we have

$$dn_1 + dn_2 = 0$$

In order to satisfy both equations under any arbitrary amount of variation of dn_1 , we must have

$$\mu_1^* = \mu_2^*$$

#

6 CRITERIA FOR EQUILIBRIUM

Criteria for chemical equilibrium depend on the condition at which certain thermodynamic properties (or property) are kept constant. For convenience

in constant-volume processes, we introduce another secondary thermodynamic function, called the *Helmholtz free energy* A , defined by

$$A \equiv U - TS \quad (1-94)$$

Physically, A represents the available useful work other than pressure-volume work, when temperature and volume are used as independent variables. This can be seen by following Rossini's approach^{18,11} in extending the formulation of the first law by writing

$$dU = \delta\hat{Q} - p dV + d\hat{\xi} \quad (1-95)$$

where $d\hat{\xi}$ designates the work other than pressure-volume work. For work done on the system, $d\hat{\xi}$ is positive. For work done by the system, $d\hat{\xi}$ is negative. Combining Eq. (1-95) with the second law of thermodynamics, we have

$$d\hat{\xi} = dU - T dS + p dV \quad (1-96)$$

and

$$d\hat{\xi} = dA + S dT + p dV \quad (1-97)$$

It is quite obvious from Eq. (1-97) that

$$d\hat{\xi} = dA \text{ at constant } T \text{ and } V \quad (1-98)$$

Hence, dA represents the available useful work, other than pressure-volume work, at constant T and V . In particular, if dA is negative, then $d\hat{\xi}$ is negative and the system under consideration will do useful work. On the other hand, if $d\hat{\xi}$ is positive for any given process, then work must be done on the system. Finally, if $d\hat{\xi} = 0$, no useful work is done on the system or by the system and the system is at equilibrium.

By the same procedure described above, one can easily obtain the following equation written in terms of Gibbs free energy G :

$$d\hat{\xi} = dG + S dT - V dp \quad (1-99)$$

Hence,

$$d\hat{\xi} = dG \text{ at constant } T \text{ and } p \quad (1-100)$$

The general equilibrium criterion $d\hat{\xi} = 0$ leads to the results summarized in Table 1.1.

For open systems, Eq. (1-64) can be rewritten to show the change of A for an open irreversible chemical reaction process as

$$dA = -S dT - p dV + \sum_{j=1}^N \mu_j dn_j \quad (1-101)$$

Table 1.1 General Equilibrium Criteria for Closed Thermodynamic Systems¹⁸

Variables Held Constant	Thermodynamic Equilibrium Criteria for Closed Systems
p	$dH - T dS = dG + S dT = 0$
V	$dU - T dS = dA + S dT = 0$
T	$d(U - TS) + p dV = dG - V dp = dA + p dV = 0$
S	$dU + p dV = dH - V dp = 0$
p, T	$dG = 0$
V, T	$dA = 0$
P, S	$dH = 0$
V, S	$dU = 0$
S, U or A, T	$dV = 0$
A, V or G, p	$dT = 0$
U, V or H, p	$dS = 0$
G, T or H, S	$dp = 0$

Equations (1-64) and (1-72) can be rearranged to give

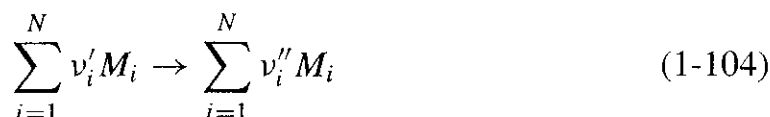
$$dU = T dS - p dV + \sum_{j=1}^N \mu_j dn_j \quad (1-102)$$

$$dH = T dS + V dp + \sum_{j=1}^N \mu_j dn_j \quad (1-103)$$

These equations together with Eq. (1-77) are very useful in chemical equilibrium studies as well as in thermochemical calculations.

7 CONSERVATION OF ATOMIC SPECIES

A generalized single-step reaction can be expressed as

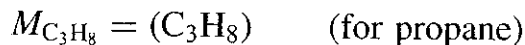
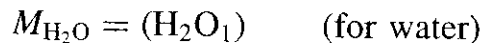


Once the values of v'_i are assigned, there is a constraint on the values of v''_i ; they cannot be arbitrary. This constraint is due to the law of conservation of atomic species.

For any molecular species M_i , we can then write its chemical formula in terms of its atomic composition as

$$M_i = (A_{1a_1} A_{2a_2} A_{3a_3} \cdots)_i \quad (1-105)$$

The symbols A_1, A_2, A_3 , etc., stand for different atomic species, and a_1, a_2, a_3 are the numbers of atoms present in the particular molecular species M_i . For example,



The generalized single-step reaction can then be written as

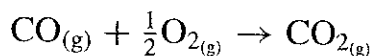
$$\sum_{i=1}^N v'_i (A_{1a_1} A_{2a_2} A_{3a_3} \cdots)_i = \sum_{i=1}^N v''_i (A_{1a_1} A_{2a_2} A_{3a_3} \cdots)_i \quad (1-106)$$

The total number of any given atomic species present in the reaction is conserved. Defining $[A_1]$ as the total number of atomic species A_1 present in the reaction, then

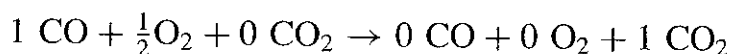
$$[A_1] \equiv \sum_{i=1}^N (v'_i a_{1i}) = \sum_{i=1}^N (v''_i a_{1i}) = \text{constant} \quad (1-107)$$

It is important to note here that if, for example, we have five atomic species in a combustion system, five equations like Eq. (1-107) can be constructed in order to solve for the numbers of moles of products.

Example 1.4. Use the law of conservation of atomic species for the evaluation of the total numbers of atomic species in the following reaction:



Solution: In a more helpful form, the above equation can be written as



Then, the total number of carbon atoms is

$$\begin{aligned} [\text{C}] &= (1 \times 1) + (0.5 \times 0) + (0 \times 1) \\ &= (0 \times 1) + (0 \times 0) + (1 \times 1) = 1 \end{aligned}$$

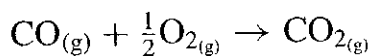
Similarly, for the oxygen atoms,

$$\begin{aligned} [\text{O}] &= (1 \times 1) + (0.5 \times 2) + (0 \times 2) \\ &= (0 \times 1) + (0 \times 2) + (1 \times 2) = 2 \end{aligned}$$

Given the definition of Avogadro's number as representing the number of molecules per mole (6.02252×10^{23} /mole), the molecular weight of the i th species, Mw_i , is the mass of 6.02252×10^{23} molecules and has the units of g/mole. In a gaseous mixture, the number of moles n_i of i th species is equal to the weight of the gas divided by its molecular weight Mw_i :

$$n_i = \frac{m_i g}{g_c Mw_i} \quad (1-108)$$

where g is the gravitational acceleration and g_c is the dimensional conversion factor for gravitation. The values of g_c are given in Appendix B. Then, for the reaction



we have

$$\begin{aligned} \sum_{i=1}^N \left(\frac{m_i g}{g_c} \right)_{\text{reactant}} &= \sum_{i=1}^N \left(\frac{m_i g}{g_c} \right)_{\text{product}} = v'_{\text{CO}} Mw_{\text{CO}} + v'_{\text{O}_2} Mw_{\text{O}_2} = v''_{\text{CO}_2} Mw_{\text{CO}_2} \\ &= (1 \times 28) + (\frac{1}{2} \times 32) = 1 \times 44 = 44 \end{aligned}$$

In general, the mass balance equation for any generalized single-step reaction can be written as

$$\sum_{i=1}^N v'_i Mw_i = \sum_{i=1}^N v''_i Mw_i \quad (1-109)$$

8 VARIOUS METHODS FOR REACTANT-FRACTION SPECIFICATION

The weight of the reactant is generally specified by means of fractions and ratios as follows:

8.1 Mole Fraction X and Mass Fraction Y

The mole and mass fractions of the i th species in a multicomponent system are defined by Eqs. (I-1) and (I-2) in the Introduction. It is useful to note that for N different species in a given system

$$\sum_{i=1}^N X_i = 1 \quad \text{and} \quad \sum_{i=1}^N Y_i = 1 \quad (1-110)$$

At low pressures, it is convenient to use Dalton's law to calculate partial pressures from mole fractions:

$$p_i V = n_i R_u T \quad (1-111)$$

Then,

$$p = \sum_{i=1}^N p_i = \frac{R_u T}{V} \sum_{i=1}^N n_i \quad (1-112)$$

Combining equations (1-111) and (1-112), we have

$$\frac{p_i}{p} = \frac{n_i}{\sum_{i=1}^N n_i} = X_i \quad (1-113)$$

8.2 Fuel–Oxidant Ratio F/O and Fuel–Air Ratio F/A

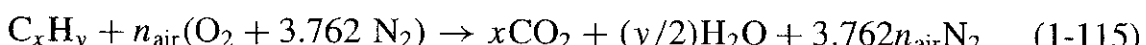
The fuel–oxidant ratio (F/O) is defined by Eq. (I-12). Similarly, the fuel–air ratio F/A can be defined as

$$F/A \equiv \frac{\text{mass of fuel}}{\text{mass of air}} \quad (1-114)$$

8.3 Equivalence Ratio ϕ

As shown in Eq. (I-13) of the Introduction, the equivalence ratio is defined as the ratio of the actual fuel–oxidant ratio (F/O) to the ratio (F/O)_{st} for a stoichiometric process. Physically, a stoichiometric reaction can be considered as a unique reaction in which the oxidizer is just the amount required to completely burn the quantity of fuel in the system. It can be regarded as the most economic reaction.

Quite often the stoichiometric reaction can be written in terms of 1 mole of hydrocarbon fuel in reaction with air. For example,



where the constant 3.762 comes from the ratio of approximately 79% nitrogen to 21% oxygen by volume in the air and

$$n_{\text{air}} = x + y/4 \quad (1-116)$$

The stoichiometric air–fuel ratio can be determined as

$$(A/F)_{\text{st}} = \left(\frac{M_{\text{air}}}{M_{\text{fuel}}} \right)_{\text{st}} = \frac{4.762 n_{\text{air}}}{1} \frac{M_{\text{wair}}}{M_{\text{wfuel}}} \quad (1-117)$$

The equivalence ratio of the fuel–air system can be evaluated from

$$\phi = \frac{(A/F)_{\text{st}}}{(A/F)} = \frac{(F/A)}{(F/A)_{\text{st}}} \quad (1-118)$$

Again, for fuel-rich mixtures, $\phi > 1$ and for fuel-lean mixtures, we have $\phi < 1$. For stoichiometric mixtures, $\phi = 1$. For a general situation, other than

stoichiometric, the mole fractions in a combustible mixture with air are calculated from Eq. (I-16).

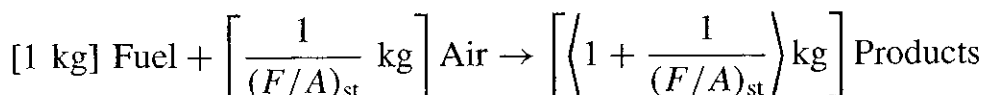
8.4 Mixture Fraction f

Mixture fraction f is a conserved scalar, which can be defined in the most general way as the mass percentage of fuel (both burned and unburned) in a gaseous mixture, i.e.,

$$f = \frac{\text{mass of material having its origin in the fuel stream}}{\text{mass of mixture}} \quad (1-119)$$

Let us consider a stoichiometric combustion process of two streams of reactants (a fuel stream and an air stream, also called the first stream and the auxiliary stream) as shown in the sketch in Fig. 1.3.

In terms of mass balance, the global reaction can be written as



Let us consider the case that the reaction may not be complete due to poor mixing or low temperature conditions. Some portion of the unburned fuel and oxidizer are contained in the "mixture," containing all three types of gases (fuel, air, and product). Assume we know the local mass fractions of these three gases at a downstream location within the mixture. We now would like to find out the fraction of the original material from the fuel stream in a small local control volume in the mixture stream and call this fraction the mixture fraction, f . The next step is to determine the relationship between f , Y_F , Y_P , and $(F/A)_{\text{st}}$. Since no fuel is present in the air stream, the mass fraction of any partially burned material having its origin in the fuel stream can be written as the sum of two parts, namely

$$f = 1 \times Y_F + \frac{1}{1 + 1/(F/A)_{\text{st}}} \times Y_P$$

$$\begin{aligned} \left(\text{Mass fraction of material having its origin in the fuel stream} \right) &= \underbrace{\left(\frac{\text{kg fuel stream}}{\text{kg fuel}} \right)}_{\text{fraction of unburned fuel in the mixture}} \times \left(\frac{\text{kg fuel}}{\text{kg mixture}} \right) \\ &\quad + \underbrace{\left(\frac{\text{kg fuel stream}}{\text{kg product stream}} \right)}_{\text{fraction of burned fuel in the mixture}} \times \left(\frac{\text{kg products}}{\text{kg mixture}} \right) \end{aligned}$$

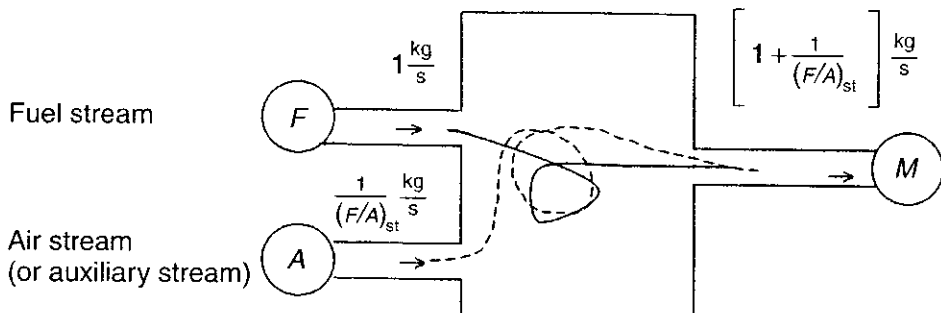


Figure 1.3 Mixing and combustion of fuel and air streams in a combustor.

Therefore, the value of mixture fracture f can be calculated from

$$f = Y_F + \left[\frac{1}{1 + (F/A)_{st}} \right] Y_P \quad (1-120a)$$

In this example, f can be considered to be a “composite” mass fraction, which is a *conserved scalar*, neither created nor destroyed by chemical reactions. As will be discussed in later chapters, the differential equation for f will not have any source terms, since it is a conserved scalar. Now let us consider the air stream that has only oxidizer; then we have

$$f = Y_F + \left[\frac{1}{1 + (F/O)_{st}} \right] Y_P \quad (1-120b)$$

It is useful to prove that the following properties are conserved scalars in this sense:

Y_{inert} —The mass fraction of a chemically inert mixture component

$[Y_F - (F/O)_{st} Y_O]$ —A “composite” mass fraction made of Y_F and Y_O

$\left[Y_F + \frac{(F/O)_{st}}{1 + (F/O)_{st}} Y_P \right]$ —Another “composite” mass fraction, where Y_P is the mass fraction of combustion product

$\left[\left(\frac{F}{O} \right)_{st} Y_O + \frac{(F/O)_{st}}{1 + (F/O)_{st}} Y_P \right]$ —Another “composite” mass fraction

It should be noted that any linear combination of conserved properties, ζ_i

$$a_0 + a_1 \zeta_1 + a_2 \zeta_2 + \cdots + a_n \zeta_n$$

is also a conserved property, where a_0, a_1, \dots, a_n are constants. It can be shown in the two-stream combustion process that the mixture fraction can be expressed as

$$f = \frac{\zeta_M - \zeta_A}{\zeta_F - \zeta_A} \quad (1-121)$$

where ζ represents any conserved property¹⁹ free from sources and sinks.

Using the composite mass fraction $[Y_F - (F/O)_{st}Y_O]$ to represent the ζ for a two-stream mixing/combustion process, the fuel and oxidant mass fractions are then linked with f as follows:

$$f = \frac{[Y_F - (F/O)_{st}Y_O]_M - [Y_F - (F/O)_{st}Y_O]_A}{[Y_F - (F/O)_{st}Y_O]_F - [Y_F - (F/O)_{st}Y_O]_A} \quad (1-121a)$$

If the F stream contains only fuel and the A stream contains oxidizer but no fuel, then we have

$$[Y_F]_A = 0, \quad [Y_F]_F = 1, \quad [Y_O]_F = 0$$

$$f = \frac{[Y_F - (F/O)_{st}Y_O]_M + (F/O)_{st}Y_{O,A}}{1 + (F/O)_{st}Y_{O,A}} \quad (1-122)$$

If chemical reaction is complete within the mixing chamber, either fuel or oxidant will have zero concentration in the M state. Therefore, the stoichiometric value of f is

$$f_{st} = \frac{(F/O)_{st}Y_{O,A}}{1 + (F/O)_{st}Y_{O,A}} \quad (1-123)$$

and

$$f = \frac{-(F/O)_{st}Y_{O,M} + (F/O)_{st}Y_{O,A}}{1 + (F/O)_{st}Y_{O,A}} \quad \text{if } f < f_{st} \text{ (fuel-lean case)} \quad (1-124a)$$

$$f = \frac{Y_{F,M} + (F/O)_{st}Y_{O,A}}{1 + (F/O)_{st}Y_{O,A}} \quad \text{if } f > f_{st} \text{ (fuel-rich case)} \quad (1-124b)$$

Equation (1-124) can be rearranged to give the following values after combustion:

$$\left. \begin{aligned} Y_{F,M} &= 0 \\ Y_{O,M} &= Y_{O,A} \frac{f_{st} - f}{f_{st}} \end{aligned} \right\} \quad \text{for } f < f_{st} \quad (1-125a)$$

$$\left. \begin{aligned} Y_{O,M} &= 0 \\ Y_{F,M} &= \frac{f - f_{st}}{1 - f_{st}} \end{aligned} \right\} \quad \text{For } f > f_{st} \quad (1-125b)$$

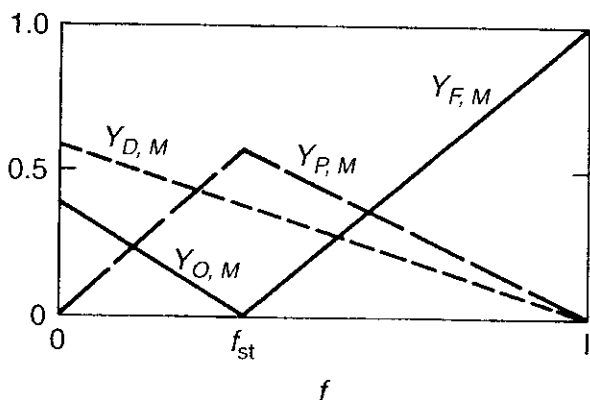


Figure 1.4 A plot of mass fractions of various species as functions of mixture fraction on the totally burned plane.

If the air stream contains some diluent gas, then we have the following relationships for any f :

$$\begin{aligned} Y_{D,M} &= Y_{D,A}(1 - f) \\ Y_{P,M} &= 1 - Y_{D,M} - Y_{O,M} - Y_{F,M} \end{aligned} \quad (1-125c)$$

where $Y_{D,M}$ represents the mass fraction of diluent in the M state. The relationship between Y_O , Y_F , Y_P , Y_D , and f on the burned plane can be expressed by the graph in Fig. 1.4, which consists *entirely of straight lines*. It should be noted that this graph is not the most general form; the F stream could have some diluent, and both streams might also be contaminated with product. It would be a useful exercise for readers to construct an unburned plane of Y_O , Y_F , Y_P , and Y_D versus f and to demonstrate that the dependence of Y_i on f is totally linear. It is important to note that the mixture fraction should be distinguished quite clearly from the mass fraction of fuel, Y_F , and the fuel–oxidant ratio.

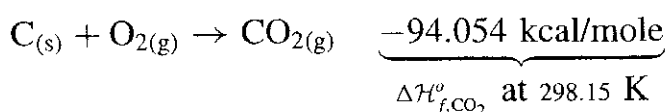
9 STANDARD ENTHALPIES OF FORMATION

The standard enthalpy of formation of the i th substance, $\Delta\mathcal{H}_{f,i}^o$ (kcal/mole), is often called the heat of formation of that substance. It is defined as the heat evolved when 1 mole of the substance is formed from its elements in their respective standard state temperature of 298.15 K and standard state pressure of 1 bar (or 100,000 N/m²). The subscript f indicates formation of the compound from elements, and the index o refers to all products and reactants in their standard states.

The *standard state of an element* is the stable form of that element at room temperature and 1 bar. The standard states of some elements are as follows: H_{2(g)}, O_{2(g)}, N_{2(g)}, Hg_(l), C_(s,graphite). For gases, the reference state is the ideal gaseous state at a pressure of 1 bar and at a given temperature (usually 298.15 K). For

pure liquids and solids, the reference state is the actual state of the substance at 1 bar pressure and a given temperature (mostly 298.15 K). By convention, each element in its standard state is assigned an enthalpy of zero or has a standard heat of formation of zero. It is worthwhile to note that other sources may use a different reference state. One must exercise great care in this regard.

Example 1.5. As an example of the standard heat of formation, reference may be made to the reaction



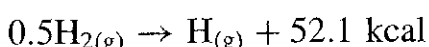
When heat is evolved (*exothermic reaction*) in the formation of the compound, then the ΔH_f^o value of that compound is a negative quantity, since heat must be taken away from the system in order to maintain an isothermal reaction process. The absolute enthalpy of 1 mole of CO_2 in any other state can be found by adding the sensible enthalpy change between the standard state (298.15 K, 1 bar) and the given state (T, p) to the chemical enthalpy, associated with the heat of formation. That is,

$$H(T, p) = \Delta H_{298.15 \text{ K}, 1 \text{ bar} \rightarrow T, p} + \Delta H_f^o \times 1 \text{ mole} \quad (1-126)$$

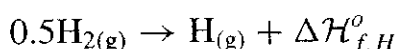
The above equation is not only valid for CO_2 but also valid for calculating the absolute enthalpy of 1 mole of any compound.

#

Now let us consider another formation reaction



which can also be written as



Note that the heat of formation of hydrogen atom is a positive value equal to 52.1 kcal/g-mole. This is due to the fact that external heat must be supplied for the reaction to proceed (*endothermic reaction*). When heat is absorbed in the formation of a compound, the heat of formation of that compound is a positive quantity, since heat must be added to the system. It is useful to note that substances with large positive standard heats of formation are usually more chemically active species.

Example 1.6. Express the heat of formation of 1 mole of a given compound at 1 bar pressure and an arbitrary temperature T , in terms of the heats of formation of the compound at the standard state and the enthalpy changes of all elements involved in the formation chemical reaction.

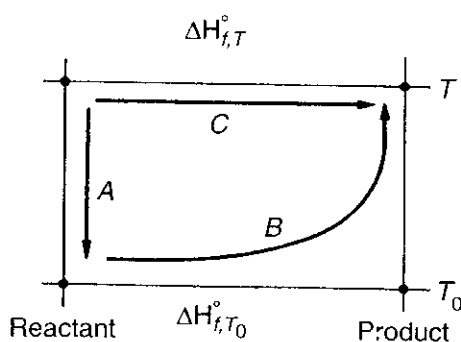


Figure 1.5 Two temperature-reaction paths.

Solution: Figure 1.5 shows that path *C* can be replaced by the sum of paths *A* and *B*; namely,

$$C = A + B = B - (-A)$$

Therefore we can write

$$\Delta H_{f,T}^o = 1 \times [(\mathcal{H}_T^o - \mathcal{H}_{T_0}^o) + \Delta H_{f,T_0}^o]_{\text{compound}} - \sum_{j \text{ elements}} v'_j (\mathcal{H}_T^o - \mathcal{H}_{T_0}^o)_j$$

where the number 1 stands for 1 mole of compound formed.

#

Table 1.2 contains the standard heats of formation of various compounds at 298.15 K. More complete information can be found either from *JANAF Thermochemical Tables*,²⁰ the *Handbook of Chemistry and Physics*,¹⁶ or the users' manual of NASA CEA code developed by McBride and Gordon.²

Table 1.2 Standard Heats of Formation of Selected Substances at 298.15 K^a

Substance	ΔH_f^o (kcal/mol)	Substance	ΔH_f^o (kcal/mol)
$\text{B}_{(s)}$	0.00	$\text{F}_{2(g)}$	0.00
$\text{B}_{(g)}$	133.8 ± 2.9	$\text{F}_{2\text{O}}_{(g)}$	5.86 ± 0.38
$\text{B}_{2(g)}$	198.3 ± 8.0	$\text{HF}_{(g)}$	-65.14 ± 0.19
$\text{B}_2\text{H}_{6(g)}$ diborane	9.8 ± 4.0	$\text{H}_{(g)}$	52.103 ± 0.001
$\text{B}_5\text{H}_{9(l)}$ pentaborane	10.24 ± 1.60	$\text{H}_{2(g)}$	0.00
$\text{BO}_{(g)}$	0 ± 1.91	$\text{OH}_{(g)}$	9.318 ± 0.289
$\text{B}_2\text{O}_{3(s)}$	-304.0 ± 0.50	$\text{H}_2\text{O}_{(g)}$	-57.798 ± 0.010
$\text{BF}_{3(g)}$	-271.41 ± 0.41	$\text{H}_2\text{O}_{(l)}$	-68.315 ± 0.010
$\text{Br}_{(g)}$	26.74 ± 0.01	$\text{H}_2\text{O}_{2(g)}$	-32.530
$\text{Br}_{2(g)}$	7.34 ± 0.03	$\text{H}_2\text{O}_{2(l)}$	-44.880
$\text{HBr}_{(g)}$	-8.71 ± 0.04	$\text{I}_{(g)}$	25.516 ± 0.01
$\text{C}_{(g)}$	171.29 ± 0.110	$\text{I}_{2(g)}$	14.919 ± 0.019
$\text{C}_{(\text{s,diamond})}$	0.45	$\text{I}_{2(s)}$	0.00

(continued overleaf)

Table 1.2 (continued)

Substance	ΔH_f° (kcal/mol)	Substance	ΔH_f° (kcal/mol)
$C_{(s, \text{graphite})}$	0.0	$\text{HI}_{(\text{g})}$	6.300 ± 0.050
$\text{CH}_2\text{N}_{2(s)}$ cyanamide	14.05	$\text{Li}_{(\text{g})}$	38.07 ± 0.240
$\text{CH}_3(\text{g})$	34.82 ± 0.19	$\text{Li}_{(\text{s})}$	0
$\text{CH}_4(\text{g})$	17.895 ± 0.08	$\text{Li}_2\text{O}_{(\text{s})}$	143.10 ± 0.50
$\text{C}_2\text{H}_6(\text{g})$	-20.041	$\text{Li}_2\text{O}_{2(\text{s})}$	151.20 ± 2.01
$\text{C}_3\text{H}_8(\text{g})$	-25.02	$\text{LiH}_{(\text{g})}$	33.610 ± 0.010
$\text{C}_4\text{H}_{10(\text{g})}$ <i>n</i> -butane	-30.065	$\text{LiH}_{(\text{s})}$	-21.660 ± 0.031
$\text{C}_4\text{H}_{10(\text{g})}$ isobutene	-32.263	$\text{LiOH}_{(\text{s})}$	115.90 ± 0.10
$\text{C}_5\text{H}_{12(\text{g})}$ <i>n</i> -pentane	-35.1	$\text{HCN}_{(\text{g})}$	32.29
$\text{C}_6\text{H}_6(\text{g})$ benzene	19.81	$\text{LiF}_{(\text{s})}$	-147.45 ± 0.191
$\text{C}_7\text{H}_8(\text{g})$ toluene	12.07	$\text{N}_{(\text{g})}$	112.97 ± 0.02
$\text{C}_8\text{H}_{10(\text{g})}$ ethylbenzene	7.146	$\text{NH}_{3(\text{g})}$	-10.97 ± 0.096
$\text{C}_8\text{H}_{10(\text{g})}$ <i>o</i> -xylene	4.565	$\text{N}_{2(\text{g})}$	0.00
$\text{C}_8\text{H}_{10(\text{g})}$ <i>m</i> -xylene	4.135	$\text{NO}_{(\text{g})}$	21.580 ± 0.041
$\text{C}_8\text{H}_{10(\text{g})}$ <i>p</i> -xylene	4.302	$\text{NO}_{2(\text{g})}$	7.911 ± 0.191
$\text{C}_6\text{H}_5\text{NH}_{2(\text{l})}$ aniline	-7.553	$\text{NO}_{3(\text{g})}$	17.00 ± 5.00
$\text{CH}_2\text{O}_{(\text{g})}$ formaldehyde	-27.7 ± 1.5	$\text{N}_2\text{O}_{(\text{g})}$	19.61 ± 0.10
$\text{CH}_3\text{OH}_{(\text{g})}$	-48.04	$\text{N}_2\text{O}_{3(\text{g})}$	19.800 ± 0.191
$\text{CH}_3\text{OH}_{(\text{l})}$	-57.01	$\text{N}_2\text{O}_{4(\text{g})}$	2.17 ± 0.41
$\text{C}_{32}\text{H}_{66(\text{s})}$	-231.65 ± 0.15	$\text{N}_2\text{O}_{5(\text{g})}$	2.700 ± 0.311
$\text{CH}_2\text{O}_2\text{N}_{4(\text{s})}$	22.14	$\text{N}_2\text{O}_{5(\text{s})}$	-10.30
$\text{CH}_3\text{ON}_{(\text{l})}$ formamide	-60.71	$\text{N}_2\text{H}_{4(\text{l})}$	12.100 ± 0.096
$\text{CH}_3\text{O}_2\text{N}_{(\text{l})}$ nitromethane	-26.91	$\text{N}_2\text{H}_4 \cdot \text{H}_2\text{O}_{(\text{l})}$	-57.95
$\text{CH}_4\text{ON}_{2(\text{s})}$ urea	-79.613	$\text{Na}_{(\text{g})}$	25.64 ± 0.17
$\text{CH}_5\text{N}_{(\text{g})}$ methylamine	-6.7	$\text{Na}_{(\text{s})}$	0
$\text{CH}_5\text{N}_{3(\text{s})}$ guanidine	-13.38	$\text{Na}_{2(\text{g})}$	33.956 ± 0.287
$\text{CH}_5\text{O}_{4(\text{s})}\text{N}_{3(\text{s})}$ urea nitrate	-114.8	$\text{NaO}_{2(\text{s})}$	-62.300 ± 0.693
$\text{CH}_6\text{O}_3\text{N}_{4(\text{s})}$ guanidine nitrate	91.4	$\text{Na}_2\text{O}_{(\text{s})}$	-99.900 ± 1.004
$\text{CO}_{(\text{g})}$	-26.42 ± 0.04	$\text{Na}_2\text{O}_{2(\text{s})}$	-122.66 ± 1.20
$\text{CO}_{2(\text{g})}$	-94.054 ± 0.012	$\text{NaH}_{(\text{g})}$	29.700 ± 4.590
$\text{C}_2\text{H}_{2(\text{g})}$	54.190 ± 0.189	$\text{NaH}_{(\text{s})}$	-13.489 ± 0.019
$\text{C}_2\text{H}_{4(\text{g})}$	12.540 ± 0.069	$\text{NaOH}_{(\text{s}, \text{II})}$	-101.800 ± 0.096
$\text{C}_2\text{H}_2\text{O}_{(\text{g})}$ ketene	-11.35	$\text{NaF}_{(\text{s})}$	-137.52 ± 0.19

Table 1.2 (continued)

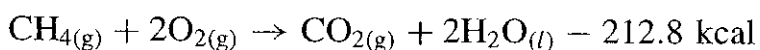
Substance	ΔH_f° (kcal/mol)	Substance	ΔH_f° (kcal/mol)
$C_2H_4O_{(g)}$ ethylene oxide	-12.580 ± 0.15	$HNO_{3(g)}$	-32.10 ± 0.10
$C_2N_{2(g)}$	73.870 ± 0.430	$NH_2OH_{(s)}$	-27.29
$C_2H_4O_{(g)}$ ethylene oxide	-12.580 ± 0.15	$NH_4NO_{3(s)}$	-87.38
$C_2H_3N_{(g)}$ acetonitrile	17.69	$NF_{3(g)}$	-31.570 ± 0.270
$C_2H_3N_{(g)}$ methyl isocyanide	39.08	$NH_4Cl_{(s)}$	-75.14
$C_2H_5O_2N_{(l)}$ nitroethane	-34.39	$NH_4ClO_4(s)$	-70.58
$C_2H_7N_{(g)}$ ethylamine	-11.35	$O_{(g)}$	59.553 ± 0.023
$C_2H_5O_3N_{(g)}$ ethyl nitrite	-36.83	$O_{2(g)}$	0.00
$C_2H_5O_3N_{(l)}$ ethyl nitrate	-45.51	$O_{3(g)}$	34.100 ± 0.406
$C_2H_4O_6N_{2(l)}$ glycol dinitrate	58	$P_{(g)}$	75.619 ± 0.239
$Cl_{(g)}$	28.992 ± 0.002	$PH_{3(g)}$	5.471 ± 0.406
$Cl_{2(g)}$	0	$S_{(g)}$	66.200 ± 0.060
$HCl_{(g)}$	-22.063 ± 0.050	$SO_{2(g)}$	-70.947 ± 0.050
$ClI_{(g)}$	4.184 ± 0.025	$SO_{3(g)}$	-94.590 ± 0.170
$F_{(g)}$	18.974 ± 0.072	$H_2S_{(g)}$	-4.900 ± 0.191

^aConstructed from data in Refs. 2, 20, and 21.

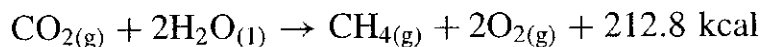
10 THERMOCHEMICAL LAWS

Pioneers A. L. Lavoisier and P. S. Laplace (1780) have been credited with the following law, stated as follows: *The quantity of heat, which must be supplied to decompose a compound into its elements, is equal to the heat evolved when the compound is formed from its elements.* A more general form of this law states that *the heat change accompanying a chemical reaction in one direction is exactly equal in magnitude, but opposite in sign, to that associated with the same reaction in the reverse direction.*

Example 1.7. Consider the following reaction occurring at 298.15 K:



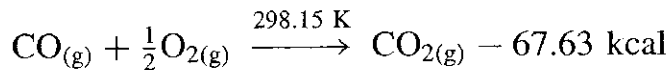
By switching the products and reactants, the sign of the heat evolved must be changed accordingly, i.e.,



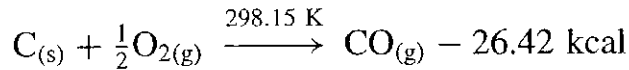
#

In 1840 G. H. Hess developed empirically what is known as the law of constant heat summation. This law states that *the resultant heat change, at constant pressure or constant volume, in a given chemical reaction is the same whether it takes place in one or in several stages*. This means that the net heat of reaction depends only on the initial and final states. As a result of Hess's law, thermochemical equations can be added and subtracted just like algebraic equations. The following example demonstrates the application of this powerful law.

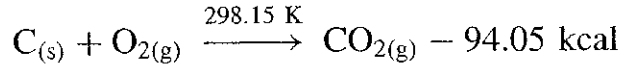
Example 1.8. Show that the standard heat of formation of carbon dioxide in the amount of $-94.05 \text{ kcal/g-mole}$ can be obtained from the known heat of formation of CO and the heat evolved from the following reaction:



Solution: Note that the heat evolved in the above reaction is not the standard heat of formation for 1 mole of $\text{CO}_{2(\text{g})}$, since the reactant $\text{CO}_{(\text{g})}$ is not an element in its standard state. In the formation reaction of 1 mole of $\text{CO}_{(\text{g})}$, we have



Adding the above two thermochemical equations like algebraic equations according to Hess's law, we have



Note that the two species on the reactant side are elements in their respective states. Therefore, this thermochemical equation is the formation reaction of 1 mole of carbon dioxide. Thus, the heat evolved is the standard heat of formation of $\text{CO}_{2(\text{g})}$ and

$$(\Delta\mathcal{H}_f^o)_{\text{CO}_{2(\text{g}), 298.15 \text{ K}}} = -94.05 \text{ kcal/mol}$$

#

11 RELATIONSHIP BETWEEN BOND ENERGIES AND HEATS OF FORMATION

The bond energy for dissociation, $D^\circ(R - X)$, is also known as the strength of a chemical bond between R and X of the molecule RX. When a molecule is dissociated into two parts by the reaction $\text{RX} \rightarrow \text{R} + \text{X}$, the energy required

to break the bond at 298.15 K is related to the heats of formation (also called enthalpies of formation) of the original molecule and its dissociated fragments by

$$D_{298}^o(R - X) = \Delta H_{f,R}^o + \Delta H_{f,X}^o - \Delta H_{f,RX}^o \quad (1-127)$$

Physically, it represents the average amount of energy, per mole, required to break that kind of bond in a molecule and separate the two fragments far apart. In general, the energy required to pull two molecular fragments (R and X) apart is a function of the distance between R and X, as shown in Fig. 1.6. The bond energy corresponds to the difference between the energy level at infinity and the minimum of the potential energy curve. Some bond energies selected from Refs. 16 and 14 are tabulated in Table 1.3. These values are given at 298.15 K rather than at 0 K.

The bond strengths in many different polyatomic molecules are tabulated in Ref. 16. The enthalpies of formation of various free radicals are also given in Ref. 16. Using these tables, it is possible to estimate the standard heats of formation for compounds that have never been synthesized or are unsuitable for burning in a calorimeter.

It is useful to note that the bond energies are based on data for substances in the gaseous state and, therefore, should be used for reactions involving gases only. Also, the bond energy has the negative value of the energy required to form a particular bond. Bond energies can be used to estimate the heats of formation of certain chemical compounds. In addition to the bond energy, one should take into account the possibility of resonance in some molecules in order to estimate their heats of formation. Bond and resonance energies can also be used to estimate the heats of combustion of certain reactions. For example, the benzene molecule C_6H_6 can resonate between the five structures¹¹ shown in Fig. 1.7.

As a result of resonance, $\Delta H_{f,C_6H_6}^o$ is much larger than the sum of three C=C, three C–C, and six C–H bond energies. The additional energy is termed the resonance energy; it must be considered in addition to the bond energies to calculate the actual heat of formation of a given chemical compound. The resonance energy of C_6H_6 is 48.9 kcal/mol. The use of resonance energy in enthalpy of formation

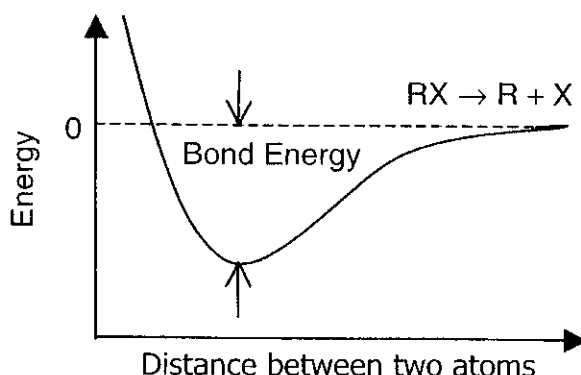


Figure 1.6 Potential energy between two molecular fragments as a function of interatomic separation distance.

Table 1.3 Some Bond and Resonance Energies
Bond Energies in Some Diatomic Molecules¹⁶

Bond	Energy, D_{298}^o (kcal/mol)	Bond	Energy, D_{298}^o (kcal/mol)
H–H	104.20	C–O	≥ 141.97
F–F	37.95	C–Cl	94.89 ± 6.93
Cl–Cl	57.98	Br–C	66.92 ± 5.02
Br–Br	46.08	C–I	49.95 ± 5.02
I–I	36.11	C–F	131.93
C–H	80.88 ± 0.29	N≡N	225.94 ± 0.14
H–N	≤ 81.02	C=C	145.08 ± 5.02
H–O	102.20	O=O	119.11
Cl–H	103.16	Al–O	122.13 ± 0.72
Br–H	87.55	C≡N	180.28 ± 2.39
H–I	71.32		

Mean Bond Energies^{14,16}

Bond	Energy (kcal/mol)	Bond	Energy (kcal/mol)
Br–Br	46	H–F	135
C–C	85	H–H	103
C=C	145	H–I	72
C≡C	194.3	H–P	76
C–Br	67	H–S	81
C–Cl	78	I–I	36
C–F	102	N–H	88
C–H	98.1	N–N	60
C–I	64	N≡N	225
C–N	81	O–H	109
C≡N	210	O–N	150
C–O	86	O–O	33.1
C=O	173	O=O	117
C–S	64	P–Br	64
Cl–Cl	57	P–Cl	78
F–F	36	P–P	48
H–Br	88	S–Cl	60
H–Cl	103	S–S	50

Resonance Energies of Selected Compounds

Compound	Resonance Energy (kcal/mol)
Benzene, C ₆ H ₆	48.9
–COOH group (carboxyl group)	28
CO ₂	33
Naphthalene, C ₁₀ H ₈	88.0
Aniline, C ₆ H ₅ NH ₂	69.6

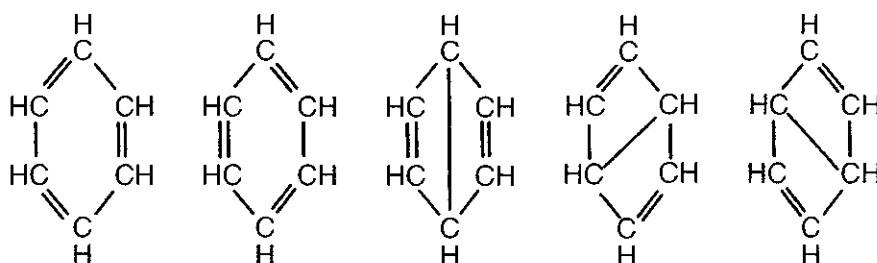


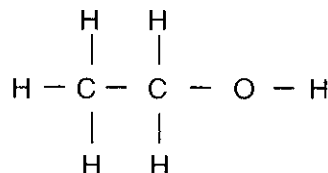
Figure 1.7 Different molecular structures of the benzene (C₆H₆) molecule.

calculation is given in Ref.¹¹. Some examples (e.g., Example 1.11) are provided in a later section to describe the use of resonance energies.

Note that Table 1.3 has three parts. Part 1 shows the bond energies of some selected diatomic molecules, part 2 gives the mean bond energies between some selected atoms, and part 3 shows the resonance energies of some particular molecules for which different molecular structures exist; their resonance energies must be considered in the estimation of their heats of formation.

Example 1.9. Use the tabulated bond energies to estimate the heat of formation of ethanol, C₂H₆O_(g).

The molecular structure of C₂H₆O_(g) is



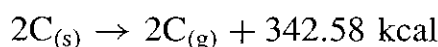
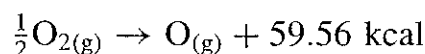
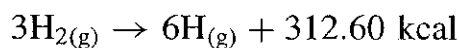
The energy required to form one mole of C₂H₆O_(g) is

$$\begin{aligned} & 5(\text{C-H}) + (\text{C-C}) + (\text{C-O}) + (\text{O-H}) \\ & = 5 \times (-98.1) + (-85.5) + (-86) + (109) = -771 \text{ kcal/mole} \end{aligned}$$

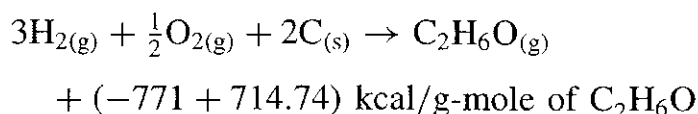
Therefore, we may write the thermochemical equation as



In order to obtain the heat of formation of C₂H₆O_(g), we must utilize Hess's law and the thermochemical equations



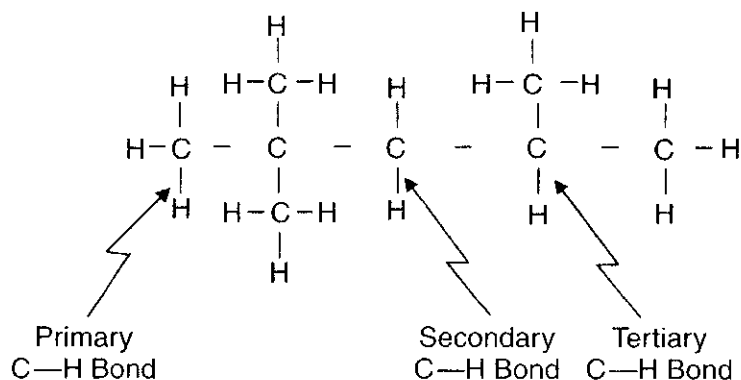
Summing up the above reaction equations, we have



Therefore, the estimated value for $\Delta H_{f,\text{C}_2\text{H}_6\text{O}(\text{g})}^o$ is -56.26 kcal/mol . The actual value of heat of formation is -56.12 kcal/mol ; the difference is attributed to the fact that the estimated value is based on average bond energies.

#

The previous example showed that the estimated heat of formation is very close to the actual value. However, this is not always true. It is important to note that the bond energy between the two atoms can vary significantly, depending on their respective locations in the molecule. For example, the molecular structure of iso-octane is



The bond strength ratios between primary, secondary, and tertiary bonds of iso-octane are 13, 5, and 1. Therefore, the enthalpy of formation estimated by the mean bond energy could differ significantly from the actual value. The reason for the difference in bond strengths is due to the fact that the tertiary C–H bond has a higher probability of forming antibonding orbitals than the primary and secondary C–H bonds. In antibonding orbitals, the electrons help to pull the nuclei apart rather than helping to pull them together.

12 HEATS OF REACTION FOR CONSTANT-PRESSURE AND CONSTANT-VOLUME COMBUSTION

The science of thermochemistry is concerned with the heat changes associated with chemical reaction; in other words, it deals essentially with the conversion of chemical energy into thermal energy, and vice versa.

The heat change associated with a chemical reaction, like that for any other process, is in general an *indefinite* quantity, depending on the path taken. However, once the process is specified (e.g., a constant-pressure process), the heat

change has a definite value, determined only by the initial and final states of the system. It is for this reason that heat changes of chemical reactions are usually measured under constant-pressure or constant-volume conditions.

There are a number of different ways in which a heat of reaction may be defined. One of the most general definitions is stated in the following section.

12.1 Constant-Pressure Combustion

If a closed system containing n_i moles of N different species at a given T and p is caused to undergo an isobaric process in which the values n_i are changed to prescribed final values and in which the initial and final values of T are the same, then the heat liberated by the system is the heat of reaction for the constant-pressure process.

When a system changes from one state to another, it may lose or gain energy in the form of heat and work. If, in a change from state A to state B , the energy content of the system is increased by ΔE , with the work done by the system being $\delta \hat{W}$ and the heat absorbed by the system $\delta \hat{Q}$, then by the first law of thermodynamics

$$\Delta E = \delta \hat{Q} - \delta \hat{W} \quad (1-128)$$

For chemical reactions under negligible change of kinetic energy and with no change in potential energy, $\Delta E = \Delta U$, and the first law becomes

$$\Delta U = \delta \hat{Q} - \delta \hat{W} \quad (1-128a)$$

If, in addition, the reaction occurs at a constant pressure, the first law is written as

$$\hat{Q}_p = \int (\delta \hat{Q})_p = \Delta U + p \Delta V \quad (1-128b)$$

For a change from state A to state B ,

$$\hat{Q}_p = (U_B - U_A) + p(V_B - V_A) = H_B - H_A \quad (1-129)$$

Therefore, for a constant-pressure, nonflow reaction,

$$\hat{Q}_p = \Delta H \quad (1-130)$$

For a constant-volume, nonflow reaction, on the other hand, no external work is done ($\delta \hat{W} = 0$), and the first law is

$$\hat{Q}_v = \Delta U \quad (1-131)$$

For a reacting flow, if there is insignificant amount of change in PE or KE, and no work other than that required for flow, then the net change in enthalpy is equal to the heat of reaction, i.e., $\hat{Q}_p = \Delta H$.

The notation for the heat content or enthalpy of a substance at standard state is H_T^o , where, as stated previously, the index o specifies standard state and the subscript T gives the temperature in kelvins. Therefore, H_0^o represents the enthalpy of a substance at the pressure of 1 bar and at the temperature of 0 K.

The ideal or perfect-gas equation of state is

$$pV = mRT = nR_uT \quad (1-132)$$

After inserting it into the definition of enthalpy,

$$H = U + pV$$

we have

$$H_T^o = U_T^o + (pV)^o = U_T^o + mRT = U_T^o + nR_uT \quad (1-133)$$

At $T = 0$ K,

$$H_0^o = U_0^o + mR(0) = U_0^o \quad (1-134)$$

Subtracting Eq. (1-134) from Eq. (1-133) gives a convenient way to calculate H_T^o from U_T^o , or vice versa:

$$H_T^o - H_0^o = (U_T^o - U_0^o) + mRT \quad (1-135)$$

From Eq. (1-129) we know that for a constant-pressure nonflow reaction,

$$\Delta H = \Delta U + p\Delta V \quad (1-136)$$

If V is the volume of 1 mole of any ideal gas at the constant temperature and pressure, then the change of pV is equal to $p\Delta V$. Using Eq. (1-132) for an ideal gas, one has

$$p\Delta V = (\Delta n)R_uT \quad (1-137)$$

Substituting Eq. (1-137) into Eq. (1-136), we have

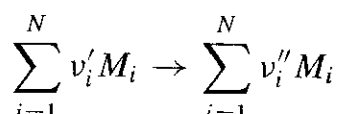
$$\Delta H = \Delta U + (\Delta n)R_uT \quad (1-138)$$

where

$$\Delta n = \left[\left(\sum_{i=1}^N n_i \right)_{\text{products}} - \left(\sum_{i=1}^N n_i \right)_{\text{reactants}} \right]_{\text{gaseous species}} \quad (1-139)$$

From Eq. (1-135) the value of the heat of reaction at constant pressure can be calculated from the value of the heat of reaction at constant volume.

Consider the generalized reaction



The heat of reaction at standard state, $\Delta H_{r,T_0}$, at T_0 is

$$\Delta H_{r,T_0} = \sum_{i=1}^N v_i'' \Delta \mathcal{H}_{f,M_i}^o - \sum_{i=1}^N v_i' \Delta \mathcal{H}_{f,M_i}^o \quad (1-140)$$

If the heat of reaction at T_1 is known, the heat of reaction at T_2 can be determined by considering the two equilibrium states as indicated in Fig. 1.8, i.e.,

$$(\text{heat change})_{\text{path } A} = (\text{heat change})_{\text{path } B}$$

or

$$\Delta H_{\text{reactants}} + \Delta H_{r,T_2} = \Delta H_{r,T_1} + \Delta H_{\text{products}}$$

$$\begin{aligned} \Delta H_{\text{reactants}} &= \sum_{i=1}^N v_i' \int_{T_1}^{T_2} C_{p,M_i} dT \quad \text{and} \quad \Delta H_{\text{products}} \\ &= \sum_{i=1}^N v_i'' \int_{T_1}^{T_2} C_{p,M_i} dT \end{aligned}$$

Therefore,

$$\Delta H_{r,T_2} = \Delta H_{r,T_1} + \sum_{i=1}^N v_i'' \int_{T_1}^{T_2} C_{p,M_i} dT - \sum_{i=1}^N v_i' \int_{T_1}^{T_2} C_{p,M_i} dT \quad (1-141)$$

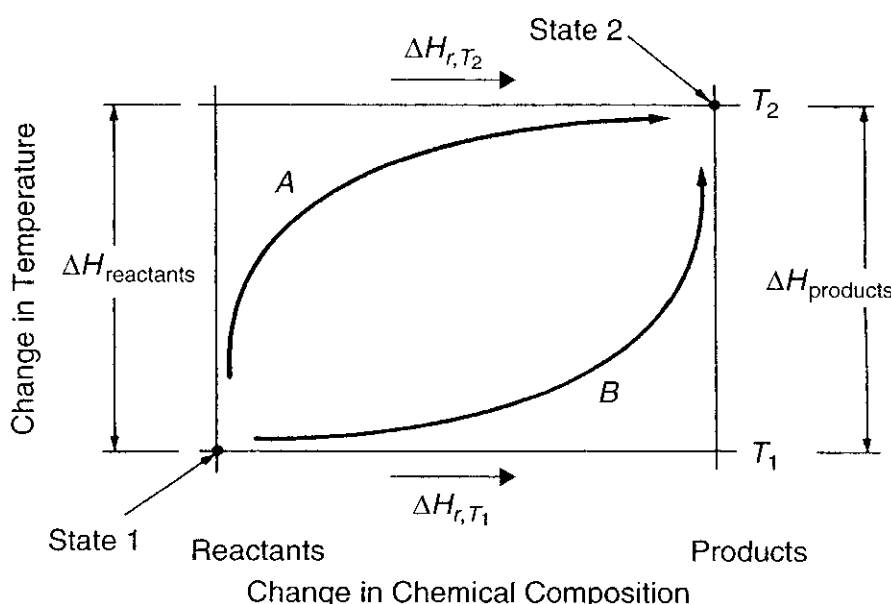


Figure 1.8 Two temperature-reaction paths, showing the relationship between heats of reaction at two different temperatures.

or

$$\Delta H_{r,T_2} = \Delta H_{r,T_1} + \sum_{\text{all products}} [H_{T_2} - H_{T_1}] - \sum_{\text{all reactants}} [H_{T_2} - H_{T_1}] \quad (1-142)$$

If we consider the reaction occurring at 1 bar pressure and set $T_1 = T_0 = 298.15$ K, $T_2 = T$, then

$$\Delta H_{r,T} = \Delta H_{r,T_0} + \sum_{\text{products}} [H_T - H_{T_0}] - \sum_{\text{reactants}} [H_T - H_{T_0}] \quad (1-143)$$

Substituting in Eqs. (1-140) and (1-141) and changing to the appropriate integration limits gives

$$\begin{aligned} \Delta H_{r,T} = & \left[\sum_{i=1}^N v_i'' \Delta \mathcal{H}_{f,M_i}^o - \sum_{i=1}^N v_i' \Delta \mathcal{H}_{f,M_i}^o \right] \\ & + \sum_{i=1}^N v_i'' \int_{T_0}^T C_{p,M_i} dT - \sum_{i=1}^N v_i' \int_{T_0}^T C_{p,M_i} dT \end{aligned} \quad (1-144)$$

Rearranging,

$$\begin{aligned} \Delta H_{r,T} = & \sum_{i=1}^N v_i'' \left(\Delta \mathcal{H}_{f,M_i}^o + \int_{T_0}^T C_{p,M_i} dT \right) \\ & - \sum_{i=1}^N v_i' \left(\Delta \mathcal{H}_{f,M_i}^o + \int_{T_0}^T C_{p,M_i} dT \right) \end{aligned} \quad (1-145)$$

As discussed in Section 3 of Appendix A, the constant-pressure specific heat C_p is highly dependent on the temperature at relatively low pressure conditions. Methods for C_p calculation at high pressures as well as mixing rules for gas mixtures are given in the same section of Appendix A. The values of C_p^o at 1 bar can be determined from

$$\frac{C_p^o}{R_u} = a_1 T^{-2} + a_2 T^{-1} + a_3 + a_4 T + a_5 T^2 + a_6 T^3 + a_7 T^4 \quad (1-146)$$

where the coefficients a_1 through a_7 are tabulated in Ref. 2. In addition, C_p^o values for various gases are tabulated in the JANAF Thermochemical Tables.²⁰ For monatomic gases, the molar heat capacities at standard states, $C_p^o(T)$, are tabulated in Ref. 21. Also, expressions for C_p in terms of temperature are given in polynomial forms for 238 different gases by Andrews and Biblarz.²² These expressions, based on least-squares polynomial approximation, are very convenient for numerical computations.

Values of C_p^o (J/mol-K) for some selected gaseous chemical species covering a broad range of temperatures are given in Table 1.4. These values are compiled

Table 1.4a Molar Heat Capacities C_p^o (cal/mol-K) for Various Substances^a

T (K)	O _{2(g)}	H _{2(g)}	N _{2(g)}	O _(g)	H _(g)	H ^{+(g)}	N _(g)	C _(graphite)
0	0.000	0.000	0.000	0.000	0.000	0.000	0.000	0.000
100	6.957	6.729	6.956	5.665	4.968	4.968	4.968	0.400
200	6.961	6.560	6.957	5.434	4.968	4.968	4.968	1.196
298.15	7.021	6.892	6.961	5.237	4.968	4.968	4.968	2.036
300	7.023	6.895	6.961	5.234	4.968	4.968	4.968	2.051
400	7.196	6.974	6.991	5.134	4.968	4.968	4.968	2.824
500	7.431	6.993	7.070	5.081	4.968	4.968	4.968	3.495
600	7.670	7.009	7.196	5.049	4.968	4.968	4.968	4.026
700	7.883	7.037	7.350	5.029	4.968	4.968	4.968	4.430
800	8.062	7.080	7.513	5.015	4.968	4.968	4.968	4.739
900	8.211	7.142	7.670	5.006	4.968	4.968	4.968	4.977
1000	8.334	7.219	7.815	4.999	4.968	4.968	4.968	5.165
1100	8.437	7.309	7.945	4.994	4.968	4.968	4.968	5.316
1200	8.525	7.407	8.060	4.990	4.968	4.968	4.968	5.441
1300	8.601	7.510	8.161	4.987	4.968	4.968	4.968	5.546
1400	8.670	7.615	8.250	4.984	4.968	4.968	4.968	5.635
1500	8.734	7.719	8.328	4.982	4.968	4.968	4.968	5.713
1600	8.794	7.821	8.396	4.980	4.968	4.968	4.968	5.782
1700	8.853	7.920	8.456	4.979	4.968	4.968	4.968	5.843
1800	8.909	8.016	8.509	4.978	4.968	4.968	4.968	5.899
1900	8.965	8.106	8.555	4.978	4.968	4.968	4.968	5.950
2000	9.020	8.193	8.597	4.978	4.968	4.968	4.969	5.998
2200	9.129	8.354	8.668	4.978	4.968	4.968	4.971	6.083
2400	9.235	8.499	8.726	4.981	4.968	4.968	4.974	6.160
2600	9.337	8.631	8.775	4.986	4.968	4.968	4.982	6.231
2800	9.435	8.752	8.815	4.994	4.968	4.968	4.993	6.297
3000	9.528	8.864	8.850	5.004	4.968	4.968	5.010	6.360
3500	9.731	9.118	8.920	5.041	4.968	4.968	5.085	6.507
4000	9.900	9.349	8.975	5.091	4.968	4.968	5.212	6.645
4500	10.048	9.564	9.020	5.149	4.968	4.968	5.390	6.777
5000	10.200	9.758	9.061	5.210	4.968	4.968	5.607	6.906
5500	10.379	9.918	9.101	5.269	4.968	4.968	5.849	7.032
6000	10.609	10.030	9.148	5.323	4.968	4.968	6.100	7.157

^aCompiled and converted from the JANAF Thermochemical Tables.²⁰

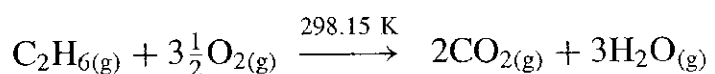
from the JANAF Tables²⁰ and Gordon and McBride's Thermodynamic Data Report.²¹ Similarly, values of the enthalpy differences ($\mathcal{H}_T^o - \mathcal{H}_{298.15}^o$) of these species are tabulated in Table 1.5 with the same temperature range as that of Table 1.4. These values are useful for equations which are expressed in terms of ($\mathcal{H}_T^o - \mathcal{H}_{298.15}^o$). The values in Tables 1.5a through 1.5f were compiled from the same sources.^{20,21}

Table 1.4b Molar Heat Capacities C_p^o (cal/mol-K) for Various Substances^a

T (K)	C _(g)	CO _(g)	NO _(g)	OH _(g)	H ₂ O _(g)	CO _{2(g)}	S _(g)	CH _{4(g)}
0	0.000	0.000	0.000	0.000	0.000	0.000	0.000	0.000
100	5.084	6.956	7.720	7.798	7.959	6.981	5.104	7.949
200	4.996	6.957	7.271	7.356	7.971	7.734	5.590	8.000
298.15	4.980	6.965	7.133	7.167	8.028	8.874	5.658	8.518
300	4.980	6.965	7.132	7.165	8.030	8.896	5.657	8.534
400	4.975	4.862	7.157	7.087	8.189	9.877	5.553	9.680
500	4.972	7.121	7.286	7.056	8.419	10.666	5.435	11.076
600	4.971	7.276	7.466	7.057	8.682	11.310	5.339	12.483
700	4.970	7.450	7.655	7.090	8.962	11.846	5.266	13.813
800	4.970	7.624	7.832	7.150	9.255	12.293	5.210	15.041
900	4.969	7.786	7.988	7.233	9.557	12.667	5.168	16.157
1000	4.969	7.931	8.123	7.332	9.863	12.980	5.136	17.159
1100	4.969	8.057	8.238	7.439	10.166	13.243	5.111	18.052
1200	4.970	8.168	8.336	7.549	10.461	13.466	5.092	18.842
1300	4.970	8.263	8.419	7.659	10.742	13.656	5.079	19.537
1400	4.972	8.346	8.490	7.766	11.007	13.815	5.069	20.149
1500	4.975	8.417	8.552	7.867	11.233	13.953	5.064	20.687
1600	4.978	8.480	8.605	7.963	11.484	14.074	5.062	21.161
1700	4.983	8.535	8.651	8.053	11.696	14.177	5.063	21.578
1800	4.990	8.583	8.691	8.137	11.890	14.269	5.068	21.946
1900	4.998	8.626	8.727	8.214	12.069	14.352	5.075	22.272
2000	5.008	8.664	8.759	8.286	12.232	14.424	5.085	22.562
2200	5.032	8.728	8.813	8.415	12.526	14.547	5.111	23.049
2400	5.060	8.681	8.858	8.526	12.773	14.648	5.144	23.440
2600	5.094	8.825	8.895	8.622	12.985	14.734	5.181	23.757
2800	5.130	8.863	8.927	8.706	13.167	14.807	5.219	24.017
3000	5.168	8.895	8.955	8.780	13.324	14.873	5.258	24.233
3500	5.261	8.961	9.012	8.933	13.637	15.006	5.347	24.632
4000	5.345	9.014	9.058	9.055	13.870	15.118	5.418	24.900
4500	5.414	9.059	9.097	9.158	14.050	15.217	5.469	25.089
5000	5.468	9.100	9.132	9.249	14.195	15.307	5.502	25.226
5500	5.509	9.100	9.164	9.336	14.336	15.415	5.520	25.329
6000	5.540	9.175	9.194	9.422	14.477	15.525	5.527	25.408

^aCompiled and converted from the JANAF Thermochemical Tables.²⁰

Example 1.10. Assume the combustion of ethane C₂H_{6(g)} with O₂ can be represented by the following global reaction without any dissociation in the final product:



Evaluate the heat of reaction of ethane.

Table 1.4c Molar Heat Capacities C_p^o (cal/mol-K) for Various Substances^a

T (K)	$\text{C}_2\text{H}_{2(\text{g})}$	$\text{C}_2\text{H}_{4(\text{g})}$	$\text{Cl}_{2(\text{g})}$	$\text{Br}_{2(\text{g})}$	$\text{I}_{2(\text{g})}$	$\text{Cl}_{(\text{g})}$	$\text{Br}_{(\text{g})}$	$\text{I}_{(\text{g})}$
0	0.000	0.000	0.000	0.000	0.000	0.000	0.000	0.000
100	7.014	7.952	7.003	7.381	7.919	4.968	4.968	4.968
200	8.505	8.451	7.581	8.265	8.619	5.038	4.968	4.968
298.15	10.539	10.250	8.114	8.616	8.816	5.219	4.968	4.968
300	10.571	10.292	8.122	8.620	8.819	5.223	4.968	4.968
400	12.065	12.679	8.436	8.777	8.904	5.370	4.968	4.968
500	13.114	14.932	8.620	8.862	8.954	5.436	4.971	4.968
600	13.931	16.889	8.735	8.915	8.989	5.445	4.979	4.968
700	14.615	18.574	8.813	8.953	9.019	5.424	4.997	4.968
800	15.239	20.038	8.869	8.983	9.046	5.389	5.026	4.968
900	15.801	21.319	8.913	9.009	9.072	5.351	5.063	4.969
1000	16.318	22.442	8.948	9.053	9.102	5.314	5.106	4.970
1100	16.789	23.427	8.978	9.053	9.138	5.279	5.153	4.973
1200	17.221	24.289	9.004	9.073	9.185	5.248	5.199	4.977
1300	17.613	25.044	9.027	9.094	9.249	5.221	5.243	4.984
1400	17.968	25.705	9.050	9.116	9.334	5.196	5.284	4.993
1500	18.291	26.284	9.071	9.139	9.442	5.175	5.320	5.004
1600	18.582	26.793	9.092	9.165	9.572	5.156	5.351	5.006
1700	18.845	27.241	9.114	9.195	9.721	5.140	5.377	5.034
1800	19.085	27.636	9.136	9.228	9.883	5.125	5.398	5.052
1900	19.302	27.985	9.159	9.266	10.051	5.112	5.415	5.072
2000	19.504	28.295	9.185	9.308	10.217	5.101	5.428	5.093
2200	19.853	28.817	9.243	9.404	10.515	5.081	5.443	5.137
2400	20.151	29.235	9.313	9.510	10.729	5.066	5.446	5.182
2600	20.404	29.574	9.395	9.619	10.835	5.053	5.442	5.226
2800	20.625	29.852	9.485	9.721	10.832	5.043	5.432	5.267
3000	20.820	30.082	9.578	9.808	10.731	5.034	5.418	5.304
3500	21.225	30.509	9.781	9.929	10.195	5.018	5.375	5.376
4000	21.557	30.796	9.872	9.896	9.496	5.007	5.329	5.420
4500	21.835	30.998	9.811	9.738	8.819	5.000	5.287	5.442
5000	22.077	31.145	9.614	9.508	8.232	4.994	5.249	5.446
5500	22.309	31.255	9.322	9.249	7.746	4.989	5.216	5.439
6000	22.521	31.339	8.980	8.992	7.350	4.986	5.188	5.425

^aCompiled and converted from the JANAF Thermochemical Tables.²⁰

Solution: To calculate ΔH_r at standard state conditions, we can use Eq. (1-140):

$$\begin{aligned}\Delta H_{r,T_0}^o &= \sum_{i=1}^N v_i'' \Delta \mathcal{H}_{f,M_i}^o - \sum_{i=1}^N v_i' \Delta \mathcal{H}_{f,M_i}^o \\ &= 0 \Delta \mathcal{H}_{f,\text{C}_2\text{H}_{6(\text{g})}}^o + 0 \Delta \mathcal{H}_{f,\text{O}_{2(\text{g})}}^o + 2 \Delta \mathcal{H}_{f,\text{CO}_{2(\text{g})}}^o + 3 \Delta \mathcal{H}_{f,\text{H}_2\text{O}_{(\text{g})}}^o \\ &\quad - (1 \Delta \mathcal{H}_{f,\text{C}_2\text{H}_{6(\text{g})}}^o + 3 \frac{1}{2} \Delta \mathcal{H}_{f,\text{O}_{2(\text{g})}}^o + 0 \Delta \mathcal{H}_{f,\text{CO}_{2(\text{g})}}^o + 0 \Delta \mathcal{H}_{f,\text{H}_2\text{O}_{(\text{g})}}^o)\end{aligned}$$

Table 1.4d Molar Heat Capacities C_p^o (cal/mol-K) for Various Substances^a

T (K)	$\text{HCl}_{(\text{g})}$	$\text{HBr}_{(\text{g})}$	$\text{HI}_{(\text{g})}$	$\text{F}_{2(\text{g})}$	$\text{F}_{(\text{g})}$	$\text{HF}_{(\text{g})}$	$(\text{FH})_{2(\text{g})}$
0	0.000	0.000	0.000	0.000	0.000	0.000	0.000
100	6.959	6.959	6.958	6.958	5.068	6.962	8.288
200	6.961	6.961	6.961	7.095	5.403	6.962	9.507
298.15	6.964	6.965	6.968	7.481	5.436	6.964	10.725
300	6.964	6.965	6.969	7.489	5.435	6.964	10.748
400	6.973	6.984	7.010	7.885	5.361	6.967	11.879
500	7.004	7.039	7.107	8.187	5.282	6.973	12.795
600	7.069	7.139	7.253	8.393	5.218	6.986	13.512
700	7.167	7.272	7.424	8.564	5.169	7.015	14.090
800	7.288	7.422	7.600	8.685	5.132	7.063	14.579
900	7.422	7.576	7.767	8.779	5.104	7.129	15.012
1000	7.559	7.724	7.919	8.857	5.083	7.211	15.404
1100	7.693	7.863	8.056	8.923	5.065	7.303	15.763
1200	7.819	7.989	8.177	8.982	5.052	7.402	16.093
1300	7.936	8.103	8.283	9.035	5.041	7.504	16.396
1400	8.043	8.205	8.376	9.084	5.032	7.606	16.673
1500	8.141	8.296	8.459	9.130	5.024	7.705	16.926
1600	8.229	8.378	8.532	9.172	5.018	7.800	17.155
1700	8.310	8.451	8.596	9.209	5.013	7.891	17.364
1800	8.382	8.517	8.654	9.241	5.008	7.977	17.553
1900	8.448	8.576	8.706	9.266	5.005	8.058	17.724
2000	8.509	8.630	8.753	9.284	5.001	8.133	17.880
2200	8.614	8.724	8.835	9.296	4.996	8.270	18.149
2400	8.702	8.803	8.904	9.272	4.992	8.389	18.371
2600	8.778	8.870	8.964	9.213	4.988	8.493	18.556
2800	8.844	8.929	9.016	9.123	4.986	8.584	18.710
3000	8.901	8.980	9.063	9.006	4.984	8.664	18.841
3500	9.020	9.088	9.162	8.641	4.979	8.829	19.087
4000	9.115	9.176	9.246	8.234	4.977	8.958	19.257
4500	9.195	9.252	9.320	7.841	4.975	9.063	19.378
5000	9.265	9.320	9.387	7.486	4.974	9.152	19.467
5500	9.328	9.383	9.451	7.176	4.973	9.230	19.534
6000	9.388	9.442	9.512	9.300	4.972	9.300	19.586

^aCompiled from the JANAF Thermochemical Tables.²⁰

Using the heats of formation tabulated in Table 1.2, we have

$$\begin{aligned}\Delta H_{r,T_0}^o &= [-(2 \times 94.05) - (3 \times 57.8)] - [-(1 \times 20.04) + (3.5 \times 0)] \\ &= -341.46 \text{ kcal}\end{aligned}$$

Table 1.5a Enthalpy Differences [$H(T) - H(T_r)$] (kcal/mol) for Various Substances^a

T (K)	$O_{2(g)}$	$H_{2(g)}$	$N_{2(g)}$	$O_{(g)}$	$H_{(g)}$	$H_{(g)}^+$	$N_{(g)}$	$C_{(graphite)}$
0	-2.075	-2.024	-2.072	-1.607	-1.481	-1.481	-1.481	-0.251
100	-1.381	-1.307	-1.379	-1.080	-0.984	-0.984	-0.984	-0.237
200	-0.685	-0.663	-0.618	-0.522	-0.488	-0.488	-0.488	-0.159
298.15	0.000	0.000	0.000	0.000	0.000	0.000	0.000	0.000
300	0.013	0.013	0.013	0.010	0.009	0.009	0.009	0.004
400	0.723	0.707	0.710	0.527	0.506	0.506	0.506	0.248
500	1.454	1.406	1.413	1.038	1.003	1.003	1.003	0.565
600	2.209	2.106	2.126	1.544	1.500	1.500	1.500	0.942
700	2.987	2.808	2.853	2.048	1.996	1.996	1.996	1.366
800	3.785	3.514	3.596	2.550	2.493	2.493	2.493	1.825
900	4.599	4.225	4.355	3.051	2.990	2.990	2.990	2.312
1000	5.426	4.943	5.130	3.552	3.487	3.487	3.487	2.819
1100	6.265	5.669	5.918	4.051	3.984	3.984	3.984	3.343
1200	7.113	6.405	6.718	4.550	4.480	4.480	4.480	3.881
1300	7.969	7.151	7.529	5.049	4.977	4.977	4.977	4.431
1400	8.833	7.907	8.350	5.548	5.474	5.474	5.474	4.990
1500	9.703	8.674	9.179	6.046	5.971	5.971	5.971	5.558
1600	10.580	9.451	10.015	6.544	6.467	6.467	6.467	6.132
1700	11.462	10.238	10.858	7.042	6.964	6.964	6.964	6.714
1800	12.350	11.035	11.706	7.540	7.461	7.461	7.461	7.301
1900	13.244	11.841	12.559	8.038	7.958	7.958	7.958	7.893
2000	14.143	12.656	13.417	8.536	8.455	8.455	8.455	8.491
2200	15.958	14.311	15.144	9.531	9.448	9.448	9.449	9.699
2400	17.795	15.996	16.883	10.527	10.442	10.442	10.443	10.924
2600	19.652	17.709	18.634	11.524	11.435	11.435	11.439	12.163
2800	21.529	19.448	20.393	12.522	12.429	12.429	12.436	13.416
3000	23.426	21.209	22.159	13.522	13.423	13.423	13.436	14.681
3500	28.242	25.706	26.603	16.032	15.907	15.907	15.958	17.899
4000	33.151	30.324	31.077	18.565	18.391	18.391	18.531	21.187
4500	38.139	35.053	35.576	21.125	20.875	20.875	21.179	24.542
5000	43.200	39.884	40.096	23.715	23.359	23.359	23.927	27.963
5500	48.343	44.805	44.637	26.335	25.843	25.843	26.791	31.448
6000	53.587	49.795	49.199	28.983	28.327	28.327	29.778	34.995

^aCompiled and converted from the JANAF Thermochemical Tables.²⁰

When the heat of reaction is negative, heat is evolved and the process is called an *exothermic process*. When the heat of reaction is positive, heat must be absorbed by the system during the chemical reaction and the process is called an *endothermic process*.

The *heating value* of a fuel is a term commonly used in discussing combustion. The heating value is a positive number that is equal to the enthalpy of combustion

Table 1.5b Enthalpy Differences [$H(T) - H(T_r)$] (kcal/mol) for Various Substances^a

T (K)	C _(g)	CO _(g)	NO _(g)	OH _(g)	H ₂ O _(g)	CO _{2(g)}	S _(g)	CH _{4(g)}
0	-1.562	-2.072	-2.197	-2.192	-2.367	-2.238	-1.591	-2.396
100	-0.992	-1.379	-1.451	-1.467	-1.581	-1.543	-1.092	-1.601
200	-0.489	-0.683	-0.705	-0.711	-0.784	-0.816	-0.554	-0.805
298.15	0.000	0.000	0.000	0.000	0.000	0.000	0.000	0.000
300	0.009	0.013	0.013	0.013	0.015	0.016	0.011	0.016
400	0.507	0.711	0.727	0.725	0.825	0.957	0.571	0.923
500	1.004	1.418	1.448	1.432	1.655	1.985	1.121	1.960
600	1.501	2.137	2.185	2.137	2.510	3.085	1.659	3.138
700	1.999	2.874	2.941	2.845	3.392	4.243	2.189	4.454
800	2.495	3.627	3.716	3.556	4.303	5.451	2.713	5.897
900	2.992	4.398	4.507	4.275	5.243	6.699	3.232	7.458
1000	3.489	5.184	5.313	5.004	6.214	7.982	3.747	9.125
1100	3.986	5.984	6.131	5.742	7.216	9.293	4.259	10.886
1200	4.483	6.795	6.960	6.491	8.247	10.629	4.769	12.732
1300	4.980	7.617	7.798	7.252	9.307	11.986	5.278	14.652
1400	5.477	8.447	8.643	8.023	10.395	13.359	5.785	16.637
1500	5.975	9.285	9.495	8.805	11.508	14.748	6.292	18.679
1600	6.472	10.130	10.353	9.596	12.645	16.147	6.798	20.772
1700	6.970	10.981	11.216	10.397	13.804	17.562	7.304	22.909
1800	7.469	11.837	12.083	11.207	14.984	18.984	7.811	25.086
1900	7.968	12.697	12.954	12.024	16.182	20.416	8.318	27.297
2000	8.469	13.562	13.829	12.849	17.397	21.854	8.826	29.539
2200	9.473	15.301	15.586	14.520	19.874	24.752	9.845	34.102
2400	10.482	17.047	17.353	16.214	22.405	27.672	10.871	38.753
2600	11.497	18.803	19.129	17.929	24.981	30.610	11.903	43.473
2800	12.519	20.572	20.911	19.662	27.597	33.564	12.943	48.252
3000	13.549	22.348	22.699	21.411	30.246	36.533	13.991	53.077
3500	16.157	26.813	27.189	25.841	36.990	44.003	16.643	65.300
4000	18.809	31.307	31.709	30.339	43.870	51.535	19.335	77.688
4500	21.499	35.826	36.248	34.893	50.852	59.119	22.058	90.188
5000	24.220	40.366	40.805	39.495	57.914	66.750	24.801	102.768
5500	26.965	44.923	45.379	44.141	65.047	74.430	27.557	115.408
6000	29.728	49.500	49.969	48.831	72.250	82.165	30.320	128.093

^aCompiled and converted from the JANAF Thermochemical Tables.²⁰

but has the opposite sign. There are many possible heating values for a fuel, depending on the phase of the water formed in the products (liquid or gas), the phase of the fuel (liquid or gas), and the conditions under which the combustion is carried out (e.g., constant pressure or constant volume).

The heat of combustion may be considered a special case of the heat of reaction. The *heat of combustion* of a substance is the heat liberated when a fuel (usually a hydrocarbon) reacts with oxygen to yield H₂O and CO₂.

Table 1.5c Enthalpy Differences [$H(T) - H(T_r)$] (kcal/mol) for Various Substances^a

T (K)	C ₂ H _{2(g)}	C ₂ H _{4(g)}	Cl _{2(g)}	Br _{2(g)}	I _{2(g)}	Cl _(g)	Br _(g)	I _(g)
0	-2.393	-2.514	-2.194	-2.324	-2.418	-1.499	-1.481	-1.481
100	-1.698	-1.719	-1.498	-1.619	-1.692	-1.002	-0.984	-0.984
200	-0.938	-0.909	-0.772	-0.831	-0.857	-0.503	-0.488	-0.488
298.15	0.000	0.000	0.000	0.000	0.000	0.000	0.000	0.000
300	0.020	0.019	0.015	0.016	0.016	0.010	0.726	0.009
400	1.155	1.167	0.844	0.887	0.903	0.540	0.506	0.506
500	2.416	2.550	1.698	1.769	1.796	1.081	1.003	1.003
600	3.769	4.143	2.566	2.658	2.693	1.625	1.500	1.500
700	5.197	5.918	3.444	3.552	3.594	2.169	1.999	1.996
800	6.690	7.851	4.328	4.448	4.497	2.710	2.500	2.493
900	8.243	9.920	5.217	5.348	5.403	3.247	3.005	2.990
1000	9.849	12.109	6.110	6.250	6.311	3.780	3.513	3.487
1100	11.505	14.404	7.006	7.154	7.223	4.310	4.026	3.984
1200	13.206	16.791	7.906	8.060	8.139	4.836	4.543	4.482
1300	14.947	19.258	8.807	8.969	9.061	5.359	5.066	4.980
1400	16.727	21.796	9.711	9.879	9.990	5.880	5.592	5.478
1500	18.540	24.396	10.617	10.792	10.929	6.399	6.122	5.978
1600	20.384	27.051	11.525	11.707	11.879	6.915	6.656	6.479
1700	22.255	29.753	12.435	12.625	12.844	7.430	7.192	6.982
1800	24.152	32.497	13.348	13.546	13.824	7.943	7.731	7.486
1900	26.072	35.279	14.263	14.471	14.821	8.455	8.272	7.992
2000	28.012	38.093	15.180	15.400	15.834	8.966	8.814	8.500
2200	31.949	43.806	17.022	17.271	17.908	9.984	9.901	9.523
2400	35.950	49.613	18.878	19.162	20.034	10.998	10.990	10.555
2600	40.006	55.495	20.748	21.075	22.193	12.010	12.079	11.596
2800	44.109	61.438	22.636	23.009	24.361	13.020	13.167	12.646
3000	48.254	67.432	24.543	24.962	26.519	14.027	14.252	13.703
3500	58.768	82.588	29.386	29.903	31.763	16.540	16.950	16.374
4000	69.466	97.918	34.305	34.865	36.687	19.046	19.626	19.074
4500	80.315	113.370	39.232	39.778	41.263	21.548	22.280	21.790
5000	91.294	128.908	44.093	44.591	45.522	24.046	24.914	24.513
5500	102.391	144.509	48.831	49.281	49.512	26.542	27.530	27.235
6000	113.600	160.158	53.407	53.841	53.283	29.036	30.131	29.951

^aCompiled and converted from the JANAF Thermochemical Tables.²⁰

The heat of reaction of a certain reaction can be determined using Hess's law to sum the related reactions for which the heats of reaction are known. Bond energies and resonance energies can also be used for evaluating the heat of reaction or heat of combustion of a reaction, as illustrated in Example 1.11.

Example 1.11. Evaluate the heat of combustion of benzoic acid, C₆H₅COOH_(g).

Solution: The reaction is

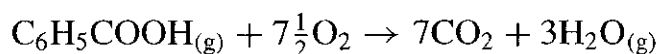
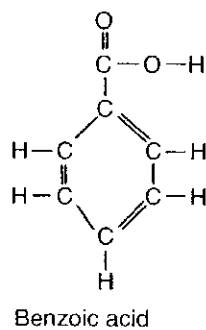


Table 1.5d Enthalpy Differences [$H(T) - H(T_r)$] (kcal/mol) for Various Substances^a

<i>T</i> (K)	HCl _(g)	HBr _(g)	HI _(g)	F _{2(g)}	F _(g)	HF _(g)	(HF) _{2(g)}
0	-2.065	-2.067	-2.069	-2.109	-1.558	-2.055	-2.684
100	-1.379	-1.379	-1.380	-1.414	-1.060	-1.380	-1.882
200	-0.683	-0.683	-0.684	-0.714	-0.534	-0.683	-0.993
298.15	0.000	0.000	0.000	0.000	0.000	0.000	0.000
300	0.013	0.013	0.013	0.014	0.010	0.013	0.020
400	0.710	0.710	0.711	0.783	0.550	0.709	1.153
500	1.408	1.411	1.417	1.588	1.082	1.406	2.388
600	2.112	2.120	2.135	2.418	1.607	2.104	3.705
700	2.823	2.840	2.868	3.267	2.126	2.804	5.086
800	3.546	3.575	3.620	4.129	2.641	3.508	6.520
900	4.281	4.324	4.388	5.003	3.153	4.217	8.000
1000	5.030	5.089	5.172	5.885	3.663	4.934	9.521
1100	5.793	5.869	5.971	6.774	4.170	5.660	11.080
1200	6.568	6.662	6.783	7.669	4.676	6.395	12.673
1300	7.356	7.466	7.606	8.570	5.180	7.140	14.298
1400	8.155	8.282	8.439	9.476	5.684	7.896	15.951
1500	8.965	9.107	9.281	10.387	6.187	8.661	17.631
1600	9.783	9.941	10.130	11.302	6.689	9.437	19.336
1700	10.610	10.782	10.987	12.221	7.190	10.221	21.062
1800	11.445	11.631	11.850	13.143	7.691	11.015	22.808
1900	12.286	12.485	12.718	14.069	8.192	11.816	24.572
2000	13.134	13.346	13.591	14.996	8.692	12.626	26.352
2200	14.847	15.082	15.350	16.855	9.692	14.267	29.956
2400	16.579	16.834	17.124	18.712	10.691	15.933	33.609
2600	18.327	18.602	18.911	20.562	11.689	17.621	37.302
2800	20.089	20.382	20.709	22.396	12.686	19.329	41.029
3000	21.864	22.173	22.517	24.209	13.683	21.054	44.784
3500	26.345	26.691	27.074	28.624	16.174	25.429	54.270
4000	30.880	31.258	31.676	32.843	18.663	29.877	63.859
4500	35.458	35.865	36.318	36.861	21.151	34.383	73.519
5000	40.073	40.508	40.995	40.690	23.638	38.937	83.231
5500	44.722	45.185	45.705	44.354	26.124	43.533	92.983
6000	49.401	49.891	50.446	47.874	28.610	48.166	102.763

^aCompiled and converted from the JANAF Thermochemical Tables.²⁰

The molecular structure of benzoic acid is given below:



For the reactants, the bond and resonance energies are

$$\begin{aligned} & 4(\text{C-C}) + 3(\text{C=C}) + 5(\text{C-H}) + 1(\text{C=O}) \\ & + 1(\text{C-O}) + 1(\text{O-H}) + 7\frac{1}{2}(\text{O=O}) \\ & + 1(\text{C}_6\text{H}_6, \text{benzene-ring resonance}) + 1(-\text{COOH}, \text{carboxyl}) \end{aligned}$$

Inserting numerical values from Table 1.3, the total bond and resonance energy of the reactants is

$$\begin{aligned} & 4 \times 85 + 3 \times 145 + 5 \times 98.1 + 173 + 86 + 109 + 7.5 \times 119.1 + 48.9 + 28 \\ & = 2603.7 \text{ kcal} \end{aligned}$$

For the products, recognizing that CO_2 is formed with two double bonds, the bond and resonance energies are

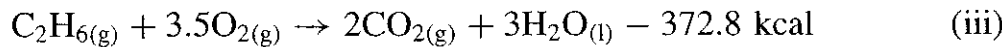
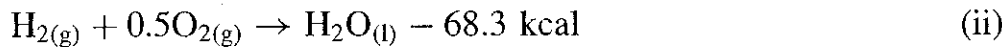
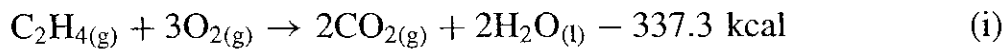
$$14(\text{C=O}) + 6(\text{O-H}) + 7(\text{CO}_2 \text{ resonance}) = 14 \times 173 + 6 \times 109 + 7 \times 33 = 3307 \text{ kcal}$$

Thus, the estimated heat of combustion of benzoic acid is

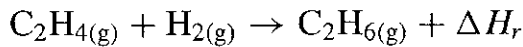
$$2603.7 - 3307 = -703.3 \text{ kcal}$$

#

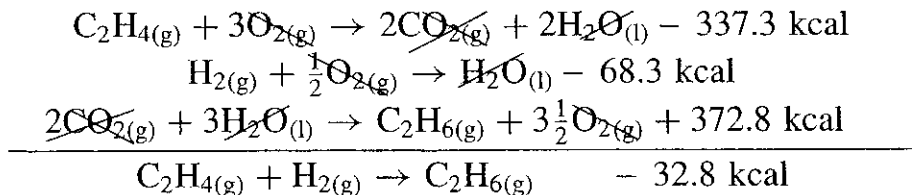
Example 1.12. Given the following three reactions at 298.15 K,



determine the heat of reaction for



Solution: The result is obtained simply by adding (i) and (ii) and subtracting (iii), or by using Lavoisier and Laplace's law on (iii) to reverse it first and add it to both (i) and (ii):



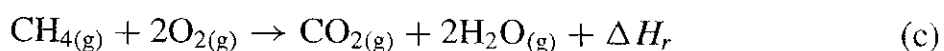
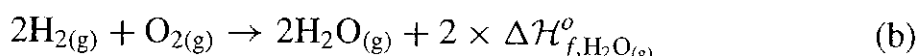
#

Heat of reactions may also be manipulated by Hess's law to arrive at heats of formation for substances. The heat of combustion of CH_4 is about 10 times

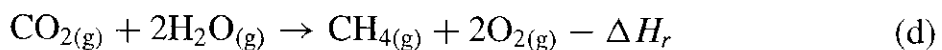
larger than the heat of formation of CH₄. Some tabulated heats of formation of compounds are deduced from heats of combustion, which can be measured experimentally in the laboratory. The heat of formation of CH₄ can be deduced from the heats of formation of CO₂ and H₂O and the heat of reaction of CH₄ + 2O₂.

Example 1.13. Deduce the heat of formation of CH₄ from those of CO₂ and H₂O and the ΔH_r of the methane–oxygen reaction.

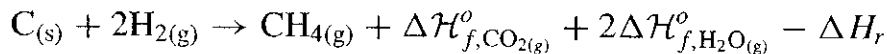
Solution: Consider the following reactions,



Using Lavoisier and Laplace's law, the last equation becomes



Summing Eqs. (a), (b), and (d) gives



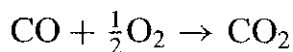
Therefore,

$$\Delta\mathcal{H}_{f,\text{CH}_{4(g)}}^o = \Delta\mathcal{H}_{f,\text{CO}_{2(g)}}^o + 2\Delta\mathcal{H}_{f,\text{H}_{2\text{O}}_{(g)}}^o - \Delta H_r$$

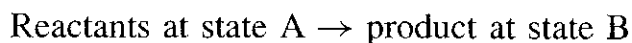
#

12.2 Constant-Volume Combustion

Let us consider the following simple reaction in a constant-volume situation:



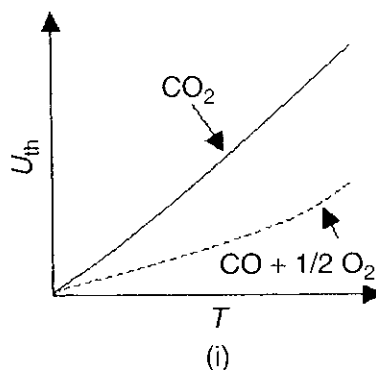
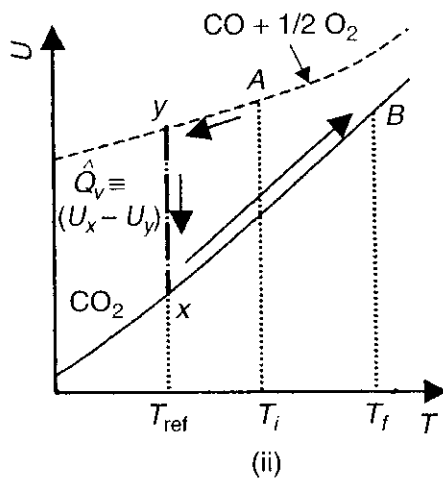
or



The sensible portion of the internal energy (without the chemical energy) of the reactants or products can be defined as

$$U_{\text{th}} \equiv \sum \int_{T_{\text{ref}}}^T n_i C_{v_i} dT$$

The U_{th} values of the reactants and products can be plotted versus temperature, as in Figure 1.9. If the chemical energy is added to both reactant and product curves, we have two new positions for these curves, as shown in Figure 1.10.

**Figure 1.9** U_{th}^f values versus T .**Figure 1.10** Addition of chemical energy to Figure 1.9.

The internal energy difference between the product at thermodynamic state B and the reactants at state A is

$$\begin{aligned}\Delta U &= U_B - U_A = (U_B - U_x) + (U_x - U_y) + (U_y - U_A) \\ &= \int_{T_{ref}}^{T_f} n_{CO_2} C_{vCO_2} dT + \hat{Q}_v - \int_{T_{ref}}^{T_i} \sum_{\text{reactants}} n_i C_{v_i} dT\end{aligned}\quad (1-147)$$

where the heat of reaction at constant volume is defined as

$$\hat{Q}_v \equiv \Delta U_r = (U_x - U_y)_{T_{ref}}$$

For an exothermic reaction, \hat{Q}_v is a negative quantity. Under the adiabatic condition, ΔU of Eq. (1-147) is zero; therefore $U_B = U_A$ and state B is at the same level as state A. If there is any heat loss from the system, $U_B < U_A$, then $\Delta U < 0$.

The temperature-reaction path of the above reaction is shown in Figure 1.11.

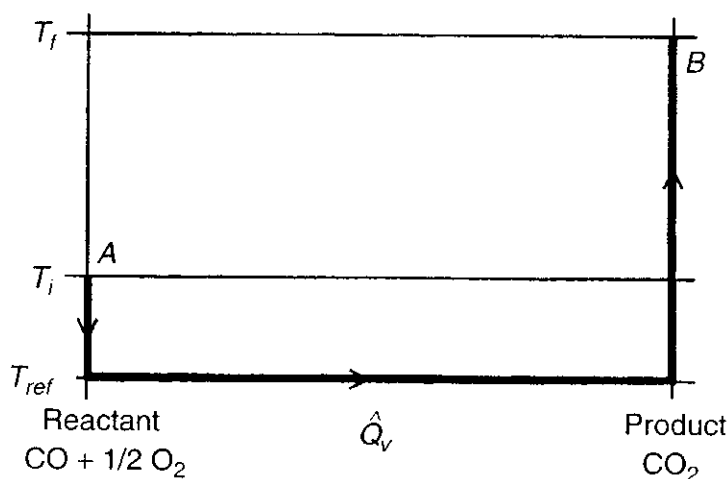


Figure 1.11 Temperature-reaction path.

The energy balance gives essentially the same equation as Eq. (1-147).

$$\Delta U = \int_{T_i}^{T_{\text{ref}}} \sum_{\text{reactants}} n_i C_{v_i} dT + \hat{Q}_v + \int_{T_{\text{ref}}}^{T_i} \sum_{\text{product}} n_i C_{v_j} dT \quad (1-147a)$$

where ΔU is equal to zero if the system is adiabatic. The value of \hat{Q}_v is related to \hat{Q}_p by

$$\hat{Q}_v = \hat{Q}_p - R_u T \Delta n \quad (1-148)$$

where Δn is defined by Eq. (1-139).

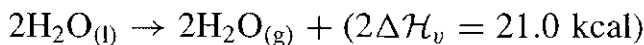
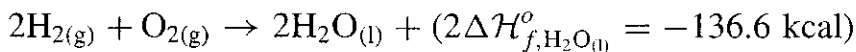
13 ENERGY BALANCE CONSIDERATIONS FOR FLAME TEMPERATURE CALCULATIONS

Consider a combustion process that takes place adiabatically in a closed system with negligible changes in kinetic and potential energies. For such a process, the temperature of the products is referred to as the *adiabatic flame temperature*. It is the maximum temperature that can be achieved for the given reactants, because any heat transfer from the reacting substances and any incomplete combustion would tend to lower the temperature of the products. The adiabatic temperature T_f can be controlled with an excess amount of air or diluent. In gas turbines, where the maximum permissible temperature is defined by metallurgical considerations in the turbine, close control of the temperature of the products is essential.

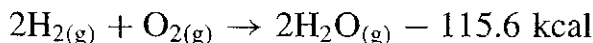
A few examples are given here to illustrate some of the steps used to calculate the adiabatic flame temperature.

Example 1.14. Calculate the adiabatic flame temperature of water vapor based on the reaction of gaseous H₂ and O₂.

Solution: The overall reaction may be broken down as



where $\Delta\mathcal{H}_v$ represents the heat of vaporization. Adding these two equations, we have



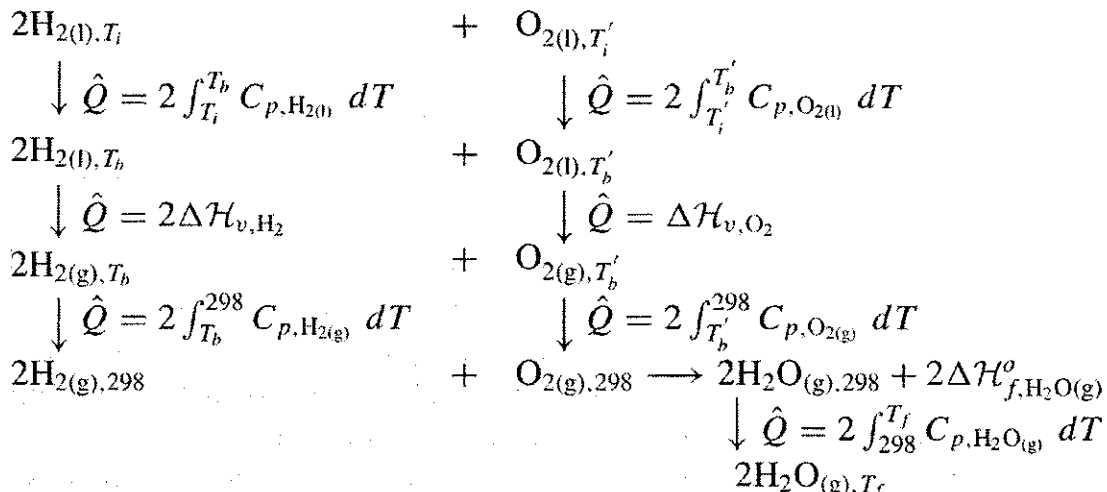
Therefore, the heat generated by the reaction is 115.6 kcal. If all of the heat is used to heat up the steam adiabatically under the assumption of no dissociation, then

$$115.6 \text{ kcal} = 2 \int_{298}^{T_f} C_{p,\text{H}_2\text{O}(\text{g})} dT \quad \text{or} \quad 57.8 \text{ kcal} = \mathcal{H}_{\text{H}_2\text{O},T_f} - \mathcal{H}_{\text{H}_2\text{O},298} \text{ K}$$

Using Table 1.5b, the approximate value of T_f is found to be around 5000 K in order to balance the above equation. At such a high temperature, dissociation of steam must occur and the actual combustion products become unknown; therefore, to obtain a realistic value of the adiabatic flame temperature, we must include the effect of dissociation and equilibrium reactions among the product species. These complications will be discussed later. The adiabatic flame temperature for nondissociating products is normally called the adiabatic frozen-flame temperature.

#

To demonstrate the usefulness of the adiabatic assumption in calculating the adiabatic frozen-flame temperature, consider a more detailed example of the combustion of liquid H₂ with liquid O₂. Let T_b represent the boiling temperature of H_{2(l)}, T'_b the boiling temperature of O_{2(l)}, and T_i the initial temperature of both reactants under cryogenic conditions. (The critical temperatures and pressures of H₂ and O₂ are 33.3 and 154.4 K and 1.3 and 5.04 MPa, respectively.) Considering the energy required for each step, we have



Since the system is assumed to be adiabatic,

$$\sum \hat{Q} = 0$$

Thus,

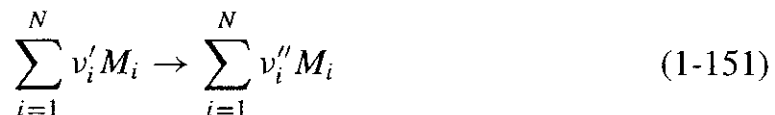
$$\begin{aligned} & 2 \int_{T_i}^{T_b} C_{p,H_2(l)} dT + \int_{T'_i}^{T'_b} C_{p,O_2(l)} dT + 2\Delta\mathcal{H}_{v,H_2} + \Delta\mathcal{H}_{v,O_2} \\ & + 2 \int_{T_b}^{298} C_{p,H_2(g)} dT + \int_{T'_b}^{298} C_{p,O_2(g)} dT \\ & + 2\Delta\mathcal{H}_{f,H_2O(g)}^o + 2 \int_{298}^{T_f} C_{p,H_2O(g)} dT = 0 \end{aligned} \quad (1-149)$$

The above equation can be written as

$$2\mathcal{H}_{H_2}|_{T_i}^{298} + \mathcal{H}_{O_2}|_{T'_i}^{298} + \Delta H_r^o + 2\mathcal{H}_{H_2O(g)}|_{298}^{T_f} = 0 \quad (1-150)$$

Either Eq. (1-149) or Eq. (1-150) can be utilized for T_f calculation.

Corresponding to the generalized chemical reaction,



flame-temperature calculations can be conducted using the following enthalpy balance equation for either frozen or equilibrium processes:

$$\overbrace{\sum_{i=1}^N v''_i \Delta\mathcal{H}_{f,M_i}^o - \sum_{i=1}^N v'_i \Delta\mathcal{H}_{f,M_i}^o}^{\Delta H_r} - \sum_{i=1}^N v'_i (\mathcal{H}_{M_i,T_i} - \mathcal{H}_{M_i,298}) + \sum_{i=1}^N v''_i (\mathcal{H}_{M_i,T_f} - \mathcal{H}_{M_i,298}) = \Delta H \quad (1-152)$$

Note that in case a change of state takes place for a given species during the combustion process, different phases are considered as different species in this equation. For an adiabatic process, the heat addition from the surroundings to the system (ΔH) is zero. The above energy balance equation allows the calculation of the adiabatic frozen-flame temperature (where ΔH is positive for heat addition).

In general, the reactants may not be at the standard-state temperature T_0 , but rather at T_i , where T_i may be higher or lower than T_0 . During the combustion,

a part of the heat evolved is used to heat the product to a temperature T_2 . The energy-balance equation can also be written as

$$\Delta H = \sum_{\substack{j=1 \\ \text{products}}}^N v_j'' \left\{ (\mathcal{H}_{T_f}^o - \mathcal{H}_{T_0}^o) + (\Delta \mathcal{H}_f^o)_{T_0} \right\}_j - \sum_{\substack{j=1 \\ \text{reactants}}}^N v_j' \left\{ (\mathcal{H}_{T_i}^o - \mathcal{H}_{T_0}^o) + (\Delta \mathcal{H}_f^o)_{T_0} \right\}_j \quad (1-153)$$

This equation says that under adiabatic condition ($\Delta H = 0$), the sum of sensible enthalpy and chemical enthalpy of product species is the same as that of the reactant species. The above energy balance can also be seen easily from the temperature-reaction path diagram in Fig. 1.12.

Let us define A , B , and C as

$$A = - \sum_{j=1}^N v_j' [(\mathcal{H}_{T_i}^o - \mathcal{H}_{T_0}^o)]_j$$

$$B = \sum_{j=1}^N v_j'' (\Delta \mathcal{H}_f^o)_{T_0,j} - \sum_{j=1}^N v_j' (\Delta \mathcal{H}_f^o)_{T_0,j}$$

$$C = \sum_{j=1}^N v_j'' [(\mathcal{H}_{T_f}^o - \mathcal{H}_{T_0}^o)]_j$$

Figure 1.12 indicates that

$$\Delta H = A + B + C$$

If $T_i < T_0$, then

$$\Delta H = A' + B + C$$

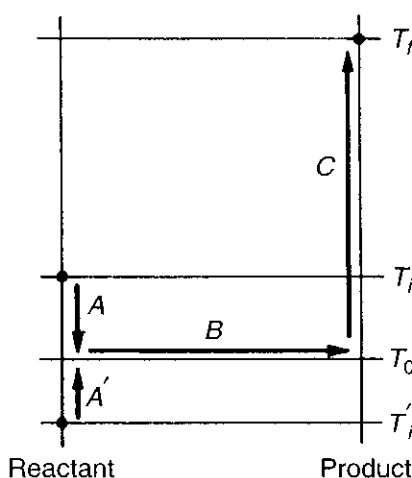
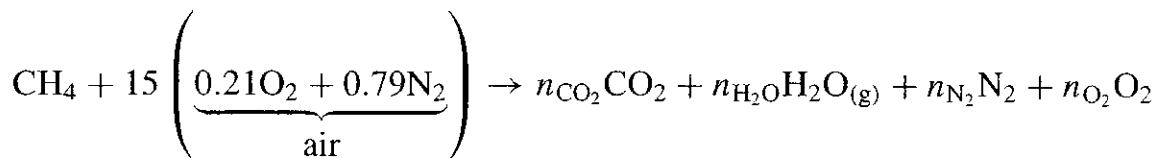


Figure 1.12 Temperature-reaction paths, showing the effect of initial reactant temperature.

Example 1.15. Assuming no dissociation of product species, determine the adiabatic flame temperature and product concentrations for the following chemical reaction at $T_i = 298$ K:



Solution: The four equations for conservation of atomic species are

$$\begin{aligned} \text{C:} \quad & 1 = n_{\text{CO}_2} \\ \text{O:} \quad & 15 \times (0.21 \times 2) = 2n_{\text{CO}_2} + n_{\text{H}_2\text{O}} + 2n_{\text{O}_2} \\ \text{N:} \quad & 15 \times (0.79 \times 2) = 2n_{\text{N}_2} \\ \text{H:} \quad & 4 = 2n_{\text{H}_2\text{O}} \end{aligned}$$

Using the above equations, the values of n_{CO_2} , $n_{\text{H}_2\text{O}}$, n_{N_2} , and n_{O_2} are determined as 1.0, 2.0, 11.85, and 1.15, respectively. The adiabatic flame temperature T_f can then be calculated by letting $\Delta H = 0$ in Eq. (1-152), i.e.,

$$\begin{aligned} & \left[1\Delta\mathcal{H}_f^o_{\text{CO}_2} + 2\Delta\mathcal{H}_f^o_{\text{H}_2\text{O}_{(\text{g})}} \right] - \left[1\Delta\mathcal{H}_f^o_{\text{CH}_4_{(\text{g})}} \right] \\ & + \{ 1(\mathcal{H}_{T_f} - \mathcal{H}_{298})_{\text{CO}_2} + 2(\mathcal{H}_{T_f} - \mathcal{H}_{298})_{\text{H}_2\text{O}_{(\text{g})}} \\ & + 11.85(\mathcal{H}_{T_f} - \mathcal{H}_{298})_{\text{N}_2} + 1.15(\mathcal{H}_{T_f} - \mathcal{H}_{298})_{\text{O}_2} \} = 0 \end{aligned}$$

Using the values of $\Delta\mathcal{H}_f^o$ in Table 1.2, we have

$$\Delta H_r = [(-94.054) + 2(-57.798)] - (-17.895) = -191.755 \text{ kcal}$$

Assuming a flame temperature of 2000 K and using Table 1.5, the thermal energy change is

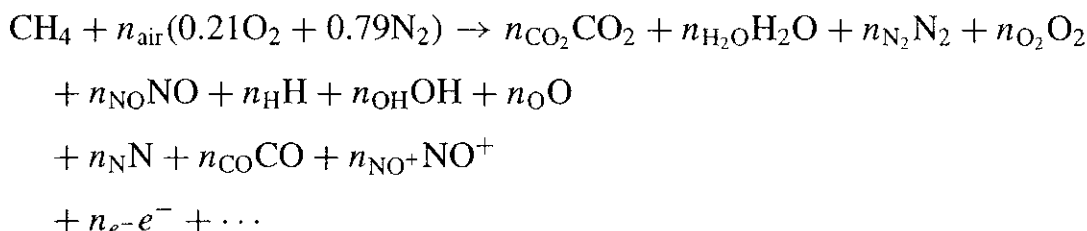
$$\begin{aligned} & 1(21.854)_{\text{CO}_2} + 2(17.397)_{\text{H}_2\text{O}} + 11.85(13.417)_{\text{N}_2} + 1.15(14.143)_{\text{O}_2} \\ & = 231.904 \text{ kcal} \end{aligned}$$

Assume a flame temperature of 1700 K, the thermal-energy change is

$$\begin{aligned} & 1(17.562)_{\text{CO}_2} + 2(13.804)_{\text{H}_2\text{O}} + 11.85(10.858)_{\text{N}_2} + 1.15(11.462)_{\text{O}_2} \\ & = 187.019 \text{ kcal} \end{aligned}$$

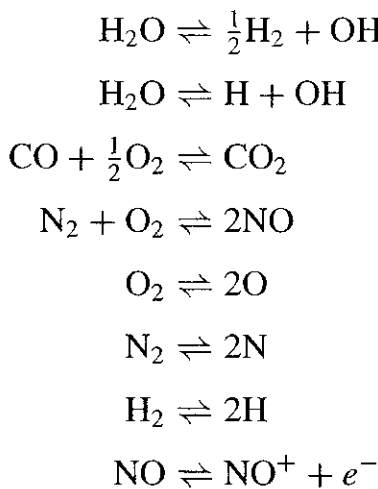
Interpolating for a value of 191.755 kcal, we arrive at $T_f = 1732$ K.

The above example shows that under the assumption of no product dissociation, there are five equations to be solved for five unknowns. It is important to note that the above method of calculation is appropriate only if T_f is low ($T_f < 1200$ K). At higher temperatures, the products dissociate and many other compounds are formed. The above chemical reaction could change into

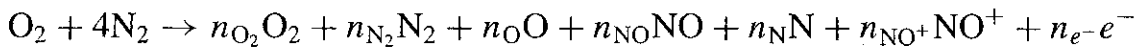


Because we still have only four equations from the conservation of atomic species, there are more unknowns than equations, and the adiabatic flame temperature cannot be calculated as in the simplified reaction.

If the products are in a condition of chemical equilibrium, we can obtain more relations between the mole fractions of the product constituents at equilibrium. Some equilibrium reactions are listed below.



The equilibrium constants (to be discussed in the next section) for each pair of equilibrium reactions will give us further information on the determination of the adiabatic flame temperature. We note here that for air at high temperatures, the reaction between O₂ and N₂ can produce many species. For example,



14 EQUILIBRIUM CONSTANTS

From previous discussion of Gibbs free energy, we have

$$G \equiv H - TS = U + pV - TS \quad (1-154)$$

Differentiating $U \equiv H - pV$ and utilizing the first law of thermodynamics, we have

$$dU = dH - p\,dV - V\,dp = T\,dS - p\,dV \quad (1-155)$$

where $p\,dV$ is the work done by the system. The differential form of Eq. (1-154) is

$$dG = dU + p\,dV + V\,dp - T\,dS - S\,dT \quad (1-156)$$

Then, substituting Eq. (1-155) into Eq. (1-156) gives

$$dG = V\,dp - S\,dT \quad (1-157)$$

Assuming the perfect-gas relation, for an isothermal process,

$$dG = V\,dp = \frac{nR_uT}{p}\,dp = nR_uT\,d(\ln p) \quad (1-158)$$

Integrating from p^o to p , Eq. (1-158) becomes

$$G - G^o = nR_uT (\ln p - \ln p^o) \quad (1-159)$$

where p is given in the unit of bar and $p^o = 1$ bar. After combining the last two terms and rearranging, we have

$$G = G^o + nR_uT \ln(p/p^o) \quad (1-160)$$

Then, for species i in the system, we have

$$G_i = G_i^o + n_i R_u T \ln(p_i/p^o) \quad (1-161)$$

Let us now consider a reaction of A with B to produce C and D in a constant-temperature bath, i.e.,



Applying Eq. (1-161) to all four species flowing in and out of the Van't Hoff equilibrium box (see Fig. 1.13), we have

$$\begin{aligned} G_A &= G_A^o + aR_uT \ln(p_A/p^o) \\ G_B &= G_B^o + bR_uT \ln(p_B/p^o) \\ G_C &= G_C^o + cR_uT \ln(p_C/p^o) \\ G_D &= G_D^o + dR_uT \ln(p_D/p^o) \end{aligned}$$

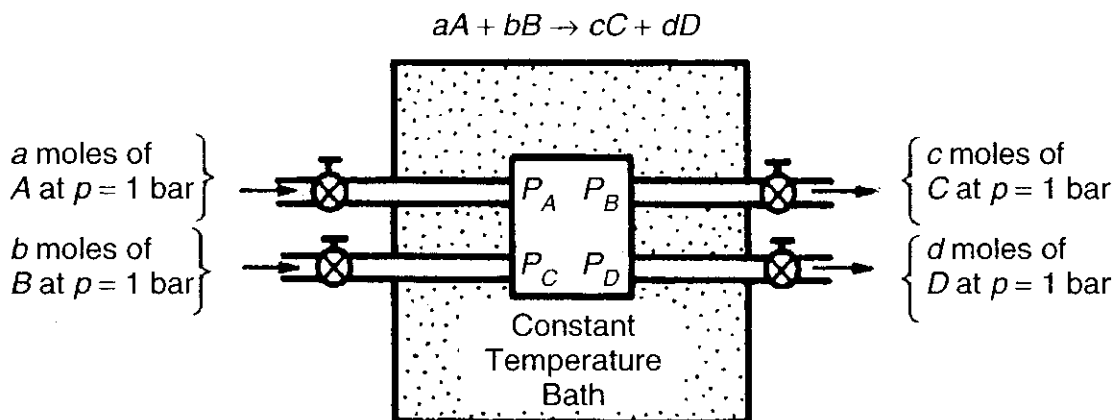


Figure 1.13 Van't Hoff equilibrium box.

Through the equilibrium box, we assume a moles of A and b moles of B are pumped into the box, the reaction occurs isothermally and equilibrium is reached, and then c moles of C and d moles of D are pumped out. From these considerations, the Gibbs free energy change can be written as

$$\begin{aligned}
 \Delta G &= G_{\text{product}} - G_{\text{reactant}} \\
 &= (G_C + G_D) - (G_A + G_B) \\
 &= [(G_C^o + G_D^o) - (G_A^o + G_B^o)] + R_u T \ln \left[\frac{p_C}{p^o} \right]^c \left[\frac{p_D}{p^o} \right]^d \\
 &\quad - R_u T \ln \left[\frac{p_A}{p^o} \right]^a \left[\frac{p_B}{p^o} \right]^b \\
 &= \Delta G^o + R_u T \ln \frac{[p_C/p^o]^c [p_D/p^o]^d}{[p_A/p^o]^a [p_B/p^o]^b} \tag{1-162}
 \end{aligned}$$

Since we have assumed the system to be at equilibrium,

$$\Delta G = 0$$

and

$$-\Delta G^o = R_u T \ln \frac{[p_C/p^o]^c [p_D/p^o]^d}{[p_A/p^o]^a [p_B/p^o]^b} \tag{1-163}$$

We can define

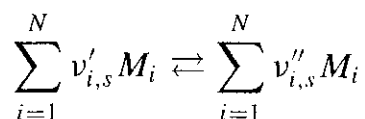
$$K_p \equiv \frac{[p_C/p^o]^c [p_D/p^o]^d}{[p_A/p^o]^a [p_B/p^o]^b} \tag{1-164}$$

$$\boxed{\Delta G^o = -R_u T \ln K_p} \tag{1-165}$$

Equation (1-165) shows the relation between the standard-free-energy change and the equilibrium constant at any arbitrary pressure and temperature. The value of K_p can be deduced from Eq. (1-165), if ΔG° is known.

It is important to note that a large negative ΔG° corresponds to a large equilibrium constant. Large K_p means that once reaction starts, the conversion of the reactants to products in their standard states will be quite complete at equilibrium with product concentrations much higher than those of reactants. Also, for any negative ΔG° , K_p must be greater than unity.

The equilibrium constant can be put into a more general form by considering the general chemical reaction

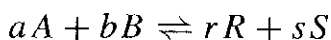


where v'_i and v''_i represent, respectively, the stoichiometric coefficients of reactants and products for the chemical species M_i , and N is the total number of chemical species involved. Then,

$$K_p = \prod_{i=1}^N \left[\frac{p_{i,e}}{p^\circ} \right]^{(v''_{i,s} - v'_{i,s})} \quad (1-166)$$

where in this product sum, the partial pressure of species i in the equilibrium mixture is raised to the power of $(v''_{i,s} - v'_{i,s})$ and the subscript s identifies the coefficients as the stoichiometric coefficients for the individual chemical equilibrium reactions. The subscript p in K_p means that the equilibrium constant is written in terms of partial pressures.

The same expression for the equilibrium constant can be obtained from thermodynamic considerations instead of from the Van't Hoff equilibrium box concept. Consider the hypothetical reaction between ideal gases



We shall now develop an expression for the free-energy change, which occurs when the reactants at partial pressures p_A and p_B are converted into products at partial pressures p_R and p_S . From earlier discussion,

$$G(p, T) = H(T) - TS(p, T) \quad (1-167)$$

Since we define the standard state at $p^\circ = 1$ bar, the Gibbs free energy at temperature T is

$$G^\circ(p^\circ, T) = H^\circ(T) - TS^\circ(p^\circ, T) \quad (1-168)$$

Subtracting Eq. (1-168) from (1-167) and noting that (since H is independent of pressure for a perfect gas) $H - H^\circ = 0$, we have

$$G - G^\circ = -T(S - S^\circ) \quad (1-169)$$

From the perfect-gas law, for an isothermal process

$$S - S^o = -nR_u \ln\left(\frac{p}{p^o}\right) \quad (1-170)$$

To see this, note that

$$\delta\hat{Q} = dE + \delta\hat{W}$$

For an isothermal process, $dE = 0$ and

$$\delta\hat{Q} = \delta\hat{W} = p \, dV \quad (1-171)$$

but

$$\begin{aligned} d_e S &= \frac{\delta\hat{Q}}{T} = \frac{p}{T} \, dV = \frac{nR_u}{V} \, dV = nR_u \, d(\ln V) \\ &= nR_u \, d\left[\ln\left(\frac{nR_u T}{p}\right)\right] \end{aligned} \quad (1-172)$$

Since we have made the isothermal assumption,

$$d_e S = -nR_u \, d(\ln p) \quad (1-173)$$

By integrating the above equation from p^o to p , we can obtain the same equation as Eq. (1-170). Substituting Eq. (1-170) into Eq. (1-169) gives

$$G(T, p) = G^o + nR_u T \ln\left(\frac{p}{p^o}\right) \quad (1-174)$$

For the mixture, then,

$$G(T, p) = \sum_{i=1}^N n_i \left\{ g_i^o + R_u T \ln\left(\frac{p_i}{p^o}\right) \right\} \quad (1-175)$$

where g_i is the molar Gibbs free energy of the i th species with units of cal/mol and p_i is the partial pressure as previously defined. At equilibrium,

$$(dG)_{T,p} = 0 \quad (1-176)$$

If we take the differential of Eq. (1-175), we get

$$0 = \sum_{i=1}^N g_i^o \, dn_i + R_u T \sum_{i=1}^N \left[\ln\left(\frac{p_i}{p^o}\right) \right] \, dn_i + R_u T \sum_{i=1}^N \mu_i \frac{dp_i^o}{p_i} \quad (1-177)$$

The last term of Eq. (1-177) vanishes because

$$\begin{aligned} \sum_{i=1}^N n_i \frac{dp_i}{p_i} &= \sum_{i=1}^N \left(\frac{n_{\text{total}}}{p} \right) dp_i = \frac{1}{p} \left(\sum_{i=1}^N n_i \right) \left(\sum_{i=1}^N dp_i \right) \\ &= \frac{1}{p} \left(\sum_{i=1}^N n_i \right) d \left(\sum_{i=1}^N p_i \right) = 0 \end{aligned} \quad (1-178)$$

since at equilibrium the system pressure is constant. The first term of Eq. (1-177) can be expressed as

$$\sum_{i=1}^N g_i^o dn_i = g_A^o dn_A + g_B^o dn_B + \cdots + g_R^o dn_R + g_S^o dn_S + \cdots \quad (1-179)$$

where

$$\begin{aligned} dn_A &= -a, & dn_B &= -b \\ dn_R &= r, & dn_S &= s \end{aligned}$$

Therefore,

$$\sum_{i=1}^N g_i^o dn_i \equiv \Delta G^o = G_{\text{products}}^o - G_{\text{reactants}}^o \quad (1-180)$$

Eq. (1-177) then becomes

$$\Delta G^o = -R_u T \ln K_p \quad (1-181)$$

where

$$K_p = \frac{(p_R/p^o)^r (p_S/p^o)^s}{(p_A/p^o)^a (p_B/p^o)^b}, \quad p^o = 1 \text{ bar} \quad (1-182)$$

and r , s , a , and b are the stoichiometric coefficients. We have thus arrived at the same result of Eq. (1-181) using two different methods.

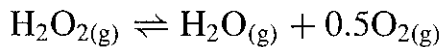
It should be noted that K_p is independent of system pressure, since K_p is related to ΔG^o and T by Eq. (1-165). Both G^o and ΔG^o are functions of T only, as can be seen from Eq. (1-168). The equilibrium constant K_p can therefore be tabulated as a unique function of temperature.

In the preceding discussion, the molar form of the free energy was introduced. We may also note that the molar standard free energy of formation Δg_f^o is known for many compounds, allowing ΔG^o to be calculated for any reaction as

$$\boxed{\Delta G^o = \sum_{i=1}^N v_i'' \Delta g_{f,i}^o - \sum_{i=1}^N v_i' \Delta g_{f,i}^o} \quad (1-183)$$

where ΔG° depends only on the nature of the reactants and products. The values of Δg_f° for some selected species are given in Table 1.6. It is important to note that the value of Δg_f° for every element in its standard state is equal to zero.

Example 1.16. The decomposition of gaseous hydrogen peroxide occurs according to the reaction



What is the value of the equilibrium constant of this reaction at 298.15 K?

Solution: The value of ΔG° for this equilibrium reaction can be calculated using Table 1.6 and Eq. (1-183) as shown below:

$$\begin{aligned}\Delta G^\circ &= \sum_{i=1}^N v_i'' \Delta g_{f,i}^\circ - \sum_{i=1}^N v_i' \Delta g_{f,i}^\circ \\ &= \left[1\Delta g_{f,\text{H}_2\text{O}_{(\text{g})}}^\circ + \frac{1}{2}\Delta g_{f,\text{O}_{2(\text{g})}}^\circ + 0\Delta g_{f,\text{H}_2\text{O}_{2(\text{g})}}^\circ \right] \\ &\quad - [0\Delta g_{f,\text{H}_2\text{O}_{(\text{g})}}^\circ + 0\Delta g_{f,\text{O}_{2(\text{g})}}^\circ + 1\Delta g_{f,\text{H}_2\text{O}_{2(\text{g})}}^\circ] \\ &= [1(-54.63) + 0.5(0) + 0] - [0 + 0 + 1(-25.2)] = -29.43 \text{ kcal}\end{aligned}$$

ΔG° is related to K_p by Eq. (1-181). Considering the decomposition of 1 g-mol of H_2O_2 , we must use 29.43 kcal/g-mol for ΔG° . After rearrangement, we have

$$\begin{aligned}K_p &= \exp\left(-\frac{\Delta G^\circ}{R_u T}\right) = \exp\left(\frac{29.43 \times 10^3 \text{ cal/g-mole}}{(1.9872 \text{ cal/g-mole K})(298.15 \text{ K})}\right) \\ &= 3.736 \times 10^{21}\end{aligned}$$

#

Let us consider the equilibrium constants for the formation reactions of H_2O , H , and OH species. Their equilibrium constants can be written in terms of the partial pressures shown below:

$$\text{H}_2 + \frac{1}{2}\text{O}_2 \rightleftharpoons \text{H}_2\text{O}, \quad K_{p,\text{H}_2\text{O}} = \frac{[\text{p}_{\text{H}_2\text{O}}/\text{p}^\circ]}{[\text{p}_{\text{H}_2}/\text{p}^\circ][\text{p}_{\text{O}_2}/\text{p}^\circ]^{1/2}}$$

$$\frac{1}{2}\text{H}_2 \rightleftharpoons \text{H}, \quad K_{p,\text{H}} = \frac{[\text{p}_{\text{H}}/\text{p}^\circ]}{[\text{p}_{\text{H}_2}/\text{p}^\circ]^{1/2}}$$

$$\frac{1}{2}\text{H}_2 + \frac{1}{2}\text{O}_2 \rightleftharpoons \text{OH}, \quad K_{p,\text{OH}} = \frac{[\text{p}_{\text{OH}}/\text{p}^\circ]}{[\text{p}_{\text{H}_2}/\text{p}^\circ]^{1/2} [\text{p}_{\text{O}_2}/\text{p}^\circ]^{1/2}}$$

Table 1.6 Free Energy of Formation^a Δg_f° (kcal/mol) at 298.15 K

<i>Gases</i>		<i>Solids</i>	
H ₂ O	-54.63	AgCl	-26.24
H ₂ O ₂	-25.20	AgBr	-23.2
O ₃	39.00	AgI	-15.81
HCl	-22.78	BaO	-124.37
HBr	-12.79	BaSO ₄	-325.6
HI	0.37	BaCO ₃	-271.1
SO ₂	-71.73	CaO	-144.24
SO ₃	-88.67	CaCO ₃	-269.9
H ₂ S	-7.97	Ca(OH) ₂	-214.73
N ₂ O	24.90	SiO ₂	-204.69
NO	20.70	Fe ₂ O ₃	-177.71
NO ₂	12.25	Al ₂ O ₃ (α crystal)	-378.17
NH ₃	-3.91	CuO	-31.00
CO	-32.78	Cu ₂ O	-34.89
CO ₂	-94.26	ZnO	-76.60
<i>Organic Compounds</i>			
GASES			
Methane, CH ₄	-12.13	Ethylene, C ₂ H ₄	16.35
Ethane, C ₂ H ₆	-7.65	Acetylene, C ₂ H ₂	59.31
Propane, C ₃ H ₈	-5.59	1-Butene, C ₄ H ₈	17.09
<i>n</i> -Butane, C ₄ H ₁₀	-3.75	<i>cis</i> -2-Butene, C ₄ H ₈	15.74
Isobutane, C ₄ H ₁₀	-4.3	<i>trans</i> -2-Butene, C ₄ H ₈	15.05
<i>n</i> -Pentane, C ₅ H ₁₂	-2.0	Isobutene, C ₄ H ₈	13.88
Isopentane, C ₅ H ₁₂	-3.5	1,3-Butadiene, C ₄ H ₆	36.01
Neopentane, C ₅ H ₁₂	-3.6	Methyl chloride, CH ₃ Cl	-14.0
LIQUIDS			
Methanol, CH ₃ OH	-39.82	Benzene, C ₆ H ₆	29.76
Ethanol, C ₂ H ₅ OH	-41.78	Chloroform, CHCl ₃	-17.6
Acetic acid, CH ₃ COOH	-93.19	Carbon tetrachloride, CCl ₄	-16.4
Water, H ₂ O	-56.68		
<i>Aqueous Ions</i>			
H ⁺	0.0	OH ⁻	-37.59
Na ⁺	-62.59	Cl ⁻	-31.35
K ⁺	-67.47	Br ⁻	-24.57
Ag ⁺	18.13	I ⁻	-12.35
Ba ²⁺	-134.0	HS ⁻	3.01
Ca ²⁺	-132.48	S ²⁻	20.0
Cu ²⁺	15.53	SO ₄ ²⁻	-177.34
Zn ²⁺	-35.18	SO ₃ ²⁻	-126.2
<i>Gaseous Atoms</i>			
H	48.58	I	16.7
F	14.9	C	160.43
Cl	25.17	N	108.87
Br	19.69	O	55.38
C ₂	186.83	S	56.52

^aCompiled and converted from the JANAF Table,²⁰ 79th edition of *Handbook of Chemistry and Physics*,¹⁶ and Mahan.⁴

We now consider an equilibrium reaction involving all three species H₂O, H, and OH:

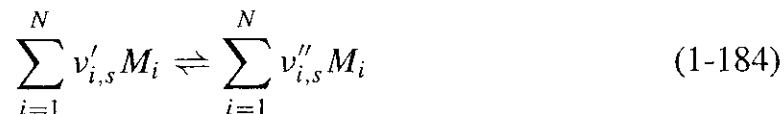


The equilibrium constant of this reaction is not tabulated as a function of T but can be evaluated from the following equation, where the last term contains the three $K_{p,i}$ which are tabulated with temperature for the formation reactions.

$$K_p = \frac{p_{\text{H}} p_{\text{OH}}}{p_{\text{H}_2\text{O}}} \frac{p_{\text{H}_2} p_{\text{O}_2}^{1/2}}{p_{\text{H}_2} p_{\text{O}_2}^{1/2}} = \frac{(p_{\text{H}}/p_{\text{H}_2}^{1/2})(p_{\text{OH}}/p_{\text{H}_2}^{1/2} p_{\text{O}_2}^{1/2})}{(p_{\text{H}_2\text{O}}/p_{\text{H}_2} p_{\text{O}_2}^{1/2})} = \frac{K_{p,\text{H}} K_{p,\text{OH}}}{K_{p,\text{H}_2\text{O}}}$$

Note that p^o is set to 1 bar for the above equation. In general, K_p of any elementary reaction can be calculated from the $K_{p,i}$ of the formation reactions of the species involved in the reaction.

Consider the following general equilibrium chemical reaction with $v'_{i,s}$ and $v''_{i,s}$ representing the stoichiometric coefficients of reactants and products for the chemical species M_i ; N is the total number of chemical species involved.



The equilibrium constant K_p expressed in terms of ratios of equilibrium partial pressures is given earlier in Eq. (1-166) as

$$K_p = K_p(T) = \prod_{i=1}^N (p_{i,e})^{(v''_{i,s} - v'_{i,s})} \quad (1-185a)$$

Other forms of the equilibrium constant are given by Eqs. (1-185b) through (1-185e)

$$K_n \equiv \prod_{i=1}^N (n_{i,e})^{(v''_{i,s} - v'_{i,s})} \quad (1-185b)$$

$$K_C \equiv \prod_{i=1}^N (C_{i,e})^{(v''_{i,s} - v'_{i,s})} \quad (1-185c)$$

$$K_X \equiv \prod_{i=1}^N (X_{i,e})^{(v''_{i,s} - v'_{i,s})} \quad (1-185d)$$

$$K_Y \equiv \prod_{i=1}^N (Y_{i,e})^{(v''_{i,s} - v'_{i,s})} \quad (1-185e)$$

For an ideal gas, we have

$$C_i = (\text{concentration of species } i) = \frac{p_i}{R_u T} \quad (1-186)$$

$$n_i \text{ (actual number of moles of species } i) = \frac{p_i V}{R_u T} = \frac{p_i}{p} n_T \quad (1-187)$$

$$X_i = (\text{mole fraction of species } i) = \frac{p_i}{p} = \frac{n_i}{n_T} \quad (1-188)$$

$$Y_i = (\text{mass fraction of species } i) = \frac{\text{Mw}_i p_i}{\rho T R_u} = \frac{\text{Mw}_i C_i}{\rho} = \frac{\rho_i}{\rho} \quad (1-189)$$

where

$$n_T = n = (\text{total number of moles in the mixture}) = \sum_{i=1}^N n_i$$

$$p = (\text{total mixture pressure}) = \sum_{i=1}^N p_i$$

$$\rho = \text{mixture density} = \sum_{i=1}^N \rho_i$$

Recall that we have defined

$$\Delta n = \sum_{i=1}^N v''_i - \sum_{i=1}^N v'_i \quad (1-190)$$

Various equilibrium constants are then related according to

$$K_p = K_C (R_u T)^{\Delta n} = K_n \left(\frac{R_u T}{V} \right)^{\Delta n} = K_n \left(\frac{p}{n_T} \right)^{\Delta n} \quad (1-191)$$

$$K_p = K_X \left(\frac{p}{p^o} \right)^{\Delta n} = K_Y \left(\frac{R_u T \rho}{p^o} \right)^{\Delta n} \prod_{i=1}^N \text{Mw}_i^{(v'_i - v''_i)} \quad (1-192)$$

When $\Delta n \neq 0$, unlike all other forms of equilibrium constants, K_p is a function of temperature only.

Now let us consider the following reaction involving only ideal gases:



Let $n^o(M_1)$, $n^o(M_2)$, $n^o(M_3)$, and $n^o(M_4)$ represent, respectively, the initial numbers of moles of M_1 , M_2 , M_3 , and M_4 before equilibrium has been reached

at a given temperature T . After equilibrium is reached, the following number of moles for each component are present in the mixture:

$$\begin{aligned} n_e(M_1) &= n^o(M_1) - v'_1 x & n_e(M_2) &= n^o(M_2) - v'_2 x \\ n_e(M_3) &= n^o(M_3) + v''_3 x & n_e(M_4) &= n^o(M_4) + v''_4 x \end{aligned}$$

They are given in the above form because for every $v''_3 x$ moles of M_3 formed, $v''_4 x$ moles of M_4 are formed, $v'_1 x$ moles of M_1 disappear, and simultaneously $v'_2 x$ moles of M_2 disappear. From the definitions of K_n and K_p , it now follows that

$$K_n = \frac{[n^o(M_3) + v''_3 x]^{v''_3} [n^o(M_4) + v''_4 x]^{v''_4}}{[n^o(M_1) - v'_1 x]^{v'_1} [n^o(M_2) - v'_2 x]^{v'_2}}$$

and

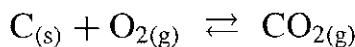
$$K_p = K_n \left(\frac{P}{n_T} \right)^{(v''_3 + v''_4 - v'_1 - v'_2)}$$

where the total number of moles in the final equilibrium mixture is

$$n_T = n^o(M_1) + n^o(M_2) + n^o(M_3) + n^o(M_4) + x(v''_3 + v''_4 - v'_1 - v'_2)$$

It is evident that for given values of K_n or K_p , the value of x can be calculated readily for given initial concentrations of the various reactants. Once the x value is known, the final equilibrium mixture composition is known.

Values of K_p for a number of formation reactions, compiled from the JANAF Thermochemical Tables,²⁰ are presented in terms of $\log_{10} K_p$ in Tables 1.7a through 1.7d. Note that the tabulated equilibrium constants are written for the formation of 1 mole of substances from their elements, for example,



When any elements are in the condensed phases, the equilibrium constants are written as in a script κ_p , that is, $\kappa_{p,\text{CO}_2} = p_{\text{CO}_2}/p_{\text{O}_2} p_{\text{C}_{(s)}}$ for the above equilibrium reaction. Since $p_{\text{C}_{(s)}}$ is very small, κ_p can be very large. Replacing $p_{\text{C}_{(s)}}$ by the vapor pressure of graphite $p_{\text{vp,C}}$, which is a known function of temperature, and rearranging the equation, we have

$$K_{p,\text{CO}_2} \equiv \kappa_{p,\text{CO}_2} p_{\text{vp,C}} = \frac{p_{\text{CO}_2}}{p_{\text{O}_2}}$$

Values of K_{p,CO_2} defined by the above equation or those defined by Eq. (1-185a) are tabulated in Tables 1.7a through 1.7d. It is useful to note that K_p usually increases with increasing temperature for endothermic reactions and decreases for exothermic reactions.

Example 1.17. Consider the chemical reaction between methane and oxygen gas under a fuel-rich condition. The thermochemical reaction can be written as

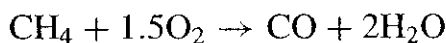


Table 1.7a Equilibrium Constants with Respect to the Elements in Their Standard States

T (K)	Log ₁₀ <i>K_{p1}</i>	Log ₁₀ <i>K_{p2}</i>	Log ₁₀ <i>K_{p3}</i>	Log ₁₀ <i>K_{p4}</i>	Log ₁₀ <i>K_{p5}</i>
0	∞	∞	∞	∞	∞
100	-126.729	-110.972	-19.438	123.579	-243.611
200	-61.986	-54.325	-9.351	60.792	-120.419
298.15	-40.599	-35.613	-6.005	40.047	-79.809
300	-40.330	-35.378	-5.963	39.785	-79.298
400	-29.469	-25.876	-4.265	29.238	-58.710
500	-22.936	-20.158	-3.246	22.884	-46.341
600	-18.570	-16.335	-2.568	18.631	-38.084
700	-15.446	-13.597	-2.085	15.582	-32.180
800	-13.098	-11.538	-1.724	13.287	-27.746
900	-11.269	-9.932	-1.444	11.496	-24.294
1000	-9.803	-8.644	-1.222	10.060	-21.530
1100	-8.603	-7.587	-1.041	8.881	-19.266
1200	-7.601	-6.705	-0.891	7.897	-17.377
1300	-6.752	-5.956	-0.764	7.063	-15.778
1400	-6.024	-5.313	-0.656	6.346	-14.407
1500	-5.392	-4.754	0.563	5.724	-13.217
1600	-4.839	-4.264	-0.482	5.179	-12.175
1700	-4.350	-3.831	-0.410	4.698	-11.256
1800	-3.915	-3.446	-0.347	4.269	-10.437
1900	-3.525	-3.100	-0.291	3.885	-9.705
2000	-3.175	-2.788	-0.240	3.540	-9.045
2200	-2.568	-2.249	-0.153	2.942	-7.905
2400	-2.062	-1.798	-0.082	2.443	-6.954
2600	-1.633	-1.415	-0.021	2.021	-6.148
2800	-1.265	-1.087	0.030	1.658	-5.457
3000	-0.946	-0.801	0.074	1.344	-4.857
3500	-0.307	-0.228	0.160	0.713	-3.655
4000	0.173	0.203	0.223	0.239	-2.751
4500	0.547	0.539	0.270	-0.131	-2.046
5000	0.846	0.809	0.307	-0.428	-1.480
5500	1.092	1.029	0.335	-0.672	-1.015
6000	1.296	1.213	0.357	-0.877	-0.625

By permission, from the JANAF Thermochemical Tables.²⁰ The equilibrium constants are defined as follows: $K_{p1} = p_O/p_{O_2}^{1/2}$, $K_{p2} = p_H/p_{H_2}^{1/2}$, $K_{p3} = p_{OH}/p_{O_2}^{1/2}p_{H_2}^{1/2}$, $K_{p4} = p_{H_2O}/p_{H_2}p_{O_2}^{1/2}$, $K_{p5} = p_N/p_{N_2}^{1/2}$. The partial pressures are those of the (ideal) gas, unless the contrary is indicated explicitly.

Let us assume that the following water-gas equilibrium reactions occur within the product species,

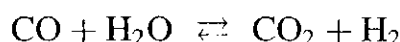


Table 1.7b Equilibrium Constants with Respect to the Elements in Their Standard States

T (K)	$\log_{10} K_{p6}$	$\log_{10} K_{p7}$	$\log_{10} K_{p8}$	$\log_{10} K_{p9}$	$\log_{10} K_{p10}$
0	∞	∞	∞	∞	∞
100	-46.460	-137.427	-365.689	62.807	205.639
200	-22.931	-65.238	-179.152	33.568	102.924
298.15	-15.172	-41.434	-117.599	24.030	69.095
300	-15.074	-41.135	-116.825	23.911	68.670
400	-11.143	-29.089	-85.606	19.110	51.539
500	-8.784	-21.932	-66.851	16.236	41.259
600	-7.210	-17.188	-54.336	14.320	34.404
700	-6.086	-13.815	-45.392	12.948	29.505
800	-5.243	-11.295	-38.681	11.916	25.829
900	-4.587	-9.405	-33.461	11.109	22.969
1000	-4.063	-8.154	-29.286	10.461	20.679
1100	-3.633	-7.128	-25.869	9.928	18.805
1200	-3.275	-6.272	-23.023	9.481	17.242
1300	-2.972	-5.548	-20.615	9.101	15.919
1400	-2.712	-4.926	-18.552	8.774	14.784
1500	-2.487	-4.386	-16.765	8.488	13.800
1600	-2.290	-3.914	-15.202	8.236	12.939
1700	-2.116	-3.497	-13.823	8.013	12.178
1800	-1.962	-3.126	-12.598	7.813	11.502
1900	-1.824	-2.793	-11.503	7.633	10.896
2000	-1.699	-2.494	-10.517	7.470	10.351
2200	-1.484	-1.977	-8.817	7.186	9.408
2400	-1.306	-1.546	-7.402	6.946	8.622
2600	-1.154	-1.180	-6.206	6.741	7.955
2800	-1.025	-0.867	-5.182	6.562	7.383
3000	-0.913	-0.595	-4.296	6.404	6.886
3500	-0.690	-0.050	-2.528	6.082	5.888
4000	-0.524	0.360	-1.207	5.830	5.134
4500	-0.396	0.680	-0.183	5.627	4.544
5000	-0.295	0.937	0.632	5.457	4.068
5500	-0.213	1.147	1.296	5.313	3.675
6000	-0.146	1.323	1.847	5.188	3.344

By permission, from the JANAF Thermochemical Tables.²⁰ The equilibrium constants are defined as follows: $K_{p6} = p_{\text{NO}}/p_{\text{N}_2}^{1/2} p_{\text{O}_2}^{1/2}$, $K_{p7} = p_{\text{S(g)}}/p_{\text{S(c)}}$, $K_{p8} = p_{\text{C(g)}}$ and $\kappa_{p8} = p_{\text{C(g)}}/p_{\text{C}_{(c,\text{graphite})}}$, $K_{p9} = p_{\text{CO}}/p_{\text{O}_2}^{1/2}$, and $\kappa_{p9} = p_{\text{CO}}/p_{\text{C}_{(c,\text{graphite})}} p_{\text{O}_2}^{1/2}$, $K_{p10} = p_{\text{CO}_2}/p_{\text{O}_2}$, $\kappa_{p10} = p_{\text{CO}_2}/p_{\text{C}_{(c,\text{graphite})}} p_{\text{O}_2}$.

Namely, a portion of the combustion product undergoes a further reaction and forms CO_2 and H_2 ; the equilibrium mixture can be assumed to consist of

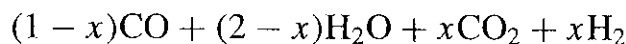


Table 1.7c Equilibrium Constants with Respect to the Elements in Their Standard States

T (K)	$\log_{10} K_{p11}$	$\log_{10} K_{p12}$	$\log_{10} K_{p13}$	$\log_{10} K_{p14}$	$\log_{10} K_{p15}$
0	∞	∞	∞	∞	∞
100	33.615	-123.562	-38.124	-60.319	-55.400
200	15.190	-63.116	-17.703	-28.855	-24.453
298.15	8.894	-43.477	-10.913	-18.449	-14.431
300	8.813	-43.232	-10.827	-18.318	-14.310
400	5.492	-33.426	-7.358	-13.028	-9.851
500	3.420	-27.626	-5.260	-9.841	-7.323
600	1.993	-23.816	-3.853	-7.709	-5.634
700	0.943	-21.138	-2.842	-6.180	-4.425
800	0.138	-19.162	-2.081	-5.029	-3.516
900	-0.500	-17.650	-1.486	-4.131	-2.808
1000	-1.018	-16.461	-1.009	-3.410	-2.239
1100	-1.447	-15.506	-0.617	-2.819	-1.773
1200	-1.807	-14.723	-0.290	-2.325	-1.384
1300	-2.115	-14.073	-0.012	-1.906	-1.054
1400	-2.379	-13.526	0.227	-1.546	-0.769
1500	-2.609	-13.061	0.435	-1.233	-0.522
1600	-2.810	-12.661	0.617	-0.959	-0.306
1700	-2.989	-12.316	0.778	-0.717	-0.114
1800	-3.147	-12.015	0.921	-0.501	0.057
1900	-3.289	-11.752	1.050	-0.307	0.211
2000	-3.416	-11.520	1.166	-0.133	0.350
2200	-3.636	-11.132	1.366	0.169	0.590
2400	-3.819	-10.823	1.534	0.422	0.792
2600	-3.973	-10.575	1.677	0.636	0.964
2800	-4.105	-10.374	1.799	0.820	1.112
3000	-4.219	-10.209	1.906	0.980	1.241
3500	-4.447	-9.914	2.121	1.301	1.500
4000	-4.619	-9.732	2.285	1.542	1.696
4500	-4.753	-9.622	2.415	1.729	1.850
5000	-4.863	-9.561	2.522	1.880	1.974
5500	-4.955	-9.533	2.612	2.003	2.076
6000	-5.034	-9.529	2.689	2.106	2.163

By permission, from the JANAF Thermochemical Tables.²⁰ The equilibrium constants are defined as follows: $K_{p11} = p_{\text{CH}_4}/p_{\text{H}_2}^2$ and $\kappa_{p11} = p_{\text{CH}_4}/p_{\text{H}_2}^2 p_{(\text{c},\text{graphite})}$, $K_{p12} = p_{\text{C}_2\text{H}_2}/p_{\text{H}_2}$ and $\kappa_{p12} = p_{\text{C}_2\text{H}_2}/p_{\text{C}_{(\text{c},\text{graphite})}}^2 p_{\text{H}_2}$, $K_{p13} = p_{\text{F}}/p_{\text{F}_2}^{1/2}$, $K_{p14} = p_{\text{Cl}}/p_{\text{Cl}_2}^{1/2}$, and $K_{p15} = p_{\text{Br}}/p_{\text{Br}_2}^{1/2}$.

Table 1.7d Equilibrium Constants with Respect to the Elements in Their Standard States

T (K)	$\log_{10} K_{p16}$	$\log_{10} K_{p17}$	$\log_{10} K_{p18}$	$\log_{10} K_{p19}$	$\log_{10} K_{p20}$
0	∞	∞	∞	∞	∞
100	-49.601	142.739	48.702	19.630	-9.927
200	-21.502	71.548	24.625	12.076	-2.596
298.15	-12.294	48.117	16.696	9.375	-0.273
300	-12.179	47.822	16.596	9.336	-0.245
400	-7.582	35.956	12.573	7.327	0.839
500	-5.245	28.831	10.151	5.957	1.054
600	-3.920	24.077	8.530	5.038	0.953
700	-2.971	20.678	7.369	4.377	0.877
800	-2.258	18.125	6.494	3.878	0.818
900	-1.702	16.137	5.812	3.489	0.770
1000	-1.256	14.544	5.265	3.176	0.732
1100	-0.890	13.240	4.817	2.919	0.699
1200	-0.584	12.151	4.442	2.704	0.672
1300	-0.325	11.229	4.124	2.522	0.649
1400	-0.103	10.438	3.852	2.366	0.629
1500	0.090	9.751	3.615	2.231	0.612
1600	0.259	9.150	3.408	2.112	0.596
1700	0.409	8.619	3.225	2.007	0.583
1800	0.542	8.146	3.062	1.914	0.570
1900	0.661	7.723	2.916	1.830	0.559
2000	0.768	7.341	2.785	1.755	0.549
2200	0.953	6.682	2.558	1.625	0.530
2400	1.107	6.131	2.368	1.516	0.514
2600	1.237	5.665	2.207	1.424	0.499
2800	1.349	5.264	2.069	1.345	0.485
3000	1.445	4.917	1.950	1.275	0.473
3500	1.638	4.221	1.709	1.136	0.445
4000	1.783	3.699	1.526	1.030	0.422
4500	1.898	3.294	1.383	0.945	0.404
5000	1.993	2.970	1.267	0.877	0.390
5500	2.073	2.707	1.171	0.821	0.379
6000	2.143	2.488	1.091	0.774	0.371

By permission, from the JANAF Thermochemical Tables.²⁰ The equilibrium constants are defined as follows: $K_{p16} = p_I/p_{I_2}^{1/2}$, $K_{p17} = p_{HF}/p_{H_2}^{1/2} p_{F_2}^{1/2}$, $K_{p18} = p_{HCl}/p_{H_2}^{1/2} p_{Cl_2}^{1/2}$, $K_{p19} = p_{HBr}/p_{H_2}^{1/2} p_{Br_2}^{1/2}$, and $K_{p20} = p_{HI}/p_{H_2}^{1/2} p_{I_2}^{1/2}$.

Write the necessary mathematical relationships required for solving the equilibrium composition and adiabatic flame temperature.

Solution: The total number of moles of product species can be calculated as

$$n_T = \sum_{i=1}^N n_i = (1-x) + (2-x) + x + x = 3$$

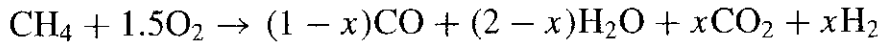
The mole fractions and partial pressures of product species are

$$\begin{aligned} X_{\text{CO}} &= \frac{1-x}{3}, & X_{\text{H}_2\text{O}} &= \frac{2-x}{3}, & X_{\text{CO}_2} = X_{\text{H}_2} &= \frac{x}{3} \\ p_{\text{CO}} &= \frac{1-x}{3} p, & p_{\text{H}_2\text{O}} &= \frac{2-x}{3} p, & p_{\text{CO}_2} = p_{\text{H}_2} &= \frac{x}{3} p \end{aligned}$$

For water–gas reaction, the equilibrium constant with $p^o = 1$ bar can be written as

$$K_p = \frac{p_{\text{CO}_2} p_{\text{H}_2}}{p_{\text{CO}} p_{\text{H}_2\text{O}}} = \frac{\left(\frac{x}{3}\right)^2 p^2}{\left(\frac{1-x}{3}\right) p \left(\frac{2-x}{3}\right) p} = \frac{x^2}{(1-x)(2-x)} \quad (\text{a})$$

For the chemical reaction



the general enthalpy balance equation for an adiabatic system can be written as

$$\Delta H = \sum_{i=1}^N v_i''(\Delta \mathcal{H}_f^o)_i - \sum_{i=1}^N v_i'(\Delta \mathcal{H}_f^o)_i + \sum_{i=1}^N v_i'' \mathcal{H}_i \Big|_{298}^{T_f} + \sum_{i=1}^N v_i' \mathcal{H}_i \Big|_{T_i}^{298} = 0$$

In terms of individual species, we have

$$\begin{aligned} &(1-x)\Delta \mathcal{H}_{f,\text{CO}}^o + (2-x)\Delta \mathcal{H}_{f,\text{H}_2\text{O}}^o + x\Delta \mathcal{H}_{f,\text{CO}_2}^o - \Delta \mathcal{H}_{f,\text{CH}_4}^o + [\mathcal{H}_{298} - \mathcal{H}_{T_i}]_{\text{CH}_4} \\ &+ 1.5[\mathcal{H}_{298} - \mathcal{H}_{T_i}]_{\text{O}_2} + (1-x)[\mathcal{H}_{T_f} - \mathcal{H}_{298}]_{\text{CO}} + (2-x)[\mathcal{H}_{T_f} - \mathcal{H}_{298}]_{\text{H}_2\text{O}} \\ &+ x[\mathcal{H}_{T_f} - \mathcal{H}_{298}]_{\text{CO}_2} + x[\mathcal{H}_{T_f} - \mathcal{H}_{298}]_{\text{H}_2} = 0 \end{aligned} \quad (\text{b})$$

Assuming a value of T_f , the equilibrium constant $K_p(T_f)$ can be determined from the equilibrium constants of the formation reactions of CO_2 , CO , and H_2O . Knowing K_p , the value of x can be solved from equation (a). Substitute the x value together with heats of formation and enthalpy changes into the left-hand side of equation (b) to see whether the sum is equal to zero. If not balanced, reassume a flame temperature and repeat the above process. Finally, the converged values of adiabatic flame temperature T_f and x can be determined through iteration, using equations (a) and (b). It is also possible to speed up the converging process using Newton-Raphson's descent method²³ for solving corrections to the initial estimated values of T_f .

Example 1.18. A mixture of 1 mole of N₂ and 0.5 mole of O₂ is heated to 4000 K at 1 atm pressure, resulting in an equilibrium mixture of N₂, O₂, and NO only. If the O₂ and N₂ were initially at 298.15 K and were heated steadily, how much heat was required to bring the final mixture to 4000 K on the basis of 1 initial mole of N₂?

Solution: The reaction is written as



The law of conservation of atomic species requires

$$\text{N} : 2 = 2a + c$$

$$\text{O} : 1 = 2b + c$$

This implies that

$$\begin{aligned} a &= 0.5(2 - c) = 1 - \frac{c}{2} \\ b &= 0.5(1 - c) = 0.5 - \frac{c}{2} \end{aligned}$$

Letting $x = c$, the reaction equation can then be written as



Considering the equilibrium reaction $0.5\text{N}_2 + 0.5\text{O}_2 \rightleftharpoons \text{NO}$ at $T_f = 4000$ K, we can obtain $\log_{10} K_p = -0.524$ from Table 1.7b or $K_p = 0.2992 \approx 0.3$; therefore,

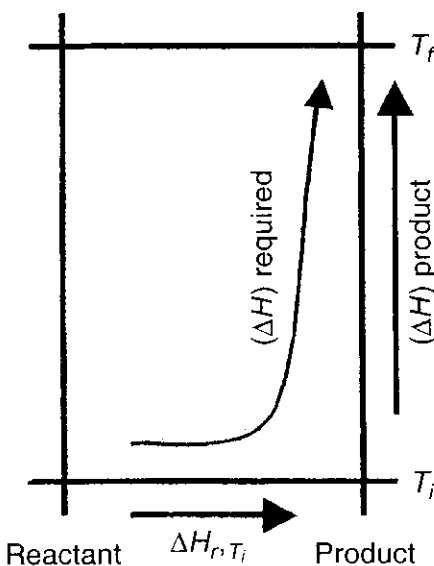
$$K_p = 0.3 = \frac{p_{\text{NO}}}{p_{\text{N}_2}^{1/2} p_{\text{O}_2}^{1/2}} = \frac{x}{(1 - x/2)^{1/2} (0.5 - x/2)^{1/2}} \left(\frac{p}{\sum n} \right)^{1-1/2-1/2}$$

Thus, $0.09 = 4x^2/[(2 - x)(1 - x)]$, or $43.5x^2 + 3x - 2 = 0$, so that

$$x = \frac{-3 \pm \sqrt{9 + 8 \times 43.5}}{2 \times 43.5} = \frac{-3 \pm 18.89}{87} = 0.1825$$

Note that the negative root of $x = -0.2516$ has no physical meaning and therefore is ignored. The final mixture is then $0.90875\text{N}_2 + 0.40875\text{O}_2 + 0.1825\text{NO}$.

The heat of formation of NO can be found from Table 1.2, i.e., $(\Delta H_{f,T_0}^\circ)_{\text{NO}} = 21.58 \text{ kcal/mol}$.



The temperature-reaction path showing
 $(\Delta H)_{\text{required}} = \Delta H_{r, T_i} + (\Delta H)_{\text{product}}$

$$\begin{aligned}
 (\Delta H)_{\text{required}} &= \underbrace{\left(\sum_{i=1}^N v''_i (\Delta \mathcal{H}_f^o)_i - \sum_{i=1}^N v'_i (\Delta \mathcal{H}_f^o)_i \right)}_{\Delta H_{r, T_i}} + (\Delta H)_{\text{product}} \\
 &= 0.1825 \times 21.58 + 0.90875(\mathcal{H}_{4000}^o - \mathcal{H}_{298.15}^o)_{\text{N}_2} \\
 &\quad + 0.40875(\mathcal{H}_{4000}^o - \mathcal{H}_{298.15}^o)_{\text{O}_2} + 0.1825(\mathcal{H}_{4000}^o - \mathcal{H}_{298.15}^o)_{\text{NO}} \\
 &= 0.1825 \times 21.58 + 0.90875 \times 31.077 + 0.40875 \times 33.151 \\
 &\quad + 0.1825 \times 31.709 \\
 &= 51.52 \text{ kcal}
 \end{aligned}$$

#

More-complicated reactions (including dissociation) will be discussed following the introduction of the concepts of fugacity and activity.

15 REAL-GAS EQUATIONS OF STATE AND FUGACITY CALCULATION

In many combustion problems, when the system pressure is at an elevated level, the ideal gas law can no longer be applied. Section 1.2 of Appendix A gives various forms of real-gas equations of state for high-pressure considerations. Section 1.3 of the same appendix describes the mixing rules for gaseous mixtures. In addition to these real-gas equations of state, it is useful to consider a thermodynamic parameter called fugacity and its usage at high pressures.

G. N. Lewis in 1901 introduced the concept of *fugacity*, which has proved of great value in representing the actual behavior of real gases, especially at high pressures. For ideal gases at a constant temperature [see Eq. (1-158)],

$$(dG)_T = nR_u T \, d(\ln p)_T \quad (1-193)$$

For a gas that does not behave ideally, the above equation will not hold, but a function f , known as the fugacity, may be defined in such a manner that the relationship

$$(dG)_T \equiv nR_u T \, d(\ln f)_T \quad (1-194)$$

is always satisfied, irrespective of whether the gas is ideal or not. Integrating Eq. (1-194) from thermodynamic state 1 to state 2, we have

$$G_2 - G_1 = nR_u T \ln \frac{f_2}{f_1} \quad (1-195)$$

Fugacity of the i th species may be considered to be the corrected partial pressure for that species:

$$\frac{f_i}{p_i} = \Gamma \text{ (proportionality factor)} \quad (1-196)$$

where Γ is a function of many parameters, such as the temperature and pressure. For an ideal gas,

$$\frac{f}{p} = 1 \quad (1-197)$$

As the pressure of the real gas is decreased, however, the behavior approaches that for an ideal gas. Therefore, the gas at very low pressure is chosen as the reference state, and it is postulated that the ratio f/p then approaches unity. Thus,

$$\lim_{p \rightarrow 0} \frac{f}{p} = 1 \quad (1-198)$$

where f has the units of pressure.

In terms of specific quantities, Eq. (1-194) can be written as

$$(dg)_T = RT \, (d \ln f)_T \quad (1-194a)$$

For a real gas, the equation of the state could be given as $pv = ZRT$, then

$$(dg)_T = ZRT(d \ln p)_T \quad (1-194b)$$

where Z represents the compressibility factor of the real gas. For an isothermal process at temperature T , the fugacity can be determined from the compressibility factor Z and the pressure p by the following relationship:

$$Z \, d(\ln p)_T = d(\ln f)_T \quad (1-199)$$

Integrating along an isothermal line from $p = 0$ to a finite pressure, we have

$$\ln \frac{f}{p} = \int_0^{P_r} (Z - 1) \, d(\ln P_r)_T \quad (1-200)$$

The reduced temperature (T_r) and reduced pressure (P_r) of a gas are defined as the ratios of temperature and pressure to their critical values, respectively. The critical temperatures (T_c) and pressures (P_c) of selected gases are shown in Table 1.8. A generalized compressibility chart for some selected gases is shown in Fig. 1.14 from Ref. 28 based on the original results of Su.²⁹

At any temperature, the right-hand side of this equation can be integrated graphically, using the generalized compressibility chart to find Z at each reduced pressure P_r ($\equiv p/p_c$). The value of f is therefore determined. The use of fugacity at high pressures is given in later chapters (e.g., Chapter 6).

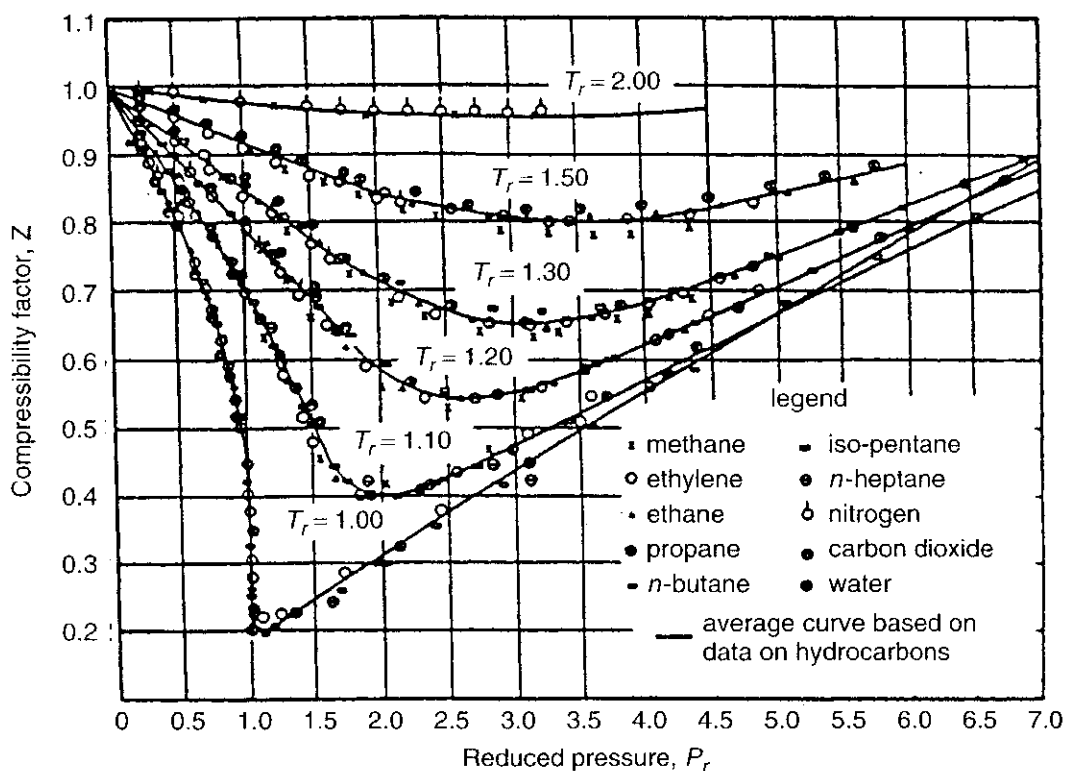


Figure 1.14 Generalized compressibility chart for selected gases.²⁸ (Gouq-Fen Su Modified Law of Corresponding States for Real Gases.²⁹ Reprinted from Ind. and Eng., Chemistry, vol. 38, p. 804, August, 1946. Copyright 1946 by the American Chemical Society and reprinted by permission of the copyright owner.).

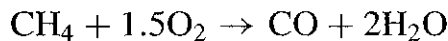
Table 1.8 Critical Temperatures and Pressures of Selected Gases^a

Gas	Formula	T_C (K)	P_C (MPa)
Air	—	132.5	3.766
Methane	CH ₄	190.56	4.592
Acetylene	C ₂ H ₂	308.3	6.138
Ethylene	C ₂ H ₄	282.34	5.041
Ethane	C ₂ H ₆	305.32	4.872
Propane	C ₃ H ₈	369.83	4.248
<i>n</i> -Butane	C ₄ H ₁₀	425.12	3.796
Isopentane	C ₅ H ₁₂	460.45	3.38
<i>n</i> -Heptane	C ₇ F ₁₆	474.8	1.62
Chlorine	Cl ₂	416.9	7.991
Carbon dioxide	CO ₂	304.13	7.375
Carbon monoxide	CO	132.91	3.499
Fluorine	F ₂	144.13	5.172
Helium	He	5.19	0.227
Hydrogen	H ₂	32.97	1.293
Neon	Ne	44.40	2.760
Nitrogen	N ₂	126.20	3.390
Hydrazine	N ₂ H ₄	653.0	14.7
Nitric oxide	NO	180.0	6.48
Nitrogen dioxide	NO ₂	430.95	10.132
Nitrous oxide	N ₂ O	309.57	7.255
Oxygen	O ₂	154.58	5.043
Ozone	O ₃	261.1	5.57
Water	H ₂ O	646.99	22.064
Xenon	Xe	289.73	5.840

^aExcerpted (with units converted) from the 79th edition of *CRC Handbook of Chemistry and Physics*.¹⁶

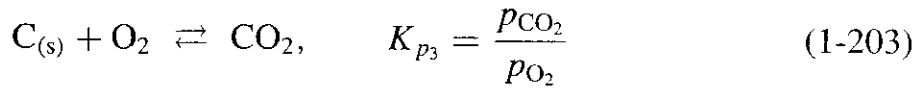
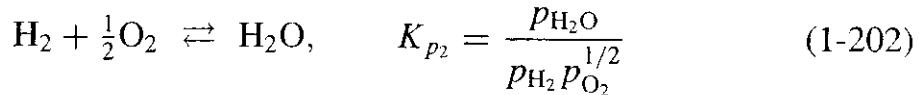
16 MORE-COMPLICATED DISSOCIATION IN THE COMBUSTION OF HYDROCARBONS

The frozen reaction process in the combustion of methane under fuel-rich conditions can be represented by

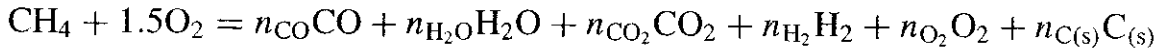


However, in reality there are more chemical product species to consider. In equilibrium, the following three equilibrium reactions should be considered:

$$\frac{1}{2}\text{O}_2 + \text{C}_{(\text{s})} \rightleftharpoons \text{CO}, \quad K_{p_1} = \frac{p_{\text{CO}}}{p_{\text{O}_2}^{1/2}} \quad (1-201)$$



The seven unknown quantities are the flame temperature and the partial pressures of the species $\text{C}_{(s)}$, CO , CO_2 , H_2 , H_2O , and O_2 , and the reaction equation can be written as



The conservation of atomic species equations for the three elements are

$$\text{C: } 1 = n_{\text{CO}} + n_{\text{CO}_2} + n_{\text{C}_{(s)}}$$

$$\text{O: } 3 = n_{\text{CO}} + n_{\text{H}_2\text{O}} + 2n_{\text{CO}_2} + 2n_{\text{O}_2}$$

$$\text{H: } 4 = 2n_{\text{H}_2\text{O}} + 2n_{\text{H}_2}$$

Recall that

$$\frac{n_i}{n_T} = \frac{p_i}{p} \quad (1-204)$$

Although n_T is unknown, it does not generally differ significantly from the stoichiometric value; the value of n_T for $\text{CH}_4 + 1.5\text{O}_2 \rightarrow \text{CO} + 2\text{H}_2\text{O}$ can be assumed to be 3 for the initial computation. With p known, we can substitute Eq. (1-204) into the atomic species conservation equations to get

$$\frac{p}{n_T} = p_{\text{CO}} + p_{\text{CO}_2} + p_{\text{C}} \quad (1-205)$$

$$3 \frac{p}{n_T} = p_{\text{CO}} + p_{\text{H}_2\text{O}} + 2p_{\text{CO}_2} + 2p_{\text{O}_2} \quad (1-206)$$

$$4 \frac{p}{n_T} = 2p_{\text{H}_2\text{O}} + 2p_{\text{H}_2} \quad (1-207)$$

Assuming $T_f = T_{f(1)}$, we can find from tables the values for $K_{p_1}(T_{f(1)})$, $K_{p_2}(T_{f(1)})$, and $K_{p_3}(T_{f(1)})$. The values of p_{C} , p_{CO} , p_{CO_2} , $p_{\text{H}_2\text{O}}$, p_{H_2} , and p_{O_2} can be obtained by solving the six simultaneous equations (1-201), (1-202), (1-203), (1-205), (1-206), and (1-207). n_{C} , n_{CO} , n_{CO_2} , $n_{\text{H}_2\text{O}}$, n_{H_2} , and n_{O_2} can be obtained from Eq. (1-204). The n_i values or v_i'' values are therefore known, and the enthalpy balance equation can be used for determination of T_f :

$$\sum_{i=1}^N v_i'' \Delta \mathcal{H}_{f,M_i}^o - \sum_{i=1}^N v_i' \Delta \mathcal{H}_{f,M_i}^o + \sum_{i=1}^N v_i'' \mathcal{H}_i|_{298}^{T_f} - \sum_{i=1}^N v_i' \mathcal{H}_i|_{298}^{T_f} = 0 \quad (1-208)$$

If Eq. (1-208) is not satisfied, we compute $n_T = \sum_{i=1}^N n_i$, reassume a value for T_f , and solve the six simultaneous equations again. This procedure is repeated until the enthalpy balance equation is satisfied. This is a general way of calculating the flame temperature and equilibrium compositions, when the combustion system is not extremely complicated. One disadvantage of this solution method is that as the partial pressure of a particular species becomes very small, errors can be introduced through very low values of partial pressure, which appears in the denominator of certain K_p expressions. Again, Newton-Raphson's descent method²³ can be used to speed up the converging process for obtaining corrections to the estimated values of T_f .

If a certain substance in an equilibrium mixture has two phases, an additional unknown is introduced. For example, if liquid water and water vapor coexist in one system, it is necessary to break $n_{H_2O_{\text{total}}}$ into $n_{H_2O_{(g)}}$ and $n_{H_2O_{(l)}}$, i.e.,

$$n_{H_2O_{\text{total}}} = n_{H_2O_{(g)}} + n_{H_2O_{(l)}}$$

and the fugacity of water vapor at relatively low pressures can be approximated by

$$f_{H_2O_{(g)}} \approx p_{H_2O_{(g)}} = \text{Known function of temperature, } T$$

Note that the vapor pressure of water is known at a certain temperature. The equilibrium constant for phase equilibrium of H₂O is known as a function of temperature:

$$K_p = \frac{p_{H_2O_{(g)}}}{p_{H_2O_{(l)}}}$$

For $\frac{1}{2}O_2 + H_2 \rightleftharpoons H_2O$, the equilibrium constant is

$$K_p = \frac{p_{H_2O_{(g)}}}{p_{O_2}^{1/2} p_{H_2}}$$

The vapor pressure in the numerator is a known quantity. Therefore, p_{O_2} can be expressed as a function of p_{H_2} or $n_{O_2} = F(n_{H_2})$.

The conservation equations of atomic species then become

$$\text{O: } [O] = 2n_{O_2} + n_{H_2O_{\text{total}}} + \dots = 2F(n_{H_2}) + n_{H_2O_{\text{total}}} + \dots$$

$$\text{H: } [H] = 2n_{H_2} + 2n_{H_2O_{\text{total}}}$$

In general, when a change in phase of certain species occurs, the adiabatic flame temperature versus F/O has a flat region. (See Fig. 1.15.) For some problems in which H₂O_(l) is present in appreciable amounts, CO₂ may dissolve in the H₂O, resulting in the fugacity of the solution being different from that of pure H₂O_(l). This phenomenon further complicates the problem of finding equilibrium composition and flame temperature.

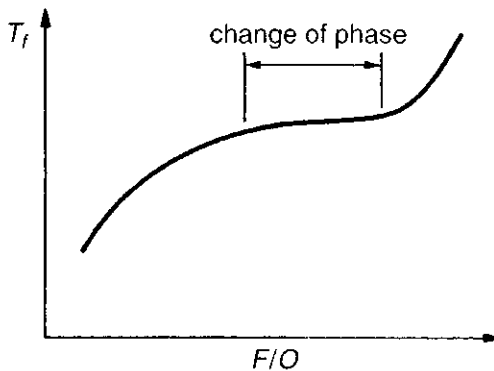


Figure 1.15 Exaggerated effect of phase change on the dependence of adiabatic flame temperature on fuel–oxidant ratio.

Some dissociation reactions are highly endothermic. This implies that T_f and equilibrium composition can be affected greatly by dissociation reactions. In general, for a C, H, O, N system, we should consider the following species in the equilibrium mixture: CO₂, H₂O, CO, H₂, O₂, OH, H, O, O₃, C_(s), CH₄, N₂, N, NO, NH₃, NO⁺, and e⁻. For low-pressure combustion systems (with $p \sim 1$ atm and $T_f > 2200$ K) or intermediate pressure systems (with $p \sim 20$ atm and $T_f > 2500$ K), the dissociation of CO₂ and H₂O by following equilibrium reactions must be considered.



The degree of dissociation will be at least 1%.

17 THE CLAUSIUS–CLAPEYRON EQUATION FOR PHASE EQUILIBRIUM

Consider any system consisting of two phases, for example, liquid and vapor. As long as both phases are present, a finite amount of vaporization of the liquid phase (represented by B) into gas phase (represented by A) will not disturb the equilibrium at constant temperature and pressure conditions, i.e.,

$$[(G_A + \Delta G_A) + (G_B - \Delta G_B)] - [G_A + G_B] = 0$$

or

$$\Delta G = 0$$

Under phase equilibrium, there is no work done other than that of expansion. Therefore, based on Eq. (1-99), dG_A and dG_B can be written as

$$dG_A = V_A \, dp - S_A \, dT \quad (1-209)$$

$$dG_B = V_B \, dp - S_B \, dT \quad (1-210)$$

where, because $\Delta G = 0$,

$$dG_A = dG_B \quad \text{and} \quad V_A \, dp - S_A \, dT = V_B \, dp - S_B \, dT \quad (1-211)$$

Therefore,

$$\frac{dp}{dT} = \frac{S_A - S_B}{V_A - V_B} = \frac{\Delta S}{\Delta V} \quad (1-212)$$

The change of entropy ΔS is related to heat of vaporization by

$$\Delta S = \frac{\Delta H_v}{T}$$

Using the molar heat of vaporization and molar volume, Eq. (1-212) becomes

$$\frac{dp}{dT} = \frac{\Delta H_v}{T \Delta v} \quad (1-213)$$

where Δv is the difference in the molar volumes of the two phases. Therefore, for liquid–vapor equilibrium, Eq. (1-213) becomes

$$\frac{dp}{dT} = \frac{\Delta H_v}{T(v_g - v_l)} \quad (1-214)$$

This is the so-called Clausius–Clapeyron equation for phase equilibrium; it effectively relates the change in vapor pressure of a substance to a very small change in temperature. If the variation of vapor pressure with temperature is known, it is possible to calculate the heat of vaporization from Eq. (1-214). If the temperature is not too near the critical point of the substance, then

$$v_g \gg v_l \quad \text{or} \quad v_g - v_l \approx v_g$$

Equation (1-214) then becomes

$$\frac{dp}{dT} \approx \frac{\Delta H_v}{T v_g} \quad (1-215)$$

Furthermore, in regions well below the critical point, the vapor pressure is relatively small, and the ideal-gas law may be assumed to be applicable, that is, $p v_g = R_u T$ where v_g is the molar volume of the vapor. Thus,

$$\frac{dp}{dT} = \frac{p \Delta H_v}{R_u T^2}$$

Therefore, the Clausius–Clapeyron equation may be written as

$$\frac{d(\ln p)}{dT} = \frac{\Delta H_v}{R_u T^2} \quad (1-216)$$

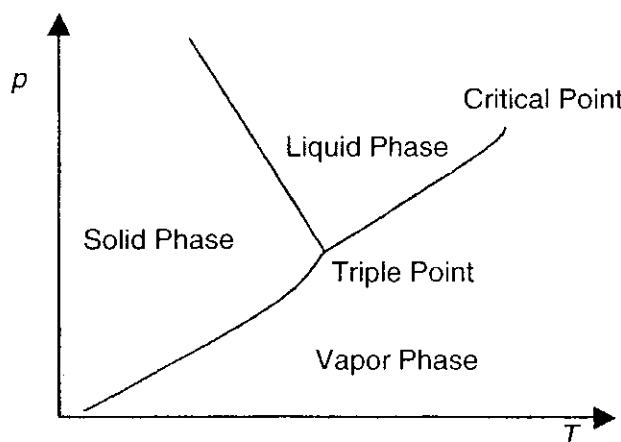


Figure 1.16 Phase diagram in terms of pressure and temperature, showing the abrupt change in slope at the triple point from solid–vapor interface to liquid–vapor interface.

If $\Delta\mathcal{H}_v$ is a constant, after integration, the algebraic form of the Clausius–Clapeyron equation is

$$\boxed{\ln \frac{p_2}{p_1} \approx -\frac{\Delta\mathcal{H}_v}{R_u} \left(\frac{1}{T_2} - \frac{1}{T_1} \right)} \quad (1-217)$$

This equation implies that the vapor pressure p_2 at T_2 can be calculated if the vapor pressure p_1 at T_1 is known. However, it should be noted that when a change of state is involved between T_1 and T_2 , the vapor-pressure-versus-temperature curve may have significant changes in slope, as shown by Fig. 1.16. If $\Delta\mathcal{H}_v$ is a function of T , then we have to integrate it analytically or numerically from Eq. (1-216).

Table 1.9 gives thermodynamic data for phase changes of many substances. These data are compiled from Ref. 16 and should be very useful in the consideration of phase-change computations.

18 CALCULATION OF EQUILIBRIUM COMPOSITIONS WITH NASA'S CEA COMPUTER PROGRAM

In various design and analysis applications to mechanical systems involving reactive mixtures, it is highly beneficial to be able to determine the chemical equilibrium compositions of the reacting media. Mechanical systems include aircraft combustors, rocket motors, gas turbines, shock tubes, heat exchangers, automobile engines, chemical processing equipment, nozzles, gun propulsion systems, and so on.

For more than four decades, Gordon,^{1,21} McBride,^{2,25} Zeleznik,²⁴ and Svehla²⁵ of NASA Lewis Research Center have made great efforts in developing methods and computer programs for calculating complex chemical equilibrium compositions, as well as thermodynamic and transport properties of the mixtures.

Table 1.9 Thermodynamic Data for Phase Changes^{a,b}

Substance	Process	Pressure (Torr)	Temperature (K)	ΔH (kcal/mol)	ΔS (cal/mol-K)	ΔC_p (cal/mol-K)
C ₂ H ₄ O (ethylene oxide)	<i>c</i> → <i>l</i> <i>l</i> → <i>g</i>	760	160.71 293.8	1.236 6.104	7.69 21.50	3.45 -9.7
C ₂ H ₆ O (dimethylether)	<i>c</i> → <i>l</i> <i>l</i> → <i>g</i>		131.66 248.4	1.180 5.141	8.96 20.70	6.8 -10.6
C ₂ H ₅ OH (ethanol)	<i>c</i> → <i>l</i> <i>l</i> → <i>g</i>	760	158.9 351.45	1.200 9.216	7.57 26.22	5.70
CO(NH ₂) ₂ (urea)	<i>c</i> → <i>l</i>		405.8	3.60	8.9	
CH ₃ NO ₂ (nitromethane)	<i>c</i> → <i>l</i> <i>l</i> → <i>g</i>		244.78 374.35	2.319 8.123	9.47	
CH ₃ ONO (methyl nitrite)	<i>l</i> → <i>g</i>	760	255	5.0	19.7	
CH ₃ NO ₃ (methyl nitrate)	<i>l</i> → <i>g</i>	760	339.7	7.8	23.0	
C ₂ H ₅ NO ₂ (nitroethane)	<i>c</i> → <i>l</i> <i>l</i> → <i>g</i>		18 17	293	9.1 31	
C ₂ H ₅ ONO (ethyl nitrite)	<i>l</i> → <i>g</i>	760	290.1	6.64	22.9	
C ₂ H ₅ NO ₃ (ethyl nitrate)	<i>c</i> → <i>l</i> <i>l</i> → <i>g</i>		171 361.9			
C ₂ H ₄ (NO ₃) ₂ (glycol dinitrate)	<i>c</i> → <i>l</i> <i>l</i> → <i>g</i>	19	250.9 378	4.5	18	
C(NO ₂) ₄ (tetrinitromethane)	<i>c</i> → <i>l</i> <i>l</i> → <i>g</i>		286 398.9			
CO	<i>l</i> → <i>g</i>	760	81.7	1.44	17.68	
CO ₂	<i>l</i> → <i>g</i>	760	194.68	6.031	30.98	
Cl ₂	<i>c</i> → <i>l</i> <i>l</i> → <i>g</i>		171.5 238.96	1.530 4.878	8.892 20.4	2.75 -8.76
ClF	<i>l</i> → <i>g</i>	760	172.9	5.34	30.88	
Cl ₂ O ₇	<i>l</i> → <i>g</i>	760	354.7	7.88	22.2	
F ₂	<i>c</i> → <i>l</i> <i>l</i> → <i>g</i>		53.6 85.04	0.122 1.58	6.74 17.7	1.86 4.27
F ₂ O	<i>l</i> → <i>g</i>	760	128.41	2.651	20.7	
H ₂	<i>c</i> → <i>l</i> <i>l</i> → <i>g</i>	54.0 760	13.9 20.29	0.029 0.22	2.0 10.6	1.9
HBr	<i>c</i> → <i>l</i> <i>l</i> → <i>g</i>		186.30 206.44	0.5751 4.210	3.087 20.39	1.64 -7.37
HCl	<i>c,I</i> → <i>l</i> <i>l</i> → <i>g</i>		158.97 188.13	0.4760 3.86	2.994 20.5	2.10 -7.14
HCN	<i>l</i> → <i>g</i>	760	298.86	6.027	20.17	
HF	<i>c</i> → <i>l</i> <i>l</i> → <i>g</i>		190.09 293.1	1.094 1.8	15.756 6.1	2.55 10.9
HI	<i>c</i> → <i>l</i> <i>c</i> → <i>g</i> <i>c</i> → <i>l</i>	0.31 222.37 48	298.16 231.6 293	14.88 2.510 9.43	49.91 10.808 32.17	
HNO ₃	<i>c</i> → <i>l</i> <i>l</i> → <i>g</i>					1.10 10.55

(continued overleaf)

Table 1.9 (continued)

Substance	Process	Pressure (Torr)	Temperature (K)	ΔH (kcal/mol)	ΔS (cal/mol-K)	ΔC_p (cal/mol-K)
H_2O	$c \rightarrow l$	760	273.16	1.436	5.2581	8.911
	$l \rightarrow g$	4.58	273.16	10.767	39.416	-10.184
	$l \rightarrow g$	23.75	298.16	10.514	35.263	9.971
	$l \rightarrow g$	760	373.16	9.716	26.040	10.021
H_2O_2	$c \rightarrow l$		272.73	2.99	9.29	
	$l \rightarrow g$	2.1	298.16	13.01	43.64	
I_2	$c \rightarrow l$		386.9	3.709	9.67	
IF_7	$c \rightarrow l$	760	276.6	7.37	26.64	
N_2	$c, I \rightarrow l$	94	63.16	0.17	2.709	
	$l \rightarrow g$	760	77.36	1.33	17.231	
NH_3	$c \rightarrow l$	45.57	195.42	1.35	6.9133	
	$l \rightarrow g$	760	239.76	5.581	23.277	
N_2H_4	$c \rightarrow l$		274.6	3.01		
	$l \rightarrow g$	764	386.71	9.99	25.9	
NH_4N_3	$c \rightarrow g$	760	407	15.1	37.11	
NH_4NO_3	$c, V \rightarrow$					
	$c, IV \rightarrow$	760	255	0.13	0.511	
	$c, IV \rightarrow$	760	305.3	0.38	1.23	
	c, III					
	c, III					
	c, II	6.32×10^5	336.5	0.20	0.594	
	$c, II \rightarrow c, I$	760	398.4	1.01	2.535	
$N_2H_4 \cdot HNO_2$	$c, I \rightarrow l$	760	442.8	1.3	12.94	
	$c \rightarrow l$		316			
$N_2H_4NO_3$	$c, I \rightarrow l$		343.9			
$N_2H_4 \cdot H_2O$	$c \rightarrow l$		233			
	$l \rightarrow g$		118.5	391.7		
	$c \rightarrow l$		306.3			
	$l \rightarrow g$	22	331			
NO	$c \rightarrow l$	164.4	109.6	0.550	5.016	6.0
	$l \rightarrow g$	760	121.42	3.305	27.113	11.8
N_2O	$c \rightarrow l$	658.9	182.4	1.56	8.5719	4.67
	$l \rightarrow g$	760	184.68	3.951	21.421	
N_2O_3	$c \rightarrow l$		162			
	$l \rightarrow g$	760	275	9.4	34.2	
N_2O_4	$c \rightarrow l$	139.78	263.9	3.501	13.368	6.12
	$l \rightarrow g$	760	294.31	9.111	30.954	
N_2O_5	$c \rightarrow g$	760	305.6	13.6	44.50	
NO_2F	$c \rightarrow l$		107.2			
	$l \rightarrow g$	760	200.8	4.314	21.46	
NO_3F	$c \rightarrow l$		92			
	$l \rightarrow g$	103	193			
O_2	$c, I \rightarrow l$	1.1	54.5	0.11	1.95	1.74
	$l \rightarrow g$	760	90.21	1.63	18.07	-6.00
O_3	$l \rightarrow g$	760	162.65	2.59	15.92	
Br_2	$c \rightarrow l$	760	266.0	2.526	9.48	0.9
	$l \rightarrow g$	214	332.0	7.16	24.6	
C	$c \rightarrow g$	760	4765	28.0		

Table 1.9 (continued)

Substance	Process	Pressure (Torr)	Temperature (K)	ΔH (kcal/mol)	ΔS (cal/mol-K)	ΔC_p (cal/mol-K)
CH_4	$c \rightarrow l$	87.7	90.8	0.225	2.48	
	$l \rightarrow g$	760	111.68	1.96	17.51	
C_2H_2 (ethyne, acetylene)	$c \rightarrow l$	900	191.7	0.9	5	
	$l \rightarrow g$	900	191.7	4.2	22	
C_2H_4 (ethane, ethylene)	$l \rightarrow g$	760	189.2	5.1	27	
	$c \rightarrow l$	0.9	104	0.801	7.702	
C_2H_6 (ethane)	$l \rightarrow g$	760	169.39	3.234	19.10	
	$c \rightarrow l$	0.006	90.4	0.684	7.597	2.2
CHF_3 (trifluoromethane)	$c \rightarrow l$		113			
	$l \rightarrow g$	760	189.0	4.4	2.3	
CH_3NH_2 (methylamine)	$c \rightarrow l$		150.0	1.41	8.16	
	$l \rightarrow g$	760	266.84	6.17	23.1	
$(\text{CH}_3)_2\text{NH}$ (dimethylamine)	$c \rightarrow l$		181.0	1.42	7.85	9.81
	$l \rightarrow g$	760	280.0	6.33	22.6	17.1
$\text{C}_2\text{H}_8\text{N}_2$ (2-dimethyl hydrazine)	$l \rightarrow g$	760	354			
CH_2O (formaldehyde)	$c \rightarrow l$		154.9			
	$l \rightarrow g$	760	253.9	5.85	23.0	
CH_3OH (methanol)	$c, l \rightarrow l$		175.48	0.760	4.32	4.2
	$l \rightarrow g$	760	337.8	8.415	24.95	
CH_4O_2 (methyl hydrogen peroxide)	$l \rightarrow g$	34	298	7.9	26.5	

^aBy permission, compiled and converted from *Selected Values of Chemical Thermodynamic Properties*³⁶ and 79th ed. of *CRC Handbook of Chemistry and Physics*.¹⁶

^b*c* denotes the solid phase or the condensed-phase material.

Many versions of their programs have been adopted broadly for research studies, development work, and chemical equilibrium computer (CEC) programs, including Zeleznik and Gordon's earlier version of 1962, Svehla and McBride's CEC73, Gordon and McBride's CEC76, Gordon, McBride, and Zeleznik's TRAN84 with calculations of transport properties, and the latest version called CEA (Chemical Equilibrium and Application) by McBride and Gordon¹ in 1996 and 2000. More information about the code can be obtained from the following web site: <http://www.lerc.nasa.gov/www/ceaweb/>.

18.1 Assumptions and Capabilities

The CEA program^{1,2} is designed to provide both thermodynamic and transport properties for a wide range of scientific and engineering applications and for a wide range of independent variables. Thermodynamic data for more than 2000 chemical species (including gases, solids, and ions) are provided with the program for a temperature range of 300 to 5000 K. Transport and relaxation data

are provided for many common species; transport data are also provided for interactions between unlike species. In contrast with the thermodynamic data, the temperature range of the transport data is not the same for all interactions.

The range of applicability of the thermodynamic calculations is approximately described by the limits of applicability of the ideal-gas law. The lower limit for temperature in the transport calculations occurs when ternary and higher-order molecular collisions become important. This also defines the upper pressure limit for the transport property calculations. The upper limit for temperature occurs when ionization becomes appreciable. Incipient ionization can be included in the calculations. For increasing ionization, however, higher approximations are needed in the transport calculations. The lower limit is given by the onset of free-molecular-flow regime, which occurs when the mean free path is of the same order of magnitude as the dimensions of the container. Under these conditions, the equations for the transport properties are no longer applicable.

Thermodynamic data contained in the CEA data file is obtained from the JANAF Thermochemical Tables²⁰ and from data generated at NASA Lewis Research Center (now called NASA Glenn Research Center). Standard-state pressure of 1 bar and temperature of 298.15 K are used as the reference conditions for computations. Heats of transition are included in the thermodynamic data, and the program automatically checks for the condensation of species. Thus, without any special instructions, the proper concentrations of gaseous, liquid, and solid phases of all species included in the THERMO library are calculated.

The usual equations for the conservation of mass, momentum, and energy are used along with the ideal-gas assumption. Composition and properties are calculated for equilibrium conditions and, in some situations, for frozen conditions (sometimes called nonreacting). The effects of chemical kinetics—that is, of finite reaction rates—are not included.

The program is capable of calculating several types of problems:

1. Equilibrium compositions for assigned thermodynamic states
2. Theoretical rocket performance
3. Chapman–Jouguet detonations
4. Shock-tube parameter calculations for both incident and reflected shocks

In the first type of problem, it can calculate the equilibrium composition of a mixture for assigned thermodynamic states. The thermodynamic states are assigned by specifying two thermodynamic state functions (code names are given in parentheses):

1. Temperature and pressure (*tp*)
2. Enthalpy and pressure (*hp*)
3. Entropy and pressure (*sp*)
4. Temperature and volume or density (*tv*)
5. Internal energy and volume or density (*uv*)
6. Entropy and volume or density (*sv*)

The *hp* problem provides constant-pressure combustion properties, and the *uv* problem gives constant-volume combustion properties. As mentioned, the ideal-gas law is taken for the equation of state for the mixture. The analysis assumes that interactions between phases are negligible. In the event that condensed species are present, it is assumed that they occupy negligible volume and exert negligible pressure compared with the gaseous species.

18.2 Equations Describing Chemical Equilibrium

Prior to 1958, all equilibrium computations were carried out using the equilibrium constant formulation of the governing equations. In 1958, White, Johnson, and Dantzig²⁶ suggested that equilibrium compositions be calculated by free-energy minimization. Their procedure soon captured the fancy of some of the researchers making thermodynamic calculations, and the world of equilibrium computations was then divided into two camps, the free-energy minimizers and the traditional equilibrium-constant formulators. Most present-day multipurpose chemical-equilibrium computer programs use the free-energy minimization procedure; however, in some special-purpose computer programs, the equilibrium-constant formulation technique is used. The two formulations reduce to the same number of nonlinear iterative equations.

There are several disadvantages of the equilibrium-constant method, which limit the versatility of a multipurpose program. Briefly, these disadvantages are more bookkeeping, numerical difficulties with the use of components, more difficulty in testing for the presence of condensed species, and more difficulties in extending the method to include the effects of nonideal equations of state. Furthermore, with the minimization-of-free-energy method, each species can be treated independently without specifying a set of reactions *a priori*, as is required with equilibrium constants. For these reasons, the free-energy minimization formulation was used in the CEA program. A very brief discussion of the development of the nonlinear iterative equations is presented in the following section. For a more complete thermodynamic and mathematical treatise, the reader is referred to Refs. 1 and 2.

18.2.1 Thermodynamic Equations As discussed earlier, it is assumed that all gases are ideal and that interactions among phases may be neglected. The equation of state for the mixture is

$$Pv = n^* R_u T \quad (1-218)$$

or

$$\frac{P}{\rho} = n^* R_u T \quad (1-218a)$$

where n^* represents the number of moles per unit mass of mixture (kg-mole/kg), and the units for the variables are those of the International System (SI). Equation (1-218) is assumed to be correct even when small amounts of condensed

species (up to several percent by weight) are present. The specific volume v and number of moles n^* refer to the gases only, while the mass in the system is for the entire mixture including condensed-phase species. The word *mixture* is used to designate the burned (reacted) mixture of species at equilibrium, to distinguish it from the mixture of unburned reactants, which is referred to as *total reactants*. The molecular weight M_w of the mixture (including condensed species) is then defined to be

$$M_w = \frac{\sum_{j=1}^N n_j^* M_{w,j}}{\sum_{j=1}^{N_g} n_j^*} = \frac{1}{\sum_{j=1}^{N_g} n_j^*} = \frac{1}{n^*} \quad (1-219)$$

where n^* is the number of kilogram-moles of species j per kilogram of mixture, and $M_{w,j}$ is the molecular weight of species j . Among the N possible species considered, gases are indexed from 1 to N_g and condensed species from $N_g + 1$ to N .

It should be noted that the molecular weight of a multicomponent mixture is conventionally defined as

$$M_{w,conv} \equiv \frac{\sum_{j=1}^N n_j^* M_{w,j}}{\sum_{j=1}^N n_j^*} \quad (1-219a)$$

CEA code gives M_w instead of $M_{w,conv}$ as the output. $M_{w,conv}$ can be calculated from M_w by means of

$$M_{w,conv} = M_w \left(1 - \sum_{j=N_g+1}^N X_j \right) \quad (1-219b)$$

18.2.2 Minimization of Gibbs Free Energy The condition for equilibrium may be stated in terms of any of several thermodynamic functions, for example, the minimization of the Gibbs free energy or Helmholtz free energy, or the maximization of the entropy. If one wishes to use temperature and pressure to characterize a thermodynamic state, the Gibbs free energy is most easily minimized, inasmuch as temperature and pressure are its natural variables. Similarly, the Helmholtz free energy is most easily minimized if the thermodynamic state is characterized by temperature and volume (or density). In the following equations, the nonlinear iterative procedure for minimization of the Gibbs free energy is presented. A parallel development for minimization of the Helmholtz free energy can be found in Ref. 1, if the thermodynamic state is characterized by temperature and volume.

For a mixture of N species, the Gibbs free energy (g) per kilogram of mixture is given by

$$g = \sum_{j=1}^N \mu_j n_j^* \quad (1-220)$$

where the chemical potential per kilogram-mole of species j is defined to be

$$\mu_j = \left[\frac{\partial g}{\partial n_j^*} \right]_{T, P, n_{i \neq j}^*} \quad (1-221)$$

The condition for chemical equilibrium is the minimization of free energy. This minimization is usually subject to certain constraints, such as the following mass-balance constraints:

$$\sum_{j=1}^N a_{ij} n_j^* - b_i^o = 0, \quad i = 1, 2, \dots, l \quad (1-222)$$

or

$$b_i - b_i^o = 0, \quad i = 1, 2, \dots, l \quad (1-222a)$$

where the coefficient a_{ij} is the number of kilogram-atoms of element i per kilogram-mole of species j , b_i^o is the assigned number of kilogram-atoms of element i per kilogram of total reactants (fuel and oxidant), and l is the number of chemical elements. If ions are considered, l is equal to the number of elements plus 1. Comparing Eq. (1-222) with Eq. (1-222a), we have

$$b_i = \sum_{j=1}^N a_{ij} n_j^*, \quad i = 1, \dots, l \quad (1-223)$$

where b_i is the number of kilogram-atoms of element i per kilogram of mixture.

To minimize G , we shall follow the well-known Lagrange method²⁷ developed by the great eighteenth-century mathematician J. L. Lagrange. Let us define

$$\tilde{G} \equiv g + \sum_{i=1}^l \lambda_i (b_i - b_i^o) \quad (1-224)$$

where λ_i are Lagrange multipliers that incorporate the l constraints in Eq. (1-222a). Treating the variations δn_j^* and $\delta \lambda_i$ as independent gives

$$\begin{aligned} \delta g &= \sum_{j=1}^N \mu_j \delta n_j^* \\ \delta \sum_{i=1}^l \lambda_i (b_i - b_i^o) &= \delta \sum_{i=1}^l \lambda_i \left(\sum_{j=1}^N a_{ij} n_j^* - b_i^o \right) = \sum_{j=1}^N \sum_{i=1}^l \lambda_i a_{ij} \delta n_j^* \\ &\quad + \sum_{i=1}^l \left(\sum_{j=1}^N a_{ij} n_j^* \right) \delta \lambda_i - \sum_{i=1}^l b_i^o \delta \lambda_i \end{aligned}$$

$$\delta \sum_{i=1}^l \lambda_i (b_i - b_i^o) = \sum_{j=1}^N \sum_{i=1}^l \lambda_i a_{ij} \delta n_j^* + \sum_{i=1}^l b_i \delta \lambda_i - \sum_{i=1}^l b_i^o \delta \lambda_i$$

$$\delta \tilde{G} = \sum_{j=1}^N \left(\mu_j + \sum_{i=1}^l \lambda_i a_{ij} \right) \delta n_j^* + \sum_{i=1}^l (b_i - b_i^o) \delta \lambda_i$$

Then, the condition for equilibrium becomes

$$\delta \tilde{G} = \sum_{j=1}^N \left(\mu_j + \sum_{i=1}^l \lambda_i a_{ij} \right) \delta n_j^* + \sum_{i=1}^l (b_i - b_i^o) \delta \lambda_i = 0 \quad (1-225)$$

$$\mu_j + \sum_{i=1}^l \lambda_i a_{ij} = 0 \quad j = 1, \dots, N \quad (1-226)$$

and the mass-balance equation (1-222a).

Based on the assumption of an ideal gas, the chemical potential may be written

$$\mu_j = \begin{cases} \mu_j^o + R_u T \ln \left(\frac{n_j^*}{n^*} \right) + R_u T \ln p \text{ (bar)} & (j = 1, \dots, N_g) \\ \mu_j^o & (j = N_g + 1, \dots, N) \end{cases} \quad (1-227)$$

where μ_j^o represents the chemical potential at the standard state for gases with $j = 1$ to N_g and for condensed phases with $j > N_g$. The numerical values of μ_j^o are generally found in JANAF Thermochemical Tables.²⁰ The pressure p in Eq. (1-227) must be in bars. Equations (1-226) and (1-222a) permit the determination of equilibrium compositions for thermodynamic states specified by an assigned temperature T_0 and pressure p_0 .

The equations required to obtain equilibrium composition are not all linear in the composition variables, and therefore an iteration procedure is generally required. Detailed iteration procedures are described in Ref. 1. Briefly speaking, the CEA program follows a widely used steepest-descent Newton-Raphson method to solve for corrections to initial estimates of compositions n_j^* , Lagrange multipliers λ_i , mole number n , and (when required) temperature T . This method involves a Taylor series expansion of the appropriate equations with all terms containing derivatives higher than the first order omitted. The correction variables used are $\Delta \ln n_j^*$ (for $j = 1, \dots, N_g$), Δn_j^* (for $j = N_g + 1, \dots, N$), $\Delta \ln n$, $\pi_i = -(\lambda_i / R_u T)$, and $\Delta \ln T$. As pointed out in Refs. 22 and 1, there is no restriction in starting iteration with an estimate of the Lagrange multipliers equal to zero, inasmuch as they appear linearly in Eq. (1-226).

For chemical systems containing many species, it would be necessary to solve a large number of simultaneous equations. They can be reduced quite simply to a much smaller number by algebraic substitution, eliminating $\Delta \ln n_j^*$

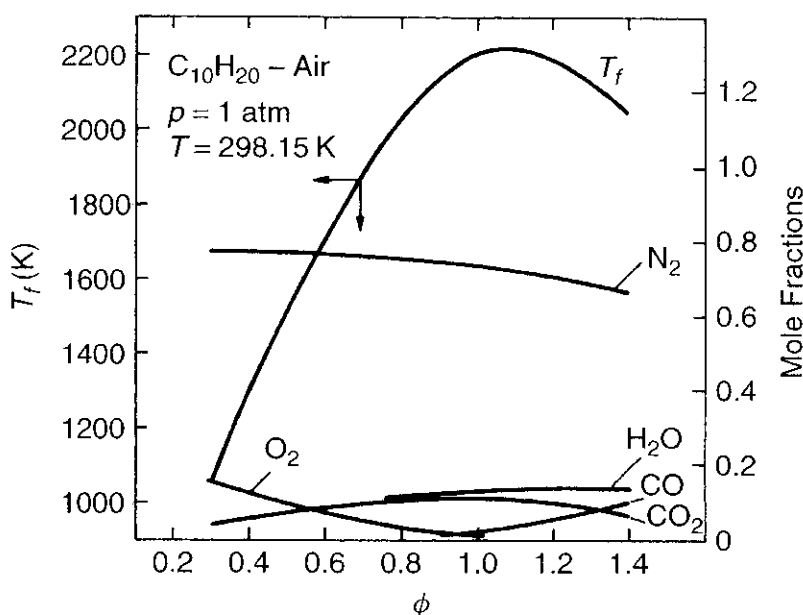


Figure 1.17 Calculated adiabatic flame temperature and equilibrium composition of products from combustion of kerosene in air.

terms for gaseous species. The resulting equations are solved through continuous iteration until the corrections become smaller than the specified tolerance. Convergence of the Newton–Raphson iterative equations with 35 iterations is permitted by the program.¹ For most problems, a typical number of iterations is 8 to 12.

A typical output for the combustion of kerosene ($C_{10}H_{20}$) in air at initial temperature of 298.15 K and at constant pressure of 1 atm is shown in Fig. 1.17. The calculated equilibrium compositions and the flame temperature of the combustion product are plotted against equivalence ratio. As we can see from this figure, the adiabatic flame temperature reaches a peak very close to the stoichiometric condition ($\phi = 1.0$) on the slightly fuel-rich side. This is due to the fact that when the system is slightly under-oxidized, the specific heat of the products is reduced and thus the flame temperature is increased. Dissociation of combustion products also contributes to this shifting effect.

19 OTHER WELL-ESTABLISHED CHEMICAL EQUILIBRIUM CODES

In addition to NASA CEA code, there are number of chemical equilibrium codes developed in the combustion and propulsion fields. These programs include, for example, BLAKE Code,³⁰ developed by Freedman of the U.S. Army Ballistic Research Lab, based on the initial development of the TIGER Code³¹ of the Stanford Research Institute; the PEP Code³² of the U.S. Navy by Cruise; the STANJAN Code³³ of Reynolds of Stanford University; and the Cheetah Code³⁴ of the Lawrence Livermore National Laboratory by Fried, Howard, and Souers. In view of limited space, no extensive discussions are given to these codes. Also, some of these codes have license requirements.

Depending on the user's application, certain codes may have some limitations based on the assumptions made in the analysis. For example, the broadly used NASA CEA code is limited to cases with system pressure below 200 bars, due to its assumption of ideal-gas law. For people interested in gun interior ballistics, the high-pressure effects become significant and the real-gas behavior must be taken into account in the analysis. In this case, the BLAKE code would be more adequate than CEA code, since it considers the real-gas effect. In general, the BLAKE code was developed for gas pressures up to 700 MPa and temperatures up to 4000 K. It uses four different equations of states (EOS), including (1) ideal-gas law; (2) truncated virial EOS; (3) Becker-Kistiakowsky-Wilson (BKW) EOS; and (4) NBS EOS proposed by Powell, Wilmot, Haar, and Klein.³⁵ Among these four different EOS, the truncated virial EOS is best suited for calculations of thermochemical equilibrium under gun environments. BLAKE code contains enthalpies of formation for 349 different ingredients most often found in military propellants. The equilibrium calculations are performed using the method based on equilibrium constants. Similar to CEA code, the BLAKE code can be executed for various combinations of thermodynamic variables, including p , v , T , ρ , e , and s problems.

To demonstrate the differences in the computed results at high pressures, BLAKE and NASA CEA were used by the author to calculate the adiabatic flame temperature and chamber pressure of a closed bomb loaded with solid propellants at various loading densities. (This is not a fair test for CEA, since the code was not designed for extremely high pressures. It is used only as a demonstration to prove a point.) Departure in calculated chamber pressure started at the propellant loading density of 0.14 gm/cm³, and the difference becomes very large (47% lower) at the propellant loading density of 0.6 gm/cm³. The calculated adiabatic flame temperature from CEA code is higher than that of the BLAKE code by about 6.5% at the propellant loading density of 0.1 to 0.4 gm/cm³. In general, one should know how to select the suitable code to perform the specific task in question. For example, for propellant burning in a very high-pressure environment such as a closed bomb or gun chamber, BLAKE code, or other high-pressure application codes should be used.

Recently, a commercial code called Cequel™ has become available for computation of equilibrium products and other propulsion related problems. Cequel™ stands for "Chemical EQUilibrium in excEL", and was developed by Software & Engineering Associates, Inc. It is based on CCET™ (Compressible Chemical Equilibrium and Transport properties) code developed as an extension of the NASA Lewis's Gordon-McBride CEA (Chemical Equilibrium with Applications) code. Cequel™ code considers Lennard-Jones Parameters (LJP) in the equation of state to treat the nonideal gas behavior. The results of the Cequel™ code are written directly in Microsoft Excel. This eliminates the need to cut and paste from external thermodynamics codes' output files into Excel and provides the additional power of allowing the parametric calculations. This allows the user to quickly evaluate many different scenarios as well as to utilize Excel's built-in solvers and optimization routines.

REFERENCES

1. S. Gordon and B. J. McBride, *Computer Program for Calculation of Complex Chemical Equilibrium Compositions, and Applications I. Analysis*, NASA Reference Pub. 1311, Oct. 1994.
2. B. J. McBride, and S. Gordon, *Computer Program for Calculation of Complex Chemical Equilibrium Compositions and Applications, II. Users Manual and Program Description*, NASA Reference Pub. 1311, June 1996.
3. G. J. Van Wylen and R. E. Sonntag, *Fundamentals of Classical Thermodynamics*, John Wiley & Sons, New York, 1973.
4. B. H. Mahan, *Elementary Chemical Thermodynamics*, W. A. Benjamin, New York, 1964.
5. G. N. Lewis and M. Randall, *Thermodynamics*, McGraw-Hill Book Company, New York, 1961.
6. C. E. Mortimer, *Chemistry: A Conceptual Approach*, D. van Nostrand Company, Princeton, NJ, 1971.
7. E. Fermi, *Thermodynamics*, Dover Publications, Inc., New York, 1956.
8. S. R. Turns, *An Introduction to Combustion*, 2nd Edition, McGraw-Hill, Inc., 2000.
9. S. Glasstone, *Thermodynamics for Chemists*, D. van Nostrand Company, Princeton, NJ, 1964.
10. R. A. Strehlow, *Fundamentals of Combustion*, International Textbook Co., Scranton, PA, 1968.
11. S. S. Penner, *Chemistry Problems in Jet Propulsion*, Pergamon Press, New York, 1957.
12. F. A. Williams, *Combustion Theory*, 2nd ed., Benjamin/Cummings Publishing Company, Menlo Park, CA, 1985.
13. I. Glassman, *Combustion*, 2nd ed., Academic Press, New York, 1987.
14. A. M. Kanury, *Introduction to Combustion Phenomena*, Gordon and Breach, New York, September 1975.
15. R. E. Sonntag, C. Borgnakke, and G. J. Van Wylen, *Fundamentals of Thermodynamics*, 5th edition, J. Wiley & Sons, Inc., 1998.
16. D. R. Lide (Editor in Chief), *Handbook of Chemistry and Physics*, 79th ed., CRC Press, Inc., Boca Raton, FL, 1998–1999.
17. Prigogine and R. Defay, *Chemical Thermodynamics*, Longmans, Green & Co., New York, 1954.
18. F. D. Rossini, *Chemical Thermodynamics*, Chapter 16, John Wiley & Sons, New York, 1950.
19. D. B. Spalding, *Combustion and Mass Transfer*, Chapter 6, Pergamon Press, New York, 1979.
20. M. W. Chase, Jr., et al., *JANAF Thermochemical Tables*, 3rd ed., Part I and Part II. Published by American Chemical Society, American Institute of Physics and National Bureau of Standards, 14, 1985.
21. S. Gordon and B. J. McBride, *Thermodynamic Data to 20,000 K for Monatomic Gases*, NASA/TP-1999-208523, June 1999.

22. J. R. Andrews and O. Biblarz, *Temperature Dependence of Gas Properties in Polynomial Form*, Naval Postgraduate School, Report **NPS67-81-001**, January 1981.
23. S. Gordon and B. J. McBride, *Computer Program for Calculation of Complex Chemical Equilibrium Compositions, Rocket Performance, Incident and Reflected Shocks, and Chapman-Jouguet Detonations*, NASA SP-273 Interim Revision **N78-17724**, March 1976.
24. F. J. Zeleznik and S. Gordon, Calculation of Complex Equilibria, *Ind. Eng. Chem.*, **60**(6), 27–57, June 1968.
25. R. A. Svehla and B. J. McBride, *Fortran IV Computer Program for Calculation of Thermodynamic and Transport Properties of Complex Chemical Systems*, NASA **TND-7056**, Jan. 1973.
26. W. B. White, S. M. Johnson, and G. B. Dantzig, *J. Chem. Phys.*, **28**, 751, 1958.
27. A. E. Taylor, *Advanced Calculus*, Chapter 6, Ginn and Co., Lexington, MA, 1955.
28. Sorenson, H. A., *Principles of Thermodynamics*, Holt, Rinehart and Winston, New York, 1961, p. 106.
29. Su, G.-F., Modified Law of Corresponding States for Real Gases, *Ind. and Eng. Chemistry*, **38**, 804, 1946.
30. E. Freedman, *BLAKE—A Thermodynamic Code Based on Tiger: User's Guide and Manual*, Technical Report **ARBRL-TR-02411**, July 1987.
31. M. Cowperthwaite and W. H. Zwisler, *User's Guide for the Tiger Computer Program*, Stanford Research Institute, Publication No. **Z106**, January 1973.
32. D. R. Cruise, *Theoretical Computations of Equilibrium Compositions, Thermodynamic Properties, and Performance Characteristics of Propellant Systems*, Naval Weapons Center Report **NWC TP-6037**, April 1979.
33. W. C. Reynolds, *The Element Potential Method for Chemical Equilibrium Analysis: Implementation in the Interactive Program STANJAN*, Unnumbered Report, Department of Mechanical Engineering, Stanford University, Stanford, CA, 1986.
34. L. E. Fried, W. M. Howard, and P. C. Souers, *Cheetah 2.0 User's Manual*, Report No. **UCRL-MA-117541** Rev. 5, August 1998.
35. E. G. Powell, G. Wilmot, L. Haar, and M. Klein, Equation of State and Thermodynamic Data for Interior Ballistics Calculations, pp. 325–348, *Interior Ballistics of Guns*, edited by H. Krier and M. Summerfield, *Progress in Astronautics and Aeronautics*, 66, 1979.
36. F. D. Rossini et. al., Selected Values of Chemical Thermodynamics, *National Bureau of Standards/Circular 500*, U.S. Government Print Office, Washington, DC, Feb. 1, 1952.

HOMEWORK

1. A mixture of 1 mole of gaseous ethane (C_2H_4) and 3 moles of oxygen at 298 K react in a constant-volume bomb. Assume the combustion products are CO_2 and $\text{H}_2\text{O}_{(g)}$ and there is insignificant amount of dissociation products. Heat is transferred out of the bomb until the products are cooled to 600 K. Determine the amount of heat transferred in cal/g-mole of the fuel.

2. Show that the rate equation of the first law for a control volume (c.v.) can be expressed as

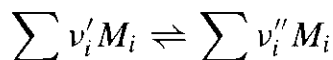
$$\dot{Q}_{\text{c.v.}} + \sum \dot{m}_i \left(h_i + \frac{|\mathbf{v}_i|^2}{2g_c} + z_i \frac{g}{g_c} \right) = \frac{dE_{\text{c.v.}}}{dt} + \sum \dot{m}_e \left(h_e + \frac{|\mathbf{v}_e|^2}{2g_c} + z_e \frac{g}{g_c} \right) + \dot{W}_{\text{c.v.}}$$

where h represents specific enthalpy ($h = u + p/\rho$) and subscripts i and e designate the inlet and exit conditions, respectively. Give the physical meaning of each term.

3. Air flows steadily through an air heater at the rate of 125 g/s. It enters at 290 K and 1.2 atm with a velocity of 15 m/s and leaves at 325 K and 1 atm with a velocity of 18 m/s. There is no shaft work done on or by the air, and the centerlines of the inlet and discharge ducts are in the same horizontal plane. The heating is accomplished with steam coils. What is the rate of heat input to the air in J/s? ($C_{p,\text{air}} = 0.24 \text{ cal/g K}$.)

ANSWER: $\dot{Q}_{\text{in}} = 4401.3 \text{ J/s}$

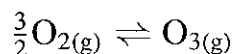
4. Consider a general chemical equilibrium reaction



established in a heterogeneous mixture containing N chemical components. Some of the components have multiple phases in phase equilibrium. Show that

$$\mu_{j(\text{g})} = \mu_{j(\text{l})} = \mu_{j(\text{s})} \quad \text{for any component } j$$

5. Suppose gaseous ozone, $\text{O}_{3(\text{g})}$, is formed from molecular oxygen, $\text{O}_{2(\text{g})}$, by the following reaction:



What is the value of the standard-free-energy change, ΔG° , of this reaction? What is the equilibrium constant of this reaction at 298 K? If the value of K_p is very small, what does that imply?

ANSWER: $\Delta G^\circ = 39.06 \text{ kcal}$, $K_p = 2.261 \times 10^{-29}$

6. A combustible mixture of air and carbon monoxide that is 10% rich [air/fuel = $\frac{100}{110}(\text{air/fuel})_{\text{st}}$] is compressed to a pressure of 8.28 bar and a temperature of 555 K. The mixture is ignited, and combustion occurs adiabatically at constant volume. When the maximum temperature is attained, analysis shows 0.228 moles of CO present for each mole of CO supplied. Show that the

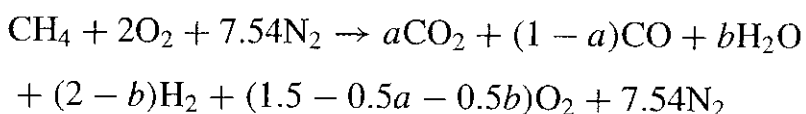
maximum temperature reached is 2950 K. If the pressure at this temperature is now doubled, calculate the amount of CO present.

ANSWER: $n_{\text{CO}} = 0.194$ when the pressure is doubled.

7. Using bond energies, determine the heat of formation of gaseous normal butane (C_4H_{10}).

ANSWER: $\Delta\mathcal{H}_{f,\text{C}_4\text{H}_{10}}^o = -32.94 \text{ kcal/mole}$

8. Methane supplied at 1 atm and 25°C is burned adiabatically in a steady-flow burner with the stoichiometric amount of air supplied at the same conditions. Assume the reaction equation is



Determine the temperature of the products.

ANSWER: $T_f = 2244.3 \text{ K}$

9. Show that the fugacity of a real gas is related to the pressure p and compressibility factor Z by

$$\ln \frac{f}{p} = \int_0^{P_r} (Z - 1) d(\ln P_r)_T$$

where P_r is the reduced pressure ($P_r = p/p_{\text{critical}}$). Discuss the use of this equation. Hint: Integrate Eq. (1-199) from $p = 0$ to a finite pressure.

10. Consider the combustion of kerosene ($\text{C}_{10}\text{H}_{20}$) in air at initial temperature 298.15 K and at constant pressure 1 atm. Use the NASA Lewis computer program (CEA) to carry out the thermochemical calculations for the equilibrium compositions and flame temperature for equivalence ratios of 0.3 to 1.4 ($\Delta\phi = 0.1$ increment). Plot T_f and the mole fractions of CO_2 , H_2O , N_2 , O_2 , CO , NO , OH , O , H , H_2 , and NO_2 versus ϕ ($\Delta\mathcal{H}_{f,\text{C}_{10}\text{H}_{20}}^o = -59 \text{ kcal/mol}$).

ANSWER: For $\phi = 1$, $T_f = 2280 \text{ K}$, $X_{\text{CO}} = 0.01455$, $X_{\text{CO}_2} = 0.1160$, $X_{\text{H}_2\text{O}} = 0.12584$, $X_{\text{N}_2} = 0.72753$, and $X_{\text{O}_2} = 0.00653$.

11. Methane is burned with 80% of stoichiometric air in a steady-flow process at 1 atm. Methane and air are both supplied at 298 K, and the products leave at 1666 K. Assuming that no CH_4 , OH , NO , or free oxygen appears in the products, determine the amount of heat transferred per kilogram of methane.

ANSWER: $Q = -2291 \text{ kcal/(kg of CH}_4)$

12. Consider the combustion of a homogeneous propellant in a closed bomb. The ingredients of this propellant together with their chemical formulas, weight fractions, and heats of formation are listed below:

Ingredients	Chemical Formula	Heats of Formation (kcal/g-mol)	Weight Fraction
NC nitrocellulose (13.25% N)	C ₆ H _{7.329} O ₅ (NO ₂) _{2.671}	-163.81	0.75
NG, nitroglycerin	C ₃ H ₅ O ₃ (NO ₂) ₃	-88.6	0.15
DBP, dibutylphthalate	C ₁₆ H ₂₂ O ₄	-201.4	0.09
DPA, diphenylamine	C ₁₂ NH ₁₁	31.07	0.01

Use the computer program NASA CEA to compute the adiabatic flame temperature, chamber pressure, and product concentrations for loading densities of 0.05, 0.25, and 0.4 g/cm³.

ANSWER: For loading density = 0.25 g/cm³, $T_f = 2773$ K, $p = 2480$ atm, $X_{CO} = 0.47251$, $X_{H_2O} = 0.17751$, $X_{H_2} = 0.17099$, $X_{N_2} = 0.10436$, and $X_{CO_2} = 0.07276$.

13. Consider the two-stream mixing and combustion system shown in the sketch below. Let us assume that both the fuel-rich stream and the oxidizer-rich stream are contaminated by a portion of combustion products and inert diluents. There is a small amount of oxidizer in the fuel stream and vice versa. Sketch the burned and unburned planes of mass fractions of fuel (F), oxidant (O), diluent (D), and combustion products (P) versus mixture fraction f , defined by the following equation.



$$f = \frac{[Y_F - (F/O)_{st} Y_O]_M - [Y_F - (F/O)_{st} Y_O]_A}{[Y_F - (F/O)_{st} Y_O]_F - [Y_F - (F/O)_{st} Y_O]_A}$$

14. The vapor pressure of liquid chlorine, in centimeters of mercury, can be represented by the expression

$$\log_{10} p = -1414.8T^{-1} + 9.91635 - 1.206 \times 10^{-2}T + 1.34 \times 10^{-5}T^2$$

The specific volume of chlorine gas at its boiling point is 269.1 cm³/g and that of the liquid is approximately 0.7 cm³/g. Calculate the heat of vaporization of liquid chlorine in cal/g at its boiling point, 239.05 K.

Note: $\frac{d(\log_{10} p)}{dT} = \frac{1}{2.303} \frac{d(\ln p)}{dT}$

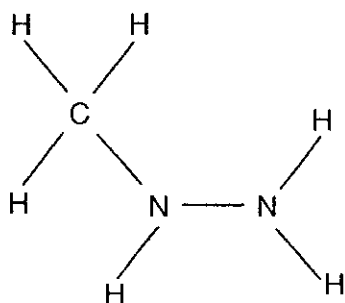
ANSWER: $\Delta H_v = 68.3$ cal/g

15. Imagine that a fuel is burned in a large excess of each of these various oxygen mixtures:

- (a) $0.21\text{O}_2 + 0.79\text{N}_2$
- (b) $0.21\text{O}_2 + 0.79\text{Ar}$
- (c) $0.21\text{O}_2 + 0.79\text{CO}_2$
- (d) pure O_2

Order the mixtures according to the adiabatic flame temperatures that you would expect, by noting the highest first, the next highest second, etc. If you believe all will give the same temperature, state so and explain. The fuel is arbitrary, of course.

16. Calculate the adiabatic flame temperature, T_f , and the equilibrium composition of the decomposition flame of pure liquid hydrazine, $\text{N}_2\text{H}_{4(l)}$. The initial temperature of the pure $\text{N}_2\text{H}_{4(l)}$ is 273 K. Total pressure on the system is 1 atm. Products to be considered are $\text{NH}_{3(g)}$, N_2 , and H_2 .
17. Find the heat of formation of gaseous monomethylhydrazine (MMH) from its bond energies. The molecular structure of MMH is shown below. Its chemical formula is $\text{CH}_3\text{NHNH}_2(\text{g})$.



Note that the heat of formation of $\text{N}_{(g)}$ is 112.97 kcal/mol. The average bond energy of the N–N bond is 60 kcal/mol. The average bond energy for the N–H bond is 88 kcal/mol. Please compare your estimated result with some reported values of heat of formation of MMH as 20.41 kcal/mol, or 22.55 kcal/mol.

PROJECTS

- 1.1 Octane vapor (C_8H_{18}) at 1 atm and 298.15 K is burned adiabatically at constant pressure with 100% excess air at the same conditions. Determine the flame temperature of the products, assuming CO_2 , H_2O , O_2 , and N_2 are produced in the reaction. Verify that the dissociation products CO, H_2 , and NO will not appear in substantial quantities.

1.2 Propane (C_3H_8) gas supplied at 1 atm and 298.15 K is burned adiabatically in a steady-flow burner with air ($O_2 + 3.762N_2$) supplied at the same pressure and temperature. Assume that the air in the combustible mixture is 10% richer (by volume) than the stoichiometric condition. Do the following:

- (a) Write the chemical reaction equation to express the full utilization of fuel and air in the generation of combustion products under the assumption of no product dissociation.
- (b) If the combustion product contains CO_2 , H_2O , CO , H_2 , O_2 , and N_2 , rewrite the chemical reaction equation to reflect the dissociation of CO_2 and water vapor. Also, express the relationships between the moles of product species.
- (c) Calculate the fuel–oxidant mass ratio.
- (d) Calculate the adiabatic flame temperature and the equilibrium composition of case (b).

2

CHEMICAL KINETICS AND REACTION MECHANISMS

Symbol	Description	Dimension
A	Arrhenius factor	$(N/L^3)^{1-m}/t$
A^* or B	Collision-frequency factor	$(N/L^3)^{1-m}/(tT^b)$
k	Specific reaction-rate constant	$(N/L^3)^{1-m}/t$
l	Length	L
N	Total number of species	—
P	Steric factor	—
RR	Reaction rate	$N/L^3 t$
r	Radius	L
z	Collision frequency	$N/L^3 t$
σ	Diameter of a molecule or collision radius	L
μ	Reduced mass	M
v'_i	Stoichiometric coefficient of i th reactant	— or N
v''_i	Stoichiometric coefficients of i th product	— or N

Subscripts

a	Activation
b	Backward
e	Equilibrium
f	Forward
p	Pressure
t	Total

In Chapter 1, a review of chemical thermodynamics is given. It is shown that if we know the initial state of a reactive gas mixture, the final state of this mixture after chemical equilibrium can be determined. However, the chemical equilibrium calculations are not able to answer some of the relevant questions such as "How does the mixture get from the initial state to the final state?" and "How long does it take to complete the reaction?" As we know, some elementary chemical reactions proceed more slowly in comparison with other elementary reactions occurring in a combustion system. These slow reactions are more important to characterize, since they control the rate of the overall reacting system. In general, most chemical reactions occur more rapidly as temperature increases. One objective of this chapter is to discuss the mechanisms and rates of chemical reactions as well as to explain certain observations. Chemical kinetics is the part of chemical science dealing with the quantitative study of the rates of chemical reactions and of the factors (such as temperature, pressure, concentrations of chemical species) upon which they depend.¹ It also deals with the interpretation of the empirical kinetic laws in terms of reaction mechanisms, describing the governing chemical pathways from reactants to products. The subject includes both the experimental study of reaction rates and theoretical models to explain experimental results and to predict the outcome of future experiments.

In terms of the physical state of the reacting chemical substances, chemical reactions can be classified into four different types: (1) gas-phase reactions, (2) liquid-phase reactions, (3) solid-phase reactions, and (4) heterogeneous reactions occurring at the interfaces of two substances of different phases, such as gas–solid interfaces. Most of the effort has been devoted to the first two types of reactions.¹ Reactions at gas–solid interfaces have received some attention. Even though there has been some emphasis in recent years, only a limited amount of work has been conducted on reactions in the solid phase.

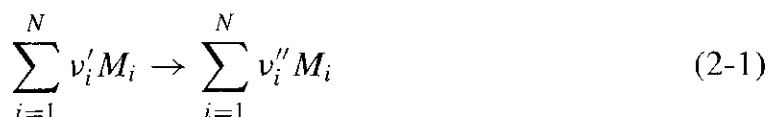
In terms of the speed of reaction, chemical reactions can be divided into two categories: (1) very fast explosive reactions and (2) relatively slow nonexplosive reactions.² The study of explosive chemical reactions involves not only the determination of conditions under which chemical systems undergo very fast reaction, but also the examination of the reaction mechanism.

Although explosions are important, the subject of nonexplosive reactions is also of great interest. For instance, many pollutants are formed in reaction zones of rather steady reactions in various combustion systems. Certain essential features of chemical kinetics, which occur frequently in combustion phenomena, will be discussed in this chapter. For a more detailed understanding of these features, attention is directed to books on chemical kinetics, such as those by Laidler¹ and Benson.³ Names of the first 10 aliphatic hydrocarbons (see Table C.1) and the systematic method for naming these organic compounds (see Table C.2) are given in Appendix C. Families of organic compounds and special functional groups are also given in Table C.3 of Appendix C.

1 RATES OF REACTION AND THEIR FUNCTIONAL DEPENDENCE

All chemical reactions take place at a definite rate, depending on the conditions of the system. Some important conditions⁴ are (1) concentrations of the chemical compounds, (2) temperature, (3) pressure, (4) presence of a catalyst or inhibitor, and (5) radiative effects. The rate of reaction may be expressed in terms of the concentration of any reactant as the rate of decrease of the concentration of that reactant (the rate of consumption of the reactant). It may also be expressed in terms of product concentration as the rate of increase of the product concentration. A conventional unit for reaction rate, R , is (mol/m³-s).

A one-step chemical reaction of arbitrary complexity can be represented by the following stoichiometric equation:



where v'_i are the stoichiometric coefficients of the reactants, v''_i the stoichiometric coefficients of the products, M_i the specification of the molecule of the i th chemical species, and N the total number of compounds involved. If a species represented by M_i does not appear as a reactant, then $v'_i = 0$; if the species does not appear as a product, then $v''_i = 0$.

The meaning of Eq. (2-1) may be illustrated for the reaction between two hydrogen atoms in the presence of a third hydrogen atom to form a hydrogen molecule, with the third hydrogen atom gaining translational energy during the collision process. Symbolically we write



Here $N = 2$, and

$$\begin{aligned} M_1 &= H, & M_2 &= H_2 \\ v'_1 &= 3, & v'_2 &= 0 \\ v''_1 &= 1, & v''_2 &= 1 \end{aligned}$$

Observe that in the present notation, no distinction is made between hydrogen atoms having different energies. Let's now consider the overall chemical reaction between gaseous hydrogen and oxygen to form water vapor. The overall reaction can be expressed by



Here $N = 3$, and

$$\begin{aligned} M_1 &= H, & M_2 &= H_2, & M_3 &= H_2O \\ v'_1 &= 2, & v'_2 &= 1, & v'_3 &= 0 \\ v''_1 &= 0, & v''_2 &= 0, & v''_3 &= 2 \end{aligned}$$

The chemical reaction (2-3) is balanced with the above sets of stoichiometric coefficients. The detailed reaction mechanism between hydrogen and oxygen is discussed in a later section. The global balance is useful but it gives no information about the reaction mechanism. Furthermore, the rate of reaction between hydrogen and oxygen cannot be deduced from this global reaction. More complicated examples in which the values of v'_i and v''_i are not necessarily integers can be given without difficulty. It is clear, however, that Eq. (2-1) is adequate to describe all possible chemical reactions (elementary reactions or global reactions).

The *law of mass action*,⁵ which is confirmed by numerous experimental observations, states that the rate of reaction (RR) of a chemical product species is proportional to the products of the concentrations of the reacting chemical species, each concentration being raised to a power equal to the corresponding stoichiometric coefficient. Thus, the reaction rate is given as

$$\text{RR} = \frac{dC_{\text{product}}}{dt} = \frac{dC_{\text{reactant}}}{dt} = k \prod_{i=1}^N (C_{M_i})^{v'_i} \quad (2-4)$$

The coefficient k is the proportionality constant called the *specific reaction-rate constant*. For a given chemical reaction, k is *independent* of the concentrations C_{M_i} and depends *only* on the temperature. In general, k is expressed as

$$k = AT^b \exp\left(-\frac{E_a}{R_u T}\right) \quad (2-5)$$

where AT^b represents the collision frequency and the exponential term is called the Boltzmann factor, specifying the fraction of collisions that have energy levels greater than the activation energy E_a . The values of A , b , and E_a are based on the nature of the elementary reaction.⁴ For a given chemical reaction, these parameters are neither functions of the concentrations nor functions of temperature. In the following section, we shall discuss the specific reaction rate constant k in more detail, in terms of theoretical chemical kinetics.

1.1 Total Collision Frequency

In the study of molecular collisions, one must consider the effect of the size of the molecules. For simplicity, let us first consider the collision of two identical spherical molecules with molecular diameter σ . When they collide, the distance between their centers must be less than or equal to σ . If the distance between the two centers is greater than σ , the two molecules do not collide. This is illustrated in Figs. 2.1a and 2.1b. In terms of collision cross-sectional area, the larger the value of σ , the greater the probability that two molecules will collide. The collision of the two molecules, each with a diameter of σ , can be considered equivalent to the collision of a molecule with diameter 2σ and another molecule

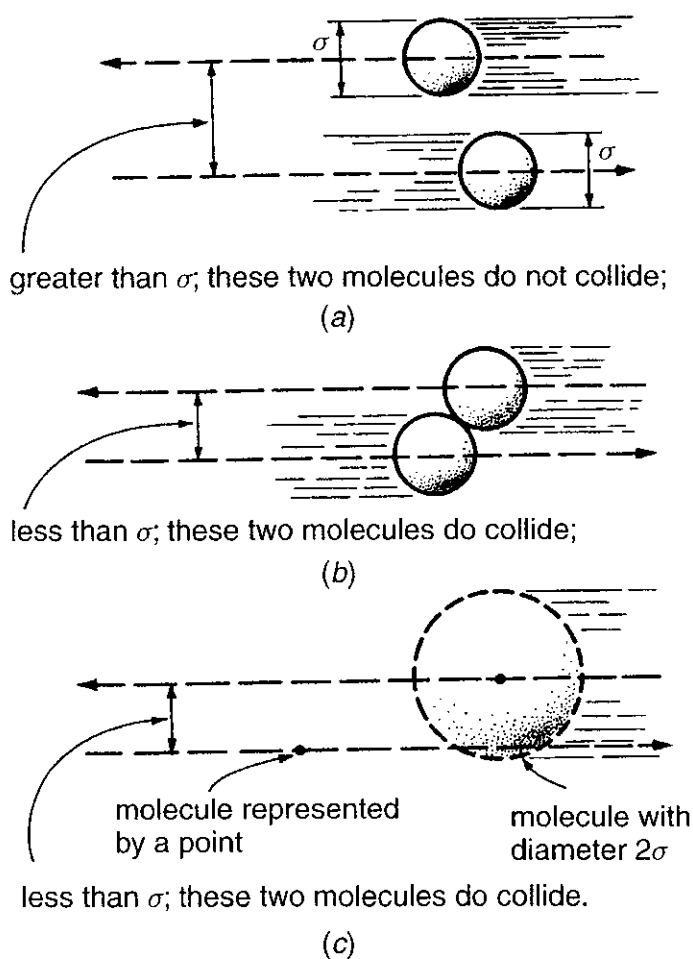


Figure 2.1 Illustration of the distance required between molecules for a collision to occur.

represented as a point (see Fig. 2.1c). In each representation, collision is judged to have occurred if the distance between the two centers of the molecules is less than σ . Calculation of the collision frequency is simpler when based on the second (substituted) representation.

As illustrated in Fig. 2.2, the average collision frequency for pairs of molecules in a gas is approximately equal to the total number of point molecules in the volume swept out in unit time by a molecule of radius σ moving with average velocity. A molecule sweeps through a cylinder of length \bar{u} in 1 s. The average molecular velocity \bar{u} can be calculated from [see Eq. (3-16)]

$$\bar{u} = \left(\frac{8R_u T}{\pi M_w} \right)^{1/2} = 1.455 \times 10^4 \left(\frac{T}{M_w} \right)^{1/2} \text{ cm/s}$$

For a molecule with $\sigma = 3.5 \times 10^{-8}$ cm and molecular weight of 130, the volume of the cylinder through which the molecule sweeps in a gas container at 773 K is

$$V = \pi r^2 l = \pi \alpha^2 \bar{u} \cdot 1 = \pi (3.5 \times 10^{-8})^2 \left[1.455 \times 10^4 \left(\frac{773}{130} \right)^{1/2} \right]$$

$$= 1.365 \times 10^{-10} \text{ cm}^3$$

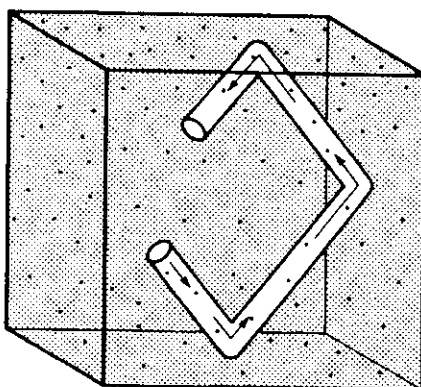


Figure 2.2 Collisions of a moving molecule of radius σ with stationary point molecules. In the volume swept out by the moving molecule, there are 12 point molecules. This is the number of collisions in the time interval in question according to this simple model.

If the concentration of gas molecules is 10^{-6} mole/cm³, there are $(10^{-6}$ mole/cm³)(1.365×10^{-10} cm³)(6.02252×10^{23} molecules/mole) = 8.22×10^7 molecules present in this volume. This is the number of collisions that the molecule in question makes in 1 s, based on the assumption that all molecules are stationary. If motion of all molecules is taken into account, the calculation leads to a $\sqrt{2}$ -fold higher collision frequency. The total frequency of collisions of pairs of molecules in 1 cm³ of gas is obtained by multiplying the collision frequency for one molecule by the number of molecules in 1 cm³ and then dividing by 2, since each collision of two molecules has been counted twice. For molecules with $\sigma = 3.5 \times 10^{-8}$ cm and molecular weight 130 at a concentration of 10^{-6} mole/cm³, the collision frequency per cm³ at 773 K is therefore

$$\begin{aligned} \text{collision frequency} &= \left(\frac{1}{2} \sqrt{2} \times 8.22 \times 10^7 \text{ collisions/molecules} \cdot \text{s} \right) \\ &\quad \times (10^{-6} \text{ mole/cm}^3) (6.02252 \times 10^{23} \text{ molecules/mole}) \\ &= 3.50 \times 10^{25} \text{ collision/(cm}^3 \cdot \text{s)} \end{aligned}$$

If the molecules react upon every collision, the collision frequency will be equal to the reaction rate. In a more familiar dimension, the rate is

$$\frac{3.50 \times 10^{25}}{6.02252 \times 10^{23}} = 58.1 \text{ mole/cm}^3 \cdot \text{s}$$

This is certainly a very high value. This corresponds to the instantaneous rate if reaction occurs at each collision. However, not all the collisions will have sufficient energy for reactions to occur, as will be explained later with the discussion of activation energy.

In the calculation of the total number of collisions of two molecules in 1 cm³ in 1 s, the concentration of the gas appears twice as a factor: the first time in the evaluation of the number of stationary point molecules, the second time in

the calculation of the overall collision frequency. The frequency of collisions of two gaseous molecules of the same kind is therefore proportional to the square of the concentration of the gas, that is

$$\text{Collision frequency, } Z \propto C_A^2$$

A reexamination of the derivation indicates that the collision frequency of two different kinds of gas molecules (B and C) is proportional to the product of the concentrations of the two gases:

$$\text{Collision frequency } Z \propto C_B C_C$$

We therefore conclude that a second-order rate law will be associated with a gas-phase reaction whose mechanism is bimolecular collisions. Notice the use of the terms *second-order* and *bimolecular*. The two are not synonymous. The reaction order pertains to the number of concentration factors in the experimentally established rate law; the molecularity pertains to the number of species taking part in a postulated reaction step. Although it may seem that reaction order and molecularity must be uniquely associated, later discussion will show that this assumption is unwarranted.

Now let's write the mathematical expression for the collision frequency as

$$Z = \sigma_{BC}^2 \left(\frac{8\pi KT}{\mu} \right)^{1/2} C_B C_C \quad (2-6)$$

where K is the Boltzmann's constant (see Appendix B for its value), μ is the reduced mass of molecules B and C [$\mu \equiv m_B m_C / (m_B + m_C)$], σ_{BC} is the collision radius of species B and C , and m_B and m_C are the molecular masses.

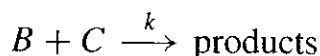
1.2 Equation of Arrhenius

The Swedish chemist and physicist Svante Arrhenius (1859–1927) stated that only those molecules that possess energy greater than a certain amount E_a will react,² and these high-energy, active molecules lead to products. Since Arrhenius was also the first scientist (1889) to introduce the Boltzmann factor $\exp(-E_a/R_u T)$ to calculate chemical reaction rates, the equation

$$k = A \exp\left(-\frac{E_a}{R_u T}\right) \quad (2-7)$$

is called the Arrhenius law; here A is assumed to include the effect of the collision terms, the steric factor associated with the orientation of the colliding molecules, and the mild temperature dependence of the preexponential factor. The preexponential parameter A corresponds to the product of AT^b in Eq. (2-5), where the exponent b lies between 0 and 1.

For a bimolecular reaction, the reaction occurs in a collision only if the relative translational energy along the line of the centers of the two molecules at the moment of impact is in excess of E_a . For the second-order reaction



the rate law is given by

$$\frac{dC_B}{dt} = -kC_B C_C = -AC_B C_C \exp\left(-\frac{E_a}{R_u T}\right) \quad (2-8)$$

According to Arrhenius,

$$\frac{dC_B}{dt} = -Z_{BC} \underline{P} \exp\left(-\frac{E_a}{R_u T}\right) \quad (2-9)$$

where T is the absolute temperature, Z_{BC} is the total collision frequency between B and C molecules, and \underline{P} is called the steric factor. The steric factor depends on the orientation of the colliding molecules. Its value is less than unity if some special orientation of colliding molecules is required (in addition to the necessary activation energy) for the reaction to occur. The meaning of the steric factor can be illustrated by considering the collision of two hydrogen iodide molecules. If the orientation of the colliding molecules is that shown in Fig. 2.3a, hydrogen and iodine molecules can be formed; if, however, the orientation is that shown in Fig. 2.3b, the colliding molecules will simply bounce off each other.

The numerical value of the steric factor for hydrogen iodide reaction is found to be approximately 0.2. For more complex molecules, the steric factor may be on the order of 0.01.

Comparing Eqs. (2-8) and (2-9) gives

$$AC_B C_C = Z_{BC} \underline{P}$$

Solving for A and substituting the value for Z_{BC} from Eq. (2-6) leads to

$$A = \sigma_{BC}^2 \left(\frac{8\pi K T}{\mu} \right)^{1/2} \underline{P} \quad (2-10)$$

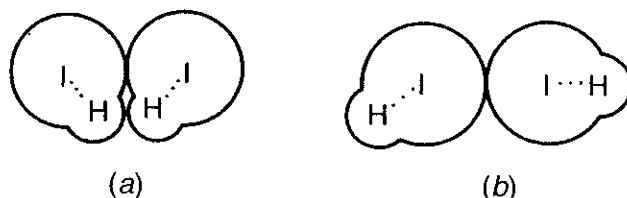


Figure 2.3 Two possible orientations for the collision of two HI molecules.

Theoretical treatment indicates that the activation energy E_a obtained from the use of Eq. (2-7) applied to reactions of other orders has significance analogous to that already indicated for bimolecular reactions; hence Eq. (2-7) can be applied to reactions of all orders.

It should be mentioned that the specific rates of many reactions follow the Arrhenius law. For these reactions, the kinetic data plotted on a graph of $\ln k$ versus T^{-1} follow a straight line. Figure 2.4 shows that in a given chemical reaction, the specific reaction rate constant k is independent of the concentrations C_{M_i} and depends only on temperature. The equation for $\ln k$, as shown in Fig. 2.4, can be derived from the natural logarithm of the Arrhenius equation (2-7), which gives

$$\ln k = \ln A - \frac{E_a}{R_u T} \quad (2-11)$$

It is important to note that the specific reaction rate constant depends on both temperature and temperature range. The Arrhenius equation generally cannot describe the combustion process over a wide temperature range. For example, a set of reactions that matches with test data at low temperatures may provide erroneous results at high temperature. There, however, another set of reactions may match the experimental results well. This is illustrated in Fig. 2.5. Caution must therefore be exercised in extrapolating the specific reaction rate to broader temperature ranges.

Although many reactions follow the Arrhenius law, there are two classes of reactions for which Eq. (2-7) does not hold. These include the following:

- Low-activation-energy free-radical reactions.* In these reactions, temperature dependence in the preexponential term assumes greater importance, and the so-called absolute theory of reaction appears to provide better correlation of kinetic data with temperature.⁵ For further information, see Benson.³
- Radical recombination.* When simple radicals recombine to form a single product, energy must be removed from the product upon its formation in

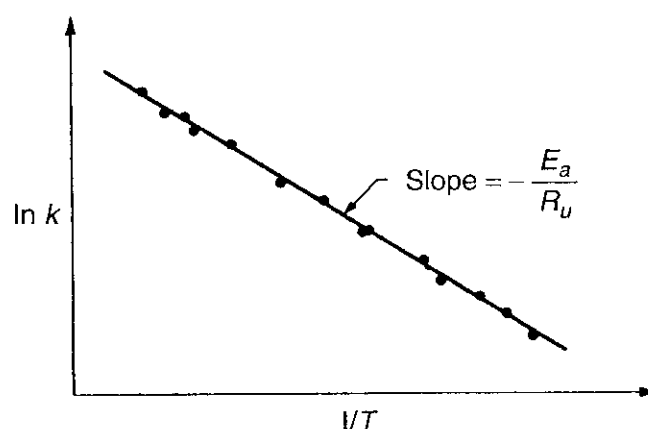


Figure 2.4 Graph showing temperature dependence of the specific reaction rate constant k .

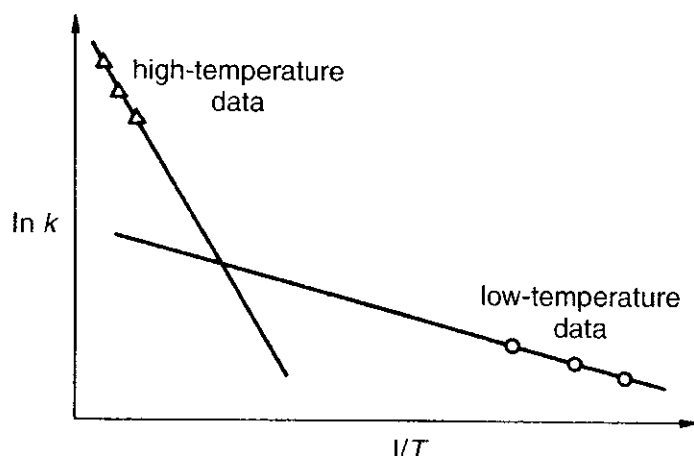


Figure 2.5 Plot illustrating that the specific reaction rate is dependent upon the temperature range as well as temperature.

order to stabilize it. A third body is necessary to remove this energy. The pressure dependence of third-body recombination reactions can be quite pronounced. Hence, the specific reaction rate does not follow Eq. (2-7).

We shall always use k to denote a specific reaction-rate constant and shall employ frequently the subscript f to identify a forward reaction, that is, a reaction in which the reactants appear on the left side of the equation and the reaction products on the right side.

1.3 Apparent Activation Energy

The theory of absolute reaction rates begins with molecular collisions. Under favorable conditions, the collisions lead to the formation of a transitory chemical species, the *activated complex*. By using the methods of quantum mechanics, it is possible, in principle, to calculate the forces between atoms and molecules. A detailed description of the activated complex will provide insight into the nature of the changes in electronic and nuclear arrangement that characterize the chemical reaction. Consider the reaction between reactants A and B to form the reaction products C and D . The formation of reaction products is preceded by the production of an aggregate, the activated complex, which is designated by the symbol X^\ddagger . Thus,



The energy between two atoms of a diatomic molecule A_2 is a function of the distance between the two atoms. (This function was plotted and discussed in Chapter 1.) When a free atom B is approaching the molecule A_2 , the distance between A and A changes. This is shown in Fig. 2.6. Immediately after the collision of B with A_2 , the activated complex BA_2^\ddagger may be formed. The activated complex has a much higher reactivity than normal atoms, and may separate in such a way as to give either the components BA and A or the initial components B and A_2 .

Initial condition:



As B approaches A_2 the configuration becomes

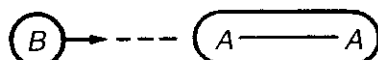


Figure 2.6 The distance between two atoms in the A_2 molecule may change as a free atom B approaches.

A *reaction coordinate* may be associated with the path from reactants to reaction products. Depending on the choice of the reaction coordinate, different amounts of energy will be required for the reaction described by Eq. (2-12). The activated complex is located at the point of highest energy on the most favorable reaction path, and the activation energy E^* per molecule is required to form X^\ddagger . For the most favorable reaction path, the highest point (X^\ddagger) has lower total energy above the reactants (namely, $E_a = N_A E^*$ per mole) than any other reaction path. Figure 2.7 illustrates the activation complex and the required activation energy for exothermic and endothermic reactions in both forward and reverse directions.

An examination of Fig. 2.7 reveals that the potential energy of the reactants, $E(\text{reactants}) > E(\text{product})$ for an exothermic reaction, while $E(\text{product}) > E(\text{reactants})$ for an endothermic reaction. Also note that the activation energy for forward and reverse reactions is not equal; that is, the forward and reverse reactions have different specific reaction rate constants.

In summary, the activation energy is the energy required for the reaction to occur; that is, it is the energy required to move the reactants over the energy barrier in order for reaction to begin. The activation energy is usually recovered by the heat generated from the reaction process. Referring to Fig. 2.7, E_a is the activation energy and ΔH_r is the energy release observed thermodynamically. For exothermic reactions, the values of ΔH_r are negative, as described in Chapter 1.

Chemists have learned that chemical reactions occur only when collisions between molecules have sufficient energy to cause a rearrangement of atoms. We can use an analogy of collisions between cars to understand the true meaning of activation energy. At very low speeds, gentle bumps between two cars may not cause any permanent damage. High-energy collisions can definitely cause auto damage. Similarly, high-energy molecular collisions cause “molecular damages” called chemical reactions. Chemical reactions take place only if the two colliding molecules bring enough energy to the collision so that rearrangement of atoms to form new molecules occurs. The minimum amount of energy is called the *threshold energy* or the *activation energy*, E_a .

1.4 Rates of Reaction

The only observable results of a chemical reaction are net rates of change for the chemical components. It is clear from Eqs. (2-1) and (2-4) that the net rate

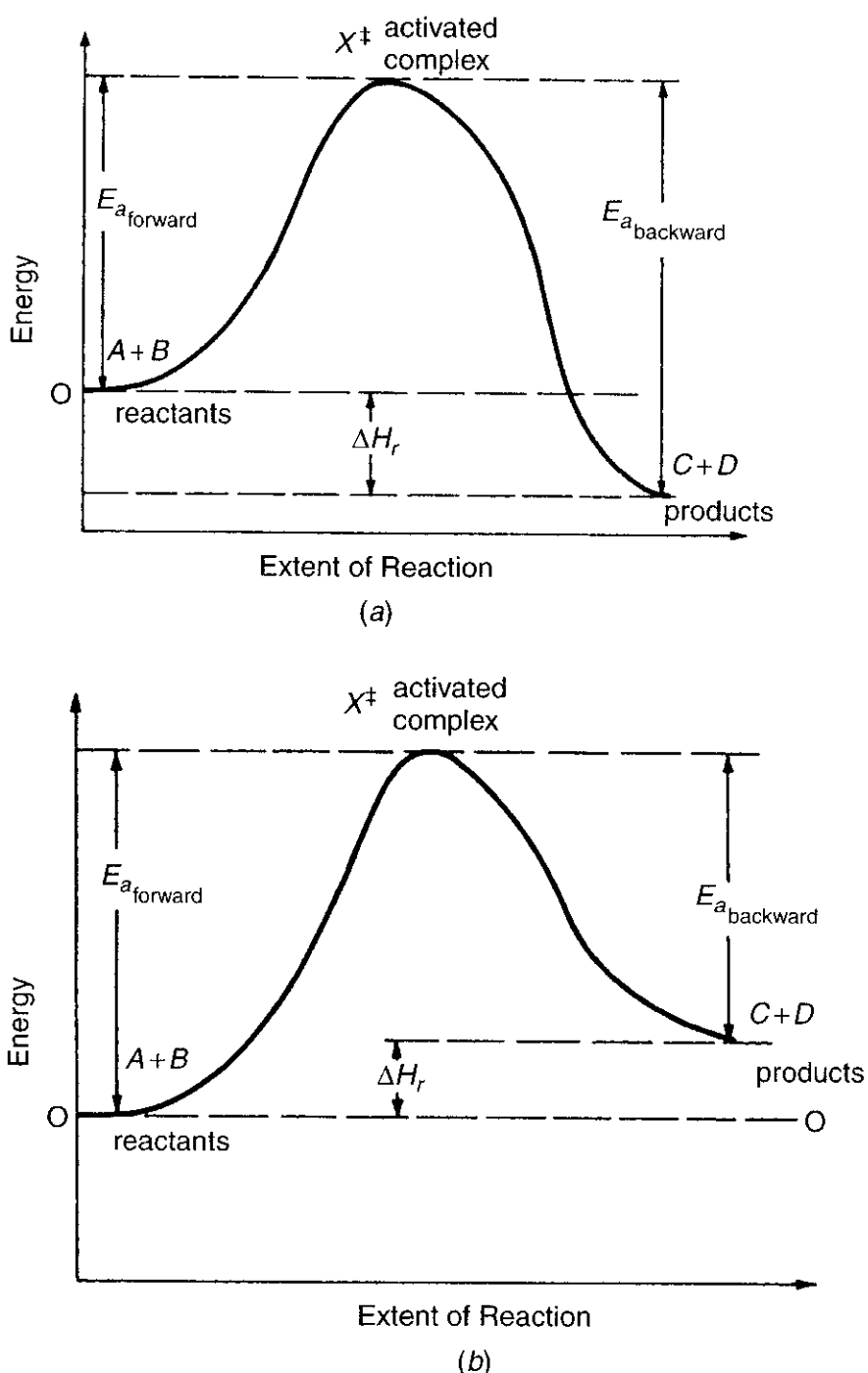


Figure 2.7 Variation of potential energy along reaction coordinate: (a) exothermic reaction, (b) endothermic reaction.

of production of M_i is

$$\frac{dC_{M_i}}{dt} = (\nu''_i - \nu'_i)RR = (\nu''_i - \nu'_i)k_f \prod_{i=1}^N (C_{M_i})^{\nu'_i} \quad (2-13)$$

Since species M_i may appear on both sides of Eq. (2-1) with different values for ν''_i and ν'_i , the difference ($\nu''_i - \nu'_i$) is multiplied by the reaction rate in the above equation.

The result of applying Eq. (2-13) to the reaction (2-2) is

$$\frac{dC_H}{dt} = (1 - 3)k_f C_H^3 = -2 k_f C_H^3$$

and

$$\frac{dC_{H_2}}{dt} = (1 - 0)k_f C_H^3 = k_f C_H^3$$

Therefore,

$$\frac{dC_H}{dt} = -2 \frac{dC_{H_2}}{dt} = -2 k_f C_H^3$$

which states that the rate of depletion of H is twice as fast as the rate of formation of H_2 .

The process represented by Eq. (2-1) is said to be of *order* v'_i with respect to M_i . The *overall order of the reaction* is

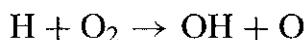
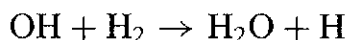
$$m = \sum_{i=1}^N v'_i \quad (2-14)$$

That is, the overall order of the reaction is equal to the sum of the exponents in the reactant concentration terms. Thus, the reaction (2-2) is of third order with respect to H and of zeroth order with respect to H_2 , and it has an overall order of three.

The hypothetical chemical reaction described by Eq. (2-3) represents a third-order process that is of second order with respect to H_2 and of first order with respect to O_2 . Equation (2-3) is an example of a valid overall chemical reaction that does not describe the reaction mechanism correctly. Thus, the overall result for reaction between 2 moles of H_2 and 1 mole of O_2 is the production of 2 moles of H_2O ; however, the conversion of H_2 and O_2 occurs by means of a series of successive, interdependent, elementary chemical-reaction steps to be discussed later. For this reason, the following rate expression obtained by applying Eq. (2-13) to Eq. (2-3) has no physical significance.

$$\frac{dC_{H_2}}{dt} = 2 \frac{dC_{O_2}}{dt} = -\frac{dC_{H_2O}}{dt} = -2 k_f C_{H_2}^2 C_{O_2}$$

The law of mass action, as expressed by Eq. (2-13), may be applied in a meaningful way *only* to elementary reaction steps that describe the correct reaction mechanism. For a number of simple chemical processes, a plausible reaction mechanism has been deduced by chemical kineticists; for some technically important reactions, chemical kineticists provide intelligent conjectures regarding the probable reaction mechanism. Detailed studies⁶ show that the production of H_2O from H_2 and O_2 involves, among others, the elementary reaction steps



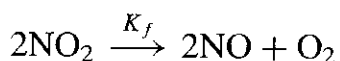
An *elementary reaction* is one that occurs on a molecular level exactly in the way described by the law of mass action given by Eq. (2-13).

The stoichiometric coefficients for elementary reactions give information about the numbers of reacting moles, but not about the weights or volumes, which are changing. If the cubic centimeter is chosen as the unit of volume, it is apparent that the units of the rate constant k_f are

$$\frac{\text{mole}}{\text{cm}^3 \cdot \text{s}} \frac{1}{(\text{mole/cm}^3)^m} = \text{mole}^{1-m} \text{cm}^{3m-3} \text{s}^{-1}$$

Thus, for a first-order reaction, the unit of k_f is a frequency.

Example 2.1. The decomposition of nitrogen dioxide in the absence of inert gas can be written as



What is the order of this reaction? What is the rate law? What is the unit of the specific reaction rate constant?

Solution: The decomposition of nitrogen dioxide is a second-order reaction, as can be seen by examining the exponent in the reaction concentration term in the rate law, given as

$$\frac{dC_{\text{NO}_2}}{dt} = -2k_f C_{\text{NO}_2}^2$$

Therefore, the unit of the specific reaction rate constant can be determined by substituting $m = 2$ into the general unit of k_f , i.e.,

$$\text{mole}^{1-2} \text{cm}^{6-3} \text{s}^{-1} = \text{cm}^3 / (\text{mole} \cdot \text{s}) \quad (2-15)$$

#

Example 2.2. Consider the following for the decomposition of nitrogen dioxide:

- At 592 K, the value of k_f is $498 \text{ cm}^3 / (\text{mole} \cdot \text{s})$. What is the rate of decomposition of nitrogen dioxide at this temperature if the concentration of nitrogen dioxide is 0.0030 mole/liter?
- Values of this rate constant at other temperatures are

T (K)	k_f ($\text{cm}^3/\text{mole} \cdot \text{s}$)
603.5	775
627.0	1810
651.5	4110
656.0	4740

What is the activation energy for this reaction?

Solution:

- a. Converting the units of concentration to mole/cm³, since 1 liter = 1000 ml = 1000 cm³, we have 0.0030 mole/liter = 3 × 10⁻⁶ mole/cm³. From Example 2.1, the rate of decomposition of nitrogen dioxide is given as

$$\frac{dC_{\text{NO}_2}}{dt} = -2k_f C_{\text{NO}_2}^2$$

which in turn gives

$$\frac{dC_{\text{NO}_2}}{dt} = -2 \times 498 \frac{\text{cm}^3}{\text{mole} \cdot \text{s}} \times \left(3 \times 10^{-6} \frac{\text{mole}}{\text{cm}^3} \right)^2 = -8.964 \times 10^{-9} \frac{\text{mole}}{\text{cm}^3 \text{s}}$$

- b. The activation energy for a reaction can be calculated directly from values of rate constants measured at two different temperatures. At T_1 ,

$$\ln k_1 = \ln A - \frac{E_a}{R_u T_1}$$

which was obtained by taking the natural logarithm of both sides of the Arrhenius law as given in Eq. (2-7). At T_2 ,

$$\ln k_2 = \ln A - \frac{E_a}{R_u T_2}$$

Subtracting these two equations yields

$$\ln \frac{k_1}{k_2} = \frac{E_a}{R_u} \left(\frac{1}{T_2} - \frac{1}{T_1} \right)$$

Upon rearranging,

$$E_a = \frac{R_u T_2 T_1}{T_1 - T_2} \ln \frac{k_1}{k_2}$$

Substituting in any two temperature values and the corresponding specific reaction rate constant, we have

$$E_a = \frac{(1.9872 \text{ cal/mole-K})(627 \text{ K})(592 \text{ K})}{(627 - 592) \text{ K}} \ln \frac{1810}{498} = 27.2 \text{ kcal/mole} \quad (2-16)$$

Experimentally, E_a is found by plotting measured values of $\ln k$ against $1/T$ and computing the slope of the best-fit straight line through the data points (slope = $-E_a/R_u$). After E_a is obtained, the factor A in the Arrhenius equation (2-7) may be calculated, using this equation and the measured values of k .

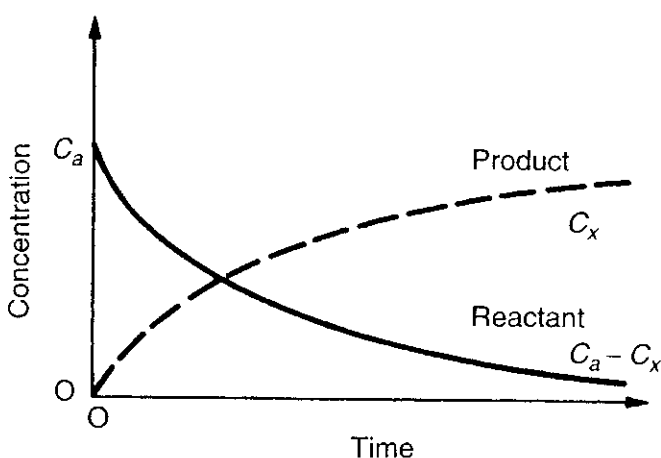


Figure 2.8 Plot of time variation of concentrations of reactant and product in terms of C_x , representing the portion of reactant consumed in chemical reaction.

In the kinetic study of a given reaction, often there is no simple way to measure the rate directly; normally the concentration of a reactant or product is determined at various times. As shown in Fig. 2.8, a smooth curve is obtained if concentration is plotted against time, where C_a is the initial concentration of the reactant. At any given time, the rate of reaction can be determined from the slope $-d(C_a - C_x)/dt$ of the instantaneous reactant concentration ($C_a - C_x$) curve, or by the rate of generation of product species concentration (dC_x/dt). In particular, the initial slope, at $t = 0$, provides the rate of the reaction corresponding to the concentrations with which the experiment was begun. Another method commonly employed involves the use of expressions relating concentration to time for reactions of various orders. Some of the useful expressions will be derived in the next section.

1.5 Methods for Measurement of Gas-Phase Reaction Rates

Measurement of reaction rate constants has always been an important issue for chemists and combustion engineers. However, it is not always easy to measure these reaction rates since some reactions can be very fast (a fraction of a millisecond, for instance) or very slow (several hours, for instance).

In this section, some common methods for measurement of reaction rate constants of gas-phase reactions are discussed. In general, there are three kinds of methods: static methods (e.g., reaction rates deduced from measured temperature/pressure-time records in closed vessels or through direct chemical analysis), dynamic methods (e.g., reaction rates measured in isothermal flow systems), and methods for very fast reactions. The degree of accuracy of measurement often depends on the method chosen. In order to conduct rate measurement of very fast reactions, some special techniques have to be utilized.

According to Eq. (2-13), the *rate of reaction* is the rate of disappearance of a reactant or the rate of appearance of a product. The purpose of all the rate measurement methods is to determine either directly or indirectly the initial state and the final state. By comparing these two states, one is able to determine

rates of reaction. To compare the efficiency of different methods, one can use the half-lives, which is the time needed for the concentration of the reactant to decrease to half of its initial concentration.

1.5.1 Static Methods The most widely used static method for determining the rate of a reaction involving gaseous reactants is to introduce the reactants into a bulb maintained at the desired temperature and to make determinations of the composition after various intervals of time. The measurement of the composition of the gas can be carried out either directly by chemical analysis or indirectly by measurement of pressure of the system. However, the measure of the pressure variation is only possible if the number of moles changes, which is not always the case. The pressure measurements can be made while the reaction is in progress by connecting a pressure-measuring device directly to the reaction vessel.

Stopping the reaction after various intervals of time by rapid cooling of the reaction system using cryogenic fluids can also be used to measure the concentration of the species in the intermediate products. The total pressure of the system can be measured. However, in many cases, the total pressure does not provide very reliable information since many intermediate products can form and disappear. Thus, the results of the static method can contain some serious errors. The classical methods of chemical analysis are seldom used today, because they are much more tedious than gas-chromatographic or mass-spectrometric techniques. Gas-phase reactions involving certain specific reactants or products are sometimes detected by observing the light absorption at a particular wavelength.

For the reaction $M_i \rightarrow \text{Products}$, the rate of change of C_{M_i} is

$$\frac{dC_{M_i}}{dt} = -k_{\text{exp}}(C_{M_i})^m$$

The temporal change of the concentration of species M_i can be calculated by integrating this differential equation, as it will be shown next for some typical cases.

For *first-order reactions* ($m = 1$), by integration of the above equation, we obtain the first-order time behavior

$$\ln \frac{C_{M_i}(t)}{C_{M_i}(0)} = \ln \frac{C_{M_i^t}}{C_{M_i^0}} = -k_{\text{exp}}(t - 0) = -k_{\text{exp}}t$$

where $C_{M_i^0}$ and $C_{M_i^t}$ denote the concentrations of species A at time 0 and t , respectively.

For *second-order reactions* ($m = 2$) the time-dependent behavior of $C_{M_i^t}$ can be expressed by

$$\frac{1}{C_{M_i^t}} - \frac{1}{C_{M_i^0}} = k_{\text{exp}}t$$

and for *third-order reactions* ($m = 3$) the time-dependent behavior of $C_{M'_i}$ can be expressed by

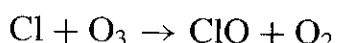
$$\frac{1}{C_{M'_i}^2} - \frac{1}{C_{M_i^0}^2} = 2k_{\text{exp}}t$$

There are several experimental techniques to determine specific rate constant using static methods. These are as follows:

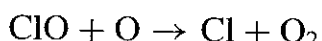
1. Flash Photolysis Resonance Fluorescence Technique (see Kurylo et al.⁶⁻⁹)
2. Relative Rate-Constant Photolysis Technique (see DeMore¹⁰)
3. Laser Photolysis/Laser Induced Fluorescence (LIF) Technique (see Kasner et al.¹¹)

Brief discussions of these static methods are given below before our discussion of dynamic methods and measurements of rapid reaction rates.

1.5.1.1 Flash Photolysis Resonance Fluorescence Technique Let's first define a *photolysis reaction* as a reaction caused by absorption of a photon; this is different from *thermolysis reactions* caused by vigorous intermolecular collisions. For example, Cl atoms can be formed by the dissociation of Cl₂ molecules because of absorption of a photon. A hypothesis under consideration states that the ultraviolet photo-dissociation of "freons" (CF₂Cl₂ and CFCl₃) to produce Cl atoms stimulates the catalytic destruction of ozone (O₃) in the stratosphere. The suggested reactions for the catalytic cycle are



and



Kinetic studies were performed on the first reaction by Kurylo and Braun⁶ with subsequent publications by Kurylo et al. in recent years.⁷⁻⁹ In their experimental setup, a stainless steel cylindrical cell is maintained at a desirable temperature, with an outer tube for circulating fluids between the walls and the cell. The interior of the cell is coated with Teflon to minimize light scattering while maintaining chemical inertness. An absorption cell is used to monitor O₃ concentrations by absorption of radiation from a low-pressure Hg source. A pulsed N₂ flash lamp produces chlorine atoms from ultraviolet flash photolysis in a vacuum environment, and a chlorine atom resonance lamp excites a small fraction of the atoms. Resonantly scattered, the atom signal is detected by a cooled photomultiplier at right angles to both of the lamps. The fluorescence decay, directly proportional to the species concentration, is then recorded on a PC-based multichannel recorder

as a summation of multiflash experiments. The expression for the rate of chlorine atom removal is given by

$$-\frac{dC_{\text{Cl}}}{dt} = k_1 C_{\text{Cl}} C_{\text{O}_3} + k_p C_{\text{Cl}} + k_M C_M C_{\text{Cl}}$$

where k_1 is the rate constant for the first catalytic cycle discussed earlier, k_p is a rate constant associated with both mechanical pumping and diffusion of atoms out of the viewing zone, and k_M is a rate constant for reaction with some impurity species M . When the above removal rate equation is integrated, the following relationship is found:

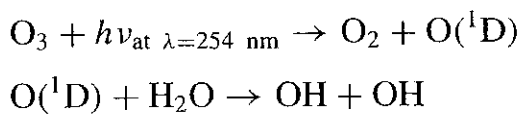
$$\ln \left(\frac{C_{\text{Cl}}(t)}{C_{\text{Cl}}(0)} \right) = (-k_1 C_{\text{O}_3} - k_p - k_M C_M) t$$

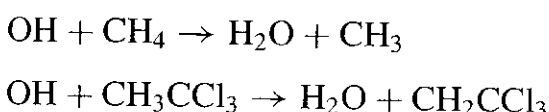
At a fixed total pressure and constant temperature, k_1 can be determined from the slope of the Arrhenius plot associated with the first-order decay rate versus C_{O_3} . By using a nonlinear least-squares fit of data, k_1 can be determined by Arrhenius plot of rate constant data. Kurylo and Braun⁶ obtained the following expression for k_1 in the unit of ($\text{cm}^3 \text{ molecule}^{-1} \text{ s}^{-1}$).

$$k_1 = (2.94 \pm 0.49) \times 10^{-11} \exp \left[\frac{-(298 \pm 39)}{T} \right]$$

They claimed the measurement of rate constants as small as $10^{-16} \text{ cm}^3 \text{ molecule}^{-1} \text{ s}^{-1}$ can be achieved using this method.

1.5.1.2 Relative Rate-Constant Photolysis Technique There is interest in predicting the atmospheric lifetimes of compounds that may be used as substitutes for chlorine-containing compounds (CFCs). The relative atmospheric lifetimes of methane and methyl chloroform are inversely proportional to the ratio of the corresponding rate coefficients. According to DeMore,¹⁰ the relative rate constants can be measured in a low-speed flow, temperature-controlled photochemical reactor and are based on rates of disappearance of the parent compounds as measured by FTIR spectroscopy. The required rate-constant ratios can be obtained from tabulations of absolute reaction rate constants. However, uncertainties in individual rate constants are usually in the range of 10–30%, and the combined error may be substantial.¹⁰ Rate-constant ratios, on the other hand, can usually be determined more accurately through relative rate techniques. The results permit the relative lifetimes of CH_3CCl_3 and CH_4 (for removal by OH in the troposphere) to be estimated within about 7% at relevant temperatures. The major reaction mechanism considered is





The depletion factor (DF) for a given chemical compound can be defined as

$$\text{DF} = \frac{\text{Initial Concentration}}{\text{Final Concentration}}$$

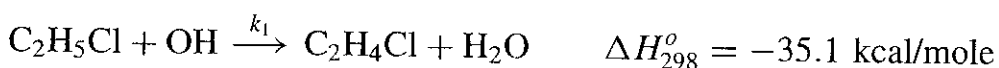
It can be determined that the reaction losses are due almost entirely to OH, and the desired rate-constant ratio can thus be estimated from

$$\frac{k(\text{CH}_3\text{CCl}_3)}{k(\text{CH}_4)} = \frac{\ln \text{DF}(\text{CH}_3\text{CCl}_3)}{\ln \text{DF}(\text{CH}_4)}$$

A temperature-controlled quartz photochemical cell was used to contain the test sample by photolysis. The concentrations of CH₄ and CH₃CCl₃ are measured by passing the effluent mixture through a small White cell on a Nicolet spectrometer. Tests based on relative flow rates were conducted to verify that the reactant concentrations measured in the White cell were proportional to those in the photolysis cell under all conditions of the experiment. DeMore¹⁰ showed that each reactant is depleted by the OH reaction in a manner similar to that of the atmosphere. The rate-constant ratio is obtained from the following relationship:

$$\frac{k_{\text{react}}}{k_{\text{reference}}} = \frac{\ln \text{DF}_{\text{react}}}{\ln \text{DF}_{\text{reference}}}$$

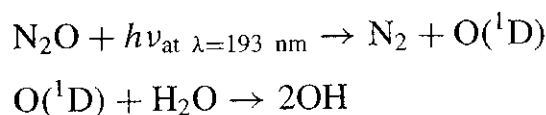
1.5.1.3 Laser Photolysis/Laser Induced Fluorescence Technique Hazardous organic wastes can be disposed through high-temperature incineration methods, which also produce considerable chlorinated hydrocarbons. Hydroxyl radicals (OH) are an important species in hydrocarbon oxidation, and reliable kinetic data for the radical species are necessary for successful modeling of high-temperature systems. Hydrogen atom metathesis rate-constant measurements for the reaction of OH with methyl chloride (CH₃Cl), methylene chloride (CH₂Cl₂), and chloroform (CHCl₃) over an extended temperature range (295–800 K) using a single apparatus were conducted by Kasner et al.¹¹ Similar measurements of the following reaction over a temperature range of 294–789 K at a total pressure of 740 ± 10 Torr were reported.



A resistively heated quartz optical test cell permits data to be acquired from room temperature to 1000 K. The gas transport time, from the onset of heating, was approximately 0.875 s. Mutually perpendicular axes of the quartz cell permitted irradiation of the reaction volume by the photolysis and probe lasers and detection of the laser induced OH fluorescence. Data were taken at a 10-Hz rate coinciding with the firing of the lasers. A linear gas velocity of 4 cm/s

was maintained through the cell to ensure that each photolysis/probe pulse pair encountered a fresh reaction volume, thus reducing the buildup of reaction products. The cell temperature was constantly monitored by a thermocouple placed 5 mm below the reaction zone. A temperature controller was used to maintain the desired cell temperature (within 2 K) during experiments. Measurements from a second retractable thermocouple inserted into the gas flow indicated no more than a ± 2 K temperature variation across the reaction volume.

In Kasner's experiment,¹¹ hydroxyl radicals were generated by the photolysis of nitrous oxide (N_2O) in the presence of water vapor (H_2O). The photolysis laser was an ArF excimer laser, which operated at 193 nm. This N_2O photolysis produced excited O atoms, which quickly reacted with H_2O to generate OH:



To ensure complete conversion of O atoms to OH, the ratio of H_2O to N_2O was typically 15:1. Once created, the relative OH population was monitored by a laser induced fluorescence device. A frequency-doubled, Nd:YAG pumped dye laser was used to produce 2–3-mJ pulses at the wave length of 282.08 nm. This light was used to excite the transition of the OH radical. Hydroxyl fluorescence was collected at 309 nm, corresponding to the 0–0 vibrational transition.

All experiments were performed under pseudo-first-order kinetic conditions with concentration of $\text{C}_2\text{H}_5\text{Cl}$ much greater than that of OH. Over the entire temperature range, OH decay profiles exhibited exponential behavior and were fit by the following nonlinear expression by Kasner¹¹:

$$C_{\text{OH}}(t) = C_{\text{OH}}(0) \exp(-k't) + c$$

where $k' = k \times \text{C}_{\text{C}_2\text{H}_5\text{Cl}} + k_d$ and c is an additional term accounting for background light levels. This expression was fitted by using the Levenberg–Marquardt method, an iterative χ^2 minimization (least squares) technique. The bimolecular rate constant, k , was separated from the diffuse rate constant, k_d , by fitting a weighted least-squares line through the data points on the plot of $\text{C}_2\text{H}_5\text{Cl}$ concentration versus k' . Observed pseudo-first-order OH decay rates, in the absence of $\text{C}_2\text{H}_5\text{Cl}$, were $80 \pm 20 \text{ s}^{-1} \times \text{C}_{\text{C}_2\text{H}_5\text{Cl}}$ at various temperatures.

1.5.2 Dynamic Methods for Reactions in Flow Systems Kinetic rates can be determined from isothermal flow reactors. One of the earliest flow reactors is described by Caldin and Trowse.^{12,1} In their setup, two reactant solutions were placed in separate containers and driven through a special mixing chamber into an observation tube. At various points along the observation tube, the composition of the solution was determined by optical, thermal, or other methods. By taking measurements at various distances, concentration–time curves were obtained, and from the concentration distribution, the rate constants were determined. In general, for flow reactor systems, the reactants (gas or liquid) are supplied at

known flow rates through a mixing section followed by a long reaction channel of known volume maintained at a desirable temperature. Sampling tubes are connected to multiple stations between the upstream and downstream ends of the reactor, allowing samples to be easily collected for chemical analysis. From the volume of the reactor vessel and the rate of flow, it is possible to calculate the mean time spent by the reaction mixture in the reactor. The difference between the compositions at an upstream station and a downstream station represents the amount of reaction that has occurred in the flow residence time between the two stations. The reaction rate is then deduced from the concentration difference divided by the flow residence time. The order of the reaction can be determined by varying the rate of flow through the reactor and the concentrations of the entering gases or solutions. One can also make measurements at a fixed station by varying the mixture flow velocity. By varying flow rates and the volume of the reaction vessel, the residence time could be varied from 0.025 to 25 s. In view of certain minimum time requirements for mixing, flow reactor techniques are not suitable for the study of reactions whose lives are smaller than about 1 ms.

For a plug-flow reactor with homogeneous reacting mixture, the flow in the reactor is treated as one-dimensional with concentration variation only in the x -direction. The spatial variation of the i th species is calculated from

$$\frac{dY_i}{dx} = \frac{\dot{\omega}_i M w_i}{\rho v_x}$$

where v_x is the average velocity of the gas in the reactor, and $\dot{\omega}_i$ is the production rate of i th species in a multiple reaction system with M elementary reactions. From the measured mass fraction gradient and the known flow rate, the production rate $\dot{\omega}_i$ is determined. The overall production rate is related to the forward and backward specific reaction rates according to following equation:

$$\dot{\omega}_i = \sum_{j=1}^M k_{fj} \prod C_{M_i}^{v'_{ji}} - \sum_{j=1}^M k_{bj} \prod C_{M_i}^{v''_{ji}}$$

1.5.3 Several Methods for Measuring Rapid Reaction Rates There are many different methods for measuring rapid reaction rates. These include, for example, stopped-flow spectrophotometric method,^{13,14} relaxation method,^{15,16} shock tube method,^{17–19} flash photolysis method^{20,21} (or kinetic spectroscopy), reaction in molecular beams,^{22–24} multiple photo ionization technique,²⁴ femtochemistry techniques,²⁴ etc.

The *stopped-flow spectrophotometric technique*¹ (developed initially for reactions in solution by Chance¹³) possesses some of the best features of both the static and the flow systems. In the experimental setup, two solutions are forced through multiple opposing jets into a mixing chamber, in which mixing is extremely rapid and accomplished within 10^{-3} s. From the mixing chamber, the solution passes immediately into a reaction vessel. In some designs, the mixing chamber and reaction vessel are one component. The flow is stopped suddenly,

and time-dependent concentration measurements are made by spectrophotometric methods. The main advantages of the stopped-flow technique over continuous-flow methods are that (1) this method is not affected by the rate and character of the flow, as long as the mixing is satisfactory; (2) the progress of the reaction, covering a wide range of rates, can be measured; and (3) the volumes of reagents used are smaller, which is particularly important when it is desired to work with substances that are difficult to obtain in large quantities. The disadvantages of the method are that it is less sensitive than continuous-flow methods, and that there are fewer convenient methods of observation. The stopped-flow technique has also occasionally been used for gas reactions. Johnston¹⁴ contributed to the initial development of spectrophotometric apparatus for gas-phase reaction measurements in stopped-flow reaction vessels.

Most chemical reactions involve either the liberation or absorption of heat; thus, it is useful to measure the temperature rise in the system. When a continuous-flow technique is employed, the products may be passed into a solution medium that quenches the reaction; chemical procedures, such as gas-phase titrations by NO₂ injection, can then be used to determine the extent of reaction. This kind of measurement can be carried out at different residence times, thus allowing the rate constant to be obtained. The method of electron-spin resonance has been applied to reactions occurring in flow systems containing free radicals as intermediate species.

To avoid the difficulties arising from mixing for reactions whose half-lives are smaller than 1 ms, *relaxation methods* have been developed.^{15,16} In this method, the reaction is allowed to compete with a physical process (such as diffusion), the rate of which is known. When the relaxation method is used, the reaction is not started by initially mixing the reactants or raising their temperature. Instead, the reaction is first allowed to go to equilibrium and is then disturbed in some way; its approach to a new equilibrium is then followed using high-speed techniques. From these measurements, the relaxation time of the process can be calculated. Through the relationships between the relaxation time and the rate constants, the reaction rates are determined. In order for the relaxation methods to be effective, the perturbation from initial equilibrium must be accomplished in a time period that is much shorter than the relaxation time. Usually, the perturbation has to take place over a period of 10⁻⁶ or 10⁻⁷ s. Various experimental techniques have been employed.¹⁶ These include the pressure-jump and temperature-jump methods, in which pressure and temperature changes are brought about rapidly. Perturbations (using, for example, high electric fields or ultrasonic vibrations) can produce oscillating temperatures. Various techniques can be used to follow the response of the system to the perturbation and to measure the relaxation time for deducing the reaction rates. This method is particularly suitable for reaction times that are longer than 10⁻⁵ s.

Fast gas-phase reactions can also be investigated by *shock tube methods*.^{17,18} The principle of this method is that the chemical reaction system of gas mixture is contained in a long metal tube, through which a shock wave is allowed to pass. As the shock wave propagates through the gaseous mixture, it raises the mixture

temperature, and reaction occurs in and behind the shock front. The species concentration and mixture temperature are determined by various methods and, in this way, knowledge of the kinetic rates can be obtained. The shock wave is usually produced by the rupture of a thin metal disc separating the high-pressure and low-pressure compartments of the shock tube. The reaction mixture is placed in the low-pressure compartment. Helium gas is usually used in the high-pressure compartment to support the displacement of the traveling shock wave into the low-pressure compartment after the mechanical rupture of the diaphragm. As the shock wave passes, the mixture is not at thermal or chemical equilibrium; the perturbation caused by the shock wave is a much stronger one than is usually employed in relaxation methods.

The problem of following the course of a chemical reaction in and behind a shock wave is a very difficult one. It is required to follow the change in concentration of at least one reactant or product species. This is usually performed by observing its absorption spectrum. Other alternative techniques can also be used. For example, Bradley and Kistiakowsky¹⁹ used a time-of-flight mass spectrometer to follow concentrations of species produced by the shock wave. Even though the time resolution of the time-of-flight mass spectrometer is relatively long (about 50 μ s), the concentration of the oxygen atoms can be measured accurately by this method. This method can also follow the concentrations of several species simultaneously. The shock wave technique has also been applied to the study of vibrational and rotational energy transfers between gaseous molecules.

Another very important method for studying very fast reactions in gas mixtures or liquid solutions is the *flash photolysis method* developed initially by Norrish and coworkers.^{20,21} This method is also called the *kinetic spectroscopy method*. The basic step in the procedure is to produce a light flash of very high intensity and very short duration ($\sim 10^{-6}$ s) in the neighborhood of a reaction vessel. The purpose is to produce atoms, free radicals, and excited species in the reaction system, and these active species will undergo further reactions, which can be followed by spectroscopic means.

Physicists and chemists have also developed *molecular beam scattering* techniques to produce mono-energetic molecular beams.^{22,23} The advantage of reactions in molecular beams is the ability to study chemical reactions under conditions in which there is no Maxwellian distribution of velocity (at a given temperature, the Maxwellian distribution of velocity is a probability function based on the number density and the mass of molecules) so that it is easier to interpret the data for determining reaction rates. By allowing two molecular beams to impinge on each other, it is convenient to study the kinetic rates of bimolecular reactions.

The molecular beam scattering experiment consists of intersecting two beams of molecules (A and B) and detecting the product molecules C in a suitable reactor. While this may be simple, there are a number of constraints that must be met in order for the experiment to be successful.²⁴ The product molecules must not undergo collisions with background gas molecules before they reach the detector. This means that the mean free path in the gas must be greater than

the distance from the scattering center to the detector, which may be on the order of 10 to 30 cm. Therefore, the molecular beam scattering chambers are operated at very low pressures on the order of 10^{-6} torr. Differential pumping is frequently employed to reduce pressure down to 10^{-10} torr or lower. Another constraint is that the beam densities should be very high, typically 10^{11} molecules/cm³, so that a sizable rate of production of C is obtained. Only a small fraction of this production rate is intercepted by the detector. The detection techniques involve making use of laser-excited fluorescence or multiphoton ionization of the product molecules. A few techniques other than laser-induced fluorescence (LIF) and Raman spectroscopy are described briefly in the following paragraphs.

Resonant Multiple Photo Ionization (REMPI) Technique²⁴ The photo ionization technique utilizes one or more pulsed visible- or ultraviolet-light lasers focused between two biased ion collection plates housed inside a sample cell. The two plates have opposite polarities. If the energy absorbed by the product molecules exceeds their ionization threshold, ions will be generated and detected by collection plates. The detected molecules, ionized using the *multiple photo ionization process* (MPI), provide the resulting signal, which represents the number density of molecules in the cell. The ionization of molecules is achieved by first exciting the product molecule from ground electronic state to an intermediate state and then ionizing the molecule from the intermediate state by one photon excitation. This technique is referred to as the $n + 1$ MPI process, in which n photons are used to reach the intermediate state and one additional photon is used to ionize the molecule from that excited state. In general, this process has high sensitivity. The concentration of product species in a reaction is proportional to the product ion signal; the specific rate parameter k can be determined by fitting the half-life of the ion-count growth to its steady-state value. The photo ionization technique is a sensitive laser technique, which is well suited for kinetic measurements. Its main advantage is that the ionization process is highly effective, so that one can ionize and identify transient or stable species at low concentration in the presence of a large excess of other species. This cannot be accomplished using LIF because fluorescence quantum yields are too low.

Reaction Product Imaging Technique²⁴ This technique is a further development of MPI. It utilizes a two-dimensional image of the product angular distribution by capturing the photo ions produced at the scattering center on a position-sensitive detector. Such a detector usually consists of an array of micro-channel plates coupled to a phosphor screen that lights up when struck by an ion; the luminescence is then captured by a charge-coupled-device (CCD) camera, which in turn transmits the data to image analysis software. This technique was originally developed to image the angular distributions of the fragmented species following photo dissociation.

Femtochemistry Technique²⁴ This is a rather different approach represented by the use of very short-pulse (and therefore wide-bandwidth) lasers to probe real-time reaction dynamics. This approach is analogous to the laser photolysis method

but uses laser pulses as short as 10^{-14} s (10 femtoseconds). Using successive delays between initiation (pump) and interrogation (probe) pulses, one can obtain a “stroboscopic” picture of a reaction as it proceeds in time. One example where it has been used is the decomposition of cyclic ketones. The reaction is initiated by absorption of two photons from a femtosecond pulse laser operating at a wavelength of 280–320 nm. This provides enough energy to eliminate CO, leaving the diradical $-\text{CH}_2\text{CH}_2\text{CH}_2\text{CH}_2-$. This diradical is ionized by a delayed femtosecond probe pulse and detected in a time-of-flight mass spectrometer. Buildup and decay occurs on a time scale of several hundred femtoseconds or 0.1 to 1.0 picoseconds. The detected signal is proportional to the product ion signal; k can be determined by fitting the half-life of the ion-count growth to its steady-state value.

In general, in order to study fast kinetic rates, the reactive atoms (such as O, H, N) and radicals (such as OH, CH₃, C₂H₅) have to be produced. Depending on the selected experimental method, generation of highly reactive species is usually achieved by using the following:

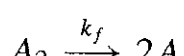
- Microwave discharge to disassociate parent molecules (such as O₂, H₂) by microwave energy input to form (O, H, etc.)
- Flash photolysis to supply light flash of very high intensity for very short duration ($\sim 10^{-6}$ s) to generate atoms, free radicals, and excited species
- Laser photolysis to dissociate molecules by energetic monochromatic waves of laser energy
- Shock-wave heating to thermally heat reactants to high temperatures by the shock wave in the test section of the shock tube

Various techniques have been adopted for chemical species measurements in the characterization of kinetic rates. These include mass spectroscopy, gas chromatography, electron spin resonance, UV/visible absorption spectroscopy, FT-IR spectroscopy, and many other kinds of optical spectroscopy. Table 2.1 summarizes the range of half-life times of chemical species corresponding to different techniques for reaction rate measurements. For very fast reactions, kinetic spectroscopy methods, REMPI, and femtochemistry techniques seem to be the most appropriate.

2 ONE-STEP CHEMICAL REACTIONS OF VARIOUS ORDERS

2.1 First-Order Reactions

The rate law for the first-order reaction, usually associated with rearrangement or dissociation of a molecule



is

$$\frac{dC_A}{dt} = -2k_f C_{A_2} = -2 \frac{dC_{A_2}}{dt} \quad (2-17)$$

Table 2.1 Typical Half-Lives of Chemical Species for Different Techniques (Partially Adapted from Laidler¹ and Hammes²⁵)

Techniques for Reaction Rate Measurements	Typical Half-Lives (s)
Conventional static methods	10^2 to 10^8
Flow reactors	10^{-3} to 10^2
Rapid mixing	10^{-4} to 1
Nuclear magnetic resonance	10^{-6} to 1
Pulse radiolysis	10^{-11} to 1
Flash photolysis	10^{-12} to 1
Relaxation methods	10^{-10} to 1
Pressure jump	10^{-6} to 1
Temperature jump	10^{-8} to 1
Shock tube method	10^{-9} to 10^{-3}
Kinetic spectroscopy methods	10^{-15} to 10^{-10}
Fluorescence decay	10^{-10} to 10^{-6}
Photo-stationary methods	10^{-10} to 1
Electrochemical methods	10^{-8} to 1
Acoustical methods	10^{-11} to 10^{-3}
Electrical pulses and waves	10^{-10} to 10^{-2}
Femtochemistry techniques	10^{-14} to 10^{-10}

After separating the variables and performing integration from time 0 to t , we have

$$-\ln C_{A_2} \Big|_{C_{A_2,0}}^{C_{A_2,t}} = k_f(t - 0)$$

or

$$\ln \left(\frac{C_{A_2,0}}{C_{A_2,t}} \right) = k_f t \quad (2-18)$$

which gives the concentration of A_2 as a function of time. The rate expression given in Eq. (2-17) also applies formally to the process



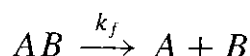
Since $C_C \gg C_A$, the rate expression is given as

$$\frac{dC_A}{dt} = -\frac{dC_D}{dt} = -k_f C_A C_C = k' C_A$$

where k' is a new specific rate constant, which can be defined because the concentration of C is approximately constant (i.e., $C_C = \text{constant}$). The decomposition of A_2 is a unimolecular reaction that obeys first-order kinetics, and the reaction $A + C \rightarrow D$ is a bimolecular reaction that also obeys first-order kinetics. Thus,

all unimolecular reactions are of order one, but not all first-order reactions are unimolecular.

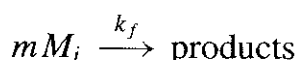
Another example of a first-order reaction is the dissociation of molecule AB



where the rate law is given as

$$\frac{dC_{AB}}{dt} = -k_f C_{AB}$$

One can also consider the following reaction as first order if $m = 1$:



The rate of change of the concentration of species M_i is

$$\frac{dC_{M_i}}{dt} = -k_f C_{M_i}$$

By integration of the above equation, we have

$$\ln \frac{C_{M_i,t}}{C_{M_i,0}} = -k_f t$$

where $C_{M_i,t}$ and $C_{M_i,0}$ denote the concentrations of species M_i at time 0 and t , respectively. Obviously, a plot of the natural log of their ratio with respect to time will yield a straight line with negative slope (see Fig. 2.9). When the time behavior ($C_{M_i,t}$) is measured, the rate constant, k_f , is determined. It is typical for first-order reactions to have this kind of time dependency, which is characteristically different from the second-order reaction as we shall discuss later. From the above reaction rate expression, we can see that when the initial concentration of the first-order reaction is doubled, the reaction rate is also doubled. This relationship is distinctly different from that of second-order reactions.

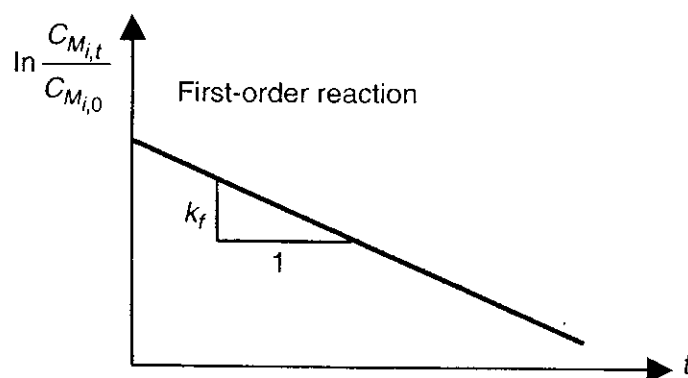


Figure 2.9 Time variation of reactant concentration for first-order reactions.

Example 2.3. Denoting the concentration of the products by C_x and the concentration of the reactants by $C_{A0} - C_x$ (where C_{A0} is the initial reactant concentration), develop an expression for the specific reaction rate constant. Also, develop an expression for C_x (see Fig. 2.8).

Solution: From Eq. (2-18)

$$\ln \left(\frac{C_{A0}}{C_{A0} - C_x} \right) = k_f t$$

Therefore,

$$k_f = \frac{1}{t} \ln \left(\frac{C_{A0}}{C_{A0} - C_x} \right)$$

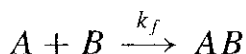
Thus, the concentration of x is

$$C_x = C_{A0}(1 - e^{-k_f t}) \quad (2-19)$$

#

2.2 Second-Order Reactions

Most chemical reactions are bimolecular and proceed as the result of reactions following binary collisions. It is therefore not surprising to see that chemical reactions frequently follow second-order kinetics. If a complex reaction process displays second-order kinetic behavior, then it indicates that the rate-determining (slow) step is a bimolecular process. For the second-order bimolecular reaction

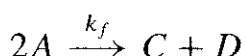


the rate law becomes

$$\frac{dC_A}{dt} = \frac{dC_B}{dt} = -\frac{dC_{AB}}{dt} = -k_f C_A C_B$$

In this reaction, if the concentration of A is equal to the concentration of B , that is, $C_A = C_B$, then the differential equation for this second-order reaction can be solved readily.

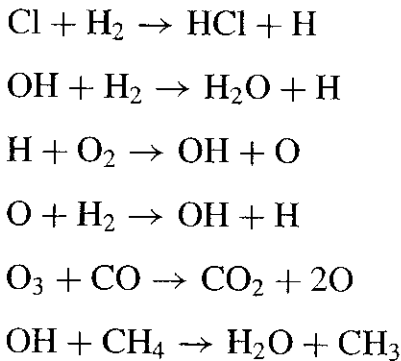
For the following second-order bimolecular reaction



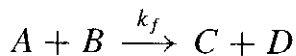
the rate law can be written as

$$\frac{dC_A}{dt} = -2 \frac{dC_c}{dt} = -2 \frac{dC_D}{dt} = -2k_f C_A^2$$

Some representative second-order processes, which have been postulated by Lewis and von Elbe²⁶ as elementary reactions occurring in flames, are given below:



The rate law can also be expressed in terms of the concentration of the consumed portion of the reactant in the reaction. For example, consider the following second-order reaction (sometimes called the atom-transfer reaction):



The concentrations of species *A* and *B* are given as

$$\begin{aligned} C_A &= C_{A_0} - C_x \\ C_B &= C_{B_0} - C_x \end{aligned}$$

where C_{A_0} and C_{B_0} are the initial concentrations and C_x is the portion of *A* and *B* that is consumed in the reaction. The rate law for this reaction is

$$\frac{dC_x}{dt} = k_f(C_{A_0} - C_x)(C_{B_0} - C_x)$$

If $C_{B_0} \neq C_{A_0}$, we can multiply both sides of the equation by

$$\frac{(C_{B_0} - C_{A_0}) dt}{(C_{A_0} - C_x)(C_{B_0} - C_x)}$$

to obtain

$$\frac{(C_{B_0} - C_{A_0}) dC_x}{(C_{A_0} - C_x)(C_{B_0} - C_x)} = k_f(C_{B_0} - C_{A_0}) dt$$

Splitting the denominator of the fraction on the left-hand side of the above equation and integrating yields

$$\ln \left(\frac{C_x - C_{B_0}}{C_x - C_{A_0}} \right) = k_f (C_{B_0} - C_{A_0}) t + \text{constant}$$

To solve for k_f , use the fact that at $t = 0$, $C_x = 0$ from the definition of C_x ; we have

$$\text{constant} = \ln\left(\frac{C_{B_0}}{C_{A_0}}\right)$$

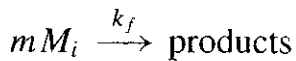
Solving for k_f , the result is

$$k_f = \frac{1}{t(C_{A_0} - C_{B_0})} \ln\left(\frac{C_{B_0}(C_{A_0} - C_x)}{C_{A_0}(C_{B_0} - C_x)}\right) \quad (2-20)$$

If $C_{B_0} = C_{A_0}$, one can show that

$$k_f = \frac{C_x}{tC_{A_0}(C_{A_0} - C_x)}$$

One can also consider the following reaction as second order if $m = 2$:



The rate of change of the concentration of species M_i is

$$\frac{dC_{M_i}}{dt} = -k_f C_{M_i}^2$$

This rate expression implies that doubling the concentration of each reaction partner quadruples the reaction rate. By integration of the above equation, we have

$$\frac{1}{C_{M_{i,t}}} - \frac{1}{C_{M_{i,0}}} = k_f t$$

where $C_{M_{i,t}}$ and $C_{M_{i,0}}$ denote the concentrations of species M_i time t and 0, respectively.

Obviously, a plot of the reciprocal of $C_{M_{i,t}}$ with respect to time will yield a straight line with positive slope. When the time behavior ($C_{M_{i,t}}$) is measured, the rate constant, k_f , is determined. The time dependency of $1/C_{M_{i,t}}$ shown in

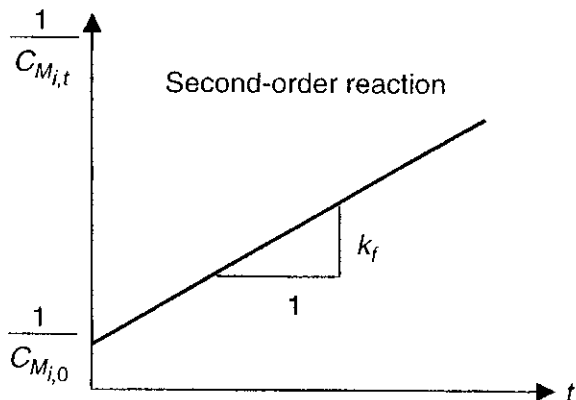


Figure 2.10 Time variation of reactant concentration for second-order reactions.

Fig. 2.10 is typical for second-order reactions, which is characteristically different from the first-order reaction as discussed earlier.

2.3 Third-Order Reactions

An example of a third-order reaction involving three molecules is



Another example representing a recombination reaction is



M is called a third body, which facilitates the recombination reaction of two A atoms to form A_2 during the collision process. After collision, the third body is designated as M^* with a slightly different characteristic from that of M , since the nature of the third body is changed by the energy transfer process. Some molecules may even emit radiation (light) after collisions. The rate law for the above reaction is given as

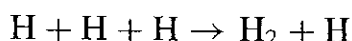
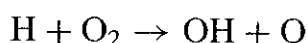
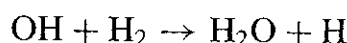
$$\begin{aligned}\frac{dC_{A_2}}{dt} &= k_f C_M C_A^2 = -\frac{1}{2} \frac{dC_A}{dt} \\ \frac{dC_A}{dt} &= -2k_f C_M C_A^2\end{aligned}$$

In case the concentration of M is truly a constant, it can then be combined with k_f to give

$$\frac{dC_{A_2}}{dt} = k' C_A^2$$

where k' can be regarded as a new rate constant. The order of the reaction is then reduced from three to two. If C_M is not truly constant, it is then a function of time, and the order of the reaction is still three.

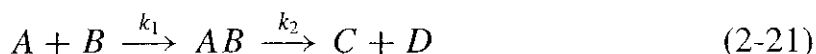
Detailed reaction mechanisms for many chemical reactions can be very complex. It is usually very difficult to measure the concentrations of every significant species. In combustion studies, most reactions we shall deal with are either second or third order. Several second- and third-order reactions in the complicated H_2/O_2 system are given below:



A more detailed reaction mechanism for the H_2/O_2 system is given in a later section.

3 CONSECUTIVE REACTIONS

Another type of complication that can occur in a reaction process is that in which the products of one reaction undergo further reaction to yield other products. A simple example of this type is



As can be seen from this equation, a consecutive reaction is a series reaction in which k_1 and k_2 are the two specific reaction rate constants. Here, the reverse reactions are neglected. The rate laws for the first and second reactions can be determined as follows.

First reaction:

$$\frac{dC_{AB}}{dt} = k_1 C_A C_B = -\frac{dC_A}{dt} = -\frac{dC_B}{dt}$$

Second reaction:

$$\frac{dC_{AB}}{dt} = -k_2 C_{AB} = -\frac{dC_C}{dt} = -\frac{dC_D}{dt}$$

The net rate of change of C_{AB} is obtained by adding the first and second rate laws:

$$\left(\frac{dC_{AB}}{dt}\right)_{\text{net}} = k_1 C_A C_B - k_2 C_{AB} \quad (2-21a)$$

As the reaction proceeds, the concentrations of A and B decrease, and the concentrations of C and D increase. The concentration of AB , therefore, may have a peak at a particular time, as shown in Fig. 2.11.

Example 2.4. Determine an equation for the concentration of the intermediate product B in a simple consecutive reaction in which both reactions are of first

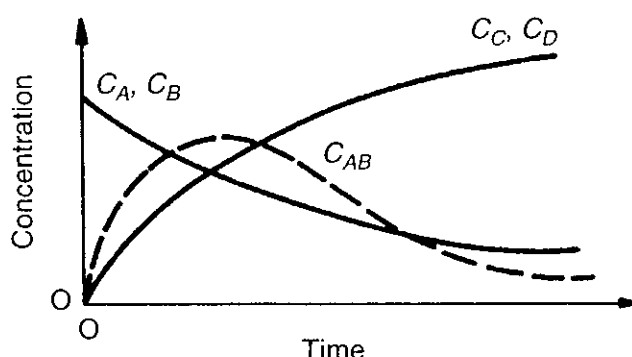


Figure 2.11 Illustration of the possibility of a concentration peak of the intermediate product AB in a consecutive reaction.

order as given by the equation



where k_1 and k_2 are the two specific rate constants.

Solution: The rate of disappearance of A is given by

$$\frac{dC_A}{dt} = -k_1 C_A$$

which integrates to

$$C_A = C_{A_0} e^{-k_1 t} \quad (2-22a)$$

where C_{A_0} is the initial concentration of A . The rate of formation of species C is given by

$$\frac{dC_C}{dt} = k_2 C_B$$

while the net rate of production of B is equal to the rate of its formation from A minus that of its destruction to produce C and D ; i.e.,

$$\frac{dC_B}{dt} = k_1 C_A - k_2 C_B \quad (2-22b)$$

Substituting Eq. (2-22a) into (2-22b) gives

$$\frac{dC_B}{dt} = k_1 C_{A_0} e^{-k_1 t} - k_2 C_B$$

which contains only the variables C_B and t . It integrates to

$$C_B = C_{A_0} \frac{k_1}{k_2 - k_1} (e^{-k_1 t} - e^{-k_2 t}) \quad (2-22c)$$

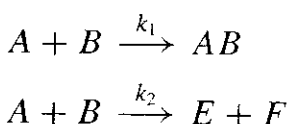
Using the above result, the rate of change of C_C can be readily obtained as

$$C_C = \frac{C_{A_0}}{k_2 - k_1} [k_2(1 - e^{-k_1 t}) - k_1(1 - e^{-k_2 t})] \quad (2-22d)$$

Once C_C is known, C_D is known, since $C_D = C_C$.

4 COMPETITIVE REACTIONS

Competitive reactions occur when two or more sets of combustion products are produced from the same set of reactants. This situation is illustrated by



The rate laws for the first and second reactions can be determined as follows:

First reaction:

$$\frac{dC_A}{dt} = -k_1 C_A C_B$$

Second reaction:

$$\frac{dC_A}{dt} = -k_2 C_A C_B$$

The net rate of disappearance of species A is found by summing the two equations given above:

$$\frac{dC_A}{dt} = -(k_1 + k_2) C_A C_B$$

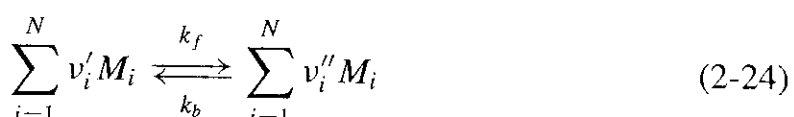
The extrapolation of the rate law to a higher temperature range can lead to incorrect results because the specific reaction rate constants are strongly dependent on temperature. One set of reactions may be dominant at lower temperatures, whereas at higher temperatures other competitive reactions may also need to be considered.

5 OPPOSING REACTIONS

In general, chemical reactions can proceed in both the forward direction (reactants forming products at the rate constant of k_f) and the reverse or backward direction (reaction products reforming the reactants at the rate constant of k_b). Under a thermodynamic equilibrium condition, there is no net change in chemical composition. The rate constants k_f and k_b must therefore be related through the equilibrium constant, K_C , expressed in terms of the ratio of concentrations raised to appropriate powers:

$$K_C = \prod_{i=1}^N C_{M_i}^{(v''_i - v'_i)} \quad (2-23)$$

The general set of opposing chemical reactions is



For a pair of opposing chemical reactions, the rate of change of concentration of i th species (dC_{M_i}/dt) can be expressed as

$$\frac{dC_{M_i}}{dt} = (v''_i - v'_i)k_f \prod_{j=1}^N (C_{M_j})^{v'_j} + (v'_i - v''_i)k_b \prod_{j=1}^N (C_{M_j})^{v''_j} \quad (2-25)$$

At thermodynamic equilibrium

$$\frac{dC_{M_i}}{dt} = 0 \quad \text{and} \quad C_{M_i} = C_{M_{i,e}} \quad (2-26)$$

where $C_{M_{i,e}}$ denotes the thermodynamic equilibrium value for species M_i .

From Eqs. (2-25) and (2-26) it follows that

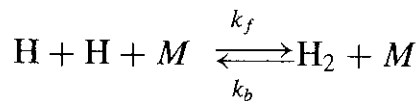
$$\frac{k_f}{k_b} = \prod_{j=1}^N (C_{M_{j,e}})^{v''_j - v'_j} \equiv K_C \quad (2-27)$$

Here K_C represents the usual equilibrium constant defined in terms of concentration chemical species in equilibrium. It is evident that Eq. (2-27) relates the ratio of the kinetic parameters k_f and k_b to the thermodynamic equilibrium constant K_C , which can be calculated quite accurately, for example, by quantum-statistical methods²⁷ from molecular properties. Equation (2-25) can be rewritten in terms of K_C as follows:

$$\frac{dC_{M_i}}{dt} = (v''_i - v'_i)k_f \prod_{j=1}^N (C_{M_j})^{v'_j} \left(1 - \frac{1}{K_C} \prod_{j=1}^N (C_{M_j})^{v''_j - v'_j} \right) \quad (2-28)$$

Knowing K_C and the measured value of dC_{M_i}/dt , it is possible to calculate the forward rate constant from Eq. (2-28).

For a third-body reaction, the third-body concentration always cancels out in the equilibrium constant expression. For example, consider

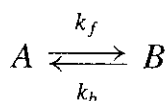


The equilibrium constant for this expression is

$$K_C = \frac{C_{\text{H}_2} C_M}{C_{\text{H}}^2 C_M} = \frac{C_{\text{H}_2}}{C_{\text{H}}^2}$$

5.1 First-Order Reaction Opposed by a First-Order Reaction

Consider the first-order reaction



for which Eq. (2-25) becomes

$$\frac{dC_x}{dt} = k_f(C_{A0} - C_x) - k_b C_x$$

where C_x is the portion of A converted to B . Therefore,

$$C_A = C_{A0} - C_x$$

$$C_B = C_x$$

$$C_{B0} = 0$$

where the subscript 0 denotes initial conditions. Also,

$$\frac{k_f}{k_b} = K_C = \frac{C_{xe}}{C_{A0} - C_{xe}} \quad (2-29)$$

where the subscript e identifies the value of C_x at thermodynamic equilibrium. If $C_x = 0$ at $t = 0$, then substituting k_b of Eq. (2-29) into the ordinary differential equation for C_x and performing integration gives

$$k_f = \frac{C_{xe}}{C_{A0}t} \ln \left(\frac{C_{xe}}{C_{xe} - C_x} \right) \quad (2-30)$$

Hence, if the equilibrium concentration $C_{xe} = C_{Be}$ is known, we can determine both k_f and k_b from experimental measurements of C_x as a function of time. Equation (2-27) can also be written in the form

$$\frac{C_{xe}}{C_{A0}} = \frac{k_f}{k_f + k_b}$$

from which Eq. (2-30) becomes

$$k_f + k_b = \frac{1}{t} \ln \left(\frac{C_{xe}}{C_{xe} - C_x} \right) \quad (2-31)$$

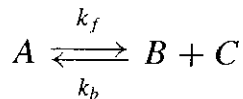
Equation (2-31) is formally identical to the first-order rate law for the forward reaction alone (see Example 2.3):

$$k_f = \frac{1}{t} \ln \left(\frac{C_{A0}}{C_{A0} - C_x} \right) \quad (2-32)$$

Equation (2-32) can be used to study the reaction rate as a function of the initial concentration C_{A0} . Equations (2-31) and (2-32) are written in the form suitable for the interpretation of experimental data for deducing forward and backward reaction rates.

5.2 First-Order Reaction Opposed by a Second-Order Reaction

A first-order reaction opposed by a second-order reaction is represented by the relation



Using Eq. (2-28), the rate of increase of product species B or C becomes

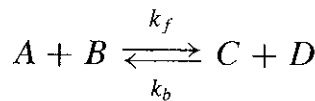
$$\frac{dC_x}{dt} = k_f(C_{A0} - C_x) - k_b C_x^2$$

if $C_{B0} = C_{C0} = 0$. The integration equation is

$$k_f = \frac{C_{xe}}{t(2C_{A0} - C_{xe})} \ln \left(\frac{C_{A0}C_{xe} + C_x(C_{A0} - C_{xe})}{C_{A0}(C_{xe} - C_x)} \right) \quad (2-33)$$

5.3 Second-Order Reaction Opposed by a Second-Order Reaction

For any second-order opposing reactions, represented symbolically by the following reaction



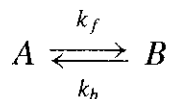
the forward rate constant can be expressed as

$$k_f = \frac{C_{xe}}{2at(a - C_{xe})} \ln \left(\frac{C_x(a - 2C_{xe}) + aC_{xe}}{a(C_{xe} - C_x)} \right) \quad (2-34)$$

where $a = C_{A0} = C_{B0}$ and $C_{C0} = C_{D0} = 0$.

Example 2.5. Develop an equation for the specific reaction rate constant for the backward reaction of a first-order reaction opposed by a first-order reaction, and a first-order reaction opposed by a second-order reaction.

Solution: For the first-order reaction opposed by a first-order reaction,



the rate law can be written as

$$\frac{dC_x}{dt} = k_f(C_{A0} - C_x) - k_b C_x$$

If C_{xe} is the equilibrium concentration of B at equilibrium when the net rate of reaction is zero, we have

$$k_f(C_{A0} - C_{xe}) = k_b C_{xe}$$

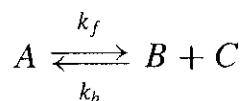
which can be rearranged to

$$k_b = \frac{k_f(C_{A0} - C_{xe})}{C_{xe}}$$

Using Eq. (2-32), we have

$$k_b = \frac{C_{A0} - C_{xe}}{tC_{xe}} \ln\left(\frac{C_{A0}}{C_{A0} - C_x}\right) \quad (2-35)$$

For the first-order reaction opposed by a second-order reaction,



the rate law is

$$\frac{dC_x}{dt} = k_f(C_{A0} - C_x) - k_b C_x^2$$

For the case in which the initial concentrations of B and C are a , while that of A is zero, the rate equation integrates to

$$k_b = \frac{C_{xe}}{t(a^2 - C_{xe}^2)} \ln\left(\frac{C_x(a^2 - C_x C_{xe})}{a^2(C_{xe} - C_x)}\right)$$

where C_{xe} is now the equilibrium concentration of A , and k_b is the specific rate of formation of A .

#

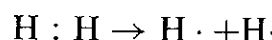
6 CHAIN REACTIONS

Chain reactions are the most common type of chemical reactions. They consist of a series of consecutive, competitive, and opposing reaction steps with different reaction rate constants. These complex chemical reactions occur in numerous combustion processes. Chain reactions can be defined as those reactions in which an intermediate product produced in one step generates a reactive intermediate species in a subsequent step, then that intermediate generates another reactive intermediate, and so on. Processes such as the H_2/O_2 system, which are understood in considerable detail, will be discussed in terms of their reaction mechanisms after the introduction of the basic chemical kinetics background. In the next section, we shall define free radical species and some initiation processes for their generation, since they play an extremely important role in chain reactions.

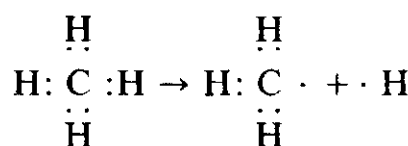
6.1 Free Radicals

In a reaction process, usually the highly reactive species are atoms (such as H , O , N , F , and Cl) or radical species (such as CH_3 , OH , CH , and C_2H_5). These

chemical species, which have unpaired electrons and can react very actively with other molecules, are called *free radicals* or sometimes just *radicals*. In chemical terminology, a free radical is either an atom or a group of atoms, charged or uncharged, that acts as a unit in chemical changes. The hydrogen atom is a free radical, as is illustrated below, where the dots symbolize electrons:



If one hydrogen atom $\text{H}\cdot$ is taken away from CH_4 , two free radicals are formed:



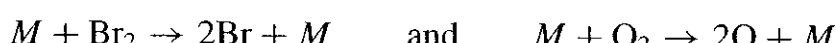
Electromagnetic theory can be used to study the nature of free radicals in the reaction process. After losing its electron, the hydrogen atom becomes a positively charged ion, denoted by H^+ . This is an example of a charged free radical. Other examples are Cl^- , Na^+ , CH_3^+ , etc. (For CH_3^+ , one electron is lost from carbon.) The chlorine atom has an electronic configuration of $1s^2 2s^2 2p^6 3s^2 3p^5$. It takes one electron from another atom to fill the 3p subshell and becomes a chloride ion, Cl^- . For simplicity in notation, we will use either “+” or “-” symbols for positively or negatively charged radicals. However, the dots for electrons will be used only in special circumstances.

Elementary reactions are called chain-initiating reactions when free radicals are produced from these reactions. Similarly, chain-terminating reactions are those in which free radicals are destroyed. Also, with regard to the ratio of the number of free radicals in the product to that in the reactant, elementary reactions are called chain-propagating (or chain-carrying) reactions if the ratio is equal to 1, and chain-branching reactions if the ratio is greater than 1. Some elementary reactions and their denominations are given below:

$M + A_2 \rightarrow 2A + M\}$	Chain-initiation reaction (A_2 has lower dissociation energy than B_2)
$A + B_2 \rightarrow AB + B$	
$B + A_2 \rightarrow AB + A$	
$A + AB \rightarrow A_2 + B$	
$B + AB \rightarrow B_2 + A$	Chain-carrying reactions (propagate very fast)
$M + 2A \rightarrow A_2 + M\}$	
$M + 2B \rightarrow B_2 + M\}$	Chain-terminating reactions

A and B are called chain carriers or free radicals and seldom build up in high concentrations.

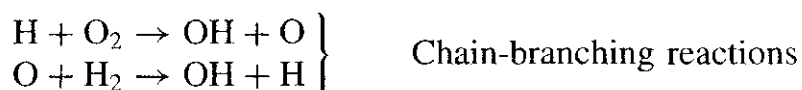
Examples of two chain-initiating reactions are given below:



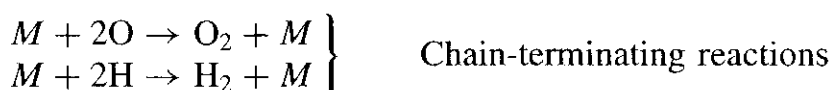
Several chain-carrying reactions (with the same number of radicals on each side) are



Two elementary chain-branching reactions are

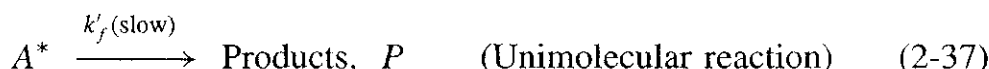
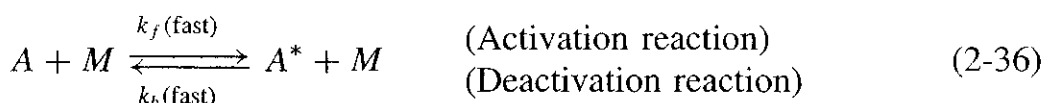


These are called chain-branching reactions, since the number of chain carriers formed is more than the number of chain carriers used up in the reaction. Chain-branching reactions are discussed in more detail in later sections. Two elementary chain-terminating reactions (with higher number of radicals on the reactant side) are



6.2 Lindemann's Theory for First-Order Reaction

According to Lindemann,²⁸ the first-order chain-initiating reaction in the aforementioned set of elementary reactions occurs as the result of the two-step reaction described below. Now we shall use the symbol A to represent the original molecule in the dissociation reaction.



He proposed that reactant molecules receive energy by collisions with collision partner molecule M , and at any given time a small fraction of the molecules have sufficient energy to pass into the reaction products without having to receive any additional energy; such molecules will be referred to as *energized* molecules, A^* . The concentration of A^* depends on the net rate of generation (rate of energization of A minus the rate of deenergization of A^*) by collision, as well as on the rate of destruction of A^* by decomposition into products. If the energized molecules are converted into products at a rate that is small compared to the rate at which they are energized by collision or that at which they are deenergized, a stationary concentration of them may be achieved. In addition, since these energized molecules are in equilibrium with the normal molecules, their concentration is proportional to that of the normal molecules. The rate of reaction is proportional to the concentration of energized molecules and is therefore proportional to the

concentration of normal molecules; the reaction is therefore of first order. That is, the overall process will obey a first-order rate law as long as the formation of A^* according to Eq. (2-36) is sufficiently rapid to maintain an equilibrium concentration of A^* . Since the frequency of binary collisions decreases as the pressure is reduced, it is reasonable to expect that the process symbolized by Eq. (2-36) will cease to be fast at reduced pressures; therefore, a first-order reaction should become of second order at sufficiently low pressures. This change of overall order with pressure has been observed in many first-order reactions.

The differential equations corresponding to the reaction processes of Eqs. (2-36) and (2-37) are

$$\frac{dC_{A^*}}{dt} = k_f C_A C_M - k_b C_{A^*} C_M - k'_f C_{A^*} \quad (2-38)$$

and

$$\frac{dC_A}{dt} = -k_f C_A C_M + k_b C_{A^*} C_M \quad (2-39)$$

These two coupled ODEs can be integrated using a standard Runge–Kutta integration routine. The product concentration can be obtained from

$$\frac{dC_P}{dt} = k'_f C_{A^*} \quad (2-40)$$

Assuming that the concentration of the energized molecule A^* is in a quasi-steady state, the classical steady-state approximation can be utilized, i.e.,

$$\frac{dC_{A^*}}{dt} = 0 \quad (2-41)$$

Then Eq. (2-38) can be expressed by

$$C_{A^*} = \frac{k_f C_A C_M}{k_b C_M + k'_f} \quad (2-38a)$$

which can be combined with Eq. (2-39) to yield the result

$$\frac{dC_A}{dt} = -\frac{k_f k'_f C_A C_M}{k_b C_M + k'_f} \quad (2-39a)$$

This equation can be integrated directly after setting $C_M = C_A$ (since the collision partner in the collision process is molecule A). To understand the effect of pressure on the order of reaction, let us substitute the C_{A^*} expression in Eq. (2-38a) into Eq. (2-40) to obtain

$$\frac{dC_P}{dt} = \frac{k_f k'_f C_A C_M}{k_b C_M + k'_f} \quad (2-42)$$

At very high pressures, the concentration of the collision partner M is high; hence $k_b C_M \gg k'_f$ and equation (2-42) becomes

$$\frac{dC_P}{dt} = \frac{k_f k'_f}{k_b} C_A = k_\infty C_A \quad (2-42a)$$

Thus, the reaction follows the first-order rate law, where k_∞ represents the equivalent specific reaction rate at very high pressures.

At low pressures, the concentration of the collision partner M is very low; hence $k_b C_M \ll k'_f$ and Eq. (2-42) becomes

$$\frac{dC_P}{dt} = k_f C_A C_M \quad (2-42b)$$

Thus, the reaction follows the second-order rate law. Based on the above difference, it is evident that the Lindemann mechanism [shown by Eqs. (2-36) and (2-37)] illustrates that the order of reaction depends on pressure. The rate law of unimolecular reactions can be rewritten from Eq. (2-42) into the following form:

$$\frac{dC_P}{dt} = \frac{k_f k'_f C_M}{k_b C_M + k'_f} C_A \equiv k C_A$$

where $k \equiv \frac{k_f k'_f C_M}{k_b C_M + k'_f} \rightarrow k_\infty \left(\equiv \frac{k_f k'_f}{k_b} \right)$ as $p \rightarrow \infty$

(2-42c)

From the above equation, it is obvious that at very high pressures k approaches k_∞ and at low pressures k approaches the system pressure, since C_M is proportional to p .

Using the above definition of k and k_∞ , we have

$$\frac{k}{k_\infty} \equiv \frac{k_b C_M}{k_b C_M + k'_f} \rightarrow 1 \quad \text{at high pressures} \quad (2-43)$$

Based on this kind of relationship, the theory of unimolecular reaction yields *fall-off* curves. A typical set of *fall-off* curves obtained by Warnatz^{29,30} for the unimolecular reaction $\text{C}_2\text{H}_6 \rightarrow \text{CH}_3 + \text{CH}_3$ is shown in Fig. 2.12, which describes the pressure dependence of k for different temperatures. The Lindemann mechanism is a relatively simplified model. Extensive coverage for the pressure dependence of unimolecular reactions can be found from Robinson and Holbrook's book³¹ or Atkin's book.³²

A steady-state postulation for reaction intermediates is sometimes justified as a first approximation for chemical reactions in flow systems. However, it is necessary to examine the conditions in any given problem in order to at least verify the fact that the steady state is possible. The limitations of the steady-state assumption can be assessed most simply by comparing the complete solution with results derived from the steady-state treatment. Before applying the steady-state approximation to a given combustion problem, considerable ingenuity and

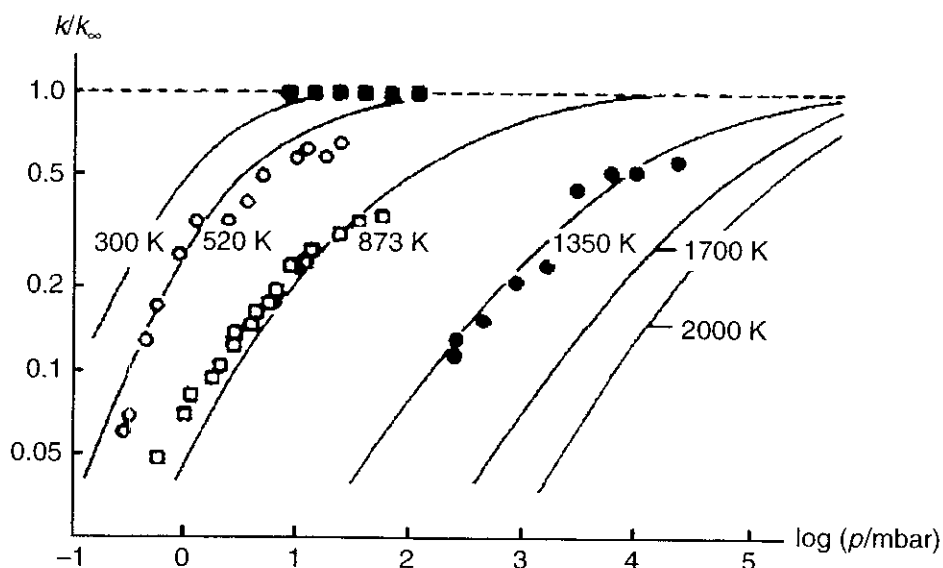
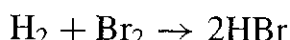


Figure 2.12 Fall-off curves for the unimolecular reaction $\text{C}_2\text{H}_6 \rightarrow \text{CH}_3 + \text{CH}_3$ (Warnatz^{29,30}).

physical insight may be required in order to obtain a rational estimate for the limits of reliability of the treatment.

6.3 Complex Reactions

6.3.1 Hydrogen–Bromine Reaction A classical example of a complex reaction mechanism is provided by the formation of HBr from H_2 and Br_2 . Bromine is a heavy, volatile, corrosive, reddish-brown, nonmetallic liquid element that has a highly irritating vapor with boiling point of 58.78°C . The global (overall) gas-phase reaction for the generation of hydrogen bromide is



The rate of production of HBr does not follow the law of mass action given by Eq. (2-13). Instead, the experimentally determined rate law for the reaction is

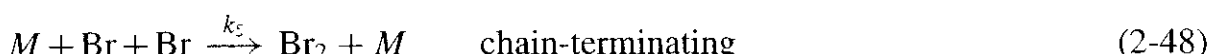
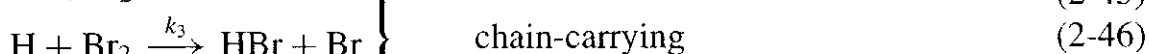
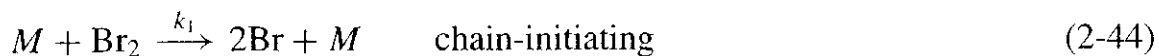
$$\frac{dC_{\text{HBr}}}{dt} = \frac{a_1 C_{\text{H}_2} C_{\text{Br}_2}^{1/2}}{1 + C_{\text{HBr}}/(a_2 C_{\text{Br}_2})}$$

where a_1 and a_2 are constants at a given temperature.

In the following, we shall first consider the detailed reaction mechanism, which consists of an interplay of various elementary reactions, then apply the steady-state treatment to free H and Br radicals, and finally derive a rate expression in the same form as that obtained experimentally. The $\text{H}_2\text{–Br}_2$ reaction also serves as an example of how a complex reaction mechanism can be proposed and verified.

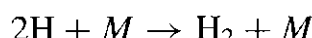
To initiate this chemical reaction, heat is added. Br_2 begins to decompose first, since H_2 is more stable than Br_2 (note: $\Delta H_{f,\text{Br}}^o = 6.71 \text{ kcal/mol}$, $\Delta H_{f,\text{H}}^o = 52 \text{ kcal/mol}$). Once bromine atoms are formed, these free radicals can react

readily with H_2 . Therefore, a series of reactions are followed:

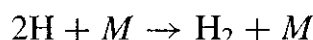
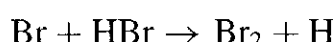


In reactions (2-44) and (2-48), the symbol M represents a third body, that is, any of the chemical species H , Br , H_2 , Br_2 , or HBr which may be present in the system. The relationships showing the effectiveness between different collision partners are called chaperon relationship [see, for example, Eq. (5-52) and (5-53)]. Initially, Br_2 or H_2 molecules are the collision partners with Br_2 molecules.

Reaction (2-44) is a chain-initiating step. Reactions (2-45) and (2-46) represent the chain-carrying reactions in which an atom (either Br or H) is produced for each atom which reacts. Reaction (2-47) is the inverse of (2-45); the inverse of (2-46) is relatively slow and is therefore unimportant. Reaction (2-46) represents the chain-terminating (also called chain-breaking or chain-killing) step. The chain-breaking step according to the recombination process



is not important in the present case, since the concentration of H atoms is generally small compared with that of Br atoms. However, at higher temperatures the following two reactions



can become quite influential. After examining the above set of opposing and consecutive reactions, it is easy to understand why the rate law derived from the global reaction has very little significance.

Following the law of mass action, a set of equations for the rate of change of concentration is obtained:

$$\frac{dC_{Br}}{dt} = 2k_1 C_M C_{Br_2} - k_2 C_{Br} C_{H_2} + k_3 C_H C_{Br_2} + k_4 C_H C_{HBr} - 2k_5 C_M C_{Br}^2 \quad (2-49)$$

$$\frac{dC_H}{dt} = k_2 C_{Br} C_{H_2} - k_3 C_H C_{Br_2} - k_4 C_H C_{HBr} \quad (2-50)$$

$$\frac{dC_{Br_2}}{dt} = -k_1 C_{Br_2} C_M - k_3 C_H C_{Br_2} + k_5 C_{Br}^2 C_M \quad (2-51)$$

$$\frac{dC_{H_2}}{dt} = -k_2 C_{Br} C_{H_2} + k_4 C_H C_{HBr} \quad (2-52)$$

$$\frac{dC_{HBr}}{dt} = k_2 C_{Br} C_{H_2} + k_3 C_H C_{Br_2} - k_4 C_H C_{HBr} \quad (2-53)$$

Applying the steady-state assumption that the mean concentrations of the free radicals H and Br remain nearly constant, we have

$$\frac{dC_H}{dt} = \frac{dC_{Br}}{dt} = 0 \quad (2-54)$$

In actuality, the concentrations of H and Br will not remain constant throughout the reaction process, but they will remain constant throughout the major portion of the reaction period, except for short initial and final periods. Thus, the concentration of the free radicals can be treated as nearly constant.

Using Eq. (2-54) to equate Eqs. (2-49) and (2-50), and then rearranging the result, we have

$$C_{Br} = \sqrt{\frac{k_1}{k_5}} \sqrt{C_{Br_2}} \quad (2-55)$$

Solving for C_H after setting the left-hand-side term of Eq. (2-50) equal to zero, we have

$$C_H = \frac{k_2 C_{Br} C_{H_2}}{k_3 C_{Br_2} + k_4 C_{HBr}} \quad (2-56)$$

Note that Eqs. (2-55) and (2-56) were obtained under the steady-state assumption. If the equilibrium assumption were used instead of the steady-state assumption, Eq. (2-56) would be different, since equilibrium-constant equations would be used to replace the rate expressions. It is obvious that these two assumptions are not interchangeable. Under either the steady-state assumption or the equilibrium assumption, the total number of unknowns is equal to six, namely



In addition to Eqs. (2-49) through (2-53), we have one enthalpy-balance equation to make the system completely defined. By solving these six simultaneous equations as a function of time, the reaction history of this combustion problem is obtained.

Now, if we follow the steady-state assumption for H and Br atoms and substitute Eqs. (2-55) and (2-56) into Eq. (2-53), we have

$$\frac{dC_{HBr}}{dt} = k_2 \sqrt{\frac{k_1 C_{Br_2}}{k_5}} C_{H_2} + \frac{k_3 C_{Br_2} - k_4 C_{HBr}}{k_3 C_{Br_2} + k_4 C_{HBr}} k_2 C_{Br} C_{H_2}$$

or

$$\frac{dC_{HBr}}{dt} = k_2 \sqrt{\frac{k_1 C_{Br_2}}{k_5}} C_{H_2} \left(\frac{2k_3 C_{Br_2}}{k_3 C_{Br_2} + k_4 C_{HBr}} \right)$$

which simplifies to

$$\frac{dC_{HBr}}{dt} = \frac{2k_2 \sqrt{k_1/k_5} \sqrt{C_{Br_2}} C_{H_2}}{1 + (k_4/k_3) C_{HBr}/C_{Br_2}} \quad (2-57)$$

Equation (2-57) matches the empirical relation obtained from experimental measurements,

$$\frac{dC_{\text{HBr}}}{dt} = \frac{2k_t C_{\text{H}_2} \sqrt{C_{\text{Br}_2}}}{1 + C_{\text{HBr}}/(10C_{\text{Br}_2})} \quad (2-58)$$

At the beginning of the reaction process, the concentration of HBr is very small, that is,

$$1 \gg \frac{C_{\text{HBr}}}{10C_{\text{Br}_2}}$$

In this case, Eq. (2-58) reduces to the Arrhenius form in which

$$\frac{dC_{\text{HBr}}}{dt} = k C_{\text{H}_2} C_{\text{Br}_2}^{1/2} \quad (2-59)$$

The overall order of the reaction is $1\frac{1}{2}$.

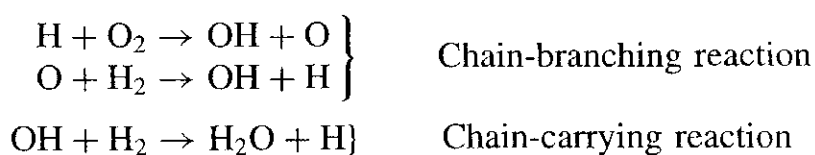
For the other case, corresponding to

$$\frac{C_{\text{HBr}}}{10C_{\text{Br}_2}} \gg 1$$

the Arrhenius form is again obtained. In general, the order of complex reactions changes as a function of time.

7 CHAIN-BRANCHING EXPLOSIONS

In a mixture of hydrogen and oxygen, it is presumed plausible that the presence of a free radical (free valence) in the form of an OH radical or H atom should result in the following reaction cycle:



The first reaction is endothermic by 17 kcal/mole. Thus, at room temperature and even at somewhat higher temperatures, a mixture of hydrogen and oxygen is very stable even if hydrogen atoms are introduced from another source. The free valence ultimately terminates at the wall through recombination processes. Above some temperatures, however, the chain-branching reaction becomes sufficiently frequent, when compared with the rate of removal of H atoms, to cause multiplication of free valences and possible explosion.

Explosions are conveniently classified into two distinct categories: *branched-chain explosions*, in which the reaction rate increases without limit because of

chain branching, and *thermal explosions*, in which there is an exponential increase in reaction rate resulting from exothermic chemical reaction, heating of reactants, and an increase in the magnitude of the specific reaction rate constants.

Consider a 1-cm³ container that contains initially one chain molecule, that is, one free radical per centimeter³. Assume that the number density in the container is 10¹⁹ molecules/cm³ and the average collision rate is 10⁸ collisions/s. If the reaction in the volume is a chain-carrying reaction [i.e., one free radical can generate another free radical in the reaction ($\alpha' = 1.0$)], then the time required for all of the molecules to react (i.e., 10¹⁹ collisions) will be

$$t = \frac{10^{19} \text{ collisions}}{10^8 \text{ collisions/s}} = 10^{11} \text{ s} \approx 30,000 \text{ years}$$

Such a slow process cannot be called combustion. If the reaction in the volume is a chain-branched reaction [i.e., one free radical or chain particle can generate two chain particles in the reaction ($\alpha' = 2.0$)], then the time required for all of the molecules to react can be estimated as follows:

$$1 + 2 + 2^2 + 2^3 + \dots + 2^N = \frac{2^{N+1} - 1}{2 - 1} = 10^{19} \text{ molecules}$$

where

$$N = 64 \text{ generations}$$

or

$$t = 64 \times 10^{-8} \text{ s} \approx 10^{-6} \text{ s} = 1 \mu\text{s}$$

This is certainly an extremely rapid combustion process. In an actual combustion process, not all reactions are chain-branched reactions. However, the reaction rate can still be very fast even for a very small portion of chain-branched reactions. For a combustion process, in which 1% ($\alpha' = 1.01$) of the elementary reactions are of the chain-branched type, the time required for all the molecules in the volume to react would be only

$$\frac{\alpha'^{N+1} - 1}{\alpha' - 1} = \frac{1.01^{N+1}}{0.01} = 10^{19} \text{ molecules/cm}^3$$

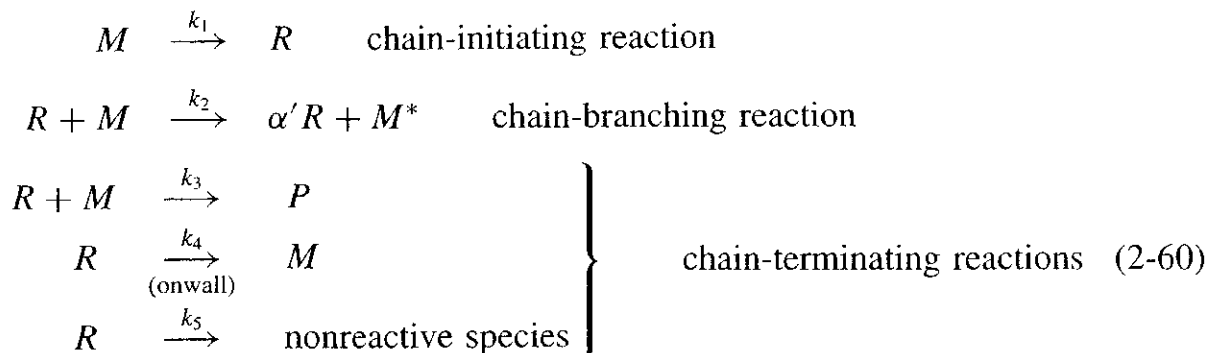
$$N = 3934$$

$$t = 3934 \times 10^{-8} \text{ s} \approx 40 \mu\text{s}$$

This is still a very fast reaction.

In general, branched-chain reactions and explosions can be studied by considering the following symbolic chemical kinetics starting with the initial dissociation

of a parent molecule M to form radical species R :



The rate equation (applying the steady-state assumption) is

$$\frac{dC_R}{dt} = 0 = k_1 C_M + (\alpha' - 1)k_2 C_R C_M - k_3 C_R C_M - k_4 C_R - k_5 C_R \quad (2-61)$$

Solving for C_R gives

$$C_R = \frac{k_1 C_M}{k_3 C_M + k_4 + k_5 - (\alpha' - 1)k_2 C_M} \quad (2-62)$$

The rate of change of the product concentration is given as

$$\frac{dC_P}{dt} = k_3 C_R C_M = \frac{k_1 k_3 C_M^2}{k_3 C_M + k_4 + k_5 - k_2(\alpha' - 1)C_M} \quad (2-63)$$

The quantity $k_2(\alpha' - 1)C_M$ is positive; as its value increases, it tends to decrease the denominator in Eq. (2-63). The critical value of α' is given as

$$\alpha'_{\text{critical}} = 1 + \frac{k_3 C_M + k_4 + k_5}{k_2 C_M} \quad (2-64)$$

and we have

$$\begin{aligned}
 \alpha' &\geq \alpha'_{\text{critical}} \Rightarrow \text{chain-branching explosion} \\
 \alpha' &< \alpha'_{\text{critical}} \Rightarrow \text{no explosion}
 \end{aligned}$$

However, it is important to note that for some actual explosion processes, because the concentration of R does not remain small, the steady-state approximation may not be valid. Other reaction steps may also become important. The postulated reaction kinetics in Eq. (2-60) may not always be applicable during an explosion. Extensive discussions of gas-phase explosions are given in later sections, after the presentation of detailed chemical kinetic mechanisms.

8 CHEMKIN ANALYSIS AND CODE APPLICATION FOR GAS-PHASE KINETICS

Chemkin package was originally developed by Kee et al.³³ at the Sandia National Laboratories and has since become a very powerful tool in combustion engineering as well as in other fields such as fluid dynamics and chemistry. The Chemkin

package (also called the Chemkin Collection) is a set of flexible and powerful programs and subroutine libraries for incorporating complex chemical kinetics into simulations of reacting flow. The software is a collection of programs that work together to facilitate the formation, solution, and interpretation of problems involving gas-phase and heterogeneous (gas-surface) chemical kinetics. This software package can be considered as a tool to the users in preparing large sets of complex equations that would otherwise be cumbersome. Chemkin prepares these equations so that they can then be readily incorporated into some other computational differential equation solver. Chemkin package allows the reexpression of the governing equations required into a FORTRAN representation and retrieves some thermodynamic data on the species involved. For reaction mechanisms involving numerous elementary reactions, Chemkin can be used very effectively by the user to write and analyze the equations involved.

Since 1980 the original Chemkin package has been modified to expand its capabilities. Chemkin-II³³ was released in 1992 and the latest package is called Chemkin-III³⁴ and is now commercially available from Reaction Design, Inc.^{35,36} One of the new capabilities of Chemkin-II and Chemkin-III is that they can handle pressure-dependent reactions, which do not follow the Arrhenius form of the rate of reaction laws. Chemkin-II and -III contain three methods of dealing with pressure-dependent reactions: the Lindemann approach,²⁸ the Troe–coworker approach³⁷ with the fall-off curves for the unimolecular reactions, and the approach developed by Stewart et al.³⁸ For reactions that involve vibrational energy transfer, the Arrhenius form of the rate expression is again invalid. These new packages have made adaptations allowing the use of the Landau–Teller formulation of the rate expressions, which consider these effects. Additionally, Chemkin-II and -III are capable of specifying more than one rate expression for a given reaction and can explicitly define a reverse rate for a reaction that may proceed in both directions.

8.1 Thermodynamic Properties

Chemkin package is capable of determining a wide range of standard-state thermodynamic properties. All thermodynamic properties are expressed in terms of polynomial fits to the specific heats at constant pressure. In general, the specific heats can be represented by a polynomial fit of arbitrary order of temperature. The C_P values of the k th species are represented by a fifth-order polynomial as

$$\frac{C_{Pk}^o}{R} = a_{1k} + a_{2k}T + a_{3k}T^2 + a_{4k}T^3 + a_{5k}T^4 \quad (2-65)$$

Chemkin code is designed to be compatible with the very extensive thermodynamic database used by the NASA chemical equilibrium code.^{39–41}

Other thermodynamic properties are given in terms of integrals of the specific heats. The standard-state enthalpy is represented as

$$H_k^o = \int_0^T C_{Pk}^o dT \quad (2-66)$$

The standard-state entropy is represented as

$$S_k^o = \int_0^T \frac{C_{Pk}^o}{T} dT \quad (2-67)$$

Many other thermodynamic data are then easily represented in terms of Eqs. (2-65), (2-66), and (2-67). The specific heat at constant volume is represented as,

$$C_{vk}^o = C_{Pk}^o - R \quad (2-68)$$

the internal energy as

$$U_k^o = H_k^o - RT \quad (2-69)$$

and the Gibbs free energy and the Helmholtz free energy as

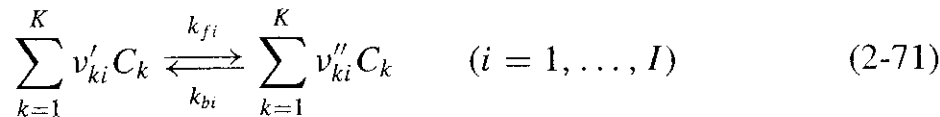
$$G_k^o = H_k^o - TS_k^o \quad \text{and} \quad A_k^o = U_k^o - TS_k^o \quad (2-70)$$

All of the above thermodynamic relations may be alternatively expressed per unit mass or on a mixture-averaged basis.

8.2 Reaction Rate Expressions

There are many reaction rate subroutines available. As mentioned earlier, Chemkin code considers, in addition to the Arrhenius temperature-dependent form, various reaction rate expressions for many special situations such as pressure-dependent reactions, vibrational energy transfer reactions, enhanced third-body reactions, and reverse reactions.

In general, I elementary reversible reactions involving a total of K species can be represented by



The production rate of the k th species can be written as a summation of the rate-of-progress variables for all reactions involving the k th species:

$$\dot{\omega}_k = \sum_{i=1}^I v_{ki} q_i = \sum_{i=1}^I (v''_{ki} - v'_{ki}) q_i \quad (k = 1, \dots, K) \quad (2-72)$$

The rate-of-progress variable for the i th reaction is given by the difference of the forward and the reverse rates as

$$q_i = k_{fi} \prod_{k=1}^K (C_{M,k})^{v'_{ki}} - k_{bi} \prod_{k=1}^K (C_{M,k})^{v''_{ki}} \quad (2-73)$$

where $C_{M,k}$ is the molar concentration of the k th species and k_{fi} and k_{bi} are the forward and backward (reverse) rate constants of the i th reaction. When a third-body reaction type is specified, its concentration must appear in the rate-of-progress variable expression(2-73). To account for this, the following expression is multiplied with the right-hand side of (2-73):

$$\sum_{k=1}^K \alpha_{ki} C_{M,k} \quad (2-74)$$

The α_{ki} coefficients are used to specify the increased efficiency of the k th species in the i th reaction. If all species contribute equally as third bodies, then all the $\alpha_{ki} = 1$. If a species has no effect as a third body for a particular reaction, the $\alpha_{ki} = 0$.

Unless otherwise noted, the forward rate constants for a given reaction are generally stated in an Arrhenius temperature-dependent form:

$$k_{fi} = A_i T^{\beta_i} \exp\left(-\frac{E_{ai}}{R_u T}\right) \quad (2-75)$$

where the preexponential factor A_i , the temperature exponent β_i , and the activation energy E_{ai} must all be specified as inputs into the rate constant subroutine. Normally, the reverse rate constant is related to the forward rate constant through the equilibrium constant by

$$k_{bi} = \frac{k_{fi}}{K_{Ci}} \quad (2-76)$$

where K_{Ci} is determined by Chemkin through the following relation:

$$K_{Ci} = \left[\frac{p_{\text{atm}}}{R_u T} \right]^{\sum_{k=1}^K (\nu''_{ki} - \nu'_{ki})} \times \exp\left[\frac{\Delta S_i^\circ}{R_u} - \frac{\Delta H_i^\circ}{R_u T} \right] \quad (2-77)$$

Chemkin-II allows the user to explicitly define an Arrhenius expression for the reverse reaction rate of the form eqnr(2-75). This option overrides the reverse rates that would normally be computed through the equilibrium constant (2-76).

As mentioned in Section 6.2, many chemical reactions are pressure dependent. At very high or low pressures, these reactions often approach different limiting reactions at both ends. At intermediate pressures, the reaction may exhibit a behavior that is a combination of the high- and low-pressure limiting cases. When such a reaction is at either limit, the Arrhenius form of the rate reaction (2-75) is applicable. If, however, the reaction falls between these two cases, the reaction rate expression is more complicated. The Chemkin manual refers to this type of reaction as a “fall-off” reaction. The code requires information on the high- and low-pressure limit rate expressions. Therefore, for each case, the preexponential factor (A_∞, A_o), the temperature exponent (β_∞, β_o), and the activation energy (Ea_∞, Ea_o) must all be specified as inputs into the rate constant subroutine.

This subroutine then determines the high-pressure limit rate constant k_∞ and the low-pressure limit rate constant k_o .

All three of the fall-off reaction rate constant methods follow the same basic structure. The rate constant at any pressure is taken to be

$$k = k_\infty \left(\frac{P_r}{1 + P_r} \right) F \quad (2-78)$$

where the reduced pressure P_r is related to the concentration of the mixture (C_M) by

$$P_r = \frac{k_0 C_M}{k_\infty} \quad (2-79)$$

In the Lindemann approach to the fall-off rate constant, the function F in (2-78) is taken as unity. The approach developed by Stewart et al.³⁸ assumes that F is given by

$$F = \left[a \exp\left(\frac{-b}{T}\right) + \exp\left(\frac{-T}{c}\right) \right]^{\frac{1}{1+\log^2 P_r}} d \times T^e \quad (2-80)$$

where the constants a , b , c , d , and e must all be specified as inputs to the subroutine. The last method is known as the Troe–coworker approach.³⁷ In this form, the function F is given by

$$\log F = \left\{ 1 + \left[\frac{\log P_r + c}{n - d \times (\log P_r + c)} \right]^2 \right\}^{-1} \log F_{\text{cent}} \quad (2-81)$$

where

$$c = -0.4 - 0.67 \log F_{\text{cent}}, \quad n = 0.75 - 1.27 \log F_{\text{cent}}$$

$$F_{\text{cent}} = (1 - a) \exp(-T/T^{***}) + a \exp(-T/T^*) + \exp(-T^{**}/T)$$

The parameters a , T^{***} , T^* , and T^{**} must all be specified as inputs to the subroutine.

The Chemkin-II package is also capable of handling vibrational energy transfer processes, where the Arrhenius expression (2-75) is not applicable. The following expression, which is often used to handle such reactions, is known as the Landau–Teller formulation:

$$k_{fi} = A_i \exp\left(\frac{B_i}{T^{1/3}} + \frac{C_i}{T^{2/3}}\right) \quad (2-82)$$

where A_i , B_i , and C_i must be specified as inputs to the subroutine.

Because the net rate of production of a particular species is the difference between the rate of creation and the rate of destruction by chemical reactions, we have

$$\dot{\omega}_k = \dot{C}_k - \dot{D}_k \quad (2-83)$$

where the chemical creation and destruction rates of a particular species are often of interest and are therefore computed in the Chemkin code as

$$\begin{aligned}\dot{C}_k &= \sum_{i=1}^I v''_{ki} k_{fi} \prod_{j=1}^K (C_{M,j})^{v'_{ji}} + \sum_{i=1}^I v'_{ki} k_{bi} \prod_{j=1}^K (C_{M,j})^{v''_{ji}} \\ \dot{D}_k &= \sum_{i=1}^I v'_{ki} k_{fi} \prod_{j=1}^K (C_{M,j})^{v'_{ji}} + \sum_{i=1}^I v''_{ki} k_{bi} \prod_{j=1}^K (C_{M,j})^{v''_{ji}}\end{aligned}\quad (2-84)$$

The net chemical production rates can also be expressed in terms of a creation rate and a corresponding characteristic time (τ_k) for the destruction rate of k th species:

$$\dot{\omega}_k = \dot{C}_k - \frac{C_{M,k}}{\tau_k} \quad \text{where} \quad \tau_k \equiv \frac{C_{M,k}}{\dot{D}_k} \quad (2-85)$$

8.3 Brief Description of Procedures in Using Chemkin Code

The Chemkin software contains five core components: (1) the gas-phase kinetics and preprocessor and subroutine libraries, (2) the surface kinetics preprocessor and subroutine libraries, (3) the transport property preprocessor and subroutine library, (4) the thermodynamic property database, and (5) a two-point boundary value problem solver. A block diagram showing the structure of the Chemkin package and its relationship to the application codes is given in Fig. 2.13. To use the Chemkin package, the user will need to provide three more components: (1) a

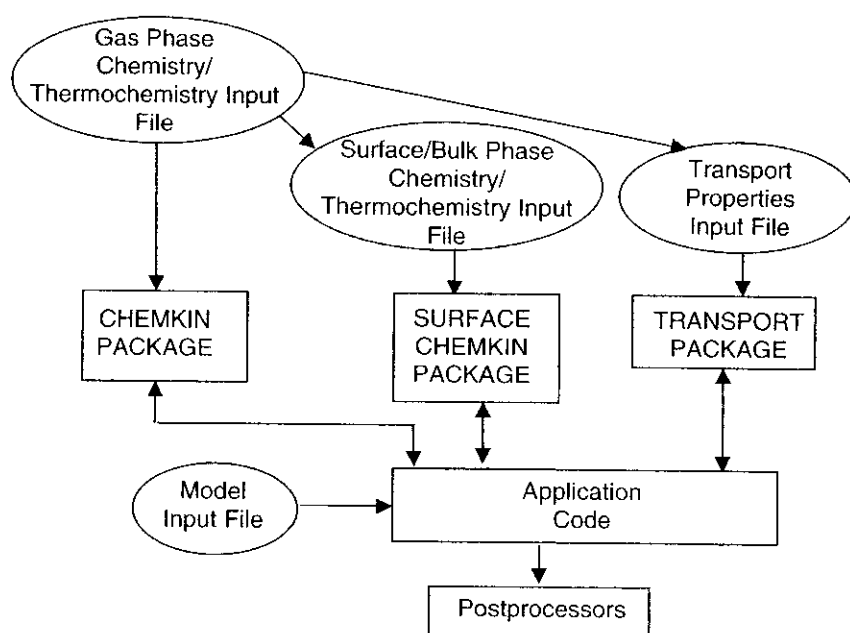


Figure 2.13 Block diagram showing the structure of the Chemkin package and its relationship to an application code.

model input file describing the system parameters and chemicals to be considered in the solution; (2) a thermodynamics database file including physical properties for every chemical ingredients listed for consideration in the input file; (3) a transport property input file. In practice, these files are loaded by including them in the user's working directory when the application is activated. Specific file placement varies depending on the operating system of the user's computer and the current version of Chemkin that is installed.

The programming involved in writing a set of governing equations is minimal because most of the required information can be found within the Chemkin subroutine library.

The symbolic reaction mechanism in the model input file is a crucial step in the problem definition and has many constituents.

A. This file must begin with a list of all chemical elements or isotopes of elements that will be involved in the reaction. The purpose of the element data is to associate atomic weights of the elements with their character symbol representation.

B. Next, a list of each species involved in the reaction must be specified. This information will be used to determine the weight of each species and to gather their thermodynamic data.

C. The largest part of this input file is the reaction mechanism description. The reaction mechanism description can contain any number of chemical reactions involving species listed at the top of the file. Each reaction specified in the reaction mechanism must contain some auxiliary information. *Every* reaction requires information on the *Arrhenius rate coefficients*. In addition to that minimal information, a reaction may be indicated as reversible or irreversible; it may be a third-body reaction, a fall-off reaction, or a vibrational energy transfer process, and it may involve photon emissions. If a backward reaction is to have an explicitly defined reverse reaction rate, the Arrhenius data for the backward (reverse) reaction must be specified in the auxiliary information. Third-body reactions may require extra information about enhanced third-body efficiencies as referred to in Eq. (2-74). For pressure-dependent reactions, the Arrhenius coefficients for both the high- and low-pressure limiting cases are required. In addition, one of the three mechanisms described in Eqs. (2-78) through (2-81) must be specified along with their corresponding inputs.

Any information specified in the auxiliary information about photon emissions or absorption will not actually be used by Chemkin, but it is available to the user for other subroutine calls. Sometimes only information about the elements and species is required and no reaction mechanism will even be specified. In these cases, Chemkin will merely return thermodynamic information for all specified data; no subroutines that require information on chemical reactions can be used.

This symbolic reaction mechanism data is then used as input to the Chemkin package, which retrieves thermodynamic information about all elements and species involved in the reaction from the Thermodynamic Database. The Chemkin

Table 2.2 A Sample Input to Interpreter of Chemkin Package

Input			
Elements H O N END			
Species H2 H O2 O OH HO2 H2O2 H2O N N2 NO END			
Reactions			
H2 + O2 = 2OH	0.170E + 14	0.00	47780
OH + H2 = H2O + H	0.117E + 10	1.30	3626 ! D-L&W
O + OH = O2 + H	0.400E + 15	-0.50	0 ! JAM 1986
O + H2 = OH + H	0.506E + 05	2.67	6290 ! KLEMM ET AL. 1986
H + O2 + M = HO2 + M	0.361E + 18	-0.72	0 ! DIXON-LEWIS
H2O/18.6/H2/2.86/N2/1.26/			
OH + HO2 = H2O + O	0.750E + 13	0.00	0 ! D-L
H + HO2 = 2OH	0.140E + 15	0.00	1073 ! D-L
O + HO2 = O2 + OH	0.140E + 14	0.00	1073 ! D-L
2OH = O + H2O	0.600E + 09	1.30	0 ! COHEN-WEST
H + H + M = H2 + M	0.100E + 19	-1.00	0 ! D-L
H2O/0.0/H2/0.0/			
H + H + H2 = H2 + H2	0.920E + 17	-0.60	0
H + H + H2O = H2 + H2O	0.600E + 20	-1.25	0
H + OH + M = H2O + M	0.160E + 23	-2.00	0 ! D-L
H2O/5/			
H + O + M = OH + M	0.620E + 17	-0.60	0 ! D-L
H2O/5/			
O + O + M = O2 + M	0.189E + 14	0.00	-1788 ! NBS
H + HO2 = H2 + O2	0.125E + 14	0.00	0 ! D-L
HO2 + HO2 = H2O2 + O2	0.200E + 13	0.00	0
H2O2 + M = OH + OH + M	0.130E + 18	0.00	45500
H2O2 + H = HO2 + H2	0.160E + 13	0.00	3800
H2O2 + OH = H2O + HO2	0.100E + 14	0.00	1800
O + N2 = NO + N	0.140E + 15	0.00	75800
N + O2 = NO + O	0.640E + 10	1.00	6280
OH + N = NO + H	0.400E + 14	0.00	0
END			

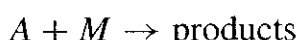
interpreter code was written so that it can read from any thermodynamic database that has the same format as the one used by the NASA Lewis chemical equilibrium code by Gordon and McBride.^{39–41} The NASA database is very extensive and offers obvious advantages. If users prefer to input their own thermodynamic data, this can be done by creating their own file, which follows the same format as the NASA database. The output from the Chemkin code is a list of all elements and species, their thermodynamic data, and all information about the reaction mechanism.

With the data about the reaction mechanism available, the user's activation of any application subroutines construct a set of governing equations from the Gas-Phase Subroutine Library. Once these equations have been established, the

last step is to use some numerical routine appropriate for solving them. Typically, equations representing chemical reactions involve one or more variables that change rapidly, while others change slowly. This is referred to as a *stiff* system of equations. The difference in time scales is due to the fact that reactions involving radicals proceed instantly while reactions involving more stable species are much slower.

There are many commercially available packages (such as IMSL's DGEAR) that are capable of handling a stiff system of equations.⁴²⁻⁴³

To understand the time constant, let us consider the following first-order decomposition reaction of species *A* in collision with *M* having a constant level of concentration:



The rate of depletion of *A* can be written as

$$\frac{dC_A}{dt} = -kC_M C_A$$

whose solution is

$$C_A(t) = C_A(0) \exp(-kC_M t)$$

The time constant *t_c* is defined as the time it takes for *C_A* to decay to *e*⁻¹ of the original concentration. In this case, inspection shows that

$$t_c = (kC_M)^{-1}$$

A complex kinetic system is usually composed of many species whose concentrations can decay (or grow) at different rates; thus, a kinetic system usually has disparity in time scales for a very broad range of time constants. In order to integrate the governing equations, it is obvious that the numerical solution is dominated by the species that have the shortest time constants. Such a system is termed stiff as defined above. Mathematically the problem of stiffness⁴⁴ lies in ensuring the numerical stability of the solution algorithm. Stability here refers to the requirement that any errors (roundoff or truncation errors) introduced during the computation should be damped by the algorithm.

The CHEMKIN Collection version (Release3.6.1) of Chemkin-III released from Reaction Design, Inc.,^{35,36} is available for a variety of UNIX and Windows operating systems. Many different problems can be addressed; these include

Reducing NO_x emissions and other pollutant emissions

Predicting performance of compression-ignition engines

Optimizing flow and process parameters for burner design

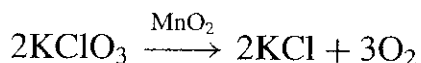
Determining auto ignition behavior for gas mixtures

Determining flame temperatures and flame speeds for flammability studies

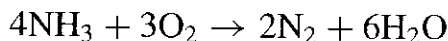
The CHEMKIN Combustion Package includes application programs for stirred reactors, plug-flow reactors, premixed and diffusion flames, and transient and steady-state analyses. The stirred reactor model includes gas-phase and surface reactions on multiple materials, as well as sensitivity analysis. The structure of opposed-flow diffusion flames in cylindrical or planar coordinate systems can also be calculated with the fuel and oxidizer streams having different temperatures.

9 SURFACE REACTIONS

Surface reactions play an important role in many combustion applications, e.g., in wall recombination processes during auto ignition, in coal combustion, in soot formation and oxidation, in catalytic combustion, or in metal combustion.^{1,30,45} The rates of many heterogeneous chemical reactions are influenced by solid surfaces. The rate of a surface reaction can be markedly increased or decreased by the presence of a small amount of some substance, which may be recovered in its original form after the reaction is completed. This phenomenon is referred to as *catalysis*, and the substance the presence of which changes the rate of the surface reaction is called a *catalyst*. Catalysis is of great importance in the refining of petroleum, the manufacturing of plastics, the oxidation of ammonia, and many industrial processes. An example of catalysis in which the rate of reaction is increased, *positive catalysis*, is the decomposition of potassium chlorate, KClO_3 , catalyzed by the presence of a little manganese dioxide, MnO_2 . The equation for this reaction may be written as



The oxidation of ammonia to nitric oxide (NO) is another example of catalysis. When ammonia burns, two independent reactions take place. These are illustrated by the following two reactions:



In the absence of a catalyst, the first of these reactions takes place almost exclusively, but if the combustion takes place on the surface of metallic platinum, the second reaction is so dominant that nearly all of the ammonia is converted to NO rather than to N_2 . In this case, the evidence indicates that the reactivity of the gases is greatly increased by their adsorption on the surface of the platinum. Thus, platinum serves as an effective catalyst for the heterogeneous reaction. In the pioneering studies in surface reaction research, the ability of platinum to facilitate reactions was noticed by Henry in 1824. He discovered that adding a platinum powder to the reacting surface in miners' safety lamps enhanced the light emitted from the reaction. One of the key results associated

with surface catalysis involving specific chemical interaction between the surface and the reacting gas molecules is that the molecules must first become adsorbed on the surface before reaction can occur. This view was first proposed in 1825 by Faraday,¹ who studied the nature of adsorption on surfaces and considered that reaction occurred in adsorbed films.

9.1 Surface Adsorption Processes

In view of the importance of adsorption forces in connection with surface catalysis, we shall first discuss the adsorption processes before addressing the issue of heterogeneous reaction. In the early 1900s, Langmuir first investigated the process of adsorption and developed the ideas of sticking and trapping. There are two main types of adsorption, and they are distinctly different. In the first type, called *physisorption*, the forces are of a physical nature and the adsorption is relatively weak. Physisorption is a process in which there is no direct chemical bond between the adsorbate and surface. The adsorbate is held by physical forces such as van der Waals forces. The heat changes found with *van der Waals adsorption* are usually less than 5 kcal/mol. According to Langmuir's original concept,⁴⁶ the second type of adsorption is considerably stronger and the adsorbed molecules are held to the surface by valence forces of the same type as those occurring between bound atoms in molecules. The heat evolved in this type of adsorption, known as *chemisorption*, is on the order of 10 to 100 kcal/mol. Chemisorption occurs when the adsorbate and surface have a direct chemical bond resulting in the sharing of electrons. Usually, the adsorbate first physisorbs and then converts to a chemisorbed state. However, at equilibrium there are always some physisorbed molecules, and they can contribute to the overall surface reaction process. The rate of adsorption by a surface has been determined to be the product of the total flux of molecules onto the surface and the sticking coefficient, which is defined as the ratio of molecules that stick to the surface to the number of impinging molecules.

An important consequence of Langmuir's concept of chemisorption is that after a surface has become covered with a single layer of adsorbed molecules it is essentially saturated. This idea of the *unimolecular layer* was proved experimentally by the existence of a definite adsorption limit for a given surface area; beyond the specific limit more molecules cannot be adsorbed readily. This result is good evidence for the theory that chemical forces are involved in chemisorption.

Taylor⁴⁷ suggested by that chemisorption is frequently associated with appreciable activation energy and may therefore be a relatively slow process. The energies of activation are often on the order of 20 kcal/mol, and consequently the adsorption is extremely slow at low temperatures; under these conditions, *van der Waals adsorption*, which requires very small or no activation energy, will predominate. Surface conditions can influence the chemisorption process. Not all surfaces are smooth, and in reality, surfaces are never smooth from the molecular viewpoint, and the kind of behavior to be expected on rough surfaces was discussed by Taylor,⁴⁸ Keier and Roginsky,⁴⁹ Kummer and Emmett,⁵⁰

Constable,⁵¹ and many others. Some surface sites will be more active than others, and chemical processes will occur predominantly on the most active sites, which are called active centers by Taylor. These active centers usually correspond to certain types of lattice defect.

Another complication that exists in connection with chemisorption is that there are interactions, usually of a repulsive nature, between atoms or molecules adsorbed side by side on a surface. The first evidence for this was obtained by Roberts,⁵² who measured heats of adsorption of hydrogen on a smooth tungsten surface. The heat was found to fall from about 45 kcal/mol for a bare surface to 15 kcal/mol for a 70%-covered surface,⁵³ and the heats of adsorption became close to zero when the surface was fully covered. If the surface is really homogeneous, this change in heat of adsorption must be due to repulsive interactions between the adsorbed molecules; when the surface is sparsely covered, the molecules are sufficiently far apart so as not to interact with each other, but the repulsive interactions become more important as the coverage increases. Additional evidence for repulsive interactions has been obtained by Emmett and Kummer⁵⁰ using an isotope method, and by Weber and Laidler⁵⁴ from measurements of rates of desorption.

The amount of gas adsorbed by chemisorption after equilibrium depends on several factors, including the nature of the surface, the adsorbate, the temperature, and the pressure. If the temperature is kept constant for a given system, the relationship between the amount of adsorption and the chamber pressure is known as an *adsorption isotherm*. A number of such isotherms have been proposed, some obtained empirically and others obtained theoretically. The simplest theoretical equation was developed by Langmuir,^{46,55} whose isotherm has the special significance of being the one that applies to the ideal case of chemisorption on a perfectly smooth surface with no interactions between adsorbed molecules. Thus, the Langmuir isotherm has an importance in adsorption theory that is equivalent to that of the ideal-gas laws. It is convenient to speak of adsorption that obeys Langmuir's isotherm as ideal adsorption. The equations for ideal adsorption play an important role in surface kinetics. These ideal adsorption equations will now be derived from several different points of view and for several different situations.

In general, the quantity of gas that can be adsorbed by a material is proportional to the surface area. Two different types of adsorption are possible, monolayer and multilayer. Figure 2.14 shows a schematic of the two types.

Monolayer adsorption is more common and is dominated by the interaction between the adsorbate and the surface. Multilayer adsorption is dominated by

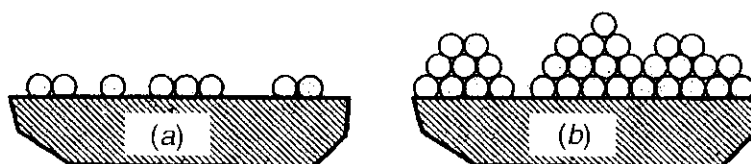


Figure 2.14 Illustration of (a) monolayer and (b) multilayer adsorption.

adsorbate–adsorbate interactions and occurs only at temperatures near the boiling point of the adsorbate. In the following derivation, we shall consider the monolayer case.

The rate of adsorption has an upper limit; it cannot exceed the rate at which gas-phase molecules collide with the surface. Using the kinetic theory of gases, the collision frequency of the *i*th molecule (in terms of mole/m²/s) on the surface can be written as

$$Z_{\max,i} = C_i \frac{\bar{u}}{4} = C_i \left(\frac{R_u T}{2\pi Mw_i} \right)^{1/2} = \frac{p_i}{R_u T} \left(\frac{R_u T}{2\pi Mw_i} \right)^{1/2} = \frac{p_i}{\sqrt{2\pi Mw_i R_u T}} \quad (2-86)$$

The maximum adsorption rate (kg/m²/s) is then equal to

$$k_{\max,i} = N_A m_i Z_{\max,i} = \frac{p_i m_i N_A}{\sqrt{2\pi Mw_i R_u T}} = \frac{p_i m_i}{\sqrt{2\pi m_i k_B T}} \quad (2-87)$$

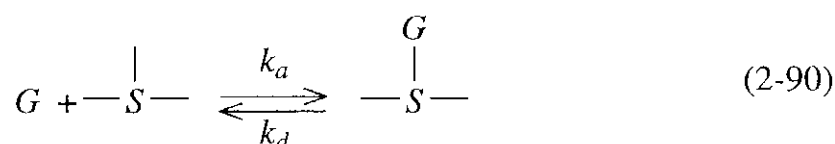
where m_i is the mass of a single *i*th molecule and k_B is the Boltzmann's constant, which is equal to R_u divided by Avogadro's number, N_A . Since only a fraction of molecular collisions on the surface will lead to surface adsorption, we can write the adsorption rate as

$$k_{\text{ads},i} = S_i k_{\max,i} = S_i p_i \sqrt{\frac{Mw_i}{2\pi R_u T}} = S_i C_i \sqrt{\frac{Mw_i R_u T}{2\pi}} \quad (2-88)$$

where S_i is the dimensionless sticking coefficient of the *i*th molecule on the surface. The value of S_i is between 0 and 1. For very low pressures, the value of S_i can be close to unity. Under other situations,³⁰ it can have extremely low values down to 10^{-6} . The specific reaction-rate constants for a surface adsorption process can be given in the following Arrhenius form³⁰:

$$k_{\text{ads}} = A_{\text{ads}} \exp \left(\frac{-E_{a,\text{ads}}}{R_u T} \right) \quad (2-89)$$

9.1.1 The Langmuir Adsorption Isotherm The simplest situation exists when the gas atoms or molecules occupy single sites on the surface and are not dissociated; the adsorption and desorption processes may then be expressed as



Let θ be the fraction of surface that is covered by the adsorbed gas molecules (G) and let $(1-\theta)$ be the fraction that is bare. The rate of adsorption is then $k_a p(1-\theta)$, where p is the gas pressure and k_a the adsorption rate constant. The

rate of desorption is $k_d\theta$. At equilibrium the adsorption rate is balanced by the desorption rate, so that

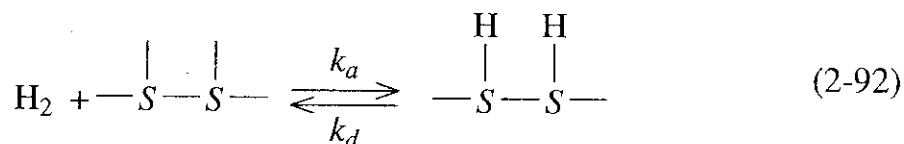
$$\frac{\theta}{1 - \theta} = \frac{k_a}{k_d} p \equiv Kp \quad (2-91)$$

where the equilibrium constant K is defined as the ratio k_a/k_d , which is a constant at a given temperature. The above equation can be rewritten as

$$\theta = \frac{Kp}{1 + Kp} \quad (2-91a)$$

One can easily plot the above Langmuir's adsorption-desorption isotherm equation to show that the value of θ increases monotonically with pressure. At very low pressures, $\theta \approx Kp$, while at high pressures, $1 - \theta \approx 1/Kp$.

9.1.2 Adsorption with Dissociation There is experimental evidence that the adsorption process can be accompanied by the dissociation of the molecule on the surface. For example, hydrogen can be adsorbed on the surfaces of many metals in the form of atoms, each of which occupies a surface site. Similarly, methane adsorbed on metals is usually dissociated into CH_3 , CH_2 , and hydrogen atoms. In the case of the dissociation of a molecule into two species (e.g., H_2 into 2H), the process may be represented as



Therefore, the process of adsorption can be considered a reaction between the gas molecule and two surface sites, and the reaction rate of adsorption may be written as

$$RR_a = k_a p(1 - \theta)^2 \quad (2-93)$$

The reaction rate of desorption, involving two adsorbed atoms, is proportional to the square of the fraction of surface covered by the gas molecule; thus,

$$RR_d = k_d \theta^2 \quad (2-94)$$

At equilibrium, these two rates are equal; therefore,

$$\frac{\theta}{1 - \theta} = \left(\frac{k_a}{k_d} p \right)^{1/2} \equiv K^{1/2} p^{1/2} \quad (2-95)$$

The above equation can be rewritten as

$$\theta = \frac{K^{1/2} p^{1/2}}{1 + K^{1/2} p^{1/2}} \quad (2-95a)$$

When the pressure is very low, the denominator approaches unity and θ is proportional to $p^{1/2}$. When the pressure is very high, $(1 - \theta)$ is inversely proportional to the square root of pressure.

9.1.3 Competitive Adsorption The isotherm for two different gases adsorbed on the same surface is of considerable interest. Let the fraction of the surface covered by molecules *A* be θ , and the fraction covered by *B* be θ' ; the bare fraction is $(1 - \theta - \theta')$. The reaction rate of adsorption of *A* may be written as

$$RR_a = k_a p(1 - \theta - \theta') \quad (2-96)$$

The reaction rate of desorption of *A* is

$$RR_d = k_d \theta \quad (2-97)$$

At equilibrium the adsorption rate is balanced by the desorption rate, so that

$$\frac{\theta}{1 - \theta - \theta'} = \frac{k_a}{k_d} p \equiv Kp \quad (2-98a)$$

where *p* is the partial pressure of *A*. From a similar step, the equilibrium condition of the *B* molecules is

$$\frac{\theta'}{1 - \theta - \theta'} = \frac{k'_a}{k'_d} p' \equiv K' p' \quad (2-98b)$$

where *p'* is the partial pressure of *B* and *K'* is the equilibrium constant for the adsorption-desorption reaction of *B*. The fractions covered by *A* and *B* can be expressed as

$$\theta = \frac{Kp}{1 + Kp + K'p'} \quad \text{and} \quad \theta' = \frac{K'p'}{1 + Kp + K'p'} \quad (2-99)$$

It can be seen from Eq. (2-99) that the fraction of the surface covered by one gas is reduced if the partial pressure of the other gas is increased; this is caused by the fact that the molecules are competing with one another for a limited number of surface sites in the competitive chemisorption process.

9.2 Surface Reaction Processes

9.2.1 Reaction Mechanism Surface reaction facilitated by catalyst (such as platinum, palladium) is called catalytic surface reaction, in which the catalyst itself increases the reaction rate without being consumed in the reaction.^{1,56} As described by Gardiner,⁵⁷ the overall process of gas–solid reactions can be divided into several subprocesses:

1. Transport of the reactant molecule to the surface by convection and/or diffusion

2. Adsorption of the reactant molecules on the surface
3. Elementary reaction steps, involving various combinations of adsorbed molecules, the surface itself, and gas-phase molecules
4. Desorption of the product molecules from the surface
5. Transport of the product molecules away from the surface by convection and/or diffusion

This concept is in fact the basis of the modern treatment of surface reactions, known as the *Langmuir–Hinshelwood mechanism*. This mechanism is described by the following reaction:

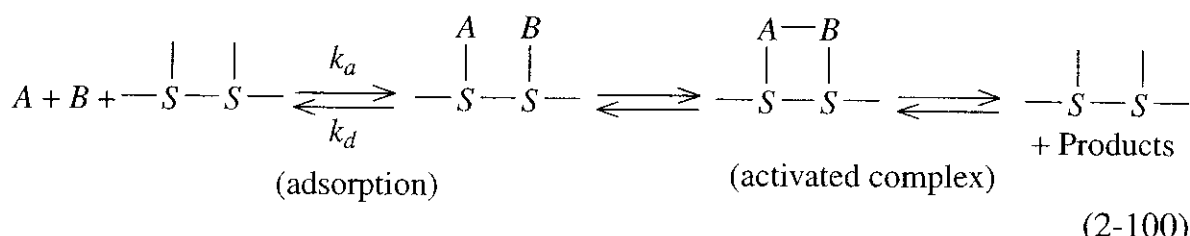
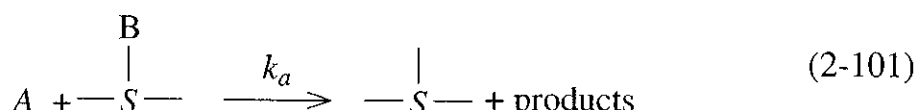


Figure 2.15 shows these three steps of an H₂ oxidation reaction on a Pt surface. First, the H₂ and O₂ are adsorbed on the surface to form H and O atoms, and then the adsorbed atoms collide and react with each other to form OH and then the adsorbed H₂O. Finally, the H₂O desorbs into the gas phase.

Another type of mechanism, initially considered by Langmuir⁵⁹ and later revised by Rideal,⁶⁰ involves the reaction between a gas molecule and an adsorbed molecule and is described by the following representative reaction:



The difference between this reaction and Eq. (2-100) is that A is not at all adsorbed on the surface. This mechanism is referred to as the *Langmuir–Rideal mechanism*¹ or *Rideal–Eley mechanism*.⁶¹ In addition to the Langmuir–Hinshelwood and

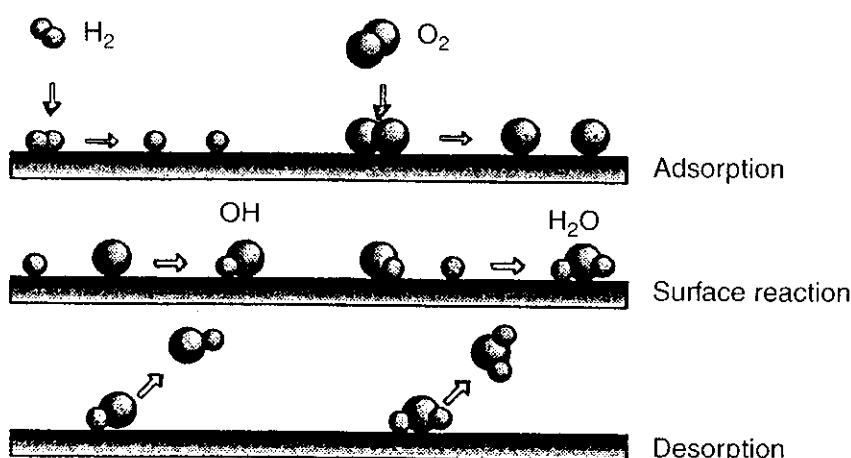


Figure 2.15 Processes of catalytic surface reaction of hydrogen oxidation.³⁰

Rideal-Eley mechanisms, a third mechanism is called the *precursor mechanism*, in which species *B* is adsorbed on the metal catalyst surface, species *A* has just a momentary residence on the surface without forming a bond on the surface, and the reaction product *AB* is immediately formed.

9.2.2 Unimolecular Surface Reactions For mechanisms associated with surface reactions, the concept of *molecularity* is important for a basic understanding. The molecularity is the number of molecules that come together during the course of a reaction. The molecularity of a surface reaction is deduced from the kinetics based on the experimental results and theoretical analysis. The simplest surface reaction involving one reactant molecule at pressure *p* is described by the Langmuir adsorption isotherm given in Eq. (2-91a). The reaction rate is proportional to θ and can therefore be written as

$$\text{RR} = k_a \theta = \frac{k_a K p}{(1 + K p)} \quad (2-102)$$

where k_a is the proportionality constant. This rate expression is based on the assumption that the adsorption equilibrium is not disturbed by the occurrence of the reaction. This assumption is generally satisfied. At sufficiently high pressures, $K p \gg 1$ and the rate of reaction is equal to k_a and is independent of pressure, which means that the kinetics are zeroth order. At low pressures, when $K p \ll 1$, Eq. (2-102) becomes $\text{RR} = k_a K p$, and the kinetics are first order.

One complication that frequently occurs in surface reactions is when an inhibitor substance *I* (also called a poison substance) other than the reactant is adsorbed on the surface. The resulting effect is the reduction of catalytic surface area and the corresponding decrease of reaction rate. If the fraction of the surface covered by *A* is θ , and that covered by *I* is θ_i , the fraction covered by *A* can be expressed by

$$\theta = \frac{K p}{1 + K p + K_i p_i} \quad (2-103)$$

where p_i is the partial pressure of the inhibitor and K_i its adsorption constant. The rate of reaction is therefore

$$\text{RR} = \frac{k_a K p}{1 + K p + K_i p_i} \quad (2-104)$$

When the partial pressure of the reactant is very low, the denominator is reduced to $(1 + K_i p_i)$. The rate of reaction is

$$\text{RR} = \frac{k_a K p}{1 + K_i p_i} \quad (2-104a)$$

If the inhibitor is very strongly adsorbed, $K_i p_i$ is large compared with unity; thus,

$$\text{RR} = \frac{k_a K p}{K_i p_i} \quad (2-104b)$$

The reaction is therefore first order. The decomposition of ammonium on platinum can be considered a good example of first-order reaction at low partial pressures of ammonia. The decomposition reaction is partially inhibited by hydrogen produced in the reaction. The rate of reaction follows the following functional dependence:

$$RR = \frac{kC_{\text{NH}_3}}{C_{\text{H}_2}} \quad (2-105)$$

9.2.3 Bimolecular Surface Reactions Bimolecular surface reactions represent reactions between two adsorbed molecules on neighboring surface sites. The mechanism involved with bimolecular surface reactions is the Langmuir–Hinshelwood mechanism. The rate of such a reaction between species *A* and *B* is proportional to the probability that *A* and *B* are adsorbed on neighboring sites, and is proportional to the fractions of the surface, θ and θ' , covered by *A* and *B*. Therefore, the reaction rate can be written as

$$RR = k\theta\theta' = \frac{kKK'pp'}{(1 + Kp + K'p')^2} \quad (2-106)$$

For sparsely covered surfaces, the above equation reduces to

$$RR \approx kKK'pp' \quad (2-107)$$

If one reactant is weakly adsorbed, Eq. (2-106) reduces to

$$RR = \frac{kKK'pp'}{(1 + K'p')^2} \quad \text{or} \quad RR = \frac{kKK'pp'}{(1 + Kp)^2} \quad (2-108)$$

The rate is then proportional to the partial pressure of *A* in the first expression. As the pressure of *B* increases, the rate first increases, passes through a maximum, and then decreases. If high concentration of reactant *B* is strongly adsorbed, $K'p'$ is much greater than unity, and the rate equation becomes

$$RR = \frac{kKp}{K'p'} \quad (2-109)$$

As mentioned before, surface reaction between a gas molecule and an adsorbed molecule can occur based on the Langmuir–Rideal mechanism¹ or Rideal–Eley mechanism.⁶¹ Let us assume that reaction occurs between an adsorbed *A* molecule and a gaseous *B* molecule. The fraction of surface covered by *A* is given by Eq. (2-99), and the rate is proportional to the partial pressure p' of *B*, namely,

$$RR = k\theta p' = \frac{kKpp'}{1 + Kp + K'p'} \quad (2-110)$$

Table 2.3 Reactions Run on Metal Catalysts

Type of Surface Reaction	Examples
Decomposition of chemical compound	$\text{NH}_3 \rightarrow \frac{1}{2}\text{N}_2 + \frac{3}{2}\text{H}_2$
Hydrogenation	$\text{N}_2 + 3\text{H}_2 \rightarrow 2\text{NH}_3$ $\text{CO} + 2\text{H}_2 \rightarrow \text{CH}_3\text{OH}$
Dehydrogenation	$\text{HCOOH} \rightarrow \text{CO}_2 + \text{H}_2$ methyl-cyclopropane \rightarrow toluene + H_2
Dehydration	$\text{HCOOH} \rightarrow \text{CO} + \text{H}_2\text{O}$
Hydrogenolysis	$\text{C}_2\text{H}_6 + \text{H}_2 \rightarrow 2\text{CH}_4$
Total oxidation	$4\text{NH}_3 + 8\text{O}_2 \rightarrow 2\text{N}_2\text{O}_5 + 6\text{H}_2\text{O}$ $2\text{CO} + \text{O}_2 \rightarrow 2\text{CO}_2$
Partial oxidation	$2\text{C}_2\text{H}_4 + \text{O}_2 \rightarrow 2\text{C}_2\text{H}_4\text{O}$
Steam reforming	$\text{C}_7\text{H}_{16} + 14\text{H}_2\text{O} \rightarrow 22\text{H}_2 + 7\text{CO}_2$

In this mechanism, B is not at all adsorbed. However, in the above equation with $K'p'$ in the denominator, B molecules do affect the rate by occupying surface that might otherwise be occupied by A . The surface reaction between ethylene and hydrogen has frequently been interpreted as occurring by the Langmuir–Rideal mechanism.¹

Table 2.3 shows different types of reactions commonly run on metal catalysts.

9.2.4 Desorption The final step in the surface reaction process is the desorption of product species. Desorption requires that the molecules have sufficient energy to overcome the bond strength between the adsorbed species and the surface. If the desorption process of product species does not occur quickly at the catalytic surface, product species can become saturated to stop the surface reaction process. The desorption process is governed by the same mechanisms as the adsorption process. The specific rate of desorption can also be given in the following Arrhenius form:

$$k_{\text{des}} = A_{\text{des}} \exp\left(\frac{-E_{a,\text{des}}}{R_u T}\right) \quad (2-111)$$

The preexponential factor A_{des} can be estimated from the vibrational frequencies of the corresponding bond. According to Warnatz et al.,³⁰ the preexponential factors for OH and H_2O desorption processes are on the order of 10^{-13} s^{-1} , which is closely related to the vibrational frequencies of the corresponding bonds. Thus, surface bond energies can be utilized to estimate the activation energy of the desorption process.

According to Ljungstrom and Kasemo,⁶² the rate of adsorption for the i th species can be expressed as

$$k_{\text{ads},i} = Z_i \cdot S_i(0) = \frac{p_i \cdot A}{\sqrt{2\pi m_i k_B T_{\text{gas}}}} \cdot S_i(0) \quad (2-112)$$

where Z_i = gas impingement rate ($i = \text{O}_2, \text{H}_2$) and $S_i(0)$ = zero-coverage sticking coefficient (on bare surface). This equation is similar to Eq. (2-87), except that the dimension of the adsorption rate is the number of i th molecules per second. If we define $f_i(\theta)$ as the coverage-dependent coefficient, then the coverage-dependent adsorption rate can be given as

$$k_{\text{ads},i} \cdot f_i(\theta) = Z_i \cdot S_i(0) \cdot f_i(\theta) = \frac{p_i \cdot A}{\sqrt{2\pi m_i k_B T_{\text{gas}}}} \cdot S_i(0) \cdot f_i(\theta) \quad (2-113)$$

One can consider the product of $f_i(\theta)$ and $S_i(0)$ as the effective coverage-dependent sticking coefficient. The rate of desorption is given by Eq. (2-111) or in terms of Boltzmann's constant as

$$k_{\text{des},i} = v_{\text{des},i} \cdot \exp\left(\frac{-E_{a_{\text{des},i}}}{k_B T}\right) \quad (2-114)$$

where $v_{\text{des},i}$ represents the vibrational frequencies of the corresponding bond to the surface and $E_{a_{\text{des},i}}$ is the surface bond energy for desorption.

The rate of surface reaction between adsorbed species is based on bimolecular reactions in the gas phase, mobility (hopping to adjacent site), Boltzmann's exponential factor, and surface coverage parameter θ_i . Therefore, the surface reaction rate for the recombination of two adsorbed A atoms to form an A_2 molecule (i.e., $A_{(\text{a})} + A_{(\text{a})} \rightarrow A_{2(\text{a})}$) is expressed as

$$\text{RR} = k_{f,i} \theta_i \theta_i \quad (2-115)$$

where the forward specific rate constant can be expressed as

$$k_{f,i} = v_i \exp\left(\frac{-E_{a,i}}{k_B T}\right) = \frac{D_i}{A} \sqrt{\frac{\pi k_B T}{2m_i}} \cdot \exp\left(\frac{-E_{a,i}}{k_B T}\right) \quad (2-116)$$

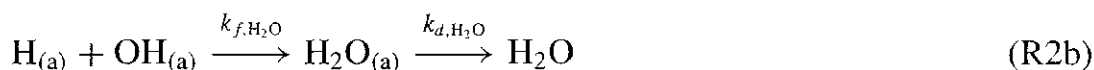
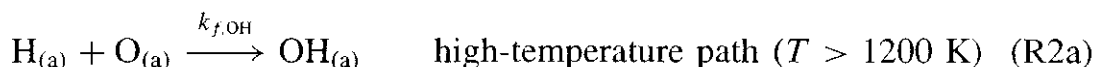
where D_i is the collision coefficient of the i th species.

9.3 Kinetic Model of Hydrogen–Oxygen Reaction on Platinum Surface

The surface reaction between H_2 and O_2 has been investigated under a variety of conditions, and many types of behavior have been observed. On a porcelain surface, the rate was found to be proportional to partial pressures of both H_2 and O_2 . On the surfaces of various metals, including silver, gold, copper, and nickel, the reaction rate has been found¹ to be first order in H_2 and zeroth order in O_2 . On a platinum surface, inhibition by O_2 was detected by Langmuir.⁵⁹ He also found that H_2O and other product species could inhibit the H_2/O_2 reaction on the surface of silver.

9.3.1 Simple Kinetic Model of H_2/O_2 Reaction on Platinum Surface

Let's consider the following elementary reaction steps for H_2/O_2 reaction on Pt surface under high-temperature conditions:



where subscript *a* is used for adsorbed species. Similarly, we shall use subscript *d* for desorption and subscript *f* for formation reaction. Several reaction steps were excluded from the above reaction mechanism in order to match these sufficiently high-temperature experimental conditions:

- $OH_{(a)} + OH_{(a)} \rightarrow O_{(a)} + H_2O_{(a)} \rightarrow O_{(a)} + H_2O$ (a low-temperature path).
- $OH_{(a)} \rightarrow H_{(a)} + O_{(a)}$ [as (R2a), and (R2b) reactions are assumed to be much faster].
- O_2 desorption neglected (due to large desorption energy, which is less likely to occur).
- H_2O is weakly adsorbed and desorbed rapidly enough, implying no coverage by $H_2O_{(a)}$.
- Due to low desorption energy, there is no coverage of surface by $H_{2(a)}$.

Equilibrium values of the coverage parameters of species are determined by steady-state solution of the coupled rate equations given below:

$$0 = \frac{d\theta_H}{dt} = 2k_{a,H_2} \cdot f_{H_2}(\theta) - k_{f,OH}\theta_H\theta_O - k_{f,H_2O}\theta_H\theta_{OH} - 2k_{d,H_2}\theta_H^2 \quad (2-117a)$$

$$0 = \frac{d\theta_O}{dt} = 2k_{a,O_2} \cdot f_{O_2}(\theta) - k_{f,OH}\theta_H\theta_O \quad (2-117b)$$

$$0 = \frac{d\theta_{OH}}{dt} = k_{f,OH}\theta_H\theta_O - k_{f,H_2O}\theta_H\theta_{OH} - k_{d,OH}\theta_{OH} \quad (2-117c)$$

where the total surface coverage parameter, $\theta = \theta_H + \theta_O + \theta_{OH}$. Making the assumption that $H_{(a)}$ is more mobile than $O_{(a)}$ and $OH_{(a)}$ would simplify the reaction rate equation with kinetic input data for E_i , $S_i(0)$, and v_i as follows:

Desorption and formation rate constants:

$$k_{f,\text{OH}} = v_{\text{H}} \cdot \exp \frac{-E_{af,\text{OH}}}{k_B T}$$

$$k_{f,\text{H}_2\text{O}} = v_{\text{H}} \cdot \exp \frac{-E_{af,\text{H}_2\text{O}}}{k_B T}$$

$$k_{d,\text{H}_2} = v_{\text{H}} \cdot \exp \frac{-E_{ad,\text{H}_2}}{k_B T}$$

$$\text{where } v_{\text{H}} = \frac{D_H}{A} \sqrt{\frac{\pi k_B T}{2m_H}} \approx 10^{13}$$

$$k_{d,\text{OH}} = v_{d,\text{OH}} \cdot \exp \frac{-E_{ad,\text{OH}}}{k_B T}$$

Adsorption rate constants:

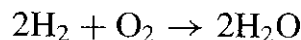
$$\left. \begin{aligned} k_{a,\text{H}_2} \cdot f_{\text{H}_2}(\theta) &= \frac{p_{\text{H}_2} \cdot A}{\sqrt{2\pi m_{\text{H}_2} k_B T_{\text{gas}}}} \cdot S_{\text{H}_2}(0) \cdot f_{\text{H}_2}(\theta) \\ k_{a,\text{O}_2} \cdot f_{\text{O}_2}(\theta) &= \frac{p_{\text{O}_2} \cdot A}{\sqrt{2\pi m_{\text{O}_2} k_B T_{\text{gas}}}} \cdot S_{\text{O}_2}(0) \cdot f_{\text{O}_2}(\theta) \end{aligned} \right\} \quad (2-118)$$

$$\text{where } f_{\text{H}_2}(\theta) = 1 - \theta, \quad f_{\text{O}_2}(\theta) = (1 - \theta)^2$$

OH and H_2O production rate: The rate of production of OH species from the surface can be calculated from the product of OH desorption rate and the coverage parameter θ_{OH} given in Eq. (2-117). The H_2O production rate can be determined from the formation rate of water and the coverage parameters θ_{OH} and θ_{H} .

$$\left. \begin{aligned} \text{RR}_{d,\text{OH}} &= k_{d,\text{OH}} \cdot \theta_{\text{OH}} \\ \text{RR}_{d,\text{H}_2\text{O}} &= k_{f,\text{H}_2\text{O}} \cdot \theta_{\text{H}} \cdot \theta_{\text{OH}} \end{aligned} \right\} \quad (2-119)$$

Maximum water production rate: The maximum water production rate occurs when H_2 and O_2 adsorption rate follows the stoichiometric relationship, i.e.,



In addition, OH and H_2 desorption are assumed to be negligible. Under these conditions, we have

$$r \equiv \frac{k_{a,\text{H}_2} f_{\text{H}_2}(\theta)}{k_{a,\text{O}_2} f_{\text{O}_2}(\theta)} = 2, \quad \text{for } \theta \leq 1$$

From Eq. (2-117b) and Eq. (2-117c), We obtain the following relationship using the condition that OH desorption and H_2 desorption are small,

$$k_{f,\text{H}_2\text{O}} \cdot \theta_{\text{H}} \theta_{\text{OH}} = k_{f,\text{OH}} \theta_{\text{H}} \theta_{\text{O}} = 2k_{a,\text{O}_2} \cdot f_{\text{O}_2}(\theta)$$

Substituting this result into Eq. (2-119)

$$RR_{\max, \text{H}_2\text{O}} = k_{f, \text{H}_2\text{O}} \cdot \theta_{\text{H}} \cdot \theta_{\text{OH}} = 2k_{a, \text{O}_2} \cdot f_{\text{O}_2}(\theta) \approx 2k_{a, \text{O}_2} = k_{a, \text{H}_2}$$

By using the definition of adsorption rate of H_2 in Eq. (2-118), we can finally get the maximum H_2O production rate:

$$RR_{\max, \text{H}_2\text{O}} = k_{a, \text{H}_2} = \frac{p_{\text{H}_2}}{\sqrt{2\pi m_{\text{H}_2} k_B T_{\text{gas}}}} \cdot S_{\text{H}_2}(0) \quad (2-120)$$

So, the maximum H_2O production rate is simply determined by either hydrogen or oxygen sticking coefficient at zero surface coverage.

9.3.2 Kinetic Rates of H_2/O_2 Reaction on Platinum Surface Warnatz et al.⁶³ studied the H_2/O_2 reactions on platinum surface. The rate constants for the elementary reactions are given in Table 2.4, which also describes the mechanisms for the hydrogen oxidation platinum-catalyzed surface reaction.

Table 2.4 Detailed Surface Reaction Mechanism of Hydrogen Oxidation on Platinum Surface (Adapted from Warnatz et al.⁶³)

Reaction	<i>S</i>	<i>A</i> (cm, mol, s)	<i>E_a</i> (kJ/mol)
1. H_2/O_2 adsorption/desorption			
$\text{H}_2 \xrightleftharpoons[\text{Pt}]{\text{Pt}} \text{H}_{2(\text{a})}$	0.1		0.0
$\text{H}_{2(\text{a})} \xrightarrow[\text{Pt}]{\text{Pt}} \text{H}_{(\text{a})} + \text{H}_{(\text{a})}$		1.5×10^{23}	17.8
$\text{O}_2 \xrightleftharpoons[\text{Pt}]{\text{Pt}} \text{O}_{2(\text{a})}$	0.046		0.0
$\text{O}_{2(\text{a})} \xrightarrow[\text{Pt}]{\text{Pt}} \text{O}_{(\text{a})} + \text{O}_{(\text{a})}$		5.0×10^{24}	0.0
2. Surface reactions			
$\text{H}_{(\text{a})} + \text{O}_{(\text{a})} \xrightarrow[\text{Pt}]{\text{Pt}} \text{OH}_{(\text{a})}$		3.7×10^{21}	19.3
$\text{H}_{(\text{a})} + \text{OH}_{(\text{a})} \xrightarrow[\text{Pt}]{\text{Pt}} \text{H}_2\text{O}_{(\text{a})}$		3.7×10^{21}	0.0
$\text{OH}_{(\text{a})} + \text{OH}_{(\text{a})} \xrightarrow[\text{Pt}]{\text{Pt}} \text{H}_2\text{O}_{(\text{a})} + \text{O}$		3.7×10^{21}	0.0
3. Product adsorption/desorption			
$\text{H} \xrightleftharpoons[\text{Pt}]{\text{Pt}} \text{H}_{(\text{a})}$	1.0		0.0
$\text{O} \xrightleftharpoons[\text{Pt}]{\text{Pt}} \text{O}_{(\text{a})}$	1.0		0.0
$\text{H}_2\text{O} \xrightleftharpoons[\text{Pt}]{\text{Pt}} \text{H}_2\text{O}_{(\text{a})}$	0.75		0.0
$\text{OH} \xrightleftharpoons[\text{Pt}]{\text{Pt}} \text{OH}_{(\text{a})}$	1.0		0.0

9.4 Experimental Methods to Study Surface Reactions

In general, there are two methods that appear to be the most suitable for studying surface phenomena: spectroscopic methods and temperature-programmed methods. This section will discuss these two methods separately with some focus on specific examples.

9.4.1 Spectroscopic Methods Christoffel⁶⁴ provides a summary of spectroscopic methods (see Table 2.5) as well as the information that each method is capable of providing. As indicated in Table 2.5, by utilizing these methods it is possible to determine the surface structure, topography, and surface composition of solid materials. In addition, the structure of adsorbed molecules and the binding between solid surface and adsorbents can be evaluated.⁶⁴ In general, spectroscopic methods utilize characteristic bands in the infrared spectra of some fractions of products, which may help identify organic compounds present.⁶⁵

One of the great advantages of these methods is that there is no interference with the flame, flow streams, or hot gases. However, one major disadvantage involved in these techniques is that all of them require that the sample be analyzed in a very low-pressure or near-vacuum condition in order to keep it from contamination. One of the main difficulties that spectroscopic methods have helped to alleviate is that it is very difficult to identify reactive intermediate species on solid surfaces because of the adsorption phenomenon of more stable molecules on the surface. The more stable species that adsorbed onto the surface are usually found in much greater concentrations than the intermediate reactive species. For this reason, it is very difficult to detect the intermediate species,⁶⁶ which in many cases have a concentration on the order of 10^{-9} g/cm². Concentration levels on this order could not be detected by traditional methods, but through the evolution of spectroscopic methods and the development of easily mountable vacuum-tight enclosures, it is now possible to measure concentrations on this order with a high precision (within a few percent).

9.4.1.1 Auger Electron Spectroscopy Perhaps the most commonly used experimental technique for the determination of surface chemical composition is Auger electron spectroscopy (AES). The basis for Auger electron spectroscopy⁶⁷ came from the discovery by P. Auger in 1925, who recognized that an atom in the excited state could return to the equilibrium state by releasing energy through ejection of an electron from an upper level—hence the name for the technique. The electrons that were ejected had characteristic energies that depended on the electronic structure of the element. Therefore, it was possible to identify the element by knowing the characteristic energy of the electron that was ejected. Basically, AES systems input a specified amount of energy through an excitation beam and count the number of electrons that are ejected. Elements can then be identified by the energy required to eject the electrons. With the ability to identify elements, and particularly elements in very small concentrations, it is very clear how Auger electron spectroscopy could be utilized in the determination of species concentrations in surface reactions.

Table 2.5 Various Types of Spectroscopy and Their Respective Uses (Adapted from Christoffel⁶⁴)

Spectroscopy (acronym)	Probe (input)	Measurement (output)	Remarks
<i>Photon Spectroscopy</i>			
Infrared spectroscopy (IR)	Monochromatic infrared photons (0.02–0.5 eV)	Absorption vs. wavelength	Occupied surface states, structure of adsorbed molecules
Optical spectroscopy	Monochromatic photons (0.5–6.5 eV)	Absorption vs. wavelength	Occupied surface states, structure of adsorbed molecules
Extended X-ray absorption fine structure (EXAFS)	Monochromatic X-ray photons (few keV from a synchrotron)	Modulation of the absorbed photon intensity vs. energy	Coordination number, atomic disturbances, nature of surrounding atoms (heavy nuclei)
<i>Ion Back-Scattering Spectroscopy</i>			
Secondary ion mass spectroscopy (SIMS)	Ions (~ 1 keV)	Sputtered ion current vs. mass-to-charge ratio	Surface composition (as function of depth)
Rutherford back-scattering spectroscopy (RBS)	Helium ions (few MeV)	Backscattered He^+ ions vs. energy	Surface states and composition
<i>Electron Emission Spectroscopy</i>			
Ultraviolet photoemission spectroscopy (UPS)	Monochromatic UV photon beam (~ 20 eV)	Electron emission vs. energy	Surface state, direction of bonds, valence state of ion
X-ray photo-emission spectroscopy (XPS or ESCA)	Monochromatic X-ray ($\sim 1, 5$ keV)	Electron emission vs. energy	Surface composition, valence state of ion
Auger electron spectroscopy (AES)	Electron beam (~ 3 keV)	Derivative electron emission vs. energy	Surface composition, valence state of ion

Table 2.5 (continued)

Spectroscopy (acronym)	Probe (input)	Measurement (output)	Remarks
Ion neutralization spectroscopy (INS)	Helium ions (5 eV)	Electron emission vs. energy	Surface states
Field emission spectroscopy (FES)	Electric field ($\sim 3 \times 10^7$ V/cm)	Electron emission vs. energy	Surface states, direction of bonds, crystal structure
<i>Electron Scattering Spectroscopy</i>			
Energy loss spectroscopy (ELS)	Monoenergetic electrons (~ 1 keV)	Derivative electron emission vs. energy loss	Transitions between surface states
Soft X-ray appearance potential spectroscopy (SAPS)	Monoenergetic electrons ($\sim 10\text{--}1000$ eV)	Derivative total X-ray yield vs. incident electron energy	Surface states, composition, valence state of ion
<i>Electron Diffraction</i>			
Low-energy electron diffraction (LEED)	Monoenergetic electrons (10–1000 eV)	Angular distribution of elastically scattered electrons	Surface crystallography

While Auger had made his discovery in 1925, it was not until the late 1960s and early 1970s that AES development really took off. During its development, there were many derivatives of the AES system, all of which were based on the same principles, depending on the needs of the individual using them. One of the recent derivatives of AES is known as the Scanning Auger Microscope or SAM. The original SAM system used an excitation beam of about 5000 Å; however, with the advances made in technology, the excitation beams have been reduced⁶⁷ to as little as 350 Å as of 1988. This reduction in the size of the excitation beam makes the system more sensitive and therefore much more accurate in its output. One of the major advantages of the SAM system over the other early AES systems was that it was able to provide a two-dimensional map of the chemical composition of the surface. Further advances in technology, such as the ability to collect and store data on computers, have also greatly improved the power of AES systems. With today's computers, it is easier to distinguish chemical species by using different colors.

9.4.2 Temperature-Controlled Methods Temperature-controlled methods have added greatly to the understanding of chemical kinetics of adsorption, but

even more so to the understanding of desorption processes. In particular, the identification of “desorption peaks” observed at controlled temperatures makes it possible to distinguish different adsorption states coexisting on a given surface and to evaluate approximately the associated energies of interaction.⁵⁸ Temperature-controlled methods are generally non-steady-state methods involving heating of a sample according to a usually linear computer-controlled temperature program. During the heating process, the sample is placed in a stream of inert gas.⁶⁴ The basic idea behind this method is that if a gas is adsorbed onto a surface, gradual heating will cause its desorption. As the temperature is increased, the desorption rate increases, reaches a maximum, and then decreases as the surface is depleted of the adsorbed species. It is possible for the gas to take more than one adsorbed form on the surface, in which case the number of so-called adsorption peaks will correspond to the number of adsorbed forms on the surface. Three common types of temperature-controlled methods are temperature-programmed desorption (TPD), thermal desorption spectroscopy (TDS), and temperature-programmed reaction spectra (TPRS). These methods can provide information on the adsorption energy, kinetic order, activation energy, and the pre exponential factors of desorption, to name a few. The desorption peaks can also provide insight regarding the order in which reactions occur and which steps in the overall reaction could be rate-determining steps.

9.4.3 Combination of Spectroscopic and Temperature-Controlled Methods

Methods Techniques have been developed to use both the spectroscopic and temperature-controlled techniques together. One example of this is scanning kinetic spectroscopy (SKS). This technique is similar to other temperature-controlled methods except that it is carried out in a high vacuum. SKS is generally used in the study of catalysis. The sample used is a catalytic crystal, which is “shot” with a molecular beam of reactant whose temperature is raised according to a computer program. A mass spectrometer is usually utilized to detect both products and reactants leaving the surface of the crystal. By continuously feeding a supply of reactants to the surface, this technique eliminates one of the main drawbacks of temperature-controlled methods: contamination of the surface due to adsorption.⁶⁴ Using the SKS technique, one can detect both positive and negative peaks, which has a great significance. Negative peaks indicate that the reactant is being consumed, while positive peaks are an indication of products being formed by chemical reaction or reactants that have left the surface due to desorption. This phenomenon is significant because it can lend insight into the overall surface reaction process. By analyzing the peaks, one can determine what reactions are taking place, or what reactions are significant to the overall reaction.

9.5 Surface Reaction Rate Determination

The experimental evaluation of the kinetics of catalytic surface reaction is a complex procedure, involving not only the determination of the overall kinetics, but also the determination of the intrinsic kinetics. Application of the law of mass

action to elementary reactions on a catalyst surface requires both identification of reactant species on the surface and measurement of their surface concentrations. For decades, the lack of means to accomplish these tasks led to reliance on equilibrium adsorption isotherms, such as the Langmuir isotherm, Temkin isotherm, and Freundlich isotherm,⁶⁸ to relate surface concentrations of reactant species to gas-phase partial pressures.⁶⁹ A breakthrough occurred in the mid-1950s with the announcement by Eischens and his coworkers that the infrared (IR) spectra of chemisorbed CO, CO₂, olefins, and acetylene, among others, can be measured under various conditions.^{70,71} Many important extensions have been developed based on this seminal discovery. Various techniques in addition to IR spectroscopy have been applied to the identification of adsorbed species in the absence of reaction. Among these techniques are Fourier transform infrared (FTIR) spectroscopy,⁷² field-emission microscopy (FEM), field-ion microscopy (FIM), low-energy electron diffraction (LEED),⁷³ secondary ion mass spectroscopy (SIMS),⁷⁴ electron energy loss spectroscopy (EELS),⁷⁵ surface extended X-ray-absorption fine structure (SEXAFS),⁷⁶ Auger electron spectroscopy (AES), X-ray photoelectron spectroscopy (XPS),⁷⁷ ultraviolet photoelectron spectroscopy (UPS),⁷⁸ electron spin resonance (ESR), and temperature-programmed desorption (TPD).⁷⁹ Many of these require ultra-high vacuum conditions.

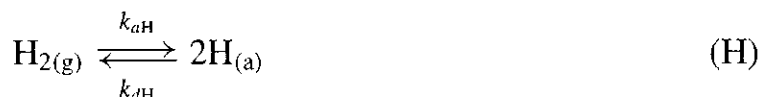
During the last decades, laser diagnostic techniques have been applied in various cases for engine-related studies. The main features of the laser techniques are their ability to offer high spatial resolution as well as temporal resolution in combination with a favorable nonintrusiveness. Laser induced thermal desorption (LITD) technique involves focusing a high-power laser pulse onto a small spot on the crystal surface in an ultra-high vacuum. The very rapid heating of the surface induces a rapid thermal desorption of adsorbate in the localized area. The desorption flux is subsequently detected by a mass spectrometer.^{80–82} Laser induced fluorescence (LIF), pioneered by Lin and coworkers,^{83–85} uses laser spectroscopic methods to detect intermediate species, which are desorbed from the surface during dynamic reaction conditions, before they react to form new species. This method offers unique possibilities to simultaneously identify the type of intermediate species, their internal quantum states, and their desorption energies.^{86–89} The advantage of this technique is that it is both extremely sensitive and unique for the radical under study. Unlike techniques involving high-energy electron impact, LIF does not cause splitting of the radical or radical precursor and hence offers a more definitive detection of radical species.

9.5.1 An Example of Application of LIF Technique in Surface Reaction

Rate Determination In the paper by Williams et al.,⁸⁹ OH radical desorption over a polycrystalline Pt foil exposed to mixtures of H₂, O₂, and H₂O for surface temperatures between 1000 and 1800 K was measured and used to determine the elementary steps in this reaction. Since hydrogen oxidation is characterized by extremely fast rates, determination of the rates of the intermediate surface reaction steps by stable species detection can be difficult. In fact, because of fast rates, much of the kinetic behavior in H₂ oxidation is determined by

mundane factors such as sticking coefficients and flux limitations. However, by probing trace amounts of desorbing OH radicals using LIF, Williams et al. have obtained essential information on the coverage of intermediate species during H₂ oxidation.

9.5.1.1 The Elementary Steps The elementary steps include three parts: adsorption, desorption, and surface reaction. Adsorption and desorption steps considered by Williams et al. are



The surface reaction steps considered are



The schematic of the reaction mechanism is shown in Figure 2.16.

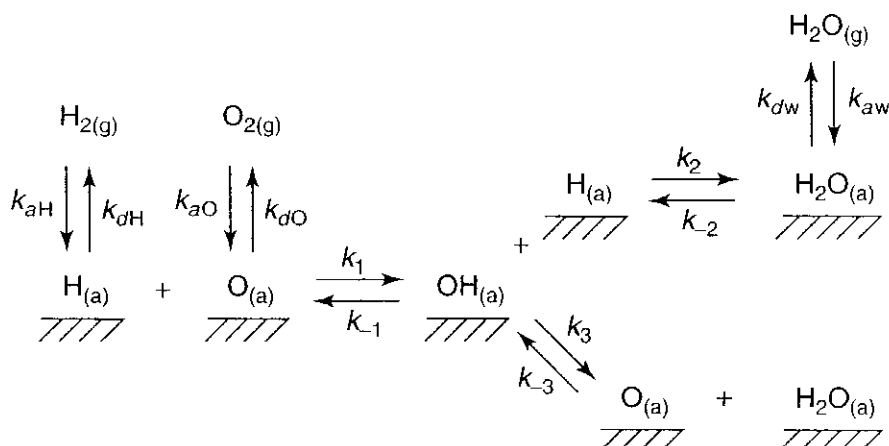


Figure 2.16 Reaction mechanism for the catalytic oxidation of H₂ on Pt foil by Williams et al.⁸⁹

9.5.1.2 Experimental Setup In their experimental setup, Williams et al.⁸⁹ used a six-way cross stainless steel reactor with a volume of 0.4 liter pumped by a mechanical pump. A resistively heated Pt foil, 0.17-cm × 3.0-cm in area, was suspended from nickel leads. Surface temperature was monitored with a thermocouple. Total pressure was measured with a capacitance manometer, and partial pressures in reaction systems were measured by leaking into a chamber equipped with a quadrupole mass spectrometer at $\sim 10^{-7}$ Torr pumped by a turbo mechanical pump. In nonreacting systems and for calibrations, partial pressures were measured by using differences in capacitance manometer measurements. Their LIF signal was filtered and detected using an RCA 1P28B photomultiplier and a boxcar integrator that integrated the fluorescence signal between 50 and 100 ns after the laser pulse. Data were taken by integrating 300 laser shots. The fluorescence was also monitored with a 175-MHz digital oscilloscope. This allowed them to monitor fluorescence lifetimes to ensure that nonradiative quenching was not affecting their results.

9.5.1.3 Experimental Results The experiments focused primarily on isothermal studies of the H₂/O₂/H₂O system. Isothermal measurements of OH desorption rates for the decomposition of H₂O over a 1700-K Pt foil as a function of H₂O pressure are shown in Fig. 2.17a. The effects of O₂ and H₂ addition on the decomposition of H₂O are shown in Fig. 2.18a and Fig. 2.19a, respectively.

Figure 2.17a shows that the rates of desorption of OH depend on H₂O pressure nearly linearly. This can be expected from the law of mass action. Assume that the forward reaction of reaction R2 is slow due to the desorption of OH and that reaction R2 gets to equilibrium with the desorption of OH. The rate of desorption of OH will then be equal to the rate of accumulation of OH due to the backward reaction of R2; therefore,

$$RR_{OH} = k_{-2}\theta_{H_2O} = k_{-2}K_W P_{H_2O}$$

For the isothermal condition, k_{-2} and K_W are constants.

Figure 2.18a shows the OH desorption versus O₂ pressure for varying H₂O pressure. The data can be fit by a curve of the form

$$C_{OH} = C_{OH,ref} + \frac{aP_{O_2}}{1 + bP_{O_2}}$$

The O₂ addition to the H₂O caused an increase of OH desorption. This is because the addition of O₂ contributes to OH due to the forward reaction of R1 and backward reaction of R3. Figure 2.19a shows the OH desorption versus H₂ pressure for varying H₂O pressure. The data can be fit by an expression of the form

$$C_{OH} = \frac{C_{OH,ref}}{1 + cP_{H_2}}$$

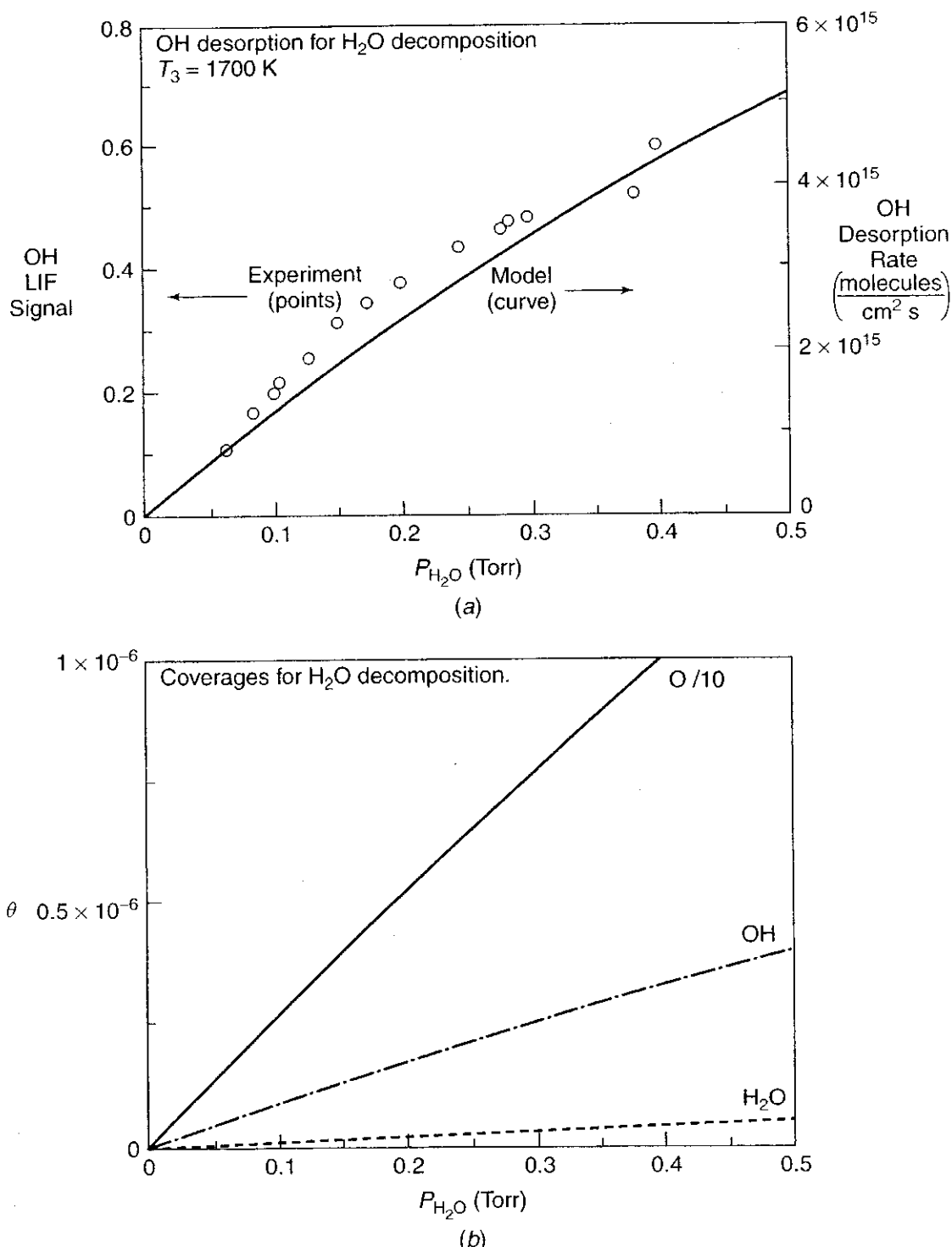


Figure 2.17 (a) Comparison of experimental and model results of OH desorption for H_2O decomposition over a 1700-K Pt surface. (b) Model predictions of surface coverage in monolayers for O_2 , H_2 , OH, and H_2O (after Williams et al.⁸⁹).

The addition of H_2 caused a decrease of OH desorption. This is because the addition of H_2 shifts the equilibrium of R2 toward water. Figures 2.17b, 2.18b, and 2.19b are the model predictions of surface coverage in monolayers for O_2 , H_2 , OH, and H_2O ; these results are useful for comparison with experimental data as well as for achieving better understanding of the surface reaction mechanism.

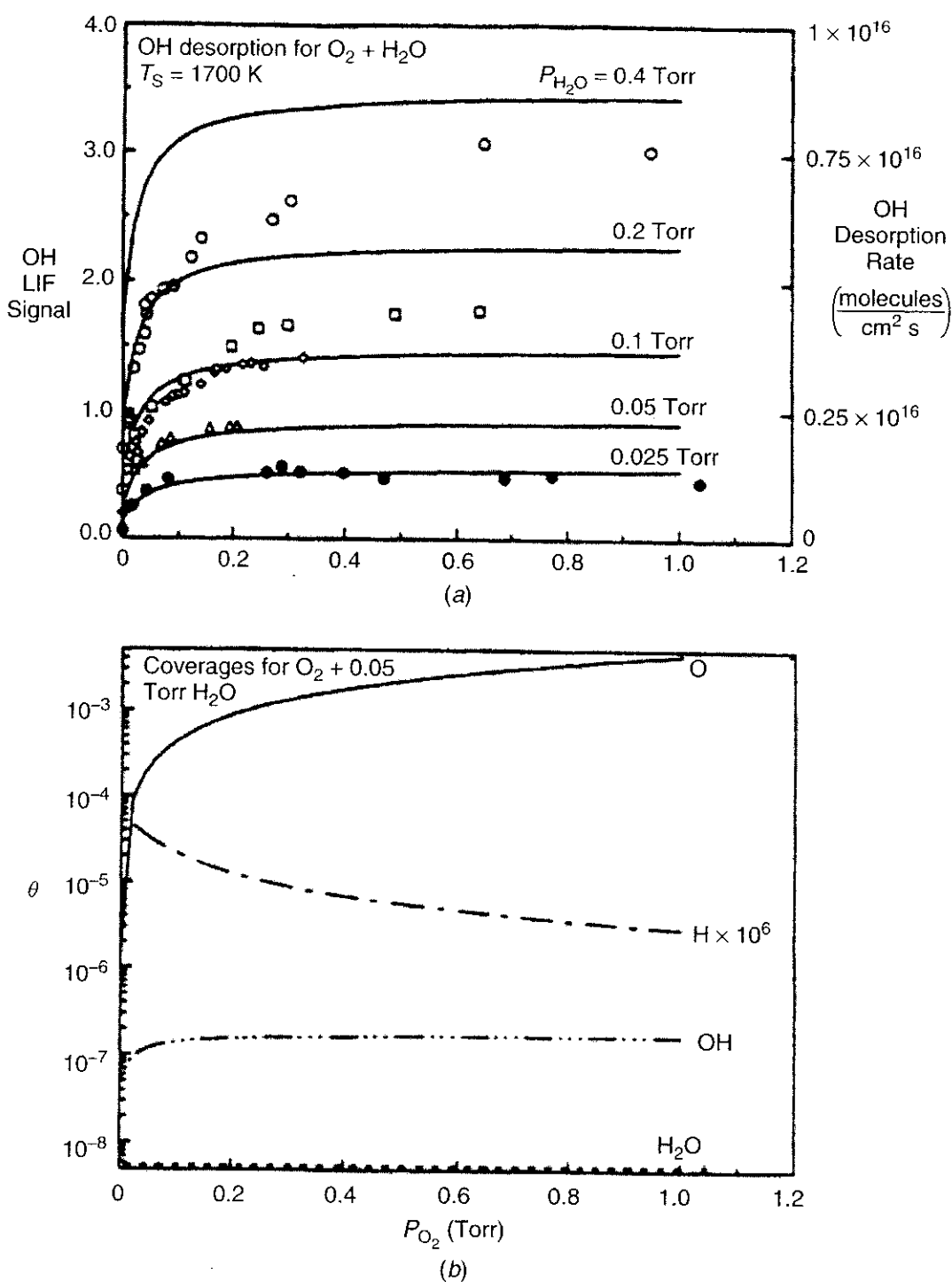


Figure 2.18 (a) Comparison of experimental and model results of OH desorption as a function of O_2 pressure added to 0.025 Torr (\bullet), 0.05 Torr (\triangle), 0.1 Torr (\diamond), 0.2 Torr (\square), and 0.4 Torr (\circ) H_2O over a 1700-K Pt surface. (b) Model predictions of surface coverage in monolayers for O_2 , H_2 , OH, and H_2O (after Williams et al.⁸⁹).

10 RATE LAWS FOR ISOTHERMAL REACTIONS UTILIZING DIMENSIONLESS PARAMETERS³

Before we talk about complex reaction mechanisms, it is useful to express the rate laws in different forms. For the sake of brevity, the following discussion will

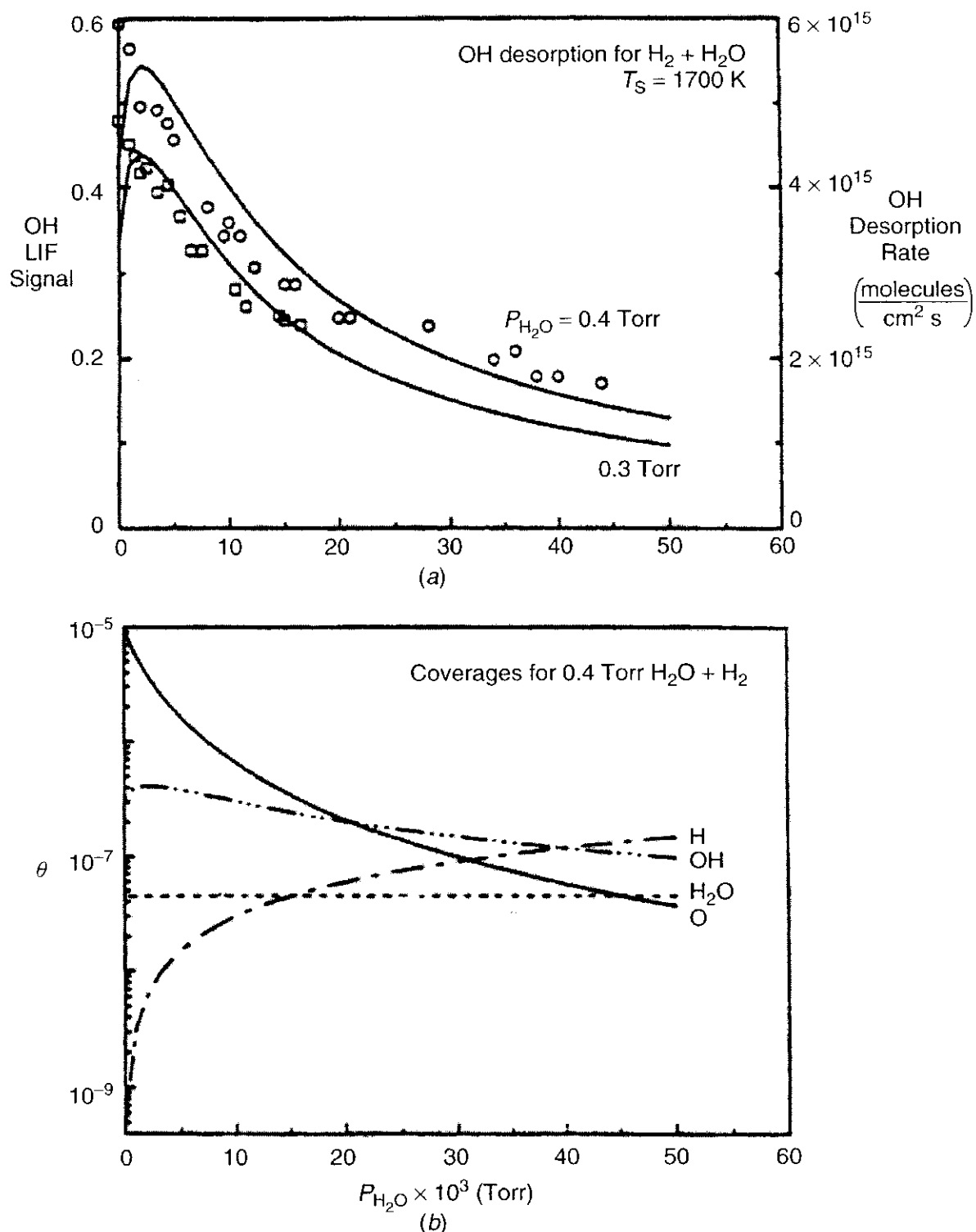


Figure 2.19 (a) Comparison of experimental and model results of OH desorption as a function of H₂ pressure added to 0.3 Torr (□) and 0.4 Torr (○) H₂O over a 1700-K Pt surface. (b) Model predictions of surface coverage in monolayers for O₂, H₂, OH, and H₂O. (After Williams et al.⁸⁹)

be restricted to a pair of opposing chemical reactions. Generalization to chain reactions can be made without difficulty.

For the most general opposing chemical reactions, expressed by Eq. (2-1), the net rate of production of species M_i is given by Eq. (2-28) based on the law of

mass action

$$\frac{dC_{M_i}}{dt} = (v''_i - v'_i)k_f \prod_{j=1}^N (C_{M_j})^{v'_j} \left(1 - \frac{1}{K_C} \prod_{j=1}^N (C_{M_j})^{v''_j - v'_j} \right) \quad (2-28)$$

where K_C was defined as the ratio of k_f to k_b , according to Eq. (2-27). A set of relations equivalent to that given above can now be formulated by replacing the concentrations with partial pressures, mole fractions, weight fractions, and so on. The transformations can be accomplished by assuming the validity of the ideal gas law, which constitutes an adequate approximation for a large class of combustion problems.

10.1 Equilibrium Constants

For ideal gases

$$C_{M_{j,e}} = \frac{p_{j,e}}{R_u T} \quad (2-121)$$

where $p_{j,e}$ denotes the equilibrium partial pressure of the chemical species identified by the symbol M_j . If the equilibrium constant K_p is defined by the relation

$$K_p = \prod_{j=1}^N \left(\frac{p_{j,e}}{p^o} \right)^{v''_j - v'_j} \quad (2-122)$$

where p^o is 1 bar and $p_{j,e}$ has a unit of bar. It is then apparent from Eqs. (2-27), (2-121), and (2-122) that

$$\frac{k_f}{k_b} = K_C = K_p (R_u T)^{-\Delta n} \quad (2-123)$$

where

$$\Delta n = \sum_{j=1}^N (v''_j - v'_j)$$

For ideal gases, the equilibrium mole fraction $X_{j,e}$ of species j is expressed as

$$X_{j,e} = \frac{p_{j,e}}{p} = \frac{C_{M_{j,e}}}{C_M} \quad (2-124)$$

where p represents the system pressure and C_M is the total number of moles per unit volume of gas mixture. From Eqs. (2-27), (2-121), (2-122), and (2-123) it can be seen that

$$\frac{k_f}{k_b} = K_C = K_p (R_u T)^{-\Delta n} = K_x \left(\frac{p}{R_u T} \right)^{\Delta n} = K_x (C_M)^{\Delta n} \quad (2-125)$$

where

$$K_X = \prod_{j=1}^N (X_{j,e})^{(v_j'' - v_j')} \quad (2-126)$$

For an ideal gas, the equilibrium mass of species j per unit volume, $\rho_{j,e}$, is

$$\rho_{j,e} = \left(\frac{P_{j,e}}{R_u T} \right) Mw_j = C_{M_{j,e}} Mw_j \quad (2-127)$$

where Mw_j represents the molecular weight of species j . The equilibrium weight fraction at species j is then

$$Y_{j,e} = \frac{\rho_{j,e}}{\rho_e} \quad (2-128)$$

where ρ_e denotes the equilibrium density of the fluid mixture. Using the preceding relations, it can be readily seen that

$$\frac{k_f}{k_b} = K_C = K_p (R_u T)^{-\Delta n} = K_x \left(\frac{P}{R_u T} \right)^{\Delta n} = K_Y F_w^{-1} \rho_e^{\Delta n} = K_\rho F_w^{-1} \quad (2-129)$$

where

$$K_\rho = \prod_{j=1}^N (\rho_{j,e})^{(v_j'' - v_j')} \quad (2-130)$$

$$F_w = \prod_{j=1}^N (Mw_j)^{(v_j'' - v_j')} \quad (2-131)$$

$$K_Y = \prod_{j=1}^N (Y_{j,e})^{v_j'' - v_j'} \quad (2-132)$$

Referring to the definitions of the various quantities involved, it is clear that only for $\Delta n = 0$; the parameters K_p , k_f/k_b , K_c , and F_w are dimensionless quantities. However, the equilibrium constants K_x defined in terms of mole fractions and K_Y defined in terms of weight fractions are always dimensionless. For substituting K_C of Eq. (2-28) by other forms of equilibrium constants given in Eqs. (2-129) through (2-132), all of the above expressions given are equivalent, since the group

$$\frac{k_b}{k_f} \prod_{j=1}^N (C_{M_j})^{v_j'' - v_j'}$$

is always dimensionless. If we consider quantities K_C^* , K_p^* , K_X^* , K_ρ^* , and K_Y^* as analogous to the equilibrium constants except that concentrations, partial pressures, and so on refer to the prevailing local concentrations, partial pressures,

and so on, rather than to equilibrium for the local conditions at T and p , then it is clear that

$$\frac{k_b}{k_f} \prod_{j=1}^N (C_{M_j})^{v''_j - v'_j} = \frac{K_C^*}{K_C} = \frac{K_p^*}{K_p} = \frac{K_X^*}{K_X} = \frac{K_\rho^*}{K_\rho} = \frac{K_Y^*}{K_Y} \equiv \frac{K^*}{K} \quad (2-133)$$

10.2 Net Rate of Production of Chemical Species

Using the definitions introduced in the preceding paragraph, it is easy to obtain the following equivalent expressions for dC_{M_i}/dt :

$$\begin{aligned} \frac{dC_{M_i}}{dt} &= (v''_j - v'_j) k_f \left[1 - \left(\frac{K^*}{K} \right) \right] \prod_{j=1}^N (C_{M_j})^{v'_j} \\ &= (v''_j - v'_j) k_f (R_u T)^{-m} \left[1 - \left(\frac{K^*}{K} \right) \right] \prod_{j=1}^N (p_j)^{v'_j} \\ &= (v''_j - v'_j) k_f (C_M)^m \left[1 - \left(\frac{K^*}{K} \right) \right] \prod_{j=1}^N (X_j)^{v'_j} \quad (2-134) \\ &= (v''_j - v'_j) k_f \left[1 - \left(\frac{K^*}{K} \right) \right] \prod_{j=1}^N \left(\frac{\rho_j}{\text{Mw}_j} \right)^{v'_j} \\ &= (v''_j - v'_j) k_f \left[1 - \left(\frac{K^*}{K} \right) \right] \rho^m \prod_{j=1}^N \left(\frac{Y_j}{\text{Mw}_j} \right)^{v'_j} \end{aligned}$$

where $m = \sum_{j=1}^N v'_j$, and the quantities p_j , X_j , ρ_j , and Y_j denote, respectively, the partial pressure, mole fraction, mass per unit volume, and weight fraction of species; these quantities are the instantaneous local properties of the reacting mixture.

11 PROCEDURE AND APPLICATIONS OF SENSITIVITY ANALYSIS

Computational capability has risen dramatically in recent years. Despite this progress, there remains a need for rapid, accurate computational methods for solving combustion problems. One way of achieving these needs for quick, accurate calculations in combustion systems involving complex chemical kinetics is in the reduction of the full chemical reaction model. Combustion analyses generally require the use of dozens or even hundreds of elementary chemical reactions. If certain of these chemical reactions can be removed from consideration while retaining accuracy, the solution becomes much more efficient.

One way of achieving this reduction of chemical reactions is by the use of chemical sensitivity analysis. Several methods can be used to determine if a

certain reaction is sensitive to changes in other parameters. Sensitivity analyses have been used with several different parameters, the most popular being species concentration or reaction rate coefficients, but may also include pressure, temperature, mass fraction, mixture molecular weight, density, mole fraction, and chemical potential.⁹⁰ Sensitivity analysis per se can be used to study the effects of any parameter change on a complex system.

11.1 Introduction to Sensitivity Analysis

Sensitivity analyses are used for three main purposes with respect to chemical kinetics: (1) to reduce the number of reactions in a given problem, (2) to identify the rate-limiting reaction steps in the system, and (3) to understand the relative importance of reactions in the system. The concept of sensitivity analysis, although not new to the field of chemical kinetics, has recently received considerable interest in chemical kinetic research due to the development of very efficient methods for obtaining sensitivity analysis information. These newer, less time-consuming methods have enabled the study of larger systems and extended use past linear gradients⁹¹ (e.g., higher-order gradients, “derived” gradients, and Green’s function gradients).

Mathematically, when the spatial dependency is negligible, the sensitivity analysis of a system of chemical reactions consists of the problem of determining the effect of uncertainties in parameters and initial conditions on the solution of a set of ordinary differential equations. Sensitivity analysis procedures may be classified as deterministic or stochastic in nature. The interpretation of system sensitivities in terms of first-order elementary sensitivity coefficients is called a *local* sensitivity analysis (a deterministic approach to sensitivity analysis). Here, the first-order elementary sensitivity coefficient is defined as the gradient, $\partial C_i / \partial \alpha_j$, where C_i is the concentration of the i th species at time t and α_j is the j th input parameter, and the gradient is evaluated at a set of nominal parameter values α . Theoretical treatments have included the “direct method,”⁹² the Green’s function method,^{93,94} and Taylor series expansion methods.⁹⁵ Although the sensitivity coefficients $\partial C_i / \partial \alpha_j$ provide direct information on the effect of a small perturbation in each parameter about its nominal value on each concentration, they do not necessarily indicate the effect of simultaneous, large variations in all parameters on each species concentration.

An analysis that accounts for simultaneous parameter variations of arbitrary magnitude can be termed a *global* sensitivity analysis. This analysis produces coefficients that have a measure of sensitivity over the entire admissible range of parameter variation. Examples of this stochastic approach are the FAST method,⁹⁶ Monte Carlo methods,⁹⁷ and pattern methods.⁹⁸ Both local and global analyses are useful in studying the behavior of a system since each has advantages and disadvantages. For excellent reviews of the different approaches, see Tilden et al.⁹⁹ and Rabitz et al.¹⁰⁰

Reaction-flow analyses discussed in Section 11.2 are especially useful in determining the characteristic reaction paths. The eigenvector analysis to be described

later in Section 11.3 is very helpful in determining the characteristic time scales and directions of the chemical reactions. Reduction procedure involves several steps, which include specifying the initial reactants and main reaction product species, determining temperature range for nonisothermal reactions, and examining the remaining species to determine if the species is necessary or redundant. In general, sensitivity analyses can be applied to nearly every parameter of the combustion process. Some of the more common parameters that have been studied by this means are temperature, pressure, and chemical potential. Another group of important parameters, which have been studied with direct connection to chemical kinetics, is the reaction rates. In sensitivity analysis theory, it is useful to define a generalized Jacobian matrix by the following definition. Given a solution \mathbf{x} that is dependent on a set of parameters \mathbf{p} , a Jacobian matrix J can be defined to describe the marginal changes in the solution \mathbf{x} as the parameters change.

$$J = \left(\frac{\partial \mathbf{x}^T}{\partial \mathbf{p}^T} \right)^T \quad (2-135)$$

This Jacobian matrix is called the *first-order sensitivity matrix*. Sensitivity matrices of higher order n are simply the Jacobian matrices of the n th derivatives. Second-order sensitivity matrices have also been used before.⁹¹ Second-order sensitivities were shown to yield valuable information on how these linear sensitivities vary when an initial condition or rate constant is varied. A normalized first-order matrix can be established to relate the rate of production of a given species f_j to the change in concentration C_i of another species by defining J as

$$J = \frac{\partial(\ln f_j)}{\partial(\ln C_i)} \quad (2-136)$$

By taking the sum of the squares of the normalized Jacobian, an expression B_i can be obtained for the concentration sensitivity as defined in Eq. (2-137).

$$B_i \equiv \sum_{j=1}^N \left(\frac{\partial \ln f_j}{\partial \ln C_i} \right)^2 \quad (2-137)$$

The concentration sensitivity B_i relates a change in i th species concentration to the rate of production of another species. The concentration sensitivity allows the determination of whether individual species are necessary or redundant, as opposed to the reactions.

The rate laws for a reaction mechanism consisting of M reactions involving N chemical species can be written as a system of first-order nonlinear ordinary differential equations

$$\begin{aligned} \frac{dC_i}{dt} &= F_i(C_1, C_2, \dots, C_N; k_1, k_2, \dots, k_M) \\ C_i(t=0) &= C_{i,0} \quad i = 1, 2, \dots, N \end{aligned} \quad (2-138)$$

where $C_{i,0}$ denotes the initial concentration of the i th species. Here only the specific rate coefficients taken into account shall be considered as parameters of the system, even though other parameters such as pressure and temperature can also be treated as system parameters. The main question of interest is “How does the $C_i(t)$ change by the change of the specific rate coefficients?” According to Warnatz et al.,³⁰ for many elementary reactions, a change in the rate coefficients has nearly no effect on the time-dependent solution (showing that quasi-steady states or partial equilibria are in force). Even if one chooses to include the reaction explicitly in the reaction mechanism, one does not need a highly accurate rate coefficient. On the other hand, for a few of the elementary reactions, changes in the rate coefficients have really pronounced effects on the solution. Accordingly, accurate rate coefficients are required. These few important reaction steps are *rate-determining steps* or *rate-limiting steps*.

The absolute and relative sensitivities can be defined as the dependence of the solution C_i on the parameter k_r by the following mathematical definitions.

$$E_{i,r} \equiv \frac{\partial C_i}{\partial k_r} \quad \text{and} \quad E_{i,r}^{\text{rel}} \equiv \frac{k_r}{C_i} \frac{\partial C_i}{\partial k_r} = \frac{\partial \ln C_i}{\partial \ln k_r} \quad (2-139)$$

Differentiating Eq. (2-138) with respect to k_r , we have

$$\begin{aligned} \frac{\partial}{\partial k_r} \left(\frac{\partial C_i}{\partial t} \right) &= \frac{\partial}{\partial k_r} F_i(C_1, C_2, \dots, C_N; k_1, k_2, \dots, k_M) \\ \frac{\partial}{\partial t} \left(\frac{\partial C_i}{\partial k_r} \right) &= \left(\frac{\partial F_i}{\partial k_r} \right)_{C_n, k_{m \neq r}} + \sum_{n=1}^N \left\{ \left(\frac{\partial F_i}{\partial C_n} \right)_{C_l \neq n, k_m} \left(\frac{\partial C_n}{\partial k_r} \right)_{k \neq r} \right\} \quad (2-140) \\ \frac{\partial}{\partial t} E_{i,r} &= \left(\frac{\partial F_i}{\partial k_r} \right)_{C_n, k_{m \neq r}} + \sum_{n=1}^N \left\{ \left(\frac{\partial F_i}{\partial C_n} \right)_{C_l \neq n, k_m} E_{n,r} \right\} \end{aligned}$$

In these equations, C_n in the subscripts of the partial derivatives means that all C_n are held constant during the differentiation, and $C_{l \neq n}$ means that all C_l are held constant, except C_n . There are software packages for solving Eq. (2-140) numerically to perform sensitivity analysis.^{101–103} Usually, the relative sensitivities of fast reactions decay rapidly with time to very low values, while the product concentrations have high relative sensitivities with respect to slow reactions and vice versa for fast reactions.

A set of rate equations for a complex system of chemical reactions can also be expressed in terms of nonlinear ordinary differential equations given by Eq. (2-141). The set of species mass fractions Y_i can be written as a vector \vec{Y} . Therefore, it is possible to rewrite the rate of change of \vec{Y} in terms of the global reaction rates \tilde{g} .¹⁰⁴

$$\frac{d\vec{Y}}{dt} = \tilde{g}(\vec{Y}) \quad (2-141)$$

The matrix quantity of global reaction rates \tilde{g} can be expressed as the sum of the contributions from the stoichiometric coefficient $v_{ij} = [(v_i'' - v_i')_j]$ and the reaction rate RR_j of the j th reaction in order to determine reaction rate sensitivity.¹⁰⁴

$$\tilde{g}(\vec{Y}) = \sum_{j=1}^M v_{ij} RR_j(\vec{Y}) \quad (2-142)$$

The goal of sensitivity analysis in general is to reduce the size of the \vec{Y} vector. There are several computation methods that can be used for this purpose. The most common method is through principal component analysis.

For the reaction rate sensitivity, the matrix \tilde{g} can be taken with the transpose of itself and decomposed into a system of eigenvalues and eigenvectors. The eigenvectors thus formed represent sets of coupled reactions. The eigenvalues represent the overall importance of these sets in the overall reaction. By defining certain numerical thresholds, it becomes possible to categorize the eigenvectors and eigenvalues.¹⁰⁵

In addition to the eigenvalue/eigenvector system, it is possible to define a normalized sensitivity coefficient for a given reaction. An overall rate sensitivity coefficient S_j for the j th reaction can be defined by taking the sum of the squares of the coefficients for that reaction with respect to a change in a given species,

$$S_j \equiv \sum_{i=1}^N \left[\frac{v_{ij} RR_j}{f_i} \right]^2 \quad (2-143)$$

where f_i represents the rate of change of the species i .

In order to be necessary, a reaction must have normalized rate sensitivity above a certain threshold value and, in addition, must have an effect on the important species. In most cases, these two conditions represent the same condition, but the sensitivity analysis does have certain flaws that occasionally allow the selection of reactions that are not required. The second condition also allows the addition of other parameters that affect the model, such as temperature or pressure. The determination of the addition of other parameters is made through a separate form of sensitivity analysis. Conversely, in order for a reaction to be redundant, its normalized rate sensitivity must be below the threshold value, and its removal from the system must not affect the important species. If the reaction fulfills these two conditions, it may be removed from the system of reactions within the model. A similar method is used for the temperature sensitivity analysis. Temperature sensitivities become important when thermodynamic effects play an important role in the chemical reactions. The temperature sensitivity can be defined as

$$TS \equiv \frac{\partial \ln(dT/dt)}{\partial \ln k_j} = \frac{-\Delta H_r \times RR_j}{C_p \rho dT/dt} \quad (2-144)$$

For combustion systems, it is possible to model the isothermal combustion process without considering thermal sensitivity, but models of this type do not

represent real processes. Most accurate nonisothermal combustion models therefore consider thermal sensitivity in the model reduction process.

The solution of the numerical model of a combustion process depends on a number of input parameters, including, for example, the initial conditions and rate constant parameters. However, the rate constants are often not known with great precision, and the experimental data are not detailed enough to estimate accurately the rate constant parameters. It is necessary, however, to know the effect of variations of inputs parameters on the solution. Sensitivity analysis can help determine the effects of the uncertainties in rate constant parameters or error in initial conditions on the model predictions. In a reaction system—in fact, only for a few of the elementary reactions, changes in the rate coefficients have large effects on the outcome of the system. Accordingly, an accurate rate coefficient is required. These few important reaction steps are the rate-limiting steps. Thus, sensitivity analysis helps identify the rate-limiting reaction steps.³⁰ As mentioned briefly before, sensitivity analysis methods fall into two categories¹⁰⁶: (1) *local* methods and (2) the *global* methods. Local methods typically produce the effect of a small change in one parameter by computing the first-order sensitivity coefficient. The first-order local sensitivity coefficients $S_{i,j}$ can be defined by

$$S_{i,j} = \left[\frac{\partial Y_i}{\partial k_j} \right]_{k_i \neq j} \quad j = 1, 2, \dots, M; i = 1, 2, \dots, N \quad (2-145)$$

In the above equation, Y_i is a variable of interest (e.g., a concentration or temperature) and k_j is a rate constant parameter (A, b, E_a) or an initial condition value. For isothermal reactions, the rate constants are time invariant; there is then no need to consider the individual rate constant parameters.

In a more general notation, if a system is described by a dependent variable $\Phi = \Phi(\mathbf{p}, \mathbf{x})$, where $\Phi \equiv (\Phi_1, \Phi_2, \dots, \Phi_N)$, \mathbf{x} is the independent variable, and \mathbf{p} is a set of parameters, the dependence of Φ on the parameters p_j for $j = 1, 2, \dots, N_k$ is described by absolute and relative sensitivities (which are local properties with respect to the independent variable \mathbf{x}):

$$S_{\Phi_i, p_j} \equiv \frac{\partial \Phi_i}{\partial p_j} \quad S_{\Phi_i, p_j}^{(rel)} \equiv \frac{p_j}{\Phi_i} \frac{\partial \Phi_i}{\partial p_j} \quad (2-146)$$

The extreme usefulness of sensitivity analysis is based on its unique ability to identify rate-limiting steps (e.g., the slowest step in a series of elementary reactions, the fastest step in a group of parallel reactions). $S^{(rel)} = 0$ implies no dependence, $S^{(rel)} = 1$ indicates linear dependence, and $S^{(rel)} = 2$ represents quadratic dependence on the parameter considered.

Global methods can account for simultaneous parameter variations of arbitrary magnitudes and can provide an average effect of all uncertainties examined. However, the computational effort for the global methods is much larger than for the local methods, since global methods require repeated solution of the chemical kinetics equations. Thus, local methods are used more often than global methods.

11.2 The Procedure for Local Sensitivity Analysis

Sensitivity analysis has been applied to problems in heat and mass transfer and combustion. The governing equation in these problems can often be modeled by a system of parabolic mixed initial-boundary value problems. The treatment for sensitivity can be organized according to the type of physical model involved:

- Time-dependent zero-dimensional problems
- Steady-state one-dimensional problems
- Time-dependent one-dimensional problems

11.2.1 Time-Dependent Zero-Dimensional Problems The governing equations for time-dependent problems are

$$\frac{\partial T}{\partial t} = - \frac{\sum \dot{\omega}_i h_i M w_i}{\rho C_p} \quad (2-147a)$$

$$\frac{\partial Y_i}{\partial t} = \frac{\dot{\omega}_i}{\rho} \quad (2-147b)$$

with $Y_i(x, 0) = Y_{i,0}(x)$, and $T(x, 0) = T_0(x)$. The above set of equations can be written in the following form:

$$\frac{\partial \Phi_i}{\partial t} = f_i[t, \Phi(t), \mathbf{K}] \quad i = 1, 2, \dots, N, N + 1 \quad (2-148)$$

with $\Phi = (Y_1, \dots, Y_m, T)$, and $\mathbf{K} = (k_1, k_2, \dots, k_M)$. Differentiation of Eq. (2-148) with respect to the parameter k_j gives

$$\frac{\partial S_{i,j}}{\partial t} - J_{i,l}(t) S_{l,j}(t) = \frac{\partial f_i(t, \Phi, \mathbf{K})}{\partial k_j} \quad (2-149)$$

where $S_{i,j}(t) = \frac{\partial \Phi_i(t)}{\partial k_j}$ and $S_{l,j}(t) = \frac{\partial \Phi_l(t)}{\partial k_j}$ are the sensitivity coefficients and $J_{i,l}(t) \equiv \frac{\partial f_i(t, \Phi, \mathbf{K})}{\partial \Phi_l}$ is the Jacobian matrix. Then, Eqs. (2-148) and (2-149) can be solved simultaneously using Runge–Kutta methods. This method for solving sensitivity coefficients is called Direct Method (DM). There are also some other methods for the temporal problems, such as Brute Force Method, Green's Function Method (GFM), Analytically Integrated Magnus (AIM), modification of the GFM or GFM/AIM,¹⁰⁶ and Decoupled Direct Method (DDM).¹⁰⁶

Hwang et al.⁹³ and Kramer et al.¹⁰⁷ showed that the Green's function method with AIM can be an efficient computational technique for determining local linear sensitivities, and it was adopted by Yetter et al.⁹¹ and coworkers^{108,109} for chemical kinetic studies. As emphasized by Rabitz¹¹⁰ and Yetter et al.,⁹¹ the real power of the local sensitivity analysis technique resides in the further

manipulation of the sensitivity coefficients to obtain new “derived” sensitivities capable of addressing literally any physically meaningful question in the system. These new derived sensitivities provide a quantitative guide and analytical tool for an intrusive analysis of the complex kinetic interactions among reactions and among species.

In the Green’s function method, the coupled first-order ordinary differential equations for describing a chemical kinetic system reacting under isothermal conditions without spatial transport [Eq. (2-136)] may be written as

$$\frac{dC_i}{dt} = f_i(\mathbf{C}, \boldsymbol{\alpha}), \quad C_i(t=0) \equiv C_{i,0} \quad (2-150)$$

where f_i is the usual nonlinear first-order, second-order, or third-order function of the species concentrations. The parameter vector $\boldsymbol{\alpha}$ includes all physically definable input parameters of interest, all of which are treated as constant.

Equation (2-150) may be differentiated with respect to the parameter α_j to yield the following set of linear coupled equations in terms of the desired linear sensitivity coefficients, $\partial C_i / \partial \alpha_j$:

$$\frac{\partial^2 C_i}{\partial t \partial \alpha_j} = \frac{\partial f_i}{\partial \alpha_j} + \sum_s \frac{\partial f_i}{\partial C_s} \frac{\partial C_s}{\partial \alpha_j} \quad (2-151)$$

This set of equations is solved in closed form to give the result⁹³

$$\frac{\partial \mathbf{C}}{\partial \alpha_j} = G(t, 0) \left[\frac{\partial \mathbf{C}}{\partial \alpha_j} \right]_0 + \int_0^t G(t, t') \left(\frac{\partial \mathbf{f}(t')}{\partial \alpha_j} \right) dt' \quad (2-152)$$

where Green’s function satisfies the following linear ODE:

$$\left[\frac{\partial}{\partial t} - J(t) \right] G(t, t') = 0, \quad t > t' \quad \text{and} \quad G(t', t') = 1 \quad (2-153)$$

where $J(t)$ is the $n \times n$ Jacobian matrix with elements $\partial f_i / \partial C_j$. The governing equations for second-order sensitivities are obtained by taking consecutive derivatives of Eq. (2-150) with respect to the input parameters α_j . The solutions of these equations are again obtained by the Green’s function technique.⁹³ One of the reasons to use Green’s function technique for solution is due to the fact that the original nonlinear differential equations are replaced by a combined linear ODE and an integral equation, which are generally more convenient to solve.

The initial conditions for Eq. (2-151) result from mathematical considerations versus physical considerations for Eq. (2-150). Here, the initial condition $(\partial C_i / \partial \alpha_j)_0$ is the zero vector, unless α_j is the initial concentration of the i th species, in which case the initial condition is a vector whose components are all zero except the i th component, which has the value 1. The kinetic equations can be solved by the stiff ODE solver code (LSODE) of Hindmarsh,¹¹¹ and the sensitivity equations by the Green’s function code (SENSIT) with AIM of Kramer et al.¹¹²

It is important to recognize that the Green's function matrix itself has an important physical interpretation. In particular, elements of the Green's function matrix may be identified as the gradients¹¹³

$$G_{ij} = \frac{\partial C_i(t)}{\partial C_j(t')}, \quad t' \leq t$$

These terms may be directly interpreted as "memory functions" in that each term represents the sensitivity of species i at time t with respect to variations of species j at prior time t' . The result is a very detailed probe for the operational mechanistic pathways of a complex chemical system. Perturbations of the chemical species can be introduced at varying times t' , and the subsequent response at later times can be studied to deduce mechanistic information.

The Green's function coefficients are, in principle, the *only* sensitivity coefficients directly measurable in the laboratory, and thus, unexpected behavioral traits as indicated by these response functions can be experimentally investigated. For instance, the response of hydroxyl radicals to a small source of molecular hydrogen can be examined. Figure 2.20 shows that when H_2 is perturbed between 0

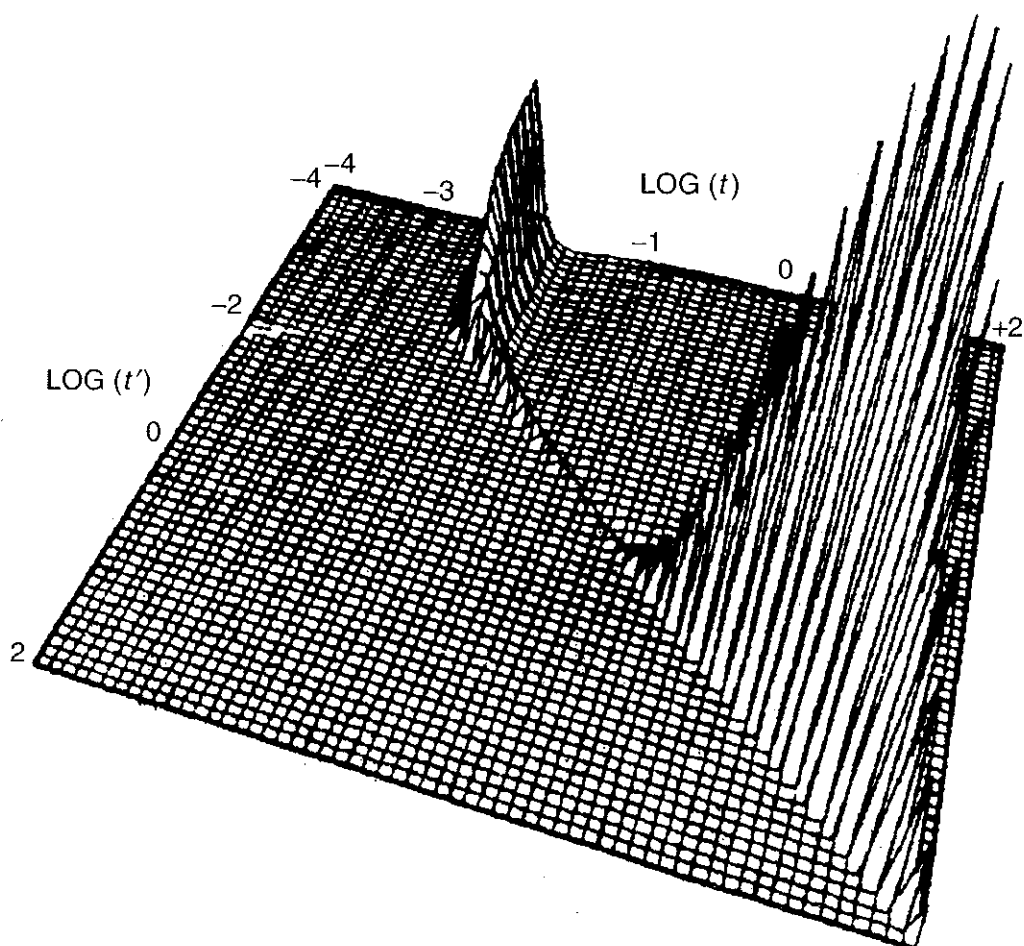


Figure 2.20 Green's function coefficient, $\partial C_{OH}(t)/\partial C_{H_2}(t')$, versus $\log_{10}(t')$ and $\log_{10}(t)$. The minimum and maximum values of $\partial C_{OH}(t)/\partial C_{H_2}(t')$ are -0.03 and 0.7, respectively (after Yetter et al.⁹¹).

and 10 ms or between 0.5 and 100 s, the OH radical concentration is disturbed at some later time. The later response in OH is significantly different from the earlier response in that it resides for a considerably longer period. That is, the H₂ is not directly converted to H₂O but exists in part as OH for a lengthy period of time prior to formation of H₂O. This results primarily from the equilibration of reactions H + H₂O ⇌ OH + H₂.

11.2.2 The Procedure for Steady-State One-Dimensional

Problems^{114,115} The governing equations for steady-state one-dimensional problems are

$$\frac{\partial T}{\partial t} = -u \frac{\partial T}{\partial x} + \frac{1}{\rho C_p} \frac{\partial}{\partial x} \left(\rho \lambda \frac{\partial T}{\partial x} \right) - \frac{\sum \dot{\omega}_i h_i M_w i}{\rho C_p} = 0 \quad (2-154)$$

$$\frac{\partial Y_i}{\partial t} = -u \frac{\partial Y_i}{\partial x} + \frac{1}{\rho} \frac{\partial}{\partial x} \left(\rho D_i \frac{\partial Y_i}{\partial x} \right) + \frac{\dot{\omega}_i}{\rho} = 0 \quad (2-155)$$

with boundary conditions

$$\nabla \mathbf{Y}|_{xL, xR} = 0 \quad \text{and} \quad \nabla T|_{xL, xR} = 0$$

The above equations can be written as

$$F_l(\Phi; \mathbf{K}) = 0 \quad l = 1, 2, \dots, N, N+1 \quad (2-156)$$

with $\Phi = (Y_1, \dots, Y_N, T)$ and $\mathbf{K} = (k_1, k_2, \dots, k_M)$. The method of Newton iteration can be used here to obtain the sensitivity coefficients. The Newton iteration can be carried out as follows:

$$\frac{\partial F_l(\Phi)}{\partial \Phi_i} (\Phi_i^{n+1} - \Phi_i^n) = 0 - F_l(\Phi_i^n); \quad n = \text{iteration parameter} \quad (2-157)$$

To perform sensitivity analysis, differentiation of Eq. (2-154) gives

$$\frac{\partial F_l}{\partial \Phi_i} \frac{\partial \Phi_i}{\partial k_j} + \frac{\partial F_l}{\partial k_j} = 0 \quad (2-158)$$

The Jacobian matrix $\frac{\partial F_l}{\partial \Phi_i}$ is already known from the Newton iteration. The derivatives of the residuum \mathbf{F} with respect to the parameter k_j can be determined numerically. The finite difference methods can be used to discretize the above equations in the x direction and reduce the given problem to the solution of a linear equation system. Solution of this linear equation system leads to sensitivities $\partial \Phi_i / \partial k_j$ or the relative sensitivities $\partial(\ln \Phi_i) / \partial(\ln k_j)$.

11.2.3 The Procedure for Time-Dependent Spatial Problems¹¹⁶ For transient spatial problems, the species and energy equations can be written as

$$\frac{\partial \Phi}{\partial t} = \mathbf{f}[\Phi(t), \mathbf{K}] \quad (2-159)$$

with $\Phi = (Y_1, \dots, Y_N, T)$ and $\mathbf{K} = (k_1, k_2, \dots, k_M)$. Starting from the initial point $t = 0$, we desire a numerical solution of (2-159) at time levels $0 = t^0 < t^1 < \dots < t^L$. Then, upon employing a backward time discretization, the equation can be written in the form

$$\mathbf{f}(\Phi^{n+1}, \mathbf{K}) = \frac{\Phi^{n+1} - \Phi^n}{\Delta t} \quad (2-160)$$

where $\Phi^n = \Phi(t^n, \mathbf{K})$ and $\Delta t = t^{n+1} - t^n$. Eq. (2-160) can also be written as

$$\mathbf{F}(\Phi^{n+1}, \Phi^n; \mathbf{K}) \equiv \mathbf{f}(\Phi^{n+1}; \mathbf{K}) - \frac{(\Phi^{n+1} - \Phi^n)}{\Delta t} = 0 \quad (2-161)$$

We can solve Eq. (2-161) using Newton's method. Thus, we write

$$\left[\mathbf{J}(\Phi_k^{n+1}) - \frac{\mathbf{I}}{\Delta t^{n+1}} \right] (\Phi_{k+1}^{n+1} - \Phi_k^{n+1}) = -\lambda_k^{n+1} [0 - \mathbf{F}(\Phi_k^{n+1}, \Phi^n; \mathbf{K})] \quad (2-162)$$

where Φ_k^{n+1} denotes the k th solution iterate, λ_k^{n+1} is the k th damping parameter ($0 < \lambda < 1$), \mathbf{I} is the identity matrix, and

$$\mathbf{J}(\Phi_k^{n+1}) \equiv \frac{\partial \mathbf{f}(\Phi_k^{n+1}; \mathbf{K})}{\partial \Phi_k^{n+1}}$$

is the Jacobian matrix.

At the $(n + 1)$ th time level, we differentiate Eq. (2-161) with respect to k_j , we have

$$\frac{d}{dk_j} \mathbf{F}(\Phi^{n+1}, \Phi^n; \mathbf{K}) = \frac{\partial \mathbf{F}}{\partial \Phi^{n+1}} \frac{\partial \Phi^{n+1}}{\partial k_j} + \frac{\partial \mathbf{F}}{\partial \Phi^n} \frac{\partial \Phi^n}{\partial k_j} + \frac{\partial \mathbf{F}}{\partial k_j} = 0 \quad (2-163)$$

Recalling the forms of Eq. (2-161) and noting that $\frac{\partial \mathbf{F}}{\partial \Phi^n} = \frac{\mathbf{I}}{\Delta t^{n+1}}$, we can rewrite Eq. (2-163) in the form

$$\left[\mathbf{J}(\Phi_k^{n+1}) - \frac{\mathbf{I}}{\Delta t^{n+1}} \right] \frac{\partial \Phi^{n+1}}{\partial k_j} = - \left(\frac{\partial \mathbf{F}}{\partial k_j} + \frac{\mathbf{I}}{\Delta t^{n+1}} \frac{\partial \Phi^n}{\partial k_j} \right) \quad (2-164)$$

The Jacobian matrix $\mathbf{J}(\Phi_k^{n+1})$ and sensitivity coefficients $\partial \Phi^n / \partial k_j$ are already known from the Newton iteration at the n th time level. The derivatives of the

residuum \mathbf{F} with respect to the parameter k_j can be determined. The finite difference methods can also be used to discretize the above equations in the x direction and reduce the given problem to the solution of a linear equation system at each time step. Solution of this linear equation system leads to sensitivities $\partial\Phi/\partial k_j$ or the relative sensitivities $\partial(\ln \Phi)/\partial(\ln k_j)$ at each time step.

11.3 The Example of Sensitivity Analysis of Aliphatic Hydrocarbon Combustion

11.3.1 Local Sensitivity Analysis in One-Dimensional Flame Fronts

Nowak and Warnatz¹⁰³ applied the sensitivity analysis to aliphatic hydrocarbon combustion. In their paper, the sensitivity analyses for steady-state one-dimensional problems have been conducted to identify the rate-limiting steps in a reaction system for aliphatic hydrocarbon combustion. Some very useful information was obtained. Figures 2.21a and 2.21b show the results of sensitivity analysis with respect to the flame velocity of stoichiometric CH₄/air and C₃H₈/air flames at atmospheric pressure, respectively. It is clearly shown that the flame velocities are relatively insensitive to reactions related specifically to methane and propane oxidation (see Section 14). However, there is a strong influence of the several elementary reactions involving oxidation of H atoms and CO reaction with OH radicals, i.e., H + O₂ → OH + O, H + O₂ + M → HO₂ + M, and CO + OH → CO₂ + H.

The similar sensitivity results between CH₄/air laminar flame and C₃H₈/air laminar flame are interesting. For both cases, only a few elementary reactions are sensitive, giving nearly the same qualitative results. This implies that some elementary reactions are always rate limiting, independent of the type of fuels considered. The effect of stoichiometric ratio on the relative sensitivity of laminar flame speed of CH₄/air laminar flame is shown in Fig. 2.22. Again, the differences between lean and rich flames are not pronounced. Therefore, the sensitivity spectra are more or less independent of the equivalence ratio of the initial mixture.

In Fig. 2.23, the sensitivity analysis of mass fractions of H and H₂O and T is demonstrated. Based on the calculated results of Nowak and Warnatz,¹⁰³ it is evident that the mass fraction of H atoms is much more sensitive to the rate coefficients of different reactions than the mass fraction of the stable species H₂O and temperature.

11.3.2 Sensitivity Analysis for Zero-Dimensional Problems Figure 2.24 shows the results of a sensitivity analysis by Nehse et al.¹¹⁷ for the OH concentration in an igniting stoichiometric dodecane (C₁₀H₂₂)/air mixture at $p = 13$ bar and a relatively low initial temperature of 800 K. For this zero-dimensional ignition delay problem, sensitivity analysis indicated that the induction time is strongly dependent on many elementary reactions. This dependency is much stronger than those results shown in Figs. 2.21 and 2.22 for stationary laminar flames. Figure 2.24 shows that more reactions are rate limiting.

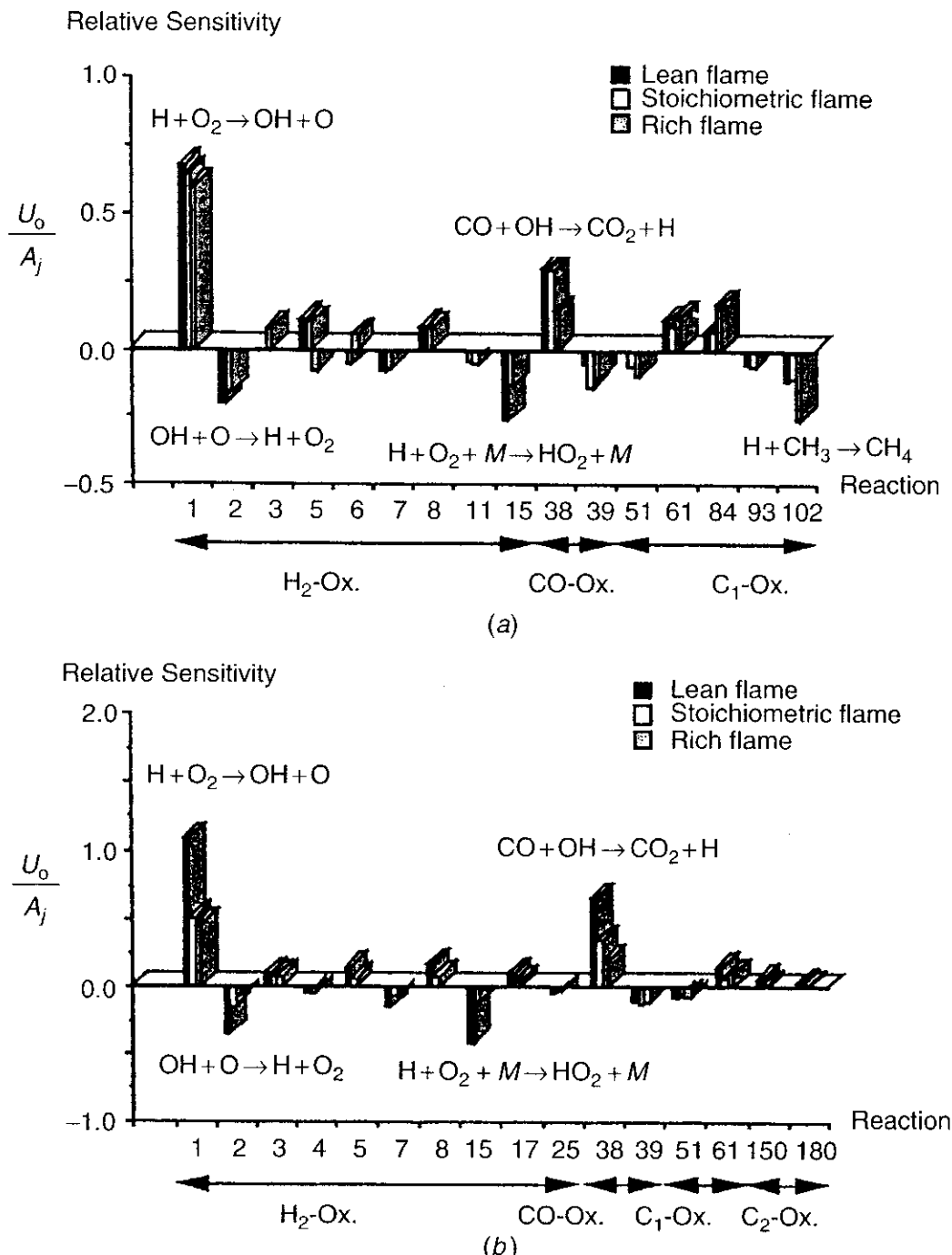


Figure 2.21 (a) Sensitivity analysis for the laminar flame velocity of a stoichiometric methane/air flame at $p = 1$ bar and $T_u = 298$ K. (b) Sensitivity analysis for the laminar flame velocity of a stoichiometric propane/air flame at $p = 1$ bar and $T_u = 298$ K (after Nowak and Warnatz¹⁰³).

12 REACTION FLOW ANALYSIS

In numerical simulations of combustion processes with complex reactions, *reaction flow analysis* can often be very helpful. There are software packages available³⁰ that automatically perform this kind of analysis. Let us consider the percentage of the contributions of different elementary reactions r ($r = 1, \dots, M$) to the formation (or consumption) of the chemical species s ($s = 1, \dots, N$), as shown in Table 2.6.

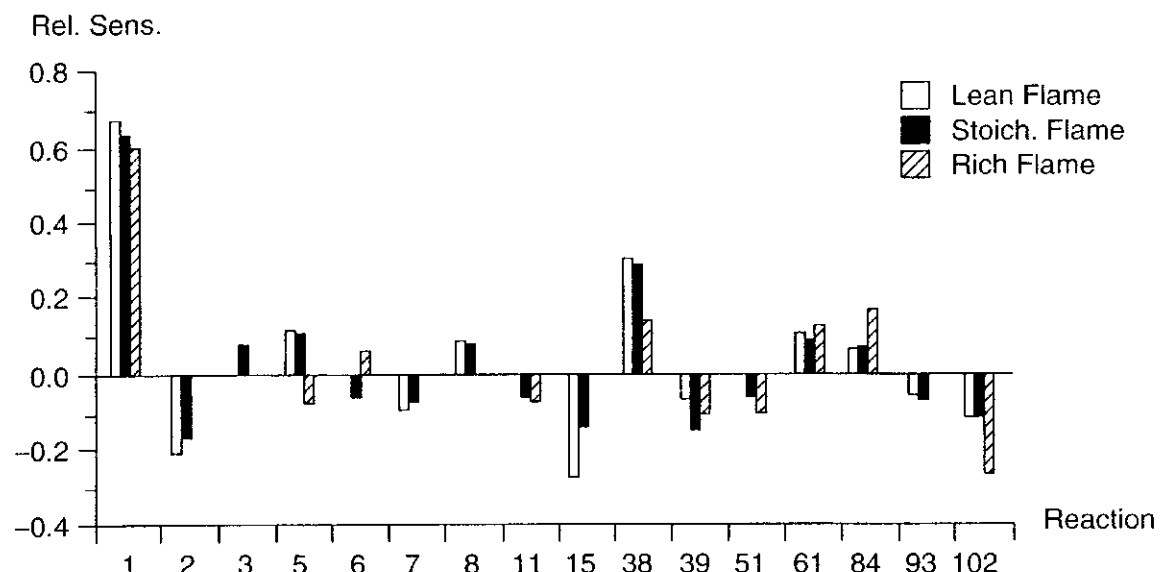


Figure 2.22 Sensitivity analysis of flame velocity V_u for methane/air laminar flame under different equivalence ratios (after Nowak and Warnatz¹⁰³).

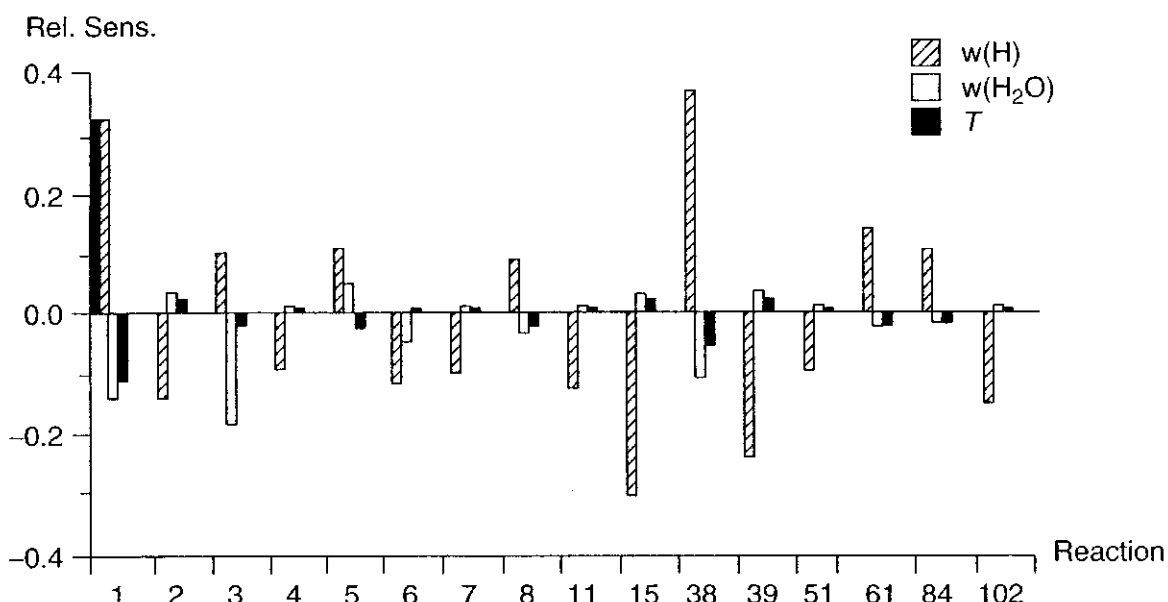


Figure 2.23 Sensitivity of mass fractions of H atoms and water vapor and flame temperature of methane/air laminar flame at $p = 1$ bar and $T_u = 298$ K to reaction rate constants (after Nowak and Warnatz¹⁰³).

In this example, 31.0% of the formation of species 1 can be attributed to reaction 1, 0.1% to reaction 2, 2.9% to reaction 3, and 66% to reaction $M - 1$. The percentages in the columns have to add to 100%. This kind of table allows the construction of highly useful *reaction flow diagrams*. An example of a *reaction flow diagram* is shown in Fig. 2.25.

After obtaining the percentage output of all species for each reaction, an integral reaction flow analysis and a local reaction flow analysis can be performed for the combustion problem. According to Warnatz et al.,³⁰ the *integral reaction*

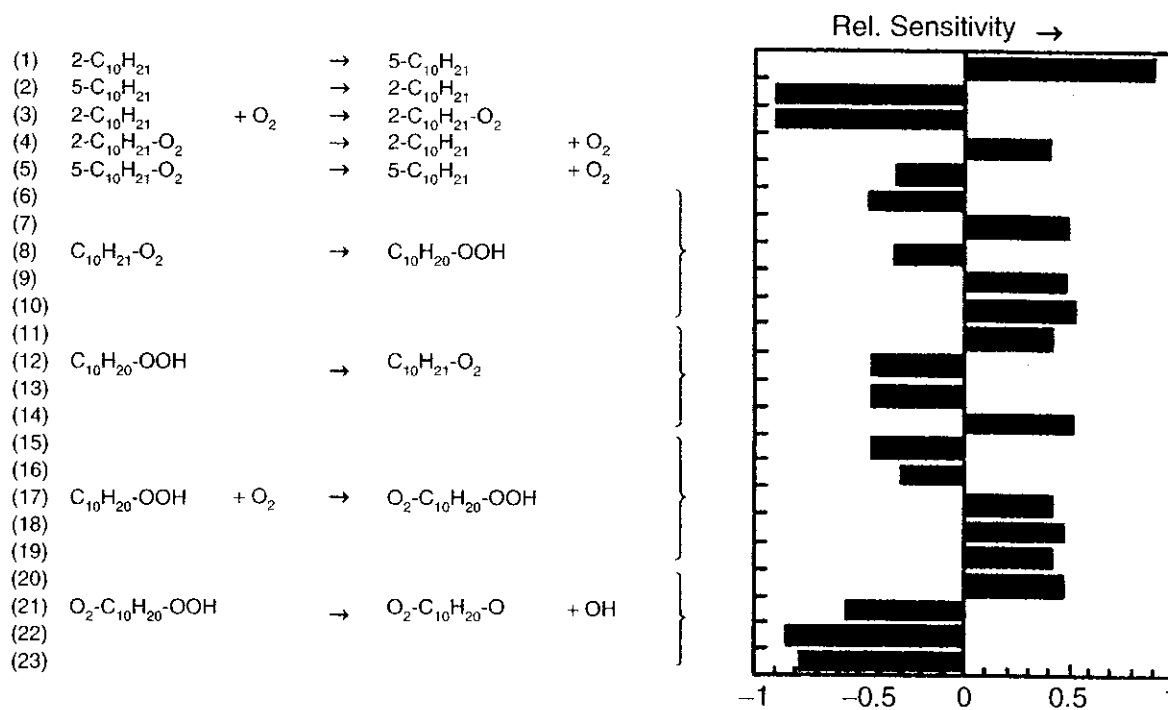


Figure 2.24 Sensitivity analysis for the OH concentration in an igniting stoichiometric $\text{C}_{10}\text{H}_{22}$ /air mixture at $p = 13$ bar and $T_u = 800$ K (after Nehse et al.¹¹⁷).

Table 2.6 Sample Output Percentage of a Reaction Flow Analysis

Reaction Number	Chemical Species					
	1	2	3	...	$N - 1$	N
1	31.0%	2.2%	0%	...	0%	0%
2	0.1%	0%	0%	...	0%	0%
3	2.9%	5.0%	0%	...	80.0%	5.0%
4	0%	0%	2.0%	...	20.0%	92.0%
:	:	:	:	...	:	:
$M - 1$	66.0%	90.4%	98.0%	...	0%	3.0%
M	0%	2.4%	0%	...	0%	0%

flow analysis considers the overall formation or consumption of chemical species during the combustion process. The results for zero-dimension homogeneously mixed time-dependent systems are integrated over the whole reaction time. The results for 1-D stationary flames are integrated over the entire reaction zone. A reaction such as reaction 2 in Table 2.6 can be regarded as unimportant if all entries in a row are below a certain limit, e.g., 1% for the formation as well as for the consumption of chemical species. The *local reaction flow analysis* considers the formation and consumption of species locally, i.e., at specific times in time-dependent problems (e.g., a homogeneous ignition process) or at specific

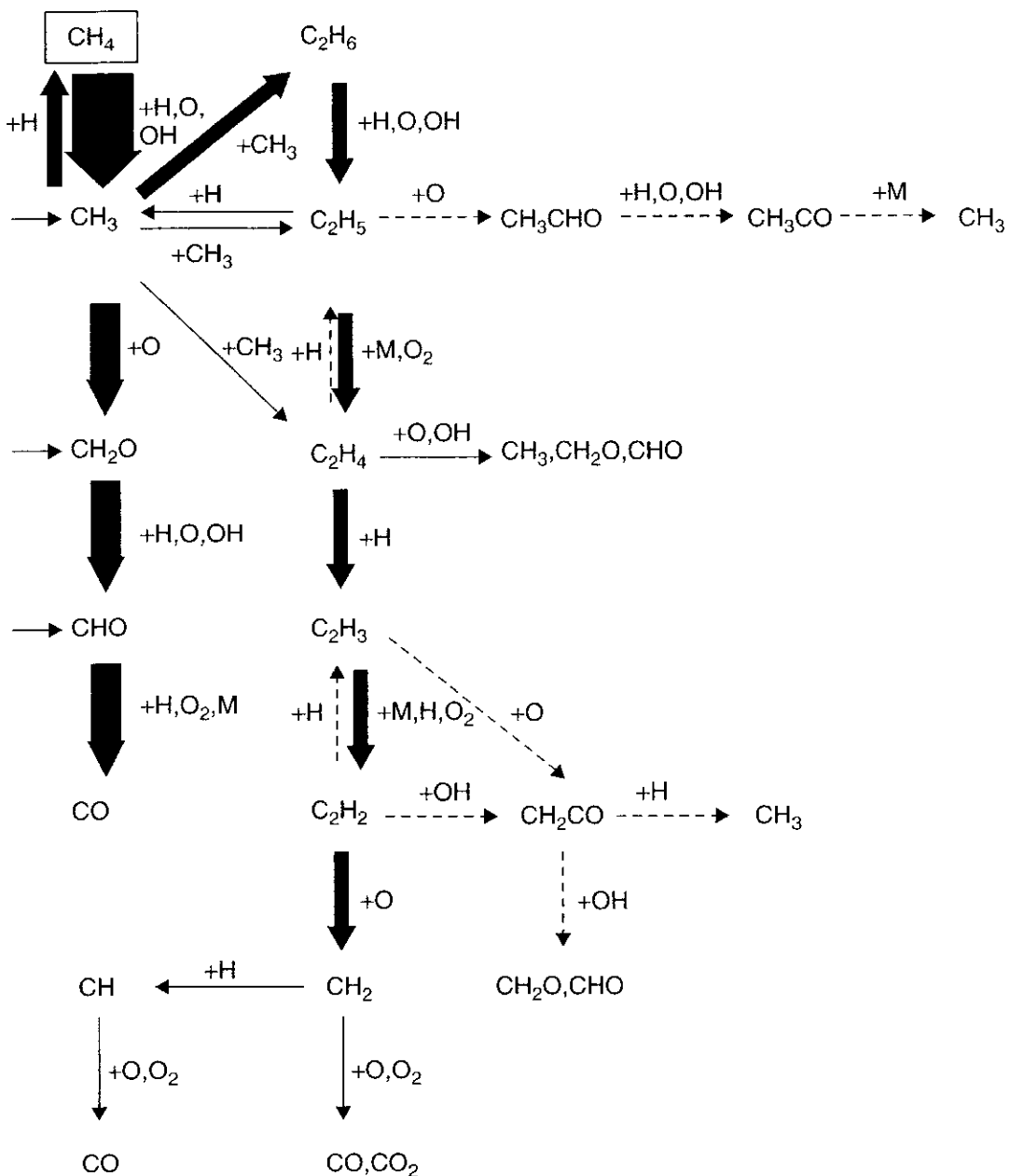


Figure 2.25 Integral reaction flow analysis in a premixed stoichiometric CH_4 /air flame at $p = 1$ bar and $T_u = 298 \text{ K}$ (after Warnatz¹¹⁸).

locations in steady processes (e.g., a flat flame). According to the local analysis, a reaction rate RR is unimportant for all times t or locations x if the reaction rate satisfies the following condition:

$$|\text{RR}_{t,r,s}| < \varepsilon |\text{Max}_{r=1,2,\dots,M} \text{RR}_{t,r,s}| \quad s = 1, 2, \dots, N, \quad t = 0, \dots, t_{\text{total}} \quad (2-165)$$

This is a much stricter requirement than in the case of integral analysis. In the above equation, ε is a limit that has to be specified arbitrarily, e.g., $\varepsilon = 1\%$.

Figure 2.25 shows integral reaction flow analysis in premixed stoichiometric methane/air flame.¹¹⁸ A different result for the premixed rich methane/air flame was also obtained by Warnatz¹¹⁸ and is shown in Fig. 2.26. It is obvious that

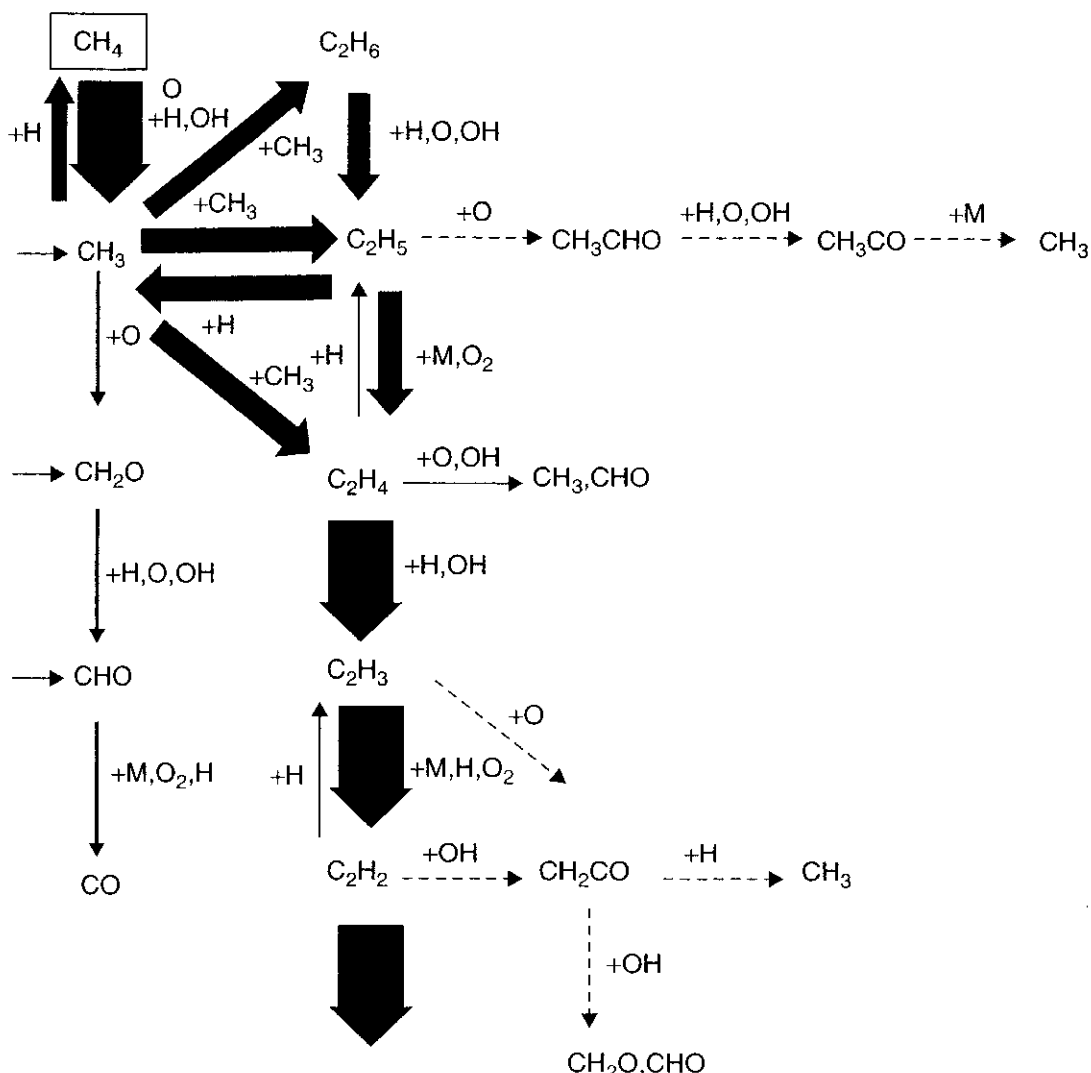


Figure 2.26 Integral reaction flow analysis in a premixed rich CH₄/air flame at $p = 1$ bar and $T_u = 298$ K (after Warnatz¹¹⁸); the analysis of acetylene is left out due to its complexity.

different reaction paths are followed, depending on the value of the equivalence ratio, even though the chemical mechanism is the same. In the stoichiometric flame, CH₄ is mainly oxidized directly, whereas methyl radicals in the rich flame recombine to form ethane (C₂H₆), which is then oxidized. Therefore, one can find the rather surprising requirement that a satisfactory mechanism for methane oxidation also demands an additional mechanism for ethane oxidation.³⁰

13 REACTION MECHANISMS OF H₂/O₂ SYSTEMS

The hydrogen/oxygen combustion systems have many attractive features, including high specific impulse (defined as the thrust per unit bipropellant weight flow rate) for rocket propulsion applications, clean-burning feature for achieving environmentally friendly combustion products, reliable ignition, and high combustion efficiency. Even though there are only two elements involved, the chemical reaction mechanisms of H₂/O₂ systems are quite complex, involving

various steps of chain reactions such as initiation, chain-propagating, and chain-branching reactions as well as chain-termination reactions. As discussed in a later section, hydrogen/oxygen reactions also play an important role in the oxidation of hydrocarbons. It is essential to understand different reaction mechanisms that have been developed under various conditions. In the following subsections, some observed phenomena of H₂/O₂ systems are reported. Different examples are shown here to illustrate how researchers proceed from a full chemistry system to a reduced number of equations to explain why emphasis is given to some particular reactions rather than others. Later, the explosion limits of this mixture are explained to underline some basic mechanisms.

13.1 Background Information about H₂/O₂ Reaction Systems

Several features of H₂/O₂ reactions are introduced here as background information. It is known that the dissociation energy of H₂ is less than that of O₂. This is why the initiation reactions are related to hydrogen dissociation and H atom generation steps. The maximum flame temperature of H₂/air reaction is around 2400 K, and maximum T_f of H₂/O₂ flame is around 3100 K. Dougherty and Rabitz¹¹⁹ modeled H₂/O₂ combustion over a wide range of temperature and pressure using nine chemical species (H₂, O₂, H₂O, OH, O, H, HO₂, H₂O₂, and O₃) and 72 reactions (see Table 2.7). Their calculations correctly predicted the explosion limit peninsula (to be discussed later) in the 650–850 K temperature range and the 1–103 Torr pressure range in addition to rank ordering quantitatively the importance of different reactions in the neighborhood of each explosion limit. Dougherty and Rabitz¹¹⁹ also considered a 47-reaction mechanism with nine species for studying oscillatory combustion phenomena of H₂/O₂ systems. To include many detailed aspects of kinetics in the simulation of combustion processes and to achieve better understanding of the complex reaction processes and to facilitate computation, we shall first discuss some basic reaction steps involved in the H₂/O₂ systems and then address different reduced models of reactions. These reduced models have been developed to determine which reactions and which species are necessary to predict the behavior of the system with high accuracy. According to Glassman,² the oxidation of H₂ can be divided into many groups of reactions (see also Turns⁴⁴). The initiation reactions are

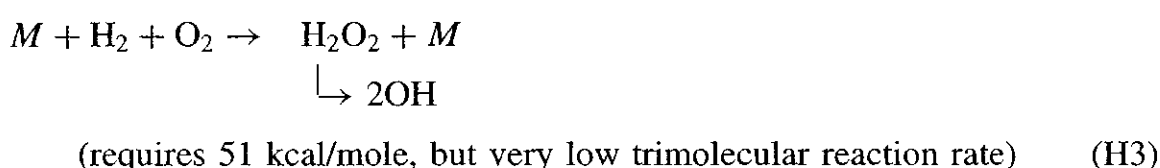
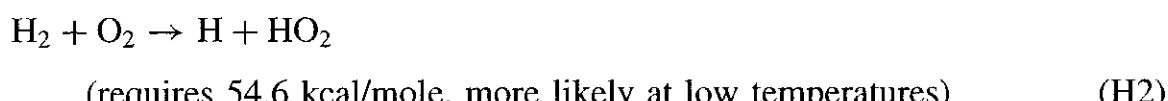


Table 2.7 H₂/O₂ Reaction Mechanism and Rate Data Considered by Dougherty and Rabitz¹¹⁹ [Reaction Set for H₂/O₂ Calculations: $k_i = A_i T^B / \exp(-C_i/T)$]

Reaction Number	Reaction ^b	A_i	B_i	C_i	$\Delta \log_{10} k_i^c$	References ^d
1	$2\text{H} + M \rightarrow \text{H}_2 + M,$ $M = \text{Ar}, \text{N}_2$	9.0(17)	-1.00		0.3	17, 29
2*	$\text{H} + \text{HO}_2 \rightarrow \text{H}_2 + \text{O}_2$	2.5(13)		350	0.8	29, 30, 31
3*	$\text{H} + \text{HO}_2 \rightarrow \text{H}_2\text{O} + \text{O}$	5.0(13)		500	1.0	32, 33
4*	$\text{H} + \text{HO}_2 \rightarrow 2\text{OH}$	2.5(14)		950	1.0	32
5	$\text{H} + \text{HO}_2 \rightarrow \text{H}_2 + \text{OH}$	1.4(14)	-0.03	10,200	0.1	29, 34
6*	$\text{H} + \text{H}_2\text{O}_2 \rightarrow \text{H}_2 + \text{HO}_2$	1.7(12)		1,900	0.8	29
7*	$\text{H} + \text{H}_2\text{O}_2 \rightarrow \text{H}_2\text{O} + \text{OH}$	5.0(14)		5,000	0.4	29, 35, 36
8	$\text{H} + \text{O} + M \rightarrow \text{OH} + M,$ $M = \text{Ar}, \text{N}_2$	7.9(15)			1.2	37
9	$\text{H} + \text{OH} \rightarrow \text{H}_2 + \text{O}$	8.3(9)	1.00	5,500	0.2	29, 38
10	$\text{H} + \text{OH} + M \rightarrow \text{H}_2\text{O} + M,$ $M = \text{Ar}$	8.4(21)	-2.00		1.5	29
10a	$\text{H} + \text{OH} + M \rightarrow \text{H}_2\text{O} + M,$ $M = \text{N}_2$	2.2(22)	-2.00		1.5	29
11*	$\text{H} + \text{O}_2 \rightarrow \text{OH} + \text{O}$	2.3(14)		8,400	0.2	39
12*	$\text{H} + \text{O}_2 + M \rightarrow \text{HO}_2 + M,$ $M = \text{Ar}$	2.1(18)	-1.00		0.4	40
12a	$\text{H} + \text{O}_2 + M \rightarrow \text{HO}_2 + M,$ $M = \text{N}_2$	3.0(18)	-1.00		0.4	40
13*	$2\text{HO}_2 \rightarrow \text{H}_2\text{O}_2 + \text{O}_2$	1.8(13)		500	1.0	41
14*	$\text{H}_2 + \text{HO}_2 \rightarrow \text{H}_2\text{O}_2 + \text{H}$	6.0(11)		9,300	0.6	29
15	$\text{HO}_2 + \text{H}_2\text{O} \rightarrow \text{H}_2\text{O}_2 + \text{OH}$	1.8(13)		15,100	0.4	42
16	$\text{OH} + \text{HO}_2 \rightarrow \text{H}_2\text{O} + \text{O}_2$	5.0(13)		500	0.5	32
17	$\text{OH} + \text{HO}_2 \rightarrow \text{H}_2\text{O}_2 + \text{O}$	5.2(10)	0.50	10,600	2.0	43
18	$\text{HO}_2 + M \rightarrow \text{H} + \text{O}_2 + M,$ $M = \text{Ar}$	2.1(15)		23,000	0.2	29
18a	$\text{HO}_2 + M \rightarrow \text{H} + \text{O}_2 + M,$ $M = \text{N}_2$	2.8(15)		23,000	0.2	29
19	$\text{HO}_2 + M \rightarrow \text{O} + \text{OH} + M,$ $M = \text{Ar}, \text{N}_2$	6.8(19)	-0.43	32,200	2.0	34, 44
20*	$\text{H}_2 + \text{O} \rightarrow \text{H} + \text{OH}$	1.8(10)	1.00	4,480	0.2	29, 45
21	$\text{O} + \text{H}_2\text{O} \rightarrow \text{H} + \text{NO}_2$	4.8(14)	0.45	28,700	2.0	32, 34
22	$\text{O} + \text{H}_2\text{O} \rightarrow 2\text{OH}$	5.8(13)		9,070	0.4	46, 47
23*	$\text{O} + \text{H}_2\text{O}_2 \rightarrow \text{OH} + \text{HO}_2$	2.0(13)		2,950	1.0	48, 49
24	$\text{O} + \text{OH} \rightarrow \text{H} + \text{O}_2$	3.0(12)	0.028		1.0	29, 34, 49
25	$\text{O} + \text{OH} + M \rightarrow \text{HO}_2 + M,$ $M = \text{Ar}, \text{N}_2$	8.0(16)			2.0	34, 44, 50
26*	$\text{H}_2 + \text{OH} \rightarrow \text{H}_2\text{O} + \text{H}$	2.5(13)		2,600	0.1	51, 52, 53
27	$\text{H}_2\text{O} + \text{OH} \rightarrow \text{H}_2\text{O}_2 + \text{H}$	2.4(14)		40,500	1.2	29
28*	$\text{OH} + \text{H}_2\text{O}_2 \rightarrow \text{H}_2\text{O} + \text{HO}_2$	1.0(13)		910	0.3	29
29	$2\text{OH} \rightarrow \text{H} + \text{HO}_2$	1.2(13)		20,200	0.8	29
30	$2\text{OH} \rightarrow \text{H}_2 + \text{O}_2$	1.7(13)		24,100	0.8	54
31	$2\text{OH} \rightarrow \text{H}_2\text{O} + \text{O}$	6.3(12)		550	0.4	29
32	$2\text{OH} + M \rightarrow \text{H}_2\text{O}_2 + M,$ $M = \text{Ar}$	2.7(14)		-2,650	0.8	51

(continued overleaf)

Table 2.7 (continued)

Reaction Number	Reaction ^b	A_i	B_i	C_i	$\Delta \log_{10} k_i^c$	References ^d
32a	$2\text{OH} + M \rightarrow \text{H}_2\text{O}_2 + M,$ $M = \text{N}_2$	8.4(14)		-2,650	0.8	29, 51
33	$\text{OH} + M \rightarrow \text{O} + \text{OH} + M,$ $M = \text{Ar}, \text{N}_2$	6.1(15)		51,100	1.5	34, 37
34	$\text{H}_2 + \text{O}_2 \rightarrow \text{H} + \text{HO}_2$	3.1(13)		28,700	0.9	55
35	$\text{H}_2 + \text{O}_2 \rightarrow 2\text{OH}$	1.7(15)		24,200	1.2	54, 56
36	$\text{H}_2\text{O} + \text{O}_2 \rightarrow \text{OH} + \text{HO}_2$	5.6(13)	0.17	36,600	1.5	32, 34
37	$\text{H}_2\text{O}_2 + \text{O}_2 \rightarrow 2\text{HO}_2$	3.0(13)		21,600	1.0	29, 55
38	$\text{H}_2 + M \rightarrow 2\text{H} + M,$ $M = \text{Ar}, \text{N}_2$	2.2(14)		48,300	0.8	17, 29
39	$\text{H}_2\text{O} + M \rightarrow \text{H} + \text{OH} + M,$ $M = \text{Ar}$	4.0(23)	-2.20	59,000	0.6	29, 51, 57
39a	$\text{H}_2\text{O} + M \rightarrow \text{H} + \text{OH} + M,$ $M = \text{N}_2$	1.0(24)	-2.20	59,000	0.6	29, 51, 57
40*	$\text{H}_2\text{O}_2 + M \rightarrow 2\text{OH} + M,$ $M = \text{Ar}$	6.0(16)		22,900	0.3	29
40a	$\text{H}_2\text{O}_2 + M \rightarrow 2\text{OH} + M,$ $M = \text{N}_2$	1.2(17)		22,900	0.3	29
41	$2\text{O} + M \rightarrow \text{O}_2 + M,$ $M = \text{Ar}$	1.9(13)		-900	0.6	58
41a	$2\text{O} + M \rightarrow \text{O}_2 + M,$ $M = \text{N}_2$	6.0(13)		-900	0.6	58
42	$\text{O}_2 + M \rightarrow 2\text{O} + M,$ $M = \text{Ar}$	1.8(18)	-1.00	59,400	0.6	58
42a	$\text{O}_2 + M \rightarrow 2\text{O} + M,$ $M = \text{N}_2$	5.4(18)	-1.00	59,400	0.6	58
43	$\text{O} + \text{HO}_2 \rightarrow \text{O}_2 + \text{OH}$	5.0(13)		500	0.8	32
44	$\text{O}_2 + \text{OH} \rightarrow \text{HO}_2 + \text{O}$	1.3(13)	0.18	28,200	1.2	32, 34
45	$\text{H}_2 + \text{HO}_2 \rightarrow \text{H}_2\text{O} + \text{OH}$	6.5(11)		9,400	1.0	59, 60
46	$\text{H}_2\text{O} + \text{OH} \rightarrow \text{H}_2 + \text{HO}_2$	7.2(9)	0.43	36,100	1.4	34, 59, 60
47*	$\text{O} + \text{H}_2\text{O}_2 \rightarrow \text{H}_2\text{O} + \text{O}_2$	8.4(11)		2,130	1.0	41
48	$\text{H}_2\text{O} + \text{O}_2 \rightarrow \text{H}_2\text{O}_2 + \text{O}$	3.4(10)	0.52	44,800	1.4	42, 56
49	$\text{O} + \text{O}_2 + M \rightarrow \text{O}_3 + M,$ $M = \text{Ar}$	4.3(12)		-1,050	0.6	61
49a	$\text{O} + \text{O}_2 + M \rightarrow \text{O}_3 + M,$ $M = \text{N}_2$	6.9(12)		-1,050	0.6	29, 61
50	$\text{O}_3 + M \rightarrow \text{O} + \text{O}_2 + M,$ $M = \text{Ar}$	2.5(14)		11,400	0.6	58
50a	$\text{O}_3 + M \rightarrow \text{O} + \text{O}_2 + M,$ $M = \text{N}_2$	4.0(14)		11,400	0.6	58
51	$\text{O} + \text{O}_3 \rightarrow 2\text{O}_2$	1.1(13)		2,300	0.4	41
52	$2\text{O}_2 \rightarrow \text{O} + \text{O}_3$	1.2(13)		50,500	0.6	41, 61
53	$\text{H} + \text{O}_3 \rightarrow \text{OH} + \text{O}_2$	2.3(11)	0.75		1.8	62
54	$\text{OH} + \text{O}_2 \rightarrow \text{H} + \text{O}_3$	4.4(7)	1.44	38,600	2.0	56, 62
55	$\text{OH} + \text{O}_3 \rightarrow \text{HO}_2 + \text{O}_2$	9.6(11)		1,000	0.6	41
56	$\text{HO}_2 + \text{O}_2 \rightarrow \text{OH} + \text{O}_3$	9.0(8)			2.0	27
57	$\text{HO}_2 + \text{O}_3 \rightarrow \text{OH} + 2\text{O}_2$	2.0(10)		1,000	1.0	63

Table 2.7 (continued)

Reaction Number	Reaction ^b	A _i	B _i	C _i	Δ log ₁₀ k _i ^c	References ^d
58 ^f	HO ₂ → wall	1.0(−1)			...	64, 65
58	H ₂ O ₂ → wall	1.0(−2)			...	64, 65
60	H → wall	3.0(0)			...	64, 65
61	O → wall	1.7(1)			...	64, 65
62	OH → wall	1.7(1)			...	64, 65

^aTemperature range: 300–2500 K. Units are in terms of moles, cm³, s, and K. Numbers in parentheses denote powers of 10. Missing entries are all zero. Some of the table entries correspond to pairs of forward and reverse reactions. In these cases, both rate constants are considered as parameters rather than invoking thermodynamic reversibility arguments.

^bM denotes all other species present as third bodies. The numerical values for the third-order reactions here are for M = Ar or N₂. We took numerical values for the A_i's for M = H, H₂, etc. to be 1.6 times those shown for the case where M = Ar. Reference 29 was used as a guide for assigning these third-body efficiencies.

^cOnly rough estimates of the rate constant uncertainties are given.

^dIn several cases, the authors made slight modifications to the numerical values of the rate constant parameters given in the references. Often a compromise was reached. This explains the reason for two or three citations for a single elementary step.

^eThe reaction numbers marked with an asterisk (*) are those of the Baldwin et al. reaction set of Ref. 27.

^fThe wall reaction rate constants (58–62) are for 4-cm spherical vessels coated with boric acid. No estimates of uncertainty are given, as the values of the parameters depend critically on many factors (see text).

Chain-reaction steps involving O, H, and OH radicals are

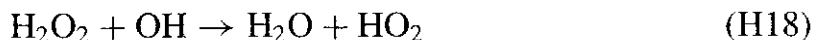
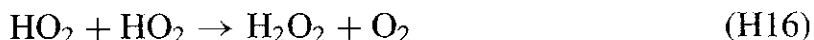


Chain-terminating steps involving O, H, and OH radicals are the three-body recombination reactions:



When the HO₂, hydroperoxyl radical and H₂O₂ species are considered in the reaction mechanism, many other elementary reactions must be included. Some of these reactions are given below.





Depending on the temperature and pressure condition of the system, many elementary reactions may be required for modeling the combustion processes of various H_2/O_2 systems. Next, we shall consider the explosion limits of a stoichiometric H_2/O_2 system.

13.2 Explosion Limits of H_2/O_2 Systems

It is experimentally observed that a pressure vessel containing hydrogen and oxygen under certain conditions can explode as the pressure is raised. Intuitively, one would assume that as the pressure is raised, the concentration of free radicals would be increased, which would lead to an explosion. However, an explosion is also experimentally observed as the pressure is lowered from a certain level. The existence of explosion limits in a closed vessel can be understood very simply from qualitative considerations of competition between chain-terminating and chain-branching reactions on surfaces and in the gas phase. Typical experimentally determined explosion limits for hydrogen-oxygen mixtures by Lewis and von Elbe²⁶ are plotted schematically in Fig. 2.27.

In Fig. 2.27 the first, or lower, explosion limit occurs at roughly the same pressure over a relatively large temperature range. The lower explosion limit is determined by a balance between the removal of chain carriers on the surface (wall effect) and production of chain carriers by gas-phase reactions. In this low-pressure range, the number of collisions and the rate of production of chain carriers are both low. From Eq. (2-64), we know that

$$\alpha'_{\text{critical}} = (1 + C_1) + \frac{C_2}{C_M} \quad \text{and} \quad C_M \propto p$$

The lower the pressure, the larger the value of $\alpha'_{\text{critical}}$, and hence the smaller the chance for explosion. However, none of the simplified analyses can predict the exact location of the explosion limits; they can only explain the mechanism of reaction in each region.

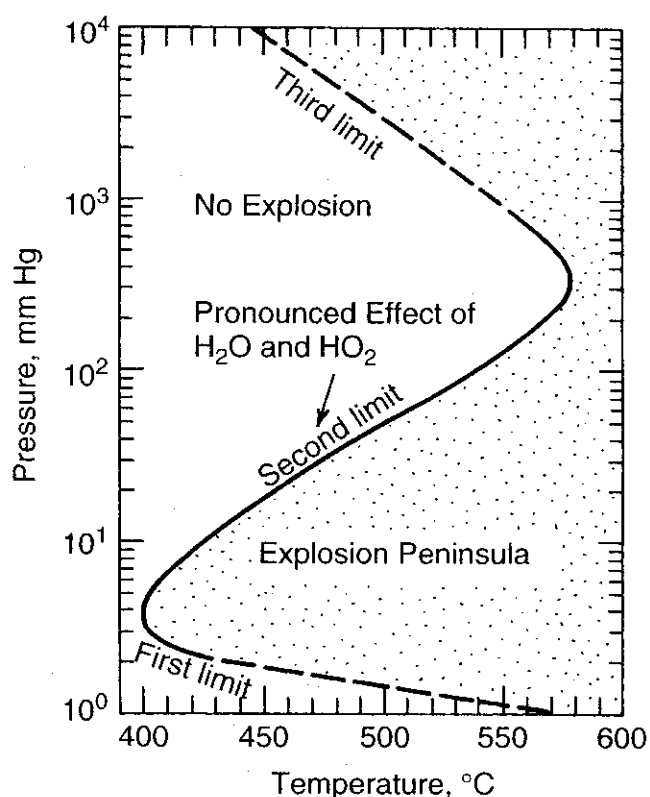


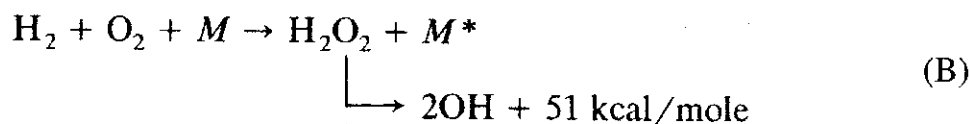
Figure 2.27 Pressure-temperature explosion diagram of a stoichiometric H₂/O₂ mixture in a spherical vessel. First and third limits are partly extrapolated. First limit is subject to erratic changes (after Lewis and von Elbe²⁶).

As the pressure is raised, the rate of production of chain carriers by gas-phase reactions increases to the point at which surface destruction is no longer sufficient to prevent a branching explosion. The first explosion limit thus defines the condition at which chain branching in the gas phase is balanced by chain termination at the surface.

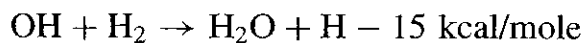
As the pressure is raised from the explosion peninsula, chain branching in the gas phase becomes important. There are two postulations about the reaction kinetics. A number of investigators in the 1920s suggested that the chain initiation reaction for H₂ dissociation started by

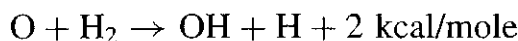
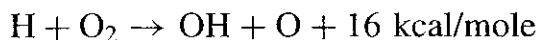


Lewis and von Elbe²⁶ thought that the following reaction is more likely to happen at relatively low initial temperatures:



After the OH radical is generated, many chain propagation reactions can follow:



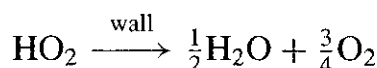
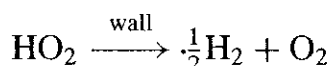


The reaction proposed in (A) is more endothermic than the reaction in (B). However, reaction (B) requires a third-body reaction, which has low reaction rates to introduce OH radicals. Reaction (B) is less endothermic; therefore, it is more likely to happen at relatively low initial temperatures. Conversely, at high temperatures, reaction (A) is more likely to cause the initiation of H atoms and the subsequent explosion.

As the chamber pressure is increased from a given point on the explosion peninsula, the second explosion limit is approached. The existence of the second explosion limit is readily explained if the three-body reaction

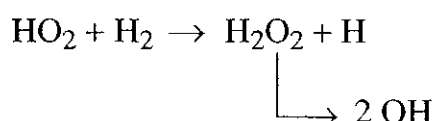


is added to the scheme. In the above elementary reaction, the symbol M denotes any third molecule that stabilizes the combination of H and O_2 . Because the metastable intermediate hydroperoxy molecule (HO_2) is relatively unreactive, it is able to diffuse to the wall. HO_2 becomes a vehicle for the destruction of free valences, and therefore the above reaction can be regarded as a chain-terminating reaction. With increasing pressure, the frequency of ternary collisions $\text{H} + \text{O}_2 + M$ increases relative to the frequency of binary collisions $\text{H} + \text{O}_2$. The destruction of the HO_2 molecule on the wall can be expressed by the reaction



Thus, there exists a particular pressure level above which the rate of removal of free radicals exceeds the rate of formation of free radicals by chain-branching reactions. This explains the existence of the second explosion limit. In the no-explosion region above the peninsula, HO_2 molecules can be assumed to play no part in chain propagation and are destroyed at the wall.

At some pressure levels above the second explosion limit, however, HO_2 can collide and react with H_2 molecules to form H_2O_2 and H atom according to the following reaction; H_2O_2 can dissociate to effectively generate OH radicals to participate in the chain propagation process:



Therefore, when the chamber pressure is at an elevated level, there is a rapid increase in the number of radicals. This pressure level defines the third explosion

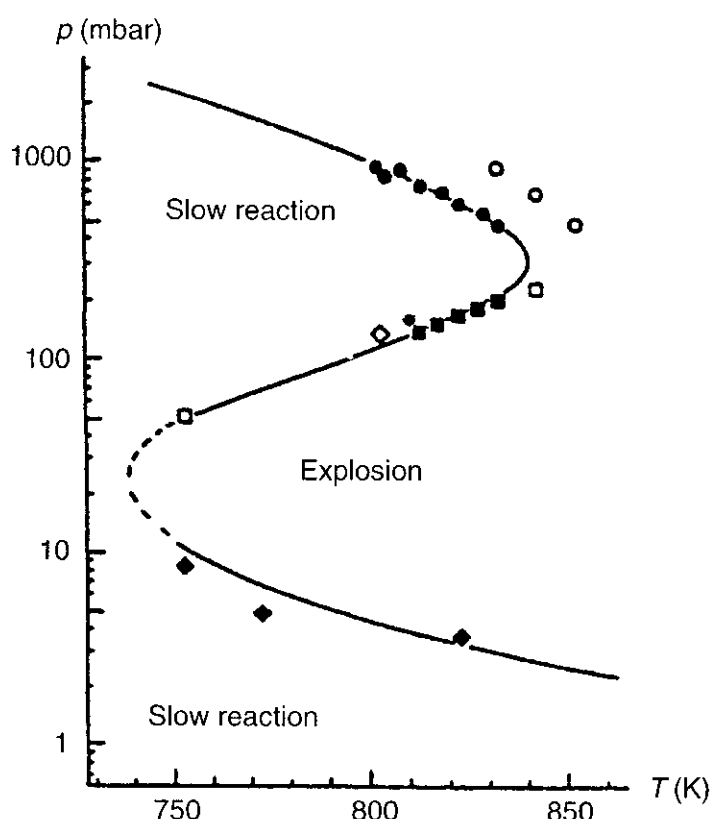


Figure 2.28 Ignition limits in the p - T explosion diagram of H_2/O_2 mixture contained in vessels of different materials: points = experiments, lines = simulations (after Maas and Warnatz¹²⁰).

limit. Another factor worth mentioning is due to the molecular structure similarity between H_2O and HO_2 . Based on their molecular structure similarity, H_2O has a bond frequency very close to that of HO_2 . Therefore, H_2O is an excellent third body for the trimolecular reaction $\text{H} + \text{O}_2 + M \rightarrow \text{HO}_2 + M$. The region for pronounced effect of H_2O and HO_2 is indicated in the explosion-limit diagram. It is useful to note that for $T > 600^\circ\text{C}$, HO_2 cannot be stabilized and therefore explosion is observed at all pressures.

The detailed numerical simulation of the explosion limits of H_2/O_2 system with different vessel materials (e.g., glass, iron, copper, palladium) was conducted by Maas and Warnatz.¹²⁰ They found that different wall materials give different explosion limits. Their calculated ignition limits in the p - T explosion diagram is shown in Fig. 2.28. The treatment of explosion limits in flow systems can be worked out through an extension of the methods developed for closed reaction vessels.

14 GAS-PHASE REACTION MECHANISMS OF ALIPHATIC HYDROCARBON AND OXYGEN SYSTEM

The combustion of a hydrocarbon fuel consists primarily of the sequential fragmentation of the initial fuel molecule into smaller intermediate species, which are ultimately converted to final products, usually dominated by H_2O and CO_2 . In

many cases, these intermediate species can be fuel themselves. For example, ethylene (C_2H_4) is an important intermediate in the combustion of propane (C_3H_8) and other higher hydrocarbons, but ethylene can be a primary fuel. Carbon monoxide (CO) and hydrogen (H_2) are common species observed during the oxidation of all hydrocarbons, and the radical species H, O, OH, HO_2 , HCO , and others are common to all hydrocarbon combustion. A mechanism can be developed systematically, beginning with the simplest species and reactions that are common subelements in the combustion of more complex species, and sequentially constructed by incorporating new species and reactions in order of increasing complexity. An excellent review of kinetic modeling of hydrocarbon combustion was given by Westbrook and Dryer.¹²¹ Detailed discussion of hydrocarbon oxidation kinetics is also given by Warnatz et al.³⁰ The hierarchical structure and overall interrelationships between oxidation mechanisms for simple hydrocarbon fuels constructed by Westbrook and Dryer¹²¹ are shown in Fig. 2.29. The hierarchical structure of the reaction mechanism of aliphatic hydrocarbon combustion shown in Fig. 2.30 was also constructed by Westbrook and Dryer.¹²²

14.1 Specific Mechanisms

As shown in Figs. 2.29 and 2.30, oxidation of H_2 and CO plays a predominant part in the hydrocarbon combustion process. On one hand, the oxyhydrogen reaction mechanism contains the chain-branched steps that produce the O, H, and OH radicals for attacking hydrocarbons. On the other hand, CO is the primary product of hydrocarbon oxidation reactions, and it is converted to CO_2 in subsequent slow secondary reactions. Before discussing small aliphatic hydrocarbon oxidation, we shall first address the gas-phase kinetics of H_2/O_2 and CO oxidation.

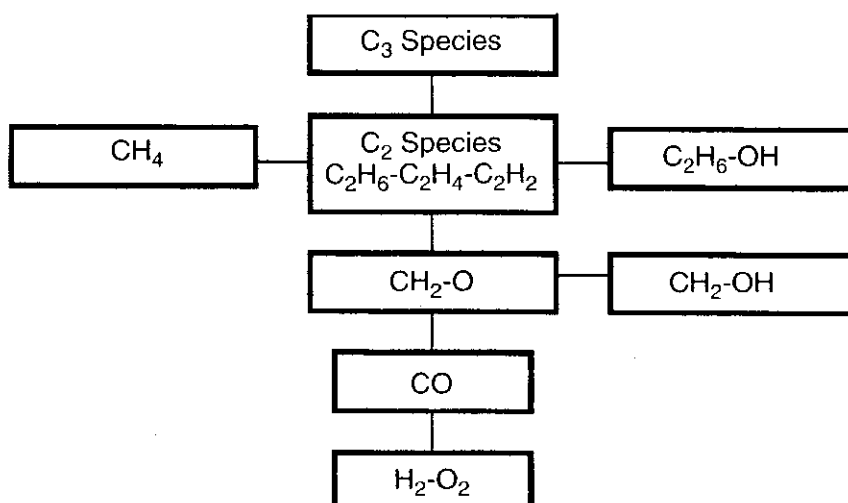


Figure 2.29 Hierarchical structure and overall interrelationships between oxidation mechanisms for simple hydrocarbon fuels (after Westbrook and Dryer¹²¹).

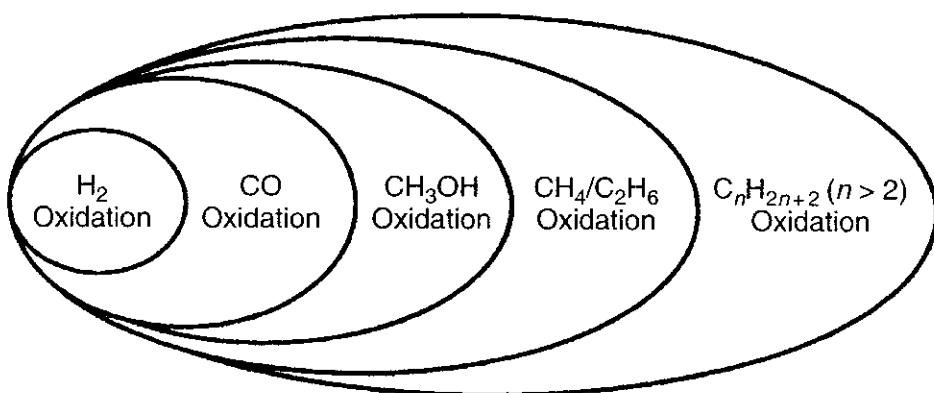


Figure 2.30 Hierarchical structure of the reaction mechanism of aliphatic hydrocarbon combustion (after Westbrook and Dryer¹²²).

14.1.1 Gas-Phase Kinetics of H₂ Oxidation The reaction mechanism of H₂ oxidation is well established by many researchers (e.g., Baulch et al.^{123,124} and Dixon-Lewis and Williams¹²⁵). The reaction mechanism required for hydrogen oxidation is much smaller than for hydrocarbon oxidation (see Table 2.8 given by Warnatz et al.³⁰). H₂-O₂ mechanisms have been used in model simulations of multidimensional chemically reacting flows, chemical kinetic studies, sensitivity analysis, detonations, and ignition problems.

For hydrogen oxidation reactions, the radical species pool is evolved among OH, O, and H by the reactions



The chain-termination reactions and their backward reactions include



where *M* refers to any available third-body species. The reaction (R8) is listed here for completeness of the kinetic mechanism. It is not as important as (R5) through (R7). Reaction (R8_b) is not likely to happen, since OH radical is highly reactive with other species. Also, the bond energy of OH molecule is high to have this dissociation.

Table 2.8 Elementary Reactions in the H₂-CO-C₁-C₂-O₂ System at p = 1 Bar for High Temperatures (T > 1200 K)

Rate coefficients are presented in the form $k = AT^b \exp(E_a/R_u T)$ as described by Eq. (2-5), $C_{M^*} = C_{H_2} + 6.5C_{H_2O} + 0.4C_{O_2} + 0.4C_{N_2} + 0.75C_{CO} + 1.5C_{CO_2} + 3.0C_{CH_4}$. → Only forward reaction is considered =: reverse reaction rate calculated via Eq. (2-123). (After Warnatz et al.³⁰)

Reaction	A (cm, mol, s)	b	E_a (kJ/mol)
<i>01.-04. H₂-CO Oxidation</i>			
<i>01. H₂-O₂ Reactions (HO₂, H₂O₂ not Included)</i>			
$O_2 + H = OH + O$	2.00×10^{14}	0.0	70.3
$H_2 + O = OH + H$	5.06×10^4	2.67	26.3
$H_2 + OH = H_2O + H$	1.00×10^8	1.6	13.8
$OH + OH = H_2O + O$	1.50×10^9	1.14	0.42
$H + H + M^* = H_2 + M^*$	1.80×10^{18}	-1.0	0.00
$O + O + M^* = O_2 + M^*$	2.90×10^{17}	-1.0	0.00
$H + OH + M^* = H_2O + M^*$	2.20×10^{22}	-2.0	0.00
<i>02. HO₂ Formation/Consumption</i>			
$H + O_2 + M^* = HO_2 + M^*$	2.30×10^{18}	-0.8	0.00
$HO_2 + H = OH + OH$	1.50×10^{14}	0.0	4.20
$HO_2 + H = H_2 + O_2$	2.50×10^{13}	0.0	2.90
$HO_2 + H = H_2O + O$	3.00×10^{13}	0.0	7.20
$HO_2 + O = OH + O_2$	1.80×10^{13}	0.0	-1.70
$HO_2 + OH = H_2O + O_2$	6.00×10^{13}	0.0	0.00
<i>03. H₂O₂ Formation/Consumption</i>			
$HO_2 + HO_2 = H_2O_2 + O_2$	2.50×10^{11}	0.0	-5.20
$OH + OH + M^* = H_2O_2 + M^*$	3.25×10^{22}	-2.0	0.00
$H_2O_2 + H = H_2 + HO_2$	1.70×10^{12}	0.0	15.7
$H_2O_2 + H = H_2O + OH$	1.00×10^{13}	0.0	15.0
$H_2O_2 + O = OH + HO_2$	2.80×10^{13}	0.0	26.8
$H_2O_2 + OH = H_2O + HO_2$	5.40×10^{12}	0.0	4.20
<i>04. CO Reactions</i>			
$CO + OH = CO_2 + H$	6.00×10^6	1.5	-3.10
$CO + HO_2 = CO_2 + OH$	1.50×10^{14}	0.0	98.7
$CO + O + M^* = CO_2 + M^*$	7.10×10^{13}	0.0	-19.0
$CO + O_2 = CO_2 + O$	2.50×10^{12}	0.0	200.
<i>10.-19. C₁-Hydrocarbon Oxidation</i>			
<i>10. CH Reactions</i>			
$CH + O = CO + H$	4.00×10^{13}	0.0	0.00
$CH + O_2 = CHO + O$	6.00×10^{13}	0.0	0.00
$CH + CO_2 = CHO + CO$	3.40×10^{12}	0.0	2.90
$CH + H_2O = CH_2O + H$	3.80×10^{12}	0.0	-3.20
$CH + H_2O = ^3CH_2 + OH$	1.90×10^{12}	0.0	-3.20
$CH + OH = CHO + H$	3.00×10^{13}	0.0	0.00

Table 2.8 (continued)

Reaction	A (cm, mol, s)	b	E_a (kJ/mol)
<i>11. CHO Reactions</i>			
$\text{CHO} + M^* = \text{CO} + \text{H} + M^*$	7.10×10^{14}	0.0	70.3
$\text{CHO} + \text{H} = \text{CO} + \text{H}_2$	9.00×10^{13}	0.0	0.00
$\text{CHO} + \text{O} = \text{CO} + \text{OH}$	3.00×10^{13}	0.0	0.00
$\text{CHO} + \text{O} = \text{CO}_2 + \text{H}$	3.00×10^{13}	0.0	0.00
$\text{CHO} + \text{OH} = \text{CO} + \text{H}_2\text{O}$	1.00×10^{14}	0.0	0.00
$\text{CHO} + \text{O}_2 = \text{CO} + \text{HO}_2$	3.00×10^{12}	0.0	0.00
$\text{CHO} + \text{CHO} = \text{CH}_2\text{O} + \text{CO}$	3.00×10^{13}	0.0	0.00
<i>12. CH₂ Reactions^a</i>			
${}^3\text{CH}_2 + \text{H} = \text{CH} + \text{H}_2$	6.00×10^{12}	0.0	-7.50
${}^3\text{CH}_2 + \text{O} \rightarrow \text{CO} + \text{H} + \text{H}$	8.40×10^{12}	0.0	0.00
${}^3\text{CH}_2 + {}^3\text{CH}_2 = \text{C}_2\text{H}_2 + \text{H}_2$	1.20×10^{13}	0.0	3.40
${}^3\text{CH}_2 + {}^3\text{CH}_2 = \text{C}_2\text{H}_2 + \text{H} + \text{H}$	1.10×10^{14}	0.0	3.40
${}^3\text{CH}_2 + \text{CH}_3 = \text{C}_2\text{H}_4 + \text{H}$	4.20×10^{13}	0.0	0.00
${}^3\text{CH}_2 + \text{O}_2 = \text{CO} + \text{OH} + \text{H}$	1.30×10^{13}	0.0	6.20
${}^3\text{CH}_2 + \text{O}_2 = \text{CO}_2 + \text{H}_2$	1.20×10^{13}	0.0	6.20
${}^1\text{CH}_2 + M^* = {}^3\text{CH}_2 + M^*$	1.20×10^{13}	0.0	0.00
${}^1\text{CH}_2 + \text{O}_2 = \text{CO} + \text{OH} + \text{H}$	3.10×10^{13}	0.0	0.00
${}^1\text{CH}_2 + \text{H}_2 = \text{CH}_3 + \text{H}$	7.20×10^{13}	0.0	0.00
${}^1\text{CH}_2 + \text{CH}_3 = \text{C}_2\text{H}_2 + \text{H}$	1.60×10^{13}	0.0	-2.38
<i>13. CH₂O Reactions</i>			
$\text{CH}_2\text{O} + M^* = \text{CHO} + \text{H} + M^*$	5.00×10^{16}	0.0	320
$\text{CH}_2\text{O} + \text{H} = \text{CHO} + \text{H}_2$	2.30×10^{10}	1.05	13.7
$\text{CH}_2\text{O} + \text{O} = \text{CHO} + \text{OH}$	4.15×10^{11}	0.57	11.6
$\text{CH}_2\text{O} + \text{OH} = \text{CHO} + \text{H}_2\text{O}$	3.40×10^9	1.2	-1.90
$\text{CH}_2\text{O} + \text{HO}_2 = \text{CHO} + \text{H}_2\text{O}_2$	3.00×10^{12}	0.0	54.7
$\text{CH}_2\text{O} + \text{CH}_3 = \text{CHO} + \text{CH}_4$	1.00×10^{11}	0.0	25.5
$\text{CH}_2\text{O} + \text{O}_2 = \text{CHO} + \text{HO}_2$	6.00×10^{13}	0.0	171.
<i>14. CH₃ Reactions</i>			
$\text{CH}_3 + M^* = {}^3\text{CH}_2 + \text{H} + M^*$	6.90×10^{14}	0.0	345.
$\text{CH}_3 + M^* = {}^3\text{CH}_2 + \text{H} + M^*$	1.00×10^{16}	0.0	379.
$\text{CH}_3 + \text{O} = \text{CH}_2\text{O} + \text{H}$	8.43×10^{13}	0.0	0.00
$\text{CH}_3 + \text{H} = \text{CH}_4$	1.93×10^{36}	-7.0	38.0
$\text{CH}_3 + \text{OH} \rightarrow \text{CH}_3\text{O} + \text{H}$	2.26×10^{14}	0.0	64.8
$\text{CH}_3\text{O} + \text{H} \rightarrow \text{CH}_3 + \text{OH}$	4.75×10^{16}	-0.13	88.0
$\text{CH}_3 + \text{O}_2 \rightarrow \text{CH}_2\text{O} + \text{OH}$	3.30×10^{11}	0.0	37.4
$\text{CH}_3 + \text{HO}_2 = \text{CH}_3\text{O} + \text{OH}$	1.80×10^{13}	0.0	0.00
$\text{CH}_3 + \text{HO}_2 = \text{CH}_4 + \text{O}_2$	3.60×10^{12}	0.0	0.00
$\text{CH}_3 + \text{CH}_3 \rightarrow \text{C}_2\text{H}_4 + \text{H}_2$	1.00×10^{16}	0.0	134.
$\text{CH}_3 + \text{CH}_3 = \text{C}_2\text{H}_6$	1.69×10^{53}	-12.	81.2

(continued overleaf)

Table 2.8 (continued)

Reaction	<i>A</i> (cm, mol, s)	<i>b</i>	<i>E_a</i> (kJ/mol)
<i>15a. CH₃O Reactions</i>			
CH ₃ O + M* = CH ₂ O + H + M*	5.00 × 10 ¹³	0.0	105.
CH ₃ O + H = CH ₂ O + H ₂	1.80 × 10 ¹³	0.0	0.00
CH ₃ O + O ₂ = CH ₂ O + HO ₂	4.00 × 10 ¹⁰	0.0	8.90
CH ₂ O + CH ₃ O → CHO + CH ₃ OH	6.00 × 10 ¹¹	0.0	13.8
CH ₃ OH + CHO → CH ₂ O + CH ₃ O	6.50 × 10 ⁹	0.0	57.2
CH ₃ O + O = O ₂ + CH ₃	1.10 × 10 ¹³	0.0	0.00
CH ₃ O + O = OH + CH ₂ O	1.40 × 10 ¹²	0.0	0.00
<i>15b. CH₂OH Reactions</i>			
CH ₂ OH + M* = CH ₂ O + H + M*	5.00 × 10 ¹³	0.0	105.
CH ₂ OH + H = CH ₂ O + H ₂	3.00 × 10 ¹³	0.0	0.00
CH ₂ OH + O ₂ = CH ₂ O + HO ₂	1.00 × 10 ¹³	0.0	30.0
<i>16. CH₃O₂ Reactions</i>			
CH ₃ O ₂ + M* → CH ₃ + O ₂ + M*	7.24 × 10 ¹⁶	0.0	111.
CH ₃ + O ₂ + M* → CH ₃ O ₂ + M*	1.41 × 10 ¹⁶	0.0	-4.60
CH ₃ O ₂ + CH ₂ O → CHO + CH ₃ O ₂ H	1.30 × 10 ¹¹	0.0	37.7
CH ₃ O ₂ H + CHO → CH ₃ O ₂ + CH ₂ O	2.50 × 10 ¹⁰	0.0	42.3
CH ₃ O ₂ + CH ₃ → CH ₃ O + CH ₃ O	3.80 × 10 ¹²	0.0	-5.00
CH ₃ O + CH ₃ O → CH ₃ O ₂ + CH ₃	2.00 × 10 ¹⁰	0.0	0.00
CH ₃ O ₂ + HO ₂ → CH ₃ O ₂ H + O ₂	4.60 × 10 ¹⁰	0.0	-10.9
CH ₃ O ₂ H + O ₂ → CH ₃ O ₂ + HO ₂	3.00 × 10 ¹²	0.0	163.
CH ₃ O ₂ + CH ₃ O ₂ → CH ₂ O + O ₂ + CH ₃ OH	1.80 × 10 ¹²	0.0	0.00
CH ₃ O ₂ + CH ₃ O ₂ → CH ₃ O + CH ₃ O + O ₂	3.70 × 10 ¹²	0.0	9.20
<i>17. CH₄ Reactions</i>			
CH ₄ + H = H ₂ + CH ₃	1.30 × 10 ⁴	3.00	33.6
CH ₄ + O = OH + CH ₃	6.92 × 10 ⁸	1.56	35.5
CH ₄ + OH = H ₂ O + CH ₃	1.60 × 10 ⁷	1.83	11.6
CH ₄ + HO ₂ = H ₂ O ₂ + CH ₃	1.10 × 10 ¹³	0.0	103.
CH ₄ + CH = C ₂ H ₄ + H	3.00 × 10 ¹³	0.0	-1.70
CH ₄ + ³ CH ₂ = CH ₃ + CH ₃	1.30 × 10 ¹³	0.0	39.9
<i>18. CH₃OH Reactions</i>			
CH ₃ OH = CH ₃ + OH	9.51 × 10 ²⁹	-4.3	404.
CH ₃ OH + H = CH ₂ OH + H ₂	4.00 × 10 ¹³	0.0	25.5
CH ₃ OH + O = CH ₂ OH + OH	1.00 × 10 ¹³	0.0	19.6
CH ₃ OH + OH = CH ₂ OH + H ₂ O	1.00 × 10 ¹³	0.0	7.10
CH ₃ OH + HO ₂ → CH ₂ OH + H ₂ O ₂	6.20 × 10 ¹²	0.0	81.1
CH ₂ OH + H ₂ O ₂ → HO ₂ + CH ₃ OH	1.00 × 10 ⁷	1.7	47.9
CH ₃ OH + CH ₃ = CH ₄ + CH ₂ OH	9.00 × 10 ¹²	0.0	41.1
CH ₃ O + CH ₃ OH → CH ₂ OH + CH ₃ OH	2.00 × 10 ¹¹	0.0	29.3
CH ₂ OH + CH ₃ OH → CH ₃ O + CH ₃ OH	2.20 × 10 ⁴	1.7	45.4

Table 2.8 (continued)

Reaction	<i>A</i> (cm, mol, s)	<i>b</i>	<i>E_a</i> (kJ/mol)
$\text{CH}_3\text{OH} + \text{CH}_2\text{O} \rightarrow \text{CH}_3\text{O} + \text{CH}_3\text{O}$	1.53×10^{12}	0.0	333.
$\text{CH}_3\text{O} + \text{CH}_3\text{O} \rightarrow \text{CH}_3\text{OH} + \text{CH}_2\text{O}$	3.00×10^{13}	0.0	0.00
<i>19. CH₃O₂H Reactions</i>			
$\text{CH}_3\text{O}_2\text{H} = \text{CH}_3\text{O} + \text{OH}$	4.00×10^{15}	0.0	180.
$\text{OH} + \text{CH}_3\text{O}_2\text{H} = \text{H}_2\text{O} + \text{CH}_3\text{O}_2$	2.60×10^{12}	0.0	0.00
<i>20.-29. C₂-Hydrocarbons Oxidation</i>			
<i>20. C₂H Reactions</i>			
$\text{C}_2\text{H} + \text{O} = \text{CO} + \text{CH}$	1.00×10^{13}	0.0	0.00
$\text{C}_2\text{H} + \text{O}_2 = \text{HCCO} + \text{O}$	3.00×10^{12}	0.0	0.00
<i>21. HCCO Reactions</i>			
$\text{HCCO} + \text{H} = {}^3\text{CH}_2 + \text{CO}$	1.50×10^{14}	0.0	0.00
$\text{HCCO} + \text{O} \rightarrow \text{CO} + \text{H} + \text{CO}$	9.60×10^{13}	0.0	0.00
$\text{HCCO} + {}^3\text{CH}_2 = \text{C}_2\text{H}_3 + \text{CO}$	3.00×10^{13}	0.0	0.00
<i>22. C₂H₂ Reactions</i>			
$\text{C}_2\text{H}_2 + M^* = \text{C}_2\text{H} + \text{H} + M^*$	3.60×10^{16}	0.0	446.
$\text{C}_2\text{H}_2 + \text{O}_2 = \text{HCCO} + \text{OH}$	2.00×10^8	1.5	126.
$\text{C}_2\text{H}_2 + \text{H} = \text{C}_2\text{H} + \text{H}_2$	6.02×10^{13}	0.0	116.
$\text{C}_2\text{H}_2 + \text{O} = {}^3\text{CH}_2 + \text{CO}$	1.72×10^4	2.8	2.10
$\text{C}_2\text{H}_2 + \text{O} = \text{HCCO} + \text{H}$	1.72×10^4	2.8	2.10
$\text{C}_2\text{H}_2 + \text{OH} = \text{H}_2\text{O} + \text{C}_2\text{H}$	6.00×10^{13}	0.0	54.2
$\text{C}_2\text{H}_2 + \text{C}_2\text{H} = \text{C}_4\text{H}_2 + \text{H}$	3.00×10^{13}	0.0	0.00
<i>23. CH₂CO Reactions</i>			
$\text{CH}_2\text{CO} + M^* = {}^3\text{CH}_2 + \text{CO} + M^*$	1.00×10^{16}	0.0	248.
$\text{CH}_2\text{CO} + \text{H} = \text{CH}_3 + \text{CO}$	3.60×10^{13}	0.0	14.1
$\text{CH}_2\text{CO} + \text{O} + \text{CHO} + \text{CHO}$	2.30×10^{12}	0.0	5.70
$\text{CH}_2\text{CO} + \text{OH} = \text{CH}_2\text{O} + \text{CHO}$	1.00×10^{13}	0.0	0.00
<i>24. C₂H₃ Reactions</i>			
$\text{C}_2\text{H}_3 = \text{C}_2\text{H}_2 + \text{H}$	4.73×10^{40}	-8.8	194.
$\text{C}_2\text{H}_3 + \text{OH} = \text{C}_2\text{H}_2 + \text{H}_2\text{O}$	5.00×10^{13}	0.0	0.00
$\text{C}_2\text{H}_3 + \text{H} = \text{C}_2\text{H}_2 + \text{H}_2$	1.20×10^{13}	0.0	0.00
$\text{C}_2\text{H}_3 + \text{O} = \text{C}_2\text{H}_2 + \text{OH}$	1.00×10^{13}	0.0	0.00
$\text{C}_2\text{H}_3 + \text{O} = \text{CH}_3 + \text{CO}$	1.00×10^{13}	0.0	0.00
$\text{C}_2\text{H}_3 + \text{O} = \text{CHO} + {}^3\text{CH}_2$	1.00×10^{13}	0.0	0.00
$\text{C}_2\text{H}_3 + \text{O}_2 = \text{CHO} + \text{CH}_2\text{O}$	5.40×10^{12}	0.0	0.00
<i>25a. CH₃CO Reactions</i>			
$\text{CH}_3\text{CO} = \text{CH}_3 + \text{CO}$	2.32×10^{26}	-5.0	75.1
$\text{CH}_3\text{CO} + \text{H} = \text{CH}_2\text{CO} + \text{H}_2$	2.00×10^{13}	0.0	0.00

(continued overleaf)

Table 2.8 (continued)

Reaction	A (cm, mol, s)	b	E_a (kJ/mol)
<i>25b. CH₂CHO Reactions</i>			
CH ₂ CHO + H = CH ₂ CO + H ₂	2.00×10^{13}	0.0	0.00
<i>26. C₂H₄ Reactions</i>			
C ₂ H ₄ + M* = C ₂ H ₂ + H ₂ + M*	7.50×10^{17}	0.0	320.
C ₂ H ₄ + M* = C ₂ H ₃ + H + M*	8.50×10^{17}	0.0	404.
C ₂ H ₄ + H = C ₂ H ₃ + H ₂	5.67×10^{14}	0.0	622.9
C ₂ H ₄ + O = H + CH ₂ CHO	1.40×10^6	2.08	0.00
C ₂ H ₄ + O = CHO + CH ₃	2.42×10^6	2.08	0.00
C ₂ H ₄ + OH = C ₂ H ₃ + H ₂ O	2.11×10^{13}	0.0	24.9
<i>27. CH₃CHO Reactions</i>			
CH ₃ CHO + M* = CH ₃ + CHO + M*	7.00×10^{15}	0.0	343.
CH ₃ CHO + H = CH ₃ CO + H ₂	2.10×10^9	1.16	10.1
CH ₃ CHO + H = H ₂ + CH ₂ CHO	2.00×10^9	1.16	10.1
CH ₃ CHO + O = CH ₃ CO + OH	5.00×10^{12}	0.0	7.60
CH ₃ CHO + O = OH + CH ₂ CHO	8.00×10^{11}	0.0	7.60
CH ₃ CHO + O ₂ = CH ₃ CO + HO ₂	4.00×10^{13}	0.0	164.
CH ₃ CHO + OH = CH ₃ CO + H ₂ O	2.30×10^{10}	0.73	-4.70
CH ₃ CHO + HO ₂ = CH ₃ CO + H ₂ O ₂	3.00×10^{12}	0.0	50.0
CH ₃ CHO + ³ CH ₂ = CH ₃ CO + CH ₃	2.50×10^{12}	0.0	15.9
CH ₃ CHO + CH ₃ = CH ₃ CO + CH ₄	2.00×10^{-6}	5.64	10.3
<i>28. C₂H₅ Reactions</i>			
C ₂ H ₅ = C ₂ H ₄ + H	1.02×10^{43}	-9.1	224.
C ₂ H ₅ + H = CH ₃ + CH ₃	3.00×10^{13}	0.0	0.00
C ₂ H ₅ + O = H + CH ₃ CHO	5.00×10^{13}	0.0	0.00
C ₂ H ₅ + O = CH ₂ O + CH ₃	1.00×10^{13}	0.0	0.00
C ₂ H ₅ + O ₂ = C ₂ H ₄ + HO ₂	1.10×10^{10}	0.0	-6.30
C ₂ H ₅ + CH ₃ = C ₂ H ₄ + CH ₄	1.14×10^{12}	0.0	0.00
C ₂ H ₅ + C ₂ H ₅ = C ₂ H ₄ + C ₂ H ₆	1.40×10^{12}	0.0	0.00
<i>29. C₂H₆ Reactions</i>			
C ₂ H ₆ + H = C ₂ H ₅ + H ₂	1.40×10^9	1.5	31.1
C ₂ H ₆ + O = C ₂ H ₅ + OH	1.00×10^9	1.5	24.4
C ₂ H ₆ + OH = C ₂ H ₅ + H ₂ O	7.20×10^6	2.0	3.60
C ₂ H ₆ + HO ₂ = C ₂ H ₅ + H ₂ O ₂	1.70×10^{13}	0.0	85.9
C ₂ H ₆ + O ₂ = C ₂ H ₅ + HO ₂	6.00×10^{13}	0.0	217.
C ₂ H ₆ + ³ CH ₂ = C ₂ H ₅ + CH ₃	2.20×10^{13}	0.0	36.3
C ₂ H ₆ + CH ₃ = C ₂ H ₅ + CH ₄	1.50×10^{-7}	6.0	25.4

^a³CH₂ is the triplet state of methylene, and ¹CH₂ is the singlet electronic excited state of methylene.

The hydroperoxyl radical HO_2 is formed primarily by (see explosion behavior of H_2/O_2 mixture section)



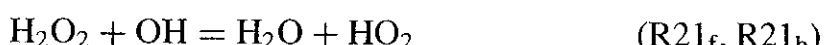
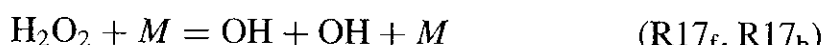
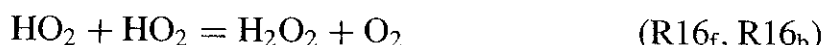
and occasionally by



The hydroperoxyl radical HO_2 is consumed by additional reactions with various radicals, including

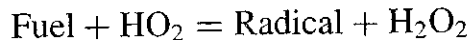


The hydrogen peroxide (H_2O_2) formation and consumption reactions include



In the high-temperature combustion of hydrogen and hydrocarbons, (R1_f) is the single most important chain-branching reaction, consuming one H atom and producing two radical species, O and OH. According to numerous evidences described by Westbrook and Dryer¹²¹ and other chemists, any type of kinetic perturbation, which increases the production of H atoms, will accelerate the overall rate of combustion by increasing the net amount of chain branching from reaction (R1_f). Conversely, processes that reduce the H atom population and reactions that compete with reaction (R1_f) for H atoms will tend to inhibit the combustion. For example, reaction (R9_f) competes directly with reaction (R1_f) for H atoms, but the rate of the third-order reaction (R9_f) is much more pressure dependent than that of (R1_f). Another example for competition of H atoms is based on the observation that the addition of small amounts of various chemicals to flammable mixtures can drastically reduce the overall rate of combustion. The addition of many halogenated species inhibits the combustion process by removing H atoms from the radical pool. The removal of H atoms means that they are then unavailable for reaction with O₂ through reaction (R1_f), thereby reducing the rate of chain branching and slowing the overall rate of combustion.

At elevated pressures ($p \geq 20$ atm) and at relatively low temperatures ($T \sim 1000$ K), reaction (R9_f) will dominate over reaction (R1_f). In such environments, the sequence of reactions (R9_f), (R16), and (R17) provides chain propagations (i.e., two H atoms consumed, and two OH radicals produced). In contrast, the sequence of reaction (R9_f) followed by



and then reaction (R17_f) results in chain branching (one H atom yields two OH radicals). Under these conditions, increased fuel concentration will therefore result in an accelerated overall rate of reaction, while at lower pressures an increased fuel concentration will generate an inhibiting effect by competing with reaction (R1_f).

Reaction (R2_f) provides additional chain branching in H₂/O₂ system. Since the O atom concentration of this reaction depends on the reaction (R1_f), the importance of the reaction (R2_f) is not as great as that of (R1_f). Reaction (R3_f) is responsible for the majority of H₂ consumption under normal circumstances; thus, when the OH level is low, H₂ oxidation will be low. The backward reaction (R12_b) provides a mechanism for the initiation reaction of H₂/O₂ mixtures, which accurately simulates experimental ignition delay measurements in shock tube and detonation condition. Reaction (R12_b) dominates over the following reaction (R22_f),



14.1.2 O₃ Decomposition Mechanism Ozone decomposition mechanism is occasionally considered in combustion of H₂/O₂ systems, since it is an oxidizer that contributes much more chemical potential energy to a given fuel-oxidizer mixture than does ordinary oxygen O₂, and its use provides significantly higher product temperatures and pressures than does O₂. The reaction mechanism for the ozone decomposition flame is the simplest one that has all of the requisite features of a truly detailed mechanism, consisting of only three species (O, O₂, and O₃) with three reactions, reaction (R6) together with



Direct coupling between the O₃ system and H₂ oxidation can be provided by reactions including

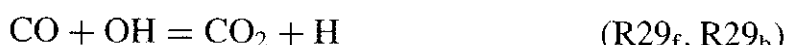


The ozone mechanism is of minor practical importance in combustion environments, but its application to model validation of laminar flame structure can make it valuable (see Chapter 5 for more detailed discussions of O₃ decomposition flame structure).

14.1.3 CO Oxidation Mechanism The oxidation mechanism for carbon monoxide is very simple, consisting of



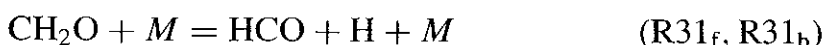
The rates of both these CO oxidation reactions are quite small at normal combustion temperatures. Thus, CO oxidation rate in hydrogen-free environments is very slow. However, if H atoms are present, even in amounts as small as 20 ppm H₂O, the CO oxidation mechanism becomes strongly coupled to that of H₂O₂, through the following reactions¹²⁶:



Reaction (R30) is rarely as important as reaction (R29), although at very high pressures or in the initial stages of hydrocarbon oxidation, the high HO₂ concentrations can make it competitive. All hydrocarbon oxidation eventually involves H₂ and CO oxidation kinetics (see Fig. 2.30), and most of the CO₂ that is produced results from reaction (R29_f). The coupling between the CO and the H₂O₂ submechanisms is further complicated by the unusually large chaperon efficiency of water molecules for some reactions. For example, Dryer and Glassman¹²⁷ found that at $T_f \sim 1000$ K and $p = 1$ atm, the rate of CO oxidation in a turbulent flow reactor depended on the concentrations of CO, O₂, and H₂O, even though the water concentration was quite small ($\sim 2.5\%$). This is due to the important role of H₂O as a third body in the recombination reaction (R9). When the chaperon efficiency for H₂O in this reaction was varied, the computed results of Yetter et al.¹²⁸ showed large variations. Their best agreement was obtained by setting the third-body efficiency of water in reaction (R9) equal to that determined from shock tube experiments by Getzinger and Schott.¹²⁹

Because reaction (R29) consumes most of the CO, which reacts with OH to produce CO₂, the rate of CO oxidation depends very much on the availability of OH radicals. The rate of reaction of (R29_f) is considerably lower than the rates of reactions between OH radicals and typical hydrocarbon species. As a result, the presence of most hydrocarbon species will effectively inhibit the oxidation reaction of CO. During the oxidation of hydrocarbons, CO is produced in substantial amounts, but the subsequent oxidation of CO to CO₂ is usually retarded until *after* the original hydrocarbon and the fragment intermediate hydrocarbon species have all been consumed. Only then does the OH concentration rise to higher levels, rapidly converting the CO to CO₂.

14.1.4 CH₂O Reaction Formaldehyde is an intermediate in the oxidation of most hydrocarbon fuels. The two possibilities for decomposition are

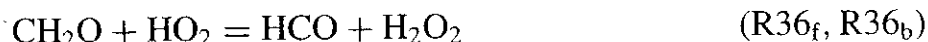


The chain-branching characteristics of these two paths are vastly different. Reaction (R31) produces one H atom directly, and in most environments the formyl radical HCO rapidly decomposes further into CO and H. Thus, the net difference between reactions (R31) and (R32) is H + H as opposed to H₂. Reaction (R31_f) with reaction (R1_f) is a very active chain-branching sequence in oxidizing environments, while reaction (R32_f) is effectively a termination sequence.

Formaldehyde is consumed primarily by reactions with OH, H, and O radicals to produce HCO.



The particular reaction environment being examined determines the relative importance of reactions (R33–R35). In fuel-rich mixtures, reaction (R34) dominates; in lean and stoichiometric condition, reactions (R33) and (R35) dominate. Another reaction that is less important but can contribute to CH₂O consumption in some cases is



The formyl radicals (HCO) produced by reaction of CH₂O and other species are in turn consumed in a variety of elementary reactions.



This pair of reactions for a hydrocarbon radical illustrates a pattern that will be repeated for many larger radicals; a reaction with O₂ competes with a thermal decomposition reaction, and their relative rates determine much of the behavior of the overall mechanism. Typically, the activation energy of the decomposition reaction (R37) is substantially higher than that of the reaction with O₂.

The formyl radical reacts also with other radical species, with rates that are close to collision rates, having negligible activation energies. These reactions include

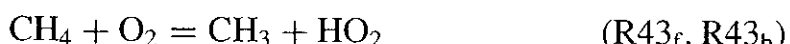


14.1.5 CH₄ Oxidation Methane is a very important practical fuel, constituting approximately 90% of the composition of natural gas. It is also a significant byproduct in many industrial processes and is produced during the combustion

of most other hydrocarbons. The thermal decomposition of CH_4 yields methyl radicals.



Another possible initiation reaction under oxidation conditions is



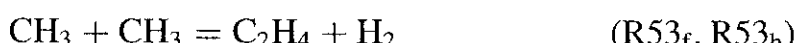
which has been shown to be much less important than reaction (R42). Hydrogen abstraction from CH_4 occurs by several reactions.



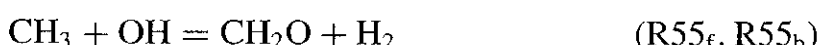
The methyl radical reacts directly with O_2 according to the reactions listed below.



Bowman¹³⁰ pointed out that reaction (R50) was probably not an elementary reaction, but rather a convenient model for simulating CH_3 oxidation. Computed model results were found to be very sensitive to variations in the rate of reaction (R50), with a rather large rate and relatively low activation energy in order to reproduce the observed combustion rate. Lately, it has been verified that the major CH_3 oxidation step takes place according to reaction (R48) as was initially suggested by Brabbs and Brokaw.¹³¹ During the pyrolysis and oxidation of methane, radical recombination reactions produce significant amounts of larger hydrocarbons containing two or more carbon atoms. These recombination reactions must be considered.



The methyl radical reacts with other radicals

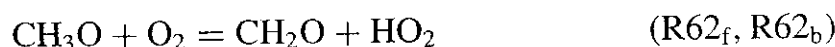
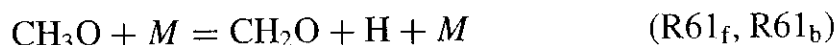




At very high temperatures, CH_3 may also dissociate



Methoxy radicals (CH_3O) generated from reactions (R56_f) and (R59_f) can react by means of



Based on Westbrook and Dryer,¹²¹ other reactions between CH_3O and radicals such as O and OH probably occur at high rates, but such paths have not yet been incorporated into detailed mechanisms. The competition between (R61) and (R62) follows the pattern discussed earlier for formyl radicals (CHO) with the reaction with O_2 competing only for very lean mixtures and at lower temperatures.

14.1.6 C_2H_6 (Ethane) Oxidation Ethane decomposition reaction (R51_b) is at neither its high- nor low-pressure limit in most combustion regimes; therefore, some treatment or estimate of its fall-off behavior is usually necessary. The following initial reaction with oxygen has been considered by chemists for low temperature and in oxidizing environments:



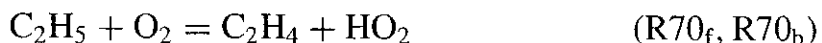
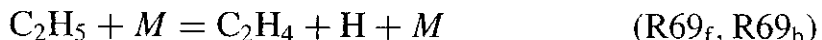
Ethane can also react relatively fast with CH_3 to produce reactive ethyl radicals by



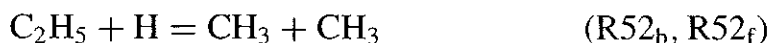
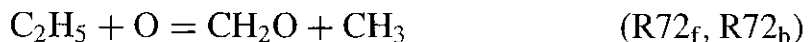
The other key reactions involving C_2H_6 include



The rates of these reactions exhibit substantial non-Arrhenius behavior. Two principal reactions involving ethyl radical (C_2H_5) are



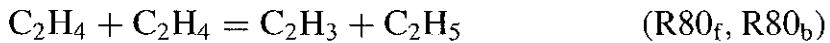
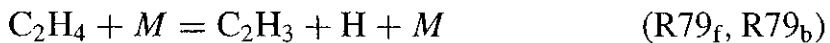
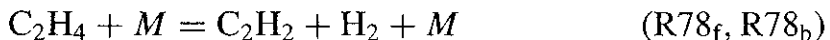
In shock-tube conditions, (R69) can be assumed to be second order, while other studies at lower temperature indicate first-order behavior. In most typical combustion situations, this reaction is in the fall-off region. Other reactions of the ethyl radicals are



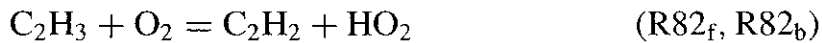
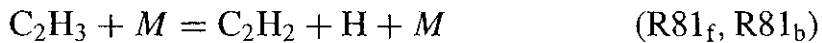
When ethane is the primary fuel, another key feature of the oxidation mechanism is the recombination of C_2 and C_1 radicals to produce C_3 and C_4 species, as shown by the following reactions:



14.1.7 C_2H_4 (Ethylene) Oxidation Ethylene is a primary fuel itself and is also produced in large amounts during the combustion of CH_4 , C_2H_6 , and other higher hydrocarbons. Three initiation reactions can be important, including



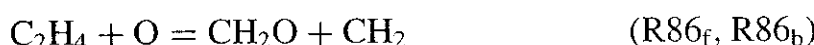
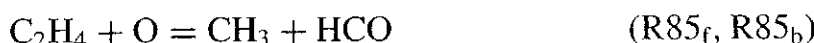
Reaction (R78) is fastest in most cases, while (R80) rarely competes except in conditions in which C_2H_4 concentrations are very high.¹²¹ The two important reactions of the vinyl radical (C_2H_3) are



Reactions of radicals with ethylene fall into two general classes. One consists of H atom abstraction reactions:

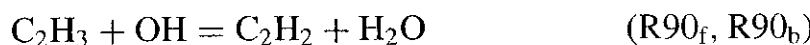
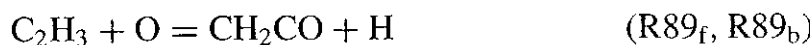


The other family of reactions (R85–R87), involving the formation of an activated complex followed by rearrangement and fragmentation, is given below. They generally have lower activation energies than those of H atom abstraction reactions.



The H atom abstraction reactions at room temperature are often negligibly slow, but under high-temperature conditions, the H atom abstraction reactions can be very important.

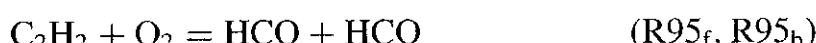
Additional reactions of vinyl radicals (C_2H_3) include



A reaction as a possible step leading to soot formation produces 1–3 butadiene (C_4H_6).



14.1.8 C_2H_2 (Acetylene) Oxidation Acetylene is a practical fuel and is also believed to be an important contributor to the formation and growth of soot. C_2H_2 and its pyrolysis and oxidation reactions are part of the reaction mechanisms for most other hydrocarbon fuels, particularly in fuel-rich conditions. The important initiation reactions include



In acetylene pyrolysis, reaction (R92) dominates under dilute conditions, while reaction (R93) is more important at high fuel concentrations. Unlike the other hydrocarbons already discussed, the pyrolysis of acetylene is *exothermic*, so

decomposition flames and detonation processes are possible even in pure C₂H₂. Under oxidation conditions, the reaction of C₂H₂ with O₂ is extremely important, but there is not yet positive identification of the product distribution.¹²¹

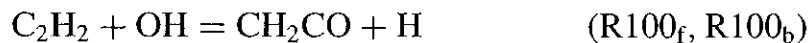
The following hydrogen atom abstraction reaction competes with the recombination reaction (R81_b) only at high temperature:



Reactions between C₂H₂ and O atoms include (R97–R99) with reaction (R98) being predominant under most conditions.



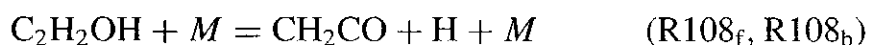
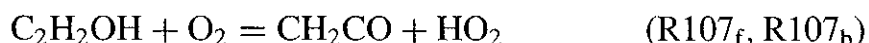
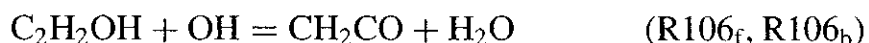
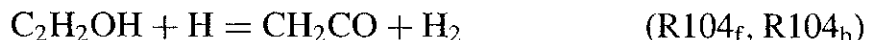
Acetylene reacts with OH radicals by the following reactions:



An additional path proposed by Miller et al.¹³² is



This reaction is then followed by several reactions involving C₂H₂OH species and other radicals or molecules:

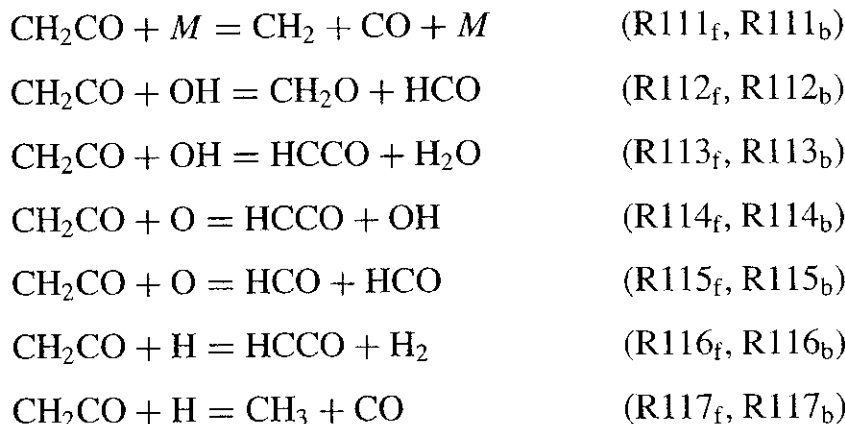


An alternative path for acetylene oxidation under rich conditions has been examined recently, proceeding by means of

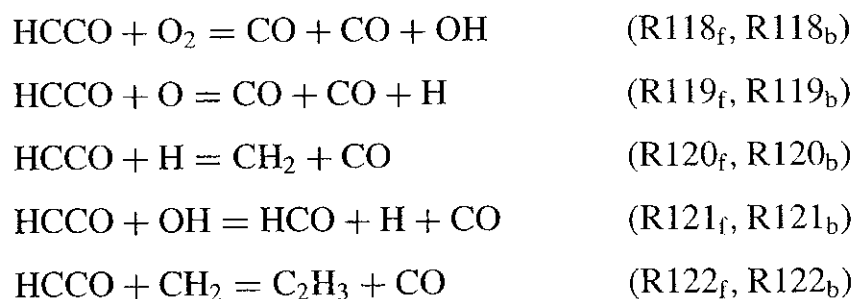


followed by reactions between C_3H_2 and radical species to give a variety of other products. Warnatz et al.¹³³ attributed as much as 35% of the fuel consumption in rich acetylene flames to this sequence, which avoids ketene formation entirely.

14.1.9 CH_2CO (Ketene) Oxidation A summary of the ketene reactions, which have been used in model simulations, includes

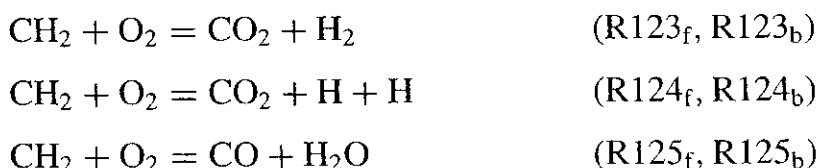


Rate expressions for reactions (R111) and (R112) have been obtained from experimental studies, but rate expressions for the other reactions represent either estimates or results of modeling studies. Ketyl radicals (HCCO) produced from ketene, directly from acetylene by reaction (R99), or by reaction (R136) between C_2H and O_2 can be consumed by the following set of reactions suggested by Miller et al.¹³²:



However, there is very little information available on these reactions at high temperatures near T_f or shock tubes. As a result, most detailed mechanisms avoid modeling the reactions involving the ketyl radical by including only reactions (R111), (R115), and (R117).

Other species produced during the oxidation of ketene and acetylene include C_2H , CH_2 , and CH . The reactions of methylene radical (CH_2) near room temperature include



$\text{CH}_2 + \text{O}_2 = \text{CO} + \text{OH} + \text{H}$	(R126 _f , R126 _b)
$\text{CH}_2 + \text{O}_2 = \text{HCO} + \text{OH}$	(R127 _f , R127 _b)
$\text{CH}_2 + \text{O} = \text{CH} + \text{OH}$	(R128 _f , R128 _b)
$\text{CH}_2 + \text{O} = \text{CO} + \text{H} + \text{H}$	(R129 _f , R129 _b)
$\text{CH}_2 + \text{O} = \text{CO} + \text{H}_2$	(R130 _f , R130 _b)
$\text{CH}_2 + \text{OH} = \text{CH} + \text{H}_2\text{O}$	(R131 _f , R131 _b)
$\text{CH}_2 + \text{H} = \text{CH} + \text{H}_2$	(R132 _f , R132 _b)
$\text{CH}_2 + \text{CH}_2 = \text{C}_2\text{H}_3 + \text{H}$	(R133 _f , R133 _b)
$\text{CH}_2 + \text{CH}_2 = \text{C}_2\text{H}_2 + \text{H}_2$	(R134 _f , R134 _b)
$\text{CH}_2 + \text{C}_2\text{H}_3 = \text{CH}_3 + \text{C}_2\text{H}_2$	(R135 _f , R135 _b)

Reaction (R127) followed by the formyl radical (HCO) deformation reaction (R37) results in the same product distribution as reaction (126) alone.

Reactions of C₂H and CH include

$\text{C}_2\text{H} + \text{O}_2 = \text{HCCO} + \text{O}$	(R136 _f , R136 _b)
$\text{C}_2\text{H} + \text{O}_2 = \text{HCO} + \text{CO}$	(R137 _f , R137 _b)
$\text{C}_2\text{H} + \text{O} = \text{CO} + \text{CH}$	(R138 _f , R138 _b)
$\text{C}_2\text{H} + \text{C}_2\text{H}_3 = \text{C}_2\text{H}_2 + \text{C}_2\text{H}_2$	(R139 _f , R139 _b)
$\text{CH} + \text{O}_2 = \text{HCO} + \text{O}$	(R140 _f , R140 _b)
$\text{CH} + \text{O}_2 = \text{CO} + \text{OH}$	(R141 _f , R141 _b)

Reactions of C₂H with alkanes and with O₂ have been examined at low temperatures.

An additional acetylene pyrolysis submechanism has been proposed as a possible factor in soot formation. The formation processes of polyacetylene species are

$\text{C}_4\text{H}_3 + M = \text{C}_4\text{H}_2 + \text{H} + M$	(R142 _f , R142 _b)
$\text{C}_2\text{H}_2 + \text{C}_2\text{H} + M = \text{C}_4\text{H}_2 + \text{H} + M$	(R143 _f , R143 _b)
$\text{C}_4\text{H}_2 + M = \text{C}_4\text{H} + \text{H} + M$	(R144 _f , R144 _b)

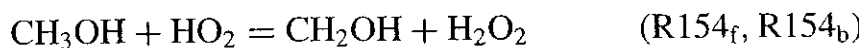
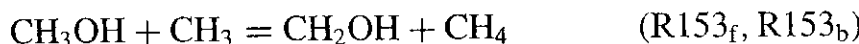
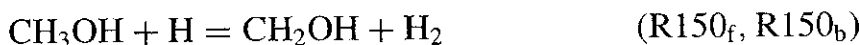
14.1.10 CH₃OH (Methanol) Reactions

The possible initial reactions include

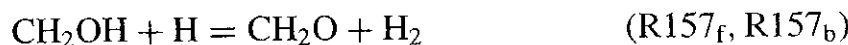
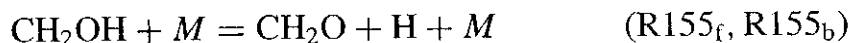
$\text{CH}_3\text{OH} + M = \text{CH}_3 + \text{OH} + M$	(R145 _f , R145 _b)
$\text{CH}_3\text{OH} + M = \text{CH}_3\text{O} + \text{H} + M$	(R146 _f , R146 _b)
$\text{CH}_3\text{OH} + M = \text{CH}_2\text{OH} + \text{H} + M$	(R147 _f , R147 _b)
$\text{CH}_3\text{OH} + \text{O}_2 = \text{CH}_2\text{OH} + \text{HO}_2$	(R148 _f , R148 _b)

Based on the relative bond energies, reactions (R146) and (R147) can be rejected from the kinetic mechanism. The addition of these two reactions to a mechanism already containing reaction (R145) had no appreciable effect on computed induction times under shock-tube oxidation conditions.¹²¹ Reaction (R148) provides a much different chain initiation function than do the alternate initiation reactions, since both the methoxy (CH_3O) and hydroperoxyl (HO_2) radicals quickly decompose, producing additional H atoms. Reaction (R145) yields only a relatively nonreactive methyl radical and the chain-propagating radical OH. The lower rates and the short period over which initiation reactions are important make reactions (R146) and (R147) negligible. Reaction (R148) becomes unimportant at high-temperature conditions relative to reaction (R145).

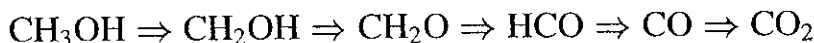
Abstraction of H atoms proceeds primarily by breaking C–H bonds rather than the O–H bond:



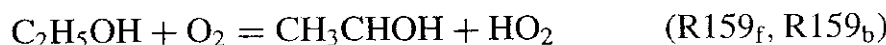
For the reactions between CH_3OH and H, reaction (R149) is faster below 650 K, while the rates reverse at higher temperatures ($T > 1000$ K). If reaction (R149) or any other faster reaction produced CH_3 radicals in large amounts, then methyl radical recombination reactions (R51–R53) would result in considerable amounts of C_2 species. However, very low concentrations of C_2 species are observed in CH_3OH –air flames. The CH_2OH radicals decompose by means of reaction (R155) or react with O_2 and H by reactions (R156) and (R157).



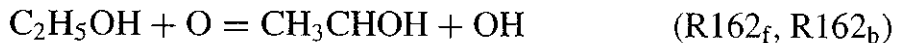
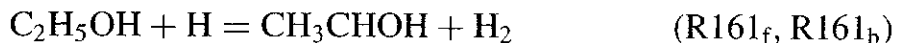
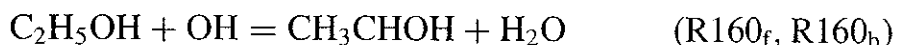
In general, the oxidation path for methanol proceeds in a sequential manner through



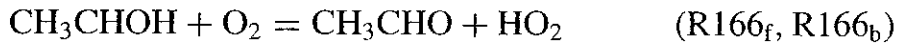
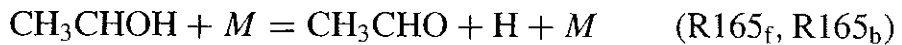
14.1.11 $\text{C}_2\text{H}_5\text{OH}$ (Ethanol) Reactions Based in principle on mechanisms for methanol oxidation, the initiation reactions are



Reactions between radical species and ethanol are



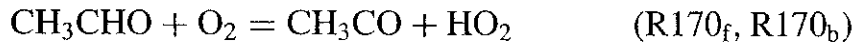
The hydroxyethyl radical (CH_3CHOH) is consumed by the same paths as CH_2OH , producing acetaldehyde:



The production of acetaldehyde as the dominant intermediate is somewhat analogous to the production of formaldehyde as the major intermediate in methanol combustion. The mechanism for subsequent oxidation of acetaldehyde is discussed in the next section. A turbulent flow reactor study of ethanol pyrolysis and oxidation¹²¹ has shown that, similar to the case for CH_3OH , two hydrogen abstraction reactions are important at high temperature, consisting of reaction (R161) as well as

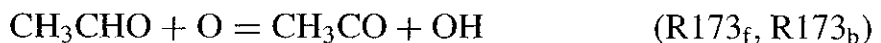
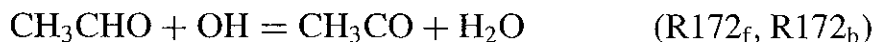


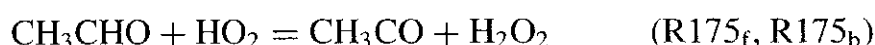
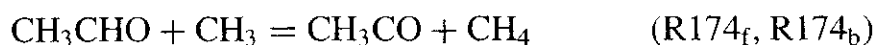
14.1.12 CH_3CHO (Acetaldehyde) Reaction Acetaldehyde is an important intermediate chemical species in the combustion of higher hydrocarbon fuels. The principal initiation reactions are



The decomposition reactions dominate at shock-tube temperatures, and reaction (R168) is more important than reaction (R169). At flow reactor temperatures around 1000 K, reactions (R170), (R9), and (R38) produce high concentrations of hydroperoxyl radicals. Much of CH_3 radical consumption can be attributed to reaction (R59) with hydroperoxyl radicals.

The principal H atom abstraction reactions are





These reactions are followed by the decomposition reaction of CH_3CO radical,

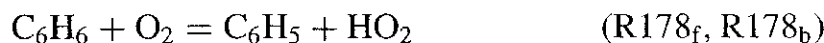
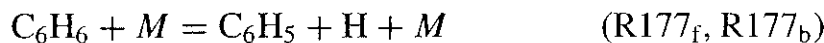


The above mechanism leads to large concentrations of CH_3 and CO. Some methyl radicals produce methane, and a fraction of methyl radicals recombine to produce C_2H_6 . Subsequent reactions of C_2H_6 lead to C_2H_4 , C_2H_2 , and other related species as already discussed.

14.2 Discussion of More Complex Cases

Chemical kinetics for oxidation and pyrolysis reactions of higher hydrocarbons are given in the excellent review paper by Westbrook and Dryer.¹²¹ Due to space limitation, these are not included in this section. As we commented earlier, the combustion properties of methane and ethane are not truly typical of higher hydrocarbon fuels. However, propane and butane exhibit many of the same properties as practical hydrocarbon fuels, including burning velocity, vapor pressure, quenching properties, ignition behavior, effects of pressure on combustion rates, and other important macroscopic properties of practical fuels.

Detailed mechanisms for the combustion of aromatic hydrocarbon fuel species have not yet been developed, although some preliminary modeling studies of benzene and polyaromatic hydrocarbon (PAH) oxidation in shock tubes have been conducted.^{134,135} In the case of benzene, the principal initiation reactions include



as well as abstraction of H atoms from the ring by various radicals



At low temperatures, it appears that these reactions are followed by



with ensuing steps leading to final products. At higher temperatures, the reaction of phenyl radicals with O₂ leads to phenoxy radicals and an O atom



with subsequent expulsion of CO leading to the next lower hydrocarbon (cyclopentadienyl) radical



This sequence is followed by similar reactions leading to butadienyl radicals, its decomposition products (vinyl acetylene and vinyl radicals), and butadiene.

In general, all of the reaction mechanisms depend on the existence of a radical pool. Chain-branching reactions accelerate the combustion process by increasing the size of the radical pool, and termination reactions slow the combustion by reducing the size of the radical pool.

15 REDUCTION OF HIGHLY COMPLEX REACTION SYSTEM TO SIMPLER REACTION MECHANISMS

Due to the complex mathematical nature of the physics and chemical kinetics, numerical computation of most combustion problems is a necessary step in obtaining solutions. Combustion problems, in general, are quite complex both in number of species involved and in the necessary dimensionality of the problem needed to obtain an accurate solution. The full equations to describe a complex combustion problem currently exist, but the means to compute the solutions in a reasonable amount of time frequently do not. The goal in finding solutions for a full solution in all cases can be approximately found by reducing the complexity of the problem by reducing the underlying kinetic mechanisms to a simpler regime. Often, the full equations are not necessary to get a reasonably close estimate by having a smaller set of equations that will approximate the full solution while reducing computing time. A second benefit to the study of mechanism reduction is that sometimes greater insight to species interaction and importance of certain mechanisms are appreciated when different reduced combustion schemes are compared to each other and to the full equations.

From the beginning, it should be stated that mechanism reduction is a field of study by itself. The effort to reduce chemical mechanisms probably started from the simple fact that sufficient computing resources were not available to handle broad-scope, multifaceted combustion problems. Even today, as computing power has increased nearly exponentially, the effort to reduce chemical mechanisms is still just as valid.

A combustion problem is set up when the equations for continuity, momentum, and energy are established. If adiabatic or other common assumptions can be made about the problem, the number of equations will be fewer. The chemical aspect of modeling lies in the laws of mass action in which the rate of

production of each possible species is written out once a full equation set is made up to describe not only initiation and termination reactions but also the chain-propagating reactions, which can involve a great number of intermediary species or radicals. These mass action equations can be numerous as well as very complicated. Large and complex equation sets are difficult to solve, but chemical problems are notoriously large, warranting efforts to reduce these equations to manageable proportions.

How a method of reduction is typically evaluated is by comparison with experimental results and not necessarily with the results of a full model. The validity of a reduced mechanism cannot be compared against the full mechanism because both mechanisms are merely models of what is thought to occur during combustion. Experimental data can be sparse and the conditions of combustion desired may be difficult to simulate, but the true test of a kinetic mechanism will usually reside with how well the model fits experimental data and over how large of a parameter range this model is valid.

15.1 Quasi-Steady-State Assumption (QSSA) and Partial Equilibrium Assumption

Quasi-steady-state assumptions are very commonly used in mechanism reduction. Many researchers use this method either by itself or in combination with other similar assumptions. This assumption is simply that the rate of production of a chemical species is close enough to its consumption rate to assume that they are both equal. This allows us to assume that the concentration of the species is low and can be neglected in analysis. As a whole, this assumption allows some of the ODEs of the full mechanism to be converted to algebraic expressions. With algebraic relations, the number of ODEs is reduced and the mechanism becomes simpler. The drawback to this type of assumption is that the modeler must have some *a priori* knowledge regarding what species are likely to exhibit this behavior and are good candidates for this assumption without compromising accuracy excessively. The other drawback is that models based entirely on this type of assumption are usually valid only under a narrow range of parameters, and thus each model tends to fit only a small number of cases.

The justification of the steady-state approximation is generally provided in physical terms by stating that the rate at which a species is consumed is much faster than the rate by which it is produced. Therefore, its concentration always stays much smaller than those of the initial reactants and the final products. Since the concentration always stays small, its time derivative also stays small compared with the time derivative of the other species. For many engineering purposes, it will be acceptable to assume those intermediate species in steady state whose concentrations are significantly less than 10% of the initial fuel concentration.

It is useful to note that partial equilibrium assumption is not to be confused with steady-state assumptions. Although these two assumptions are both frequently used in combinations with each other, it should not be assumed that they are the same thing. At high temperatures, the forward and backward reactions are

so fast that we can assume partial equilibria for certain reactions; for example,



From these equilibrium reactions, the concentrations of reactive species (such as H, O, and OH), which are difficult to measure, can be expressed in terms of concentrations of stable species such as H₂, O₂, and H₂O, which are easier to measure. Usually, partial equilibrium assumption is valid only at very high temperatures.^{30,136}

15.2 Computational Singular Perturbation Methods for Stiff Equations

In the formulation of a reduced reaction mechanism, traditionally theoreticians always try to simplify an originally complex system of elementary reactions as much as possible. This is usually done by neglecting unimportant terms, which is justified by the use of order-of-magnitude estimates, or by asymptotic expansions, by matching of such expansions, or by skillful use of ad hoc assumptions guided by experience and intuition.

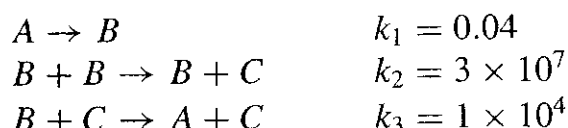
A major advancement in computational singular perturbation (CSP) theory was developed by Lam and Goussis.^{137,138} They introduced and exploited the new concept of optimal representation of the rate of change of species mass fraction and temperature (represented by a vector \mathbf{G}) and used numerical computation to monitor directly and continuously the contribution to \mathbf{G} by each of its components, representing linearly independent reaction groups. At any given time, we can easily identify which terms are nearly constant, which terms are controlling the reaction, and which chemical species are nearly exhausted.

$$\mathbf{G} = \frac{dy}{dt} = \begin{pmatrix} \frac{dy_1}{dt} \\ \frac{dy_2}{dt} \\ \vdots \\ \frac{dy_N}{dt} \end{pmatrix} = \mathbf{S}_r F_r \quad \text{where } y_i = Y_i \text{ or } T \quad (2-166)$$

where \mathbf{S}_r and F_r are called the stoichiometric vector and reaction rate of the r th reaction, respectively. The summation index r spans from 1, 2, ..., M , where M is the total number of physically meaningful reactions. Under CSP, we no longer neglect a term in the a priori manner; we simply discard it when it has become numerically too small to make any difference. The investigator sets the

criterion of smallness for the characteristic chemical reaction times to discard the fast reactions.

15.2.1 Stiff Equations Basically, stiffness is caused by the widely varying characteristic reaction times in the rate equations. For very fast reactions, the rates of decay of species concentrations are rapid and require extremely small timescales for integration. Although these fast reaction rates are of no interest (since the slower reactions are the rate-controlling ones), they cause most numerical methods to become unstable, because any inaccuracies become magnified. A historically important example is the following chemical reaction. Here there are three chemical reactions with their rate of reaction constants known.



Let $y_1(t)$, $y_2(t)$, and $y_3(t)$ be the concentrations of A , B , and C , respectively [i.e., $y_1(t) = C_A$, $y_2(t) = C_B$, and $y_3(t) = C_C$]. Then, by using the law of mass action, it can be shown that $y_1(t)$, $y_2(t)$, and $y_3(t)$ satisfy the following three differential equations:

$$Y'(t) = \begin{bmatrix} y'_1(t) \\ y'_2(t) \\ y'_3(t) \end{bmatrix} = \begin{bmatrix} -k_1 y_1(t) & & +k_3 y_2(t) y_3(t) \\ k_1 y_1(t) & -k_2 y_2(t)^2 & -k_3 y_2(t) y_3(t) \\ & +k_2 y_2(t)^2 & \end{bmatrix}$$

The initial conditions for these three ODEs are

$$Y(0) = [1, 0, 0]^T$$

In this system, species A is converted to B via the slow first reaction, since k_1 is much lower than k_2 and k_3 . The much faster second and third reactions then rapidly convert even small amounts of B to C . The vastly different rates of reaction occurring in the same system cause the ODEs to be stiff.

15.2.2 Chemical Kinetic Systems as Stiff Equations As defined above in Eq. (2-166), the vector \mathbf{G} represents the rate of change of instantaneous state variable, $y(t)$. As shown in Eq. (2-13), \mathbf{G} can be expressed as follows:

$$\mathbf{G}(y) = \mathbf{S}_r F_r \quad (2-167)$$

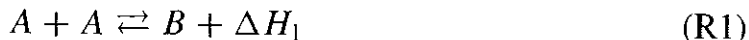
or

$$\mathbf{G}_i = \left(\sum_{r=1}^M \mathbf{S}_r F_r \right)_i \quad (2-167a)$$

It is understood that $F_r(y)$ carries the main y dependence and \mathbf{S}_r is independent of y . We are interested in the case when the system of equations (2-166) is

known to be stiff with respect to the desired time step Δt for obtaining the numerical solution.

Example: Let the state vector be $\mathbf{y} = [C_A, C_B, T]^T$ where C_A and C_B are chemical concentrations and T is temperature. The reaction system consists of three elementary reactions:



where ΔH_1 , ΔH_2 , and ΔH_3 are the heats of reaction of the respective reactions. The generalized stoichiometric vectors and the reaction rates are

$$\begin{aligned} s_1 &= [-2, 1, \Delta H_1]^T, & F_1 &= k_1(C_A^2 - K_{C_1}C_B), \\ s_2 &= [-1, 1, \Delta H_2]^T, & F_2 &= k_2(C_A - K_{C_2}C_B), \\ s_3 &= [1, -2, \Delta H_3]^T, & F_3 &= k_3(C_B^2 - K_{C_3}C_A). \end{aligned}$$

where the reaction rate coefficients k_1 , k_2 , k_3 are the forward reaction rate constants and the equilibrium constants K_{C_1} , K_{C_2} , K_{C_3} are known. Without loss of generality, the M stoichiometric vectors \mathbf{S}_r are linearly independent and in this case are equal to N . Physically, when some of the reactions are much faster than others, partial equilibria are established between the fast forward and reverse reactions after a certain transient time period, leaving the slower reactions to control the overall reaction rate thereafter.

15.2.3 Formulation of the Problem

15.2.3.1 The Fast Subspace We shall formally split vector space $\mathbf{G}(\mathbf{y})$ into a fast and a slow subspace. We shall represent the fast subspace by a set of fast basis vectors \mathbf{a}_I and its dual \mathbf{b}^J , where $I = 1, 2, \dots, m$ and $J = 1, 2, \dots, m$ with $m < M$. A method to determine these basis vectors and parameter m is described in a later section. Assume that they are known; some useful relationships are stated here. We have used the convention that uppercase superscripts and subscripts run from 1 to m while lowercase superscripts and subscripts run from 1 to M .

The fast basis vectors are required to satisfy the usual orthonormal relations:

$$\mathbf{b}^J \cdot \mathbf{a}_I = \delta_I^J, \quad I, J = 1, 2, \dots, m \quad (2-168)$$

Note that for a given set of fast basis vectors \mathbf{b}^J , Eq. (2-168) does not uniquely determine its set of dual basis vectors \mathbf{a}_I , and vice versa.

With the above developments, $\mathbf{G}(\mathbf{y})$ can be split into its fast and slow components as follows:

$$\mathbf{G}(\mathbf{y}) = \mathbf{G}_{\text{fast}} + \mathbf{G}_{\text{slow}} \quad (2-169)$$

where

$$\mathbf{G}_{\text{fast}} \equiv \mathbf{a}_I f^I = \sum_{I=1}^m \mathbf{a}_I f^I \quad (2-170)$$

The physical meaning of f^I is the reaction rate of I th fast reaction. The projection of \mathbf{G}_{slow} in the fast subspace \mathbf{b}^J should be zero, i.e.,

$$\mathbf{b}^J \cdot \mathbf{G}_{\text{slow}} = 0 \quad (2-171)$$

It is clear that \mathbf{G}_{slow} has no projection in the fast subspace. The basis vector sets for the fast subspace \mathbf{a}_I and \mathbf{b}^J are yet to be determined.

The I th component of \mathbf{G} in the fast subspace can be computed as follows:

$$\begin{aligned} f^I &\equiv \mathbf{b}^I \cdot \mathbf{G} = \mathbf{b}^I \cdot (\mathbf{G}_{\text{fast}} + \mathbf{G}_{\text{slow}}) = \mathbf{b}^I \cdot \mathbf{G}_{\text{fast}} = \mathbf{b}^I \cdot \mathbf{a}_I f^I = \delta_I^I f^I \\ I &= 1, 2, \dots, m \end{aligned} \quad (2-172)$$

15.2.3.2 The Equations for f^I It is seen that \mathbf{a}_I is the stoichiometric vector and f^I is the reaction rate for the I th fast mode. When a fast mode exhausts itself and reaches quasi-equilibrium, its forward reaction rate will nearly be balanced by the reverse reaction rate. Computationally, this means that in this quasi-equilibrium time period, Eq. (2-170) will suffer severe loss of significant figures if used to evaluate f^I . Thus, Eq. (2-170) is computationally useful only before such severe cancellations occur. In order to avoid using Eq. (2-170) directly, we can derive differential equations for f^I by differentiating Eq. (2-172) with respect to time to obtain

$$\begin{aligned} \frac{df^I}{dt} &= \frac{d\mathbf{b}^I}{dt} \cdot \mathbf{G} + \mathbf{b}^I \cdot \frac{d\mathbf{G}}{dt} = \frac{d\mathbf{b}^I}{dt} \cdot \mathbf{a}_J f^J + \mathbf{b}^I \cdot \frac{d\mathbf{a}_J f^J}{dt} \\ &= \frac{d\mathbf{b}^I}{dt} \cdot \mathbf{a}_J f^J + \mathbf{b}^I \cdot \frac{d(\mathbf{a}_J f^J + \mathbf{G}_{\text{slow}})}{dt} = \frac{d\mathbf{b}^I}{dt} \cdot \mathbf{a}_J f^J + \mathbf{b}^I \cdot \frac{d\mathbf{S}_r F_r(\mathbf{y})}{dt} \\ &= \frac{d\mathbf{b}^I}{dt} \cdot \mathbf{a}_J f^J + \mathbf{b}^I \cdot \mathbf{S}_r \frac{dF_r(\mathbf{y})}{dt} = \frac{d\mathbf{b}^I}{dt} \cdot \mathbf{a}_J f^J + \mathbf{b}^I \cdot \mathbf{S}_r \frac{\partial F_r(\mathbf{y})}{\partial y^k} \frac{dy^k}{dt} \\ &= \frac{d\mathbf{b}^I}{dt} \cdot \mathbf{a}_J f^J + b_n^I S_r^n \frac{\partial F_r(\mathbf{y})}{\partial y^k} a_J^k f^J \equiv \frac{db_n^I}{dt} a_J^n f^J + b_n^I J_k^n a_J^k f^J \\ &\equiv \Omega_J^I f^J \end{aligned} \quad (2-173)$$

where

$$I, J = 1, 2, \dots, m$$

$$\Omega_J^I \equiv \frac{db_n^I}{dt} a_J^n + b_n^I J_k^n a_J^k, \quad I, J = 1, 2, \dots, m \quad \text{and} \quad k, n = 1, 2, \dots, N \quad (2-174)$$

$$J_k^n \equiv S_r^n \frac{\partial F_r}{\partial y^k} \quad r = 1, 2, \dots, M \quad \text{and} \quad k, n = 1, 2, \dots, N \quad (2-175)$$

The matrix J_k^n is the Jacobian of \mathbf{G} . J_k^n is in general not a constant matrix (in nonlinear case with $v_i' > 1$). At any moment in time, the eigenvalues of J_k^n can be computed. For problems arising from chemical kinetics, they are essentially real when the problems are of the boundary-layer type. The reciprocal of an eigenvalue, called the timescale, has the dimension of time. The i th timescale is denoted by $\tau(i)$ for the i th reaction. By placing them in ascending order, we have

$$|\tau(1)| < \dots < |\tau(i)| < \dots < |\tau(M)|$$

15.2.3.3 Determination of m , the Choice of \mathbf{a}_I and \mathbf{b}^J At any t , and particularly at $t = 0$, the $N \times N$ matrix J_k^n is available and its N eigenvalues and eigenvectors can be computed. The number of large eigenvalues of J_k^n determines the value of m .

An eigenvalue λ is considered large if $|\lambda \Delta t|$ is larger than 1.0, where Δt is the desired time resolution of the numerical solutions.

Each of the m right eigenvectors ($\beta^i = \beta^1, \beta^2, \dots, \beta^m$) of J_k^n with m large eigenvalues can be solved from the following equation:

$$\beta^i J_k^n = \lambda(i) \beta^i \quad (2-176)$$

Similarly, each of m left eigenvectors ($\alpha_i = \alpha_1, \alpha_2, \dots, \alpha_m$) of J_k^n can be solved from Eq. (2-177):

$$J_k^n \alpha_i = \alpha_i \lambda(i) \quad (2-177)$$

Basis vectors for the fast subspace \mathbf{a}_I and \mathbf{b}^J are defined as follows:

$$\mathbf{a}_I = \begin{bmatrix} \beta^1 \\ \beta^2 \\ \beta^3 \\ \vdots \\ \beta^m \end{bmatrix} \quad \text{and} \quad \mathbf{b}^J = [\alpha_1, \alpha_2, \alpha_3, \dots, \alpha_m] \quad (2-178)$$

Note that if complex eigenvalues (in conjugate pairs) are encountered, these eigenvalues can be replaced by the sum of the conjugate pairs and the real number of the imaginary part of the corresponding difference of the conjugate pairs.

When all of the eigenvalues of Ω_J^I have large negative real parts, all of the f^I 's will decay exponentially and \mathbf{G}_{fast} will become insignificant numerically very rapidly. It is now not a matter of "neglecting" anything; the contribution of \mathbf{G}_{fast} after some initial transient period will simply and naturally fade away numerically. When the \mathbf{G}_{fast} is dropped from Eq. (2-169), the system is said to be in *quasi-equilibrium* and the resulting (approximate) equation is theoretically equivalent to the so-called partial-equilibrium approximation commonly used in manual singular perturbation analysis, carrying as many terms as necessary to maintain "exactness" consistent with the precision of the numerical method used.

15.2.4 Procedures for Solving the Chain Reaction Problems A numerical demonstration of the use of the computational singular perturbation (CSP) method for the solution of stiff ordinary differential equations is demonstrated.

The use of CSP method to study a problem involves the following steps:

1. Identify S_r and $\mathbf{F}_r(y)$ from given $\mathbf{G}(y)$, assigning physical meaning to each r th reaction as much as possible.
2. Determine m and decide whether to use the optimal or the physical choice for the fast subspace.
3. Integrate Eqs. (2-166) and (2-173) using suitably small time steps until \mathbf{G}_{fast} is insignificant, and then bypass this term in the integration of Eq. (2-166) with an appropriately larger time step while solving for \mathbf{b}^J .
4. Whenever the value of m changes, repeat step 2.
5. The values of \mathbf{a}_I , \mathbf{b}^J , and S_r are physically meaningful and should be part of the output to provide useful (physically meaningful) information about the system under study.

Lu, Ju, and Law¹³⁹ employed the CSP method to generate a four-step and a ten-step reduced mechanism for the high-temperature H₂/air and CH₄/air oxidation, respectively. The validity of these reduced mechanisms was evaluated based on the responses of the perfectly stirred reactors and the one-dimensional planar propagating premixed flames. Comparisons between the reduced and detailed chemistries over a wide range of pressures and equivalence ratios show very good agreement on the flame speed, flame temperature, and flame structure. A software package based on the CSP algorithm was compiled to generate reduced mechanisms for complex chemical mechanisms. The validity and efficiency of the CSP algorithm was demonstrated. Results are shown in Figs. 2.31 and 2.32.

In general, the computational singular perturbation (CSP) method is a method that shows great promise in the realm of sensitivity analysis. This technique is held to be able to detect important and nonessential reactions and systematically eliminate them with minimal input or advance knowledge from the user. The CSP method of mechanism reduction is gaining popularity among combustion researchers. Many papers were written describing applications of this numerical procedure for specific combustion mechanism reduction or addressing variations very similar to CSP. Maas and Pope¹⁴⁰ have a similar scheme to create what they call low-dimensional manifolds of composition rates. These manifolds generate a graphic representation of reaction rates, and although they are in only a few dimensions because people can visualize no more than three dimensions, the trends are shown more clearly. The primary advantage to using CSP is that no advance knowledge is needed, but one should be cautious about blindly applying any numerical method without paying attention to the results and what they mean.

15.3 Some Observations of the CSP Method

One of the most undesirable aspects of the sensitivity analyses is the fact that no general methodology of mechanism reduction exists. Every author seems to

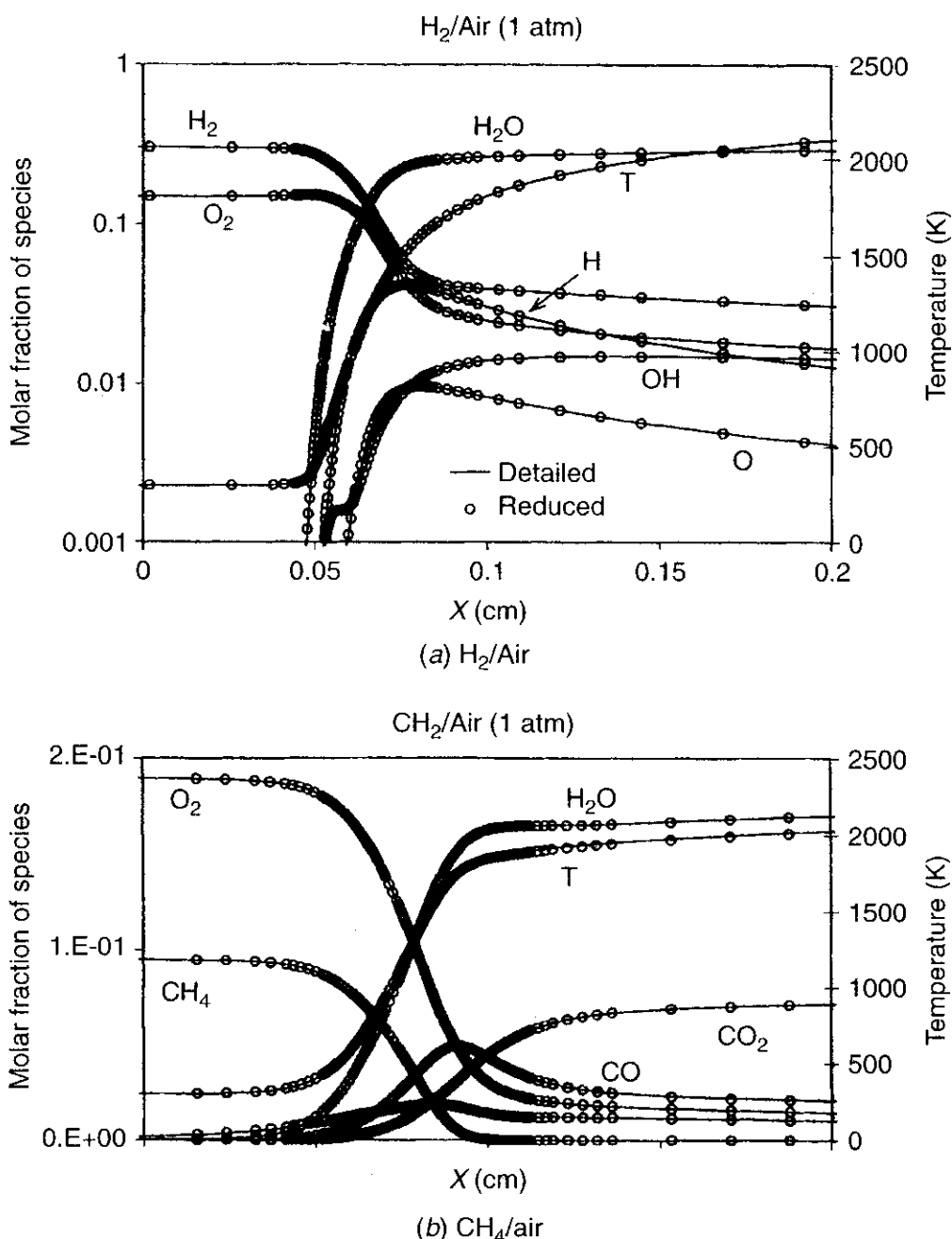


Figure 2.31 Comparison of the flame structures of temperature and species predicted by the reduced and detailed mechanisms, respectively, for stoichiometric flames at 1 atm. (a) H₂/air; (b) CH₄/air (after Lu, Ju, and Law¹³⁹).

have a preferred approach. Implementation of one specific approach or a hybrid mixture of several techniques is very typical. Some mathematically based studies have given some insight to the validity of the technique and details of how the mathematics involved works and tell in vague terms what the methods are capable of determining. The CSP technique described the previous section seems to be winning approval among the experts. The detailed treatment serves to illustrate how this approach can reduce mechanisms in general with minimal input from the user. However, there is no substitute for human evaluation of the results of any analysis.

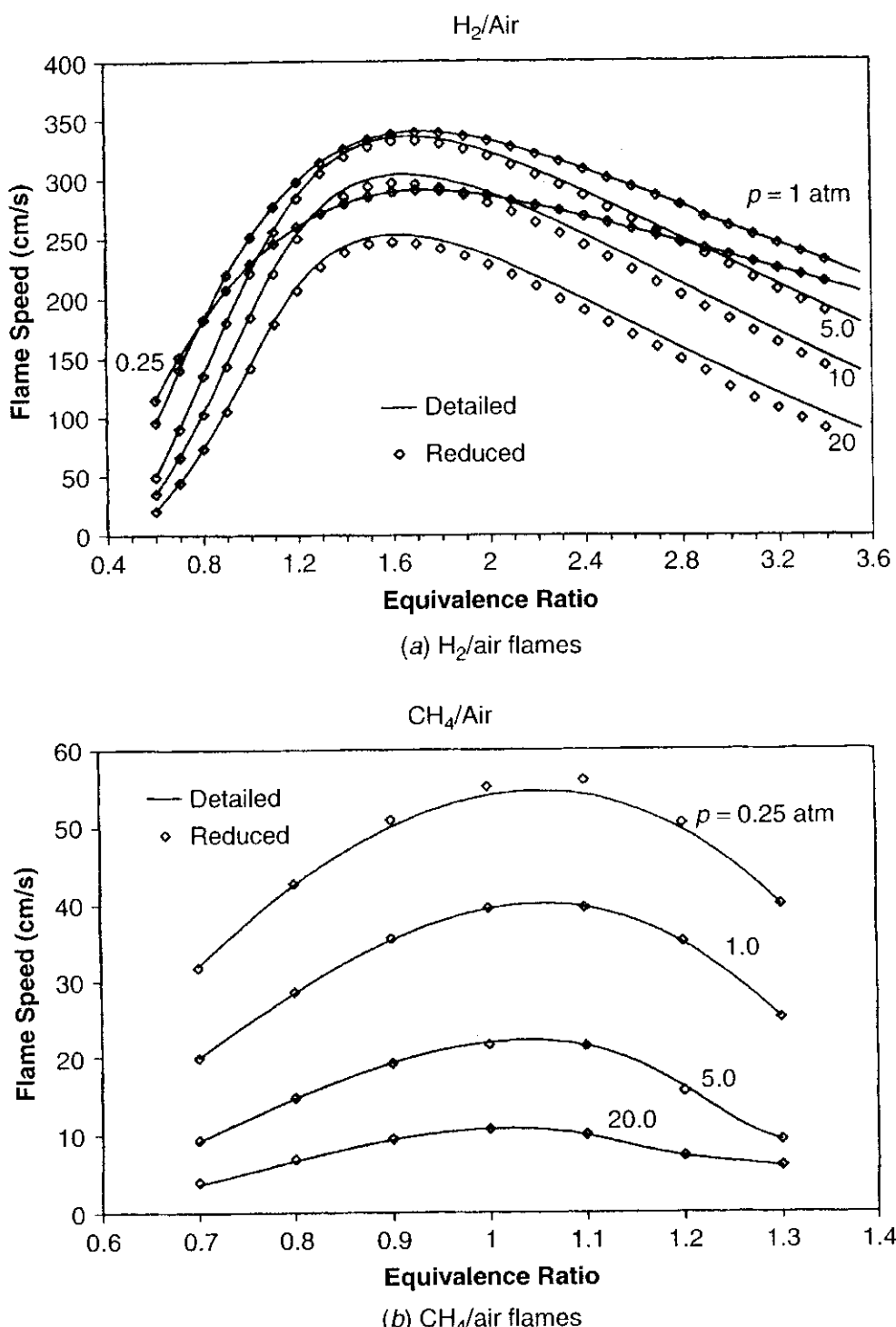


Figure 2.32 Comparison of the dependence of flame speed on the equivalence ratio between reduced and detailed mechanisms for (a) H₂/air flames and (b) CH₄/air flames at various pressures (after Lu, Ju, and Law¹³⁹).

Some might say that it is only a matter of time before the raw computing power necessary to tackle the full mechanisms in combustion is available. A quick consideration of how far computing power has come in recent years attests to this statement very well. But if one considers the fact that experimentation is the only trusted methodology to confirm whatever numerical assumption or scheme that

is produced, the full mechanism solution is not truly the end solution. Reduced mechanism study will probably continue even after full mechanism studies are possible with multidimensional, fluid-equation-coupled situations. Reduced mechanism study, which has its primary focus on reduction of work-time for the user, will also continue to have its merit in highlighting specific features within comprehensive models.

16 FORMATION MECHANISM OF NITROGEN OXIDES

Formation mechanism of oxides of nitrogen has been a topic of intensive research for many decades. The importance of this mechanism stems from the fact that nitrogen oxides are one of the principal contaminants emitted by combustion processes. Oxides of nitrogen damage the environment severely; thus, government agencies are passing stringent laws to control the emissions of pollutants. An in-depth understanding of the mechanism of formation of the oxides of nitrogen is essential when automotive and other industrial devices are designed. Suitable schemes must be developed for controlling the amount of NO_x generated from combustion products of various engines and other energy-conversion systems. Another motivation for the study of NO_x formation mechanism arises from the fact that energetic materials, such as explosives, always contain nitrogen compounds, and nitrogen oxides are always present in their combustion products. Therefore, knowledge of the NO_x formation mechanism is essential for understanding combustion of energetic materials.

The first major work on the kinetics of NO_x was performed by Zel'dovich¹⁴¹ in 1946, who postulated the thermal NO mechanism, now known as the Zel'dovich NO mechanism. Later on, Fenimore¹⁴² in 1979 proposed the prompt NO mechanism to explain the additional NO being produced over and above the Zel'dovich thermal NO in hydrocarbon flames. Recently, researchers identified some additional routes through which NO and other oxides of nitrogen are formed. These different routes are categorized below:

1. Thermal NO route, also known as the Zel'dovich NO mechanism
2. Prompt NO route, also known as the Fenimore NO mechanism
3. Fuel-bound nitrogen (FN) route
4. NO_2 route
5. N_2O route

Their individual mechanisms are described in the following sections.

16.1 Thermal NO Mechanism (Zel'dovich Mechanism)

In the combustion of clean fuels (which do not contain nitrogen compounds) with air (which contains atmospheric N_2) NO is formed mainly by the Zel'dovich

mechanism. This mechanism consists of three principal reactions as follows:



$$k_{1,f} = 1.8 \times 10^{11} \exp(-38,370/T) \text{ m}^3/(\text{kmol} \cdot \text{s})$$

$$k_{1,r} = 3.8 \times 10^{10} \exp(-425/T) \text{ m}^3/(\text{kmol} \cdot \text{s})$$



$$k_{2,f} = 1.8 \times 10^{10} \exp(-4,680/R_u T) \text{ m}^3/(\text{kmol} \cdot \text{s})$$

$$k_{2,r} = 3.8 \times 10^9 \exp(-20,820/T) \text{ m}^3/(\text{kmol} \cdot \text{s})$$



$$k_{3,f} = 7.1 \times 10^{10} \exp(-450/T) \text{ m}^3/(\text{kmol} \cdot \text{s})$$

$$k_{3,r} = 1.7 \times 10^{11} \exp(-24,560/T) \text{ m}^3/(\text{kmol} \cdot \text{s})$$

The chain nature of this mechanism can be observed in Fig. 2.33. The Zel'dovich mechanism is also known as the “thermal” mechanism, because reaction (N1) has very high activation energy (319 kJ/mol) due to the strong triple bond in the N₂, and so it is sufficiently fast only at high temperatures. Because of the low reaction rate constant, reaction (N1) is the rate-determining step in the Zel'dovich reaction mechanism. As a rule-of-thumb, the thermal mechanism is usually unimportant at temperatures below 1800 K. NO is generally considered to be formed in the post-flame gases.

In general, this mechanism is coupled with the fuel combustion chemistry through the O₂, O, and OH species. Since the overall rate of NO formation by the thermal mechanism generally is slow compared with the fuel oxidation reactions, it often is assumed, following the suggestion of Zel'dovich, that the

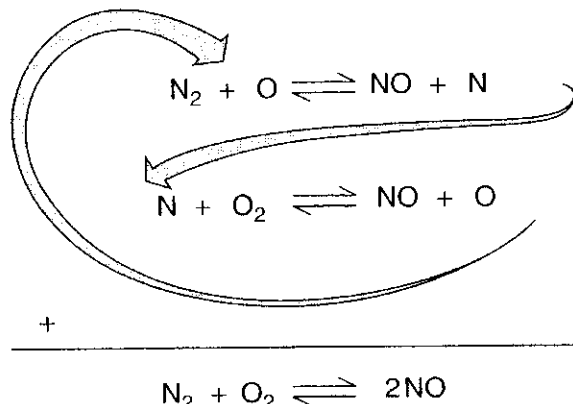


Figure 2.33 Chain nature of the thermal NO formation mechanism.

NO formation reactions can be decoupled from the fuel oxidation process. The concentration of NO cannot be predicted well by considering it to be in equilibrium in reaction (N1), because the reaction (N1) is so slow that equilibrium is reached only for times that are much longer than typical residence times in the high-temperature range.

Quasi-steady-state assumption for N atom can be used to simplify the rate expression of NO formation. If the assumption that the NO concentrations are much less than the equilibrium values is made, the reverse reactions can be neglected. These assumptions greatly simplify the calculation of NO formation rate. Using reactions (N1), (N2), and (N3), we have

$$\frac{dC_{\text{NO}}}{dt} = k_{1,f} C_{\text{O}} C_{\text{N}_2} + k_{2,f} C_{\text{N}} C_{\text{O}_2} + k_{3,f} C_{\text{N}} C_{\text{OH}} \quad (2-179)$$

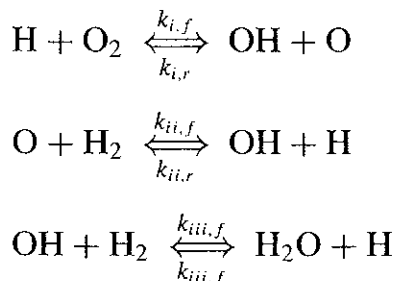
Assuming N atoms to be in quasi steady state [because of fast reactions (N2) and (N3)], $dC_N/dt = 0$; thus,

$$\frac{dC_{\text{N}}}{dt} = 0 = k_{1,f} C_{\text{O}} C_{\text{N}_2} - k_{2,f} C_{\text{N}} C_{\text{O}_2} - k_{3,f} C_{\text{N}} C_{\text{OH}} \quad (2-180)$$

Solving Eq. (2-180) for C_N and substituting it into Eq. (2-179), we get

$$\frac{dC_{\text{NO}}}{dt} = 2k_{1,f} C_{\text{O}} C_{\text{N}_2} \quad (2-181)$$

Hence, it can be observed that NO formation rate depends on the concentrations of N_2 and O. The concentration of N_2 can be accurately measured with a probe or can be estimated assuming equilibrium in the burnt gases. If the relevant timescales are sufficiently long, one can assume that the N_2 , O_2 , O, and OH concentrations are at their equilibrium values and N atoms are in quasi steady state. In flame zone proper and in certain short-timescale post-flame processes, the equilibrium assumption is not truly valid. According to Warnatz et al.,³⁰ *super-equilibrium concentrations* of O atoms, up to several orders of magnitude greater than equilibrium, can greatly increase NO formation. *Partial-equilibrium* assumption for O atoms gives better estimate of O atom concentration as has been verified from experiments. Consider partial equilibrium for the following reactions:



For each of the reactions, the forward and backward reaction rates are equal. Therefore, we get

$$\begin{aligned} k_{i,f} C_H C_{O_2} &= k_{i,r} C_{OH} C_O \\ k_{ii,f} C_O C_{H_2} &= k_{ii,r} C_{OH} C_H \\ k_{iii,f} C_{OH} C_{H_2} &= k_{iii,r} C_{H_2O} C_H \end{aligned}$$

Solving for O-atom concentration, we obtain,

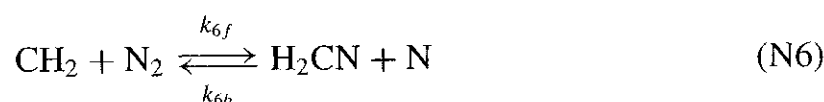
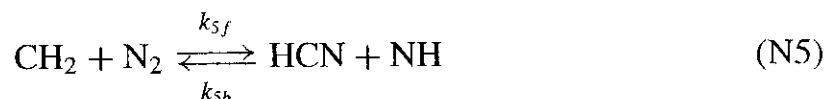
$$C_O = \frac{k_{i,f} k_{iii,f} C_{O_2} C_{H_2}}{k_{i,r} k_{iii,r} C_{H_2O}} \quad (2-182)$$

Therefore, the O atom concentration can be calculated from the concentrations of H₂O, O₂, and H₂, which can be measured or estimated easily, since they are stable species.

16.2 Prompt NO Mechanism (Fenimore Mechanism)

Fenimore^{142,143} discovered that some NO was promptly produced in the flame zone of laminar premixed flames long before there would be time to form NO by the thermal mechanism, and he termed this rapidly formed NO the “prompt” NO. Numerous studies have shown that prompt NO in hydrocarbon flames is formed primarily by a reaction sequence that is indicated by the rapid reaction of hydrocarbon radicals (CH, CH₂, C₂, C₂H, C) with molecular nitrogen, leading to formation of amines or hydrocyanic acid (HCN) that subsequently reacts to form NO. Therefore, prompt NO reaction mechanism is of paramount importance in hydrocarbon fuels, especially in fuel-rich conditions.

The following reactions are considered principal reactions, although there might also be other reactions:



Reaction (N4) is the primary path and is the rate-limiting step in the sequence. The rate constant $k_{4,f}$ correlated from many sets of experimental data can be

expressed as

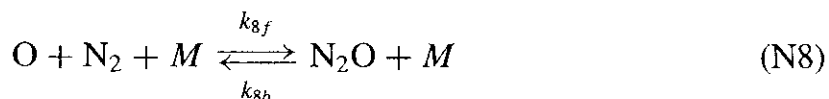
$$k_{4,f} = 4.4 \times 10^{12} \exp(-11,060K/T) \text{ cm}^3/(\text{mol} \cdot \text{s}) \quad (2-183)$$

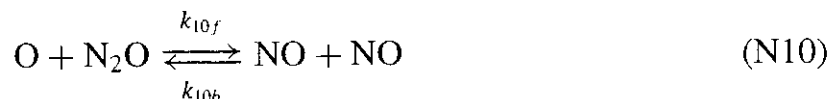
Reaction (N4) leads to prompt NO. There have been indirect measurements of k_4 from flame, shock-tube, and stirred-reactor data and one direct shock-tube measurement. The estimated accuracy of k_4 from Eq. (2-183) is about a factor of 2 at the present time. The activation energy for reaction (N4) is between 75 and 92 kJ/mol, which is much lower than 319 kJ/mol for the formation of thermal NO. Thus, reaction (N4) is very important for NO formation through the production of HCN species. For readers interested in comparison of various rate constants of k_4 obtained by different research groups, the review paper by Miller and Bowman,¹⁴⁴ which gives the detailed information in tabular form, is highly recommended.

Now let's consider the reaction (N5) in the mechanism. This reaction is endothermic. The suggested activation energy for this reaction is approximately 356 kJ/mol, a very high value. The rate coefficient expression used by Glarborg and coworkers is $k_5 = 10^{13} \exp(-310,000/R_u T) \text{ cm}^3/\text{mol-s}$, though a value of $k_5 = 10^{12} \exp(-356,000/R_u T) \text{ cm}^3/\text{mol-s}$ is suggested by Miller and Bowman¹⁴⁴ to be more likely. Due to the high value of activation energy, this reaction is an insignificant contributor to prompt NO.

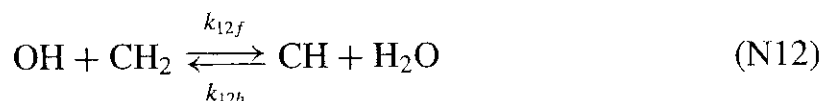
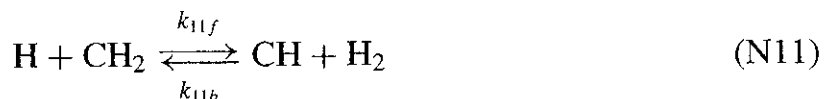
The reaction (N6) is endothermic by 330.5 kJ/mol. The rate coefficient expression k_6 is estimated to be essentially the same as $k_{1,f}$ of the Zel'dovich mechanism. This reaction is also an insignificant contributor to prompt NO. The last prompt-NO reaction considered in the mechanism is reaction (N7). Experiments indicate that the reverse of this reaction is very fast according to Miller and Bowman¹⁴⁴; hence, reaction (N7) is a minor, but non-negligible, contributor to prompt NO under most conditions. This reaction is highly endothermic. Thus, its importance with respect to reaction (N4) increases with increasing temperature.

Overall, prompt-NO formation involves three separate kinetic issues, including (1) the CH concentration and how it is established; (2) the rate of molecular nitrogen fixation (i.e., value of k_4); and (3) the rate of interconversion among fixed nitrogen fragments. From sensitivity analysis conducted by Miller and Bowman,¹⁴⁴ it was found that reaction (N4) is an important rate-limiting step for NO, HCN, and TFN (total fixed nitrogen, TFN = NO + HCN + NH₃) production under all conditions investigated. The reaction has sensitivity coefficients for these species approaching unity in rich mixtures. Even under lean conditions ($\phi < 0.8$), it plays a major role in NO formation. The thermal NO mechanism is the dominant source of NO only in the equivalence-ratio range ($\phi = 0.8-1.0$). For $\phi < 0.8$, the temperature becomes sufficiently low and the following reactions become an important source of NO formation:

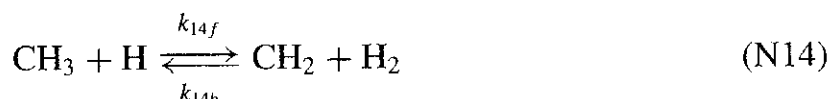
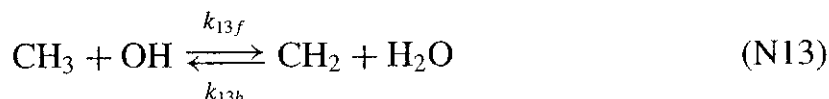




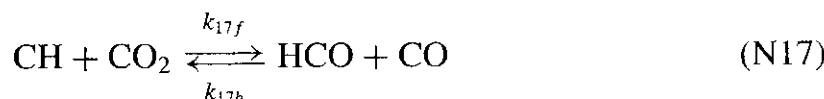
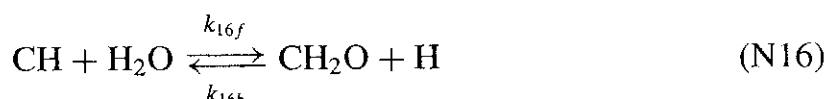
CH is formed as an intermediate at the flame front only. The mechanism of CH formation depends slightly on the fuel. In all cases, CH is formed from methylene (CH_2) by reaction with H and OH , i.e.,



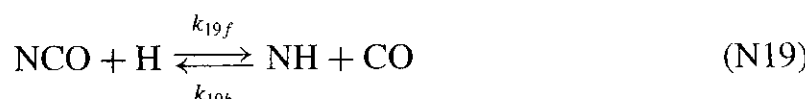
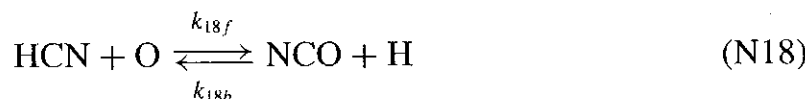
The CH_2 can be formed either from methyl radical (CH_3) or from acetylene. For $\phi < 1.5$, the CH_3 is the dominant source.



The most important CH -consuming steps are the following reactions:



Up to an equivalence ratio of approximately $\phi = 1.2$, the HCN and N produced by reaction (N4) are converted rapidly to NO , primarily by the following reactions:

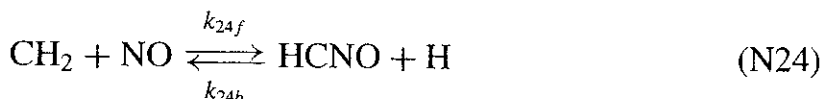
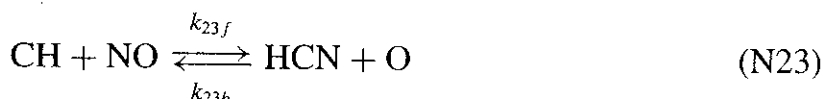




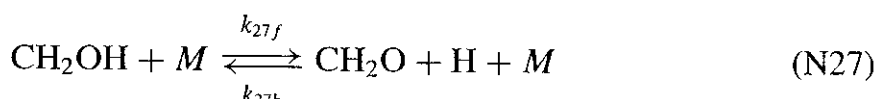
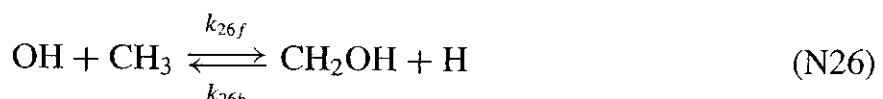
Beyond $\phi = 1.2$, several factors¹⁴⁴ combine to cause the NO concentration to decrease relative to HCN:

1. The conversion of HCN to NO by the above mechanism is no longer rapid.
2. The “recycle” of NO to HCN by the mechanism discussed below begins to inhibit NO production.
3. The reaction $\text{N} + \text{NO} \rightleftharpoons \text{N}_2 + \text{O}$ shifts direction from reverse to forward.

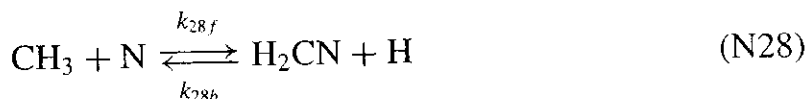
A decrease in the O atom concentration contributes to all three of the above occurrences. Under rich conditions, reactions that convert CH_3 to CH_2 become more competitive with the oxidation reaction of CH_3 according to $\text{CH}_3 + \text{O} \rightleftharpoons \text{CH}_2\text{O} + \text{H}$, thereby producing the radicals C, CH, and CH_2 and allowing the following recycle reactions to be more effective:



From their calculations, Miller and Bowman¹⁴⁴ found that at $\phi = 1.4$ the peaks in the CH and TFN (total fixed nitrogen) concentrations occur simultaneously. Beyond $\phi = 1.4$, the fixed nitrogen concentration is limited by the availability of the chain carriers (H and OH) required for producing CH from methane. The following chain-branching reactions occur



In this regime, the following reaction



appears as a competitor for nitrogen atoms, competing with



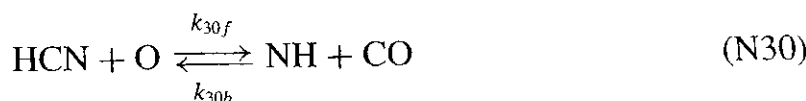
The dissociation of H_2CN following reaction (N28) results in the formation of hydrogen cyanide, rather than nitric oxide, from the N atom in reaction (N28).

From experiments and calculations, it has been found that at low temperatures ($T < 2000$ K) the hydrocarbon–nitrogen prompt-NO channel dominates the rate of NO formation. As the temperature increases, the relative importance of the hydrocarbon–nitrogen prompt-NO channel decreases, so that for temperatures above 2500 K, NO formation is controlled mainly by the thermal mechanism. Miller and Bowman¹⁴⁴ also showed that, for a series of premixed methane/air flames ($1.37 \geq \phi > 1.06$), the transition from the hydrocarbon–nitrogen prompt-NO mechanism to the thermal mechanism occurs as conditions become leaner.

16.3 NO Production from Fuel-Bound Nitrogen

In fossil fuels (coal and coal-derived fuels), nitrogen is present as the chemically bound nitrogen. It is the primary source of production of nitrogen oxides formed on their combustion. From different experiments, it has been found that the extent of conversion of fuel-bound nitrogen (FN) into NO is strongly dependent on the local combustion environment (temperature and stoichiometric conditions) and on the initial level of nitrogen compounds in the fuel-air mixture. Available data suggest that the gas-phase fuel-nitrogen reaction sequence is initiated by a rapid conversion of the fuel nitrogen compounds to hydrogen cyanide (HCN) and ammonia (NH_3). HCN appears to be the principal product when the fuel nitrogen is bound in an aromatic ring, NH_2 when the fuel nitrogen is in the form of amines. Thus, the mechanism of NO production is essentially the mechanism of oxidation of HCN and NH_3 . The important paths are shown in Fig. 2.34, along with the prompt mechanism.

16.3.1 The Oxidation of HCN The removal of HCN is controlled by the reaction of HCN with O atoms, even in rich flames.



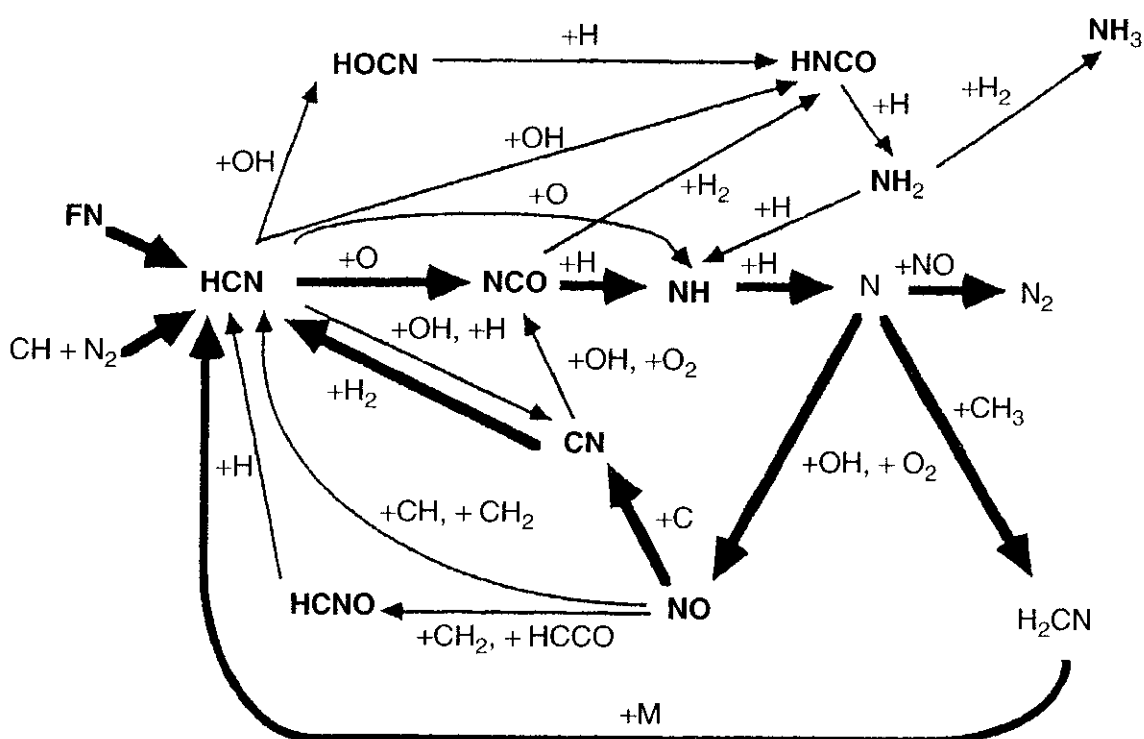
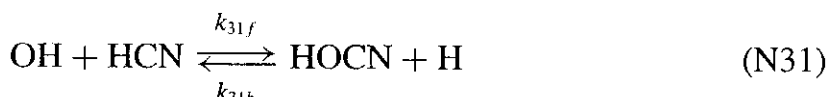


Figure 2.34 Reaction path diagram showing the major steps in prompt NO and conversion of fuel nitrogen to NO (after Miller and Bowman¹⁴⁴).

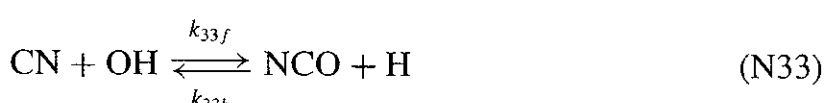
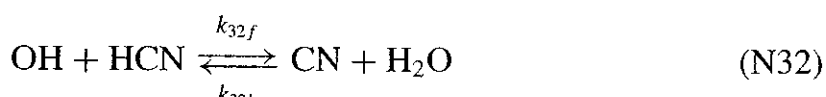
The subsequent reactions of NCO and NH with hydrogen atoms, producing N, are relatively fast and have little influence on the observed species profiles. The distribution of NO and N₂ in the flame is governed by the N atom reactions,



In the post-flame gases of very rich atmospheric-pressure flames, HCN is removed primarily by reaction with OH. Two routes have been suggested by Miller and Bowman,¹⁴⁴ one that is first order in OH,



and one that is second order,



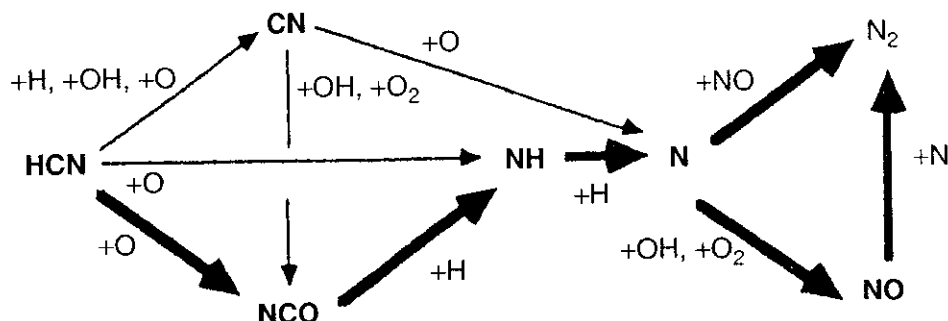
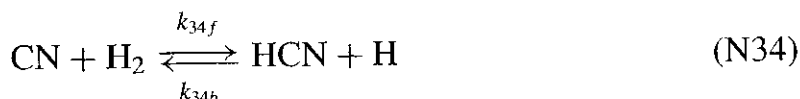


Figure 2.35 Reaction path diagram illustrating the reaction mechanism by which HCN is converted to NO and N₂ (after Miller and Bowman¹⁴⁴).

under the partially equilibrated conditions prevalent in the post-flame gases of atmospheric-pressure flames. The first route is dominant below 2300 K and the second route above 2300 K.

Accumulated experience by chemists in modeling a variety of flames, stirred reactors, and flow reactors indicates that the O + HCN sequence shown in Fig. 2.35 always plays a major role in the conversion to NO and N₂. The OH + HCN reactions normally come into play only under conditions that are both rich and nearly equilibrated. If HCN conversion takes place in a highly nonequilibrated reaction zone, even under very rich conditions, the O + HCN sequence still is likely to be dominant according to Miller and Bowman.¹⁴⁴

16.3.2 The NO → HCN → N₂ Mechanism In rich combustion systems, there is the possibility of reaction of NO with hydrocarbon free radicals, leading to the formation of HCN and, eventually, of molecular nitrogen N₂. The main reaction paths involved in converting NO to N₂ through HCN and CN is shown in Fig. 2.36. As shown in this figure, there is no direct interaction between hydrocarbon and nitrogen chemistry. There are different routes of production of HCN. Based on experiments conducted on low-pressure premixed flames ($\phi = 1.5$, H₂/O₂/Ar flames), to which small quantities of acetylene, HCN, and NO were added in various combinations, researchers found that CN concentration has a sharp peak at a few millimeters above the flame. From such observations, it can be concluded that CN is produced and destroyed in this region of the flame by the sequence



Another sequence for HCN production is the following reaction:



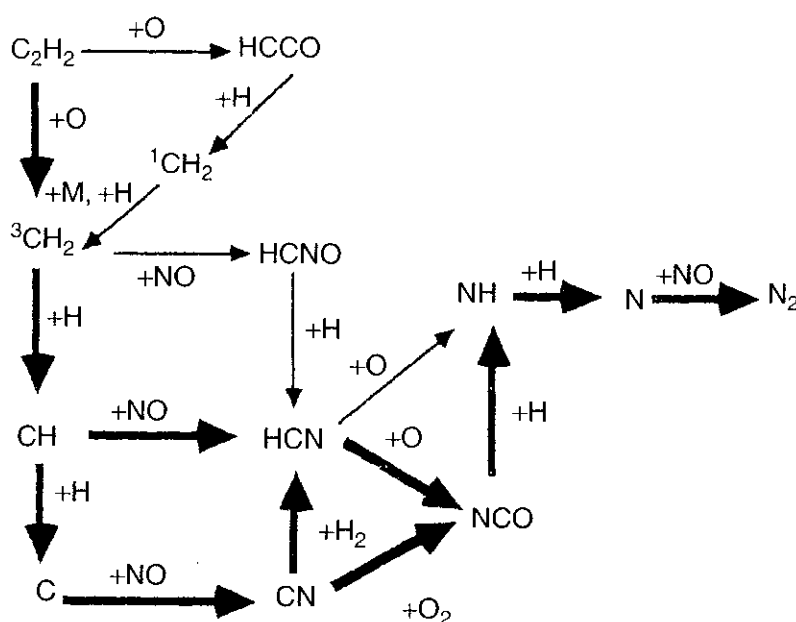
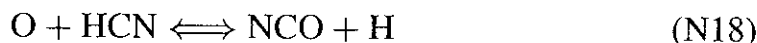
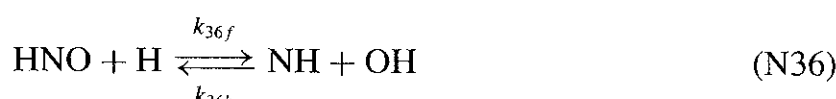
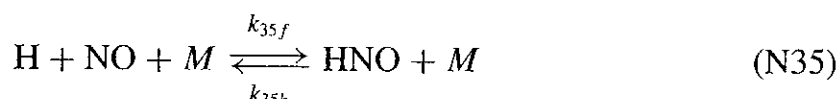


Figure 2.36 Reaction path diagram illustrating the $\text{NO} \rightarrow \text{HCN} \rightarrow \text{N}_2$ conversion mechanism proposed by Miller and Bowman¹⁴⁴ for NO added flames.

HCN is partially converted to N_2 in the flame by the following sequence of reactions:



Bowman and co workers have shown that in atmospheric-pressure, fuel-rich $\text{H}_2/\text{O}_2/\text{Ar}$ flames to which small amounts of NO were added, significant removal of NO ($\geq 40\%$) occurs by the following reaction sequence:



16.3.3 The Oxidation of NH_3 Figure 2.37 shows the principal reactions through which ammonia is oxidized to NO and then NO is converted to molecular nitrogen in NH_3/O_2 flames. Ammonia is converted to NH_2 by hydrogen

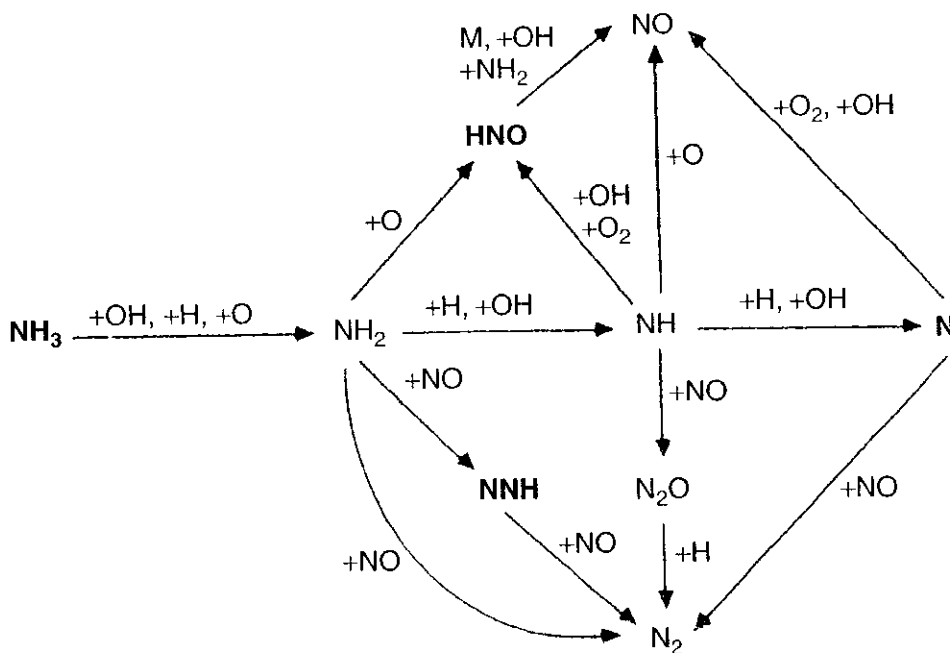
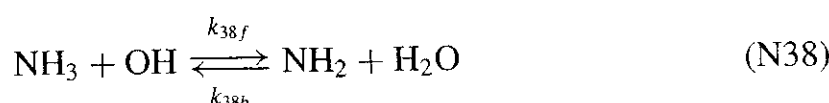
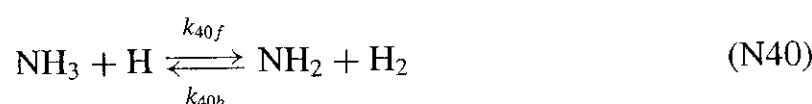
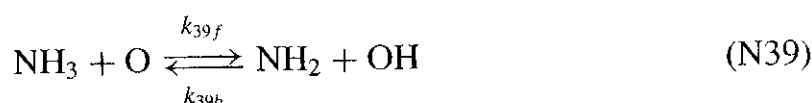


Figure 2.37 Reaction path diagram showing the major routes for the oxidation of NH_3 (after Miller and Bowman¹⁴⁴).

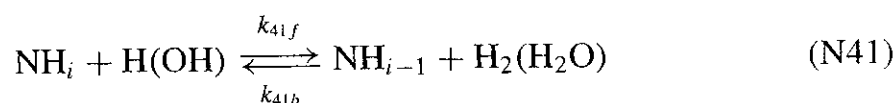
abstraction. The primary abstraction reaction is



The NH_3 reaction with O atom under fuel-lean conditions and the NH_3 reaction with H atom under fuel-rich conditions are both significant for NH_2 formation:



Successive smaller amine free radicals are formed by reaction with H atoms and to a lesser extent by reaction with OH,



$$i = 1, 2$$

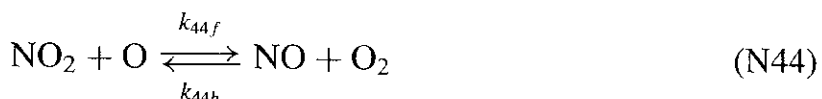
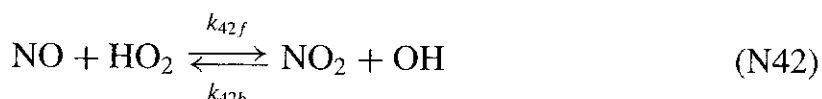
Each NH_i free radical can undergo subsequent reaction by one of two mechanisms:

1. oxidation leading to NO formation;
2. reaction with NO leading to the formation of molecular nitrogen.

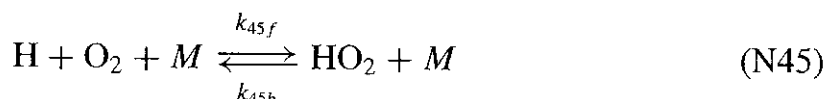
Whether N, NH, or NH₂ is the primary radical in determining NO/N₂ product distribution depends on the equivalence ratio (ϕ). For very lean flames, NH₂ is the critical amine radical. As ϕ increases, the greater availability of H atoms results in a shift in the critical radical species from NH₂ to NH to N. Normally all three radicals play same role. However, in rich flames the N atom is more dominant. It is interesting to note that there are reactions other than those shown in Fig. 2.37 that form N₂ but do not involve NO.

16.4 NO₂ Mechanism

It has been observed that NO₂ can have significant concentration in certain combustion conditions, especially near the flame zone. Kinetic calculations have indicated that the NO₂ formation and destruction in flames can occur according to the following sequence.



In the low-temperature regions of flames, significant HO₂ concentrations are found that can react with NO formed in the high-temperature regions and transported by diffusion to the low-temperature region. The NO₂ removal reactions are rapid, and in the presence of high radical concentrations, NO₂ will be converted rapidly back to NO. The most important reaction for NO₂ formation is reaction (N42). Since the rate of this reaction depends on the HO₂ concentration, NO₂ formation is also sensitive to reactions forming and removing HO₂. The following is the principal HO₂ formation reaction in the low-temperature region of the flame.



The H atoms needed for this reaction are transported from the high-temperature regions by molecular diffusion. Since H atoms play an important role in HO₂ production, NO₂ formation is also sensitive to reaction (N25). This phenomenon can be observed in Fig. 2.38. The principal NO₂ removal step is reaction (N43), while reaction (N44) is not so important.

16.5 N₂O Mechanism

N₂O is an important nitrogen oxide under fuel-lean conditions. Studies indicate that N₂O is a very short-lived species in hot combustion gases and that the

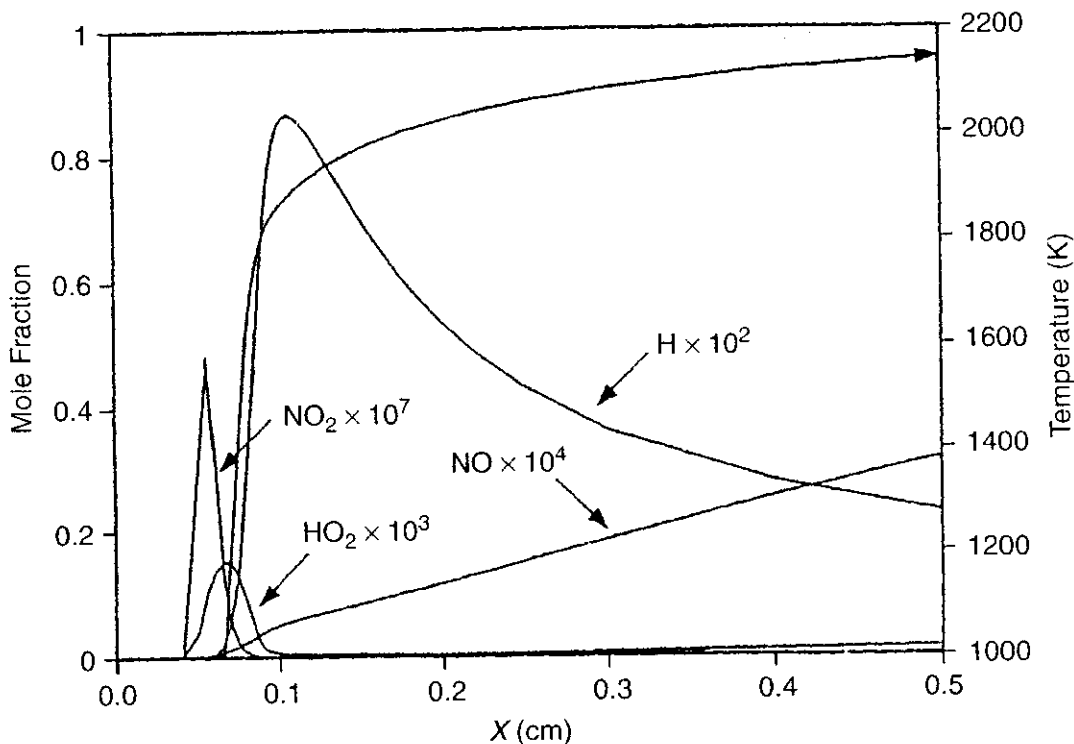
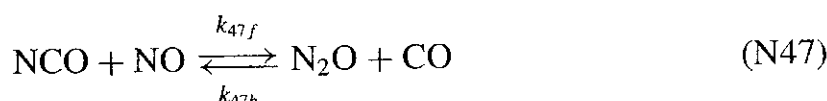


Figure 2.38 Flame structure showing the large concentration of nitric oxide near the flame zone of atmospheric-pressure 10% methane in air flame. Profiles of H, NO, and HO₂ are also seen (after Miller and Bowman¹⁴⁴).

principal N₂O formation reactions involve NO and various nitrogen-containing radicals such as



The principal N₂O formation reaction is reaction (N46). For rich mixtures, both reactions (N46) and (N47) are important in N₂O formation. The forward reaction rate coefficient for reaction (N46) is estimated to be $k_{46f} = 2.46 \times 10^{15} T^{-0.8} \text{ cm}^3/\text{mol-s}$ and that of reaction (N47) is $k_{47f} = 1.0 \times 10^{13} (390 \text{ cal}/R_u T) \text{ cm}^3/\text{mol-s}$.

The N₂O formed in these reactions rapidly reacts with H atoms to form N₂:



In fuel-lean flames, the primary N₂O removal reaction is reaction (N48). While the removal is done by reaction (N48), there is another mechanism first postulated by Wolfrum (1972) for the formation of N₂O and subsequent conversion to NO (see Warnatz et al.³⁰). This mechanism is analogous to the thermal mechanism

in that O atom attacks N_2 . In the presence of a third body, M , the outcome of this reaction is N_2O .



The N_2O may subsequently react with O atoms to form NO



The activation energy of this reaction is around 97 kJ/mol. Under fuel-lean conditions, CH formation is suppressed, leading to less Fenimore prompt NO, and at low-temperatures, Zel'dovich thermal NO is also less. What remains is NO generated via N_2O , which is promoted at high pressures because of the three-body reaction. Since the activation energy for the three-body reaction is low, low temperature does not affect the formation rate of NO. Due to the characteristic of the reaction mechanism, this route is the major source of NO in lean premixed combustion in gas turbine engines.

16.6 Overall Remarks on NO_x Formation

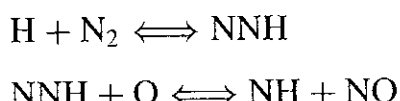
In general, the formation of NO is a complex process that involves many elementary chemical reactions. It involves both equilibrium and nonequilibrium processes that take place in the precombustion, combustion, and post-flame regions. The primary nitrogen oxide formed in combustion systems is NO, although in some systems, appreciable NO_2 is produced, usually because of $\text{NO} \rightarrow \text{NO}_2$ conversion in low-temperature mixing regions of non-premixed systems.

The formation of NO is for the most part determined by the peak temperature achieved during combustion. In turn, the peak temperature depends on a number of variables, including equivalence ratio ϕ , quantity of diluents present, fuel composition, and the initial temperature of the fuel-air mixture. Prompt NO is produced at low temperatures (about 1000 K). This is because the activation energy of the rate-limiting reaction of the prompt-NO mechanism, $\text{CH} + \text{N}_2 \rightarrow \text{HCN} + \text{N}$, is about 92 kJ/mol ($T_a = 11,060$ K), compared with 319 kJ/mol ($T_a = 38,400$ K) for the rate-limiting reaction of the thermal-NO mechanism.

In laminar flames at low pressures, NO yield is dominated by the Fenimore and super-equilibrium O/OH Zel'dovich route. At high pressures, the equilibrium concentrations of O, OH, and H have strong influence on the formation rate, and the Zel'dovich thermal-NO mechanism dominates. For fuel-rich mixtures, Fenimore prompt-NO mechanism dominates. For sufficiently fuel-rich mixtures, however, this route no longer dominates. At ultra-lean conditions, it has been suggested by Correa and Smooke that N_2O intermediate route dominates. Lean conditions can suppress the formation of CH radicals, hence leading to less Fenimore prompt NO, and low temperature can suppress the Zel'dovich NO. What remains is NO generated via N_2O route. The fuel-bound nitrogen route is important in non-premixed flames.

Although the NO_x mechanism has been extensively investigated, one cannot conclude that all of the formation routes have already been found. There could be

additional mechanisms involved. For example, the mechanism proposed by Dean and Bozzelli in 1995 considered the following reactions for NO production¹⁴⁵:

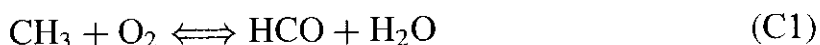


These reactions predict formation of significant amounts of NO in flames burning in air. Using the results from numerous research investigations on NO_x formation mechanism, engineers have made various modifications to combustion devices to minimize the amount of NO_x generated. These techniques are called *primary methods* of NO_x control.

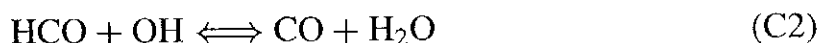
17 FORMATION AND CONTROL OF CO AND PARTICULATES

17.1 Carbon Monoxide

Carbon monoxide is a colorless, odorless, and tasteless gas that is a noncorrosive gaseous material with density of 1.25 g/L at room temperature and ambient pressure. CO is mainly emitted from passenger cars and traffic-related sources (~ 22%), domestic heating (~ 21%), combustion of biomass (~ 18%), anthropogenic oxidation (~ 15%), industry exhaust (~ 14%), vegetation (~ 4%), and other miscellaneous sources (~ 6%). At present, the detailed kinetics of CO formation is not fully understood. In most studies, high-temperature oxidation of the methyl radical is considered to be the principal intermediate reaction, i.e.,



It is then proposed that carbon monoxide is mainly formed from the reaction



Another possibility is



Currently, about 77% of the nationwide CO emissions are from transportation sources. The largest emissions contribution comes from highway motor vehicles. Thus, the focus of CO monitoring has been on traffic-oriented sites in urban areas where the main source of CO is motor vehicle exhaust. Thus, in newer vehicles the following modifications are made to reduce CO emissions:

Choke modulated closer to lean limit

Retarded ignition timing

Improved combustion chamber design to reduce flame quenching

Overall leaner mixture ratios for automobile engines

Other major CO sources are wood-burning stoves, incinerators, and industrial sources. These are controlled by simple techniques of making CO burn completely to form CO₂. This increases the amount of gas to be handled; however, subsequent explosions can be reduced. The National Ambient Air Quality Standard for carbon monoxide is 9 ppm for 8-hour nonoverlapping average not to be exceeded more than once per year. The rounding convention in the standard specifies that values of 9.5 ppm or greater are counted as exceeding the level of the standard. A steady increase in amount of CO emitted (in millions of tons per year) was noted from 1940 to 1970. In 1970, the Clean Air Act was passed, which put stringent conditions on CO emissions. Thus, a drastic decrease of CO emission was made possible from 1970 to 1995. In the absence of this act, the amount of CO emission was heading to almost 200 millions tons in 1995, whereas now it's less than half of that.

17.2 Particulate Matter

Air pollutants called particulate matter include dust, dirt, soot, smoke, and liquid droplets directly emitted into the air by sources such as factories, power plants, cars, construction activity, fires, and natural windblown dust. Particles formed in the atmosphere by condensation or the transformation of emitted gases such as SO₂ are also considered particulate matter. The nature of particulate matter can be described by the following specifications:

Particulate matter ranges in size from about half a millimeter down to molecular dimensions.

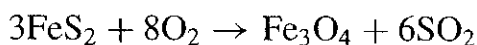
Particulate matter makes for visible and obvious forms of air pollution.

Atmospheric aerosols are solid or liquid particles smaller than 100 μm in diameter.

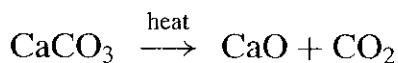
Pollutant particles in the 0.001 to 10 μm range are commonly suspended in the air near sources such as the urban atmosphere, industrial plants, highways, and power plants.

The chemical processes of formation of particulate matter include

Inorganic particles—Metal oxides constitute a major class of inorganic particles formed from burning fuels containing metals:



Calcium carbonate is converted to calcium oxide:



A common process for the formation of aerosol mists involves the oxidation of atmospheric sulfur dioxide to sulfuric acid, a hygroscopic substance that

accumulates atmospheric water to form small liquid droplets:



17.2.1 Major Types of Particulates

Soot Carbonaceous particles produced in the gaseous fuels or generated from the volatilized components of liquid or solid fuels are called soot. Soot particles are agglomerates of small, roughly spherical particles. They vary in size from 0.005 to 0.2 μm but most commonly lie in the size range of 0.01 to 0.05 μm . Typically, they consist of large numbers of lamellar crystals that usually have 5–10 sheets containing roughly 100 carbon atoms each. Formation and growth of polycyclic aromatic hydrocarbons (PAH) and soot were studied extensively by Frenklach and Warnatz¹⁴⁶, Frenklach and Wang¹⁴⁷, Santoro et al.¹⁴⁸ Basic mechanisms and processes are discussed in the book by Warnatz, Mass, and Dibble.³⁰

Ash Coal is a natural dark-brown to black solid used as a fuel and is formed from fossilized plants. Coal contains amorphous carbon with various organic and some inorganic compounds. The inorganic compounds are called minerals. Mineral inclusions are dispersed in the coal matrix. The mean diameter of the mineral inclusions is typically about 1 μm (0.1 to several microns). Coal is usually crushed to 70–80% through 200 mesh or 75 μm . Coal particles are heated to about 1500 K. Particles undergo pyrolysis, char formation, fragmentation, and burnout. Because of porosity, fissures, and structural imperfections, particles disintegrate into a number of fragments. This is how ash is formed.

17.2.2 Harmful Effects Based on studies of human populations exposed to high concentrations of particles (sometimes in the presence of SO_2) and laboratory studies of animals and humans, there are major effects of concern for human health. These include effects on breathing and respiratory symptoms and aggravation of existing respiratory and cardiovascular diseases. Exposure also causes alterations in the body's defense systems against foreign materials, damage to lung tissue, carcinogenesis, and premature death. The major subgroups of the population that appear to be most sensitive to the effects of particulate matter include individuals with chronic obstructive pulmonary or cardiovascular disease or influenza, asthmatics, the elderly, and children. Particulate matter also soils and damages materials and is a major cause of visibility impairment in industrialized countries.

17.2.3 Particulate Matter Control Methods There are many methods for controlling particulate matter. In general, the particulate-laden gas is forced to change direction. As the gas changes direction, the inertia of the particles causes them to travel continuously in their original directions. In this way, particles can be separated from the gas stream. Different methods are described briefly below.

Gravity Settlers The cross-sectional area of the duct on the gravity settler is much larger than that of the duct approaching it or leading the gas away from it,

so the gas velocity inside is much lower than that in either of those two ducts. Baffles have been used to evenly spread the flow across the chamber.

Cyclones Particles enter the cyclone entrained in the gas stream, which is forced into a vortex by the shape of the cyclone. The inertia of the particles resists the change in the direction of the gas, and they move radially outward. It provides a low-cost, low-maintenance method of removing larger particulates from the gas stream. A cyclone reduces dust loading and removes larger abrasive particles, extending the life of the final dust collection device. Inertial separators have been used for the collection of medium-sized to coarse particles. Their construction and absence of moving parts mean that both capital and maintenance costs are lower than those for bag houses or electrostatic precipitators; their efficiency is low, and therefore they are mainly used as precleaners.

Electrostatic Precipitators (ESPs) An electrostatic precipitator is a device that uses electrical forces by imparting an electric charge to particles and moving the particles from the gas stream onto collector plates. The particles are given an electric charge by forcing them to pass through a corona, a region in which gaseous ions flow. The electric field that forces the charged particles to the walls comes from electrodes maintained at high voltage in the center of the flow lane. The particles collected are removed from the plates by knocking them loose from the plates either by mechanically tapping or by washing with water.

Fabric Filters Fabric filters remove dust from a gas stream by passing the stream through a porous fabric. Dust particles form a porous cake on the surface of the fabric. This cake actually helps the filtration. The manner in which the dust is removed from the fabric is a crucial factor in the performance of the fabric filter system. If the cake is not removed, the pressure drop will increase to an excessive amount. Fabric filters are often referred to as bag filters. Generally, there are two types: (1) reverse-air and (2) pulse-jet. In the reverse-airflow type, dust-laden gas is passed from inside the bag to outside, and thus dust accumulates in the bag. As required, the flow of air is reversed to clean the bags. For the pulse-jet type, bags are designed with internal frame structures, called cages, to allow collection of the dust on the outside of the bags. The dust is periodically removed by a pulse of air into the bag, causing sudden expansion. Dust is removed primarily by inertial forces when the bag reaches its maximum expansion.

Wet Scrubbers As the name implies, wet collectors or wet scrubbers are devices that use a liquid for removing particles or polluted gases from an exhaust stream. They are used when one of the following conditions applies:

- The contaminant cannot be removed easily in a dry form.
- Soluble gases or wettable particulates are present.
- The contaminant will undergo some subsequent wet process.
- The pollution control system must be compact.
- The contaminants are most safely handled wet rather than dry.

Wet scrubbing typically has been used to control sticky emissions that would otherwise plug filter-type collectors, to control both particulate and gaseous emissions simultaneously, to control acid gases, to recover soluble dusts and powders, to scrub particulate from incinerator exhausts, and to control metallic powders such as aluminum dust that tend to explode if handled dry.

REFERENCES

1. K. J. Laidler, *Chemical Kinetics*, 2nd ed., McGraw-Hill Book Co., New York, 1965.
2. I. Glassman, *Combustion*, 2nd ed., Academic Press, New York, 1987.
3. S. W. Benson, *The Foundations of Chemical Kinetics*, McGraw-Hill Book Co., New York, 1960.
4. S. S. Penner, *Introduction to the Study of Chemical Reactions in Flow Systems*, Agardograph No. 7, Butterworth Scientific Publications, London, 1955.
5. F. A. Williams, *Combustion Theory*, Addison-Wesley Publishing Co., Reading, MA, 1965.
6. M. J. Kurylo and W. Braun, "Flash Photolysis Resonance Fluorescence Study of the Reaction $\text{Cl} + \text{O}_3 \rightarrow \text{ClO} + \text{O}_2$ Over the Temperature Range 213–298 K," *Chem. Phys. Lett.* **37**, 232 (1976).
7. Z. Zhang, S. Padmaja, R. D. Saini, R. E. Huie, and M. J. Kurylo, "Reactions of Hydroxyl Radicals with Several Hydrofluorocarbons: The Temperature Dependencies of the Rate Constants for $\text{CHF}_2\text{CF}_2\text{CH}_2\text{F}$ (HFC-245ca), $\text{CF}_3\text{CHFCH}_2\text{F}$ (HFC-236ea), $\text{CF}_3\text{CHFCF}_3$ (HFC-227ea), and $\text{CF}_3\text{CH}_2\text{CH}_2\text{CF}_3$ (HFC-356ffa)," *J. Phys. Chem.* **98**, 4312 (1994).
8. R. Liu, R. E. Huie, and M. J. Kurylo, "Rate Constants for the Reactions of the OH Radical with Some Hydrochlorofluorocarbons over the Temperature Range 270–400 K," *J. Phys. Chem.* **94**, 3247 (1990).
9. V. L. Orkin, R. E. Huie, and M. J. Kurylo, "Atmospheric Lifetimes of HFC-143a and HFC-245fa: Flash Photolysis Resonance Fluorescence Measurements of the OH Reaction Rate Constants," *J. Phys. Chem.* **100**, 8907 (1996).
10. W. B. DeMore, "Relative Rate Constants for the Reactions of OH with Methane and Methyl Chloroform," *Geophys. Res. Lett.* **19**, 1367 (1992).
11. J. H. Kasner, P. H. Taylor, and B. Dellinger, "Laser Photolysis/Laser Induced Fluorescence Study of OH- $\text{C}_2\text{H}_5\text{Cl}$ Rate Constants from 294 to 789 K," *J. Phys. Chem.* **94**, 3250 (1990).
12. E. F. Caldin and F. W. Trowse, *Discussions Faraday Soc.* **17**, 133 (1954).
13. B. Chance, *J. Franklin Inst.*, 229, 455, 613, 737 (1940).
14. H. S. Johnston, *Discussions Faraday Soc.* **17**, 14 (1954).
15. M. Eigen and J. S. Johnson, *Ann. Rev. Phys. Chem.* **11**, 307 (1960).
16. M. Eigen and K. Kustin, *ICSU Rev.* **5**, 97 (1963).
17. H. O. Pritchard, *Quart. Rev. (London)* **14**, 46 (1960).
18. A. G Gaydon and I. R. Hurle, *The Shock Tube in High-Temperature Chemical Physics*, Reinhold Publishing Corporation, New York, 1963.
19. J. N. Bradley and G. B. Kistiakowsky, *J. Chem. Phys.* **35**, 256 (1961).

20. R. G. W. Norrish and B. A. Thrush, *Quart. Rev. (London)* **10**, 149 (1956).
21. R. G. W. Norrish, *Proc. Chem. Soc.*, 247 (1958).
22. D. R. Herschbach, *Vortex* **22**, 8 (1961).
23. D. Beck, E. F. Greene, and J. Ross, *Vortex* **37**, 2895 (1962).
24. J. I. Steinfeld, J. S. Francisco, and W. L. Hase, *Chemical Kinetics and Dynamics*, 2nd ed., Prentice Hall, 1999.
25. G. G. Hammes, *Principles of Chemical Kinetics*, Academic Press, New York, 1978.
26. E. Lewis and G. von Elbe, *Combustion, Flames, and Explosions of Gases*, Academic Press, New York, 1951.
27. J. E. Mayer and M. G. Mayer, *Statistical Mechanics*, John Wiley & Sons, New York, 1940.
28. F. A. Lindemann, *Trans. Faraday Soc.* **17**, 598 (1922).
29. J. Warnatz, "The Mechanism of High Temperature Combustion of Propane and Butane," *Comb. Sci Tech.* **34**, 177 (1983).
30. J. Warnatz, U. Mass, and R. W. Dibble, *Combustion: Physical and Chemical Fundamentals, Modeling and Simulation, Experiments, Pollutant Formation*, 2nd ed., Springer-Verlag, Berlin Heidelberg, New York, 1999.
31. P. J. Robinson and K. A. Holbrook, *Unimolecular Reactions*, Wiley-Interscience, New York, 1972.
32. P. W. Atkins, *Physical Chemistry*, 5th ed. Freeman, New York.
33. R. J. Kee, F. M. Rupley, and J. A. Miller, "CHEMKIN-II: A FORTRAN Chemical Kinetics Package for the Analysis of Gas-Phase Chemical Kinetics," Sandia National Laboratories Report, SAND89-8009B, 1992.
34. URL: http://www.ca.sandia.gov/chemkin/docs/CHEMKIN_III.pdf
35. URL: http://www.reactiondesign.com/chemkin_combustionpkg.html
36. URL: http://www.reactiondesign.com/ps_software.html
37. R. G. Gilbert, K. Luther, and J. Troe, "Theory of Unimolecular Reactions in the Fall-Off Range," *Ber. Bunsenges. Phys. Chem.* **87**, 169–177 (1983).
38. P. H. Stewart, C. W. Larson, and D. Golden, "Pressure and Temperature Dependence of Reactions Proceeding via a Bound Complex. 2. Application to $2\text{CH}_3 \rightarrow \text{C}_2\text{H}_5 + \text{H}$," *Comb. and Flame* **75**, 25 (1989).
39. S. Gordon and B. J. McBride, "Computer Program for Calculation of Complex Chemical Equilibrium Compositions, Rocket Performance, Incident and Reflected Shocks and Chapman-Jouguet Detonations," NASA SP-273, 1971.
40. S. Gordon and B. J. McBride, "Computer Program for Calculation of Complex Chemical Equilibrium Compositions, and Applications I. Analysis," NASA Reference Pub. 1311, October 1994.
41. B. J. McBride and S. Gordon, "Computer Program for Calculation of Complex Chemical Equilibrium Compositions and Applications, II. Users Manual and Program Description," NASA Reference Pub. 1311, June 1996.
42. C. W. Gear, "The Automatic Integration of Ordinary Differential Equations," *Comm. ACM* **14**, 176–179 (1971).
43. C. W. Gear, "DIFSUB for Solution of Ordinary Differential Equations," (Algorithm 407), *Comm. ACM* **14**, 185–189 (1971).

44. S. R. Turns, *An Introduction to Combustion: Concepts and Applications*, 2nd ed., McGraw-Hill, 2000, pp. 120–1121.
45. R. I. Masel, *Principles of Adsorption and Reaction on Solid Surfaces*, John Wiley and Sons, Inc., New York, 1996.
46. I. Langmuir, *J. Am. Chem. Soc.* **38**, 2221 (1916).
47. H. S. Taylor, *J. Am. Chem. Soc.* **53**, 578 (1931); *Rev.* **9**, 1 (1931).
48. H. S. Taylor, *Proc. Roy. Soc (London)* **A108** (1925); *J. Phys. Chem.* **30**, 145 (1926); H. S. Taylor and S. C. Liang, *J. Am. Chem. Soc.* **69**, 1306 (1947); H. Sadek and H. S. Taylor, *J. Am. Chem. Soc.* **72**, 1168 (1950).
49. N. P. Keier and S. Z. Roginsky, *Dokl. Akad. Nauk. SSSR* **57**, 151 (1947); *J. Phys. Chem. USSR* **23**, 897 (1949).
50. J. T. Kummer and P. H. Emmett, *J. Am. Chem. Soc.* **73**, 2886 (1951); P. H. Emmett and J. T. Kummer, *J. Chem. Phys.* **47**, T67 (1950).
51. H. Constable, *Proc. Roy. Soc. (London)* **A105**, 355 (1925).
52. J. K. Roberts, *Proc. Roy. Soc. (London)* **A152**, 445 (1935).
53. K. Rideal and B. M. W. Trapnell, *J. Chem. Phys.* **47**, 126 (1950).
54. J. Weber and K. J. Laidler, *J. Chem. Phys.* **18**, 1418 (1950); **19**, 1089 (1951).
55. I. Langmuir, *J. Am. Chem. Soc.* **40**, 1361 (1918).
56. M. Ciureanu, H. Wang, and Z. Qi, “Electrooxidation of H₂ and H₂/CO Mixtures on Pt/Ru-Based Gas-Diffusion Electrodes,” *J. Phys. Chem.* **103** (1999).
57. W. C. Gardiner, Jr., *Rates and Mechanisms of Chemical Reactions*, Benjamin, Menlo Park, CA, 1972.
58. G. J. Minkoff and C. F. H. Tipper, *Chemistry of Combustion Reactions*, Butterworth Inc., Washington, D.C., 1962.
59. I. Langmuir, *Trans. Faraday Soc.* **17**, 621 (1922).
60. K. Rideal, *Proc. Cambridge Phil. Soc.* **35**, 130 (1939); *Chem. Ind. (London)* **62**, 335 (1943).
61. D. D. Eley and E. K. Rideal, *Proc. Royal Soc. (London)* **A178**, 429 (1941).
62. S. Ljungstrom and B. Kasemo, *Surface Science* **216**, 63 (1989).
63. J. Warnatz, M. D. Allendorf, R. J. Kee, and M. E. Coltrin, *Comb. and Flame* **96**, 393 (1994).
64. E. G. Christoffel, *Laboratory Studies of Heterogeneous Catalytic Processes*, Elsevier Scientific Publishing Company, Amsterdam-Oxford-New York, 1989.
65. J. Benard, *Adsorption on Metal Surfaces an Integrated Approach*, Elsevier Scientific Publishing Company, Amsterdam-Oxford-New York, 1983.
66. G. J. Minkoff and C. F. H. Tipper, *Chemistry of Combustion Reactions*, Butterworth Inc., Washington, D.C., 1962.
67. D. F. Stein, “The Historical Development of Auger Electron Spectroscopy,” *Auger Electron Spectroscopy*, Academic Press Inc., 1988, pp. 1–15.
68. C. Bond, *Heterogeneous Catalysis: Principles and Applications*, 2nd ed., Oxford, 1987.
69. W. Willer, “Kinetics of Heterogeneous Catalyzed Reactions,” *Catal. Rev.* **34**(3), 227 (1992).
70. R. P. Eischens, S. A. Pliskin, and S. A. Francis, “Infrared Spectra of Chemisorbed Carbon Monoxide,” *J. Chem. Phys.* **22**, 1786 (1954).

71. R. P. Eischens, S. A. Francis, and W. A. Pliskin, "The Effect of Surface Coverage on the Spectra of Chemisorbed CO," *J. Phys. Chem.* **60**, 194 (1956).
72. S. Krishnamoorthy and M. D. Amiridis, "Kinetic and In Situ FTIR Studies of the Catalytic Oxidation of 1,2-dichlorobenzene over V₂O₅/Al₂O₃ Catalysts," *Catalysis Today* **51**, 203 (1999).
73. A. Spitzer and H. Luth, "The Adsorption of Oxygen on Copper Surfaces," *Surf. Sci.* **118**, 121 (1982).
74. J. R. Creighton, J. M. White, "SIMS and TDS Study of the Reaction of Water and Oxygen on Pt(111)," *Surf. Sci.* **122**, L648 (1982).
75. J. F. Wendelken, "The Chemisorption of Oxygen on Cu(110) Studied by EELS and LEED," *Surf. Sci.* **108**, 605 (1981).
76. U. Dobler, K. Baberschke, I. Stohr, and D. A. Outka, "Structure of C(2*2) Oxygen on Cu(100): A Surface Extended X-ray Absorption Fine-Structure Study," *Phys. Rev. B* **31**, 2532 (1985).
77. G. B. Fisher and J. L. Gland, "The Interaction of Water with the Pt(111) Surface," *Surf. Sci.* **94**, 446 (1980).
78. V. P. Belash, I. N. Klimova, V. Ti. Kormilets, V. Yu. Trubitsin, and L. D. Finkelstein, "Transformation of the Electronic Structure of Cu into Cu₂O in the Adsorption of Oxygen," *Surf. Rev. and Lett.* **6**(3), 383 (1999).
79. O. Dewaele and G. F. Froment, "TAP Study of the Mechanism and Kinetics of the Adsorption and Combustion of Methane on Ni/Al₂O₃ and NiO/Al₂O₃," *J. Catalysis* **184**, 499 (1999).
80. V. J. Kwasniewski and L. D. Schmidt, "Steps in the Reaction H₂ + O₂ = H₂O on Pt(111): Laser-Induced Thermal Desorption at Low Temperature," *J. Phys. Chem.* **96**(14), 5931 (1992).
81. T. E. Caldwell, I. M. Abdelrehim, and D. P. Land, "Pre-Adsorbed Oxygen Atoms Affect the Product Distribution and Kinetics of Acetylene Cyclization to Benzene on Pd(111): A Laser-Induced Thermal Desorption/Fourier Transform Mass Spectrometry Study," *J. Phys. Chem.* **102**, 562 (1998).
82. F. E. Livingston, J. A. Smith, S. M. George, "Origin of Non-Zero-Order H₂O Desorption Kinetics from Crystalline Ice Multilayers on Ru(001)," *Surf. Sci.* **423**, 145 (1999).
83. D. E. Tevault, L. D. Talley, and M. C. Lin, "Matrix Isolation and Laser Diagnostic Studies of Catalytic Oxidation of H₂ and D₂ on Platinum," *J. Chem. Phys.* **72**(5), 3314 (1980).
84. L. D. Talley, W. A. Saunders, D. J. Bogan, and M. C. Lin, "Dynamics of hHdroxyl Radical Desorption from a Polycrystalline Platinum Surface," *J. Chem. Phys.* **75**, 3107 (1981).
85. G. S. Selwyn, G. T. Fujimoto, and M. C. Lin, "Catalytic Removal of NH and NH₂ Free Radicals by Polycrystalline Pt and Fe Surfaces," *J. Phys. Chem.* **86**, 760 (1982).
86. A. Rosen, S. Ljungstrom, T. Wahnstrom, and B. Kasemo, "Laser Diagnostics of Radicals in Catalytic Reactions," *J. Electron Spectroscopy and Related Phenomena* **39**, 15 (1986).
87. S. Ljungstrom, J. Halc, B. Kasemo, A. Rosen, and T. Wahnstrom, "A Comparative Study of OH Radical Desorption in the H₂ + O₂ Reaction on Pt, Pd, Rh, Ir, and Ni," *J. Catalysis* **107**, 548 (1987).

88. S. Ljungstrom, B. Kasemo, A. Rosen, T. Wahnstrom, and E. Fridell, "An Experimental Study of the Kinetics of OH and H₂O Formation on Pt in the H₂ + O₂ Reaction," *Surf. Sci.* **216**, 63 (1989).
89. W. R. Williams, C. M. Marks, and L. D. Schmidt, "Steps in the Reaction H₂ + O₂ = H₂O on Pt: OH Desorption at High Temperatures," *J. Phys. Chem.* **96**, 5922 (1992).
90. W. R. Smith and R. W. Missen, *Chemical Reactions: Equilibrium Analysis Theory and Algorithms*, Copyright, 1982, pp. 173–198.
91. R. A. Yetter, F. L. Dryer, and H. Rabitz, "Some Interpretive Aspects of Elementary Sensitivity Gradients in Combustion Kinetics Modeling," *Comb. and Flame* **59**, 107–133 (1985).
92. R. P. Dickinson and R. J. Gelinas, *J. Computational Phys.* **21**, 123 (1976).
93. J. Hwang, E. P. Dougherty, S. Rabitz, and H. Rabitz, *J. Chem. Phys.* **69**, 5180 (1978).
94. M. D. Greenberg, *Application of Green's Functions in Science and Engineering*, Prentice-Hall, Inc., 1971.
95. R. W. Atherton, R. B. Schinker, and E. R. Ducot, *Al. Chem. E. J.* **21**, 441 (1975).
96. R. I. Cukier, C. M. Fortuin, K. E. Shuler, A. G. Petschek, and J. H. Schaibly, *J. Chem. Phys.* **59**, 3873 (1973).
97. R. S. Stolarski, D. M. Butler, and R. D. Rundel, *J. Geophys. Res.* **83**, 3074 (1978).
98. M. C. Dodge and T. A. Hecht, *Int. J. Chem. Kinet.* **1**, 155 (1975).
99. J. W. Tilden, V. Costanza, G. J. McRae, and J. H. Seinfeld, in K. H. Ebert, P. Deuffhard, and W. Jager, eds., *Modelling of Chemical Reaction Systems*, Springer-Verlag, Berlin, 1981, p. 69.
100. H. Rabitz, M. A. Kramer, and D. Dacol, *Ann. Rev. Phys. Chem.* **34**, 417 (1983).
101. M. A. Kramer, R. J. Kee, and H. Rabitz, "CHEMSEN: A Computer Code for Sensitivity Analysis of Elementary Reaction Models," SANDIA Report SAND82-8230, Sandia National Laboratories, Livermore, CA, 1982.
102. A. E. Lutz, R. J. Kee, and J. A. Miller, "A FORTRAN Program to Predict homogeneous Gas-Phase Chemical Kinetics Including Sensitivity Analysis," Sandia Report SAND87-8248, Sandia National Laboratories, Livermore, CA, 1987.
103. U. Nowak and J. Warnatz, "Sensitivity Analysis in Aliphatic Hydrocarbon Combustion," in A. L. Kuhl et al., eds., *Dynamics of Reactive Systems*, Vol. 1, Part I, AIAA, 1988, p. 87.
104. S. H. Lam, Lecture notes for *Aerothermochemistry for Hypersonic Technology*, 1994–1995 Lecture Series Programme, the Von Karman Institute for Fluid Dynamics, April 24–25, 1995.
105. S. A. Tomlin, M. Pilling, T. Turányi, J. Merkin, and J. Brindley, "Mechanism Reduction for the Oscillatory Oxidation of Hydrogen: Sensitivity and Quasi-Steady-State Analyses," *Comb. and Flame* **91**, 107–130 (1992).
106. K. Radhakrishnan, "Combustion Kinetics and Sensitivity Analysis Computations," in E. S. Oran and J. P. Boris, eds., *Numerical Approaches to Combustion Modeling*, AIAA, 1991, pp. 83–128.
107. M. A. Kramer, J. M. Calo, and H. Rabitz, *Appl. Math. Modelling* **5**, 432 (1981).

108. M. Mishra, L. Peiperl, Y. Reuven, H. Rabitz, R. A. Yetter, and M. D. Smooke, "Use of Green's Functions for the Analysis of Dynamic Couplings: Some Examples from Chemical Kinetics and Quantum Dynamics," *J. Phys. Chem.* **95**, 3109 (1991).
109. M. Mishra, R. A. Yetter, Y. Reuven, H. Rabitz, and M. D. Smooke, *Int. J. Chem. Kinetics* **26**(4), 437–453 (1994).
110. H. Rabitz, *Computers and Chem.* **5**, 167 (1981).
111. A. C. Hindmarsh, *ACM Sigum Newsletter* **15**(4) (1980).
112. M. A. Kramer, J. M. Calo, H. Rabitz, and R. J. Kee, Sandia Tech. Rep. 82–923 1, Sandia National Lab., Livermore, CA, 1982.
113. M. Dermilap and H. Rabitz, *J. Chem. Phys.* **74**, 3362 (1981).
114. M. D. Smooke, H. Rabitz, Y. Reuven, F. L. Dyrer, "Application of Sensitivity Analysis to Premixed Hydrogen-Air Flames," *Comb. Sci. Tech.* **59**, 295–319 (1988).
115. Y. Reuven, M. D. Smooke, and H. Rabitz, "Sensitivity Analysis of Boundary Value Problems: Application to Nonlinear Reaction-Diffusion Systems," *J. Comp. Phys.* **64**, 27–55 (1986).
116. Y. Reuven, M. D. Smooke, H. Rabitz, "Sensitivity Analysis of One-Dimensional Mixed Initial-Boundary Value Problems: Application to Freely Propagating Premixed Laminar Flames," *J. Scient. Comput.* **2**(4), 345 (1987).
117. M. Nehse, J. Warnatz, and C. Chevalier, "Kinetic Modelling of the Oxidation of Large Aliphatic Hydrocarbons," *26th Symposium (Intl.) on Combustion*, The Combustion Institute, Pittsburgh, PA, 1996, p. 773.
118. J. Warnatz, "Critical Survey of Elementary Reaction Rate Coefficients in the C/H/O System," in W. C. Gardiner, Jr., ed., *Combustion Chemistry*, Springer-Verlag, New York, 1984.
119. E. P. Dougherty and H. Rabitz, "Computational Kinetics and Sensitivity Analysis of Hydrogen-Oxygen Combustion," *J. Chem. Phys.* **72**, 6571 (1980).
120. U. Maas and J. Warnatz, "Ignition Processes in Hydrogen-Oxygen Mixtures," *Comb. and Flame* **74**, 53 (1988).
121. C. K. Westbrook and F. L. Dryer, "Chemical Kinetic Modeling of Hydrocarbon Combustion," *Prog. Energy Combust. Sci.* **10**, 1–57 (1984).
122. C. K. Westbrook and F. L. Dryer, "Chemical Kinetic and Modeling of Combustion Processes," *18th Symposium (Intl.) on Combustion*, The Combustion Institute, 1981, p. 749.
123. D. L. Baulch, C. J. Cobos, R. A. Cox, C. Esser, P. Frank, T. Just, J. A. Kerr, M. J. Pilling, J. Troe, R. W. Walker, and J. Warnatz, (Ref Data), *J. Phys. Chem.* **23**, 847 (1994).
124. D. L. Baulch, D. D. Drysdale, and D. G. Horne, *Homogeneous Gas Phase Reactions of the H₂-O₂-N₂ System*, Butterworths, London, 1973.
125. G. Dixon-Lewis and D. J. Williams, in C. H. Bamford and C. H. F. Tipper, eds., *Comprehensive Chemical Kinetics*, Vol. 17, 1. Elservier, Oxford, 1977.
126. R. S. Brokaw, *11th Symposium (Intl.) on Combustion*, The Combustion Institute, Pittsburgh, PA, 1967, p. 1063.
127. F. L. Dryer and I. Glassman, *4th Symposium (Intl.) on Combustion*, The Combustion Institute, Pittsburgh, PA, 1973, p. 987.
128. R. A. Yetter, F. L. Dryer, and H. Rabitz, *7th International Symposium on Gas Kinetics*, Gottingen, 1982.

129. R. W. Getzinger and G. L. Schott, *J. Chem. Phys.*, **43**, 3237 (1965).
130. C. T. Bowman, *5th Symposium (Intl.) on Combustion*, The Combustion Institute, Pittsburgh, PA, 1975, p. 869.
131. T. A. Brabbs and R. S. Brokaw, *5th Symposium (Intl.) on Combustion*, The Combustion Institute, Pittsburgh, PA, 1975, p. 893.
132. J. A. Miller, R. E. Mitchell, M. D. Smooke, and R. J. Kee, *9th Symposium (Intl.) on Combustion*, The Combustion Institute, Pittsburgh, PA, 1983, p. 181.
133. J. Warnatz, et al., *9th Symposium (Intl.) on Combustion*, The Combustion Institute, Pittsburgh, PA, 1983, p. 197.
134. N. Fuji and T. Asaba, *14th Symposium (Intl.) on Combustion*, The Combustion Institute, Pittsburgh, PA, 1993, p. 433.
135. R. P. Lindstedt and K. A. Rizos, *29th Symposium (Intl.) on Combustion*, The Combustion Institute, Pittsburgh, PA, 2002, p. 2291.
136. R. L. G. M. Eggels and L. P. H. de Goey, "Mathematically Reduced Reaction Mechanisms Applied to Adiabatic Flat Hydrogen/Air Flames," *Comb. and Flame* **100**, 559–570 (1995).
137. S. H. Lam and D. A. Goussis, "Research on Computational Singular Perturbation," Progress Report #1, Report #1749(a)-MAE, Department of Mechanical and Aerospace Engineering, Princeton University, 1987.
138. S. H. Lam and D. A. Goussis, "The CSP Method for Simplifying Kinetics," *Int'l. J. Chem. Kinetics* **26**, 461–486 (1994).
139. T. Lu, Y. Ju, and C. K. Law, "Complex CSP for Chemistry Reduction and Analysis," *Comb. and Flame* **126**, 1445–1455 (2001).
140. U. Maas and S. B. Pope, "Simplifying Chemical Kinetics: Intrinsic Low-Dimensional Manifolds in Composition Space," *Comb. and Flame* **88**, 239 (1992).
141. Yu. B. Zel'dovich, "The Oxidation of Nitrogen in Combustion and Explosives," *Acta Physicochim USSR* **21**, 577 (1946).
142. C. P. Fenimore, "Studies of Fuel-Nitrogen Species in Rich Flame Gases," *17th Symposium (Intl.) on Combustion*, The Combustion Institute, Pittsburgh, PA, 1979, pp. 661–670.
143. C. P. Fenimore, "Formation of Nitric Oxide in Premixed Hydrocarbon Flames," *13th Symposium (Intl.) on Combustion*, The Combustion Institute, Pittsburgh, PA, 1970, pp. 373–380.
144. J. A. Miller and C. T. Bowman, "Mechanism and Modeling of Nitrogen Chemistry in Combustion," *Prog. in Energy and Comb. Sci.* **15**, 287–338 (1989).
145. A. M. Dean and J. W. Bozzelli, "Combustion Chemistry of Nitrogen," in W. C. Gardiner, Jr., ed., *Gas-Phase Combustion Chemistry*, 2000, pp. 125–341.
146. M. Frenklach and J. Warnatz, "Detailed Modeling of PAH Profiles in a Sooting Low Pressure Acetylene Flame", *Combustion Science & Technology* **51**; 265 (1987).
147. M. Frenklach and H. Wang, "Detailed Modeling of Soot Particle Nucleation and Growth", *23rd Symp. (Intl.) Combustion*, The Combustion Institute, Pittsburgh, p. 1559 (1991).
148. R. J. Santoro, T. T. Yeh, J. J. Horvath, and H. H. Semerjian, "The Transport and Growth of Soot Particles in Laminar Diffusion Flames," *Combustion Science of Technology*, **53**; 89 (1987).

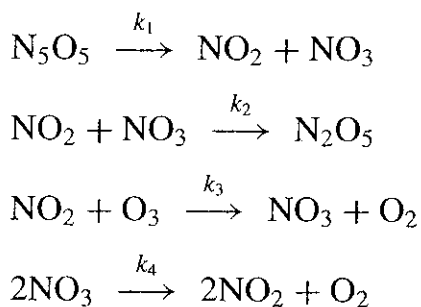
HOMEWORK

- 1.** For the rate expression

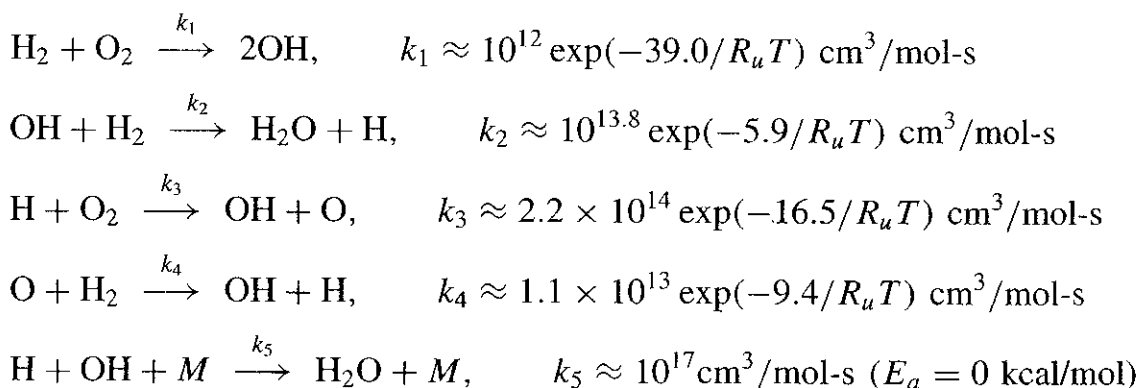
$$-\frac{dC_A}{dt} = k C_A^2 C_M$$

where M represents all of the constituents of the mixture.

- (a) What is the order of the reaction?
 - (b) How would the rate of reaction depend on pressure? Show this explicitly.
- 2.** The rate of a given reaction doubles for a 10°C rise in temperature from T_0 to $T_0 + 10$. Develop an expression for the activation energy of the reaction. Do not solve for a numerical answer.
- 3.** Develop an expression for the half-life time at which an initial concentration $C(0)$ decreases to $\frac{1}{2}$ its original value for a first-order reaction.
- 4.** For the reaction sequence



- (a) Write equations for the rates of formation of N_2O_5 , NO_2 , NO_3 , O_2 , and O_3 .
 - (b) Assume that the species NO_2 and NO_3 are in steady state. Solve for their concentrations.
 - (c) What do the results of the steady-state assumption imply with respect to the rate of N_2O_5 formation?
- 5.** At low pressure, assuming no wall reaction, the $\text{H}_2\text{-O}_2$ reaction may be accounted for by the mechanism



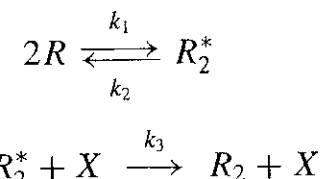
Using the steady-state hypothesis, derive the differential equations expressing $dC_{\text{H}_2\text{O}}/dt$ in terms of C_{H_2} and C_{O_2} .

$$\text{ANSWER: } dC_{\text{H}_2\text{O}}/dt = 2k_2 C_{\text{O}_2} C_{\text{H}_2} \left[\frac{k_1}{k_2} + \frac{k_3}{(k_5 C_M)} \right]$$

6. The combustion chamber in a certain rocket contains H atoms and OH radicals at equal concentrations of 4×10^{-6} mole/cm³ and 3000 K. The total gas concentration is 4×10^{-4} mole/cm³. Supposing the gases to be exhausted from the chamber at 1000 K (where H₂O is essentially undissociated) and at a density equal to $\frac{1}{40}$ of the density in the chamber, calculate how far in the exhaust stream, moving at 3048 m/s, one will have to probe before finding that the H and OH are 99% recombined. Ignore recombination reactions other than $\text{H} + \text{OH} + M \rightarrow \text{H}_2\text{O} + M$, for which k is given as 10^{16} cm⁶/mol²-s, independent of temperature (this is a typical figure for a three-body recombination rate constant).

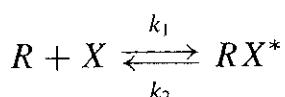
$$\text{ANSWER: } x = 30.8 \text{ m}$$

7. One of the mechanisms of atom and radical combinations, called the *energy-transfer mechanism*, is described by the following chemical steps:

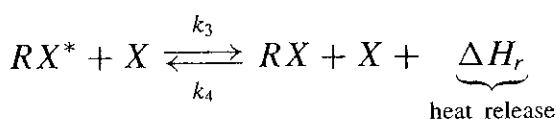


where R represents a radical or an atom and X is a third body. Use the steady-state treatment for R_2^* to determine the rate of consumption of R . What is the order of the recombination reaction when the concentration of X is sufficiently large such that $k_3 C_X \gg k_2$? What is the order of the recombination reaction at very low pressures?

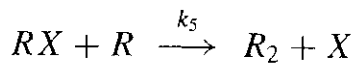
8. Another mechanism of atom and radical combination is called the *atom-molecule* or *radical-molecule-complex mechanism*. This mechanism is particularly likely for atom combinations when the third body X is a molecule that can readily form a complex with one of the atoms. The reaction steps may be represented as



The resulting complex retains the energy released in its formation and may be deenergized by collision with another molecule X :



Finally, RX may react with R , giving rise to



Apply the steady-state treatment to determine the rate of consumption of R . What is the order of the combination reaction when the concentration of R is sufficiently small? Does the reaction become second-order at high pressures (high concentrations of X)?

- 9.** A mixture of high-temperature gases flows over a horizontal graphite slab. Some of the species $H_2O_{(g)}$, $CO_{2(g)}$, $H_{2(g)}$ in the mixture can react with graphite surface by heterogeneous reaction and cause thermochemical erosion of the solid. Consider the following heterogeneous reactions:



Determine the heats of reaction of the above three reactions at 2000 K. Are these reactions exothermic or endothermic?

- 10.** Suppose the order of reaction of a chemical reacting system is n , that is,

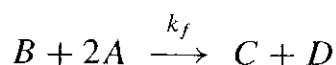
$$\frac{dC}{dt} = -kC^n$$

where C is the concentration of the reacting species. Show that the rate of change of mole fraction of reacting species, dX/dt , is proportional to $-kX^n\rho^{n-1}$. What is the pressure dependence of dX/dt ? List your assumptions. Can we say that

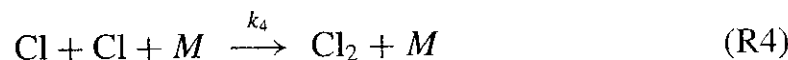
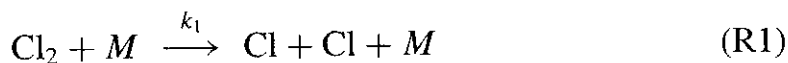
$$\frac{d\varepsilon}{dt} \propto -k\varepsilon^n \rho^{n-1}$$

where ε is the reaction progress variable defined by Eq. (1–12) in Chapter 1?

- 11.** Express the concentration of the i th species, C_i , in terms of following parameters:
- (a) ρ_i , Mw_i
 - (b) ρ , Y_i , Mw_i
 - (c) C , X_i
 - (d) p , Y_i , T , Mw_i
 - (e) p , T , X_i
- 12.** Express the reaction rate of the following third-order reaction in terms of consumed portion of reactant concentration (C_x) in the reaction



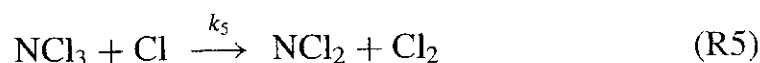
13. Consider the following set of elementary reactions between hydrogen and chlorine:



- (a) Show that this scheme leads to the rate expression

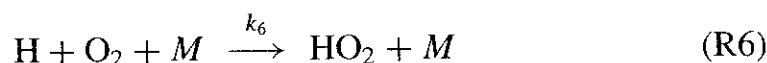
$$\frac{dC_{\text{HCl}}}{dt} = 2k_2 \sqrt{\frac{k_1}{k_4}} (C_{\text{Cl}_2})^{1/2} C_{\text{H}_2}$$

- (b) NCl_3 is a potential inhibitor for the reaction, according to



Derive the kinetic rate expression for the scheme including reaction (R5). What is the form of the rate expression when $k_5 \gg k_1$?

- (c) O_2 also inhibits the reaction through



Why should NCl_3 be a much stronger inhibitor than O_2 ?

3

THE CONSERVATION EQUATIONS FOR MULTICOMPONENT REACTING SYSTEMS

Symbol	Description	Dimension
B_i	Body force per unit volume in i -direction	F/L^3
C	Molar concentration	N/L^3
d	Molecular diameter	L
D_{AB}	Binary diffusivity for $A-B$ system	L^2/t
e_{ij}	Strain rate tensor	t^{-1}
Ea_k	Activation energy for the k th reaction	Q/N
f_i	External force per unit mass on species i	F/M
\mathbf{F}	Force	F
\mathbf{F}_S	Surface force	F
h	Enthalpy per unit mass	Q/M
h_t	Total enthalpy per unit mass [Eq. (3-80)]	Q/M
\mathbf{I}	Identity matrix or vector form of Kronecker delta δ_{ij}	—
\mathbf{J}_i	Mass flux of species i relative to mass-average velocity	M/L^2t

(continued overleaf)

Symbol	Description	Dimension
\mathbf{J}_i^*	Molar flux of species i relative to molar-average velocity	N/L^2t
K	Boltzmann constant	$(Q/T)/\text{molecule}$
l	Mean free path	L
$\dot{\mathbf{m}}$	Mass flux	M/L^2t
M_{w_i}	Molecular weight of i th species	M/N
$\dot{\mathbf{n}}$	Molar flux	N/L^2t
N_i	Number of moles of species i	—
N_A	Avogadro's number, 6.02252×10^{23} molecules/mole	N^{-1}
\mathbf{q}	Heat-flux vector	Q/L^2t
T°	Fixed standard reference temperature, at 298.15 K	T
\bar{u}	Arithmetic-mean molecular speed	L/t
u_i	Velocity component in i -direction	L/t
\mathbf{v}	Mass-average velocity	L/t
V	Control volume	L^3
\mathbf{v}_i	Velocity of i th species with respect to stationary coordinate axes	L/t
\mathbf{v}^*	Molar-average velocity	L/t
\mathbf{V}_i	Mass diffusion velocity of i th species	L/t
\mathbf{V}_i^*	Molar diffusion velocity of i th species	L/t
y	Space coordinate in y -direction	L
z	Space coordination in z -direction	L
Z	Frequency of molecular collisions of gaseous species per unit surface area	$L^{-2}t^{-1}$

Greek Symbols

α	Thermal diffusivity	L^2/t
α_i	Thermal diffusion coefficient for species i	L^2/t
λ	Thermal conductivity or second viscosity	Q/tLT
μ	Dynamic viscosity or first viscosity	Ft/L^2
μ'	Bulk viscosity	Ft/L^2
μ_{ij}	Reduced mass of molecules of species i and j	M
$\sigma_{ij}, \tilde{\sigma}$	Total stress tensor	F/L^2
τ_{ij}	Viscous stress tensor	F/L^2
Ω_i	Molar rate or production of species i	$N/(tL^3)$
$\dot{\omega}_i$	Mass rate of production of species i	$M/(tL^3)$

Subscripts

A, B	Species in binary system
i, j, k	Species in multicomponent systems
x, y	Fluxes in x and y directions
$\mathbf{i}, \mathbf{j}, \mathbf{k}$	Unit vectors in x , y , and z directions

1 DEFINITIONS OF CONCENTRATIONS, VELOCITIES, AND MASS FLUXES

The concentration of various species in a multicomponent system may be expressed in numerous ways, as discussed in the Introduction. This chapter will consider four such ways: *mass concentration* ρ_i , which is the mass of the i th species per unit volume of mixture or solution; *molar concentration* $C_i = \rho_i/Mw_i$, which is the number of moles of i th species per unit volume; *mass fraction* $Y_i = \rho_i/\rho$, which is the mass concentration of i th species divided by the total mass density of the mixture; and *mole fraction* $X_i = C_i/C$, which is the molar concentration of the i th species divided by the total molar density of the gaseous mixture or liquid solution.

In a multicomponent system, various chemical species will move at different velocities. Let us use \mathbf{v}_i to denote the velocity of the i th species with respect to the stationary coordinate axes. Thus, for a mixture of N species, the local bulk mass-average velocity \mathbf{v} can be defined as

$$\mathbf{v} = \frac{\sum_{i=1}^N \rho_i \mathbf{v}_i}{\sum_{i=1}^N \rho_i} = \frac{\sum_{i=1}^N \rho_i \mathbf{v}_i}{\rho} = \sum_{i=1}^N Y_i \mathbf{v}_i \quad (3-1)$$

Similarly, a local bulk *molar-average velocity* \mathbf{v}^* may be defined as

$$\mathbf{v}^* = \frac{\sum_{i=1}^N C_i \mathbf{v}_i}{\sum_{i=1}^N C_i} = \frac{\sum_{i=1}^N C_i \mathbf{v}_i}{C} = \sum_{i=1}^N X_i \mathbf{v}_i \quad (3-2)$$

In general, \mathbf{v}^* differs from \mathbf{v} in both magnitude and direction, since their weighting factors are different, as indicated by the above two equations.

In multicomponent reacting flow systems, we are frequently interested in the velocity of a given species with respect to the local bulk mass-average velocity \mathbf{v} of the mixture in an infinitesimal bulk control volume or with respect to the local bulk molar-average velocity \mathbf{v}^* rather than with respect to stationary coordinates. This leads to the definition of the *diffusion velocities* (see Figure 3.1).

The mass diffusion velocity of i th species can be defined as

$$\mathbf{V}_i = \mathbf{v}_i - \mathbf{v} \quad (3-3)$$

Similarly, the molar diffusion velocity of i th species can be defined as

$$\mathbf{V}_i^* = \mathbf{v}_i - \mathbf{v}^* \quad (3-4)$$

These diffusion velocities indicate the average motion of component i relative to the local bulk motion of the mixture in the fluid stream. To illustrate the meaning of various kinds of velocities, let's consider a simple case of a binary system in which $X_A = \frac{1}{3}$ and velocity vectors are colinear. In addition, the magnitudes of

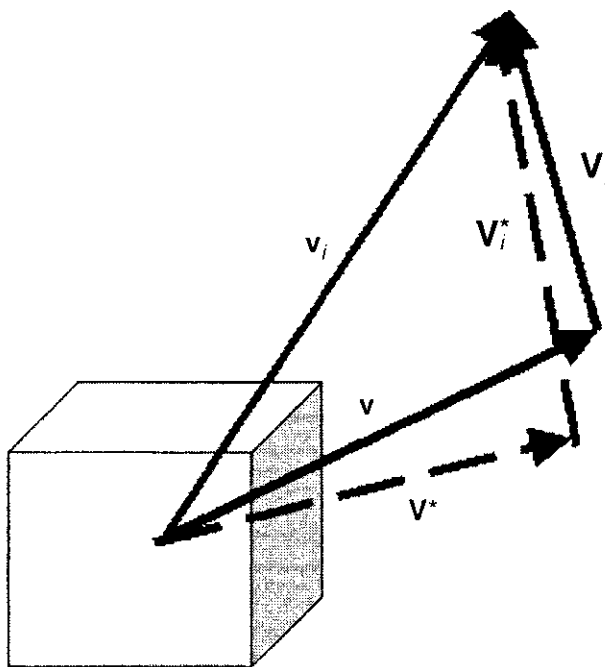


Figure 3.1 Diagram of velocity vectors.

two vector quantities are $|\mathbf{v}^*| = 10$, $|\mathbf{v}_A - \mathbf{v}^*| = 2$, and $Mw_A = 3 Mw_B$:

$$|\mathbf{v}^*| = \frac{\sum_{i=1}^N C_i |\mathbf{v}_i|}{\sum_{i=1}^N C_i} = \sum_{i=1}^N X_i |\mathbf{v}_i| = \frac{1}{3} \times 12 + \frac{2}{3} |\mathbf{v}_B|$$

Note that

$$X_i = \frac{C_i}{C}, \quad \sum_{i=1}^N X_i = \frac{\sum_{i=1}^N C_i}{C} = \frac{C}{C} = 1, \quad \text{and} \quad Y_i = \frac{X_i Mw_i}{\sum_{i=1}^N X_i Mw_i}$$

Using the relationships given above, one obtains $|\mathbf{v}_B| = 9$. Further, from the definition of molar concentration and mass-averaged velocity, one obtains $|\mathbf{v}| = 10.8$. Thus, in general, \mathbf{v} and \mathbf{v}^* differ not only in magnitude but also in direction.

Now that concentrations and velocities have been discussed, we are in a position to define mass and molar fluxes. The mass (or molar) flux of species i is a vector quantity denoting the mass (or number of moles) of species i that passes through a unit area per unit time. Thus, the mass and molar fluxes relative to stationary coordinates are

$$\dot{\mathbf{m}}_i \equiv \rho_i \mathbf{v}_i \quad (\text{mass flux}) \quad (3-5)$$

$$\dot{\mathbf{n}}_i \equiv C_i \mathbf{v}_i \quad (\text{molar flux}) \quad (3-6)$$

The relative mass and molar fluxes are defined as

$$\mathbf{J}_i \equiv \rho_i (\mathbf{v}_i - \mathbf{v}) = \rho_i \mathbf{V}_i \quad (3-7)$$

$$\mathbf{J}_i^* \equiv C_i (\mathbf{v}_i - \mathbf{v}^*) = C_i \mathbf{V}_i^* \quad (3-8)$$

Example 3.1. Relations among the molar fluxes:

- How are the fluxes \mathbf{J}_i^* and $\dot{\mathbf{n}}_i$ related in an N -component system?
- Show that the sum of the fluxes \mathbf{J}_i^* is zero.

Solution: Using the definitions of \mathbf{v}^* and \mathbf{J}_i^* , one obtains

$$\mathbf{J}_i^* \equiv C_i(\mathbf{v}_i - \mathbf{v}^*) = C_i\mathbf{v}_i - \frac{C_i}{C} \sum_{j=1}^N C_j \mathbf{v}_j$$

Using the definitions of $\dot{\mathbf{n}}_i$ and X_i , we have

$$\mathbf{J}_i^* = \dot{\mathbf{n}}_i - X_i \sum_{j=1}^N \dot{\mathbf{n}}_j \quad (3-9)$$

Summation of Eq. (3-9) from $i = 1$ to $i = N$ gives

$$\sum_{i=1}^N \mathbf{J}_i^* = 0 \quad (3-10)$$

#

2 FICK'S LAW OF DIFFUSION

In a binary system with two chemical species, species A always diffuses in the direction from high concentration of A to low concentration of A . The same is true for species B . The binary mass diffusivity can be expressed by either \mathcal{D}_{AB} or \mathcal{D}_{BA} . Then, Fick's first law of diffusion, written in terms of the molar diffusion flux \mathbf{J}_A^* for the binary system, is

$$\mathbf{J}_A^* = -C \mathcal{D}_{AB} \nabla X_A \quad (3-11)$$

This equation states that species A diffuses (moves relative to the mixture) in the direction of decreasing mole fraction of A , just like heat transfer by conduction in the direction of decreasing temperature. The dimension of \mathcal{D}_{AB} is (L^2/t) , usually given in (m^2/s) .

The molar flux relative to stationary coordinates can now be given as the sum of two terms

$$\dot{\mathbf{n}}_A = C_A \mathbf{v}^* - C \mathcal{D}_{AB} \nabla X_A \quad (3-12)$$

The first term represents the molar flux of A resulting from the bulk motion of the fluid. The second term with the minus sign represents the relative molar flux of A resulting from the diffusion species A . The net molar flux of species A

relative to stationary coordinates should therefore be determined from the sum by superimposing the relative diffusing effect onto the bulk flow. In terms of mass flux, Fick's first law can be written as

$$\mathbf{J}_A = -\rho \mathcal{D}_{AB} \nabla Y_A \quad (3-13)$$

Similar to Eq. (3-12), the mass flux of A relative to the stationary coordinates can be expressed as

$$\dot{\mathbf{m}}_A = \rho_A \mathbf{v} - \rho \mathcal{D}_{AB} \nabla Y_A \quad (3-14)$$

Again, the first term is the mass flux of species A due to bulk fluid motion. The second term including the minus sign represents the mass diffusion effect of species A , which is driven by the mass fraction gradient.

It is useful to note that the mathematical form of Fick's law of mass transport for constant-density situation in the transverse direction (y -direction) of a binary system is very similar to Newton's law of momentum transport and Fourier's law of energy transport in the transverse direction. These equations are given here:

$$J_{Ay} = -\mathcal{D}_{AB} \frac{\partial}{\partial y} (\rho_A) \quad \text{(Fick's law for constant } \rho\text{)}$$

$$\tau_{yx} = -\nu \frac{\partial}{\partial y} (\rho v_x) \quad \text{(Newton's law for constant } \rho\text{)}$$

$$q_y = -\alpha \frac{\partial}{\partial y} (\rho C_p T) \quad \text{(Fourier's law for constant } \rho C_p\text{)}$$

The dimensions of mass diffusivity (\mathcal{D}), momentum diffusivity (ν), and thermal diffusivity (α) are the same. Therefore, the three dimensionless parameters Schmidt number, Prandtl number, and Lewis number can be defined as the ratios made from different combinations of these diffusivities. More detailed discussion of these parameters is given in Section 11.

$$Sc \equiv \frac{\nu}{\mathcal{D}}, \quad Pr \equiv \frac{\nu}{\alpha}, \quad \text{and} \quad Le \equiv \frac{\alpha}{\mathcal{D}} \quad (3-15)$$

3 THEORY OF ORDINARY DIFFUSION IN GASES AT LOW DENSITY

The mass diffusivity \mathcal{D}_{AB} for binary mixtures of nonpolar gases is predictable within about 5% by kinetic theory. By definition, nonpolar gases contain molecules that have zero permanent electric dipole moment; however, they may temporarily acquire a dipole moment in an electric field as a result of the distortion of their electronic distributions and the locations of their nuclei.

Consider a nonpolar gas containing two molecular species A and A^* , both species having the same mass m_A and the same size and shape. Assume temperature T and molar concentration C to be constant. From kinetic theory of gases,

the random motion molecular velocity relative to fluid velocity v has an average magnitude, \bar{u} :

$$\bar{u} = \sqrt{\frac{8KT}{\pi m_A}} \quad (3-16)$$

K is the Boltzmann constant = (universal gas constant)/(Avogadro's number). The frequency of molecular collisions per unit area (Z) on a stationary surface exposed to the gas is

$$Z = \frac{1}{4} \tilde{n} \bar{u} \quad (3-17)$$

where \tilde{n} represents the molecules per unit volume. The value of \tilde{n} is a constant, since the molar concentration of the mixture C is a constant and $\tilde{n} = C \times N_A$, where N_A is Avogadro's number. The mean free path l , from kinetic theory, is

$$l = \frac{1}{\sqrt{2\pi} d_A^2 \tilde{n}} \quad (3-18)$$

where d_A is the diameter of the molecule A . The molecules reaching any $y =$ constant plane in the gas have, on the average, had their last collision at a distance a from that plane (see Fig. 3.2):

$$a = \frac{2}{3} l \quad (3-19)$$

The relative molar flux \mathbf{J}_A^* of species A across any plane of constant y is found by counting the molecules of A that cross a unit area of the plane in the positive y -direction and subtracting the number that cross in the negative y -direction.

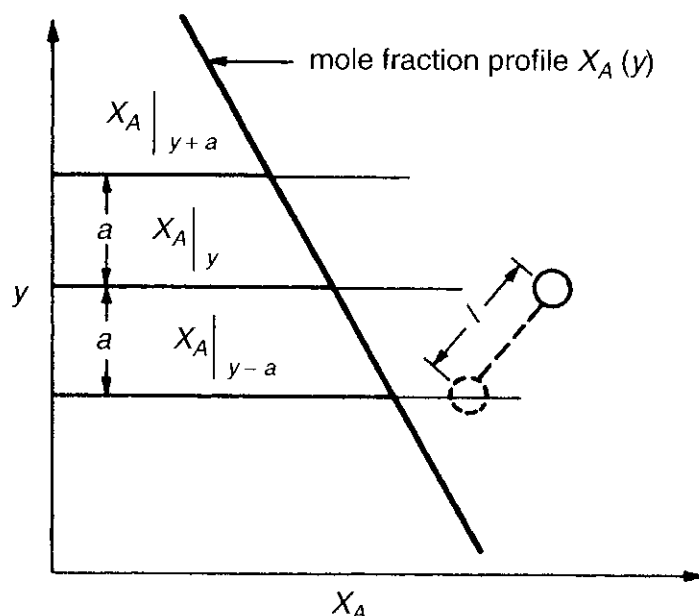


Figure 3.2 Molecular transport of species A from plane at $y-a$ to plane at y .

Thus, if the concentration profile $X_A(y)$ is assumed to be essentially linear near $y = \text{constant}$ plane, we have

$$\mathbf{J}_A^* = \frac{ZX_A|_{y-a} - ZX_A|_{y+a}}{N_A} \mathbf{j} \quad (3-20)$$

As a further consequence of this assumption,

$$\begin{aligned} \frac{dX_A}{dy} &= \frac{X_A|_y - X_A|_{y-a}}{a} = \frac{X_A|_{y+a} - X_A|_y}{a} \\ X_A|_{y-a} &= X_A|_y - \frac{2}{3}l \frac{dX_A}{dy} \end{aligned} \quad (3-21a)$$

$$X_A|_{y+a} = X_A|_y + \frac{2}{3}l \frac{dX_A}{dy} \quad (3-21b)$$

Substituting Eqs. (3-21a) and (3-21b) into Eq. (3-20), we have

$$\begin{aligned} \mathbf{J}_{Ay}^* &= \frac{Z}{N_A} \left(-\frac{4}{3}l \frac{dX_A}{dy} \right) \mathbf{j} = - \left(\frac{1}{3} \frac{\tilde{n}}{N_A} \bar{u}l \right) \frac{dX_A}{dy} \mathbf{j} \\ \mathbf{J}_{Ay}^* &= -C \left(\frac{1}{3} \bar{u}l \right) \frac{dX_A}{dy} \mathbf{j} \end{aligned} \quad (3-22)$$

This equation corresponds to the Fick's law of diffusion in the y -direction, with the following approximate value for \mathcal{D}_{AA^*} :

$$\mathcal{D}_{AA^*} = \frac{1}{3} \bar{u}l \quad (3-23)$$

Using Eq. (3-16) for \bar{u} and Eq. (3-18) for l , Eq. (3-23) becomes

$$\begin{aligned} \mathcal{D}_{AA^*} &= \frac{1}{3} \sqrt{\frac{8KT}{\pi m_A}} \frac{1}{\sqrt{2\pi d_A^2 \tilde{n}}} = \frac{2}{3} \sqrt{\frac{K^3}{\pi^3 m_A}} \frac{T^{3/2}}{d_A^2} \frac{1}{\tilde{n}KT} \\ &= \frac{2}{3} \sqrt{\frac{K^3}{\pi^3 m_A}} \frac{T^{3/2}}{d_A^2} \frac{1}{\tilde{n}KT} \end{aligned}$$

Using the perfect-gas law $p = CR_u T = \tilde{n}KT$, approximate value for \mathcal{D}_{AA^*} can be calculated from

$$\mathcal{D}_{AA^*} = \frac{2}{3} \sqrt{\frac{K^3}{\pi^3 m_A}} \frac{T^{3/2}}{pd_A^2} \quad (3-24)$$

The parameter \mathcal{D}_{AA^*} represents the mass diffusivity of a mixture of two species of rigid spheres of identical mass and diameter. The calculation of \mathcal{D}_{AB} for

rigid spheres of unequal mass and diameter is slightly more complicated; the corresponding result is

$$\mathcal{D}_{AB} = \frac{2}{3} \left(\frac{K^3}{\pi^3} \right)^{1/2} \left(\frac{1}{2m_A} + \frac{1}{2m_B} \right)^{1/2} \frac{T^{3/2}}{p \left(\frac{d_A + d_B}{2} \right)^2} \quad (3-25)$$

4 CONTINUITY EQUATION AND SPECIES MASS CONSERVATION EQUATIONS

To derive the mass conservation equation of each species in a multicomponent mixture, we begin by making a mass balance over an arbitrary differential fluid element in a binary mixture. We apply the law of conservation of mass of species A to a volume element $\Delta x \Delta y \Delta z$ fixed in space through which a binary mixture of A and B is flowing (see Fig. 3.3).

Within this infinitesimal control volume, species A can be produced or consumed by chemical reaction at rate $\dot{\omega}_A$ ($\text{kg m}^{-3} \text{s}^{-1}$). If $\dot{\omega}_A < 0$, species A is consumed. Various terms describing their respective contributions to the mass balance are given below:

The rate of accumulation of mass of species A in the control volume is

$$\frac{\partial \rho_A}{\partial t} \Delta x \Delta y \Delta z$$

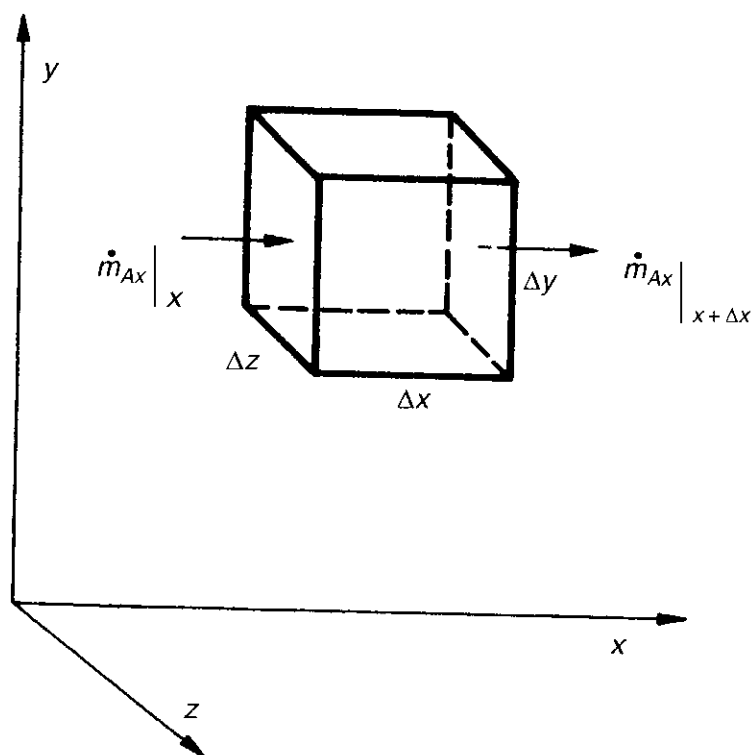


Figure 3.3 A fixed infinitesimal control volume $\Delta x \Delta y \Delta z$ through which a fluid is flowing.

The rate of mass input of A due to the x -direction mass flux at x station is

$$\dot{m}_{Ax}|_x \Delta y \Delta z$$

The rate of mass output of A due to the x -direction mass flux at $x + \Delta x$ station is

$$\dot{m}_{Ax}|_{x+\Delta x} \Delta y \Delta z = \dot{m}_{Ax}|_x \Delta y \Delta z + \frac{\partial \dot{m}_{Ax}}{\partial x} \Delta x \Delta y \Delta z$$

The rate of production of A by chemical reaction is

$$\dot{\omega}_A \Delta x \Delta y \Delta z$$

There are also input and output terms in the y and z directions. When the entire mass balance is divided through by $\Delta x \Delta y \Delta z$, one obtains

$$\frac{\partial \rho_A}{\partial t} + \left(\frac{\partial \dot{m}_{Ax}}{\partial x} + \frac{\partial \dot{m}_{Ay}}{\partial y} + \frac{\partial \dot{m}_{Az}}{\partial z} \right) = \dot{\omega}_A \quad (3-26)$$

This is the *equation of continuity for component A* in a binary mixture. It is also called the mass conservation equation for species A . The quantities \dot{m}_{Ax} , \dot{m}_{Ay} , \dot{m}_{Az} are the scalar components of the mass flux vector, $\dot{\mathbf{m}}_A$, in the rectangular coordinates. In vector notation, the equation may be rewritten as

$$\frac{\partial \rho_A}{\partial t} + (\nabla \cdot \dot{\mathbf{m}}_A) = \dot{\omega}_A \quad (3-27)$$

Similarly, the equation of continuity for component B is

$$\frac{\partial \rho_B}{\partial t} + (\nabla \cdot \dot{\mathbf{m}}_B) = \dot{\omega}_B \quad (3-28)$$

Adding Eq. (3-27) to Eq. (3-28) gives

$$\frac{\partial \rho}{\partial t} + \nabla \cdot (\rho \mathbf{v}) = 0 \quad (3-29)$$

which is the *equation of continuity for the mixture*. In arriving at Eq. (3-29), we have made use of both the relation $\dot{\mathbf{m}}_A + \dot{\mathbf{m}}_B = \rho \mathbf{v}$ and the law of conservation of mass in the form $\dot{\omega}_A + \dot{\omega}_B = 0$. For a fluid of constant mass density ρ , Eq. (3-29) becomes

$$\nabla \cdot \mathbf{v} = 0 \quad (3-30)$$

The development given above could have been made equally well in terms of molar units. If $\dot{\Omega}_A$ is the molar rate of production of A per unit volume, then the molar analog of Eq. (3-27) is

$$\frac{\partial C_A}{\partial t} + \nabla \cdot \dot{\mathbf{n}}_A = \dot{\Omega}_A \quad (3-31)$$

Substituting Eq. (3-14) into Eq. (3-27), we obtain

$$\frac{\partial \rho_A}{\partial t} + \nabla \cdot \rho_A \mathbf{v} = \nabla \cdot \rho \mathcal{D}_{AB} \nabla Y_A + \dot{\omega}_A \quad (3-32)$$

Substituting Eq. (3-12) into Eq. (3-31), we obtain

$$\frac{\partial C_A}{\partial t} + \nabla \cdot C_A \mathbf{v}^* = \nabla \cdot C \mathcal{D}_{AB} \nabla X_A + \dot{\Omega}_A \quad (3-33)$$

If no chemical reactions occur, $\dot{\omega}_A$, $\dot{\omega}_B$, $\dot{\Omega}_A$, and $\dot{\Omega}_B$ are all zero. If, in addition, \mathbf{v} is zero in Eq. (3-32) or \mathbf{v}^* is zero in Eq. (3-33), we get

$$\frac{\partial C_A}{\partial t} = \mathcal{D}_{AB} \nabla^2 C_A \quad (3-34)$$

which is called *Fick's second law of diffusion*. This equation is generally used for diffusion in solids or stationary liquids and for equimolar counter-diffusion in gases. Its usage in combustion is extremely limited. This equation is similar to the heat conduction equation

$$\frac{\partial T}{\partial t} = \alpha \nabla^2 T$$

Using the relationships that $\rho_i = Y_i \rho$ and $\mathbf{v}_i = \mathbf{v} + \mathbf{V}_i$ for a multicomponent system, Eq. (3-27) becomes

$$\frac{\partial(\rho Y_i)}{\partial t} + \nabla \cdot [\rho Y_i (\mathbf{v} + \mathbf{V}_i)] = \dot{\omega}_i \quad (3-35)$$

The above equation in its divergence form can be reduced to the Euler form by the following procedure. Expanding parts of the terms on the left-hand side, we have

$$\rho \frac{\partial Y_i}{\partial t} + Y_i \frac{\partial \rho}{\partial t} + Y_i \nabla \cdot (\rho \mathbf{v}) + \rho \mathbf{v} \cdot \nabla Y_i + \nabla \cdot (\rho Y_i \mathbf{V}_i) = \dot{\omega}_i$$

Table 3.1 Equation of Continuity in Several Coordinate Systems

Rectangular coordinates (x, y, z):

$$\frac{\partial \rho}{\partial t} + \frac{\partial}{\partial x}(\rho u_x) + \frac{\partial}{\partial y}(\rho u_y) + \frac{\partial}{\partial z}(\rho u_z) = 0 \quad (\text{A})$$

Cylindrical coordinates (r, θ, z)^a:

$$\frac{\partial \rho}{\partial t} + \frac{1}{r} \frac{\partial}{\partial r}(\rho r u_r) + \frac{1}{r} \frac{\partial}{\partial \theta}(\rho u_\theta) + \frac{\partial}{\partial z}(\rho u_z) = 0 \quad (\text{B})$$

Spherical coordinates (r, θ, ϕ)^b:

$$\frac{\partial \rho}{\partial t} + \frac{1}{r^2} \frac{\partial}{\partial r}(\rho r^2 u_r) + \frac{1}{r \sin \theta} \frac{\partial}{\partial \theta}(\rho u_\theta \sin \theta) + \frac{1}{r \sin \theta} \frac{\partial}{\partial \phi}(\rho u_\phi) = 0 \quad (\text{C})$$

^a $r \geq 0, 2\pi \geq \theta \geq 0$.

^b $r \geq 0, 2\pi \geq \phi \geq 0, \pi \geq \theta \geq 0$.

Table 3.2 Mass Conservation Equation for i th Species in Several Coordinate Systems

Rectangular coordinates (x, y, z):

$$\rho \left(\frac{\partial Y_i}{\partial t} + u_x \frac{\partial Y_i}{\partial x} + u_y \frac{\partial Y_i}{\partial y} + u_z \frac{\partial Y_i}{\partial z} \right) + \frac{\partial}{\partial x}(\rho Y_i V_{ix}) + \frac{\partial}{\partial y}(\rho Y_i V_{iy}) + \frac{\partial}{\partial z}(\rho Y_i V_{iz}) = \dot{\omega}_i \quad (\text{A})$$

$$+ \frac{\partial}{\partial x}(\rho Y_i V_{ix}) + \frac{\partial}{\partial y}(\rho Y_i V_{iy}) + \frac{\partial}{\partial z}(\rho Y_i V_{iz}) = \dot{\omega}_i$$

where mass diffusion velocities are $V_{ix} = -\frac{\mathcal{D}}{Y_i} \frac{\partial Y_i}{\partial x}$, $V_{iy} = -\frac{\mathcal{D}}{Y_i} \frac{\partial Y_i}{\partial y}$, $V_{iz} = -\frac{\mathcal{D}}{Y_i} \frac{\partial Y_i}{\partial z}$

Cylindrical coordinates (r, θ, z):

$$\rho \left(\frac{\partial Y_i}{\partial t} + u_r \frac{\partial Y_i}{\partial r} + \frac{u_\theta}{r} \frac{\partial Y_i}{\partial \theta} + u_z \frac{\partial Y_i}{\partial z} \right) + \frac{1}{r} \frac{\partial}{\partial r}(r \rho Y_i V_{ir}) + \frac{1}{r} \frac{\partial}{\partial \theta}(r \rho Y_i V_{i\theta}) + \frac{\partial}{\partial z}(\rho Y_i V_{iz}) = \dot{\omega}_i \quad (\text{B})$$

$$+ \frac{1}{r} \frac{\partial}{\partial r}(r \rho Y_i V_{ir}) + \frac{1}{r} \frac{\partial}{\partial \theta}(r \rho Y_i V_{i\theta}) + \frac{\partial}{\partial z}(\rho Y_i V_{iz}) = \dot{\omega}_i$$

where mass diffusion velocities are $V_{ir} = -\frac{\mathcal{D}}{Y_i} \frac{\partial Y_i}{\partial r}$, $V_{i\theta} = -\frac{\mathcal{D}}{Y_i r} \frac{\partial Y_i}{\partial \theta}$, $V_{iz} = -\frac{\mathcal{D}}{Y_i} \frac{\partial Y_i}{\partial z}$

Spherical coordinates (r, θ, ϕ):

$$\rho \left(\frac{\partial Y_i}{\partial t} + u_r \frac{\partial Y_i}{\partial r} + \frac{u_\theta}{r} \frac{\partial Y_i}{\partial \theta} + \frac{u_\phi}{r \sin \theta} \frac{\partial Y_i}{\partial \phi} \right) + \frac{1}{r^2} \frac{\partial}{\partial r}(r^2 \rho Y_i V_{ir}) + \frac{1}{r \sin \theta} \frac{\partial}{\partial \theta}(\sin \theta \rho Y_i V_{i\theta}) + \frac{1}{r \sin \theta} \frac{\partial}{\partial \phi}(\rho Y_i V_{i\phi}) = \dot{\omega}_i \quad (\text{C})$$

$$+ \frac{1}{r \sin \theta} \frac{\partial}{\partial \theta}(\sin \theta \rho Y_i V_{i\theta}) + \frac{1}{r \sin \theta} \frac{\partial}{\partial \phi}(\rho Y_i V_{i\phi}) = \dot{\omega}_i$$

where mass diffusion velocities are $V_{ir} = -\frac{\mathcal{D}}{Y_i} \frac{\partial Y_i}{\partial r}$, $V_{i\theta} = -\frac{\mathcal{D}}{Y_i r} \frac{\partial Y_i}{\partial \theta}$,

$$V_{i\theta} = -\frac{\mathcal{D}}{Y_i r \sin \theta} \frac{\partial Y_i}{\partial \phi}$$

After using the overall continuity equation (3-29), the Euler form of Eq. (3-35) is obtained

$$\rho \frac{\partial Y_i}{\partial t} + \rho \mathbf{v} \cdot \nabla Y_i + \nabla \cdot (\rho Y_i \mathbf{V}_i) = \dot{\omega}_i \quad i = 1, 2, \dots, N \quad (3-36)$$

In a general multicomponent system, there are N equations of this kind. In the numerical solution, all the values of Y_i are considered as unknown. Since $\sum_{i=1}^N Y_i = 1$, it is not necessary to solve all N partial differential equations for Y_i . One of these N equations can be replaced by the simple algebraic relationship. Usually, $N - 1$ independent equations for Y_i are solved with other conservation equations for the chemically reacting mixture.

It may be noted for simplicity that the above derivations have been made in rectangular coordinates. However, rectangular coordinates are not always the most convenient for solving various combustion problems. To facilitate the use of the governing conservation equations in different coordinate systems, several forms of the equation of continuity for the gas mixture are given in Table 3.1. Also, the mass conservation equations for individual species in different coordinate systems are listed in Table 3.2.

5 CONSERVATION OF MOMENTUM

In this section we shall derive and discuss the momentum equations in partial differential equation forms. The basic assumption is that we are dealing with continuous, isotropic, and homogeneous fluids. We shall consider the special case of a Newtonian fluid, that is, a fluid exhibiting a linear relationship between shear stress and rate of deformation, resulting in the Navier–Stokes equations. We derive first the momentum equation in terms of stress. Then, we shall consider the constitutive relationships between stress and fluid deformation.

5.1 Momentum Equation in Terms of Stress

We shall derive the momentum equation in terms of stress using three different approaches; each of these approaches exists in the literature. Even though these different approaches will end up with the same results, different derivations could be very helpful to the beginners in the combustion field. The basis for *any* derivation of the momentum conservation equations is Newton's second law of motion,

$$\sum \mathbf{F} = \frac{d(m\mathbf{v})}{dt} \quad (3-37)$$

Basically, the three approaches are as follows:

1. *Infinitesimal Particle Approach.* A fluid particle is considered to move through space relative to a fixed coordinate system. This approach was

adopted in several textbooks on chemically inert fluid mechanics written by Hinze,⁵ Shames,⁶ Li and Lam,⁷ and Aris.⁸ In this approach, Eq. (3-37) describes the motion of the fluid particle with a fixed mass. In fact, we are taking the “Lagrangian” approach by following the motion of a distinct fluid particle as it moves through space.

2. *Infinitesimal Control Volume Approach.* This approach is also called the “Eulerian” approach or the field approach. This method was presented in many textbooks, for example, the textbook by Bird, Stewart, and Lightfoot.¹ Usually a cubical infinitesimal volume element fixed in space is taken to be the control volume for derivation. The net momentum flux out of the control volume plus the time rate of change of momentum in the control volume is equated to the net force on the mass within the control volume. The observer is always fixed in space to examine the flow pattern going through numerous control volumes.
3. *Finite Control Volume Approach.* In this approach, a gas-permeable control volume of finite size is considered. Landau and Lifshitz⁹ adopted this method in their derivation of momentum equation by considering a fixed control volume of finite size and an arbitrary shape. Gauss’s theorem was used to relate the surface and volume integrals, resulting in an equation involving only volume integrals all collected on one-side of the equation. Since the integration is over an arbitrary shaped volume, the integrand must be equal to zero. This results in the desired differential momentum equation.

5.1.1 Momentum Equation Derivation by Infinitesimal Particle Approach

Consider a particle of mass dm moving through space with velocity \mathbf{v} , as shown in Fig. 3.4. If a net force $d\mathbf{F}$ is acting on the particle, the momentum is

$$d\mathbf{F} = \frac{d}{dt}[(dm)\mathbf{v}]$$

For the fluid particle of fixed mass, the above equation becomes

$$d\mathbf{F} = dm \frac{d\mathbf{v}}{dt} \quad (3-37a)$$

This equation describes the motion of the particle as it moves through space relative to the fixed coordinate system. Thus, $d\mathbf{v}/dt$ represents the acceleration of a particular fluid particle as it moves from point to point through space.

Next, we shall relate the derivative of the velocity to conditions at a fixed point in space. In considering the description of fluid motion, we need to describe the position, velocity, and acceleration throughout the flow for all fluid particles of interest.

Considering the Lagrangian viewpoint in Eq. (3-17a), we follow a particle and observe changes as it moves in space. Then, the expression for velocity $\mathbf{v}(x_1, x_2, x_3, t)$ does not refer to fixed coordinates, but allows for changes

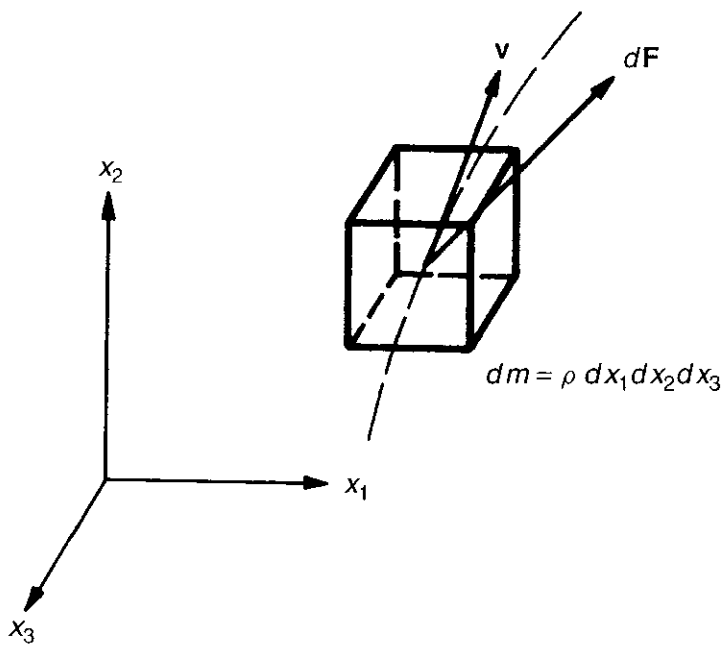


Figure 3.4 An infinitesimal fluid particle moving in a three-dimensional space.

in coordinates to locate a distinct particle at various times. The positions are given by

$$x_1 = x_1(t), \quad x_2 = x_2(t), \quad x_3 = x_3(t)$$

because the time t is the only independent variable in the Lagrangian approach. Based on the above relationships, we have

$$\mathbf{v} = \mathbf{v}[x_1(t), x_2(t), x_3(t), t] = \mathbf{v}(t)$$

where \mathbf{v} refers to the velocity of a distinct particle for different times (as a function of time). Similarly, for acceleration of the particle, we have

$$\mathbf{a} = \mathbf{a}[x_1(t), x_2(t), x_3(t), t] = \mathbf{a}(t)$$

or

$$\mathbf{a} = \frac{d\mathbf{v}}{dt} = \frac{\partial \mathbf{v}}{\partial x_1} \frac{dx_1}{dt} + \frac{\partial \mathbf{v}}{\partial x_2} \frac{dx_2}{dt} + \frac{\partial \mathbf{v}}{\partial x_3} \frac{dx_3}{dt} + \frac{\partial \mathbf{v}}{\partial t}$$

However,

$$\frac{dx_1}{dt} = u_1, \quad \frac{dx_2}{dt} = u_2, \quad \frac{dx_3}{dt} = u_3$$

where

$$\mathbf{v} = u_1 \mathbf{i} + u_2 \mathbf{j} + u_3 \mathbf{k} = [u_1, u_2, u_3]$$

The acceleration then becomes

$$\frac{du_i}{dt} = u_1 \frac{\partial u_i}{\partial x_1} + u_2 \frac{\partial u_i}{\partial x_2} + u_3 \frac{\partial u_i}{\partial x_3} + \frac{\partial u_i}{\partial t}$$

The above quantity is the acceleration of a distinct particle moving through space. However, the quantities $u_1, u_2, u_3, \partial u_i / \partial x_1$, etc., represent the flow conditions of the particle at a fixed point in space at a specific time. That is, they represent conditions from a field point of view (Eulerian point of view) as

$$u_i = u_i(x_1, x_2, x_3, t) = u_i(\mathbf{x}, t)$$

To link the Eulerian point of view with the Lagrangian parameters, let us consider the material derivative D/Dt , which is also called the *substantial derivative*. In the Lagrangian point of view, this time derivative is taken while following the motion of the fluid particle with a fixed mass. It is the same as the d/dt in Eq. (3-37a). In the Eulerian point of view, the D/Dt operator can be expressed by the sum of four terms on the right-hand side of the following equation, since there are four independent variables in the Eulerian coordinates. Thus,

$$\frac{d}{dt} \equiv \frac{D}{Dt} \equiv u_1 \frac{\partial}{\partial x_1} + u_2 \frac{\partial}{\partial x_2} + u_3 \frac{\partial}{\partial x_3} + \frac{\partial}{\partial t}$$

In terms of Eulerian independent variables, Eq. (3-37) can now be written as

$$dF_i = dm \left[u_1 \frac{\partial u_i}{\partial x_1} + u_2 \frac{\partial u_i}{\partial x_2} + u_3 \frac{\partial u_i}{\partial x_3} + \frac{\partial u_i}{\partial t} \right]$$

or

$$dF_1 = dm \frac{Du_1}{Dt}, \quad dF_2 = dm \frac{Du_2}{Dt}, \quad dF_3 = dm \frac{Du_3}{Dt}$$

To write in Cartesian tensor notation, we have

$$dF_i = dm \frac{Du_i}{Dt}$$

or

$$dF_i = dm \left[u_j \frac{\partial u_i}{\partial x_j} + \frac{\partial u_i}{\partial t} \right] \quad (3-38)$$

If we consider a particle of mass dm , which is cubical in shape and has sides of length dx_1, dx_2 , and dx_3 , then

$$dm = \rho dx_1 dx_2 dx_3$$

The force acting on the particle is split into a surface force df_i and a body force B_i (force per unit volume). In a mixture of N species, the body forces acting on different chemical species may differ. Thus, for a multicomponent system, we have

$$B_i = \rho \sum_{k=1}^N Y_k (f_k)_i \quad (3-39)$$

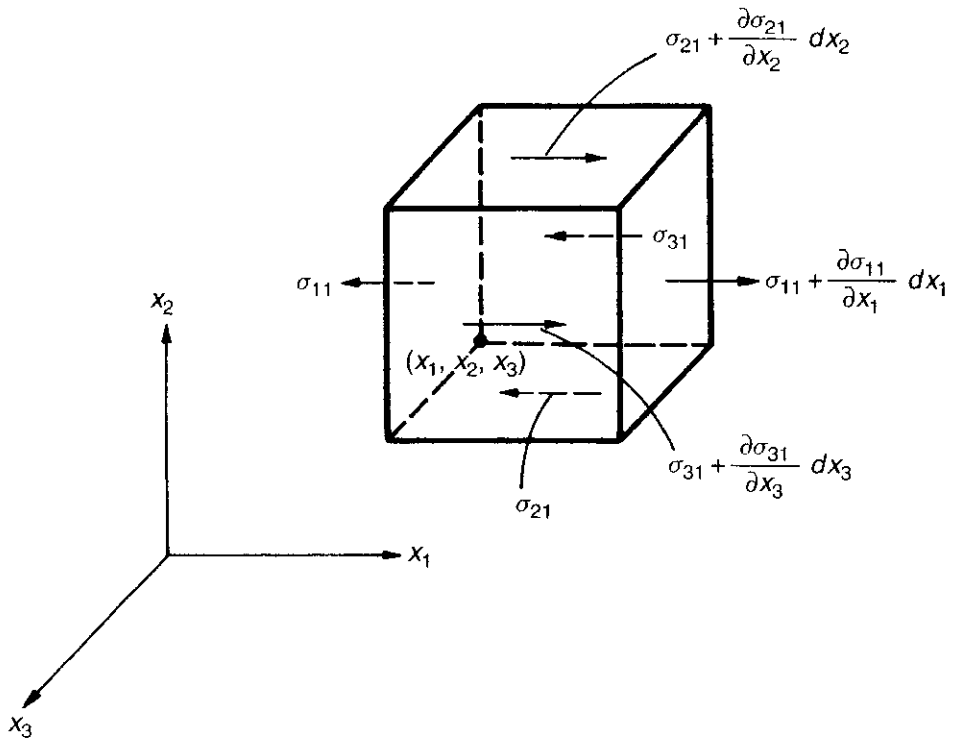


Figure 3.5 Surface-stress components acting on the fluid particle in the x_1 -direction.

where f_k is the force per unit mass acting on the k th species, and

$$dF_i = df_i + B_i dx_1 dx_2 dx_3 \quad (3-40)$$

Now we shall express the net surface force in terms of the stress acting on the different faces of the particle. Consider the surface forces acting on the cube of Fig. 3.5. In this case, the surface forces for the three directions are

$$\begin{aligned} df_1 &= \left(\frac{\partial \sigma_{11}}{\partial x_1} + \frac{\partial \sigma_{21}}{\partial x_2} + \frac{\partial \sigma_{31}}{\partial x_3} \right) dx_1 dx_2 dx_3 \\ df_2 &= \left(\frac{\partial \sigma_{12}}{\partial x_1} + \frac{\partial \sigma_{22}}{\partial x_2} + \frac{\partial \sigma_{32}}{\partial x_3} \right) dx_1 dx_2 dx_3 \\ df_3 &= \left(\frac{\partial \sigma_{13}}{\partial x_1} + \frac{\partial \sigma_{23}}{\partial x_2} + \frac{\partial \sigma_{33}}{\partial x_3} \right) dx_1 dx_2 dx_3 \end{aligned}$$

where $\sigma_{21} \times dx_1 dx_3$ represents the stress force in the x_1 -direction and acting on the $x_2 = \text{constant}$ plane. After dividing the terms by $dx_1 dx_2 dx_3$, the momentum equation becomes

$$\underbrace{\rho \left[u_j \frac{\partial u_i}{\partial x_j} + \frac{\partial u_i}{\partial t} \right]}_{\text{Inertia Force}} = \underbrace{\frac{\partial \sigma_{ji}}{\partial x_j}}_{\text{Surface Stress Force}} + \underbrace{\rho \sum_{k=1}^N Y_k (f_k)_i}_{\text{Body Force}} \quad (3-41)$$

This equation is also called the equation of motion in terms of the stress tensor.

5.1.2 Momentum Equation Derivation by Infinitesimal Control Volume

Approach Let's now reuse Fig. 3.4 in the Eulerian approach by considering the cubical volume to be our control volume, fixed in space and allowing fluid to move through its surfaces. For this control volume, we can consider the momentum equation to have the following physical meaning:

$$\left\{ \begin{array}{l} \text{rate of} \\ \text{momentum} \\ \text{increase} \\ \text{in the control} \\ \text{volume} \end{array} \right\} = \left\{ \begin{array}{l} \text{net rate} \\ \text{of momentum} \\ \text{into the control} \\ \text{volume} \end{array} \right\} + \left\{ \begin{array}{l} \text{sum of forces} \\ \text{acting on the} \\ \text{control volume} \end{array} \right\}$$

Considering only the x_1 -direction, the net momentum flux is

$$\begin{aligned} & \left\{ \rho u_1 u_1 - \left[\rho u_1 u_1 + \frac{\partial(\rho u_1 u_1)}{\partial x_1} dx_1 \right] \right\} dx_2 dx_3 \\ & + \left\{ \rho u_2 u_1 - \left[\rho u_2 u_1 + \frac{\partial(\rho u_2 u_1)}{\partial x_2} dx_2 \right] \right\} dx_1 dx_3 \\ & + \left\{ \rho u_3 u_1 - \left[\rho u_3 u_1 + \frac{\partial(\rho u_3 u_1)}{\partial x_3} dx_3 \right] \right\} dx_1 dx_2 \end{aligned}$$

After simplifying, the above group becomes

$$- \left[\frac{\partial(\rho u_1 u_1)}{\partial x_1} + \frac{\partial(\rho u_2 u_1)}{\partial x_2} + \frac{\partial(\rho u_3 u_1)}{\partial x_3} \right] dx_1 dx_2 dx_3$$

The increase of the rate of momentum in the volume for the x_1 -direction is

$$\frac{\partial(\rho u_1)}{\partial t} dx_1 dx_2 dx_3$$

After combining with the body force and surface stress forces derived previously and dividing each term by $dx_1 dx_2 dx_3$, we have for the momentum equation in the x_1 -direction

$$\left[\frac{\partial(\rho u_1)}{\partial t} + \frac{\partial(\rho u_1 u_1)}{\partial x_1} + \frac{\partial(\rho u_2 u_1)}{\partial x_2} + \frac{\partial(\rho u_3 u_1)}{\partial x_3} \right] = \left(\frac{\partial \sigma_{11}}{\partial x_1} + \frac{\partial \sigma_{21}}{\partial x_2} + \frac{\partial \sigma_{31}}{\partial x_3} \right) + B_1$$

The equations for the x_2 and x_3 directions can be obtained in a similar manner. The final result is

$$\frac{\partial(\rho u_i)}{\partial t} + \frac{\partial(\rho u_j u_i)}{\partial x_j} = \frac{\partial \sigma_{ji}}{\partial x_j} + B_i \quad (3-42)$$

After differentiating the left-hand-side terms, Eq. (3-42) becomes

$$u_i \left[\frac{\partial \rho}{\partial t} + \frac{\partial(\rho u_j)}{\partial x_j} \right] + \rho \left[\frac{\partial u_i}{\partial t} + u_j \frac{\partial u_i}{\partial x_j} \right] = \frac{\partial \sigma_{ji}}{\partial x_j} + B_i$$

The first group on the left side is zero due to the continuity equation. The final equation becomes

$$\rho \left[\frac{\partial u_i}{\partial t} + u_j \frac{\partial u_i}{\partial x_j} \right] = \frac{\partial \sigma_{ji}}{\partial x_j} + B_i = \frac{\partial \sigma_{ji}}{\partial x_j} + \rho \sum_{k=1}^N Y_k (f_k)_i \quad (3-43)$$

which is the same result as that of the previous section.

5.1.3 Finite Control Volume Using Newton's second law, the momentum equation for a finite control volume fixed in space can be written in the following form (see Shames⁶ or Landau and Lifshitz⁹):

$$\frac{\partial}{\partial t} \int_V \rho \mathbf{v} dV + \int_A \mathbf{v} (\rho \mathbf{v} \cdot d\mathbf{A}) = \mathbf{F}_s + \int_V \mathbf{B} dV \quad (3-44)$$

The physical meaning of the above equation is

$$\left\{ \begin{array}{l} \text{rate of increase} \\ \text{of momentum} \\ \text{in the control} \\ \text{volume} \end{array} \right\} + \left\{ \begin{array}{l} \text{net rate} \\ \text{of momentum} \\ \text{flux out of} \\ \text{control volume} \end{array} \right\} = \left\{ \begin{array}{l} \text{sum of surface} \\ \text{and body forces} \\ \text{acting on fluid} \\ \text{within control volume} \end{array} \right\}$$

In tensor notation, Eq. (3-44) is

$$\frac{\partial}{\partial t} \int_V \rho u_i dV + \int_A \rho u_i u_j dA_j = \int_A \sigma_{ij} dA_j + \int_V B_i dV \quad (3-45)$$

Applying Gauss's theorem to the second term to change it to a volume integral, we have

$$\int_A \rho u_i u_j dA_j = \int_V \frac{\partial(\rho u_i u_j)}{\partial x_j} dV$$

Similarly, applying Gauss's theorem to the third term, we have

$$\int_A \sigma_{ij} dA_j = \int_V \frac{\partial \sigma_{ij}}{\partial x_j} dV$$

Combining these with Eq. (3-45), we now obtain an equation that involves only volume integrals:

$$\int_V \left[\frac{\partial(\rho u_i)}{\partial t} + \frac{\partial(\rho u_i u_j)}{\partial x_j} \right] dV = \int_V \left[\frac{\partial \sigma_{ij}}{\partial x_j} + B_i \right] dV \quad (3-46)$$

Since the integrands are continuous functions and the volume integration is performed over an arbitrary shaped fluid element, we have

$$\frac{\partial(\rho u_i)}{\partial t} + \frac{\partial(\rho u_i u_j)}{\partial x_j} = \frac{\partial \sigma_{ji}}{\partial x_j} + B_i \quad (3-47)$$

Note that we utilized the symmetric relationship for the stress tensor in the last step (i.e., $\sigma_{ij} = \sigma_{ji}$). This symmetric relationship will be discussed in the next section. Equation (3-47) gives the momentum equation in the divergence form, which is identical to that obtained in the previous section [see Eq. (3-42)]. Following the method of simplification used in the previous section, Eq. (3-47) can be converted to the following Euler form of the momentum equation:

$$\rho \left[\frac{\partial u_i}{\partial t} + u_j \frac{\partial u_i}{\partial x_j} \right] = \frac{\partial \sigma_{ji}}{\partial x_j} + B_i = \frac{\partial \sigma_{ji}}{\partial x_j} + \rho \sum_{k=1}^N Y_k (f_k)_i \quad (3-48)$$

Thus, with three similar but different approaches, we have arrived at the momentum equations in terms of stress tensors. Perhaps three derivations are no more convincing than one. However, it is believed that a better understanding of the momentum equations may be achieved by looking at the three different approaches. Our next task is to establish a relationship between stress and strain, so that the momentum equations can be written in terms of velocity gradients in different directions.

5.2 Stress–Strain Rate Relationship (Constitutive Relationship)

Before we develop the constitutive relationship, it is important to point out a fundamental difference between solids and fluids. For solid elastic bodies, shear stress is proportional to the *magnitude* of angular deformation through Hooke's law, whereas for a fluid, shear stress is proportional to the *rate of angular deformation* through Stokes' law.

A fluid deforms when subjected to a shear stress. The rate of deformation varies for different fluids, and it is also dependent upon the thermodynamic state for a given fluid. Low resistance to deformation is a natural characteristic property of the fluid.

There are several ways to establish stress–strain relationships. The approach used in classical texts such as Schlichting³ is to write the stress–strain relationships for solid elastic bodies and then replace the displacement vector by a time derivative of the displacement. This approach is lengthy but has a strong physical basis. We want to relate the terms such as σ_{ij} in some way to the mean velocity gradients. In other words, we want to relate the stress tensor σ_{ij} to the rate of deformation of a fluid element.

The second-order stress tensor σ_{ij} in a three-dimensional space has nine components. It can be written as

$$\sigma_{ij} = \begin{Bmatrix} \sigma_{11} & \sigma_{12} & \sigma_{13} \\ \sigma_{21} & \sigma_{22} & \sigma_{23} \\ \sigma_{31} & \sigma_{32} & \sigma_{33} \end{Bmatrix} = -p \delta_{ij} + \tau_{ij} \quad (3-49)$$

The components with $i = j$ are σ_{11}, σ_{22} , and σ_{33} ; they represent the normal stresses and are thus related to pressure and linear deformation. The components

with $i \neq j$ represent tangential stress. (Note that σ_{21} , for example, is the stress component acting on the $x_2 = \text{constant}$ surface in the x_1 -direction.) The stress tensor σ_{ij} can also be written into the sum of two terms; one is associated with the hydrostatic compressive stress tensor and the other is defined as the viscous stress tensor τ_{ij} as indicated by Eq. (3-49).

It is known that the stress tensor is symmetric; i.e.,

$$\sigma_{ij} = \sigma_{ji}$$

or specifically, $\sigma_{12} = \sigma_{21}$, $\sigma_{13} = \sigma_{31}$, $\sigma_{23} = \sigma_{32}$. This can be shown easily by summing moments and is left as an exercise for the reader.

5.2.1 Strain Rate Consider the special case of a fluid undergoing strain as shown in Fig. 3.6a. The fluid is contained between parallel walls with the lower plate stationary and the upper plate moving at a constant velocity U . The fluid experiences angular deformation at the rate of

$$\frac{d\gamma}{dt} = \frac{U}{h}$$

In the case of a nonlinear velocity distribution as shown in Fig. 3.6b, an infinitesimal fluid element experiences a strain rate as shown in Fig. 3.7.

The total angular strain in time dt is

$$d\gamma = \frac{[u_1 + (\partial u_1 / \partial x_2) dx_2] dt - u_1 dt}{dx_2}$$

so the strain rate is

$$\frac{d\gamma}{dt} = \frac{\partial u_1}{\partial x_2}$$

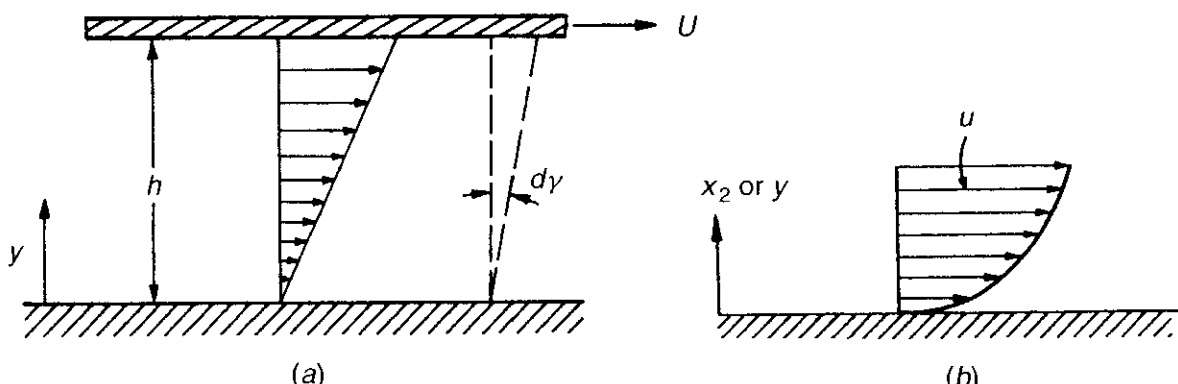


Figure 3.6 (a) Fluid between two parallel plates with the lower one stationary and the upper one moving at constant velocity (the linear velocity profile corresponding to zero pressure gradient in the flow direction). (b) Velocity distribution of a parallel flow having a nonlinear velocity profile.

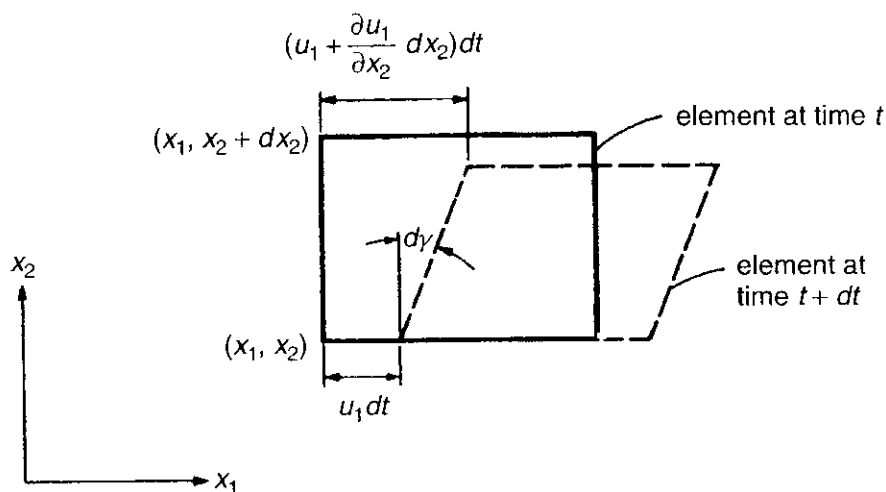


Figure 3.7 Deformation of an infinitesimal fluid element in a two-dimensional parallel flow.

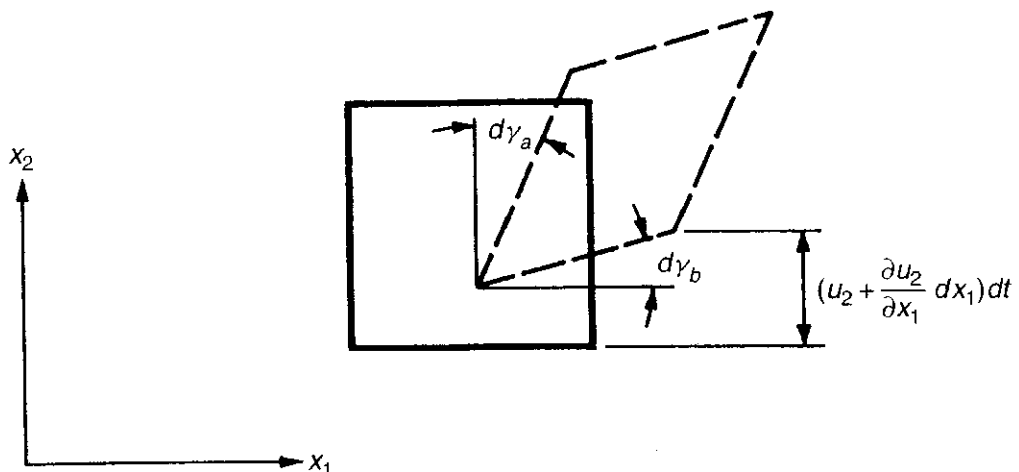


Figure 3.8 Deformation of an infinitesimal fluid element in a two-dimensional flow (angular deformations are allowed for both vertical and horizontal segments).

The above result corresponds to the shear deformation of any small fluid element between two parallel plates allowing angular deformation of this fluid element in one direction. In the case of angular deformation in two directions (i.e., due to the existence of a nonzero velocity in the x_2 -direction, u_2), we have angular deformation as shown in Fig. 3.8. The total angular deformation is then the sum of $d\gamma_a$ and $d\gamma_b$, i.e.,

$$d\gamma = d\gamma_a + d\gamma_b = \frac{[u_1 + (\partial u_1 / \partial x_2) dx_2] dt - u_1 dt}{dx_2} + \frac{[u_2 + (\partial u_2 / \partial x_1) dx_1] dt - u_2 dt}{dx_1}$$

so

$$\frac{d\gamma}{dt} = \frac{\partial u_1}{\partial x_2} + \frac{\partial u_2}{\partial x_1} \equiv 2e_{12} = 2e_{21}$$

where the general strain-rate tensor is

$$e_{ij} \equiv \frac{1}{2} \left(\frac{\partial u_i}{\partial x_j} + \frac{\partial u_j}{\partial x_i} \right) \quad (3-50)$$

5.2.2 Stress Tensor Now let's make the important Newtonian fluid assumption, which requires that the shear stress be linearly proportional to the rate of angular deformation. For a parallel-flow system, we have

$$\tau \propto \frac{d\gamma}{dt} = \frac{\partial u_1}{\partial x_2}$$

or in terms of stress tensor component σ_{21} , we have

$$\sigma_{21} = \sigma_{12} = \mu \frac{\partial u_1}{\partial x_2}$$

For the case of both velocities u_1 and u_2 being nonzero, we have

$$\tau_{12} = \mu \left(\frac{\partial u_1}{\partial x_2} + \frac{\partial u_2}{\partial x_1} \right) \quad (3-51)$$

Further, if we consider the $x_1 - x_3$ and $x_2 - x_3$ planes in the same way, we obtain the general shear stress tensor for a Newtonian fluid,

$$\sigma_{ij} = \mu \left(\frac{\partial u_i}{\partial x_j} + \frac{\partial u_j}{\partial x_i} \right) = 2\mu e_{ij}, \quad i \neq j \quad (3-52)$$

The evaluation of the off-diagonal elements of the general stress tensor σ_{ij} is now complete. This leaves the task of determining the diagonal elements of the stress tensor in terms of pressure and velocity gradient. We have considered angular deformation. Let us consider next the linear deformation of a fluid particle as shown in Fig. 3.9. The linear deformation in time dt is

$$\frac{[u_1 + (\partial u_1 / \partial x_1) dx_1] dt - u_1 dt}{dx_1} = \frac{\partial u_1}{\partial x_1} dt$$

The rate of linear deformation is

$$e_{11} = \frac{\partial u_1}{\partial x_1}$$

and for the x_2 and x_3 directions, we have

$$e_{22} = \frac{\partial u_2}{\partial x_2} \quad \text{and} \quad e_{33} = \frac{\partial u_3}{\partial x_3}$$

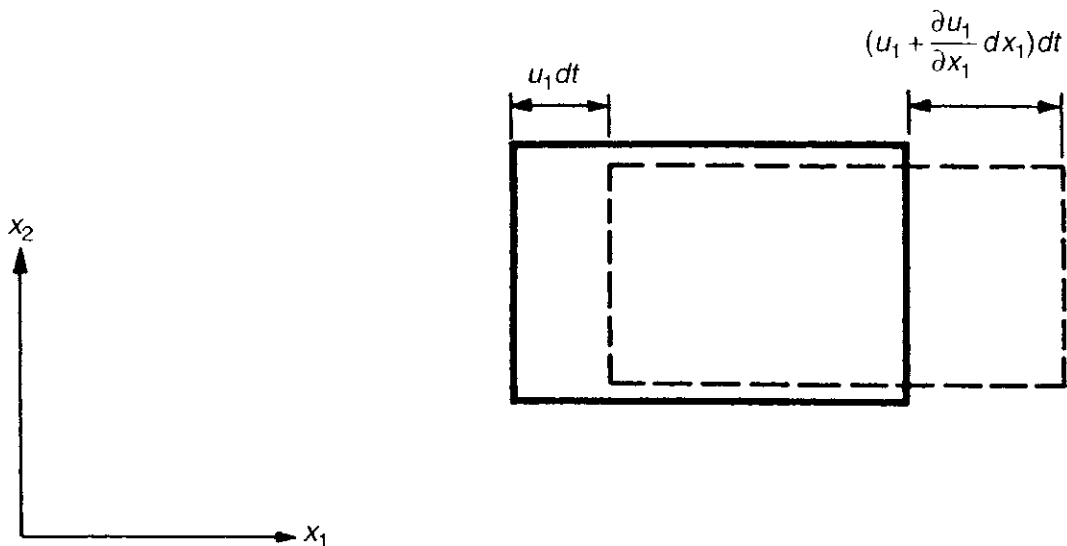


Figure 3.9 Linear deformation of a fluid particle.

The total rate-of-deformation tensor is

$$\frac{\partial u_i}{\partial x_j}$$

where we have linear deformation for $i = j$ and angular deformation for $i \neq j$. We group the deformation tensor in two parts:

$$\frac{\partial u_i}{\partial x_j} = \frac{1}{2} \left(\frac{\partial u_i}{\partial x_j} + \frac{\partial u_j}{\partial x_i} \right) + \frac{1}{2} \left(\frac{\partial u_i}{\partial x_j} - \frac{\partial u_j}{\partial x_i} \right)$$

The first group is a symmetric tensor representing $\frac{1}{2}$ of the angular-deformation tensor. The second group is an antisymmetric tensor representing rotation of a fluid without deformation.

Now, we consider the following relationship between stress and strain for the normal stress components:

$$\begin{aligned}\sigma_{11} &= -p + ce_{11} + \lambda e_{22} + \lambda e_{33} \\ \sigma_{22} &= -p + \lambda e_{11} + ce_{22} + \lambda e_{33} \\ \sigma_{33} &= -p + \lambda e_{11} + \lambda e_{22} + ce_{33}\end{aligned}\tag{3-53}$$

These equations state that there is a linear relationship between stress, say σ_{11} , and strain rate in the same direction, e_{11} (see Fig. 3.10). Also, the normal stress in x_1 direction causes strain rates in the other two directions, e_{22} and e_{33} . Since there is no preferred direction, they are related by the same coefficient λ ; that is, the fluid is assumed to be isotropic.

In Eq. (3-53), p represents the hydrostatic pressure, which must be included, since when there is no linear deformation ($e_{11} = e_{22} = e_{33} = 0$), we still have a

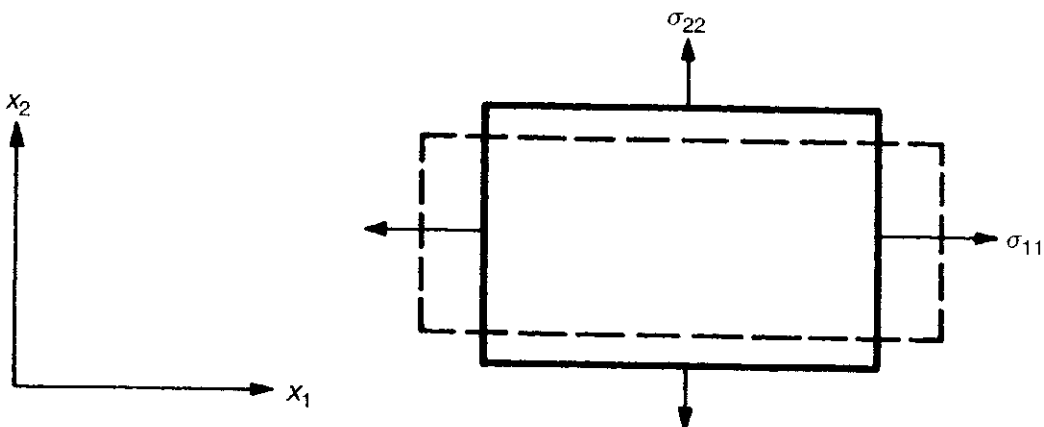


Figure 3.10 Normal stresses acting on a two-dimensional fluid particle.

normal stress in all directions and Eq. (3-53) reduces to

$$\sigma_{11} = -p, \quad \sigma_{22} = -p, \quad \text{and} \quad \sigma_{33} = -p$$

The normal stress-strain relationships may be written as

$$\begin{aligned}\sigma_{11} &= -p + \lambda(e_{11} + e_{22} + e_{33}) + (c - \lambda)e_{11} \\ \sigma_{22} &= -p + \lambda(e_{11} + e_{22} + e_{33}) + (c - \lambda)e_{22} \\ \sigma_{33} &= -p + \lambda(e_{11} + e_{22} + e_{33}) + (c - \lambda)e_{33}\end{aligned}\quad (3-53a)$$

The above two coefficients λ and c can be replaced by two other coefficients μ and μ' according to the following relations:

$$\begin{aligned}c - \lambda &= 2\mu \\ \lambda &= \mu' - \frac{2}{3}\mu\end{aligned}\quad (3-54)$$

of which the first relationship can be shown to be valid for an isotropic Newtonian fluid. Here μ is usually called the dynamic viscosity or the first viscosity, μ' is sometimes called the bulk viscosity,² and λ is called the second viscosity. (It should be noted that some authors call λ the bulk viscosity, since it is associated with volume expansion.) For monatomic gas mixtures, kinetic theory shows that $\mu' = 0$. Up to now, there are no direct and conclusive data on μ' . The usual practice is to employ the following hypothesis made by Stokes in 1845:

$$\lambda + \frac{2}{3}\mu = 0, \quad \text{or} \quad \mu' = 0 \quad (3-55)$$

Physically, the nonzero values of μ' for polyatomic gases, as explained by Williams,² are caused by the relaxation effects between the translational motion and the various internal degrees of freedom. These effects lead to a positive value of μ' . So far, no theoretical computations or reliable experimental measurements of μ' exist, and in fact μ' is usually negligible in combustion processes.

Substituting Eq. (3-54) into Eq. (3-53) and recognizing $e_{kk} = e_{11} + e_{22} + e_{33}$ from index notation, we have

$$\begin{aligned}\sigma_{11} &= -p + (\mu' - \frac{2}{3}\mu)e_{kk} + 2\mu e_{11} \\ \sigma_{22} &= -p + (\mu' - \frac{2}{3}\mu)e_{kk} + 2\mu e_{22} \\ \sigma_{33} &= -p + (\mu' - \frac{2}{3}\mu)e_{kk} + 2\mu e_{33}\end{aligned}$$

and the general stress-strain-rate relationship becomes

$$\sigma_{ij} = -p\delta_{ij} + (\mu' - \frac{2}{3}\mu)e_{kk}\delta_{ij} + 2\mu e_{ij} \quad (3-56)$$

In the above equation, the Kronecker delta function, δ_{ij} , is defined in such way that

$$\delta_{ij} = \begin{cases} 1, & i = j \\ 0, & i \neq j \end{cases} \quad (3-57)$$

The stress tensor can therefore be written as

$$\boxed{\sigma_{ij} = -p\delta_{ij} + \left(\mu' - \frac{2}{3}\mu\right) \frac{\partial u_k}{\partial x_k} \delta_{ij} + \mu \left(\frac{\partial u_i}{\partial x_j} + \frac{\partial u_j}{\partial x_i} \right)} \quad (3-58)$$

5.3 Navier–Stokes Equations

The stress-strain relationship (3-58) can be substituted into the momentum equation (3-48) to give the following Navier–Stokes equation as the momentum equation in the x_i direction.

$$\begin{aligned}\rho \left[\frac{\partial u_i}{\partial t} + u_j \frac{\partial u_i}{\partial x_j} \right] &= \frac{\partial}{\partial x_j} \left[-p\delta_{ij} + \left(\mu' - \frac{2}{3}\mu \right) \frac{\partial u_k}{\partial x_k} \delta_{ij} \right. \\ &\quad \left. + \mu \left(\frac{\partial u_i}{\partial x_j} + \frac{\partial u_j}{\partial x_i} \right) \right] + \rho \left(\sum_{k=1}^N Y_k f_k \right)_i \quad (3-59)\end{aligned}$$

If the flow is assumed incompressible, the volume dilatation term $\partial u_k / \partial x_k$ is zero, and the above momentum equation then becomes

$$\rho \left[\frac{\partial u_i}{\partial t} + u_j \frac{\partial u_i}{\partial x_j} \right] = -\frac{\partial p}{\partial x_i} + \frac{\partial}{\partial x_j} \left[\mu \left(\frac{\partial u_i}{\partial x_j} + \frac{\partial u_j}{\partial x_i} \right) \right] + \rho \sum_{k=1}^N Y_k (f_k)_i \quad (3-60)$$

It should be noted that for most combustion problems, the density variations are very pronounced; therefore, the incompressible form of the Navier–Stokes

Table 3.3 The Equation of Motion in Rectangular Coordinates (x, y, z)^a

In terms of τ :

$$\begin{aligned} x\text{-component}, \quad & \rho \left(\frac{\partial u_x}{\partial t} + u_x \frac{\partial u_x}{\partial x} + u_y \frac{\partial u_x}{\partial y} + u_z \frac{\partial u_x}{\partial z} \right) \\ & = -\frac{\partial p}{\partial x} + \left(\frac{\partial \tau_{xx}}{\partial x} + \frac{\partial \tau_{yx}}{\partial y} + \frac{\partial \tau_{zx}}{\partial z} \right) + B_x \end{aligned} \quad (\text{A})$$

$$\begin{aligned} y\text{-component}, \quad & \rho \left(\frac{\partial u_y}{\partial t} + u_x \frac{\partial u_y}{\partial x} + u_y \frac{\partial u_y}{\partial y} + u_z \frac{\partial u_y}{\partial z} \right) \\ & = -\frac{\partial p}{\partial y} + \left(\frac{\partial \tau_{xy}}{\partial x} + \frac{\partial \tau_{yy}}{\partial y} + \frac{\partial \tau_{zy}}{\partial z} \right) + B_y \end{aligned} \quad (\text{B})$$

$$\begin{aligned} z\text{-component}, \quad & \rho \left(\frac{\partial u_z}{\partial t} + u_x \frac{\partial u_z}{\partial x} + u_y \frac{\partial u_z}{\partial y} + u_z \frac{\partial u_z}{\partial z} \right) \\ & = -\frac{\partial p}{\partial z} + \left(\frac{\partial \tau_{xz}}{\partial x} + \frac{\partial \tau_{yz}}{\partial y} + \frac{\partial \tau_{zz}}{\partial z} \right) + B_z \end{aligned} \quad (\text{C})$$

In terms of velocity gradients for Newtonian fluid with constant ρ and μ :

$$\begin{aligned} x\text{-component}, \quad & \rho \left(\frac{\partial u_x}{\partial t} + u_x \frac{\partial u_x}{\partial x} + u_y \frac{\partial u_x}{\partial y} + u_z \frac{\partial u_x}{\partial z} \right) \\ & = -\frac{\partial p}{\partial x} + \mu \left(\frac{\partial^2 u_x}{\partial x^2} + \frac{\partial^2 u_x}{\partial y^2} + \frac{\partial^2 u_x}{\partial z^2} \right) + B_x \end{aligned} \quad (\text{D})$$

$$\begin{aligned} y\text{-component}, \quad & \rho \left(\frac{\partial u_y}{\partial t} + u_x \frac{\partial u_y}{\partial x} + u_y \frac{\partial u_y}{\partial y} + u_z \frac{\partial u_y}{\partial z} \right) \\ & = -\frac{\partial p}{\partial y} + \mu \left(\frac{\partial^2 u_y}{\partial x^2} + \frac{\partial^2 u_y}{\partial y^2} + \frac{\partial^2 u_y}{\partial z^2} \right) + B_y \end{aligned} \quad (\text{E})$$

$$\begin{aligned} z\text{-component}, \quad & \rho \left(\frac{\partial u_z}{\partial t} + u_x \frac{\partial u_z}{\partial x} + u_y \frac{\partial u_z}{\partial y} + u_z \frac{\partial u_z}{\partial z} \right) \\ & = -\frac{\partial p}{\partial z} + \mu \left(\frac{\partial^2 u_z}{\partial x^2} + \frac{\partial^2 u_z}{\partial y^2} + \frac{\partial^2 u_z}{\partial z^2} \right) + B_z \end{aligned} \quad (\text{F})$$

^a Adapted from Ref. 1.

equations has very limited usage. We must consider the compressible form of Navier–Stokes equations even for low Mach number situations.

Various forms of the equation of motion written in rectangular, cylindrical, and spherical coordinates are given in Tables 3.3–3.5. The components of the stress tensor for Newtonian fluids in these coordinates are given in Tables 3.6–3.8. To facilitate readers' application of the conservation equations in vector form and to

Table 3.4 The Equation of Motion in Cylindrical Coordinates (r, θ, z)^a

In terms of τ :

$$\begin{aligned} r\text{-component,}^b \quad & \rho \left(\frac{\partial u_r}{\partial t} + u_r \frac{\partial u_r}{\partial r} + \frac{u_\theta}{r} \frac{\partial u_r}{\partial \theta} - \frac{u_\theta^2}{r} + u_z \frac{\partial u_r}{\partial z} \right) \\ & = -\frac{\partial p}{\partial r} + \left(\frac{1}{r} \frac{\partial}{\partial r} (r \tau_{rr}) + \frac{1}{r} \frac{\partial \tau_{r\theta}}{\partial \theta} - \frac{\tau_{\theta\theta}}{r} + \frac{\partial \tau_{rz}}{\partial z} \right) + B_r \quad (\text{A}) \end{aligned}$$

$$\begin{aligned} \theta\text{-component,}^c \quad & \rho \left(\frac{\partial u_\theta}{\partial t} + u_r \frac{\partial u_\theta}{\partial r} + \frac{u_\theta}{r} \frac{\partial u_\theta}{\partial \theta} + \frac{u_r u_\theta}{r} + u_z \frac{\partial u_\theta}{\partial z} \right) \\ & = -\frac{1}{r} \frac{\partial p}{\partial \theta} + \left(\frac{1}{r^2} \frac{\partial}{\partial r} (r^2 \tau_{r\theta}) + \frac{1}{r} \frac{\partial \tau_{\theta\theta}}{\partial \theta} + \frac{\partial \tau_{\theta z}}{\partial z} \right) + B_\theta \quad (\text{B}) \end{aligned}$$

$$\begin{aligned} z\text{-component,} \quad & \rho \left(\frac{\partial u_z}{\partial t} + u_r \frac{\partial u_z}{\partial r} + \frac{u_\theta}{r} \frac{\partial u_z}{\partial \theta} + u_z \frac{\partial u_z}{\partial z} \right) \\ & = -\frac{\partial p}{\partial z} + \left(\frac{1}{r} \frac{\partial}{\partial r} (r \tau_{rz}) + \frac{1}{r} \frac{\partial \tau_{\theta z}}{\partial \theta} + \frac{\partial \tau_{zz}}{\partial z} \right) + B_z \quad (\text{C}) \end{aligned}$$

In terms of velocity gradients for Newtonian fluid with constant ρ and μ :

$$\begin{aligned} r\text{-component,}^b \quad & \rho \left(\frac{\partial u_r}{\partial t} + u_r \frac{\partial u_r}{\partial r} + \frac{u_\theta}{r} \frac{\partial u_r}{\partial \theta} - \frac{u_\theta^2}{r} + u_z \frac{\partial u_r}{\partial z} \right) = -\frac{\partial p}{\partial r} \\ & + \mu \left[\frac{\partial}{\partial r} \left(\frac{1}{r} \frac{\partial}{\partial r} (r u_r) \right) + \frac{1}{r^2} \frac{\partial^2 u_r}{\partial \theta^2} - \frac{2}{r^2} \frac{\partial u_\theta}{\partial \theta} + \frac{\partial^2 u_r}{\partial z^2} \right] + B_r \quad (\text{D}) \end{aligned}$$

$$\begin{aligned} \theta\text{-component,}^c \quad & \rho \left(\frac{\partial u_\theta}{\partial t} + u_r \frac{\partial u_\theta}{\partial r} + \frac{u_\theta}{r} \frac{\partial u_\theta}{\partial \theta} + \frac{u_r u_\theta}{r} + u_z \frac{\partial u_\theta}{\partial z} \right) = -\frac{1}{r} \frac{\partial p}{\partial \theta} \\ & + \mu \left[\frac{\partial}{\partial r} \left(\frac{1}{r} \frac{\partial}{\partial r} (r u_\theta) \right) + \frac{1}{r^2} \frac{\partial^2 u_\theta}{\partial \theta^2} + \frac{2}{r^2} \frac{\partial u_r}{\partial \theta} + \frac{\partial^2 u_\theta}{\partial z^2} \right] + B_\theta \quad (\text{E}) \end{aligned}$$

$$\begin{aligned} z\text{-component,} \quad & \rho \left(\frac{\partial u_z}{\partial t} + u_r \frac{\partial u_z}{\partial r} + \frac{u_\theta}{r} \frac{\partial u_z}{\partial \theta} + u_z \frac{\partial u_z}{\partial z} \right) \\ & = -\frac{\partial p}{\partial z} + \mu \left[\frac{1}{r} \frac{\partial}{\partial r} \left(r \frac{\partial u_z}{\partial r} \right) + \frac{1}{r^2} \frac{\partial^2 u_z}{\partial \theta^2} + \frac{\partial^2 u_z}{\partial z^2} \right] + B_z \quad (\text{F}) \end{aligned}$$

^a Adapted from Ref. 1.

^b The term $\rho u_\theta^2/r$ is the *centrifugal force*. It gives the effective force in the r -direction resulting from fluid motion in the θ -direction. This term arises automatically on transformation from rectangular to cylindrical coordinates; it does not have to be added on physical grounds.

^c The term $\rho u_r u_\theta/r$ is the *Coriolis force*. It is an effective force in the θ -direction when there is flow in both the r and θ directions. This term also arises automatically in the coordinate transformation. The Coriolis force arises in the problem of flow near a rotating disk (see, for example, Ref. 3).

Table 3.5 The Equation of Motion in Spherical Coordinates (r, θ, ϕ) ^a

In terms of τ :

$$\begin{aligned} r\text{-component, } \rho & \left(\frac{\partial u_r}{\partial t} + u_r \frac{\partial u_r}{\partial r} + \frac{u_\theta}{r} \frac{\partial u_r}{\partial \theta} + \frac{u_\phi}{r \sin \theta} \frac{\partial u_r}{\partial \phi} - \frac{u_\theta^2 + u_\phi^2}{r} \right) \\ & = -\frac{\partial p}{\partial r} + \left(\frac{1}{r^2} \frac{\partial}{\partial r} (r^2 \tau_{rr}) + \frac{1}{r \sin \theta} \frac{\partial}{\partial \theta} (\tau_{r\theta} \sin \theta) \right. \\ & \quad \left. + \frac{1}{r \sin \theta} \frac{\partial \tau_{r\phi}}{\partial \phi} - \frac{\tau_{\theta\theta} + \tau_{\phi\phi}}{r} \right) + B_r \end{aligned} \quad (\text{A})$$

$$\begin{aligned} \theta\text{-component, } \rho & \left(\frac{\partial u_\theta}{\partial t} + u_r \frac{\partial u_\theta}{\partial r} + \frac{u_\theta}{r} \frac{\partial u_\theta}{\partial \theta} + \frac{u_\phi}{r \sin \theta} \frac{\partial u_\theta}{\partial \phi} + \frac{u_r u_\theta}{r} - \frac{u_\phi^2 \cot \theta}{r} \right) \\ & = -\frac{1}{r} \frac{\partial p}{\partial \theta} + \left(\frac{1}{r^2} \frac{\partial}{\partial r} (r^2 \tau_{r\theta}) + \frac{1}{r \sin \theta} \frac{\partial}{\partial \theta} (\tau_{\theta\theta} \sin \theta) \right. \\ & \quad \left. + \frac{1}{r \sin \theta} \frac{\partial \tau_{\theta\phi}}{\partial \phi} + \frac{\tau_{r\theta}}{r} - \frac{\cot \theta}{r} \tau_{\phi\phi} \right) + B_\theta \end{aligned} \quad (\text{B})$$

$$\begin{aligned} \phi\text{-component, } \rho & \left(\frac{\partial u_\phi}{\partial t} + u_r \frac{\partial u_\phi}{\partial r} + \frac{u_\theta}{r} \frac{\partial u_\phi}{\partial \theta} + \frac{u_\phi}{r \sin \theta} \frac{\partial u_\phi}{\partial \phi} + \frac{u_\phi u_r}{r} + \frac{u_\theta u_\phi}{r} \cot \theta \right) \\ & = -\frac{1}{r \sin \theta} \frac{\partial p}{\partial \phi} + \left(\frac{1}{r^2} \frac{\partial}{\partial r} (r^2 \tau_{r\phi}) + \frac{1}{r} \frac{\partial \tau_{\theta\phi}}{\partial \theta} + \frac{1}{r \sin \theta} \frac{\partial \tau_{\phi\phi}}{\partial \phi} \right. \\ & \quad \left. + \frac{\tau_{r\phi}}{r} - \frac{2 \cot \theta}{r} \tau_{\theta\phi} \right) + B_\phi \end{aligned} \quad (\text{C})$$

In terms of velocity gradients for a Newtonian fluid with constant ρ and μ :^b

$$\begin{aligned} r\text{-component, } \rho & \left(\frac{\partial u_r}{\partial t} + u_r \frac{\partial u_r}{\partial r} + \frac{u_\theta}{r} \frac{\partial u_r}{\partial \theta} + \frac{u_\phi}{r \sin \theta} \frac{\partial u_r}{\partial \phi} - \frac{u_\theta^2 + u_\phi^2}{r} \right) \\ & = -\frac{\partial p}{\partial r} + \mu \left(\nabla^2 u_r - \frac{2}{r^2} u_r - \frac{2}{r^2} \frac{\partial u_\theta}{\partial \theta} - \frac{2}{r^2} u_\theta \cot \theta \right. \\ & \quad \left. - \frac{2}{r^2 \sin \theta} \frac{\partial u_\phi}{\partial \phi} \right) + B_r \end{aligned} \quad (\text{D})$$

$$\begin{aligned} \theta\text{-component, } \rho & \left(\frac{\partial u_\theta}{\partial t} + u_r \frac{\partial u_\theta}{\partial r} + \frac{u_\theta}{r} \frac{\partial u_\theta}{\partial \theta} + \frac{u_\phi}{r \sin \theta} \frac{\partial u_\theta}{\partial \phi} + \frac{u_r u_\theta}{r} - \frac{u_\phi^2 \cot \theta}{r} \right) \\ & = -\frac{1}{r} \frac{\partial p}{\partial \theta} + \mu \left(\nabla^2 u_\theta + \frac{2}{r^2} \frac{\partial u_r}{\partial \theta} - \frac{u_\theta}{r^2 \sin^2 \theta} - \frac{2 \cos \theta}{r^2 \sin^2 \theta} \frac{\partial u_\phi}{\partial \phi} \right) + B_\theta \end{aligned} \quad (\text{E})$$

Table 3.5 (continued)

$$\begin{aligned}
 \phi\text{-component}, \quad & \rho \left(\frac{\partial u_\phi}{\partial t} + u_r \frac{\partial u_\phi}{\partial r} + \frac{u_\theta}{r} \frac{\partial u_\phi}{\partial \theta} + \frac{u_\phi}{r \sin \theta} \frac{\partial u_\phi}{\partial \phi} + \frac{u_\phi u_r}{r} + \frac{u_\theta u_\phi}{r} \cot \theta \right) \\
 & = -\frac{1}{r \sin \theta} \frac{\partial p}{\partial \phi} + \mu \left(\nabla^2 u_\phi - \frac{u_\phi}{r^2 \sin^2 \theta} + \frac{2}{r^2 \sin \theta} \frac{\partial u_r}{\partial \phi} \right. \\
 & \quad \left. + \frac{2 \cos \theta}{r^2 \sin^2 \theta} \frac{\partial u_\theta}{\partial \phi} \right) + B_\phi
 \end{aligned} \tag{F}$$

^a Adapted from Ref. 1.

^b In these equations $\nabla^2 = \frac{1}{r^2} \frac{\partial}{\partial r} \left(r^2 \frac{\partial}{\partial r} \right) + \frac{1}{r^2 \sin \theta} \frac{\partial}{\partial \theta} \left(\sin \theta \frac{\partial}{\partial \theta} \right) + \frac{1}{r^2 \sin^2 \theta} \left(\frac{\partial^2}{\partial \phi^2} \right)$

Table 3.6 Components of the Stress Tensor for Newtonian Fluids in Rectangular Coordinates (x, y, z)^a

$$\tau_{xx} = \mu \left[2 \frac{\partial u_x}{\partial x} - \frac{2}{3} (\nabla \cdot \mathbf{v}) \right] \tag{A}$$

$$\tau_{yy} = \mu \left[2 \frac{\partial u_y}{\partial y} - \frac{2}{3} (\nabla \cdot \mathbf{v}) \right] \tag{B}$$

$$\tau_{zz} = \mu \left[2 \frac{\partial u_z}{\partial z} - \frac{2}{3} (\nabla \cdot \mathbf{v}) \right] \tag{C}$$

$$\tau_{xy} = \tau_{yx} = \mu \left[\frac{\partial u_x}{\partial y} + \frac{\partial u_y}{\partial x} \right] \tag{D}$$

$$\tau_{yz} = \tau_{zy} = \mu \left[\frac{\partial u_y}{\partial z} + \frac{\partial u_z}{\partial y} \right] \tag{E}$$

$$\tau_{zx} = \tau_{xz} = \mu \left[\frac{\partial u_z}{\partial x} + \frac{\partial u_x}{\partial z} \right] \tag{F}$$

$$\nabla \cdot \mathbf{v} = \frac{\partial u_x}{\partial x} + \frac{\partial u_y}{\partial y} + \frac{\partial u_z}{\partial z} \tag{G}$$

^a Adapted from Ref. 1.

enhance their understanding of vector operations in various coordinate systems, the differential operations involving the ∇ -operator in rectangular, cylindrical, and spherical coordinates are listed in Tables 3.9–3.11, respectively. All operations involving the viscous stress tensor τ are valid for symmetrical τ only. The expressions for $(\tau : \nabla \mathbf{v})$ are useful for the energy equation to be discussed in the next section.

Table 3.7 Components of the Stress Tensor for Newtonian Fluids in Cylindrical Coordinates $(r, \theta, z)^a$

$$\tau_{rr} = \mu \left[2 \frac{\partial u_r}{\partial r} - \frac{2}{3} (\nabla \cdot \mathbf{v}) \right] \quad (\text{A})$$

$$\tau_{\theta\theta} = \mu \left[2 \left(\frac{1}{r} \frac{\partial u_\theta}{\partial \theta} + \frac{u_r}{r} \right) - \frac{2}{3} (\nabla \cdot \mathbf{v}) \right] \quad (\text{B})$$

$$\tau_{zz} = \mu \left[2 \frac{\partial u_z}{\partial z} - \frac{2}{3} (\nabla \cdot \mathbf{v}) \right] \quad (\text{C})$$

$$\tau_{r\theta} = \tau_{\theta r} = \mu \left[r \frac{\partial}{\partial r} \left(\frac{u_\theta}{r} \right) + \frac{1}{r} \frac{\partial u_r}{\partial \theta} \right] \quad (\text{D})$$

$$\tau_{\theta z} = \tau_{z\theta} = \mu \left[\frac{\partial u_\theta}{\partial z} + \frac{1}{r} \frac{\partial u_z}{\partial \theta} \right] \quad (\text{E})$$

$$\tau_{rz} = \tau_{zr} = \mu \left[\frac{\partial u_z}{\partial r} + \frac{\partial u_r}{\partial z} \right] \quad (\text{F})$$

$$\nabla \cdot \mathbf{v} = \frac{1}{r} \frac{\partial}{\partial r} (r u_r) + \frac{1}{r} \frac{\partial u_\theta}{\partial \theta} + \frac{\partial u_z}{\partial z} \quad (\text{G})$$

^a Adapted from Ref. 1.

Table 3.8 Components of the Stress Tensor for Newtonian Fluids in Spherical Coordinates $(r, \theta, \phi)^a$

$$\tau_{rr} = \mu \left[2 \frac{\partial u_r}{\partial r} - \frac{2}{3} (\nabla \cdot \mathbf{v}) \right] \quad (\text{A})$$

$$\tau_{\theta\theta} = \mu \left[2 \left(\frac{1}{r} \frac{\partial u_\theta}{\partial \theta} + \frac{u_r}{r} \right) - \frac{2}{3} (\nabla \cdot \mathbf{v}) \right] \quad (\text{B})$$

$$\tau_{\phi\phi} = \mu \left[2 \left(\frac{1}{r \sin \theta} \frac{\partial u_\phi}{\partial \phi} + \frac{u_r}{r} + \frac{u_\theta \cot \theta}{r} \right) - \frac{2}{3} (\nabla \cdot \mathbf{v}) \right] \quad (\text{C})$$

$$\tau_{r\theta} = \tau_{\theta r} = \mu \left[r \frac{\partial}{\partial r} \left(\frac{u_\theta}{r} \right) + \frac{1}{r} \frac{\partial u_r}{\partial \theta} \right] \quad (\text{D})$$

$$\tau_{\theta\phi} = \tau_{\phi\theta} = \mu \left[\frac{\sin \theta}{r} \frac{\partial}{\partial \theta} \left(\frac{u_\phi}{\sin \theta} \right) + \frac{1}{r \sin \theta} \frac{\partial u_\theta}{\partial \phi} \right] \quad (\text{E})$$

$$\tau_{\phi r} = \tau_{r\phi} = \mu \left[\frac{1}{r \sin \theta} \frac{\partial u_r}{\partial \phi} + r \frac{\partial}{\partial r} \left(\frac{u_\phi}{r} \right) \right] \quad (\text{F})$$

$$\nabla \cdot \mathbf{v} = \frac{1}{r^2} \frac{\partial}{\partial r} (r^2 u_r) + \frac{1}{r \sin \theta} \frac{\partial}{\partial \theta} (u_\theta \sin \theta) + \frac{1}{r \sin \theta} \frac{\partial u_\phi}{\partial \phi} \quad (\text{G})$$

^a Adapted from Ref. 1.

Table 3.9 Summary of Differential Operations Involving the ∇ -Operator in Rectangular Coordinates (x, y, z) ^a

$$\nabla \cdot \mathbf{v} = \frac{\partial u_x}{\partial x} + \frac{\partial u_y}{\partial y} + \frac{\partial u_z}{\partial z} \quad (\text{A})$$

$$\nabla^2 s = \frac{\partial^2 s}{\partial x^2} + \frac{\partial^2 s}{\partial y^2} + \frac{\partial^2 s}{\partial z^2} \quad (\text{B})$$

$$\begin{aligned} \tau : \nabla \mathbf{v} = & \tau_{xx} \left(\frac{\partial u_x}{\partial x} \right) + \tau_{yy} \left(\frac{\partial u_y}{\partial y} \right) + \tau_{zz} \left(\frac{\partial u_z}{\partial z} \right) + \tau_{xy} \left(\frac{\partial u_x}{\partial y} + \frac{\partial u_y}{\partial x} \right) \\ & + \tau_{yz} \left(\frac{\partial u_y}{\partial z} + \frac{\partial u_z}{\partial y} \right) + \tau_{zx} \left(\frac{\partial u_z}{\partial x} + \frac{\partial u_x}{\partial z} \right) \end{aligned} \quad (\text{C})$$

$$[\nabla s]_x = \frac{\partial s}{\partial x} \quad (\text{D}) \quad [\nabla \times \mathbf{v}]_x = \frac{\partial u_z}{\partial y} - \frac{\partial u_y}{\partial z} \quad (\text{G})$$

$$[\nabla s]_y = \frac{\partial s}{\partial y} \quad (\text{E}) \quad [\nabla \times \mathbf{v}]_y = \frac{\partial u_x}{\partial z} - \frac{\partial u_z}{\partial x} \quad (\text{H})$$

$$[\nabla s]_z = \frac{\partial s}{\partial z} \quad (\text{F}) \quad [\nabla \times \mathbf{v}]_z = \frac{\partial u_y}{\partial x} - \frac{\partial u_x}{\partial y} \quad (\text{I})$$

$$[\nabla \cdot \boldsymbol{\tau}]_x = \frac{\partial \tau_{xx}}{\partial x} + \frac{\partial \tau_{xy}}{\partial y} + \frac{\partial \tau_{xz}}{\partial z} \quad (\text{J})$$

$$[\nabla \cdot \boldsymbol{\tau}]_y = \frac{\partial \tau_{yx}}{\partial x} + \frac{\partial \tau_{yy}}{\partial y} + \frac{\partial \tau_{yz}}{\partial z} \quad (\text{K})$$

$$[\nabla \cdot \boldsymbol{\tau}]_z = \frac{\partial \tau_{zx}}{\partial x} + \frac{\partial \tau_{zy}}{\partial y} + \frac{\partial \tau_{zz}}{\partial z} \quad (\text{L})$$

$$[\nabla^2 \mathbf{v}]_x = \frac{\partial^2 u_x}{\partial x^2} + \frac{\partial^2 u_x}{\partial y^2} + \frac{\partial^2 u_x}{\partial z^2} \quad (\text{M})$$

$$[\nabla^2 \mathbf{v}]_y = \frac{\partial^2 u_y}{\partial x^2} + \frac{\partial^2 u_y}{\partial y^2} + \frac{\partial^2 u_y}{\partial z^2} \quad (\text{N})$$

$$[\nabla^2 \mathbf{v}]_z = \frac{\partial^2 u_z}{\partial x^2} + \frac{\partial^2 u_z}{\partial y^2} + \frac{\partial^2 u_z}{\partial z^2} \quad (\text{O})$$

$$[\mathbf{v} \cdot \nabla \mathbf{v}]_x = u_x \frac{\partial u_x}{\partial x} + u_y \frac{\partial u_x}{\partial y} + u_z \frac{\partial u_x}{\partial z} \quad (\text{P})$$

$$[\mathbf{v} \cdot \nabla \mathbf{v}]_y = u_x \frac{\partial u_y}{\partial x} + u_y \frac{\partial u_y}{\partial y} + u_z \frac{\partial u_y}{\partial z} \quad (\text{Q})$$

$$[\mathbf{v} \cdot \nabla \mathbf{v}]_z = u_x \frac{\partial u_z}{\partial x} + u_y \frac{\partial u_z}{\partial y} + u_z \frac{\partial u_z}{\partial z} \quad (\text{R})$$

Table 3.9 (continued)

For Newtonian fluids

$$\begin{aligned} \frac{\tau : \nabla \mathbf{v}}{\mu} = & 2 \left[\left(\frac{\partial u_x}{\partial x} \right)^2 + \left(\frac{\partial u_y}{\partial y} \right)^2 + \left(\frac{\partial u_z}{\partial z} \right)^2 \right] \\ & + \left[\frac{\partial u_y}{\partial x} + \frac{\partial u_x}{\partial y} \right]^2 + \left[\frac{\partial u_z}{\partial y} + \frac{\partial u_y}{\partial z} \right]^2 + \left[\frac{\partial u_x}{\partial z} + \frac{\partial u_z}{\partial x} \right]^2 \\ & - \frac{2}{3} \left[\frac{\partial u_x}{\partial x} + \frac{\partial u_y}{\partial y} + \frac{\partial u_z}{\partial z} \right]^2 \end{aligned} \quad (\text{S})$$

^a Adapted from Ref. 1. Operations involving the tensor τ are given for symmetrical τ only.

Table 3.10 Summary of Differential Operations Involving the ∇ -Operator in Cylindrical Coordinates (r, θ, z) ^a

$$\nabla \cdot \mathbf{v} = \frac{1}{r} \frac{\partial}{\partial r} (r u_r) + \frac{1}{r} \frac{\partial u_\theta}{\partial \theta} + \frac{\partial u_z}{\partial z} \quad (\text{A})$$

$$\nabla^2 s = \frac{1}{r} \frac{\partial}{\partial r} \left(r \frac{\partial s}{\partial r} \right) + \frac{1}{r^2} \frac{\partial^2 s}{\partial \theta^2} + \frac{\partial^2 s}{\partial z^2} \quad (\text{B})$$

$$\begin{aligned} \tau : \nabla \mathbf{v} = & \tau_{rr} \left(\frac{\partial u_r}{\partial r} \right) + \tau_{\theta\theta} \left(\frac{1}{r} \frac{\partial u_\theta}{\partial \theta} + \frac{u_r}{r} \right) + \tau_{zz} \left(\frac{\partial u_z}{\partial z} \right) \\ & + \tau_{r\theta} \left[r \frac{\partial}{\partial r} \left(\frac{u_\theta}{r} \right) + \frac{1}{r} \frac{\partial u_r}{\partial \theta} \right] + \tau_{\theta z} \left(\frac{1}{r} \frac{\partial u_z}{\partial \theta} + \frac{\partial u_\theta}{\partial z} \right) + \tau_{rz} \left(\frac{\partial u_z}{\partial r} + \frac{\partial u_r}{\partial z} \right) \end{aligned} \quad (\text{C})$$

$$[\nabla s]_r = \frac{\partial s}{\partial r} \quad (\text{D}) \quad [\nabla \times \mathbf{v}]_r = \frac{1}{r} \frac{\partial u_z}{\partial \theta} - \frac{\partial u_\theta}{\partial z} \quad (\text{G})$$

$$[\nabla s]_\theta = \frac{1}{r} \frac{\partial s}{\partial \theta} \quad (\text{E}) \quad [\nabla \times \mathbf{v}]_\theta = \frac{\partial u_r}{\partial z} - \frac{\partial u_z}{\partial r} \quad (\text{H})$$

$$[\nabla s]_z = \frac{\partial s}{\partial z} \quad (\text{F}) \quad [\nabla \times \mathbf{v}]_z = \frac{1}{r} \frac{\partial}{\partial r} (r u_\theta) - \frac{1}{r} \frac{\partial u_r}{\partial \theta} \quad (\text{I})$$

$$[\nabla \cdot \tau]_r = \frac{1}{r} \frac{\partial}{\partial r} (r \tau_{rr}) + \frac{1}{r} \frac{\partial}{\partial \theta} \tau_{r\theta} - \frac{1}{r} \tau_{\theta\theta} + \frac{\partial \tau_{rz}}{\partial z} \quad (\text{J})$$

$$[\nabla \cdot \tau]_\theta = \frac{1}{r} \frac{\partial \tau_{\theta\theta}}{\partial \theta} + \frac{\partial \tau_{r\theta}}{\partial r} + \frac{2}{r} \tau_{r\theta} + \frac{\partial \tau_{\theta z}}{\partial z} \quad (\text{K})$$

$$[\nabla \cdot \tau]_z = \frac{1}{r} \frac{\partial}{\partial r} (r \tau_{rz}) + \frac{1}{r} \frac{\partial \tau_{\theta z}}{\partial \theta} + \frac{\partial \tau_{zz}}{\partial z} \quad (\text{L})$$

Table 3.10 (continued)

$$[\nabla^2 \mathbf{v}]_r = \frac{\partial}{\partial r} \left(\frac{1}{r} \frac{\partial}{\partial r} (ru_r) \right) + \frac{1}{r^2} \frac{\partial^2 u_r}{\partial \theta^2} - \frac{2}{r^2} \frac{\partial u_\theta}{\partial \theta} + \frac{\partial^2 u_r}{\partial z^2} \quad (\text{M})$$

$$[\nabla^2 \mathbf{v}]_\theta = \frac{\partial}{\partial r} \left(\frac{1}{r} \frac{\partial}{\partial r} (ru_\theta) \right) + \frac{1}{r^2} \frac{\partial^2 u_\theta}{\partial \theta^2} + \frac{2}{r^2} \frac{\partial u_r}{\partial \theta} + \frac{\partial^2 u_\theta}{\partial z^2} \quad (\text{N})$$

$$[\nabla^2 \mathbf{v}]_z = \frac{1}{r} \frac{\partial}{\partial r} \left(r \frac{\partial u_z}{\partial r} \right) + \frac{1}{r^2} \frac{\partial^2 u_z}{\partial \theta^2} + \frac{\partial^2 u_z}{\partial z^2} \quad (\text{O})$$

$$[\mathbf{v} \cdot \nabla \mathbf{v}]_r = u_r \frac{\partial u_r}{\partial r} + \frac{u_\theta}{r} \frac{\partial u_r}{\partial \theta} - \frac{u_\theta^2}{r} + u_z \frac{\partial u_r}{\partial z} \quad (\text{P})$$

$$[\mathbf{v} \cdot \nabla \mathbf{v}]_\theta = u_r \frac{\partial u_\theta}{\partial r} + \frac{u_\theta}{r} \frac{\partial u_\theta}{\partial \theta} + \frac{u_r u_\theta}{r} + u_z \frac{\partial u_\theta}{\partial z} \quad (\text{Q})$$

$$[\mathbf{v} \cdot \nabla \mathbf{v}]_z = u_r \frac{\partial u_z}{\partial r} + \frac{u_\theta}{r} \frac{\partial u_z}{\partial \theta} + u_z \frac{\partial u_z}{\partial z} \quad (\text{R})$$

For Newtonian fluids

$$\begin{aligned} \frac{\tau : \nabla \mathbf{v}}{\mu} = & 2 \left[\left(\frac{\partial u_r}{\partial r} \right)^2 + \left(\frac{1}{r} \frac{\partial u_\theta}{\partial \theta} + \frac{u_r}{r} \right)^2 + \left(\frac{\partial u_z}{\partial z} \right)^2 \right] \\ & + \left[r \frac{\partial}{\partial r} \left(\frac{u_\theta}{r} \right) + \frac{1}{r} \frac{\partial u_r}{\partial \theta} \right]^2 + \left[\frac{1}{r} \frac{\partial u_z}{\partial \theta} + \frac{\partial u_\theta}{\partial z} \right]^2 \\ & + \left[\frac{\partial u_r}{\partial z} + \frac{\partial u_z}{\partial r} \right]^2 - \frac{2}{3} \left[\frac{1}{r} \frac{\partial}{\partial r} (ru_r) + \frac{1}{r} \frac{\partial u_\theta}{\partial \theta} + \frac{\partial u_z}{\partial z} \right]^2 \end{aligned} \quad (\text{S})$$

^a Adapted from Ref. 1. Operations involving the tensor τ are given for symmetrical τ only.

Table 3.11 Summary of Differential Operations Involving the ∇ -Operator in Spherical Coordinates (r, θ, ϕ)^a

$$\nabla \cdot \mathbf{v} = \frac{1}{r^2} \frac{\partial}{\partial r} (r^2 u_r) + \frac{1}{r \sin \theta} \frac{\partial}{\partial \theta} (u_\theta \sin \theta) + \frac{1}{r \sin \theta} \frac{\partial u_\phi}{\partial \phi} \quad (\text{A})$$

$$\nabla^2 s = \frac{1}{r^2} \frac{\partial}{\partial r} \left(r^2 \frac{\partial s}{\partial r} \right) + \frac{1}{r^2 \sin \theta} \frac{\partial}{\partial \theta} \left(\sin \theta \frac{\partial s}{\partial \theta} \right) + \frac{1}{r^2 \sin^2 \theta} \frac{\partial^2 s}{\partial \phi^2} \quad (\text{B})$$

$$\begin{aligned} \tau : \nabla \mathbf{v} = & \tau_{rr} \left(\frac{\partial u_r}{\partial r} \right) + \tau_{\theta\theta} \left(\frac{1}{r} \frac{\partial u_\theta}{\partial \theta} + \frac{u_r}{r} \right) + \tau_{\phi\phi} \left(\frac{1}{r \sin \theta} \frac{\partial u_\phi}{\partial \phi} + \frac{u_r}{r} + \frac{u_\theta \cot \theta}{r} \right) \\ & + \tau_{r\theta} \left[\frac{\partial u_\theta}{\partial r} + \frac{1}{r} \frac{\partial u_r}{\partial \theta} - \frac{u_\theta}{r} \right] + \tau_{r\phi} \left(\frac{\partial u_\phi}{\partial r} + \frac{1}{r \sin \theta} \frac{\partial u_r}{\partial \phi} - \frac{u_\phi}{r} \right) \\ & + \tau_{\theta\phi} \left(\frac{1}{r} \frac{\partial u_\phi}{\partial \theta} + \frac{1}{r \sin \theta} \frac{\partial u_\theta}{\partial \phi} - \frac{\cot \theta}{r} u_\phi \right) \end{aligned} \quad (\text{C})$$

Table 3.11 (continued)

$[\nabla s]_r = \frac{\partial s}{\partial r}$	(D)	$[\nabla \times \mathbf{v}]_r = \frac{1}{r \sin \theta} \frac{\partial}{\partial \theta} (u_\phi \sin \theta) - \frac{1}{r \sin \theta} \frac{\partial u_\theta}{\partial \phi}$	(G)
$[\nabla s]_\theta = \frac{1}{r} \frac{\partial s}{\partial \theta}$	(E)	$[\nabla \times \mathbf{v}]_\theta = \frac{1}{r \sin \theta} \frac{\partial u_r}{\partial \phi} - \frac{1}{r} \frac{\partial}{\partial r} (r u_\phi)$	(H)
$[\nabla s]_\phi = \frac{1}{r \sin \theta} \frac{\partial s}{\partial \phi}$	(F)	$[\nabla \times \mathbf{v}]_\phi = \frac{1}{r} \frac{\partial}{\partial r} (r u_\theta) - \frac{1}{r} \frac{\partial u_r}{\partial \theta}$	(I)
$[\nabla \cdot \boldsymbol{\tau}]_r = \frac{1}{r^2} \frac{\partial}{\partial r} (r^2 \tau_{rr}) + \frac{1}{r \sin \theta} \frac{\partial}{\partial \theta} (\tau_{r\theta} \sin \theta) + \frac{1}{r \sin \theta} \frac{\partial \tau_{r\phi}}{\partial \phi} - \frac{\tau_{\theta\theta} + \tau_{\phi\phi}}{r}$			(J)
$[\nabla \cdot \boldsymbol{\tau}]_\theta = \frac{1}{r^2} \frac{\partial}{\partial r} (r^2 \tau_{r\theta}) + \frac{1}{r \sin \theta} \frac{\partial}{\partial \theta} (\tau_{\theta\theta} \sin \theta) + \frac{1}{r \sin \theta} \frac{\partial \tau_{\theta\phi}}{\partial \phi} + \frac{\tau_{r\theta}}{r} - \frac{\cot \theta}{r} \tau_{\phi\phi}$			(K)
$[\nabla \cdot \boldsymbol{\tau}]_\phi = \frac{1}{r^2} \frac{\partial}{\partial r} (r^2 \tau_{r\phi}) + \frac{1}{r} \frac{\partial \tau_{\theta\phi}}{\partial \theta} + \frac{1}{r \sin \theta} \frac{\partial \tau_{\phi\phi}}{\partial \phi} + \frac{\tau_{r\phi}}{r} + \frac{2 \cot \theta}{r} \tau_{\theta\phi}$			(L)
$[\nabla^2 \mathbf{v}]_r = \nabla^2 u_r - \frac{2u_r}{r^2} - \frac{2}{r^2} \frac{\partial u_\theta}{\partial \theta} - \frac{2u_\theta \cot \theta}{r^2} - \frac{2}{r^2 \sin \theta} \frac{\partial u_\phi}{\partial \phi}$			(M)
$[\nabla^2 \mathbf{v}]_\theta = \nabla^2 u_\theta + \frac{2}{r^2} \frac{\partial u_r}{\partial \theta} - \frac{u_\theta}{r^2 \sin^2 \theta} - \frac{2 \cos \theta}{r^2 \sin^2 \theta} \frac{\partial u_\phi}{\partial \phi}$			(N)
$[\nabla^2 \mathbf{v}]_\phi = \nabla^2 u_\phi - \frac{u_\phi}{r^2 \sin^2 \theta} + \frac{2}{r^2 \sin \theta} \frac{\partial u_r}{\partial \phi} + \frac{2 \cos \theta}{r^2 \sin^2 \theta} \frac{\partial u_\theta}{\partial \phi}$			(O)
$[\mathbf{v} \cdot \nabla \mathbf{v}]_r = u_r \frac{\partial u_r}{\partial r} + \frac{u_\theta}{r} \frac{\partial u_r}{\partial \theta} + \frac{u_\phi}{r \sin \theta} \frac{\partial u_r}{\partial \phi} - \frac{u_\theta^2 + u_\phi^2}{r}$			(P)
$[\mathbf{v} \cdot \nabla \mathbf{v}]_\theta = u_r \frac{\partial u_\theta}{\partial r} + \frac{u_\theta}{r} \frac{\partial u_\theta}{\partial \theta} + \frac{u_\phi}{r \sin \theta} \frac{\partial u_\theta}{\partial \phi} + \frac{u_r u_\theta}{r} - \frac{u_\phi^2 \cot \theta}{r}$			(Q)
$[\mathbf{v} \cdot \nabla \mathbf{v}]_\phi = u_r \frac{\partial u_\phi}{\partial r} + \frac{u_\theta}{r} \frac{\partial u_\phi}{\partial \theta} + \frac{u_\phi}{r \sin \theta} \frac{\partial u_\phi}{\partial \phi} + \frac{u_\phi u_r}{r} + \frac{u_\theta u_\phi \cot \theta}{r}$			(R)

For Newtonian fluids

$$\begin{aligned}
 \frac{\boldsymbol{\tau} : \nabla \mathbf{v}}{\mu} = & 2 \left[\left(\frac{\partial u_r}{\partial r} \right)^2 + \left(\frac{1}{r} \frac{\partial u_\theta}{\partial \theta} + \frac{u_r}{r} \right)^2 + \left(\frac{1}{r \sin \theta} \frac{\partial u_\phi}{\partial \phi} + \frac{u_r}{r} + \frac{u_\theta \cot \theta}{r} \right)^2 \right] \\
 & + \left[r \frac{\partial}{\partial r} \left(\frac{u_\theta}{r} \right) + \frac{1}{r} \frac{\partial u_r}{\partial \theta} \right]^2 + \left[\frac{\sin \theta}{r} \frac{\partial}{\partial \theta} \left(\frac{u_\phi}{\sin \theta} \right) + \frac{1}{r \sin \theta} \frac{\partial u_\theta}{\partial \phi} \right]^2 \\
 & + \left[\frac{1}{r \sin \theta} \frac{\partial u_r}{\partial \phi} + r \frac{\partial}{\partial r} \left(\frac{u_\phi}{r} \right) \right]^2 - \frac{2}{3} \left[\frac{1}{r^2} \frac{\partial}{\partial r} (r^2 u_r) \right. \\
 & \left. + \frac{1}{r \sin \theta} \frac{\partial}{\partial \theta} (u_\theta \sin \theta) + \frac{1}{r \sin \theta} \frac{\partial u_\phi}{\partial \phi} \right]^2
 \end{aligned} \tag{S}$$

^a Adapted from Ref. 1. Operations involving the tensor $\boldsymbol{\tau}$ are given for symmetrical $\boldsymbol{\tau}$ only.

6 CONSERVATION OF ENERGY

Before deriving the conservation of energy equation for a multicomponent system, we must be aware of the various effects that contribute to the heat flux. It is known from Fourier's law of heat conduction that the temperature gradient (∇T) in the flow field is the main cause of heat flux (\mathbf{q}), as shown by Fig. 3.11. There are two additional effects besides conduction heat flux ($-\lambda \nabla T$), which can contribute to the heat flux in a multicomponent system. When the average velocity \mathbf{v}_i of component i differs from the mass-average velocity of the mixture, there is then a diffusion mass flux $\rho_i V_i$ of component i relative to the bulk mass flux of the mixture flowing at the mass-average velocity in the local control volume. If the average enthalpy (per unit mass) associated with the i th component is h_i , then the extra enthalpy flux carried by the i th molecules across the control surface per unit time is equal to $h_i \rho_i V_i$ or $\rho h_i Y_i \mathbf{V}_i$. The overall enthalpy flux carried by all different chemical species per unit time flowing relative to the mass average motion of the mixture is $\rho \sum_{i=1}^N h_i Y_i \mathbf{V}_i$. This enthalpy flux term, caused by interdiffusion processes, constitutes an additional component to the energy flux ($\mathbf{q}_{\text{interdiffusion}}$) in binary and/or multicomponent systems.

Based on Onsager's reciprocal relations for irreversible thermodynamic processes, if temperature gradient ∇T gives rise to diffusion velocities (the "thermal-diffusion effect" or the "Soret effect"), concentration gradients (represented by ∇X_i) must produce a heat flux (see Fig. 3.11). This reciprocal effect, known as the *Dufour effect*, provides an additional contribution to the total heat flux \mathbf{q} . It is conventional to express the concentration gradients in terms of differences in diffusion velocities. In terms of diffusion velocities, the Dufour heat flux can be expressed as

$$\mathbf{q}_{\text{Dufour}} = R_u T \sum_{i=1}^N \sum_{j=1}^N \left(\frac{X_j \alpha_i}{M_w i \mathcal{D}_{ij}} \right) (\mathbf{V}_i - \mathbf{V}_j).$$

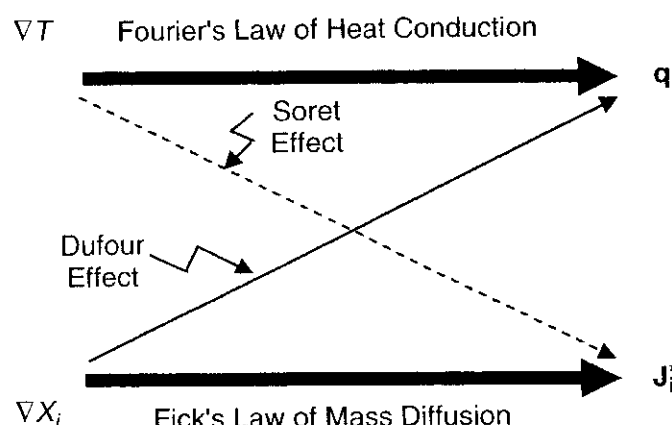


Figure 3.11 Dufour and Soret effects in comparison with the major energy flux by heat conduction and mass flux by species diffusion.

In most cases, the Dufour effect is so small that it is negligible even when thermal diffusion is not negligible. Although it is omitted in most applications, the term is retained in the general equation for completeness.

Conduction and the above two effects yield the heat-flux vector as

$$\begin{aligned}\mathbf{q} &= \mathbf{q}_{\text{conduction}} + \mathbf{q}_{\text{interdiffusion}} + \mathbf{q}_{\text{Dufour}} \\ &= -\lambda \nabla T + \rho \sum_{i=1}^N h_i Y_i \mathbf{V}_i + R_u T \sum_{i=1}^N \sum_{j=1}^N \left(\frac{X_j \alpha_i}{M_w_i \mathcal{D}_{ij}} \right) (\mathbf{V}_i - \mathbf{V}_j) \quad (3-61)\end{aligned}$$

We can now proceed to derive the conservation of energy equation. The stored energy per unit mass e_t is defined as

$$e_t = e + \frac{u_i u_i}{2} \quad (3-62)$$

where e , the specific internal energy, is defined as

$$e = h - \frac{p}{\rho} = \sum_{i=1}^N h_i Y_i - \frac{p}{\rho} \quad (3-63)$$

where

$$h_i = \Delta h_{f,i}^o + \int_{T^o}^T C_{p,i} dT \quad (3-64)$$

Beginning with a stationary differential volume element ($\Delta x \Delta y \times 1$) through which a pure fluid is flowing, we then write the law of conservation of energy for the fluid contained within the control volume by the balance of the following terms:

$$\underbrace{\left\{ \begin{array}{l} \text{rate of} \\ \text{accumulation} \\ \text{of internal and} \\ \text{kinetic energy} \\ \text{in control volume} \end{array} \right\}}_I = \underbrace{\left\{ \begin{array}{l} \text{net rate of} \\ \text{influx of} \\ \text{internal and} \\ \text{kinetic energy} \\ \text{by convection} \end{array} \right\}}_II + \underbrace{\left\{ \begin{array}{l} \text{net rate of} \\ \text{heat addition} \\ \text{due to} \\ \text{heat flux } \mathbf{q} \end{array} \right\}}_III$$

$$+ \underbrace{\left\{ \begin{array}{l} \text{rate of} \\ \text{heat added by} \\ \text{heat source} \end{array} \right\}}_IV + \underbrace{\left\{ \begin{array}{l} \text{net rate of work} \\ \text{done on fluid element} \\ \text{by surroundings} \end{array} \right\}}_V$$

The rate of work term V consists of two parts. One is due to the total surface stress tensor acting on the boundary of the control volume (such as $\sigma_{xx} u \Delta y \cdot 1, \sigma_{yy} v \Delta y \cdot 1, \sigma_{yx} u \Delta x \cdot 1$ shown in Fig. 3.12); the other is due to the body force. The body force acting on the k th species in the x -direction is $\rho Y_k f_{k,x}$. The rate

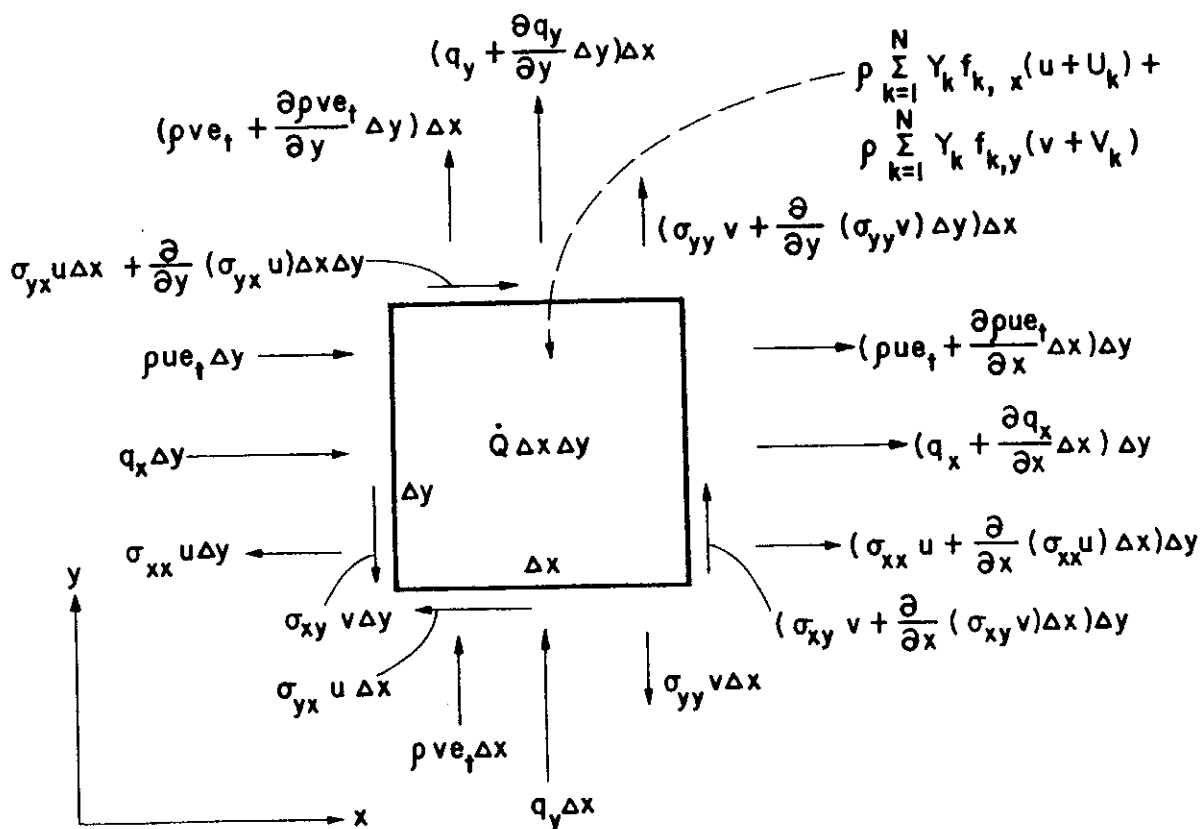


Figure 3.12 Terms in the energy-flux balance for a two-dimensional flow.

of work done on the fluid due to this force component is the product of this force component with the x -component of the average velocity of the k th species, that is, $\rho Y_k f_{k,x} u_k$, or $\rho Y_k f_{k,x} (u + U_k)$. Summing over all species in the mixture, we have $\rho \sum_{k=1}^N Y_k f_{k,x} (u + U_k)$ as the total contribution of the body force in the x -direction.

The reason for considering a two-dimensional reacting flow in Fig. 3.12 is to be able to fit all the terms around the infinitesimal control volume $\Delta x \cdot \Delta y \cdot 1$ in the same diagram. After obtaining the conservation of energy equation, we shall then generalize it to a three-dimensional space. Based on the energy-balance statement, the energy equation made of the corresponding terms I through V for a two-dimensional unsteady reacting flow is shown below:

$$\begin{aligned}
 \underbrace{\frac{\partial}{\partial t}(\rho e_t)}_I &= -\underbrace{\frac{\partial}{\partial x}(\rho u e_t)}_{II} - \underbrace{\frac{\partial}{\partial y}(\rho v e_t)}_{III} - \underbrace{\frac{\partial q_x}{\partial x}}_{IV} - \underbrace{\frac{\partial q_y}{\partial y}}_{IV} + \dot{Q} \\
 &+ \underbrace{\rho \sum_{k=1}^N Y_k f_{k,x} (u + U_k) + \rho \sum_{k=1}^N Y_k f_{k,y} (v + V_k) + \frac{\partial \sigma_{xx} u}{\partial x} + \frac{\partial \sigma_{yx} u}{\partial y} + \frac{\partial \sigma_{yy} v}{\partial y} + \frac{\partial \sigma_{xy} v}{\partial x}}_V
 \end{aligned} \tag{3-65}$$

where U_k, V_k are relative mass-diffusion velocity components.

To generalize Eq. (3-65) to a three-dimensional space, we have

$$\begin{aligned}
 & \frac{\partial}{\partial t}(\rho e_t) + \frac{\partial}{\partial x}(\rho u e_t) + \frac{\partial}{\partial y}(\rho v e_t) + \frac{\partial}{\partial z}(\rho w e_t) \\
 &= -\frac{\partial q_x}{\partial x} - \frac{\partial q_y}{\partial y} - \frac{\partial q_z}{\partial z} + \dot{Q} + \frac{\partial \sigma_{xx} u}{\partial x} + \frac{\partial \sigma_{yx} u}{\partial y} + \frac{\partial \sigma_{zx} u}{\partial z} \\
 &+ \frac{\partial \sigma_{xy} v}{\partial x} + \frac{\partial \sigma_{yy} v}{\partial y} + \frac{\partial \sigma_{zy} v}{\partial z} + \frac{\partial \sigma_{xz} w}{\partial x} + \frac{\partial \sigma_{yz} w}{\partial y} + \frac{\partial \sigma_{zz} w}{\partial z} \\
 &+ \rho \sum_{k=1}^N Y_k f_{k,x}(u + U_k) + \rho \sum_{k=1}^N Y_k f_{k,y}(v + V_k) + \rho \sum_{k=1}^N Y_k f_{k,z}(w + W_k)
 \end{aligned} \tag{3-66}$$

Writing the equation in vector-tensor notation, it becomes

$$\frac{\partial}{\partial t}(\rho e_t) + \frac{\partial}{\partial x_i}(\rho u_i e_t) = -\frac{\partial q_i}{\partial x_i} + \dot{Q} + \frac{\partial \sigma_{ji} u_i}{\partial x_j} + \rho \sum_{k=1}^N Y_k f_{k,i}(u_i + V_{k,i}) \tag{3-67}$$

The above energy equation is given in the divergence form. Using the following continuity equation in the index form,

$$\frac{\partial \rho}{\partial t} + \frac{\partial \rho u_i}{\partial x_i} = 0$$

Eq. (3-67) is simplified to

$$\rho \frac{\partial e_t}{\partial t} + \rho u_i \frac{\partial e_t}{\partial x_i} = -\frac{\partial q_i}{\partial x_i} + \dot{Q} + \frac{\partial \sigma_{ji} u_i}{\partial x_j} + \rho \sum_{k=1}^N Y_k f_{k,i}(u_i + V_{k,i})$$

(3-68)

The energy equation is given in the Euler form.

In the following, we shall use the momentum equation (3-48) to obtain the mechanical-energy equation. Multiplying the momentum equation by u_i and making a slight rearrangement, we have

$$\rho \frac{\partial (\frac{1}{2} u_i u_i)}{\partial t} + \rho u_j \frac{\partial (\frac{1}{2} u_i u_i)}{\partial x_j} = u_i \frac{\partial \sigma_{ji}}{\partial x_j} + \rho \sum_{k=1}^N Y_k f_{k,i} u_i$$

(3-69)

This equation is called the mechanical-energy equation. Subtracting Eq. (3-69) from Eq. (3-68), we get

$$\rho \frac{De}{Dt} = -\frac{\partial q_i}{\partial x_i} + \sigma_{ji} \frac{\partial u_i}{\partial x_j} + \dot{Q} + \rho \sum_{k=1}^N Y_k f_{k,i} V_{k,i}$$

(3-70)

The above equation can be rewritten in vector form as

$$\rho \frac{\partial e}{\partial t} + \rho \mathbf{v} \cdot \nabla e = -\nabla \cdot \mathbf{q} + \tilde{\sigma} : \nabla \mathbf{v} + \dot{Q} + \rho \sum_{k=1}^N Y_k \mathbf{f}_k \cdot \mathbf{V}_k \quad (3-71)$$

The deformation tensor can be written in two parts, i.e.,

$$\frac{\partial u_i}{\partial x_j} = \frac{1}{2} \left(\frac{\partial u_i}{\partial x_j} + \frac{\partial u_j}{\partial x_i} \right) + \frac{1}{2} \left(\frac{\partial u_i}{\partial x_j} - \frac{\partial u_j}{\partial x_i} \right) = e_{ij} + \hat{\omega}_{ij} \quad (3-72)$$

The first part is the strain-rate tensor (e_{ij}), which is symmetric. The second part represents the angular-velocity tensor ($\hat{\omega}_{ij}$), which is antisymmetric. It is useful to note that

$$(\text{a symmetric tensor}) \times (\text{an antisymmetric tensor}) = 0$$

Therefore,

$$\sigma_{ji} \hat{\omega}_{ij} = 0$$

and

$$\begin{aligned} \sigma_{ji} \frac{\partial u_i}{\partial x_j} &= \sigma_{ji} (e_{ij} + \hat{\omega}_{ij}) = \sigma_{ji} e_{ij} = \frac{1}{2} \left(-p - \frac{2}{3} \mu \frac{\partial u_k}{\partial x_k} \right) \\ &\quad \times \delta_{ij} \left(\frac{\partial u_i}{\partial x_j} + \frac{\partial u_j}{\partial x_i} \right) + 2\mu e_{ij} e_{ij} \end{aligned} \quad (3-73)$$

In the above operations, we have neglected the bulk viscosity (μ') term. Thus Eq. (3-70) reduces to

$$\begin{aligned} \underbrace{\rho \frac{De}{Dt}}_{\substack{\text{increase of} \\ \text{internal} \\ \text{energy}}} &= \underbrace{-\frac{\partial q_i}{\partial x_i}}_{\substack{\text{heat influx} \\ \text{due to} \\ \text{conduction,} \\ \text{diffusion,} \\ \text{and Dufour effect}}} - p \underbrace{\frac{\partial u_j}{\partial x_j}}_{\text{flow work}} - \underbrace{\frac{2}{3} \mu \left(\frac{\partial u_j}{\partial x_j} \right)^2}_{\Phi, \text{dissipation by viscous stress}} + 2\mu e_{ij} e_{ij} \\ &+ \underbrace{\dot{Q}}_{\substack{\text{heat input}}} + \rho \underbrace{\sum_{k=1}^N Y_k f_k V_{k,i}}_{\text{body-force work}} \end{aligned} \quad (3-74)$$

$$\rho \frac{De}{Dt} + p \frac{\partial u_j}{\partial x_j} = -\nabla \cdot \mathbf{q} + \Phi + \dot{Q} + \rho \sum_{k=1}^N Y_k \mathbf{f}_k \cdot \mathbf{V}_k \quad (3-75)$$

Since

$$h = e + \frac{p}{\rho}$$

$$\frac{De}{Dt} = \frac{Dh}{Dt} - \frac{1}{\rho} \frac{Dp}{Dt} + \frac{p}{\rho^2} \frac{D\rho}{Dt} \quad (3-76)$$

From the continuity equation, we have the following relationship between the percentage increase of mixture density and the negative amount of volume dilatation:

$$\frac{1}{\rho} \frac{D\rho}{Dt} = -\frac{\partial u_j}{\partial x_j} \quad (3-77)$$

Using Eqs. (3-76) and (3-77), Eq. (3-75) becomes

$$\rho \frac{Dh}{Dt} - \frac{Dp}{Dt} = -\nabla \cdot \mathbf{q} + \Phi + \dot{Q} + \rho \sum_{k=1}^N Y_k \mathbf{f}_k \cdot \mathbf{V}_k \quad (3-78)$$

Adding the mechanical-energy equation (3-69) to the above equation, we obtain

$$\rho \frac{D}{Dt} \left(h + \frac{u_i u_i}{2} \right) - \frac{Dp}{Dt} = u_i \frac{\partial \sigma_{ji}}{\partial x_j} + \Phi + \dot{Q} - \nabla \cdot \mathbf{q} + \rho \sum_{k=1}^N Y_k \mathbf{f}_k \cdot (\mathbf{u} + \mathbf{V}_k) \quad (3-79)$$

Using Eq. (3-58) and the following definition of total enthalpy

$$h_t \equiv h + \frac{u_i u_i}{2} \quad (3-80)$$

we have

$$\rho \frac{Dh_t}{Dt} - \frac{\partial p}{\partial t} - u_i \frac{\partial p}{\partial x_i} = -u_i \frac{\partial p}{\partial x_j} \delta_{ij} + u_i \frac{\partial \tau_{ji}}{\partial x_j} + \Phi + \dot{Q} - \nabla \cdot \mathbf{q}$$

$$+ \rho \sum_{k=1}^N Y_k \mathbf{f}_k \cdot (\mathbf{u} + \mathbf{V}_k) \quad (3-81)$$

where

$$\tau_{ij} = -\frac{2}{3} \mu \frac{\partial u_k}{\partial x_k} \delta_{ij} + \mu \left(\frac{\partial u_i}{\partial x_j} + \frac{\partial u_j}{\partial x_i} \right) = \rho_{ij} + p \delta_{ij}$$

Now,

$$u_i \frac{\partial p}{\partial x_j} \delta_{ij} = u_i \frac{\partial p}{\partial x_i}$$

and from Eq. (3-73) and from the definition of τ_{ij} it follows that

$$\Phi = \tau_{ij} \frac{\partial u_i}{\partial x_j} \quad (3-82)$$

Table 3.12 Energy Equation^a in Several Coordinate Systems

Rectangular coordinates (x, y, z):

$$\begin{aligned}
 & \rho C_p \left(\frac{\partial T}{\partial t} + u_x \frac{\partial T}{\partial x} + u_y \frac{\partial T}{\partial y} + u_z \frac{\partial T}{\partial z} \right) - \left(\frac{\partial p}{\partial t} + u_x \frac{\partial p}{\partial x} + u_y \frac{\partial p}{\partial y} + u_z \frac{\partial p}{\partial z} \right) \\
 &= \lambda \left(\frac{\partial^2 T}{\partial x^2} + \frac{\partial^2 T}{\partial y^2} + \frac{\partial^2 T}{\partial z^2} \right) - \sum_{i=1}^N \dot{\omega}_i \Delta h_{f,i}^o \\
 & - \left[\frac{\partial}{\partial x} \left(\rho T \sum_{i=1}^N C_{pi} Y_i V_{ix} \right) + \frac{\partial}{\partial y} \left(\rho T \sum_{i=1}^N C_{pi} Y_i V_{iy} \right) + \frac{\partial}{\partial z} \left(\rho T \sum_{i=1}^N C_{pi} Y_i V_{iz} \right) \right] \\
 &+ \mu \left\{ 2 \left[\left(\frac{\partial u_x}{\partial x} \right)^2 + \left(\frac{\partial u_y}{\partial y} \right)^2 + \left(\frac{\partial u_z}{\partial z} \right)^2 \right] + \left[\frac{\partial u_y}{\partial x} + \frac{\partial u_x}{\partial y} \right]^2 \right. \\
 &+ \left. \left[\frac{\partial u_z}{\partial y} + \frac{\partial u_y}{\partial z} \right]^2 + \left[\frac{\partial u_x}{\partial z} + \frac{\partial u_z}{\partial x} \right]^2 - \frac{2}{3} \left[\frac{\partial u_x}{\partial x} + \frac{\partial u_y}{\partial y} + \frac{\partial u_z}{\partial z} \right]^2 \right\} \quad (\text{A}) \\
 &+ \rho \sum_{i=1}^N Y_i (f_{ix} V_{ix} + f_{iy} V_{iy} + f_{iz} V_{iz})
 \end{aligned}$$

Cylindrical coordinates (r, θ, z):

$$\begin{aligned}
 & \rho C_p \left(\frac{\partial T}{\partial t} + u_r \frac{\partial T}{\partial r} + \frac{u_\theta}{r} \frac{\partial T}{\partial \theta} + u_z \frac{\partial T}{\partial z} \right) - \left(\frac{\partial p}{\partial t} + u_r \frac{\partial p}{\partial r} + \frac{u_\theta}{r} \frac{\partial p}{\partial \theta} + u_z \frac{\partial p}{\partial z} \right) \\
 &= \lambda \left[\frac{1}{r} \frac{\partial}{\partial r} \left(r \frac{\partial T}{\partial r} \right) + \frac{1}{r^2} \frac{\partial^2 T}{\partial \theta^2} + \frac{\partial^2 T}{\partial z^2} \right] - \sum_{i=1}^N \dot{\omega}_i \Delta h_{f,i}^o \\
 & - \left[\frac{1}{r} \frac{\partial}{\partial r} \left(r \rho T \sum_{i=1}^N C_{pi} Y_i V_{ir} \right) + \frac{1}{r} \frac{\partial}{\partial \theta} \left(\rho T \sum_{i=1}^N C_{pi} Y_i V_{i\theta} \right) \right. \\
 &+ \left. \frac{\partial}{\partial z} \left(\rho T \sum_{i=1}^N C_{pi} Y_i V_{iz} \right) \right] + \mu \left\{ 2 \left[\left(\frac{\partial u_r}{\partial r} \right)^2 + \left(\frac{1}{r} \frac{\partial u_\theta}{\partial \theta} + \frac{u_r}{r} \right)^2 + \left(\frac{\partial u_z}{\partial z} \right)^2 \right] \right. \\
 &+ \left[r \frac{\partial}{\partial r} \left(\frac{u_\theta}{r} \right) + \frac{1}{r} \frac{\partial u_r}{\partial \theta} \right]^2 + \left[\frac{1}{r} \frac{\partial u_z}{\partial \theta} + \frac{\partial u_\theta}{\partial z} \right]^2 + \left[\frac{\partial u_r}{\partial z} + \frac{\partial u_z}{\partial r} \right]^2 \\
 &- \frac{2}{3} \left[\frac{1}{r} \frac{\partial}{\partial r} (r u_r) + \frac{1}{r} \frac{\partial u_\theta}{\partial \theta} + \frac{\partial u_z}{\partial z} \right]^2 \Big\} \quad (\text{B}) \\
 &+ \rho \sum_{i=1}^N Y_i (f_{ir} V_{ir} + f_{i\theta} V_{i\theta} + f_{iz} V_{iz})
 \end{aligned}$$

Table 3.12 (continued)

Spherical coordinates (r, θ, ϕ):

$$\begin{aligned}
& \rho C_p \left(\frac{\partial T}{\partial t} + u_r \frac{\partial T}{\partial r} + \frac{u_\theta}{r} \frac{\partial T}{\partial \theta} + \frac{u_\phi}{r \sin \theta} \frac{\partial T}{\partial \phi} \right) - \left(\frac{\partial p}{\partial t} + u_r \frac{\partial p}{\partial r} + \frac{u_\theta}{r} \frac{\partial p}{\partial \theta} + \frac{u_\phi}{r \sin \theta} \frac{\partial p}{\partial \phi} \right) \\
&= \lambda \left[\frac{1}{r^2} \frac{\partial}{\partial r} \left(r^2 \frac{\partial T}{\partial r} \right) + \frac{1}{r^2 \sin \theta} \frac{\partial}{\partial \theta} \left(\sin \theta \frac{\partial T}{\partial \theta} \right) + \frac{1}{r^2 \sin^2 \theta} \frac{\partial^2 T}{\partial \phi^2} \right] - \sum_{i=1}^N \dot{\omega}_i \Delta h_{f,i}^o \\
&\quad - \left[\frac{1}{r^2} \frac{\partial}{\partial r} \left(r^2 \rho T \sum_{i=1}^N C_{pi} Y_i V_{ir} \right) + \frac{1}{r \sin \theta} \frac{\partial}{\partial \theta} \left(\rho T \sin \theta \sum_{i=1}^N C_{pi} Y_i V_{i\theta} \right) \right. \\
&\quad \left. + \frac{1}{r \sin \theta} \frac{\partial}{\partial \phi} \left(\rho T \sum_{i=1}^N C_{pi} Y_i V_{i\phi} \right) \right] + \mu \left\{ 2 \left[\left(\frac{\partial u_r}{\partial r} \right)^2 + \left(\frac{1}{r} \frac{\partial u_\theta}{\partial \theta} + \frac{u_r}{r} \right)^2 \right. \right. \\
&\quad \left. \left. + \left(\frac{1}{r \sin \theta} \frac{\partial u_\phi}{\partial \phi} + \frac{u_r}{r} + \frac{u_\theta \cot \theta}{r} \right)^2 \right] + \left[r \frac{\partial}{\partial r} \left(\frac{u_\theta}{r} \right) + \frac{1}{r} \frac{\partial u_r}{\partial \theta} \right]^2 \right. \\
&\quad \left. + \left[\frac{\sin \theta}{r} \frac{\partial}{\partial \theta} \left(\frac{u_\phi}{\sin \theta} \right) + \frac{1}{r \sin \theta} \frac{\partial u_\theta}{\partial \phi} \right]^2 + \left[\frac{1}{r \sin \theta} \frac{\partial u_r}{\partial \phi} + r \frac{\partial}{\partial r} \left(\frac{u_\phi}{r} \right) \right]^2 \right. \\
&\quad \left. - \frac{2}{3} \left[\frac{1}{r^2} \frac{\partial}{\partial r} (r^2 u_r) + \frac{1}{r \sin \theta} \frac{\partial}{\partial \theta} (u_\theta \sin \theta) + \frac{1}{r \sin \theta} \frac{\partial u_\phi}{\partial \phi} \right]^2 \right\} \tag{C} \\
&\quad + \rho \sum_{i=1}^N Y_i (f_{ir} V_{ir} + f_{i\theta} V_{i\theta} + f_{i\phi} V_{i\phi})
\end{aligned}$$

^aBased on the following assumptions: (1) all species in the mixture follow the ideal-gas equation of state, (2) C_p and λ are constant, (3) Dufour effect is negligible, and (4) there is no radiation effect.

Substituting in Eq. (3-81), it follows that

$$\rho \frac{Dh_t}{Dt} - \frac{\partial p}{\partial t} = \frac{\partial(u_i \tau_{ji})}{\partial x_j} + \dot{Q} - \nabla \cdot \mathbf{q} + \rho \sum_{k=1}^N Y_k \mathbf{f}_k \cdot (\mathbf{u} + \mathbf{V}_k) \tag{3-83}$$

From the above equation, it follows that if (1) flow is inviscid and steady, (2) there is no heat flux due to conduction, diffusion, or Dufour effect, (3) there is no body force, and (4) there is no energy input, then h_t will be constant.

The energy equation written in terms of temperature in several coordinate systems is given in Table 3.12.

7 PHYSICAL DERIVATION OF THE MULTICOMPONENT DIFFUSION EQUATION

In order to render the conservation equations soluble for a multicomponent system, the diffusion velocities \mathbf{V}_i appearing in these equations must be determined. In general, there are two ways to evaluate the diffusion velocities. The approximate way is to employ Fick's law of mass diffusion and to replace the diffusion velocities by the concentration gradient times some appropriate coefficient [see Eqs. (3-5) to (3-8) and Eqs. (3-11) to (3-14)]. The more exact method is to find \mathbf{V}_i from the multicomponent diffusion equation, which is derived in the following through physical arguments.

The binary-collision problem has been studied extensively in classical mechanics.⁴ The three-dimensional dynamical problem of binary collision between two particles with masses m_i and m_j is found to be mathematically equivalent to a one-body problem in a plane, with the reduced mass

$$\mu_{ij} \equiv \frac{m_i m_j}{m_i + m_j}$$

The average momentum transferred from a molecule of type i to a molecule of type j must be equal to the negative of that transferred from j to i molecules. It is expected that on the average, the momentum transferred to an i molecule in a collision between i and j molecules is approximately

$$\mu_{ij}(\mathbf{V}_j - \mathbf{V}_i)$$

where μ_{ij} is the reduced mass and $\mathbf{V}_j - \mathbf{V}_i$ is the average relative velocity between molecules of species i and j . The body force acting on molecules of type i in a unit volume element is $\rho Y_i \mathbf{f}_i$ or $\rho Y_i \mathbf{f}_i \sum_{j=1}^N Y_j$, since $\sum_{i=1}^N Y_i = 1$. Hence, the net rate of change of momentum of molecules of type i per unit volume is

$$\Gamma_i = \sum_{j=1}^N \mu_{ij} Z_{ij}(\mathbf{V}_j - \mathbf{V}_i) + \sum_{j=1}^N \rho Y_i Y_j \mathbf{f}_i \quad \text{for } i = 1, 2, \dots, N \quad (3-84)$$

where Z_{ij} is the total number of collisions per unit volume per second between the molecules of types i and j .

This change of momentum of species i is evident in changes in both the random velocity and ordered velocity of the molecules. The rate of change of the ordered momentum is $\rho Y_i D\mathbf{v}/Dt$. The partial pressure p_i of species i represents physically the momentum of molecules of type i transported per second across a surface of unit area, traveling with the mass-average velocity of the fluid. Thus, ∇p_i is the rate of change of momentum associated with the random motion of

molecules of type i per unit volume. The quantity Γ_i is therefore given by the relation

$$\Gamma_i = \rho Y_i \frac{D\mathbf{v}}{Dt} + \nabla p_i, \quad i = 1, 2, \dots, N \quad (3-85)$$

According to Dalton's law of partial pressures,

$$p_i = X_i p, \quad i = 1, 2, \dots, N$$

Hence,

$$\nabla p_i = p \nabla X_i + X_i \nabla p, \quad i = 1, 2, \dots, N \quad (3-86)$$

Neglecting the viscous forces, the momentum equation can be used to show that

$$\rho \frac{D\mathbf{v}}{Dt} = -\nabla p + \rho \sum_{j=1}^N Y_j \mathbf{f}_j \quad (3-87)$$

Substituting Eqs. (3-85), (3-86), and (3-87) into Eq. (3-84) yields

$$\nabla X_i = \sum_{j=1}^N \frac{\mu_{ij} Z_{ij}}{p} (\mathbf{V}_j - \mathbf{V}_i) + (Y_i - X_i) \frac{\nabla p}{p} + \frac{\rho}{p} \sum_{j=1}^N Y_i Y_j (\mathbf{f}_i - \mathbf{f}_j) \quad (3-88)$$

The product $\mu_{ij} Z_{ij}$ may be related to the binary diffusion coefficient by considering the limiting case of a constant-pressure process in a two-component system with no body forces, for which Eq. (3-88) reduces to

$$\nabla X_A = \frac{\mu_{AB} Z_{AB}}{p} (\mathbf{V}_B - \mathbf{V}_A) \quad (3-89)$$

Using Eq. (3-9), one can show that the relative molar flux \mathbf{J}_A^* can be expressed in terms of the mole fractions of species A and B , and the velocity-vector difference between B and A as

$$\mathbf{J}_A^* = -C X_A X_B (\mathbf{V}_B - \mathbf{V}_A) \quad (3-90)$$

Substituting $\mathbf{V}_B - \mathbf{V}_A$ of Eq. (3-90) into Eq. (3-89) and comparing it with Eq. (3-11), we have $\mathcal{D}_{AB} = (X_A X_B p)/(\mu_{AB} Z_{AB})$, which implies that, in general,

$$\mathcal{D}_{ij} = \frac{X_i X_j p}{\mu_{ij} Z_{ij}} \quad (3-91)$$

Utilizing Eq. (3-91), Eq. (3-88) becomes

$$\begin{aligned} \nabla X_i &= \sum_{j=1}^N \frac{X_i X_j}{\mathcal{D}_{ij}} (\mathbf{V}_j - \mathbf{V}_i) + (Y_i - X_i) \frac{\nabla p}{p} + \frac{\rho}{p} \sum_{j=1}^N Y_i Y_j (\mathbf{f}_i - \mathbf{f}_j), \\ i &= 1, 2, \dots, N \end{aligned} \quad (3-88a)$$

The multicomponent diffusion equation obtained through more rigorous derivation from the kinetic theory is

$$\begin{aligned} \nabla X_i &= \sum_{j=1}^N \frac{X_i X_j}{\mathcal{D}_{ij}} (\mathbf{V}_j - \mathbf{V}_i) + (Y_i - X_i) \frac{\nabla p}{p} \\ &\quad + \frac{\rho}{p} \sum_{j=1}^N Y_i Y_j (\mathbf{f}_i - \mathbf{f}_j) + \sum_{j=1}^N \frac{X_i X_j}{\rho \mathcal{D}_{ij}} \left(\frac{\alpha_j}{Y_j} - \frac{\alpha_i}{Y_i} \right) \frac{\nabla T}{T}, \\ i &= 1, 2, \dots, N \end{aligned} \quad (3-88b)$$

where α_j is the thermal diffusion coefficient of species j . This equation is a vector balance equation. For a given chemical species in a three-dimensional space, Eq. (3-88b) can be expressed as three individual equations for vector component balance in all three directions. It may be noted that the last summation of the above equation was absent in Eq. (3-88a), since we did not consider the thermal-diffusion (Soret) effect⁴ in the derivation. Opposite to the Dufour effect (see Fig. 3.11), the Soret effect describes the mass diffusion resulting from temperature gradients. Physically, Eq. (3-88b) states that concentration gradients may be supported by diffusion velocities, pressure gradients, the differences in the body force per unit mass on molecules of different species, and thermal-diffusion effects.

The diffusion equation [Eq. (3-88b)] reduces to Fick's law of diffusion for binary mixtures when (a) thermal diffusion is negligible, (b) the body force per unit mass is the same for each species ($\mathbf{f}_A = \mathbf{f}_B$), and (c) either the pressure is a constant or the molecular weights of both species are the same.

For a multicomponent system, which assumes that thermal diffusion, body forces, and pressure-induced diffusions are negligible, the diffusion equation simplifies to

$$\nabla X_i = \sum_{j=1}^N \frac{X_i X_j}{\mathcal{D}_{ij}} (\mathbf{V}_j - \mathbf{V}_i) \quad (3-92)$$

By using Eqs. (3-3) and (3-6), it can be shown easily that the above equation can be written as

$$\nabla X_i = \sum_{j=1}^N \frac{X_i X_j}{C \mathcal{D}_{ij}} (X_i \dot{\mathbf{n}}_j - X_j \dot{\mathbf{n}}_i) \quad (3-93)$$

In performing calculations for multicomponent systems, it is often convenient to define an effective binary diffusion \mathcal{D}_{im} for the diffusion of species i in a mixture. Equation (3-12) then becomes

$$\dot{\mathbf{n}}_i = C_i \mathbf{v}^* - C \mathcal{D}_{im} \nabla X_i \quad (3-94)$$

This equation, simpler than Eq. (3-93), also relates $\dot{\mathbf{n}}_i$ to ∇X_i .

8 OTHER NECESSARY EQUATIONS IN MULTICOMPONENT SYSTEMS

The term $\dot{\omega}_i$ in each species continuity equation [Eq. (3-36)] is determined by the phenomenological chemical reaction rate expression

$$\dot{\omega}_i = Mw_i \sum_{k=1}^M (v''_{i,k} - v'_{i,k}) B_k T^{\alpha_k} \exp\left(-\frac{E_{ak}}{R_u T}\right) \prod_{j=1}^N \left(\frac{X_j p}{R_u T}\right)^{v'_{j,k}} \quad (3-95)$$

where M is the total number of chemical reactions occurring and N is the total number of chemical species present. The ideal-gas equation of state for a multicomponent system can be written as

$$p = \rho R_u T \sum_{i=1}^N \frac{Y_i}{Mw_i} \quad (3-96)$$

The relationship between X_i and Y_i is

$$X_i = \frac{Y_i / Mw_i}{\sum_{j=1}^N (Y_j / Mw_j)} \quad \text{or} \quad Y_i = \frac{X_i Mw_i}{\sum_{j=1}^N X_j Mw_j}, \quad i = 1, 2, \dots, N \quad (3-97)$$

9 SOLUTION OF A MULTICOMPONENT-SPECIES SYSTEM

If \mathbf{V}_i can be substituted by Fick's law in the species and energy equations, then in a system with N species there are $N + 6$ unknowns. They are

$$Y_1, Y_2, Y_3, \dots, Y_N, \rho, T, p, u, v, w$$

The $N + 6$ equations to be solved are

- 1 overall mass continuity [Eq. (3-29)]
- 3 momentum equations [Eq. (3-60)]
- 1 energy equation [Eq. (3-75)]
- $N - 1$ species equations [Eq. (3-36)]
- 1 equation of state [Eq. (3-96)]
- 1 equation relating all Y_i [$Y_1 + Y_2 + \dots + Y_N = 1$]

If \mathbf{V}_i must be solved from the diffusion equation for a multicomponent system, there will be $5N + 6$ unknowns. They are

$$Y_1, Y_2, Y_3, \dots, Y_N, \rho, T, p, u, v, w$$

$$X_1, X_2, X_3, \dots, X_N$$

and

$$\begin{aligned} & V_{1,x}, V_{1,y}, V_{1,z} \\ & V_{2,x}, V_{2,y}, V_{2,z} \\ & \vdots \\ & V_{N,x}, V_{N,y}, V_{N,z} \end{aligned}$$

There are $5N + 6$ equations. In addition to the $N + 6$ equations listed above, there are $4N$ equations coming from

$3N$ diffusion equations [Eq. (3-88b)]

N equations relating X_i to Y_i [Eq. (3-97)]

To avoid solving a large number of differential equations for a given problem, usually Fick's law of mass diffusion is adopted for a broad range of combustion problems.

10 SHVAB-ZEL'DOVICH FORMULATION

A very useful technique was developed by Shvab¹⁰ and Zel'dovich¹¹ to express the equations for conservation of energy and of chemical species in a common form. Their formulation enables the chemical-source terms to be removed from many equations by considering certain linear combinations of dependent variables. Their general procedure is called the Shvab–Zel'dovich formulation. Let's first understand that a number of effects in the governing equations are unimportant for a large class of combustion problems and can therefore be omitted in many applications. These include

- a. Body forces (\mathbf{f}_i terms)
- b. Soret and Dufour effects (terms involving α_i)
- c. Pressure gradient diffusion $[(Y_i - X_i)\nabla p/\rho]$ [term in Eq. (3-88b)]
- d. Bulk viscosity (μ')

In order to proceed with the Shvab–Zel'dovich formulation of the conservation equations, additional assumptions have to be made. These assumptions are discussed below.

For *steady flow*, the overall continuity equation [Eq. (3-29)] reduces to

$$\nabla \cdot \rho \mathbf{v} = 0 \quad (3-98)$$

For *low-speed* steady-flow problems, viscous effects are often negligible, and the momentum equation (3-60) reduces to

$$\frac{\partial p}{\partial x_i} \approx 0 \quad (3-99)$$

In other words, the pressure can be taken to be constant for the combustion zone; i.e.,

$$p = \text{constant} \quad (3-100)$$

The energy equation (3-78) reduces to

$$\rho \mathbf{v} \cdot \nabla h = \nabla \cdot (\lambda \nabla T) - \nabla \cdot \left(\rho \sum_{i=1}^N h_i Y_i \mathbf{V}_i \right) + \dot{Q} \quad (3-101)$$

because $\Phi = 0$ and the pressure gradient is also zero.

Adding $\sum_{i=1}^N h_i Y_i \nabla \cdot \rho \mathbf{v} = 0$ on the left-hand side of Eq. (3-101), noting that $h = \sum_{i=1}^N h_i Y_i$, and setting the external heat addition $\dot{Q} = 0$, one obtains

$$\nabla \cdot \left[\rho \sum_{i=1}^N h_i Y_i (\mathbf{v} + \mathbf{V}_i) - \lambda \nabla T \right] = 0 \quad (3-102)$$

The conservation of species equation (3-35) for steady flow reduces to

$$\nabla \cdot [\rho Y_i (\mathbf{v} + \mathbf{V}_i)] = \dot{\omega}_i, \quad i = 1, 2, \dots, N \quad (3-103)$$

When the *mass-diffusion coefficients of all pairs of species are equal*, the diffusion equation (3-92) reduces to

$$\mathcal{D} \nabla X_i = X_i \sum_{j=1}^N X_j \mathbf{V}_j - X_i \mathbf{V}_i, \quad i = 1, 2, \dots, N \quad (3-104)$$

Multiplying the above equation by Y_i/X_i and summing over i , we obtain

$$\sum_{i=1}^N \frac{Y_i}{X_i} \mathcal{D} \nabla X_i = \sum_{i=1}^N Y_i \sum_{j=1}^N X_j \mathbf{V}_j - \sum_{i=1}^N Y_i \mathbf{V}_i \quad (3-105)$$

Using the fact that

$$\sum_{i=1}^N Y_i = 1 \quad \text{and} \quad \sum_{i=1}^N Y_i \mathbf{V}_i = 0$$

we obtain

$$\sum_{j=1}^N X_j \mathbf{V}_j = \sum_{i=1}^N Y_i \mathcal{D} \nabla \ln X_i = \sum_{j=1}^N Y_j \mathcal{D} \nabla \ln X_j \quad (3-106)$$

Substituting Eq. (3-106) into Eq. (3-104) and dividing by X_i , we obtain

$$\mathcal{D} \left[\nabla \ln X_i - \sum_{j=1}^N Y_j \nabla \ln X_j \right] = -\mathbf{V}_i, \quad i = 1, 2, \dots, N \quad (3-107)$$

Substituting Eq. (3-97) for X_i in the above equation, we obtain Fick's law

$$\mathbf{V}_i = -\mathcal{D} \nabla \ln Y_i, \quad i = 1, 2, \dots, N \quad (3-108)$$

Substituting Eqs. (3-103), (3-108), and (3-64) into Eq. (3-102), we obtain

$$\begin{aligned} \nabla \cdot \left[\rho \mathbf{v} \int_{T^o}^T \left(\sum_{i=1}^N Y_i C_{p,i} \right) dT - \rho \mathcal{D} \sum_{i=1}^N \nabla Y_i \int_{T^o}^T C_{p,i} dT - \rho \mathcal{D} \frac{\lambda}{\rho C_p \mathcal{D}} C_p \nabla T \right] \\ = - \sum_{i=1}^N \dot{\omega}_i \Delta h_{f,i}^o \end{aligned} \quad (3-109)$$

Assuming that the Lewis number is unity, that is,

$$\text{Le} = \frac{\lambda}{\rho C_p \mathcal{D}} = 1 \quad (3-110)$$

and using the fact that

$$\sum_{i=1}^N Y_i C_{p,i} = C_p \quad (3-111)$$

and also noting that

$$\begin{aligned} \nabla \int_{T^o}^T C_p dT &= \nabla \sum_{i=1}^N Y_i \int_{T^o}^T C_{p,i} dT \\ &= \sum_{i=1}^N (\nabla Y_i) \int_{T^o}^T C_{p,i}(T^*) dT^* + \sum_{i=1}^N Y_i \nabla \int_{T^o}^T C_{p,i}(T^*) dT^* \\ &= \sum_{i=1}^N (\nabla Y_i) \int_{T^o}^T C_{p,i} dT + \sum_{i=1}^N Y_i C_{p,i}(T) \nabla T \\ &= \sum_{i=1}^N (\nabla Y_i) \int_{T^o}^T C_{p,i} dT + C_p \nabla T \end{aligned} \quad (3-112)$$

Eq. (3-109) then becomes

$$\nabla \cdot \left\{ \rho \mathbf{v} \int_{T^o}^T C_p dT - \rho \mathcal{D} \overbrace{\left[\sum_{i=1}^N \nabla Y_i \int_{T^o}^T C_{p,i} dT + C_p \nabla T \right]}^{\nabla \int_{T^o}^T C_p dT} \right\} = - \sum_{i=1}^N \dot{\omega}_i \Delta h_{f,i}^o \quad (3-113)$$

Substituting Eq. (3-112) into Eq. (3-113), we obtain the Shvab-Zel'dovich energy equation:

$$\nabla \cdot \left\{ \rho \mathbf{v} \int_{T^o}^T C_p dT - \rho \mathcal{D} \nabla \int_{T^o}^T C_p dT \right\} = - \sum_{i=1}^N \dot{\omega}_i \Delta h_{f,i}^o \quad (3-114)$$

Substituting Eq. (3-108) in Eq. (3-103), we obtain the Shvab-Zel'dovich species equation:

$$\nabla \cdot \{ \rho \mathbf{v} Y_i - \rho \mathcal{D} \nabla Y_i \} = \dot{\omega}_i \quad (3-115)$$

Note the similarity in Eqs. (3-114) and (3-115). In deriving these equations, we have not assumed that the specific heat (or any transport coefficient) of the mixture is a constant or that the specific heats of all the species are equal.

The Shvab-Zel'dovich form of the conservation equations is particularly useful when one may assume that chemical changes occur by a single-step forward reaction

$$\sum_{i=1}^N v'_i M_i \rightarrow \sum_{i=1}^N v''_i M_i \quad (3-116)$$

In this case,

$$\frac{\dot{\omega}_i}{M w_i (v''_i - v'_i)} \equiv \dot{\omega}, \quad i = 1, 2, \dots, N \quad (3-117)$$

Defining two new parameters η_T and η_i such that

$$\eta_T \equiv \frac{\int_{T^o}^T C_p dT}{\sum_{i=1}^N \Delta h_{f,i}^o M w_i (v'_i - v''_i)} \quad (3-118)$$

$$\eta_i \equiv \frac{Y_i}{M w_i (v''_i - v'_i)}, \quad i = 1, 2, \dots, N \quad (3-119)$$

then the energy equation (3-114) becomes

$$\nabla \cdot [\rho \mathbf{v} \eta_T - \rho \mathcal{D} \nabla \eta_T] = \dot{\omega} \quad (3-120)$$

and the species equation (3-115) becomes

$$\nabla \cdot [\rho \mathbf{v} \eta_i - \rho \mathcal{D} \nabla \eta_i] = \dot{\omega} \quad (3-121)$$

The nonlinear rate term $\dot{\omega}$ may be eliminated from N of the $N + 1$ equations corresponding to

$$L(\eta) = \dot{\omega} \quad (3-122)$$

where L is a linear operator if $\rho \mathcal{D}$ is independent of η

$$L(\eta) \equiv \nabla \cdot [\rho \mathbf{v} \eta - \rho \mathcal{D} \nabla \eta] \quad (3-123)$$

where η can be $\eta_T, \eta_1, \eta_2, \dots$, or η_N . If we select $\eta = \eta_1$ to be solved from the inhomogeneous differential equation, then

$$L(\eta_1) = \dot{\omega} \quad (3-124)$$

The other N variables are then determined by the linear homogeneous differential equation

$$L(\beta) = 0 \quad (3-125)$$

where β can be defined as $\beta_T, \beta_2, \beta_3, \dots, \beta_N$:

$$\begin{aligned} \beta_T &\equiv \eta_T - \eta_1 \\ \beta_2 &\equiv \eta_2 - \eta_1 \\ &\vdots \\ \beta_N &\equiv \eta_N - \eta_1 \end{aligned} \quad (3-126)$$

It should be noted that $\rho \mathcal{D}$ may depend on β_T or β_i . Under such conditions, the operator L depends implicitly on β and Eq. (3-125) becomes nonlinear. As we will see in laminar premixed flames in Chapter 5 and laminar diffusion flames in Chapter 6, through use of the Shvab-Zel'dovich formulation we can obtain many important relationships. For systems in which the reactants are initially unmixed, combustion rates can even be determined by solving a homogeneous differential equation like (3-125), bypassing the handling of an inhomogeneous differential equation like (3-124).

11 DIMENSIONLESS RATIOS OF TRANSPORT COEFFICIENTS

In flow problems, the conservation equations can often be written in forms involving dimensionless ratios of various transport coefficients. The *Lewis number* (or Lewis–Seminov number) is defined as

$$\text{Le} \equiv \frac{\lambda}{\rho C_p \mathcal{D}} = \frac{\alpha}{\mathcal{D}} = \frac{\text{rate of energy transport}}{\text{rate of mass transport}}$$

(3-127)

It should be noted that in a small fraction of combustion articles, Le is defined as the reciprocal of the definition given in Eq. (3-127). To avoid confusion, it is recommended to use the above equation for Lewis number.

The *Prandtl number* is defined as

$$\text{Pr} \equiv \frac{C_p \mu}{\lambda} = \frac{C_p \rho(\mu/\rho)}{\lambda} = \frac{\nu}{\alpha} = \frac{\text{rate of momentum transport}}{\text{rate of energy transport}} \quad (3-128)$$

The *Schmidt number* is defined as

$$\text{Sc} \equiv \frac{\nu}{D} = \frac{\text{rate of momentum transport}}{\text{rate of mass transport}} \quad (3-129)$$

Le and Sc may be defined for each pair of species in multicomponent mixtures. From the above, we see that

$$\text{Le} \equiv \frac{\text{Sc}}{\text{Pr}} \quad (3-130)$$

In certain combustion systems, Lewis numbers are close to unity. The approximation $\text{Le} = 1$ is frequently very helpful in theoretical combustion analyses. However, Le can also differ significantly from unity. Researchers should examine their combustible materials before making the assumption of $\text{Le} = 1$ for their analyses and/or modeling work.

12 BOUNDARY CONDITIONS AT AN INTERFACE

In the formulation of a combustion problem, besides the consideration of the governing differential equations, one also has to formulate the boundary and initial conditions adequately. The specification of boundary conditions is not always trivial. The number of boundary conditions required for a set of governing differential equations depends quite often on the flow conditions of the reactive mixture, in other words, on the type (based on the characteristic values or eigenvalues) of the governing equations. Either under- or over-specifying the boundary conditions will make the overall formulation ill posed. The boundary condition specification for various types of combustion problems is discussed in many circumstances in later chapters. The purpose for describing boundary conditions here is to familiarize readers with the formal way of specifying them through the use of conservation conditions at material interfaces, where the boundary conditions are usually more complex than those for far fields.

Relations expressing the conservation of mass, momentum, and energy at an interface may be derived by converting conservation equations in differential form to integral form and then passing to the limit in which the volume of integration approaches a surface.

Based on *Reynolds' Transport Theorem*, the time rate of change of the integral of an arbitrary function $f(x, t)$ over a given volume V can be written as the sum of two parts:

$$\frac{d}{dt} \left(\iiint_v f dV \right) = \iiint_v \frac{\partial f}{\partial t} dV + \iint_{\delta} \mathbf{v}_B \cdot \mathbf{n} f d\delta \quad (3-131)$$

The first term represents the contribution due to the time rate of change of the integrand. The second term represents the contribution due to the motion of the control surface Σ bounding the volume ς . Here \mathbf{n} is the local outward normal unit vector to the surface δ , and \mathbf{v}_B is the velocity of the boundary of the control volume. In general, both \mathbf{n} and \mathbf{v}_B can vary from point to point on the control surface δ . Equation (3-131) can be proved² and is used here as a mathematical identity.

Now, let us derive the mass conservation condition at an interface by first considering the continuity equation (3-29):

$$\frac{\partial \rho}{\partial t} + \nabla \cdot (\rho \mathbf{v}) = 0$$

Upon integration of this equation over v , we have

$$\iiint_v \left[\frac{\partial \rho}{\partial t} + \nabla \cdot (\rho \mathbf{v}) \right] dV = 0$$

Using Eq. (3-131) and the divergence theorem,

$$\iiint_v \nabla \cdot (\rho \mathbf{v}) dV = \iint_{\delta} \rho \mathbf{v} \cdot \mathbf{n} dS$$

we obtain

$$\frac{d}{dt} \iiint_v \rho dV - \iint_{\delta} \mathbf{v}_B \cdot \mathbf{n} \rho dS + \iint_{\delta} \rho \mathbf{v} \cdot \mathbf{n} dS = 0$$

or

$$\frac{d}{dt} \left(\iiint_v \rho dV \right) + \iint_{\delta} \rho (\mathbf{v} - \mathbf{v}_B) \cdot \mathbf{n} dS = 0 \quad (3-132)$$

Equation (3-132) represents the integral form of the continuity equation.

Example 3.2. If the right surface of a solid material is burning at a rate of v_b , show that [from Eq. (3-131)] the mass burning rate is

$$\frac{dM}{dt} = -v_b \rho_s A_b$$

where A_b is the burning surface area and ρ_s is the density of the solid. If one lets the control volume on both sides move at the same rate as v_b , show that the rate of change of mass in the control volume is zero.

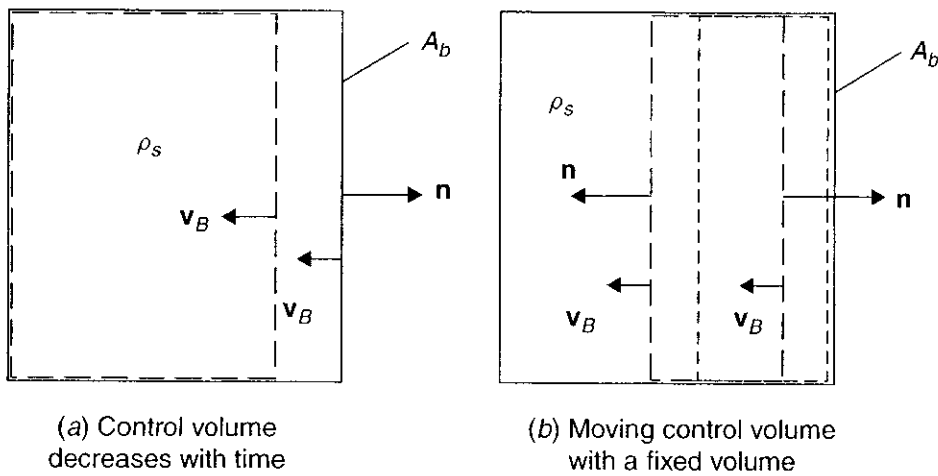


Figure 3.13 Regressing surface of a burning solid material.

Solution: We first let ρ_s be equal to the arbitrary function f given in the *Reynolds' Transport Theorem* given by Eq. (3-131). The density of the solid can be treated as constant; thus, from Fig. 3.13(a), we have

$$\underbrace{\frac{d}{dt} \iiint_V \rho_s dV}_M = \iiint_V \frac{\partial \rho_s^0}{\partial t} dV + \underbrace{\iint_S \mathbf{v}_B \cdot \mathbf{n} \rho_s dS}_{-v_b \rho_s A_b}$$

$$\therefore \frac{dM}{dt} = -v_b \rho_s A_b$$

If the solid material is burning away, but we avoid changing the size of the control volume by moving the boundaries of the control volume at the same rate as the burning rate, then according to Fig. 3.13(b), we have

$$\begin{aligned} \frac{d}{dt} \iiint_V \rho_s dV &= \iiint_V \frac{\partial \rho_s^0}{\partial t} dV + \iint_S \mathbf{v}_B \cdot \mathbf{n} \rho_s dS \\ &= +v_{b\text{left}} \rho_s A_b - v_{b\text{right}} \rho_s A_b \\ &= v_b \rho_s A_b - v_b \rho_s A_b = 0 \end{aligned}$$

The momentum equation (3-48) is

$$\rho \frac{\partial \mathbf{v}}{\partial t} + \rho \mathbf{v} \cdot \nabla \mathbf{v} = \nabla \cdot \tilde{\boldsymbol{\sigma}} + \rho \sum_{i=1}^N Y_i \mathbf{f}_i \quad (3-133)$$

Multiplying the continuity equation (3-29) by \mathbf{v} , we obtain

$$\mathbf{v} \frac{\partial \rho}{\partial t} + \mathbf{v} \nabla \cdot (\rho \mathbf{v}) = 0 \quad (3-134)$$

Adding Eqs. (3-133) and (3-134) gives

$$\frac{\partial}{\partial t} (\rho \mathbf{v}) + \nabla \cdot (\rho \mathbf{v} \mathbf{v}) = \nabla \cdot \tilde{\boldsymbol{\sigma}} + \rho \sum_{i=1}^N Y_i \mathbf{f}_i \quad (3-135)$$

We may integrate this over ς to show that

$$\frac{d}{dt} \iiint_V \rho \mathbf{v} dV + \iint_S \rho \mathbf{v} [(\mathbf{v} - \mathbf{v}_B) \cdot \mathbf{n}] dS = \iint_S \tilde{\boldsymbol{\sigma}} \cdot \mathbf{n} dS + \iiint_V \rho \sum_{i=1}^N Y_i \mathbf{f}_i dV \quad (3-136)$$

The above equation represents the integral form of the momentum equation.

The energy equation (3-67) can be written in vector notation as

$$\frac{\partial}{\partial t} (\rho e_t) + \nabla \cdot (\rho e_t \mathbf{v}) = -\nabla \cdot \mathbf{q} + \dot{Q} + \nabla \cdot (\tilde{\boldsymbol{\sigma}} \cdot \mathbf{v}) + \rho \sum_{i=1}^N Y_i \mathbf{f}_i \cdot (\mathbf{v} + \mathbf{V}_i) \quad (3-137)$$

After integration, we obtain

$$\begin{aligned} & \frac{d}{dt} \iiint_V \rho e_t dV + \iint_S \rho e_t [(\mathbf{v} - \mathbf{v}_B) \cdot \mathbf{n}] dS \\ &= \iiint_V \dot{Q} dV - \iint_S \mathbf{q} \cdot \mathbf{n} dS + \iint_S \mathbf{v} \cdot \tilde{\boldsymbol{\sigma}} \cdot \mathbf{n} dS + \iiint_V \rho \sum_{i=1}^N Y_i \mathbf{f}_i \cdot (\mathbf{v} + \mathbf{V}_i) dV \end{aligned} \quad (3-138)$$

Equation (3-138) represents the integral form of the energy equation.

The vector form of the conservation of chemical species equation (3-35) is

$$\frac{\partial}{\partial t} (\rho Y_i) + \nabla \cdot [\rho Y_i (\mathbf{v} + \mathbf{V}_i)] = \dot{\omega}_i$$

Upon integration, we obtain

$$\frac{d}{dt} \left(\iiint_v \rho Y_i dV \right) + \iint_{\delta} \rho Y_i (\mathbf{v} + \mathbf{V}_i - \mathbf{v}_B) \cdot \mathbf{n} dS = \iiint_v \dot{\omega}_i dV \quad (3-139)$$

We now consider the control volume v to be a thin slab, the thickness of which is made to approach zero (see Fig. 3.14). In the limit, the integrals over δ are composed of two parts, namely integrals over each face of the slab.

Let us arbitrarily choose one face as the “positive” side of the slab, identifying quantities on this side by the subscript $+$ and those on the other side by the subscript $-$. It is clear that \mathbf{n}_- is equal to $-\mathbf{n}_+$ at corresponding points on the two faces; in the limit, the integral over the surface of v may be replaced by an integral over the interface area δ_I , and hence Eq. (3-132) becomes

$$\iint_{\delta_I} [\rho_+ (\mathbf{v}_+ - \mathbf{v}_{B+}) - \rho_- (\mathbf{v}_- - \mathbf{v}_{B-})] \cdot \mathbf{n}_+ dS = - \lim_{v \rightarrow 0} \left[\frac{d}{dt} \iiint_v \rho dV \right] \quad (3-140)$$

Integrating over the same interfacial volume, Eq. (3-136) becomes

$$\begin{aligned} & \iint_{\delta_I} \{ \rho_+ \mathbf{v}_+ [(\mathbf{v}_+ - \mathbf{v}_{B+}) \cdot \mathbf{n}_+] - \rho_- \mathbf{v}_- [(\mathbf{v}_- - \mathbf{v}_{B-}) \cdot \mathbf{n}_+] - (\tilde{\sigma}_+ - \tilde{\sigma}_-) \cdot \mathbf{n}_+ \} dS \\ &= \lim_{v \rightarrow 0} \left[\iiint_v \rho \sum_{i=1}^N Y_i \mathbf{f}_i dV - \frac{d}{dt} \iiint_v \rho \mathbf{v} dV \right] \end{aligned} \quad (3-141)$$

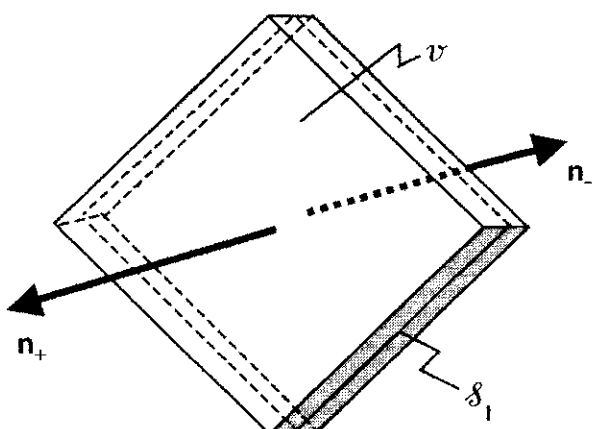


Figure 3.14 Control volume and interface δ_I for the derivation of interface conditions.

Using the same integration procedure, the energy equation (3-138) becomes

$$\begin{aligned} & \iint_{\delta_I} [\rho_+ e_{t+}(\mathbf{v}_+ - \mathbf{v}_{B+}) - \rho_- e_{t-}(\mathbf{v}_- - \mathbf{v}_{B-}) + \mathbf{q}_+ - \mathbf{q}_- - \mathbf{v}_+ \cdot \tilde{\sigma}_+ \\ & \quad + \mathbf{v}_- \cdot \tilde{\sigma}_-] \cdot \mathbf{n}_+ dS \\ &= \lim_{\nu \rightarrow 0} \left\{ \iiint_V \dot{Q} dV + \iiint_V \rho \sum_{i=1}^N Y_i \mathbf{f}_i \cdot (\mathbf{v} + \mathbf{V}_i) dV - \frac{d}{dt} \iiint_V \rho e_t dV \right\} \end{aligned} \quad (3-142)$$

Similarly, the species equation (3-139) becomes

$$\begin{aligned} & \iint_{\delta_I} [\rho_+ Y_{i+}(\mathbf{v}_+ + \mathbf{V}_{i+} - \mathbf{v}_{B+}) - \rho_- Y_{i-}(\mathbf{v}_- + \mathbf{V}_{i-} - \mathbf{v}_{B-})] \cdot \mathbf{n}_+ dS \\ &= \lim_{\nu \rightarrow 0} \left(\iiint_V \dot{\omega}_i dV - \frac{d}{dt} \iiint_V \rho Y_i dV \right), \quad i = 1, 2, \dots, N \end{aligned} \quad (3-143)$$

The last term in the equation represents surface reactions as well as the nonzero time rate of accumulation of the i th chemical species at the interface.

For example, if the interface is taken to be a solid surface at which chemical reactions are proceeding at a finite rate, then

$$\dot{\omega}_i \rightarrow \dot{\omega}'_i \delta(y - y_I)$$

The parameter $\dot{\omega}'_i$ represents the surface reaction rate for producing i th species with a dimension of $[M/(L^2 t)]$, while $\dot{\omega}_i$ has a dimension of $[M/(L^3 t)]$. The Dirac delta function δ is nonzero when the y coordinate normal to the surface is equal to y_I on the surface. Thus, we can replace the volume integral for the species production by a surface integral, namely,

$$\lim_{\nu \rightarrow 0} \iiint_V \dot{\omega}_i dV = \iint_{\delta_I} \dot{\omega}'_i dS$$

If ρ'_i represents the mass of species i per unit area, then

$$\rho Y_i \rightarrow \rho'_i \delta(y - y_I)$$

The last term of Eq. (3-143) can be written as

$$\lim_{\nu \rightarrow 0} \frac{d}{dt} \iiint_V \rho Y_i dV = \frac{d}{dt} \lim_{\nu \rightarrow 0} \iiint_V \rho'_i \delta(y - y_I) dV = \frac{d}{dt} \iint_{\delta_I} \rho'_i dS \quad (3-144)$$

Thus, the physical meaning of Eq. (3–143) can be expressed by the following species mass-flux balance statement:

$$\begin{aligned} & \left[\begin{array}{l} \text{mass flux of} \\ i\text{th species} \\ \text{leaving the surface} \end{array} \right] - \left[\begin{array}{l} \text{mass flux of} \\ i\text{th species} \\ \text{entering the surface} \end{array} \right] \\ & = \left[\begin{array}{l} \text{production rate} \\ \text{of } i\text{th species} \\ \text{at the surface} \end{array} \right] - \left[\begin{array}{l} \text{rate of accumulation} \\ \text{of } i\text{th species on the} \\ \text{control surface} \end{array} \right] \end{aligned}$$

Similar interpretations can be given for the continuity equation of a mixture's mass flux [Eq. (3–140)], the momentum flux-balance equation [Eq. (3–141)], and the energy flux-balance equation [Eq. (3–142)]. In many combustion problems, all terms in Eqs. (3–140) through (3–142) involving $\lim_{v \rightarrow 0}$ are zero. If it is further assumed that the interface is stationary, i.e.,

$$\mathbf{v}_B = 0$$

and that viscosity is negligible, then Eqs. (3–140) through (3–143) can be simplify considerably to give

$$\rho_+ \mathbf{v}_+ \cdot \mathbf{n}_+ = \rho_- \mathbf{v}_- \cdot \mathbf{n}_+ \quad (3-145)$$

$$\rho_+ \mathbf{v}_+ (\mathbf{v}_+ \cdot \mathbf{n}_+) + p_+ \mathbf{n}_+ = \rho_- \mathbf{v}_- (\mathbf{v}_- \cdot \mathbf{n}_+) + p_- \mathbf{n}_+ \quad (3-146)$$

$$\begin{aligned} & \left\{ \rho_+ \left[h_{t+} \mathbf{v}_+ + \sum_{i=1}^n h_{i+} Y_{i+} \mathbf{V}_{i+} \right] - \lambda_+ (\nabla T)_+ + \mathbf{q}_{R+} \right\} \cdot \mathbf{n}_+ \\ & = \left\{ \rho_- \left[h_{t-} \mathbf{v}_- + \sum_{i=1}^n h_{i-} Y_{i-} \mathbf{V}_{i-} \right] - \lambda_- (\nabla T)_- + \mathbf{q}_{R-} \right\} \cdot \mathbf{n}_+ \end{aligned} \quad (3-147)$$

where \mathbf{q}_{R+} and \mathbf{q}_{R-} represent the radiative heat-flux contribution. These terms have been included because radiative losses from surfaces are often substantial. If there is no surface reaction to generate species i , then the terms on the right-hand side of Eq. (3–143) are also zero and the species mass-flux balance at the interface gives

$$\rho_+ Y_{i+} (\mathbf{v}_+ + \mathbf{V}_{i+}) \cdot \mathbf{n}_+ = \rho_- Y_{i-} (\mathbf{v}_- + \mathbf{V}_{i-}) \cdot \mathbf{n}_+ \quad (3-148)$$

Example 3.3. Write the momentum flux balance at a gas–solid interface.

Solution: If the viscous effect is negligible, the total stress tensor $\tilde{\sigma}$ in the gas phase becomes

$$\tilde{\sigma} = -p \mathbf{I}$$

$$\therefore \sigma_{ij} = -p \delta_{ij} + \left(\mu' - \frac{2}{3} \mu \right) \frac{\partial u_k}{\partial x_k} \delta_{ij} + \mu \left(\frac{\partial u_i}{\partial x_j} + \frac{\partial u_j}{\partial x_i} \right)$$

or

$$\tilde{\sigma} = -p\mathbf{I} + \left(\overset{\circ}{\mu}' - \frac{2}{3}\overset{\circ}{\mu} \right) (\nabla \cdot \mathbf{v})\mathbf{I} + \overset{\circ}{\mu} [(\nabla \mathbf{v}) + (\nabla \mathbf{v})^T]$$

where the superscript T means the transpose. The stress tensor in a linear viscoelastic solid material can be written as

$$\sigma_{ij}(t) = \int_{-\infty}^t G_1(t-t') \frac{d}{dt'} \varepsilon_{ij}(t') dt' - \frac{1}{3} \delta_{ij} \int_{-\infty}^t G_1(t-t') \frac{d\varepsilon_{kk}}{dt'} dt' + \delta_{ij} K \varepsilon_{kk}$$

where $G_1(t-t')$ is called the relaxation modulus in shear, ε_{ij} and ε_{kk} are the strain-rate tensor components, and K is the bulk modulus. Note that if the solid material is either a solid fuel or a solid propellant, such material can usually be assumed to be viscoelastic in shear and elastic in bulk. For most viscoelastic materials, we can express G_1 as a function of time t according to the following exponential series:

$$G_1 = g_0 + \sum_{m=1}^M g_m e^{-\beta_m t}$$

For simplicity, let us denote the normal stress in the solid phase by $\sigma_p \mathbf{I}$. Note that σ_p is positive for tension. Then, the normal-stress tensor in the solid phase becomes

$$\tilde{\sigma} = \sigma_p \mathbf{I}$$

Now, we shall assume the interface is stationary (i.e., fixed in space by feeding the solid material upward at its burning rate r_b as shown in Figure 3.15) and the body-force and viscous effects are negligible. Following Eq. (3-141), we have

$$\begin{aligned} & A\rho_{g+}\mathbf{v}_{g+} \cdot (\mathbf{n}_+) - A\rho_{s-}\mathbf{r}_{b-} \cdot (\mathbf{n}_+) - (-p_+\mathbf{I} - \sigma_p \mathbf{I}) \cdot \mathbf{n}_+ A \\ &= \lim_{v \rightarrow 0} \left[\iiint_v \rho \sum_{i=1}^N Y_i \mathbf{f}_i dV - \frac{d}{dt} \iiint_v \rho \mathbf{v} dV \right] \rightarrow 0 \end{aligned}$$

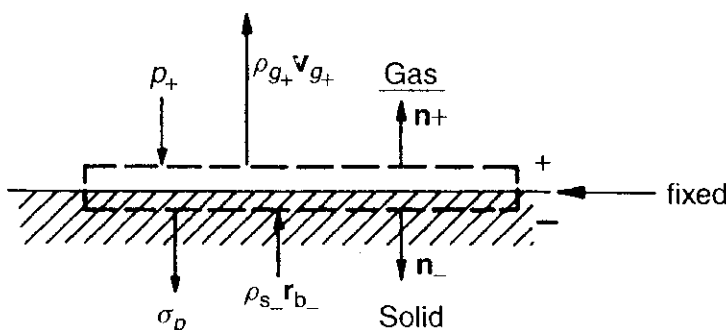


Figure 3.15 An infinitely thin control volume at the gas-solid interface of a burning solid material.

or

$$\underbrace{\frac{A\rho_g + \mathbf{v}_{g+}}{\left(\frac{M}{t}\right)\left(\frac{L}{t}\right)} \underbrace{v_{g+}}_{\text{Momentum flux leaving control surface}} - \underbrace{\frac{A\rho_s - \mathbf{r}_{b-}}{\left(\frac{M}{t}\right)\left(\frac{L}{t}\right)} \underbrace{r_{b-}}_{\text{Momentum flux entering control surface}}}_{(F)} + \underbrace{\frac{Ap_+ \mathbf{n}_+}{(F)}}_{\text{Force exerted on top surface of control volume}} + \underbrace{\frac{A\sigma_{p-} \mathbf{n}_+}{(F)}}_{\text{Force exerted on bottom surface of control volume}} = 0$$

\mathbf{n}_+ can be eliminated from the above equation because

$$\mathbf{v}_g = v_g \mathbf{n}_+, \quad \mathbf{r}_{b-} = r_{b-} \mathbf{n}_+$$

Thus, we have

$$\rho_g v_{g+}^2 + p_+ = \rho_s r_{b-}^2 - \sigma_{p-}$$

Because $\rho_g v_{g+} = \rho_s r_{b-}$ and usually $v_{g+} \gg r_{b-}$, we can accept the approximation that $\rho_g v_{g+}^2 \gg \rho_s r_{b-}^2$; then,

$$-\sigma_{p-} = p_+ + \rho_g v_{g+}^2$$

Therefore, the normal compressive stress ($-\sigma_{p-}$) in the solid phase immediately below the interface is approximately equal to the sum of the hydrostatic pressure and the momentum of the gas leaving the burning surface.

#

Example 3.4. Write the species mass-flux balance at a gas–solid interface, by adopting the following three assumptions:

1. The interface location is fixed in space.
2. Fick's law of mass diffusion is valid.
3. There is no subsurface diffusion.

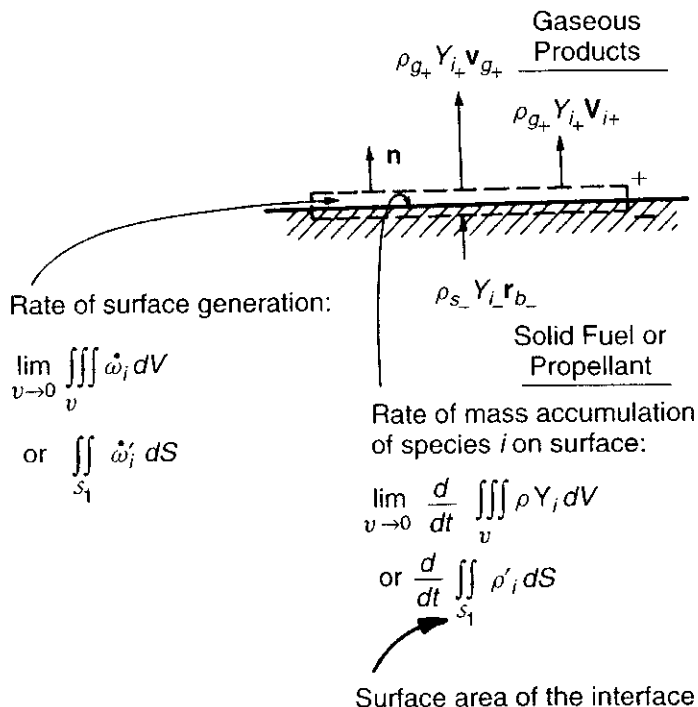
Solution: Let's now consider the diagram containing different mass fluxes at the interface.

Following Eq. (3-143) and Eq. (3-144), we have

$$A\rho_{g+} Y_{i+} (\mathbf{v}_{g+} + \mathbf{V}_{i+}) \cdot \mathbf{n}_+ - A\rho_{s-} Y_{i-} \mathbf{r}_{b-} \cdot \mathbf{n}_+ = \iint_{S_I} \dot{\omega}'_i dS - \frac{d}{dt} \iint_{S_I} \rho'_i dS$$

where

$$\mathbf{V}_{i+} = -\frac{\mathcal{D}}{Y_{i+}} \frac{\partial Y_i}{\partial y} \Big|_+ \mathbf{n}_+$$

**Figure 3.16** Mass-flux balance of i th species at the gas-solid interface.

so that

$$\underbrace{\rho_{g+} Y_{i+} v_{g+}}_{\text{mass flux of species } i \text{ convected out}} - \underbrace{\rho_{g+} \mathcal{D} \left. \frac{\partial Y_i}{\partial y} \right|_+}_{\text{mass flux of species } i \text{ diffused out}} = \underbrace{\rho_{s-} Y_{i-} r_{b-}}_{\text{mass flux of species } i \text{ supplied to burn at surface by feeding solid material from bottom}}$$

$$+ \underbrace{\dot{\omega}'_i}_{\text{net rate of generation of species } i \text{ at surface per unit area by heterogeneous reaction, decomposition, or condensation}} - \underbrace{\frac{1}{A} \frac{d}{dt} \iint_{S_1} \rho'_i dS}_{\text{mass accumulation at surface}}$$

If we further assume that the mass-accumulation term is negligible, then we have

$$\rho_{g+} Y_{i+} v_{g+} - \rho_{g+} \mathcal{D} \left. \frac{\partial Y_i}{\partial y} \right|_+ = \rho_{s-} Y_{i-} r_{b-} + \dot{\omega}'_i$$

In general, a gaseous species i in the product does not exist in the same form in the solid; hence $Y_{i-} = 0$. Therefore,

$$\underbrace{\rho_{g+} Y_{i+} v_{g+}}_{\text{mass flux of species } i \text{ convected out}} - \underbrace{\rho_{g+} \mathcal{D} \left. \frac{\partial Y_i}{\partial y} \right|_+}_{\text{mass flux of species } i \text{ diffused out}} = \underbrace{\dot{\omega}'_i}_{\text{mass flux of species } i \text{ generated on the surface}}$$

Example 3.5. Write the energy-flux balance at a gas–liquid interface.

Solution: Following Eq. (3-142), if the body-force work is zero and if there is no net accumulation of total stored energy inside the interfacial control volume, we have

$$\begin{aligned} & \iint_{\delta_I} \rho_{g+} \left(e_{g+} + \frac{v_{g+}^2}{2} \right) v_{g+} dS - \iint_{\delta_I} \rho_{l-} \left(e_{l-} + \frac{r_{b-}^2}{2} \right) r_{b-} dS \\ & + \iint_{\delta_I} \mathbf{q}_+ \cdot \mathbf{n}_+ dS - \iint_{\delta_I} \mathbf{q}_- \cdot \mathbf{n}_+ dS \\ & - \iint_{\delta_I} v_{g+} (-p_{g+} + \tau_{ii+}) dS - \iint_{\delta_I} r_{b-} p_{l-} dS = \lim_{V \rightarrow 0} \iiint_V \dot{Q} dV \end{aligned} \quad (\text{A})$$

Figure 3.17 shows many different energy flux terms in and out of the interfacial control volume.

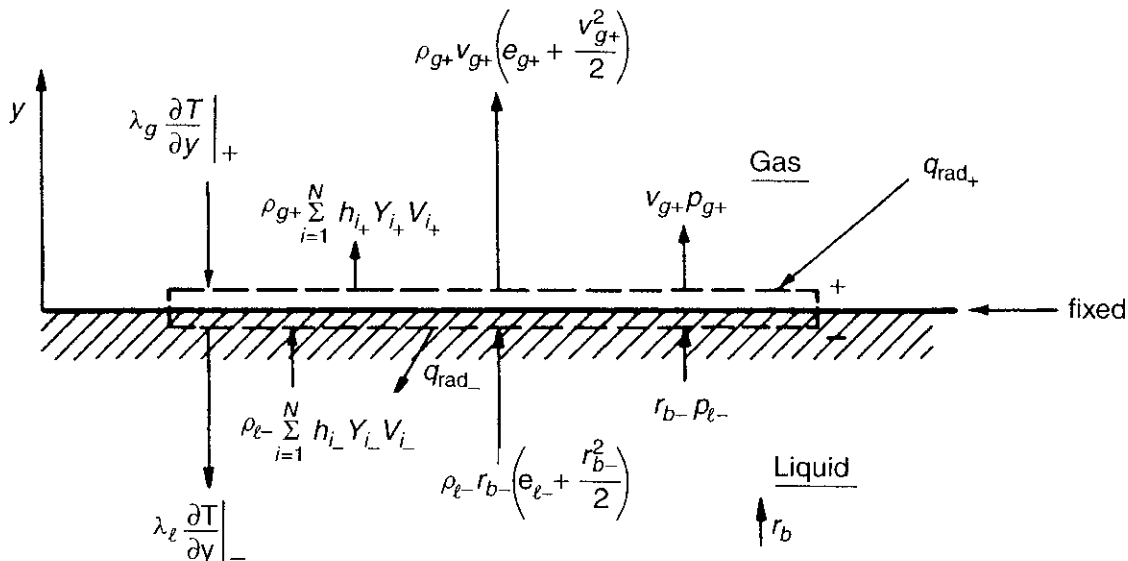


Figure 3.17 Energy-flux balance at the gas–liquid interface.

Let's recall that the gas-phase energy flux \mathbf{q}_+ can be written as the sum of three terms:

$$\mathbf{q}_+ = -\lambda \nabla T + \rho \sum_{i=1}^N h_i Y_i \mathbf{V}_i + \mathbf{q}_{\text{Dufour}}$$

where $\mathbf{q}_{\text{Dufour}}$ can be neglected; also, the nonhydrostatic normal stresses, τ_{ii+} ($\approx \frac{4}{3} \mu \nabla \cdot \mathbf{v}$), can be neglected in comparison with p_{g+} .

Now $\lim_{v \rightarrow 0} \iint_v \dot{Q} dV$ is equal to $\iint_{\delta_l} (\mathbf{q}_{\text{rad}-} - \mathbf{q}_{\text{rad}+}) \cdot \mathbf{n}_+ dS$, which represents the net rate of energy absorption at the interface. Thus, the energy-flux balance becomes

$$\begin{aligned} & \rho_{g+} v_{g+} \left(e_{g+} + \frac{p_{g+}}{\rho_{g+}} + \frac{v_{g+}^2}{2} \right) + \rho_{g+} \sum_{i=1}^N h_{i+} Y_{i+} V_{i+} - \lambda_g \left. \frac{\partial T}{\partial y} \right|_+ - q_{\text{rad}+} \\ & = \rho_{l-} r_{b-} \left(e_{l-} + \frac{p_{l-}}{\rho_{l-}} + \frac{r_{b-}^2}{2} \right) + \rho_{l-} \sum_{i=1}^N h_{i-} Y_{i-} V_{i-} - \lambda_l \left. \frac{\partial T}{\partial y} \right|_- - q_{\text{rad}-} \end{aligned} \quad (\text{B})$$

Note that

$$e \equiv h - \frac{p}{\rho} = \sum_{i=1}^N h_i Y_i - \frac{p}{\rho} \quad (\text{C})$$

Substituting Eq. (C) into (B), we have

$$\begin{aligned} & \left[\underbrace{\rho_{g+} v_{g+} \left(h_{g+} + \frac{v_{g+}^2}{2} \right)}_{\text{total enthalpy flux of gaseous mixture leaving surface by bulk motion of gases at surface}} + \underbrace{\rho_{g+} \sum_{i=1}^N h_{i+} Y_{i+} V_{i+}}_{\text{enthalpy flux of gaseous mixture leaving surface by mass diffusion}} \right] - \underbrace{\lambda_g \left. \frac{\partial T}{\partial y} \right|_+} - \underbrace{q_{\text{rad}+}}_{\substack{\text{energy flux to surface due to heat conduction} \\ \text{energy flux to surface due to radiation}}} \\ & = \left[\underbrace{\rho_{l-} r_{b-} \left(h_{l-} + \frac{r_{b-}^2}{2} \right)}_{\text{total enthalpy flux of liquid material arriving at interface by bulk motion of liquid at surface}} + \underbrace{\rho_{l-} \sum_{i=1}^N h_{i-} Y_{i-} V_{i-}}_{\text{enthalpy flux of liquid arriving at interface by mass diffusion}} \right] - \underbrace{\lambda_l \left. \frac{\partial T}{\partial y} \right|_-} - \underbrace{q_{\text{rad}-}}_{\substack{\text{energy flux from interface to subsurface due to heat conduction} \\ \text{energy flux leaving interface by radiation}}} \end{aligned} \quad (\text{D})$$

It should be noted that the enthalpy contains not only the sensible enthalpy but also the chemical enthalpy, that is,

$$h_i = \Delta h_{f,i}^o + \int_{T^o}^T C_{p_i} dT \quad (\text{E})$$

Recall that the species mass-flux balance can be written as

$$\rho_{g+} Y_{i+} v_{g+} - \rho_{g+} \mathcal{D} \left. \frac{\partial Y_i}{\partial y} \right|_+ = \rho_{l-} Y_{i-} r_{b-} - \rho_{l-} \mathcal{D} \left. \frac{\partial Y_i}{\partial y} \right|_- + \dot{\omega}'_i \quad (\text{F})$$

or

$$\rho_{g+}[Y_{i+}v_{g+} + Y_{i+}V_{i+}] = \rho_{l-}[Y_{i-}r_{b-} + Y_{i-}V_{i-}] + \dot{\omega}'_i \quad (\text{F}')$$

Since usually $h_{g+} \gg v_{g+}^2/2$ and $h_{l-} \gg r_{b-}^2/2$, we can drop the kinetic-energy terms from Eq. (D). After using Eqs. (C) and (E), Eq. (D) becomes

$$\begin{aligned} & \rho_{g+} \sum_{i=1}^N h_{i+} Y_{i+} (v_{g+} + V_{i+}) - \lambda_g \left. \frac{\partial T}{\partial y} \right|_+ - q_{\text{rad}_+} \\ &= \rho_{l-} \sum_{i=1}^N h_{i-} Y_{i-} (r_{b-} + V_{i-}) - \lambda_l \left. \frac{\partial T}{\partial y} \right|_- - q_{\text{rad}_-} \end{aligned} \quad (\text{G})$$

or

$$\begin{aligned} & \sum_{i=1}^N \left[\Delta h_{f,i}^o + \int_{T^o}^T C_{p_i} dT \right]_+ \rho_{g+} Y_{i+} (v_{g+} + V_{i+}) - \lambda_g \left. \frac{\partial T}{\partial y} \right|_+ - q_{\text{rad}_+} \\ &= \sum_{i=1}^N \left[\Delta h_{f,i}^o + \int_{T^o}^T C_{p_i} dT \right]_- \rho_{l-} Y_{i-} (r_{b-} + V_{i-}) - \lambda_l \left. \frac{\partial T}{\partial y} \right|_- - q_{\text{rad}_-} \end{aligned} \quad (\text{H})$$

or

$$\begin{aligned} & \underbrace{\lambda_l \left. \frac{\partial T}{\partial y} \right|_-}_{\substack{\text{conductive heat} \\ \text{flux immediately} \\ \text{below interface} \\ \text{to liquid}}} = \underbrace{\lambda_g \left. \frac{\partial T}{\partial y} \right|_+}_{\substack{\text{heat-flux} \\ \text{feedback} \\ \text{at interface}}} + \underbrace{(q_{\text{rad}_+} - q_{\text{rad}_-})}_{\substack{\text{net radiation flux} \\ \text{absorbed at} \\ \text{interface}}} \\ & + \underbrace{\sum_{i=1}^N \rho_{l-} Y_{i-} (r_{b-} + V_{i-}) \Delta h_{f,i-}^o - \sum_{i=1}^N \rho_{g+} Y_{i+} (v_{g+} + V_{i+}) \Delta h_{f,i+}^o}_{\substack{\text{net heat release at interface} [\approx \rho_{l-} r_{b-} Q_s \text{ if } V_i \text{ are small for all species}]}}, \\ & + \underbrace{\sum_{i=1}^N \rho_{l-} Y_{i-} (r_{b-} + V_{i-}) \int_{T^o}^T C_{p_{i-}} dT - \sum_{i=1}^N \rho_{g+} Y_{i+} (v_{g+} + V_{i+}) \int_{T^o}^T C_{p_{i+}} dT}_{\substack{\text{enthalpy change across interface}}} \end{aligned}$$

The last term for the enthalpy change across the interface is equal to

$$\sum_{i=1}^N \rho_{l-} Y_{i-} (r_{b-} + V_{i-}) (C_{p_{i-}} - C_{p_{i+}}) (T_s - T^o)$$

if $C_{p_i}(T_s - T^o) = \int_{T^o}^{T_s} C_{p_i} dT$ for all i species; this term also can be further simplified to

$$\rho_l - r_{b-}(C_{pl} - C_{pg})(T_s - T^o)$$

if $V_i = 0$ for all i .

#

REFERENCES

1. R. B. Bird, W. E. Stewart, and E. N. Lightfoot, *Transport Phenomena*, John Wiley & Sons, New York, 1960.
2. F. A. Williams, *Combustion Theory*, Addison-Wesley Publishing Co., Reading, Mass., 1965.
3. H. Schlichting, *Boundary-Layer Theory*, 6th ed., Chapter 5, McGraw-Hill Book Company, New York, 1968.
4. J. O. Hirschfelder, C. F. Curtiss, and R. B. Bird, *Molecular Theory of Gases and Liquids*, Chapter 1, John Wiley & Sons, New York, 1954.
5. J. O. Hinze, *Turbulence*, McGraw-Hill Book Company, New York, 1975.
6. I. H. Shames, *Mechanics of Fluids*, McGraw-Hill Book Company, New York, 1962.
7. W. H. Li and S. H. Lam, *Principles of Fluid Mechanics*, Addison-Wesley Publishing Co., Reading, Mass., 1964.
8. R. Aris, *Vectors, Tensors, and the Basic Equations of Fluid Mechanics*, Prentice-Hall, Englewood Cliffs, N.J., 1962.
9. L. C. Landau and E. M. Lifshitz, *Fluid Mechanics*, Pergamon Press, New York, 1959.
10. V. A. Shvab, *Gos. Energized.*, Moscow-Leningrad, 1948.
11. Y. B. Zel'dovich, *Zhur. Tekhn. Fiz.* **19**, 1199 (1949), English translation, NACA Tech. Memo **1296**, 1950.

HOMEWORK

1. Use Eq. (3-9) to show that the molar flux of species A can be expressed as

$$\mathbf{J}_A^* = -CX_AX_B(\mathbf{V}_B - \mathbf{V}_A)$$

in a binary system with species A and B .

2. Evaluate the following sums for a multicomponent system with N species:

- | | | |
|---------------------------------|-----------------------------------|-----------------------------------|
| (a) $\sum_{i=1}^N Y_i$ | (b) $\sum_{i=1}^N X_i$ | (c) $\sum_{i=1}^N \rho_i$ |
| (d) $\sum_{i=1}^N \mathbf{J}_i$ | (e) $\sum_{i=1}^N \mathbf{J}_i^*$ | (f) $\sum_{i=1}^N \dot{\omega}_i$ |

3. For a multicomponent flow of reactive mixture with N species, show that

$$\sum_{i=1}^N Y_i \mathbf{V}_i = 0$$

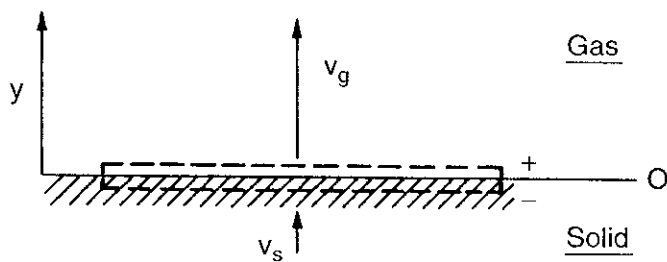
where Y_i represents the mass fraction of species i , and \mathbf{V}_i represents the relative mass diffusion velocity of species i . If the x -component of \mathbf{V}_i , V_{x_i} , is substituted for \mathbf{V}_i in the above equation, will it still be valid?

4. Show that the total stress tensor τ_{ij} for an isotropic Newtonian fluid is symmetric.
5. Show that for any isotropic Newtonian fluid, the relationship $c - \lambda = 2\mu$ given in Eq. (3-54) is valid, where μ is the dynamic viscosity of the fluid. Hint: Consider a coordinate transformation between the principal stress axes and some arbitrary axes x_1, x_2, x_3 for which the shear stresses are not zero.
6. Express the quantity \dot{Q} in the energy equation in terms of the heat of formation and the rate of local production of all the species considered in reacting flow systems, if the internal energy e in the following equation contains *no* chemical energy:

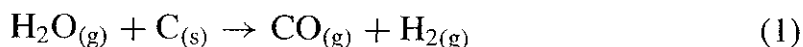
$$\rho \frac{\partial e}{\partial t} + \rho \mathbf{v} \cdot \nabla e = -\nabla \cdot \mathbf{q} + \tilde{\sigma} : \nabla \mathbf{v} + \dot{Q} + \rho \sum_{k=1}^N Y_k \mathbf{f}_k \cdot \mathbf{V}_k$$

ANSWER: $\dot{Q} = - \sum_{i=1}^N \dot{\omega}_i \Delta h_{f,i}^o$

7. If a solid fuel is gasifying at a fixed surface by feeding it in the upward direction at its regression rate, write down the boundary conditions for the balance of mass flux at the interface.



8. If the interface control volume moves at the regression rate of the solid in the above problem, what is the mass-flux balance equation across this interface?
9. A mixture of high-temperature gases flows over a horizontal graphite slab. Some of species $[H_2O_{(g)}, CO_{2(g)}, \text{ and } H_{2(g)}]$ in the mixture can react with graphite surface by heterogeneous reaction and cause thermochemical erosion of the solid. Consider the following heterogeneous reactions:





- (a) Write the species mass-flux balance at the gas–solid interface for species $\text{H}_2\text{O}_{(\text{g})}$, $\text{CO}_{2(\text{g})}$, $\text{CO}_{(\text{g})}$, and $\text{H}_{2(\text{g})}$. Give the physical meanings of each term in the mass-flux balance for $\text{H}_2\text{O}_{(\text{g})}$. The rates of consumption of graphite due to H_2O , CO_2 , and H_2 can be denoted as $-\dot{\omega}_{\text{C},\text{H}_2\text{O}}$, $-\dot{\omega}_{\text{C},\text{CO}_2}$, and $-\dot{\omega}_{\text{C},\text{H}_2}$, respectively. These rates are assumed to be known functions of T_{wall} and the partial pressure of each reacting species.
- (b) What is the energy-flux balance at the gas–solid interface? Give the physical meaning of each term.
- (c) Sketch the vertical concentration profiles of the gaseous species near the gas–solid interface.
10. Derive a continuity equation to describe the local balance of the mass fraction of atomic element i , Z_i , in a chemically reacting flow where Z_i is defined as

$$Z_i = \frac{\text{mass of atomic element } i \text{ in all chemical species}}{\text{total mass of the mixture}}$$

Note that $Z_i = \sum_{j=1}^N a_{ij} Y_j$ where Y_j represents the mass fraction of the j th molecule and a_{ij} represents the mass fraction of the i th atom in the j th molecule.

11. Write the conservation of energy equation in terms of temperature in the following coordinates:
- Rectangular Cartesian coordinates (x , y , z)
 - Cylindrical coordinates (r , θ , z)
 - Spherical coordinates (r , θ , ϕ)
12. Consider a solid fuel slab sublimating into fuel gases; the fuel gases generated from the surface then react with the ambient oxidizer gases.
- Express the species mass-flux boundary condition in terms of $\left. \frac{\partial Y_F}{\partial y} \right|_+$, $\left. \frac{\partial Y_O}{\partial y} \right|_+$, and $\left. \frac{\partial Y_P}{\partial y} \right|_+$ if the sublimating surface is held at a fixed location. The global reaction can be regarded as: $F + O \rightarrow P$.
 - Express the species mass-flux boundary condition in terms of $\left. \frac{\partial Y_F}{\partial y} \right|_+$, $\left. \frac{\partial Y_O}{\partial y} \right|_+$, and $\left. \frac{\partial Y_P}{\partial y} \right|_+$ if the sublimating surface is allowed to regress at the rate of v_s .
13. Write the energy flux balance at the interface of a burning solid propellant that contains both oxidizer and fuel ingredients. The propellant can be treated as a homogeneous material.

- 14.** Consider the combustion of a porous solid material with porosity (void fraction) ϕ . The solid material regresses at the rate of r_b .
- Write the mass-flux balance equation at the interface.
 - Write the energy-flux balance equation at the interface.

PROJECTS

- 3.1.** In the process of modeling certain complex combustion problems, it is often helpful to consider some simpler problems that are similar or closely related to the combustion problems under investigation. For example, in order to formulate the pyrolysis process of a solid fuel under radiative heating, one could start with a simpler problem by considering the sublimation of ice under radiative heating. In this project, let us consider a very thick layer of ice on a large pond.
- Assuming the air is still (no wind), formulate the ice melting and evaporation problem under solar heating. The initial temperature of ice, T_i , could be much below its melting point (273 K). Write the governing equations for the temperature profiles in ice and air. Specify the initial and boundary conditions so that the problem can be solved numerically. Please list all assumptions and define all important variables. (The radiation heat flux could be solved from a two-flux model.)
 - Reformulate the above problem, allowing air to flow over the ice surface.
- 3.2.** The parameter Z_i is defined as the mass fraction of the i th element of a multicomponent gaseous mixture containing N molecular species (see homework 10). Starting from the element conservation equation in the divergence form of the partial differential equation, derive an interfacial element mass flux balance equation for the solid–gas boundary at the surface of a burning solid fuel that generates gaseous product species. To facilitate the formulation, it is more convenient to consider the burning surface to be kept at a fixed location.
- 3.3.** Consider a sublimating solid fuel in the form of a rod burning in an air atmosphere. The rod can be considered infinitely long. It burns axially downward. For the case of vapor-phase combustion (without any heterogeneous surface reaction), formulate this combustion problem by giving the necessary governing equations and boundary conditions. The edge effects can be neglected and the flame can be treated as one-dimensional. Also, the initial ignition transient variations can be neglected.

4

DETONATION AND DEFLAGRATION WAVES OF PREMIXED GASES

Additional Symbols

Symbol	Description	Dimension
c	Local sonic velocity	L/t
\bar{C}_p	Average specific heat	Q/MT
D	Detonation wave speed	L/t
V_w	Wave velocity (Fig. 4.3)	L/t
h	Enthalpy per unit mass (thermal plus chemical)	Q/M
M	Mach number	—
q	Heat release per unit mass [Eq. (4-16)]	Q/M
q_{cond}	Conductive heat flux [Eq. (4-4)]	$Q/L^2 \cdot t$
R	Specific gas constant	Q/T
s	Entropy per unit mass	Q/MT
u	Relative gas velocity to the combustion wave (Fig. 4.1)	L/t
v	Absolute gas velocity (Fig. 4.3)	L/t
Δe_f^o	Specific energy of formation	Q/M
Δh_c	Enthalpy increase per unit mass due to combustion	Q/M
Δh_s	Enthalpy increase per unit mass due to shock heating	Q/M
$\Delta h_{f,i}^o$	Specific enthalpy of formation of i th species at standard states	Q/M

Symbol	Description	Dimension
α	Constant defined by [Eq. (4-146)]	—
β	Constant defined by [Eq. (4-146)]	—
γ	Specific-heat ratio	—
λ	Thermal conductivity	Q/LTt
λ	Detonation cell width	L
τ	Induction time	t
<i>Superscript</i>		
o	Standard state condition	
<i>Subscripts</i>		
C-J	Taken at Chapman-Jouguet points	
HC	Taken along Hugoniot curve	
j	j th species	
L	Taken at lower Chapman-Jouguet point J	
k	Index of summation	
min	Minimum value of quantity	
s	Taken at constant entropy	
t	Total	
U	Taken at upper Chapman-Jouguet point Y	
0	Initial state	
$1/\rho$	Taken at constant $1/\rho$	
1	Condition of unburned gases in region I (Fig. 4.1)	
2	Condition of burned gases in region II (Fig. 4.1)	

The chemical-reaction zone is often called the “flame zone,” “flame front,” “reaction wave,” or the like. Within the flame zone, rapid reactions take place and light is usually (but not always) emitted from the flame. In general, there are two types of flames:

- a. *Premixed Flame.* Reactants are perfectly mixed before chemical reaction.
- b. *Diffusion Flame.* Reactants diffuse into each other during the chemical reaction.

In this chapter, we shall concentrate on the premixed flame.

Depending on the existence of a combustion wave and the speed of wave propagation through a reacting mixture, reactions of premixed gases are generally divided into three categories:

1. *Explosion.* Rate of heat generation is extremely fast, but it does not require the passage of a combustion wave through the exploding medium. Chemical kinetics associated with explosion of premixed gases such as H_2/O_2 systems are discussed in Chapter 2.

2. *Deflagration.* A combustion wave propagating at subsonic speed. Detailed discussions of laminar premixed flame structure are given in Chapter 5. A portion of the reaction mechanism is given in Chapter 2.
3. *Detonation.* A combustion wave propagating at supersonic speed. Formation of a detonation wave from deflagration-to-detonation or shock-to-detonation transition processes and discussion of detonation wave structure are given in a later portion of this chapter.

In the following, we shall discuss the general characteristics of the deflagration and detonation waves, and derive the Rankine–Hugoniot equations to relate the properties on either side of the wave. The method of calculating the speed and structure of the detonation wave will also be discussed.

1 QUALITATIVE DIFFERENCES BETWEEN DETONATION AND DEFLAGRATION

The waves we consider in the first part of this chapter will be limited to one-dimensional (1D) planar waves. A schematic diagram of a one-dimensional combustion wave is shown in Fig. 4.1 to help visualize the physical situation. In this figure, we are following the motion of a one-dimensional planar combustion wave in a very long duct with constant area. The combustion wave is moving to the left at a constant velocity u_1 . In a reference frame following the wave motion, the stationary unburned gases ahead of the wave can be considered to move at velocity u_1 toward the wave front. The selection of this frame of reference is convenient for working with a stationary wave. In Fig. 4.1, the subscript 1 designates conditions of the unburned gases ahead of the wave, and subscript 2 indicates conditions of the burned gases behind the wave. Velocities u_1 and u_2 are defined with respect to the coordinate system fixed relative to the stationary wave.

Typical data on the upstream and downstream conditions can give us a good notion of the physical situation associated with a deflagration and detonation wave. A comparison of data between typical deflagration and detonation waves, taken from Friedman,¹ is shown in Table 4.1.

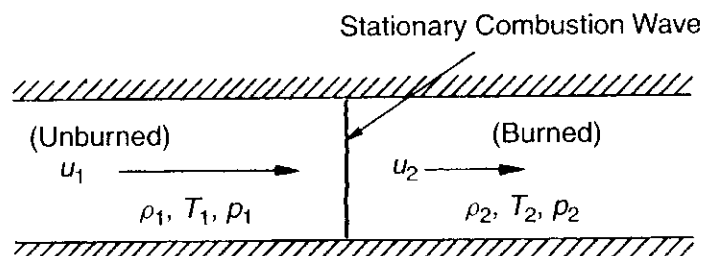


Figure 4.1 Schematic diagram of a stationary one-dimensional combustion wave (deflagration or detonation wave).

Table 4.1 Qualitative Differences between Detonation and Deflagration in Gases^a

	Detonation	Deflagration
u_1/c_1	5–10	0.0001–0.03
u_2/u_1	0.4–0.7 (deceleration)	4–6 (acceleration)
p_2/p_1	13–55 (compression)	≈ 0.98 (slight expansion)
T_2/T_1	8–21 (heat addition)	4–16 (heat addition)
ρ_2/ρ_1	1.7–2.6	0.06–0.25

^aData taken by Friedman.¹

In the following section, we shall consider some basic relationships between the unburned and burnt properties of the premixed gaseous mixtures contained in a constant-area tube. The combustion wave is assumed to propagate at a steady-state speed with no heat loss to the surrounding tube wall. Although these idealized conditions are somewhat difficult to achieve, the results derived from the basic 1D conservation equations are important. Essentially, the solution of any steady-state deflagration and detonation waves lie on the Hugoniot curve, which can be divided into several branches and regimes, corresponding to the different types of combustion waves.

2 THE HUGONIOT CURVE

The conservation equations for steady one-dimensional flow, with no body forces, no external heat addition or heat loss, and negligible Dufour and species inter-diffusion effects, are as follows:

Continuity.

$$\frac{d(\rho u)}{dx} = 0 \quad (4-1)$$

Momentum.

$$\rho u \frac{du}{dx} = -\frac{dp}{dx} + \frac{d}{dx} \left[\left(\frac{4}{3}\mu + \mu' \right) \frac{du}{dx} \right] \quad (4-2)$$

Energy.

$$\rho u \left[\frac{d}{dx} \left(h + \frac{u^2}{2} \right) \right] = -\frac{d}{dx} q_{\text{cond}} + \frac{d}{dx} \left[u \left(\frac{4}{3}\mu + \mu' \right) \frac{du}{dx} \right] \quad (4-3)$$

where

$$q_{\text{cond}} = -\lambda \frac{dT}{dx} \quad (4-4)$$

$$h = C_p T + h^o \quad (4-5)$$

The viscosity $(\frac{4}{3}\mu + \mu')$ in the momentum equation is due to

$$\tau_{ij} = \mu \left(\frac{\partial u_i}{\partial x_j} + \frac{\partial u_j}{\partial x_i} \right) + \left(\mu' - \frac{2}{3}\mu \right) \frac{\partial u_k}{\partial x_k} \delta_{ij} \quad (4-6)$$

$$\tau_{11} = \left(2\mu + \mu' - \frac{2}{3}\mu \right) \frac{du}{dx} = \left(\frac{4}{3}\mu + \mu' \right) \frac{du}{dx} \quad (4-7)$$

The bulk viscosity μ' is usually very small and can be neglected.

By integrating Eq. (4-1) to Eq. (4-3) we have

$$\rho u = \text{constant} \equiv \dot{m} \quad (4-8)$$

$$\rho u \frac{du}{dx} + u \frac{d}{dx}(\rho u) = -\frac{dp}{dx} + \frac{d}{dx} \left(\frac{4}{3}\mu \frac{du}{dx} \right) \quad (4-2)$$

From continuity

$$\frac{d}{dx}(\rho u) = 0 \quad (4-1)$$

Equation (4-2) becomes

$$\frac{d}{dx} \left[\rho u^2 + p - \frac{4}{3}\mu \frac{du}{dx} \right] = 0 \quad (4-9)$$

After integration with respect to x , we have

$$\rho u^2 + p - \frac{4}{3}\mu \frac{du}{dx} = \text{constant} \quad (4-10)$$

The energy equation after integrating once with respect to x becomes

$$\rho u \left(C_p T + h^o + \frac{1}{2}u^2 \right) - \lambda \frac{dT}{dx} - u \left(\frac{4}{3}\mu \frac{du}{dx} \right) = \text{constant}' \quad (4-11)$$

Because du/dx and dT/dx are both equal to zero in the fully burned and unburned regions, the following conservation equations provide the relationships between the flow properties in these two regions:

$$\rho_1 u_1 = \rho_2 u_2 = \dot{m} \quad (4-12)$$

$$p_1 + \rho_1 u_1^2 = p_2 + \rho_2 u_2^2 \quad (4-13)$$

$$C_p T_1 + \frac{1}{2}u_1^2 + q = C_p T_2 + \frac{1}{2}u_2^2 \quad (4-14)$$

or

$$h_1 + \frac{1}{2}u_1^2 = h_2 + \frac{1}{2}u_2^2 \quad (4-14a)$$

and

$$p_2 = \rho_2 R_2 T_2 \quad (4-15)$$

where

$$q \equiv h_1^o - h_2^o \quad (4-16)$$

and

$$h^o = \sum_{i=1}^N Y_i \Delta h_{f,i}^o \quad (4-17)$$

Equation (4-15) is simply the equation of state of the burned mixture, assuming the ideal-gas law is applicable. There are four equations [Eqs. (4-12) through (4-15)] relating the five unknowns: $u_1, u_2, \rho_2, T_2, p_2$. Through algebraic substitutions and manipulations, these four equations can be reduced to a single equation involving only two unknowns, p_2 and ρ_2 . This final result is called the (Rankine-) Hugoniot relation for constructing the Hugoniot plot. Before presenting this relationship, it is useful to examine some intermediate steps.

The combining of Eq. (4-12) and Eq. (4-13) gives

$$p_2 - p_1 = \rho_1 u_1^2 - \rho_2 u_2^2 = \frac{(\rho_1 u_1)^2}{\rho_1} - \frac{(\rho_2 u_2)^2}{\rho_2} = \left(\frac{1}{\rho_1} - \frac{1}{\rho_2} \right) \dot{m}^2 \quad (4-18)$$

$$\therefore \rho_1^2 u_1^2 = \frac{p_2 - p_1}{1/\rho_1 - 1/\rho_2} = \dot{m}^2 \quad (4-19)$$

Equation (4-19) is generally referred to as the *Rayleigh-line relation*. This can also be written in terms of the Mach number $M_1 \equiv u_1/c_1$. We have

$$c_1 \equiv \sqrt{\gamma R_1 T_1} = \sqrt{\gamma \left(\frac{p_1}{\rho_1} \right)} \quad (4-20)$$

$$\frac{\gamma \rho_1^2 u_1^2}{\gamma \rho_1 p_1} = \frac{p_2/p_1 - 1}{1 - \rho_1/\rho_2} \quad (4-21)$$

Combining, the Rayleigh-line relation becomes

$$\gamma M_1^2 = \frac{p_2/p_1 - 1}{1 - \rho_1/\rho_2} \quad (4-22)$$

Using the definitions for C_p and γ , we have

$$C_p - C_v = R \quad (4-23)$$

or

$$C_p = \frac{\gamma}{\gamma - 1} R \quad (4-24)$$

Substituting the equation of state and Eq. (4-24) into Eq. (4-14), the conservation of energy equation can be rewritten in the following form:

$$\frac{\gamma}{\gamma - 1} \left(\frac{p_2}{\rho_2} - \frac{p_1}{\rho_1} \right) - \frac{1}{2} (u_1^2 - u_2^2) = q \quad (4-25)$$

Rearranging Eq. (4-13) to obtain expressions for u_1^2 and u_2^2 and substituting these expressions into Eq. (4-25), we have

$$\frac{\gamma}{\gamma - 1} \left(\frac{p_2}{\rho_2} - \frac{p_1}{\rho_1} \right) - \frac{1}{2} \underbrace{\left(\frac{p_2 - p_1}{\rho_1} + \frac{\rho_2}{\rho_1} u_2^2 \right)}_{u_1^2} - \underbrace{\left(\frac{p_2 - p_1}{\rho_2} - \frac{\rho_1}{\rho_2} u_1^2 \right)}_{-u_2^2} = q \quad (4-26)$$

Rearranging Eq. (4-12) and combining with Eq. (4-26), we have

$$\frac{\gamma}{\gamma - 1} \left(\frac{p_2}{\rho_2} - \frac{p_1}{\rho_1} \right) - \frac{1}{2} (p_2 - p_1) \left(\frac{1}{\rho_1} + \frac{1}{\rho_2} \right) = q \quad (4-27)$$

Equation (4-27) is known as the (*Rankine–*) *Hugoniot relation*. The plot of p_2 versus $1/\rho_2$ for a fixed heat release per unit mass, q , is called the *Hugoniot curve* and is shown in Fig. 4.2. Alternatively, the Hugoniot relation can be expressed in terms of total (thermal plus chemical) enthalpy h .

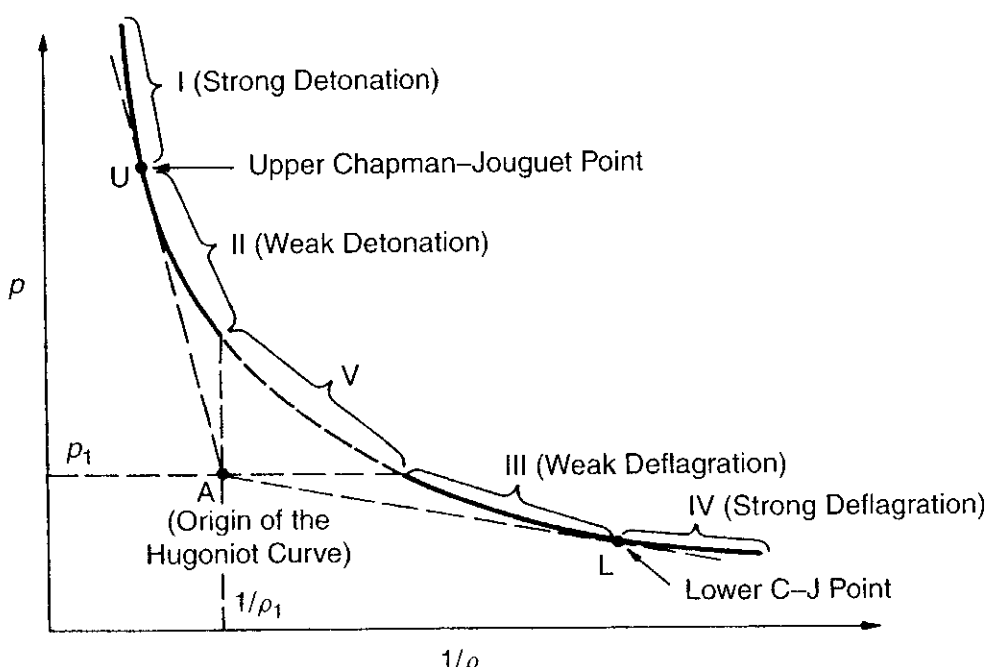


Figure 4.2 Hugoniot curve on p -versus- $1/\rho$ plane, showing various sections of the curve corresponding to the solution domains of various combustion conditions.

Combining Eq. (4-5) with Eq. (4-24) and the ideal-gas law, we have

$$h = \left(\frac{\gamma}{\gamma - 1} \right) \frac{p}{\rho} + h^o \quad (4-28)$$

Combining Eq. (4-16) and Eq. (4-28) gives

$$h_2 - h_1 = \frac{\gamma}{\gamma - 1} \frac{p_2}{\rho_2} + h_2^o - \frac{\gamma}{\gamma - 1} \frac{p_1}{\rho_1} - h_1^o = \frac{\gamma}{\gamma - 1} \left(\frac{p_2}{\rho_2} - \frac{p_1}{\rho_1} \right) - q \quad (4-29)$$

Substituting into Eq. (4-27) gives the equivalent Hugoniot relation:

$$h_2 - h_1 = \frac{1}{2} (p_2 - p_1) \left(\frac{1}{\rho_1} + \frac{1}{\rho_2} \right) \quad (4-30)$$

3 PROPERTIES OF THE HUGONIOT CURVE

The Hugoniot is essentially a plot of all the possible values of $(1/\rho_2, p_2)$ for a given value of $(1/\rho_1, p_1)$ and q . The point $(1/\rho_1, p_1)$, which is usually called the *origin* of the Hugoniot plot, is designated by the symbol A . Regions of possible solutions are constructed by drawing tangents to the curve through the point A , and vertical and horizontal lines from A . The curve is thus divided into five regions, specified as Roman numerals in Fig. 4.2. The two tangent points to the curve are called Chapman–Jouguet points,^{2,3} generally referred to as C–J points, and denoted by U for the upper C–J point and L for the lower C–J point.

It must be noted that although the curve represents all the *possible* solutions of the Hugoniot equation for the burned mixture, not all the solutions are valid, for physical reasons. We shall establish which regions of the curve represent valid solutions.

In region V, $p_2 > p_1$ and $1/\rho_2 > 1/\rho_1$. The Rayleigh-line expression (4-19) implies that u_1 is imaginary. Thus, region V is shown to be a physically impossible region.

To study the characteristic nature at the C–J points, let us consider q to be fixed and differentiate the Hugoniot relation (4-27) with respect to $1/\rho_2$:

$$\begin{aligned} & \frac{1}{\rho_2} \left(\frac{\gamma}{\gamma - 1} \right) \frac{dp_2}{d(1/\rho_2)} + \left(\frac{\gamma}{\gamma - 1} \right) p_2 - \frac{1}{2} (p_2 - p_1) \\ & - \frac{1}{2} \frac{dp_2}{d(1/\rho_2)} \left(\frac{1}{\rho_1} + \frac{1}{\rho_2} \right) = 0 \end{aligned} \quad (4-31)$$

After rearranging, we have

$$\frac{dp_2}{d(1/\rho_2)} = \frac{(p_2 - p_1) - \left(\frac{2\gamma}{\gamma - 1} \right) p_2}{\left(\frac{2\gamma}{\gamma - 1} \right) \frac{1}{\rho_2} - \left(\frac{1}{\rho_1} + \frac{1}{\rho_2} \right)} \quad (4-32)$$

The slopes at the tangent points U and L can also be represented as

$$\left[\frac{dp_2}{d(1/\rho_2)} \right]_{C-J} = \frac{p_2 - p_1}{1/\rho_2 - 1/\rho_1} \quad (4-33)$$

Equating the right-hand side of Eq. (4-32) to that of Eq. (4-33) and rearranging, we have

$$\frac{p_2 - p_1}{(1/\rho_2 - 1/\rho_1)} = -\gamma \rho_2 p_2 \quad \text{at C-J points} \quad (4-34)$$

Combining Eq. (4-34) with Eq. (4-19), we have

$$u_2^2 = \frac{\gamma p_2}{\rho_2} = c_2^2, \quad \text{or} \quad |u_2| = c_2 \quad (4-35)$$

Therefore, at the C-J points the Mach number of the burned gas is $M_2 = 1$.

In the detonation branch of the Hugoniot curve (regions I and II), $1/\rho_2 < 1/\rho_1$; therefore,

$$u_2 - u_1 = \dot{m} \left(\frac{1}{\rho_2} - \frac{1}{\rho_1} \right) < 0$$

or

$$u_1 > u_2 \quad (4-36)$$

where u_1 and u_2 are the velocities of the unburned and burned gases relative to the detonation wave (Fig. 4.1). If we now consider a laboratory coordinate system in which the detonation wave is moving at velocity V_w relative to the stationary duct, the direction of the absolute velocities of the gases before and behind the detonation wave is shown in Fig. 4.3. The algebraic relationships between the absolute and relative velocities are

$$\begin{aligned} v_1 &= V_w - u_1 \\ v_2 &= V_w - u_2 \end{aligned} \quad (4-37)$$

While u_1 and u_2 are positive in the direction shown in Fig. 4.1, v_1 and v_2 are positive in the direction shown in Fig. 4.3.

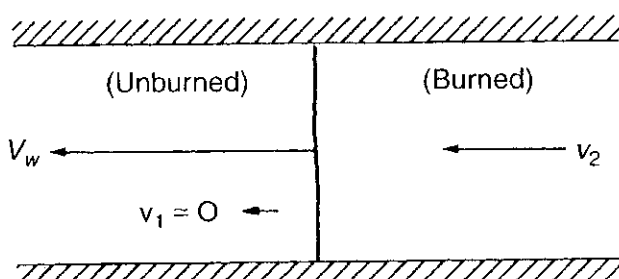


Figure 4.3 Detonation wave in the laboratory coordinate system.

Since the absolute velocity of the unburned gases is assumed to be zero, $V_w = u_1$, and from the inequality (4-36) we have

$$v_2 = V_w - u_2 = u_1 - u_2 > 0 \quad (4-38)$$

Physically, this means that the burned gases behind a detonation wave try to follow the wave motion. We shall next examine the magnitude of v_2 with respect to V_w to see whether the burned gases can catch up with the wave motion or not. First of all, the detonation-wave speed V_w can be expressed as the sum of u_2 and v_2 by rearranging Eq. (4-37), i.e.,

$$V_w = u_2 + v_2$$

For the upper C-J point, $u_2 = c_2$ and we have

$$V_w = c_2 + v_2 > c_2 \quad (4-39)$$

This implies that the C-J detonation wave is traveling at supersonic speed. Also, because $V_w > v_2$, the burned gases, although traveling in the same direction as the detonation wave, can never catch up with it.

Region I is called the strong-detonation region; within this region, the pressure of the burned gases is greater than that of the C-J detonation wave, that is, $p_2 > p_U$. In passing through a strong detonation wave, the gas velocity relative to the wave front is slowed down substantially from supersonic speed to subsonic (shown later). At the same time, the pressure and density increase significantly. In general, a strong detonation wave is seldom observed, since it requires a special experimental setup for generating overdriven shock waves in a very strong confinement.

Region II is called the weak-detonation region; within it, the pressure of the burned gases is smaller than that of the C-J detonation wave, that is $p_2 < p_U$. In passing through a weak detonation wave, the gas velocity relative to the wave front is slowed down, but the burned mixture still has a velocity greater than that of sound. It is interesting to note that the isochoric ($1/\rho_2 \approx 1/\rho_1$) weak detonation corresponding to infinite wave velocity [see Eq. (4-19)] is physically unattainable. In general, a weak detonation wave is seldom observed; it requires a gas mixture chosen specially to have extremely fast chemical kinetics.

Under most experimental conditions, detonations are Chapman-Jouguet waves (at the upper C-J point). A part of the reason for ruling out regions I and II also stems from the structure of the detonation wave, which will be discussed in a later section. The upper C-J point, U in Fig. 4.4, therefore represents the usual solution on the detonation branch of the Hugoniot curve. The wave speed at U corresponds to the minimum detonation wave speed, since a straight line through the origin $(1/\rho_1, p_1)$ will not intersect the detonation branch anywhere if the magnitude of its slope is less than that of the tangent line shown in Fig. 4.4.

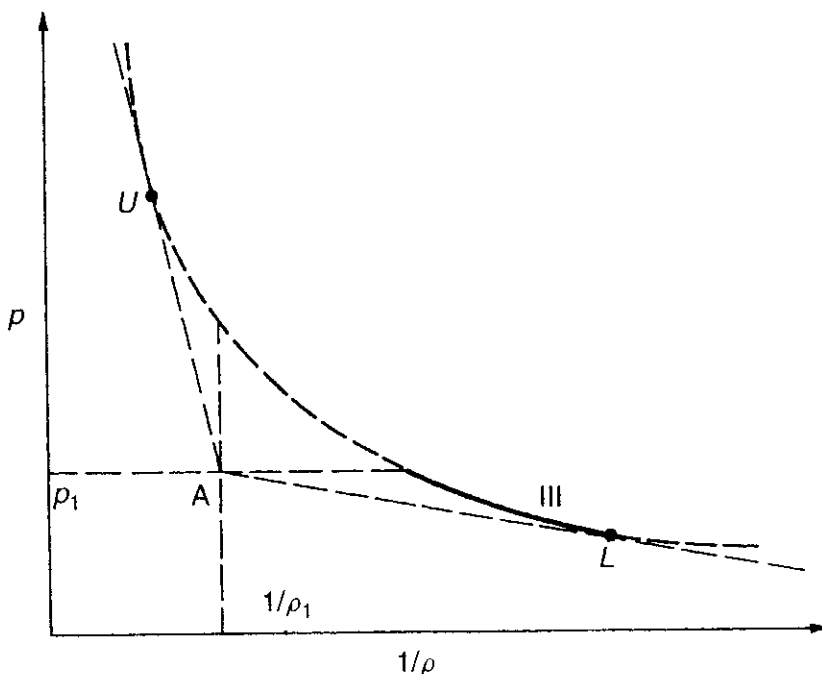


Figure 4.4 Solution regions on the Hugoniot curves.

In contrast to the upper C-J point, the lower C-J deflagration (corresponding to point L on the Hugoniot curve) has the maximum wave speed of all deflagrations [see Eq. (4-19)]. This is because a straight line through the origin A fails to intersect the deflagration branch if the magnitude of its slope exceeds that of the tangent line, and it intersects the deflagration branch at two points (once in region III and once in region IV) if its slope is less than that of the tangent line (see Fig. 4.2).

Region III is called the weak-deflagration region; within it $p_1 \geq p_2 > p_L$ and $1/\rho_2 < 1/\rho_L$. In passing through a weak deflagration wave, the gas velocity relative to the wave front is accelerated from a subsonic velocity to a higher subsonic velocity. The isobaric weak deflagration ($p_s = p_1$) corresponds to zero propagation velocity. The solution in region III is often observed; in most experimental conditions, the pressure in the burned-gas zone is slightly lower than that of the unburned gases. The detailed wave structure and methods for determining the wave speed as the eigenvalue of the problem (laminar flame speed of premixed gases) are discussed in detail in Chapter 5.

Region IV is called the strong-deflagration region. In passing through a strong deflagration wave, the gas velocity relative to the wave front must be accelerated substantially from subsonic to supersonic. Considerations of wave structure forbid a change from subsonic to supersonic flow in a constant-area duct.⁴ Consequently, strong deflagration is never observed experimentally; the possible solution in the deflagration branch is shown in Fig. 4.4 as the solid line on the Hugoniot curve. The C-J deflagration, corresponding to point L , is also not observed experimentally; hence it is excluded from the solid curve.

In the realizable deflagration-solution region, the burned gases move away from the combustion wave front. This can be shown by using the continuity

equation (4-12) and the conditions $1/\rho_2 > 1/\rho_1$ and $\dot{m} \geq 0$; we have

$$u_2 - u_1 = \dot{m} \left(\frac{1}{\rho_2} - \frac{1}{\rho_1} \right) > 0$$

Using Eq. (4-37) and substituting V_w for u_1 , the above inequality becomes

$$v_2 < 0$$

This shows that the burned gases, unlike those shown in Fig. 4.3 for a detonation wave, flow away from the deflagration wave. This is one of the characteristic differences between deflagration and detonation waves.

3.1 Entropy Distribution along the Hugoniot Curve

Now we shall consider the entropy variation along the Hugoniot curve and show that the entropy has a minimum at U and a maximum at L . Let us recall that

$$h \equiv e + \frac{p}{\rho} \quad (4-40)$$

where e represents internal energy including chemical energy:

$$h_2 - h_1 = (e_2 - e_1) + \left(\frac{p_2}{\rho_2} - \frac{p_1}{\rho_1} \right) \quad (4-41)$$

From Eq. (4-30) we know that

$$e_2 - e_1 = \frac{1}{2}(p_2 - p_1) \left(\frac{1}{\rho_1} + \frac{1}{\rho_2} \right) - \frac{p_2}{\rho_2} + \frac{p_1}{\rho_1} \quad (4-42)$$

After rearranging, we have

$$e_2 - e_1 = \frac{1}{2}(p_2 + p_1) \left(\frac{1}{\rho_1} - \frac{1}{\rho_2} \right) \quad (4-43)$$

From the first and second laws of thermodynamics we have

$$T_2 ds_2 = de_2 + p_2 d \left(\frac{1}{\rho_2} \right) \quad (4-44)$$

Differentiating Eq. (4-43), we have

$$de_2 = \frac{1}{2}(dp_2) \left(\frac{1}{\rho_1} - \frac{1}{\rho_2} \right) - \frac{1}{2}(p_2 + p_1) d \left(\frac{1}{\rho_2} \right) \quad (4-45)$$

Substituting Eq. (4-45) into Eq. (4-44) and rearranging, we have

$$T_2 ds_2 = \frac{1}{2} \left(\frac{1}{\rho_1} - \frac{1}{\rho_2} \right) dp_2 + \frac{1}{2} (p_2 - p_1) d \left(\frac{1}{\rho_2} \right)$$

or

$$T_2 \frac{ds_2}{d(1/\rho_2)} = \frac{1}{2} \left(\frac{1}{\rho_1} - \frac{1}{\rho_2} \right) \left(\frac{dp_2}{d(1/\rho_2)} - \frac{p_2 - p_1}{1/\rho_2 - 1/\rho_1} \right) \quad (4-46)$$

Using Eq. (4-33) for the slopes at the C-J points, Eq. (4-46) gives

$$\left[\frac{ds_2}{d(1/\rho_2)} \right]_{C-J} = 0 \quad (4-47)$$

Thus, we can conclude that the entropy has a maximum or minimum at the C-J points. In order to determine which it is, we have to obtain the second derivative of s_2 with respect to $1/\rho_2$. Differentiating Eq. (4-46), we have

$$T_2 \left[\frac{d^2 s_2}{d(1/\rho_2)^2} \right]_{C-J} = \frac{1}{2} \left(\frac{1}{\rho_1} - \frac{1}{\rho_2} \right) \times \left[\frac{d^2 p_2}{d(1/\rho_2)^2} - \frac{1}{1/\rho_2 - 1/\rho_1} \frac{dp_2}{d(1/\rho_2)} \right. \\ \left. + \frac{p_2 - p_1}{(1/\rho_2 - 1/\rho_1)^2} \right]_{C-J} \quad (4-48)$$

or

$$\left[\frac{d^2 s_2}{d(1/\rho_2)^2} \right]_{C-J} = \frac{1}{2T_2} \left(\frac{1}{\rho_1} - \frac{1}{\rho_2} \right) \left[\frac{d^2 p_2}{d(1/\rho_2)^2} \right]_{C-J} \\ + \frac{1}{2} \left\{ \frac{dp_2}{d(1/\rho_2)} - \frac{p_2 - p_1}{1/\rho_2 - 1/\rho_1} \right\}_{C-J} \frac{1}{T_2}$$

Using Eq. (4-33), the last term in the above equation vanishes, so we have

$$\left[\frac{d^2 s_2}{d(1/\rho_2)^2} \right]_{C-J} = \frac{1}{2T_2} \left(\frac{1}{\rho_1} - \frac{1}{\rho_2} \right) \left[\frac{d^2 p_2}{d(1/\rho_2)^2} \right]_{C-J} \quad (4-49)$$

From the shape of the Hugoniot curve (Fig. 4.2), we observe that

$$\frac{d^2 p_2}{d(1/\rho_2)^2} > 0 \quad \text{for every point} \quad (4-50)$$

This inequality will be shown later after we have introduced the asymptotes of the Hugoniot curve.

For the upper C-J point U , we have $1/\rho_1 > 1/\rho_2$, and Eq. (4-49) gives

$$\left[\frac{d^2 s_2}{d(1/\rho_2)^2} \right]_U > 0 \quad (4-51)$$

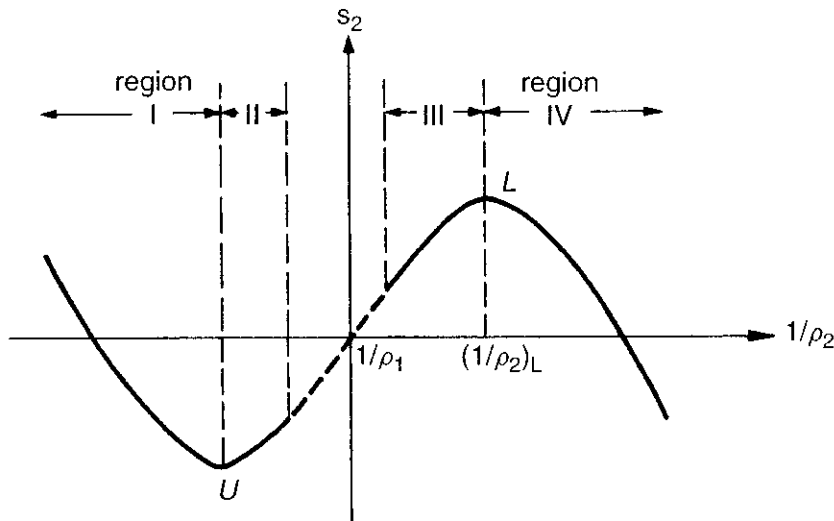


Figure 4.5 Solution regions on the Hugoniot curves.

This shows that entropy has a minimum at point U . For the lower C-J point L , we have $1/\rho_1 < 1/\rho_2$, and Eq. (4-49) gives

$$\left[\frac{d^2 s_2}{d(1/\rho_2)^2} \right]_L < 0 \quad (4-52)$$

This shows that entropy has a maximum at point L . The entropy distribution thus appears as shown in Fig. 4.5.

3.2 Comparison of the Burned-Gas Velocity behind a Detonation Wave with the Local Speed of Sound

Since the entropy s is a function of p and $1/\rho$,

$$ds = \left[\frac{\partial s}{\partial(1/\rho)} \right]_p d\left(\frac{1}{\rho}\right) + \left[\frac{\partial s}{\partial p} \right]_{1/\rho} dp \quad (4-53)$$

The speed of sound of the burned gases can be obtained from the consideration of an adiabatic reversible (isentropic) process. By setting $ds = 0$, Eq. (4-53) reduces to

$$\left[\frac{\partial p}{\partial(1/\rho)} \right]_s = - \frac{[\partial s / \partial(1/\rho)]_p}{[\partial s / \partial p]_{1/\rho}} \quad (4-54)$$

We use the subscript HC to represent that the derivative is being taken along the Hugoniot curve. From Eq. (4-53) we know that

$$\left[\frac{\partial s}{\partial(1/\rho)} \right]_{HC} = \left[\frac{\partial s}{\partial(1/\rho)} \right]_p + \left[\frac{\partial s}{\partial p} \right]_{1/\rho} \left[\frac{\partial p}{\partial(1/\rho)} \right]_{HC} \quad (4-55)$$

After rearranging, we have

$$\left[\frac{\partial p}{\partial(1/\rho)} \right]_{HC} = \frac{1}{[\partial s/\partial p]_{1/\rho}} \left\{ \left[\frac{\partial s}{\partial(1/\rho)} \right]_{HC} - \left[\frac{\partial s}{\partial(1/\rho)} \right]_s \right\} \quad (4-55a)$$

Subtracting Eq. (4-54) from Eq. (4-55a) yields

$$\left[\frac{\partial p}{\partial(1/\rho)} \right]_{HC} - \left[\frac{\partial p}{\partial(1/\rho)} \right]_s = \frac{[\partial s/\partial(1/\rho)]_{HC}}{[\partial s/\partial p]_{1/\rho}} \quad (4-56)$$

At C-J points, we have

$$\left[\frac{\partial s}{\partial(1/\rho)} \right]_{HC} = 0 \quad (4-57)$$

Thus, Eqs. (4-56) implies that

$$\left[\frac{\partial p}{\partial(1/\rho)} \right]_{HC} = \left[\frac{\partial p}{\partial(1/\rho)} \right]_s \quad \text{at C-J points} \quad (4-58)$$

This means that the tangent lines to the Hugoniot curve on a p -versus- $1/\rho$ plot at C-J points are also the tangents to the constant-entropy line.

After rearranging Eq. (4-46) and combining with Eq. (4-56), we have

$$\frac{2T_2}{1/\rho_1 - 1/\rho_2} \left[\frac{\partial s}{\partial(1/\rho)} \right]_{HC} + \frac{p_2 - p_1}{1/\rho_2 - 1/\rho_1} - \left[\frac{\partial p}{\partial(1/\rho)} \right]_s = \frac{[\partial s/\partial(1/\rho)]_{HC}}{[\partial s/\partial p]_{1/\rho}} \quad (4-59)$$

Using Eq. (4-19) and rearranging the above equation, we get

$$-\rho_2^2 u_2^2 + \rho_2^2 \left[\frac{\partial p_2}{\partial \rho_2} \right]_s = \left[\frac{\partial s}{\partial(1/\rho)} \right]_{HC} \left[\frac{-2T_2}{1/\rho_1 - 1/\rho_2} + \frac{1}{[\partial s/\partial p]_{1/\rho}} \right] \quad (4-60)$$

Based on the definition of the speed of sound, we know that

$$\rho_2^2 \left[\frac{\partial p_2}{\partial \rho_2} \right]_s = \rho_2^2 c_2^2 \quad (4-61)$$

Substituting Eq. (4-61) into Eq. (4-60), we have

$$-\rho_2^2 u_2^2 + \rho_2^2 c_2^2 = \left[\frac{\partial s}{\partial(1/\rho)} \right]_{HC} \left[\frac{-2T_2}{1/\rho_1 - 1/\rho_2} + \frac{1}{[\partial s/\partial p]_{1/\rho}} \right] \quad (4-62)$$

We note that if the right-hand side of Eq. (4-62) is positive in region I, then

$$c_2^2 > u_2^2 \quad (4-63)$$

which implies that the burned-gas velocity is subsonic.

From Fig. 4.5 we know that in region I

$$\left[\frac{\partial s}{\partial(1/\rho)} \right]_{\text{HC}} < 0 \quad (4-64)$$

and the right-hand side of Eq. (4-62) will be positive if

$$\frac{2T_2}{1/\rho_1 - 1/\rho_2} > \frac{1}{[\partial s/\partial p]_{1/\rho}} \quad (4-65)$$

In order to prove the above inequality, the partial derivative term on the right-hand side of inequality (4-65) must be first replaced by an algebraic term involving the properties of the gases at the burned end, since $[\partial s/\partial p]_{1/\rho}$ represents the change of entropy of the burned gases with respect to p_2 when $1/\rho_2$ is held constant. Differentiating Eq. (4-40), we have

$$dh = de + p d\left(\frac{1}{\rho}\right) + \frac{1}{\rho} dp \quad (4-66)$$

The first law of thermodynamics gives

$$dh = T ds + \frac{1}{\rho} dp \quad (4-67)$$

For mixtures with constant C_p , we have

$$C_p dT = T ds + \frac{1}{\rho} dp \quad (4-68)$$

From the perfect-gas law,

$$T = \frac{p}{\rho R} \quad (4-69)$$

$$dT = \frac{1}{\rho R} dp + \frac{p}{R} d\left(\frac{1}{\rho}\right) \quad (4-70)$$

Substituting Eq. (4-70) and Eq. (4-24) into Eq. (4-68) yields

$$\frac{\gamma}{\gamma-1} R \left[\frac{1}{\rho R} dp + \frac{p}{R} d\left(\frac{1}{\rho}\right) \right] = T ds + \left(\frac{1}{\rho} \right) dp \quad (4-71)$$

Substituting Eq. (4-69) into Eq. (4-71) to eliminate T , and solving for ds , we have

$$ds = \frac{\gamma R}{\gamma - 1} \rho d \left(\frac{1}{\rho} \right) + \frac{1}{(\gamma - 1)\rho T} dp \quad (4-72)$$

$$\left[\frac{\partial s}{\partial p} \right]_{1/\rho} = \frac{1}{(\gamma - 1)\rho T} \quad (4-73)$$

Using Eq. (4-73), the second factor on the right-hand side of Eq. (4-62) becomes

$$\frac{-2T_2}{1/\rho_1 - 1/\rho_2} + \frac{1}{[\partial s / \partial p]_{1/\rho}} = \frac{-2T_2}{1/\rho_1 - 1/\rho_2} + (\gamma - 1)\rho_2 T_2 \quad (4-74)$$

It can also be written in the following form after some algebraic manipulations:

$$\frac{-2T_2}{1/\rho_1 - 1/\rho_2} + \frac{1}{[\partial s / \partial p]_{1/\rho}} = \frac{p_2}{R} \left[\gamma - \frac{1 + (\rho_1/\rho_2)}{1 - (\rho_1/\rho_2)} \right] \quad (4-75)$$

In order to prove that $c_2 > u_2$ in region I, we need to show that

$$\gamma - \frac{1 + (\rho_1/\rho_2)}{1 - (\rho_1/\rho_2)} < 0 \quad (4-76)$$

The Rankine-Hugoniot relation given by Eq. (4-27) can be arranged to give

$$\frac{\gamma + 1}{2(\gamma - 1)} \frac{p_2}{\rho_2} - \frac{1}{2} \frac{p_2}{\rho_1} + \frac{p_1}{2\rho_2} - \frac{\gamma + 1}{2(\gamma - 1)} \frac{p_1}{\rho_1} - q = 0 \quad (4-77)$$

This is the equation of a hyperbola in the $p_2 - 1/\rho_2$ plane. To represent p_2 in terms of $1/\rho_2$, we have

$$p_2 = \frac{q + \frac{\gamma + 1}{2(\gamma - 1)} \frac{p_1}{\rho_1} + \left[-\frac{p_1}{2} \right] \frac{1}{\rho_2}}{-\frac{1}{2} \frac{1}{\rho_1} + \left[\frac{\gamma + 1}{2(\gamma - 1)} \right] \frac{1}{\rho_2}} = \frac{a + \frac{b}{\rho_2}}{c + \frac{d}{\rho_2}} \quad (4-78)$$

where

$$a = q + \frac{\gamma + 1}{2(\gamma - 1)} \frac{p_1}{\rho_1} \quad (4-79)$$

$$b = -\frac{p_1}{2} \quad (4-80)$$

$$c = -\frac{1}{2\rho_1} \quad (4-81)$$

$$d = \frac{\gamma + 1}{2(\gamma - 1)} \quad (4-82)$$

Solving Eq. (4-78) for $1/\rho_2$, we have

$$\frac{1}{\rho_2} = \frac{a - cp_2}{-b + dp_2} \quad (4-83)$$

The vertical asymptote of the Hugoniot curve is determined by setting the denominator of Eq. (4-78) equal to zero, i.e.,

$$c + \frac{d}{\rho_2} = 0$$

or

$$\left(\frac{1}{\rho_2}\right)_{\min} = -\frac{c}{d} = \frac{(\gamma - 1)}{(\gamma + 1)} \frac{1}{\rho_1} \quad (4-84)$$

Similarly, the horizontal asymptote is determined by $p_2 = b/d$, or

$$(p_2)_{\min} = -\left(\frac{\gamma - 1}{\gamma + 1}\right) p_1 \quad (4-85)$$

From the vertical asymptote, we know that any solution on the Hugoniot curve must satisfy the following inequality:

$$\frac{1}{\rho_2} > \left(\frac{\gamma - 1}{\gamma + 1}\right) \frac{1}{\rho_1} \quad (4-86)$$

or

$$(\gamma + 1) \frac{\rho_1}{\rho_2} > \gamma - 1 \quad (4-86a)$$

or

$$\left(1 + \frac{\rho_1}{\rho_2}\right) > \gamma \left(1 - \frac{\rho_1}{\rho_2}\right) \quad (4-86b)$$

For region I,

$$1 - \frac{\rho_1}{\rho_2} > 0 \quad (4-87)$$

Dividing both sides of Eq. (4-86b) by this positive quantity, we have

$$\frac{1 + (\rho_1/\rho_2)}{1 - (\rho_1/\rho_2)} > \gamma \quad \text{for region I} \quad (4-88)$$

The above inequality together with Eqs. (4-75) and (4-62) shows that

$$c_2 > u_2 \quad \text{for region I} \quad (4-89)$$

This means that the velocity of the burned gas at any point above the upper C-J point U is subsonic. If we consider the laboratory coordinates, then V_w is

the speed of the detonation wave relative to the tube, and $V_w = v_2 + u_2$ [see Eq. (4-37)]. Using this relationship, Eq. (4-89) becomes

$$c_2 > V_w - v_2$$

or

$$c_2 + v_2 > V_w \quad \text{for region I} \quad (4-90)$$

This equation implies that the resultant propagation velocity of any disturbance in the wave motion direction (as the sum of gas particle velocity v_2 and any disturbance propagation velocity c_2) can catch up with the wave propagation velocity, V_w . Physically, it means that any rarefaction disturbances behind the detonation wave can propagate at a higher speed than the wave. Therefore, they catch up with the detonation wave and reduce its strength. Thus, any solution in region I falls back to the upper C-J point, U .

In the previous derivation, we assumed that the shape of the Hugoniot curve satisfying the inequality given by Eq. (4-50). This inequality can be proved by using the asymptotic limits. By differentiating Eq. (4-78) with respect to $1/\rho_2$, we have

$$\frac{dp_2}{d(1/\rho_2)} = \frac{bc - ad}{(c + d/\rho_2)^2} \quad (4-91)$$

and

$$\frac{d^2 p_2}{d(1/\rho_2)^2} = \frac{-2d(bc - ad)}{(c + d/\rho_2)^3} \quad (4-92)$$

From the vertical asymptote (4-84), it can be shown that $c/d = -(1/\rho_2)_{\min}$; therefore,

$$\left(\frac{c}{d} + \frac{1}{\rho_2}\right) > 0 \quad \text{or} \quad \left(c + \frac{d}{\rho_2}\right)^3 > 0 \quad (4-93)$$

Also,

$$\begin{aligned} bc - ad &= \frac{p_1}{4\rho_1} - \frac{\gamma + 1}{2(\gamma - 1)}q - \frac{(\gamma + 1)^2}{4(\gamma - 1)^2} \frac{p_1}{\rho_1} \\ &= - \left[\frac{\gamma}{(\gamma - 1)^2} \frac{p_1}{\rho_1} + \frac{\gamma + 1}{2(\gamma - 1)}q \right] \end{aligned} \quad (4-94)$$

Since the quantity in the square brackets is always positive for exothermic reactions, $bc - ad$ is less than zero. Based on Eqs. (4-93), (4-94), and (4-82), we have

$$\frac{d^2 p_2}{d(1/\rho_2)^2} > 0 \quad (4-95)$$

The solution in region II is ruled out in view of the ZND detonation wave structure,⁵ which will be discussed in Section 5. In summary, the commonly

observed detonation waves usually correspond to the upper C–J point, and the commonly observed deflagration waves lie in region III of the Hugoniot curve as shown in Fig. 4.4. Chapter 5 is devoted to the determination of the eigenvalue (the actual laminar flame speed) on the weak-deflagration branch.

4 DETERMINATION OF CHAPMAN-JOUQUET DETONATION-WAVE VELOCITY

The detonation velocity u_1 is obviously of great interest to combustion scientists and engineers. Many articles describe methods for the calculation of C–J detonation-wave velocities.^{5–15} The calculation methods can be divided into two categories. First are trial-and-error methods,^{5–9} and second are Newton–Raphson iteration methods.^{10–15} The trial-and-error calculations are generally inferior to Newton–Raphson calculations for two reasons. First, the former give less precision for an equivalent amount of calculation. Second, their success often depends on the intuition of the person performing the calculations in obtaining successive approximations to the solution. To understand their differences, we shall discuss both methods in the following.

4.1 Trial-and-Error Method

The speed of sound behind a detonation wave is given by

$$c_2 = \sqrt{\left[\frac{\partial p_2}{\partial \rho_2} \right]_s} \quad (4-96)$$

Since $u_2 = c_2$ at the upper C–J point, using Eqs. (4-12) and (4-96), we have

$$u_1 = \frac{1}{\rho_1} c_2 \rho_2 = \frac{1}{\rho_1} \sqrt{\rho_2^2 \left[\frac{\partial p_2}{\partial \rho_2} \right]_s} = \frac{1}{\rho_1} \sqrt{- \left[\frac{\partial p_2}{\partial (1/\rho_2)} \right]_s} \quad (4-97)$$

The isentropic relation for the burned gas can be written as

$$p_2 \left(\frac{1}{\rho_2} \right)^{\gamma_2} = \text{constant} \quad (4-98)$$

Differentiating the above equation and rearranging, we obtain

$$-\left[\frac{\partial p_2}{\partial (1/\rho_2)} \right]_s = \frac{\gamma_2 p_2}{1/\rho_2} \quad (4-99)$$

Substituting this expression into Eq. (4-97), we have

$$u_1 = \frac{1/\rho_1}{1/\rho_2} \sqrt{\gamma_2 p_2 \frac{1}{\rho_2}} = \frac{\rho_2}{\rho_1} \sqrt{\gamma_2 R_2 T_2} \quad (4-100)$$

This equation is useful, but insufficient to determine u_1 , since the properties at the burned end are not known. A different form of Eq. (4-100) can be written as

$$\rho_1^2 u_1^2 = \gamma_2 p_2 \rho_2 \quad (4-101)$$

Substituting into the Rayleigh-line relation (4-19), we get

$$\frac{1}{\rho_1} - \frac{1}{\rho_2} = \frac{p_2 - p_1}{\gamma_2 p_2 \rho_2} \quad (4-102)$$

Substituting Eq. (4-102) into Eq. (4-43), we have

$$e_2 - e_1 = \frac{1}{2} (p_2^2 - p_1^2) \frac{1}{\gamma_2 p_2 \rho_2} \quad (4-103)$$

Making an acceptable approximation for the detonation wave that

$$p_2^2 \gg p_1^2$$

then Eq. (4-103) becomes

$$e_2 - e_1 \approx \frac{1}{2} p_2 \frac{1}{\gamma_2 \rho_2} = \frac{R_2 T_2}{2 \gamma_2} \quad (4-104)$$

The molar form of Eq. (4-104) can be obtained by multiplying the above equation by the molecular weight M_{w2} :

$$e_2 M_{w2} - \frac{M_{w2}}{M_{w1}} e_1 M_{w1} = \frac{1}{2} \frac{R_u T_2}{\gamma_2} \quad (4-105)$$

where $e_2 M_{w2}$ and $e_1 M_{w1}$ represent the molar internal energy of the products and reactants, respectively.

Multiplying Eq. (4-102) by a factor of $(p_2 + p_1)$, we have

$$(p_1 + p_2) \left(\frac{1}{\rho_1} - \frac{1}{\rho_2} \right) = (p_2^2 - p_1^2) \frac{1}{\gamma_2 p_2 \rho_2} \quad (4-106)$$

Again assuming that $p_2^2 \gg p_1^2$, and expanding the left-hand side, Eq. (4-106) becomes

$$\frac{p_1}{\rho_1} - \frac{p_1}{\rho_2} + \frac{p_2}{\rho_1} - \frac{p_2}{\rho_2} = \frac{p_2}{\gamma_2 \rho_2} \quad (4-107)$$

Using the equation of state to eliminate p_1 and p_2 , the above equation becomes

$$R_1 T_1 - \frac{\rho_1}{\rho_2} R_1 T_1 + \frac{\rho_2}{\rho_1} R_2 T_2 - R_2 T_2 = \frac{R_2 T_2}{\gamma_2} \quad (4-108)$$

Multiplying by $\rho_2/(\rho_1 R_2 T_2)$ and rearranging, the approximate Rayleigh-line relation gives

$$\left(\frac{\rho_2}{\rho_1}\right)^2 - \left(\frac{1}{\gamma_2} + 1 - \frac{R_1 T_1}{R_2 T_2}\right) \left(\frac{\rho_2}{\rho_1}\right) - \frac{R_1 T_1}{R_2 T_2} = 0 \quad (4-109)$$

Equation (4-109) allows us to solve for ρ_2/ρ_1 in terms of T_2 . Also, using the equation of state, p_2 is related to ρ_2/ρ_1 and T_2 by

$$p_2 = \left(\frac{\rho_2}{\rho_1}\right) \left(\frac{R_2 T_2}{R_1 T_1}\right) p_1 \quad (4-110)$$

Using the above relations, the C–J detonation velocity u_1 can be determined according to the following iteration procedure:

1. Assume p_2 .
2. Assume T_2 .
3. Calculate the equilibrium composition based on T_2 and p_2 .
4. From the equilibrium composition, find γ_2 , R_2 , e_2 .
5. Check the approximate Rankine–Hugoniot equation [Eq. (4-104)] to see whether the calculated e_2 , γ_2 , and R_2 and the assumed T_2 satisfy the equation. If not, go back to step 2 and reassume another T_2 . If equation is satisfied, proceed to step 6.
6. Solve for ρ_2/ρ_1 from Eq. (4-109).
7. Find p_2 from Eq. (4-110). If the calculated p_2 equals the assumed p_2 , then the iteration sequence has converged. Otherwise, go to step 1 and assume a new p_2 .
8. Calculate the detonation velocity u_1 from Eq. (4-100).

Note: A quick way to have a good guess of the value of ρ_2/ρ_1 is to assume that $p_2 \gg p_1$ (see Table 4.1). By doing so, Eq. (4-102) reduces to

$$\frac{1}{\rho_1} - \frac{1}{\rho_2} = \frac{1}{\gamma_2 \rho_2} \quad (4-111)$$

or

$$\frac{\rho_2}{\rho_1} \approx \frac{\gamma_2 + 1}{\gamma_2} \quad (4-112)$$

This equation is useful, since an excellent guess of the value of γ_2 can be easily made. One can thus obtain a good guess for p_2 .

4.2 The Newton–Raphson Iteration Method

The general iterative method for obtaining the C–J detonation-wave velocity to be described below is based on those of Refs. 14 and 15. The method of Eisen^{10,11}

also uses the Newton–Raphson iteration procedure¹⁶ for obtaining successive approximations to roots of algebraic equations. However, Eisen's method requires at least four and often more separate solutions of the detonation equations to obtain the desired C–J solution. His interpolation scheme can easily lead to inaccurate estimates of the detonation velocity. The methods used by McGill¹² and Luker,¹³ although following the same general Newton–Raphson iteration method, encounter some severe oscillations due to the omission of the changes in composition and heats of reaction with respect to temperature and pressure. The method developed by Zeleznik and Gordon,¹⁴ and programmed by Gordon and McBride,¹⁵ is considered to be the best among all the Newton–Raphson iteration methods and is described below.

There are three steps in the Gordon–McBride calculation procedure. The first step is an initial estimation of the detonation pressure and temperature. The second is an improved estimation of these parameters by means of a recursion formula. The third is obtaining the correct values by means of a Newton–Raphson iteration procedure. The derivation of the required equations is given in Ref. 14, and they are summarized here in slightly modified form. The conservation equations (4-12), (4-13), and (4-14a) for continuity, momentum, and energy, with the additional constraint $u_2 = c_2$, were reduced to the following two equations:

$$\frac{p_1}{p_2} = \underbrace{1 - \gamma_{s,2} \left(\frac{\rho_2}{\rho_1} - 1 \right)}_{p''} \quad (4-113)$$

$$h_2 = h_1 + \frac{R_u \gamma_{s,2} T_2}{2 M w_2} \left[\left(\frac{\rho_2}{\rho_1} \right)^2 - 1 \right] = h'' \quad (4-114)$$

where γ_s represents the exponent used in Eq. (4-98) for an isentropic process; it can be expressed as

$$\gamma_s = \left[\frac{\partial \ln p}{\partial \ln \rho} \right]_s \quad (4-115)$$

It should be noted that γ_s in general is not equal to the ratio of specific heats. Equations (4-113) and (4-114) can be rearranged to give the well-known Rankine–Hugoniot equation (4-30). However, in order to facilitate numerical calculations of detonation velocity, Zeleznik, Gordon, and McBride^{14,15} chose to use Eqs. (4-113) and (4-114) rather than use the Hugoniot equation directly.

For convenience in writing the iteration equations, the symbols p'' and h'' are used to represent the right sides of Eqs. (4-113) and (4-114), respectively. These equations then become

$$p'' - \frac{p_1}{p_2} = 0 \quad (4-116)$$

$$h'' - h_2 = 0 \quad (4-117)$$

Applying the Newton-Raphson method to Eqs. (4-116) and (4-117) divided by R_u , and using the logarithms of the temperature ratio and the pressure ratio across the detonation wave as independent variables, we have

$$\frac{\partial(p'' - p_1/p_2)}{\partial \ln(p_2/p_1)} \Delta \ln \frac{p_2}{p_1} + \frac{\partial(p'' - p_1/p_2)}{\partial \ln(T_2/T_1)} \Delta \ln \frac{T_2}{T_1} = \frac{p_1}{p_2} - p'' \quad (4-118)$$

$$\frac{\partial[(h'' - h_2)/R_u]}{\partial \ln(p_2/p_1)} \Delta \ln \frac{p_2}{p_1} + \frac{\partial[(h'' - h_2)/R_u]}{\partial \ln(T_2/T_1)} \Delta \ln \frac{T_2}{T_1} = \frac{h_2 - h''}{R_u} \quad (4-119)$$

where $\Delta \ln(p_2/p_1)$ represents the difference $\ln(p_2/p_1)_{k+1} - \ln(p_2/p_1)_k$, and the subscript k stands for the k th iteration. A similar expression is used for $\Delta \ln(T_2/T_1)$.

The partial derivatives appearing in Eqs. (4-118) and (4-119) can be evaluated if γ_s is taken to be independent of temperature and pressure. Within the accuracy of this assumption, the partial derivatives are

$$\frac{\partial(p'' - p_1/p_2)}{\partial \ln(p_2/p_1)} = \frac{p_1}{p_2} - \gamma_{s,2} \left(\frac{\rho_2}{\rho_1} \right) \left(\frac{\partial \ln \rho}{\partial \ln p} \right)_{T,2} \quad (4-120)$$

$$\frac{\partial(p'' - p_1/p_2)}{\partial \ln(T_2/T_1)} = -\gamma_{s,2} \left(\frac{\rho_2}{\rho_1} \right) \left(\frac{\partial \ln \rho}{\partial \ln T} \right)_{p,2} \quad (4-121)$$

$$\begin{aligned} \frac{\partial[(h'' - h_2)/R_u]}{\partial \ln(p_2/p_1)} &= \frac{\gamma_{s,2} T_2}{2Mw_2} \left\{ \left(\frac{\rho_2}{\rho_1} \right)^2 - 1 + \left(\frac{\partial \ln \rho}{\partial \ln p} \right)_{T,2} \left[1 + \left(\frac{\rho_2}{\rho_1} \right)^2 \right] \right\} \\ &\quad - \frac{T_2}{Mw_2} \left[\left(\frac{\partial \ln \rho}{\partial \ln T} \right)_{p,2} + 1 \right] \end{aligned} \quad (4-122)$$

$$\frac{\partial[(h'' - h_2)/R_u]}{\partial \ln(T_2/T_1)} = \frac{\gamma_{s,2} T_2}{2Mw_2} \left[\left(\frac{\rho_2}{\rho_1} \right)^2 - 1 \right] \left(\frac{\partial \ln \rho}{\partial \ln T} \right)_{p,2} - \frac{T_2(C_p)_2}{R_u} \quad (4-123)$$

To perform calculations, the equation of state for the products of reaction must be known. In Refs. 14 and 15, consideration is given only to the case where the products of reaction obey the perfect-gas law $pMw = \rho R_u T$. From the equation of state, it follows that

$$\left[\frac{\partial \ln \rho}{\partial \ln p} \right]_T = \left[\frac{\partial \ln Mw}{\partial \ln p} \right]_T + 1 \quad (4-124)$$

$$\left[\frac{\partial \ln \rho}{\partial \ln T} \right]_p = \left[\frac{\partial \ln Mw}{\partial \ln T} \right]_p - 1 \quad (4-125)$$

The evaluation of the derivatives of the molecular weight appearing in the above equations is discussed in detail in Ref. 17. It should be noted that derivatives of the molecular weight generally have some effect on the convergence and

cannot be neglected unless they are small relative to unity. Zeleznik and Gordon¹⁴ showed that the omission of these derivatives can result in oscillations.

Gordon and McBride¹⁵ reported that a good initial estimate for the pressure ratio is not as important as a good estimate for the temperature ratio. For a number of chemical systems that were investigated, an initial estimate of $(p_2/p_1)_0 = 15$ has been found to be satisfactory. An initial estimate for the temperature ratio is found by calculating the flame temperature T_2 corresponding to the following enthalpy (see Ref. 14 for details):

$$h_2 = h_1 + \frac{3}{4} \frac{R_u T_1}{\text{Mw}_1} \left(\frac{p_2}{p_1} \right)_0 \quad (4-126)$$

Improved initial assumed values of $(p_2/p_1)_0$ and estimated values of $(T_2/T_1)_0$ corresponding to h_2 in Eq. (4-126) can be obtained by the use of the following recursion formulas:

$$\left(\frac{p_2}{p_1} \right)_{k+1} = \frac{1 + \gamma_{s,2}}{2\gamma_{s,2}\alpha_k} \left\{ 1 + \left[1 - \frac{4\gamma_{s,2}\alpha_k}{(1 + \gamma_{s,2})^2} \right]^{1/2} \right\} \quad (4-127)$$

$$\begin{aligned} \left(\frac{T_2}{T_1} \right)_{k+1} &= \left(\frac{T_2}{T_1} \right)_0 - \frac{3}{4} \frac{R_u}{\text{Mw}_1(C_p)_2} \left(\frac{p_2}{p_1} \right)_0 \\ &\quad + \frac{R_u \gamma_{s,2}}{2\text{Mw}_1(C_p)_2} \left(\frac{r_{k+1}^2 - 1}{r_{k+1}} \right) \left(\frac{p_2}{p_1} \right)_{k+1} \end{aligned} \quad (4-128)$$

where

$$\alpha_k \equiv \left(\frac{T_1}{T_2} \right)_k \left(\frac{\text{Mw}_2}{\text{Mw}_1} \right) \quad (4-129)$$

$$r_{k+1} \equiv \alpha_k \left(\frac{p_2}{p_1} \right)_{k+1} \quad (4-130)$$

The quantities Mw_2 , $\gamma_{s,2}$, and $(C_p)_2$ in Eqs. (4-127) to (4-129) are the equilibrium values for $(p_2/p_1)_0$ and $(T_2/T_1)_0$. Repeating the use of Eqs. (4-127) to (4-130) three times in the NASA-CEA program generally provides excellent initial estimates for the Newton-Raphson iteration.

An arbitrary control factor f_c is applied to the corrections obtained from solution of Eqs. (4-118) and (4-119) before getting improved estimates of $\ln(p_2/p_1)$ and $\ln(T_2/T_1)$ for the new iteration step. The value of f_c used by Gordon and McBride permits a maximum correction of 1.5 of the previous estimates of p_2/p_1 and T_2/T_1 . This is the same as permitting a maximum absolute correction of 0.4054652 on $\ln(p_2/p_1)$ and $\ln(T_2/T_1)$. The control factor is determined by the following equation:

$$f_c = \min \left[\frac{0.4054652}{|\Delta \ln(p_2/p_1)|}, \frac{0.4054652}{|\Delta \ln(T_2/T_1)|}, 1 \right] \quad (4-131)$$

Improved estimates are then obtained by using f_c and the following equations:

$$\begin{aligned}\ln\left(\frac{p_2}{p_1}\right)_{k+1} &= \ln\left(\frac{p_2}{p_1}\right)_k + f_c \left[\Delta \ln\left(\frac{p_2}{p_1}\right) \right]_k \\ \ln\left(\frac{T_2}{T_1}\right)_{k+1} &= \ln\left(\frac{T_2}{T_1}\right)_k + f_c \left[\Delta \ln\left(\frac{T_2}{T_1}\right) \right]_k\end{aligned}\quad (4-132)$$

The iteration process is continued until corrections obtained from Eqs. (4-118) and (4-119) meet the following criteria:

$$\begin{aligned}\left| \Delta \ln\left(\frac{p_2}{p_1}\right) \right| &< 0.00005 \\ \left| \Delta \ln\left(\frac{T_2}{T_1}\right) \right| &< 0.00005\end{aligned}\quad (4-133)$$

Convergence of Gordon and McBride's program can generally be reached in three to five iterations.

4.3 Comparison of Calculated Detonation-Wave Velocities with Experimental Data

The first critical test of the C-J theory for its prediction of the experimentally measured detonation velocity was carried out by Lewis and Friauf¹⁸ on mixtures of hydrogen and oxygen diluted with various gases. The dissociation equilibria considered were

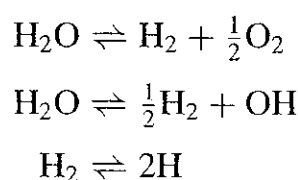


Table 4.2 gives a summary of the results for $p_1 = 1$ atm, $T_1 = 298$ K. It is quite evident that except for large excess of hydrogen, the agreement between the calculated and experimental velocities is very good.

Table 4.2 Comparison of Lewis and Friauf's Detonation-Velocity Data with the Calculated Results Based on Chapman-Jouquet Theory

Explosive Mixture	p_2 (atm)	T_2 (K)	u_1 (calc.) (m/s)	u_1 (expt.) (m/s)	Dissociation (mole %)
(2H ₂ + O ₂)	18.0	3583	2806	2819	32
(2H ₂ + O ₂) + O ₂	17.4	3390	2302	2314	30
(2H ₂ + O ₂) + N ₂	17.4	3367	2378	2407	18
(2H ₂ + O ₂) + 5N ₂	14.4	2685	1850	1822	2
(2H ₂ + O ₂) + 6H ₂	14.2	2650	3749	3532	1

The influence of species dissociation on the u_1 cannot be neglected. If dissociation is neglected (no H or OH species present), the calculated velocities are considerably larger, by several hundred meters per second, than the experimental data. The equilibrium concentrations of radicals (amount of dissociation shown in the last column) suggest that the chain-carrying concentration in the reaction zone must be very large indeed. This, together with the high temperature, provides an explanation for the extreme rapidity of the reaction (which supports the supersonic wave).

It is seen from Table 4.2 that dilution of the stoichiometric mixture with hydrogen results in an increase in the detonation velocity, despite the reduced temperature T_2 . This reflects the influence of the much-reduced density of the mixture, a result that suggests the performance of experiments with helium and argon as diluents. The addition of helium to a stoichiometric mixture should increase the velocity because of the decreased density of the initial mixture. On the other hand, the addition of argon should decrease the detonation velocity. These two inert gases are identical in their thermal effect, but affect the detonation velocity in opposite directions. How well this prediction is fulfilled can be seen from Table 4.3, obtained by Lewis and Friauf.¹⁸ The experimental fact that dilution with the inert gas helium increases the detonation velocity provides a particularly clear confirmation of the predictability of the detonation wave velocity by the simple theory.

Berets, Greene, and Kistiakowsky¹⁹ repeated the calculations made by Lewis and Friauf,¹⁸ using more accurate spectroscopic data, and obtained good agreement with the theoretical values of detonation velocities reported in Ref. 18 (about 1% difference). They further showed that the measured and calculated u_1 agree closely except for lean mixtures in the neighborhood of the limits of detonability. Under those conditions, the measured data are significantly below the theoretical values. These discrepancies were attributed²⁰ in early days to the lateral heat losses, which are not considered in the one-dimensional theory. More comparisons between the experimentally measured detonation velocities

Table 4.3 Effect of Diluent Concentration and Initial Density on Detonation-Wave Velocity^a

Explosive Mixture	p_2 (atm)	T_2 (K)	u_1 (calc.) (m/s)	u_1 (expt.) (m/s)
(2H ₂ + O ₂) + 5Ar	16.3	3097	1762	1700
(2H ₂ + O ₂) + 3Ar	17.1	3265	1907	1800
(2H ₂ + O ₂) + 1.5Ar	17.6	3412	2117	1950
(2H ₂ + O ₂)	18.0	3583	2806	2819
(2H ₂ + O ₂) + 1.5He	17.6	3412	3200	3010
(2H ₂ + O ₂) + 3He	17.1	3265	3432	3130
(2H ₂ + O ₂) + 5He	16.3	3097	3617	3160

^aData extracted from Lewis and Friauf¹⁸ and Lewis and von Elbe²⁰ with $P_1 = 1$ atm and $T_1 = 291$ K.

and theoretical results based upon the classical C-J theory can be found in the books by Lewis and von Elbe²⁰ and Strehlow.⁴⁸

In general, the classical C-J theory predicts properties of the bulk flow which ordinarily are in good agreement with measured values.²¹ However, poor agreement has been found for initial pressures, mixture compositions, and tube dimensions that are near the limit values for the occurrence of a constant-velocity propagating wave, as indicated by Strehlow.²¹ This disagreement has been attributed to multidimensional transverse structure, which is much more pronounced under these marginal conditions. Such detonation is termed *marginal*, and average frontal velocities as low as 85–90% of the C-J velocity are observed.

5 DETONATION-WAVE STRUCTURE

The understanding of detonation-wave structure has gone through a revolution due to great advances made in the 1960s by various researchers. The evolution from the classical one-dimensional point of view to the modern concepts of multidimensional wave structure can be found in several excellent comprehensive review papers, including those of Oppenheim, Manson, and Wagner,²² Strehlow,²³ Lee, Soloukhin, and Oppenheim,²⁴ Schott,²⁵ Shchelkin,²⁶ van Tiggenlen and de Soete,²⁷ and Oran.²⁸ Different numerical solution methods for detonation wave structures are discussed by Oran²⁸ and Oran, Boris, and Kailasanath.²⁹ To introduce some commonly used terminology in the field of detonation and also to appreciate the efforts involved in reaching this current understanding of detonation, we shall discuss both the classical and modern views.

5.1 Zel'dovich-von Neumann-Döring (ZND) One-Dimensional Wave Structure

A detonation wave can be produced in a long shock tube with combustible gaseous mixture loaded in the low-pressure (driven) side of the shock tube. The high-pressure (driver) side of the shock tube can be charged initially with a low-molecular-weight gas (such as helium) to facilitate the expansion process. At time zero, the diaphragm separating the driver and driven sides of the shock tube is ruptured and a shock wave of known strength is propagating into the combustible mixture. The passage of the incident shock raises the temperature and pressure of the reactive gas. When the shock hits the wall at the end of the tube, it reflects and raises the temperature and pressure of the gas behind the shock even higher. A strong igniter is initiated a very short time after the reflected shock wave starts to travel in the reverse direction. After a short ignition delay time, the gas mixture first ignites near the reflecting wall and a reaction wave is formed behind the propagating shock wave. This reaction wave travels at a higher speed than the shock wave. After some time, the reaction wave catches up with the propagating shock wave and merges with it to form a detonation wave of a constant speed. This steady-state detonation wave can propagate continuously

into the combustible mixture at a supersonic speed. Finally, it meets the contact discontinuity between the helium and reactive gas mixture.

Extending the classical C-J theory,^{2,3} Zel'dovich,³⁰ von Neumann,³¹ and Döring³² independently assumed that the flow is strictly one-dimensional and steady relative to the detonation front. They postulated that the detonation wave consisted of a shock wave moving at the detonation velocity, with chemical reactions occurring behind the shock in a region much thicker than that of a typical shock wave. They considered that the shock wave initially heats the reactants to a temperature at which they can react at a rate high enough for the ensuing deflagration to propagate as fast as the shock wave. Their assumption of very limited reactions in the shock-wave region itself was based on the fact that the thickness of a shock wave is usually very small, in the order of a few mean free paths of the gas molecules. In view of the very small number of collisions between molecules within the shock wave, the major amount of heat release in a detonation wave was believed to occur in a thick region behind the shock wave.

Figure 4.6 shows the variation of physical properties through a one-dimensional ZND detonation wave. The magnitude of the pressure, temperature, and density immediately behind the shock (at station 1') depends on the fraction of gaseous mixture reacted. If the reaction rate follows the Arrhenius law, then the rate of reaction increases slowly in the region immediately behind the shock, where the temperature is not extremely high. As a result, the pressure, temperature, and density profiles are relatively flat in the region immediately behind the shock front. This region is therefore called the induction zone. After the induction period, the gas properties change sharply as the reaction rate increases drastically to high values. When the reaction is completed, the thermodynamic properties reach their equilibrium values. The physical distance between the shock front and the fully reacted station is on the order of 1 cm.

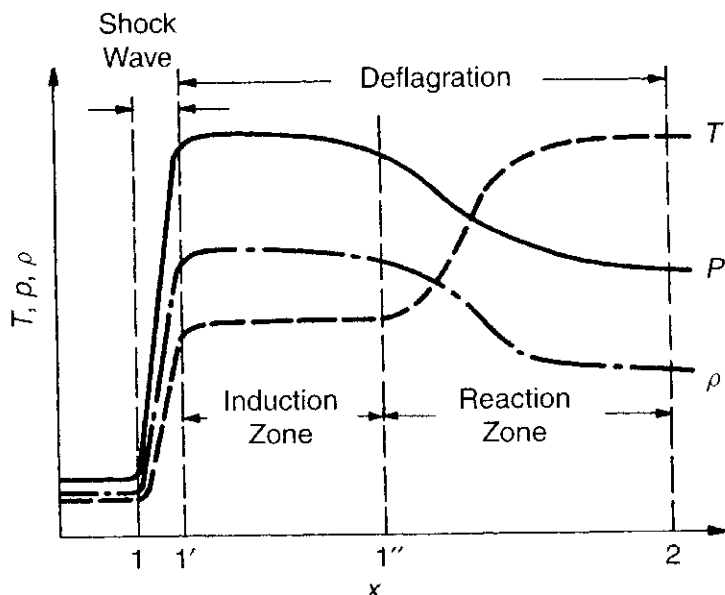


Figure 4.6 Variation of physical properties through a ZND detonation wave.

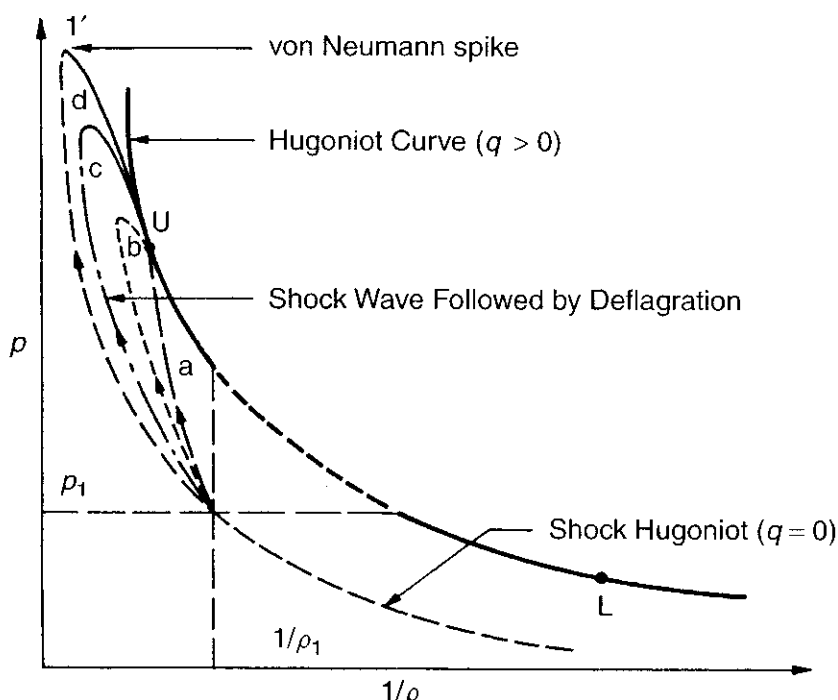


Figure 4.7 ZND detonation structure on $(p, 1/\rho)$ diagram.

The locus of the reacting mixture is shown on the Hugoniot plot in Fig. 4.7. As shown in the figure, there are many paths by which a reacting mixture may pass through the detonation wave from the unreacted state to the fully reacted state. All paths (*a*, *b*, *c*, etc.) can satisfy the conservation equations.

A gaseous mixture may enter the detonation wave in the state corresponding to the initial point $(l/\rho_1, p_1)$ and move directly to the upper C-J point by path *a*. However, this path would demand that reaction occur everywhere along the path. Since there is no significant compression in the beginning part of this path, there cannot be sufficient temperature to initiate any reaction. Thus, path *a* is very unlikely to have enough energy release to sustain the wave. Path *b* represents a possible locus for mixtures with fast chemical kinetics. For slow chemical kinetics, the path may be *c*. In the limit of zero chemical-energy release in the shock wave, the initial portion of path *d* will coincide with the shock Hugoniot curve. The peak pressure behind the shock wave in the ZND model is called the *von Neumann spike*.

According to the ZND model, there exist sharp pressure and density gradients at the front of the detonation wave. For detonations propagating into subatmospheric initial pressures, the sharp rises in pressure and density have been confirmed experimentally by several investigators, notably Kistiakowsky and his students,^{33,34} Wagner and his coworkers,³⁵⁻³⁸ Edwards and his coworkers,³⁹⁻⁴¹ White,⁴²⁻⁴⁴ and Fay.^{45,46}

However, the crucial question, whether the so-called von Neumann spike has been attained or not, could not be answered by these experiments, because their effective spatial resolution was insufficient. An extrapolation of the density profile, measured by the X-ray absorption technique,^{33,34} to the front of the reaction

zone demonstrated that a peak density of about 70% of the expected von Neumann spike was probably attained. Just and Wagner⁴⁷ measured, by means of a schlieren technique, a peak density that was 70 to 90% of the von Neumann spike value. The preliminary records of the pressure profile, obtained by Edwards et al.,⁴¹ can be extrapolated to a pressure peak that seems to be in fair agreement with the von Neumann spike.

It is worth pointing out that the state at the von Neumann spike is usually evaluated assuming complete equilibrium for different degrees of freedom. However, it is known in particular that the vibrational relaxation times of several species appearing in the vicinity of the von Neumann spike are on the order of a microsecond. In these cases, lower peak densities and higher pressures than those of the equilibrium von Neumann state can be expected to occur.

5.2 Multidimensional Detonation-Wave Structure

According to Strehlow,⁴⁸ the first evidence of multidimensional wave structure was obtained in 1926 by Campbell and Woodhead.⁴⁹ By observing spin in lean mixtures in circular tubes, they showed that detonation waves might prefer to travel in a manner that is locally three-dimensional and nonsteady. For more than 25 years after their discovery, spinning detonation was thought to be a phenomenon peculiar to lean mixtures. The detailed wave structure of self-sustaining detonation waves was not studied until Denisov and Troshin⁵⁰ adapted an experimental technique used initially by Antolik⁵¹ in 1875. Antolik used soot-coated plates near a spark discharge and recorded many thin lines on the smoked foil. These lines were interpreted much later as being caused by the intersection of "sound waves." Denisov and Troshin revived the technique in 1959 and first applied it to the observation of transverse waves in detonations. In effect, the smoked-foil method exploits the fact (realized by Denisov and Troshin) that the detonation, unlike any other singular wave process, could actually "write on the walls"; that is, it could leave a record of its passage in the form of an imprint on a film-coated wall, the most convenient material for this purpose being a thin layer of soot. Since 1959, the smoked-foil method has been extensively applied to the study of detonation structure. According to Strehlow,⁴⁸ wood smoke deposited in an almost opaque layer on the surface produces the best smoked-foil records. The foil may be "frozen" after firing by spraying it with a clear lacquer.

A few examples of smoked-foil records obtained with self-sustaining propagating detonation^{48,52} are shown in Figs. 4.8, 4.9, and 4.10. The reason that a propagating detonation wave is able to write on the walls is the presence of triple points at the intersecting lines of triple shock waves. The triple point (line) can be described using Fig. 4.11. In this figure, a steady supersonic two-dimensional flow, passing through a convergent ramp section from right to left, produces a shock-wave pattern as shown in the schematic diagram, when the ramp angle is very steep. The triple point (line) is the intersection point (line) of Mach-stem, incident, and reflected shocks. A slipstream is also generated in this situation. A detailed description of such flow configurations can be found in the book by Shapiro.⁵³



Figure 4.8 Smoked-foil record of equilibrium-configuration detonation (rectangular mode). The active width of this smoked foil is 8.26 cm. The detonation propagation from left to right: H₂-O₂ system, 40% argon, $p_1 = 60$ Torr, $\phi = 1$ (after R. A. Strehlow⁵²).



Figure 4.9 Smoked-foil record of a time-average steady detonation, illustrating the lack of an equilibrium configuration. The active width of this smoked foil is 8.26 cm. The detonation is propagating from left to right. 20% C₃H₈ - 80% O₂ system, $p_1 = 50$ Torr (after R. A. Strehlow⁵²).

The detonation-wave structure is characterized by a nonplanar leading shock wave, which at every instant consists of many curved shock sections that are convex toward the incoming flow. The lines of intersection of these curved shock segments are propagating in various directions at high velocities (see Fig. 4.10). The third shock (R in Fig. 4.11) of these intersections extends back into the reactive flow regime and is required for the flow to be balanced at the intersection of the two convex leading shock waves. In general, the flow in the neighborhood of the shock front is quite complex. The schematic diagram of symmetric planar interaction is shown in Fig. 4.10.

In agreement with the above wave-structure description, the interferogram of a self-sustained detonation (Fig. 4.12) obtained by White⁴³ (1961) shows an irregular pattern of the fringes in and behind the reaction zone, whereas the shock front itself is quite smooth and planar. Flash schlieren pictures taken by Fay⁴⁵

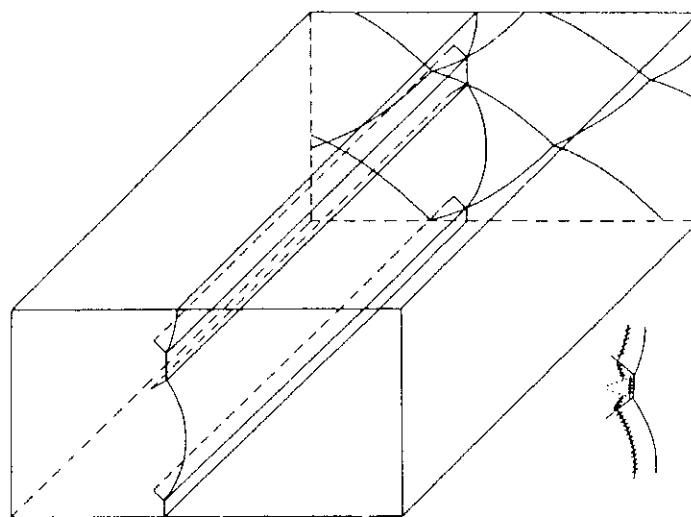
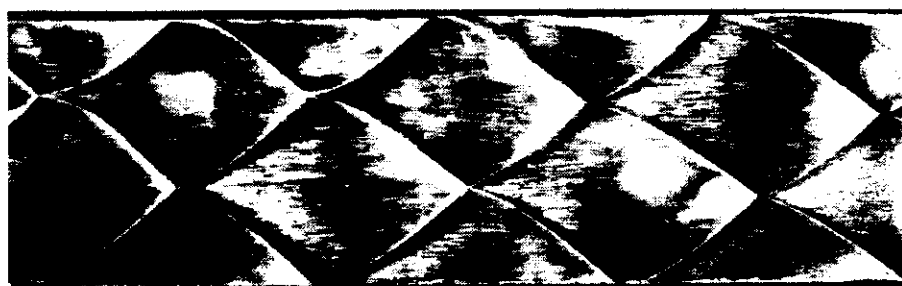
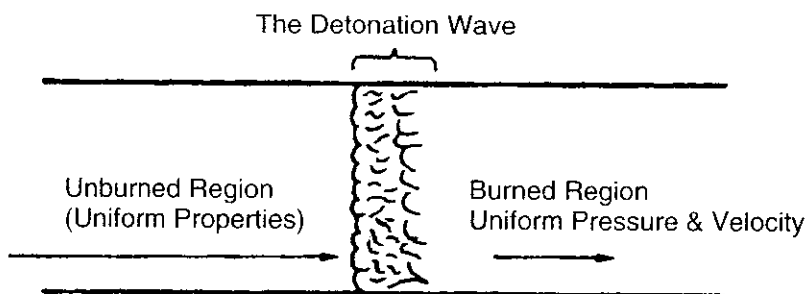


Figure 4.10 Smoked-foil record and schematic diagram of symmetric planar interaction (after R. A. Strehlow⁴⁸).

and Fay and Opel⁵⁴ demonstrated also that the shape of the reaction zone is irregular. On the basis of optical reflectivity measurements, Sastri et al.⁵⁵ concluded that detonations in $\text{H}_2 + 3\text{O}_2$ mixture show the wave front is neither planar nor smoothly curved.

5.3 Numerical Simulation of Detonations

Taki and Fujiwara⁵⁶ performed the first numerical simulations of the evolution to the triple point structure in detonations for low-pressure, stoichiometric H_2-O_2 mixtures heavily diluted with Ar. Their calculated results demonstrated that computer simulations could reproduce the types of shock and reaction-front structures characterizing detonations. Oran²⁸ indicated that there are some unreacted pockets of material behind the detonation front. Experiments also showed such pockets. The existence of unreacted pockets provides a multidimensional fluid-dynamic mechanism by which a detonation wave can become weaker or even die in a situation where, in one-dimension assumption, it might be expected to propagate. The cellular structure of the detonation front is shown in Fig. 4.13, based on the calculated pressure, temperature, density, and reaction variable contours by Oran.²⁸



Background : Mach Stem Structure in a Reactive Gas

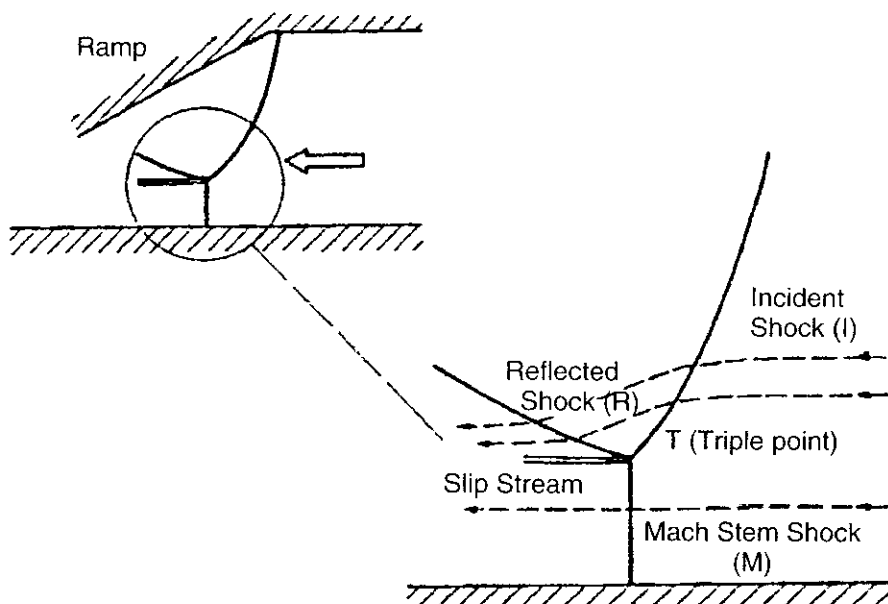


Figure 4.11 Schematic diagram showing the shock-wave pattern and triple point in a two-dimensional supersonic flow passing through a convergent ramp section.

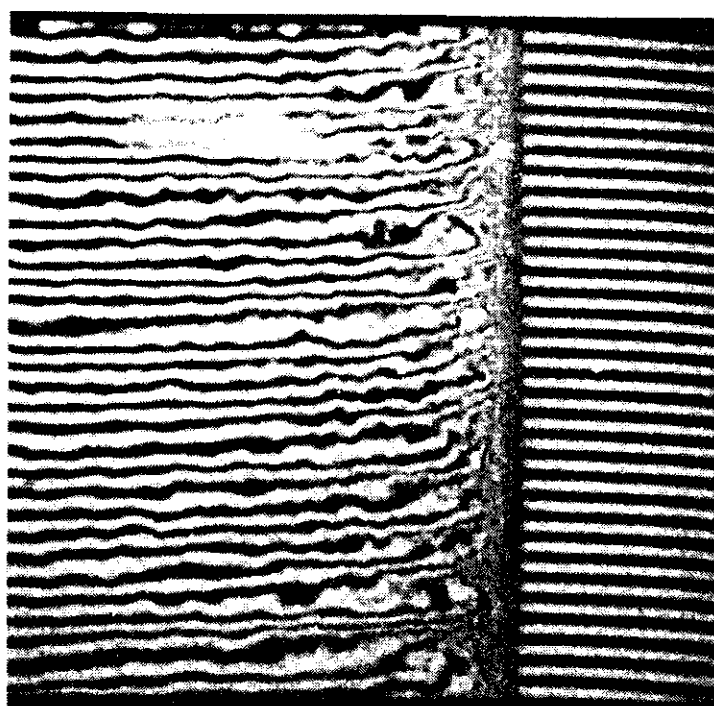


Figure 4.12 Interferogram, obtained by White,⁴³ of a self-sustained detonation in a $2\text{H}_2 + \text{O}_2 + 2\text{CO}$ mixture initially at 0.3-atm pressure and room temperature.

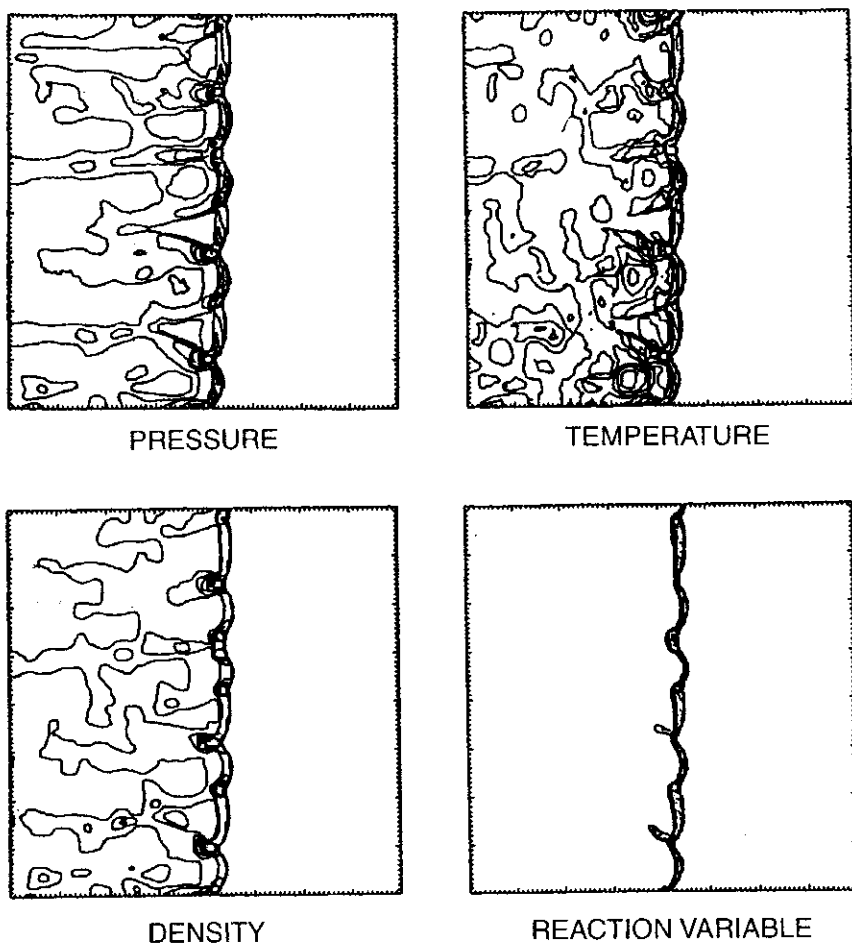


Figure 4.13 Pressure, temperature, density, and reaction variable contours showing the cellular structure of the detonation front (after Oran²⁸).

6 THE MECHANISM OF DEFLAGRATION-TO-DETONATION TRANSITION (DDT) IN GASEOUS MIXTURES

The current understanding of the DDT mechanism is presented in an excellent review by Oppenheim, Manson, and Wagner.²² This understanding has been achieved due largely to the recent development of laser schlieren photography, which has permitted the attainment of extremely short (less than 0.01 μs) light pulses at ultrahigh (up to $10^6/\text{s}$) repetition rate. This technique generates a stroboscopic set of still photographs that reveal many details of the DDT processes that could not be observed by any other means. Urtiew and Oppenheim⁵⁷ reported some detailed experimental observations of DDT in explosive gases.

The sequence of events leading to detonation in a tube containing explosive gases can be seen in Figs. 4.14–4.17, which are streak and flash schlieren photographs with interpretations. The development of detonation can be summarized as follows:

- Generation of compression waves ahead of an accelerating laminar flame (see Fig. 4.14). The laminar flame front is wrinkled at this stage.

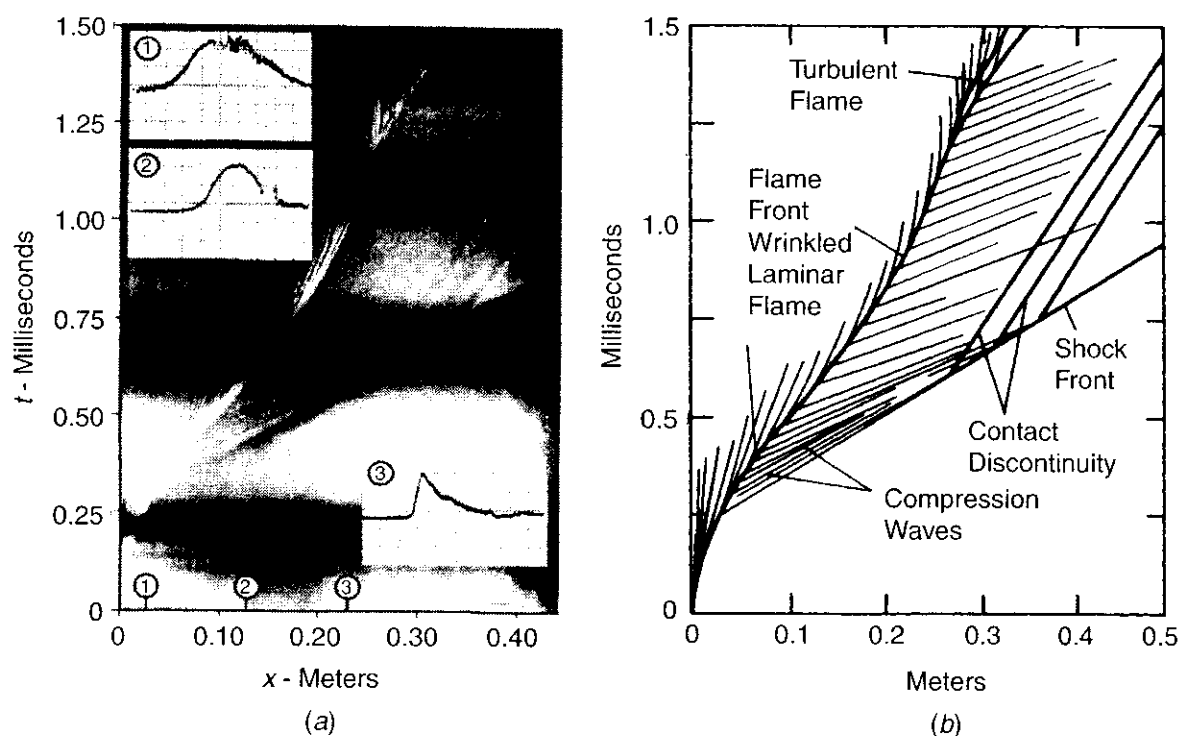


Figure 4.14 Streak schlieren photograph of the development of detonation in stoichiometric hydrogen–oxygen mixture initially at normal temperature and pressure, showing the generation of pressure waves ahead of the accelerating flame. Spark ignition by discharging 1.0 mJ across a $\frac{1}{32}$ -in. gap. Electrodes located at closed end of a $1 \times 1\frac{1}{2}$ -in.-cross-section tube. Pressure records at positions 1, 2, and 3 shown as inserts. Vertical grid: 5.2 (lb/in.²)/div for insert 1, 10.4 (lb/in.²)/div for inserts 2 and 3. Horizontal grid: 0.10 ms/div for inserts 1 and 2, 0.20 ms/div for insert 3, from left to right.²²

- Formation of a shock front due to coalescence of compression waves (see Fig. 4.14).
- Movement of gases induced by shock, causing the flame to break into a turbulent brush (see Fig. 4.14).
- Onset of “an explosion in an explosion” at a point within the turbulent reaction zone, producing two strong shock waves in opposite directions and transverse oscillations in between. These oscillations are called transverse waves (see Fig. 4.15). The forward shock is referred to as *superdetonation* and moves into unburned gases. In the opposite direction, a shock moves into the burned gases and is known as *retonation*.
- Developments of spherical shock wave at the onset of the “explosion in an explosion,” with a center located in the vicinity of the boundary layer (see Fig. 4.16).
- Interaction of transverse waves with shock front, retonation wave, and reaction zone (see Fig. 4.17).
- Establishment of a final “steady wave” as a result of a long sequence of wave interaction processes that lead finally to the shock-deflagration ensemble: the self-sustained C–J detonation wave.

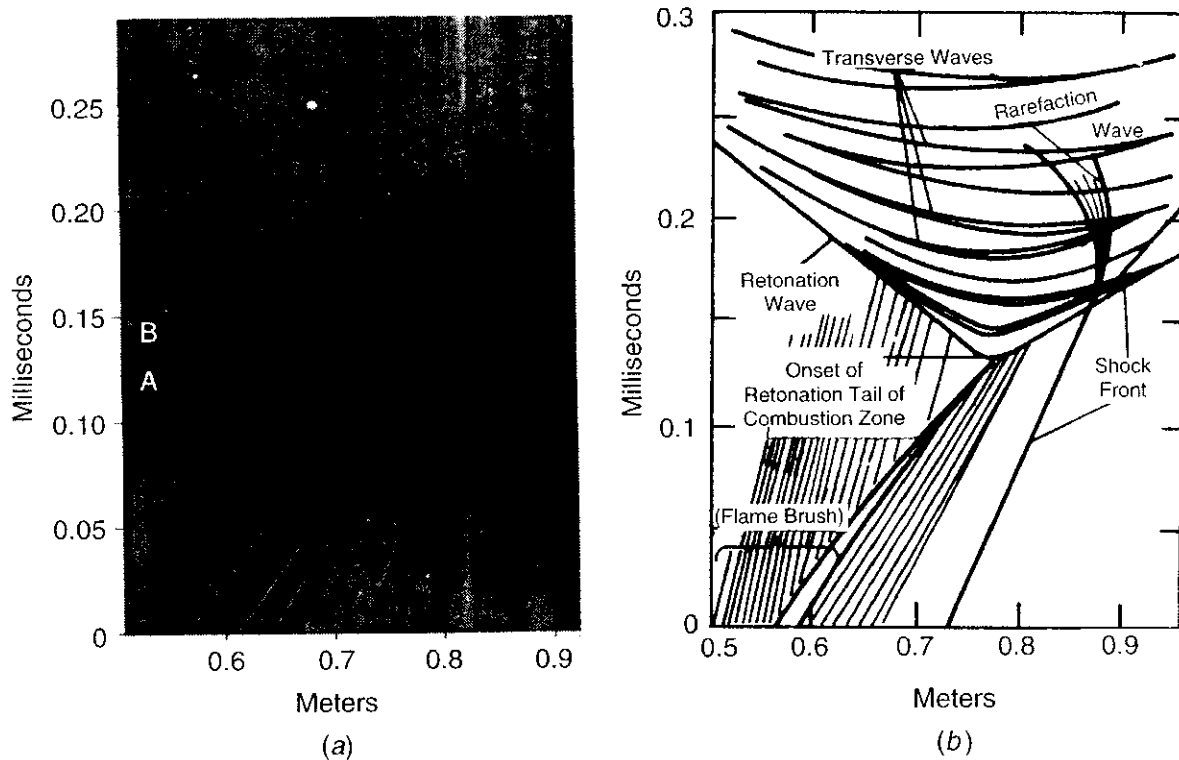


Figure 4.15 Streak schlieren photograph of the onset of retonation in a stoichiometric hydrogen–oxygen mixture initially at normal temperature and pressure. Hot-wire ignitor, made up of a $\frac{1}{2}$ -in.-long by $\frac{1}{8}$ -in.-diameter electrically heated coil, located at closed end of a $1 \times 1\frac{1}{2}$ -in.-cross-section tube. The abscissa scale denotes the distance from the end of the tube. Symbols A and B mark instants at which the accompanying flash schlieren photographs were obtained.²²

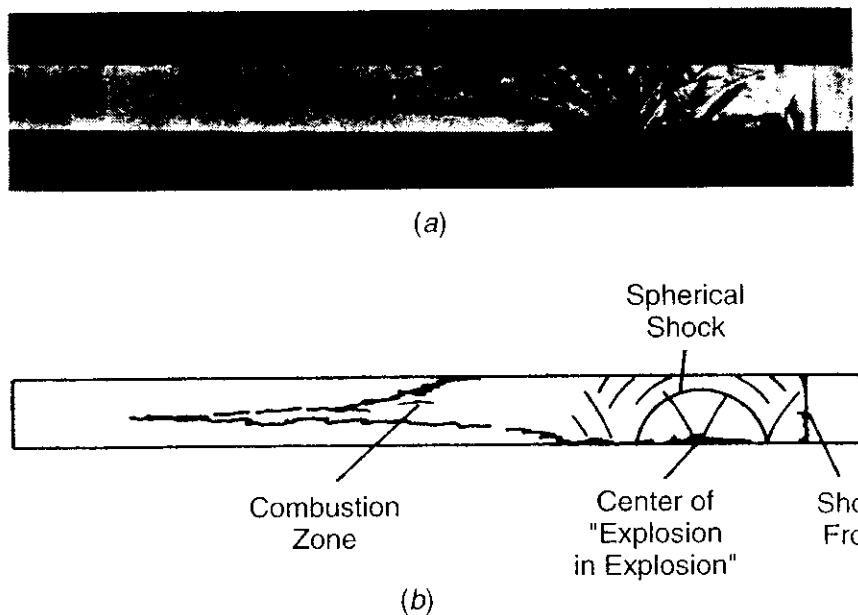


Figure 4.16 Flash schlieren photograph of the onset of retonation in a stoichiometric hydrogen–oxygen mixture initially at normal temperature and pressure at an instant marked by A on the streak schlieren photograph (Fig. 4.15).

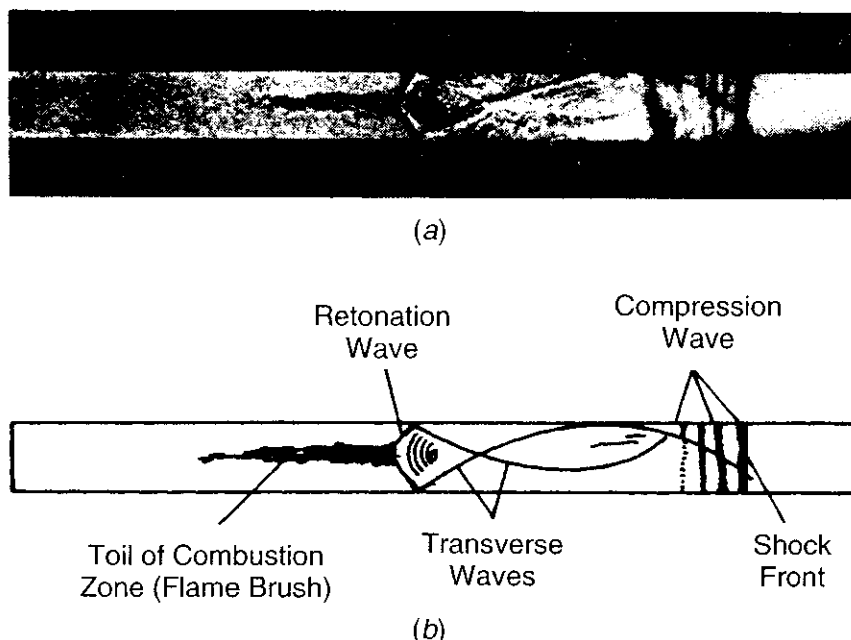


Figure 4.17 Flash schlieren photograph of transverse waves set up at the onset of retonation in an stoichiometric hydrogen–oxygen mixture initially at normal temperature and pressure, shown at an instant marked by *B* on the streak schlieren photograph (Fig. 4.15).

A typical example of DDT in a $2\text{H}_2 + \text{O}_2$ mixture ignited by a glow coil in a 1-m-long tube is shown in Fig. 4.18, obtained by Urtiew and Oppenheim.⁵⁷ Occupying the major part of the figure is a streak recorded with a slit located along the centerline of the tube, and the knife edge oriented in the direction perpendicular to the main wave motion. Above it is a single-flash photograph that, as demonstrated by the two chain-dotted lines, matches the events of the streaks as if it were taken concurrently. A pressure record, obtained simultaneously with the streak photography by means of a transducer located at a position corresponding to about 0.24 m of the distance scale of Fig. 4.18, is included as an insert.

The nature of the transverse waves can be seen clearly in Fig. 4.18. The minima of the hyperbolic traces indicate the instant the transverse waves crossed the tube centerline. The minima of the hyperbolic traces remain nearly at the same spatial location in Fig. 4.18. This implies that the center of the “explosion in an explosion” must have been brought practically to rest. The forward-moving wave was studied using wall imprints of the detonation process, an example of which is shown in Fig. 4.19. The characteristic fish-scale pattern, which corresponds to inception of the forward shock, is a distinguishing feature of a self-sustained detonation front (see Fig. 4.19⁵⁷).

In giving these general descriptions of the detonation development, it must be pointed out that there are several different modes of transition processes. The detailed mechanism of each mode depends strongly on the action of the pressure waves that are generated in the course of the transition. Four different modes

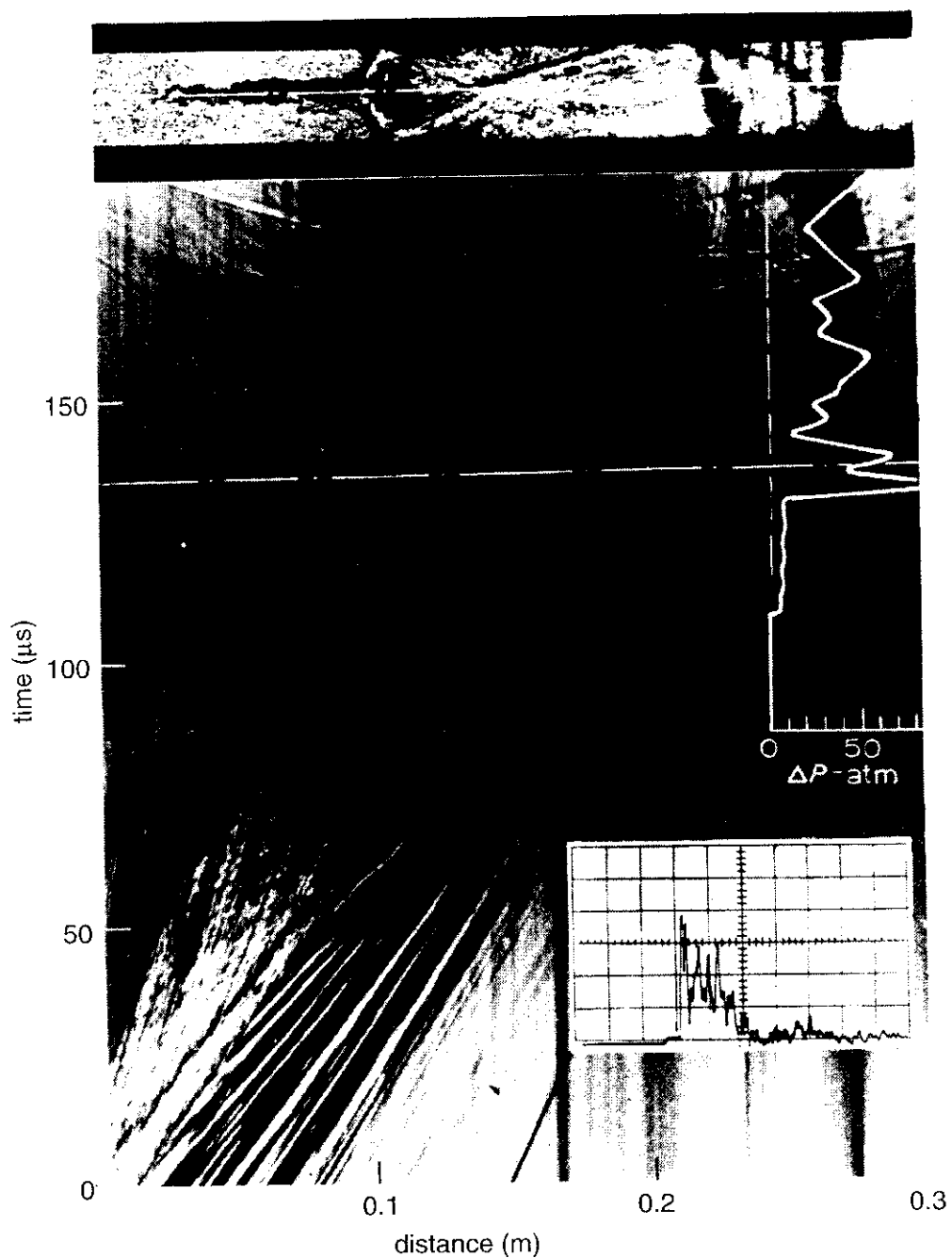


Figure 4.18 Streak schlieren record of wave processes associated with transition to detonation and a matching single-flash photograph of the wave pattern. $2\text{H}_2 + \text{O}_2$ initially at atmospheric pressure. Pressure record shown in insert. Vertical scale: 1 div = 260 lb/in.². Horizontal scale: 1 div = 50 μs. Oscilloscope sweep leads the streak photograph by 18 μs.⁵⁷

are generally observed and classified, based on the location of the onset of an “explosion in an explosion,” as follows:

- Mode 1.* Between flame and shock front (see Figs. 4.20 and 4.21*a*)
- Mode 2.* At flame front (see Fig. 4.21*b*)
- Mode 3.* At shock front (see Fig. 4.21*c*)
- Mode 4.* At contact discontinuity (see Fig. 4.21*d*)

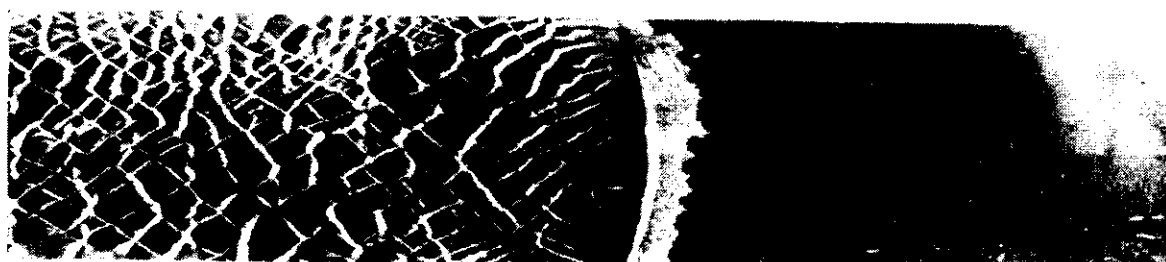


Figure 4.19 Wall imprints of the transition process.

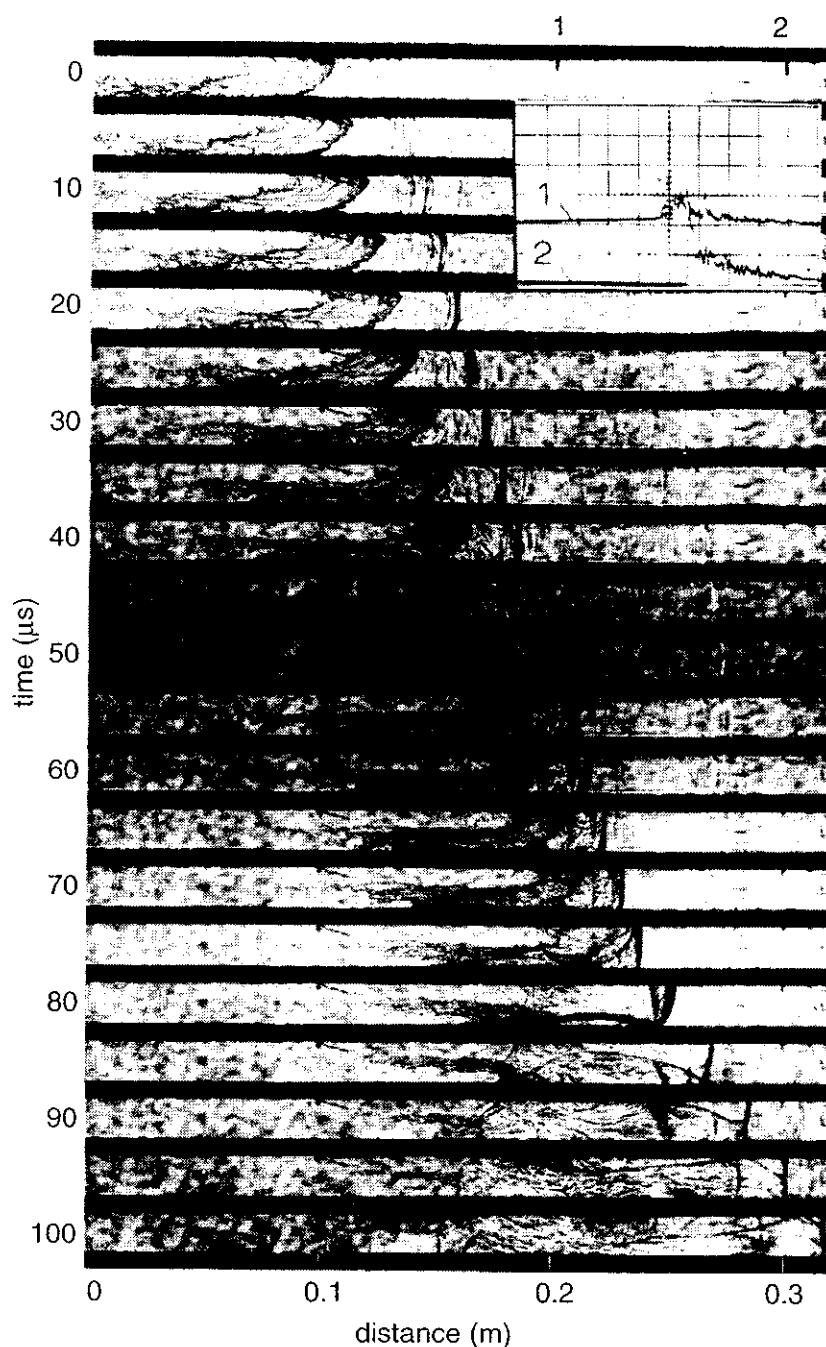


Figure 4.20 Stroboscopic schlieren record of the transition to detonation with onset between flame and shock. $2\text{H}_2 + \text{O}_2$ initially at a pressure of 554 Torr. Pressure record shown in insert. Vertical scale: 1 div = 200 lb/in^2 . Horizontal scale: 1 div = $50 \mu\text{s}$. Oscilloscope sweep leads the photographic record by $180 \mu\text{s}$. (After Urtiew and Oppenheim.⁵⁷)

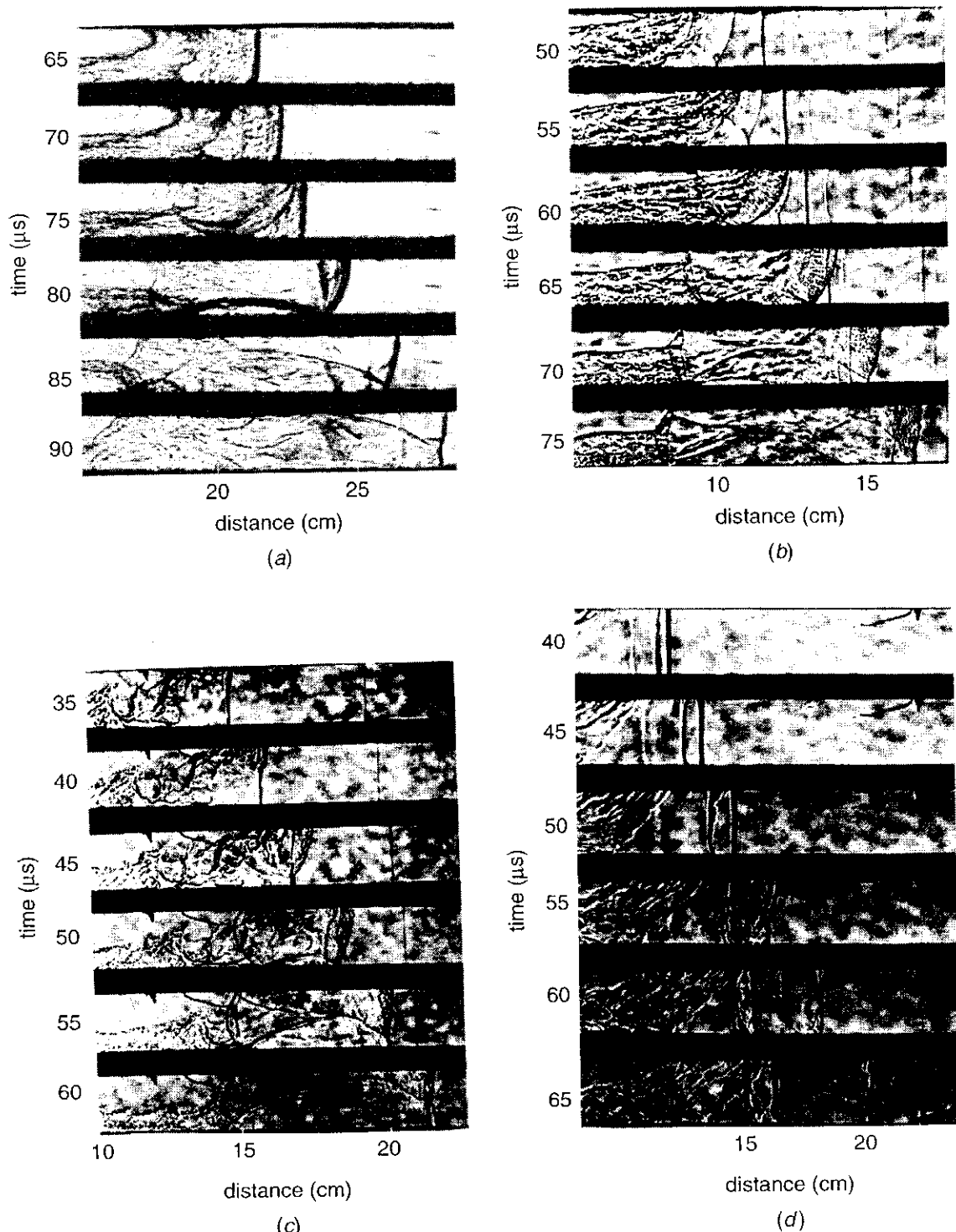


Figure 4.21 Various modes of transition to detonation observed in $2\text{H}_2 + \text{O}_2$ mixtures (after Urtiew and Oppenheim⁵⁷): (a) mode 1 with onset occurring between flame and shock, (b) mode 2 with onset occurring at flame front, (c) mode 3 with onset occurring at shock front, (d) mode 4 with onset occurring at contact discontinuity.

In view of the existence of various modes, the onset of detonation depends on the particular pattern of shock fronts created by the accelerating flame. Since the generation of any particular pattern depends on some minute inhomogeneities in its development, the process of transition to detonation is nonreproducible in its detailed sequence of events.

7 DETONABILITY AND CHEMICAL KINETICS: LIMITS OF DETONABILITY

The detonability limits of a reactive mixture are “the critical conditions for the propagation of a self-sustained detonation.” The critical conditions are the initial and boundary conditions of the explosive mixture. The initial conditions refer to the fuel’s initial characteristics, concentration, thermodynamic state, fluid mechanical state (mean flow and turbulence characteristics), ignition source properties, and all other relevant parameters that characterize the explosive mixture prior to ignition. The boundary conditions refer to the size and geometry of the mixture volume, the degree of confinement, the surface characteristics of the walls, and all other relevant parameters that specify the boundary of the explosive mixture.

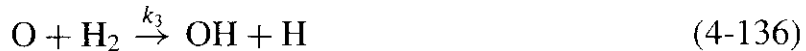
Unlike the flammability tube of Coward and Jones,⁵⁸ usually considered as the standard equipment for determining flammability limits of premixed gases, detonability limits are subject to variations in experimental setup, apparatus, and ignition source strength. Despite this lack of standardization, the detonability limits are generally measured as the critical fuel concentrations beyond which no detonation can propagate independently.

7.1 Classical Model of Belles⁵⁹

Currently, there is no theory derived directly from first principles that can accurately predict detonability limits. This problem is compounded by the fact that there is no standard method for measuring detonability limits. Despite this fact, Belles⁵⁹ developed a model based on chemical kinetics for studying the detonability limits of hydrogen–oxygen mixtures. Belles combined kinetic data with the observed wave behavior during the transition from flame to detonation and developed a useful technique for predicting the limits of detonability of hydrogen–oxygen mixtures. His analysis was based on the premise that the transition to detonation occurs when the preflame shock becomes strong enough to cause the mixture to explode. The prediction of limits of detonability was based on the following considerations and procedures:

1. The chemical kinetics condition for branched-chain explosion of hydrogen was defined in terms of temperature, pressure, and mixture composition.
2. Standard shock-wave equations were used to express the temperature and pressure of the shock-heated gas in terms of the shock strength, represented by the Mach number.
3. Steps 1 and 2 were combined so as to express the explosion condition in terms of shock strength and mixture composition. Critical shock strengths for explosion were then determined.
4. Conservation of energy was used to show that some mixtures, on burning, can produce enough energy to support a shock of the critical strength, whereas others cannot. Thus, the limits of detonability can be found.

The following gas-phase kinetics for the oxidation of hydrogen were considered by Belles:



where k_1, k_2, k_3, k_4 are the rate constants for the reactions represented by Eqs. (4-134) to (4-137), respectively, and M represents the third body in the formation of HO_2 . Since the diffusion time of a free radical to the cold wall is much longer than the characteristic time of detonation, the chain-killing reactions on the wall were neglected.

The steady-state assumption was used for the free radicals. Thus

$$\frac{dC_{\text{H}_2\text{O}}}{dt} = k_1 \frac{C_{\text{H}_2}^2 C_X}{k_4 C_M - 2k_2} \quad (4-138)$$

where C_X is the effective concentration of third bodies for the formation of HO_2 in the fourth reaction. The branched-chain explosion limit condition is therefore

$$\frac{2k_2}{k_4 C_M} = 1 \quad (4-139)$$

Using the rate constants of Lewis and von Elbe,²⁰ an expression for the concentration C_M in terms of temperature and pressure, and the gas law, Eq. (4-139) becomes

$$\frac{(3.11)T \exp(-8550/T)}{X_M p} = 1 \quad (4-140)$$

where X_M is the effective mole fraction of the third bodies in the formation of HO_2 in Eq. (4-137). Recall that the mole fraction X_M is related to the concentration by the following equation:

$$C_M = \frac{X_M p}{R_u T} \quad (4-141)$$

where X_M is given by the following empirical equation²⁰:

$$X_M = X_{\text{H}_2} + 0.35X_{\text{O}_2} + 0.43X_{\text{N}_2} + 0.2X_{\text{Ar}} + 1.47X_{\text{CO}_2} \quad (4-142)$$

The numerical factors in Eq. (4-142) express ratios of the rates of reaction for Eq. (4-137) with various third bodies, to the rate with H_2 as the third body.

Rewriting Eq. (4-140) in the logarithmic form, we have

$$\frac{3.71}{T} - \log_{10}\left(\frac{T}{p}\right) = \log_{10}\left(\frac{3.11}{X_M}\right) \quad (4-143)$$

As soon as a given H₂-O₂ mixture (having characteristic value of X_M dependent upon its composition) is raised to a temperature and pressure that satisfy Eq. (4-143), the mixture will explode. The pressure and temperature behind an incident shock may be calculated from the following equations:

$$p = \frac{p_1}{\alpha} \left(\frac{M^2}{\beta} - 1 \right) \quad (4-144)$$

$$T = \frac{T_1}{\alpha^2 \beta M^2} \left(\frac{M^2}{\beta} - 1 \right) \left(\beta M^2 + \frac{1}{\gamma} \right) \quad (4-145)$$

where

$$\alpha \equiv \frac{\gamma + 1}{\gamma - 1}, \quad \beta \equiv \frac{\gamma - 1}{2\gamma} \quad (4-146)$$

and T_1 and p_1 are the initial temperature and pressure. Equations (4-144) and (4-145) apply to the ideal case in which $C_p = \text{constant}$. However, the shock strengths required to cause explosion in hydrogen mixtures are sufficiently low that real-gas effects are usually not very important.

The critical Mach number may be found by combining Eqs. (4-143) through (4-145). One obtains

$$\begin{aligned} & \frac{3.710 \alpha^2 \beta M^2}{T_1(M^2/\beta - 1)(\beta M^2 + 1/\gamma)} - \log_{10} \left[\frac{T_1(\beta M^2 + 1/\gamma)}{p_1 \alpha \beta M^2} \right] \\ &= F(T_1, p_1, \gamma, M) = \log_{10}\left(\frac{3.11}{X_M}\right) \end{aligned} \quad (4-147)$$

Equation (4-147) may be solved graphically. Figure 4.22 shows typical plots of the left-hand side of Eq. (4-147) against Mach number, for different hydrogen-oxygen mixtures.

Conservation of energy provides the link between the calculated critical shock Mach numbers for explosion and the prediction of limits of detonability. The preflame shock provides a mechanism whereby some of the energy released by combustion is distributed to unburned gas ahead of the flame. Ultimately, this energy is recovered by the burned gas, when the flame consumes the shock-heated mixture. But if the enthalpy increase in the shock-heated state corresponding to the critical shock Mach number is greater than the heat of combustion, an impossible situation arises. No transition to detonation could ever occur, even if the duct were infinitely long. The criterion for detonability is therefore

$$\Delta h_s \leq \Delta h_c \quad (4-148)$$

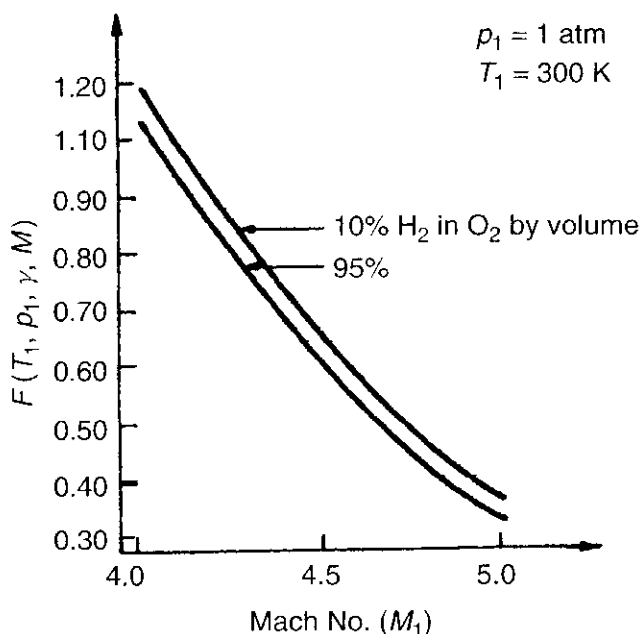


Figure 4.22 Critical Mach number as a function of T_1 , P_1 , and γ .

where Δh_s is the enthalpy rise across a shock of critical Mach number, and Δh_c the heat of combustion. Both Δh_s and Δh_c are expressed as the energy per unit mass of mixture. The energy increase of the shocked state is obtained from

$$\Delta h_s = \bar{C}_p (T_t - T_0) \quad (4-149)$$

where the total temperature T_t is given by

$$T_t = T_0 \left(1 + \frac{\gamma - 1}{2} M_c^2 \right) \quad (4-150)$$

and \bar{C}_p , the average specific heat of the mixture, which has dimension of $(Q/M/T)$. The average molar heat capacity of the mixture can be evaluated from

$$\tilde{C}_p = \sum_{i=1}^N X_i \tilde{C}_{p,i} \quad (4-151)$$

where $\tilde{C}_{p,i}$ is the average molar heat capacity at constant pressure of species i .

Figure 4.23 is a plot of Δh_s and Δh_c versus the percentage of H_2 in the mixture. The two curves intersect at two concentrations. The criterion of detonability [Eq. (4-148)] is satisfied only between these two concentrations. Hence, they are the predicted limits of detonability. The calculated results of Belles' study⁵⁹ showed good agreements with measured detonability limits (see Table 4.4). This implies that the limits of detonability of H_2 are well accounted for by the kinetic requirements for explosion. However, one interesting discrepancy between the theoretical model and the experimental treatment is the method of ignition. The

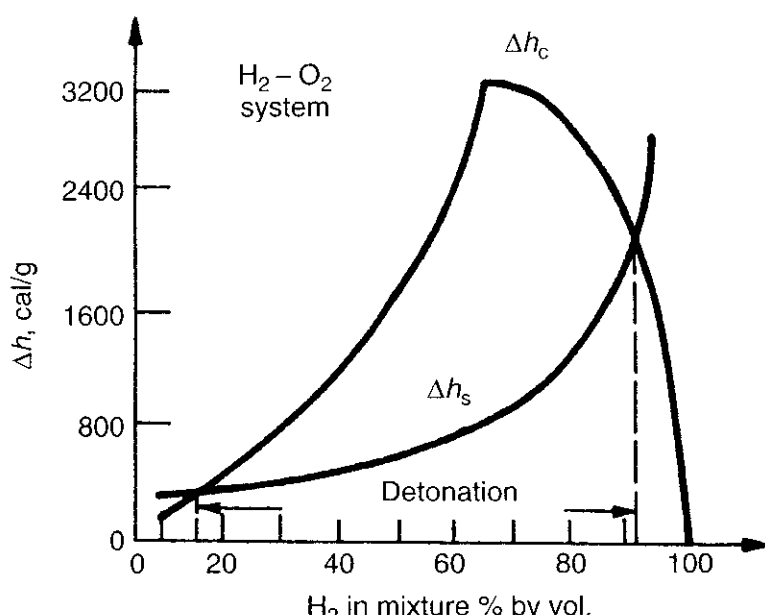


Figure 4.23 Δh_s and Δh_c versus percentage of H_2 in mixture, and the limits of detonability.

Table 4.4 Comparison of Belles' Theory⁵⁹ and Experimental Results for Hydrogen Mixtures

	Lean Limit, % H_2^a		Rich Limit, % H_2^a	
	Exptl.	Theory (Belles)	Exptl.	Theory (Belles)
Detonation in air	18.3	15.8	59	59.7
Flammability limit	14	—	70	—
Detonation in O_2	15	16.3	90	92.3

^aBy volume.

theoretical predictions were based on flame transformation to a detonation. The experimentally observed detonations were initiated by an explosive charge or a detonation in an adjoining stoichiometric H_2-O_2 mixture. Despite this discrepancy, the calculated and observed results agree and no ignition source dependence seems to be influential.

Another feature of the Belles model worth noting is the assumption of no dissociation. This assumption allowed for a simplification of calculations due to the utilization of constant specific heats and the absence of dissociation kinetic equations from the reaction scheme. This assumption proved to be valid due to the occurrence of the detonability limits at low temperatures and pressures.

Since the calculated detonation velocity is usually very accurate, many researchers have used the detonation-wave velocity to determine the bond energies of certain chemical species. It should be noted that the departure between theory and experiment becomes significant when the concentration of the fuel is decreased below the lean limit as shown in Fig. 4.24. As shown in Table 4.5,

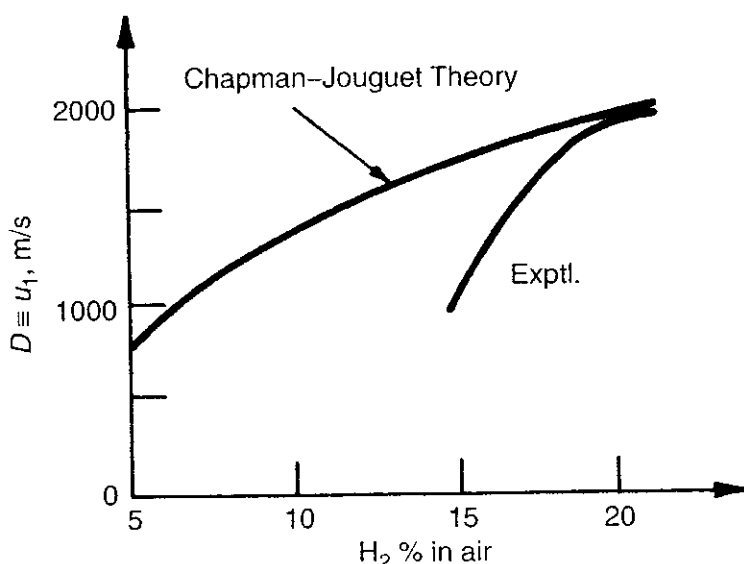


Figure 4.24 Comparison of calculated detonation-wave velocity with experimentally measured velocities as a function of H₂ concentration.

Table 4.5 Experimental Deflagration and Detonation Limits for Different Fuels

Mixture	Deflagration Lean Limit (% Fuel) ^a	Detonation Lean Limit (% Fuel) ^a	Detonation Rich Limit (% Fuel) ^a	Deflagration Rich Limit (% Fuel) ^a
H ₂ -O ₂	4.6	15	90	93.9
H ₂ -air	4	18.3	59	74
CO-O ₂ (moist)	15.5	38	90	93.9
(CO + H ₂)-O ₂	12.5	17.2	91	92
(CO + H ₂)-air	6.05	19	59	71.8
NH ₃ -O ₂	13.5	25.4	75	79
C ₃ H ₈ -O ₂	2.4	3.2	37	55
C ₂ H ₂ -O ₂	2.8	3.5	92	93
C ₄ H ₁₀ O-air	1.85	2.8	4.5	36.5

^aBy volume.

there exist limits of detonability, analogous to limits of flammability, beyond which a stable detonation is not observed. In comparison with the deflagration limits, one can see that the deflagration limits are wider than the detonation limits. It is also interesting to note that hydrocarbon mixtures such as C₃H₈/O₂ (see Fig. 4.25) and C₂H₂/O₂ mixtures (see Fig. 4.26) show maximum detonation velocities that are widely displaced from those for the stoichiometric composition for combustion to CO₂ and H₂O; instead they are fairly close to compositions corresponding to combustion to CO and H₂O. This is because the reaction time in the detonation process is very short; the time to form stoichiometric CO and H₂O mixtures is much shorter than that for CO₂ and H₂O. The oxidation process from

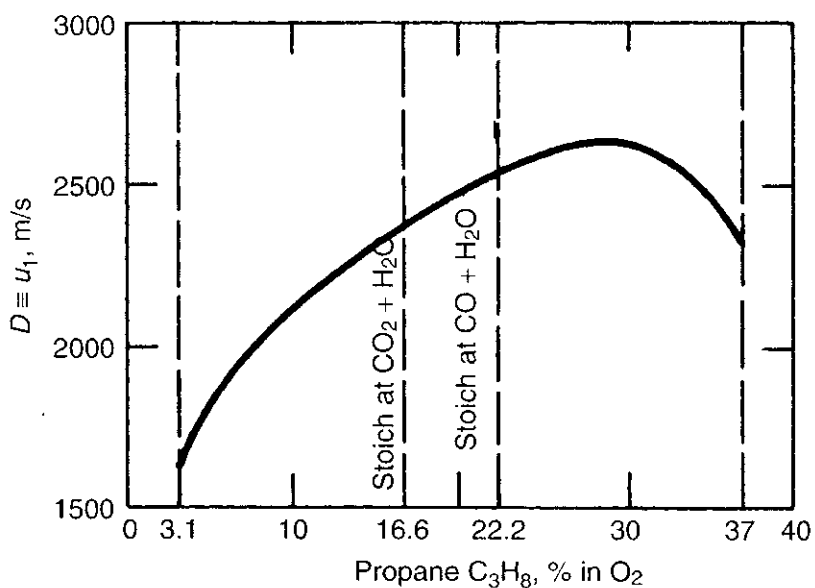


Figure 4.25 Detonation-wave velocity as a function of the percentage of propane in O_2 .

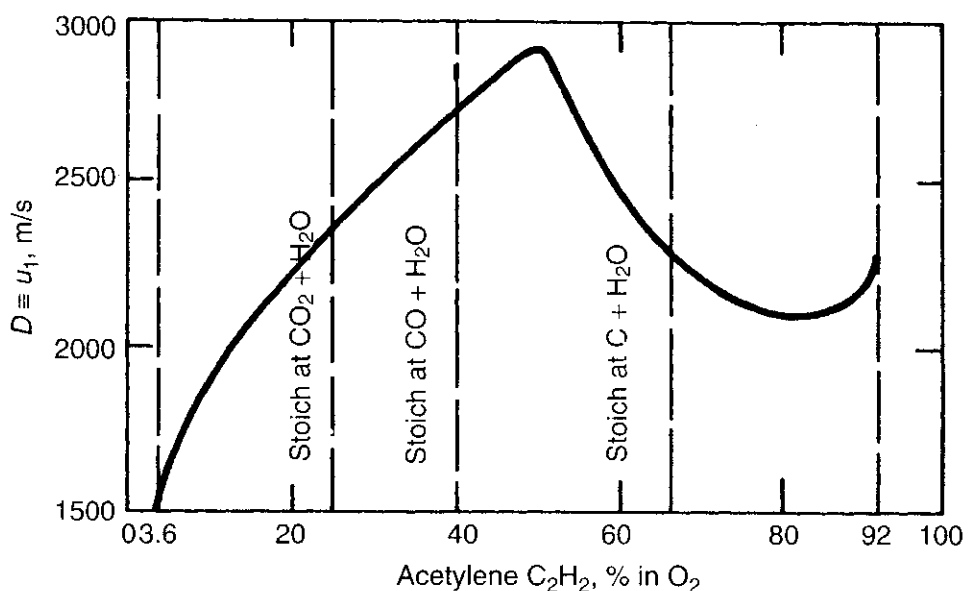


Figure 4.26 Detonation-wave velocity as a function of the percentage of acetylene in O_2 .

CO to CO_2 is relatively slow. The change of detonation with mixture composition is further illustrated in Figs. 4.25 and 4.26.

7.2 Detonability Limits of Confined Fuel Mixtures

This section discusses the dependence of detonability limit on initial and boundary conditions of confined mixtures. As the detonation limits are approached, the critical energy density required to ignite the mixture increases exponentially. We shall see that for larger tube diameters, the detonation limits are wider. Certain detonability limit criteria have been found for specific apparatus based on a few characteristics of the detonation as the limits are approached. One limit criterion

characteristic is the transition from a multi-headed detonation to a single-headed spin detonation as the limits are approached. Fuel concentration is also coupled to tube diameter. At each fuel concentration, there is a specific tube diameter at which a multi-headed detonation becomes a single-headed spin detonation. The detonation structure of the single-headed spin detonation is unstable to finite perturbations as it loses and then recovers its structure immediately after a perturbation obstacle. Mixtures slightly leaner or richer than that for the onset of the single-headed spin demonstrate the destruction-reformation phenomenon, known as galloping, when detonated. The detonability limits of confined mixtures can, therefore, be defined as the critical fuel concentrations or critical tube diameters that produce single-head spinning detonations. Another limit criterion characteristic is the cell size associated with the detonation structure. The detonation limit occurs when the detonation cell width is approximately equal to the tube circumference. If the tube diameter is less than this critical diameter, no detonation wave can propagate. It is also known that the critical diameter increases with percent dilution.

As discussed before, the detonability limits of a reactive mixture are defined as “the critical conditions for the propagation of a self-sustained detonation.” The critical conditions are functions of the initial and boundary conditions of the explosive mixture. The initial conditions refer to the fuel’s initial characteristics, concentration, thermodynamic state, fluid mechanical state or mean flow and turbulence characteristics, ignition source properties, and all other relevant parameters that characterize the explosive mixture prior to ignition. The boundary conditions refer to the size and geometry of the mixture volume, the degree of confinement, the surface characteristics of the walls, and all other relevant parameters that characterize the boundary of the explosive mixture. For simplicity, the following discussions of the detonability limit will be restricted for confined mixtures in smooth-walled circular tubes.

7.2.1 Initial Condition Dependence In order to demonstrate the detonability limit dependence on the initial condition of the reactive mixture, the results of Wolanski et al.⁶⁰ on the detonation of methane–air mixtures are considered. In their study, the amount of ignition energy density or critical energy density (MJ/m^2), defined as the total chemical energy in the initiator divided by the main tube cross-sectional area, was varied through the fuel concentration range where detonations can occur in methane–air mixtures. It was demonstrated that, as the detonation limits are approached, the critical energy density required to initiate detonation of the mixture increases exponentially. Essentially, they showed a U-shaped curve dependency of critical energy density on percentage of CH_4 in the initial mixtures. In their experiments using a 6.35-cm tube, they found that the limits of detonation were associated with 8 and 14.5% methane in the CH_4 –air mixture.

7.2.2 Boundary Condition Dependence Theoretically speaking, the detonability limits of *unconfined* mixtures should be regarded as the “true” detonability limits of the mixture because spherical detonations are supposedly free

from boundary effects. In practice, however, detonability limits of any mixture are always influenced by the boundary conditions of the experimental setup. Therefore, it is only meaningful to speak of detonability limits associated with a given apparatus, such as a smooth cylindrical tube of a given diameter.

In order to demonstrate the dependency on boundary condition and the need for standardization, results of three hydrogen detonability limit experiments are compared. Wendland⁶¹ showed that for tube diameter of 1.4 cm, the detonation limits of H₂-O₂ system range from 18.3 to 59% of H₂ by mole. Kogarko and Zel'dovich⁶² reported that for a tube with a diameter of 30.5 cm, the detonation limits of H₂-O₂ system range from 15.0 to 63.5% of H₂ by mole. Lee and coworkers⁶³ used an even larger tube with a diameter of 43 cm and found that detonation limits of H₂-O₂ system range from 13.6 to 70.0% of H₂ by mole. It is quite obvious that as the tube diameter increases, the detonation limits become wider. Therefore, detonability limits of confined mixtures are not unique, but strongly dependent on the boundary conditions of the medium in which the detonation propagates.

7.2.3 Single-Head Spin Detonation Over the range of detonable concentrations of a given fuel-oxidizer mixture, the wave structure is called multi-head wave front. This wave is characterized by relatively weak transverse waves in comparison to the axial component, which allows it to be considered roughly one-dimensional as modeled by Zel'dovich, von Neumann, and Döring in the ZND model. It has been observed that, in a given smooth circular tube, as the mixture composition becomes leaner or richer, the multi-head, self-sustained detonation becomes a single-head spinning detonation propagating at about the C-J velocity. This single-head spinning detonation is characterized by an increase in transverse wave strength, a three-dimensional structure, and mixture gases that are rotated about the tube axis. Figure 4.27 shows a typical path of the single-head detonation wave propagation. Dove and Wagner⁶⁴ studied this spin phenomenon quite early. They proposed that the single-head spinning detonation is the lowest possible stable mode in a given tube as the detonation limits of confined mixtures are approached.

Not only are the single-head detonations associated with the detonability limits for a given fuel-oxidizer mixture, coupled to fuel concentration, they are also coupled to tube diameter. In an experimental study performed by Moen et al.,⁶⁵

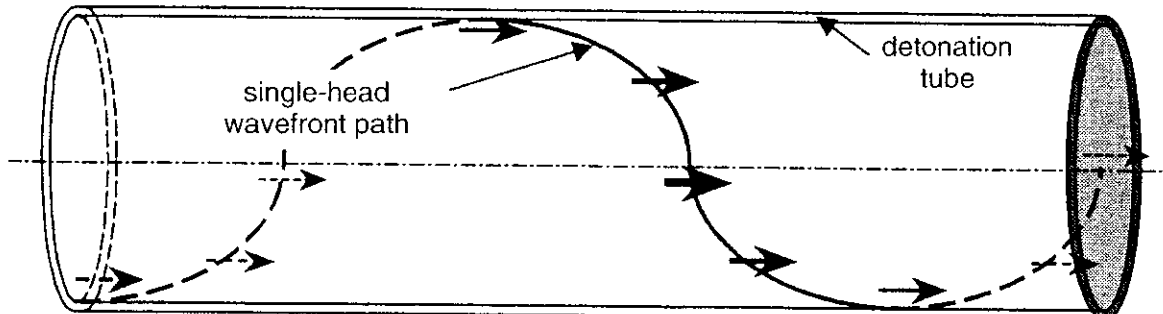


Figure 4.27 Path of a single-head detonation wave front in a straight tube.

three tubes of diameters 28, 48, and 145 mm were used to detonate ethylene–air mixtures at 1-atm pressure near their lean limits. They showed that for each fuel concentration, there is a specific tube diameter at which the multi-head detonation becomes a single-head detonation. For a given fuel concentration, that specific diameter is defined as the “critical tube diameter, d_c .” The general trend obtained by Moen et al. follows that shown in Fig. 4.29 to be discussed later. Mitrofanov and Soloukhin⁶⁶ discovered that d_c for oxy-acetylene systems is related to the characteristic transverse wave spacing λ by:

$$d_c = 13\lambda \quad \text{for a circular tube} \quad (4-152a)$$

$$d_c = 10\lambda \quad \text{for a planar channel} \quad (4-152b)$$

A schematic illustration of wave motion in a detonation cell is shown in Fig. 4.28. In this figure, the detonation wave is propagating upward and the transverse waves are indicated; the reaction-zone thicknesses are given by the widths of the shaded areas. Edwards et al.⁶⁷ showed that these two results are equivalent and have provided further experimental support for these simple relationships. They also suggested that the relations should apply to all detonative systems. In

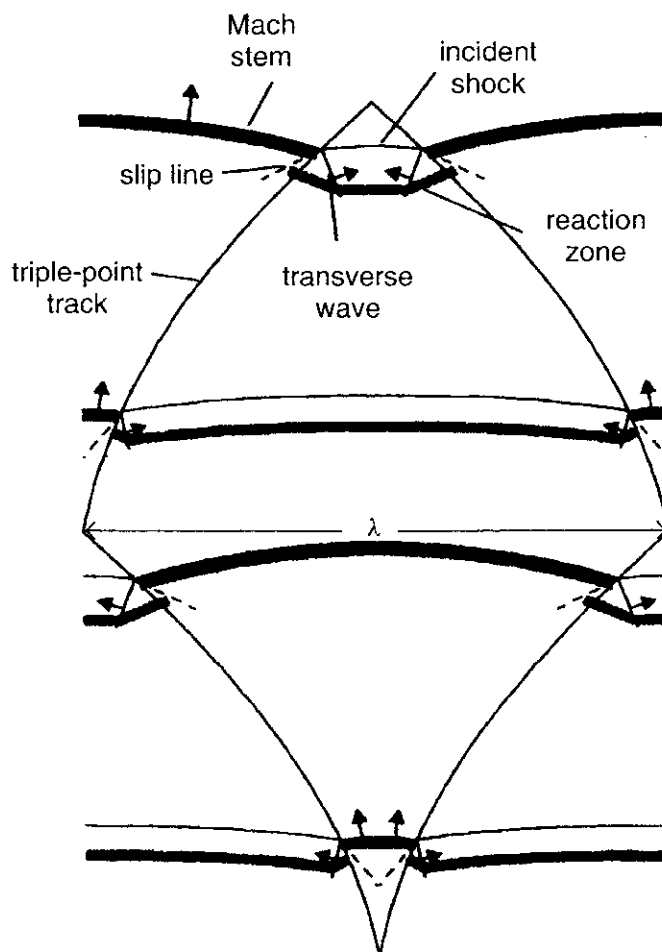


Figure 4.28 Schematic illustration of wave motion in a detonation cell; detonation wave propagates upwards. (Modified from Gavrikov et al.^{75a})

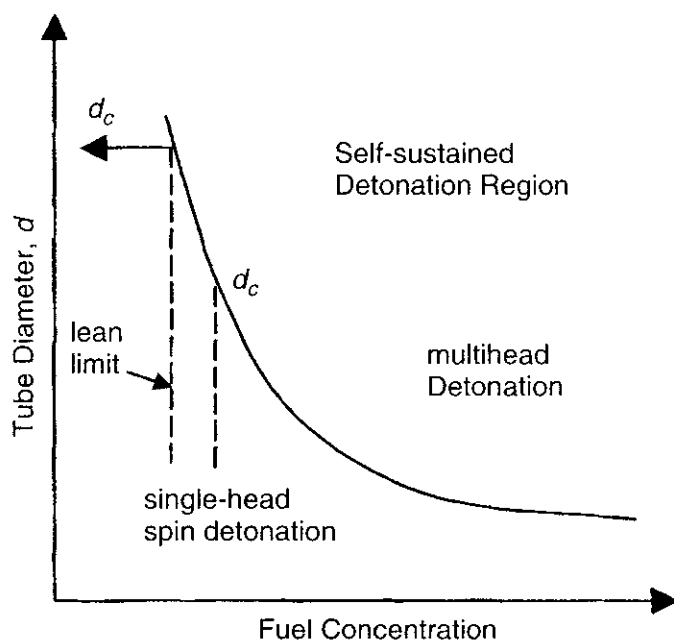


Figure 4.29 Effects of fuel concentration and tube diameter on the onset of single-head spin detonation.

other words, a minimum of 10 to 13 transverse waves are required for a self-sustained detonation to be established even in an unconfined situation, thus indicating that the lower transverse modes, which are observed in tubes near the detonability limits, are stabilized by the tube walls. In Fig. 4.29, the tube diameter d is plotted against fuel concentration around the lean limit. In the region above the curve, known as the “self-sustained” detonation region, multi-head detonations readily propagate. In the region below the curve, known as the “detonation-like” region, single-head detonations can propagate, but only with powerful igniters.

Moen et al.⁶⁵ also showed that the detonation structure of the single-head detonation is unstable to finite perturbations. In their experiments, a short length of surface obstacle called Shchelkin spiral was used to perturb the detonation. It was observed that for mixture compositions near the onset of single-head spinning, the detonation recovers its structure immediately after the obstacle. For mixtures slightly leaner or richer than that for the onset of the single-head spin detonation, the detonation fails and then recovers its spinning structure far downstream of the Shchelkin spiral. This behavior is similar to the galloping detonations observed by Mooradian and Gordon⁶⁸ and Edwards and Morgan.⁶⁹ The “galloping” mode is a longitudinal mode with periodic destruction and formation of the detonation. This reformation process is not stable and eventually dies out. Therefore, the detonability limits of confined mixtures can be defined as the compositions for the onset of single-head spinning detonation.

7.3 Detonability Criteria and Detonation Cell Size

The detonation cell width is defined as the width of one of the cells formed by the slipstream associated with the interaction of the transverse and longitudinal

waves of the detonation. The cellular structure can be mapped during a detonation with the use of soot-covered sheets called smoke foils. A typical cellular structure left on a smoke foil and its corresponding cell width, λ , is shown in Fig. 4.28.

As early as 1948, Kogarko and Zel'dovich⁶² proposed without any derivation that, at the onset of single-head spin in a smooth circular tube, the detonation cell width, λ , must be equal to the tube circumference,

$$\lambda = \pi d^* \quad (4-153)$$

This limiting tube diameter is designated as d^* . Lee⁷⁰ provided a derivation of this criterion. In his paper, it is stated that because the tube circumference, πd , represents the largest characteristic dimension for the tube, the longest characteristic acoustic time is $\pi d/c$, where c is the sound speed of the detonation products. Assuming a resonant coupling between the acoustic vibration and the periodic chemical processes in the detonation cell, the characteristic acoustic time, $\pi d^*/c$, must be equal to the characteristic chemical timescale, λ/c . Therefore, the detonation cell width is proportional to the tube circumference, $\lambda \cong \pi d^*$. Moen et al.⁶⁵ formulated another limit criterion based on the acoustic theories of Manson⁷¹ and Fay.⁷² These theories predict the ratio of spin pitch (P) to the limiting tube diameter, which can be written as

$$\frac{P}{d^*} = \frac{\pi U}{K_1 c} \quad (4-154)$$

Here, U is the C-J detonation velocity and $K_1 = 1.841$. In order to arrive at the limit criterion, $\lambda \cong 1.7 d^*$, it was arbitrarily assumed that the pitch angle equals the cell length and $U/c \cong 1$ for most fuel-air mixtures. Therefore, it can be inferred from all of the aforementioned limit criteria that, in smooth round tubes, the detonability limits occur when the tube perimeter is on the order of the cell size.

The $\lambda = \pi d^*$ criterion was also suggested by Dupre et al.⁷³ as being the most suitable for their data. Their experiments were conducted using five smooth round tubes of decreasing diameters, 15.2 to 3.8 cm, with lean hydrogen-air mixtures at ambient initial conditions and concentrations of 15–25% H₂. In addition to confirming this detonability limit criterion, it was found that the single-head detonation is highly unstable to finite perturbations with velocity fluctuations in excess of 10% of the C-J value. Therefore, the detonability limits for stable propagation of a reactive mixture detonation initiated by a strong source in a cylindrical rigid smooth-walled tube can be written in terms of the limiting tube diameter, d^* . This can be estimated directly with the detonation cell size data using the relationship

$$d^* = \lambda/\pi \quad (4-155)$$

Guirao, Knystautas, and Lee^{74b} studied the variations of d_c for H₂-air and H₂-air-CO₂ mixtures at 25°C and H₂-air-steam mixtures at 100°C as a function of the fuel concentration. Knystautas et al.^{74c} further conducted extensive

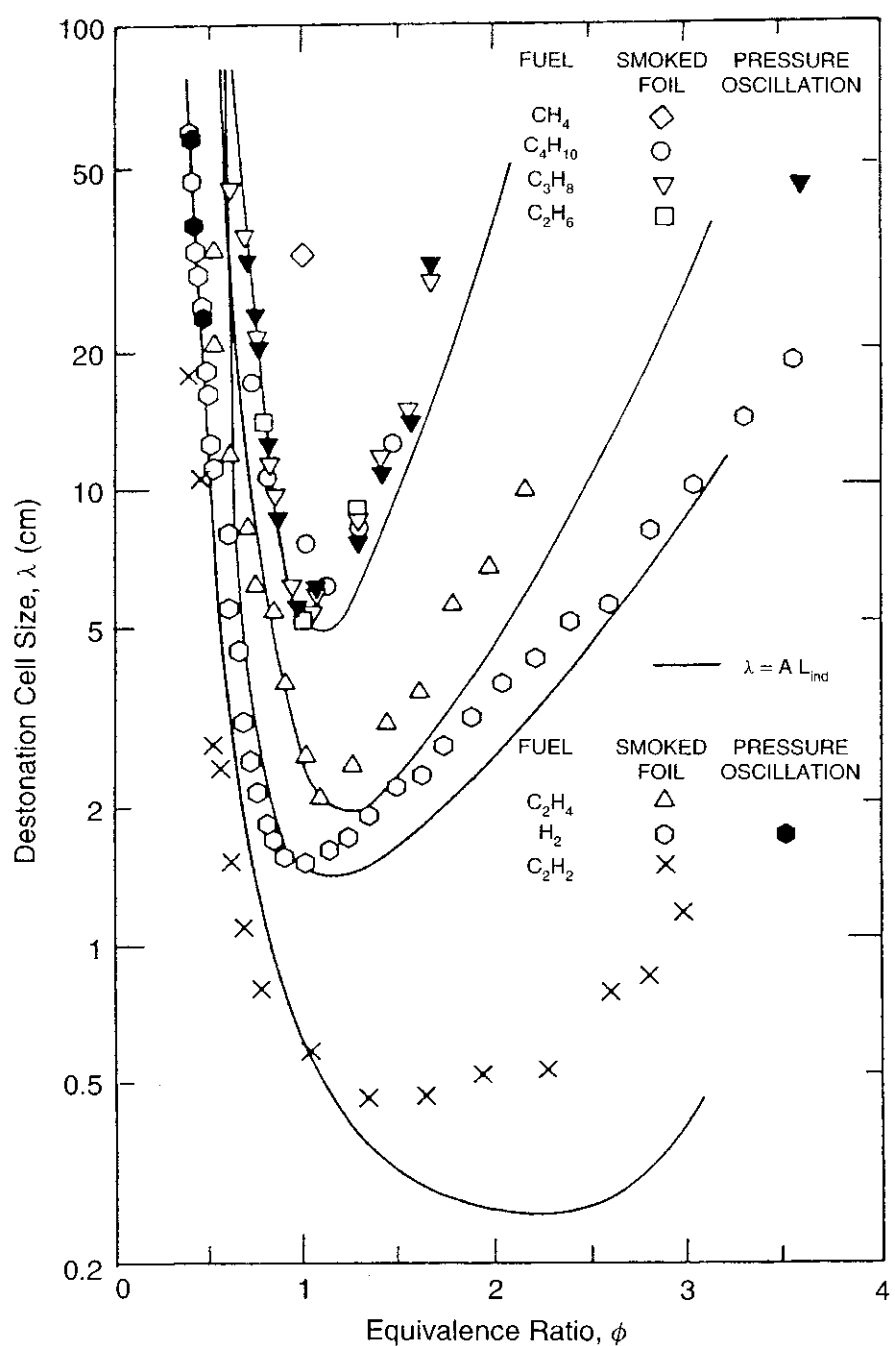


Figure 4.30 Variation of measured detonation cell size λ with fuel-air composition and correlation with induction length, L_{ind} . (Modified from Knystautas et al.^{74c})

measurements of detonation cell sizes in mixtures of H_2 , C_2H_2 , C_2H_4 , C_2H_6 , C_3H_8 , and C_4H_{10} with air over a range of fuel concentrations. Their results of the cell size are plotted in Fig. 4.30. As expected, acetylene (C_2H_2) is found to be the most sensitive fuel with a minimum cell size $\lambda \approx 0.57$ cm as compared to $\lambda \approx 1.5$ cm for H_2 , $\lambda \approx 2.6$ cm for C_2H_4 , and $\lambda \approx 5.35$ cm for the alkane group (C_2H_6 , C_3H_8 , and C_4H_{10}). It is useful to note that the width of the typical U-shaped curves for cell size versus the fuel composition decreases with decreasing sensitivity of the fuel. Also, the increase in cell size as the equivalence approaches the rich limit ($\phi > 1$) is in general much slower than towards

the lean limit ($\phi < 1$). According to Knystautas et al.,^{74c} this universal behavior is reflected in practically all dynamic detonation parameters that are dependant on the induction time (or length) of the mixture itself.

Based on cell size data given in Fig. 4.30, the critical tube diameter (d_c) can be estimated from the empirical relationship [Eq. (4-152a)]. The solid curves shown in Fig. 4.31 represent critical tube diameters estimated from the cell-sized data obtained from Knystautas et al.^{74c} In view of the interest in H₂-air mixtures in various industrial safety considerations, a large-scale experiment on the measurement of d_c for both lean and rich mixtures were conducted by Guirao et al.^{74b} As can be seen from Fig. 4.31, the agreement with the estimates of d_c from cell size data via the empirical law $d_c = 13\lambda$ is extremely good for the case of H₂. For hydrocarbon-air mixtures, the results from direct measurements of d_c are in reasonable agreement with those estimated from the empirical law. However, the "bottle-to-bottle" variations of the purity of the commercial C₂H₂ could account

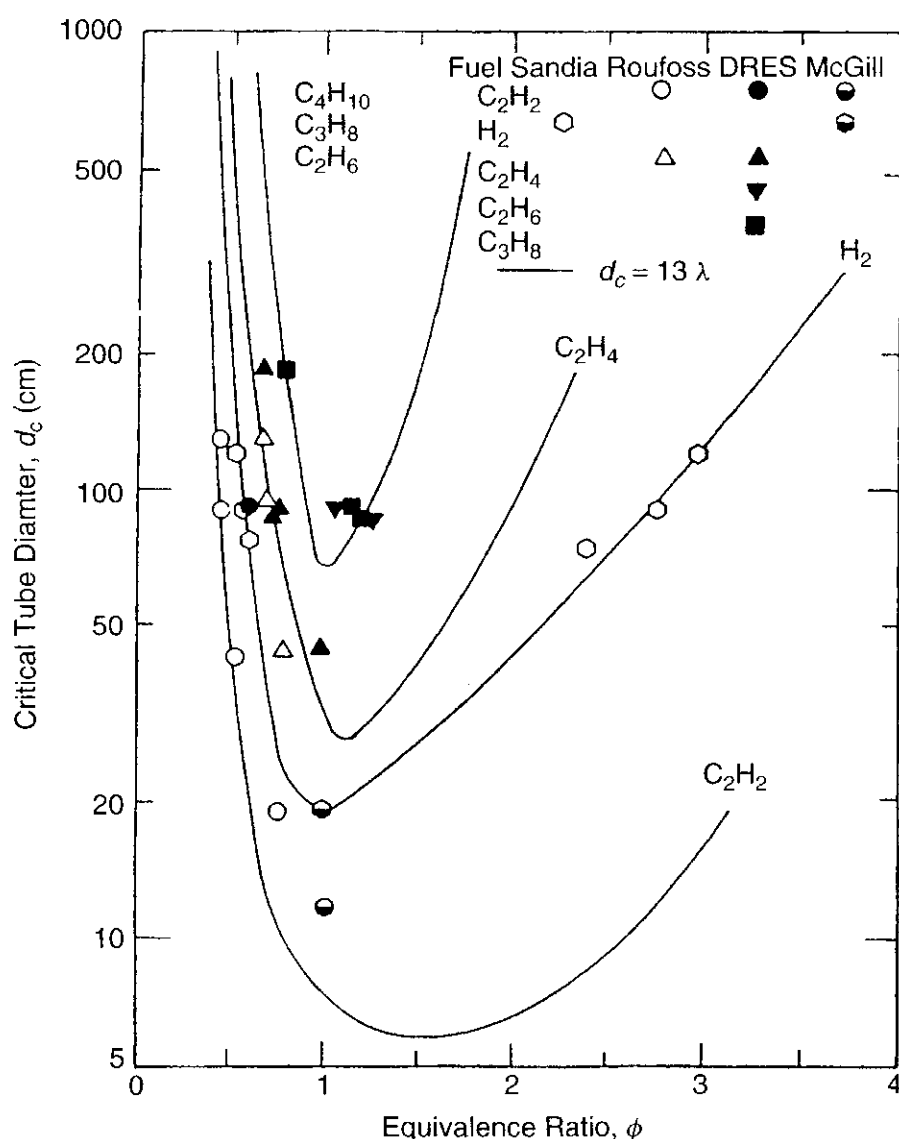


Figure 4.31 Correlation of a critical tube diameter d_c with the empirical law $d_c = 13\lambda$ for a range of fuel-air mixtures. (Modified from Knystautas et al.^{74c})

for the observed deviations, especially in view of the highly sensitive nature of the C_2H_2 -air mixture.

Adopting the criterion that the outset of single-head spinning waves in a given tube should correspond to the detonability limits for that tube, the limits in the circular tubes can be estimated when cell size data are available. Since the onset of single-head spin corresponds to a cell size of the order of the tube circumference [see Eq.(4-155)]. The composition limits for a given circular tube can be estimated if λ is known. Figure 4.32 gives the limiting tube diameter d^* as function of equivalence ration for various fuels studied by Knystautas et al.^{74c} For a given fuel composition of known equivalence ratio, stable detonations cannot be propagated in tubes with a diameter $d < d^*$. For the case of stoichiometric

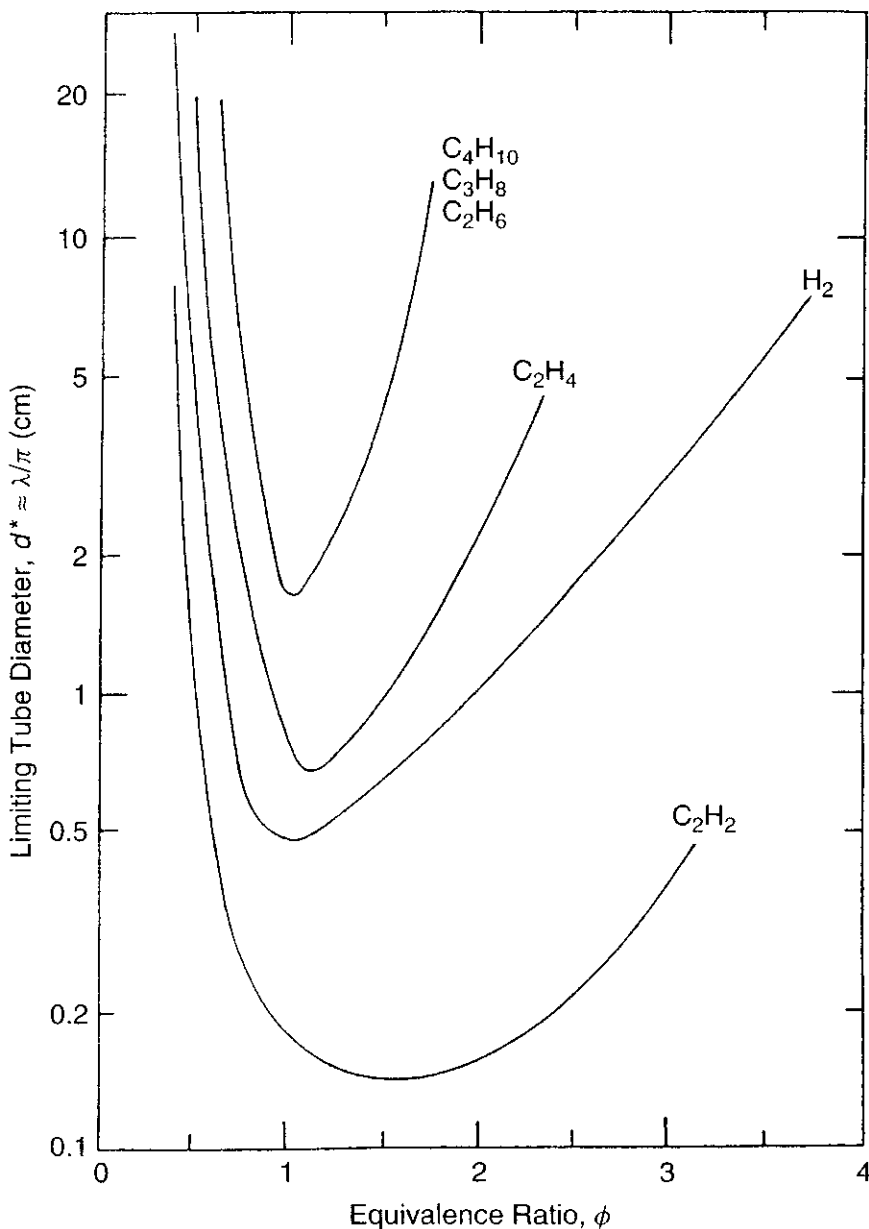


Figure 4.32 Variation of the minimum limiting tube diameter $d^* \approx \lambda/\pi$ for stable propagation of detonation waves in tubes as a function of fuel-air composition. (Modified from Knystautas et al.^{74c})

H_2 -air mixtures, $d^* \approx 0.5$ cm when compared to $d^* \approx 0.2$ cm for C_2H_2 -air mixtures and $d^* \approx 1.7$ cm for the alkanes-air mixtures.

As reported by Guirao et al.,^{74b} for the stoichiometric composition, 29.6% H_2 , initially at 298°C and 1 atm, the limiting tube diameter is $d^* \approx 0.5$ cm. This value increases by 12.2 times to $d^* \approx 6.1$ cm when 15% CO_2 dilution is added. For hot H_2 -air mixtures initially at 100°C and superatmospheric pressure, the limiting tube diameter for the stoichiometric composition is $d^* \approx 0.16$ cm. This value increases by 60 times to $d^* \approx 9.6$ cm when 30% steam diluent is added. Again, the d^* values for hydrocarbon-air mixtures are expected to be higher for cases with diluent addition.

Based on the discussion in this section, it is evident that the detonability limit depends on initial and boundary conditions. As the detonation limits are approached, the critical energy density required to ignite the mixture increases exponentially. It was also demonstrated that as the tube diameter increases, the detonation limits become wider. Certain detonability limit criteria have been found for specific apparatus based on a few characteristics of the detonation as the limits are approached. One limit criterion characteristic is the transition from a multi-head detonation wave to a single-head detonation wave as the limits are approached. The onset of a single-head detonation is not only associated with the detonability limit for a given fuel concentration in the fuel-oxidizer mixture but also determined by the tube diameter. For each fuel concentration, there is a specific tube diameter in which the multi-head detonation transforms into a single-head detonation wave. It was noted that the detonation structure of the single-head detonation is unstable to finite perturbations as it loses and then recovers its structure immediately after perturbation obstacles. For mixtures slightly leaner or richer than that for the onset of the single-head spin detonation, the detonation demonstrates the phenomenon known as galloping. Therefore, the detonability limits of confined mixtures can be defined as the critical fuel concentrations or critical tube diameters that produce the onset of single-head spinning detonations.

Another limit criterion characteristic is the cell size on the smoke foil. It has been shown that at the onset of single-head spin in a smooth circular tube, the detonation cell width is approximately equal to the tube circumference. It has also been shown that for hydrogen-air mixtures at ambient conditions, the single-headed detonation is highly unstable to finite perturbations with velocity fluctuations in excess of 10% of the C-J value. Finally, it has been shown that critical tube diameter increases with percent dilution in the mixture.

7.4 Chemical Kinetics of Detonation in H_2 -Air-Diluent Mixtures

The relationship between calculated reaction zone length and measured cell size was studied by Shepherd^{74a} for H_2 -air-diluent detonations. Several different means of calculating reaction zone length were considered. The possibility of using detailed chemical kinetic models and simple correlations to predict the detonation cell size for H_2 -air-diluent detonations was explored. He utilized a set of 23 reactions and 11 species (H_2 , O_2 , H , O , OH , H_2O , HO_2 , H_2O_2 , N_2 ,

Table 4.6 Hydrogen Oxidation Mechanism and Rate Constants^a (after J. E. Shepherd^{74a})

	Reaction	A	β	E^a
1.	$H_2 + O_2 \rightleftharpoons OH + OH$	1.70×10^{13}	0.00	47,780
2.	$OH + H_2 \rightleftharpoons H_2O + H$	1.17×10^9	1.30	3,626
3.	$H + O_2 \rightleftharpoons OH + O$	5.13×10^{16}	-0.82	16,507
4.	$O + H_2 \rightleftharpoons OH + H$	1.80×10^{10}	1.00	8,826
5.	$H + O_2 + M \rightleftharpoons HO_2 + M$	2.10×10^{18}	-1.00	0
6.	$H + O_2 + O_2 \rightleftharpoons HO_2 + O_2$	6.70×10^{19}	-1.42	0
7.	$H + O_2 + N_2 \rightleftharpoons HO_2 + N_2$	6.70×10^{19}	-1.42	0
8.	$OH + HO_2 \rightleftharpoons H_2O + O_2$	5.00×10^{13}	0.00	1,000
9.	$H + HO_2 \rightleftharpoons OH + OH$	2.50×10^{14}	0.00	1,900
10.	$O + HO_2 \rightleftharpoons O_2 + OH$	4.80×10^{13}	0.00	1,000
11.	$OH + OH \rightleftharpoons O + H_2O$	6.00×10^8	1.30	0
12.	$H_2 + M \rightleftharpoons H + H + M$	2.23×10^{12}	0.50	92,600
13.	$O_2 + M \rightleftharpoons O + O + M$	1.85×10^{11}	0.50	95,560
14.	$H + OH + M \rightleftharpoons H_2O + M$	7.50×10^{23}	-2.60	0
15.	$H + HO_2 \rightleftharpoons H_2 + O_2$	2.50×10^{13}	0.00	700
16.	$HO_2 + HO_2 \rightleftharpoons H_2O_2 + O_2$	2.00×10^{12}	0.00	0
17.	$H_2O_2 + M \rightleftharpoons OH + OH + M$	1.30×10^{17}	0.00	45,500
18.	$H_2O_2 + H \rightleftharpoons HO_2 + H_2$	1.60×10^{12}	0.00	3,800
19.	$H_2O_2 + OH \rightleftharpoons H_2O + HO_2$	1.00×10^{13}	0.00	1,800
20.	$HO_2 + CO \rightleftharpoons CO_2 + OH$	1.51×10^{13}	0.00	22,934
21.	$CO + O + M \rightleftharpoons CO_2 + M$	3.20×10^{13}	0.00	-4,200
22.	$CO + OH \rightleftharpoons CO_2 + H$	1.51×10^7	1.30	-758
23.	$CO + O_2 \rightleftharpoons CO_2 + O$	1.60×10^{13}	0.00	41,000

^aReaction rate coefficients are in the form $k_f = AT^\beta \exp(-E_a/R_u T)$. Units are moles, cubic centimeters, seconds, Kelvins, and calories/mole. Third body efficiencies: $k_5 C_{H_2O} = 21k_5 C_{Ar}$; $k_5 C_{H_2} = 3.3k_5 C_{Ar}$; $k_5 C_{CO_2} = 5k_5 C_{Ar}$; $k_5 C_{CO} = 2k_5 C_{Ar}$; $k_{12} C_{H_2O} = 6k_{12} C_{Ar}$; $k_{12} C_H = 2k_{12} C_{Ar}$; $k_{12} C_{H_2} = 3k_{12} C_{Ar}$; $k_{14} C_{H_2O} = 20k_{14} C_{Ar}$

CO_2 , and CO) in the kinetic model for hydrogen oxidation (see Table 4.6). Even with detailed kinetic rates, Shepherd concluded that an appropriate theory still was not developed at the time of his investigation. Lacking a sound theoretical basis for multidimensional effects, a simple linear proportionality relationship was used to correlate cell size to reaction zone lengths. He reported that single parameter correlations were accurate only to within $\pm 200\%$ over an equivalence ratio range of 0.38 to 5.56 for H_2 -air mixtures initially at ambient conditions. He found that an improved correlation using existing data could predict within $\pm 50\%$ the effects of dilution with CO_2 and H_2O and the effects of simultaneously changing the initial condition. The dramatic inhibition effect of CO_2 and H_2O was explained in terms of both thermal and chemical effects and a secondary effect due to a switch in the rate-limiting kinetic step.

The detonation cell width (λ) is commonly used to measure the ease with which a mixture can be detonated (detonation sensitivity). Numerous criteria have

been developed to correlate the possibility of detonation initiation and propagation in a given geometry and known mixture composition. For the above reason, many studies have attempted to assess the cell sizes of different mixtures, using both measurements and theoretical models.

Shchelkin and Troshin^{75b} first proposed that the experimentally measured detonation cell size could be correlated with the reaction zone width, calculated on the basis of the ZND model of 1D detonation wave. In the ZND model, reaction starts behind the leading shock at the von Neumann temperature T_{vn} and pressure P_{vn} . The reaction is accompanied by expansion, and chemical equilibrium is approached with thermodynamic parameters coming to the C-J values (T_{C-J} , P_{C-J}). The local flow Mach number with respect to the shock front reaches unity at the C-J conditions $M_{C-J} = 1$. A characteristic reaction zone width, δ , can be defined in this model. Shepherd^{74a} has discussed in detail several definitions of δ . Usually this value was defined by the location characterized by the maximum temperature gradient behind the leading shock ($dT/dx = \text{max}$, corresponding to the point of the maximum heat release rate) or by a certain value of local Mach number (e.g., $M = 0.75$). Some simplifications were also used in the calculations of reaction zone widths.⁷⁶ In some of them, integrations of the governing equations were not made along the Rayleigh line. The reaction was assumed to proceed at either constant volume or constant pressure conditions. Shepherd^{74a} showed that the length of the reaction zone for constant-volume calculation behind the detonation front is very close to that for the constant-pressure case.

Attempts have been made to relate the characteristic reaction widths predicted by the ZND model to the measured cell widths using detailed chemical reaction mechanisms. Detailed ZND analyses of gaseous detonable mixtures have been made by Westbrook,⁷⁷ Westbrook and Urtiew,⁷⁶ Moen et al.,⁷⁸ Shepherd,^{74a} and Ciccarelli et al.⁷⁹ Calculations have covered hydrogen and hydrocarbon fuels, mixed with oxygen and diluted with different gases (nitrogen, steam, argon, helium, and carbon dioxide). The results have shown that the ZND model captures qualitatively the effects of mixture composition, temperature, and pressure on cell width, provided that a suitable choice is made for the value of A —defined as the ratio of detonation cell width to the reaction zone width. If the value of A is determined from the ratio of measured cell width to the calculated reaction zone width, it appears to depend on the mixture composition and initial conditions and varies over a range of about two orders of magnitude. This range is much wider than that of the accuracy of the cell width measurements. The detonation cell width, thus, appeared to be not proportional to a characteristic reaction zone width determined in the framework of the ZND model. This is because the reaction times or characteristic reaction lengths determined with the ZND model cannot be used directly as representative parameters to characterize the multidimensional wave.

Gavrikov et al.^{75a} developed a simple model to generalize the correlation between characteristic reaction zone width (δ) and cell widths (λ). They proposed that the ratio (A) of the detonation cell width to the characteristic reaction zone

width be considered a function of two stability parameters (a dimensionless effective activation energy, $E_a/R_u T_{ps}$, using the post-shock temperature corresponding to the average shock-wave speed through the detonation cell $D = (D_1 + D_2)/2$, and dimensionless temperature T_{vn}/T_0 , representing the ratio of the von Neumann temperature to the initial combustible gas mixture temperature). These parameters introduce adequate reaction time sensitivity to changes of the initial reaction condition after the shock heating of the mixture to the von Neumann state. They took into account multi-dimensional structure of real detonations, since their model was based on the characteristic reaction zone width calculated from initial conditions behind a shock with velocity exceeding that of the stationary 1D C-J detonation. The effective activation energy was defined as an average parameter describing reaction time sensitivity to the strength of lead shock in a range of shock speeds $D_1 = 1.0D_{C-J}$ and $D_2 = 1.6D_{C-J}$ representative for reaction conditions in a multi-dimensional detonation wave with hydrogen mixtures. Gavrikov et al.^{75a} developed a semiempirical correlation to relate the ratio A and the above two stability parameters. The results computed from their correlation are in reasonable agreement with experimental data for a wide range of conditions.

The effective temperature sensitivity of reaction time in multi-dimensional detonations was found to be weaker than those in 1D detonation models. The effective activation energy was found to decrease with an increase of initial reaction temperature, at least for the types of mixtures considered. Such a behavior appeared to be important in the λ/δ correlation. The changes of effective activation energy over the range of reaction conditions also may play a role in the dynamic behavior of detonations. For hydrogen-air mixtures, the range of $E_a/R_u T_{ps}$ is from 3 to 16, and T_{vn}/T_0 from 1.5 to 8.0. For $C_nH_m/O_2/N_2$ mixtures, the range of $E_a/R_u T_{ps}$ is narrower, varying between 5 and 10 with $T_{vn}/T_0 = 4.5$ to 6.5.

8 NONIDEAL DETONATIONS

This section confines itself to available information on gaseous detonations summarized in a review by Gelfand, Frolov, and Nettleton,⁸⁰ including those in aerosols, clouds of flammable dusts, and hybrid mixtures, from the standpoint of safety of chemical processing plants. Some recent extensions to work based on the concept of an ideal front with losses (nonideal theory) are discussed, showing how this may be applied to derive guidelines on the effects of tube diameter, wall roughness, and initial pressure of the mixture on the velocity of a steady front. Further extension to the prediction of limits is considered for conditions likely to be experienced in an actual plant, where walls are unlikely to be smooth and the presence of inert particles in the explosive medium is a possibility.

A comparison is made between the one-dimensional ZND theory with the real detonations with respect to the losses. The mechanisms of detonations in rough pipes and the aspect of the critical pipe diameter are discussed. The limits of detonations in various detonable media are studied. The last part of this section deals with various methods available for prevention and suppression of detonations.

8.1 Definition of Nonideal Detonation and Zel'dovich and Shchelkin's Detonation Mechanisms in Rough Tubes

The term *nonideal detonation* implies a detonation wave characterized by momentum and energy losses resulting from the interaction of the gas with rough walls and particles dispersed in it. Since the major assumption of the ZND model of detonation is that the wave structure is one-dimensional, it is obvious that this assumption cannot be applied to practical cases with rough walls. Clearly obstacles (e.g., roughness elements at channel walls or dispersed particles) can disturb the flow field, distort the three-dimensional nonsteady pattern of detonation cells, and generate additional hot spots. The latter may lead to the reaction proceeding in a more active fashion, or result in the formation of zones with a relatively low temperature (as a result of decrease in the wave velocity) and generate the opposite effect of reaction quenching. There is a consensus view, based on comprehensive studies, that not only should momentum and energy losses be taken into account but so also should the nonsteady nature of shock wave-reaction zone complex. It is also known that energy losses are more important in mixtures of fuel-air than in mixtures of fuel-oxygen, as the reaction zone for the former is much larger than that for the latter. Moreover, these enhanced losses may well modify the relationship between the multi-dimensional nature of a real front and its degree of unsteadiness.

Unfortunately, a comprehensive analysis of multi-dimensional flow in detonation waves with detailed consideration of energy and momentum losses is not yet available. Moreover, available information on specific features of detonations in systems with losses is far from systematic. Nevertheless, a qualitative generalization of quasi-detonations in tubes with barriers has been suggested recently,^{81–83} which allows the identification of some special features of the phenomenon.

Shchelkin's^{84–86} original experiments on detonations in rough tubes have resulted in several mechanisms proposed to interpret the significant velocity deficit between propagation in rough and smooth walled tubes. Zel'dovich^{87,88} postulated that for rough tubes the temperature behind the shock wave traveling at a moderate velocity (less than the ideal detonation velocity) may be insufficient for ignition of the mixture, depending upon the amount of heat loss. On the other hand, in a rough tube, local hot spots come into play and result in reflections of the leading shock from protuberances on the wall. These hot spots can promote local ignition of the mixture and the spread of flame across the tube cross section. The flame traveling from the periphery towards the axis of the tube generates compression waves, which overtake the leading shock front, allowing its propagation without attenuation. The leading flame front has the form of a cone with its base on the shock wave and its apex directed toward the site of initiation. Since the time for burnout of the mixture increases and the drag coefficient of a rough tube is higher than that of a tube with smooth walls, the total losses in the reaction zone grow considerably. Therefore, in rough tubes, detonation waves propagate at lower velocities than those in smooth tubes. The velocity of the wave in a rough tube is such that after its reflection from a protuberance, the

resultant ignition delay is close to the value typical for ideal detonation in a tube with smooth walls.

Babkin and Kozachenko^{89,90} obtained clear photographs of a failing detonation front in a rough tube filled with a mixture of 33.75% H₂ + 13.9% O₂ + 52.35% N₂ showing the existence of hot spots behind a shock wave. They demonstrated that the luminous flame front lagged significantly behind the shock wave, which was followed by many localized ignition spots near the channel wall. These spots were clearly distinguishable and distributed between the shock-wave station and the flame-front station. Some bow shocks were also visible in that region. As explained by Borisov et al.,⁹¹ it is not possible to exclude the influence of focusing shock waves by protuberances in the processes of the formation of hot spots.

An alternative mechanism for the propagation of detonations in rough-walled tubes was suggested by Shchelkin.⁸⁴⁻⁸⁶ This mechanism is associated with turbulence generated by the interaction of the flow with bumps on the wall surface. When the appropriate intensity of turbulence is achieved behind the leading shock, ignition occurs on account of mixing of pure unburnt mixture with hot combustion products. Combustion can start at a certain distance from the wave front, and as turbulent reactants burn out, it spreads across the cross section of the channel. The reaction zone can be much thicker compared with that of an ideal detonation. This feature could contribute to observed detonation waves with lower propagation velocity than C-J detonation. Since the shock wave itself does not ignite the combustible mixture, such a process is not a true detonation in the traditional sense. For these waves, many researchers have observed wedge-shaped flame tongues near the wave front. Flame propagating from the periphery of the tube cross section towards its center have been distinctly recorded. In addition, combustion centers near the axis of a tube and long tails of burning mixture behind the main combustion zone have been observed. Some lengths of the reaction zone are on the order of a few tube diameters. In general, it appears that both mechanisms are involved in the propagation of detonations in rough tubes. In this case, ignition of a combustible mixture takes place both behind reflected shock waves and due to turbulent mixing of the unburnt mixture with hot combustion products.

8.2 Theoretical Considerations of Energy and Momentum Losses

With all the aforementioned factors present in actual conditions, the nonideal detonation process can be called the “quasi-detonation process.” We can assume that ignition occurs due to interaction of the shock front with protuberances on the internal walls of the channel and reaction proceeds under highly turbulent conditions. The first successful attempt in treating the problem analytically was conducted by Ribnin.⁹² He adopted a number of suggestions from the pioneering work by Zel'dovich^{87,88} and the phenomenological considerations of Shchelkin⁸⁴⁻⁸⁶ in his model and obtained quantitative results. Ribnin⁹² suggests that the reaction zone of a detonation can be divided into two subzones. In the first

subzone, attached to the leading front, the flame propagates from the tube walls toward the tube axis (i.e., boundary layer combustion takes place); in the second subzone, located downstream of the first, the unburnt mixture is consumed in pockets, spreading later throughout the cross section of the tube (i.e., bulk combustion takes place after the merging of the boundary layers). Essentially, the two submodels are based on the concept of Zel'dovich,⁸⁸ involving peripheral self-ignition of the mixture behind reflected shocks, and that by Shchelkin,⁸⁴ involving ignition of the mixture due to mixing with highly turbulent combustion products. According to Ribavin,⁹² for the limiting situation when the combustion zone occupies the whole cross section of a tube, the minimum value of the detonation can be calculated from

$$(D/D_0)^2 = \frac{\gamma}{2(\gamma + 1)[1 + (\gamma - 1)\Omega]} \quad (4-156)$$

Here, Ω is the ratio of heat losses to momentum losses, defined as

$$\Omega = \frac{2 \int_0^x \alpha_H \Delta T dx}{D \int_0^x C_f \rho (D - u)^2 dx} \quad (4-157)$$

where α_H is the heat transfer coefficient, C_f is the drag coefficient, and γ is the ratio of the specific heats. According to Zel'dovich,^{87,88} $\Omega = 1$ applies only to tubes with hydrodynamically smooth walls. In tubes with rough walls, $\Omega \ll 1$, and hence (for example, for $\gamma = 1.2$) the normalized velocity deficit $(D/D_0) \approx 0.52$. Of practical importance is the existence of a limiting value of the self-sustaining steady propagation of a detonation wave in a rough tube. It is of interest that the limiting value of the drag coefficient is independent of tube diameter. When the drag coefficient attains its limiting value, the combustion products are shown to decelerate completely relative to channel walls. Consequently, this limit is frequently named the gasdynamic limit. The detonation velocity at this limit is close to the sound velocity in the combustion products. The effect of incomplete combustion was also considered by Ribavin,⁹² who proposed that

$$(D/D_0)^2 \approx \frac{\gamma(1 - \beta_*)}{2(\gamma + 1)[1 + \Omega(\gamma - 1)]} \quad (4-158)$$

where β_* is the unburned portion of a detonable mixture on the C–J plane. With properly chosen heat-transfer and drag coefficients, the predicted quasi-detonation wave velocities were in close agreement with the measured data of C_2H_2 –air, C_2H_4 –air, and C_3H_8 –air mixtures.

8.3 Critical Pipe Diameter Consideration

The Zel'dovich theory⁸⁷ relates the detonation limit to the occurrence of severe losses in energy and momentum with decreasing diameter of the confinement. An

attempt has been made by Gelfand et al.⁹³ to relate this theory with experimental observations. The model incorporates enhanced values for drag and heat-transfer coefficients over those describing steady flow in the conservation equations for momentum and energy. Experimental values for the C-J velocity and the ignition delay were used in the model. This ensures that the predicted critical diameter matches closely with the experimental observations for a wide range of mixture ratios. Specifically, the predicted effect of initial pressure and composition on the limiting diameter agrees well with experimental data. The limits of detonation are attributed to the increasing energy losses with decreasing tube diameters.

The empirical determination of the critical diameter involves measurements of the cell size, in the appropriate ranges of pressure, temperature, and mixture compositions. However, there were large discrepancies in certain media, in the sizes measured and those predicted by models. In general, the one-dimensional models⁸⁷ give a good qualitative explanation. The use of a more sophisticated treatment of chemical kinetics and realistic values of drag and heat-transfer coefficients gives a better agreement than the one-dimensional model.

The kinetics can be described in two ways: (1) the use of ignition delays measured in shock-tube experiments and (2) the use of comprehensive reaction schemes for the chain-branching process. Gelfand et al.⁹³ used the ignition-delay approach and considered the momentum loss in the growing boundary layer behind the wave front. From their study, reliable drag coefficients were derived for use in the induction zone. The kinetic parameters of fuel-air and fuel-oxygen mixtures were chosen by comparison of the well-known expression for an adiabatic induction period. A comparison was made between the correlations for adiabatic induction period (ignition delay)

$$\tau_i = \frac{C_v}{k} \frac{R_u T^2}{QE_a} \beta_0^{-(n-1)} \exp\left(\frac{E_a}{R_u T}\right) \quad (4-159)$$

with an empirical correlation:

$$\tau_i = AC_F^a C_{Ox}^b C_{In}^c \exp\left(\frac{E_*}{R_u T}\right) \quad (4-160)$$

Here, C_v is the constant-volume specific heat constant, k the pre-exponential factor in the Arrhenius-type reaction, Q the heat release, E_a the activation energy, β_0 the initial concentration of the reactant, n the reaction order, and E^* the experimental value of activation energy. C_F , C_{Ox} , and C_{In} are the molar concentrations of fuel, oxidizer, and inert species, respectively.

A comparison between these correlations leads to the following result:

$$n = 1 - (a + b + c) \quad (4-161)$$

$$k = \frac{C_v R_u T_{sf}^2}{A \rho_{sf}^{1-n} QE_a} \left[\left(\frac{Y_F}{\mu_F} \right)^a \left(\frac{Y_{Ox}}{\mu_{Ox}} \right)^b \left(\frac{Y_{In}}{\mu_{In}} \right)^c \right]_0^{-1} \quad (4-162)$$

$$E_a = E^* \quad (4-163)$$

where Y and μ are the mass fraction and the molecular mass of a given species. The subscript 0 denotes the undisturbed upstream condition of the leading shock and ρ_{sf} and T_{sf} are the density and temperature at the shock front, defined by the detonation velocity D . The γ value is assumed to be constant and equal to the average value between the initial mixture and the combustion products.

A single-step reaction was assumed by Gelfand et al.⁹³ without any dissociation. The heat release is calculated as

$$Q = \frac{D_0^2}{2(\gamma^2 - 1)} \quad (4-164)$$

where D_0 is the ideal C-J detonation velocity.

The kinetics of the chemical process can be expressed in terms of the reactant concentration as

$$\frac{d\beta}{dx} = -\frac{k\beta^n}{U} \exp\left(-\frac{E_a}{R_u T}\right) \quad (4-165)$$

where x is the distance to the lead shock front of the steady-state detonation wave traveling with velocity U .

The drag coefficient C_f is normally related to the hydraulic drag coefficient f by $C_f = f/4$. Gelfand et al.⁹³ found that in nonstationary flow conditions behind a shock wave, it is adequate to represent the drag coefficient C_f by the hydraulic drag coefficient f (i.e., $C_f = f$). Also, the drag coefficient in a rough tube holds for a tube with smooth walls. According to the Blasius law, we have

$$C_f = 0.3164/\text{Re}_d^{0.25} \quad (4-166)$$

where $\text{Re}_d = Wd/\nu$; note that the C-J condition implies that $D - W = c$. The kinematic viscosity is calculated using the kinetic theory of gases, i.e.,

$$\nu = 26.7 \times 10^{-6} \frac{(\mu T_{sf})^{0.5}}{r_m \rho_{sf}} \quad (4-167)$$

where r_m is the “radius” of a mixture molecule (\AA) in a model of hard spheres. The heat-transfer coefficient can be obtained through the use of Reynolds’ analogy. Essentially, the heat-transfer coefficient C_H can be calculated from

$$C_H \equiv \frac{h_c}{C_p \rho W} = \frac{C_f}{2} \quad (4-168)$$

The detonation velocity is calculated by an iterative process of Eq. (4-165) together with the following conservation equations written in a frame attached to the detonation wave front:

$$\frac{d(\rho u)}{dx} = 0 \quad (4-169)$$

$$\frac{d}{dx}[p + \rho u^2] = \frac{4\sigma}{d} \quad (4-170)$$

$$\frac{d}{dx} \left[\rho u \left(h + \frac{u^2}{2} \right) \right] + Q \frac{d\beta}{dx} = -\frac{4q}{d} + \frac{4\sigma D}{d} \quad (4-171)$$

The drag force is determined by the expression

$$\sigma = C_f \rho |D - u| \frac{D - u}{2} \quad (4-172)$$

The heat flux is calculated as

$$q = h_c(T_{st} - T_0) \quad (4-173)$$

where T_{st} is the stagnation temperature of the gas. The following boundary conditions are applicable to the problem:

$$\begin{aligned} x = 0, \quad \rho &= \rho_{sf}, \quad p = p_{sf}, \quad \beta = 1 \\ x \rightarrow \infty, \quad \rho &= \rho_0, \quad p = p_0 \end{aligned} \quad (4-174)$$

Using the above model and assuming that the number of moles does not change, the calculated results of Gelfand et al.⁸⁰ were compared with many sets of detonation mixtures. Their chosen values of A , a , b , c , and E^* resulted in ignition delays that produced satisfactory agreement between the limiting tube diameter and λ/π , especially for such readily detonable mixtures as C_2H_2 , H_2 , and C_2H_4 with oxygen or air. They showed that at the limit of propagation, there is a reduction in wave velocity; also $(D_0 - D)/D_0$ does not exceed 10–15%.

8.4 Effect of Several Physical and Chemical Parameters on Detonability

In an early stage, the most severe difficulty encountered in an attempt to produce a comprehensive list of detonable media is that potential hazards are recognized only after the accident has taken place. Also, it cannot be confidently said that the damage in question was caused totally due to detonation. Furthermore, at elevated pressures and temperatures, the relation between the original combustible mixture and the one that caused the detonation cannot be determined. Thus, at higher temperatures, some compounds can be formed to cause detonation, but they were not present in the initial mixture. The experiments carried out are usually on a small scale, much smaller than actual conditions in chemical plants. The extrapolation of these results can be erroneous, according to Nettleton.⁹⁴ There are some materials that can form detonation waves by themselves (i.e., ozone and acetylene). Due to these reasons, it is almost impossible to produce a comprehensive list of detonable media.

In practical conditions, confined detonations are much more likely to occur than unconfined detonations. Confinement allows pressure buildup and the development of viscous boundary layer on the wall surface. A turbulent boundary layer can be formed on the wall surface, which promotes the transition from deflagration to detonation. Though the wall roughness is responsible for transition to detonation, the detonation velocity is, in general, lower due to energy and momentum losses. In general, unconfined detonations can be produced due to leakage of explosive gases into the atmosphere. When unconfined detonations are studied, it should be borne in mind that they may not be exactly spherical in nature.

There are a number of gases and vapors that decompose exothermically and can support a detonation wave even in the absence of an oxidant. Examples of such gases are acetylene, ozone, ethylene, and high-concentration hydrogen peroxide. There are common features in the decomposition of derivatives of acetylene; hence, they can also be detonable. In general, all compounds that decompose exothermically should be given due consideration. It is worth noting that there are very few recorded examples of detonations of self-decomposing materials in unconfined medium.

The concentration of the fuel in the mixture may not be a cause for detonations to cease. If the pressure is sufficiently high, the detonation can be produced either by exothermic decomposition of gaseous mixture or due to its oxidation reactions. Thus, the detonation limits in terms of equivalence ratio are wider for higher-pressure conditions.

Tables 4.4 and 4.5 give some comparison of data on flammability and detonation limits. These limits are for both confined and unconfined detonations in mixtures with air and oxygen. It can be observed that the detonation limits are narrower than the flammability limits for each fuel with air as well as oxygen. The detonation limits for unconfined detonations are narrower than those for confined detonations.

Many studies were conducted to determine the influence of initial pressure on the detonability of self-decomposing fuels. Most researchers show that for a given combustible mixture (e.g., acetylene–O₂), the initial pressure does have an effect on the critical diameter. For initial pressures exceeding a threshold level, detonation is possible if the pipe is long enough. For pressures below the threshold level, the flame propagates as a deflagration wave no matter what the length of the pipe is. It is difficult to study the effect of initial temperature on detonation. This is due to the fact that the autoignition temperature for most fuel–air mixtures is pretty low. For alkane–air mixtures, it starts from 540°C and reduces with an increase in fuel molecular weight. Thus, the experiments can only be carried out over a small range of temperature. In general, it can be said that higher initial temperatures will lead to a higher flame velocity and the transition from deflagration to detonation will take place faster.

8.5 Possible Measures for Reducing Potential of Detonation Wave Generation

The minimal conditions required for the development of a detonation wave are the occurrence of a flammable mixture and an ignition source in the case of

fuel–oxidant mixtures, or sufficiently high pressures with an ignition source for exothermically self-decomposing fuels. It is not possible to altogether eliminate such conditions in chemical plants. Hence, several mechanisms have been developed to inhibit flames from spreading.

Halogen-containing compounds, products of their pyrolysis, sulfur dioxide, etc., inhibit flame spreading by combination with radicals such as H, OH, and O. These chemical species halt the chain-branching reactions and stop flame spreading. The mechanism involved in the flame inhibition by sodium or potassium salts of organic materials is not fully known. It could be due to a combination of endothermic decomposition and reactions with radicals such as H, OH, etc.

Spraying of water curtains can be effective in many cases and offers the obvious advantage of cost effectiveness; thus, it is widely used. In the inhibition of accelerating flames, the time factor is of importance. For flames with high velocities, the time available for the suppressants to act is indeed very small. There are several different strategies in the prevention of detonation:

Inhibition of flames of normal burning velocity—This is performed mostly by injection of a flame suppressant into the pipes. This requires some kind of flame detection mechanism, which triggers the injection of the suppressants. As the length of the pipes is usually very large in industrial plants, an array of such units is required. For slow-burning flames with burning velocity not exceeding 10 m/s, there is ample time for flame detection and suppression injection. The most widely used inhibitor is mono-ammonium phosphate. Halogenated hydrocarbons are generally used in commercially supplied suppressant equipment. The disadvantage in this family of suppressants is that the products of decomposition of such materials are highly corrosive. Thus, a decision has to be made between the effectiveness of the suppressant and the damage caused due to an accidental injection. Suppression of flames in spherical or cylindrical vessels is more difficult as the time available is much less. Precautions should be taken against central ignition, which is the most harmful. Flames can also be arrested by insertion of sintered metal discs, honeycombs, etc. The choice depends on the allowable pressure drop. These are usually cost effective, as they do not require much maintenance. But the positioning could prove crucial, as in the later stages of flame spread, such structures could actually enhance the flame due to generation of turbulence.

Venting in the early stages of an explosion—An alternative form of prevention of a detonation wave is some form of pressure relief. Bursting diaphragms and hinged or spring-loaded explosion doors can be used. These are much cheaper. An unwanted consequence of such pressure release could be that turbulence could be created that could actually accelerate the flame. This design option could introduce pressure oscillations in the vessel, which could be equally harmful. There are many suggestions available for the placing of pressure reliefs in pipes. In general, it can be said that pressure relief is favored in systems with low working pressures.

Quenching of flame-shock complex—Most methods used to quench low-velocity flames are also effective at a stage when the flame has accelerated to near-detonation velocity. An example is the use of ceramic packings. This method has been adopted by some plants in the German chemical industry. The pipelines were designed to sustain the maximum pressure developed, and the packings prevented the transition to detonation.

In addition, there are other methods for reducing the chance for deflagration-to-detonation transition to occur. For example, in mine galleries, trays containing limestone dust or water were supported on ledges on walls that could be easily dislodged by turbulence, thus introducing the inert material just before the flame zone. Injection of a suppressant is perhaps the most effective in all the stages of flame spreading. The choice and design of the system depends on the type and dimensions of the plant and also the nature of the detonable media.

9 CONSIDERATION OF SPONTANEOUS DETONATION INITIATION

Bartenev and Gelfand⁹⁵ presented a very recent review article describing the process of detonation initiation within the scope of the spontaneous flame concept, originally proposed by Zel'dovich.^{96,97} The basis of the concept is that the origin of certain combustion modes is conditioned by the spatial gradients of self-ignition delay time in the system. Considerable recent attention has been focused on applying this concept to real physical systems. Their overview summarizes the essential results of numerical, analytical, and experimental works on the spontaneous detonation initiation performed over the past decade.

According to Bartenev and Gelfand,⁹⁵ presently there are two extreme points of view on the problem under consideration. One is the recognition of the problem from the standpoint of mathematical proof of the appropriate solutions of chemically reacting gasdynamics, and the other is the phenomenological recognition of some combustion processes that cannot be adequately explained within the framework of the laminar flame theory or the classical theory of detonation.

Following Zel'dovich,^{96,97} the general problem of spontaneous detonation initiation can be formulated. The solution of this problem can be applied to numerous combustion studies covering various spontaneous flame propagation regimes. Let us consider a closed space Σ , filled with a reactive mixture described by self-ignition induction time value $\tau_i(x, y, z)$. The induction period $\tau_i(x, y, z)$ in the general case is a function of the mixture composition and thermodynamic parameters. The particular expression of this function is not as important. It is sufficient to state that after some self-ignition delay time, the chemical energy release will take place at a point (x, y, z) . The evolution of a surface $\tau_i(x, y, z)$ with time will correspond to the propagation of a wave of chemical energy release in space. The velocity vector of this spontaneous wave can be written as

$$\vec{u}_{sp} = \frac{\text{grad } \tau_i(x, y, z)}{[\text{grad } \tau_i(x, y, z)]^2} \quad (4-175)$$

The basis of Eq. (4-175) is that the chemical energy is released consequently in accordance with the spatial distribution of ignition delay (more exactly, its inverse value). This energy release is accompanied by the temperature increase and change of mixture composition, thus displaying the wave of chemical transformation. The magnitude of the spontaneous wave speed is the absolute value of \vec{u}_{sp} , which can be defined as $u_{sp} \equiv |\vec{u}_{sp}|$. This speed can be compared to magnitudes of other speeds of known combustion processes to form the basis for classification of Zel'dovich's spontaneous regimes,^{96,97} described in the following:

1. At $u_{sp} > D$ (speed of C-J detonation), there is a propagation of an underdriven detonation wave; in this case, no shock front is formed, although the velocity is higher than the detonation speed. In the limit, when the constant-volume explosion takes place, $u_{sp} \rightarrow \infty$.
2. If $u_{sp} \leq D$, then after self-ignition and consumption of some part of the initial substance, a shock wave can form in the space occupied by fresh gas, transforming into detonation through a transient process.
3. If S_L (laminar flame speed) $< u_{sp} \ll c$ (speed of sound) $< D$, this case corresponds to the propagation of a subsonic deflagration wave.
4. If $u_{sp} < S_L$, the laminar flame propagation is realized in a system. This mode of flame propagation is controlled by the processes of heat conduction and mass diffusion.

Thus, the basic problem of the theory of spontaneous propagation of explosive processes can be formulated as follows: if the distribution of $\tau_i(x, y, z)$ in a region Σ at the initial time ($t = 0$) is known, then the behavior of the system should be determined at the subsequent moment of time, namely the regime of the combustion process propagation.

At first glance, it is rather simple to find the answer using Zel'dovich's classification. For this purpose, it is sufficient to calculate the fields of spontaneous flame speed $u_{sp}(x, y, z)$ and to compare their magnitudes to known characteristic speeds S_L , c , and D . However, in a real system (even greatly simplified), there is a whole spectrum of spontaneous speeds at the initial moment of time; it is related to the continuity of the initial conditions in the physical system. The gradients of parameters responsible for self-ignition can be smoothed, for example, by the processes of mass diffusion and heat transfer.

Another feature of the spontaneous behavior of explosive processes is the uncertainty of distribution function $\tau_i(x, y, z)$ [and, therefore, the field of spontaneous speeds $u_{sp}(x, y, z)$] after the expiration of the self-ignition delay time in some spatial points in the space (where $\tau_i(x, y, z)$ is minimal at $t = 0$). The inevitability of the generation of the pressure perturbations in the system after the first act of ignition is the reason that the behavior of a field of spontaneous speeds is not solely determined by initial conditions any longer, but also depends on the intensity of interaction with gasdynamic processes (from acoustic fluctuations to shock waves). The nonstationary character of such interaction results in the transition from one mode of combustion to another. Thus, the aforementioned

is the global problem of the theory of spontaneous regimes of flame propagation that resulted in consideration of the following particular problems.

1. Formation of a zone with nonuniform distribution of an induction period in physical systems: this case includes works devoted to the formation of isolated initiating centers of reaction, and those works in which the occurrence of extended zones with nonuniform distribution of thermodynamic parameters (e.g., Lee, et al.⁹⁸).
2. Determination of the connection between initial distribution $\tau_i(x, y, z)$ and the regime of flame propagation in a system: in these investigations the gradients of various parameters on which τ_i depends are taken as the initial conditions, and with the help of numerical modeling the possibility of realization of any mode of flame propagation is determined. Therefore, the attempt to obtain the criteria of explosive processes generation is made on the basis of an initial distribution and absolute magnitudes of these parameters (e.g., Lee and Moen⁹⁹).
3. Examination of gasdynamic perturbations influencing the process of spontaneous ignition: these studies consider the process of amplification of gasdynamic perturbations in a chemically reacting environment, and the formation of transient complex pressure fronts plus reaction fronts, providing the mechanism for transition from one mode of flame propagation to another (e.g., Clarke¹⁰⁰).
4. Theoretical research of real physical systems from the point of view of spontaneous explosive processes: such research makes it possible to relate the investigations of ignition phenomena behind the incident, and reflected shock waves, as well as the process of deflagration to detonation transition (e.g., Wolanski¹⁰¹).
5. Experimental studies, directly or indirectly confirming the concept of spontaneous regimes of flames propagation (e.g., Lee and Moen,⁹⁹ Dorofeev et al.¹⁰²).

9.1 Functional Form of Distribution of Ignition Delay

The formation of spatial zones with nonuniform distribution of ignition delay $\tau_i(x, y, z)$ implies the analysis of nonuniform distribution of parameters included in the expression for $\tau_i(x, y, z)$:

$$\tau_i(x, y, z) = \frac{c_v R_u [T_0(x, y, z)]^2 \exp [E_a / R_u T_0(x, y, z)]}{t_0^{-1} Q C_0(x, y, z) E_a} \times \left[1 + \frac{2 R_u T_0(x, y, z)}{E_a} \right] \quad (4-176)$$

where t_0 represents the frequency factor in the Arrhenius law, C the concentration of the reacting substances, and Q the heat of reaction. This equation was derived by Frank-Kamenetsky¹⁰³ by integrating the energy balance equation for a system containing reactive gas obeying the temperature dependency of the rate of chemical reaction according to the Arrhenius law.

Equation (4-176) indicates that the most appropriate variables for the generation of nonuniformity are temperature, T , and concentration, C , of a combustible component, because it is difficult to realize in practice the system with variable activation energy, E_a , or heat of reaction, Q . Thus, the expression for the field of spontaneous wave speed can be presented in the following form.

$$\vec{u}_{sp} = \frac{\text{grad } \tau_i(x, y, z)}{[\text{grad } \tau_i(x, y, z)]^2} = \frac{[(\partial \tau_i / \partial T_0)_{C_0} \nabla T_0 + (\partial \tau_i / \partial C_0)_{T_0} \nabla C_0]}{[(\partial \tau_i / \partial T_0)_{C_0} \nabla T_0 + (\partial \tau_i / \partial C_0)_{T_0} \nabla C_0]^2} \quad (4-177)$$

Many reacting systems with different initial temperature and concentration distribution have been analyzed. Most frequently the linear distribution of temperature was analyzed as the simplest case having the least number of governing parameters. The linear distribution of concentration of a combustible component of a mixture was also considered. However, in real physical systems, there often exists parabolic or Gaussian distribution of temperature, as a result of the propagation of a thermal wave in reacting flows or in systems with external energy deposition. Despite various types of nonuniformities and distributions of controlling parameters, the fields of spontaneous speeds of a flame have exponential character in all cases, because the speed of chemical reaction generally obeys the Arrhenius rate dependency on temperature. Hence, it is reasonable to expect that there are some similarities in the development of chemically reacting flows.

9.2 Experimental Verification of Processes of Nonexplosive Detonation Initiation

Direct experimental illustrations of the detonation initiation phenomena are not as well developed as theoretical studies. This is caused by the difficulty of setting initial conditions for the realization of certain planned combustion processes, extreme sensitivity of considered processes to accidental fluctuations of gasdynamic parameters, instability of chemically reacting flows, etc.

9.2.1 Photochemical Initiation of Detonation in Mixtures with Nonuniform Concentration Usually the initiation of a detonation is connected to heating some mass of reactive mixture beyond the temperature of self-ignition and maintaining the mixture at this high temperature for some time interval, long enough for initiation of a local thermal explosion that escalates and results in the onset of detonation. However, the phenomenon of direct detonation initiation can be realized in the case when the temperature of the mixture is lower than the temperature of self-ignition. In a set of experiments, Lee and coworkers^{98,99} exposed acetylene–oxygen, hydrogen–oxygen, and hydrogen–chlorine mixtures, placed in a chamber with quartz windows, to ultraviolet radiation. The absorption of ultraviolet radiation by O_2 or Cl_2 molecules resulted in dissociation of these molecules to form free radicals O or Cl , respectively. At sufficient concentrations of these radicals, the chain reactions began, resulting in local thermal explosion in the system. Depending on the intensity of ultraviolet radiation, three different

modes were observed. At a low intensity, the ultraviolet radiation penetrated through the window and heated the mixture only in a small region with shallow depth. In the near-window space, a layer of the radicals is formed, resulting in initiation of a combustion wave (deflagration), propagating from the adjacent wall inside the chamber. At a very high intensity of incident ultraviolet radiation, the energy of the light was absorbed throughout the mixture, providing high concentrations of radicals to the whole volume of the chamber and resulting in explosion at constant-volume conditions. In this case, explosion in the system was not preceded by the propagation of any shock waves.

At an intermediate level of ultraviolet radiation, a detonation wave can be formed instantly and propagated from quartz windows inside the chamber; this phenomenon is associated with the attainment of high concentrations of radicals directly near the window of the chamber, and the development of a gradient of free radicals concentration at the wall of the chamber. If the profiles of radicals' concentration have the suitable form and thickness, the thermal explosion in a layer near the wall can produce a pressure wave, promoting the increase of pressure in the following layers of the mixture and reducing the ignition delay in these layers. Such an amplification of a pressure wave proceeds until the stationary C-J detonation is generated, though the pressure wave development as a result of explosion of one particular layer in itself cannot ensure the initiation of chemical reaction in the next layer.

9.2.2 Gasdynamic Jet as a Method of Creating Temperature-Concentration Nonuniformity Another interesting example of the mechanism of detonation excitation without occurrence of shock waves was investigated by Knystautas et al.¹⁰⁴ This phenomenon is closely connected to a problem of spontaneous explosion. It appears that by changing the outflow conditions of combustion products from a circular hole (or a perforated orifice plate) of the small closed chamber, it is possible to cause onset of detonation without the occurrence of strong shock waves. After the ignition of an equimolar $C_2H_2-O_2$ mixture, by a spark source in the center of a small, round chamber, the first event is the outflow of some unburned cold mixture through the circular hole into the adjacent chamber of large volume. After a short delay, the products of combustion begin to flow into the large chamber and intense mixing of the hot combustion products with the unburned gas in the large chamber takes place; this can initiate the onset of a detonation wave. Large-scale eddies were found to be essential for detonation. These eddies were considered to provide the main mechanism of entrainment, and were also responsible for providing energy to maintain the intensity of the small-scale turbulence.

The study by Knystautas et al.¹⁰⁴ demonstrates conclusively that DDT can be achieved when an appropriate obstruction is placed in the path of a propagating flame. Although their experiments were performed using equimolar acetylene–oxygen mixture (perhaps the most sensitive gaseous explosive) there is no reason to believe that the same mechanisms would not apply to less sensitive fuel–air mixtures if the length and time scales involved were chosen appropriately. The role of the obstruction is to first create a turbulent flow of displaced

unburned gases. Then, as the flame emerges into this turbulent region, rapid mixing between the hot combustion products and the unburned gases occurs. Auto ignition conditions can be achieved in the turbulent eddies by mixing, and the pressure generated from these explosion centers within eddies amplifies rapidly to become detonation wavelets, which then grow to engulf the entire turbulent mixing region. The requirements for DDT by the turbulent mixing mechanism are (1) generation of large-scale energetic eddies of unburned gases in the turbulent wake of the obstruction, (2) sufficiently intense fine-scale turbulence to promote mixing of hot combustion products entrained into large eddies, and (3) generation of a gradient field in induction time inside the eddy to produce the so-called shock wave amplification by the coherent energy release (SWACER) mechanism. The scale of the required large eddies are estimated to be at least of the order of detonation kernel size (i.e., transverse wave spacing) of the gaseous mixture. The generation of these large eddies by the obstruction is also necessary for feeding the fine-scale turbulence and keeping up the turbulence intensity to facilitate rapid mixing of fluid entrained into turbulent eddies. It was suggested by Knystautas et al.¹⁰⁴ that the large eddies must be at least on the order of the size of the detonation kernel, so that the total chemical energy contained in the volume of the eddy must be sufficient to maintain a shock at a strength capable of auto ignition for a distance of the order of the induction zone length corresponding to that shock strength. Although shock waves with less than the auto ignition strength, generated by sufficiently closely spaced exploding eddies, may coalesce and result in the onset of detonation, their measured results indicate that the SWACER mechanism is probably more effective, since a gradient field in induction time is always generated in a turbulent eddy when hot products are entrained into the eddy and drawn out into spiral "filaments" of fluid before mixing with the unburned gases via turbulent diffusion. Thus, the entrainment and mixing mechanisms in a turbulent eddy are ideal in the sense that they produce a gradient of induction time from the center of the vortex outward, thus making the SWACER mechanism most effective.

Based on their physical considerations, it can be shown that the maximum mixing rate in the eddy is inversely proportional to the induction time of the mixture. Thus, for fuel-air mixtures where induction times are about two orders of magnitude larger than that of fuel-oxygen systems, the corresponding maximum mixing rate should also be two orders of magnitude slower inside the eddy for the reaction not to be quenched. The detonation kernel size depends linearly on the induction time, and fuel-oxygen mixtures typically have induction times one or two orders of magnitude larger than fuel-air mixtures (i.e., few hundreds of microseconds versus a few microseconds under auto ignition limit conditions). Therefore, the critical eddy sizes required for DDT in fuel-air mixture must be about 10 to 100 times larger (i.e., of the order of a few centimeters to 0.5 m) than those of fuel-oxygen mixtures. Thus, we may expect that DDT will occur only in very large-scale experiments with the appropriate large obstruction to generate the large eddies. This may also explain the lack of experimental evidence of DDT in unconfined fuel-air experiments.

9.3 General Observation and Status of Understanding

The investigations of the spontaneous initiation of intensive explosion regimes in gaseous combustible mixtures with the nonuniform distribution of initial thermodynamic properties have been performed intensively over the past 20 years. The most detailed research has been conducted in the theoretical description of the phenomena, while technology gaps exist in experimental confirmation of the ideas developed. It is generally established that the process of spontaneous detonation initiation proceeds through four separate stages, including (1) primary explosion, (2) propagation of adiabatic auto ignition wave, (3) development of a complex detonation-like structure, and (4) its disintegration. According to Bartenev and Gelfand,⁹⁵ except the third stage, each of these stages can be described by a corresponding mathematical model. The third stage still has no mathematical solution to follow the trajectory and intensity of the amplifying shock wave.

A close interrelation between the phenomena of different modes of ignition and the spontaneous ignition concept (applied to exothermic centers) has been demonstrated. Thus, it is possible to assume that most events, admitting self-ignition and further escalation to detonation, occur in the frame of spontaneous mechanism. Moreover, such physical phenomena as deflagration-to-detonation transition in long channels or unconfined clouds can also be explained from the positions of spontaneous initiation. The basic exothermic reaction concept suggested by Zel'dovich^{96,97} is generally applicable to problems, where the gasdynamic flow and the source of fast energy release (chemical, radiation, or atomic) exist simultaneously.

REFERENCES

1. R. Friedman, *Am. Rocket Soc. J.* **24**, 349 (November 1953).
2. D. L. Chapman, "On the Rate of Explosion of Gases," *Phil. Mag.* **47**, 90–103 (1899).
3. E. Jouguet, *J. Mathematique* **347**, 6 (1905); O. Doin, *Mécanique des Explosifs*, Paris, (1917).
4. F. A. Williams, *Combustion Theory*, Addison-Wesley Publishing Co., Reading, Mass., 1965.
5. I. Glassman, *Combustion*, Academic Press, New York, 1977.
6. B. T. Wolfson and R. G. Dunn, "The Calculation of Detonation Parameters for Gaseous Mixtures," *Proc. Propellant Thermodynamics and Handling Conf. Special Rept. 12*, 397–440, Eng. Exp. Station, Ohio State University (June 1960).
7. M. P. Moyle, *Effect of Temperature on the Detonation Characteristics of Hydrogen–Oxygen Mixtures*, Ph.D. Thesis, University of Michigan, 1956.
8. R. L. Gealer, *Influence of High Pressure on the Properties of Hydrogen–Oxygen Detonation Waves*. Ph.D. Thesis, University of Michigan, 1958.
9. L. E. Bollinger and R. Edse, "Thermodynamic Calculations of Hydrogen–Oxygen Detonation Parameters for Various Initial Pressures," *ARS J.* **31**, 251–256 (1961).

10. C. L. Eisen, R. A. Gross, and T. J. Rivlin, *Theoretical Calculations in Gaseous Detonations*, TN 58-326, Office of Scientific Research, March 15, 1958.
11. C. L. Eisen, "Theoretical Calculations in Gaseous Detonations," *Proc. Propellant Thermodynamics and Handling Conf. Special Rept. 12*, 345-356, Eng. Exp. Station, Ohio State University, June 1960.
12. P. L. McGill and J. A. Luker, *Detonation Pressures of Stoichiometric Hydrogen-Oxygen Mixtures Saturated with Water at High Initial Temperatures and Pressures*, Rept. ChE273-5611F, Research Institute, Syracuse University, December 1956.
13. J. A. Luker, L. B. Adler, and E. C. Hobaica, *The Formation of Detonation in Saturated Mixtures of Knallgas-Steam and in Stoichiometric Mixtures of Deuterium-Oxygen (Heavy Knallgas) Saturated with Deuterium Oxide (Heavy Water)*, Rept. ChE273-591F, Research Institute, Syracuse University, January 23, 1959.
14. F. J. Zeleznik and S. Gordon, "Calculation of Detonation Properties and Effect of Independent Parameters on Gaseous Detonations," *ARS J.* **32(4)**, 606-615 (April 1962).
15. S. Gordon and B. J. McBride, *Computer Program for Calculation of Complex Chemical Equilibrium Compositions, Rocket Performance, Incident and Reflected Shocks, and Chapman-Jouguet Detonations*, NASA SP-273, 1971.
16. F. B. Hildebrand, *Advanced Calculus for Applications*, Chapter 7, Prentice-Hall, Englewood Cliffs, N.J., 1962.
17. S. Gordon, F. J. Zeleznik, and V. N. Huff, *A General Method for Automatic Computation of Equilibrium Compositions and Theoretical Rocket Performance of Propellants*, NASA TN D-132, 1959.
18. B. Lewis and J. B. Friauf, *J. Am. Chem. Soc.* **52**, 3905 (1930).
19. D. G. Berets, E. F. Greene, and G. B. Kistiakowsky, *J. Am. Chem. Soc.* **72**, 1080 (1950).
20. B. Lewis and G. von Elbe, *Combustion, Flames and Explosion of Gases*, 2nd ed., Chapter VIII, Academic Press, New York, 1961.
21. R. A. Strehlow, "Detonation Structure and Gross Properties," *Combustion Sci. Technol.* **4**, 65-71 (1971).
22. A. K. Oppenheim, N. Manson, and H. Gg. Wagner, "Recent Progress in Detonation Research," *AIAA J.* **1**, 2243-2252 (1963).
23. R. A. Strehlow, "Gas Phase Detonations: Recent Developments," *Combustion and Flame* **12(2)**, 81-101 (1968).
24. J. H. Lee, R. I. Soloukhin, and A. K. Oppenheim, "Current Views on Gaseous Detonation," *Astronautica Acta* **14**, 565-584 (1969).
25. G. L. Schott, "Structure, Chemistry and Instability of Detonation in Homogeneous Low-Density Fluids—Gases," paper presented at the Fourth International Symposium on High Explosive Detonation, White Oak, Maryland, 1964.
26. K. I. Shchelkin, *Usp. Akad. Nauk* **80**, 525 (1963); Translation, *Soviet Physics Uspekhi* **6**, 523 (1964).
27. A. van Tiggelen and G. de Soete, *Rev. Inst. Franc. Petrole, Ann. Combust. Liquides* **21**, 239-284, 455-486, 604-678 (1966).
28. E. S. Oran, "The Structure of Detonation Waves," Chapter 12 in J. R. Bowen, ed., *Dynamics of Exothermicity*, Gordon and Breach Publishers, 1996, pp. 253-290.

29. E. S. Oran, J. P. Boris, and K. Kailasanath, "Studies of Detonation Initiation, Propagation and Quenching," Chapter 13 in E. S. Oran and J. P. Boris, eds., *Numerical Approaches to Combustion Modeling, Progress in Astronautics and Aeronautics*, Vol. 135, 1991, pp. 421–445.
30. Y. B. Zel'dovich, "The Theory of the Propagation of Detonation in Gaseous Systems," *Expt. Theor. Phys. S.S.S.R.* **10**, 542 (1940); Translation, NACA TM 1261 (1950).
31. J. von Neumann, *Theory of Detonation Waves*, Project Report No. 238, April 1942; OSRD Report No. 549, 1942.
32. W. Döring, "Über den Detonationvorgang in Gasen," *Ann. Phys. Lpz.* **43**, 421–436 (1943).
33. J. P. Chesick and G. B. Kistiakowsky, "Gaseous Detonations X—Study of Reaction Zones," *J. Chem. Phys.* **28**, 956–961 (1958).
34. G. B. Kistiakowsky and J. P. Kydd, "Gaseous Detonations. IX. A Study of the Reaction Zone by Gas Density Measurements," *J. Chem. Phys.* **25**, 824 (1956).
35. W. Jost, Th. Just, and H. Gg. Wagner, "Investigation of the Reaction Zone of Gaseous Detonations," Proceedings of the *Eighth Symposium (International) on Combustion*, 1962, pp. 582–588.
36. Th. Just, F. J. Luig, and H. Gg. Wagner, "Untersuchungen der Reaktionszone von Detonationen in Knallgas verschiedener Zusammensetzung," *Z. Elektrochem.* **65**, 403 (1961).
37. W. Pusch and H. Gg. Wagner, "Investigation of the Dependence of the Limits of Detonability on Tube Diameter," *Combustion and Flame* **6**, 157–162 (1962).
38. H. Gg. Wagner, "Reaction Zone and Stability of Gaseous Detonations," Proceedings of the *Ninth Symposium (International) on Combustion*, 1963, pp. 454–460.
39. D. H. Edwards, G. T. Williams, and J. C. Breeze, "Pressure and Velocity Measurements on Detonation Waves in Hydrogen–Oxygen Mixtures," *J. Fluid Mech.* **6**, 497–517 (1959).
40. D. H. Edwards and T. G. Jones, "Vibration Phenomena in Detonation Waves in Hydrogen–Oxygen Mixtures," *Brit. J. Appl. Phys.* **11**, 190–194 (1960).
41. D. H. Edwards, G. T. Williams, and B. Price, "Pressure Measurements on Detonation Waves in Hydrogen–Oxygen Mixtures," *Les Ondes de Detonation*, CNRS, Paris, 1962, pp. 249–256.
42. F. J. Martin and D. White, "The Formation and Structure of Gaseous Detonation Waves," Proceedings of the *Seventh Symposium (International) on Combustion*, 1959, pp. 856–865.
43. D. R. White, "Turbulent Structure of Gaseous Detonation," *Phys. Fluids* **4**, 465–480 (1961).
44. D. R. White and K. H. Cary, "Structure of Gaseous Detonation, II. Generation of Laminar Detonation," *Phys. Fluids* **6**, 749–750 (1963).
45. J. A. Fay, "Two-Dimensional Gaseous Detonations: Velocity Deficit," *Phys. Fluids* **2**, 283–289 (1959).
46. J. A. Fay, "The Structure of Gaseous Detonation Waves," Proceedings of the *Eighth Symposium (International) on Combustion*, 1962, pp. 30–40.

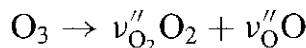
47. Th. Just and H. Gg. Wagner, "Die Reaktionszone in Gasdetonationen, I," *Z. Physik. Chem.* **13**, 241–243 (1957); Th. Just and H. Gg. Wagner, "Reaktionszone von Knallgasdetonationen," *Z. Physik. Chem.* **19**, 250 (1959); Th. Just and H. Gg. Wagner, "Untersuchung der Reaktionszone von Detonationen in Knallgas," *Z. Elektrochem.* **64**, 501 (1960).
48. R. A. Strehlow, *Fundamentals of Combustion*, Chapter 9, McGraw-Hill International Textbook Company, 1984.
49. C. Campbell and D. W. Woodhead, *J. Chem. Soc.*, 3010 (1926); 1572 (1927).
50. Y. H. Denisov and Y. K. Troshin, *Dokl. Akad. Sci. SSSR* **125**, 110 (1959); translation, *Phys. Chem. Sect.* **125**, 217 (1960).
51. K. Antolik, *Pogg. Ann.* **230**, Series 2, **154**, 14 (1875).
52. R. A. Strehlow, "Multi-Dimensional Detonation Wave Structure," *Astronautica Acta* **15**, 345–357 (1970).
53. A. H. Shapiro, *Compressible Fluid Flow*, Vol. I, Chapter 16, The Ronald Press Company, New York, 1953.
54. J. A. Fay and G. L. Opel, "Two-Dimensional Effects in Gaseous Detonation Waves, *J. Chem. Phys.* **29**, 955–958 (1958).
55. M. L. N. Sastri, L. M. Schwartz, B. F. Myers, and D. F. Homing, "Optical Studies of the Structure of Gaseous Detonation Waves," Proceedings of the *Ninth Symposium (International) on Combustion*, 1963, pp. 470–473.
56. S. Taki and T. Fujiwara, *AIAA J.* **16**, 73–77 (1978).
57. P. A. Urtiew and A. K. Oppenheim, "Experimental Observations of the Transition to Detonation in an Explosive Gas," *Proc. Roy. Soc. A*, **295**, 13–28 (1966).
58. H. F. Coward and C. W. Jones, U.S. Bureau of Mines, Bulletin 503, 1952.
59. F. E. Belles, *Seventh Symposium on Combustion (International)*. Butterworths, London, 1959, p. 745.
60. P. Wolanski, C. W. Kauffman, M. Sichel, and J. A. Nicholls, "Detonations of Methane-Air Mixtures," Proceedings of the *Eighteenth Symposium (International) on Combustion*, 1981, pp. 1651–1660.
61. R. Wendlant, "Experimentelle Untersuchungen zur Detonationsgrenze gasformiger," *Gemische. Zeitschrift Fur Physik. Chemie* **110**, 637–655 (1924).
62. S. M. Kogarko and Y. B. Zel'dovich. Doklady Akad. Nauk SSSR NS **63**, 1948, p. 553.
63. S. R. Tieszen, M. P. Sherman, W. B. Benedick, R. Knystautas, and J. H. Lee, "Detonation Cell Size Measurements in H₂-Air-H₂O Mixtures," *Progr. in Aeronautics and Astronautics* **106**, 205–219 (1985).
64. J. E. Dove and H. Gg. Wagner, "A Photographic Investigation of the Mechanism of Spinning Detonation," Proceedings of the *Eighth Symposium (International) on Combustion*, 1961, pp. 589–600.
65. I. O. Moen, M. Donato, M. R. Knystautas, and J. H. Lee, Proceedings of the *Eighteenth Symposium (International) on Combustion*, 1981, p. 1615.
66. V. V. Mitrofanov and R. I. Soloukhin, *Soviet Phys.* **9**, 1055 (1964).
67. D. H. Edwards, M. A. Nettleton, and G. O. Thomas, *J. Fluid Mech.*, **95**, 79 (1979).
68. A. J. Mooradian and W. E. Gordon, "Gaseous Detonation. I. Initiation of Detonation," *J. Chem. Physics* **19**, 1166–1172 (1951).

69. D. H. Edwards and J. M. Morgan, "Instabilities in Detonation Waves Near the Limits of Propagation," *J. Phys. D: Applied Physics* **10**, 2377–2387 (1977).
70. J. H. Lee, "On the Transition from Deflagration to Detonation," *Progr. in Aeronautics and Astronautics* **106**, 3–18 (1985).
71. N. Manson, *Comte Rendu* **222**, 46 (1946).
72. J. A. Fay, "The Mechanical Theory of Spinning Detonation," *J. Chem. Physics* **20**, 942–950 (1952).
73. G. Dupre, R. Knystautas, and J. H. Lee, "Near-Limit Propagation of Detonations in Tubes," *Progr. in Aeronautics and Astronautics* **106**, 244–259 (1985).
- 74a. J. E. Shepherd, "Chemical Kinetics of H₂–Air–Diluent Detonations," *Progr. in Astronautics and Aeronautics* **106**, 263–293 (1986).
- 74b. C. M. Guirao, R. Knystautas, J. H. Lee, W. Benedick, and M. Berman, "Hydrogen–Air Detonations," Proceedings of the *Nineteenth Symposium (International) on Combustion*, The Combustion Institute, Pittsburgh, 583–590 (1982).
- 74c. R. Knystautas, C. M. Guirao, J. H. Lee, and A. Sulmistras, "Measurement of Cell size in Hydrocarbon–Air Mixtures and Predictions of Critical Tube Diameter, Critical Energy, and Detonability Limits," *Progr. in Astronautics and Aeronautics* **94**, 23–37 (1984).
- 75a. A. I. Gavrikov, A. A. Efimenko, and S. B. Dorofeev, *Combustion and Flame* **120**, 19–33 (2000).
- 75b. Shchelkin, K. I. and Troshin, Y. K., *Gasdynamics of Combustion*, Mono Book Corp., Baltimore, 1965.
76. C. K. Westbrook and P. A. Urtiew, Proceedings of the *Nineteenth Symposium (International) on Combustion*, The Combustion Institute, Pittsburgh, 1982, p. 615.
77. C. K. Westbrook, *Combustion and Flame* **46**, 191 (1982).
78. I. O., Moen, S. A. Ward, P. A. Thibault, J. H. Lee, R. Knystautas, T. Dean, and C. K. Westbrook, Proceedings of the *Twentieth Symposium (International) on Combustion*, 117 (1984).
79. G. Ciccarelli, T. Ginsberg, C. Finfrock, J. Boccio, C. Economos, and M. Kinoshita, *Combustion and Flame* **99**, 212 (1994).
80. B. E. Gelfand, S. M. Frolov, and M. A. Nettleton, "Gaseous Detonations: A Selective Review," *Prog. Energy Combustion Sci.* **17**, 327–371 (1991).
81. J. H. Lee, "The Propagation of Turbulent Flames and Detonations in Tubes," *Adv. in Chem. React. Dynamics*, D. Reidel Publ. Co., London, 1986, p. 345.
82. J. H. Lee, "On the Universal Role of Turbulence in the Propagation of Deflagrations and Detonations," in B. Engquist et al., eds., *IMA Volumes in Mathematics and Its Applications*, Springer Verlag, Berlin, 1988; *Computational Fluid Dynamics and Reacting Gas Flows* **12**, 169 (1988).
83. O. Peraldi, R. Knystautas, and J. H. S. Lee, "Criteria for Transition for Detonation in Tubes," Proceedings of the *21st Symposium (International) on Combustion*, The Combustion Institute, Pittsburgh, PA, 1986, p. 1629.
84. K. I. Shchelkin, "Effect of Tube Surface Roughness on Origin and Propagation of Detonation in Gases," *Sov. J. Exp. Theor. Phys.* **10**, 823 (1940).
85. K. I. Shchelkin, *High-Speed Combustion and Spin Gaseous Detonation*, Veonizdat, Moscow, 1949.

86. V. E. Ditsent, and K. I. Shchelkin, "High-Speed Combustion in Tubes with Rough Walls," *Sov. J. Phys. Chem.* **19**, 221 (1945).
87. Ya. B. Zel'dovich, "On the Theory of Detonation Propagation in Gaseous Systems," *Sov. J. Exp. Theor. Phys.* **10**, 542 (1940); *Natl. Adr. Comm. Aeronaut. Technol. Mem.* No. 1261, 1950.
88. Ya. B. Zel'dovich and A. S. Kompaneets, *Theory of Detonation*, Gostechteorizdat, Moscow, 1955; Academic Press, New York, 1960.
89. V. S. Babkin, and L. S. Kozachenko, "The Onset of Detonation in a Gas in Tubes with Rough Walls," *Sov. J. Appl. Mech. Tech. Phys.* **3**, 165 (1960).
90. L. S. Kozachenko and V. S. Babkin, "The Mechanism of Predetonation Flame Propagation in Tubes with Rough Walls," *Dokl. Akad. Nauk U.S.S.R.* **131**, 591 (1960).
91. A. A. Borisov, B. E. Gelfand, V. N. Zamanskiy, V. V. Lisyanskiy, G. I. Skachkov, and K. Ya. Troshin, "Ignition of Combustible Gaseous Mixtures in Conditions of Reflected Shock Wave Focusing," *Sov. J. Chem. Phys.* **7**, 1387 (1988).
92. S. S. Ribanin, "On the Theory of Detonation in Tubes with Rough Walls," *Sov. J. Fiz. Gorenija Vzriva* **5**, 395 (1969).
93. B. E. Gelfand, S. M. Frolov, S. P. Medvedev, and S. A. Tsyganov, "Quenching of Shock Waves in Channels-rough Tubes," *Prepr. Dep. Inst. Chem. Phys. Acad. Sci. U.S.S.R.*, Chernogolovka, 1989.
94. M. A. Nettleton, *Gaseous Detonations: Their Nature, Effect and Control*, Chapman and Hall, 1987.
95. A. M. Bartenev and B. E. Gelfand, "Spontaneous Initiation of Detonations," *Progr. in Energy and Combustion Science* **26**, 29–55 (2000).
96. Ya. B. Zel'dovich, "Classification of Regimes of Exothermic Reaction in Accordance with Initial Conditions," *Chernogolovka*, Preprint IChPh USSR Ac Sci, 1978 (in Russian).
97. Ya. B. Zel'dovich, "Regime Classification of an Exothermic Reaction with Non-Uniform Initial Conditions," *Combustion and Flame* **39(2)**, 21 (1980).
98. J. H. Lee, R. Knystautas, and N. Yoshikawa, "Photochemical Initiation of Gaseous Detonations," *Astron. Acta* **5**, 971–982 (1978).
99. J. H. Lee and I. O. Moen, "The Mechanism of Transition from Deflagration to Detonation in Vapor Cloud Explosions," *Progr. in Energy and Combustion Sci.* **6**, 359–389 (1980).
100. J. F. Clarke, "Fast Flame, Waves, and Detonation," *Progr. in Energy and Combustion Sci.* **15**, 241–271 (1989).
101. P. Wolanski, "Influence of Non-Isentropic Processes on Transition from Deflagration to Detonation in Combustible Mixtures," *Archivum Combustionis* **11(3–4)**, 143–149 (1991).
102. S. B. Dorofeev, A. V. Bezmel'ntsins, and V. P. Sidorov, "Transition to Detonation in Vented Hydrogen–Air Explosion," *Combustion and Flame* **103**, 243–246 (1995).
103. D. A. Frank-Kamenetsky, "Diffusion and Heat Transfer in Chemical Kinetics," *Nauka*, Moscow, 1967, p. 490.
104. R. Knystautas, J. H. Lee, I. O. Moen, and H. Gg. Wagner, "Direct Initiation of Spherical Detonation by a Hot Turbulent Gas Jet," Proceedings of the *Seventeenth Symposium (International) on Combustion*, Pittsburgh, PA, 1979, pp. 1235–1245.

HOMEWORK

- Calculate the steady-state detonation-wave velocity in gaseous ozone at initial pressure of 1 atm and initial temperature of 298 K:



Compare your solution with numerical results obtained from the NASA/Lewis code (CEA).

ANSWER: $U_1 = 1911$ m/s

- Suppose the perfect-gas law is replaced by the Noble–Abel dense-gas law

$$p \left(\frac{1}{\rho} - b \right) = RT$$

where b represents the covolume (the volume occupied by gaseous molecules themselves). Develop a Rankine–Hugoniot relation using the above equation of state for the gases behind the detonation wave front.

- A mixture of hydrogen, oxygen, and nitrogen, having partial pressures in the ratio 2:1:5 in the order listed, is observed to detonate with a speed of 1890 m/s when the initial temperature is 293 K and the initial pressure is 1 atm. Assuming fully relaxed conditions, calculate the peak pressure in the detonation wave, and calculate the pressure and temperature of the gas just after the passage of the wave. Prove that the observed speed corresponds to the C–J condition. Reasonable approximations are allowed, such as neglect of dissociation, the assumption that the pressure after the wave passes is much greater than the initial pressure, the use of existing gas-dynamics tables designed for pure air to analyze processes inside the wave, and specific heats independent of pressure.
- Estimate the steady-state detonation-wave velocity for the premixed gaseous mixture $2\text{H}_2 + \text{O}_2 + 3\text{N}_2$ (assuming no dissociation of the product gases). The initial temperature and pressure of the reactants are $T_1 = 298.15$ K and $p_1 = 1$ atm, respectively.
- Derive the equations expressing the pressure ratio p_2/p_1 , the temperature ratio T_2/T_1 , and the velocity ratio u_2/u_1 in terms of the Mach number M_1 , M_2 and the specific-heat ratio γ for the combustion wave shown in Fig. 4.1. Assume (1) ideal-gas behavior, (2) steady state, (3) no body force, (4) no external heat addition or heat loss, (5) Dufour effect negligible, (6) interdiffusion negligible.
- Consider a stationary combustion wave in a constant-area tube. Assume that there is no external heat transfer across the walls and that the problem can be treated as one-dimensional and steady state. There are no body forces or Dufour effect.

- (a) Derive an expression to relate the change of entropy to the pressure ratio in this problem, for example, $\Delta S = F(p_2/p_1)$.
- (b) Use the above relationship to comment about the difference between detonation and deflagration waves.
7. Verify the following C-J condition: *The C-J condition implies that when the Hugoniot curve is tangent to the Rayleigh line passing through the origin, it is also tangent to the isentrope. Hence, the local Mach number at the upper C-J point and the lower C-J point is unity irrespective of the thermodynamic properties of the medium.*
8. Assume the conditions at the unburned side of a stationary one-dimensional combustion wave are

$$p_1 = 1 \text{ atm} \quad \text{and} \quad \rho_1 = 1.185 \text{ kg/m}^3$$

- (a) Derive an equivalent Hugoniot relation in terms of compression ratio, $\varepsilon(v_1/v_2)$, and pressure ratio, $\pi_r (\equiv p_2/p_1)$.
- (b) Calculate the heat release per unit mass using the data given in Table 4.1 for both detonation and deflagration waves, and compare the calculated results.

PROJECT

The interferograms of both Chapman–Jouguet and slightly overdriven detonations of initial pressures up to 0.3 atm show that without exception the shock front reaction zone structure is not planar and that the following flow has variations in refractive index that we can interpret as being due to turbulence.* Show, by resolving the burned gas properties U_2 (velocity), ρ_2 (density), p_2 (pressure), and E_2 (energy) into mean and fluctuating quantities, the form of the Rayleigh and Rankine–Hugoniot functions when turbulence is considered. You may make the following assumptions:

- (a) The detonation wave occurs as a statistically steady process in a constant-area tube (see Fig. 4.33).

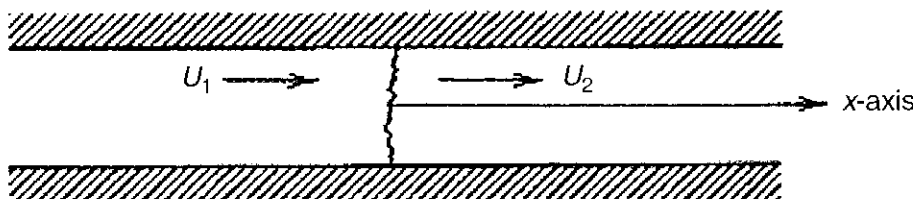


Figure 4.33 Detonation wave in a constant-area tube.

* D. R. White, "Turbulent Structure of Gaseous Detonation," *The Physics of Fluids* 4(4), 465–480, (1961).

- (b) The flow ahead of the detonation wave is nonturbulent.
- (c) The mean gas velocity U is parallel to the axis of the tube (x -axis), and the transverse derivatives of any time-averaged quantity vanish.
- (d) Neglect velocity fluctuation terms of third order or higher.
- (e) Assume isotropic turbulence $\overline{u'_i u'_j} = \frac{1}{3} u^2 \delta_{ij}$.

5

PREMIXED LAMINAR FLAMES

Symbol	Description	Dimension
a	Number of molecules of reactant per unit volume	L^{-3}
C_t	Total number of moles per unit volume	NL^{-3}
d_p	Penetration distance [see Eq. (5-143)]	L
d_q	Quenching distance	L
g	Boundary velocity gradient	t^{-1}
G	Total mass velocity per unit area	$M/t \cdot L^2$
H_{R_A}	Standard heat of reaction of A	Q/M
N_A	Avogadro's number	N^{-1}
n_r	Number of moles of reactant	N
n_p	Number of moles of product	N
r_{BA}	Stoichiometric ratio	—
R_A	Consumption rate of A	$M/L^3 \cdot t$
S_L	Laminar flame speed	L/t
T_f	Flame temperature	T
$T_{i \text{ nf}}$	Temperature at point of inflection	T
δ_{ph}	Length of preheat zone	L
δ_r	Length of reaction zone	L

1 INTRODUCTION AND FLAME SPEED MEASUREMENT METHODS

From the Hugoniot plot (Fig. 4.2) we have learned that there are two types of combustion waves: detonation waves (regions I and II of the Hugoniot curve) and deflagration waves (regions III and IV). Detonation waves are supersonic waves supported by combustion, while deflagration waves are subsonic waves propagated by heat release from chemical reactions. As mentioned earlier, solutions in region IV do not exist, because combustion products cannot depart from the wave at supersonic speeds. The unique solution in region III is the main subject of this chapter. One of the major tasks in the laminar-flame studies is to determine the laminar flame speed as the unique solution of the deflagration wave under a given set of conditions. The detailed flame structure in terms of concentration and temperature distributions are also of great interest.

The flame velocity has been defined as the velocity of the unburned gases through the combustion wave in the direction normal to the wave surface. Various measurement techniques for this quantity have been developed. Some common techniques are briefly discussed in the following sections. For more detailed information on techniques for measuring the speed and structure of laminar premixed flames, the reader is referred to the books by Glassman,¹ Gaydon and Wolfhard,³⁰ Beer and Chigier,³⁹ Weinberg,³¹ and Kanury.³³

1.1 Bunsen Burner Method

The first laboratory premixed-flame burner was invented by Bunsen around 1855. Figure 5.1 shows a schematic diagram of the Bunsen burner. The fuel gas enters the burner through a feedline near the bottom. The gaseous fuel jet induces the entrainment of primary air through a number of ports on the control ring. As fuel and air flow up the barrel tube, they mix, and before reaching the top of the burner, the gases are well mixed and can be considered to be homogeneous. At the port, the flame is anchored near the top of the burner. As long as the fuel feeding rate remains constant, the premixed flame in a quiescent ambient atmosphere will remain stationary and steady.

A photograph of a conical premixed ethylene-air flame by Gaydon and Wolfhard³⁰ is shown in Fig. 5.2a. A shadowgraph of a conical premixed laminar flame from Weinberg³¹ is shown in Fig. 5.2b. A simultaneous photograph of visible (outer cone) and schlieren (inner cone) cones of a premixed flame from Weinberg³¹ is shown in Fig. 5.2c.

These photographs indicate clearly that there is a luminous conical region within which reaction and heat release are taking place. Underneath the luminous cone, there is a dark zone (marked in Fig. 5.1) within which the unburned gas molecules change their flow direction from the initially vertical direction to outward directions. Immediately beneath the luminous cone, the unburned gases are heated to a critical temperature at which rapid chemical reaction starts. The burned gases expand as they leave the flame zone and are diluted and cooled by the surrounding air. A few streamlines are sketched in Fig. 5.1 to show the general flow characteristics near a Bunsen burner flame.

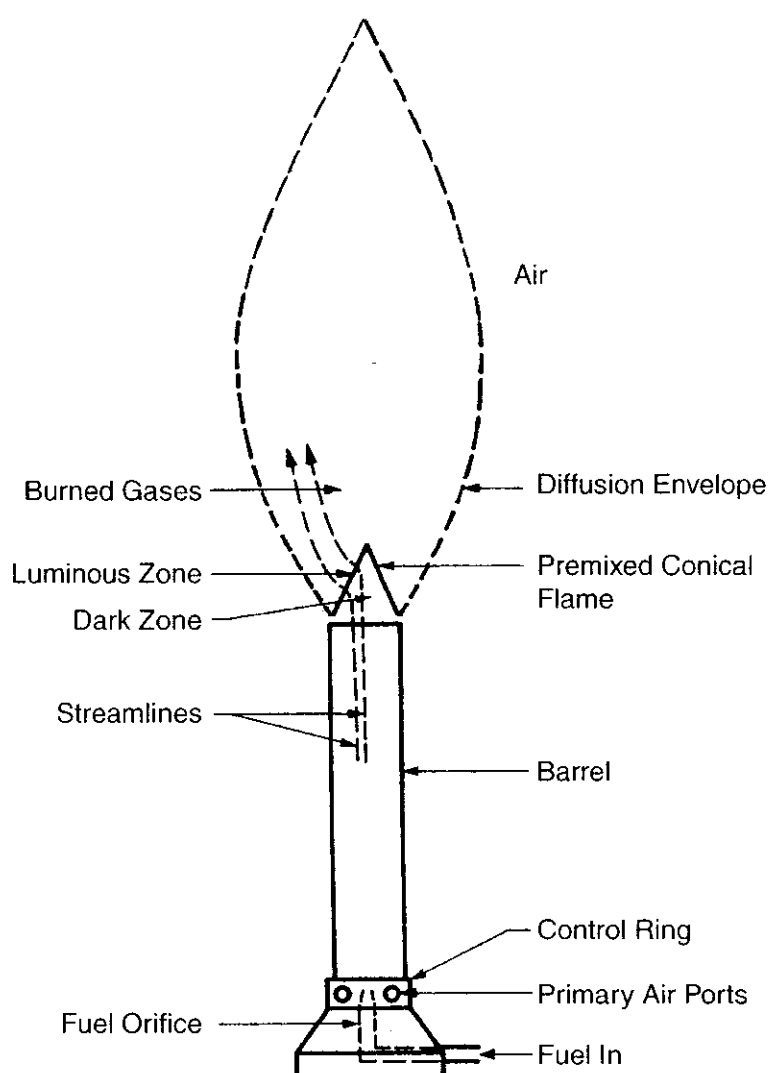


Figure 5.1 Schematic of a premixed laminar flame shown above a Bunsen burner.

The luminous zone is usually no more than 1 mm thick. The color of the luminous zone, according to Glassman,¹ changes with the fuel–air ratio. When the mixture is fuel-lean, the color of the cone surface is deep violet due to large concentrations of excited CH radicals. When the mixture is fuel-rich, the color of the cone surface is green due to large concentrations of C₂ molecules. The high-temperature burned gases usually show a reddish glow that arises from radiation from CO₂ and water vapor. When the mixture is highly fuel-rich, carbon particles form and an intense yellow radiation appears. It is yellow because the blackbody radiation curve peaks in the yellow for the temperatures that normally exist in these premixed flames.

In comparison with diffusion flames, the premixed flames from Bunsen burners are relatively clean and give much more intense combustion with higher effective temperatures. In the simple type of Bunsen burner, as shown in Fig. 5.1, the fuel gas issues from a small nozzle or orifice and entrains some air (primary air). The mixture of gas and primary air passes up the burner tube at a speed that is sufficient to prevent the flame flashback down the tube. The mixture thus burns at the top of the burner. For good air entrainment, the air holes must be of sufficient

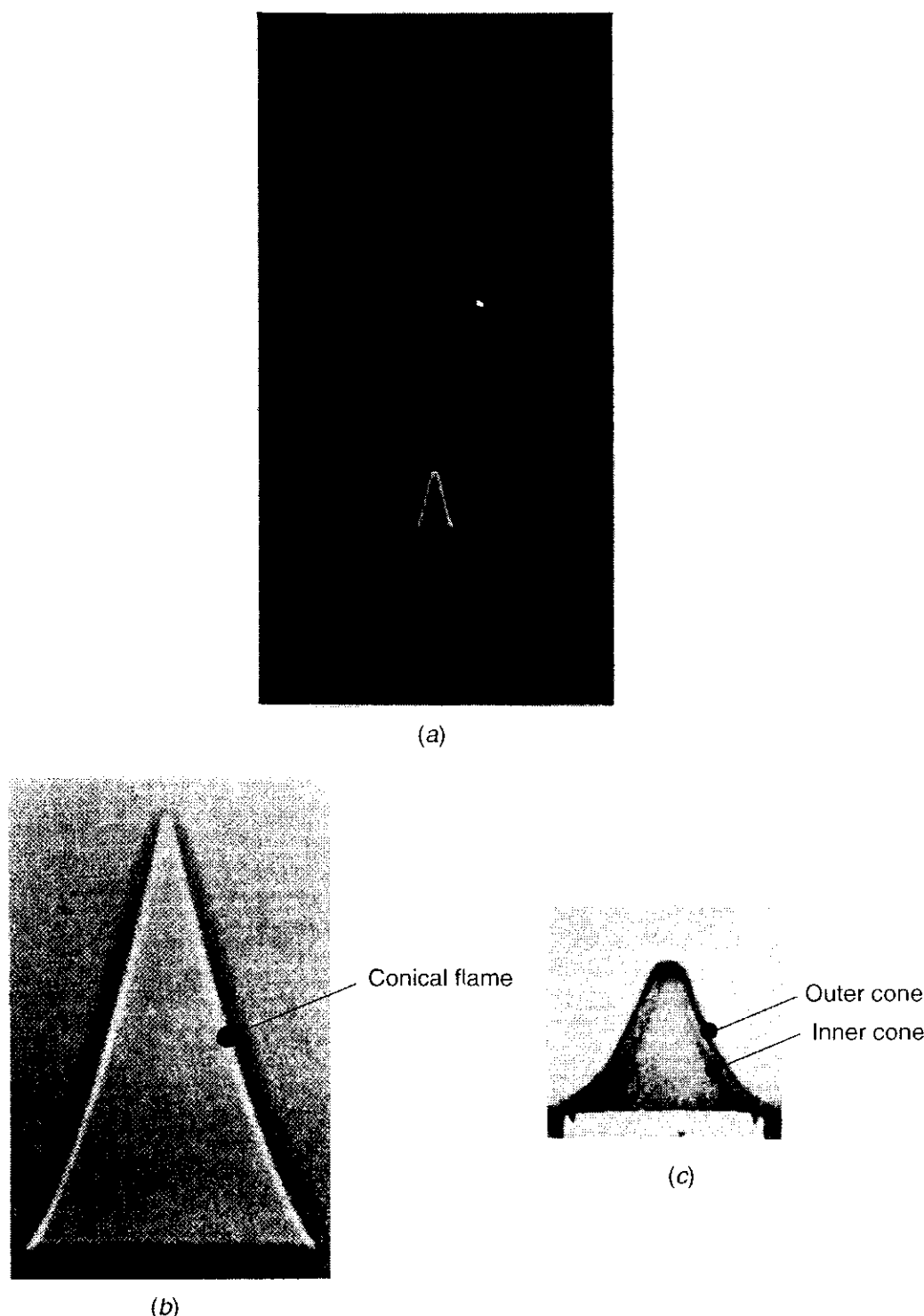


Figure 5.2 (a) Photograph of a premixed ethylene–air flame (from Gaydon and Wolfhard³⁰). (b) Shadowgraph of conical premixed laminar flame (Modified from Weinberg,³¹ photographed by J. W. Anderson). (c) Simultaneous photographs of visible (outer) and schlieren (inner) cones of a premixed flame (Modified from Weinberg;³¹ photographed by J. W. Linnett).

size. The amount of air entrained is usually well below that needed for complete combustion of the gas.

There are limits to the size of Bunsen burners. The lower limit of tube diameter is set by the quenching distance (a term to be discussed later) of the gas–air mixture. The upper limit is set by the increasing tendency toward flashback

with large burners. To maintain the flame at the port, there is a maximum gas velocity for a given supply pressure. To obtain sufficient velocity at all points in the tube and to prevent flashback, the average velocity must be increased for larger burners.

To obtain good mixing and allow time for the turbulence created by the gas jet to die down, it is desirable to have a long burner, but if it is too long, it will cause unnecessary resistance to flow and reduce the air entrainment. For natural gases, the length in general should be about 6 times the inner diameter of the mouth. For premixed gas mixtures with higher burning velocities, a longer burner is required, usually 10 times the diameter. The inner diameter of the tube is usually on the order of 1 cm. The aforementioned simple design principle of the Bunsen burner has been adopted in many gas appliances such as cooking stoves and gas burners.

A sketch of the flow configuration through the conical laminar flame is shown in Fig. 5.3. Let us call the conical surface area of the innermost cone A_f , the tube cross-sectional area A_t , and the average flow velocity in the tube V_t . Then, the laminar flame speed S_L , defined as the magnitude of the velocity of the unheated premixed gas just before entering the flame zone, can be determined from the mass continuity:

$$S_L = V_t \frac{A_t}{A_f} \quad (5-1)$$

Since the conical surface area A_f is greater than A_t , S_L must be less than V_t .

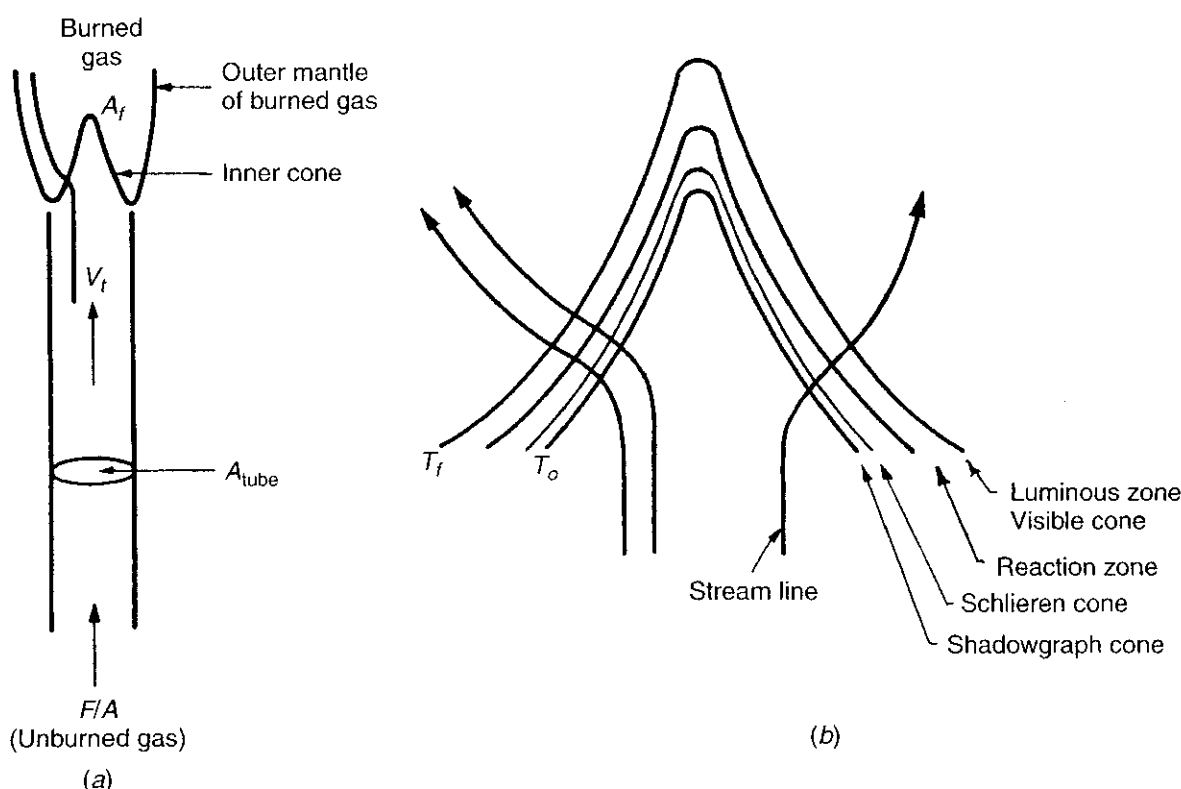


Figure 5.3 (a) Flow configuration near the mouth of a Bunsen burner. (b) Relative locations of different conical surfaces (differences exaggerated).

Although Eq. (5-1) is a very simple equation, there are some difficulties in determining S_L . This is due to the uncertainty of the surface area A_f . Depending on the optical method used, the conical area varies in the manner shown in Fig. 5.3b. Many experimentalists have used the shadow cone because it is simpler than the schlieren techniques. The shadow cone, being cooler, gives a more correct result than the visible cone.

Experiments with fine magnesium oxide particles entrained in the gaseous stream have shown that the flow streamlines remain fairly straight until the schlieren cone is reached, and then the flow diverges from the burner axis before reaching the visible cone. These experiments have led many investigators to use the schlieren cone for flame-speed evaluation. In general, the thicker the flame zone, the greater the measurement error in the determination of S_L .

The major advantage of the Bunsen burner method for premixed laminar flame study is that the equipment is simple, flexible, and easily adapted for measurements at initial temperature and pressure conditions. However, there are several disadvantages, including the following:

1. The diffusional interchange of chemical species with those in the surrounding atmosphere, through the circumferential edge near the base of the conical flame, alters the fuel–oxidant ratio, so that the flame velocity observed may not represent the measured fuel–air ratio.
2. It is difficult to completely eliminate wall-quenching effects on flame speed.
3. The flame cone can act as a lens in a shadow measurement; this causes uncertainties in the proper cone size determination.
4. There may be inadequate entrainment of air and resultant tendency toward flashback with large-diameter burners.

The accuracy of S_L measurement by the Bunsen burner method is on the order of $\pm 20\%$.

1.2 Constant-Volume Spherical Bomb Method

It should be noted that a laminar flame does not have to be stationary like the Bunsen burner flame shown in Fig. 5.3; it can be a traveling flame in a spherical windowed chamber. In the closed constant-volume spherical bomb method, the combustible mixture is ignited at the center of a rigid spherical vessel, which is usually on the order of 30 cm in diameter. As the flame progresses, the expansion of the burned gas causes both the pressure and temperature of the unburned gas to increase because of the adiabatic compression. The temperature increase causes the flame velocity to increase continuously from the center toward the wall. In this method, simultaneous records of the size of the spherical zone of the burned gas and of the pressure in the vessel must be made to determine S_L . It can be shown from the consideration of the time variation of the instantaneous mass of the unburned gas that laminar flame speed of the spherical deflagration wave is

related to dp/dt and dr/dt according to

$$S_L = \left(1 - \frac{R^3 - r^3}{3p\gamma_u r^2} \frac{dp}{dr} \right) \frac{dr}{dt} = \frac{dr}{dt} - \frac{R^3 - r^3}{3p\gamma_u r^2} \frac{dp}{dt} \quad (5-2)$$

where p and r are the instantaneous chamber pressure and spherical flame radius, R is the inner radius of the spherical vessel, and γ_u is the specific heat ratio of the unburned gas. In Eq. (5-2), S_L is obtained as a difference of two time derivatives, which are of comparable magnitude; therefore, errors in these derivatives can be magnified in the S_L calculation.

An alternative method of evaluating the burning velocity is to determine the rate of change of the mass fraction Y of burned gas. That is,

$$S_L = \frac{1}{3} \frac{R^3}{r^2} \left(\frac{p_i}{p} \right)^{1/\gamma_u} \frac{dY}{dt} \quad (5-3)$$

where p_i is the initial pressure of the unreacted gas mixture. For small values of Y , the value of Y can be calculated from

$$Y \equiv \frac{p - p_i}{p_e - p_i}$$

where p_e is the pressure corresponding to equilibrium chamber pressure based on constant-volume combustion condition, which can be computed thermochemically. The flame speed deduced according to the constant-volume spherical bomb method assumes complete equilibrium behind the flame front and no heat losses. Any delay in attaining equilibrium in a rather large volume immediately behind the flame front can cause error; the value of S_L calculated using the above expression is usually less than the actual value.

1.3 Soap-Bubble (Constant-Pressure Bomb) Method

In the soap-bubble method, a homogeneous combustible mixture is used to blow a soap bubble around a pair of spark electrodes. At time zero, the gas mixture contained in the spherical soap bubble is ignited by the spark (see Fig. 5.4). An approximate way to calculate the flame velocity is to use

$$S_L = \frac{V_{\text{flame}} r_i^3}{r_f^3} \quad (5-4)$$

where V_{flame} is the average spatial velocity of the spherical flame front, r_i is the initial radius of the soap bubble, and r_f is the final radius of the sphere of burned gas. In general, we can assume that (1) the spherical flame spreads uniformly in radial direction in gaseous mixture; (2) the pressure remains constant; and (3) the growth of the flame front can be followed by some photographic means.

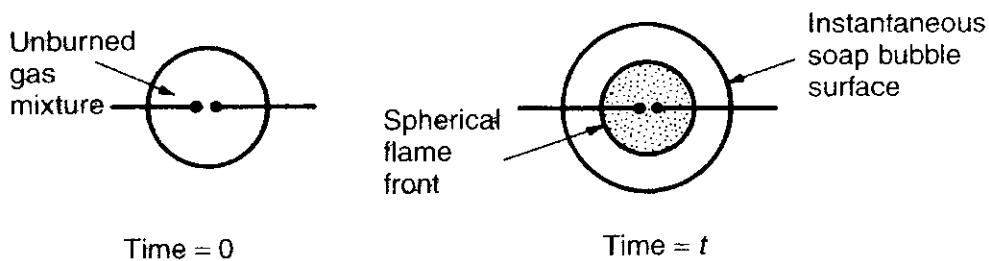


Figure 5.4 Experimental setup of the soap-bubble method.

The instantaneous flame speed can be deduced by equating the mass flux in front of the flame front to that behind the flame front, i.e.,

$$S_L A \rho_u = u_r A \rho_b \quad (5-5)$$

or

$$S_L = u_r \frac{\rho_b}{\rho_u} = u_r \frac{T_u}{T_b} \quad (5-6)$$

where u_r represents the recorded flame velocity.

If the effective mean reaction-zone temperature is constant and the reaction mechanism does not change with composition, the true effects of fuel and oxidant concentrations on laminar flame speed and hence on the overall reaction rate can be expressed as

$$S_L^2 \propto X_F^a X_0^c \quad (5-7)$$

where X_F is the mole fraction of fuel in unburned gas and X_0 is the mole fraction of oxidant in unburned gas. The exponents a and c are empirical constants.

One obvious disadvantage of this method is the large uncertainty in the temperature ratio T_u/T_b needed for obtaining ρ_b/ρ_u . Although one can assume that the gases reach the theoretical flame temperature, comparison of measured and calculated expansion ratios often reveals serious discrepancies. Also, for use in Eq. (5-4), the initial and final sizes of the bubble must be known very accurately because they are raised to the third power in the calculation. In fact, however, the final size is difficult to measure. There are several other problems in using the soap-bubble method, namely the following:

- (a) The method is not suitable for studying the flame spread of dry mixtures, since they can be moistened by evaporation from the soap solution.
- (b) There is inevitably some heat loss to the electrodes.
- (c) For slow flames, the flame front may not remain spherical; also, the thickness of the reaction zone becomes large.
- (d) For very fast flames, the flame front is no longer smooth, due to the formation of cellular flame structure.

1.4 Particle-Track Method

With conical flames on round burners, it is inevitable that flame surfaces are nonflat, making it difficult to film particle streak lines. To overcome this difficulty, Lewis and von Elbe⁴⁰ made a very useful investigation using rectangular burners. A particle-track method was devised in which small magnesium oxide particles in a gas stream were illuminated intermittently from the side. A photograph of the track of a particle then shows its direction. Typical results are shown in Fig. 5.5. The velocity of the particle can also be deduced from consecutive photographs.

The width of their burner was 0.755 cm, which was rather small; the propagation of the flame front with uniform burning velocity would be faster if larger burners were employed. They showed that the burning velocity is a genuine physical constant (observe the flat region in Fig. 5.5b).

A distinct weakness of this method is that the introduction of solid particles may, by catalytic effects at the surface, modify the combustion processes and hence alter S_L . Errors may also occur if the particles are too large to follow the gas flow accurately. The particle-track method is generally too laborious for regular measurement of burning velocities.

1.5 Flat-Flame Burner Method

The flat-flame burner method is usually attributed to Powling's invention.⁴¹ It is probably the most accurate method, because it offers the simplest flame front

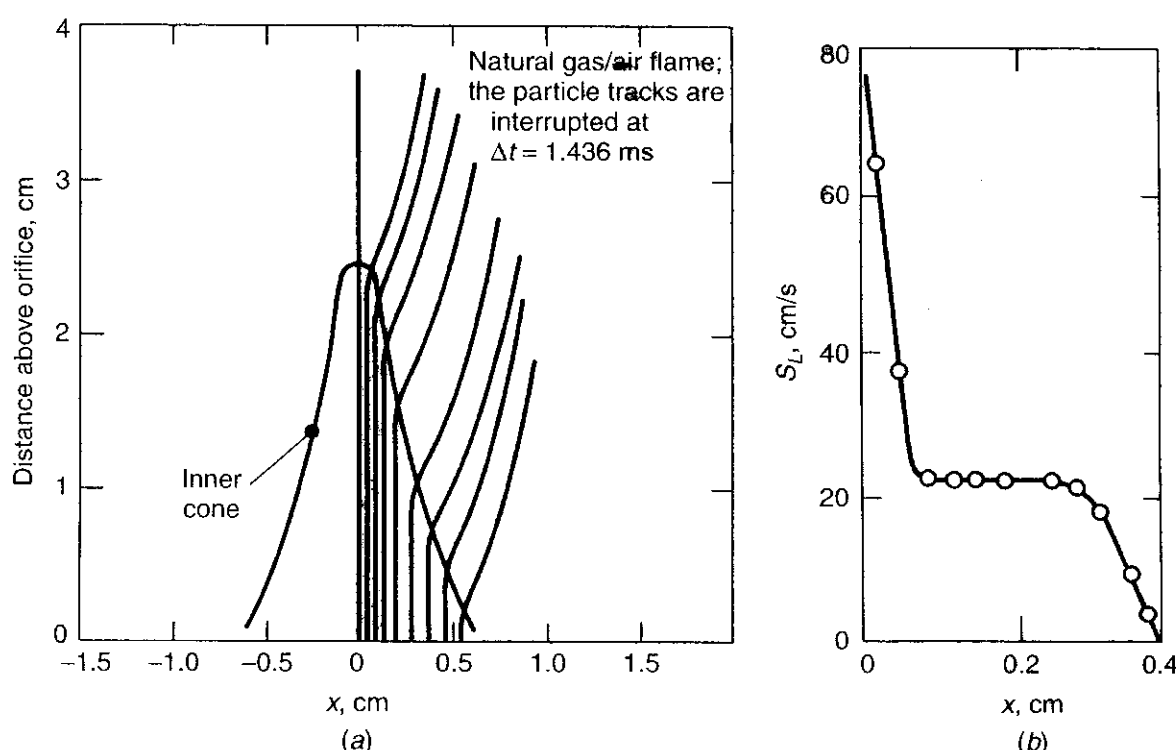


Figure 5.5 (a) Particle trajectory lines through the inner cone of a natural gas-air flame from particle-track measurements. (b) Burning velocity of flame determined from the particle path lines shown in (a) (modified from Lewis and von Elbe⁴⁰).

and one in which the areas of the shadow, schlieren, and visible fronts are all the same. It is achieved by placing a porous metal disk or a series of small tubes of 1-mm diameter or less at the exit of the larger flow tube. A modern flat-flame burner (see Fig. 5.6) usually consists of a sintered, porous bronze (or 316 stainless steel) water-cooled burner surrounded by a sintered, porous shroud ring for the introduction of a shielding gas (usually nitrogen), both enclosed in a precision-machined housing assembly with connections for water cooling, combustion gas, and shielding gas.

The gaseous mixture is usually ignited at high flow rate and adjusted until the flame is flat. By controlling the rate of efflux of burned gases with a grid above the flame, a more stable flame can be obtained. This method is applicable only to mixtures having low burning velocities, on the order of 15 cm/s or less. At

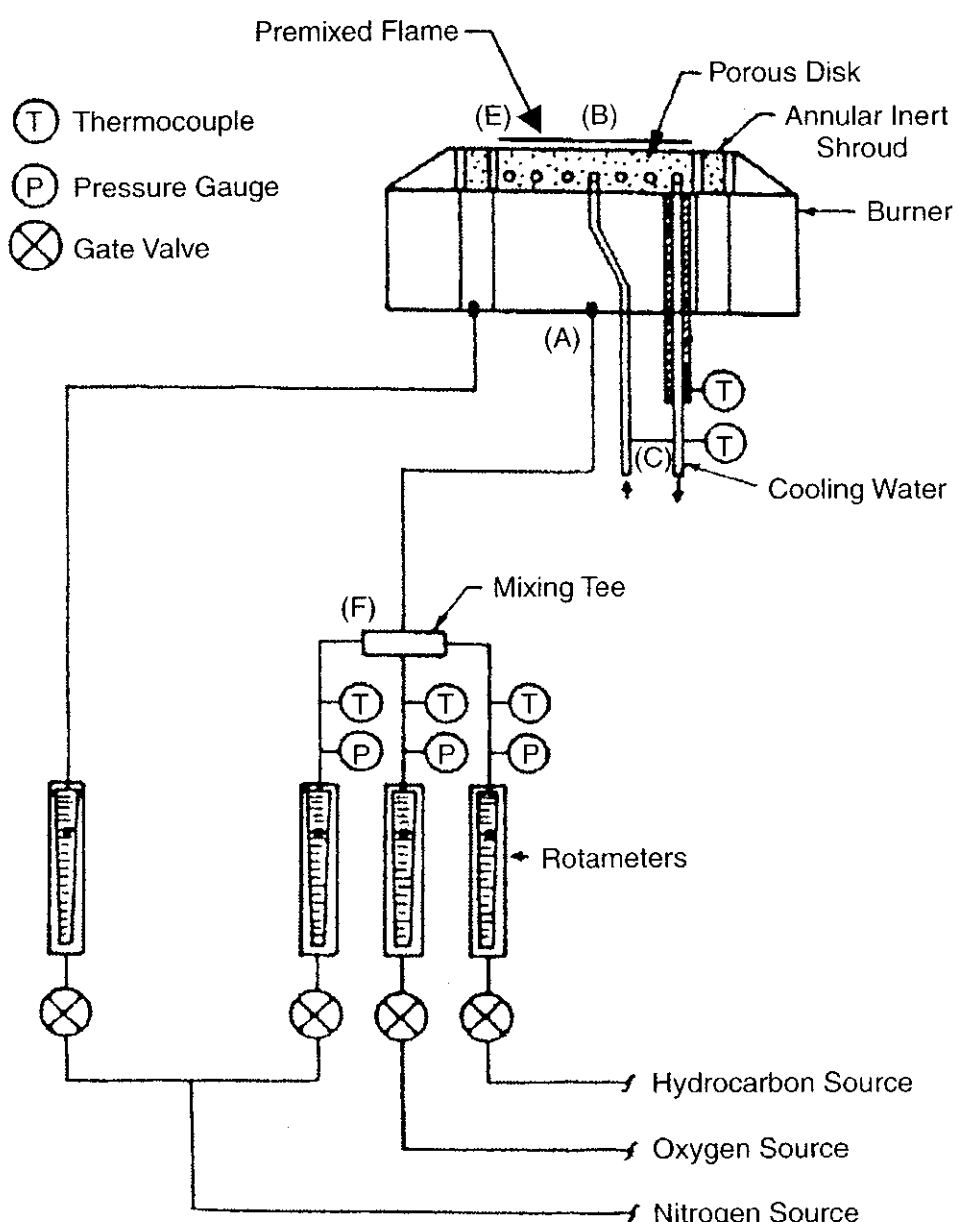


Figure 5.6 A flat-flame burner setup with (A) reactant gas supply line; (B) a flat premixed flame; and (C) a cooling water passage through sintered metal disk.

higher S_L , the flame front positions itself far from the burner and forms conical shapes. Spalding and Botha⁴² extended the flat-flame burner method to higher flame speeds by cooling the porous disk. The cooling brings the flame front closer to the porous disk and stabilizes it. In order to obtain the adiabatic laminar flame speed, several tests at different cooling rates are made. The values of S_L are plotted against the cooling rates. The curve is then extrapolated to zero cooling rate to obtain adiabatic flame speed S_L . This procedure can be utilized for all mixture ratios within the flammability limits.

1.6 Diagnostic Method for Flame Structure Measurements

In the last 20 years, there have been substantial developments in nonintrusive combustion diagnostic techniques. Advances in diagnostics have been due largely to the rapid development of laser-based optical techniques, computer-coupled data acquisition systems, and digital image capture and analysis. The nonintrusive character of these methods is essential to prevent perturbation of the flow systems under study and thus provide more realistic and accurate measurements than those provided by intrusive techniques. Advanced diagnostic techniques have been applied to various flame structure studies for measurements of concentrations of chemical species, temperatures of gaseous mixtures and particles, the velocity field of chemically reacting flows, etc. Using advanced nonintrusive diagnostic techniques, engineers and scientists are much better equipped to study combustion problems.

Experimental measurements are needed for a variety of purposes, including achieving a better understanding of flame and flow field structures in order to improve the design of existing combustion systems, validating theoretical models and numerical codes, studying the formation mechanism of undesirable species in emission control, and conducting performance evaluations of combustion systems.

Although the design of many modern combustion systems leans toward calculation and simulation rather than extensive hardware fabrication and testing, diagnostic techniques are still very important. Indeed, the rise in computational fluid dynamics (CFD) is beginning to allow evaluation of complex flow and combustion systems over a wide range of design parameters more quickly, inexpensively, and thoroughly than can be accomplished with actual hardware tests. Reactive flows including multistep kinetic considerations have become computationally tractable. However, these computational models often require adequate input of kinetic information in the form of submodels, which are based on specific measurements or basic understanding of the chemical and physical mechanisms derived from experimental observations. In particular, experimental validation of computed results will be necessary to prove the predictive capability of theoretical models and computer codes before they are used for guiding actual designs. Advanced nonintrusive combustion diagnostics are an excellent way to provide required input and measured data for comparison with CFD results. Many modern diagnostic techniques allow multiparameter measurements, which

further improve the validation of CFD results. These multiparameter diagnostic measurements are even more valuable for some systems that, due to complicated geometries or operating conditions, are beyond the capability of current CFD calculations. For such systems, improvement of the design beyond simple trial and error can be enhanced greatly by nonintrusive diagnostic measurements of properties of chemically reacting flow fields.

Many technical papers and books (e.g., Eckbreth,⁵⁰ Thorne,⁵¹ Kuo and Parr,⁵² Warnatz, Maas, and Dibble⁵³) are available in the laser spectroscopic area. It is too broad to be covered in this section or even in many sections. The purpose here is to indicate some available modern and conventional methods for measurements of reacting gas properties without detailed description of each method. The average pressure of a reacting flow system can be measured by conventional manometers. Any time variations of pressure can be measured by piezoelectric pressure transducers. We now list the methods for other flow property measurement without any detailed descriptions in order to keep the text short.

1.6.1 Velocity Measurements

Hot-wire anemometer

Laser Doppler anemometry (LDA), also called laser Doppler velocimetry (LDV)

Particle-tracking methods

Particle image velocimetry (PIV) with pulsed thin laser sheet

1.6.2 Density Measurements

Laser-beam extinction measurement

Laser Rayleigh-scattering technique

Filter Rayleigh-scattering (FRS) technique

1.6.3 Concentration Measurements

Probe methods coupled with chemical analysis

Raman spectroscopies

Coherent and anti-Stokes Raman spectroscopies (CARS spectroscopies)

Laser-induced fluorescence (LIF) technique

Planar laser-induced fluorescence (PLIF) technique

1.6.4 Temperature Measurements

Thermocouples

Sodium-line-reversal method

Absorption and emission spectroscopies

Coherent and anti-Stokes Raman spectroscopies (CARS spectroscopies)

Laser induced fluorescence (LIF) technique

Since this chapter deals with laminar premixed flame, techniques associated with other combustion problems are not included here, such as diagnostics and

image analyses of combustion of liquids and solids, particle distribution and sizing measurements, and particle ignition diagnostics.

2 CLASSICAL LAMINAR-FLAME THEORIES

In laminar-flame theory, we are mostly interested in determining the laminar-flame speed S_L , defined as the velocity of the unburned gases normal to the combustion wave surface as these gases move into the combustion front. S_L is also called burning velocity, flame velocity, or normal combustion velocity.

In the last 100 years, many physical and chemical processes involved in steady-state flame propagation have been studied. A variety of methods of attack have been developed. An extensive review of the classical laminar-flame theories was conducted by Evans.² On the basis of the major assumptions, classical theories are divided into three groups:

1. Thermal theory

- Mallard and LeChatelier's development³
- The Damköhler theory⁴
- The theory of Bartholomé⁵
- The theory of Emmons, Harr, and Strong⁶
- The theory of Bechert⁷

2. Comprehensive theory

- The theory of Lewis and von Elbe⁸
- The theory of Zel'dovich, Frank-Kamenetsky, and Semenov⁹
- The theory of Boys and Corner¹⁰
- The theory of Hirschfelder and Curtiss¹¹
- The theory of von Karman and Penner¹²

3. Diffusion theory

- The theory of Tanford and Pease¹³
- The theory of Van Tiggelen¹⁴
- The theory of Manson¹⁵
- The theory of Gaydon and Wolfhard¹⁶

For detailed information on these theories, the reader should refer to the original paper of each theory or the discussions in Evans's review paper. In the following, one theory is selected from each group to show the special considerations in the development of each group.

2.1 Thermal Theory: Mallard and LeChatelier's Development² (1883)

The objective of laminar-flame theory is to find the laminar-flame speed S_L . The temperature variation across the flame can be plotted as shown in Fig. 5.7. Mallard and LeChatelier divided the flame into two zones. Zone I is the preheat zone, in which the gases are heated by conduction and reach ignition at the

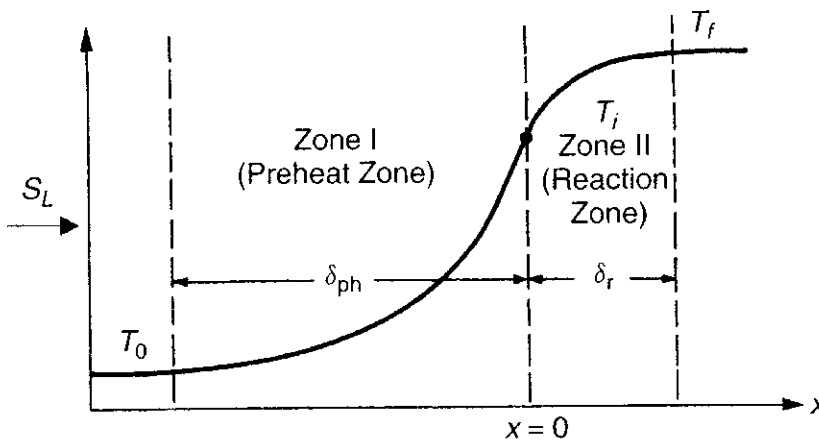


Figure 5.7 Schematic diagram of the temperature variation across a typical laminar flame.

ignition boundary. Zone II is the chemical reaction zone, in which chemical enthalpy is converted into sensible enthalpy.

The energy balance of zone I gives

$$S_L \rho C_p (T_i - T_0) = \lambda \frac{T_f - T_i}{\delta_r} \quad \text{or} \quad S_L = \frac{\lambda}{\rho C_p} \frac{T_f - T_i}{T_i - T_0} \frac{1}{\delta_r} \quad (5-8)$$

where the left-hand side of the equation represents the amount of energy absorbed as the unburned mixture flows into the entrance of the preheat zone at T_0 and is heated to T_i at the exit of the preheat zone, and the right-hand side is the heat flux to the interface. The value of S_L can be determined from Eq. (5-8), if the reaction zone thickness δ_r is known. Let's define τ_r to be the reaction time; then

$$\delta_r = S_L \tau_r = S_L \frac{1}{d\varepsilon/dt} \quad \text{or} \quad \delta_r \propto S_L \frac{1}{RR} \quad (5-9)$$

where ε is the reaction-progress variable discussed in Chapter 1 and $d\varepsilon/dt$ is the rate of reaction (RR). Substituting Eq. (5-9) into Eq. (5-8), we get

$$S_L = \sqrt{\left(\frac{\lambda}{\rho C_p}\right) \frac{T_f - T_i}{T_i - T_0} \left(\frac{d\varepsilon}{dt}\right)} \propto \sqrt{\alpha \cdot RR} \quad (5-10)$$

where T_i represents the ignition temperature. Mallard and LeChatelier did not specify the specific temperature at which the reaction rate RR should be determined. However, their analysis suggests that the flame speed is proportional to the square root of the product of thermal diffusivity and reaction rate. This result is one of the most important relationships in laminar-flame theories.

As seen in Problem 2.10, for an n th-order chemical reaction, we have

$$\frac{d\varepsilon}{dt} = k \varepsilon^n p^{n-1} = A e^{-E_a/R_u T} \varepsilon^n p^{n-1} \quad (5-11)$$

For the pressure dependence, we have

$$S_L \propto \sqrt{\frac{1}{\rho} p^{n-1}} \propto \sqrt{p^{n-2}} \quad (5-12)$$

This equation implies that for second-order chemical reactions, the laminar-flame speed should be independent of pressure. Based on Eq. (5-10) and the Arrhenius law for RR, the temperature dependence can be expressed:

$$S_L \propto \sqrt{e^{-E_a/R_u T}} = e^{-E_a/2R_u T} \quad (5-13)$$

As we shall see later, in order to obtain realistic values of S_L , one needs to replace the temperature T in Eq. (5-13) by T_f , since most chemical reaction takes place around T_f .

2.2 Comprehensive Theory: The Theory of Zel'dovich, Frank-Kamenetsky, and Semenov

These investigators have adopted Mallard and LeChatelier's idea^{2,3} of dividing the flame into two zones (preheat and reaction zones). However, instead of considering the energy equation alone, they have used the species-conservation equation together with the energy equation. They propose that the ignition temperature is very close to the adiabatic flame temperature and consequently replace T_i with T_f in their estimation of reaction rates. Their basic assumptions are as follows:

- (a) The pressure is constant.
- (b) The number of moles does not vary during the reaction. This restriction is later removed to allow the number to change in the mole ratio

$$\frac{n_r}{n_p} \equiv \frac{\text{moles of reactant}}{\text{moles of product}}$$

according to the stoichiometric reaction.

- (c) C_p and λ are constant.
- (d) $\lambda/C_p = \mathcal{D}\rho$. This implies that $\text{Le} = 1$, and has the effect of reducing the number of differential equations from two to one by replacing one of the differential equations with an algebraic equation. Later this restriction is modified to allow $\text{Le} = \text{constant}$.
- (e) The flame is one-dimensional and steady-state.

The equations of species continuity and energy conservation are first written in their most general forms and then simplified according to the above assumptions:

The general species conservation equation derived in Chapter 3 can be written as

$$\frac{\partial \rho_r}{\partial t} + \nabla \cdot \rho_r \mathbf{v} = \nabla \cdot (\rho \mathcal{D} \nabla Y_r) - \dot{\omega}_r \quad (5-14)$$

$\dot{\omega}_r$ is positive for rate of destruction of reactants, and $\dot{\omega}_r$ has the dimension of $Mt^{-1}L^{-3}$. Under assumption (e), Eq. (5-14) becomes

$$\frac{d}{dx} \left(\frac{\rho_r}{\rho} \cdot \rho u \right) = \frac{d}{dx} \left[\rho \mathcal{D} \frac{d}{dx} \left(\frac{\rho_r}{\rho} \right) \right] - \dot{\omega}_r$$

or

$$\frac{\rho_r}{\rho} \frac{d(\rho u)}{dx} + \rho u \frac{d(\rho_r/\rho)}{dx} = \rho \mathcal{D} \frac{d^2}{dx^2} \left(\frac{\rho_r}{\rho} \right) - \dot{\omega}_r \quad (5-14a)$$

From continuity equation $d(\rho u)/dx = 0$, Eq. (5-14a) becomes

$$\rho u \frac{d(\rho_r/\rho)}{dx} = \rho \mathcal{D} \frac{d^2}{dx^2} \left(\frac{\rho_r}{\rho} \right) - \dot{\omega}_r \quad (5-14b)$$

ρ_r can be written in terms of the number density a of reactant molecules (molecules/m^3) as

$$\rho_r = \frac{a}{N_A} \cdot \text{Mw}_r \quad (5-15)$$

where N_A is Avogadro's number, and Mw_r is the reactant molecular weight (g/mole or kg/kmol). Equation (5-14b) then becomes

$$\rho u \frac{d(a \text{Mw}_r / \rho N_A)}{dx} = \rho \mathcal{D} \frac{d^2}{dx^2} (a \text{Mw}_r / \rho N_A) - \dot{\omega}_r \quad (5-14c)$$

Multiplying through by N_A/Mw_r and rearranging the terms, we have

$$\rho \mathcal{D} \frac{d^2(a/\rho)}{dx^2} - \rho u \frac{d(a/\rho)}{dx} - \dot{\omega} = 0 \quad (5-16)$$

The inhomogeneous term in Eq. (5-16) is denoted by $\dot{\omega} \equiv N_A \cdot \dot{\omega}_r / \text{Mw}_r$, which represents the rate of change of the number of molecules of reactant per unit volume by chemical reaction. The first term of the species equation represents the rate of mass diffusion of reactant species and the second term the rate of mass convection of reactant species.

From Chapter 3 we have learned that the general form of the energy equation in terms of enthalpy is

$$\rho \frac{Dh}{Dt} - \frac{Dp}{Dt} = -\nabla \cdot \mathbf{q} + \Phi + \dot{Q} + \rho \sum_{K=1}^N Y_K \mathbf{f}_K \cdot \mathbf{v}_K \quad (3-78)$$

Neglecting dissipation, body-force work, and unsteady terms, and also using

$$q = -\lambda \frac{dT}{dx}, \quad h = C_p T$$

we have the following energy equation in one-dimensional form:

$$\rho C_p u \frac{dT}{dx} = \lambda \frac{d^2 T}{dx^2} + \dot{Q}$$

or

$$\frac{\lambda}{\rho C_p} \frac{d^2 T}{dx^2} = u \frac{dT}{dx} - \frac{\dot{Q}}{\rho C_p} \quad (5-17)$$

where $\dot{Q} = -\sum_{i=1}^N \dot{\omega}_i \Delta h_{f,i}^\theta = \dot{\omega} Q$ (Q represents the heat of reaction per molecule of reactant). Equation (5-17) can be written as

$$\frac{\lambda}{C_p} \frac{d^2 T}{dx^2} - \rho u \frac{dT}{dx} + \frac{\dot{\omega} Q}{C_p} = 0 \quad (5-18)$$

where the product ρu is the eigenvalue of the problem.

Following the Shvab-Zel'dovich formulation (see Chapter 3), two new variables θ and α are defined as

$$\theta \equiv C_p \frac{T - T_0}{Q} \quad (5-19)$$

$$\alpha \equiv \frac{a_0}{\rho_0} - \frac{a}{\rho} \quad (5-20)$$

where the subscript 0 designates initial values at an undisturbed station. Substituting Eqs. (5-19) and (5-20) into Eqs. (5-18) and (5-16), we have

$$\frac{\lambda}{C_p} \frac{d^2 \theta}{dx^2} - \rho u \frac{d\theta}{dx} + \dot{\omega} = 0 \quad (5-21)$$

$$\rho \mathcal{D} \frac{d^2 \alpha}{dx^2} - \rho u \frac{d\alpha}{dx} + \dot{\omega} = 0 \quad (5-22)$$

These two equations are identical if $Le = 1$.

The boundary conditions for (5-21) and (5-22) are prescribed as follows: For $x = -\infty$ (cold boundary),

$$\alpha = 0, \quad \theta = 0$$

For $x = +\infty$ (hot boundary),

$$\alpha = \frac{a_0}{\rho_0}, \quad \theta = C_p \frac{T_f - T_0}{Q}$$

It is interesting to note that the solutions of Eqs. (5-21) and (5-22) are identical (i.e., $\alpha = \theta$) over the entire combustion wave zone if

$$\frac{a_0}{\rho_0} = C_p \frac{T_f - T_0}{Q}$$

The above relationship can be satisfied if the flame is adiabatic. Under this assumption, the following algebraic equation can be introduced to replace one of the two differential equations [say, Eq. (5-22)]:

$$C_p T + \frac{aQ}{\rho} = C_p T_0 + \frac{a_0 Q}{\rho_0} = C_p T_f \quad (5-23)$$

The meaning of this equation is that the sum of the thermal (sensible) and chemical energies per unit mass of mixture is constant throughout the combustion zone. This implies that only one ordinary differential equation, (5-21) or (5-17), need be solved. Let's now use the energy equation. In region I ($\dot{\omega} = 0$), the energy equation can be written as

$$\frac{d^2T}{dx^2} - \frac{(\rho u)C_p}{\lambda} \frac{dT}{dx} = 0 \quad (5-24)$$

with the boundary conditions

$$x = -\infty, \quad T = T_0$$

$$x = 0^-, \quad T = T_i$$

In region II, the convective term was considered by these researchers to be negligible in comparison with the heat generation term, since T_i is usually very close to T_f . Then, the energy equation can be written as

$$\frac{d^2T}{dx^2} + \frac{\dot{\omega}Q}{\lambda} = 0 \quad (5-25)$$

with boundary conditions

$$x = \infty, \quad T = T_f, \quad \frac{dT}{dx} = 0$$

$$x = 0^+, \quad T = T_i$$

In order to have heat-flux balance at the interface of the two zones, it is required that

$$\left(\frac{dT}{dx} \right)_{x=0^-} = \left(\frac{dT}{dx} \right)_{x=0^+} \quad (5-26)$$

By integrating Eq. (5-24) with respect to x , we have

$$\frac{dT}{dx} = \frac{(\rho u)C_p}{\lambda} T + \text{constant}$$

Since at $x = -\infty$ we have $T = T_0$, $dT/dx = 0$, it follows that

$$\frac{dT}{dx} = \frac{(\rho u)C_p}{\lambda}(T - T_0)$$

This gives

$$\left(\frac{dT}{dx} \right)_{x=0^-} = \frac{(\rho u)C_p(T_i - T_0)}{\lambda} \approx \frac{(\rho u)C_p(T_f - T_0)}{\lambda} \quad (5-27)$$

if T_i is very close to T_f .

In order to obtain the temperature gradient on the 0^+ side, we need to integrate Eq. (5-25) by first multiplying it by $2 dT/dx$ and rearrange it to give

$$\frac{d}{dx} \left(\frac{dT}{dx} \right)^2 = -2 \left(\frac{dT}{dx} \right) \frac{Q\dot{\omega}}{\lambda}$$

Integrating from $x = 0^+$ to $x = \infty$, and applying the boundary conditions, we have

$$0 - \left(\frac{dT}{dx} \right)_{x=0^+}^2 = - \int_{T_i}^{T_f} \frac{2Q\dot{\omega}}{\lambda} dT$$

or

$$\left(\frac{dT}{dx} \right)_{x=0^+}^2 = \int_{T_i}^{T_f} \frac{2Q\dot{\omega}}{\lambda} dT \quad (5-28)$$

Substituting both (5-27) and (5-28) into (5-26), we have

$$\frac{(\rho u)^2 C_p^2 (T_f - T_0)^2}{\lambda^2} = \frac{2Q}{\lambda} \int_{T_i}^{T_f} \dot{\omega} dT$$

or

$$(\rho u)^2 = \frac{2\lambda Q}{C_p^2 (T_f - T_0)^2} \int_{T_i}^{T_f} \dot{\omega} dT$$

Also, we know that $a_0 Q / \rho_0 = C_p (T_f - T_0)$; then

$$(\rho u)^2 = \rho_0^2 S_L^2 = \rho_0^2 u_0^2 = \frac{2\lambda}{C_p (T_f - T_0)} \frac{\rho_0}{a_0} \int_{T_i}^{T_f} \dot{\omega} dT$$

Therefore,

$$S_L = u_0 = \sqrt{\left(\frac{\lambda}{\rho_0 C_p}\right) \frac{2}{(T_f - T_0)} \left(\frac{1}{a_0} \int_{T_i}^{T_f} \dot{\omega} dT\right)} = \sqrt{\left(\frac{\lambda}{\rho_0 C_p}\right) \frac{2}{(T_f - T_0)} I} \quad (5-29)$$

where

$$I \equiv \frac{1}{a_0} \int_{T_i}^{T_f} \dot{\omega} dT = \frac{1}{a_0} \int_{T_0}^{T_f} \dot{\omega} dT \quad (5-30)$$

The two integral quantities in the above equation are equal because there is no reaction between T_0 and T_i . Now, let $\dot{\omega}$ be a function of T , according to the expression for a zero-order chemical reaction for simplicity:

$$\dot{\omega} = A e^{-E_a/R_u T} \quad (5-31)$$

where A , the Arrhenius factor, is considered a constant that does not depend on the concentration. For most hydrocarbon fuels, $E_a/R_u T \gg 1$. Since $E_a \approx 30,000\text{--}40,000 \text{ cal/mole}$, $T_f \approx 1500\text{--}2000 \text{ K}$, and $R_u = 1.987 \text{ cal/mole K}$, then

$$\frac{E_a}{R_u T_f} \sim 10 \gg 1$$

Set $\sigma \equiv T_f - T$; its values range from $\sigma_1 \equiv T_f - T_i$ down to 0 for zone II. Then,

$$T = T_f - \sigma = T_f \left(1 - \frac{\sigma}{T_f}\right)$$

Since σ/T_f is generally small, we have

$$\begin{aligned} e^{-E_a/R_u T} &= \exp\left[-\frac{E_a}{R_u T_f (1 - \sigma/T_f)}\right] \approx \exp\left[-\frac{E_a}{R_u T_f} \left(1 + \frac{\sigma}{T_f}\right)\right] \\ &= e^{-E_a/R_u T_f} e^{-E_a \sigma / R_u T_f^2} \end{aligned} \quad (5-32)$$

The expression for ω is now introduced into (5-30) to give

$$I = \frac{A e^{-E_a/R_u T_f}}{a_0} \int_{T_i}^{T_f} e^{-E_a \sigma / R_u T_f^2} dT = -\frac{A e^{-E_a/R_u T_f}}{a_0} \int_{\sigma_1}^0 e^{-E_a \sigma / R_u T_f^2} d\sigma \quad (5-33)$$

Let

$$\beta \equiv \frac{E_a \sigma}{R_u T_f^2} \quad \text{and} \quad \beta_1 \equiv \frac{E_a \sigma_1}{R_u T_f^2} \quad (5-34)$$

Substitute (5-34) into (5-33):

$$I = \frac{A e^{-E_a/R_u T_f}}{a_0} \frac{R_u T_f^2}{E_a} \int_0^{\beta_1} e^{-\beta} d\beta \approx \frac{A e^{-E_a/R_u T_f}}{a_0} \frac{R_u T_f^2}{E_a} j$$

where $j = \int_0^{\beta_1} e^{-\beta} d\beta = 1 - e^{-\beta_1} \approx 1$. Therefore,

$$I \approx \frac{Ze^{-E_a/R_u T_f}}{a_0} \left(\frac{R_u T_f^2}{E_a} \right) \quad (5-35)$$

According to Eq. (5-29), u_0 for a zero-order reaction can be written as

$$S_L = u_0 = \sqrt{\frac{2\lambda}{C_p \rho_0} \frac{1}{a_0} \left(\frac{Ae^{-E_a/R_u T_f}}{T_f - T_0} \right) \frac{R_u T_f^2}{E_a}} \quad (5-36)$$

Since $a_0 \propto p$ and $\rho_0 \propto p$, then $S_L \propto \sqrt{p^{-2}}$ for a zero-order reaction. This agrees with the result obtained before, that $S_L \propto \sqrt{p^{n-2}}$.

Note: This theory is valid only when $E_a/R_u T_f \gg 1$, in other words for high-activation-energy reactions. Reactions in which $\dot{\omega}$ is a function of reactant concentration as well as temperature have been considered. For first-order (unimolecular) reactions

$$\dot{\omega} = CAe^{-E_a/R_u T} \quad (C = \text{concentration}) \quad (5-37)$$

and for second-order (bimolecular) reactions

$$\dot{\omega} = C^2 Ae^{-E_a/R_u T} \quad (5-38)$$

Some of the restricting assumptions may now be removed. If we allow the number of molecules to change in the ratio n_r/n_p , assign λ and C_p the mean values $\bar{\lambda}$ and \bar{C}_p in region I and the value for the burned gases λ_f and C_{pf} in region II, and set $(\lambda/C_p)/\rho D = Le$, then the equation for a first-order reaction becomes

$$S_L = u_0 = \sqrt{\frac{2\lambda_f C_{pf} A}{\rho_0 \bar{C}_p^2} \left(\frac{T_0}{T_f} \right) \left(\frac{n_r}{n_p} \right) (Le) \left(\frac{R_u T_f^2}{E_a} \right)^2 \frac{e^{-E_a/R_u T_f}}{(T_f - T_0)^2}} \quad (5-39)$$

and for a second-order reaction

$$S_L = u_0 = \sqrt{\frac{2\lambda_f (C_{pf})^2 A a_0}{\rho_0 \bar{C}_p^3} \left(\frac{T_0}{T_f} \right) \left(\frac{n_r}{n_p} \right)^2 (Le)^2 \left(\frac{R_u T_f^2}{E_a} \right)^3 \frac{e^{-E_a/R_u T_f}}{(T_f - T_0)^3}} \quad (5-40)$$

The theory does not give very accurate results, but it does predict the trend of the flame propagation speed. Note that we still have the basic relationship

$$S_L \propto \sqrt{\alpha(\text{RR})_{T_f}} \quad (5-41)$$

The difference between this theory and that of Mallard and LeChatelier is that the reaction rate is based on the flame temperature.

2.3 Diffusion Theory: The Theory of Tanford and Pease

Tanford and Pease¹³ assumed that for certain reactions in laminar flames the rate of diffusion of active radicals into the unburned gas governs the magnitude of the flame speed. Their work was reported in three parts. The first part^{13a} gave calculations of the equilibrium atom and free-radical concentrations in a moist carbon monoxide flame. The results indicated that the equilibrium concentration of the hydrogen atoms is an important factor in determining the flame velocity. In the second part, Tanford^{13b} presented calculations to establish the relative importance of mass diffusion and heat conduction in creating the hydrogen atoms in the flame zone. The conclusion was that diffusion is the controlling process. The third paper^{13c} developed an equation for the flame velocity based on this conclusion.

They plotted their calculated equilibrium concentration of H in the moist CO–O₂–N₂ flame versus the flame velocities reported by Jahn¹⁷ and showed a linkage between S_L and C_H , suggesting that S_L is a function of hydrogen-atom concentration. Two mechanisms were considered by which radicals appear throughout the flame zone, and an evaluation of the relative importance of the two mechanisms was made. The mechanisms considered were as follows:

1. Local production by thermal dissociation, the radical concentrations being functions of temperature and hence dependent upon the heat-conduction process.
2. Supply by diffusion from a station at which the reaction has reached equilibrium.

The concentration of hydrogen atoms, C_H , as a function of x was evaluated for the first mechanism by setting up an energy equation, which upon solution gives T as a function of x . From the $T(x)$ curve, the maximum possible values of C_H as a function of x were calculated. The distribution of C_H throughout the combustion wave was evaluated according to the second mechanism by solving the species-continuity equation and applying boundary conditions at both burned and unburned stations.

Comparison was made between the two C_H distributions obtained by using the two different mechanisms. It was found that the concentration of hydrogen atoms from thermal dissociation is less than 10% of that due to mass diffusion at a small distance away from the fully reacted station for both the carbon monoxide flame and hydrogen flame. On the basis of these results, a formula for the flame velocity was developed on the assumption that the determining factor is the diffusion of active species, chiefly hydrogen atoms, from the station at which the combustion has reached equilibrium. Several further assumptions were used in the development of their diffusion theory: (1) zero activation energy for radical species, (2) exponential concentration distribution for all active free radicals,

(3) a constant mean temperature = $0.7T_f$ for the whole combustion zone, (4) a constant mass diffusion coefficient for gases in the combustion zone, (5) a first-order chemical-reaction expression for the source term in the species equation, and (6) no chain-branching reactions.

Using these assumptions, an expression for the laminar-flame speed was derived as

$$S_L \equiv u_0 = \sqrt{\frac{C_r}{X_P} \sum_i \frac{k_i p_i \mathcal{D}_{i,0}}{B'_i}} \quad (5-42)$$

where p_i is the equilibrium partial pressure of free-radical species i ; $\mathcal{D}_{i,0}$ is the mass diffusivity of i th species at the initial temperature of the unburned mixture; k_i is the specific rate constant for the consumption of i th species; C_r is the concentration of the reactant mixture; X_P is the mole fraction of products; and B'_i is a function of the mass diffusivity of the gases in the reaction zone, the kinetic parameter, and the laminar-flame speed. One obvious defect of the above equation is that the flame velocity of the dry carbon monoxide mixture goes to zero with free-radical concentration or partial pressure. Tanford and Pease therefore assumed that there is a constant contribution to the flame velocity independent of the radical concentration, and this constant (17 cm/s) is added to Eq. (5-42). By considering only H and OH radicals in moist carbon monoxide flames, they obtained

$$S_L = 17 \text{ cm/s} + \sqrt{\frac{C_r}{X_P} \left(\frac{k_H p_H \mathcal{D}_{H,0}}{B'_H} + \frac{k_{OH} p_{OH} \mathcal{D}_{OH,0}}{B'_{OH}} \right)} \quad (5-43)$$

Since both B'_H and B'_{OH} are functions of S_L , Eq. (5-43) is an implicit equation for calculating S_L .

Flame velocities for moist CO–O₂–N₂ mixtures typically vary from 25 to 106 cm/s. The calculated values of S_L from Eq. (5-43) generally have errors less than 25%. Equation (5-42) was applied to the combustion of H₂ in a similar way, with results of the same degree of accuracy.

Dugger¹⁸ measured the velocity as a function of initial temperature for propane–air and ethylene–air flames and compared the curves for the experimental data with curves calculated by the Zel'dovich–Frank–Kamenetsky theory as well as with curves calculated according to the Tanford–Pease theory. In this comparison, Dugger assumed that the controlling step was a bimolecular reaction. To examine the temperature dependence, he rearranged the second-order Zel'dovich–Frank–Kamenetsky–Semenov equation and approximated the temperature-dependent terms with those for air. In this way, he reduced Eq. (5-40) to the form

$$S_L \propto \sqrt{\frac{T_0^2 T_f^{4.9} e^{-E_a/R_u T_f}}{(T_f - T_0)^3}} \quad (5-44)$$

In using the Tanford–Pease equation, Dugger assumed that only p_i , $\mathcal{D}_{i,m}$, and the number density of the reactant molecules are temperature-dependent.

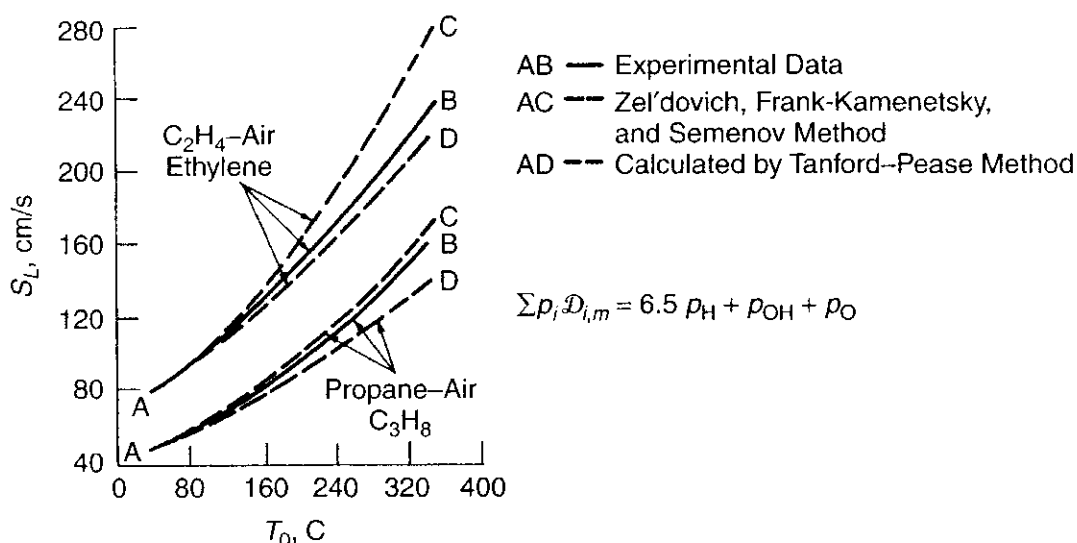


Figure 5.8 Comparison of calculated S_L versus T_0 with the measured data (adapted from Evans²).

Dugger's expression for predicting the relative effect of temperature on flame speed according to the Tanford-Pease theory is

$$S_L \propto \sqrt{\left(\sum k_i p_i \mathcal{D}_{i,m} \right) T_0^2 T_f^{-1.33}} \quad (5-45)$$

where $\mathcal{D}_{i,m}$ is the mass diffusivity at $0.7T_f$. Figure 5.8 shows the results for the Tanford-Pease theory as well as for the Zel'dovich-Frank-Kamenetsky-Semenov theory. The effect of the initial temperature on the flame velocity appears to be explained equally well or equally badly by the two theories.

Simon¹⁹ found the calculated flame velocities of 35 hydrocarbons from the diffusion flame theory to be consistent with those measured by Gerstein, Levine, and Wong.²⁰ Equilibrium concentrations of H, O, and OH radicals were calculated at compositions giving the maximum flame velocity. The sum of the active radical concentrations each multiplied by the respective diffusion coefficient was plotted against S_L as shown in Fig. 5.9. It should be noted that Eq. (5-42) was modified for application to hydrocarbons by including a factor r for the total number of moles of water vapor and carbon dioxide that form per mole of hydrocarbon, and by assuming that H, OH, and O are equally effective as chain carriers.

Then Eq. (5-42) becomes

$$S_L = \sqrt{\frac{r C_r}{X_P} k \left(\frac{\mathcal{D}_H p_H}{B'_H} + \frac{\mathcal{D}_{OH} p_{OH}}{B'_{OH}} + \frac{\mathcal{D}_O p_O}{\beta'_O} \right)} \quad (5-46)$$

From Eq. (5-46) k was found for all hydrocarbons except ethylene to have a value of $(1.4 \pm 0.1) \times 10^{11} \text{ cm}^3/\text{mole} \cdot \text{s}$. This constancy of k suggests that the rate constants for the oxidation of different hydrocarbons are either the same or closely related. This stipulation is in agreement with the general observed hydrocarbon oxidation reaction mechanism discussed in Chapter 2.

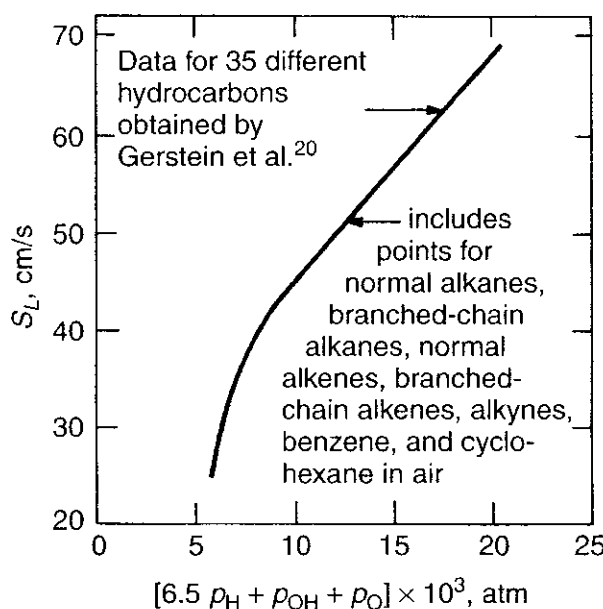


Figure 5.9 S_L versus radical concentrations as calculated by Simon.¹⁹

Simon¹⁹ points out that a correlation between laminar-flame speed and flame temperature exists for these hydrocarbons, and that a flame mechanism, which depended strongly on flame temperature, might have given an equally good correlation with flame speed. Therefore, a thermal mechanism cannot be ruled out.

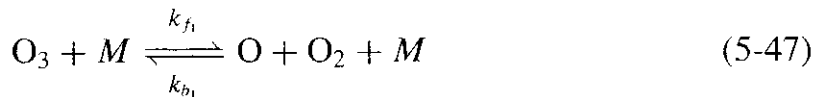
The consistency of the calculated results with experimental data does not prove the validity of these simple theories developed in the 1940s. Indeed, the researchers then were handicapped by not having any advanced computers and sophisticated numerical schemes to solve nonlinear coupled partial or ordinary differential equations. The above classical theories were presented for the basic understanding of the historical development of the laminar-flame theory as well as to introduce the fundamental physicochemical mechanism of flame propagation in premixed gases. The current approach to this type of problem is quite different from those in the pioneering age. A formulation using crude assumptions like those of Tanford and Pease would be inexcusable in today's research work. We shall follow several examples to show a modern approach to laminar-flame problems.

3 CONTEMPORARY METHOD FOR SOLVING LAMINAR-FLAME PROBLEMS

3.1 Premixed O₃/O₂ Laminar Flames

With the advent of high-speed digital computers, the solution of laminar-flame problems has changed significantly from the traditional methods discussed previously. We shall use one of the papers by Heimerl and Coffee²¹ as one of the examples of the contemporary method. A one-dimensional, premixed, laminar, steady-state ozone/oxygen flame was considered in their theoretical model. One

reason for choosing this mixture was its simplicity; it involves only three species: O, O₂, and O₃. The chemical reactions between these species are



where *M* represents the third body, which could be either O, O₂, or O₃. The kinetic coefficients for these reactions are given as a function of temperature in Table 5.1.

The rate coefficient may vary with the identity of the chaperon third body *M*. The chaperon relationships used are

$$k_{f_1}(M = \text{O}) = k_{f_1}(M = \text{O}_2) = 0.44 \quad k_{f_1}(M = \text{O}_3) \quad (5-50)$$

$$k_{f_3}(M = \text{O}) = 3.6 \quad k_{f_3}(M = \text{O}_2) = 3.6 \quad k_{f_3}(M = \text{O}_3) \quad (5-51)$$

Table 5.1 Kinetic Coefficients

Coefficient	Expression	Reference	Remarks
k_{f_1}	$4.31 \times 10^{14} \exp\left(-\frac{11,161}{T}\right) \frac{\text{cm}^3}{\text{mole s}}$	Heimerl and Coffee ²² (1979)	$M = \text{O}_3, 300 < T < 3000 \text{ K}$
k_{b_1}	$1.2 \times 10^{13} \exp\left(\frac{+976}{T}\right) \frac{\text{cm}^6}{\text{mole}^2 \text{s}}$	—	Derived from equilibrium constant
k_{f_2}	$1.14 \times 10^{13} \exp\left(-\frac{2300}{T}\right) \frac{\text{cm}^3}{\text{mole s}}$	Hampson ²³ (1973)	$200 < T < 1000 \text{ K}$
k_{b_2}	$1.19 \times 10^{13} \exp\left(-\frac{50,600}{T}\right) \frac{\text{cm}^3}{\text{mole s}}$	—	Derived from equilibrium constant
k_{f_3}	$1.38 \times 10^{18} T^{-1} \exp\left(-\frac{171}{T}\right) \frac{\text{cm}^6}{\text{mole}^2 \text{s}}$	Johnston ²⁴ (1968)	$M = \text{O}_2, 1000 < T < 8000 \text{ K}$
k_{b_3}	$2.75 \times 10^{19} T^{-1} \exp\left(-\frac{59,732}{T}\right) \frac{\text{cm}^3}{\text{mole s}}$	Johnston ²⁴ (1968)	$M = \text{O}_2, 1000 < T < 8000 \text{ K}$

Equation (5-50) is based on the work of Johnston,²⁴ and Eq. (5-51) is based on the work of Baulch et al.²⁵

The rate of production of species i for Eqs. (5-47) to (5-49) can be given as

$$\dot{\omega}_i = Mw_i \sum_{k=1}^6 (v''_{i,k} - v'_{i,k}) \underbrace{B_k T^{\alpha_k} e^{-E_a/R_u T}}_{k_k} \prod_{j=1}^3 \left(\frac{X_j}{R_u} \frac{p}{T} \right)^{v'_{j,k}} \quad (5-52)$$

which considers all six chemical reactions [Eqs. (5-47) to (5-49)] and all three chemical species. Note that this equation has the same form as Eq. (3-95).

In addition to the kinetic coefficients, there are two sets of data required as inputs to the model: the thermodynamic and transport coefficients. By means of the thermodynamic coefficients, the sensible enthalpy and constant-pressure specific heat are related to the temperature by the following equations:

$$h = R_u \left(a_0 + \sum_{n=1}^5 a_n \frac{T^n}{n} \right) \quad (5-53)$$

$$C_p = R_u \sum_{n=1}^5 a_n T^{n-1} \quad (5-54)$$

For each species, two sets of coefficients are given in Ref. 21 for two temperature ranges. The transport coefficients λ and μ are given as functions of temperature. The mass diffusivity $D_{i,j}$ is assumed to be a function of both temperature and pressure.

The governing equations used in the model are given in one-dimensional and time-dependent forms as follows:

Overall continuity equation:

$$\frac{\partial \rho}{\partial t} + \frac{\partial (\rho u)}{\partial x} = 0 \quad (5-55)$$

Species continuity equation:

$$\rho \frac{\partial Y_k}{\partial t} + \rho u \frac{\partial Y_k}{\partial x} = -\frac{\partial}{\partial x} (\rho Y_k V_k) + \dot{\omega}_k \quad (5-56)$$

where $k = 1, 2$, or 3 for O , O_2 , or O_3 respectively.

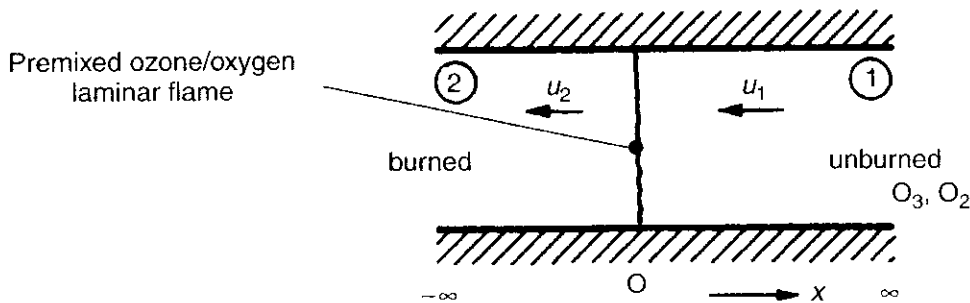
Energy equation:

$$\rho C_p \frac{\partial T}{\partial t} + \rho u C_p \frac{\partial T}{\partial x} = \frac{\partial}{\partial x} \left(\lambda \frac{\partial T}{\partial x} \right) - \sum_{k=1}^N \dot{\omega}_k \Delta h_{f_k}^o - \rho \sum_{k=1}^N C_{p,k} Y_k V_k \frac{\partial T}{\partial x} \quad (5-57)$$

This energy equation was arrived at under the assumptions that the pressure is constant in the reaction zone, the viscous dissipation is negligible, and there is no body-force work.

Diffusion equation:

$$\frac{\partial X_k}{\partial x} = \sum_{j=1}^N \frac{X_k X_j}{D_{kj}} (V_j - V_k) \quad (5-58)$$



The boundary conditions for the totally unburned end are

$$x \rightarrow \infty : \quad T = T_1, \quad Y_k = Y_{k1} \quad \text{for } k = 1, 2, 3 \quad (5-59)$$

The boundary conditions for the totally burned end are

$$x \rightarrow -\infty : \quad \frac{\partial T}{\partial x} = \frac{\partial Y_k}{\partial x} = 0 \quad (5-60)$$

In order to avoid solving the continuity Eq. (5-55) along with the other equations, Heimerl and Coffee²¹ used a Langrangian coordinate ψ and a new time coordinate τ defined by

$$\psi \equiv \int_0^x \rho(x', t) dx', \quad \tau \equiv t \quad (5-61)$$

By the chain rule, we have

$$\frac{\partial}{\partial t}(\cdot) = \frac{\partial \psi}{\partial t} \frac{\partial (\cdot)}{\partial \psi} + \frac{\partial \tau}{\partial t} \frac{\partial (\cdot)}{\partial \tau} = [(\rho u)_0 - (\rho u)] \frac{\partial (\cdot)}{\partial \psi} + \frac{\partial (\cdot)}{\partial \tau} \quad (5-62)$$

$$\frac{\partial}{\partial x}(\cdot) = \frac{\partial \psi}{\partial x} \frac{\partial (\cdot)}{\partial \psi} + \frac{\partial \tau}{\partial x} \frac{\partial (\cdot)}{\partial \tau} = \rho \frac{\partial (\cdot)}{\partial \psi} \quad (5-63)$$

In arriving at the final expressions in Eqs. (5-62) and (5-63), we have used the following relationships, which come directly from the definition given in Eq. (5-61):

$$\begin{aligned} \frac{\partial \psi}{\partial x} &= \rho, & \frac{\partial \tau}{\partial x} &= 0 \\ \frac{\partial \psi}{\partial t} &= (\rho u)_{x=0} - (\rho u)_x, & \frac{\partial \tau}{\partial t} &= 1 \end{aligned} \quad (5-64)$$

One can easily show that by integrating the overall continuity equation (5-55) from 0 to x , one obtains

$$\frac{\partial}{\partial t} \int_0^x \rho dx + [(\rho u)_x - (\rho u)_0] = 0 \quad (5-65)$$

which automatically satisfies one of the relationships given in Eq. (5-64). Therefore, the overall continuity equation need not be solved in the (ψ, τ) coordinate system.

It is important to point out that the product ρu at $x = 0$ is the eigenvalue of the problem. It is defined as

$$m_0 \equiv (\rho u)_0 \quad (5-66)$$

After the transformation and replacement of τ by t , we have

$$\frac{\partial Y_k}{\partial t} + m_0 \frac{\partial Y_k}{\partial \psi} = -\frac{\partial}{\partial \psi} (\rho Y_k V_k) + \frac{\dot{\omega}_k}{\rho} \quad \text{for } k = 1, 3 \quad (5-67)$$

For O_2 , the mass fraction Y_2 can be determined from

$$Y_2 = 1 - Y_1 - Y_3 \quad (5-68)$$

The energy equation in the new coordinate system becomes

$$\frac{\partial T}{\partial t} + m_0 \frac{\partial T}{\partial \psi} = \frac{1}{C_p} \frac{\partial}{\partial \psi} \left(\rho \lambda \frac{\partial T}{\partial \psi} \right) - \frac{1}{\rho C_p} \sum_{k=1}^N \dot{\omega}_k \Delta h_{f_k}^o - \sum_{k=1}^N \frac{C_{p,k}}{C_p} \rho Y_k V_k \frac{\partial T}{\partial \psi} \quad (5-69)$$

The eigenvalue of m_0 or S_L was determined from the steady-state solution of the problem, that is,

$$\frac{\partial Y_k}{\partial t} = 0 \quad \text{and} \quad \frac{\partial T}{\partial t} = 0 \quad (5-70)$$

Under the steady-state condition,

$$\rho u = \text{constant} = \rho(\infty)u(\infty) = -\rho_1 S_L \quad (5-71)$$

Integrating Eq. (5-56) over any interval (a, b) , one obtains

$$\rho u [Y_k(b) - Y_k(a)] = \int_a^b \dot{\omega}_k dx - \rho Y_k V_k \Big|_a^b \quad (5-72)$$

or

$$S_L = -\frac{\int_a^b \dot{\omega}_k dx - \rho Y_k V_k \Big|_a^b}{\rho_1 [Y_k(b) - Y_k(a)]} = -\frac{\int_{x=a}^{x=b} (\dot{\omega}_k / \rho) d\psi - \rho Y_k V_k \Big|_a^b}{\rho_1 [Y_k(b) - Y_k(a)]} \quad (5-73)$$

In the numerical solution, Heimerl and Coffee²¹ used a general PDE solver (PDECOL), developed by Madsen and Sincovec.²⁶ In the solution procedure, the spatial discretization is accomplished by finite-element collocation methods

based on B -splines, developed by de Boor.²⁷ The solution was written in the form of a finite series

$$\begin{aligned} Y_k &\approx \sum_{i=1}^{\text{NC}} C_k^{(i)}(t) B_i(\psi), \quad k = 1, 3 \\ T &\approx \sum_{i=1}^{\text{NC}} C_T^{(i)}(t) B_i(\psi) \end{aligned} \quad (5-74)$$

where $C_k^{(i)}$ and $C_T^{(i)}$ are time-dependent coefficients, $B_i(\psi)$ are basis functions of the B -splines, and NC is the number of collocation points. The time-dependent coefficients are determined uniquely by requiring that the preceding expansions satisfy the given boundary conditions and that they satisfy Eqs. (5-67) and (5-69) exactly at interior collocation points.

The predicted flame velocities are in reasonable agreement with the measurements of Streng and Grosse,²⁸ as shown in Fig. 5.10 and Table 5.2. The calculated results of Heimerl and Coffee²¹ are also in good agreement (within $\pm 12\%$) with the computed results of Warnatz,²⁹ even though he used quite different expressions for some of the kinetic coefficients (see Table 5.3). The calculated temperature and atomic oxygen profiles are quite different from those of Warnatz. The comparison of temperature profiles is shown in Fig. 5.11.

A typical set of calculated profiles of temperature and concentration are shown in Fig. 5.12. As depicted in this figure, the major variations of temperature and concentrations are within a distance of 0.1 mm.

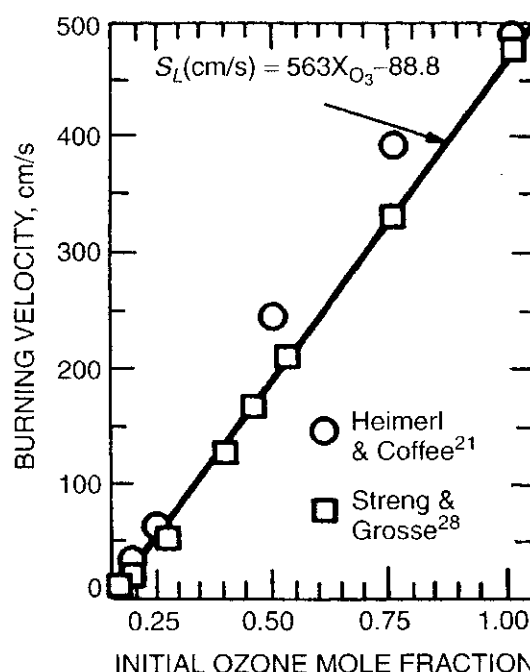


Figure 5.10 Comparison of theoretical results of Heimerl and Coffee²¹ with experimental data of Streng and Grosse.²⁸

Table 5.2 Comparison of Computed Burning Velocities by Heimerl and Coffee²¹ with the Measurements of Streng and Grosse²⁸

Mole Fraction	Initial Ozone		Burning Velocity (cm/s)	Ratio
	Heimerl	Streng and Grosse ^a		
1.00	497	474		1.05
0.75	396	333		1.19
0.50	248	193		1.28
0.25	64	52		1.23
0.20	33	24		1.38

^aDetermined from Streng and Grosse's equation in Fig. 5.10.

Table 5.3 Comparison of Burning Velocities Computed by Warnatz²⁹ and by Heimerl and Coffee²¹

Mole Fraction	Initial Ozone		Burning Velocity (cm/s)	Ratio
	Warnatz	Heimerl and Coffee		
1.00	445	497		0.90
0.75	350	396		0.88
0.50	225	248		0.91
0.25	65	64		1.02
0.20	37	33		1.12

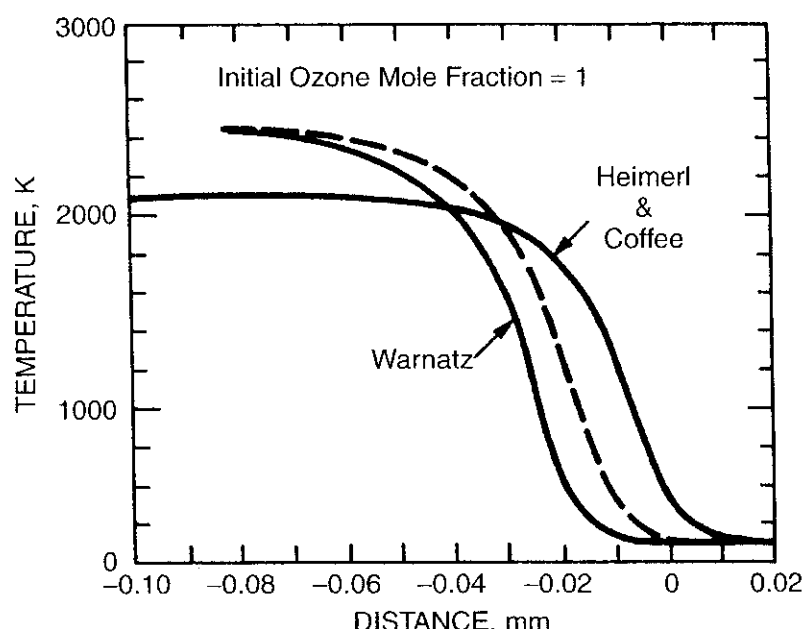


Figure 5.11 Comparison of calculated temperature profiles by Warnatz²⁹ and Heimerl and Coffee.²¹ (Dashed profile represents the result obtained by substituting Warnatz's expressions for k_{f1} and k_{f2} into the Heimerl-Coffee model.)

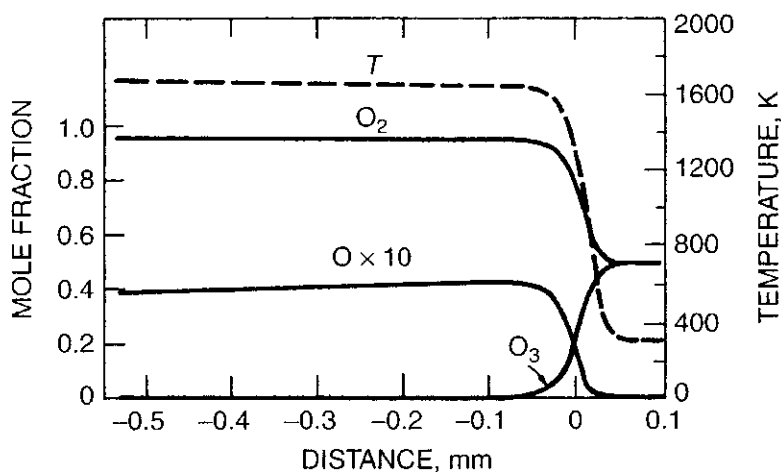


Figure 5.12 Calculated temperature and concentration profiles.

Heimerl and Coffee²¹ stressed that profile measurements for temperature and concentrations are vital to test the model's output coefficients and so validate the model. They further indicated that agreement with burning velocities, even over a wide range of initial ozone mole fractions, is a necessary but insufficient condition to ensure that the input coefficients are realistic.

3.2 Chemkin Code for Solving Premixed Laminar-Flame Structures

The Chemkin Code written in Fortran was developed by Kee et al.⁵⁴ of the Sandia National Laboratories in Livermore, California, in an attempt to model the exact processes in various types of flames, with the consideration of detailed chemical kinetics. This numerical simulation is important because it facilitates the understanding of flame structure under different operating conditions. The temperature and species profiles in various flame configurations can be analyzed by this code. Their report⁵⁴ specifically discussed two types of flames: steady-state burner-stabilized flames and freely propagating premixed laminar flames.

For the burner-stabilized flames, the mass flow rate is treated to be known. There are two cases for this type of flame. One case corresponds to problems with known (measured) temperature profiles. For the other case, the temperature profile must be determined by solving the energy equation. Naturally, the results for flames with known temperature profiles through experimental measurements are more accurate. For the freely propagating adiabatic flames, there is no heat loss and the temperature profile can be computed from the conservation of energy equation.

The equations for steady-state, isobaric, quasi-one-dimensional flames are given below.

$$\dot{M} = \rho u A \quad (5-75)$$

$$\dot{M} \frac{dT}{dx} - \frac{1}{C_p} \frac{d}{dx} \left(\lambda A \frac{dT}{dx} \right) + \frac{A}{C_p} \sum_{k=1}^N \rho Y_k V_k C_{pk} \frac{dT}{dx} + \frac{A}{C_p} \sum_{k=1}^N \dot{\omega}_k h_k M_w k = 0 \quad (5-76)$$

$$\dot{M} \frac{dY_k}{dx} + \frac{d}{dx}(\rho A Y_k V_k) - A \dot{\omega} M w_k = 0 \quad (5-77)$$

and

$$\rho = p \overline{Mw} / (R_u T) \quad (5-78)$$

In the above formulation, x is the spatial coordinate and A represents the cross-sectional area of tube encompassing the flame. The diffusion velocity V_k is the sum of three parts, including the ordinary diffusion velocity, thermal diffusion velocity, and a correction velocity.

Once the governing equations have been established, boundary conditions must be applied. These boundary conditions vary between the two types of flames considered. For the burner-stabilized flames, \dot{M} is a known constant, the temperature and mass flux fractions are specified at the cold boundary, and vanishing gradients are imposed at the hot boundary. For the freely propagating flames, \dot{M} must be determined. This means that additional constraints must be applied in order to solve for the \dot{M} value. To account for this, the temperature is specified at one point.

Now that the equations and boundary conditions have been established, numerical methods must be applied to solve these flame problems. The first step in this numerical process is to use the finite-difference approximation. Specifically, the central difference formula is used to solve the differential equations. The following approximates have been adopted in Chemkin.

$$\left(\dot{M} \frac{dT}{dx} \right)_j \simeq \dot{M}_j \left[\frac{h_{j-1}}{h_j(h_j + h_{j-1})} T_{j+1} + \frac{h_j - h_{j-1}}{h_j h_{j-1}} T_j - \frac{h_j}{h_{j-1}(h_j + h_{j-1})} T_{j-1} \right] \quad (5-79)$$

where the spatial increment, $h_j \equiv x_{j+1} - x_j$. The second derivative term in the energy equation can be approximated by

$$\begin{aligned} \frac{d}{dx} \left(\lambda A \frac{dT}{dx} \right)_j &\simeq \left(\frac{2}{x_{j+1} - x_{j-1}} \right) \\ &\times \left[\lambda A_{j+1/2} \left(\frac{T_{j+1} - T_j}{x_{j+1} - x_j} \right) - \lambda A_{j-1/2} \left(\frac{T_j - T_{j-1}}{x_j - x_{j-1}} \right) \right] \end{aligned} \quad (5-80)$$

The derivative of the diffusion velocity term is calculated by

$$\frac{d}{dx} (\rho A Y_k V_k)_j \simeq \frac{(\rho A Y_k V_k)_{j+1/2} - (\rho A Y_k V_k)_{j-1/2}}{x_{j+1/2} - x_{j-1/2}} \quad (5-81)$$

In order for the numerical methods to begin their iterative process to find the solution, initial guesses of the various flame parameters must be made. These include thickness of the reaction zone and estimates of the product species. In addition, intermediate species must be identified. The general form of the starting estimates can be a ramping rise of the product species from zero to an equilibrium

value and a ramping decay of the reactant species from its initial mole fraction to an equilibrium value. The profile of any intermediate species can be assumed to rise from zero level at the start of the reactant concentration decay to reach a peak value and then go down to zero mole fraction when the reactant species levels off to its equilibrium value. For the case of unknown temperature profile, the energy equation must be solved and the program requires initial guesses of the temperature profile. This initial guess also speeds up the computational process. In general, when more temperature data are provided, the more accurate the solution will be.

The Chemkin Code is divided into two sections: a numeric solution module and a flame-specific piece of code. The latter contains all the input and output routines as well as the equations governing flame properties. Figure 5.13 is a simplified version of the block diagram of Fig. 2.13 showing the structure of this code for flame structure calculation. The numeric solution module is a generic numerical solver. The first step in running the code is to execute the CHEMKIN Interpreter. This interpreter reads the user's data and extracts further information from a thermodynamic properties database. The next step is to run TRANSFIT, which computes polynomial representations of the temperature-dependent parts of the individual species viscosities, thermal conductivities, and diffusion coefficients. The final step is to run the flame code, which actually computes the temperature profile and species distribution from data obtained in the previous two programs.

The user is required to write a short program that runs the above subroutines. The first thing that the flame code does is to verify that there is enough space to solve the problem. Naturally, the more grid points the user desires, the more storage space that is required. The user must also provide an area subroutine for describing the physical area of the flame as a function of the distance from the burner. It is recommended that users of Chemkin Code for laminar-flame study follow the Keyword Input and a couple of examples with typical input data. The output provides the axial distributions of temperature, density, composition, and velocity at different grid points. The number of grid points and the thickness of the reaction zone are specified in the input file.

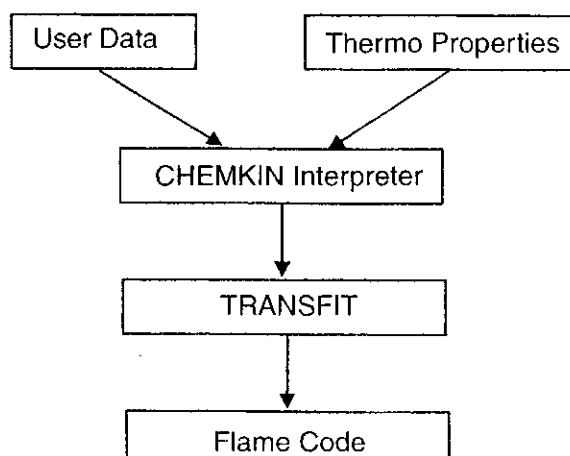


Figure 5.13 Structure of the Chemkin Code.

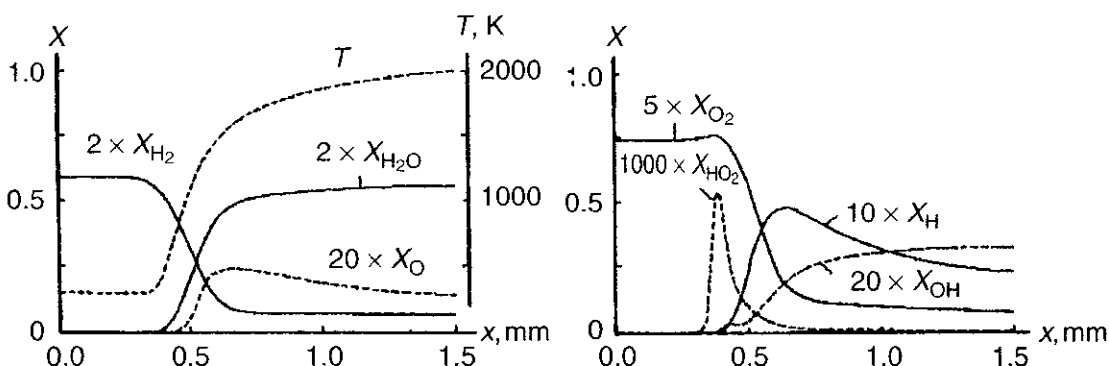


Figure 5.14 Computed profiles of the mole fractions in a stoichiometric H_2/O_2 flame at $p = 1 \text{ atm}$ and $T_u = 298 \text{ K}$ (modified from Warnatz⁵⁵).

The computed profiles of the mole fractions in a stoichiometric H_2/O_2 flame at $p = 1 \text{ atm}$ and $T_u = 298 \text{ K}$ are shown in Fig. 5.14. This computation was conducted by Warnatz⁵⁵ with chemical kinetic rates given in Table 2.8.

Some other representative computed results for H_2/air flame and CH_4/air flame at 1 atm obtained by Lu, Ju, and Law⁵⁶ can be seen from Figs. 2.31 and 2.32.

4 DYNAMIC ANALYSIS OF STRETCHED LAMINAR PREMIX FLAMES

4.1 Definition of Flame Stretch Factor and Karlovitz Number

A flame surface propagating in a nonuniform flow field is submitted to strain and curvature effects leading to changes in the frontal area. Karlovitz et al.⁵⁷ and Markstein⁵⁸ initiated the study of stretched premixed flames and demonstrated the importance of aerodynamic stretching and preferential diffusion on the flame response in terms of flame-front instability. The flame stretch factor (κ) is defined as “the relative rate of change of flame surface area” (also designated as the fractional rate of change of flame surface area).

$$\kappa \equiv \frac{1}{\delta A} \frac{d(\delta A)}{dt} = \frac{1}{A} \frac{dA}{dt} \quad (5-82)$$

The effect of stretch on the flame is to reduce the thickness of the flame front and hence the flame speed and influence the flame structure through its coupled effect with mass and heat diffusion. The concept of flame stretch can be applied to (1) flame stabilization, (2) laminar-flame speed determination, (3) flammability limits, and (4) modeling of turbulent flames.

More recently, several important papers were given by Buckmaster,⁵⁹ Matalon,⁶⁰ Chung and Law,^{61,62} Law,⁶³ and Candel and Poinsot⁶⁴ to elucidate the mathematical relationships and physical processes associated with flame stretch behavior. Let's first derive the basic relationship between the flame stretch rate and the strain rate, dilatation of the fluid element, and the curvature of the flame surface. The three perpendicular coordinates on a curved flame surface are shown in Fig. 5.15, which has two unit vectors (ν and η) tangent to the flame surface and an outward normal

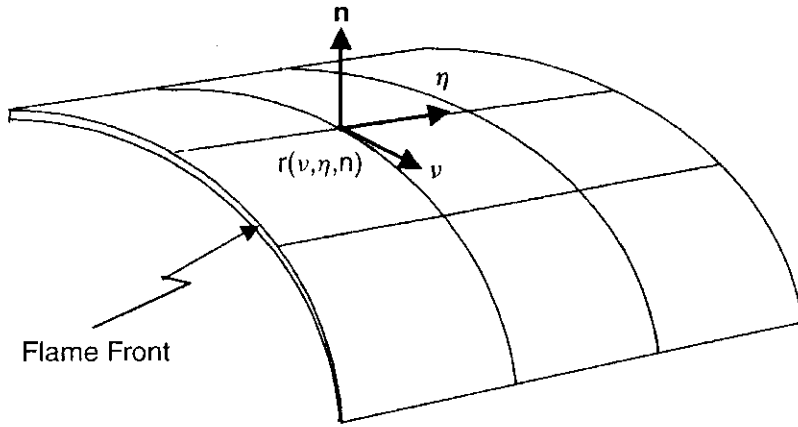


Figure 5.15 Curved laminar-flame front with three perpendicular curvilinear coordinates.

unit vector \mathbf{n} at the spatial point $\mathbf{r}(v, \eta, n)$ as a function of the three independent coordinates.

The elemental arc $(ds)_v$ in the v direction and the elemental arc $(ds)_\eta$ in the η direction are given by

$$(ds)_v = \left(\frac{\partial \mathbf{r}}{\partial v} \right) dv, \quad (ds)_\eta = \left(\frac{\partial \mathbf{r}}{\partial \eta} \right) d\eta \quad (5-83)$$

The incremental flame surface area can be approximated by

$$dA(t) = \left(\frac{\partial \mathbf{r}}{\partial v} \times \frac{\partial \mathbf{r}}{\partial \eta} \right) \cdot \mathbf{n} (dv)(d\eta) \quad (5-84)$$

In the orthogonal curvilinear coordinate system, the two unit vectors (\mathbf{e}_v in the v direction and \mathbf{e}_η in the η direction) can be given by

$$\mathbf{e}_v \equiv \frac{\partial \mathbf{r}/\partial v}{|\partial \mathbf{r}/\partial v|}, \quad \mathbf{e}_\eta \equiv \frac{\partial \mathbf{r}/\partial \eta}{|\partial \mathbf{r}/\partial \eta|}, \quad \text{and} \quad \mathbf{e}_v \times \mathbf{e}_\eta = \mathbf{n} \quad (5-85)$$

Thus,

$$dA(t) = \left| \frac{\partial \mathbf{r}}{\partial v} \right| \left| \frac{\partial \mathbf{r}}{\partial \eta} \right| (dv)(d\eta) \quad (5-86)$$

Now let another surface that is close to the flame surface be represented by $\mathbf{r}^*(v, \eta, n^*)$ such that

$$\mathbf{r}^* = \mathbf{r} + \mathbf{a}, \quad \frac{\partial \mathbf{r}^*}{\partial v} = \frac{\partial \mathbf{r}}{\partial v} + \frac{\partial \mathbf{a}}{\partial v}, \quad \frac{\partial \mathbf{r}^*}{\partial \eta} = \frac{\partial \mathbf{r}}{\partial \eta} + \frac{\partial \mathbf{a}}{\partial \eta} \quad (5-87)$$

where \mathbf{a} is a small-magnitude displacement vector; then

$$dA^*(t) = \left(\frac{\partial \mathbf{r}^*}{\partial v} \times \frac{\partial \mathbf{r}^*}{\partial \eta} \right) \cdot \mathbf{n}^* (dv)(d\eta) = \left| \frac{\partial \mathbf{r}^*}{\partial v} \right| \left| \frac{\partial \mathbf{r}^*}{\partial \eta} \right| (dv)(d\eta)$$

$$\approx \left| \frac{\partial \mathbf{r}}{\partial v} \right| \left| \frac{\partial \mathbf{r}}{\partial \eta} \right| [1 + \nabla_t \cdot \mathbf{a}] (dv) (d\eta) = [1 + \nabla_t \cdot \mathbf{a}] dA(t) \quad (5-88)$$

where $\nabla_t \equiv \mathbf{e}_v \frac{\partial}{\partial v} + \mathbf{e}_\eta \frac{\partial}{\partial \eta}$, which represents the gradient operator along the tangential plane of the flame surface.⁶²

It is useful to note that we can always decompose the any arbitrary velocity into two parts with one part tangent to the flame surface (\mathbf{v}_t) and the other part normal to the flame surface, i.e.,

$$\mathbf{v} = \mathbf{v}_n + \mathbf{v}_t = (\mathbf{v} \cdot \mathbf{n})\mathbf{n} + \mathbf{v}_t \quad (5-89)$$

Now consider a curved flame surface $A(t)$ in Fig. 5.16 moving in space with the local velocity \mathbf{w} (note that each spatial point has its own velocity). Then, the rate of change of the flux of a vector \mathbf{G} across the flame surface is given by the following equation based on the Reynolds' transport theorem.

$$\frac{d}{dt} \int_{A(t)} \mathbf{G} \cdot \mathbf{n} dA = \int_{A(t)} \left[\frac{\partial \mathbf{G}}{\partial t} + \mathbf{w} \cdot \nabla \mathbf{G} - \mathbf{G} \cdot \nabla \mathbf{w} + \mathbf{G} \nabla \cdot \mathbf{w} \right] \cdot \mathbf{n} dA \quad (5-90)$$

By specifying $\mathbf{G} = \mathbf{n}$, Eq. (5-90) yields

$$\frac{d}{dt} \int_{A(t)} dA = \int_{A(t)} \left[\frac{\partial \mathbf{n}}{\partial t} + \mathbf{w} \cdot \nabla \mathbf{n} - \mathbf{n} \cdot \nabla \mathbf{w} + \mathbf{n} \nabla \cdot \mathbf{w} \right] \cdot \mathbf{n} dA \quad (5-91)$$

Since \mathbf{n} is the unit normal vector, we have

$$\frac{\partial \mathbf{n}}{\partial t} \cdot \mathbf{n} = \frac{1}{2} \frac{\partial n^2}{\partial t} = 0 \quad (5-92)$$

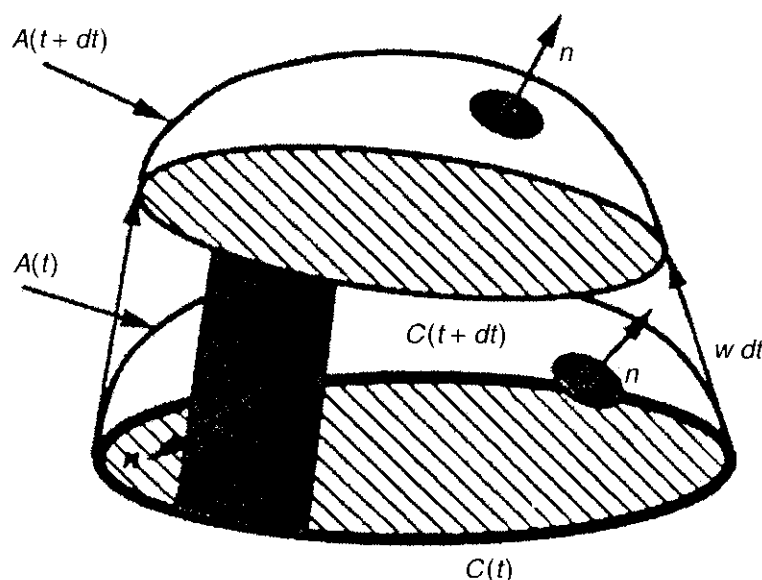


Figure 5.16 Displacement of curved laminar flame front from time t to $t + dt$ with local velocity \mathbf{w} .

$$(\mathbf{w} \cdot \nabla \mathbf{n}) \cdot \mathbf{n} = \mathbf{w} \cdot \nabla \left(\frac{n^2}{2} \right) = 0 \quad (5-93)$$

Therefore, the transport equation (5-91) becomes

$$\frac{d}{dt} \int_{A(t)} dA = \int_{A(t)} (-\mathbf{n} \mathbf{n} : \nabla \mathbf{w} + \nabla \cdot \mathbf{w}) dA \quad (5-94)$$

Note that in tensor notation, the first term on the right hand side of Eq. (5-94) can be written as

$$-\mathbf{n} \mathbf{n} : \nabla \mathbf{w} = -n_i n_j \frac{\partial w_i}{\partial x_j}$$

If we consider a surface element, then $A(t)$ can be replaced by δA . The flame stretch rate κ can then be expressed as

$$\kappa \equiv \frac{1}{\delta A} \frac{d(\delta A)}{dt} = -\mathbf{n} \mathbf{n} : \nabla \mathbf{w} + \nabla \cdot \mathbf{w} \quad (5-95)$$

The general velocity \mathbf{w} can be considered to have two components: one in the normal direction at a speed of S_L and the other is the local fluid velocity \mathbf{v} . Then, we have \mathbf{w} decomposed as

$$\mathbf{w} = \mathbf{v} + S_L \mathbf{n} \quad (5-96)$$

Several vector operations can be applied to the above equation to give

$$\nabla \mathbf{w} = \nabla \mathbf{v} + S_L \nabla \mathbf{n} + \mathbf{n} \nabla S_L \quad (5-97)$$

$$\mathbf{n} \mathbf{n} : \nabla \mathbf{w} = \mathbf{n} \mathbf{n} : \nabla \mathbf{v} + \mathbf{n} \cdot \nabla S_L \quad (5-98)$$

$$\nabla \cdot \mathbf{w} = \nabla \cdot \mathbf{v} + S_L \nabla \cdot \mathbf{n} + \mathbf{n} \cdot \nabla S_L \quad (5-99)$$

After substituting these equations into Eq. (5-95), we have

$$\begin{aligned} \kappa &\equiv \frac{1}{\delta A} \frac{d(\delta A)}{dt} = -\mathbf{n} \mathbf{n} : \nabla \mathbf{v} + \nabla \cdot \mathbf{v} + S_L \nabla \cdot \mathbf{n} \\ &= \underbrace{-n_i n_j \frac{\partial v_i}{\partial x_j}}_{\text{Associated with strain rate tensor}} + \underbrace{-\frac{1}{\rho} \frac{\partial \rho}{\partial t}}_{\text{Associated with dilatation}} + \underbrace{\frac{S_L}{R}}_{\text{Associated with flame curvature}} \end{aligned} \quad (5-100)$$

where R is the local radius of the flame curvature. Based on the physical description of the terms on the right-hand side of Eq. (5-100), it is evident that the flame can be stretched by the combined effect of strain, volume expansion of the fluid (dilatation), and the curvature of the flame, which arise from the nonuniformities of the flow and the normal propagation of the front. From the geometric

considerations, the above expression can also be expressed in other forms, such as

$$\kappa \equiv \frac{1}{\delta A} \frac{d(\delta A)}{dt} = (\mathbf{v}\mathbf{v} + \boldsymbol{\eta}\boldsymbol{\eta}) : \nabla \mathbf{v} + S_L \nabla \cdot \mathbf{n} \quad (5-101)$$

Note that we can write it in this form, since

$$\mathbf{n} = \mathbf{v} \times \boldsymbol{\eta} \equiv \mathbf{e}_v \times \mathbf{e}_\eta$$

[see Eq. (5-85)] and

$$v_j v_i + \eta_j \eta_i = \delta_{ji} - n_j n_i$$

In terms of tangential velocity of the flame surface (\mathbf{v}_t), the stretch factor was shown by Chung and Law⁶¹ to have the following expression:

$$\kappa \equiv \frac{1}{A} \frac{dA}{dt} = \nabla_t \cdot \mathbf{v}_t + (\mathbf{v} \cdot \mathbf{n})(\nabla_t \cdot \mathbf{n}) \quad (5-102)$$

The first term on the right-hand side of Eq. (5-102) is the stretch due to nonuniform tangential velocity field, and the second term represents the effect of curvature of the propagating flame. If we further assume that the tangential velocity of the flame is equal to the tangential component of the fluid velocity at the flame \mathbf{v}_{ft} , then

$$\mathbf{v}_t = \mathbf{n} \times (\mathbf{v}_{ft} \times \mathbf{n}) \quad (5-103)$$

Substituting Eq. (5-103) into Eq. (102), we have

$$\kappa \equiv \frac{1}{A} \frac{dA}{dt} = \nabla_t \cdot [\mathbf{n} \times (\mathbf{v}_{ft} \times \mathbf{n})] + (\mathbf{v} \cdot \mathbf{n})(\nabla_t \cdot \mathbf{n}) \quad (5-104)$$

The above equation can be alternatively expressed as

$$\kappa \equiv \frac{1}{A} \frac{dA}{dt} = -\nabla \times (\mathbf{v}_{ft} \times \mathbf{n}) \cdot \mathbf{n} + (\mathbf{v} \cdot \mathbf{n})(\nabla \cdot \mathbf{n}) \quad (5-105)$$

using $(\nabla \times \mathbf{n}) = 0$ and the fact that the operands of the vector operator are defined on the flame surface such that $\partial/\partial n = 0$ and thereby ∇_t can be changed to ∇ . This equation is identical to the expression derived by Matalon.⁶⁰

The Karlovitz number (Ka) has been defined as the nondimensional stretch factor, using the thickness of the unstretched flame (δ_{L0}) and the normal unstretched laminar-flame speed (S_{L0}) to form a reference time, i.e.,

$$Ka \equiv \frac{\delta_{L0}}{S_{L0}} \kappa = \frac{\text{Residence time for crossing an unstretched flame}}{\text{Characteristic time for flame stretching}} \quad (5-106)$$

For convenience, the Karlovitz number can be written as a sum of two parts due to the contribution from strain and curvature

$$Ka \equiv Ka_s + Ka_c \quad (5-107)$$

where

$$Ka_s \equiv \frac{\delta_{L0}}{S_{L0}} (\mathbf{v} \cdot \nabla \mathbf{v} + \boldsymbol{\eta} \cdot \boldsymbol{\eta}) : \nabla \mathbf{v} \quad \text{and} \quad Ka_c \equiv \frac{\delta_{L0}}{S_{L0}} S_L \nabla \cdot \mathbf{n} = \frac{\delta_{L0}}{R} \frac{S_L}{S_{L0}} \quad (5-108)$$

4.2 Balance Equation for Premixed Laminar-Flame Area

In this section we shall follow Candel and Poinsot's procedure⁶⁴ in utilizing the Reynolds' transport theorem and several aforementioned mathematical relationships to derive a balance equation for premixed laminar-flame area. This equation describes the rate of change of the flame surface density under transient conditions. It not only is useful for laminar flames but also can be applied to turbulent flame studies, using the flamelet concept. Now let us first define the flame surface density as Σ .

$$\Sigma \equiv \delta A / \delta V \quad (5-109)$$

From the Reynolds transport theorem for a moving volume $V(t)$, we have

$$\frac{d}{dt} \int_{V(t)} f dV = \int_{V(t)} \frac{\partial f}{\partial t} dV + \int_{S(t)} f \mathbf{w} \cdot \mathbf{n} dA \quad (5-110)$$

Substituting $f = 1$ in the above equation yields

$$\frac{d}{dt} \int_{V(t)} dV = \int_{V(t)} \nabla \cdot \mathbf{w} dV \quad (5-111)$$

For a volume element δV , the above equation becomes

$$\frac{1}{\delta V} \frac{d(\delta V)}{dt} = \nabla \cdot \mathbf{w} \quad (5-112)$$

From Eqs. (5-109), (5-95), (5-112), and (5-98), we have

$$\begin{aligned} \frac{1}{\Sigma} \frac{d\Sigma}{dt} &= \frac{1}{A} \frac{dA}{dt} - \frac{1}{V} \frac{dV}{dt} = [-\mathbf{n} \cdot \nabla \mathbf{w} + \nabla \cdot \mathbf{w}] - [\nabla \cdot \mathbf{w}] \\ &= -\mathbf{n} \cdot \nabla \mathbf{w} = -\mathbf{n} \cdot \nabla \mathbf{v} - \mathbf{n} \cdot \nabla S_L \end{aligned} \quad (5-113)$$

Since we can write the following relationship based on Eq. (5-96)

$$\frac{d\Sigma}{dt} = \frac{\partial \Sigma}{\partial t} + \mathbf{w} \cdot \nabla \Sigma = \frac{\partial \Sigma}{\partial t} + \mathbf{v} \cdot \nabla \Sigma + S_L \mathbf{n} \cdot \nabla \Sigma$$

Eq. (5-113) can be rewritten in the equivalent form

$$\frac{\partial \Sigma}{\partial t} + \nabla \cdot (\mathbf{v} \Sigma) = -(\mathbf{n} \cdot \nabla \mathbf{v} - \nabla \cdot \mathbf{v}) \Sigma - \mathbf{n} \cdot \nabla (S_L \Sigma) \quad (5-114)$$

Based on the relationships between Eqs. (5-100) and (5-101), the above equation can also be written as

$$\frac{\partial \Sigma}{\partial t} + \nabla \cdot (\mathbf{v}\Sigma) = [(\mathbf{v}\mathbf{v} + \boldsymbol{\eta}\boldsymbol{\eta}) : \nabla \mathbf{v}] \Sigma - \mathbf{n} \cdot \nabla (S_L \Sigma) \quad (5-115)$$

The flame area balance equation can also be written in terms of flame area per unit mass, a_f , which is defined as

$$a_f \equiv \frac{\Sigma}{\rho} \quad (5-116)$$

We then have

$$\frac{\partial(\rho a_f)}{\partial t} + \nabla \cdot (\rho \mathbf{v} a_f) = \rho[(\mathbf{v}\mathbf{v} + \boldsymbol{\eta}\boldsymbol{\eta}) : \nabla \mathbf{v}] a_f - \mathbf{n} \cdot \nabla(\rho S_L a_f) \quad (5-117)$$

The effect of flame curvature can be seen from the following balance equation, which can be shown to be consistent with Eq. (5-117):

$$\frac{\partial(\rho a_f)}{\partial t} + \nabla \cdot [\rho(\mathbf{v} + S_L \mathbf{n}) a_f] = \rho[(\mathbf{v}\mathbf{v} + \boldsymbol{\eta}\boldsymbol{\eta}) : \nabla \mathbf{v}] a_f + \rho a_f S_L \nabla \cdot \mathbf{n} \quad (5-118)$$

Using the expression of flame stretch factor given by Eq. (5-101), the above equation becomes

$$\frac{\partial(\rho a_f)}{\partial t} + \nabla \cdot [\rho(\mathbf{v} + S_L \mathbf{n}) a_f] = \rho \kappa a_f \quad (5-119)$$

4.3 The Use of Expanding Spherical Flames to Determine Burning Velocities and Stretch Effects in Hydrogen/Air Mixtures

To understand how expanding spherical flames can be used to determine burning velocities and stretch effects in hydrogen/air mixtures, Dowdy et al.⁶⁵ developed a useful technique for determining burning velocities and stretch effects in laminar flames. It has been found by various researchers that flame stretching can significantly affect the flame speed. Various methods to measure the stretch effect on the flame speed have been devised. However, very few experiments yield test data that can be utilized conveniently to deduce the flame speed with reference to the 1-D planar case, so that the stretch effect can be compared with data from other sources.

Because of the simple geometry for computer simulation, Dowdy et al.⁶⁵ used expanding spherical flames to determine burning velocities and stretch effects. They presented a new analysis of expanding flames and established its validity by comparing it with results of detailed computer modeling. The stretch effect in spherical flames is relatively easy to determine, and pertinent quantities can be derived from the measured values. There have been various measurements

for determining burning velocities using expanding flames, at either constant-pressure or constant-volume conditions, but in these measurements stretch effect has not been considered prior to their study. They quantify the stretch effect by deducing the Markstein length, to be discussed below.

In their analysis, an expression for the time variation of the radius of an expanding spherical flame at constant pressure is derived as follows, with the flame stretch effect. The flame structure is assumed to be one-dimensional. Therefore, the analysis generally holds for large radii but is not valid for very small radii, where the quasi-1D assumption fails.

For expanding spherical flame with instantaneous surface area $A = 4\pi r^2$, the flame stretch is solely due to the change in curvature with time. The stretch factor can be evaluated from

$$\kappa = \frac{1}{A} \frac{dA}{dt} = \frac{2}{r} \frac{dr}{dt} \quad (5-120)$$

where r is the instantaneous radius of the flame. Asymptotic analyses^{66,67} and detailed modeling^{68,69} show a linear relationship between stretch factor and burning velocity in the low-stretch regime. Thus, it is assumed that

$$S_{u,r} = S_u^0 - L\kappa \quad (5-121)$$

where $S_{u,r}$ is the burning velocity associated with the reference flame surface, S_u^0 is the 1-D burning velocity that is to be determined, and L is the Markstein length. It has been shown that L is independent of whether stretch is manifested as strain or curvature.

The reference surface must be well defined when applying the conventional 1-D definition of burning velocity to flames in divergent flows. Dowdy et al.⁶⁵ selected the reference surface by comparing a 1-D planar flame with a stationary spherical flame that, although in a divergent flow, is unstretched. Its position is considered to be the place where the local mass flux in the spherical flame equals the constant value of the 1-D planar flame. $S_{u,r}$ is considered to be the mass flux at this surface divided by the cold-gas density ρ_u .

The mass inside the expanding flame is given by

$$m = \frac{4}{3}\pi r^3 \bar{\rho}_b \quad (5-122)$$

where $\bar{\rho}_b$ is the mean burnt gas density. The mass flux crossing this surface is

$$\dot{m}'' = \left(\frac{dm}{dt} \right) \frac{1}{4\pi r^2} = \left[\bar{\rho}_b + \frac{r}{3} \frac{d\bar{\rho}_b}{dr} \right] \frac{dr}{dt} = \rho_b^0 f(r) \frac{dr}{dt} \quad (5-123)$$

where ρ_b^0 is the 1-D burnt gas density and

$$f(r) \equiv \left[\bar{\rho}_b + \frac{r}{3} \frac{d\bar{\rho}_b}{dr} \right] \frac{1}{\rho_b^0} \quad (5-124)$$

$f(r)$ can be regarded as the density correction factor. From geometrical considerations, this function can be assumed to have the following form

$$f(r) = 1 + \frac{c}{r} \quad (5-125)$$

where c is a constant determined by modeling the flame. This parameter varies slightly with the radius. The mean value of c is determined over the range $r = 5$ to 40 mm. The standard deviation of c over this range is about 5%.

The mass flux at the reference surface differs from its 1-D value because of stretch. Using Eqs. (5-120) and (5-121) and the conservation of mass across the flame ($\rho_b^0 S_b^0 = \rho_u S_u^0$), the following relationship is obtained:

$$\dot{m}'' = \rho_b^0 S_b^0 - \left(\frac{2\rho_u L}{r} \right) \frac{dr}{dt} \quad (5-126)$$

where S_b^0 is the 1-D burnt gas velocity. Equating (5-123) and (5-126) and after some algebra, we obtain

$$\frac{dr}{dt} = \frac{S_b^0}{f(r) + \ell/r} \quad (5-127)$$

where $\ell \equiv 2L\rho_u/\rho_b^0$. Substituting (5-125) into (5-127) gives

$$\frac{dr}{dt} = \frac{S_b^0}{1 + b/r} \quad (5-128)$$

where $b \equiv c + \ell$.

Equation (5-128) does not hold for $r \leq -b$; it can be applied only for large radii. Integrating Eq. (5-128) with respect to time, we have

$$r + b \ln r = S_b^0 t + \text{constant} \quad (5-129)$$

The true value of S_b^0 from the experimental data is obtained by fitting a curve in the form of Eq. (5-129) to the data, where S_b^0 appears as a fitting parameter. For the experimental data shown in Fig. 5.17, the value of this parameter obtained was 18.31 m/s, compared with the traditional best-fit straight-line value of 16.36 m/s. The burning velocity S_u^0 is then obtained by multiplying S_b^0 by the calculated density ratio $\sigma = \rho_b^0/\rho_u$. From the fitting procedure, b is also obtained. Markstein length is therefore obtained from

$$L = \frac{(b - c)\sigma}{2} \quad (5-130)$$

where c was obtained from computer modeling for each flame.

In experimental work, flames were burned in a spherical bomb of radius 300 mm with central ignition, using a spark gap of about 0.7 mm. Data were

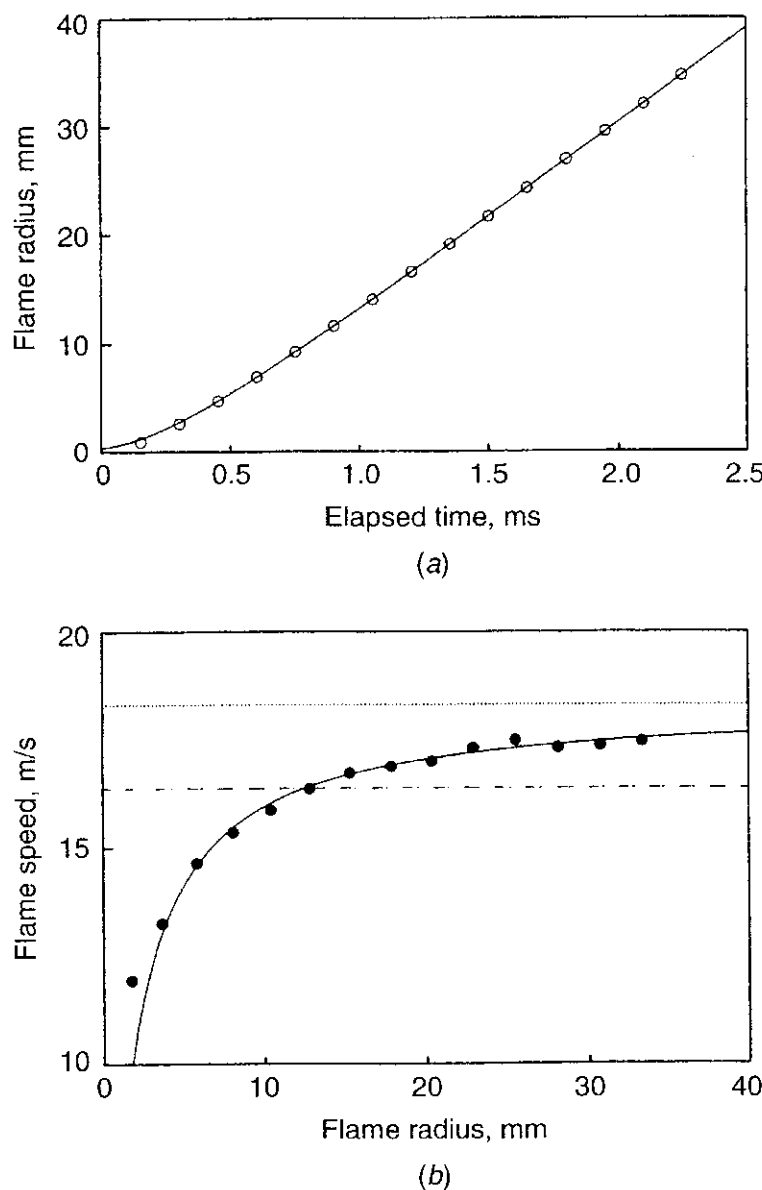


Figure 5.17 (a) Typical radius vs. time data for expanding spherical flame. Points: experimental data. Line: Eq. (5-129) with $S_b^0 = 18.31 \text{ m/s}$, $b = 1.49 \text{ mm}$. Stoichiometry = 1.4 (or 41% H₂).⁶⁵ (b) Typical flame speed vs. radius data. Points: time derivative calculated from radius vs. time. Solid line: Eq. (5-128) with $S_b^0 = 18.31 \text{ m/s}$, $b = 1.49$. Dotted line: limiting flame speed S_b^0 . Dashed line: Flame speed obtained by fitting straight line to data in Fig. 5.17a.⁶⁵

obtained in the prepressure period, with flame radius limited to 35 mm. Flame propagation was recorded by high-speed cinephotography of the schlieren image, from which the radius as a function of time was obtained. Hydrogen (99.95% purity) and compressed air were used to form combustible mixtures. All tests were performed at 1 atm and initial temperature of $296 \pm 1 \text{ K}$.

Dowdy et al.⁶⁵ also conducted modeling work for three types of flames, including planar 1-D, stationary spherical, and expanding spherical flames. The first two types were carried out by using the Sandia Laboratories' PREMIX program,⁵⁴ slightly modified to include thermal diffusion (the Soret effect) because it is important in hydrogen combustion. For modeling expanding spherical flames,

a new program was developed from the Sandia code, preserving the use of a reference frame attached to the flame. In order to allow for changes in the flame structure with time, a regridding strategy was utilized to increase computational efficiency. In all the modeling work, the following important reactions were included: $\text{H} + \text{O}_2 = \text{OH} + \text{O}$, $\text{O} + \text{H}_2 = \text{OH} + \text{H}$, $\text{OH} + \text{H}_2 = \text{H}_2\text{O} + \text{H}$, and $\text{H} + \text{O}_2 + M = \text{HO}_2 + M$.

The results of Dowdy et al.⁶⁵ from the modeling of the expanding spherical flames agreed well with experimental data. Figure 5.18 shows that flame speed (dr/dt) as a function of radius is in good agreement with experimental data and the modeling work for most of the radius range. Also, the "limiting" flame speed predicted by Eq. (5-129) is very close to that obtained by the detailed model in a planar geometry.

Figure 5.19 shows burning velocity against the equivalence ratio or stoichiometry, defined as (mole % of H_2)/(mole % of H_2)_{stoich}. The maximum burning velocity obtained was 2.85 m/s at a stoichiometry of 1.4 (41% H_2). At stoichiometry of 1.0, the value was 2.13 m/s. This figure also shows the burning velocities predicted by planar 1-D modeling. The agreement with experimental data is very good. The inaccuracy at very lean mixtures is attributed to errors in the experimental data arising from inapplicability of the simple model.

Figure 5.20 shows the value of b as a function of stoichiometry from both the experimental data and the model. It also shows the value of c calculated by

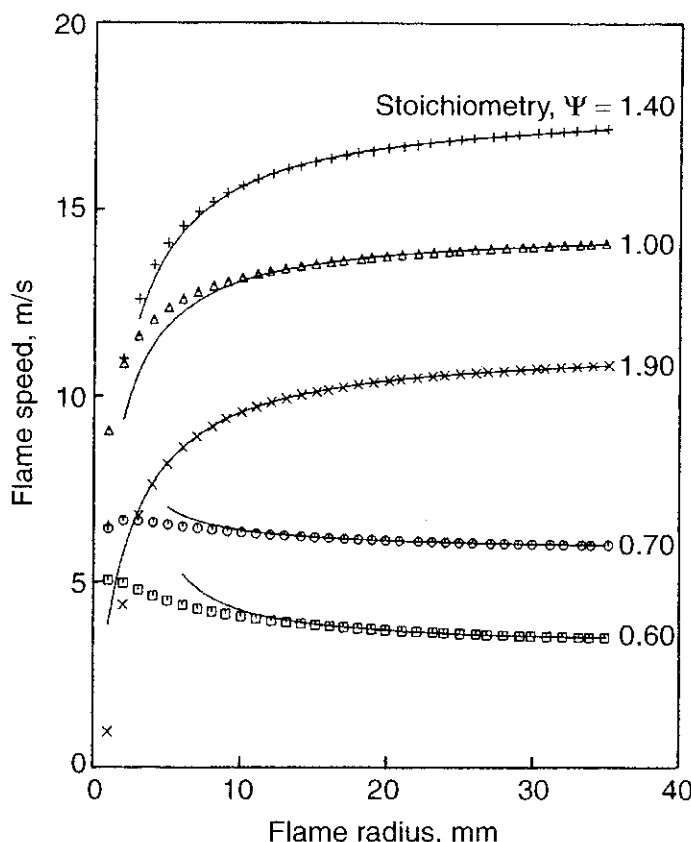


Figure 5.18 Calculated flame speed vs. radius. Symbols: detailed model. Lines: Eq. (5-128) with fitted values of S_b^0 and b (modified from Dowdy et al.⁶⁵).

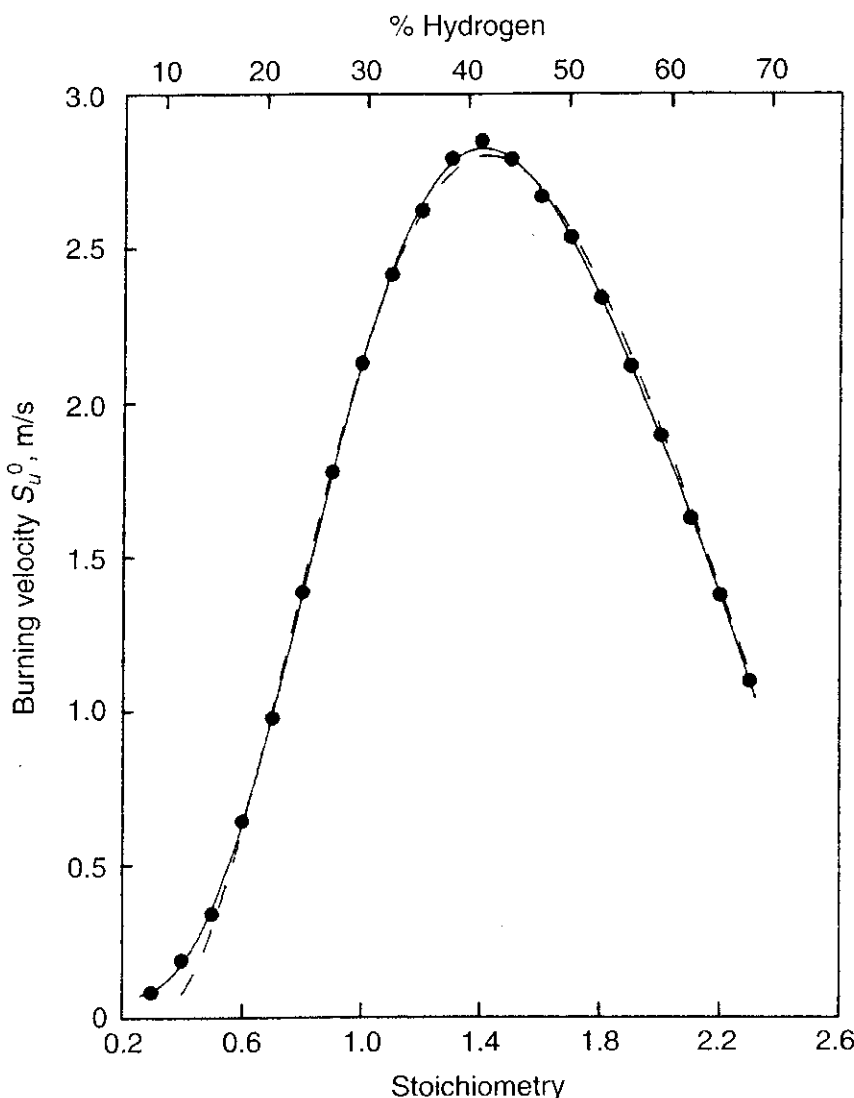


Figure 5.19 Burning velocity as a function of stoichiometry. Points: experimental result. Solid line: best-fit polynomial through experimental data. Broken line: best-fit polynomial through planar modeling results (modified from Dowdy et al.⁶⁵).

the model. The modeled b values agree well with the experimentally obtained b values by curve fitting. The b values are converted into Markstein lengths by the following steps:

Step 1. The reference surface (where the mass fluxes of stationary spherical and planar 1-D flames have the same value) is located by modeling.

Step 2. Values of c were derived by determining the average gas density inside the reference surface of spherical flames at various radii and by applying Eqs. (5-124) and (5-125). In this step, density profiles from planar 1-D modeling were employed.

Step 3. Markstein lengths were derived from the experimental b value and the computed c value using Eq. (5-130).

Markstein lengths are plotted against stoichiometry in Fig. 5.21. Values are negative (i.e., burning velocity increases with stretch) on the lean side, and positive

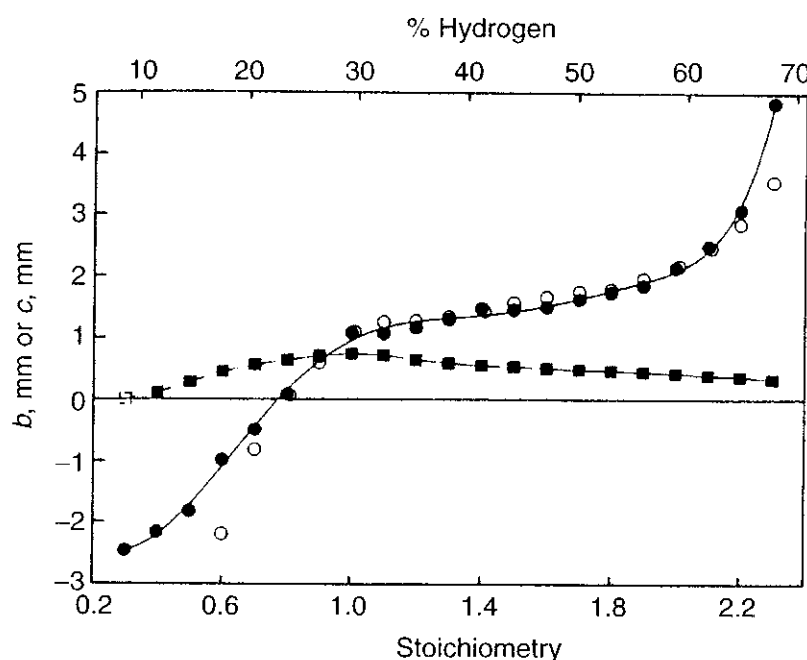


Figure 5.20 Parameter b and density constant c as a function of stoichiometry. Black circle: b derived from experiments. Open circle: b derived from detailed model. Black square: calculated values of c (after Dowdy et al.⁶⁵).

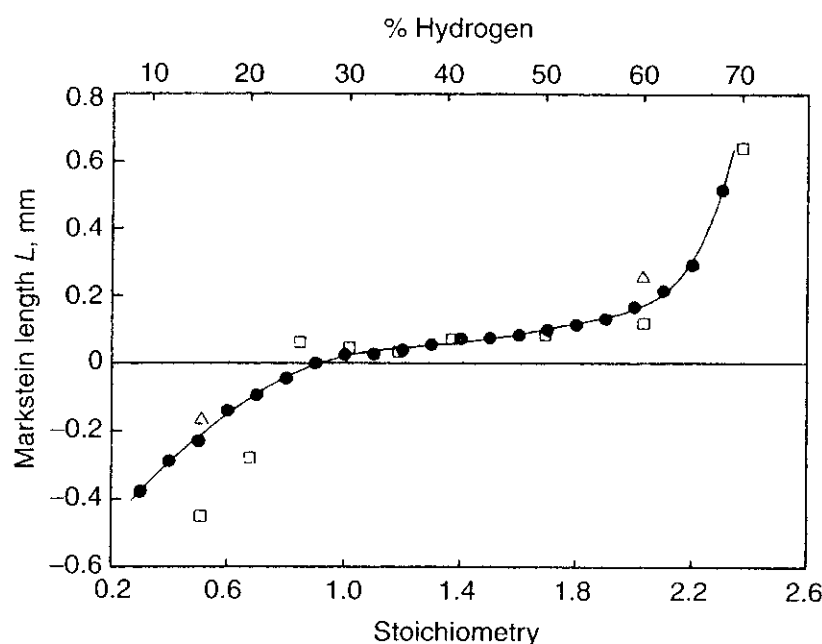


Figure 5.21 Markstein lengths for hydrogen/air as a function of stoichiometry. Black circle: the experimental data of Dowdy et al.⁶⁵ The unfilled symbols are from modeling work by Dixon-Lewis⁷⁰ and by Warnatz and Peters⁶⁸ (after Dowdy et al.⁶⁵).

on the rich side. The authors have observed similar behavior in methane/air and the opposite in propane/air mixtures.

The above results show that measured burning velocities can be utilized to obtain the true 1-D laminar-flame speed. The assumptions in the simple model appear to be justified; thus valid Markstein lengths can be derived. The modeling

also showed that the simple model does not hold below a certain radius. This is because the assumptions are likely to fail at high stretch rate and curvature. Through the investigation of Dowdy et al.,⁶⁵ burning velocities for hydrogen/air mixtures are obtained for a very broad stoichiometric range. The maximum value of the reported burning velocity is 2.85 ± 0.07 m/s at a stoichiometry of 1.4 (41% hydrogen). Markstein lengths for hydrogen/air premixed flames were reported across a broad stoichiometric range. The Markstein length is negative (i.e., burning velocity increases with stretch) on the lean side, and positive (burning velocity decreases with stretch) on the rich side.

4.4 Laminar Burning Velocities and Markstein Numbers of Hydrocarbon/Air Flames

Tseng, Ismail, and Faeth⁷¹ studied the effect of flame stretch on laminar burning velocities of hydrocarbon/air mixtures, using outward-propagating spherical flames. Their selected hydrocarbon fuels were methane, ethane, ethylene, and propane. The laminar-flame speeds and Markstein numbers (Ma) for these hydrocarbon/air flames were measured over a variety of equivalence ratios, at atmospheric pressures, and at ambient initial temperatures. In their study, Karlovitz numbers were less than 0.3 so that the flames were remote from quenching conditions.

In terms of the effect of flame stretch rate on laminar-flame speed, Markstein proposed a relationship given in Eq. (5-121), which can also be written as

$$S_L = S_{L0} - L\kappa \quad (5-131)$$

where S_L is the flame propagation rate relative to the unburned gas, S_{L0} is the flame speed for the unstretched flame, κ is the stretch factor, and L is the Markstein length. Kwon et al.⁷² suggest that the Markstein length is proportional to the characteristic flame thickness, δ_L , because both are representative of the scale of distances over which the diffusion of mass and heat occurs in the flame. This assumption leads to the dimensionless parameter Markstein number (Ma) defined as

$$\text{Ma} \equiv \frac{L}{\delta_L} \quad (5-132)$$

The dimensionless Karlovitz number (Ka) defined earlier in Eq. (5-106) can be written as

$$\text{Ka} = \frac{\delta_L}{S_L} \kappa \quad (5-133)$$

Substituting Eqs. (5-132) and (5-133) into (5-131) gives the dimensionless relationship

$$\frac{S_{L0}}{S_L} = 1 + \text{MaKa} \quad (5-134)$$

where S_{L0} is the laminar-flame speed at the unstretched condition. By Eq. (5-134) the apparent flame speed is related to the Karlovitz and Markstein numbers.

Faeth and coworkers⁷¹ used an outward-propagating spherical flame in order to investigate the effects of stretch on laminar-flame speed. Their experimental apparatus is a windowed test chamber that is “near-spherical” with a volume of 0.011 m³ and a 260-mm cross-sectional diameter at its center. The chamber is optically accessible via two 92-mm diameter quartz windows. For ignition, they used electrodes extending from the top and bottom of the chamber to two tungsten wires. The length of the wires was 25 mm, the tips of the electrodes were 250 μm in diameter, and the gap between the wires was 500 μm. The spark was supplied with a variable capacitance (100–5000 pF) high-voltage (3–5 kV) circuit. The discharge time was approximately 5 μs. The spark energies were adjusted by trial and error so that they were close to the minimum energy to have the spark jump across the given gap. The spark energies were minimized in order to minimize disturbances created by the spark. The chamber was prepared for the experiment by adding fuel and air at the desired partial pressures to reach a desired equivalence ratio and have the total pressure equal to 1 atm. The mixture was then allowed to settle to a quiescent atmosphere prior to ignition. The diagnostic for flame observation was a high-speed (3000 frames per second) motion picture shadowgraph. The exposure time was adjusted to approximately 35 μs. The framing rate and the ignition pulse were recorded using a digital oscilloscope so that the film records could be synchronized.

Several assumptions were made in their data analysis. The flame is assumed to be a spherical deflagration wave propagating away from the ignition source. The motion of the unburned gas was considered negligible. Also, the time variations of unsteady flame thickness were regarded as negligible. To minimize the transient effects of flame thickness, it was necessary to have $\delta_L/r_f \ll 1$. This implies that an estimate of δ_L is needed. Faeth et al.⁷¹ approximated δ_L as shown in Eq. (5-135). The mass diffusivity in the equation was chosen to be the binary diffusivity of fuel into the diluent (i.e., nitrogen). Based on the above assumptions, the laminar burning velocity S_L and stretch factor κ can be calculated by measuring the flame radius r_f as a function of time and the derivative of r_f , using Eqs. (5-136) and (5-120).

$$\delta_L = \frac{\mathcal{D}_u}{S_L} \quad (5-135)$$

$$S_L = \frac{\rho_b}{\rho_u} \frac{dr_f}{dt} \quad (5-136)$$

where Eq. (5-136) is based on the work of Strehlow and Savage.⁷³

Figure 5.22 shows their recorded $r_f(t)$ data for propane/air mixtures for all equivalence ratios tested. The open circles indicate the stable preferential-diffusion conditions ($Ma > 0$); the dark circles show neutral and unstable preferential diffusion ($Ma \leq 0$). For a stable preferential diffusion, the slope (dr_f/dt) increases with increasing r_f and becomes roughly constant at higher values of r_f . According

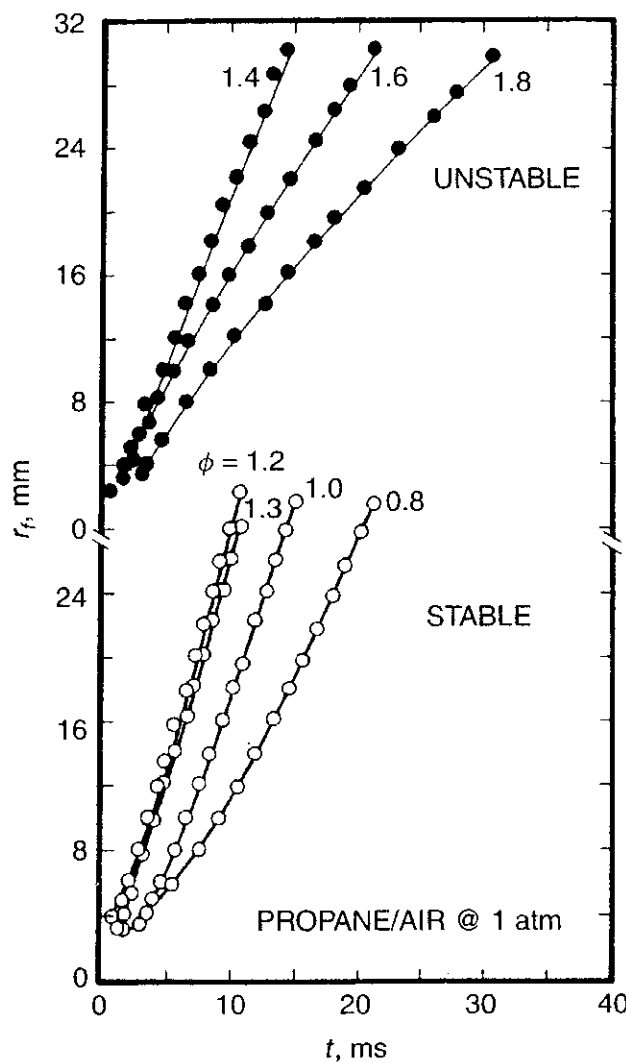


Figure 5.22 Measured flame radius as a function of time for propane/air mixtures (after Tseng et al.⁷¹).

to Eq. (5-136), S_L also increases with r_f , while stretch factor κ decreases as r_f becomes larger. The flames for unstable preferential-diffusion conditions, however, developed irregular surfaces at larger radii. The opposite trend for the slope (dr_f/dt) variations of unstable preferential-diffusion can be seen from Fig. 5.22.

Figure 5.23 shows the resulting laminar-flame speeds deduced from the data shown in Fig. 5.22. A comparison of the propane/air mixture data with that of other researchers for outward-propagating spherical flames is shown in Fig. 5.24. The data appear to agree within experimental error. A discrepancy between the data of Tseng, Ismail, and Faeth⁷¹ and those of most of the other researchers is observed with the data of Palm-Leis and Strehlow.⁷⁴ The data of Palm-Leis and Strehlow appear to be shifted to higher equivalence ratios. This was also noted by Kwon and Faeth.⁷⁵ Similar comparisons were made⁷¹ for the burning velocities of ethane/air, methane/air, and ethylene/air mixtures as a function of fuel-equivalence ratio.

Based on Eq. (5-135), the ratio of S_{L0}/S_L is linearly dependent on K_a . Figure 5.25 shows this linear dependency for various values of ϕ for laminar premixed

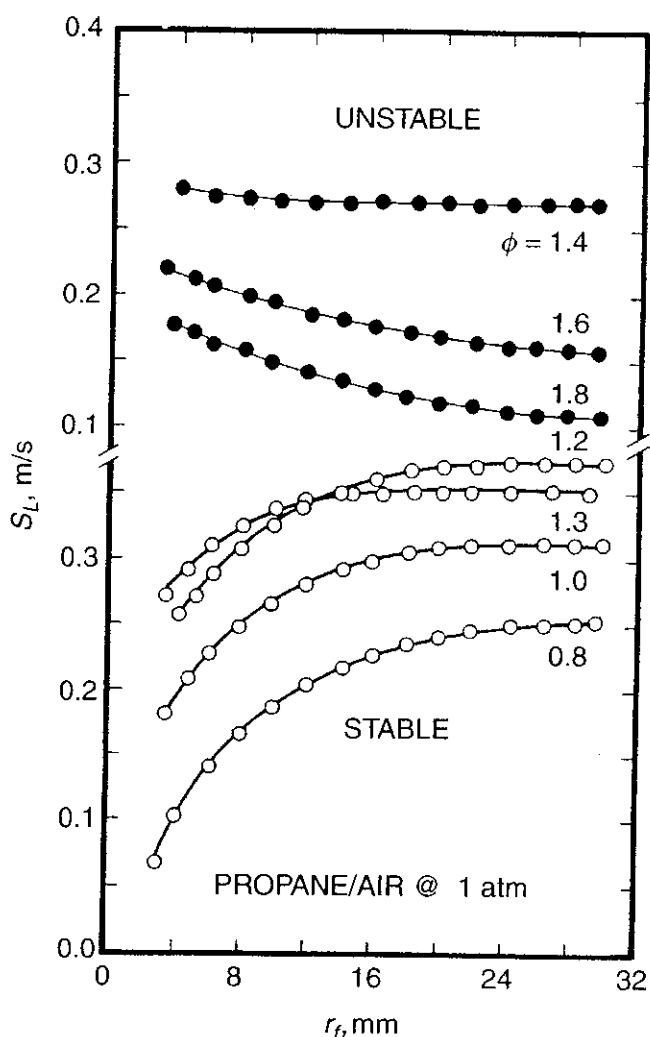


Figure 5.23 Deduced laminar-flame velocity as a function of flame radius for propane/air mixtures (after Tseng et al.⁷¹).

propane/air flames. When K_a is zero, S_L must be the same as S_{L0} or their ratio is equal to unity. One can consider that the value of S_{L0} was determined by extrapolating the S_L data to a K_a of zero as shown in Fig. 5.25, and therefore Ma does not depend on K_a . In view of the straight-line nature of the data for different values of ϕ , one can consider that the Markstein number (Ma) is independent of K_a . This implies, from Eq. (5-134), that Ma governs the slopes of the data lines in Fig. 5.25. A correlation taking the form of Eq. (5-137) is based on this data. Tseng et al.⁷¹ indicated that due to the large scatter of the data, it is difficult to justify more than a linear correlation.

$$Ma = S(\phi - \phi_n) \quad (5-137)$$

where the slope S can also be regarded as the sensitivity of Ma to variations of ϕ , and ϕ_n is the neutral preferential-diffusion condition where $Ma = 0$. The slope S can have positive or negative values depending on whether the reactant mixture exhibits unstable preferential-diffusion behavior at a fuel-equivalence ratio lower or higher than ϕ_n . A least-square fit using Eq. (5-137), based on the data of

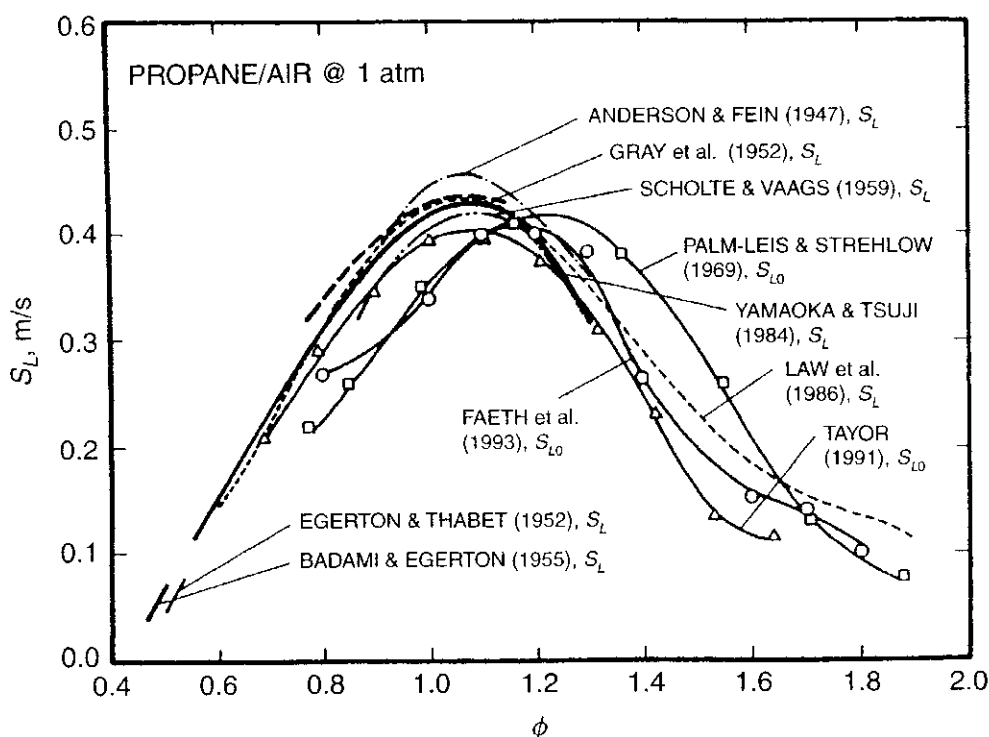


Figure 5.24 Laminar burning velocity as a function of fuel equivalence ratio for propane/air mixtures. Measurements of Tseng, Ismail, and Faeth,⁷¹ Palm-Leis and Strehlow,⁷⁴ Taylor,⁷⁶ Law et al.,⁷⁷ Yamaoka and Tsuji,⁷⁸ Scholte and Vaags,⁷⁹ Anderson and Fein,⁸⁰ Gray et al.,⁸¹ Harris et al.,⁸² and Egerton and coworkers.^{83,84} (Modified from Tseng et al.⁷¹)

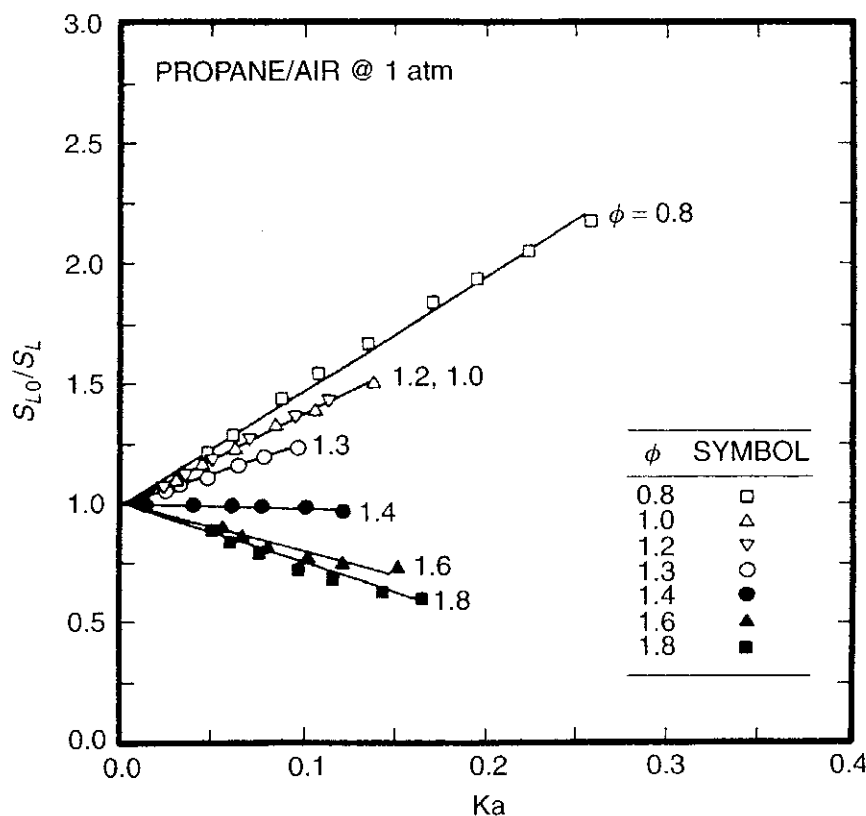


Figure 5.25 Laminar burning velocity as a function of Karlovitz number and fuel-equivalence ratio for propane/air mixtures. (Modified from Tseng et al.⁷¹)

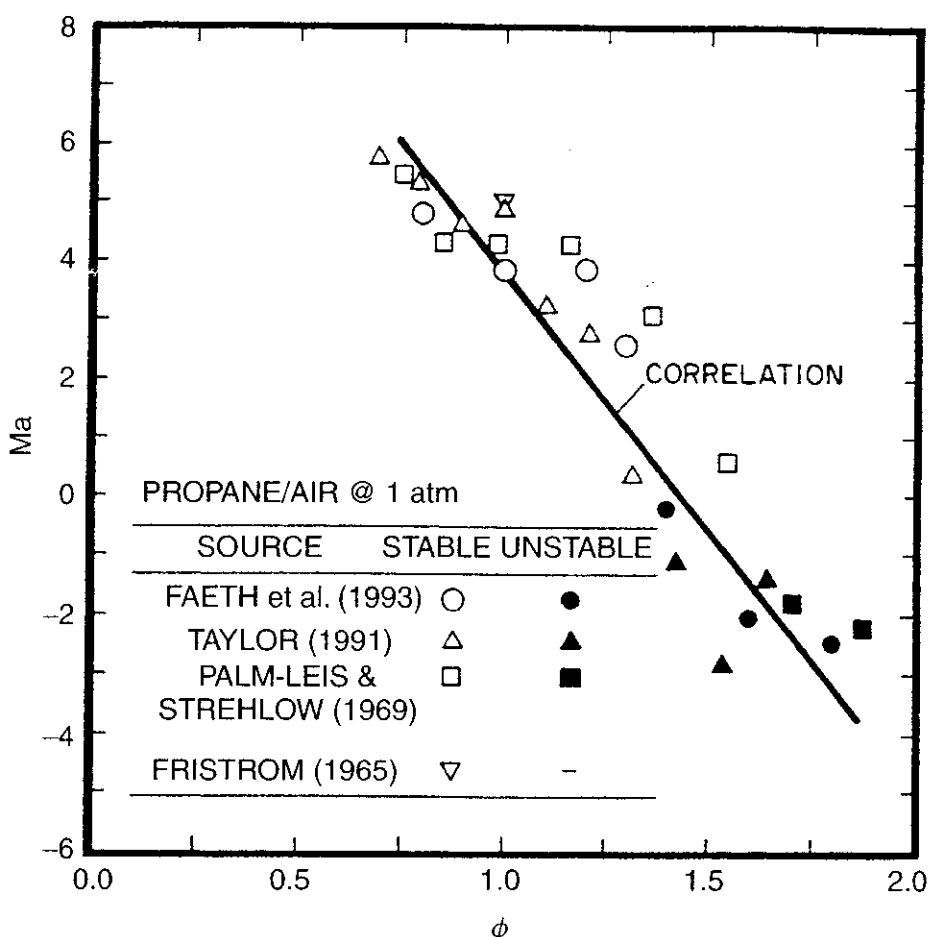


Figure 5.26 Markstein number as a function of fuel-equivalence ratio for propane/air mixtures. (Modified from Tseng et al.⁷¹)

Tseng, Ismail, and Faeth,⁷¹ Palm-Leis and Strehlow,⁷⁴ Taylor,⁷⁶ and Fristrom,⁸⁵ is also illustrated in Fig. 5.26. The slope S is -8.8 ± 0.8 and the intercept (ϕ_n) is 1.44 ± 0.11 . The maximum value of K_a of the data is 0.25. For laminar premixed CH_4/air , $\text{C}_2\text{H}_6/\text{air}$, and $\text{C}_2\text{H}_4/\text{air}$ flames, similar plots to Figs. 5.25 and 5.26 were developed by Tseng, Ismail, and Faeth.⁷¹ Their summary of Markstein number correlations for four different hydrocarbon fuels burning with air, Taylor's results,⁷⁶ and data of Kwon et al.⁷² for $\text{H}_2/\text{O}_2/\text{N}_2$ flames are given in Table 5.4. It is noted that S is positive for both CH_4/air flames and $\text{H}_2/\text{O}_2/\text{N}_2$ flames. This is because these fuel/air mixtures exhibit unstable preferential-diffusion at equivalence ratios greater than ϕ_n .

Based on the results of Tseng et al.⁷¹ on outwardly propagating spherical flames for the hydrocarbons methane, ethane, ethylene, and propane in air at atmospheric pressure and initially at room temperature, the following major findings are noted:

1. Effects of preferential-diffusion/stretch interactions could be correlated according to Eq. (5-134).
2. Effects of flame stretch on laminar burning velocities were substantial, yielding Markstein numbers in the range -2.5 to 7.2 and corresponding

Table 5.4 Summary of Markstein Number Correlations for Four Different Hydrocarbon Fuels Burning with Air and for H₂/O₂/N₂ Flames^a

Reactants	Slope (S)	Intercept (ϕ_n)	Maximum Ka	ϕ Range	Std. Dev. of S	Std. Dev. of ϕ_n	Correl. Coef. of Fit
C ₃ H ₈ /Air	-8.8	1.44	0.25	0.8–1.8	0.8	0.11	0.95
CH ₄ /Air	10.2	0.74	0.30	0.6–1.35	1.1	0.09	0.93
C ₂ H ₆ /Air	-4.0	1.68	0.25	0.8–1.6	0.7	0.22	0.83
C ₂ H ₄ /Air	-2.9	1.95	0.24	0.8–1.8	0.4	0.22	0.86
H ₂ /O ₂ /N ₂	3.9	1.50	0.21	1.00–4.83	0.2	0.22	0.99

^a Assuming a linear correlation between Ma and ϕ . Hydrocarbon/air results from Tseng et al.,⁷¹ Taylor⁷⁶ for H₂/O₂/N₂ flames at 1 atm and 298 ± 3 K, and results from Kwon et al.⁷² at 3 atm and 298 ± 3 K with 12.5–21.0% O₂ by volume in the O₂/N₂ mixture (modified from Tseng et al.⁷¹).

varyations of S_{L0}/S_L in the range of 0.4–2.7, implying significant effects of flame stretch on laboratory measurements of laminar burning velocities.

3. Markstein numbers varied linearly with equivalence ratio from the neutral preferential-diffusion condition, according to Eq.(5-137), although there was significant scatter in the data. This could be due to the fact that multiple derivatives of measurements are needed to calculate Ma.
4. Equivalence ratios for neutral preferential diffusion were shifted toward the unstable side of stoichiometry. The ϕ ranges for the unstable preferential-diffusion (negative Markstein numbers) behavior include propane, $\phi > 1.44$; methane, $\phi < 0.74$; ethane, $\phi > 1.68$; and ethylene, $\phi > 1.95$.

It is easily conceived that properties of strongly turbulent premixed flames in the thin-flamelet regime can be affected by flame stretch. The interaction between the stretched flame surface and preferential diffusion of species and heat is responsible for affecting the dynamic behavior of these flames. Turbulent distortion of the flame surface can either be retarded for stable preferential-diffusion conditions or enhanced for unstable preferential-diffusion conditions. These will be explained further in the premixed turbulent flame chapter.

4.5 Burning Rates of Ultra-Lean to Moderately Rich H₂/O₂/N₂ Laminar Flames with Pressure Variations

Egolfopoulos and Law⁸⁶ recognize that literature values of the laminar flame speeds for H₂/air mixtures exhibit a great deal of “scatter.” This scatter can cause uncertainty in assessing the applicability of various kinetic schemes for flame propagation. In order to obtain accurate experimental data on laminar-flame speeds, they employed the counterflow flame technique to experimentally determine the laminar-flame speeds of H₂/O₂/N₂ mixtures in the oxygen concentration range of 7.4 to 30 molar percent of oxidizer and a pressure range of

0.2 to 2.25 atm. The counterflow technique was originally established by Law et al.⁷⁷ The technique involves the establishment of two symmetrical, planar, nearly adiabatic flames in a nozzle-generated counterflow and the determination of the axial velocity profile along the centerline of the flow by using an LDV. By identifying the minimum point of the velocity profile as a reference upstream flame speed S_u , and the velocity gradient ahead of it as the imposed stretch rate κ , S_u can be determined as a function of κ for a given mixture concentration and pressure.

By considering the counterflow conditions, it is useful to indicate that the velocity vector in the vicinity of a stagnation-point flow field can be written for a 2-D planar case ($\sigma = 0$) as

$$\mathbf{v} = [v_x, v_y, v_z] = \left[\frac{ax}{(\sigma + 1)}, -ay, 0 \right] = [ax, -ay, 0] \quad (5-138)$$

or for an axisymmetric case ($\sigma = 1$) as

$$\mathbf{v} = [v_r, v_z, v_\theta] = \left[\frac{ar}{(\sigma + 1)}, -az, 0 \right] = \left[\frac{a}{2}r, -az, 0 \right] \quad (5-139)$$

The stretch rate for a premixed laminar flame in the vicinity of stagnation-point flow can be shown to be

$$\kappa = a \quad (5-140)$$

where a is the constant in the velocity field. A sketch of the laminar flame in the stagnation-point flow regimes of 2-D and axisymmetric flow situations are shown in Fig. 5.27. For this type of flame, at least three diffusivities must be considered: diffusion of heat governed by the magnitude of α , mass diffusion of deficient reactant species i (e.g., oxidizer species for a fuel-rich mixture) governed by \mathcal{D}_i , and mass diffusion of excess reactant species j (e.g., excess fuel for a fuel-rich mixture) governed by \mathcal{D}_j . Two effects associated with these diffusion coefficients should be considered: the nonunity Lewis number ($Le \equiv \alpha/\mathcal{D}_i$) effect and the differential diffusion ($\mathcal{D}_i/\mathcal{D}_j$) effect.

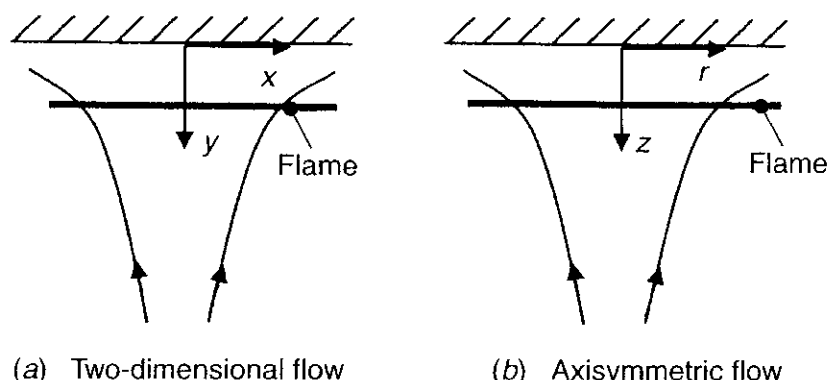


Figure 5.27 Laminar premixed flames in the vicinity of stagnation-point flows.

The control volume around the flame loses thermal energy by conduction to the incoming reactants in the positive y -direction but can gain chemical energy from an increase in the deficient reactant concentration. If $\text{Le} = 1$, the flame temperature of a stretched flame can stay the same as the adiabatic flame temperature. If $\text{Le} > 1$, the heat loss effect can exceed the reactant mass species gain effect and $T_f < T_{f,\text{ad}}$; conversely, $T_f > T_{f,\text{ad}}$ if $\text{Le} < 1$. Due to these diffusion effects, for flames with $\text{Le} > 1$, increasing the stretch rate will lower the T_f until extinction occurs due to incomplete reaction. However, for $\text{Le} < 1$ flames, increasing stretch rate increases T_f , and extinction will occur only when the reaction zone is quenched by the stagnation surface.

In Egolfopoulos and Law's experimental measurements using a counterflow premixed flame setup,⁸⁶ the stretch-free flame speed S_u^0 (same as S_{L0}) can then be determined by linearly extrapolating $S_u(\kappa)$ to $\kappa = 0$. The entire burner assembly is housed in a large stainless-steel chamber with continuous air ventilation, thereby allowing for pressure adjustments. It is also believed that upstream and downstream heat losses are minimized because the flow is nozzle generated and is highly symmetrical. In addition, buoyancy effects are automatically included in the flow-field influences because the LDV-determined velocities are the local values experienced by the specific flame segment under measurement. They estimate that the experimental data determined using this technique are accurate to within 1 to 2 cm/s for S_u^0 less than 60 cm/s, 2 to 5 cm/s for S_u^0 between 70 and 150 cm/s, and 10 cm/s for S_u^0 above 170 cm/s.

Experiments were conducted using $\text{H}_2/\text{O}_2/\text{N}_2$ mixtures with 99.995% purity, at room temperature. The fuel equivalence ratio was varied from 0.153 to 2.2, and the system pressure was varied from 0.2 to 2.25 atm. The nozzles used were 5, 7, 10, 12, 14, and 23 mm in diameter, with smaller ones used for "strong flames" and larger ones used for "weak flames." The diameter of the largest flames was about 35 to 40 mm. In addition, the visualization of the nonluminous hydrogen flame was achieved first by "doping" the mixture with trace amounts of methane, which was removed during the data-taking period.

For the numerical simulation, Egolfopoulos and Law adopted a flame code developed by Kee et al.⁵⁴ This Fortran code employs a hybrid time-integration/Newtonian-iteration technique to solve the steady-state equations of mass and energy conservation, and outputs the complete flame structure together with the sensitivities of the local concentrations of species and the mass burning rates of all reactions involved. In performing the comparison between the numerical results with experimental data, Egolfopoulos and Law used five kinetic schemes proposed by Maas and Warnatz,⁸⁷ Dixon-Lewis,⁸⁸ Glarborg et al.,⁸⁹ Tsang and Hampson,⁹⁰ and Yetter et al.⁹¹ The last scheme was modified with the input of Yetter and is called the modified Yetter scheme, which is given in Table 5.5. The modifications include reaction R3 being given by the slightly faster rate of Ref. 90, reaction R7 by the slow rate of Ref. 88, and most importantly, reactions R9 and R10 by those of Hsu et al.⁹² and Slack.⁹³

For atmospheric H_2/air flames, Fig. 5.28 provides the comparison of the experimental data with the calculated results using various kinetic schemes. The

Table 5.5 Selected Reactions of the Modified Yetter Kinetic Scheme and Their Net Normalized Sensitivities on the Mass Burning Rate of Atmospheric H₂/Air Mixtures at $\phi = 0.8, 0.5$, and 0.29 (after Egolfopoulos and Law⁸⁶)

Reaction	Rate Constants ^a			Normalized Sensitivities		
	A	β	E_a	$\phi = 0.80$	$\phi = 0.50$	$\phi = 0.29$
1. H + O ₂ = O + OH	1.91E14	0.00	16440	0.10E + 00	0.11E + 00	0.44E + 00
2. O + H ₂ = H + OH	5.01E4	2.67	6290	0.16E + 00	0.25E + 00	0.27E + 00
3. OH + H ₂ = H + H ₂ O	6.38E6	2.00	2959	0.36E + 00	0.57E + 00	0.69E + 00
4. OH + OH = O + H ₂ O	2.10E8	1.40	-397	-0.25E - 01	-0.40E - 01	0.19E - 01
5. H ₂ + M = H + H + M	4.57E19	-1.40	104380	-0.19E - 01	-0.57E - 02	-0.30E - 03
<i>Enhanced Third-body Efficiencies^b: H₂/2.5/H₂O/16.0/</i>						
6. O + O + M = O ₂ + M	6.17E15	-0.50	0	-0.73E - 03	-0.96E - 03	-0.32E - 03
<i>Enhanced Third-body Efficiencies^b: H₂/2.5/H₂O/16.0/</i>						
7. O + H + M = OH + M	6.10E16	-0.60	0	-0.33E - 02	-0.20E - 02	-0.26E - 03
<i>Enhanced Third-body Efficiencies^b: H₂O/5.0/</i>						
8. H + OH + M = H ₂ O + M	2.19E22	-2.00	0	-0.12E + 00	-0.82E - 01	-0.17E - 01
<i>Enhanced Third-body Efficiencies^b: H₂/2.5/H₂O/16.0/</i>						
9. H + O ₂ + H ₂ O = HO ₂ + H ₂ O	6.89E15	0.00	-2085.3	-0.29E - 01	-0.13E + 00	-0.33E + 00
10. H + O ₂ + M = HO ₂ + M	6.70E19	-1.42	0	0.20E - 01	-0.14E + 00	-0.57E + 00
<i>Enhanced Third-body Efficiencies^b: H₂O/0.0/H₂/2.5/</i>						
11. HO ₂ + H = H ₂ + O ₂	6.61E13	0.00	2130	-0.96E - 01	-0.15E + 00	-0.15E + 00
12. HO ₂ + H = OH + OH	1.66E14	0.00	870	0.13E + 00	0.23E + 00	0.38E + 00
13. HO ₂ + O = OH + O ₂	1.74E13	0.00	-400	-0.23E - 02	-0.88E - 02	-0.56E - 01
14. HO ₂ + OH = H ₂ O + O ₂	1.45E16	-1.00	0	-0.34E - 01	-0.70E - 01	-0.14E + 00
15. HO ₂ + HO ₂ = H ₂ O ₂ + O ₂	3.02E12	0.00	1390	-0.44E - 03	-0.21E - 02	-0.11E - 01
16. H ₂ O ₂ + M = OH + OH + M	1.20E17	0.00	45500	-0.19E - 01	-0.24E - 01	-0.20E - 01
<i>Enhanced Third-body Efficiencies^b: H₂/2.5/H₂O/16.0/</i>						
17. H ₂ O ₂ + H = H ₂ O + OH	1.00E13	0.00	3590	0.41E - 03	0.27E - 03	0.14E - 02
18. H ₂ O ₂ + H = H ₂ + HO ₂	4.79E13	0.00	7950	-0.22E - 02	-0.21E - 02	-0.12E - 02

(continued overleaf)

Table 5.5 (continued)

Reaction	Rate Constants ^a			Normalized Sensitivities		
	A	β	E_a	$\phi = 0.80$	$\phi = 0.50$	$\phi = 0.29$
19. $\text{H}_2\text{O}_2 + \text{O} = \text{OH} + \text{HO}_2$	9.55E6	2.00	3970	-0.73E - 03	-0.12E - 02	0.14E - 02
20. $\text{H}_2\text{O}_2 + \text{OH} = \text{H}_2\text{O} + \text{HO}_2$	7.08E12	0.00	1430	-0.12E - 02	-0.29E - 02	-0.50E - 02

^aReaction mechanism rate coefficients in the form $k_i = AT^\beta \exp(-E_a/R_u T)$ (units are moles, cubic centimeters, seconds, Kelvins, and calories/mole).

^bOnly species with nonunity collision efficiency are specified.

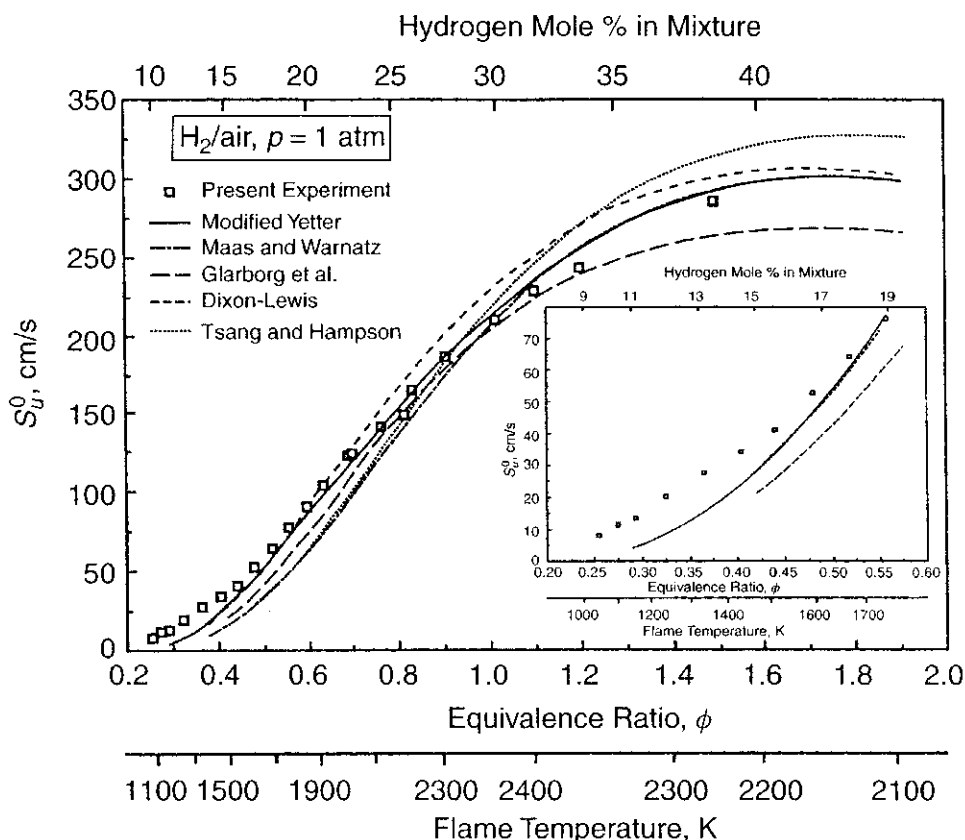


Figure 5.28 Comparison of experimentally and numerically determined $S_y^0(\phi)$ for atmospheric H_2/air mixtures using various kinetic schemes (after Egolfopoulos and Law⁸⁶).

modified Yetter scheme gives better prediction than other schemes. An interesting observation of this plot shows that all of the kinetic schemes underpredict the flame speed as ϕ becomes increasingly smaller. Egolfopoulos and Law⁸⁶ believe that the reason for this lies in the lack of understanding of the kinetics required to characterize the combustion of very weak flames with low flame temperatures.

Egolfopoulos and Law also studied the effects of nitrogen-diluted flames to determine the effects of temperature, oxygen concentration, and stoichiometry on flame speed. Nitrogen dilution was used in order to maintain low flame

temperatures even as the equivalence ratio was increased. Again, the kinetic schemes underpredicted the flame speeds for very lean conditions. However, for fuel-rich conditions, the kinetic schemes still predicted the flame speed quite well, even though the flame temperatures were kept in the same range as the lean cases by nitrogen dilution. This result clearly indicates the importance of both the temperature and oxygen concentration in influencing the kinetic mechanism responsible for their observed disagreements.

In addition to the above effects, Egolfopoulos and Law⁸⁶ also investigated the pressure effect on very lean H₂/air flames. They suggest that the proper indicator for flame response to the effects of chemistry is the mass burning rate, $m^0 = \rho_u S_u^0$, since mixture density varies with pressure. Figure 5.29 shows the mass burning rate as a function of pressure, while Fig. 5.30 shows the pressure exponent n (if we consider $m^0 \sim p^n$) as a function of pressure as well.

It is seen in Fig. 5.29 that m^0 monotonically increases with pressure for the largest value of ϕ tested. However, for all lower values of ϕ , there appears to be an inflection point, at which m^0 first increases, then decreases, and finally increases again. This result can be seen more clearly in Fig. 5.30 as the pressure increases, the pressure exponent starts with a positive value, then decreases (in some cases even becoming less than zero), and finally increases again. One possible explanation given by Egolfopoulos and Law⁸⁶ is the shift of the importance of some two-body reactions to three-body chain-terminating reactions as pressure increases. Starting from the low-pressure regime, increasing pressure increases the collision rate and thereby promotes the overall reaction rate. The increase of pressure, however, simultaneously enhances the temperature-insensitive three-body chain-terminating reactions of R9 and R10 (of Table 5.5) relative to the temperature-sensitive two-body branching reaction R1. This shift of importance

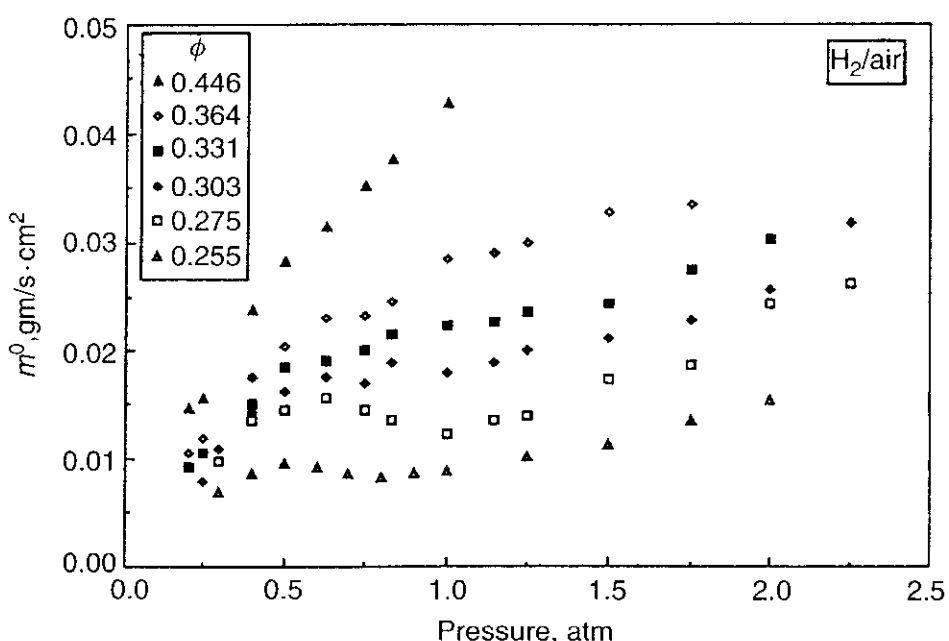


Figure 5.29 Variation of experimentally determined mass burning rate (m^0) with pressure for lean H₂/O₂/N₂ mixtures (after Egolfopoulos and Law⁸⁶).

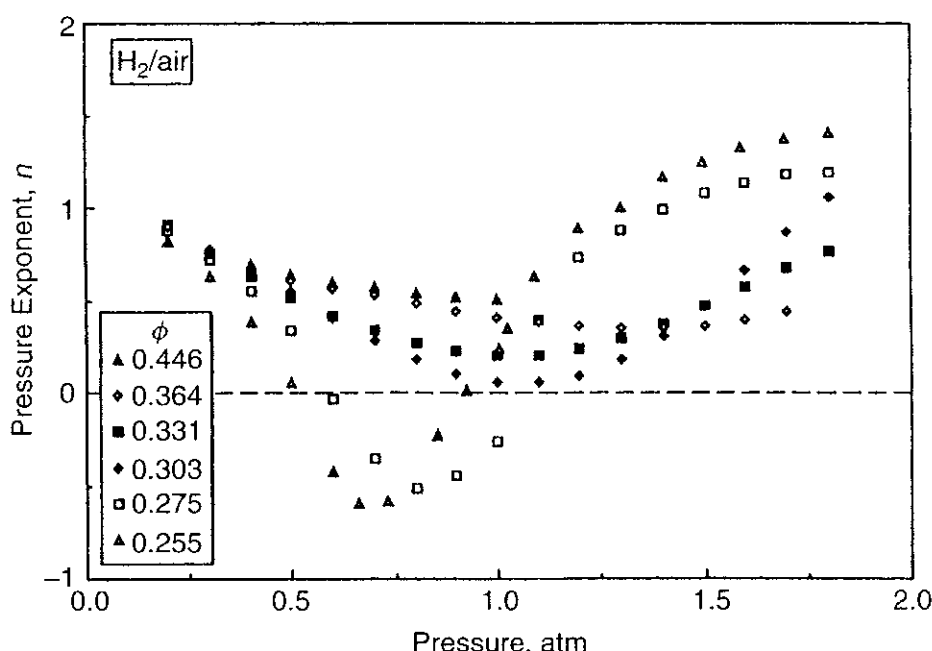


Figure 5.30 Variation of experimentally determined pressure exponent, n , with pressure for lean $\text{H}_2/\text{O}_2/\text{N}_2$ mixtures (after Egolfopoulos and Law⁸⁶).

of reactions results in a weaker dependence of m^0 on p , as indicated by the continuously decreasing values of n . Eventually, however, the decreasing trend is arrested such that with further increasing of p , another reaction channel is activated, producing additional radicals, which again facilitate the overall reaction and thereby cause n to increase with p . Egolfopoulos and Law also tried to use numerical simulation to predict m^0 and n for some of their mixtures without any success. Their simulation failed to predict the results with acceptable accuracy. Their simulation substantially underpredicted the experimental results for weakly burning flames, and calculated results were unable to represent the response of a laminar flame to the increase in pressure. The primary cause of these problems, in their opinion, is the lack of detailed understanding of the importance of HO_2 and H_2O_2 chemistry for ultra-lean burning conditions.

5 EFFECT OF CHEMICAL AND PHYSICAL VARIABLES ON FLAME SPEED

5.1 Chemical Variables

5.1.1 Effect of Mixture Ratio The variation of the laminar-flame speed with fuel–oxidant ratio is governed predominantly by the variation of the temperature with the mixture ratio. For hydrocarbon fuels, the peak of the flame speed occurs near stoichiometric or slightly fuel-rich mixtures. Some typical results of hydrocarbon/air laminar flame speeds as a function of fuel volume percentage in air are shown in Fig. 5.31 based on the data of Warnatz.⁹⁴ These data trends are the same as those measured by Hartmann.³²

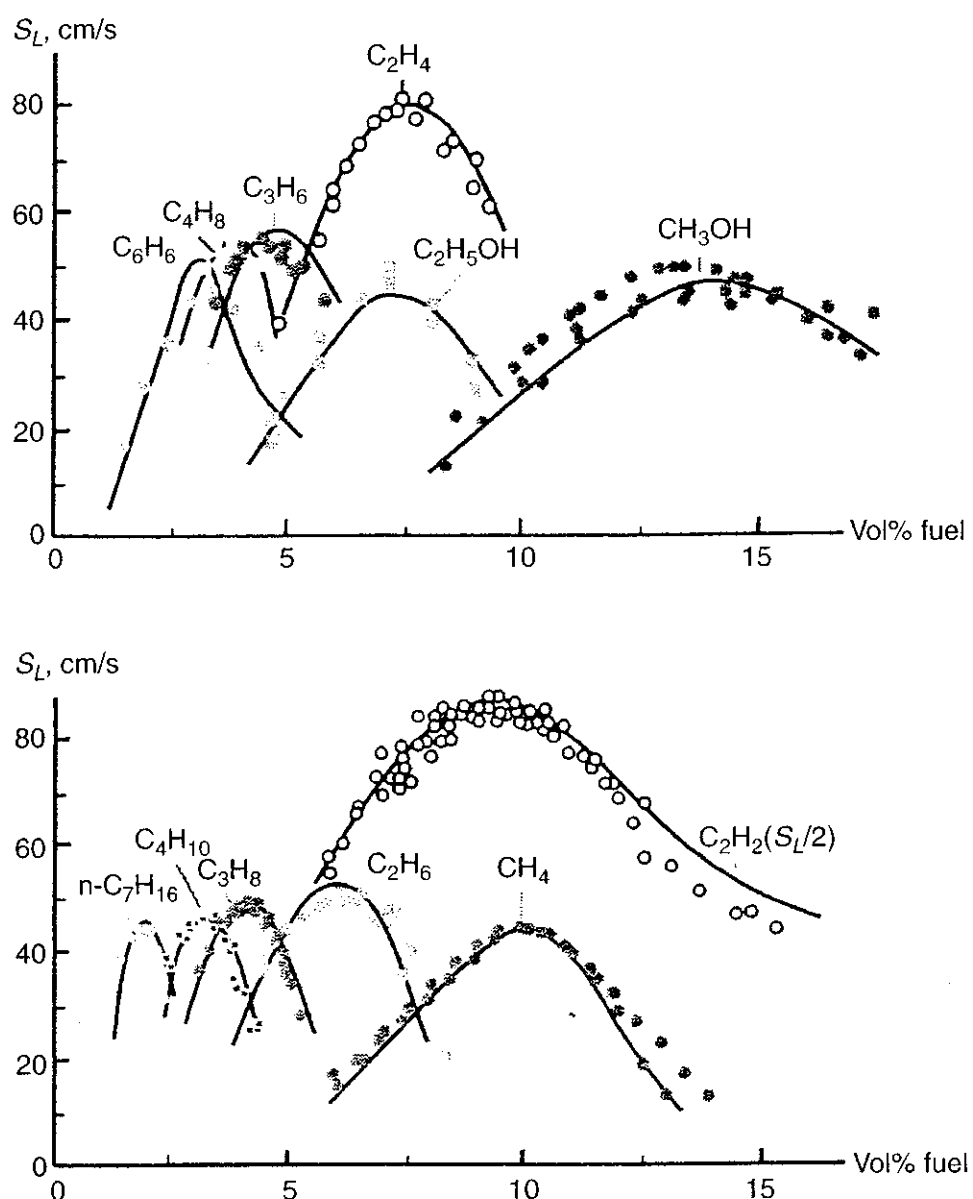


Figure 5.31 Dependence of laminar-flame speed on mixture composition for different fuel–air mixtures (modified from Warnatz⁹⁴).

It is generally acceptable to assume that a mixture with maximum flame temperature is also a mixture with maximum flame speed.³³ In very lean or very rich mixtures, it is impossible to propagate a flame because there is too little fuel or oxidant to maintain a steady deflagration wave. Thus, there exist upper and lower flammability limits. The deflagration limits for some fuel–oxidant mixtures are listed in Table 5.8 (to be discussed in a later section).

5.1.2 Effect of Fuel Molecular Structure Attempts have been made to correlate the flame speed with the fuel structure.^{20,34} The variation of flame speed with respect to the number of substituted methyl groups is shown in Fig. 5.32.

Gerstein et al.²⁰ and Reynolds³⁴ found that as the fuel molecular weight increases, the range of flammability becomes narrower (also shown in Fig. 5.31). Figure 5.33 shows the maximum flame speed as a function of the number of

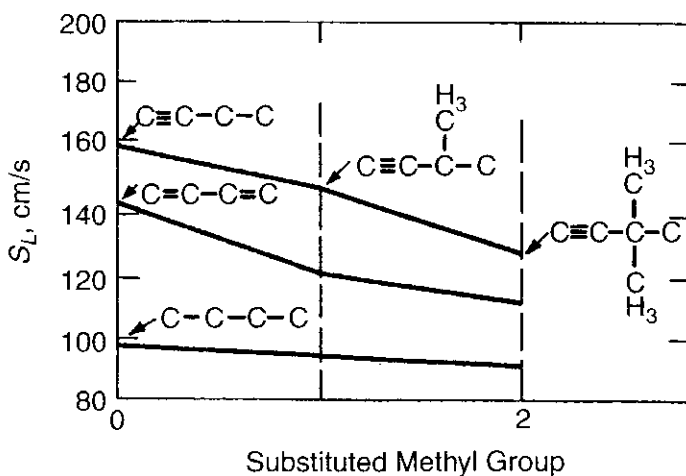


Figure 5.32 Variation of flame speed with respect to the number of substituted methyl groups.

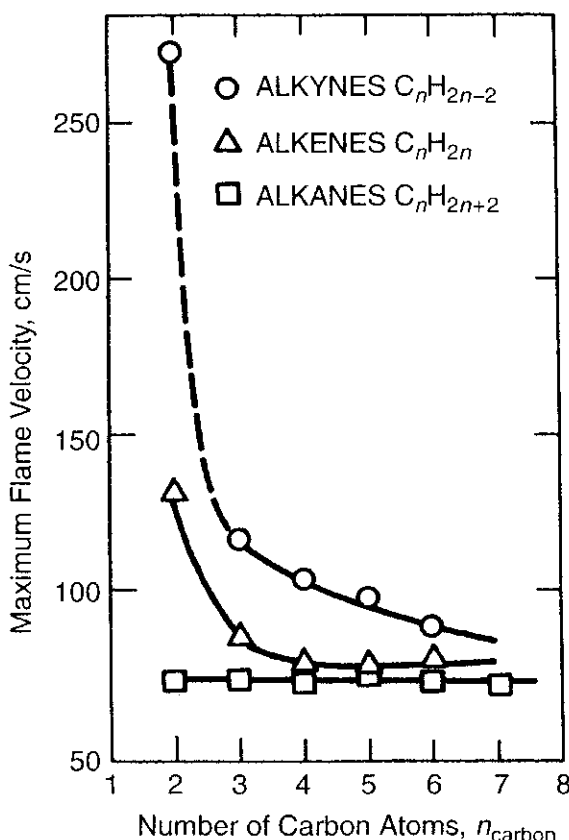


Figure 5.33 Effect of the number of carbon atoms in the chain on maximum flame velocity (after Reynolds and Gerstein³⁴).

carbon atoms in the fuel molecule for three families. For saturated hydrocarbons [alkanes (also known as paraffins) such as C_2H_6 (ethane), C_3H_8 (propane), C_4H_{10} (butane), C_5H_{12} (pentane), and C_6H_{14} (hexane)], the maximum flame speed (70 cm/s) is nearly independent of the number of carbon atoms in the molecule. For unsaturated hydrocarbons [either alkenes (also known as olefins) such as C_2H_4 (ethylene) and C_3H_6 (propylene), or alkynes (also known as the acetylene

series) such as C_2H_2 (acetylene), C_3H_4 (propyne), C_4H_6 (butyne), and C_5H_8 (pentyne)], the laminar-flame speed is higher for fuels with a smaller number of carbon atoms. The values of S_L fall steeply as n_{carbon} increases to 4 and then fall slowly with further increases in n_{carbon} , approaching the value of S_L of saturated fuels when $n_{\text{carbon}} \geq 8$.

From the above results, it seems that the number of substituted methyl groups and the structure of the fuel have a strong influence on S_L (Figs. 5.32 and 5.33). It is concluded by Gerstein et al.²⁰ that the variation of flame speed with respect to different substitutions of methyl groups is believed to be due to the flame temperature rather than the molecular structure. The influence of the number of carbon atoms in various fuels on laminar-flame speed, however, is not due to the flame temperature, since the adiabatic flame temperature of most fuels is around 2200 K; the activation energies for most fuels reacting with oxygen are within a narrow range around 40 kcal/mol. The difference in S_L for fuels containing different numbers of carbon atoms is mainly due to the changes in thermal diffusivity, which is a function of the fuel molecular weight.

So far, we have kept saying that $S_L \propto \sqrt{\alpha RR}$. However, this is true only for similar chemical compounds. The reactivity of the fuel may affect the flame velocity drastically. For example, there is a significant difference between the reactivity of a C–Si bond and a Si–H bond. This can be seen in Table 5.6. Therefore, for different chemical compounds, the reactivity of the combustion system should be considered.

5.1.3 Effects of Additives The main purpose of using an additive is to raise the ignition temperature and reduce the tendency to preignition, as well as knocking. It only slightly affects the flame speed. However, studies with moist carbon monoxide show that its flame speed can be raised appreciably by addition of small amounts of hydrogen or hydrogen-containing fuels. The pronounced effect of small amounts of H_2O on the reaction of CO gas was noticed by Tanford and Pease¹³ and has been discussed in the diffusion theories (see Section 2.3 of this chapter). The antiknocking compound is used to slow down the low-temperature oxidation and is also used as a diluent. It does not have a strong effect on the flame speed, which is mainly controlled by high-temperature reactions. Mixing of different fuels usually does not have a significant effect on

Table 5.6 Effect of Fuel Reactivity on Flame Speed

Fuel	S_L (cm/s)	T_F (K)	Reactivity
$(\text{CH}_3)_4\text{C}$	33	2254	
$(\text{CH}_3)_4\text{Si}$	60	2247	Greater than that of $(\text{CH}_3)_4\text{C}$
$(\text{C}_2\text{H}_5)_2\text{SiH}_2$	111	2278	Higher reactivity
$(\text{C}_4\text{H}_9)\text{SiH}_3$	148	2290	↓
SiH_4	Spontaneously flammable		Extremely reactive

S_L . However, if the inert substance added does change the thermal diffusivity α of the fuel, then it can affect the flame speed significantly.

5.2 Physical Variables

5.2.1 Effect of Pressure The nonmonotonic pressure dependency of S_L for the $H_2/O_2/N_2$ flame is given in Section 4.5. For various hydrocarbon/ O_2 mixtures containing N_2 , Ar, or He, Lewis³⁵ studied the effect of pressure on the laminar-flame speed. A power law, $S_L \propto p^n$, was developed, where the exponent n is referred to as the Lewis pressure index n . He observed that when $S_L < 50$ cm/s, the exponent n is usually negative, implying that S_L increases with decreasing pressure; for $50 < S_L < 100$ cm/s, S_L is independent of pressure, and when $S_L > 100$ cm/s, S_L increases with increasing pressure.

Based on the thermal and the comprehensive theories discussed in Sections 2 and 3, we know that $S_L \propto p^{(n-2)/2}$, where this n is the order of chemical reaction. The pressure dependence observed by Lewis implies that the overall order of the reaction is less than 2 for flames with $S_L < 50$ cm/s, equal to 2 for those with $50 < S_L < 100$ cm/s, and greater than 2 for those with $S_L > 100$ cm/s. The relationship $S_L \propto p^{(n-2)/2}$ is supported by much experimental evidence. For example, the first-order decomposition reaction for ethylene oxide monopropellant (C_2H_4O) is shown to follow $S_L \propto \sqrt{p^{-1}}$. For many hydrocarbon fuels undergoing second-order reactions, the laminar-flame speeds were found to be

Table 5.7 Empirical Fit to Laminar Burning Velocity Data in a Constant-Volume Chamber (Based on Metghalchi and Keck⁹⁵)

Fuel Type	<i>Flame Speed, S_{L0} (cm/s)</i>		
	$\phi = 0.8$	$\phi = 1.0$	$\phi = 1.2$
<i>Temperature Exponent, m</i>			
Methanol	25.6	32.7	38.1
Propane	23.2	31.9	33.8
Isooctane	19.2	27.0	27.6
RMFD-303 ^a	19.1	25.2	28.1
<i>Pressure Exponent, n</i>			
Methanol	-0.21	-0.13	-0.11
Propane	-0.23	-0.17	-0.17
Isooctane	-0.22	-0.18	-0.11
RMFD-303 ^a	-0.17	-0.13	-0.087

^aSynthetic gasoline (45% toluene, 14% undecene, and 41% isoctane).

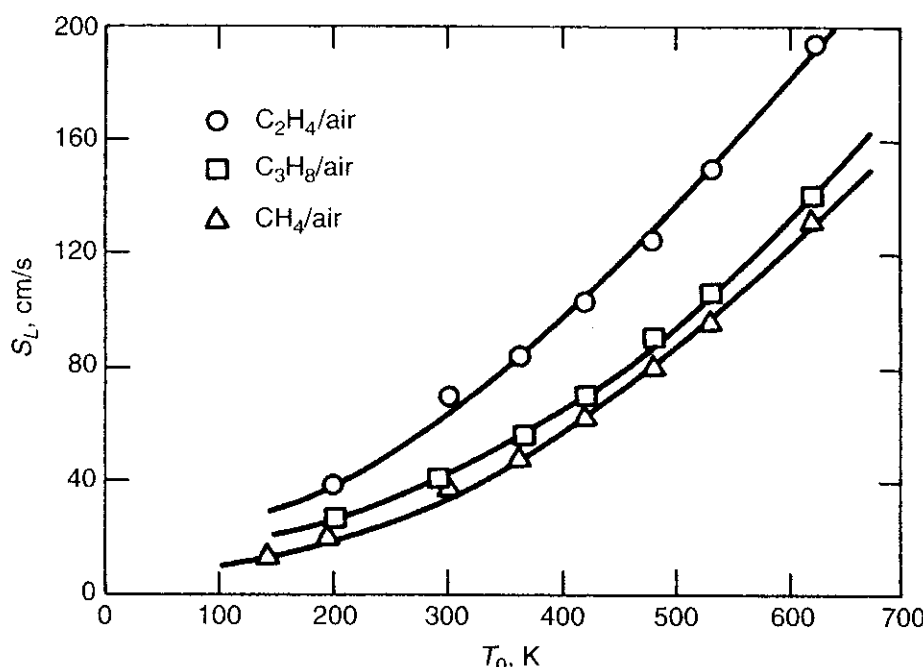


Figure 5.34 Effect of initial temperature on flame speed (adapted with permission of the American Chemical Society, from Dugger, Heimel, and Weast³⁶).

independent of pressure. Table 5.7 shows the empirical fit to laminar burning velocity data in a constant-volume chamber. The fit formula can be represented by

$$S_L = S_{L0}(\text{cm/s}) \left[\frac{T \text{ (K)}}{298 \text{ K}} \right]^m \left[\frac{p \text{ (atm)}}{1 \text{ atm}} \right]^n \quad (5-141)$$

The values of pressure exponent n for these four types of hydrocarbon fuels are all negative for three different equivalence ratios.

5.2.2 Effect of Initial Temperature The initial temperature effect on the laminar burning velocity of several types of hydrocarbon fuels combusting with air in a constant-volume chamber is shown in Table 5.7 and Eq. (5-141). Dugger et al.³⁶ also conducted a series of experiments showing the dependence of S_L on T_0 for three mixtures under constant-pressure conditions. Figure 5.34 shows that S_L (or u_0) increases with T_0 for all three hydrocarbon/air mixtures. The results can be represented by the following relationship:

$$S_L \propto T_0^m \quad (5-142)$$

where the exponent m ranges between 1.5 and 2. The increase of S_L with T_0 is mainly due to the preheating effect. In general, the change of T_f caused by preheating the initial mixture is not significant. This is due to the fact that the heat-release term $a_0 Q / \rho_0$ is more or less fixed, and this term is also much larger than $C_p T_0$. From Eq. (5-23), we can see that T_f cannot change much by the preheating effect. Nevertheless, even a slight change in T_f may alter S_L significantly, as shown in the next section.

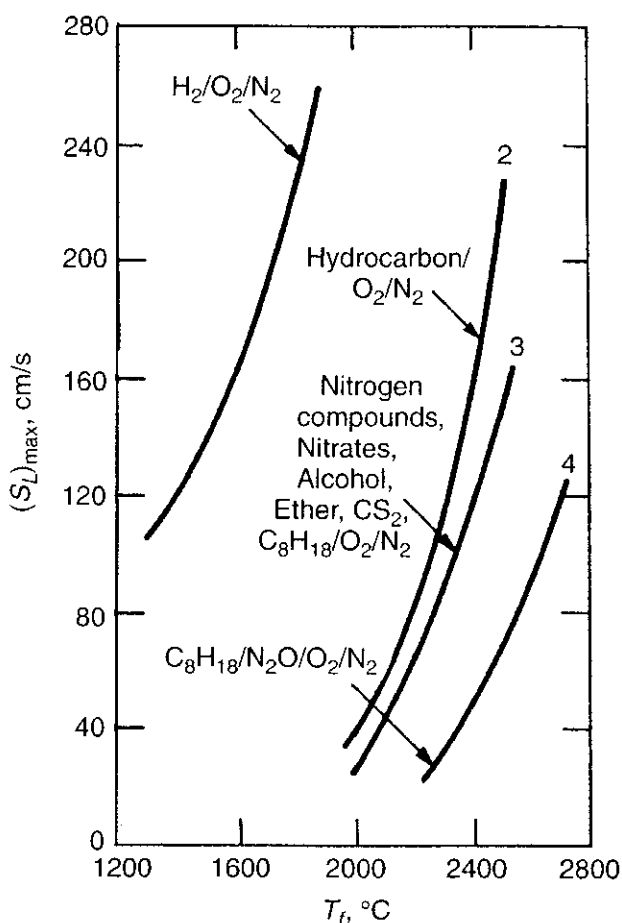


Figure 5.35 Effect of flame temperature on maximum flame speed (modified from Bartholomé⁵ and Bartholomé and Sachsse³⁷).

5.2.3 Effect of Flame Temperature The maximum flame speed for several mixtures as a function of flame temperature is shown in Fig. 5.35. The effect of T_f on S_L is obviously very strong.

From these data, we can conclude that the laminar-flame speed S_L is essentially determined by the value of T_f ; this is consistent with the idea of Zel'dovich^{9a–9c} that the reaction rate is based on T_f . At high temperatures, dissociation reactions are favored. These reactions can introduce numerous free radicals into the flame, and these free radicals act as chain carriers to promote the reaction and hence the propagation speed of the flame. The lighter these free radicals are, the more easily they are able to diffuse to the preflame zone. This is why H atoms can significantly enhance flame speeds. This concept of radical-species diffusion is the same as that of Tanford and Pease.¹³

5.2.4 Effect of Thermal Diffusivity and Specific Heat Clingman et al.³⁸ performed a set of experiments to elucidate the dominant effects of the thermal diffusivity and reaction rates on S_L . They measured the flame propagation speed of methane in various oxygen/inert-gas mixtures. The volumetric ratio of oxygen to inert gas was set at 0.21 : 0.79 for all cases studied. The inert gases chosen were nitrogen (N_2), helium (He), and argon (Ar). Their results are shown in Fig. 5.36.

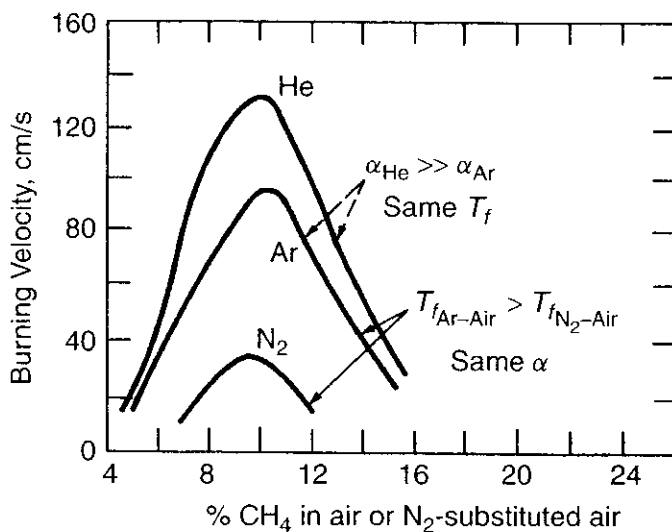


Figure 5.36 Methane flame velocities in various O₂/inert-gas mixtures (modified from Clingman et al.³⁸).

The results can be explained as follows: By comparing the two top curves, we can see that S_L in CH₄/O₂/He mixtures is higher than that in CH₄/O₂/Ar mixtures. This is due to the fact that the thermal diffusivity of helium is much larger than that of argon because the molecular weight of helium is much smaller. Recall the relationship given by Eq. (5-41): If the flame temperatures are the same in both cases, then the higher the thermal diffusivity, the higher the S_L . Helium and argon are both monatomic gases, and thus their C_p s and flame temperatures are equal. Consequently, S_L for CH₄/O₂/He mixtures is greater than that for CH₄/O₂/Ar mixtures.

In comparing the middle curve with the bottom curve of Fig. 5.36, we can see that S_L in CH₄/O₂/Ar mixtures is higher than that in CH₄/O₂/N₂ mixtures (regular air). This is due to the fact that Ar and N₂ have nearly the same values of thermal diffusivity. However, Ar is a monatomic gas, which has a lower specific heat [$(C_p)_{Ar} = \frac{5}{2}R$] than the diatomic gas N₂ [$(C_p)_{N_2} = \frac{9}{2}R$]. Since the heat release on all systems is the same, the flame temperature will be higher in the CH₄/O₂/Ar mixture than that in the CH₄/O₂/N₂ mixture. Thus, based on Eq. (5-41), S_L is higher in CH₄/O₂/Ar mixtures than in CH₄/O₂/N₂ mixtures.

6 PRINCIPLE OF STABILIZATION OF COMBUSTION WAVES IN LAMINAR STREAMS

A Bunsen burner flame provides a common example of the fixation of a combustion wave in a gas stream. We shall now examine the mechanism by which the inner cone maintains a fixed position with respect to the burner rim. Near the fringe of the combustion wave in the vicinity of the burner rim, the mixture gas velocity can be represented by an approximately linear profile. Figure 5.37 shows four different situations, which should be considered in order to study the mechanism of flame anchoring near the rim of a Bunsen burner. Let us now

compare the radial profiles of the near-surface region of the approach velocity of the unburned gas mixture (dotted line profile) and flame propagation velocity (solid line profile) adjacent to the burner rim to show how the flame is anchored to the burner rim. When the premixed-gas flow is weak [case (a)], S_L is greater than u_{supply} not only in the near surface region but also over almost the entire cross section of the barrel; hence, the flame propagates into the barrel to produce the *flashback* situation. On the other hand, when the flow is very strong [case (b)], u_{supply} is greater than S_L over the entire cross section, producing the *blowoff* situation. The critical condition for blowoff arises when the S_L and u_{supply} profiles are tangent at a certain radial location [case (c)]. Stable combustion is shown as case (d) in Fig. 5.37.

Consider a velocity profile slightly inside the barrel and assume that the flame has just entered the tube (see Fig. 5.38). The distance d_p from the tube wall is called the penetration distance, which is half of the quenching distance, d_q . Below d_q , no flame can propagate into the tube supplying the premixed combustible gases. If \bar{u}_1 is the mean velocity profile of the premixed gas near the tube wall, then there is no place where the local flame velocity is greater than the local gas velocity. Therefore, any flame that finds itself inside the tube will then be blown out of the tube. Then, the critical flashback condition is reached if u_{supply} is represented by \bar{u}_2 . The profile for the mean velocity \bar{u}_3 corresponds to the case for which the flame does flashback. The critical value of boundary velocity gradient g at which the *flashback* condition is first realized is denoted by g_F . That is,

$$g_F = \frac{S_L}{d_p} \quad (5-143)$$

where the *penetration distance* $d_p = 0.5 d_q$; the quenching distance (or quenching diameter) is discussed in a later section.

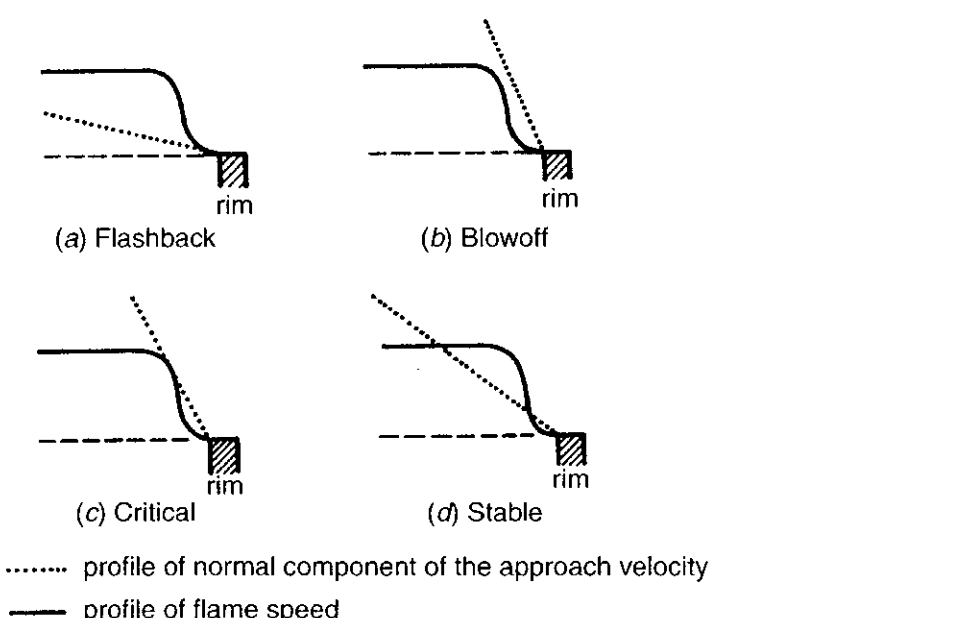


Figure 5.37 Four different radial distributions of velocity profiles in the consideration of laminar-flame stability near the rim of a Bunsen burner (modified from Kanury³³).

When the gas flow is increased, the equilibrium position of the flame shifts upward from the burner rim. Then, the premixed, unburned gas becomes progressively diluted by interdiffusion of surrounding gases (see Fig. 5.39). The critical value of velocity gradient g corresponding to *blowoff* is denoted by g_B and given by

$$g_B = \lim_{r \rightarrow R} \left(-\frac{du}{dr} \right)_{\bar{u}_{\text{average}}} \quad (5-144)$$

The critical boundary velocity gradients g_F and g_B are given by the shapes of curves 1 and 3, respectively, in Fig. 5.39. The values of g_F and g_B that define the flame stability on laminar jets are determined experimentally. It is clear from this discussion that the velocity gradients have definite influences on flame stability. A qualitative sketch of critical boundary velocity gradients versus fuel–oxidant ratio is shown in Fig. 5.40. For rich mixtures, the blow off curve continues to rise instead of decreasing after the stoichiometric value is reached. The cause for this trend is that the experiments are performed in air, and the diffusion of air into the premixed gaseous mixture as the flame lifts off the burner rim increases the local flame speed of the initially fuel-rich mixture.

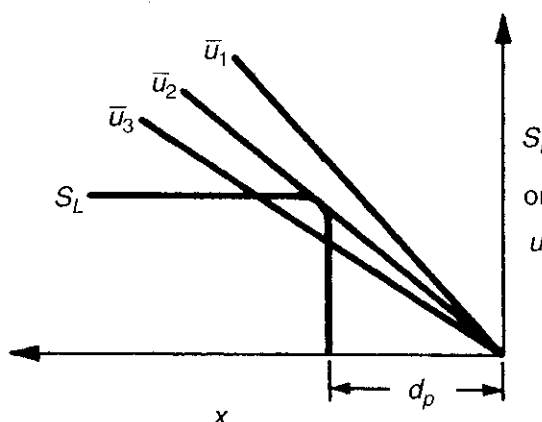


Figure 5.38 Burning velocity and gas velocity inside a Bunsen tube (after Lewis and von Elbe⁴⁰).

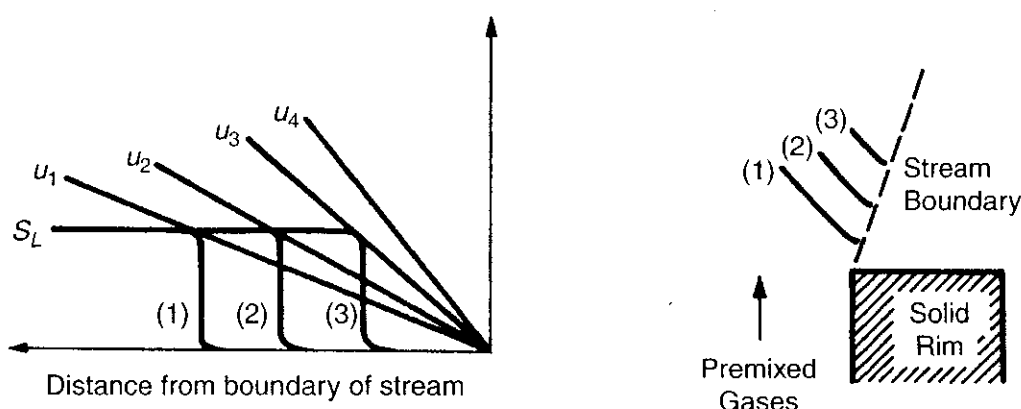


Figure 5.39 Burning velocity and gas velocity above a Bunsen tube rim (after Lewis and von Elbe⁴⁰).

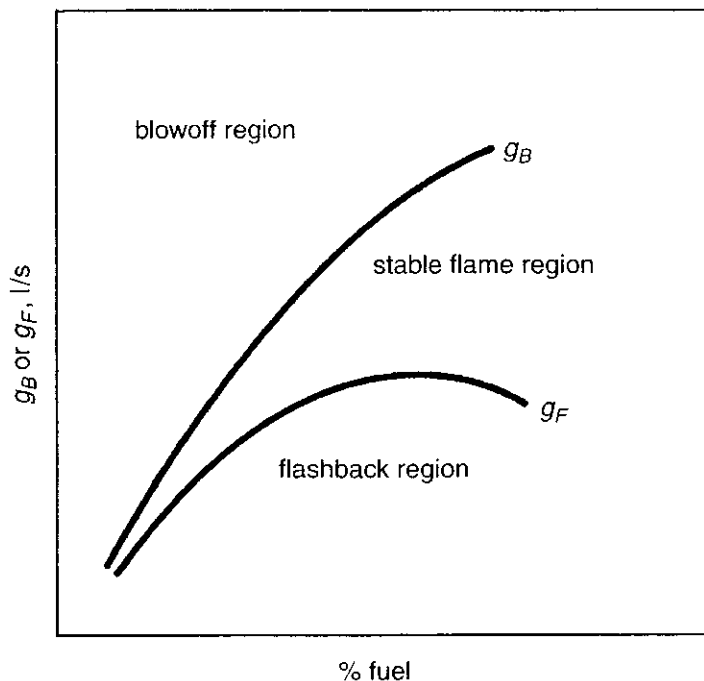


Figure 5.40 Effect of critical boundary velocity gradient and fuel percentage on flame stability (adapted from Kanury³³).

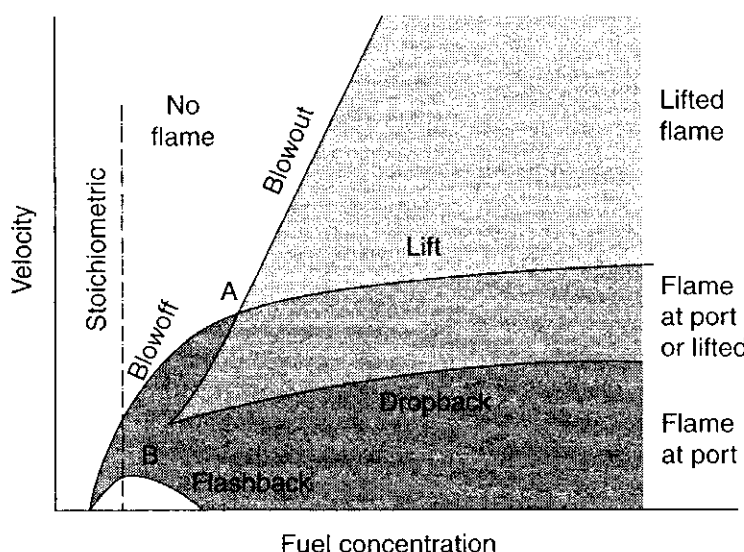


Figure 5.41 Characteristic stability diagram for a premixed open burner flame (after Wohl et al.⁹⁶).

A characteristic stability diagram for a premixed flame burning at the end of a cylindrical tube was established by Wohl et al.⁹⁶ and is given in Fig. 5.41. In this plot, the stability boundaries are given as functions of fuel concentration in the mixture and the premixed gas supply velocity. When the approach (supply) velocity to a seated flame (represented by a point in the dark shaded region) is decreased until the flame velocity exceeds the approach velocity over some portion of the burner port, the flame flashes back into the burner (unshaded area of Fig. 5.41). On the other hand, if the magnitude of the approach velocity is

increased until it exceeds that of the downward flame propagation velocity at every point, the flame will either be entirely extinguished beyond the blowoff limit or it will be lifted until a new stable position in the gas stream above the burner is reached as a result of dilution with secondary air from the surroundings. The lift curve, based on either Wohl et al.⁹⁶ or Borman and Ragland,⁹⁷ is a continuation of the blowoff curve beyond point A in Fig. 5.41. The blowout curve corresponds to the velocity required to extinguish a lifted flame. Once the flame has lifted, the approach velocity must be decreased well below the original lift velocity before the flame will drop back and be reseated on the burner rim. Between fuel concentrations A and B, the blowout of a lifted flame occurs at a lower velocity than the flame blowoff from the port.

7 FLAME QUENCHING

Flame quenching can significantly affect the process of flame propagation. Let us first define a quenching distance by considering the following phenomena. After a flame has been established on the Bunsen burner port, if the mixture is suddenly cut off, the flame flashes back and propagates down the burner tube. We then replace the barrel with a narrower one. The experiment is repeated until the tube just barely permits the flame to propagate. The diameter of the last tube is called the quenching distance (or quenching diameter) for the given fuel–oxidant mixture under the specified conditions of temperature and pressure. Below this diameter, the flame is quenched by the tube wall and the flame cannot flash back.

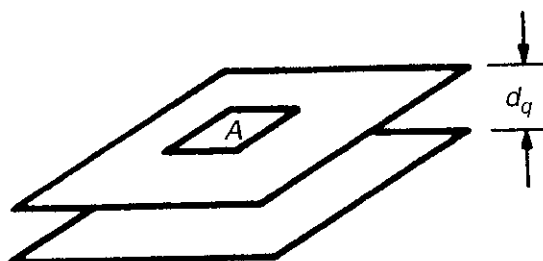
For the two-dimensional problem of a pair of parallel plates, the quenching distance d_q can be defined as the distance between the plates such that the rate of heat generation, \dot{q}_R , is exactly equal to the rate of heat removal, \dot{q}_L . For the control volume (Ad_q), the rate of heat generation can be expressed as

$$\dot{q}_R = \phi_0(RR)(Ad_q)Q_R \quad (5-145)$$

where

d_q is the distance between the two parallel plates (L)

A is a small element of area (L^2)



ϕ_0 is the stoichiometric mole fraction of the combustible mixture

Q_R is the heat of reaction per mole of stoichiometric mixture (Q/mole)

RR is the reaction rate ($\text{mole}/t L^3$)

Also,

$$\dot{q}_L = \lambda A \frac{dT}{dx} \quad (5-146)$$

Let T_q signify the lowest temperature at which the flame can propagate. Let T_0 signify the temperature at the cold boundary. Approximating the temperature distribution in the gas phase by two linear straight-line segments with a maximum temperature T_q at the center, and equating \dot{q}_R , we get

$$2A\lambda \frac{T_q - T_0}{d_q/2} = \phi_0 Q_R \text{RR } Ad_q$$

or

$$d_q^2 = \frac{4\lambda(T_q - T_0)}{\phi_0 \text{RR } Q_R} \quad (5-147)$$

From the energy balance, we have

$$Q_R = C_p(T_f - T_0) \quad (5-148)$$

Substituting Eq. (5-148) into Eq. (5-147), we have

$$d_q^2 = \frac{4\lambda}{\phi_0 C_p \text{RR}} \left(\frac{T_q - T_0}{T_f - T_0} \right) \quad (5-149)$$

Since α can be expressed as $\lambda/C_p\rho_0$, then

$$d_q \propto \sqrt{\frac{\alpha}{\text{RR}}} \quad (5-150)$$

Combining Eq. (5-150) with Eq. (5-41), we have

$$\frac{S_L}{d_q} \propto \text{RR} \quad (5-151)$$

and

$$S_L d_q \propto \alpha \quad (5-152)$$

It is important to note that Eq. (5-149) is derived under the assumption of negligible heat loss from the flame to the cold gas. Because of this assumption, Eq. (5-149) cannot satisfy the limiting condition at $\text{RR} \rightarrow 0$. If one sets the reaction rate equal to zero in Eq. (5-149), the quenching diameter approaches infinity; however, from experiments, we know that the quenching diameter is finite.

Equation (5-151), in general, is useful in determining trends in reaction rate. The ratio S_L/d_q can also be related to the boundary velocity gradient at flashback

[see Eq. (5-143)]. Lewis and von Elbe⁴⁰ suggest that twice the depth of penetration of quenching ($2d_p$) should be equal to the quenching distance between parallel plates. For cylindrical tubes (the usual experimental configuration), d_p should be about $\frac{1}{3}$ the quenching distance.^{43,44} One can thus write

$$g_F = 3 \frac{S_L}{d_q} \quad (5-153)$$

for cylindrical tubes. The results of Berlad and Potter⁴³ for a series of examinations using different fuel–oxidant mixtures are shown in Fig. 5.42. The best line through the data has the equation

$$q_F = 14.125 \left(\frac{S_L}{d_q} \right)^{1.168} \quad (5-154)$$

Equation (5-153) is also sketched in Fig. 5.42. Considering the variety of mixtures included in the correlation, the agreement with Eq. (5-153) is not so unacceptable. It would be difficult to decide whether the deviations are due to the lack of precision of the experimental data or of the analytical expression. Both are probably involved. In general, the quenching distance is smaller for more reactive fuels. The typical quenching distance for hydrocarbon fuel between parallel plates is around 0.18 cm. It has been found that a very small centerbody has a large quenching action in the annular case. For a given fuel/oxidant combination in the

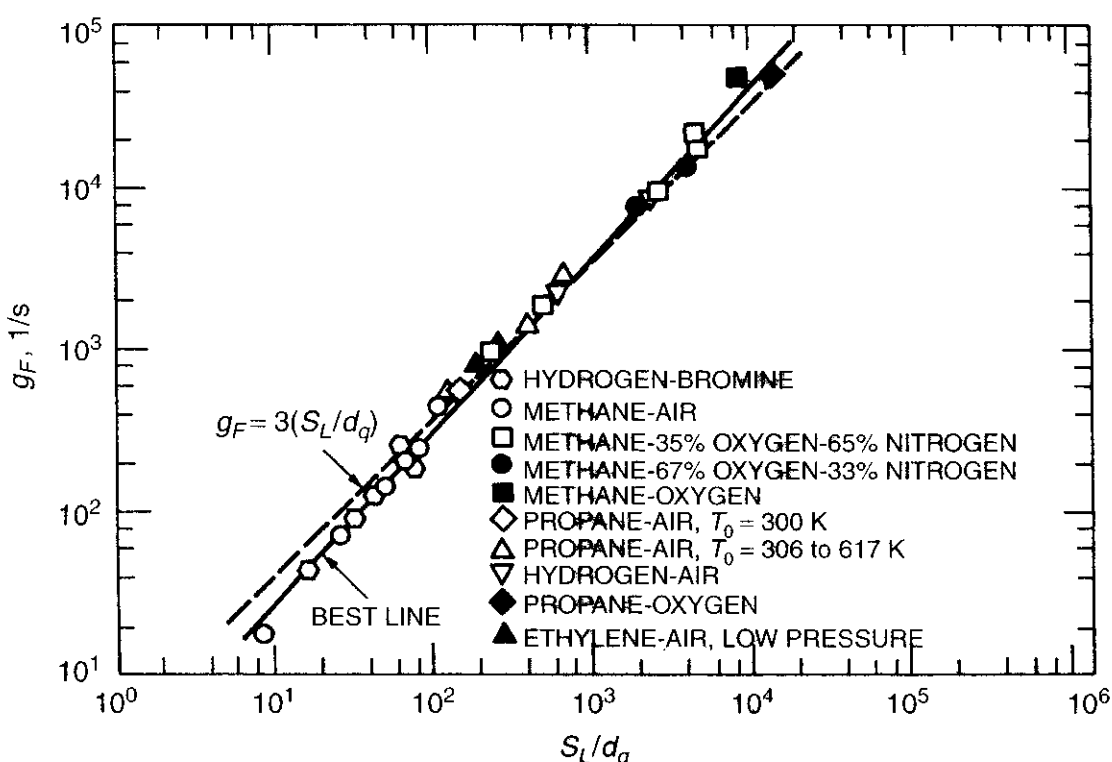


Figure 5.42 Correlation of g_F with S_L/d_q (after Berlad and Potter⁴³).

mixture, the quenching distance depends on the inert diluent used in the mixture in the following order

$$d_{q_{\text{He}}} > d_{q_{\text{Ar}}} > d_{q_{\text{N}_2}} > d_{q_{\text{CO}_2}}$$

This implies that the flame is, in effect, more insulated from the walls by CO₂ than by helium. The reason is that

$$\alpha_{\text{He}} > \alpha_{\text{Ar}} \approx \alpha_{\text{N}_2} > \alpha_{\text{CO}_2}$$

As the initial temperature of the unburned mixture is increased, the flame is able to pass through smaller openings, and hence the quenching distance is decreased. The quenching distance also depends on pressure; it increases as pressure decreases. We can see this dependency from the following equations:

$$\alpha = \frac{\lambda}{\rho C_p} \propto \frac{1}{p} \quad (5-155)$$

$$\text{RR} \propto p^n \quad (5-156)$$

$$d_q = \sqrt{\frac{\alpha}{\text{RR}}} = \sqrt{\frac{1}{p^{n+1}}} \propto \frac{1}{p^b} \quad (5-157)$$

A rough approximation for hydrocarbon burning in air is

$$d_q \propto \frac{1}{p} \quad (\text{second-order reaction}) \quad (5-158)$$

8 FLAMMABILITY LIMITS OF PREMIXED LAMINAR FLAMES

In this section, we shall discuss the stability limits of premixed laminar flames. On this subject, there are two groups of studies. One group concentrates on the laminar-flame propagation as a function of the mixture ratio; the other studies the relationship of flammability limits with flow conditions. The latter addresses flame stabilization phenomena such as flashback, blowoff, onset of turbulence, and so on. A portion of the second group study is discussed in Section 6.

8.1 Flammability Limits Determined from a Standard Glass Tube

To measure the lean and rich concentration limits of flammability, we need to exclude all external effects so that it is a property of the fuel–oxidant mixture and test conditions, which usually are specified in terms of temperature and pressure. In the early 1950s, a standard vertical glass tube of 1.22-m (4-ft) length with an inner diameter of 5 cm was selected as a standard tube for observing whether a mixture is truly capable of propagating a flame indefinitely away from the ignition

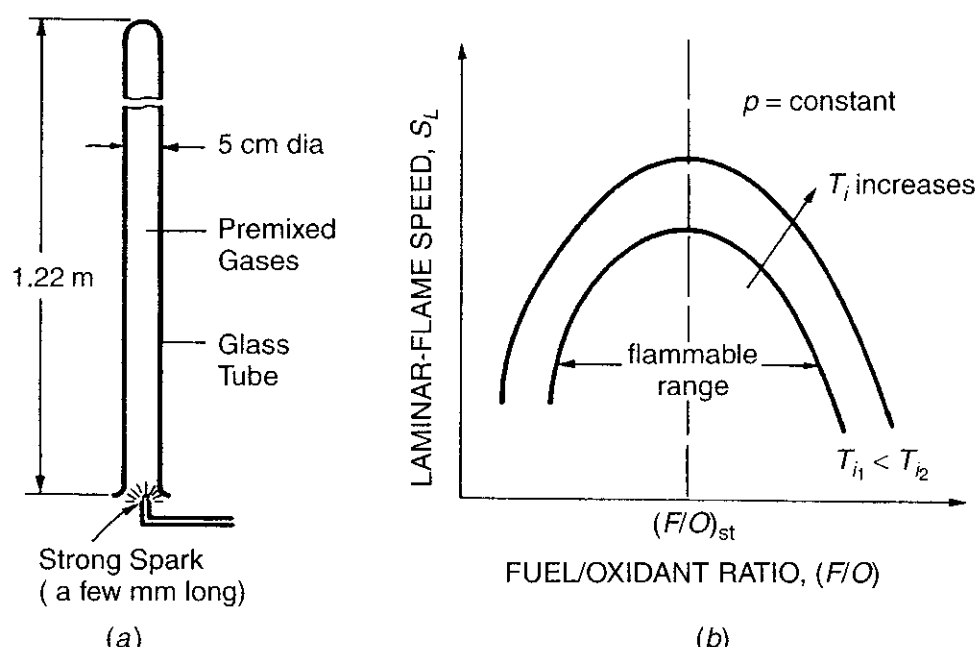


Figure 5.43 Standard glass tube for testing flammability limits of premixed gases and the laminar-flame speed as functions of fuel–oxidant ratio and initial temperature.

Table 5.8 Flammability Limits of Certain Fuel–Air Mixtures

Compound	Lower (Lean) Limits, Vol. (%) in Air	Upper (Rich) Limits, Vol. (%) in Air	Stoichiometric, Vol. (%) in Air
Methane, CH ₄	5	15	9.47
Ethane, C ₂ H ₄	2.82	13	5.64
Propane, C ₃ H ₈	2.05	11.38	4.02
Butane, C ₄ H ₁₀	1.86	8.41	3.13
Pentane, C ₅ H ₁₂	1.40	7.80	2.56
Hexane, C ₆ H ₁₄	1.18	7.40	2.16
Heptane, C ₇ H ₁₆	1	6	1.87
Isooctane, C ₈ H ₁₈	0.95	6.0	1.65
Acetylene, C ₂ H ₂	2.5	80	7.72
Hydrogen, H ₂	4	74.2	29.2
Carbon monoxide, CO	12.5	74.2	29.5
Ethylene oxide, C ₂ H ₄ O	3.0	80	7.72
Methanol (g), CH ₃ OH	5.88	49.94	12.24

source. The ignition source is a spark plug located at the bottom of the tube and can generate a strong spark of a few millimeters in length (see Fig. 5.43a).

Typical variations of laminar-flame speed as functions of F/O and initial temperature of the gaseous mixture are shown in Fig. 5.43b. When the initial temperature of the mixture is increased, the flammable F/O range becomes wider, or the flammability limits are broadened. The upper and lower flammability limits of mixtures of certain fuels with air are listed in Table 5.8. These are assembled

from data of Smith and Stinson,⁴⁵ Kanury,⁴⁶ and NACA Report 1300.⁴⁷ For other fuel compounds, the numerous flammability limits can be found from Lewis and von Elbe⁴⁰ or *Handbook of Chemistry and Physics*.

8.2 Effect of Pressure and Temperature on Flammability Limits

Pressure has a definite effect on flammability limits. As discussed in Chapter 2 (Section 6.2), the rich limits become much wider with increasing pressure (see Figs. 5.44 and 5.50 to be discussed later). As indicated by Fig. 5.50, the pressure does not appreciably affect the lean limits. This is especially valid for hydrocarbon–air mixtures. The change of slope at the upper (rich) limit in Fig. 5.50 is caused by the change of second-order reaction at low pressures to first-order reaction at high pressures.

For simple hydrocarbons such as ethane, propane, butane, and pentane, it appears that the rich limits extend linearly with increasing pressure. The lean limits, on the other hand, are at first extended slightly and approach asymptotic values thereafter as pressure is increased. A sketch of the above dependence is shown in Fig. 5.44. The measured flammability data⁴⁰ of natural gas–air mixtures are shown in Fig. 5.45. It is interesting to note that the limits shown in this figure are as wide at subatmospheric pressures as those at 1 atm. These low-pressure limits are sometimes called “flame propagation limits in a tube with specified diameter.”

It is useful to point out that the size of the test vessel has a nonnegligible effect on the relationship between pressure and flammability limits. As the size of the test vessel decreases, the effect of pressure on flammability limits becomes more

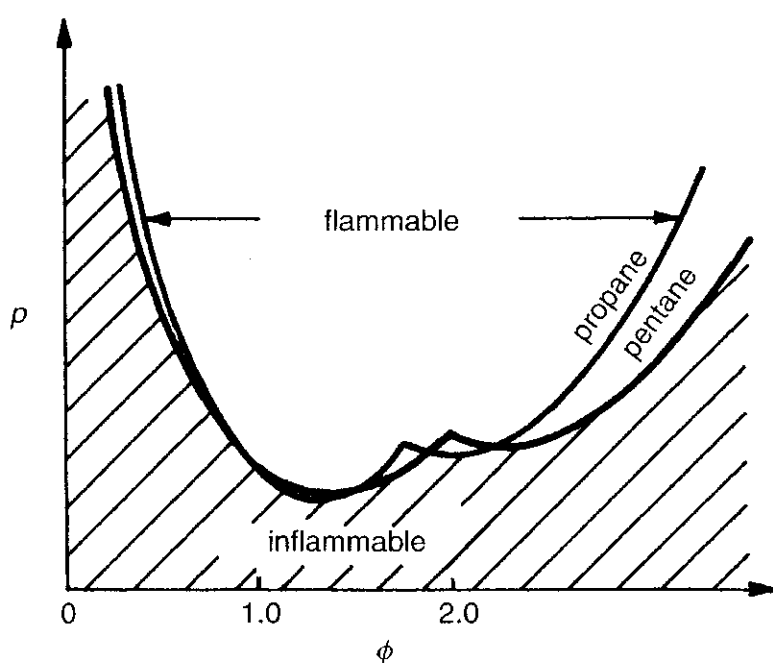


Figure 5.44 Dependence of flammability limits on pressure and stoichiometric ratio of hydrocarbon–air mixture.

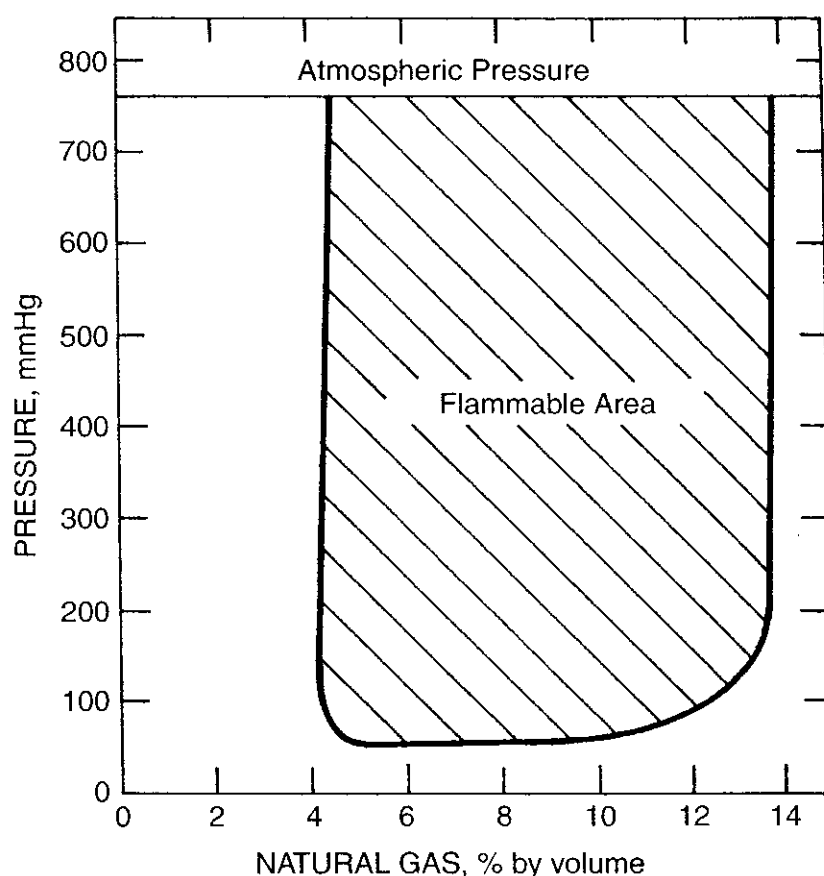


Figure 5.45 Flammable zone of natural gas–air mixture (adapted from Lewis and von Elbe,⁴⁰ based on the original work of Jones and Kennedy of Bureau of Mines, Report of Investigation No. 3798, 1945).

important; this is due to the quenching process, which is governed by the density or pressure level of the gaseous mixture. Similarly, as pressure is reduced, the mixture becomes more difficult to ignite unless the test vessel is increased to a larger size (or diameter). The minimum diameter of the test vessel is therefore found to increase with a decrease in pressure. This relationship is given by Eq. (5-158).

If the temperature is increased, the flammability limits will be broadened. That is, the lean limit will lie at a lower *F/O* equivalence ratio whereas the rich limit will lie at a higher one (Fig. 5.43b). It is observed experimentally that the limits vary linearly with temperature. For example, the lean limit of *n*-pentane drops from 1.53% in volume at room temperature to 1.22% at 572 K at a slope of 11.4×10^{-4} vol%/K. The rich limit increases at a steeper slope of 30.6×10^{-4} vol%/K. Hence, by raising the temperature of hydrocarbon–air mixture, the flammability limits become broader; nevertheless, the temperature effect on flammability limits is usually less significant than that of pressure.

8.3 Spalding's Theory of Flammability Limits and Flame Quenching

A theoretical approach of predicting the flammability limit trends was developed by Spalding.⁴⁸ This theory was supposed to be able to predict the following:

- a. The fact that below certain concentrations of combustible gas or oxygen, flame will be unable to propagate
- b. The lower limit concentration
- c. The burning velocity at the limit.

In his model, heat exchange between the gas and its solid surroundings is considered. It was demonstrated that combustible mixtures have, in general, two possible burning velocities. Only the upper one is stable in ordinary circumstances. At the inflammability limits, two burning velocities coincide; beyond the limits, they are just imaginary. Spalding claimed that the conclusions of the theory are independent of whether the reaction proceeds by a single step or by a chain mechanism. They are also independent of particular assumptions as to the dependence of reaction rate on concentration and temperature. It was also considered that the latter dependence should be steeper than that of the heat-transfer process.

In Spalding's mathematical model, a single-step forward reaction is considered:



The mass flow rate of the unburned mixture stream $A + B$ is assumed to maintain at a constant value of G in the positive x -direction. In case the species B is in excess, a part of unreacted B will exist. Even though B may exist in the product, it is still adequate to define C as the combustion product. The conservation equations under the one-dimensional steady-state assumption have the following forms:

Energy equation:

$$\frac{d}{dx} \left(\lambda \frac{dT}{dx} \right) - C_p G \frac{dT}{dx} + H_{r_A}^o \dot{R}_A = \dot{Q}_{\text{loss}} \quad (5-160)$$

Species equation:

$$\frac{d}{dx} \left(\frac{\lambda}{C_p} \frac{dY_A}{dx} \right) - G \frac{dY_A}{dx} - \dot{R}_A = 0 \quad (5-161)$$

Stoichiometric equation:

$$Y_{B_u} - Y_B = (Y_{A_u} - Y_A)r_{BA} \quad (5-162)$$

where G = total mass flux ($\text{g}/\text{s} \cdot \text{m}^2$) in x -direction

Y = mass fraction of component in mixture

\dot{R}_A = mass consumption rate of species A ($\text{g}/\text{m}^3 \cdot \text{s}$)

$H_{r_A}^o$ = standard heat of reaction of A (J/g of A)

\dot{Q}_{loss} = rate of heat loss per unit volume ($\text{J}/\text{s} \cdot \text{m}^3$)

r_{BA} = ratio of reacted amount of B to that of A (g/g)

λ = thermal conductivity ($\text{J}/\text{m} \cdot \text{s} \cdot \text{K}$)

The subscripts u and b denote completely unburned and completely burned situations, respectively.

For convenience, the following dimensionless forms are employed:

$$\tau = \frac{T - T_u}{T_b - T_u} \quad (5-163)$$

$$\xi \equiv \exp \left(C_p \frac{Gx}{\lambda} \right) \quad (5-164)$$

$$\alpha \equiv \frac{Y_A}{Y_{A_u}} \quad (5-165)$$

$$\lambda^+ = \frac{H_{r_A}^o \dot{R}_A^* \lambda_b}{(T_b - T_u)(C_p G)^2} \quad (5-166)$$

$$\phi = \frac{\lambda \dot{R}_A}{\lambda_b \dot{R}_A^*} \quad (5-167)$$

$$\psi = \frac{\lambda \dot{Q}_{\text{loss}}}{\lambda_b \dot{Q}_{\text{loss}}^*} \quad (5-168)$$

$$K = \frac{\dot{Q}_{\text{loss}}^*}{\dot{R}_A^* H_{r_A}^o} \quad (5-169)$$

where

\dot{R}_A^* is the value of \dot{R}_A when $T = T_b$ and $Y_A = Y_{A_u}$

\dot{Q}_{loss}^* is the value of \dot{Q}_{loss} at $T = T_b$

Upon substitutions, Eqs. (5-160) and (5-161) become two second-order ordinary differential equations:

$$\frac{d^2\tau}{d\xi^2} = -\frac{\lambda^+}{\xi^2}(\phi - K\psi) \quad (5-170)$$

$$\frac{d^2\alpha}{d\xi^2} = \frac{\lambda^+}{\xi^2}\phi \quad (5-171)$$

Here, ξ is a distorted space variable chosen so as to eliminate the first derivatives in Eqs. (5-160) and (5-161). From the definition of ξ , we have $\xi = 0$ corresponding to the cold unburned condition at $x \rightarrow -\infty$. Boundary conditions in terms of ξ are

$$\begin{aligned} \xi = 0 : \quad & \tau = 0, \quad \alpha = 1 \\ \xi = \infty : \quad & \frac{d\tau}{d\xi} = 0, \quad \alpha = 0 \text{ (assuming } B \text{ is in excess)} \end{aligned} \quad (5-172)$$

The question now is to find the eigenvalue λ^+ that satisfies these conditions. With λ^+ known, the burning mass flux G can be evaluated from Eq. (5-166). We shall consider two cases: $K \times \psi = 0$, corresponding to the adiabatic case, and $K \times \psi > 0$, corresponding to the nonadiabatic case.

Case I: $K \times \psi = 0$ (i.e., Zero Heat Loss)

Equations (5-170) and (5-171) become almost identical except for having opposite signs for the right-hand-side terms. Using the boundary conditions described by Eq. (5-172) and the definitions of τ and α given by Eqs. (5-163) and (5-165), τ and α can be related by the following algebraic equation:

$$\alpha + \tau = 1 \quad (5-173)$$

Therefore, only one of the two ordinary differential equations needs to be solved. The boundary condition that $\xi = \infty$ at $\tau = 1$ is somewhat inconvenient mathematically, since ξ approaches ∞ . Thus, a new boundary condition was taken by Spalding as

$$\xi = 1 : \quad \alpha = 0, \quad \frac{d\tau}{d\xi} = -\frac{d\alpha}{d\xi} = \left(\frac{d\tau}{d\xi} \right)_1 \quad (5-174)$$

This corresponds physically to supposing that an adiabatic porous catalyst plug is situated at $\xi = 1$ and reduces the concentration of species A to zero, with the result that it has the temperature $\tau = 1$ and there is a finite gradient at the catalyst surface. A set of solutions for τ versus ξ and α versus ξ is sketched in Fig. 5.46.

This catalyst plug postulation restricts the infinite domain to a finite domain with $0 < \xi \leq 1$. Solution of Eq. (5-170) yields a different profile of τ for each

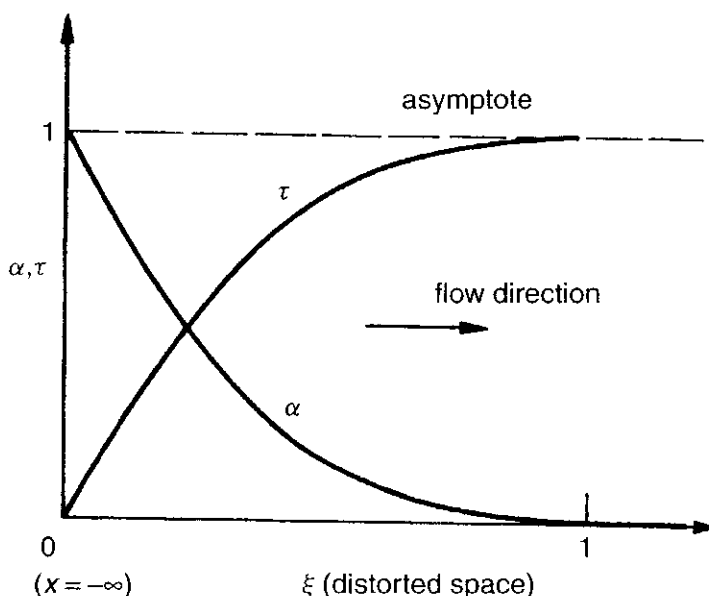


Figure 5.46 Calculated temperature and fuel concentration profiles in flame (adapted from Spalding⁴⁸).

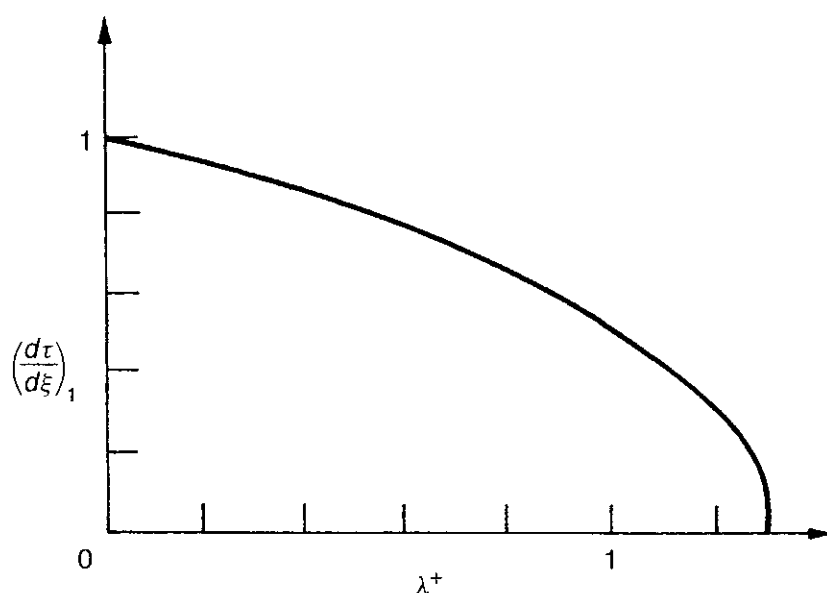


Figure 5.47 Relation between temperature gradient at catalyst plug and value of λ^+ for a particular flame (adapted from Spalding⁴⁸).

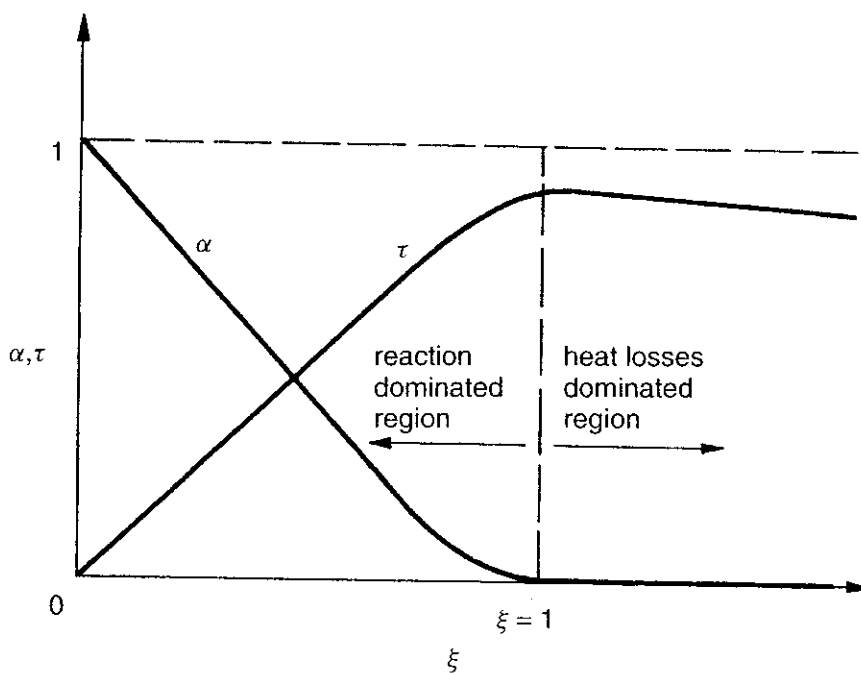


Figure 5.48 τ and α profiles in flame with heat losses from the burned gas (adapted from Spalding⁴⁸).

value of $(d\tau/d\xi)_1$. The required value of λ^+ for $(d\tau/d\xi)_1 = 0$ can then be obtained by extrapolating the curve in Fig. 5.47 to $(d\tau/d\xi)_1 = 0$.

Case II: $K \times \psi > 0$ (Heat Losses Considered)

The solution differs from Case I in that τ , after reaching a peak at $\xi = 1$, falls gradually to zero as ξ increases beyond the reaction zone (see Fig. 5.48). In this case, τ and α profiles are not similar; both Eqs. (5-170) and (5-171) must

be solved simultaneously. The line $\xi = 1$ serves to separate the region where reaction rate is dominant from that where heat losses are dominant.

In order to permit an analytical solution, attention was restricted to reacting gas mixtures characterized by

$$\phi = \alpha \tau^n \quad (5-175)$$

which signifies that the reaction rate is proportional to the concentration of A (fuel). According to Spalding, this is usually close to the truth for limit mixtures in which the other reactant, B , is in large excess. Usually, the value of temperature exponent n is between 6 and 15. The heat-loss parameter ψ was taken as another power law of temperature τ for the heat loss zone, for example,

$$\begin{aligned} \psi &= \tau^m && \text{for } \xi > 1 \\ \psi &= 0 && \text{for } \xi \leq 1 \end{aligned} \quad (5-176)$$

The exponent m varies between approximately 1 and 5 according to whether the heat transfer is predominantly by conduction or radiation. The heat-loss term ψ is neglected upstream of the line $\xi = 1$ in comparison with chemical reaction. This assumption will be justified later. In the following, we shall see that solutions are developed in two parts and patched at $\xi = 1$.

For the region $0 < \xi \leq 1$, we have

$$\frac{d^2\tau}{d\xi^2} = -\lambda^+ \frac{\alpha \tau^n}{\xi^2} \quad (5-177)$$

$$\frac{d^2\alpha}{d\xi^2} = \lambda^+ \frac{\alpha \tau^n}{\xi^2} \quad (5-178)$$

with boundary conditions

$$\begin{aligned} \xi = 0 : \quad \alpha &= 1, & \tau &= 0 \\ \xi = 1 : \quad \alpha &= 0, & \frac{d\alpha}{d\xi} &= 0 \\ \tau &= \tau_1, & \frac{d\tau}{d\xi} &= \left(\frac{d\tau}{d\xi} \right)_1 \end{aligned} \quad (5-179)$$

From the similarity of Eqs. (5-177) and (5-178), we can see that α and τ must be linearly related by

$$\alpha = -\tau + a\xi + b \quad (5-180)$$

One can easily verify this by differentiating Eq. (5-180) twice with respect to ξ and then comparing the results with Eqs. (5-177) and (5-178). It is interesting to note that the boundary conditions for α and τ are not similar. The coefficients a and b must be determined from the boundary conditions

$$\text{at } \xi = 0 : \quad 1 = 0 + 0 + b \quad \therefore b = 1$$

$$\text{at } \xi = 1 : \quad 0 = -\tau_1 + a + 1 \quad \therefore a = \tau_1 - 1$$

Substituting a and b into Eq. (5-180), we have

$$\alpha = 1 - \tau - (1 - \tau_1)\xi \quad (5-181)$$

After rearranging and differentiating with respect to ξ and setting $\xi = 1$, we have

$$\left(\frac{d\tau}{d\xi} \right)_1 = (\tau_1 - 1) \quad (5-182)$$

Multiplying Eq. (5-178) by $(d\tau/d\xi) d\xi$, we have

$$\frac{d\tau}{d\xi} \frac{d^2\alpha}{d\xi^2} d\xi = \lambda^+ \frac{\alpha \tau^n}{\xi^2} \frac{d\tau}{d\xi} d\xi$$

Substituting Eqs. (5-181) and (5-182) into the above equation and integrating from $\xi = 0$ to 1, we have

$$\begin{aligned} \int_0^1 \frac{d^2\alpha}{d\xi^2} (\tau_1 - 1) d\xi - \int_0^1 \frac{d\alpha}{d\xi} \frac{d^2\alpha}{d\xi^2} d\xi &= \lambda^+ \int_0^{\tau_1} \frac{[1 - \tau - (1 - \tau_1)\xi]}{\xi^2} \tau^n d\tau \\ (\tau_1 - 1) \int_{\xi=0}^{\xi=1} d \left(\frac{d\alpha}{d\xi} \right) - \frac{1}{2} \int_{\xi=0}^{\xi=1} d \left(\frac{d\alpha}{d\xi} \right)^2 &= \lambda^+ \int_0^{\tau_1} \frac{[1 - \tau - (1 - \tau_1)\xi]}{\xi^2} \tau^n d\tau \\ \therefore \lambda^+ &= - \frac{\frac{1}{2} \left[\left(\frac{d\alpha}{d\xi} \right)_1^2 - \left(\frac{d\alpha}{d\xi} \right)_0^2 \right] + (1 - \tau_1) \left[\left(\frac{d\alpha}{d\xi} \right)_1 - \left(\frac{d\alpha}{d\xi} \right)_0 \right]}{\int_0^{\tau_1} \frac{[1 - \tau - (1 - \tau_1)\xi]}{\xi^2} \tau^n d\tau} \end{aligned} \quad (5-183)$$

The value of n is so large that the reaction is confined to the upper temperature levels. This means that where the integrand in Eq. (5-183) is finite, ξ may be taken as unity without appreciable error. In the region beyond the small neighborhood of $\xi = 1$, the heat release term is nearly zero. From Eq. (5-178), we have

$$\left(\frac{d^2\alpha}{d\xi^2} \right) = 0 \quad \text{or} \quad \frac{d\alpha}{d\xi} = \text{constant}$$

This means that α is linear with respect to ξ . Connecting $\alpha = 1$ at $\xi = 0$ to $\alpha = 0$ at $\xi = 1$, a rough approximation for the slope at $\xi = 0$ can be given as

$$\left(\frac{d\alpha}{d\xi} \right)_0 \cong -1 \quad (5-184)$$

Also, since

$$\left(\frac{d\alpha}{d\xi} \right)_1 = 0 \quad (5-185)$$

and

$$\tau_1 - 1 = \left(\frac{d\tau}{d\xi} \right)_1 \cong 0 \quad (5-186)$$

Eq. (5-183), after the substitution of the above relationships, becomes

$$\lambda^+ \cong \frac{1}{2 \int_0^{\tau_1} (1-\tau) \tau^n d\tau} \cong \frac{1}{2 \int_0^{\tau_1} (\tau_1 - \tau) \tau^n d\tau} \quad (5-187)$$

Before evaluating the integral, it is worth noting that for the particular case when $\tau_1 = 1$, this is the well-known formula of Zel'dovich and Frank-Kamenetsky.^{9a,48} Evaluating Eq. (5-187) gives

$$\lambda^+ \cong \frac{(n+1)(n+2)}{2\tau_1^{(n+2)}} \quad (5-188)$$

When τ_1 is known, as for example when heat losses are zero so that $\tau_1 = 1$; thus λ^+ and the flame speed can be evaluated immediately. When heat losses are present, τ_1 must first be determined by considering the region beyond $\xi = 1$. Thus we have the following equation:

$$\xi \geq 1 : \quad \frac{d^2\tau}{d\xi^2} = \lambda^+ \frac{K \tau^m}{\xi^2} \quad (5-189)$$

The boundary conditions for the heat-loss region are

$$\xi = 1 : \quad \tau = \tau_1, \quad \frac{d\tau}{d\xi} = \left(\frac{d\tau}{d\xi} \right)_1 \quad (5-190)$$

$$\xi = +\infty : \quad \frac{d\tau}{d\xi} = 0 \quad (5-191)$$

Equation (5-189) has a simple solution if $m = 1$. However, if $\lambda^+ K$ is small, τ^m can be treated as a constant close to $\xi = 1$ (i.e., $\tau^m \cong \tau_1^m$) and upon integration, we have

$$\frac{d\tau}{d\xi} = -\lambda^+ K \frac{\tau_1^m}{\xi} \quad (5-192)$$

Putting $\xi = 1$ in Eq. (5-192) and postulating that the gradients on both sides of the $\xi = 1$ line are equal, we have from Eq. (5-182)

$$\lambda^+ K = \tau_1^{-m} (1 - \tau_1) \quad (5-193)$$

and so from Eq. (5-188) we have the required relations between K and τ_1 as

$$K = \frac{2\tau_1^{n+2-m}}{(n+1)(n+2)} (1 - \tau_1) \quad (5-194)$$

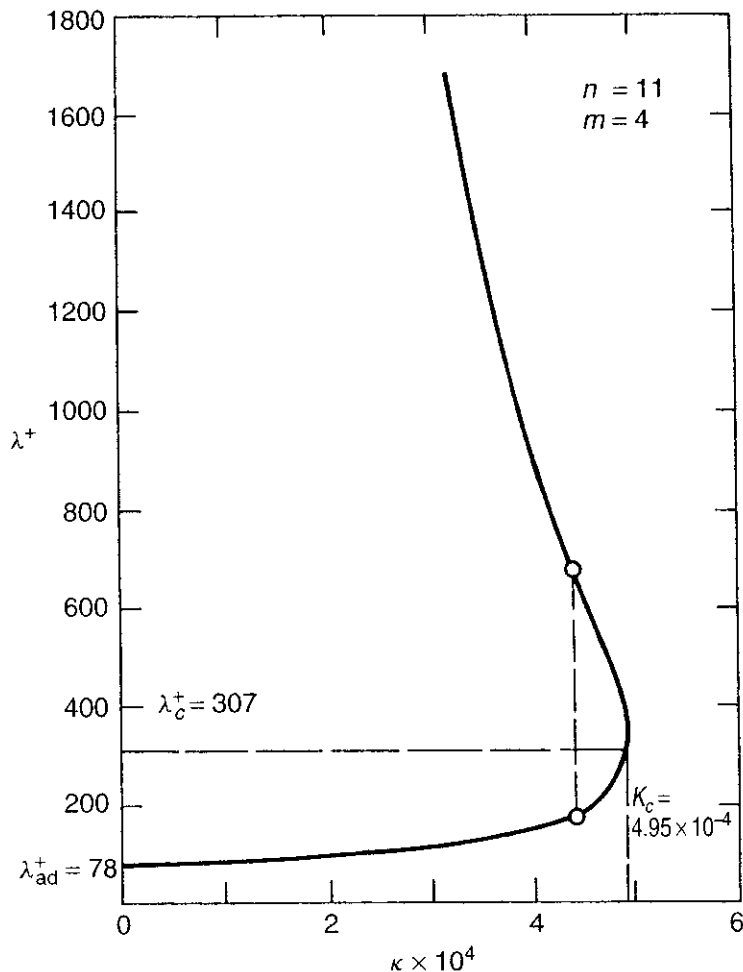


Figure 5.49 Relationship between λ^+ and K for a particular flame with $n = 11$ and $m = 4$ (after Spalding⁴⁸).

When K exceeds a critical value K_c , however, the τ_1 values are imaginary. A relation between K and λ^+ can be obtained by eliminating τ_1 from Eqs. (5-194) and (5-188). A relationship for $m = 4$, $n = 11$ is plotted in Fig. 5.49.

It can be seen that for any value of the heat-loss parameter less than K_c , two values exist for λ^+ and thus two possible flame speeds. If K exceeds K_c , however, there are no real values of λ^+ , which means no steadily propagating flame is possible. K_c therefore represents the magnitude of the ratio of heat-loss rate to chemical-reaction rate, which corresponds to the critical condition at the flammability limit. The magnitude of the flame speed at flammability limit $S_{L,c}$ can be obtained using Eqs. (5-166) and (5-169) leading to

$$S_{L,c} = \frac{1}{C_p \rho_u} \sqrt{\frac{H_{r_A}^o \dot{R}_{A_c}^* \lambda_b}{(T_b - T_u) \lambda_c^+}} = \frac{1}{C_p \rho_u} \sqrt{\frac{\lambda_b \dot{Q}_{\text{loss}}^*}{(T_b - T_u) K_c \lambda_c^+}} \quad (5-195)$$

For the particular flame under consideration, K_c and λ_c^+ are fixed. Their product, $K_c \lambda_c^+$, equals 0.169. For a weak hydrocarbon-air flame with an adiabatic temperature of 1500 K, a value of $\dot{Q}_{\text{loss}} = 0.1 \text{ cal}/(\text{cm}^3 \cdot \text{s})$ was reported by

Fishenden and Saunders⁴⁹ and used by Spalding.⁴⁸ Inserting the gas properties and the above value of $K_c \lambda_c^+$ into Eq. (5-195), the magnitude of $S_{L,c}$ is found to be 1.2 cm/s.

The effect of pressure on $S_{L,c}$ can also be seen from Eq. (5-195). Since both ρ_u and \dot{Q}_{loss} are proportional to P , we obtain the relation

$$S_{L,c} \propto \frac{1}{P^{1/2}} \propto P^{-1/2} \quad (5-196)$$

It is evident that $S_{L,c}$ does not depend on the order of reaction whereas S_L does depend on the order of reaction [see Eq. (5-7)]. This explains the generally observed trend in Fig. 5.50 of the boundary variation of the flammability region with respect to pressure. It is clear that in order to have flame propagation, we must have $S_L > S_{L,c}$ or $S_L/S_{L,c} > 1$:

$$\begin{aligned} \text{For } n = 1, \frac{S_L}{S_{L,c}} &\text{ is independent of } p \\ \text{For } n = 2, \frac{S_L}{S_{L,c}} &= \text{constant} \times \sqrt{p} \end{aligned} \quad (5-197)$$

Hence, the flammable region is widened with increasing pressure in the case of second-order reactions and maintains constant width for first-order reactions.

The above theory was also extended by Spalding to consider the wall-quenching effect as a flame travels through a stagnant gaseous mixture in a duct. Readers are referred to the original paper⁴⁸ for detailed discussions on this aspect.

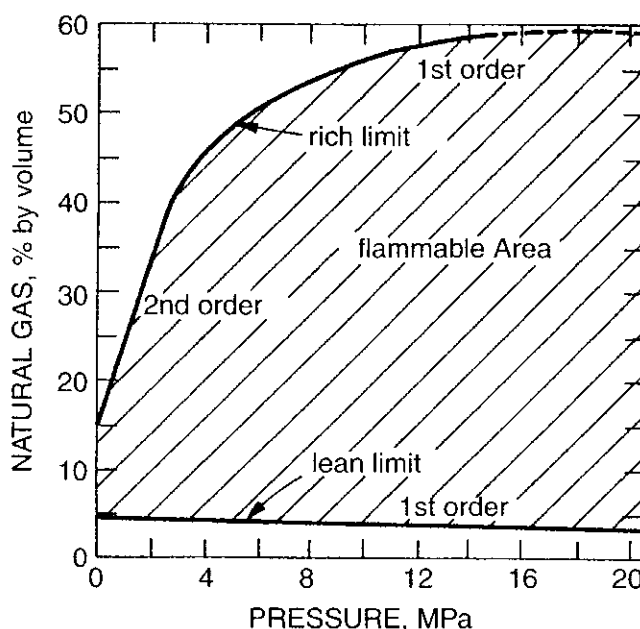


Figure 5.50 Dependence of the width of flammable region on pressure and the order of chemical reactions (after Lewis and von Elbe,⁴⁰ based on the original work of Jones, Kennedy, and Spolan of Bureau of Mines, Report of Investigation No. 4557, 1949).

8.4 Flame Structure near the Flammability Limits of Premixed Hydrogen–Oxygen Flames

He and Clavin¹⁰¹ made an extensive numerical investigation of the flammability limits and structure of adiabatic planar flames in premixed H₂/O₂ gases by considering detailed chemistry. The reaction mechanisms and the explosion limits of the H₂/O₂ system are given in Section 13 of Chapter 2. Explosion limits define the pressure and temperature boundaries for a specific mixture ratio of H₂ and O₂ and separate the regions of fast reaction for supporting “flame propagation” and slow reaction region for “no flame propagation.” A fuel/oxidizer mixture, within the explosion limits, is able to support premixed flame propagation for only a certain range of fuel concentration. Fuel concentrations outside of this range cannot propagate a flame for any significant distance from the ignition source before being quenched. The upper fuel concentration limit is called the rich flammability limit or the upper flammability limit. Likewise, the lower fuel concentration limit is called the lean flammability limit or the lower flammability limit. As the flammability limits are approached, the flame velocity decreases drastically and the flame is inevitably extinguished due to inherent instabilities caused by heat loss and flame stretching. In He and Clavin’s analysis,¹⁰¹ these effects were neglected, and therefore much smaller flame velocities near the flammability limits than the experimentally observed values were predicted based on these assumptions. Based on the important role of H atom in the reaction mechanism, the flammability limits can be described as the fuel/oxygen ratio (lean or rich) that corresponds to the balance of production and consumption rates of the H radical. A crossover temperature can be defined as the temperature at which the production rate of the hydrogen radical by chain branching balances the consumption rate of hydrogen radicals by chain terminating. The one-dimensional laminar-flame structure and the burning velocity were studied by them using direct numerical simulation close to the flammability limits. Their analysis focuses only on the major chemical reactions responsible for supporting flame propagation under adiabatic conditions.

Many studies have been conducted to analyze one-dimensional planar flame propagation with detailed chemistry for H₂/O₂ mixtures near stoichiometric conditions. However, very little research was conducted to analyze the flame structure near the flammability limits prior to their study. Part of the reason for this is that near the flammability limits the flame speed becomes significantly small, complicating the numerical analysis. Another reason is because the flame structure near the flammability limits has been observed experimentally to be multidimensional and transient, thus making the one-dimensional planar wave approximation questionable, if not totally invalid.

He and Clavin¹⁰¹ used a numerical method developed by Sermange^{102,103} and further improved by Ghilani and Larroutuou,¹⁰⁴ with the coupling of CHEMKIN¹⁰⁵ and TRANSPORT¹⁰⁶ codes. An adaptive mesh was implemented to determine flame structure. The chemical reaction scheme proposed by Warnatz¹⁰⁷ was adopted (see Table 5.9). Their numerical solution utilizes this full set of chemical reactions

Table 5.9 Reaction Mechanism of H₂/O₂ System, $k_f = AT^b \exp(-E_a/R_u T)$ (after He and Clavin,¹⁰¹ based on the proposed mechanism of Warnatz¹⁰⁷)

No.	Reaction	A	b	E	ΔH_{f298}^a
		(cm ³ /mol) ⁿ⁻¹ s ⁻¹		(cal/mol)	(cal/mol)
(1)	H + O ₂ = OH + O	2.00E + 14	0.00	16818	16769
(2)	O + H ₂ = H + OH	1.50E + 07	2.00	7553	1867
(3)	H ₂ + OH = H ₂ O + H	1.00E + 08	1.60	3300	-15020
(4)	OH + OH = H ₂ O + O	1.50E + 09	1.14	0	-16880
(5) ^b	H + O ₂ + M = HO ₂ + M	2.30E + 18	-0.80	0	-47105
(6)	H + HO ₂ = O ₂ + H ₂	2.50E + 13	0.00	694	-57103
(7)	H + HO ₂ = OH + OH	1.50E + 14	0.00	1005	-38467
(8)	H + HO ₂ = H ₂ O + O	3.00E + 13	0.00	1722	-55347
(9)	OH + HO ₂ = H ₂ O + O ₂	6.00E + 13	0.00	0	-72116
(10)	O + HO ₂ = OH + O ₂	2.00E + 13	0.00	0	-55236
(11) ^c	H ₂ + O ₂ = 2OH	1.00E + 14	0.00	69680	18636
(12)	H ₂ + M = 2H + M	2.23E + 14	0.00	95634	104206
(13)	O ₂ + M = 2O + M	1.81E + 18	-1.00	117612	119108
(14)	H + O + M = OH + M	1.00E + 16	0.00	0	-102339
(15)	H + OH + M = H ₂ O + M	2.20E + 22	-2.00	0	-119219
(16)	2HO ₂ = H ₂ O ₂ + O ₂	2.00E + 12	0.00	0	-42530
(17)	H ₂ + HO ₂ = H ₂ O ₂ + H	7.30E + 11	0.00	18684	14573
(18)	H ₂ O ₂ + M = 2OH + M	3.00E + 17	0.00	45455	51166
(19)	H ₂ O ₂ + H = H ₂ O + OH	1.00E + 13	0.00	3588	-68053
(20)	H ₂ O ₂ + O = OH + HO ₂	2.80E + 13	0.00	6411	-12706
(21)	H ₂ O ₂ + OH = H ₂ O + HO ₂	7.00E + 12	0.00	1435	-29586

^aCalculated according to JANAF Tables.^bC_M = C_{H₂} + 0.4C_{O₂} + 6.5C_{H₂O} based on Warnatz.¹⁰⁷^cBased on Kordylewski and Scott.¹⁰⁸

to analyze the dependence of flame velocity on unburned mixture temperature, ambient pressure, and equivalence ratio.

The initial temperature dependence of the burning velocity is shown in Fig. 5.51 for four mixtures ($\phi = 0.09, 0.5, 1$, and 4) at $p = 1$ atm, compared with the numerical results of Warnatz (broken line)¹⁰⁷ and the experimental results of Edse and Lawrence¹⁰⁹ (•) for $\phi = 1$. The agreement is very good. For the stoichiometric mixture, the T_u dependence of the burning mass flux is weak (see Fig. 5.52b). For this case, the flame temperature is high ($T_f \sim 2500$ K), the radical concentrations are large, and the heat release rate is essentially controlled by T_f , which is not very sensitive to T_u . However, this is not true near the flammability limits where the initial temperature T_u of the cold mixture could strongly influence the burning mass flux (see Fig. 5.52b for $\phi = 0.09$).

Figure 5.52a shows the pressure dependence of the burning velocity at $T_u = 100$ K for three equivalence ratios ($\phi = 0.5, 1$, and 4). Close to stoichiometric

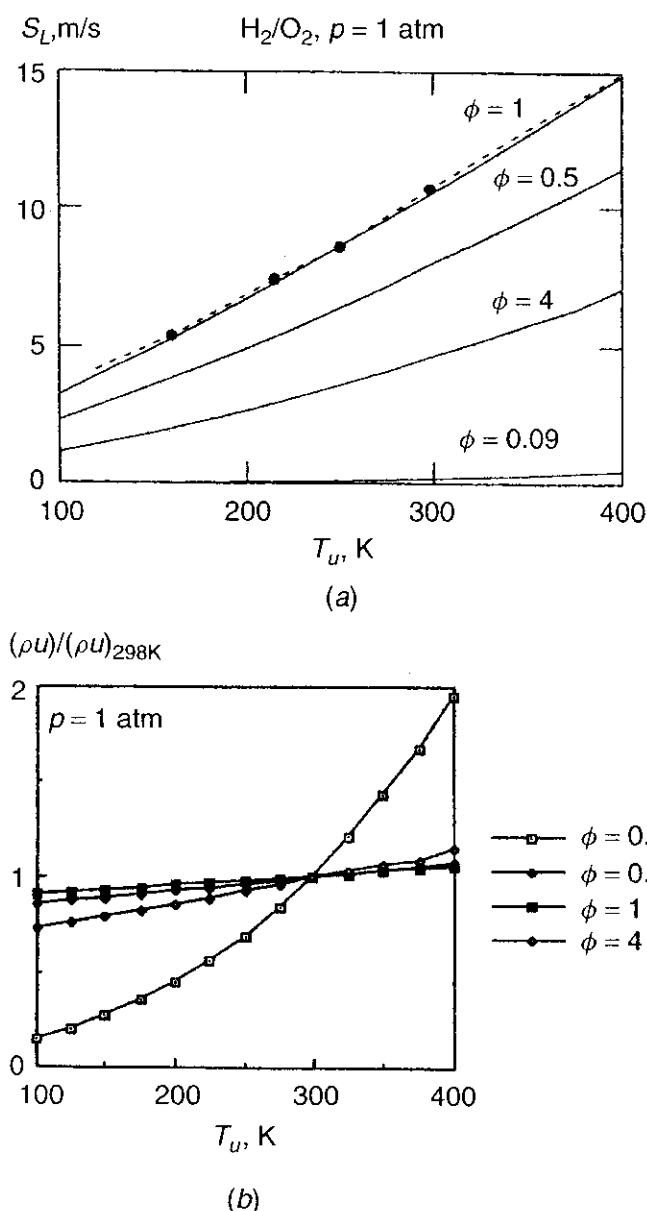


Figure 5.51 (a) Temperature dependence of burning velocity obtained numerically with detailed chemistry (solid line) for H_2/O_2 mixtures with different equivalence ratios, compared with the numerical results of Warnatz (broken line)¹⁰⁷ and the experimental results of Edse and Lawrence¹⁰⁹ (\bullet) for $\phi = 1$. (b) Reduced mass flux as a function of initial temperature T_u for different H_2/O_2 mixtures, $\phi = 0.09, 0.5, 1$, and 4 (after He and Clavin¹⁰¹).

mixtures, the burning velocity increases with the pressure between 0.1 and 10 atm. But this tendency is inverted when the flammability limits are approached because the chain-breaking reaction 5f of Table 5.9 becomes increasingly important as p increases. When the H_2/O_2 mixture is sufficiently diluted by helium, the pressure dependence shows a transition in the propagation regimes. A relatively sharp transition occurs between 8 and 12 atm (see Fig. 5.52b).

Figure 5.53 shows the burning velocity of pressure dependence of H_2/O_2 mixtures versus the mole fraction of H_2 at $T_u = 100 \text{ K}$ for three pressures ($p = 0.2, 1$, and 2 atm). The maximum velocity is located slightly on the hydrogen-rich side; this observation is the same as the H_2/O_2 flames with initial temperatures

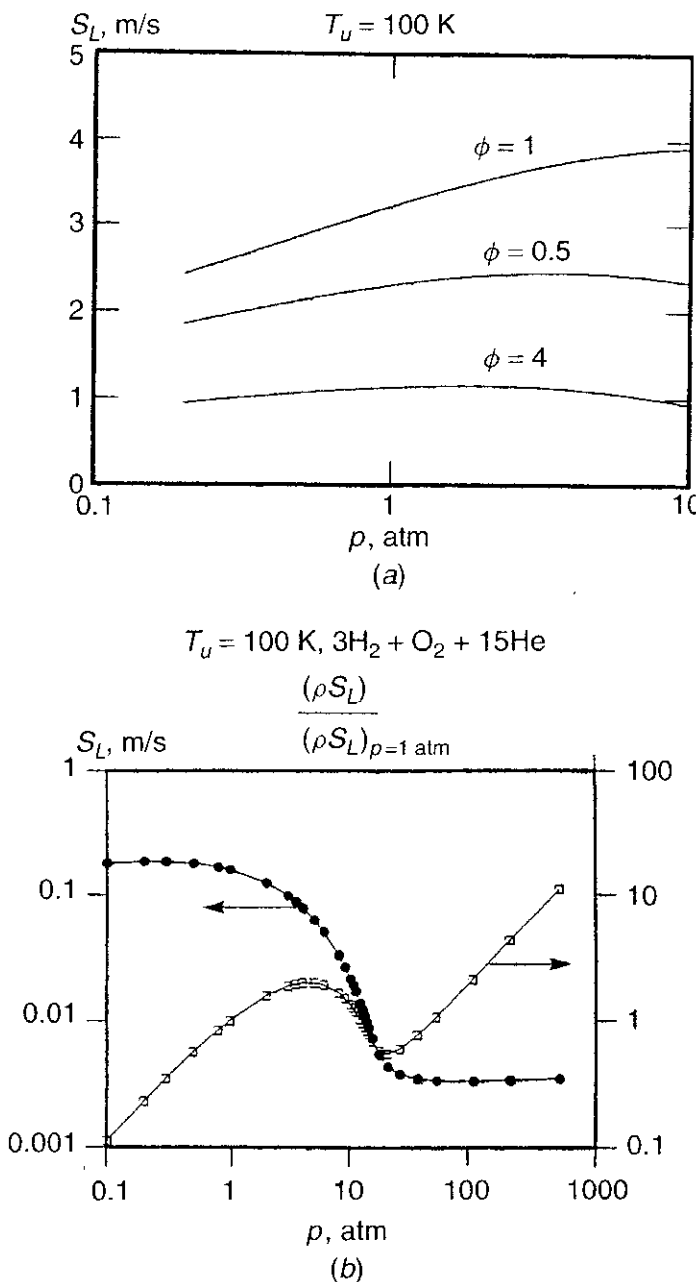


Figure 5.52 (a) Pressure dependence of burning velocity for H_2/O_2 mixtures with different equivalence ratios, $\phi = 0.5$, 1, and 4 at $T_u = 100$ K. (b) Pressure dependence of burning velocity and the mass flux for the mixture $3\text{H}_2 + \text{O}_2 + 15\text{He}$ at $T_u = 100$ K (after He and Clavin¹⁰¹).

equal to the room temperature. For the scale of Fig. 5.53, the flammability limits seem well defined. But in He and Clavin's computation,¹⁰¹ zero burning velocity was never achieved. As shown in Fig. 5.54, their minimum burning velocities are on the order of 1 mm/s (so low that any external perturbation could quench the flame). This figure shows the burning velocity variations near the rich and lean flammability limits at $T_u = 298$ K and $p = 0.2$, 1, and 2 atm. According to Lewis and von Elbe,¹¹⁰ the H_2 -rich flammability limit that is observed experimentally corresponds to $X_{\text{H}_2} \approx 0.94$. The lean flammability limit observed at microgravity condition by Ronney¹¹¹ is $X_{\text{H}_2} \approx 0.06$. He and Clavin claimed that

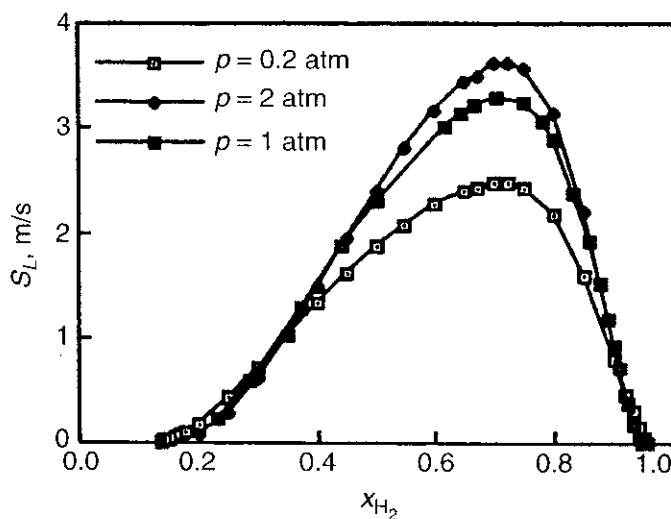


Figure 5.53 Equivalence ratio dependence of burning velocity of H_2/O_2 mixtures at different pressures $p = 0.2, 1$, and 2 atm and at $T_u = 100 \text{ K}$ (after He and Clavin¹⁰¹).

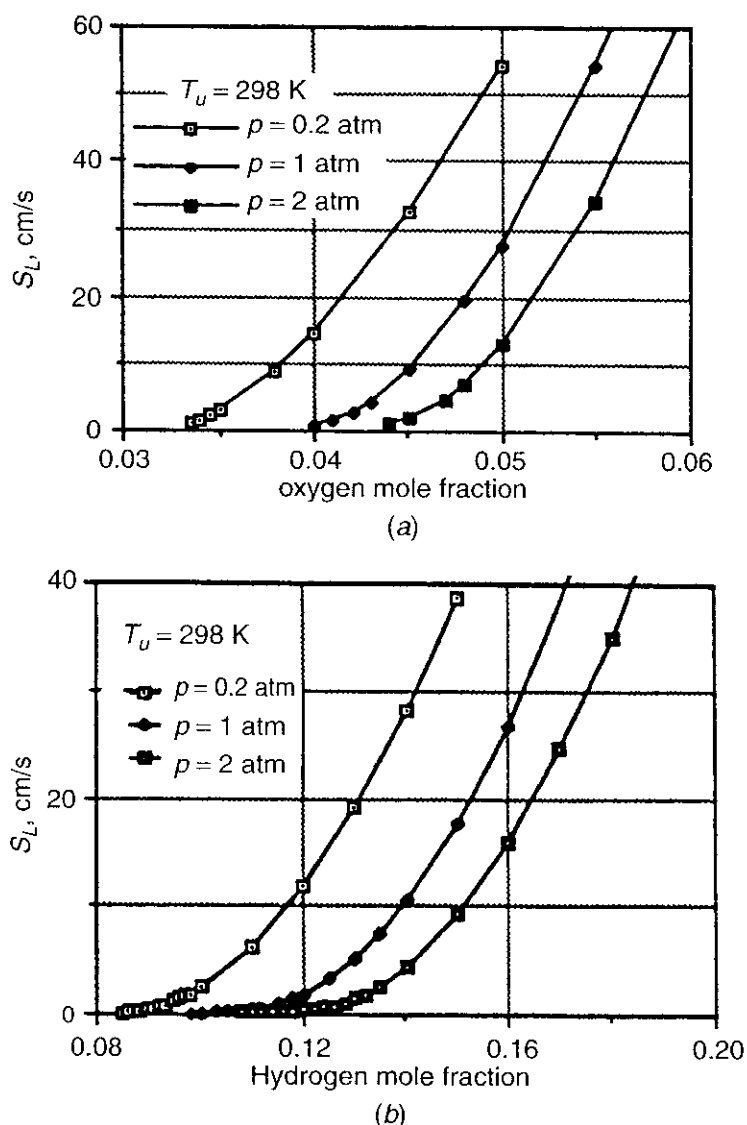


Figure 5.54 (a) Burning velocity of H_2/O_2 mixtures near rich flammability limits at $T_u = 298 \text{ K}$ and $p = 0.2, 1$, and 2 atm . (b) Burning velocity of H_2/O_2 mixtures near lean flammability limits at $T_u = 298 \text{ K}$ and $p = 0.2, 1$, and 2 atm (after He and Clavin¹⁰¹).

Table 5.10 Global Activation Energy of H₂/O₂ Mixtures^a at T_u = 298 (after He and Clavin¹⁰¹)

X _{H₂}	E _a (p = 0.2 atm)	E _a (p = 1 atm)	E _a (p = 2 atm)	T _f (K)
0.15	14.75	24.30	34.11	1432
0.94	12.70	15.2	21.07	1293
0.952	12.91	30.12	47.05	1100

^aThe unit of activation energy is kcal/mol.

typical kinetic effects of the flammability limits must be coupled with preferential diffusion mechanisms in order to represent the observed phenomena at the lean flammability limit. Even though their results did not predict exactly the flammability limits, their study using detailed chemical kinetic considerations aids in the understanding of how the flame velocity is affected by changes in the initial unburned mixture temperature, system pressure, and the equivalence ratio.

The burning velocity of the H₂/O₂ flame is related to the global activation energy and the adiabatic flame temperature of burned gases by

$$S_L \sim \exp\left(-\frac{E_a}{2R_u T_f}\right) \quad (5-198)$$

The numerical results of He and Clavin¹⁰¹ are listed in Table 5.10. It can be seen that the activation energy increases as the flammability limits are approached. For H₂/O₂/N₂ mixtures near the flammability limits, the global activation energy measured by Mitani and Williams¹¹² at T_u = 298 K and p = 1 atm is 40 kcal/mol for H₂-rich mixtures and 24 kcal/mol for lean mixtures. Considering the difference with the experimental situation, the agreement between the numerical values of Table 5.10 and these experimental data can be considered as satisfactory.

REFERENCES

1. I. Glassman, *Combustion*, Academic Press, New York, 1987.
2. M. W. Evans, "Current Theoretical Concepts of Steady-State Flame Propagation," *Chem. Rev.* **51**, 363–429 (1952).
3. E. Mallard and H. L. LeChatelier, *Ann. Mines* **4**, 379 (1883).
4. G. Damköhler, *Z. Elektrochem.* **46**, 601 (1940); translation, N.A.C.A. Tech. Memo. 1112.
5. E. Bartholomé, *Naturwissenschaften* **36**, 171 (1949); **36**, 206 (1949).
6. H. W. Emmons, J. A. Harr, and P. Strong, *Thermal Flame Propagation*, Computation Laboratory of Harvard University, December 1949.
7. K. Bechert, *Z. Naturforsch.* **3A**, 584 (1948); *Portugaliae Phys.* **3**, 29 (1949); *Ann. Physik* **6**(4), 191 (1949); *Naturwissenschaften* **37**, 112 (1950).

8. B. Lewis and G. von Elbe, *J. Chem. Phys.* **2**, 537 (1934).
- 9a. Ya. B. Zel'dovich and D. A. Frank-Kamenetsky, *Compt. Rend. Acad. Sci. USSR* **19**, 693 (1938).
- 9b. Ya. B. Zel'dovich and N. Semenov, *J. Expt. Theoret. Phys. USSR* **10**, 1116 (1940); translation, N.A.C.A. Tech. Memo. 1084.
- 9c. Ya. B. Zel'dovich, *J. Phys. Chem. USSR* **22**(1) (1948).
10. S. F. Boys and J. Corner, *Proc. Roy. Soc. London* **A197**, 90 (1949).
- 11a. J. O. Hirschfelder and C. F. Curtiss, *Third Symposium on Combustion, Flame, and Explosion Phenomena*, p. 121, The Williams and Wilkins Company, Baltimore, 1949.
- 11b. J. O. Hirschfelder and C. F. Curtiss, *J. Chem. Phys.* **17**, 1076 (1949).
12. Th. von Karman and S. S. Penner, *Selected Combustion Problems, Fundamentals, and Aeronautical Applications*, AGARD, Butterworths Scientific Publications, London, 1954, pp. 5-41.
- 13a. C. Tanford and R. N. Pease, *J. Chem. Phys.* **15**, 431 (1947).
- 13b. C. Tanford, *J. Chem. Phys.* **15**, 433 (1947).
- 13c. C. Tanford and R. N. Pease, *J. Chem. Phys.* **15**, 861 (1947).
- 14a. A. Van Tiggelen, *Bull. Soc. Chim. Belg.* **55**, 202 (1946).
- 14b. A. Van Tiggelen, *Bull. Soc. Chim. Belg.* **58**, 259 (1949).
15. N. Manson, *J. Chem. Phys.* **17**, 837 (1949).
- 16a. A. G. Gaydon and H. G. Wolfhard, *Proc. Roy. Soc. London* **A194**, 169 (1948).
- 16b. A. G. Gaydon and H. G. Wolfhard, *Fuel* **29**, 15 (1950).
17. G. Jahn, *Der Zündvorgang in Gasgemischen*, Oldenbourg, Berlin, 1942.
18. G. L. Dugger, *J. Am. Chem. Soc.* **73**, 2308 (1951).
19. D. M. Simon, *J. Am. Chem. Soc.* **73**, 422 (1951).
20. M. Gerstein, O. Levine, and E. L. Wong, *J. Am. Chem. Soc.* **73**, 418 (1951).
21. J. M. Heimerl and T. P. Coffee, "The Detailed Modeling of Premixed, Laminar, Steady-State Flames. I. Ozone," *Combust. and Flame* **39**, 301-315 (1980).
22. J. M. Heimerl and T. P. Coffee, "The Unimolecular Ozone Decomposition Reaction," *Combust. and Flame* **35**, 117-123 (1979).
23. R. F. Hampson (Ed.), "Survey of Photochemical Rate Data for Twenty-Eight Reactions of Interest in Atmospheric Chemistry," *J. Phys. Chem. Ref. Data* **2**, 267-312 (1973).
24. H. S. Johnston, *Gas Phase Reaction Kinetics of Neutral Oxygen Species*, NSRDS-NBS-20, September 1968.
25. D. L. Baulch, D. D. Drysdale, J. Duxbury, and S. J. Grant, *Evaluated Kinetic Data for High Temperature Reactions 3, Homogeneous Gas Phase Reactions of the O₂/O₃ System, the CO/O₂/H₂ System and of Sulphur Containing Species*, Butterworths, Boston, 1976.
26. B. K. Madsen and R. F. Sincovec, "PDECOL: General Collocation Software for Partial Differential Equations," Preprint UCRL-78263 (Rev 1), Lawrence Livermore Laboratory, 1977.
27. C. de Boor, "Package for Calculating with B-Splines," *SIAM J. Numer. Anal.* **14**, 441-472 (1977).

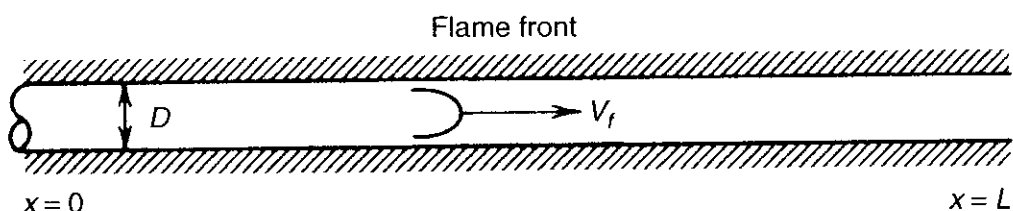
28. A. G. Streng and A. V. Grosse, "The Ozone to Oxygen Flame," *Sixth Symp. (Intl.) on Combust.*, Reinhold, New York, 1957, pp. 264–273.
29. J. Warnatz, *Berechnung der Flammengeschwindigkeit und der Struktur von laminaren flachen Flammen*, Habilitationsschrift, Darmstadt, 1977.
30. A. G. Gaydon and H. G. Wolfhard, *Flames: Their Structure, Radiation and Temperature*, 2nd ed., Chapman and Hall, London, 1960.
31. F. J. Weinberg, *Optics of Flames*, Butterworths, London, 1963.
32. E. Hartmann, thesis, Karlsruhe, 1931.
33. A. M. Kanury, *Introduction to Combustion Phenomena*, Chapter 8, Gordon and Breach, New York, 1975.
34. T. W. Reynolds and M. Gerstein, "Influence of Molecular Structure of Hydrocarbons on Rate of Flame Propagation," *Third Symp. (Intl.) on Combustion*, 1949, pp. 190–194.
35. B. Lewis, "Discussion," *Selected Combustion Problems*, AGARD, Butterworths, London, 1954, p. 177.
36. G. L. Dugger, S. Heimel, and R. C. Weast, *Ind. and Engr. Chem.* **47**, 114 (1955).
37. E. Bartholomé and H. Sachsse, *Z. Electrochem.* **53**, 183 (1949).
38. W. H. Clingman, Jr., R. S. Brokaw, and R. N. Pease, *Fourth Symp. (Intl.) on Combust.*, Combustion Inst., Pittsburgh, 1953, p. 310.
39. J. M. Beer and N. A. Chigier, *Combustion Aerodynamics*, Applied Science Publishers, London, 1974.
40. B. Lewis and G. von Elbe, *Combustion, Flames and Explosions of Gases*, 2nd ed., Chapter V, Academic Press, New York, 1961.
41. J. Powling, *Fuel* **28**, 25 (1949).
42. D. B. Spalding and J. P. Botha, *Proc. Roy. Soc. London A* **225**, 71 (1954).
43. A. L. Berlad and A. E. Potter, "Relation of Boundary Velocity Gradient for Flashback to Burning Velocity and Quenching Distance," *Combust. and Flame* **1**(1), 127–128 (1957).
44. M. Gerstein, "Review of Some Recent Combustion Experiments," *Third AGARD Symp.*, 1958, pp. 307–332.
45. M. L. Smith and K. W. Stinson, *Fuels and Combustion*, McGraw-Hill, New York, 1952.
46. A. M. Kanury, *Introduction to Combustion Phenomenon*, Chapter 4, Gordon and Breach Science Publishers, New York, 1975.
47. NACA Report 1300, "Basic Considerations in the Combustion of Hydrocarbon Fuels in Air," National Advisory Committee for Aeronautics, 1957.
48. D. B. Spalding, "A Theory of Inflammability Limits and Flame Quenching," *Proc. Roy. Soc. London A* **240**, 83–100 (1957).
49. M. Fishenden and O. A. Saunders, *Introduction to Heat Transfer*, Oxford University Press, Oxford, 1950, p. 21.
50. A. C. Eckbreth, *Laser Diagnostics for Combustion Temperature and Species*, 2nd ed., in W. A. Sirignano, ed., Combustion Science and Technology Book Series Vol. 3, Gordon and Breach, 1996.
51. A. P. Thorne, *Spectrophysics*, 2nd ed., Chapman and Hall, London/New York, 1988.

52. K. K. Kuo and T. P. Parr (eds.), *Non-Intrusive Combustion Diagnostics*, Begell House, Inc., 1994.
53. J. Warnatz, U. Maas, and R. W. Dibble, *Combustion*, 2nd ed., Springer, 1999.
54. R. J. Kee, J. F. Grcar, M. D. Smooke, and J. A. Miller, "A FORTRAN Program for Modeling Steady Laminar One-Dimensional Premixed Flames," Sandia National Laboratories, December, 1985.
55. J. Warnatz, "Concentration-, Pressure-, and Temperature Dependence of the Flame Velocity in the Hydrogen-Oxygen-Nitrogen Mixtures," *Combust. Sci. Tech.* **26**, 203 (1981).
56. T. Lu, Y. Ju, and C. K. Law, "Complex CSP for Chemistry Reduction and Analysis," *Combust. and Flame* **126**, 1445–1455 (2001).
57. B. Karlovitz, D. W. Denniston, Jr., D. H. Knappschafer, and F. E. Wells, *Fourth Symp. (Intl.) on Combustion*, The Combustion Institute, 1953, p. 613.
58. G. H. Markstein, *Nonsteady Flame Propagation*, Pergamon Press, Oxford, 1964.
59. J. D. Buckmaster, *Acta Astronautica* **6**, 741 (1979).
60. M. Matalon, *Combust. Sci. Tech.* **31**, 169 (1983).
61. S. H. Chung and C. K. Law, "An Invariant Derivation of Flame Stretch," *Combust. and Flame* **55**, 123–125 (1984).
62. S. H. Chung and C. K. Law, "An Integral Analysis of the Structure and Propagation of Stretched Premixed Flames," *Combust. and Flame* **72**, 325–336 (1988).
63. C. K. Law, Dynamics of Stretched Flames, *Twenty-Second Symp. (Intl.) on Combust.*, The Combustion Institute, 1988, pp. 1381–1402.
64. S. M. Candel and T. J. Poinsot, "Flame Stretch and the Balance Equation for the Flame Area," *Combust. Sci. Tech.* **70**, 1–15 (1990).
65. D. R. Dowdy, D. B. Smith, S. C. Taylor, and A. Williams, "The Use of Expanding Spherical Flames to Determine Burning Velocities and Stretch Effects in Hydrogen/Air Mixtures," *23rd Symp. (Intl.) on Combust.*, 1990, pp. 325–332.
66. P. Clavin, *Prog. Energy Combust. Sci.* **11**, 1 (1985).
67. M. Matalon and B. J. Matkowsky, *J. Fluid Mech.* **124**, 239 (1982).
68. J. Warnatz and N. Peters, *Prog. Astron. and Aeronaut.* **95**, 61 (1984).
69. B. Rogg, *Combust. and Flame* **73**, 45 (1988).
70. G. Dixon-Lewis, *Combust. Sci. Tech.* **43**, 1 (1983).
71. L.-K. Tseng, M. A. Ismail, and G. M. Faeth, "Laminar Burning Velocities and Markstein Numbers of Hydrocarbons/Air Flames," *Combust. and Flame* **95**, 410–426 (1993).
72. S. Kwon, L.-K. Tseng, and G. M. Faeth, *Combust. and Flame* **90**, 230–246 (1992).
73. R. A. Strehlow and L. D. Savage, *Combust. and Flame* **31**, 209–211 (1978).
74. A. Palm-Leis and R. A. Strehlow, *Combust. and Flame* **13**, 111–129 (1969).
75. S. Kwon and G. M. Faeth, *24th Symp. (Intl.) on Combust.*, 1992, p. 451.
76. S. C. Taylor, Ph.D. thesis, University of Leeds, Leeds, 1991.
77. C. K. Law, D. L. Zhu, and G. Yu, *21st Symp. (Intl.) on Combust.*, 1986, p. 1419.
78. I. Yamaoka and H. Tsuji, *20th Symp. (Intl.) on Combust.*, 1984, p. 1883.
79. T. G. Scholte and P. B. Vaags, *Combust. and Flame* **3**, 495–501 (1959).
80. J. W. Anderson and R. S. Fein, *J. of Chem. Physics* **17**, 1268–1273 (1949).

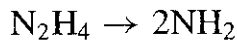
81. K. L. Gray, J. W. Linnett, and C. E. Mellish, *Trans. Farad. Soc.* **48**, 115 (1952).
82. M. E. Harris, J. Grumer, G. von Elbe, and B. Lewis, 3rd Symp. on Combust., Flame and Explosion Phenomena, Williams & Wilkins, Baltimore, 1949, p. 80.
83. A. Egerton and S. K. Thabet, *Proc. Roy. Soc. London* **A211**, 445–471 (1952).
84. G. N. Badami and A. Egerton, *Proc. Roy. Soc. London* **A228**, 297–332 (1955).
85. R. M. Fristrom, *Phys. Fluid*, **8**, 273–280 (1965).
86. F. N. Egolfopoulos and C. K. Law, 23rd Symp. (Intl.) on Combust., 1990, pp. 333–340.
87. U. Maas and J. Warnatz, *Combust. and Flame* **74**, 53 (1988).
88. G. Dixon-Lewis, *Proc. Roy. Soc. London* **A330**, 219 (1972).
89. P. Glarborg, J. A. Miller, and R. J. Kee, *Combust. and Flame* **65**, 177 (1986).
90. W. Tsang and R. F. Hampson, *J. Physical Chem. Ref. Data* **15**, 1087 (1986).
91. R. A. Yetter, F. L. Dryer, and H. Rabitz, “A Comprehensive Reaction Mechanism for Carbon Monoxide/Hydrogen/Oxygen Kinetics,” *Combust. Sci. Tech.* **79**, 97–128 (1991).
92. K.-J. Hsu, S. M. Anderson, J. L. Durant, and F. J. Kaufman, *Intl. Phys. Chem.* **93**, 1018 (1989).
93. M. W. Slack, *Combust. and Flame* **28**, 241 (1977).
94. J. Warnatz, 24th Symp. (Intl.) on Combust., 1993, p. 553.
95. M. Metghalchi and J. C. Keck, *Combust. and Flame* **48**, 191–210 (1982).
96. K. Wohl, N. M. Kapp, and C. Gazley, 3rd Symp. (Intl.) on Combust., 1949, pp. 1–16.
97. G. L. Borman and K. W. Ragland, *Combustion Engineering*, McGraw-Hill, Chapter 5, 1998.
98. S. T. Lee and J. S. T’ien, *Combust. and Flame* **48**, 273–285 (1982).
99. F. A. Williams, *Combustion Theory*, Addison Wesley, 1965, pp. 191–196.
100. F. A. Williams, *Combustion Theory*, 2nd ed., Chapter 8, Addison Wesley, 1985.
101. L. He and P. Clavin, *Combust. and Flame* **93**, 391–407 (1993).
102. M. Sermange, *Proceedings of the Symp. on Numerical Simulation of Combust. Phenomena*, INRIA, May 1985, Springer Verlag, New York, 1985.
103. M. Sermange, *Appl. Math. Opt.* **14**, 131–154 (1986).
104. M. Ghilani and B. Larroutuou, *Mod. Math Anal.* **25**, 67 (1991).
105. R. J. Kee, J. A. Miller, and T. H. Jeff, Report No. SAND 80–8003, Sandia National Laboratories, 1980.
106. R. J. Kee, J. Warnatz, and J. N. Miller, Report No. SAND 83–8209, Sandia National Laboratories, 1983.
107. J. Warnatz, in W. C. Gardiner *Combustion Chemistry*, Springer Verlag, New York, 1984.
108. W. Kordylewski and S. K. Scott, *Combust. and Flame* **57**, 127–139 (1984).
109. R. Edse and J. R. Lawrence, *Combust. and Flame* **13**, 479 (1969).
110. B. Lewis and G. von Elbe, *Combustion, Flames and Explosions of Gases*, 3rd ed., Academic Press, New York, 1987.
111. P. D. Ronney, *Combust. and Flame* **82**, 1 (1990).
112. T. Mitani and F. A. Williams, *Combust. and Flame* **39**, 169–190 (1980).

HOMEWORK

1. A long cylindrical tube of length L and diameter D is initially filled with a premixed combustible gaseous mixture of methane and oxygen. Before ignition, the mixture is stagnant with a pressure of 1 atm and a temperature of 298 K. Ignition at the left end of the tube is achieved by a spark. The flame front then moves toward the right. If the heat loss to the tube wall is *not* negligible, the flame front will not be a planar surface. The shape of the flame front is approximately parabolic, as shown in the following figure:

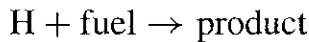


- (a) If we are interested in studying the transient flame propagation process and the detailed combustion-wave structure, list the assumptions you would make in order to formulate this problem.
 - (b) Give the governing equations.
 - (c) What chemical reaction equations should you consider in order to provide sufficient information for the source terms in your governing equations?
 - (d) Give initial and boundary conditions necessary to complete the model.
 - (e) What kind of empirical inputs and/or correlations are needed to complete the formulation?
 - (f) Sketch your anticipated results for the following:
 - (i) Axial temperature distributions at various times along the centerline of the tube
 - (ii) Axial concentration distributions at various times along the centerline of the tube
 - (iii) Radial temperature and concentration profiles near the flame front
 - (g) If the tube diameter becomes very small, what will happen to the flame propagation process?
2. A numerical analysis is to be done for a laminar premixed flame in a Bunsen burner to predict the flashback characteristics of a stoichiometric mixture of air and methane. Give the governing equations and initial and boundary conditions required to solve the problem. List all assumptions.
3. Consider the following one-step hydrazine decomposition reaction



in a laminar flame. Formulate the governing equations for species and temperature, and solve for the laminar burning velocity as the eigenvalue of the problem.

4. A gas mixture is contained in a soap bubble and ignited by a spark so that a spherical flame spreads radially. It is assumed that the soap bubble can expand. The growth of a flame front along a radius is followed by some photographic means. Relate the velocity of the flame front as determined from the photographs to the laminar-flame speed. If this method were used to measure flame speeds, what would you consider its advantages and disadvantages?
 5. In each of the cases below, properly order the flame speeds:
 - (a) Stoichiometric H₂ with
 - 21% O₂-79% He
 - 21% O₂-79% N₂
 - 21% O₂-70% Ar
 - (b) Wet CO-O₂ and dry CO-O₂, both at the same mixture ratio
 - (c) A monopropellant decomposition flame and a hydrocarbon-oxygen flame
 - (d) A hydrocarbon-air flame at high pressure and the same flame at low pressure
 6. A constant-volume spherical combustion chamber of radius R is filled initially with premixed combustible gaseous mixture. At time zero, a spark is produced at the center of the combustion chamber, and a spherical flame propagates radially outward. If the instantaneous radius of the flame is r , derive the laminar-flame speed given by Eq. (5-2), of which the instantaneous pressure is measured from a pressure transducer mounted on the wall of a spherical combustion chamber.
- (Hint: The compression of unburned gas by the burned gas can be considered to be adiabatic.)*
7. Assume that the temperature profile across a premixed laminar flame of overall thickness δ can be approximated by a linear relationship between T and x . The unburned gas temperature is T_u and the fully reacted gas temperature is T_b . Derive expressions for δ and S_L in terms of heat of reaction per molecule of reactant Q and $(T_b - T_u)$, using the energy conservation equation (5-18). Describe their functional relationships with pressure.
 8. Develop an expression for laminar-flame speed based on the species diffusion theory using the following reaction:



where the fuel could be CH₄ or any other hydrocarbon compounds. Note that in this derivation, the high rates of diffusion of H atoms from the burned zone

to the flame front must be emphasized. The activation energy of the above reaction can be treated as a very small number (~ 0 kcal/mol) for this exercise.

PROJECTS

- 5.1** The flashback phenomena of premixed laminar flame in a circular tube can be studied in more detail by considering the flow-field structure in cylindrical coordinates with a fully developed laminar flow. Examine the nonmonotonic wall velocity gradient effect as a function of tube radius. A good reference article on this topic was given by Lee and T'ien.⁹⁸
- 5.2** Consider a large amount of combustible mixture in an unconfined space. Assume that the mixture is ignited quickly along a wire and the laminar flame propagates in the radial direction only. Perform a detailed analysis to determine the flame propagation speed of the cylindrical laminar flame.
- 5.3** Develop a simplified thermal theoretical model to study the planar one-dimensional, nonadiabatic laminar flame. It would be useful to follow Williams' analysis^{99,100} for heat loss effect on flammability limits.
- 5.4** A straight cylindrical ramjet-type combustion duct is supplied with a stream of premixed fuel and air at an inlet pressure and velocity such that sonic velocity is just barely established at the exit. A spherical bluff body type of flameholder is used to anchor the flame.
 - (a) Calculate the smallest diameter of the spherical flameholder that will be able to stabilize the flame in the duct, using the following correlation obtained by Spalding:

$$\frac{V_{BO}D}{\alpha} = C \left[\frac{S_L D}{\alpha} \right]^2$$

where V_{BO} is the blowoff velocity and D is the diameter of the spherical flameholder. The fuel is natural gas (mostly methane) and the flame temperature can be taken as 2213 K for a lean mixture with 80% stoichiometric condition. The laminar-flame speed can be taken as 20 cm/s. Let us assume that the combustion efficiency is 90% and the free-stream gas temperature upstream of the flameholder is 300 K. There is no flameholder drag and all other losses can be regarded as negligible. Also, the thermal properties of gas mixtures before and after combustion can be treated as pure air with constant specific heat.

- (b) Consider a rather lean premixed air–hydrocarbon fuel mixture stabilized on a 3D spherical-type flame holder in the flow stream. Predict whether the blowoff velocity will rise or fall if

1. The pressure level throughout the combustor is raised
2. A small amount of fuel is injected in the wake of the stabilizer
3. A small amount of air is injected in the wake of the stabilizer
4. An inert gas is injected in the wake of the stabilizer
5. The thermal conductivity of the gases in the recirculation zone is drastically increased by an additive while the other conditions remain the same

6

GASEOUS DIFFUSION FLAMES AND COMBUSTION OF A SINGLE LIQUID FUEL DROPLET

Symbol	Description	Dimension
a	Acceleration of a droplet	L/t^2
b	A dimensionless parameter defined in Eq. (6-108)	—
B	Spalding transfer number defined by Eqs. (6-116), (6-129), and (6-147a–c)	—
Bo	Bond number defined in Eq. (6-161)	—
f_i	Fugacity of species i	F/L^2
G_F	Mass burning rate of fuel droplet per unit area	$M/t \cdot L^2$
h_c	Convective heat-transfer coefficient	$Q/tL^2 \cdot T$
I_f	Jet invariant based on the fuel mass consideration	L
I_h	Jet invariant based on the energy consideration	QL/M
I_u	Jet invariant based on the momentum consideration	L^2/t
J_0	Zeroth order Bessel functions of the first kind	—

(continued overleaf)

Symbol	Description	Dimension
J_1	First order Bessel functions of the first kind	—
J_m	The m th-order Bessel functions of the first kind	—
\dot{m}_{ss}	Droplet mass evaporation rate under spherically symmetric condition	M/t
Nu	Nusselt number based on particle radius	—
$r_{1/2}$	The radius at which the velocity is half of centerline velocity	L
r_{jb}	Radius at the jet boundary	L
v_{ent}	Entrainment velocity at jet boundary	L/t
We	Weber number, see Eq. (6-160)	—
z_f	Flame height	L
Z	Compressibility factor	—
α_j	Moles of j th species per mass of reacting mixture, defined in Eq. (6-12)	N/M
α_T	A parameter similar to α_j but obtained from the enthalpy associated with the moles of j th species per mass of reacting mixture	N/M
β	Coupling function used in Shvab-Zel'dovich formulation	N/M
β_v	Evaporation coefficient	L^2/t
Δh_v	Heat of vaporization of liquid fuel	Q/M
ζ	A conserved property defined by Eq. (6-83)	—
η	Dimensionless axial distance defined by Eq. (6-25)	—
ξ	Dimensionless radius defined by Eq. (6-25) or dimensionless variable defined by Eq. (6-59)	—
ϕ_m	Molar stoichiometric oxidizer-to-fuel ratio $\equiv v'_O/v'_F$	—
$\tilde{\omega}_i$	Acentric factor of pure component i	—
ϖ	The average depth of species penetration by diffusion	L
ω	Vorticity defined in Eq. (6-95)	t^{-1}

In the broadest sense, a diffusion flame may be defined as any flame in which the fuel and oxidizer are initially separated (non-premixed). For example, a pan of oil burning in air, a lighted candle, a fuel droplet burning in oxygen, a solid particle burning in oxidizer-rich environment, and pure solid fuel burning in a ramjet engine all produce diffusion flames. In a restricted sense, a diffusion flame may be defined as a non-premixed, steady or unsteady, nearly isobaric flame in which most of the reaction occurs in a narrow zone that sometimes can be approximated as a surface. The mixing rate is lower than the chemical reaction rate, or the characteristic time for mixing is much longer than chemical reaction time. This corresponds to high Damköhler numbers (defined as the ratio of diffusion or mixing time to chemical reaction time). Diffusion flames can either be laminar or turbulent; in this chapter, we shall concentrate on laminar ones.

1 BURKE AND SCHUMANN'S THEORY OF LAMINAR DIFFUSION FLAMES

A classical example of a laminar diffusion flame, which was first described quantitatively by Burke and Schumann,¹ is provided by a system in which fuel and air flow with the same linear flow velocity in coaxial cylindrical tubes.

The observed shapes of diffusion flames may be divided into two classes. If the ratio of the duct radii r_s to r_j is such that more air is available than what is required for complete combustion, then an *overventilated* flame is formed and the flame boundary converges to the cylinder axis. On the other hand, if the air supply is insufficient for complete burning, then an *underventilated* flame is produced in which the flame surface expands to the outer tube wall. (See Fig. 6.1.)

The gross features of diffusion flames can often be described by postulating the existence of a surface (assumed to be coincident with the luminous "combustion surface") at which chemical reactions occur instantaneously. A typical composition profile of a hydrogen–air diffusion flame is shown in Fig. 6.2.

Of particular interest is the fact that very little fuel and oxygen penetrate through the luminous flame boundary, a result which shows that the chemical reactions are completed in a very narrow region and which suggests that the flame surface may be identified, in first approximation, as the surface to which the fuel and oxygen rates of delivery are in stoichiometric proportions.

The time-dependent conservation-of-species equations given in Eq. (3-32) can be written as

$$\frac{\partial \rho_A}{\partial t} + \nabla \cdot (\rho_A \mathbf{v}) = \nabla \cdot \left[\rho \mathcal{D} \nabla \left(\frac{\rho_A}{\rho} \right) \right] - \dot{\omega}_A$$

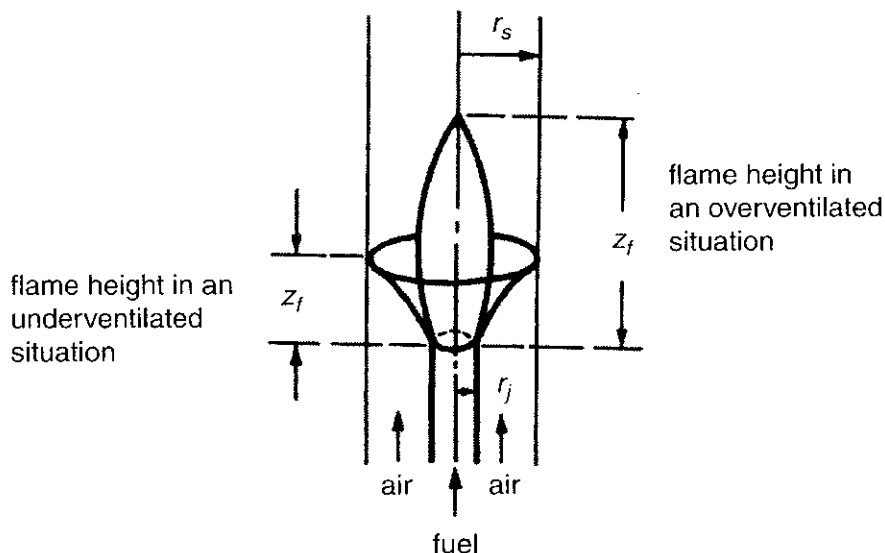


Figure 6.1 The shapes of diffusion flame under over- and underventilated situations.

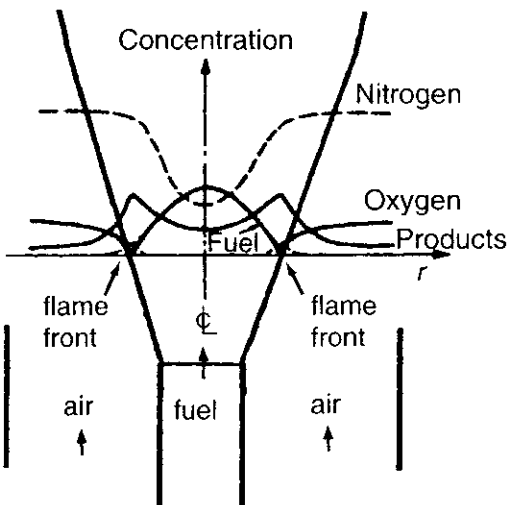


Figure 6.2 Species variation through a diffusion flame at a fixed height above the fuel jet tube.

There is a negative sign in front of ω_A , since it now represents the rate of consumption of mass of species A . For cylindrical geometry under axisymmetric condition, the above species continuity equation becomes

$$\underbrace{\frac{\partial \rho_A}{\partial t}}_{\text{rate of increase of mass } A} = \underbrace{\frac{1}{r} \frac{\partial}{\partial r} \left[\mathcal{D} \rho r \frac{\partial Y_A}{\partial r} \right]}_{\text{rate of mass } A \text{ diffused into control volume (based on Fick's law)}} - \underbrace{\left[\frac{1}{r} \frac{\partial (r \rho_A v_r)}{\partial r} + \frac{\partial v_z \rho_A}{\partial z} \right]}_{\text{rate of mass } A \text{ flowing out of control volume by advection}} - \underbrace{\dot{\omega}_A}_{\text{rate of mass consumption of } A} \quad (6-1)$$

Here the axial diffusion is neglected, since it is considered to be small in comparison with the radial diffusion term; i.e.,

$$\frac{\partial^2 Y_A}{\partial z^2} \ll \frac{\partial^2 Y_A}{\partial r^2}$$

where Y_A is mass fraction of the A species and ρ_A is density of the A species. The dependence of the product $\mathcal{D} \rho$ on the temperature can be deduced from the expressions for the random molecular velocity \bar{u} and mean free path l :

$$\mathcal{D} \rho = \frac{1}{3} \bar{u} l \rho = \frac{1}{3} \bar{u} \frac{kT}{\sqrt{2\pi\sigma^2 p}} \frac{p}{RT} = \frac{1}{3} \sqrt{\frac{8kT}{\pi m}} \frac{k}{\sqrt{2\pi R\sigma^2}}$$

Since the product $\mathcal{D} \rho$ is a weak function of temperature, as a first-order approximation it can be considered to be independent of temperature. By following the Shvab-Zel'dovich procedure described in Section 10 of Chapter 3, we will show that the species conservation equation can be expressed in the same form as the energy equation. The advection terms of Eq. (6-1) can be rearranged to give

$$\frac{1}{r} \frac{\partial (r \rho_A v_r)}{\partial r} = \frac{1}{r} \frac{\partial [r \rho v_r (\rho_A / \rho)]}{\partial r} = \rho v_r \frac{\partial (Y_A)}{\partial r} + \frac{Y_A}{r} \frac{\partial (r \rho v_r)}{\partial r}$$

$$\frac{\partial v_z \rho_A}{\partial z} = \frac{\partial v_z \rho Y_A}{\partial z} = Y_A \frac{\partial \rho v_z}{\partial z} + \rho v_z \frac{\partial Y_A}{\partial z}$$

Considering the steady-state condition for ρ_A to be independent of time and using the overall continuity equation

$$\frac{1}{r} \frac{\partial(r \rho v_r)}{\partial r} + \frac{\partial(\rho v_z)}{\partial z} = 0$$

to simplify the advection terms, Eq. (6-1) becomes

$$\frac{\mathcal{D}\rho}{r} \frac{\partial}{\partial r} \left(r \frac{\partial Y_A}{\partial r} \right) - \left(\cancel{\frac{\rho v_z}{r}} \right)^{\text{small}} r \frac{\partial Y_A}{\partial r} - \rho v_z \frac{\partial Y_A}{\partial z} = \dot{\omega}_A \quad (6-2)$$

If a single-step forward reaction $A + F \rightarrow P$ is used to represent the overall chemical reaction in the diffusion flame, then the species continuity equation for F can be written as

$$\frac{\mathcal{D}\rho}{r} \frac{\partial}{\partial r} \left(r \frac{\partial Y_F}{\partial r} \right) - (\rho v_z) \frac{\partial Y_F}{\partial z} = \dot{\omega}_F = \frac{\dot{\omega}_A}{\phi} \quad (6-3)$$

where ϕ is the stoichiometric mass ratio of A to F .

The general form of the energy equation from Eq. (3-78) can be simplified by first neglecting the viscous dissipation term and the body force term

$$\rho \frac{Dh}{Dt} - \frac{Dp}{Dt} = -\nabla \cdot \mathbf{q} + \Phi^0 + \dot{Q} + \rho \sum_{k=1}^n Y_k \mathbf{f}_k^0 \cdot \mathbf{v}_k$$

Assuming steady state, constant pressure, small v_r , and negligible axial-direction heat conduction, then

$$\begin{aligned} & \rho \frac{\partial h^0}{\partial t} + \rho v_r \frac{\partial h^0}{\partial r} + \rho v_z \frac{\partial h^0}{\partial z} - \frac{\partial p^0}{\partial t} - v_r \frac{\partial p^0}{\partial r} - v_z \frac{\partial p^0}{\partial z} \\ &= \lambda \frac{\partial}{\partial r} \left(r \frac{\partial T}{\partial r} \right) + \lambda \frac{\partial}{\partial z} \left(\frac{\partial T}{\partial z} \right)^0 + \dot{\omega}_F \Delta H_r \end{aligned}$$

The energy equation after simplification becomes

$$\frac{\lambda}{C_p} \frac{1}{r} \frac{\partial}{\partial r} \left[r \frac{\partial(C_p T)}{\partial r} \right] - \rho v_z \frac{\partial(C_p T)}{\partial z} = -\dot{\omega}_F \Delta H_r = -\frac{\dot{\omega}_A}{\phi} \Delta H_r = \dot{H} \quad (6-4)$$

where ΔH_r is the heat of reaction per unit mass of fuel (F). Recall that in the Shvab-Zel'dovich formulation we used

$$\text{Le} = 1 \quad \text{or} \quad \mathcal{D}\rho = \frac{\lambda}{C_p} \quad (6-5)$$

The energy equation, after setting the Lewis number equal to 1, becomes

$$\frac{\mathcal{D}\rho}{r} \frac{\partial}{\partial r} \left[\frac{r \partial(C_p T)}{\partial r} \right] - \rho v_z \frac{\partial(C_p T)}{\partial z} = -\frac{\dot{\omega}_A}{\phi} \Delta H_r \quad (6-6)$$

Multiplying Eq. (6-2) by $\Delta H_r/\phi$ and combining with Eq. (6-6), we get

$$\frac{1}{r} \frac{\partial}{\partial r} \left\{ \mathcal{D}\rho \left[r \frac{\partial}{\partial r} \left(C_p T + \frac{Y_A \Delta H_r}{\phi} \right) \right] \right\} - \rho v_z \frac{\partial}{\partial z} \left(C_p T + \frac{Y_A \Delta H_r}{\phi} \right) = 0 \quad (6-7)$$

This is a homogeneous differential equation written in terms of the sum of sensible and chemical enthalpy.

For more complex chemical reactions in diffusion flames, one can still follow the Shvab-Zel'dovich procedure to obtain equations of the same form as Eq. (6-7). Some detailed procedures are given below.

In general coordinate systems, the energy and mass equations are

$$\nabla \cdot \left[(\rho \mathbf{v})(C_p T) - \frac{\lambda}{C_p} \nabla(C_p T) \right] = -\dot{H} = \sum_j \Delta h_{f,j}^o \dot{\omega}_j \quad (6-8)$$

and

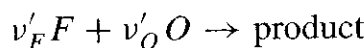
$$\nabla \cdot [(\rho \mathbf{v}) Y_j - \rho \mathcal{D} \nabla Y_j] = -\dot{\omega}_j \quad (6-9)$$

where $\dot{\omega}_j$ is the rate of consumption of species j , and $\Delta h_{f,j}^o$ is the heat of formation per unit mass of species j .

Sometimes we can consider the global reaction as follows:



or



with

$$\phi_m = \text{molar stoichiometric oxidizer-to-fuel ratio} = \frac{v'_O}{v'_F}$$

If we divide Eq. (6-9) by $Mw_j(v''_j - v'_j)$, we get the general species equation as

$$\nabla \cdot \left[(\rho \mathbf{v}) \frac{Y_j}{Mw_j(v''_j - v'_j)} - (\rho \mathcal{D}) \nabla \frac{Y_j}{Mw_j(v''_j - v'_j)} \right] = -\frac{\dot{\omega}_j}{Mw_j(v''_j - v'_j)} = -\dot{M} \quad (6-11)$$

Note that in the global reaction, if we let j represent the oxidizer, then

$$v''_j - v'_j = -v'_O = -\phi_m$$

and if we let j represent fuel, we have

$$\nu_j'' - \nu_j' = -\nu_F' = -1$$

The mass diffusion equation for all the species present in a general system can be put into the same form by setting

$$\alpha_j \equiv \frac{Y_j}{Mw_j(\nu_j'' - \nu_j')} \quad (6-12)$$

Then Eq. (6-11) reduces to

$$\nabla \cdot [(\rho \mathbf{v})\alpha_j - \rho \mathcal{D} \nabla \alpha_j] = -\dot{M} \quad (6-13)$$

Following the Shvab-Zel'dovich formulation given in Section 10 of Chapter 3, we can arrange the energy equation in the following form:

$$\begin{aligned} & \nabla \cdot \left[\rho \mathbf{v} \frac{C_p T}{\Delta H_r Mw_j(\nu_j'' - \nu_j')} - \frac{\lambda}{C_p} \nabla \frac{C_p T}{\Delta H_r Mw_j(\nu_j'' - \nu_j')} \right] \\ &= \frac{-\dot{\omega}_j}{Mw_j(\nu_j'' - \nu_j')} = -\dot{M} \end{aligned}$$

Let

$$\alpha_T \equiv \frac{C_p T}{\Delta H_r Mw_j(\nu_j'' - \nu_j')}$$

then

$$\nabla \cdot [(\rho \mathbf{v})\alpha_T - \rho \mathcal{D} \nabla \alpha_T] = -\dot{M} \quad (6-14)$$

Comparing Eq. (6-14) with Eq. (6-13), we notice that both α_j and α_T satisfy the same differential equation.

Equation (6-13) and Eq. (6-14) may both be expressed as

$$L(\alpha) = -\dot{M} \quad (6-15)$$

where the linear operator L is defined by

$$L(\alpha) \equiv \nabla \cdot [(\rho \mathbf{v})\alpha - \rho \mathcal{D} \nabla \alpha] \quad (6-16)$$

The inhomogeneous nonlinear rate term may be eliminated from all except one of the relations corresponding to Eq. (6-15). Selecting α_1 to be the dependent variable for the inhomogeneous equation, we have

$$L(\alpha_1) = -\dot{M} \quad (6-17)$$

Other variables are then determined by the linear homogeneous equation through the use of coupling functions β :

$$L(\beta) = 0 \quad (6-18)$$

with $\beta = \alpha_T - \alpha_1 \equiv \beta_T$ or $\beta = \alpha_j - \alpha_1 \equiv \beta_j (j \neq 1)$. This Shvab-Zel'dovich formulation procedure is quite important in solving diffusion-flame problems, since in these problems one often finds that by solving the linear equations for relations between flow variables, burning rates may eventually be determined without actually solving the nonlinear differential equation. Equation (6-18) is deceptively simple in appearance; it is usually hard to solve unless additional approximations are made. In general, ρv and $\rho \mathcal{D}$ do depend on β_j or β_T ; thus the operator L depends implicitly on β , and Eq. (6-18) is actually nonlinear.

1.1 Basic Assumptions and Solution Method

Burke and Schumann assumed the following:

1. At port position, the velocities of air and fuel are constant, equal, and uniform across their respective tubes. This is accomplished by varying the radii of the tubes to control the molar fuel ratio, which is given by $r_j^2/(r_s^2 - r_j^2)$.
2. The velocity of the fuel and air up the duct in the region of the flame is the same as the velocity at the port.
3. $\rho \mathcal{D}$ is constant.
4. Diffusion in the axial direction is negligible in comparison with that in the radial direction:

$$\frac{\partial^2 Y_j}{\partial r^2} \gg \frac{\partial^2 Y_j}{\partial z^2}$$

5. Mixing is caused mainly by diffusion process; however, the bulk radial velocity component is nearly zero, i.e., $v_r \doteq 0$.
6. Reaction takes place at $\phi = 1$ (at the flame surface).

The only differential equation that we need to consider for the mass-fraction distribution is Eq. (6-18):

$$L(\beta) = 0$$

with

$$\beta = \alpha_F - \alpha_O \quad (6-19)$$

$$\alpha_F = \frac{-Y_F}{Mw_F v'_F}, \quad \alpha_O = \frac{-Y_O}{Mw_O v'_O} \quad (6-20)$$

In cylindrical coordinates, this differential equation is

$$\left(\frac{v_z}{\mathcal{D}}\right) \frac{\partial \beta}{\partial z} - \frac{1}{r} \frac{\partial}{\partial r} \left(r \frac{\partial \beta}{\partial r}\right) = 0 \quad (6-21)$$

The boundary conditions for Eq. (6-21) are

$$\beta = -\frac{(Y_F)_{z=0}}{Mw_F v'_F} \quad \text{at } z = 0, \quad 0 \leq r \leq r_j \quad (6-22)$$

$$\beta = +\frac{(Y_O)_{z=0}}{Mw_O v'_O} \quad \text{at } z = 0, \quad r_j \leq r \leq r_s \quad (6-23)$$

and

$$\frac{\partial \beta}{\partial r} = 0 \quad \text{at } r = 0, \quad z > 0, \text{ and at } r = r_s, z > 0 \quad (6-24)$$

Burke and Schumann utilized the following dimensionless coordinates for r and z :

$$\xi \equiv \frac{r}{r_s} \quad \text{and} \quad \eta \equiv \frac{z \mathcal{D}}{v_z r_s^2} \quad (6-25)$$

They also defined several reduced parameters in their solution process

$$C \equiv \frac{r_j}{r_s} \quad \text{and} \quad \nu \equiv \frac{(Y_O)_{z=0} Mw_F v'_F}{(Y_F)_{z=0} Mw_O v'_O} \quad (6-26)$$

The parameter β in the governing equation was replaced by the reduced dependent variable γ , where

$$\gamma \equiv \beta \frac{Mw_F v'_F}{(Y_F)_{z=0}} \quad (6-27)$$

In terms of these parameters, Eqs. (6-21) through (6-24) become

$$\frac{\partial \gamma}{\partial \eta} = \frac{1}{\xi} \frac{\partial}{\partial \xi} \left(\xi \frac{\partial \gamma}{\partial \xi} \right) \quad (6-28)$$

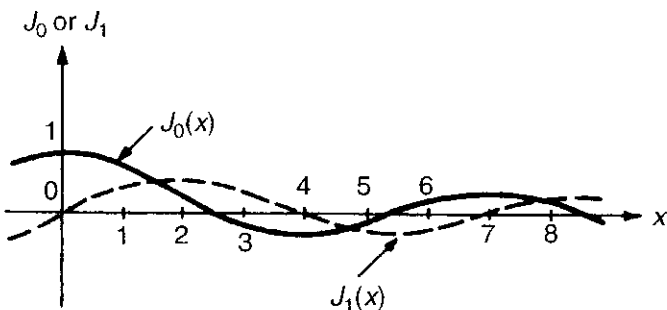
$$\gamma = \begin{cases} 1 & \text{at } \eta = 0, \quad 0 \leq \xi < C \\ -\nu & \text{at } \eta = 0, \quad C < \xi < 1 \end{cases} \quad (6-29)$$

$$\frac{\partial \gamma}{\partial \xi} = 0 \quad \text{at } \xi = 0 \quad \text{and at } \xi = 1, \quad \text{for } \eta > 0 \quad (6-30)$$

By the method of separation of variables, it can be shown that a part of the decomposed solution satisfies the Bessel's differential equation of order n :

$$\frac{d^2 y}{dx^2} + \frac{1}{x} \frac{dy}{dx} + \left(1 - \frac{n^2}{x^2}\right) y = 0$$

The functions J_0 and J_1 shown in the accompanying graph are solutions of the above differential equation; they are called the Bessel functions of the first kind (of order 0 and 1, respectively). The mathematical forms of the Bessel functions are



Bessel function of the first kind of order 0 and 1.

$$\begin{aligned} J_0(x) &= 1 - \frac{x^2}{2^2} + \frac{x^4}{2^4(2!)^2} - \cdots + (-1)^n \frac{x^{2n}}{2^{2n}(n!)^2} \\ &= \sum_{n=0}^{\infty} (-1)^n \frac{(x/2)^{2n}}{n!n!} \end{aligned}$$

and the m th order function J_m is defined as

$$J_m(x) = \sum_{n=0}^{\infty} \frac{(-1)^n x^{m+2n}}{2^{m+2n} n! \Gamma(m+n+1)}, \quad m > 0$$

The final solution for the reduced dependent variable γ in power-series form is

$$\gamma = (1+\nu)C^2 - \nu + 2(1+\nu)C \sum_{n=1}^{\infty} \frac{1}{\phi_n} \frac{J_1(C\phi_n)}{[J_0(\phi_n)]^2} J_0(\phi_n \xi) e^{-\phi_n^2 \eta} \quad (6-31)$$

where ϕ_n represent successive roots of the equation $J_1(\phi) = 0$ (with ordering convention $\phi_n > \phi_{n-1}$, $\phi_0 = 0$).

1.2 Flame Shape and Flame Height

To determine the flame shape, Burke and Schumann assumed that the entire reaction occurs on the flame surface; then

$$\beta = 0, \quad \text{or} \quad \gamma = 0$$

defines the flame surface. Hence, setting $\gamma = 0$ in Eq. (6-31) provides a relation between ξ and η that provides the locus of the flame surface [$\eta = f(\xi)$, or $z = g(r)$]. The shape of the flame surface obtained in this manner is shown in Fig. 6.1 for two different values of ν .

The flame height is obtained by solving Eq. (6-31) for η after setting the dimensionless radius $\xi = 0$ for overventilated flames or $\xi = 1$ for underventilated flames (and, of course, $\gamma = 0$ in either case). Since the flame heights are generally large enough to cause the factor $e^{-\phi_n^2 \eta}$ to decrease rapidly as n increases at these

values of η , it usually suffices to retain only the first few terms of the sum in Eq. (6-31) for this calculation. Neglecting all the terms except $n = 1$, we obtain the rough approximation

$$\eta = \frac{1}{\phi_1^2} \ln \left\{ \frac{2(1+\nu)C J_1(C\phi_1)}{[\nu - (1+\nu)C^2]\phi_1 J_0(\phi_1)} \right\} \quad (6-32)$$

for the dimensionless flame height of an underventilated flame. The first zero of $J_1(\phi)$ is $\phi_1 = 3.83$.

The flame shapes and flame heights obtained from Eq. (6-32) by Burke and Schumann (Fig. 6.3) are in surprisingly good agreement with experiments, considering the drastic nature of some of their assumptions.

In several follow-up works, Penner and Bahaduri²⁴ and Chung and Law²⁵ reexamined the Burke-Schumann problem and retained the axial diffusion terms. In Penner and Bahaduri's study,²⁴ they considered diffusion flames with arbitrary transport coefficients and chemical reactions. The closed-form solution obtained is slightly more complex than that of Burke and Schumann.¹ In Chung and Law's work,²⁵ the solution was obtained by a perturbation method under the assumption that the Lewis number is very close to unity. The zeroth order solution was obtained by separation of variables, and the first-order problem was solved using Green's functions. Their results showed that the flame is made longer and narrower by including stream-wise diffusion transport. They also showed that the Burke-Schumann solution is generally valid for large Peclet numbers (defined as the product of Reynolds number and Prandtl number or physically the convective heat flux over the conductive heat flux).

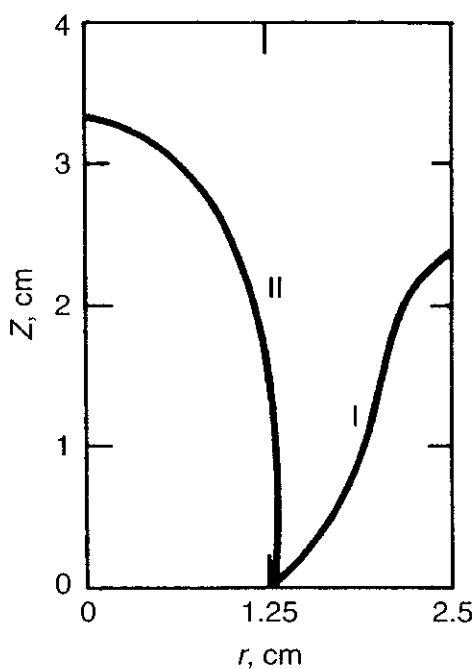


Figure 6.3 Calculated diffusion flame contour by Burke and Schumann: curve I, underventilated bowl-shaped flame; curve II, overventilated conical flame.

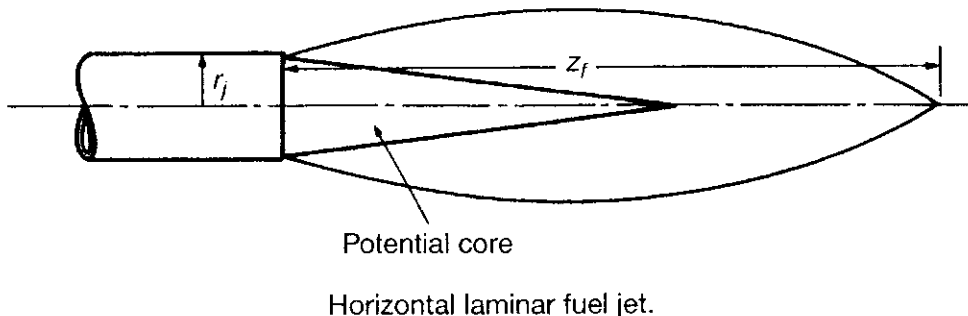
2 PHENOMENOLOGICAL ANALYSIS OF FUEL JETS

In engineering work, sometimes it is very useful to obtain quick solutions by phenomenological analyses. In the following, we shall use a simple phenomenological approach to show that for a laminar flame, the flame height is proportional to the volumetric flow rate and inversely proportional to the mass diffusivity:

$$(z_f)_{\text{laminar}} \propto \frac{\text{volumetric flow rate}}{\mathcal{D}} \quad (6-33)$$

We will also show that for a turbulent flame

$$(z_f)_{\text{turbulent}} \propto \text{port size} \quad (6-34)$$



If one can capture the main mechanism governing the physicochemical process in question, very useful information can quickly be obtained from simple phenomenological reasoning. For a horizontal fuel jet, the fundamental assumption that needs to be made here is that the combustion process does not affect the mixing rate between the fuel jet and the surrounding oxidizer. In essence, as soon as the oxidizer mixes into the fuel, it reacts. For this cylindrically asymmetric problem, there are two characteristic times we have to consider; one is associated with radial-direction diffusion of the oxidizer species from the surrounding to the centerline of the jet, the other is the convection time associated with the fuel species from the exit port of the injector to the tip of the diffusion flame. At the flame height station, one can consider that the fuel is completely burned due to the diffusion of the required oxidizer gas from the surrounding region.

Since the basic problem is simply the laminar diffusion mixing of the fuel jet with its surrounding oxidizer, some general results can be obtained using a phenomenological approach. Based on kinetic theory of gases, the average transverse displacement of a molecule due to molecular diffusion process can be given by

$$\frac{1}{2} \frac{d\bar{X}^2}{dt} = \mathcal{D} \quad (6-35)$$

where $\mathcal{D} = \frac{1}{2} \bar{u} l$ is the molecular diffusion coefficient (evaluated from the product of the gas random motion velocity and the mean free path) and \bar{X}^2 is the mean square of the transverse displacement of the gas molecules in the time t . In an

integrated form, the above equation can be written as

$$\bar{\omega}^2 = 2\mathcal{D}t \quad (6-36)$$

where $\bar{\omega}^2$ denotes the mean squared displacement of a molecule from its initial location due to diffusion during time t . The length of the flame is assumed to correspond to the condition that at the point on the stream axis where combustion is complete, the average depth of penetration of air into fuel must be approximately equal (or proportional, if one likes) to the radius of the burner tube. As an approximation, $\bar{\omega}$ is identified with the average depth of penetration. The radial diffusion time can be approximated by $t_{\text{diffusion}} = \bar{\omega}^2/2\mathcal{D}$ or $r_j^2/2\mathcal{D}$.

The gas velocity \bar{V} (inside the port) is taken as constant, so that the flow residence time $t_{\text{residence}}$ from the injector port exit to the flame tip is given by

$$t_{\text{residence}} = \frac{z_f}{\bar{V}} \quad (6-37)$$

Assuming that the residence time is of the same order of the diffusion time, we have

$$z_{f,L} \propto \frac{r_j^2 \bar{V}}{2\mathcal{D}} \propto \frac{(\pi r_j^2) \bar{V}}{2\pi \mathcal{D}} \propto \frac{\text{volumetric flow rate}}{\mathcal{D}} \quad (6-38)$$

This result is very meaningful; it clearly indicates that the height of a laminar diffusion flame ($z_{f,L}$) is proportional to the volumetric flow rate and inversely proportional to the mass diffusivity. This relationship has been supported by numerous experimental data; some representative data are given in a later section, after our discussion of the dependency of the height of turbulent fuel jet on injector diameter.

Let us now consider the extension of the above relationship for studying turbulent fuel jets. First, let us recall that the Schmidt number is defined as ν/\mathcal{D} . For constant Schmidt number, we have $\mathcal{D} \propto \nu$. Hence, Eq. (6-38) can be rewritten as

$$z_{f,L} \propto \frac{r_j^2 \bar{V}}{\nu}$$

For the turbulent case, we can use the same reasoning to arrive at a relationship similar to the above, except that instead of the molecular viscosity ν , we must use the turbulent eddy viscosity ν_T in the denominator, since $\nu_T \gg \nu$. Thus,

$$z_{f,T} \propto \frac{r_j^2 \bar{V}}{\nu_T} \quad (6-39)$$

Note that $\nu_T \propto l u'_{\text{rms}}$, where l is the scale of turbulence and is proportional to the tube diameter (or tube radius) and u'_{rms} is the intensity of turbulence, which is approximately proportional to the mean flow velocity at the axis; thus,

$$\nu_T \propto r_j \bar{V} \quad (6-40)$$

Combining Eqs. (6-39) and (6-40), we have

$$z_{f,T} \propto \frac{r_j^2 V}{r_j V} \propto r_j \quad (6-41)$$

This relationship says that the height of a turbulent diffusion flame is proportional to the port radius only. It is a very important practical conclusion that has been

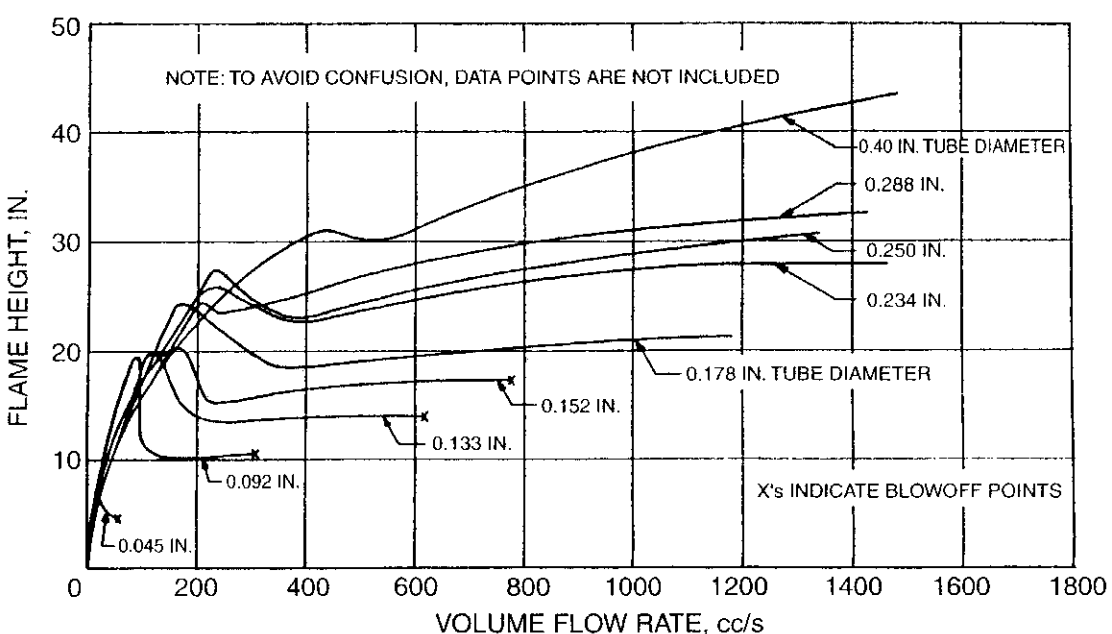
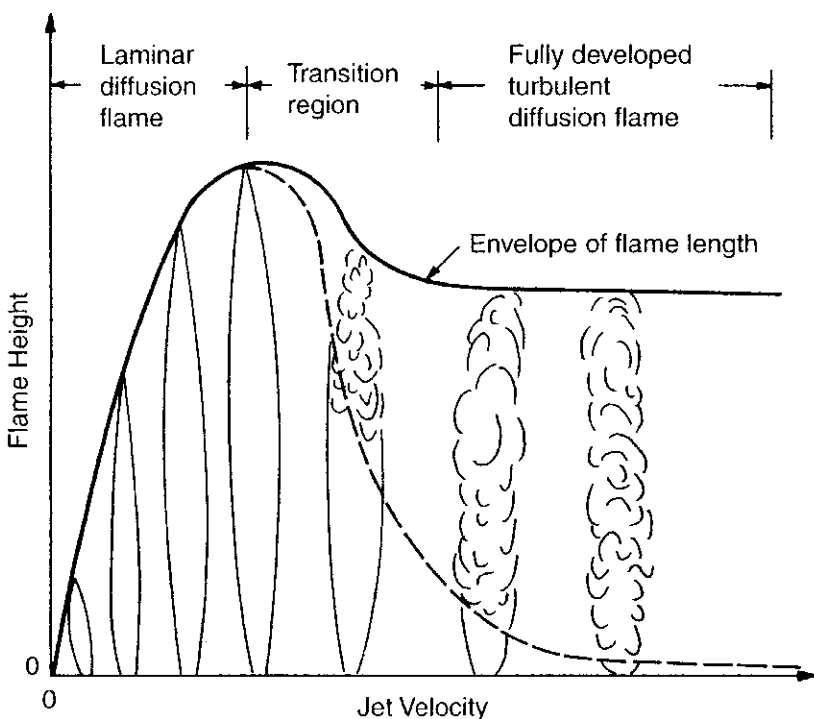


Figure 6.4 (a) The variation of flame height and character as a function of jet velocity (after Hottel and Hawthorne²). (b) Effect of volumetric flow rate and tube diameter on height of diffusion flame of city gas (after Wohl, Gazley, and Kapp, 1949, from A.G. Gaydon and H.G. Wolfhard⁹⁹).

verified in many ways. Schematically, the variation of diffusion flame height as a function of jet velocity is shown in Fig. 6.4a. The laminar diffusion flame height follows the functional dependence shown in Eq. (6-38), while the turbulent diffusion height follows Eq. (6-41). The experimentally determined effect of volumetric flow rate and tube diameter on height of diffusion flame of city gas by Wohl, Gazley, and Kapp (1949) is shown in Fig. 6.4b. More discussion of laminar diffusion flame jet is given in the following section.

3 LAMINAR DIFFUSION FLAME JETS

Injection of fuel jets into a combustor containing oxidizers is a common practice in many combustion systems such as industrial furnaces, gas-turbine engines, and ramjet engines. Under the condition when there is no crossflow or buoyancy effect and also the fuel jet and the ambient air (or oxidizer) are parallel, the diffusion flame is essentially the same as the Burke–Schumann laminar diffusion flame we discussed in Section 2. The only difference is that the effect of the outer tube becomes negligible when the combustor diameter becomes very large in comparison with the fuel-jet diameter. The schematic diagram of a single fuel jet under the above condition is shown in Fig. 6.5a. When the buoyancy or crossflow effect is significant, the flame geometry and the boundary of the hot gases will not be axisymmetric (see Fig. 6.5b). Before we study the detailed structure of these diffusion flames, we shall provide some background on laminar jet mixing.

3.1 Laminar Jet Mixing

Consider a gaseous fuel jet with a uniform (top-hat) velocity profile issuing from a circular hole of radius r_0 into quiescent air. Mixing will occur between the gaseous fuel jet and ambient air as shown in Fig. 6.6. At some downstream location, the velocity profile has a maximum value at the centerline and a gradual decay to zero at the boundary of the mixing zone. The air is entrained through the boundary of the mixing zone.

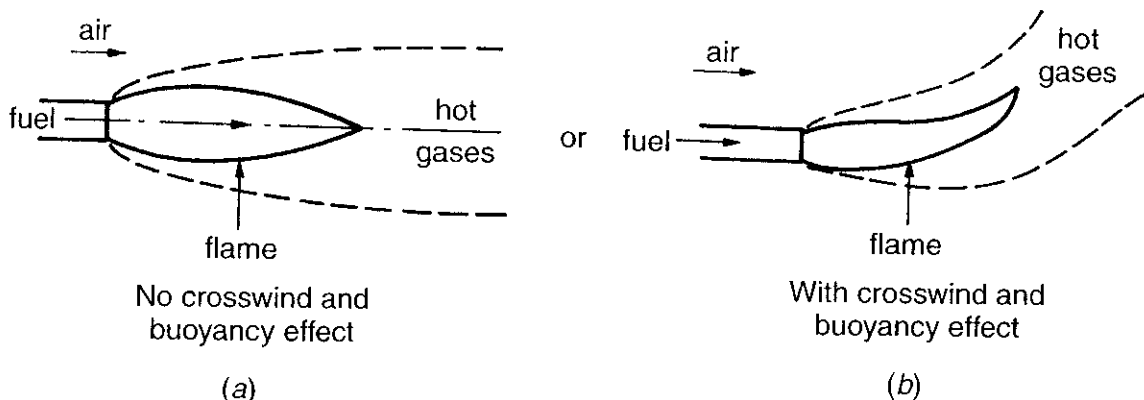


Figure 6.5 Laminar diffusion flame jets (a) without and (b) with crosswind and buoyancy effect.

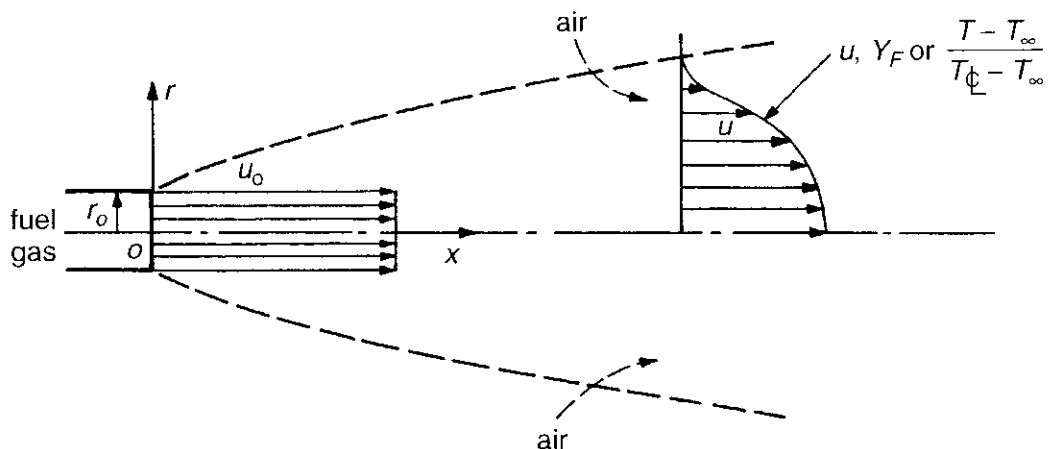


Figure 6.6 Velocity and concentration profile distributions in a laminar jet.

For simplicity of a mixing analysis, let us make the following assumptions:

1. The surrounding air far from the jet is at rest.
2. Chemical reaction is absent.
3. ρ , μ , and other properties of the gases are uniform (uniform property flow).
4. The flow is steady.
5. The effect of buoyancy is absent.
6. The pressure in the fluid is uniform.
7. Mass diffusion, heat conduction, and viscous action in the axial direction are negligible.
8. $Sc = Pr = 1$.

For large values of x/r_o , the profiles of u , Y_F , and $(T-T_\infty)/(T_o-T_\infty)$ can be shown to be “self-similar” and depend on r/x alone.

The overall mass conservation equation can be written as

$$\frac{\partial}{\partial x}(\rho u r) + \frac{\partial}{\partial r}(\rho v r) = 0 \quad (6-42)$$

The x -momentum equation is

$$\frac{\partial}{\partial x}(\rho u r u) + \frac{\partial}{\partial r}(\rho v r u) = \frac{\partial}{\partial r} \left(\mu r \frac{\partial u}{\partial r} \right) \quad (6-43)$$

The fuel species conservation equation written in terms of mixture fraction f is

$$\frac{\partial}{\partial x}(\rho u r f) + \frac{\partial}{\partial r}(\rho v r f) = \frac{\partial}{\partial r} \left(\rho \mathcal{D} r \frac{\partial f}{\partial r} \right) \quad (6-44)$$

where the mixture fraction f has been defined in Section 8 of Chapter 1. Taking ρ , μ , and \mathcal{D} to be uniform and applying the assumption that $Sc = Pr = Le = 1$,

the above equations can be reduced to

$$\frac{\partial u}{\partial x} + \frac{\partial v}{\partial r} + \frac{v}{r} = 0 \quad (6-45)$$

$$u \frac{\partial u}{\partial x} + v \frac{\partial u}{\partial r} = \frac{v}{r} \frac{\partial}{\partial r} \left(r \frac{\partial u}{\partial r} \right) \quad (6-46)$$

$$u \frac{\partial f}{\partial x} + v \frac{\partial f}{\partial r} = \frac{v}{r} \frac{\partial}{\partial r} \left(r \frac{\partial f}{\partial r} \right) \quad (6-47)$$

The boundary conditions at the entrance station are

$$x = 0, \quad r \leq r_0 : \quad u = u_0 \quad (6-48)$$

$$f = 1 \quad (6-49)$$

$$x = 0, \quad r > r_0 : \quad u = 0 \quad (6-50)$$

$$f = 0 \quad (6-51)$$

At large radius, one has

$$r \rightarrow \infty : \quad u = 0 \quad (6-52)$$

$$f = 0 \quad (6-53)$$

There are two jet invariants based on the conservation of momentum and mass of fuel species. These jet invariants are defined as follows:

$$I_u \equiv \frac{1}{\nu} \int_0^\infty u^2 r dr = \frac{1}{\nu} \left(\frac{1}{2} u_o^2 r_o^2 \right) \quad (6-54)$$

$$I_f \equiv \frac{1}{\nu} \int_0^\infty u f r dr = \frac{1}{\nu} \left(\frac{1}{2} u_o r_o^2 \right) \quad (6-55)$$

According to Spalding³ and Schlichting,⁴ the following equations satisfy the governing partial differential equations and boundary conditions at the far field:

$$u = \frac{3}{4} \frac{I_u}{x} \left(1 + \frac{\xi^2}{4} \right)^{-2} \quad (6-56)$$

or

$$\frac{u}{u_o} = \frac{3}{32} \left[\frac{\text{Re}_{d_o} d_o}{x} \right] \left(1 + \frac{1}{4} \xi^2 \right)^{-2} \quad (6-56a)$$

$$v = \left(\frac{3}{8} I_u \nu \right)^{1/2} \frac{\xi}{x} \left(1 - \frac{\xi^2}{4} \right) \left(1 + \frac{\xi^2}{4} \right)^{-2} \quad (6-57)$$

or

$$\frac{v}{u_o} = \frac{\sqrt{3}}{8} \frac{d_o}{x} \left(\xi - \frac{1}{4} \xi^3 \right) \left(1 + \frac{1}{4} \xi^2 \right)^{-2} \quad (6-57a)$$

and

$$f = \frac{3}{4} \frac{I_f}{x} \left(1 + \frac{\xi^2}{4} \right)^{-2} \quad (6-58)$$

where the dimensionless variable ξ is defined as

$$\xi \equiv \left(\frac{3}{8} \frac{I_u}{\nu} \right)^{1/2} \frac{r}{x} = \frac{\sqrt{3}}{8} \left(\frac{r}{d_o} \right) \left[\frac{\text{Re}_{d_o} d_o}{x} \right]^{1/2} \quad (6-59)$$

It is quite evident from the above solution that the velocity and concentration profiles are self-similar; that is, they depend on r/x alone. Based on Eqs. (6-56) and (6-58), when ξ is set to zero, the centerline values of u and f are

$$\begin{aligned} u_{\xi=0} &= \frac{3}{4} I_u \\ f_{\xi=0} &= \frac{3}{4} I_f \end{aligned} \quad (6-60)$$

Since the centerline velocity is less than the jet exit velocity (u_o) and the mixture fraction at the centerline in the downstream location is less than 1, we can conclude from Eq. (6-60) that the x -value satisfying the above far-field solution must obey the following inequality:

$$x > \frac{3}{4} \frac{I_u}{u_o}, \quad \text{or} \quad \frac{x}{r_o} > \frac{3}{8} \frac{u_o r_o}{\nu} \quad (6-61)$$

The radial values of u and f , when normalized by their respective centerline values, are

$$\frac{u}{u_{\xi=0}} = \frac{f}{f_{\xi=0}} = \frac{1}{\left(1 + \frac{1}{4} \xi^2 \right)^2} \quad (6-62)$$

The sketch shown in Fig. 6.7 represents the velocity or concentration profiles qualitatively. It should be noted that

$$\frac{u}{u_{\xi=0}} = 0.5 \quad \text{for} \quad \xi = 1.287$$

The radius at which the velocity has one-half of its centerline velocity is denoted $r_{1/2}$. From Eq. (6-59), we have

$$\frac{r_{1/2}}{x} = 1.287 \left(\frac{8\nu}{3I_u} \right)^{1/2} = 2.97 \left(\frac{\nu}{u_o r_o} \right)^{1/2} \quad (6-63)$$

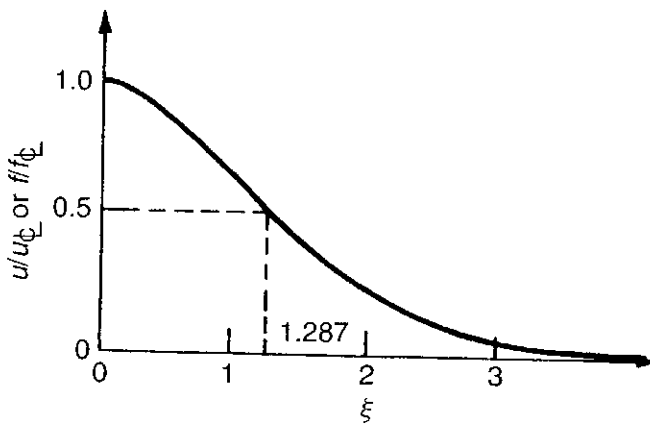


Figure 6.7 Self-similarity profile of velocity or concentration as a function of dimensionless variable ξ .

This equation implies that the angle of the spreading of the jet is inversely proportional to the Reynolds number.

The total mass flow rate in the jet, \dot{m} , can be obtained from the following integration:

$$\dot{m} \equiv \int_0^\infty 2\pi r \rho u dr \quad (6-64)$$

Substituting Eq. (6-56) into Eq. (6-64) and carrying our the integration, we have

$$\dot{m} = 2\pi\rho x^2 \left(\frac{8}{3} \frac{\nu}{I_u} \right) \left(\frac{3}{4} \frac{I_u}{x} \right) \int_0^\infty \frac{\xi d\xi}{(1 + \frac{1}{4}\xi^2)^2} = 8\pi\mu x \quad (6-65)$$

The entrainment rate can be obtained by differentiating Eq. (6-65), i.e.,

$$\frac{d\dot{m}}{dx} = 8\pi\mu \quad (6-66)$$

Associated with the entrainment process, an entrainment velocity can be defined by

$$v_{\text{ent}} \equiv -\frac{1}{2\pi r_{\text{jb}}\rho} \frac{d\dot{m}}{dx} = -\frac{4\mu}{r_{\text{jb}}\rho} = -4\frac{\nu}{r_{\text{jb}}} \quad (6-67)$$

where r_{jb} represents the radius at the jet boundary. In dimensionless form, Eq. (6-57) can be written as

$$\frac{\nu}{v_{\text{ent}}} = -\frac{\sqrt{3}}{16} \frac{u_o r_o}{\nu} \frac{\xi}{x} \left(1 - \frac{\xi^2}{4} \right) \left(1 + \frac{\xi^2}{4} \right)^{-2} r_{\text{jb}} \quad (6-68)$$

According to Schlichting,⁴

$$r_{\text{jb}} \cong \frac{16}{\sqrt{3}} \left(\frac{x}{\text{Re}_{d_o} d_o} \right) d_o \quad (6-69)$$

Using the above expression, the radial velocity can be expressed as

$$\frac{v}{v_{\text{ent}}} = -\frac{\xi^2}{4} \left(1 - \frac{\xi^2}{4}\right) \left(1 + \frac{\xi^2}{4}\right)^{-2} \quad (6-70)$$

It is interesting to note that at large ξ , $v/v_{\text{ent}} \rightarrow 1$ and at small ξ , $v/v_{\text{ent}} \rightarrow -\xi^2/4$.

The equations describing lines of constant u and f can be found by rearranging Eq. (6-56) or (6-58).

$$r = \frac{16}{\sqrt{3} \text{Re}_{d_o}} \frac{x}{\sqrt{\sqrt{\frac{3}{32}} \left(\frac{\text{Re}_{d_o} d_o}{x}\right) \frac{u_o}{u} - 1}} \quad (6-71)$$

where

$$\text{Re}_{d_o} \equiv \frac{u_o d_o}{\nu}$$

Curves obeying Eq. (6-71), for fixed values of u/u_0 (or f), have the form shown in Fig. 6.8.

Since there is exact similarity between the processes of mass transfer and momentum transfer, we can write

$$f = \frac{u}{u_o} \quad (6-72)$$

If we further assume that $\text{Le} = 1$ and consider the energy equation, we find that the temperature field is related to the concentration field by

$$\frac{T - T_\infty}{T_o - T_\infty} = f \quad (6-73)$$

Thus, the curves in Fig. 6.8 can also be interpreted as isotherms.

If the Schmidt number is not equal to unity but equal to some constant, then one can show that

$$\frac{f}{f_\infty} = \left(\frac{u}{u_\infty}\right)^{\text{Sc}} \quad (6-74)$$

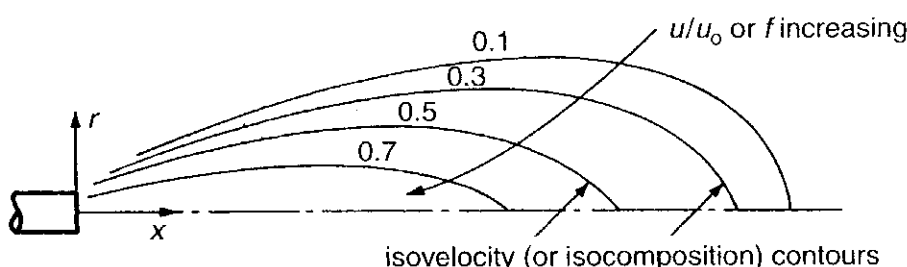


Figure 6.8 Isovelocity or isocomposition contours of a laminar jet.

This equation implies that for $Sc < 1$, the concentration profile is broader than the velocity profile. It should also be noted that, under this condition, the centerline mixture fraction f_{Φ} is smaller than that with $Sc = 1$. Furthermore, the value of f_{Φ} for $Sc \neq 1$ no longer obeys Eq. (6-60).

It is worthwhile to point out that when μ , ρ , and \mathcal{D} vary with f and T , the analytical solution of the governing equations ceases to be possible, and we must adopt numerical methods. Under these circumstances, the quantitative values will be different from those with constant transport properties; however, no qualitative change in the behavior of the jet is anticipated.

The buoyancy effect may be important in some cases. For upward vertical jets with the density of the injected fluid lower than that of the surroundings, buoyancy effects can cause the momentum flux in the jet to increase with vertical distance. Also, when buoyancy forces have components at right angles to the jet axis, the flow will no longer be axisymmetric. The solutions of these problems are more complex and one usually has to rely on numerical methods.

3.2 Laminar Jet with Chemical Reactions

In many industrial furnaces, flares, and combustors of propulsive devices, one needs to predict the shape and structure of the diffusion flame resulting from the injection of fuel gases into an oxidizing atmosphere. In order to achieve good predictive ability, the laminar diffusion flame jets must be modeled. Let us consider a steady, axisymmetric, vertical laminar jet with low Mach number but fast chemical reaction rates. We further assume that the pressure is uniform and the buoyancy effect is negligible. Under these specified conditions, the governing differential equations are given as follows:

Overall continuity equation:

$$\frac{\partial}{\partial x}(\rho ur) + \frac{\partial}{\partial r}(\rho vr) = 0 \quad (6-75)$$

Axial-momentum conservation equation:

$$\frac{\partial}{\partial x}(\rho uru) + \frac{\partial}{\partial r}(\rho vru) = \frac{\partial}{\partial r}\left(\mu r \frac{\partial u}{\partial r}\right) \quad (6-76)$$

Fuel species continuity equation:

$$\frac{\partial}{\partial x}(\rho urY_F) + \frac{\partial}{\partial r}(\rho vurY_F) = \frac{\partial}{\partial r}\left(\rho \mathcal{D}_{Fr} r \frac{\partial Y_F}{\partial r}\right) + r \dot{\omega}_F \quad (6-77)$$

Oxidant species continuity equation:

$$\frac{\partial}{\partial x}(\rho urY_O) + \frac{\partial}{\partial r}(\rho vurY_O) = \frac{\partial}{\partial r}\left(\rho \mathcal{D}_{Or} r \frac{\partial Y_O}{\partial r}\right) + r \dot{\omega}_O \quad (6-78)$$

Energy-conservation equation:

$$\frac{\partial}{\partial x}(\rho u rh) + \frac{\partial}{\partial r}(\rho vr h) = \frac{\partial}{\partial r}\left(\lambda r \frac{\partial T}{\partial r}\right) + (\Delta H_r) \frac{\partial}{\partial r}\left(\rho \mathcal{D}_F r \frac{\partial Y_F}{\partial r}\right) \quad (6-79)$$

where

$$h \equiv C_p T + Y_F \Delta H_r \quad (6-80)$$

and ΔH_r is the heat of reaction per mass of fuel.

To facilitate our discussion and theoretical solution, let us define a term introduced initially by Spalding³ for many combustion problems: in a *simple chemically reacting system* (SCRS), the pure fuel and pure oxidant are imagined to always unite in fixed proportions, the specific heats of all components are equal, and the transport properties are equal at any point in the mixture but need not be uniform. For such systems, a sketch of mixture state as a function of mixture fraction and reactedness is shown in Fig. 6.9. The symbols $Y_{F,F}$ and $Y_{F,M}$ in Fig. 6.9 represent the mass fractions of fuel in the fuel stream and in the burned mixture stream, respectively.

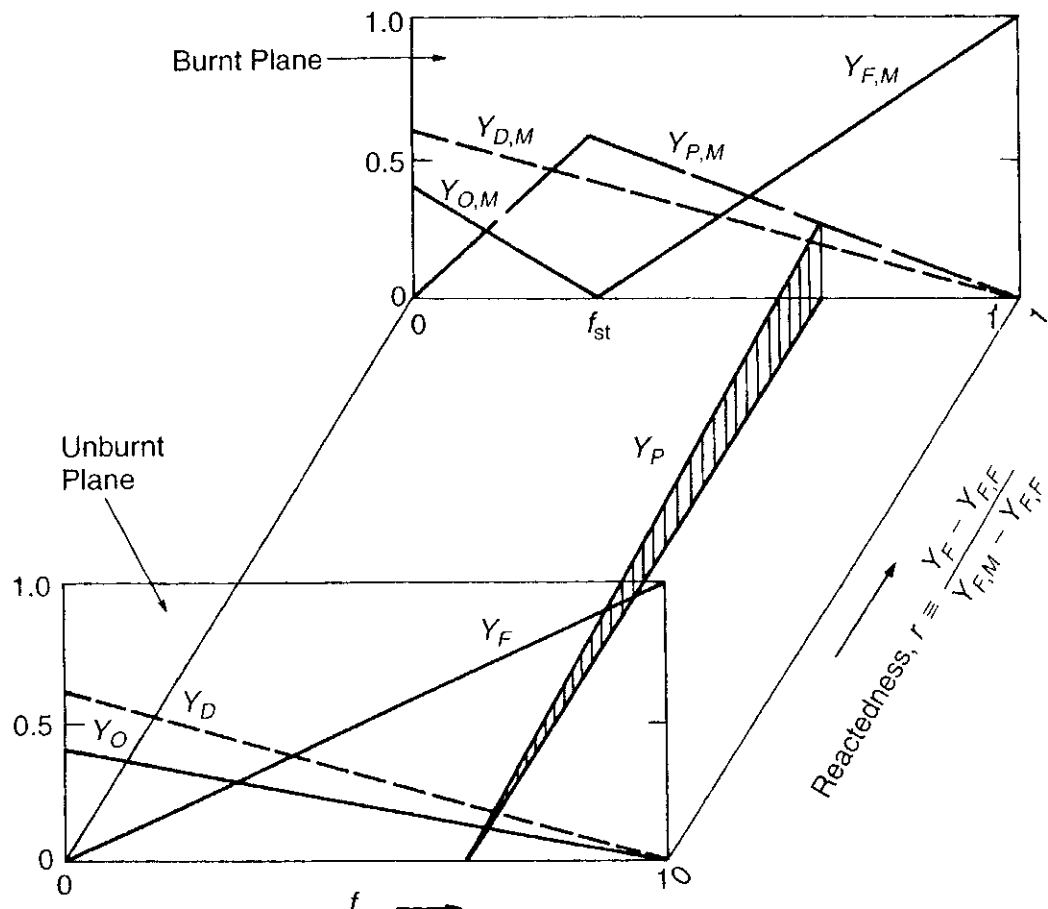


Figure 6.9 Sketch of the mixture state as a function of mixture fraction and reactedness.

If the fuel and the oxidizer are presumed to form a SCRS, one can relate the rate of production of fuel to that of oxidizer by

$$\dot{\omega}_F = \left(\frac{F}{O} \right)_{st} \dot{\omega}_O \quad (6-81)$$

Since $v = D = \alpha$ for a SCRS, so that $Sc = Pr = Le = 1$, then Eqs. (6-77) and (6-78) can be combined to form

$$\frac{\partial}{\partial x} (\rho u r \zeta) + \frac{\partial}{\partial r} (\rho v r \zeta) = \frac{\partial}{\partial r} \left(\mu r \frac{\partial \zeta}{\partial r} \right) \quad (6-82)$$

where

$$\zeta \equiv Y_F - \left(\frac{F}{O} \right)_{st} Y_O \quad (6-83)$$

Since ζ is a conserved property and related to the mixture fraction defined by Eq. (1-121a), the mixture fraction f also satisfies Eq. (6-82). Namely,

$$\frac{\partial}{\partial x} (\rho u r f) + \frac{\partial}{\partial r} (\rho v r f) = \frac{\partial}{\partial r} \left(\mu r \frac{\partial f}{\partial r} \right) \quad (6-84)$$

One can also show that Eq. (6-79) can be reduced to

$$\frac{\partial}{\partial x} (\rho u r h) + \frac{\partial}{\partial r} (\rho v r h) = \frac{\partial}{\partial r} \left(\mu r \frac{\partial h}{\partial r} \right) \quad (6-85)$$

The similarity of the equations for u , f , and h permits a single form of solution to serve for all three equations. The solutions for the set of governing equations with uniform properties (with constant values of μ and ρ) are identical to those of inert laminar jet as discussed in Section 3.1.

The far-field solution, which satisfies the boundary conditions at large r

$$r \rightarrow \infty : \quad \begin{cases} u = 0 \\ f = 0 \\ h = h_\infty \end{cases} \quad (6-86)$$

can be written as

$$\frac{ux}{I_u} = \frac{fx}{I_f} = \frac{(h - h_\infty)x}{I_h} = \frac{3}{4} \frac{1}{\left(1 + \frac{1}{4}\xi^2\right)^2} \quad (6-87)$$

where ξ is defined as before by Eq. (6-59) and the third jet invariant I_h is defined by

$$I_h \equiv \frac{1}{v} \int_0^\infty u(h - h_\infty)r dr = \frac{u_o(h_o - h_\infty)r_o^2}{2v} \quad (6-88)$$

In terms of the Reynolds number Re_{d_o} ($\equiv u_o d_o / \nu$) of the jet at the exit station, Eq. (6-87) can be written as

$$\begin{aligned} \frac{ux}{u_o r_o} \frac{1}{\text{Re}_{d_o}} &= \frac{fx}{r_o} \frac{1}{\text{Re}_{d_o}} = \frac{h - h_\infty}{h_o - h_\infty} \frac{x}{r_o} \frac{1}{\text{Re}_{d_o}} \\ &= \frac{3/16}{[1 + (3/256)(\text{Re}_{d_o}^2)(r^2/x^2)]^2} \end{aligned} \quad (6-89)$$

By examining Eqs. (6-87), (6-56), and (6-58), one can see that there is no primary effect of combustion on the distribution of velocity and of conserved properties such as f and h . The secondary effects are caused mainly by the influence of temperature on density and transport properties. It can be seen from Eq. (6-89) that the centerline values of velocity, mixture fraction, and enthalpy difference $h_\infty - h_\infty$ fall off as the reciprocal of x . The radical profiles fall asymptotically to zero as r/x increases.

If the reaction rates are infinitely fast, fuel and oxidizer cannot be simultaneously present in finite concentration; then the reaction zone is a surface (no overlapping region for Y_F and Y_O). The surface is located at

$$Y_F - \left(\frac{F}{O} \right)_{st} Y_O = 0 \quad (6-90)$$

or

$$f = f_{st} = \frac{(F/O)_{st} Y_{O,A}}{1 + (F/O)_{st} Y_{O,A}} \quad (6-90a)$$

Note that $Y_{O,A}$ represents the mass fraction of the oxidizer in the ambient gas and the form of Eq. (6-90a) is identical to Eq. (1-123). In practice, the overlapping region for many hydrocarbon fuels and air systems is very small, as shown in Fig. 6.10. The flame radius at any particular x station can be found by inserting f_{st} into Eq. (6-89) and rearranging; the result is

$$\frac{r_{\text{flame}}}{x} = \frac{16}{\sqrt{3}\text{Re}_{d_o}} \sqrt{\sqrt{\frac{3}{16} \frac{\text{Re}_{d_o} r_o}{x f_{st}}} - 1} \quad (6-91)$$

The flame contour is sketched in Fig. 6.11. The flame length can be obtained by equating r_{flame} to zero in Eq. (6-91). The flame length can then be expressed as

$$\frac{x_{\text{flame}}}{r_o} = \frac{3}{16} \frac{\text{Re}_{d_o}}{f_{st}} \quad (6-92)$$

or

$$x_{\text{flame}} = \frac{3 u_o r_o^2}{8 f_{st} \nu} = \frac{3}{8\pi} \frac{1}{f_{st}} \frac{\pi r_o^2 u_o}{\nu}$$

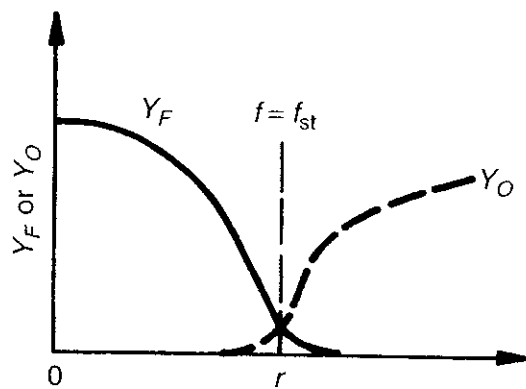


Figure 6.10 Radical distribution of mass fractions.

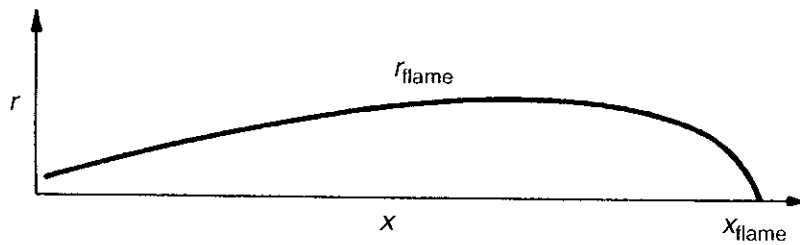


Figure 6.11 Contour of a laminar diffusion flame.

Thus, from the above equation, we showed again that the flame height is proportional to the volumetric flow rate and inversely proportional to the mass diffusivity. Namely,

$$x_{\text{flame}} \propto \frac{\text{volumetric flow rate}}{\mathcal{D}} \quad (6-92a)$$

Expressing f_{st} in terms of $Y_{O,A}$, Eq. (6-92) becomes

$$\frac{x_{\text{flame}}}{r_o} = \frac{3}{16} \text{Re}_{d_o} \left[1 + \frac{1}{(F/O)_{\text{st}} Y_{O,A}} \right] \quad (6-93)$$

This equation says that as $Y_{O,A}$ (or $Y_{O,\infty}$) decreases, the flame length increases, which implies that fuel has to go farther to find its oxidizer. Short flame lengths are often preferred in rocket motors; to obtain them, Eq. (6-93) suggests the use of a small injector radius. This is why many liquid rocket-engine combustors have numerous tiny fuel-injector nozzles. In industrial furnaces, on the other hand, long flames are often desired for uniformity of heat transfer over the furnace length, and so the fuel is often supplied through a large single nozzle.

3.3 Numerical Solution of Two-Dimensional Axisymmetric Laminar Diffusion Flames

Smooke et al. (1989) conducted a numerical simulation of a two-dimensional, axisymmetric laminar diffusion flame in which a cylindrical fuel stream is surrounded by a coflowing oxidizer jet. In their theoretical model, detailed chemical

kinetics of the combustion process and complex transport phenomena were considered. Both confined and unconfined systems were studied. In both cases, the cylindrical fuel jet was discharged into a laminar air stream. The fully elliptic problem was treated in the analysis and numerical solution. Part of their objective was to achieve a better predictive capability of pollutant formation processes and to identify the important reactions controlling extinction.

In general, a large portion of the detailed chemistry used in computational combustion studies is based on the literature focusing on one-dimensional configurations, i.e., freely propagating or burner-stabilized premixed flames and counterflow premixed or diffusion flames. In diffusion flames of practical interest, however, the oxidation of the fuel to form intermediates and products proceeds through a simultaneous mixing and diffusion process. In other words, there is a strong coupling between the fluid dynamic and the chemistry kinetics processes in the multidimensional solution fields.

Traditionally, modeling of chemically reacting flows proceeds along two independent paths: (1) chemistry is given priority over fluid mechanical effects to access the important elementary reaction paths, or (2) multidimensional fluid dynamic effects are emphasized with chemistry receiving little priority. In their study, Smooke et al. attempted to combine both of these analytical processes. They considered both the confined and unconfined configurations and utilized the following set of assumptions:

1. Two-dimensional axisymmetric flow,
2. Combustion takes place at a finite rate,
3. Fuel and oxidizer may coexist on either side of the reaction zone,
4. Steady flow,
5. Newtonian fluid characteristics,
6. Gases obey the ideal gas law,
7. Bulk viscosity is negligibly small,
8. Dufour and Soret effects are negligible,
9. Negligible viscous dissipation,
10. Adiabatic system, and
11. Pressure of the system is constant.

In their model formulation, they considered a set of 2D axisymmetric governing equations, including the continuity equation, radial-momentum equation, axial-momentum equation, K species conservation equations, an energy equation, and an equation of state, written in terms of perfect-gas law. A set of boundary conditions was specified at the injection station ($z = 0$), along the centerline ($r = 0$), at the edge of the outer zone ($r = R_o$), and at the far-field station ($z \rightarrow \infty$). To simplify the solution procedure, they considered the stream function ψ , which is defined in terms of the radial and axial components of the velocity vector. Using the stream function as one of the dependent variables, the continuity equation is

automatically satisfied.

$$\rho r v_r = - \frac{\partial \psi}{\partial z} \quad (6-94a)$$

$$\rho r v_z = \frac{\partial \psi}{\partial r} \quad (6-94b)$$

Furthermore, they considered the vorticity (ω) equation in the solution to replace the two momentum equations. In this problem, there is only one component of vorticity, which is defined as

$$\omega \equiv \frac{\partial v_r}{\partial z} - \frac{\partial v_z}{\partial r} \quad (6-95)$$

A partial differential equation for stream function can be obtained by direct substitution of Eq. (6-94a) and Eq. (6-94b) into Eq. (6-95). Finally, they used $3 + K$ partial differential equations in their solution of ψ , ω , T , and Y_i for $i = 1, 2, \dots, K$ in the chemically reacting flow field. The diffusion velocities in the radial and axial directions are assumed to obey Fick's law. The diffusion coefficients of the i th species against the mixture were calculated using the following relationship given by Curtiss and Hirschfelder,²⁹

$$\mathcal{D}_i = \frac{1 - Y_i}{\sum_{j \neq i}^K X_j / \mathcal{D}_{ji}} \quad (6-96)$$

The source term for the i th species equation is the same as that given by Eq. (3-95). The specific rate constants were evaluated using a modified Arrhenius equation with a temperature-dependent preexponential term:

$$k_j = A_j T^{\beta_j} \exp\left(-\frac{E_j}{R_u T}\right) \quad (6-97)$$

The preexponential factor A_j , the temperature exponent β_j , and the activation energy E_j for a 42-reaction mechanism involving 15 chemical species were obtained from a compilation of published experimental work gathered by Smooke et al.²⁸ The binary diffusion coefficients, the viscosity, the thermal conductivity of the mixture, and the chemical production rates are evaluated using the code CHEMKIN developed by Kee et al.³⁰

A discrete solution of the derived system is obtained by applying Newton's method in two dimensions and adaptive gridding to a mesh formed by the intersection of radial and axial lines. For convergence, Newton's method generally requires an initial estimate of flame sheet location that is sufficiently close to the actual solution. Adaptive gridding is required due to the highly nonlinear characteristics of the system, which indicates that regions of high spatial activity (e.g., steep fronts, sharp peaks) exist in the solution.

An initial estimate of flame sheet location was obtained by assuming a global, infinitely fast reaction model with assumptions that allow the system to be solved using the Shvab-Zel'dovich formulation. For this purpose, several additional assumptions must be made:

1. Infinitely fast kinetics.
2. The fuel and oxidizer are separated by a thin exothermic reaction zone.
3. Inside the reaction zone, the fuel and oxidizer are in stoichiometric proportion.
4. The fuel and oxidizer obey a single-step reaction process.

A steady-state and computationally time-dependent solution method was employed. The time-dependent approach was used to help obtain a converged numerical solution on an initial coarse grid using the initial estimate. Grid points are then inserted adaptively, and the steady-state solution procedure was used to recompute the finer grid. Grid points were inserted at the midpoint of each subinterval in question in both the r and z directions. The coarse grid solution was then interpolated linearly to serve as an initial solution estimate for the iteration procedure on the finer grid. The process was continued on finer and finer grids until several termination criteria were satisfied.

The data from the experimental studied by Mitchell³¹ on confined methane-air coflowing diffusion flame were used to validate the model and numerical solution of Smooke et al. The experimental configuration had an inner fuel jet radius of $R_i = 0.635$ cm and an outer oxidizer jet radius of $R_o = 2.54$ cm, and the length of the tubular pyrex shield was $Z = 30$ cm. Detailed transport coefficients and the 42-reaction, 15-species mechanism were used in the calculations. Figures 6.12 through 6.15 compare the experimental data with the numerical results. Figure 6.12 is a comparison of the experimentally measured and theoretically calculated radial temperature profiles at a height of 1.2 cm above the burner. Excellent agreement between the measured and calculated profiles is observed from the axis of symmetry to the low temperature coflow region. Figures 6.13a and 6.13b compare the measured and calculated radial mole fraction profiles for the major species in the flame (CH_4 , O_2 , N_2 , H_2O , CO_2 , CO , and H_2) at a height of 1.2 cm above the burner. The agreement between these computed and measured profiles is very good. Similar profiles for the temperature and major species are illustrated in Figs. 6.14 and 6.15 at a height of 2.4 cm above the burner. The experimentally measured temperature profile is somewhat narrower than that computed, but peak values and trends in the major species profiles are again in close agreement.

Their study has demonstrated the numerical capability of the model; however, more work can be performed to determine the cause of the under/overpredictions of the numerical solution. A limitation of the solution technique developed by Smooke et al.²⁸ is that it cannot be extended to three-dimensional applications

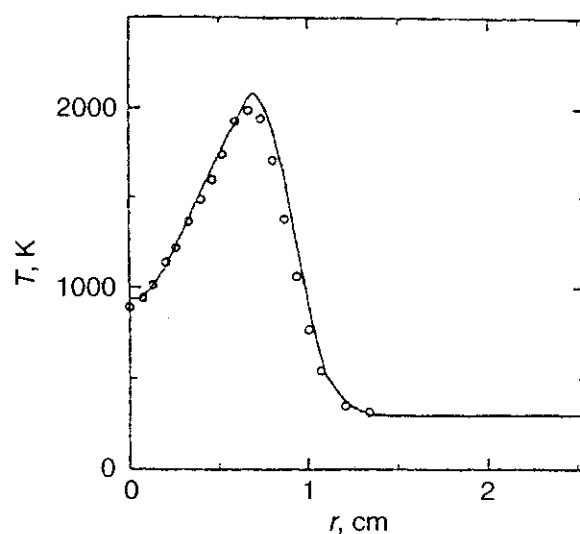


Figure 6.12 Comparison of measured (o) and calculated (solid line) radial temperature profiles for the confined coflowing methane–air laminar diffusion flame at a height of 1.2 cm above the burner inlet (after Smooke et al.²⁸).

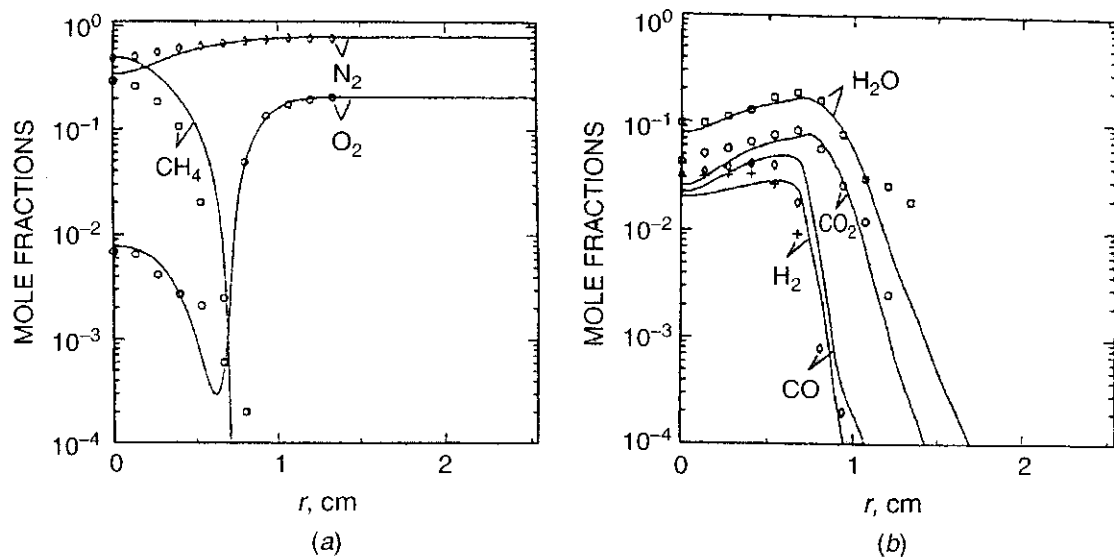


Figure 6.13 (a) Comparison between measured CH_4 (□), O_2 , (○), and N_2 (◊) profiles and corresponding computational values (solid line) for the confined coflowing methane–air laminar diffusion flame at a height of 1.2 cm above the burner inlet (after Smooke et al.²⁸). (b) Comparison between measured H_2O (□), CO_2 , (○), CO (◊), and H_2 (+) profiles and corresponding computational values (solid line) for the confined coflowing methane–air laminar diffusion flame at a height of 1.2 cm above the burner inlet (after Smooke et al.²⁸).

since the problem formulation depends on the stream function, which can only be defined properly in two-dimensional conditions. Formulation of the initial flame sheet estimate for the numerical solution required an equally rigorous formulation of the Shvab–Zel’dovich model. This exemplifies the usefulness of such models for numerical applications capable of more accurate results.

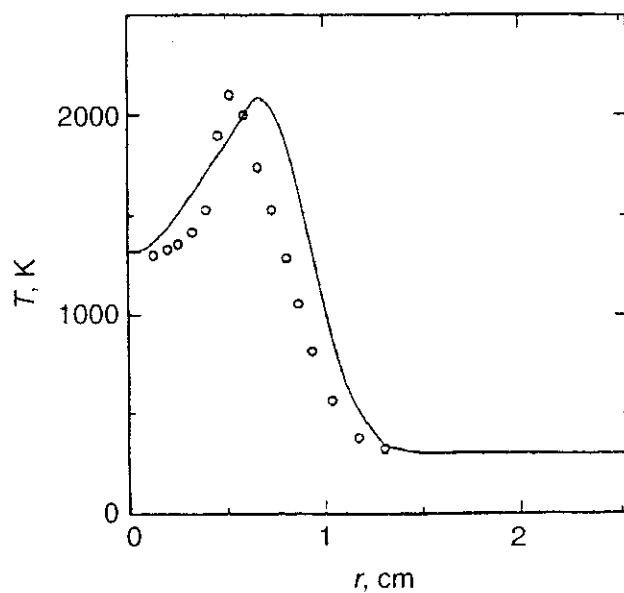


Figure 6.14 Comparison of measured (\circ) and calculated (solid line) radial temperature profiles for the confined coflowing methane–air laminar diffusion flame at a height of 2.4 cm above the burner inlet (after Smooke et al.²⁸).

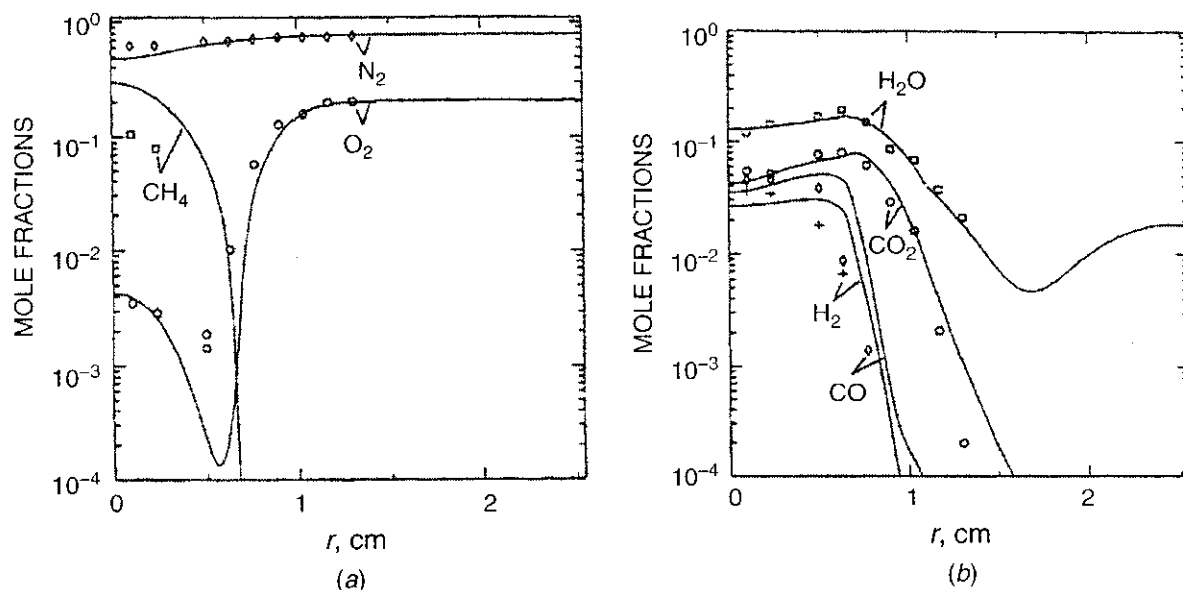


Figure 6.15 (a) Comparison between measured CH_4 (\square), O_2 , (\circ), and N_2 (\diamond) profiles and corresponding computational values (solid line) for the confined coflowing methane–air laminar diffusion flame at a height of 2.4 cm above the burner inlet (after Smooke et al.²⁸). (b) Comparison between measured H_2O (\square), CO_2 , (\circ), CO (\diamond), and H_2 (+) profiles and corresponding computational values (solid line) for the confined coflowing methane–air laminar diffusion flame at a height of 2.4 cm above the burner inlet (after Smooke et al.²⁸).

3.4 Effect of Preferential Diffusion of Species and Heat in Laminar Diffusion Flames

Takagi and Xu³² studied the effect of preferential diffusion of chemical species and heat on the structure of laminar diffusion flame. They performed numerical

computations of axisymmetric laminar jet diffusion flame with detailed chemical kinetics and multicomponent diffusion. They considered that the fuel jet is composed of 30% H₂ and 70% N₂ by mole with an average velocity of 5.2 m/s at the injection port. The surrounding air jet has an average velocity of 1.7 m/s. For hydrogen combustion, they took into consideration 10 species of H₂, O₂, H₂O, N₂, O, H, OH, HO₂, N, and NO. These species were allowed to engage in 16 elementary chemical reactions. The mass diffusion coefficients were determined from Eq. (6-96). They compared their solution with those experimental data obtained by Takagi, Tada, and Komiyama.³³ The comparison of calculated results with experimental data are shown in Figs. 6.16 and 6.17. It is quite obvious that the calculated results are in close agreement with the measured data.

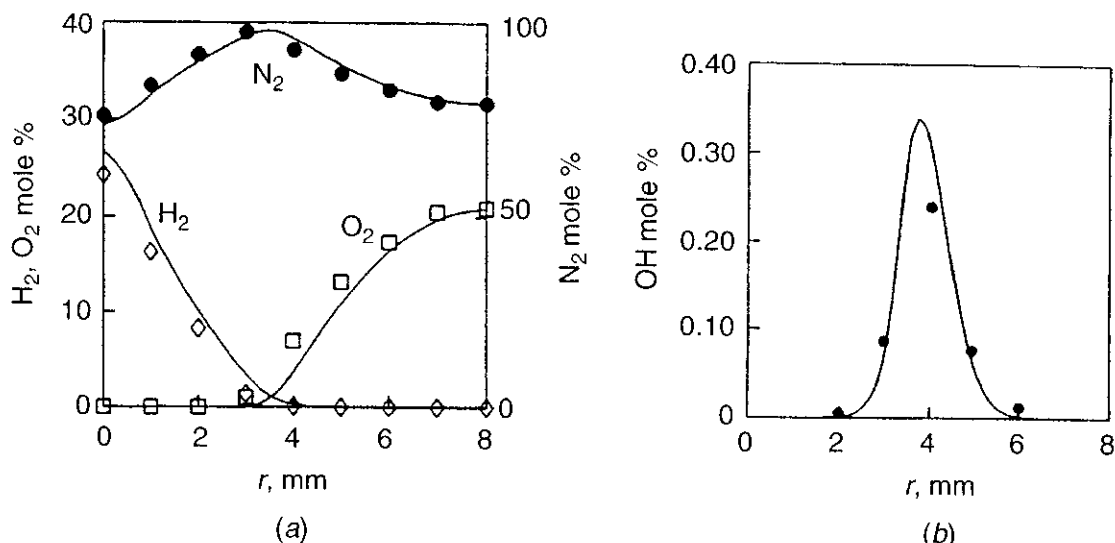


Figure 6.16 (a) Comparison of calculated radial profiles of H₂, O₂, and N₂ with measured data at a height of 30 mm above the burner inlet (after Takagi and Xu³²). (b) Comparison of calculated radial profile of OH with measured data at a height of 30 mm above the burner inlet (after Takagi and Xu³²).

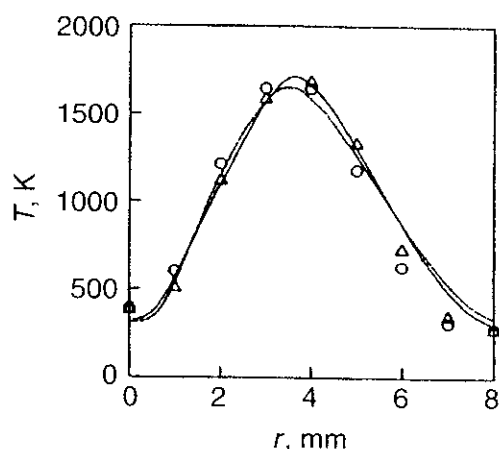


Figure 6.17 Comparison of calculated radial profile of temperature with measured data at a height of 30 mm above the burner inlet (modified from Takagi and Xu³²).

Takagi and Xu showed that preferential diffusion of heat and species causes significant amount of excess and deficit of enthalpy and change of H₂ mole fraction in the fuel before combustion. These effects induce higher flame temperature than the maximum adiabatic flame temperature for the original fuel in the upstream region. Effects of pressure were also investigated by computations. As shown in Fig. 6.18, the temperature profiles at 0.1 and 4.4 MPa are very different, not only in radial distribution but also in peak values, resulting from the difference in preferential diffusion effects. Furthermore, NO concentration profiles at these two different pressures are very different, as shown in Fig. 6.19. Higher pressure induces higher flame temperature, which is the main factor responsible for the increase of NO formation.

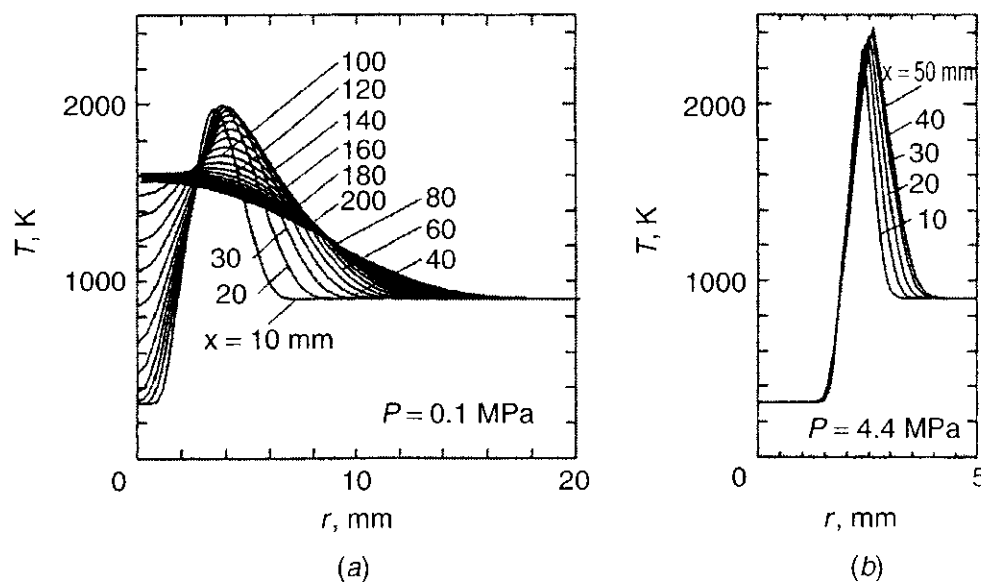


Figure 6.18 Temperature profiles at two different pressures (Modified from Takagi and Xu³²).

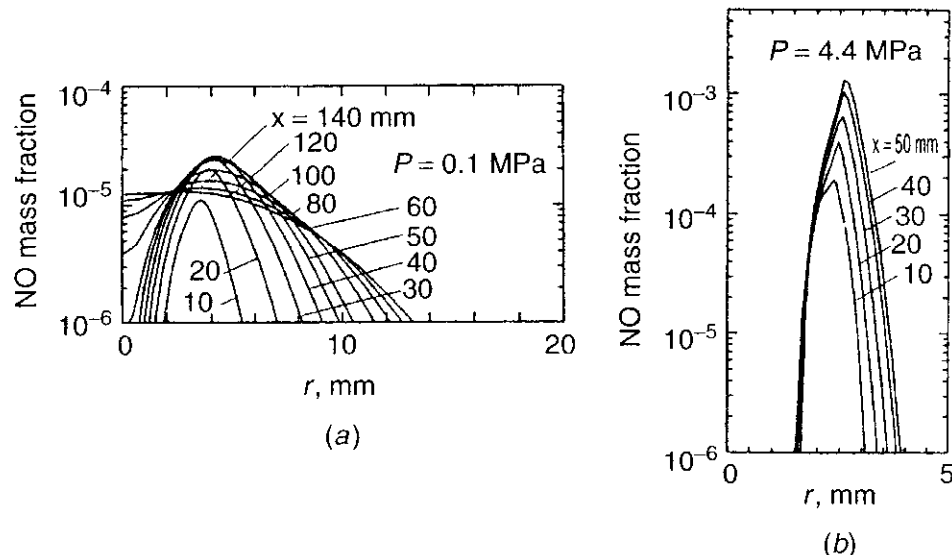


Figure 6.19 NO concentration profiles at two different pressures (modified from Takagi and Xu³²).

4 EVAPORATION AND BURNING OF A SINGLE DROPLET IN A QUIESCENT ATMOSPHERE

In the burning of a single fuel droplet in an oxidizing atmosphere, fuel is evaporated from the liquid surface and the fuel vapor diffuses to the flame front, while the oxygen moves from the surroundings to the flame front. The shape of the envelope flame can either be spherical or nonspherical (Fig. 6.20). Nonspherical flames are generally caused by the convection effect due to the relative motion between the surrounding gases and droplet. When the droplet is very small, the surrounding gases can entrain it easily and the relative velocity between the droplet and nearby gases becomes small; then, the diffusion flame surrounding the droplet becomes nearly spherical.

The rate at which the droplet evaporates and burns is generally considered to be determined by the rate of heat transfer from the flame front to the fuel surface. In the pioneering development of a theoretical model describing the gaseous diffusion flames surrounding the burning droplet, Spalding⁷ proposed a *double-film model* for the temperature and chemical species distributions around the single droplet. One film covers the region between the droplet surface and the infinitely thin flame front, and the other film lies between the flame front and the surrounding oxidizer (see Fig. 6.21). The chemical reaction processes in the gaseous flame are assumed to occur so rapidly that the droplet burning rate is determined solely by mass and heat transfer rates.

In most model developments, the liquid surface is assumed to be at the normal boiling point temperature of the fuel. Surveys of the temperature fields in burning liquids indicate that in fact the temperature is only slightly below the boiling temperature.^{3,5} In the following analysis, the temperature distribution within the droplet is assumed to be uniform and is slightly below the normal boiling point. In film I, heat is conducted from the flame front to the liquid, where it vaporizes the fuel. Most analyses assume that the fuel is heated to the flame temperature before it chemically reacts and that the vaporized fuel species does not react until it reaches the flame front. It is interesting to note that it was not necessary to determine T_f in the process to obtain the droplet burning rate. The value of T_f can, however, be determined rather easily by assuming an infinitely thin reaction

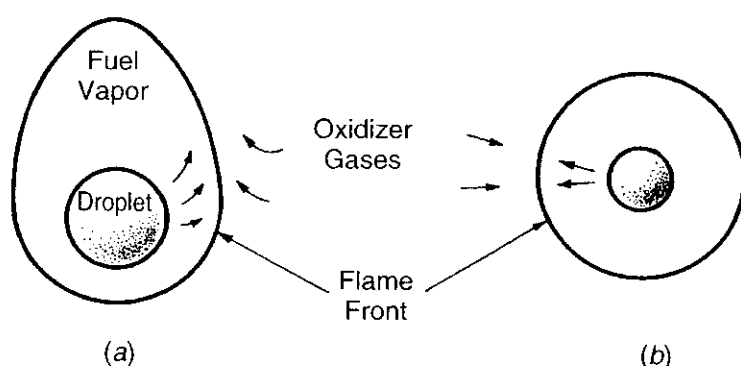


Figure 6.20 Shapes of diffusion flames surrounding a burning spherical fuel droplet: (a) non-spherical, (b) spherical.

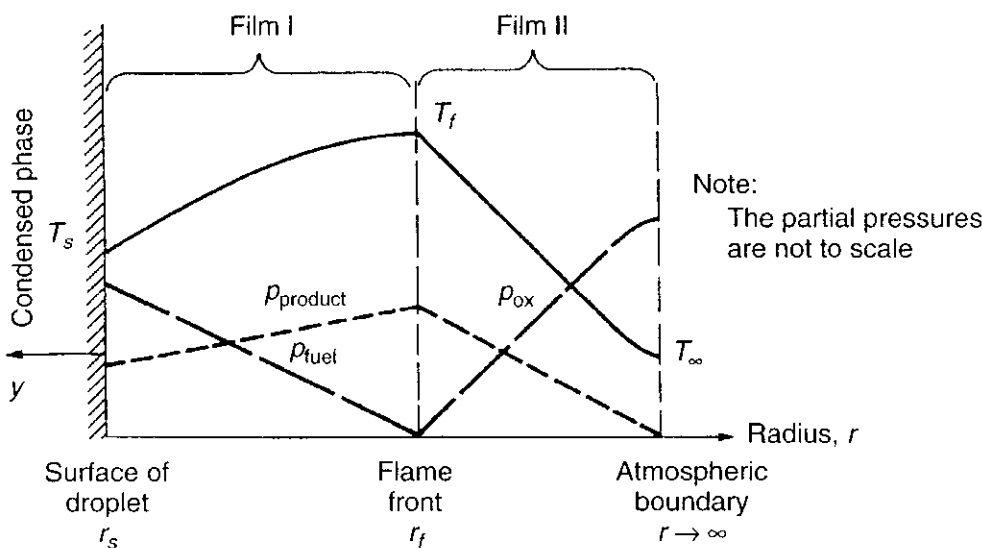


Figure 6.21 Radial variations of temperature and species partial pressures in double-film model.

zone at the stoichiometric position. In film II, oxygen diffuses to the flame front, while combustion products and heat are transported to the surrounding atmosphere. The position of this far-field boundary, designated by ∞ , is determined by the outward bulk flow condition. Strictly speaking, for a droplet burning in a stagnant environment, this boundary could be located at very far distance from the fuel surface. However, for practical purpose, this boundary can be quite close to the fuel surface, as long as the temperature is asymptotically close to the ambient hot-gas temperature, T_∞ .

In droplet burning, there are several important questions to consider. How long is the lifetime of a droplet? Which parameters govern the rate of consumption of a fuel droplet? How does the burning rate of a droplet depend on the heat of a reaction and flame temperature? What are the effects of relative motion between the droplet and surrounding gases? What is the effect of buoyancy? Is there an internal recirculation within the droplet? What is the effect of ambient pressure on the lifetime of the droplet and other parameters? Three parameters are generally evaluated to answer some of the above questions: the mass burning rate, the flame-front location, and the flame temperature. The most important parameter for engineering design is of course the mass-burning rate of the droplet, since it depicts the rate of heat release in a combustor. It also permits the evaluation of the so-called evaporation coefficient, which is most readily measured experimentally.

The use of the term *evaporation coefficient* comes about from mass- and heat-transfer experiments on evaporation without combustion, as generally used in spray drying and humidification. Basically the evaporation coefficient β_v is defined by the following d^2 -evaporation law, which has been verified by numerous experimental data:

$$d^2 = d_0^2 - \beta_v t \quad (6-98)$$

where d_0 is the original drop diameter, and d the drop diameter after time t . It will be shown later that the same expression has been found to hold true for burning droplets with mass- and heat-transfer processes involving chemical reactions.

Here we concern ourselves with the burning of droplets, but the concepts to be used are just as applicable to the evaporation of liquids, sublimation of solids, ablation heat transfer, transpiration cooling, and so on. In all cases, we are interested in the mass consumption, or the rate of regression of condensed material. The condensed phase must be gasified, and consequently there must be an energy input into the condensed phase material. The heat flux balance at the droplet surface is

$$q_s|_{r_s^+} = \dot{r} \rho_l \Delta h_v + q_s|_{r_s^-} \quad (6-99)$$

The $q_s|_{r_s^+}$ term represents the heat flux on the gas side of the droplet surface. This term can have contributions from conduction and radiation energy transfer. It has the dimension of (Q/tL^2) . The $q_s|_{r_s^-}$ term represents the heat flux on the liquid side of the droplet surface. This term is associated with the conduction heat transfer due to the temperature gradient beneath the droplet surface. It also has the dimension of (Q/tL^2) . \dot{r} is the regression rate and is equal to $|dr_s/dt|$ with the dimension of (L/t) . The parameter Δh_v represents the latent heat of vaporization of the liquid fuel, having the dimension of (Q/M) . The $q_s|_{r_s^-}$ term under quasi-steady regression condition can be estimated from

$$\underbrace{q_s|_{r_s^-}}_{\substack{\text{energy flux} \\ \text{beneath droplet} \\ \text{surface}}} = \underbrace{\dot{r} \rho_l C_l (T_s - T_0)}_{\substack{\text{rate of thermal enthalpy} \\ \text{increase from } T_0 \text{ to } T_s \\ \text{per unit surface area}}} \quad (6-100)$$

The heat flux at the surface (assuming no radiation) is

$$q_s|_{r_s^+} = \lambda_g \left(\frac{\partial T}{\partial r} \right)_{r_s^+} = \lambda_g \left(\frac{\partial T}{\partial r} \right)_s \quad (6-101a)$$

where the subscript s is used to designate the position just above the droplet surface. The energy flux balance equation (6-99) holds true even if there is mass evolution from the surface and even if convection effects prevail. For convective cases, one can write the surface heat flux in terms of the heat-transfer coefficient \bar{h}_c , averaged over the whole surface of the sphere, as

$$q_s|_{r_s^+} \equiv q_s = \bar{h}_c (T_\infty - T_s) \quad (6-101b)$$

Equating Eqs. (6-101a) and (6-101b), we have

$$q_s = \lambda_g \left(\frac{\partial T}{\partial r} \right)_s = \bar{h}_c (T_\infty - T_s) \quad (6-101c)$$

Note that when radiation becomes important, the surface heat flux can be written as the sum of two terms:

$$q_s = \lambda_g \left(\frac{\partial T}{\partial r} \right)_s + q_{\text{rad}} \quad (6-101d)$$

It is useful to understand that the mathematical procedure for obtaining the solution of the problem does not become much more difficult, since the radiation effects are only involved in the boundary condition and the differential equations describing the processes are not altered.

The heat-transfer coefficient \bar{h}_c in Eq. (6-101c) is often expressed in terms of Nusselt number

$$\overline{\text{Nu}}_d \equiv \frac{\bar{h}_c d_0}{\lambda_g} \quad (6-102)$$

where d_0 is the initial diameter of the droplet. The Nusselt number can be considered as a dimensionless heat-transfer coefficient; it is usually correlated with the Reynolds number and Prandtl number as

$$\overline{\text{Nu}}_d = f(\text{Re}_d, \text{Pr}) \quad (6-103)$$

A specific form⁶ suitable for spherical droplets is

$$\overline{\text{Nu}}_d = \frac{\bar{h}_c d}{\lambda_g} = 2 + 0.6 \left[\frac{|U_g - U_p|d}{v_g} \right]^{1/2} \left(\frac{v_g}{\alpha_g} \right)^{1/3} \quad (6-103a)$$

where $U_g - U_p$ is the relative velocity between the nearby gases and the fuel particle.

4.1 Evaporation of a Single Fuel Droplet

Before we talk about the more complicated modern approaches, we shall first follow Spalding's initial classical approach^{7,8} to treat a single fuel droplet in a quiescent (nonconvective) atmosphere of a given temperature and pressure. A *quasi-steady assumption* is utilized in Spalding's analysis for determining the distributions of fuel vapor mass fraction and temperature around the evaporating spherical droplet. The main advantage of this assumption is to temporarily avoid the consideration of time variations associated with the droplet regression process. The justification of this assumption is based on the relatively slow regression rate of the fuel droplet. Using this assumption, one can imagine that the droplet evaporates so slowly that the droplet can be replaced by a porous sphere of a fixed diameter; the surface of this sphere is wetted by the liquid fuel, and the mass evaporation rate of fuel from its surface into the warm surrounding is equal to the feeding rate of the liquid fuel from a small feeding tube to the porous sphere. For a spherical droplet of fixed size with radius r_s , the steady-state species and energy equations can then be written as

Fuel species continuity equation:

$$r^2 \rho v \frac{dY_F}{dr} = \frac{d}{dr} \left(r^2 \mathcal{D} \rho \frac{dY_F}{dr} \right) \quad (6-104)$$

Energy equation:

$$r^2 \rho v \frac{dC_p T}{dr} = \frac{d}{dr} \left(\frac{\lambda}{C_p} r^2 \frac{dC_p T}{dr} \right) \quad (6-105)$$

Let us further assume that the ambient gases do not dissolve into the fuel droplet; just below the droplet surface, only fuel (F) exists. For the vaporizing droplet, the total fuel mass flow rate leaving the droplet surface must be equal to the sum of the fuel mass flow rates due to the bulk convective motion of the gaseous mixture at the surface and the mass diffusion rate of the fuel vapor in the radial direction caused by the existence of fuel concentration gradient above the droplet surface.

$$\underbrace{\rho_s v_s}_{\substack{\text{total gaseous} \\ \text{mass flux of} \\ \text{fuel species} \\ \text{leaving} \\ \text{surface}}} = \underbrace{\rho_s (Y_F)_s v_s}_{\substack{\text{mass flux of fuel} \\ \text{species due to} \\ \text{bulk velocity of} \\ \text{mixture at} \\ \text{surface}}} + \underbrace{\rho_s (Y_F)_s (V_F)_s}_{\substack{\text{mass flux of fuel species} \\ \text{due to mass diffusion}}} = \rho_s (Y_F)_s v_s - \rho_s \mathcal{D}_s \left(\frac{dY_F}{dr} \right)_s \quad (6-106)$$

After rearranging Eq. (6-106), we have

$$v_s = \frac{\mathcal{D}(dY_F/dr)_s}{(Y_F)_s - 1} \quad (6-107)$$

Spalding defined a b parameter as

$$b \equiv \frac{Y_F}{Y_{Fs} - 1} \equiv - \frac{\text{mass fraction of } F \text{ at any location } r}{\text{mass fraction of species other than } F \text{ at surface } r = r_s} \quad (6-108)$$

Then v_s becomes

$$v_s = \mathcal{D} \left(\frac{db}{dr} \right)_s \quad (6-109)$$

Using parameter b , the fuel species conservation equation (6-104) becomes

$$r^2 \rho v \frac{db}{dr} = \frac{d}{dr} \left(r^2 \mathcal{D} \rho \frac{db}{dr} \right) \quad (6-110)$$

The boundary condition at $r = \infty$ is $Y_F = Y_{F\infty}$, or

$$r = \infty : \quad b = b_\infty = \frac{Y_{F\infty}}{Y_{Fs} - 1} \quad (6-111)$$

From the integrated continuity equation, we have

$$r^2 \rho v = \text{constant} = r_s^2 \rho_s v_s \quad (6-112)$$

Using Eq. (6-112) and integrating Eq. (6-110) with respect to r , we get

$$r^2 \rho v b = r^2 \rho \mathcal{D} \frac{db}{dr} + \text{constant}$$

Applying the boundary condition (6-109) at the surface, we have

$$r_s^2 \rho_s v_s (b - b_s + 1) = r^2 \rho \mathcal{D} \frac{db}{dr}$$

By separating variables, we have

$$\frac{r_s^2 \rho_s v_s}{r^2 \rho \mathcal{D}} dr = \frac{db}{b - b_s + 1}$$

Taking the product $\rho \mathcal{D}$ to be constant ($= \rho_s \mathcal{D}_s$) and integrating again, we have

$$-\frac{r_s^2 v_s}{r \mathcal{D}_s} = \ln(b - b_s + 1) + \text{constant} \quad (6-113)$$

Using the boundary condition (6-111), we have

$$\frac{r_s^2 v_s}{r \mathcal{D}_s} = \ln\left(\frac{b_\infty - b_s + 1}{b - b_s + 1}\right) \quad (6-114)$$

At $r = r_s$,

$$\frac{r_s v_s}{\mathcal{D}_s} = \ln[1 + (b_\infty - b_s)] \quad (6-115)$$

The difference $b_\infty - b_s$ is called the *Spalding transfer number B or B_M* , where the subscript M stands for mass, i.e.,

$$B \equiv B_M \equiv b_\infty - b_s = \frac{Y_{F_s} - Y_{F\infty}}{1 - Y_{F_s}} \quad (6-116)$$

Then Eq. (6-115) becomes

$$r_s v_s = \mathcal{D}_s \ln(1 + B_M) \quad (6-117)$$

The mass flow rate per unit area is usually called G_F :

$$G_F \equiv \frac{\dot{m}_F}{4\pi r_s^2} = \rho_s v_s \quad (6-118)$$

The fuel evaporation-rate expression (6-117) can be rearranged to give

$$G_F \equiv \frac{\dot{m}_F}{4\pi r_s^2} = \rho_s \mathcal{D}_s \frac{\ln(1 + B_M)}{r_s} \quad (6-119)$$

In order to calculate the mass evaporation rate from Eq. (6-119), the value of B_M must be evaluated; before that, Y_F (or p_F) must be determined. A reasonable assumption would be that the gas surrounding the droplet is saturated by the fuel vapor at the surface temperature. Thus, the problem now becomes to determine T_s , since the vapor-pressure data for most fuels are available.

In order to determine the surface temperature T_s , we must consider the energy equation. Using the integrated continuity equation of (6-112) and assuming C_p of the gas around the droplet is independent of temperature, Eq. (6-105) becomes

$$r_s^2 \rho_s v_s C_p \frac{dT}{dr} = \frac{d}{dr} \left(r^2 \lambda \frac{dT}{dr} \right) \quad (6-120)$$

Integrating the above equation with respect to r , we have

$$r_s^2 \rho_s v_s C_p T = r^2 \lambda \frac{dT}{dr} + \text{constant} \quad (6-121)$$

The integration constant is determined from algebraic manipulations, using boundary condition at the droplet surface (see Fig. 6.22):

$$\lambda \left(\frac{dT}{dr} \right)_s \doteq \rho_s v_s \Delta h_v, \quad T(r = r_s) = T_s \quad (6-122)$$

After applying the boundary condition at the droplet surface, we have

$$r_s^2 \rho_s v_s C_p \left(T - T_s + \frac{\Delta h_v}{C_p} \right) = r^2 \lambda \frac{dT}{dr} \quad (6-123)$$

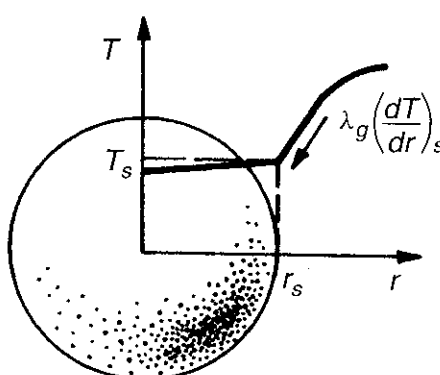


Figure 6.22 Temperature distribution of an evaporating liquid droplet.

After separating the variables and integrating the above equation, we have

$$-\frac{r_s^2 \rho_s v_s C_p}{r \lambda} = \ln \left(T - T_s + \frac{\Delta h_v}{C_p} \right) + \text{constant}' \quad (6-124)$$

Using the boundary condition that $T \rightarrow T_\infty$ as $r \rightarrow \infty$, we have

$$\frac{r_s^2 \rho_s v_s C_p}{r \lambda} = \ln \left(\frac{T_\infty - T_s + \Delta h_v / C_p}{T - T_s + \Delta h_v / C_p} \right) \quad (6-125)$$

Setting r equal to r_s at the surface, we have

$$\frac{r_s \rho_s v_s C_p}{\lambda} = \ln \left(1 + \frac{C_p(T_\infty - T_s)}{\Delta h_v} \right) \quad (6-126)$$

Since $\alpha \equiv \lambda / \rho C_p$,

$$r_s v_s = \alpha_s \ln \left[1 + \frac{C_p(T_\infty - T_s)}{\Delta h_v} \right] \equiv \alpha_s \ln[1 + B_T] \quad (6-127)$$

Comparing Eq. (6-127) with Eq. (6-117), we have

$$r_s v_s = \alpha_s \ln \left[1 + \frac{C_p(T_\infty - T_s)}{\Delta h_v} \right] \equiv \mathcal{D}_s \ln \left[1 + \frac{Y_{F\infty} - Y_{Fs}}{Y_{Fs} - 1} \right]$$

or

$$r_s v_s = \alpha_s \ln[1 + B_T] \equiv \mathcal{D}_s \ln[1 + B_M] \quad (6-128)$$

If $\alpha_s = \mathcal{D}_s$ (i.e., $\text{Le} = 1$), then

$$B_T = B_M$$

or

$$B_T = \frac{C_p(T_\infty - T_s)}{\Delta h_v} = \frac{Y_{F\infty} - Y_{Fs}}{Y_{Fs} - 1} = B_M = B \quad (6-129)$$

This equation relates the two unknowns T_s and Y_{Fs} ; one additional equation is needed to solve for them. The following equation relates Y_F to the partial pressure p_F :

$$Y_F = \frac{\rho_F}{\rho} = \frac{n_F M_w F}{n M_w} = \frac{p_F}{p} \frac{M_w F}{M_w} \quad \text{or} \quad Y_{Fs} = \frac{p_{Fs}}{p} \frac{M_w F}{M_w} \quad (6-130)$$

This equation is helpful, since we can further relate the partial pressure of fuel to the surface temperature T_s by the Clausius–Clapeyron vapor-pressure equation discussed in Section 17 of Chapter 1. In a form similar to Eq. (1-216), the

Clausius–Clapeyron equation can be written as

$$\frac{d \ln p_{Fs}}{dT_s} = \frac{\Delta h_v}{RT_s^2} \quad (6-131)$$

or

$$\ln \frac{p_{Fs}}{p_{Fs,\text{ref}}} = \frac{\Delta h_v}{R} \left(\frac{1}{T_{s,\text{ref}}} - \frac{1}{T_s} \right) \quad (6-132)$$

Now we have three equations [Eqs. (6-129), (6-130), and (6-132)] for three unknowns: Y_{Fs} , T_s , and p_{Fs} . Once the solution is obtained, the transfer number B_M and mass evaporation rate can be calculated from Eq. (6-116) and Eq. (6-119).

The lifetime or evaporation time, t_v , of a liquid droplet can be calculated using Eq. (6-119). The droplet evaporation time is an important parameter in combustion-chamber design, since the lifetime of the largest droplet in a spray determines the minimum time the droplet must be allowed to reside in the combustion chamber. Also, the residence time is related to other design parameters such as the air-stream velocity through the combustor, the velocity of the spray injection, the angle of injection, and the combustor geometry. Using the mass continuity at the droplet surface ($-\rho_l dr_s/dt = \rho_s v_s$) and rearranging Eq. (6-119), we have

$$\frac{dr_s}{dt} = -\frac{\rho_s \mathcal{D}_s}{\rho_l r_s} \ln(1 + B) \quad (6-133)$$

After integration and expressing the result in terms of droplet diameter, we have

$$d^2 = d_0^2 - \left[\frac{8\rho_s \alpha_s}{\rho_l} \ln(1 + B) \right] t \quad (6-134)$$

Comparing Eq. (6-134) with the d^2 -evaporation law given by Eq. (6-98), we obtain

$$\beta_v = \frac{8\rho_s \alpha_s}{\rho_l} \ln(1 + B) \quad (6-135)$$

where the evaporation coefficient β_v represents the magnitude of the negative slope of the straight line on the d^2-t plot shown in Fig. 6.23. The lifetime of the droplet is therefore equal to

$$t_{\text{life}} \equiv t_v = \frac{d_0^2}{\beta_v} = \frac{\rho_l d_0^2}{8\rho_s \alpha_s \ln(1 + B)} \quad (6-136)$$

This implies that t_v is longer for larger droplets, and also that lighter fuels evaporate faster. The effect of gas density and thermal diffusivity on droplet evaporation time can also be seen clearly from Eq. (6-136). It will be shown later that even though Eq. (6-136) was derived for evaporating droplets, it is also applicable to burning droplets. Godslove¹¹ and many other experimentalists have found in

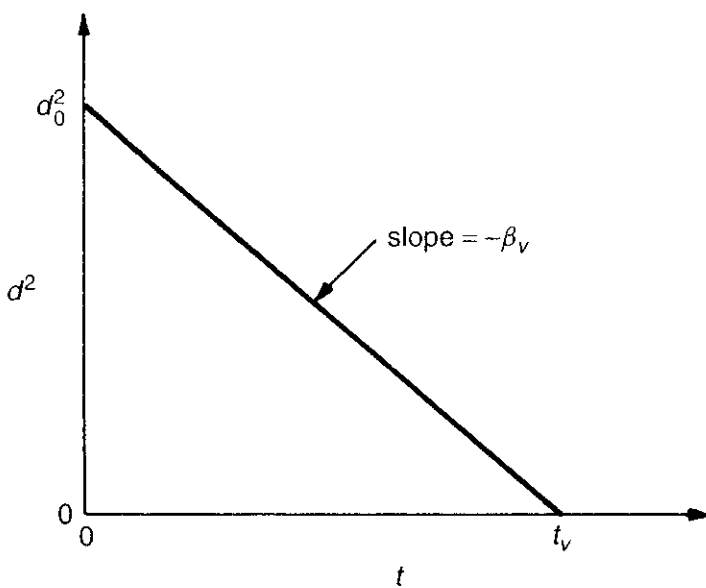


Figure 6.23 The d^2 -evaporation law for liquid fuel droplets.

droplet-burning studies⁵ that the time variation of the droplet diameter was the same as that for evaporation.

4.2 Mass Burning Rate of a Single Fuel Droplet

For a burning droplet, the fuel vapor species conservation equation is very similar to that of Eq. (6-104), except that we have to add a source term on the right-hand side, which corresponds to the generation of fuel species by chemical reaction. Since the fuel species is consumed by chemical reactions, this source term is generally negative.

$$r^2 \rho v \frac{dY_F}{dr} = \frac{d}{dr} \left(r^2 \mathcal{D} \rho \frac{dY_F}{dr} \right) + r^2 \dot{\omega}_F \quad (6-137)$$

Similarly, one can write a species conservation equation for the oxidizer, i.e.,

$$r^2 \rho v \frac{dY_O}{dr} = \frac{d}{dr} \left(r^2 \mathcal{D} \rho \frac{dY_O}{dr} \right) + r^2 \dot{\omega}_O \quad (6-138)$$

Again, the source term for this equation is generally negative due to the consumption of oxidizer species by chemical reactions. The energy conservation equation can be written as

$$r^2 \rho v \frac{dC_p T}{dr} = \frac{d}{dr} \left(\frac{\lambda}{C_p} r^2 \frac{dC_p T}{dr} \right) + r^2 \dot{Q} \quad (6-139)$$

In the following droplet-burning analysis, we shall assume that the fuel and oxidant depletion rates are related in stoichiometric proportions. Consequently,

the following relationship holds:

$$\dot{\omega}_F = \dot{\omega}_O(F/O)_{st} \quad (6-140a)$$

$$\dot{\omega}_F \Delta h_{r,F} = \dot{\omega}_O \Delta h_{r,F}(F/O)_{st} = -\dot{Q} \quad (6-140b)$$

where $\Delta h_{r,F}$ represents the heat of reaction per unit mass of fuel. If one defines the following Shvab-Zel'dovich variables

$$b_{F,O} \equiv \frac{Y_F - Y_O(F/O)_{st}}{(Y_{Fs} - 1) + Y_{Os}(F/O)_{st}} \quad (6-141a)$$

$$b_{F,T} \equiv \frac{Y_F \Delta h_{r,F} + C_p T}{\Delta h_v + \Delta h_{r,F}(Y_{Fs} - 1)} \quad (6-141b)$$

$$b_{O,T} \equiv \frac{Y_O(F/O)_{st} \Delta h_{r,F} + C_p T}{\Delta h_v + (F/O)_{st} Y_{Os} \Delta h_{r,F}} \quad (6-141c)$$

then the energy and species conservation equations can be combined (assuming $Le = 1$) to give the following homogeneous equation without any source terms:

$$r^2 \rho v \frac{db}{dr} = \frac{d}{dr} \left(r^2 \rho \mathcal{D} \frac{db}{dr} \right) \quad (6-142)$$

where b can be either $b_{F,O}$ or $b_{F,T}$ or $b_{O,T}$ defined by Eqs. (6-141a) through (6-141c). Since the product $\rho \mathcal{D}$ is considered to be independent of temperature and $r^2 \rho v = \text{constant}$, Eq. (6-142) can be integrated twice with the boundary conditions

$$r = r_s : \quad v_s = \mathcal{D} \left(\frac{db}{dr} \right)_s \quad (6-143)$$

$$r \rightarrow \infty : \quad b = b_\infty \quad (6-144)$$

to obtain the solution

$$\frac{r^2 \rho v}{\mathcal{D} \rho r} = \ln \left(\frac{b_\infty - b_s + 1}{b - b_s + 1} \right) \quad (6-145)$$

At $r = r_s$

$$r_s \rho_s v_s = \mathcal{D}_s \rho_s \ln[1 + (b_\infty - b_s)] = \mathcal{D}_s \rho_s \ln(1 + B)$$

or

$$G_F = \frac{\dot{m}_F}{4\pi r_s^2} = \mathcal{D}_s \rho_s \frac{\ln(1 + B)}{r_s} \quad (6-146)$$

Note that this equation is identical to Eq. (6-119) for the evaporation case. The only difference is that the transfer number B in Eq. (6-146) can be obtained from

one of the following:

$$B_{F,O} = \frac{(Y_{F\infty} - Y_{Fs}) + (Y_{Os} - Y_{O\infty})(F/O)_{st}}{(Y_{Fs} - 1) + (F/O)_{st}(Y_O)_s} = \frac{\underbrace{(F/O)_{st}Y_{O\infty} + Y_{Fs}}_{\text{with combustion}}}{\underbrace{1 - Y_{Fs}}_{\text{without combustion}}} \quad (6-147a)$$

$$B_{F,T} = \frac{\Delta h_{r,F}(Y_{F\infty} - Y_{Fs}) + C_p(T_\infty - T_s)}{\Delta h_v + \Delta h_{r,F}(Y_{Fs} - 1)} = \frac{\underbrace{C_p(T_\infty - T_s) - Y_{Fs}\Delta h_{r,F}}_{\text{with combustion}}}{\underbrace{\Delta h_v + \Delta h_{r,F}(Y_{Fs} - 1)}_{\text{without combustion}}} \quad (6-147b)$$

$$\begin{aligned} B_{O,T} &= \frac{(F/O)_{st}(Y_{O\infty} - Y_{Os})\Delta h_{r,F} + C_p(T_\infty - T_s)}{\Delta h_v + (F/O)_{st}Y_{Os}\Delta h_{r,F}} \\ &= \frac{\underbrace{C_p(T_\infty - T_s) + Y_{O\infty}(F/O)_{st}\Delta h_{r,F}}_{\text{with combustion}}}{\Delta h_v} \end{aligned} \quad (6-147c)$$

where for the combustion case $Y_{Os} = Y_{F\infty} = 0$.

Because $B_{F,O} = B_{O,T}$, we have

$$\frac{Y_{O\infty}(F/O)_{st} + Y_{Fs}}{1 - Y_{Fs}} = \frac{\Delta h_{r,F}(F/O)_{st}Y_{O\infty} + C_p(T_\infty - T_s)}{\Delta h_v} \quad (6-148)$$

The unknowns in this equation are T_s and Y_{Fs} . These two unknowns together with the vapor pressure of the fuel can be calculated by the same method outlined above for a noncombusting liquid droplet. Once these parameters are known, \dot{m}_F can be determined from Eq. (6-146).

Values of B taken from both Spalding⁸ and Blackshear⁹ for various condensed combustible substances are given in Table 6.1. The most convenient form of B is $B_{O,T}$, which can be expressed as

$$B_{O,T} = \frac{C_p(T_\infty - T_s) + (F/O)_{st}Y_{O\infty}\Delta h_{r,F}}{\Delta h_v} \approx \frac{Y_{O\infty}\Delta h_{r,F}}{\Delta h_v}(F/O)_{st} \quad (6-149)$$

As soon as $Y_{O\infty}$ is known, $B_{O,T}$ can be calculated from Eq. (6-149) and the burning rate of the droplet can be determined from Eq. (6-146). In general, the surface temperature has less effect on the burning rate than that of the mass fractions Y_{Fs} and $Y_{O\infty}$. It is interesting to note that for most hydrocarbon fuels, B does not change too much and is in the range of $1.7 < B < 6.5$. It can be seen clearly from Eq. (6-146) that the controlling term for the difference in mass burning rates between various fuels is due to the magnitude of the product $\mathcal{D}_s \rho_s$. Since $(1 + B)$ is inside a natural logarithm, a tenfold variation in B results in only an approximately twofold variation in burning rate. Therefore, the

Table 6.1 Values of the Transfer Number for Various Condensed Combustible Substances⁸⁻¹⁰

Combustible in Air	<i>B</i>
iso-Octane	6.41
Benzene	5.97
<i>n</i> -Heptane	5.82
Toluene	5.69
Aviation gasoline	≈5.5
Automobile gasoline	≈5.3
Kerosene	≈3.4
Gas oil	≈2.5
Light fuel oil	≈2.0
Heavy fuel oil	1.7
Carbon	0.12

$\Delta h_{r,F}$ does not have a strong influence on the magnitude of the mass consumption rate.

If it is assumed that the flame exists at the position where $Y_O = Y_F = 0$, then the temperature of the flame and its position can be determined. However, it is important to show that the burning rate can be determined *without* knowing where the flame front is. Equation (6-145) may be written in the following form:

$$\frac{r^2 \rho v}{\mathcal{D} \rho r} = \frac{r_s^2 \rho_s v_s}{\mathcal{D}_s \rho_s r} = \ln \left[\frac{Y_{F\infty} - Y_{Fs} - (F/O)_{st}(Y_{O\infty} - Y_{Os}) + (Y_{Fs} - 1)}{Y_F - Y_{Fs} - (F/O)_{st}(Y_O - Y_{Os}) + (Y_{Fs} - 1)} \right] \quad (6-150)$$

At the flame surface $Y_F = Y_O = 0$ and $Y_{F\infty} = Y_{Os} = 0$; thus Eq. (6-150) becomes

$$\frac{r_s^2 \rho_s v_s}{\mathcal{D}_s \rho_s r_{\text{stoich}}} = \ln[1 + (F/O)_{st} Y_{O\infty}] \quad (6-151)$$

Since $4\pi r_s^2 \rho_s v_s = \dot{m}_F$ is known, r_{stoich} can be solved for. The flame temperature at r_{stoich} can be obtained by setting $b = b_{O,T}$ in Eq. (6-145) and making use of Eq. (6-151). It is interesting to note that the flame temperature T_f can be *higher* than the adiabatic flame temperature, since the nitrogen diffused into film I is preheated, which can in turn heat the fuel vapor before its reaction with the oxidizer.

5 FUEL DROPLET IN A CONVECTIVE STREAM

5.1 Correlation Development for Nearly Spherical Droplets in Convective Streams

When the droplets are not at rest relative to the oxidizing atmosphere, the results for quiescent flow will no longer hold true and effects of forced convection must

be considered; especially when $\text{Re}_d > 20$, there exists a boundary-layer flow region around the front of the droplet and a wake region behind the droplet. The boundary condition at the droplet surface can be expressed as

$$\bar{h}_c(\Delta T) = \rho_s v_s \Delta h_v = \frac{\dot{m}_f}{4\pi r_s^2} \Delta h_v = \frac{\mathcal{D}_s \rho_s}{r_s} \Delta h_v \ln(1 + B) \quad (6-152)$$

where the driving potential (ΔT) for convective heat transfer is

$$\Delta T \equiv \left[T_\infty + \frac{(F/O)_{st} Y_{O\infty} \Delta h_{r,F}}{C_p} \right] - T_s \quad (6-153)$$

The second term in the square bracket of Eq. (6-153) represents the increase of temperature from T_∞ due to chemical reaction around the droplet. Essentially, the thermal driving potential in Eq. (6-153) is expressed as the ambient temperature T_∞ plus the rise in temperature due to the chemical-energy release minus the surface temperature.

Substituting the ΔT expression of Eq. (6-153) into Eq. (6-152), we have

$$\begin{aligned} \bar{h}_c \frac{(F/O)_{st} Y_{O\infty} \Delta h_{r,F} + C_p(T_\infty - T_s)}{C_p} &= \frac{\mathcal{D}_s \rho_s}{r_s} \Delta h_v \ln(1 + B) \\ &= \frac{\lambda_s}{C_p r_s} \Delta h_v \ln(1 + B) \end{aligned} \quad (6-154)$$

After rearranging, we have

$$\frac{\bar{h}_c r_s}{\lambda_s} = \left[\frac{(F/O)_{st} Y_{O\infty} \Delta h_{r,F} + C_p(T_\infty - T_s)}{\Delta h_v} \right]^{-1} \ln(1 + B) \quad (6-155)$$

Recalling the definition of B [see Eq. (6-149)] and the Nusselt number, the above equation becomes

$$\text{Nu}_{r_s} \equiv \frac{\bar{h}_c r_s}{\lambda_s} = \frac{\ln(1 + B)}{B} \quad (6-156)$$

This is why the quantity $[\ln(1 + B)]/B$ has been commonly used as an empirical correction factor to the Nusselt number for problems with high Reynolds numbers. A classical expression¹⁰ for Nu_{r_s} of a sphere in convective stream is

$$\text{Nu}_{r_s} = \frac{\ln(1 + B)}{B} [1 + 0.39 \text{Re}_{r_s}^{1/2} \text{Pr}^{1/3}] \quad (6-157)$$

It is interesting to note that as Re_{r_s} approaches 0, Eq. (6-157) reduces to Eq. (6-156). Also, if $\text{Pr} = 1$ and $\text{Re}_{r_s} \gg 1$, Eq. (6-157) becomes

$$\text{Nu}_{r_s} = 0.39 \left[\frac{\ln(1 + B)}{B} \right] \text{Re}_{r_s}^{1/2} \quad (6-158)$$

Using Eqs. (6-152), (6-153), and (6-147) and setting $\text{Pr} = 1$ (or $C_p\mu = \lambda_s$), we have

$$\begin{aligned}\frac{\bar{h}_c r_s}{\lambda_s} &= \frac{\bar{h}_c \Delta T r_s}{\Delta T \lambda_s} = \frac{\rho_s v_s \Delta h_v r_s C_p \mu}{\Delta T \lambda_s C_p \mu} \\ &= \frac{\rho_s v_s r_s}{\mu} \frac{\Delta h_v}{(F/O)_{st} Y_{O\infty} \Delta h_{r,F} + C_p(T_\infty - T_s)} = \frac{\rho_s v_s r_s}{\mu} \frac{1}{B}\end{aligned}$$

Hence, Eq. (6-158) becomes

$$\left(\frac{\rho_s v_s r_s}{\mu}\right) \frac{1}{\ln(1+B)} = 0.39 \text{ Re}_{r_s}^{1/2} \quad (6-159)$$

Due to the fact that a wake region exists behind the droplet, this equation, deduced from Eq. (6-158), is not likely to give accurate quantitative predictions. However, it has been found that after multiplying the left-hand side of the above equation by $B^{0.15}$, the following two dimensionless parameters can often be used to correlate experimental data:

$$\left(\frac{\rho_s v_s r_s}{\mu}\right) \frac{B^{0.15}}{\ln(1+B)} \quad \text{and} \quad \text{Re}_{r_s}^{1/2}$$

The above relationship implies that droplet-burning rate under a laminar convective flow condition follows a $d^{3/2}$ -burning-rate law. As we shall discuss in a later section, droplet burning follows a power law in the diameter with exponent on the order of 1 in turbulent flows.

5.2 Simulation of Deformed Droplet Dynamics

Jeng and Deng²⁶ developed a comprehensive computational model based on the Arbitrary Lagrangian Eulerian (ALE) numerical algorithm for the numerical simulation of nonspherical evaporating droplet dynamics in viscous convective flows. Their model has the ability to simulate deforming, evaporating droplet dynamic behavior under convective flows when surface tension, phase change, and mass and heat transfer are influential.

There are several dimensionless parameters controlling the droplet deformation and breakup process. Besides the Reynolds number (based on the relative velocity between the particle and gas), the special Weber number used by Borisov et al.²⁷ has the following definition:

$$\text{We} \equiv \frac{\rho |v_p - v_g|^2 d}{2\sigma_s} = \frac{\text{aerodynamic force}}{\text{surface tension force}} \quad (6-160)$$

This definition of We is somewhat unusual since it has a factor of 2 in the denominator. When the value of We is much less than 10, droplets are nearly spherical. The Bond number (Bo) is associated with the onset of instability on

the liquid surface due to droplet acceleration. The Bond number is defined as

$$Bo \equiv \frac{a\rho_f d^2}{\sigma_s} = \frac{\text{acceleration force}}{\text{surface tension force}} \quad (6-161)$$

where a represents droplet acceleration. According to Borisov et al.,²⁷ there are three secondary droplet-breakup regimes:

Parachute type (bag type): Droplet flattens perpendicular to flow and eventually forms a shroud. This shroud either breaks off, forming a group of small droplets, or several parachutes are formed from one droplet. In the final stage, the breakup process produces a group of fine droplets. This usually happens when

$$\begin{aligned} 8 &\leq We \leq 40 \\ 0.2 &\leq We Re_d^{-0.5} \leq 1.6 \end{aligned}$$

Stripping type: Droplet flattens perpendicular to flow, and the gas flow tears off shrouds from the flattened droplet, followed by disk-shaped droplet reaching its critical deformation and breaking into smaller droplets.

$$\begin{aligned} 20 &\leq We \leq 2.0 \times 10^4 \\ 1.0 &\leq We Re_d^{-0.5} \leq 20 \end{aligned}$$

Explosion type: Droplet instantly shatters into many fine particles.

$$\begin{aligned} 2.0 \times 10^3 &\leq We \leq 2.0 \times 10^5 \\ 20 &\leq We Re_d^{-0.5} \leq 200 \end{aligned}$$

It is useful to note that the critical value of We depends on the time over which the relative velocity between the droplet and the surrounding gas acts on the droplet. Since the breakup process takes a finite amount of time, the length of time that the flow acts on the droplet may determine whether breakup will actually occur, even though the breakup criteria may be satisfied.

In Jeng and Deng's study,²⁶ they showed that the numerically predicted breakup modes agree well with experimentally derived criteria. Their computational results on evaporating droplets indicated that the dynamics of droplet deformation are basically unaffected by the evaporation process. However, deformation effects on the evaporation rate are significant. The evaporation rates per unit area of deformed droplets are smaller (e.g., $\sim 85\%$) than those of nondeformed droplets. This is due to the larger recirculation zone at the back of the deformed droplet, where the evaporation rate is significantly decreased. For droplets with severe deformation, more and more energy must be fed into the liquid droplet to raise its temperature. Nevertheless, the total evaporation rate of the severely deformed droplet can be

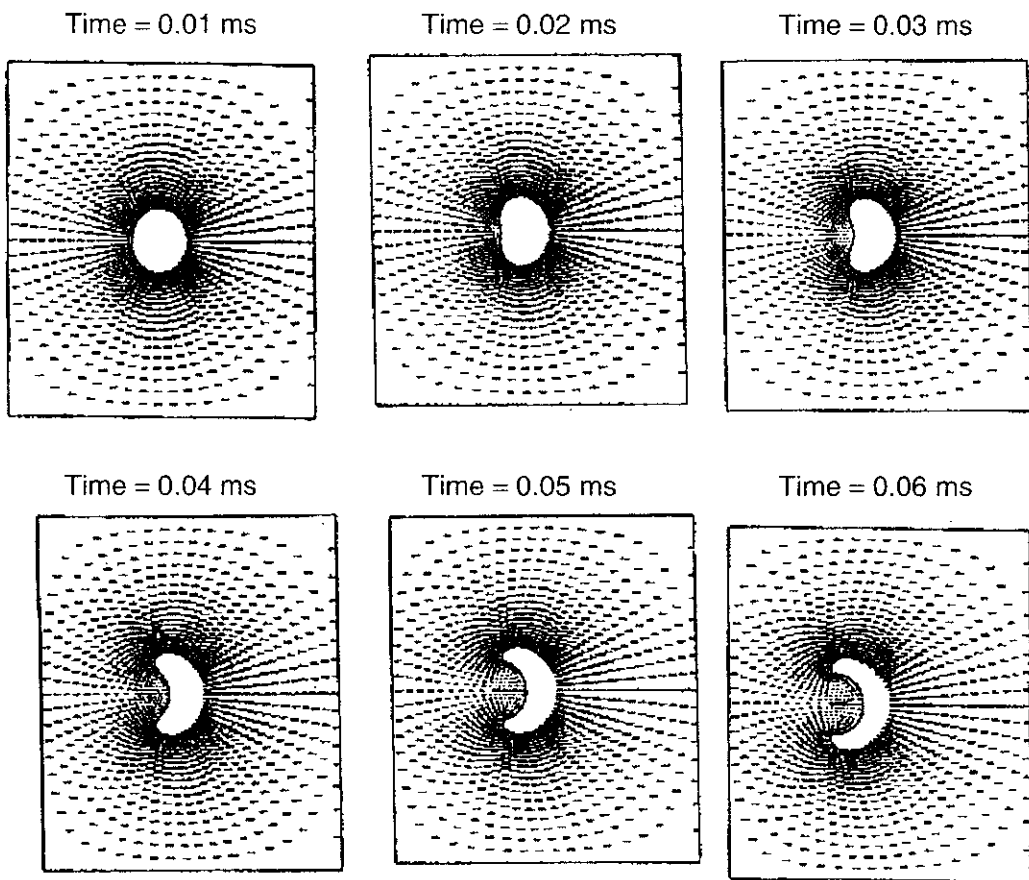


Figure 6.24 Calculated droplet deformation when it is undergoing stripping-type breakup (after Jeng and Deng²⁶).

larger than that of the undeformed spherical droplet, since the surface area of the deformed droplet is much larger than that of undeformed spherical droplet. A set of typical calculated results of Jeng and Deng²⁶ for stripping-type breakup ($Re_d = 36$ and $We = 298$) are shown in Fig. 6.24. In this figure, the gases are flowing from right to left.

5.3 Effect of Internal Circulation on Droplet Vaporization Rate

In many practical high-pressure combustors, the Reynolds number based on the relative velocity between gas and droplet is on the order of 100 or higher. This implies that the shear stress at the gas–liquid interface can be large enough to induce internal liquid-phase circulation. The liquid motion can then be important in determining the heat and mass transfer processes within the droplet and thereby modify the vaporization rate. Prakash^{18–20} and Sirignano^{19,20} developed a theoretical model for the prediction of droplet vaporization rate, considering the effect of internal circulation within a droplet.

They demonstrated that boundary layers exist in both the gas and liquid phases near the droplet surface over most of its lifetime and that convection is an important transport mode within the droplet. They considered a thin boundary layer near the surface of the droplet in the liquid phase. The liquid motion in the core

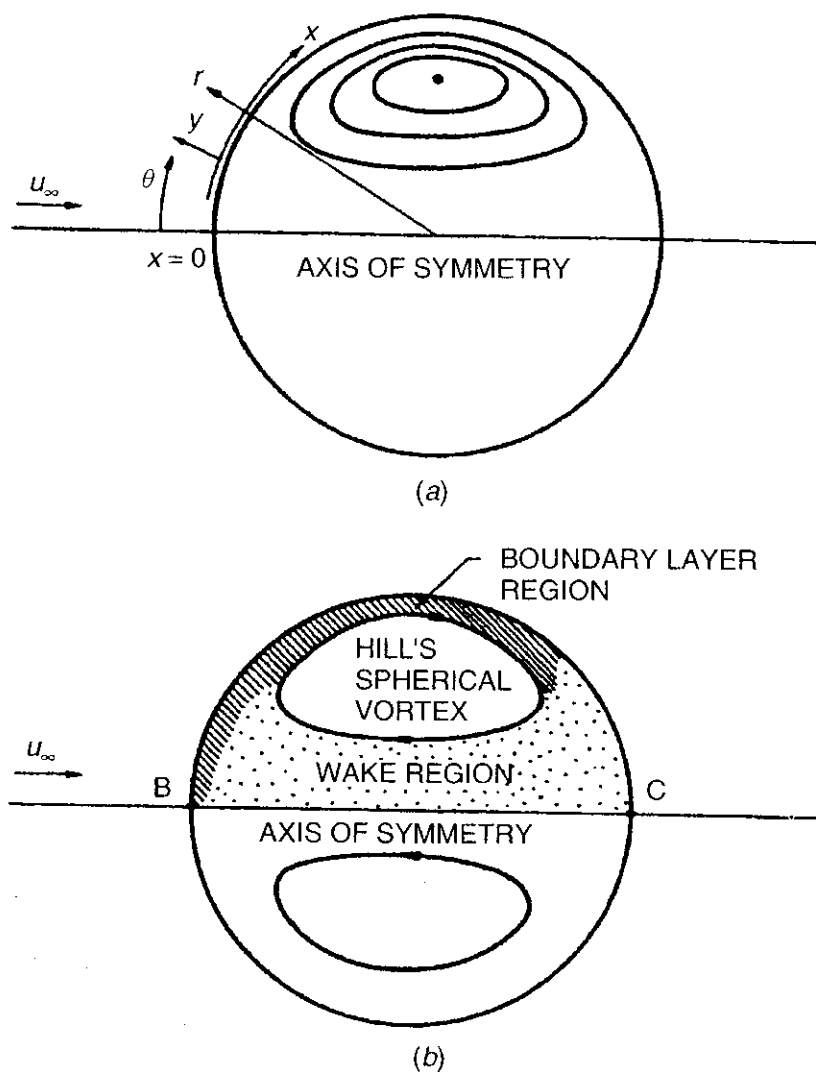


Figure 6.25 (a) Hill's spherical vortex and orthogonal boundary-layer coordinate system used by Prakash and Sirignano.^{19,20} (b) Various regions considered in Prakash and Sirignano's model.¹⁸⁻²⁰

region was approximated by Hill's spherical vortex as shown in Fig. 6.25a. The third liquid-phase region considered in their physical model was an inviscid wake near the axis of symmetry shown in Fig. 6.25b. The gas-phase motion near the surface was analyzed for three different regions: a front stagnation region, a boundary-layer region, and a separation region. For the boundary layer, the Karman-Pohlhausen integral approach⁴ was used. The matching with the front stagnation region was performed by requiring that the gradient of momentum and energy along the droplet surface be continuous. In the separation region, the boundary-layer equations cannot be used. The heat flux in this region was neglected in comparison with the fluxes in the boundary layer.

The gas-phase flow over a vaporizing droplet, rigorously speaking, is unsteady due to the temporal change in the size of the droplet. However, the characteristic time for changes in the gas phase is the residence time in the neighborhood of the droplet, and the time is usually much shorter than the droplet lifetime. Therefore, the quasi-steady gas-phase assumption was employed in Prakash and Sirignano's

model. It should be noted that although the conditions in many combustors are turbulent, a locally laminar boundary layer exists over the spherical droplet surface, since the typical size of a droplet is much smaller than a typical large eddy size. This is why laminar gas-phase equations are considered in their model.

In brief, for evaluating the heating of the droplet, the thermal-boundary-layer equations were solved in a way similar to the viscous-boundary-layer equations. The heating of the core has been shown to be essentially normal to the closed streamlines of the Hill's vortex, and the heating process is unsteady. In the solution of this coupled gas–liquid problem, the gas-phase boundary layer is first treated using the initial guess or the relaxed previous iterated values for surface velocity and surface temperature. With the shear stress and the heat flux from the gas-phase solution, the liquid-phase viscous and thermal boundary layer and then the thermal core are resolved. The gas-phase and liquid-phase solutions are iterated until convergence is reached. The new droplet radius corresponding to the next time step is calculated, and the process is repeated at the advanced time. Since the droplet becomes heated as time increases, the liquid viscosity and thus the strength of the Hill's vortex are updated in time. The overall vaporization rate at any instant is calculated by integrating the vaporizing flux over the droplet surface.

Three hydrocarbon fuels (*n*-hexane, *n*-decane, and *n*-hexadecane) evaporating in air were considered for $T = 1000$ K and $p = 10$ atm. The results for *n*-decane are shown in Fig. 6.26, which shows the variation of $(r_s/r_{s0})^{3/2}$ and the dimensionless average vaporizing mass flux. A comparison of the calculated results of Prakash and Sirignano with those based on the Ranz–Marshall correlation²¹ and the Spalding correlation²² are shown in this figure. The Ranz–Marshall correlation is

$$\dot{m} = \dot{m}_{ss}(1 + 0.276\text{Re}_d^{1/2}\text{Pr}^{1/3}) \quad (6-162)$$

where \dot{m}_{ss} is the mass vaporization rate with spherically symmetric vaporization. The Spalding correlation is given in terms of the Spalding transfer number B and the Reynolds number based on droplet diameter, that is,

$$\frac{\dot{m}}{4\pi r_s \mu} = 0.265 B^{3/5} \text{Re}_d^{1/2} \quad \text{for } 0.6 < B < 5 \quad (6-163)$$

Spalding's correlation was based on experiments with Reynolds numbers between 800 and 4000, and the scatter of the experimental results was about 15–20%.

In using these correlations, the heat of vaporization was modified by Prakash and Sirignano to take into account the heat flux into the liquid phase. The modified heat of vaporization was calculated using their results for the average heat flux into the liquid phase. Figure 6.26 shows that the solution of Prakash and Sirignano is in good agreement with the Ranz–Marshall correlation during the initial part of the lifetime when the vaporization rate is small. The numerical results are lower than Spalding's correlation by about 15–20% towards the end of the lifetime of the droplet. According to Prakash and Sirignano, the difference could be due

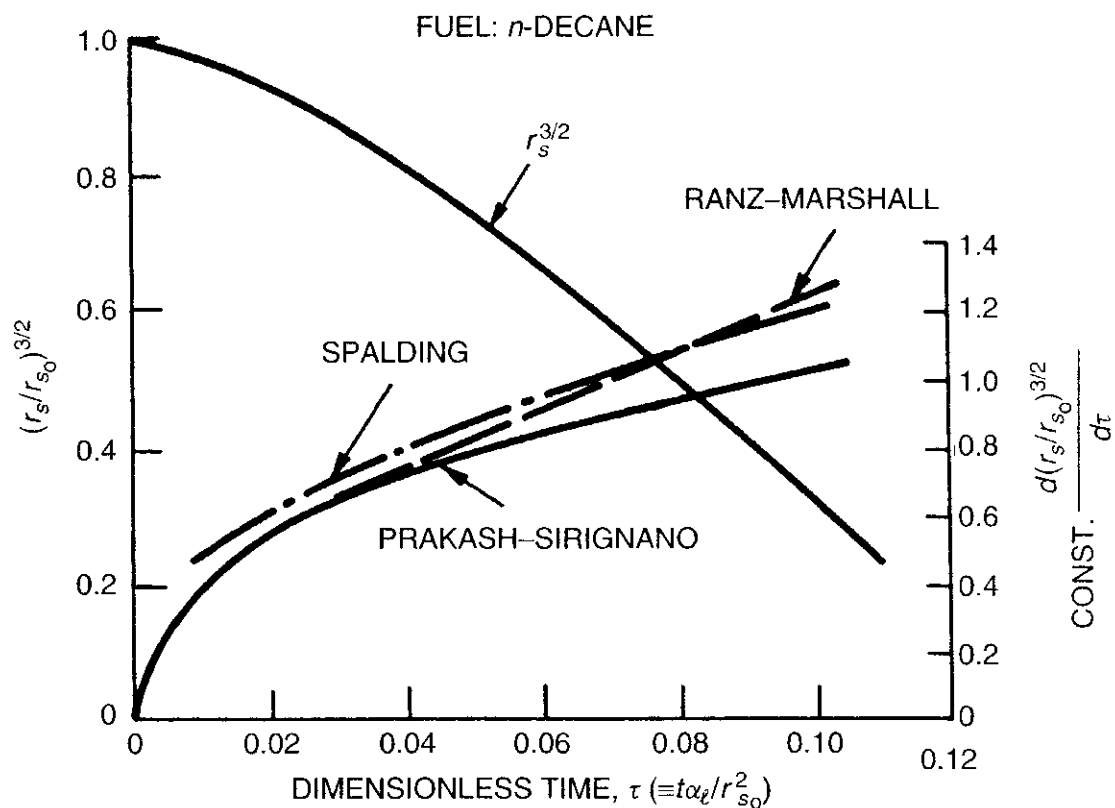


Figure 6.26 Droplet size and vaporization rate versus time (adapted from Prakash and Sirignano²⁰).

to the wake region's contribution to vaporization, which was neglected in their model. The contribution may be important when the droplet is heated. A part of the disagreement could also be due to the experimental error in the correlation.

For a comparison of the droplet lifetime for the three fuels, the change of droplet radius with respect to time is plotted on the same graph in Fig. 6.27. The timescale is nondimensionalized by the thermal diffusion time r_{s0}^2/α_l of the liquid droplet. It can be seen from this figure that the variations in the lifetimes for the three fuels are only about 10%, although their volatilities are quite different. It is also interesting to note from this figure that the vaporization rates in the initial part of the lifetime are substantially smaller for the less-volatile fuels. To understand why the lifetimes of these fuels are about the same, we need to examine the temperature–time history of these fuel droplets. A plot of the surface temperature variation (at $\theta = 90^\circ$) and vortex-center temperature variation versus dimensionless time is given in Fig. 6.28. The surface temperature rises sharply during the initial heating period, and then the change becomes smaller at later times. The surface temperature for each of the three fuels is less than the boiling point of the fuel even at the end of the droplet lifetime. This effect is strongest for the least-volatile fuel (hexadecane). The temperature at the center of the vortex of each fuel droplet is considerably lower than the droplet surface temperature during the earlier part of the lifetime. At the end of the droplet lifetime, the vortex center temperature is about 20 K lower for hexadecane and about 6 K lower for *n*-hexane (the most volatile fuel).

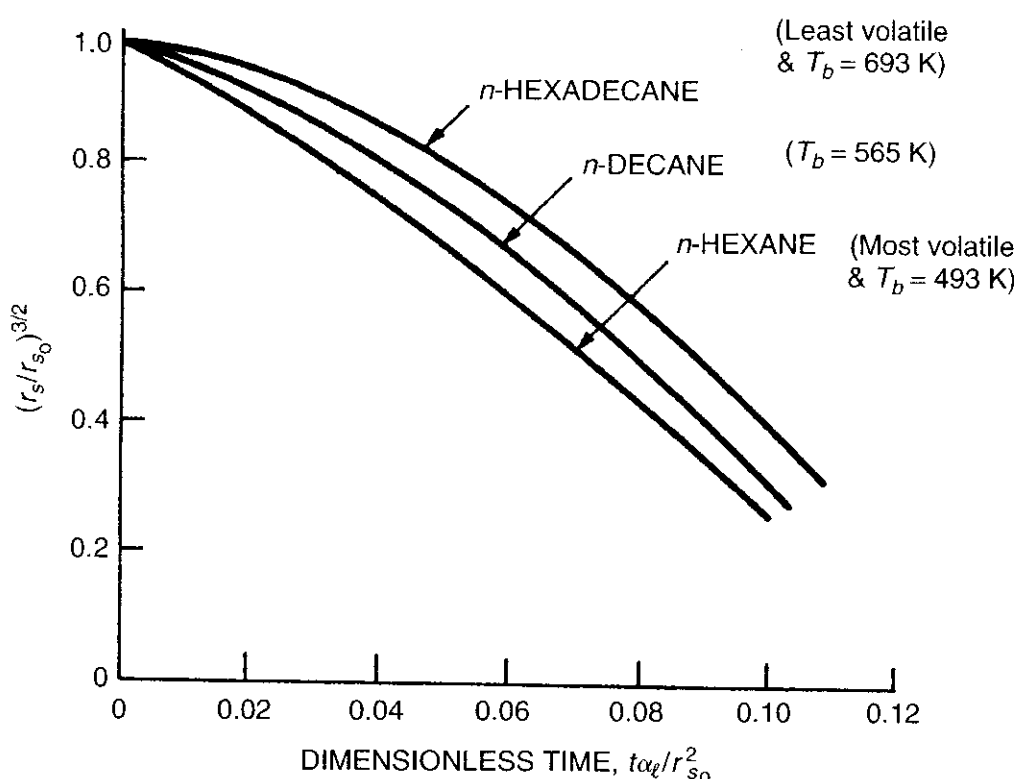


Figure 6.27 Comparison of droplet lifetimes of three hydrocarbon fuels (after Prakash and Sirignano²⁰).

The reason for the small variation in the overall lifetime of a single droplet is that the surface temperature for the less-volatile fuel rises quickly to a high value in a very short time, during which the quasi-steady thermal boundary layer is established. After the initial establishment of the thermal boundary layer, the surface temperature rises slowly, so that the less-volatile fuel is always at a higher temperature at any time, and hence the droplet lifetime is not significantly affected by the differences in volatility.

According to Prakash and Sirignano,^{19,20} the internal circulation model lies between two extreme models: (a) a pure conduction model without any circulation, and (b) a rapid-mixing model. The pure conduction model has a zero vortex strength, while the rapid-mixing model has an infinite circulation rate. Their model showed that internal circulation leads to a shorter characteristic heating length than in the pure conduction case. In particular, the distance from the droplet surface to the vortex center is about $\frac{1}{3}$ of the droplet radius. This implies that the characteristic heating time (which is proportional to the length squared) decreases by about an order of magnitude due to internal circulation. The heating time can be defined as the time required to reach a nearly uniform temperature profile in the droplet. In general, it is expected that the internal circulation via increased heat transfer rates to the droplet interior will yield lower surface temperatures and lower vaporization rates during the initial portion of the droplet lifetime than would be achieved with pure conduction only. The rapid-mixing model should yield still lower vaporization rates during this initial time interval. For an isolated droplet, Prakash and Sirignano concluded that the unsteadiness

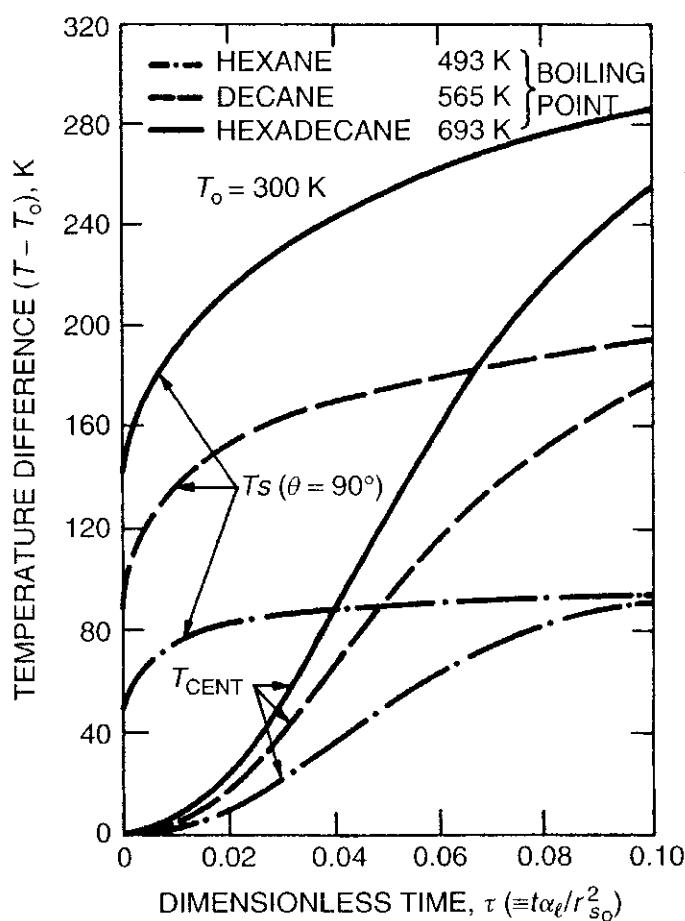


Figure 6.28 Surface and vortex-center temperature variation with respect to time (modified from Prakash and Sirignano²⁰).

in droplet vaporization persists for most of the droplet lifetime, especially for the less-volatile fuels. The temperature distribution inside the droplet is nonuniform for most of the lifetime; the difference between the surface temperature and the temperature in the interior is higher for the heavier and less-volatile fuels.

6 SUPERCRITICAL BURNING OF LIQUID DROPLETS IN A STAGNANT ENVIRONMENT

Liquid droplet vaporization and combustion in supercritical environments have attracted the interest and attention of many researchers due to their direct application to the development of high-pressure combustion devices such as liquid-propellant rockets, gas-turbine engines, diesel engines, pulse-detonation engines, liquid-fuel ramjets, underwater propulsion systems, etc. Liquid fuels and/or oxidizers are usually delivered to combustion chambers as a spray of droplets, which then undergo a sequence of vaporization, mixing, ignition, flame spreading, and combustion processes. Very often, combustion processes take place at pressure levels well above the thermodynamic critical points of the reactant fluids. Even though the reactant liquids are usually injected initially at subcritical temperatures, they can be heated up quickly and experience a thermodynamic state

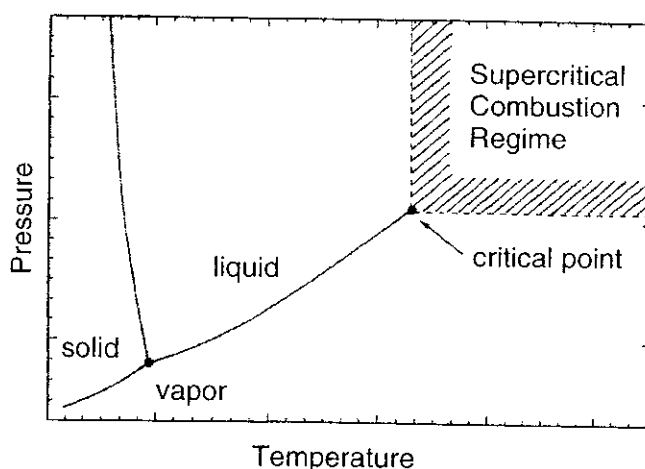


Figure 6.29 Phase diagram of a liquid fuel.

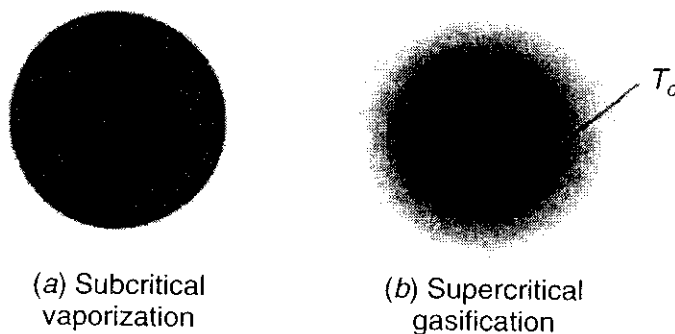


Figure 6.30 Subcritical and supercritical droplet vaporization (after Yang³⁴).

transition into the supercritical regime during their lifetimes. The critical pressure (P_c), critical temperature (T_c), and the supercritical combustion regime are shown in a phase diagram in Fig. 6.29. The surface condition of a droplet under supercritical gasification is very different from that of subcritical gasification as shown in Fig. 6.30.

The supercritical process exhibits many characteristic differences from those of subcritical conditions. First of all, as the pressure exceeds the critical pressure of the injected fuel, the latent heat of vaporization (Δh_v) becomes zero and the quasi-steady Eqs. (6-149) and (6-119) correspondingly predict a vaporization rate that rises to infinity. Second, the gaseous mass in the region influenced by the droplet increases with pressure; therefore, the transient term in the energy equation is no longer negligible. Third, the situation of abrupt change of liquid phase to gas phase at the droplet outer radius for the subcritical evaporation/burning condition is replaced by the gradual density change situation for the supercritical gasification/burning condition, as shown in the figure adopted from Yang.³⁴ The surface tension also vanishes under supercritical conditions.

In addition to the above difference, there are several reasons why conventional quasi-steady analysis and results for low-pressure applications are inappropriate for supercritical combustion at high pressures. These are caused by the necessary

consideration of (1) thermodynamic nonideality at high pressures, (2) significant transport and thermal property variations with pressure and temperature beyond the critical point, (3) ambient gas solubility into the dense “liquid” material, and (4) transient diffusion process of gas-phase species. These distinct factors render conventional approaches developed for low-pressure applications invalid.

The transient burning of a composite solid propellant was studied by Summerfield.¹² Extending Summerfield’s approach to transient-burning problems, Spalding¹³ developed a theory to predict the rate of combustion of liquid droplets under high pressure. The basic equations used by Spalding were based on the conservation of elements. Rosner¹⁴ and Dominicis¹⁵ modified Spalding’s analysis and used conservation of chemical compounds. The basic model consists of a pocket of fuel vapor surrounded by a spherical flame zone. Outside the flame zone is an environment containing an oxidant. Fuel diffuses outward to the flame zone, and oxidant diffuses inward to the flame, where they react instantly to form combustion products. In recent years, there have been significant advances in supercritical droplet analyses by various groups of researchers; these are summarized in Table 6.2.

The influences of convection, density variation, and finite-rate chemical kinetics on supercritical combustion were studied by Brzustowski,³⁵ Chervinsky,¹⁶

Table 6.2 Approaches and Emphases of Different Researchers on Supercritical Droplet Gasification/Burning (modified from Yang³⁴)

Date and Research Groups	Approaches and Emphases
1959 Spalding ¹³	Pocket of dense fuel gas with constant physical properties; studied effect of finite-rate chemical kinetics
1967 Rosner, ¹⁴ Brzustowski, ³⁵ Chervinsky, ¹⁶ Polymeropoulos & Peskin ³⁶	
1969 Manrique and Borman ³⁷	Pressure effect on interfacial thermodynamics
1971 Faeth, ^{38,39} Lazar, ³⁸ Canada, ³⁹ Kadota & Hiroyasu, ⁴¹ Rosner & Chang ⁴⁰	
1986 Umemura ⁶⁰	Effect of criticality
1991 Hsieh, Shuen, & Yang ⁴²	Effect of property variation
1992 Curtis & Farrel, ⁴³ Jia & Gogos ⁴⁴	
1993 Delpanque & Sirignano ⁴⁵	
1994 Jiang & Chiang, ^{46,47}	
1995 Daou, Haldenwang, & Nicoli ⁴⁸	
1995 Hsiao, ⁵¹ Lafon, ⁵² Yang ⁷⁵	Unified treatment of thermophysical properties
1996 Haldenwang, Daou, & Nicoli ⁵⁴	
1998 Harstad & Bellan, ^{56,57} Meng & Yang, ⁵⁵ Umemura & Shimada ⁶²	Improved treatment of thermodynamics and transport phenomena

Polymeropoulos and Peskin,³⁶ and Manrique and Borman,³⁷ who found that the effects of thermodynamic nonidealities, property variations, and high-pressure corrections for phase equilibrium could influence the vaporization mechanisms significantly. Based on these findings, Lazar and Faeth³⁸ and Canada and Faeth³⁹ conducted a series of experimental and theoretical studies on droplet combustion in both stagnant and forced convective environments, with special attention focused on the high-pressure phenomena of phase equilibrium. The effects of forced convection in the gas phase were treated by conventional multiplicative corrections. Their assumptions of quasi-steadiness and uniform property distributions^{38,39} were later relaxed. In studies by Rosner and Chang⁴⁰ and Kadota and Hiroyasu,⁴¹ the effects of transient processes, natural convection, and the conditions under which a droplet may be driven to its critical point were examined.

Several research groups⁴²⁻⁴⁸ recently employed numerical techniques to simulate high-pressure droplet vaporization and combustion with considerable success. All of these models, however, adopted certain basic assumptions and empirical formulas for fluid properties extrapolated from low-pressure cases, with their accuracy for high-pressure applications subject to question. Furthermore, according to Yang,³⁴ no effort was made by these groups to treat the thermodynamic phase transition through the critical point. In order to remedy these deficiencies, a series of fundamental studies⁴⁹⁻⁵⁹ were conducted using the state-of-the-art treatment of thermodynamic and transport phenomena. Of particular importance is the unified analyses of thermophysical properties^{50,51,56-59} based on fundamental thermodynamic theories. These approaches allow for a self-consistent solution from first principles, thereby enabling a systematic investigation into underlying mechanisms involved in supercritical droplet gasification and combustion. The effect of nonequilibrium phase transition on droplet behavior was further addressed by Harstad and Bellan,⁵⁶⁻⁵⁹ using Keizer's fluctuation theory. In addition, Umemura and Shimada⁶⁰⁻⁶² constructed approximate analyses to elucidate many intriguing characteristics of supercritical droplet gasification. Extensive reviews of supercritical droplet gasification and burning were conducted recently by Givler and Abraham⁶³ and Bellan.⁶⁴

6.1 Thermodynamic and Transport Properties

Due to the continuous variations of fluid properties in supercritical environments, classical techniques dealing with liquids and gases individually often lead to erroneous results of droplet dynamics. The problem becomes even more exacerbated when the droplet surface approaches the critical condition. The thermal properties usually exhibit anomalous variations and are very sensitive to both temperature and pressure in the vicinity of the critical point, a phenomenon commonly referred to as near-critical enhancement. Thus, an essential prerequisite of any realistic treatment of supercritical droplet behavior is the establishment of a unified property evaluation scheme capable of treating thermal properties of the system and its constituent species over the entire fluid thermodynamic state, from compressed liquid to dilute gas.

As described in Appendix A, the fluid density as one of the thermal properties can be derived from a modified Benedict–Webb–Rubin (BWR) equation of state proposed by Jacobsen and Stewart⁶⁵ due to its superior performance over conventional cubic equations of state.⁶⁶ This equation of state is extremely valuable in correlating both liquid and vapor thermodynamic and volumetric data; however, the temperature constants involved are available only for a limited number of pure substances.⁶⁷ To overcome this constraint, an extended corresponding-state (ECS) principle described by Ely and Hanley^{68,69} is used. The basic idea is to assume that the properties of a single-phase fluid can be evaluated via conformal mappings of temperature and density to those of a given reference fluid. As a result, only the BWR constants for the reference fluid are needed. For a multicomponent system, accounting for changes in properties due to mixing is much more complicated (see Appendix A for mixing rules). A pseudo pure-substance model is adopted to evaluate the properties of a mixture, treating the mixture as a single-phase pure substance with its own set of properties evaluated via the ECS principle. This method improves prediction accuracy and requires only limited data (i.e., critical properties and Pitzer's acentric factor) for each constituent component. Successful application of the corresponding-state argument for the evaluation of fluid p - V - T properties also encourages similar improvement in the prediction of thermal data. In the following section, a brief summary of the corresponding-state method in conjunction with the mixture-combining rule is first given, followed by the BWR equation of state for the reference fluid. In a later section, the techniques for evaluating thermal and transport properties are addressed.

6.1.1 Extended Corresponding-State Principle The extended corresponding-state model of Ely and Hanley^{68,69} is used to evaluate volumetric and transport properties of a mixture over its entire thermodynamic fluid state. The scheme assumes that the configurational properties (such as temperature, density, viscosity, thermal conductivity, etc.) of a single-phase mixture can be equated to those of a hypothetical pure fluid, which are then evaluated via corresponding-state principles with respect to a given reference fluid. For example, the viscosity of a mixture, μ_m , can be related to that of a reference fluid, μ_0 , at the corresponding thermodynamic state as

$$\mu_m(\rho, T) = \mu_0(\rho_0, T_0) F_\mu \quad (6-164)$$

where F_μ represents the mapping function. The correspondence of temperature and density between the mixture of interest and the reference fluid can be characterized by the following two scaling factors.

$$f_m = \frac{T}{T_0}; \quad \hbar_m = \frac{\rho_0}{\rho} \quad (6-165)$$

The f_m parameter represents the conformation of potential distribution of energy, while the \hbar_m function characterizes the effect of mixture molecular size. Assuming that all components in a mixture obey the ECS principle, the mixing rules

for a multicomponent system can be expressed as

$$\hbar_m = \sum_i^N \sum_j^N X_i X_j \hbar_{ij} \quad (6-166)$$

$$f_m = \hbar_m^{-1} \sum_i^N \sum_j^N X_i X_j f_{ij} \hbar_{ij} \quad (6-167)$$

where N is the number of species in the system and X_i the mole fraction of species i . The two binary factors, f_{ij} and \hbar_{ij} , are defined as

$$f_{ij} = (f_i f_j)^{1/2} (1 - k_{ij}) \quad (6-168)$$

$$\hbar_{ij} = \frac{1}{8} (\hbar_i^{1/3} + \hbar_j^{1/3})^3 (1 - l_{ij}) \quad (6-169)$$

where k_{ij} and l_{ij} are binary interaction parameters reflecting the effects of energy and molecular size, respectively. The conformal mapping for each individual component can be obtained by the two-parameter corresponding state principle,

$$f_i = (T_i^c / T_0^c) \theta_i(T_i^*, V_i^*, \omega_i) \quad (6-170)$$

$$\hbar_i = (V_i^c / V_0^c) \phi_i(T_i^*, V_i^*, \omega_i) \quad (6-171)$$

where θ_i and ϕ_i are the so-called shape factors, which are functions of Pitzer's acentric factor ω_i , and T_i^* and V_i^* are the reduced temperature and specific molar volume.

6.1.2 Equation of State Under the assumption of the ECS principle, the density of a mixture can be evaluated by

$$\rho_m(T, p) = \frac{\rho_0(T_0, p_0)}{\hbar_m(T, p)} \quad (6-172)$$

where ρ_0 , T_0 , and p_0 denote the corresponding density, temperature, and pressure of the reference fluid, respectively. Since the temperature at the conformal state is calculated by Eq. (6-165), the corresponding pressure can be derived based on the general compressibility theory,

$$p_0 = p \left(\frac{\hbar_m}{f_m} \right) \quad (6-173)$$

To ensure the accuracy of the density prediction, a generalized BWR equation of state⁶⁵ is adopted for the reference fluid.

$$p_0(T, \rho) = \sum_{n=1}^9 a_n(T) \rho^n + \sum_{n=10}^{15} a_n(T) \rho^{2n-17} e^{-\gamma \rho^2} \quad (6-174)$$

where γ is 0.04, and the temperature coefficients $a_i(T)$ depend on the reference fluid used.

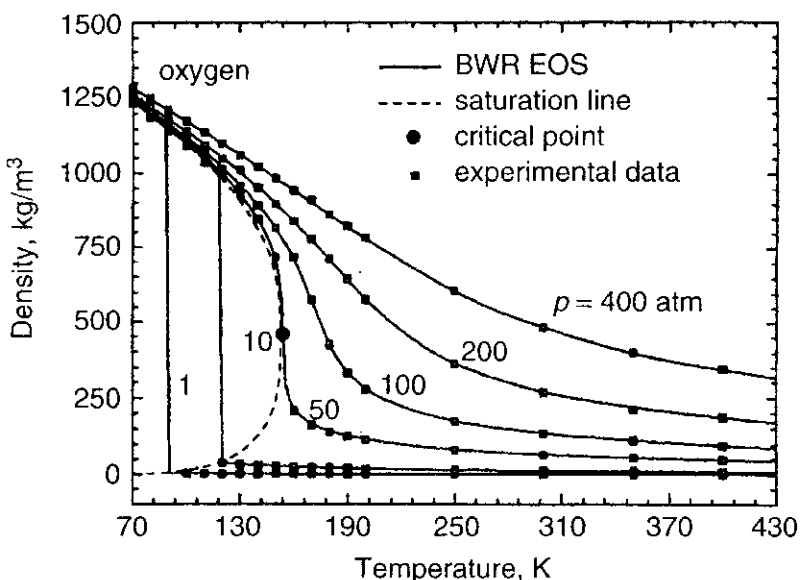


Figure 6.31 Comparison of oxygen density predicted by the BWR equation of state and measured by Sychev et al.⁷⁰ (after Yang³⁴).

Although this equation of state must be solved iteratively for density at given pressure and temperature, the prediction covers a wide range of thermodynamic states, and as such promotes the establishment of a unified evaluation scheme of thermophysical properties. Figure 6.31 shows the comparison of oxygen density between experimental data⁷⁰ and the prediction by the BWR equation of state in conjunction with the ECS principle. The reference fluid is selected to be propane due to the availability of sufficiently reliable data correlated over a wide range of experimental conditions for this substance. The result shows excellent agreement over the entire fluid state. Yang³⁴ compared the relative errors of density prediction based on three commonly used equations of state, namely, the Benedict–Webb–Rubin (BWR), Peng–Robinson (PR), and Soave–Redlich–Kwong (SRK). The ECS principle was embedded into the evaluation procedure of the BWR equation of state and showed its superior performance with the maximum relative error of 1.5% for the pressure and temperature ranges under consideration. On the other hand, the SRK and PR equations of state yield maximum errors around 13% and 17%, respectively.

6.1.3 Thermodynamic Properties Thermodynamic properties such as enthalpy, internal energy, and specific heat can be expressed as the sum of ideal-gas properties at the same temperature and departure functions, which take into account the dense-fluid correction. Thus,

$$h = h^o + \left\{ \int_{\infty}^v \left[T \left(\frac{\partial p}{\partial T} \right)_v - p \right] dv + RT(Z - 1) \right\} \quad (6-175)$$

$$e = e^o + \left\{ \int_{\infty}^v \left[T \left(\frac{\partial p}{\partial T} \right)_v - p \right] dv \right\} \quad (6-176)$$

$$C_p = C_p^o + \left\{ \int_{\infty}^v T \left(\frac{\partial^2 p}{\partial T^2} \right)_v dv - T \left(\frac{\partial p}{\partial T} \right)_v^2 / \left(\frac{\partial p}{\partial v} \right)_T - R \right\} \quad (6-177)$$

where superscripts ^o refer to ideal-gas properties. The second terms on the right sides of Eqs. (6-175) through (6-177) represent the thermodynamic departure functions and can be obtained from the equation of state described previously. The compressibility factor Z is a function of reduced pressure (p_r) and reduced temperature (T_r) described in many thermodynamics books.

6.1.4 Transport Properties Estimation of viscosity and thermal conductivity can be made by means of the ECS principle. The corresponding-state argument for the viscosity of a mixture can be written in its most general form as

$$\mu_m(\rho, T) = \mu_0(\rho_0, T_0) F_\mu \chi_\mu \quad (6-178)$$

where F_μ is the scaling factor. The correction factor χ_μ accounts for the effect of noncorrespondence and has a magnitude always close to unity based on the modified Enskog theory.⁷¹

Because of the lack of a complete molecular theory for describing transport properties over a broad regime of fluid phases, it is generally accepted that viscosity and thermal conductivity can be divided into three contributions and correlated in terms of density and temperature.⁷² For instance, the viscosity of the reference fluid is written as follows:

$$\mu_0(\rho_0, T_0) = \mu_0^0(T_0) + \Delta\mu_0^{\text{exc}}(\rho_0, T_0) + \Delta\mu_0^{\text{crit}}(\rho_0, T_0) \quad (6-179)$$

The first term on the right-hand side represents the value at the dilute-gas limit, which is independent of density and can be accurately predicted by equations derived from kinetic theory of gases. The second term is the excess viscosity, which, with the exclusion of unusual variations near the critical point, characterizes the deviation from μ_0 for a dense fluid. The third term refers to the critical enhancement, which accounts for the anomalous increase above the background viscosity (i.e., the sum of μ_0^0 and $\Delta\mu_0^{\text{exc}}$) as the critical point is approached. However, the theory of nonclassical critical behavior predicts that, in general, properties that diverge strongly in pure fluids near the critical points diverge only weakly in mixtures due to the different physical criteria for criticality in a pure fluid and a mixture.⁷³ Because the effect of critical enhancement is not well defined for a mixture and is likely to be small, the third term $\Delta\mu_0^{\text{crit}}$ is usually not considered in most analyses of supercritical droplet gasification.

Calculation of thermal conductivity must be carefully conducted for two reasons: (1) the one-fluid model must ignore the contribution of diffusion to conductivity, and (2) the effect of internal degrees of freedom on thermal conductivity cannot be correctly taken into account by the corresponding-state argument. As a result, thermal conductivity of a pure substance or mixture is generally divided

into two contributions,⁶⁹

$$\lambda_m(\rho, T) = \lambda'_m(T) + \lambda''_m(\rho, T) \quad (6-180)$$

The first term, $\lambda'_m(T)$, arises from transfer of energy via the internal degrees of freedom, while the second term, $\lambda''_m(\rho, T)$, is due to the effects of molecular collision or translation, which can be evaluated by means of the ECS method. For a mixture, $\lambda'_m(T)$ can be evaluated by a semiempirical mixing rule.

Estimation of the binary mass diffusivity for a mixture gas at high density represents a more challenging task than evaluating the other transport properties, due to the lack of a formal theory or even a theoretically based correlation. Takahashi⁷⁴ suggested a simple scheme for predicting the binary mass diffusivity of a dense fluid by means of a corresponding-state approach. The approach appears to be the most complete to date and has demonstrated moderate success in the limited number of tests conducted. The scheme proceeds in two steps. First, the binary mass diffusivity of a dilute gas is obtained using the Chapman–Enskog theory in conjunction with the intermolecular potential function. The calculated data are then corrected in accordance with a generalized chart in terms of reduced temperature and pressure (see Appendix A for more details). The following equation has been used extensively for calculating the effective mass diffusivity of *i*th species with the mixture.

$$\mathcal{D}_{im} = \frac{1 - X_i}{\sum_{j \neq i}^N (X_j / \mathcal{D}_{ij})} \quad i = 1, 2, \dots, N \quad (6-181)$$

6.2 Vapor–Liquid Phase Equilibrium

The result of vapor–liquid phase equilibrium is required to specify the droplet surface behavior prior to the occurrence of critical conditions. According to Yang,³⁴ the analysis usually consists of two steps. First, an appropriate equation of state as described in Section 6.1.2 is employed to calculate fugacity of each constituent species in both gas and liquid phases. The second step lies in the determination of the phase equilibrium conditions by requiring equal fugacities for both phases of each species. Namely, the high-pressure vapor–liquid equilibria for each component can be expressed as

$$f_i^{(v)} = f_i^{(l)} \quad (6-182a)$$

$$T^{(v)} = T^{(l)} \quad (6-182b)$$

$$P^{(v)} = P^{(l)} \quad (6-182c)$$

where the superscripts (*v*) and (*l*) stand for vapor and liquid, respectively. Variable f_i is the fugacity for species *i* and can be integrated through the following relation.⁶⁶

$$R_u T \ln \left(\frac{f_i}{X_i P} \right) = \int_V^\infty \left[\left(\frac{\partial P}{\partial n_i} \right)_{T, V, n_j} - \frac{R_u T}{V} \right] dV - R_u T \ln Z \quad (6-183)$$

This equation indicates that f_i can be determined by the properties of the constituent components, the concentrations in both phases, and the temperature and pressure of the system. To compute the integral of the above equation, a real-gas equation of state, such as Redlich–Kwong (R-K) equation of state [see Eq. (A-4)] can be employed. The parameters *a* and *b* in the cubic-type equation of state Eq. (A-4) can be expressed in terms of composition and pure component parameters.

$$a = \sum_{i=1}^N \sum_{j=1}^N X_i X_j a_{ij}, \quad b = \sum_{i=1}^N X_i b_i \quad (6-184)$$

The constants a_{ij} and b_i are essentially dependent on the critical properties of each species. In addition, the following quantum-gas mixing rules must be used to consider mixtures comprising one or more quantum gases.⁶⁶ Similar to Eq. (A-5) we have

$$a_{ii} = \frac{0.42748 R_u^2 T_{c_i}^{2.5}}{P_{c_i}}, \quad a_{ij} = \frac{0.42748 R_u^2 T_{c_{ij}}^{2.5}}{P_{c_{ij}}}, \quad b_i = \frac{0.08664 R_u T_{c_i}}{P_{c_i}} \quad (6-185)$$

where

$$T_{c_{ij}} = \frac{T_{c_{ij}}^*}{1 + [C_1 / (\text{Mw}_{ij} T)]}, \quad P_{c_{ij}} = \frac{P_{c_{ij}}^*}{1 + [C_2 / (\text{Mw}_{ij} T)]} \quad (6-186a)$$

$$T_{c_{ij}}^* = \sqrt{T_{c_i} T_{c_j}} (1 - K_{ij}), \quad P_{c_{ij}}^* = \frac{Z_{c_{ij}} R_u T_{c_{ij}}^*}{\bar{v}_{c_{ij}}} \quad (6-186b)$$

$$\bar{v}_{c_{ij}}^{1/3} = \frac{\bar{v}_{c_i}^{1/3} + \bar{v}_{c_j}^{1/3}}{2}, \quad Z_{c_{ij}} = 0.291 - 0.04(\omega_i - \omega_j) \quad (6-186c)$$

$$\frac{1}{\text{Mw}_{ij}} = \frac{1/\text{Mw}_i + 1/\text{Mw}_j}{2}, \quad K_{ij} = 1 - \frac{8(\bar{v}_{c_i} \bar{v}_{c_j})^{1/2}}{(\bar{v}_{c_i}^{1/3} + \bar{v}_{c_j}^{1/3})^3} \quad (6-186d)$$

Note that the values of C_1 and C_2 in Eq. (6-186a) are 21.8 and 44.2, respectively. The critical properties and acentric factors (ω_i) of several pure components are given in Table 6.3.

Table 6.3 Critical Properties and Acentric Factors of Several Pure Components

Species	T_c (K)	P_c (bar)	\bar{v}_c (cm ³ /mol)	Z_c	ω
Oxygen	154.6	50.4	73.4	0.288	0.025
Hydrogen	33.2	13.0	65.1	0.306	-0.218
Helium	5.19	2.27	57.4	0.302	-0.365

After substituting Eq. (A-4) into Eq.(6-183) and carrying out the partial differentiation and integration, Eq.(6-183) can be written into the following form:

$$\ln f_i = \ln X_i + \ln P + \frac{b_i}{b}(Z - 1) - \ln(Z - B) \\ - \frac{A}{B} \left[\frac{2 \sum_{j=1}^N X_j a_{ij}}{a} - \frac{b_i}{b} \right] \ln \left(1 + \frac{B}{Z} \right) \quad (6-187)$$

which is valid for both vapor and liquid phases. The parameters A and B are defined as

$$A = \frac{aP}{R_u^2 T^{5/2}}, \quad B = \frac{bP}{R_u T} \quad (6-188)$$

The mixture compressibility factor Z can be solved from the following equation, which is related to the R-K equation of state.

$$Z^3 - Z^2 + (A - B - B^2)Z - AB = 0 \quad (6-189)$$

As mentioned previously, Eq. (6-187) can be applied to both vapor and liquid phases. If we have a two-component, two-phase system in equilibrium at a given temperature and pressure, then we have four mole fractions ($X_1^{(v)}$, $X_2^{(v)}$, $X_1^{(l)}$, $X_2^{(l)}$) as unknowns for the phase equilibrium system. These unknowns must be solved from four separate equations. One of these equations can be obtained by first using Eq. (6-187) for $f_1^{(v)}$ of species 1 in the vapor phase and then use the same equation again for $f_1^{(l)}$ of species 1 in the liquid phase. Then, equate the left-hand side of both of these equation based on the fact that $f_1^{(v)} = f_1^{(l)}$ at equilibrium [see Eq. (6-182a)]. After keeping only the right-hand sides of these equation, we obtained one relationship between $X_1^{(v)}$ and $X_1^{(l)}$. Following the same procedure, we can obtain a similar relationship between $X_2^{(v)}$ and $X_2^{(l)}$. Two more relationships can be obtained from the following identities:

$$X_1^{(v)} + X_2^{(v)} = 1, \quad X_1^{(l)} + X_2^{(l)} = 1 \quad (6-190)$$

Using these four relationships, the four unknowns ($X_1^{(v)}$, $X_2^{(v)}$, $X_1^{(l)}$, $X_2^{(l)}$) are then solved. A typical result of such calculation is shown in Fig. 6.32. This figure gives the equilibrium compositions for a binary mixture of oxygen and hydrogen as a function of pressure, where P_r represents the reduced pressure of oxygen. In the subcritical regime, the amount of hydrogen dissolved in the liquid

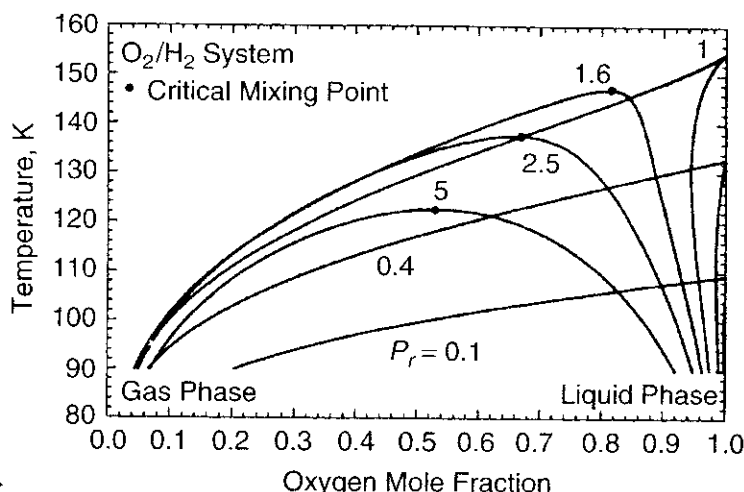


Figure 6.32 Vapor-liquid phase equilibrium compositions for O_2/H_2 system at various pressures (after Yang³⁴).

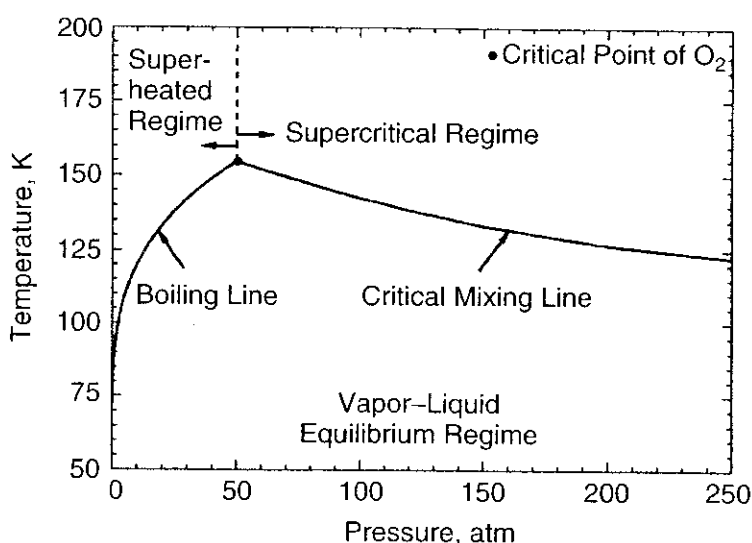


Figure 6.33 Pressure-temperature diagram for phase behavior of O_2/H_2 system in equilibrium (after Yang³⁴).

oxygen is quite limited, decreasing progressively with increasing temperature and reducing to zero at the boiling point of oxygen. At supercritical pressures, however, the hydrogen gas solubility becomes substantial and increases with temperature. Because of the distinct differences in thermophysical properties between the two species, the dissolved hydrogen may appreciably modify the liquid properties and, subsequently, the vaporization behavior. The phase equilibrium results also indicate that the critical mixing temperature decreases with pressure. Namely, the peak temperature of each curve (called the critical mixing point) decreases with the increase of pressure for $P_r > 1$. Yang, Hsieh, and Kuo⁹⁸ obtained a similar plot for an O_2/He system; the results compared very closely with the experimental data in the literature.

The pressure-temperature diagram in Fig. 6.33 shows the phase equilibrium behavior under different thermodynamic conditions. The boiling line is made up

of boiling points for subcritical pressure. At a fixed pressure, as the temperature increases, an equilibrium vapor–liquid mixture will transit to superheated vapor across this line. The critical mixing line registers the variation of the critical mixing temperature with pressure. It intersects the boiling line at the critical point of pure oxygen, the highest temperature at which the vapor and liquid phases of an O_2/H_2 binary system can coexist in equilibrium.

To understand better the significance of critical mixing point, we can consider the differences between the following two conditions:

Condition 1: When $T_s < T_{\text{critical mixing point}}$ —The droplet surface provides a well-defined interfacial boundary, which separates the liquid phase from the ambient gases. Under this condition, the liquid and gas phases can be treated separately in the theoretical formulation and then coupled together through the relationships at the droplet surface. These relationships include liquid–vapor phase equilibrium, mass, and energy flux balance at interface. The heat of vaporization is nonzero as shown in Fig. 6.34.

Condition 2: When $T_s \geq T_{\text{critical mixing point}}$ —There is no abrupt phase change near the so-called droplet surface. In fact, the definition of the interfacial boundary is very vague. The heat of vaporization is zero as shown by the heavy dots in Fig. 6.34. Under this condition, temperature and density vary continuously across the interfacial region. The interior of the droplet could still be at a subcritical condition. The regression is best characterized by the motion of the “surface,” which has a temperature equal to the critical mixing temperature of the system.

As shown by Fig. 6.34, the enthalpy of vaporization is a function of both temperature and pressure. At a given temperature, the enthalpy of vaporization decreases as P_r increases. Also, at a fixed value of P_r , the enthalpy of vaporization

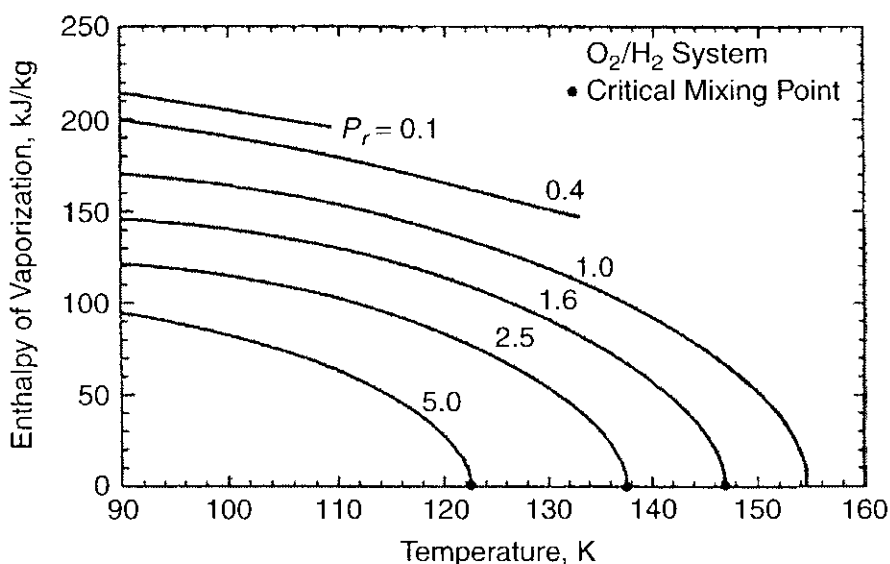


Figure 6.34 Effect of pressure on enthalpy of vaporization of O_2 in an equilibrium mixture of O_2 and H_2 (after Yang et al.⁵⁰).

decreases to zero when the temperature reaches the critical mixing point. The molar-based enthalpy of vaporization (or the heat of vaporization) of each species can be determined from

$$\Delta \overline{H}_{v,i} = \overline{h}_i^{(v)} - \overline{h}_i^{(l)} \quad (6-191)$$

where the overbar is used for all partial molar quantities. The values of $\overline{h}_i^{(v)}$ and $\overline{h}_i^{(l)}$ can be calculated from the following thermodynamic relation:

$$\frac{\overline{h}_i^0 - \overline{h}_i}{R_u T^2} = \frac{\partial}{\partial T} \left[\ln \frac{f_i}{X_i P} \right] \quad (6-192)$$

where \overline{h}_i^0 designates ideal partial molar enthalpy under standard conditions. Substituting Eq. (6-187) into Eq. (6-192) and taking differentiation with respect to temperature, we have

$$\begin{aligned} \frac{\overline{h}_i^0 - \overline{h}_i}{R_u T^2} &= \frac{b_i \partial Z}{b \partial T} - \frac{1}{Z - B} \left(\frac{\partial Z}{\partial T} - \frac{\partial B}{\partial T} \right) \\ &- \left[\frac{2 \sum_{j=1}^N X_j a_{ij}}{a} - \frac{b_i}{b} \right] \left\{ \begin{aligned} &\ln \left(1 + \frac{B}{Z} \right) \left(\frac{1}{B} \frac{\partial A}{\partial T} - \frac{A}{B^2} \frac{\partial B}{\partial T} \right) \\ &+ \left(\frac{A}{B} \right) \left(\frac{Z}{Z + B} \right) \left(\frac{1}{Z} \frac{\partial B}{\partial T} - \frac{B}{Z^2} \frac{\partial Z}{\partial T} \right) \end{aligned} \right\} \end{aligned} \quad (6-193)$$

where

$$\frac{\partial Z}{\partial T} = \frac{(B - Z) \partial A / \partial T + (Z + 2BZ + A) \partial B / \partial T}{3Z^2 - 2Z + (A - B - B^2)} \quad (6-194a)$$

$$\frac{\partial A}{\partial T} = -\frac{5aP}{2R_u^2 T^{7/2}}, \quad \frac{\partial B}{\partial T} = -\frac{bP}{R_u T^2} \quad (6-194b)$$

Besides solubility of ambient gases in the liquid phase and the enthalpy of vaporization, the thermodynamic analysis can further be used to calculate the species concentrations at the droplet surface, conditions for criticality, and even surface tension.

6.3 Droplet Vaporization in Quiescent Environments

Several theoretical works have recently been conducted to improve the understanding of droplet vaporization and combustion under high-pressure conditions. Both hydrocarbon droplets in air^{42–44,49,58,59} and liquid oxygen (LOX) droplets in hydrogen^{45,48,50–57,75} were treated comprehensively, with emphasis placed on the effects of transient diffusion and interfacial thermodynamics. The works of

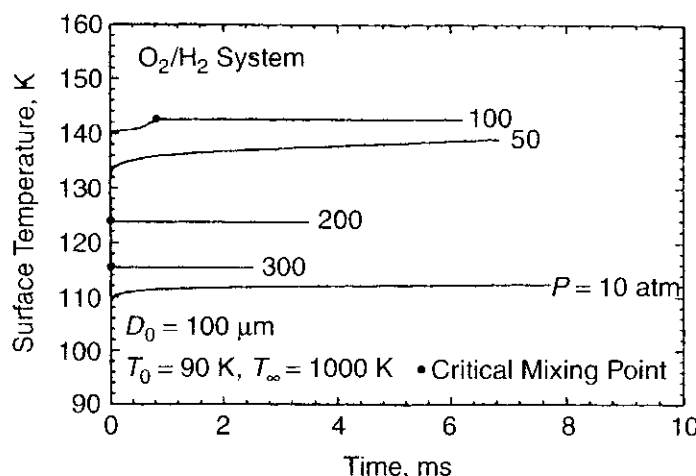


Figure 6.35 Time variations of droplet surface temperature at various pressures; $T_\infty = 1000$ K; $T_0 = 90$ K; $D_0 = 100$ μm (after Yang³⁴).

Lafon et al.,^{53,75} Hsiao and Yang,^{51,76} and Harstad and Bellan^{56–59} appear to be the most comprehensive to date because of the employment of a unified property evaluation scheme as outlined in Section 6.1.

Let us first consider the vaporization of LOX droplet in either pure hydrogen or mixed hydrogen/water environments^{53,75} due to its broad applications in cryogenic rocket engines using hydrogen and oxygen as propellants.⁷⁷ Figure 6.35 shows the time variations of droplet surface temperature at various pressures. The ambient hydrogen temperature is taken to be 1000 K. Three different scenarios are noted. First, at low pressures (i.e., $p = 10$ atm), the surface temperature rises quickly and levels off at the pseudo wet-bulb state, which is slightly lower than the oxygen boiling temperature because of the presence of hydrogen on the gaseous side of the interface. For higher pressures (i.e., $p = 50$ atm), the surface temperature rises continuously. The pseudo wet-bulb state disappears, and the vaporization process becomes transient in nature during the entire droplet lifetime. For $p = 100$ atm, the droplet surface even reaches its critical state around 1 ms. At higher pressures, the surface temperature is lower due to the decay of critical mixing line with the increase of pressure.

Figure 6.36 shows representative curves of droplet diameter versus time for a spherical oxygen droplet gasifying in a supercritical nonconvective hydrogen environment at various pressures. These data were obtained by means of direct numerical simulations at conditions with $T_\infty = 1000$ K; $T_0 = 90$ K; and $D_0 = 100$ μm .

An extensive series of numerical simulations were conducted by Yang and coworkers³⁴ for a broad range of ambient temperatures ($500 \leq T_\infty \leq 2500$ K) and pressures up to 300 atm. The calculated LOX droplet lifetime in pure hydrogen can be well correlated using an approximate analysis that takes into account the effect of transient heat diffusion in terms of the reduced critical temperature, defined as

$$T_c^* \equiv \frac{T_\infty - T_c}{T_\infty - T_0} \quad (6-195)$$

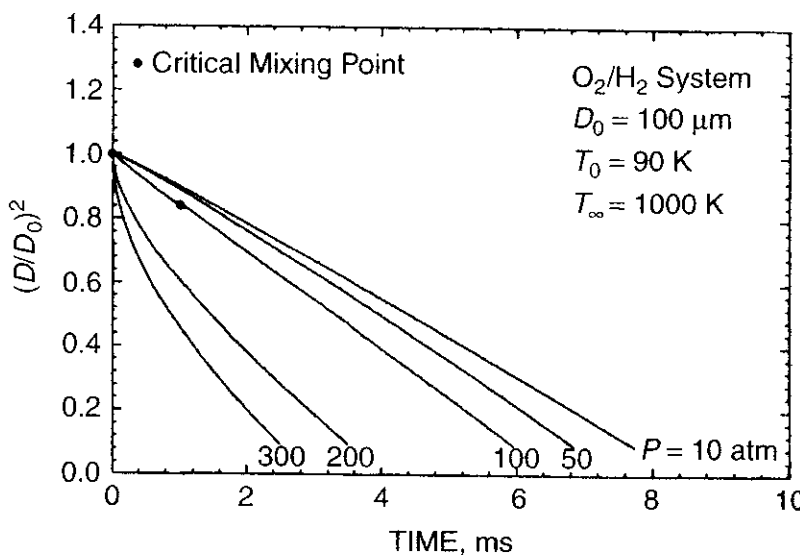


Figure 6.36 Droplet diameter vs. time for a spherical oxygen droplet gasifying in a supercritical nonconvective hydrogen environment at various pressures; $T_{\infty} = 1000 \text{ K}$; $T_0 = 90 \text{ K}$; $D_0 = 100 \mu\text{m}$ (after Lafon et al.⁵³).

The resultant expression of the droplet lifetime takes the form

$$\tau = [0.0115 + 0.542(1 - T_c^*)] \frac{R_0^2}{\alpha_0} f\left(\frac{\alpha_{\infty}}{\alpha_0}\right) \quad (6-196)$$

where the correction factor is chosen as

$$f\left(\frac{\alpha_{\infty}}{\alpha_0}\right) = 1 + 3.9 \left\{ 1 - \exp \left[-0.035 \left(\frac{\alpha_{\infty}}{\alpha_0} - 1 \right) \right] \right\} \quad (6-197)$$

and α_{∞}/α_0 represents the ratio of the thermal diffusivity of the gas mixture to that of the droplet. In contrast to the low-pressure case, where the enthalpy of vaporization is rate controlling, the thermal diffusion processes prevail at high pressures. The high-pressure Spalding transfer number, B_T , can be defined to be related to critical mixing temperature T_c by the following algebraic equation:

$$B_T = \frac{T_{\infty} - T_c}{T_c - T_0} = \frac{T_c^*}{1 - T_c^*} \quad (6-198)$$

Using the definition of the reduced critical temperature T_c^* , B_T can also be expressed in terms of T_c^* as shown in the above equation. Thus, the correlation given in Eq. (6-196) clearly shows that pressure affects the droplet lifetime through its influence on the mixture critical temperature (or critical mixing temperature, T_c) and the ambient thermal diffusivity, α_{∞} . Figure 6.37 shows the dependency of spherical oxygen droplet lifetime on reduced critical mixing temperature in a nonconvective hydrogen environment at various pressures. At high pressures, T_c^* decreases and therefore the lifetimes of the droplets are shorter.

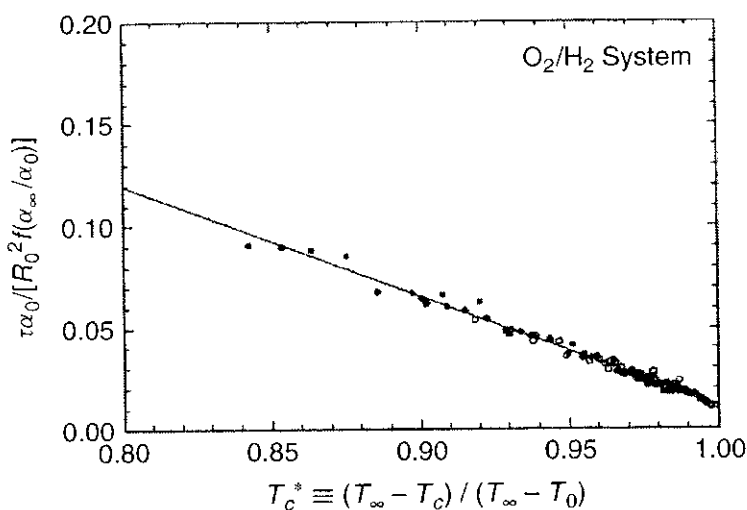


Figure 6.37 Dependency of oxygen droplet lifetime on critical mixing temperature in a non-convective hydrogen environment (after Lafon et al.⁵³).

The gasification behavior of hydrocarbon fuel droplets at supercritical conditions basically follows the same trend as cryogenic droplets. In general, the droplet lifetime decreases gradually with increasing pressure, and no discernible variation occurs across the critical transition. In the subcritical regime, as pressure increases, the enthalpy of vaporization decrease thereby facilitates the vaporization process and consequently leads to a decrease in droplet lifetime. The situation is different at supercritical conditions, at which the interfacial boundary disappears with the enthalpy of vaporization being zero. In this case, the decrease in droplet lifetime is mainly attributed to the increase in thermal diffusivity of the surrounding gas near the droplet surface.

6.4 Droplet Combustion in Quiescent Environments

Recently, much effort was devoted to the study of supercritical droplet combustion.^{48,49,53} In spite of the presence of chemical reactions in the gas phase, the general characteristics of a burning droplet are similar to those involving only vaporization. The combustion of a hydrocarbon (e.g., *n*-pentane) fuel droplet in air was studied with the droplet initial temperature of 300 K and the ambient air temperature of 1000 K.⁴⁹ Figure 6.38 shows the time history of the calculated droplet surface temperature at various pressures for $D_0 = 100 \mu\text{m}$. Once ignition is achieved in the gas phase, energy feedback from the flame causes a rapid increase in droplet surface temperature. At low pressures ($p \leq 20 \text{ atm}$), the surface temperature varies very slowly following onset of flame development and almost levels off at the pseudo wet-bulb temperature. As the ambient pressure increases, the high concentrations of oxygen in the gas phase and the fuel vapor issued from the droplet surface result in a high chemical reaction rate, consequently causing a progressive decrease in ignition and flame-development time. Furthermore, the magnitude of the surface temperature jump during the flame-development stage increases with increasing pressure. Since the critical mixing

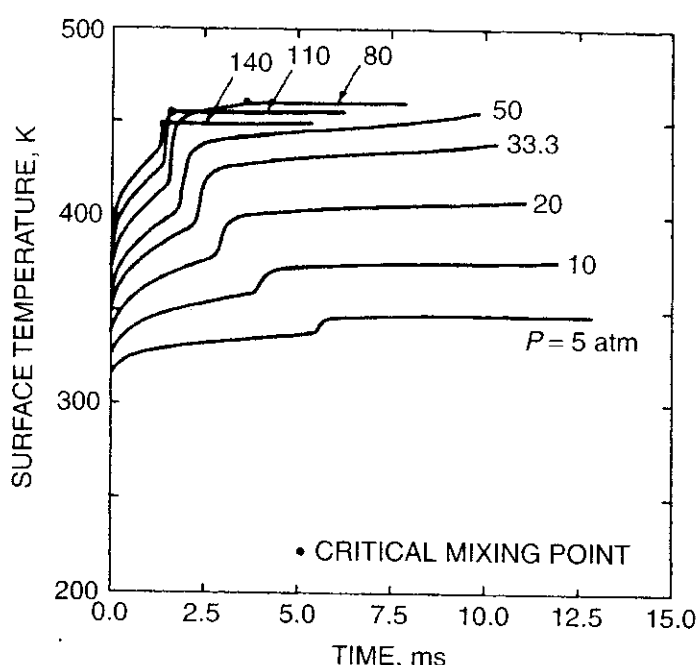


Figure 6.38 Time variations of *n*-pentane droplet surface temperature at various pressures, $D_0 = 100 \mu\text{m}$, $T_0 = 300 \text{ K}$, combustion occurring in hot-air environment, $T_\infty = 1000 \text{ K}$ (after Shuen et al.⁴⁹).

temperature decreases as pressure increases, the droplet reaches its critical condition more easily at higher pressures, almost immediately following establishment of the diffusion flame in the gas phase for $p \geq 110 \text{ atm}$.

Figure 6.39 shows the time variations of droplet surface temperature and calculated temperature distributions⁴⁹ around an *n*-pentane droplet burning in air at 80 atm. Corresponding to the six time locations on the surface temperature trace, there are six plots of temperature profiles from the center of the droplet to the surrounding air with colored temperature scale adjacent to these plots.

Figure 6.40 presents the effect of pressure on various milestone times associated with droplet gasification and burning process for both $D_0 = 100 \mu\text{m}$ and $D_0 = 1000 \mu\text{m}$.⁴⁹ Here, gasification lifetime is defined as the time required for complete gasification. The droplet-burning lifetime is defined as the gasification lifetime minus ignition time. The single-phase combustion lifetime is the time duration from complete gasification to burnout of all fuel vapors. The combustion lifetime is therefore the sum of single-phase combustion lifetime and droplet-burning lifetime. The gasification lifetime decreases continuously as pressure increases partly due to the decay of the critical mixing line, whereas the single-phase vapor combustion lifetime increases progressively with pressure due to the reduction of species mass diffusion at higher pressures. Furthermore, as discussed above, the enthalpy of vaporization of the droplet is a function of pressure and temperature. Resulting from these complicated effects, the pressure dependence of the burnout time or combustion lifetime exhibits nonmonotonic behavior as shown in Fig. 6.40*a* and *b*.

The droplet size has a pronounced effect on the burning characteristics, since the timescales for diffusion processes are inversely proportional to the droplet

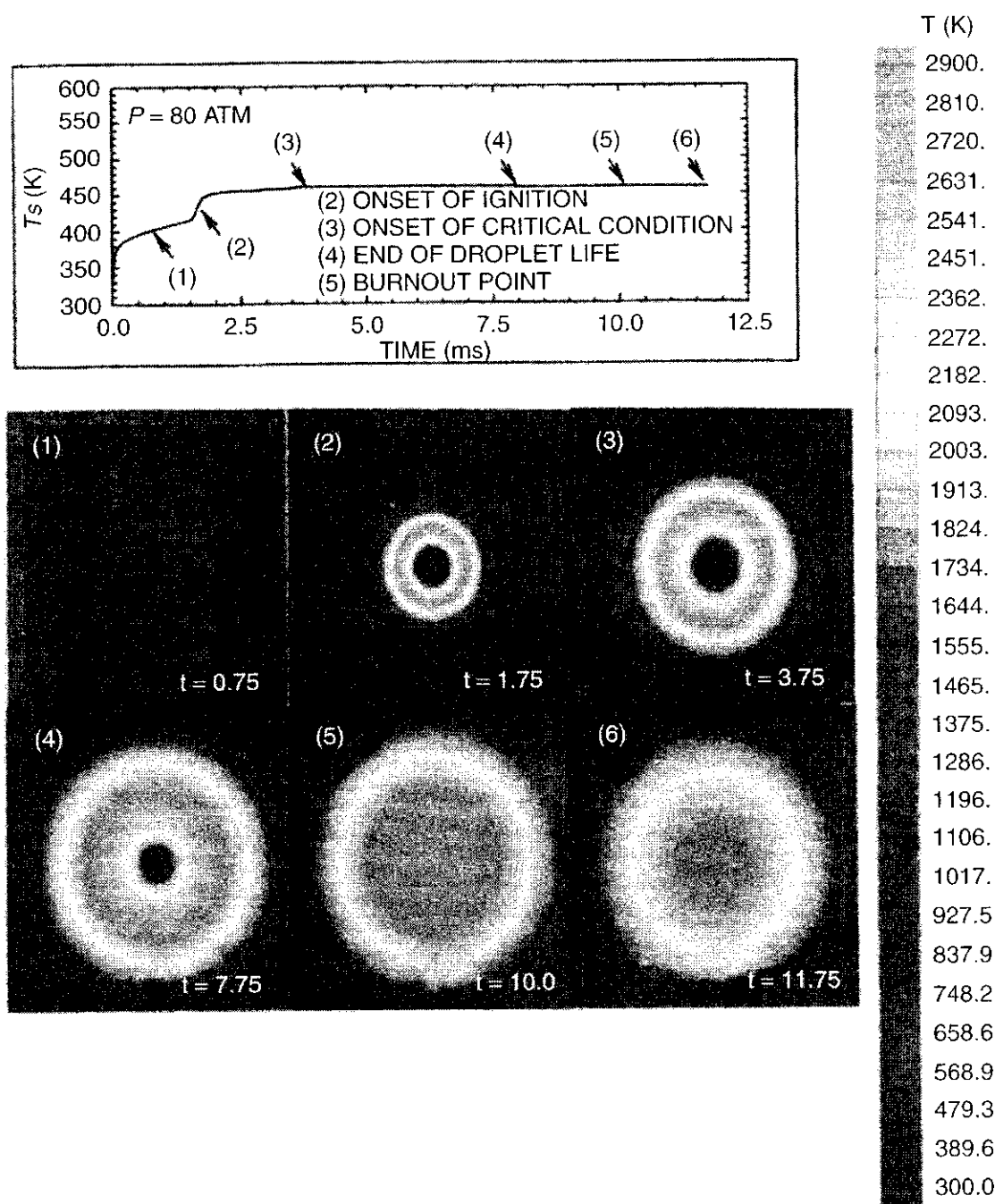
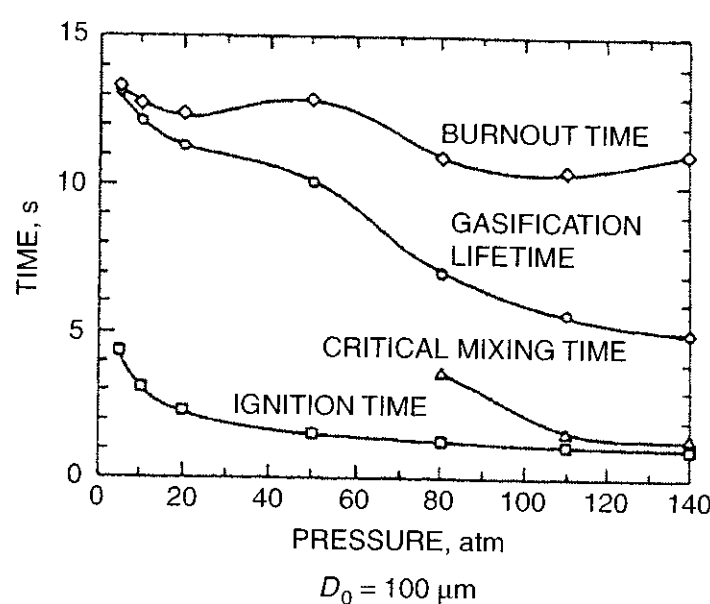
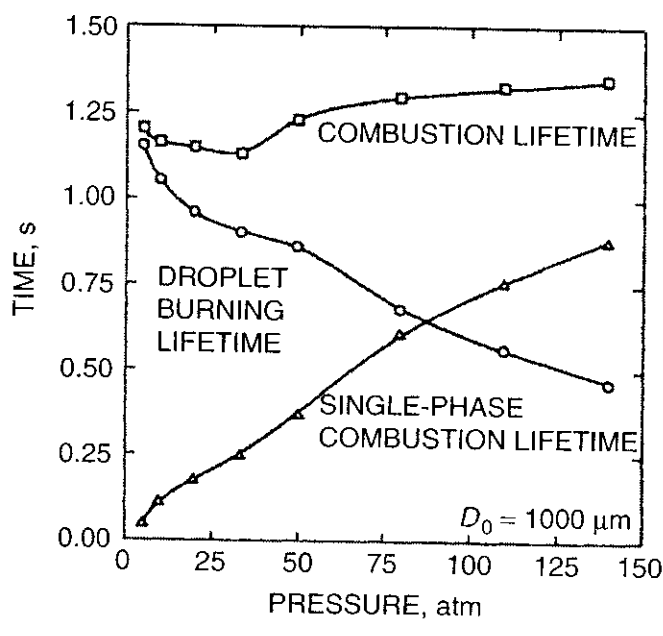


Figure 6.39 Time variations of droplet surface temperature and temperature distributions around an *n*-pentane droplet burning in air at 80 atm, $D_0 = 100 \mu\text{m}$, $T_0 = 300 \text{ K}$, $T_\infty = 1000 \text{ K}$ (after Shuen et al.⁴⁹). Note: The droplet lifetime ended near 8 ms, but the burning of supercritical *n*-pentane material continued beyond the droplet lifetime.

diameter squared. The large-droplet-size case with an initial diameter of $1000 \mu\text{m}$ is comparable to the sizes considered in most experimental studies of supercritical droplet combustion by Faeth et al.¹⁷ and Sato et al.^{78,79} For this case, the ignition delay occupies only a very small fraction of the entire droplet lifetime; therefore, the ignition time curve is not shown in plot (b). The combustion behavior of a large droplet reveals several characteristics distinct from those of a small droplet. First, as mentioned above, ignition for large droplets occurs in the very early stage of the entire droplet lifetime. The influence of gasification prior to



(a)



(b)

Figure 6.40 Effect of pressure and droplet diameter on milestone times associated with droplet gasification and burning processes of *n*-pentane/air system, $T_0 = 300$ K and $T_\infty = 1000$ K (Fig. 6.40a obtained from Yang and Fig. 6.40b after Shuen et al.⁴⁹).

ignition on the overall burning mechanisms appears to be quite limited. Second, the combustion lifetime decreases with increasing pressure at lower pressures, reaching a minimum near the critical pressure of the liquid fuel (~ 33 atm). As the pressure further increases, the combustion time increases due to the reduction of mass diffusivity at high pressures. The droplet burning lifetime decreases continuously with pressure, whereas the single vapor phase combustion lifetime increases progressively with pressure.

In general, at low pressures, the gasification of liquid fuel primarily controls the time of combustion process, whereas in a supercritical environment, the transient gas-phase diffusion process plays a more important role.

6.5 Droplet Vaporization in Supercritical Convective Environments

As discussed in Section 5, when a droplet is introduced into a crossflow of gases, the forced convection results in increases of heat and mass transfer between the droplet and surrounding gases, which consequently enhances the gasification process. Although many studies have been conducted to examine droplet vaporization in forced-convective environments, effects of pressure and free-stream velocities on droplet dynamics, especially for rocket engine applications, which involve supercritical conditions, have not yet been addressed in detail. Hsiao and Yang^{51,76} developed a comprehensive analysis of liquid-oxygen (LOX) droplet vaporization in a supercritical hydrogen stream, covering a pressure range of 100–400 atm. The model takes into account multidimensional flow motions and enables a thorough examination of droplet behavior during its entire lifetime, including dynamic deformation, viscous stripping, and secondary breakup. Detailed flow structures and thermodynamic properties are obtained to reveal mechanisms underlying droplet gasification as well as deformation and breakup dynamics.

Figure 6.41 shows six frames of isotherms and isopleths of oxygen concentration at a convective velocity of 2.5 m/s and an ambient pressure of 100 atm. The free-stream Reynolds number Re_{D_0} is 31 based on the initial droplet diameter. Soon after the introduction of the droplet into the hydrogen stream, the flow adjusts to form a boundary layer near the surface. The gasified oxygen is carried downstream through convection and mass diffusion. The evolution of the temperature field exhibits features distinct from that of the concentration field due to the disparate timescales associated with thermal and mass diffusion processes (i.e., Lewis number $\neq 1$). The thermal wave penetrates into the droplet interior with a pace faster than does the surrounding hydrogen species. Since the liquid core possesses large momentum inertia and moves slower compared with the gasified oxygen, at $t = 0.79$ ms, the droplet (delineated by the dark region in the temperature contours) reveals an olive shape while the oxygen concentration contours deform into a crescent shape with the edge bent to the streamwise direction. At $t = 1.08$ ms, the subcritical liquid core disappears, leaving behind a puff of dense oxygen fluid, which travels further downstream with increasing velocity until it reaches the momentum equilibrium with the ambient hydrogen flow.

Figure 6.42 shows the streamline patterns and oxygen concentration contours of the four different modes commonly observed in supercritical droplet gasification simulated numerically by Hsiao^{51,76} and Yang.⁷⁶ The droplet can remain in a spherical configuration, deform to an olive shape, or even break up into fragments, depending on the local flow conditions. Unlike low-pressure cases in which the large shear stress at the gas–liquid interface induces internal flow circulation in the liquid core reported by Prakash and Sirignano,⁸⁰ no discernible recirculation takes place in the droplet interior, regardless of the Reynolds number and deformation mode. This may be attributed to the diminishment of surface

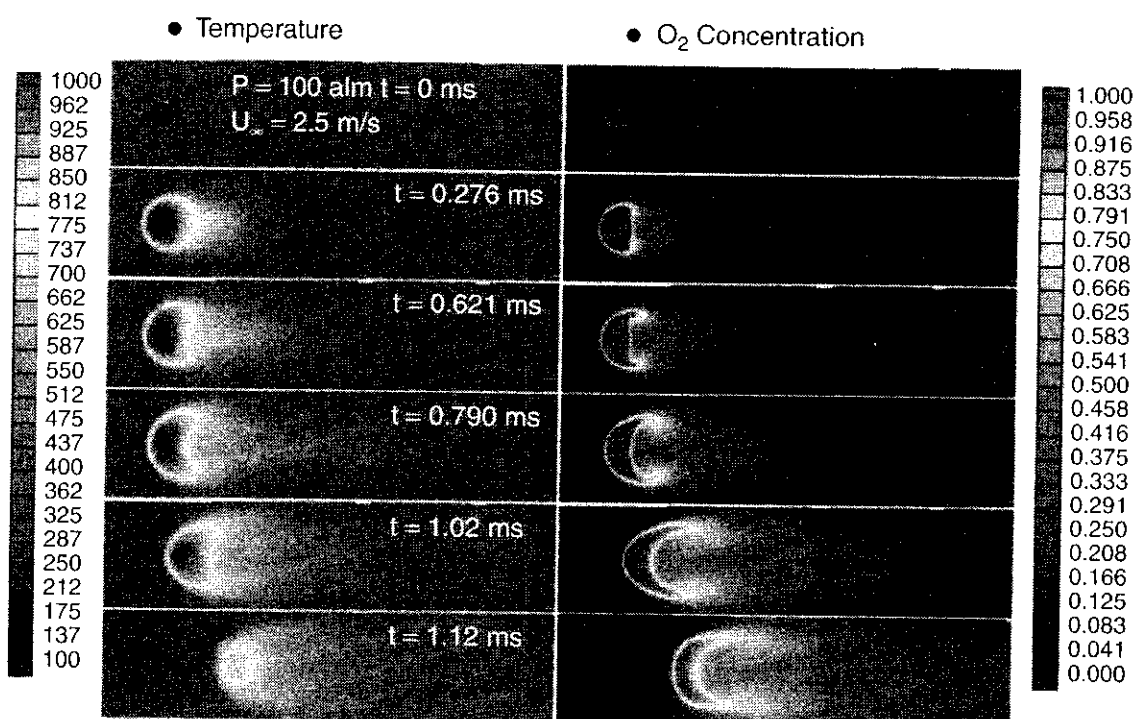


Figure 6.41 Calculated LOX droplet gasification in supercritical hydrogen flow, $p = 100$ atm, $U_{\infty} = 2.5$ m/s (after Yang³⁴).

tension at supercritical conditions. In addition, the droplet regresses so fast that a fluid element in the interfacial region may not acquire the time sufficient for establishing an internal vortical flow before it gasifies. The rapid deformation of the droplet configuration further precludes the existence of stable shear stress in the liquid core and consequently obstructs the formation of recirculation.

The spherical mode shown in Fig. 6.42a typically occurs at very low Reynolds numbers. Although flow separation is encouraged by LOX gasification, no recirculating eddy is found in the wake behind the droplet. The vorticity generated is too weak to form any confined eddy. When the ambient velocity increases to 1.5 m/s, the droplet deforms into an olive shape with a recirculating ring attached behind it, as shown in Fig. 6.42b. Owing to the droplet deformation and gasification, the threshold Reynolds number above which the recirculating eddy forms is considerably lower than that for a hard sphere. Figure 6.42c depicts the flow structure with viscous stripping at an ambient velocity of 5 m/s, showing an oblate droplet with a stretched vortex ring. The flattened edge of the droplet enhances the strength of the recirculating eddies and as such increases the viscous shear stress drastically. Consequently, a thin sheet of fluid is stripped off the edge of the droplet and swept toward the outer boundary of the recirculating eddy. At a very high ambient velocity of 15 m/s, droplet breakup takes place, as clearly shown in Fig. 6.42d. The hydrogen flow penetrates through the liquid phase and divides the droplet into two parts: the core disk and surrounding ring. The vortical structure in the wake region expands substantially as a result of the strong shear stress.

The effect of ambient pressure and Reynolds number on droplet lifetime can be correlated⁷⁶ with respect to the reference value at zero Reynolds number. The

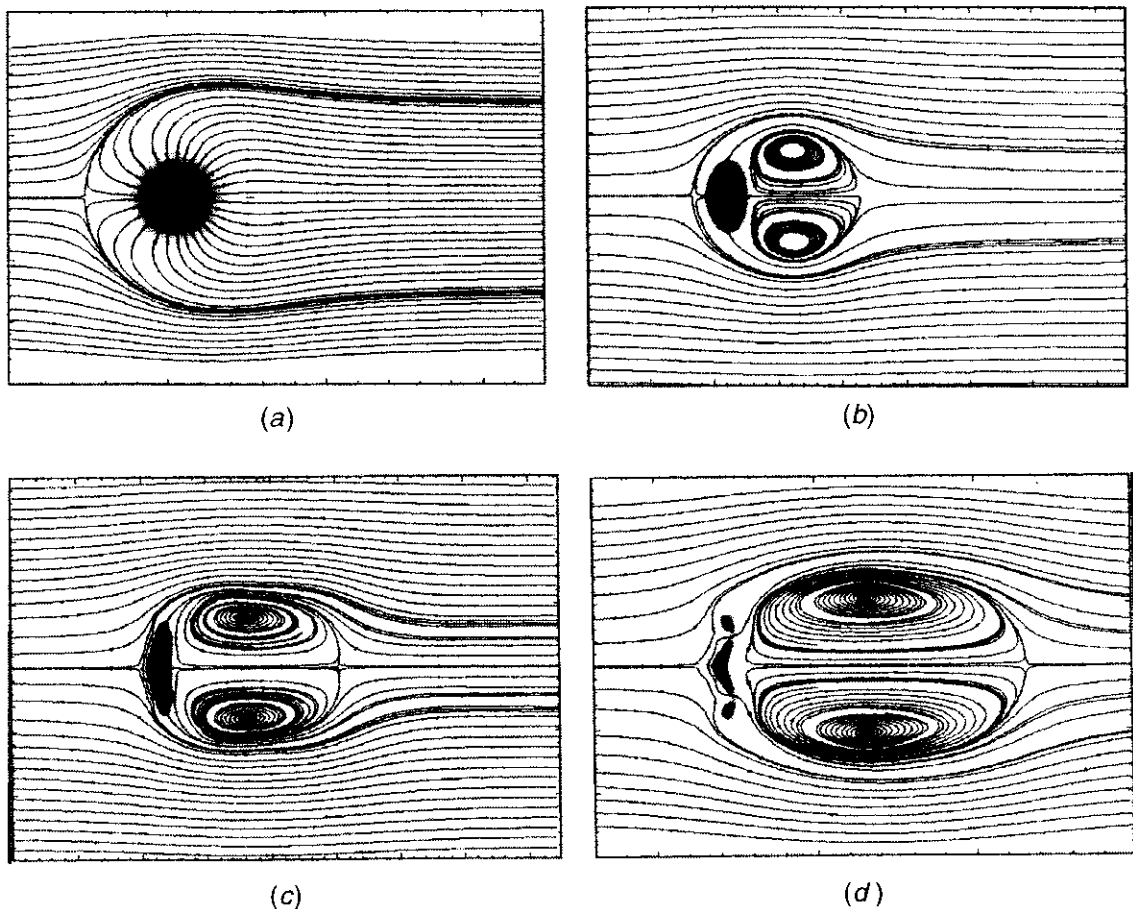


Figure 6.42 LOX Droplet gasification in supercritical hydrogen flow at $p = 100$ atm. (a) Spherical mode; $U_{\infty} = 0.2$ m/s, $t = 0.61$ ms. (b) Deformation mode; $U_{\infty} = 1.5$ m/s, $t = 0.61$ ms. (c) Stripping mode; $U_{\infty} = 5$ m/s, $t = 0.17$ ms. (d) Breakup mode; $U_{\infty} = 15$ m/s, $t = 0.17$ ms (after Yang³⁴).

result takes the form

$$\frac{\tau_f}{\tau_{f, \text{Re}_{D_0}=0}} = \frac{1}{1 + 0.17 \text{Re}_{D_0}^{1.1} (p_{r, \text{O}_2})^{-0.88}} \quad (6-199)$$

where Re_{D_0} and p_{r, O_2} refer to the Reynolds number based on the initial droplet diameter and the reduced pressure of oxygen, respectively. This correlation bears a resemblance to the popular Ranz-and-Marshall correlation²¹ for droplet heat-transfer correction due to convective effect. The Ranz-and-Marshall correlation applies only to low-pressure flows and has a weaker Reynolds number dependency.

Drag coefficient has been generally adopted as a dimensionless parameter to measure the drag force acting on a droplet. Chen and Yuen⁸¹ found that the drag coefficient of an evaporating droplet is smaller than that of a nonvaporizing solid sphere at the same Reynolds numbers. Several researchers (Renksizbulut and Haywood,⁸² Chiang et al.⁸³) numerically analyzed evaporating droplet motion by solving the Navier-Stokes equations and proposed the following correlation,

$$C_D = \frac{C_D^o}{(1 + B)^b} \quad (6-200)$$

where C_D° denotes the drag coefficient for a hard sphere, and the exponent b has a value of 0.2 for Renksizbulut and Haywood's model and 0.32 for Chiang's correlation. A transfer number B is adopted to account for the effect of blowing on momentum transfer to the droplet. For droplet vaporization at low to moderate pressures ($p_r \leq 0.5$), the Spalding transfer number is widely used to characterize the vaporization rate.

$$B = \frac{C_p(T_\infty - T_s)}{\Delta h_v} \quad (6-201)$$

The enthalpy of vaporization Δh_v becomes zero at the critical point, rendering an infinite value for the transfer number. This deficiency may be remedied by introducing a transfer number suited for supercritical droplet vaporization.^{51,76}

$$B_D = \left(\frac{T_\infty - T_c}{T_c - T_l} \right) \quad (6-202)$$

where T_l is the instantaneous average temperature of droplet, and T_c the critical mixing temperature. Since B_D diverges at $T_c = T_l$ at the end of droplet lifetime, the calculation of drag force was terminated when $(T_c - T_l)$ becomes less than 1 K, at which the droplet residual mass is usually less than one-thousandth of the initial mass. The influence on the accuracy of data reduction is quite limited. Following the procedure leading to Eq. (6-200), a correlation for LOX droplet drag coefficient was obtained by Hsiao and Yang⁷⁶:

$$C_D = \frac{C_D^\circ}{(1 + aB_D)^b} \quad (6-203)$$

where a and b are selected to be 0.05 and $1.592(P_{r,O_2})^{-0.7}$, respectively. The data clusters along the classical drag curve, Eq. (6-200), in the low Reynolds-number region but deviates considerably at high Reynolds numbers (i.e., $Re > 10$). Although a shape factor may be employed to account for this phenomenon arising from the increased form drag due to droplet deformation, the difficulty of calculating this factor and conducting the associated data analysis precludes its use in correlating the drag coefficient herein. Instead, a simple correction factor $Re_{D_0}^{0.3}$ is incorporated into Eq. (6-203) to provide the compensation. The final result is given below.

$$C_D = \frac{C_D^\circ Re_{D_0}^{0.3}}{(1 + aB_D)^{1.592(P_{r,O_2})^{-0.7}}}, \quad 0 < Re_{D_0} < 300 \quad (6-204)$$

6.6 Droplet Response to Ambient Flow Oscillation

Although unsteady droplet vaporization and combustion have long been recognized as a crucial mechanism for driving combustion instabilities in liquid-fueled propulsion systems,⁸⁴ they are extremely difficult to measure experimentally. In particular, the measurement of the effect of transverse oscillations on

instantaneous evaporation and/or burning rates is quite formidable. The droplet volume dilatation arising from rapid temperature increase may overshadow the surface regression associated with vaporization and thereby obscure the data analysis, especially in the early stage of the droplet lifetime. Furthermore, conventional suspended-droplet experiments may not be feasible in the presence of gravity due to reduced or diminished surface tension. In view of these difficulties, it is advantageous to rely on theoretical analyses to study the responses of droplet vaporization and combustion to ambient flow oscillations. The model is based on the general approach described in Refs. 51 and 75, but with a periodic pressure oscillation superimposed in the gas phase. Both cases involving hydrocarbon droplets in nitrogen⁵¹ and LOX droplets in hydrogen⁵³ are examined carefully. The purpose of these studies is to assess the effect of flow oscillation on vaporization process as a function of frequency and amplitude of the imposed oscillation, as well as its type.

The most significant result is the enhanced droplet vaporization response with increasing ambient mean pressure. Among the various factors contributing to this phenomenon, the effect of pressure on enthalpy of vaporization plays a decisive role. At high pressures, the enthalpy of vaporization decreases substantially and becomes sensitive to variations of ambient pressure and temperature. Any small fluctuations in the surrounding gases may considerably modify the interfacial thermodynamics and consequently enhance the droplet vaporization response. This phenomenon is most profound when the droplet surface reaches its critical condition at which a rapid amplification of vaporization response function is observed. The enthalpy of vaporization and related thermophysical properties exhibit abnormal variations in the vicinity of the critical point, thereby causing a sudden increase in the vaporization response. On the other hand, the effect of mean pressure on the phase angle of response function appears quite limited. The phase angle decreases from zero at the low-frequency limit to -180° at high frequency, a phenomenon that can be easily explained by comparing various timescales associated with fluid transport and ambient disturbances.

There are many characteristic times associated with the ignition and combustion of a single liquid fuel droplet. Project 6.2 asks for the mathematical forms of six different characteristic times in terms of adequate physical and chemical quantities under the condition of subcritical burning. It is also of great interest to extend the problem to the supercritical burning conditions.

REFERENCES

1. S. P. Burke and T. E. W. Schumann, "Diffusion Flames," *Indust. Eng. Chem.* **20**(10), 998 (1928).
2. H. C. Hottel and W. R. Hawthorne, *3rd Internat. Symp. Comb.*, 1949, p. 255.
3. D. B. Spalding, *Combustion and Mass Transfer*, 1st ed., Chapters 7, 9, 10, Pergamon Press, New York, 1979.
4. H. Schlichting, *Boundary Layer Theory*, 6th ed., Chapter XI, McGraw-Hill Book Co., New York, 1968.

5. G. M. Faeth, "Current Status of Droplet and Liquid Combustion," *Prog. Energy Combustion Sci.* **3**, 191–224 (1977).
6. A. M. Kanury, *Introduction to Combustion Phenomena*, Chapter 5, Gordon and Breach Science Publishers, New York, 1977.
7. D. B. Spalding, *4th Internat. Symp. Comb.*, 1953, p. 847.
8. D. B. Spalding, *Some Fundamentals of Combustion*, Chapter 4, Butterworths, London, 1955.
9. P. L. Blackshear, Jr., *An Introduction to Combustion*, Chapter IV, Dept. of Mech. Engr., University of Minnesota, Minneapolis, 1960.
10. I. Glassman, *Combustion*, Chapter 6, Academic Press, New York, 1977.
11. G. A. E. Godsake, *4th Internat. Symp. Comb.*, 1953, p. 818.
12. M. Summerfield, "Theory of Burning of a Composite Solid Propellant," ARS preprint, 1958.
13. D. B. Spalding, "Theory of Particle Combustion at High Pressure," *ARS J.*, 828–835 (November 1959).
14. D. E. Rosner, "On Liquid Droplet Combustion at High Pressures," *AIAA J.* **5**(1), 163–166 (1967).
15. D. P. Dominicis, *An Experimental Investigation of Near Critical and Supercritical Burning of Bipropellant Droplets*, NASA CR-72399, 1968.
16. A. Chervinsky, *AIAA J.* **7**, 1815–1817 (1969).
17. G. M. Faeth, D. P. Dominicis, J. F. Tulpinsky, and D. R. Olson, "Supercritical Bipropellant Droplet Combustion," *12th Intl. Symp. Combust.*, 1969, pp. 9–18.
18. S. Prakash, *Unsteady Theory of Droplet Vaporization with Large Gas and Liquid Reynolds Numbers*, Ph.D. thesis, Princeton University, 1978.
19. S. Prakash and W. A. Sirignano, "Liquid Fuel Droplet Heating with Internal Circulation," *Intl. J. Heat Mass Transfer* **21**, 885–895 (1978).
20. S. Prakash and W. A. Sirignano, "Theory of Convective Droplet Vaporization with Unsteady Heat Transfer in the Circulating Liquid Phase," *Intl. J. Heat Mass Transfer* **23**(3), 253–268 (1980).
21. W. E. Ranz and W. R. Marshall, "Evaporation from Drops," *Chem. Engr. Progr.* **48**(3), 141–173 (1952).
22. D. B. Spalding, "Experiments on Burning and Extinction of Liquid Fuel Spheres," *Fuel(London)* **32**(2), 169–185 (1953).
23. R. C. Reid and T. K. Sherwood, *The Properties of Gases and Liquids*, Chapters 3 & 8, McGraw-Hill, New York, 1958.
24. S. S. Penner and M. Y. Bahadori, "Laminar Diffusion Flames: Revisiting a Classical Combustion Problem," *International Colloquium on Gas Dynamics of Explosions and Reactive Systems, Poitier, France*, 1983.
25. S. H. Chung and C. K. Law, "Burke-Schumann Flame with Streamwise and Preferential Diffusion," *Combust. Sci. Tech.* **37**, 21 (1984).
26. S. M. Jeng and Z. Deng, "Numerical Simulation of Deformed Droplet Dynamics and Evaporation," Chapter 12 in K. K. Kuo, ed., *Recent Advances in Spray Combustion, Vol. II: Spray Combustion Measurements and Model Simulation*, Volume 171 of *Progress in Astronautics and Aeronautics*, September, 1996, pp. 305–328.

27. A. A. Borisov, B. E. Gel'fand, M. S. Natanzon, and O. M. Kossov, "Droplet Breakup Regimes and Criteria for Their Existence," *J. Engr. Phys.* **40**(1), (1981).
28. M. D. Smooke, R. E. Mitchell, and D. E. Keyes, "Numerical Solution of Two-Dimensional Axisymmetric Laminar Diffusion Flames," *Combust. Sci. Tech.* **67**, 85–122 (1989).
29. C. F. Curtiss and J. O. Hirschfelder, "Transport Properties of Multicomponent Gas Mixtures," *J. Chem. Phys.* **17**, 550 (1949).
30. Kee et al., "CHEMKIN: A General-Purpose, Transportable, Fortran Chemical Kinetics Code Package," Sandia National Laboratories Report, SAND80-8003, 1980.
31. R. E. Mitchell, *Nitrogen Oxide Formation in Laminar Methane-Air Diffusion Flames*, Sc.D. Thesis, Massachusetts Institute of Technology, 1975.
32. T. Takagi and Z. Xu, "Effect of Preferential Diffusion of Heat and Species in Diffusion Flames," in T. Takeno, ed., *Turbulence and Molecular Processes in Combustion*, Elsevier Science Publishers, 1993, pp. 393–402.
33. T. Takagi, K. Tada, and M. Komiyama, *Bulletin of JSME* **56**, 2109 (1990).
34. V. Yang, "Modeling of Supercritical Vaporization, Mixing, and Combustion Processes in Liquid-Fueled Propulsion Systems," *Proceedings of the Combustion Institute*, Vol. 28, Pt. 1, 200, pp. 925–942.
35. T. A. Brzustowski, *Canadian J. Chem. Engr.* **43**, 30–36 (1965).
36. C. E. Polymeropoulos and R. L. Peskin, *Combust. Sci. Tech.* **5**, 165–174 (1972).
37. J. A. Manrique and G. L. Borman, *Intl. J. Heat Mass Transfer*, **12**, 1081–1094 (1969).
38. R. S. Lazar and G. M. Faeth, *13th Intl. Symp. Combust.*, 1971, pp. 801–811.
39. G. S. Canada and G. M. Faeth, *15th Intl. Symp. Combust.*, 1975, pp. 418–428.
40. D. E. Rosner and W. S. Chang, *Combust. Sci. Tech.* **7**, 145–158 (1973).
41. T. Kadota and H. Hiroyasu, *Bulletin Japan Soc. Mech. Engr.*, 1515–1521 (1976).
42. K. C. Hsieh, J. S. Shuen, and V. Yang, *Combust. Sci. Tech.* **76**, 111–132 (1991).
43. E. W. Curtis and P. V. Farrel, *Combust. Flame* **90**, 85–102 (1992).
44. H. Jia and G. Gogos, *J. Thermophy. Heat Transfer* **6**, 739–745 (1992).
45. J. P. Delpanque and W. A. Sirignano, *Intl. J. Heat Mass Transfer* **36**, 303–314 (1993).
46. T. L. Jiang and W. T. Chiang, *Combust. Flame* **97**, 17–34 (1994).
47. T. L. Jiang and W. T. Chiang, *Combust. Flame* **97**, 355–362 (1994).
48. J. Daou, P. Haldenwang, and C. Nicoli, *Combust. Flame* 153–169 (1995).
49. J. S. Shuen, V. Yang, and G. C. Hsiao, *Combust. Flame* **89**, 299–319 (1992).
50. V. Yang, N. N. Lin, and J. S. Shuen, *Combust. Sci. Tech.* **97**, 247–270 (1994).
51. G. C. Hsiao, *Supercritical Droplet Vaporization and Combustion in Quiescent and Forced-Convection Environments*, Ph.D. thesis, Pennsylvania State University, University Park, PA, 1995.
52. P. Lafon, *Modélisation et Simulation Numérique de L'Evaporation et de la Combustion de Gouttes à Haute Pression*, Ph.D. thesis, à L'Université D'Orléans, 1995.
53. P. Lafon, V. Yang, and M. Habiballah, *AIAA Paper* 95–2432, 1995.
54. P. Haldenwang, C. Nicoli, and J. Daou, *Intl. J. Heat Mass Transfer* **39**, 3453–3464 (1996).

55. H. Meng and V. Yang, *AIAA Paper* 98-3537, 1998.
56. K. Harstad and J. Bellan, *Intl. J. Heat Mass Transfer* **41**, 3537-3550 (1998).
57. K. Harstad and J. Bellan, *Intl. J. Heat Mass Transfer* **41**, 3551-3558 (1998).
58. K. Harstad and J. Bellan, *Intl. J. Heat Mass Transfer* **42**, 961-970 (1999).
59. K. Harstad and J. Bellan, *Intl. J. Multiphase Flow* **26**, 1675-1706 (2000).
60. A. Umemura, *21st Intl. Symp. Combust.*, 1986, pp. 463-471.
61. A. Umemura and Shimada, *26th Intl. Symp. Combust.*, 1996, pp. 1621-1628.
62. A. Umemura and Shimada, *27th Intl. Symp. Combust.*, 1998, pp. 2659-2665.
63. S. D. Givler and J. Abraham, *Prog. Energy Combust. Sci.* **22**, pp. 1-28 (1996).
64. J. Bellan, *Prog. Energy Combust. Sci.* **26**, 329-366 (2000).
65. R. T. Jacobsen and R. B. J. Stewart, *J. Phys. Chem. Ref. Data* **2**, 757-922 (1973).
66. J. M. Prausnitz, R. N. Lichtenthaler, and E. G. de Azevedo, *Molecular Thermodynamics of Fluid-Phase Equilibria*, Prentice-Hall, Englewood Cliffs, NJ, 1986.
67. R. H. Perry, D. W. Gree, and J. O. Maloney, *Perry's Chem. Eng. Handbook*, McGraw-Hill, New York, 1984.
68. J. F. Ely and H. J. M. Hanley, *Indus. Engr. Chem. Fundamentals* **20**, 323-332 (1981).
69. J. F. Ely and H. J. M. Hanley, *Indus. Engr. Chem. Fundamentals* **22**, 90-97 (1983).
70. V. V. Sychev, A. A. Vasserman, A. D. Kozlov, and G. A. Spiridonov, *Property Data Update: Official Standards of the National Standard Reference Data Service of the USSR*, Vol. 1, Hemisphere Publishing Corp., 1987, pp. 529-536.
71. J. F. Ely, *J. Res. Nat'l Bureau Standards* **6**, 597-604 (1981).
72. V. Vesovic and W. A. Wakeham, "Transport Properties of Supercritical Fluids and Fluid Mixtures," in T. J. Bruno and J. F. Ely, eds., *Supercritical Fluid Technology*, CRC Press, Boca Raton, Florida, 1991, p. 253.
73. J. M. H. Levelt Sengers, "Thermodynamics of Solutions Near the Solvent's Critical Point," in T. J. Bruno and J. F. Ely, eds., *Supercritical Fluid Technology*, CRC Press, Boca Raton, Florida, 1991, p. 25.
74. S. Takahashi, *J. Chem. Engr. (Japan)* **7**, 417-420 (1974).
75. P. Lafon, V. Yang, and M. Habiballah, "Pressure-Couples Vaporization and Combustion Responses of Liquid Oxygen (LOX) Droplets in Supercritical Hydrogen Environments," *31st AIAA/ASME/SAE/ASEE Joint Propulsion Conference*, AIAA Paper 95-2432, July 1995.
76. G. C. Hsiao and V. Yang, *AIAA Paper* 95-0383, 1995.
77. V. Yang, M. Habiballah, J. Hulka, and M. Popp, eds., *Liquid-Propellant Rocket Combustion Devices*, Progress in Aeronautics and Astronautics, AIAA, Washington, DC, 2001.
78. J. Sato, M. Tsue, M. Niwa, and M. Kono, *Combust. Flame* **82**, 142-150 (1990).
79. J. Sato, *AIAA Paper* 93-0813, 1993.
80. S. Prakash and W. A. Sirignano, *Intl. J. Heat Mass Transfer* **23**, 253-268 (1995).
81. L. W. Chen and M. C. Yuen, *Combust. Sci. Tech.* **14**, 147-154 (1976).
82. M. Renksizbulut and R. J. Haywood, *Intl. J. Multiphase Flow* **14**, 189-202 (1988).
83. C. H. Chiang, M. S. Raju, and W. A. Sirignano, *Intl. J. Heat Mass Transfer* **35**, 1307-1324 (1992).

84. V. Yang and W. E. Anderson, eds., *Liquid Rocket Engine Combustion Instability*, Vol. 169, Progress in Aeronautics and Astronautics, AIAA, Washington, DC, 1995.
85. J. C. Oefelein and V. Yang, in K. K. Kuo, ed., *Recent Advances in Spray Combustion: Spray Combustion Measurements and Model Simulation*, Progress in Aeronautics and Astronautics **171**, AIAA, 1996, pp. 263–304.
86. J. C. Oefelein, *Simulation and Analysis of Turbulent Multiphase Combustion Processes at High Pressures*, Ph.D. thesis, Pennsylvania State University, University Park, PA, 1997.
87. J. C. Oefelein and V. Yang, *J. Prop. Power* **14**, 843–857 (1998).
88. W. Mayer and H. Tamura, *J. Prop. Power* **12**, 1137–1147 (1996).
89. W. O. H. Mayer, A. H. A. Schik, B. Vielle, C. Chauveau, I. Gokalp, D. G. Talley, and R. D. Woodward, *J. Prop. Power* **14**, 835–842 (1998).
90. W. Mayer, B. Ivancic, A. Schik, and U. Hornung, *AIAA Paper* 98–3685, 1998.
91. B. Ivancic, W. Mayer, G. Kruelle, and D. Brueggemann, *AIAA Paper* 99–2211, 1999.
92. S. Candel, G. Herding, R. Snyder, P. Scouflaire, C. Rolon, L. Vingert, M. Habiballah, F. Grisch, M. Pealat, P. Boudchardy, D. Stepowski, A. Cessou, and P. Colin, *J. Prop. Power* **14**, 826–834 (1998).
93. D. Kendrick, G. Herding, P. Scouflaire, C. Rolon, and S. Condel, *Combust. Flame* **118**, 327–339 (1999).
94. R. D. Woodward and D. G. Talley, *AIAA Paper* 96–0468, 1996.
95. J. J. Hutt and J. M. Cramer, *AIAA Paper* 96–4266, 1996.
96. G. Erlebacher, M. Y. Hussaini, C. G. Speziale, and T. A. Zang, *J. Fluid Mech.* **238**, 155–185 (1992).
97. G. M. Faeth, *Progr. Energy Combust. Sci.* **13**, 293–345 (1987).
98. A. S. Yang, W. H. Hsieh, and K. K. Kuo, “Combustion of Liquid Oxygen with Hydrogen Under High-Pressure Conditions,” *J. Propulsion and Power* **12**, 1001–1004, (September-October 1996).
99. A. G. Gaydon and H. G. Wolfhard, *Flames, Their Structure, Radiation and Temperature*, Chapman and Hall, Ltd., 1960.

HOMEWORK

1. Integrate the x -momentum equation (6-43) from $r = 0$ to $r = \infty$, and show that I_u of an axisymmetric jet is an invariant. Discuss the physical meaning of I_u .
2. Show that I_f of a cylindrical jet is an invariant. What is the physical meaning of I_f ?
3. Derive Eq. (6-179) by considering the total amount of fuel mass (burned and unburned) to be constant.
4. A turbojet engine has a flight speed of 200 m/s. If the combustor length is 2 m and if the temperature in the combustor is 1000 K, what is the maximum allowable size of *n*-pentane droplet if they have to be totally consumed by

(a) vaporization alone and (b) vaporization and combustion, before they exit the combustor? The densities of the *n*-pentane vapor and liquid at 310 K are 2.451×10^{-3} and 0.631 g/cm^3 , respectively. The thermal diffusivity and C_p of the vapor are $0.039 \text{ cm}^2/\text{s}$ and $0.397 \text{ cal/g} \cdot \text{K}$.

5. Find (a) the evaporation time; (b) the rate of evaporation per unit area; and (c) the temperature of the surface at $t = 0$, for a 4-mm-diameter water droplet evaporating in dry air at 760 Torr if the ambient temperature is 288 K. Repeat the problem for ambient temperature equal to 1273 K. Use the following data:

$$\Delta H_v = 590 \text{ kcal/kg}$$

$$C_{p,g} = 0.24 \text{ kcal/kg} \cdot \text{K}$$

$$\rho_l = 1000 \text{ kg/m}^3$$

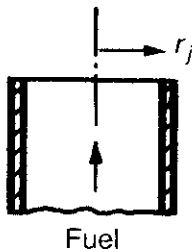
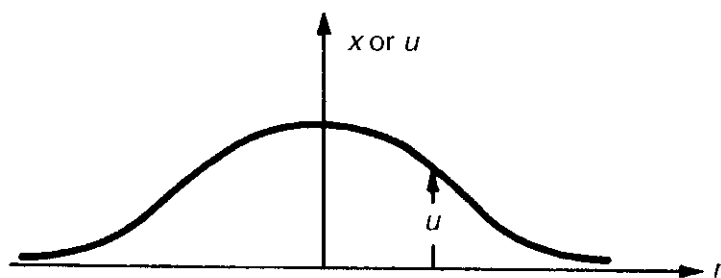
$$C_{p,l} = 1 \text{ kcal/kg} \cdot \text{K}$$

$$\text{at } 288 \text{ K, } \rho_g = 1.264 \text{ kg/m}^3 \text{ and } \alpha_g = 2.06 \times 10^{-2} \text{ m}^2/\text{s}$$

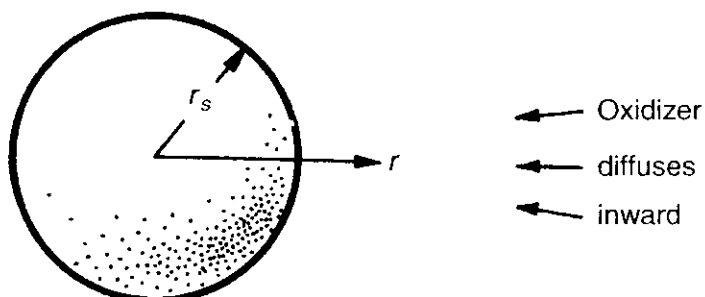
$$\text{at } 1273 \text{ K, } \rho_g = 0.2707 \text{ kg/m}^3 \text{ and } \alpha_g = 0.2583 \text{ m}^2/\text{s}$$

6. For a laminar jet diffusion flame burning in a still atmosphere, the flame surface can be considered as a source of heat and a source (or sink) of chemical species dividing the flow into two regions containing either fuel or oxidant.

- (a) Specify the governing equations (in cylindrical coordinates) that are needed for the solution for concentration, temperature, and velocity distributions throughout the entire flow field.
- (b) State the fundamental assumptions.
- (c) Give the necessary boundary conditions.
- (d) Suggest a method of simplification in the solution of this problem.

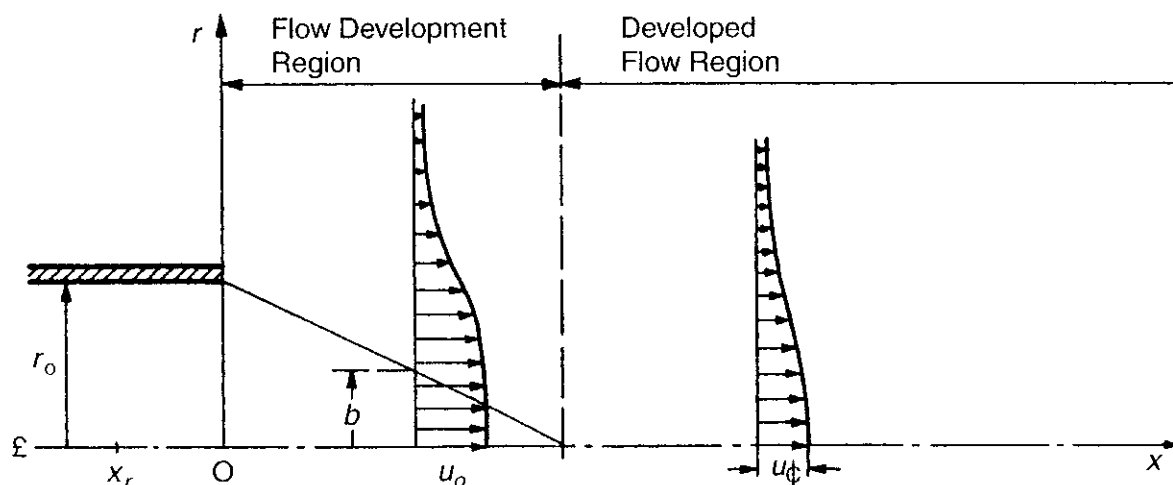


7. Consider a spherical metal particle that burns on the surface and forms a nonvolatile oxide that immediately dissolves upon formation in the metal itself. The surface reaction and dissolving rates are very fast compared with the oxidizer diffusion rate. Derive an expression for the burning rate of this metal.



PROJECTS

- 6.1 The laminar jet flow field can be divided into a developing region and a developed region (see figure below). In the developing region, a potential core can be assumed to exist. The potential core, having uniform velocity u_0 and local radius b , is bounded by an annular free-shear layer. Make the following assumptions:



Velocity profiles in flow development region and developed flow region.

- The surrounding air far from the jet is at rest.
- Chemical reaction is absent.
- The flow is steady and axisymmetric.
- The pressure in the flow field is uniform.
- The jet issues from a virtual origin x_v inside the cylindrical tube having radius r_0 .

Consider the following Schlichting jet velocity profile in the free-shear layer surrounding the potential core:

$$\frac{u}{u_0} = 1 \quad \text{for } 0 \leq R \leq B \quad (\text{A})$$

$$\frac{u}{u_0} = \frac{2(\Gamma/\text{Re})^2}{X + X_v} \left[1 + \frac{(\Gamma/\text{Re})^2(R - B)^2}{4(X + X_v)^2} \right] \quad \text{for } B \leq R \leq \infty \quad (\text{B})$$

where

$$\begin{aligned} B &\equiv \frac{b}{2r_0} \\ R &\equiv \frac{r}{2r_0}, \quad X \equiv \frac{x}{\text{Re} \cdot 2r_0} \\ \text{Re} &\equiv \frac{2u_0 r_0}{v}, \quad X_v \equiv \frac{x_v}{\text{Re} \cdot 2r_0} \end{aligned}$$

where x_v is the distance between the virtual origin and the jet exit, and

$$\Gamma \equiv \left(\frac{3}{8} \frac{I_u}{v} \right)^{1/2}$$

is the jet spread-angle parameter. In the above expression, the centerline velocity of the Schlichting jet has been shifted to the edge of the potential core. In order to ensure velocity continuity at $R = B$, we must have

$$2 \left(\frac{\Gamma}{\text{Re}} \right)^2 = X + X_v$$

Therefore,

$$\frac{u}{u_0} = \left[1 + \frac{(R - B)^2}{16(\Gamma/\text{Re})^2} \right]^{-1/2} \quad \text{for } B \leq R < \infty \quad (\text{C})$$

1. Derive Eq. (B) by rearranging Eq. (6-56) and replacing r with $r - b$ and x with $x + x_v$.
2. Using Eqs. (A) and (C) and the fact that I_u and $\int_0^\infty u^3 r dr$ are jet invariants, derive the ordinary differential equations for B and Γ/Re as functions of X .
3. Show that the above two differential equations can be combined and integrated to give

$$k_1 \ln \left[\frac{12\eta^2 + 15\pi\eta + 64}{(512 + 70\pi\eta)^2} \right] + k_2 \tan^{-1} \left[\frac{24\eta + 15\pi}{\sqrt{3072 - 225\pi^2}} \right] \\ + \frac{k_3\eta + k_4}{12\eta^2 + 15\pi\eta + 64} + k_5 = X \quad (D)$$

where

$$k_1 = -0.10395, \quad k_2 = 0.02699$$

$$k_3 = -0.51613, \quad k_4 = 2.81768$$

$$k_5 = -0.90537,$$

$$\eta \equiv \frac{B}{\Gamma/\text{Re}} \quad (E)$$

4. Plot the flow field (velocity profiles) and potential core boundary using Eqs. (D), (A), (C), and (E).

- 6.2** Consider the burning of a single spherical liquid fuel droplet of radius r_s in a quiescent environment with a sinusoidal pressure oscillation at frequency of f Hz and peak-to-peak amplitude of 20% of the average pressure, P . Express the following characteristic times in mathematical forms in terms of adequate physical and chemical quantities under the condition of subcritical burning:

- (a) τ_p —Characteristic time associated with pressure oscillation
- (b) τ_r —Characteristic time associated with the regression of liquid fuel droplet
- (c) τ_g —Characteristic time associated with the relaxation time of the gas-phase region surrounding the droplet
- (d) τ_l —Characteristic time associated with the relaxation time of the liquid fuel droplet
- (e) τ_h —Characteristic time associated with the heating up of the droplet surface to a critical pyrolysis temperature when the droplet with an initial temperature of T_o was first introduced to the hot environment at temperature T_∞
- (f) τ_{life} —Lifetime of the liquid fuel droplet

It would be useful to formulate the problem and then nondimensionalize the problem to obtain these characteristic time expressions. Also, describe the conditions for the quasi-steady gas-phase assumption to be valid.

- 6.3** To examine the evaporation and combustion behavior of a single droplet in convective stream environment, develop a set of governing equations that describe the rate of change of drop size, velocity, temperature, and composition as the droplet moves along in a dilute spray.

APPENDIX A

EVALUATION OF THERMAL AND TRANSPORT PROPERTIES OF GASES AND LIQUIDS

Symbol	Description
C_p	Constant-pressure (isobaric) specific heat, J/kg · K
C_v	Constant-volume (isochoric) specific heat, J/kg · K
$C_v^{(m)}$	Constant-volume (isochoric) specific heat of a molecule, J/K · molecule
$D_{A,B}$	Binary diffusion coefficient of species A into B, cm ² /s
$D_{A,B}^o$	Binary diffusion coefficient at very low concentrations of species A in solvent B, cm ² /s
f	Fugacity, bar
F_c	Correction factor used by Chung et al. for viscosity calculation
k	Boltzmann's constant = R_u /Avogadro's number
k_{ij}	Binary interaction parameter
L	Mean free path, m or Å
m	Mass of gas or liquid, kg
M_d	Dimensionless dipole moment
M_w	Molecular weight of gas or liquid, kg/kmol or g/mol
n	Number of moles of gas, mol
n^*	Number density of molecules, total number of molecules per unit volume
N_A	Avogadro's number, 6.02252×10^{23} molecules/mol
N^*	Equivalent chain length of carbon-based molecule
P	Pressure, usually bar
P_j	Parachor of component j , defined by Eq. (A-217)
$P_r^{(0)}$	Parameter used in Riedel vapor pressure correlation

(continued overleaf)

Symbol	Description
$P_r^{(1)}$	Parameter used in Riedel vapor pressure correlation
P_s	Saturated vapor pressure, usually bar
R	Gas constant, J/(kg · K)
R_u	Universal gas constant, 8.3144 J/(mol · K)
T	Temperature, K
T_b	Normal boiling point at 1 atm, K
T_r	Reduced temperature, T/T_c
\bar{u}	Average magnitude of the molecular velocity due to random motion, m/s
v	Specific volume, usually m ³ /kg
v	Specific molar volume, cm ³ /mol
V	Total volume, usually m ³
V^*	Characteristic volume, liter/mole
$V_r^{(0)}$	Corresponding states function for normal fluids
$V_r^{(\delta)}$	Deviation function for new correlation
V_s	Saturated liquid molar volume, mol
X	Mole fraction
Z	Compressibility factor
Z_{RA}	Rackett parameter used in Spencer-Danner correlation

Greek Letters

α	Function in Riedel vapor pressure equation
ε	Characteristic energy for molecular interaction, J/molecule
η_r	Dimensionless dipole moment for viscosity calculations
Θ_v	Characteristic temperature for vibration
κ	Special correction factor for viscosity calculations of highly polar substances
μ	Dynamic viscosity, N · s/m ² or kg/m · s or centipoise (0.001 N · s/m ²)
ν	Kinematic viscosity, m ² /s
ρ	Density of gas or liquid, kg/m ³
σ	Hard sphere diameter of gas molecule, Å
σ_s	Surface tension of a liquid, 10 ⁻³ N/m ²
N	Volume fraction
Φ	Dimensionless association factor of solvent B
ψ	Intermolecular potential function
ω	Pitzer's acentric factor
ω_{SRK}	Soave equation of state acentric factor, used in HBT correlation
Ω_D	Dimensionless collision integral for mass diffusivity consideration
Ω_v	Dimensionless collision integral for viscosity consideration
λ	Thermal conductivity, usually W/mK
λ^o	Low-pressure thermal conductivity, usually W/mK

Superscripts

L	Pertaining to liquid
o	Ideal-gas state
fr	Freezing point

Symbol	Description
<i>Subscripts</i>	
<i>c</i>	Critical conditions
<i>i</i>	<i>i</i> th chemical species
<i>j</i>	<i>j</i> th chemical species
<i>m</i>	Mixture
<i>s</i>	Saturation
SRK	Obtained using Soave–Redlich–Kwong equation of state

INTRODUCTION

In the simulation of many combustion processes, it is important to evaluate accurately the thermal and transport properties of both pure substances and mixtures of multiple chemical species in gas and liquid phases. The thermal properties include density and specific heat, while the transport properties include viscosity, thermal conductivity, and binary mass diffusivity. The accuracy of the numerical simulation depends strongly on how well these thermal and transport properties are evaluated. For low to moderate pressures, baseline methods have been developed for evaluating these properties for pure substances. For high pressures, there are techniques for correcting the baseline methods to determine the variations of the thermal and transport properties under extremely high-pressure conditions. Mixing rules have also been developed to evaluate these properties when multiple chemical species are present in a gaseous or liquid mixture.

The purpose of this appendix is to illustrate different techniques for evaluating these thermal and transport properties in a broad range of operating conditions. Table A-1 summarizes the baseline methods, high-pressure correction techniques, and mixing rules for different thermal and transport properties. Detailed procedures for evaluating each property are discussed below. For more detailed information about property evaluation of gases and liquids, the readers are recommended to consult an excellent reference book by Reid, Prausnitz, and Poling.¹ Some thermophysical properties of a number of selected gases and liquids can be obtained using the NIST web site: <http://webbook.nist.gov/chemistry/fluid/>.

1 GAS DENSITY

Gas density for pure substances and gaseous mixtures can be calculated from several accurate equations of state, which relate density to temperature and pressure. Most equations of state are accurate only when the density is substantially lower

Table A.1 Methods for Evaluating Thermal and Transport Properties

Property	Baseline Method (for Pure Substances)	High-Pressure Correction (for Pure Substances)	Mixing Rules (for Mixtures of Gases or Liquids)
Gas density	Ideal-gas law	Many different real-gas eqs. of state by van der Waals, Redlich–Kwong (RK), Soave (SRK), Peng–Robinson (PR), Beattie–Bridgeman, Benedict–Webb–Rubin (BWR), and virial eq. of state	Mixtures coefficients are evaluated from RK, SRK, PR, or BWR mixing rules
Liquid density	Spencer–Danner correlation (1972), Hankinson & Thomson's corresponding states liquid density correlation (1979)	Hankinson, Brobst, & Thomson (HBT) model (1982), Thomson et al. (1982), modified Chang–Zhao eq. (1990), model of Aalto et al. (1996)	Hankinson and Thomson's mixing rules (1979), HBT mixing rule, Aalto et al. (1996)
Gas specific heat	Daubert and Danner (1989), Joback (1984), and Thinh and Trong (1976)	Benedict, Webb, & Rubin (1940); Lee and Kesler (1975)	Mass fraction weighted averaging
Liquid specific heat	Group contribution methods of Chueh–Swanson (1973) and Missenard (1965), corresponding states method of Rowlinson (1969)	Sychev et al. (1987)	Mass fraction weighted averaging
Gas viscosity	Chapman and Enskog (1939), Reichenberg (1975), Lucas (1981), & Chung et al. (1986)	Reichenberg (1975, 77, 79), Lucas (1980, 81)	Lucas (1980, 81)

Table A.1 (continued)

Property	Baseline Method (for Pure Substances)	High-Pressure Correction (for Pure Substances)	Mixing Rules (for Mixtures of Gases or Liquids)
Liquid viscosity	van Velzen et al. (1972), Przezdziecki et al. (1985), Letsou & Stiel (1973), Starling et al. (1984)	Lucas (1981)	Grunberg & Nissan (1949), Isdale et al. (1979, 85), Teja and Rice (1981)
Gas thermal conductivity	Daubert & Danner (1989), McBride & Gordon (1996)	Stiel & Thodos (1964)	Mason & Saxena (1958), Yorizane et al. (1983)
Liquid thermal conductivity	Miller et al. (1976), Baroncini et al. (1981)	Missenard (1970)	Li (1976)
Gas binary diffusivity	Chapman & Enskog (1939), Wilke & Lee (1955)	Takahashi (1974)	Wilke (1950)
Liquid binary diffusivity	Wilke & Chang (1955), Tyn & Calus (1975), Hayduk & Minhas (1982), Tyn (1981)	Easteal (1984)	Perkins & Geankoplis (1969)

than the critical density of the substance, although several have been developed to maintain accuracy up to 2.5 times the critical density. Most equations fall into one of three categories: generalized, empirical, or theoretical. P - v - T equations of state may be of two types: *volume-explicit*, in which v is given as a function of T , P , and composition, and *pressure-explicit*, in which case P is given as a function of v , T , and composition.

1.1 Baseline Method^{1,2}

Ideal-Gas Equation of State The simplest equation of state is that for an ideal gas. The ideal-gas law, which applies to both pure components and mixtures, has been established from empirical observation and is accurate for gases at low density or up to about 2 atm for most compounds. For nondissociating molecules,

this relationship holds for low to moderate pressures.

$$PV = mRT = m \frac{R_u}{M_w} T = nR_u T \quad \text{or} \quad Pv = RT \quad \text{or} \quad P = \rho RT \quad (\text{A-1})$$

The values for the universal gas constant R_u in various units are given in Appendix B.

1.2 High-Pressure Correction

Van der Waals Equation of State The van der Waals equation² of state is one of the best-known generalized equations of state. It is essentially a modified version of the ideal-gas law, expressed by Eq. (A-1), except that it accounts for the intermolecular forces that exist between molecules (represented by the term a/v^2) and also corrects for the covolume, b , occupied by the molecules themselves. The van der Waals equation of state is

$$\left(P + \frac{a}{v^2} \right) (v - b) = RT \quad (\text{A-2})$$

where a and b are evaluated from the general behavior of gases. These constants are related to the critical temperatures and pressures of pure substances by

$$a = \frac{27}{64} \frac{R^2 T_c^2}{P_c} \quad \text{and} \quad b = \frac{RT_c}{8P_c} \quad (\text{A-3})$$

Redlich–Kwong Equation of State The Redlich–Kwong equation of state² (and many of its variants) is representative of the commonly used *empirical* cubic equations of state. It is considerably more accurate than the van der Waals equation and has been shown to be very successful for not only pure substances but also mixture calculations and phase equilibrium correlations. The original Redlich–Kwong equation is given as

$$P = \frac{R_u T}{\bar{v} - b} - \frac{a}{\bar{v}(\bar{v} + b)^{1/2}} \quad (\text{A-4})$$

where

$$a = \frac{0.42748 R_u^2 T_c^{2.5}}{P_c} \quad \text{and} \quad b = \frac{0.08664 R_u T_c}{P_c} \quad (\text{A-5})$$

Soave (SRK) and Peng–Robinson Equations of State The Soave (SRK) equation and the Peng–Robinson equations of state are both “cubic” equations of state developed to improve the Redlich–Kwong form. Both approaches have used the same method to set the parameters a and b . That is, both the first and second partial derivatives of pressure with respect to specific volume are set

Table A.2 Summary of Four Common “Cubic” Equations of State and Their Constants

Equation	<i>u</i>	<i>w</i>	<i>b</i>	<i>a</i>
van der Waals	0	0	$\frac{R_u T_c}{8 P_c}$	$\frac{27}{64} \frac{R_u^2 T_c^2}{P_c}$
Redlich–Kwong	1	0	$\frac{0.08664 R_u T_c}{P_c}$	$\frac{0.42748 R_u^2 T_c^{2.5}}{P_c T^{0.5}}$
Soave	1	0	$\frac{0.08664 R_u T_c}{P_c}$	$\frac{0.42748 R_u^2 T_c^2}{P_c} [1 + f(\omega)(1 - T_r^{0.5})]^2$ where $f(\omega) = 0.48 + 1.574\omega - 0.176\omega^2$
Peng–Robinson	2	-1	$\frac{0.07780 R_u T_c}{P_c}$	$\frac{0.42748 R_u^2 T_c^2}{P_c} [1 + f(\omega)(1 - T_r^{0.5})]^2$ $f(\omega) = 0.37464 + 1.5423\omega - 0.26992\omega^2$

Note: Values of ω for various substances can be found in Appendix A of Reference 1. Also, in the general form of Eq. (A-6), the coefficient *a* of the Redlich–Kwong equation of state given in this table is slightly different from that of Eq. (A-4).

to zero, as was done previously for the Redlich–Kwong equation of state. For brevity, the cubic form of the equations and their coefficients are provided in the summary table for common cubic equations of state (Table A-2). Both equations rely heavily on computations based primarily on the compressibility factor, *Z*, which is not treated in this text; however, the equations will be provided without the required tables.

The last four equations of state treated can be classified as “cubic equations of state”; that is, if expanded, the equations would contain volume terms raised to either the first, second, or third power. These two-parameter (containing *a* and *b*) equations can be expressed by the following equation:

$$P = \frac{R_u T}{\bar{v} - b} - \frac{a}{\bar{v}^2 + ub\bar{v} + wb^2} \quad (\text{A-6})$$

Virial Equation of State The virial equation of state,³ expressed in a polynomial series in reciprocal volume, is a theoretical equation of state derived from kinetic theory and statistical mechanics.

$$P = \frac{R_u T}{\bar{v}} + \frac{R_u T B}{\bar{v}^2} + \frac{R_u T C}{\bar{v}^3} + \dots \quad (\text{A-7})$$

where *B*, *C*, ... are called the second, third, ... virial coefficients and are functions of temperature and type of pure substance. The number of terms required for accurate predictions is highly dependent on pressure: As pressure increases, more terms must be used. Considerable amounts of information exist on second

virial coefficients;³ however, very little is known about the third coefficients, and essentially nothing about the fourth and higher coefficients.³

Beattie–Bridgeman Equation of State The Beattie–Bridgeman equation of state^{1,2} is an empirical, pressure-explicit equation requiring five constants and is reasonably accurate for densities of less than about 0.8 times the critical density.

$$P = \frac{R_u T(1 - \varepsilon)}{v^2} (v + B) - \frac{A}{v^2} \quad (\text{A-8})$$

where $A = A_0(1 - a/v)$, $B = B_0(1 - b/v)$, $\varepsilon = c/vT^3$, and a , b , and c are constants for different gases. The values of these constants for several substances are given in Table A-3.

Benedict–Webb–Rubin (BWR) Equation of State The Benedict, Webb, and Rubin equation of state^{1,3} is an extension of the Beattie–Bridgeman equation of state through the addition of high-density terms. It requires eight empirical constants. Its popularity stems from its ability to calculate both liquid and vapor properties, and it is accurate for those compounds and mixtures for which constants have been determined. Expressed in terms of molar density ρ , the BWR equation is

$$\begin{aligned} P = R_u T \rho + & \left(B_0 R_u T - A_0 - \frac{C_0}{T^2} \right) \rho^2 + (b R_u T - a) \rho^3 + a \alpha \rho^6 \\ & + \left(\frac{c \rho^3}{T^2} \right) (1 + \gamma \rho^2) \exp(-\gamma \rho^2) \end{aligned} \quad (\text{A-9})$$

where A_0 , B_0 , C_0 , b , a , α , c , and γ are the eight constants. Values for these constants can be found in Ref. 3. When solved for density, this equation can have up to six roots. The lowest value is the vapor density, and the highest is the liquid density. A more complex form of the BWR equation of state is given in Eq. (6-174).

Table A.3 Constants for Beattie–Bridgeman Equation of State² (pressure in kPa; specific volume in m³/kmol; temperature in Kelvin; $R_u = 0.08206$ atm-liters/g-mole · K)

Gas	A_0	a	B_0	b	$10^{-4}c$
Helium	0.0216	0.05984	0.01400	0.0	0.0040
Argon	1.2907	0.02328	0.03931	0.0	5.99
Hydrogen	0.1975	-0.00506	0.02096	-0.04359	0.0504
Nitrogen	1.3445	0.02617	0.05046	-0.00691	4.20
Oxygen	1.4911	0.02562	0.04624	0.004208	4.80
Air	1.3012	0.01931	0.04611	-0.001101	4.34
CO ₂	5.0065	0.07132	0.10476	0.07235	66.00

1.3 Mixing Rules

Ideal-Gas Mixing Rules The mixing rule most commonly used for the ideal-gas equation is Dalton's Law of Partial Pressures,² which is applicable only to ideal gases. In Dalton's model, the properties of each component are evaluated as though each component existed separately at the volume and temperature of the mixture.

Considering a mixture consisting of two components, *A* and *B*, where both the mixture and each individual component behave as ideal gases, then, for the mixture,

$$PV = nR_uT \quad (\text{A-10})$$

where

$$n = n_A + n_B \quad (\text{A-11})$$

For the components,

$$P_A V = n_A R_u T, \quad P_B V = n_B R_u T \quad (\text{A-12})$$

On substituting Eq. (A-12) into Eq. (A-11), we have

$$\frac{PV}{R_u T} = \frac{P_A V}{R_u T} + \frac{P_B V}{R_u T} \quad (\text{A-13})$$

which yields

$$P = P_A + P_B \quad (\text{A-14})$$

Thus, for a mixture of ideal gases, the pressure is the sum of the partial pressures of the individual components. It must be stressed that this approximation only holds for ideal gases and assumes that no interactions between different components take place.

Mixing Rules for Redlich–Kwong Type of Equation of State The mixing rules recommended by Redlich–Kwong for all two-constant cubic equations of state (i.e., van der Waals, Redlich–Kwong, Soave, and Peng–Robinson) are broadly used.¹ The constants a_m and b_m for the mixture, with N components, can be calculated from

$$a_m = \sum_i^N \sum_j^N X_i X_j (a_i a_j)^{1/2} (1 - \bar{k}_{ij}) \quad (\text{A-15})$$

$$b_m = \sum_i X_i b_i \quad (\text{A-16})$$

where a_i and b_i are constants calculated in Table A-2. The binary interaction coefficients \bar{k}_{ij} for the Soave and Peng–Robinson equations are given in Table A-4. For hydrocarbon pairs, \bar{k}_{ij} is usually taken as zero.

Table A.4 \bar{k}_{ij} Values for Soave (SRK) and Peng–Robinson (PR) Equations

	Carbon Dioxide		Hydrogen Sulfide		Nitrogen		Carbon Monoxide	
	SRK	PR	SRK	PR	SRK	PR	SRK	PR
Methane	0.093	0.092	—	—	0.028	0.031	0.032	0.030
Ethylene	0.053	0.055	0.085	0.083	0.080	0.086	—	—
Ethane	0.136	0.132	—	—	0.041	0.052	-0.028	-0.023
Propylene	0.094	0.093	—	—	0.090	0.090	—	—
Propane	0.129	0.124	0.088	0.088	0.076	0.085	0.016	0.026
Isobutane	0.128	0.120	0.051	0.047	0.094	0.103	—	—
<i>n</i> -Butane	0.143	0.133	—	—	0.070	0.080	—	—
Isopentane	0.131	0.122	—	—	0.087	0.092	—	—
<i>n</i> -Pentane	0.131	0.122	0.069	0.063	0.088	0.100	—	—
<i>n</i> -Hexane	0.118	0.110	—	—	0.150	0.150	—	—
<i>n</i> -Heptane	0.110	0.100	—	—	0.142	0.144	—	—
<i>n</i> -Decane	0.130	0.114	—	—	—	—	—	—
Carbon dioxide	—	—	0.099	0.097	-0.032	-0.017	—	—
Cyclohexane	0.129	0.105	—	—	—	—	—	—
Benzene	0.077	0.077	—	—	0.153	0.164	—	—
Toluene	0.113	0.106	—	—	—	—	—	—

Benedict–Webb–Rubin Mixing Rules For mixtures of N components, the eight constant parameters in Eq. (A-9) are functions of composition in the mixture.¹ The parameter of the mixture, φ_{mix} , can be calculated from

$$\varphi_{\text{mix}} = \sum_{i=1}^N X_i \varphi_i^{1/r} \quad (\text{A-17})$$

where r , the inverse exponential integer, is based on the type of constant represented by φ , as shown below:

φ	A_0	B_0	C_0	b	a	c	α	γ
r	2	1	2	3	3	3	3	2

Virial Equation Mixing Parameters Because the second virial coefficient is the most used, it will be the only one treated here, as very little is known about the third and fourth virial coefficients. The second virial coefficient for mixtures of N components, B_{mix} , is obtained from the following expression^{1,3}:

$$B_{\text{mix}} = \sum_{i=1}^N \sum_{j=1}^N X_i X_j B_{ij} \quad (\text{A-18})$$

where B_{ii} represents the pure-component second virial coefficient of component i , and B_{ij} is the binary-interaction second virial coefficient for components i and j (Note that $B_{ij} = B_{ji}$).

For example, in a ternary system with mixture components 1, 2, and 3,

$$B_{\text{mix}} = X_1^2 B_1 + X_2^2 B_2 + X_3^2 B_3 + 2X_1 X_2 B_{12} + 2X_1 X_3 B_{13} + 2X_2 X_3 B_{23} \quad (\text{A-19})$$

Extensive treatment of interaction coefficients and combination rules can be found in Ref. 3.

2 LIQUID DENSITY

Prediction of liquid density is needed in many engineering problems. A good correlation should be accurate and reliable over the whole temperature range from the freezing point of the liquid to its critical point. Usually, cubic equations of state are not accurate enough in predicting liquid densities, and many special methods for predicting liquid densities have been developed. Models are divided into two categories: for saturated liquids and for compressed liquids. When calculating densities of compressed liquids, the density of the saturated liquid is calculated first. The saturated liquid densities are then corrected with the appropriate pressure-dependence relation to obtain density at the given pressure.

A good correlation for predicting liquid density must be both accurate and reliable. For computer applications, computation times should be short, and the functions in the correlation should be continuous and single valued. Where iterative calculations are required, the calculation algorithm should converge reliably. A correlation for the densities of compressed liquids must also be predictive, since the given experimental data may be scarce.

2.1 Baseline Method

Spencer–Danner Correlation and Other Modifications Spencer and Danner⁴ conducted a critical review of 13 correlations for predicting the effect of temperature on the saturated liquid densities of pure fluids. Of those correlations, Spencer and Danner demonstrated that the correlations of Yen and Woods,⁵ Gunn and Yamada,⁶ and Rackett⁷ were the best. Spencer and Danner also modified the Rackett correlation to give more accurate predicted saturated liquid densities over the entire temperature range from the triple point to the critical point.

$$V_s = \frac{RT_c}{P_c} Z_{RA}^{[1+(1-T_r)^{2/7}]} \quad (\text{A-20})$$

This model requires the critical properties and a characteristic parameter Z_{RA} for the component of interest. Reid et al.¹ have listed the values of Z_{RA} for numerous compounds. R is the molar gas constant. The Spencer–Danner correlation can be applied from the triple point to the critical point of a substance, but the molar volume at the critical point is not correct unless $Z_{RA} = Z_c$.¹ Spencer and Danner obtained a set of data with 3595 points of saturated liquid data for 111 compounds, of which 2795 points were for hydrocarbons. They reported an average absolute deviation of 0.5% for hydrocarbons.

Campbell and Thodos⁸ made a modification to the method of Spencer and Danner, where the parameter Z_{RA} in Eq. (A-20) was replaced by a temperature-dependent function:

$$Z_{RA} = \alpha + \beta(1 - T_r) \quad (\text{A-21})$$

The parameters α and β were fitted and reported for 62 substances. Correlations for estimating α and β from T_c , T_b , P_c and molar mass were developed. Correlations for nonpolar compounds are

$$\alpha = 0.3883 - 0.0179s \quad (\text{A-22})$$

The parameter s is calculated from

$$s = \frac{T_{Rb} \ln(P_c)}{1 - T_{Rb}} \quad (\text{A-23})$$

where $T_{Rb} = T_b/T_c$, and P_c is the critical pressure.

For estimating β , the Λ parameter is defined:

$$\Lambda = \frac{P_c^{1/3}}{\text{Mw}^{1/2} T_c^{5/6}} \quad (\text{A-24})$$

where Mw is the molar weight. β is obtained from

$$\beta = 0.00318s - 0.0211 + 0.625\Lambda^{1.35} \quad (\text{A-25})$$

Chang and Zhao⁹ used both the original and this modified Spencer–Danner equation when they developed their model for compressed liquids. The parameters required for the Chang–Zhao equation were fitted using the Spencer–Danner correlation for calculating the saturated molar volume.

COSTALD (Hankinson–Thomson Correlation) Hankinson and Thomson¹⁰ developed COSTALD (Corresponding States Liquid Density), where the baseline method and mixing rules were originally described. Hankinson and Thomson attempted to use the desirable features of the three general-purpose correlations recommended by Spencer and Danner and to eliminate the least desirable ones. The equation to predict densities of saturated liquids, V_s , is given by

$$\frac{V_s}{V^*} = V_R^{(0)}(1 - \omega_{SRK} V_R^{(\delta)}) \quad (\text{A-26})$$

where ω_{SRK} is the acentric factor and V^* is a pure compound characteristic molar volume generally within 1 to 4% of the critical volume. The V^* values of various pure components are given in Reid et al.¹ Also, V^* can be estimated from Eq. (A-33). $V_r^{(0)}$ is a spherical molecule function, and $V_r^{(\delta)}$ represents the

deviation from spherical molecule behavior.

$$V_R^{(0)} = 1 + a(1 - T_r)^{1/3} + b(1 - T_r)^{2/3} + c(1 - T_r) + d(1 - T_r)^{4/3} \quad \text{for } 0.25 < T_r < 0.95 \quad (\text{A-27})$$

$$V_r^{(\delta)} = \frac{e + fT_r + gT_r^2 + hT_r^3}{T_r - 1.00001} \quad \text{for } 0.25 < T_r < 1.0 \quad (\text{A-28})$$

The coefficients a through h for the above two equations are given below.

$$a = -1.52816, b = 1.43907, c = -0.81446, d = 0.190454,$$

$$e = -0.296123, f = 0.386914, g = -0.0427258, h = -0.0480645.$$

2.2 High-Pressure Correction

Hankinson–Brobst–Thomson (HBT) Model Hankinson, Brobst, and Thomson^{11,1} developed the high-pressure correction using the modified Tait equation (extended and generalized to permit the calculations of densities of compressed liquids and their mixtures to a pressure of 68.95 MPa) and utilized the acentric factor from the Soave–Redlich–Kwong equation of state (Section 1.2). Their final correlation is called the HBT model. In their model, once the saturated molar volume V_s is determined from the chosen temperature T and the vapor pressure P_s , the molar volume V can be calculated at a higher pressure P by the following equation:

$$V = V_s \left[1 - c \ln \left(\frac{\beta + P}{\beta + P_s} \right) \right] \quad (\text{A-29})$$

A Guggenheim temperature dependence is assigned to β , and since $\beta \rightarrow -P_c$ as $T \rightarrow T_c$, the terms β and c are obtained from Eqs. (A-30) through (A-32).

$$\beta = P_c[-1 + a(1 - T_r)^{1/3} + b(1 - T_r)^{2/3} + d(1 - T_r) + e(1 - T_r)^{4/3}] \quad (\text{A-30})$$

$$e = \exp(f + g\omega_{\text{SRK}} + h\omega_{\text{SRK}}^2) \quad (\text{A-31})$$

$$c = j + k\omega_{\text{SRK}} \quad (\text{A-32})$$

P_c is the critical pressure of the component of interest, and the parameters a through k are given in the following table. Thomson et al. had a database consisting of 7690 points of compressed liquid density data for 42 pure compounds, of which 6338 points were for nonpolar liquids. An average absolute deviation of 0.446% was reported for this group.

$$a = -9.070217, b = 62.45326, d = -135.1102, f = 4.79594,$$

$$g = 0.250047, h = 1.14188, j = 0.0861488, k = 0.0344483.$$

Generalized COSTALD If a single experimental datum point is available for a fluid, the entire saturated liquid density curve and the characteristic volume curve can be obtained using Eqs. (A-26), (A-27), and (A-28). Often, however, a single datum point may not be available. Consequently, to provide an accurate prediction for such cases, the characteristic volumes have been correlated with the following expression:

$$V^* = \frac{RT_c(a + b\omega_{SRK} + c\omega_{SRK}^2)}{P_c} \quad (A-33)$$

Table A-5 presents the values of the coefficients a , b , and c for nine classes of fluids.¹ Since the expected error in calculated volume or density is directly proportional to the error in characteristic volume, the average percentage error is given for each case.

Chang–Zhao Equation In 1990, Chang and Zhao⁹ presented a new equation for compressed liquids. In general, this equation works the same way as the Tait equation; it needs the saturated molar volume V_s and the vapor pressure P_s as the input variables, and it produces the molar volume V at a given pressure P . The parameters required for Chang–Zhao were fitted using the Spencer–Danner correlation for calculating the saturated molar volume. The Chang–Zhao equation is given as

$$V = V_s \left[\frac{A + C^{(D-T_r)B}(P_r - P_{s,r})}{A + C(P_r - P_{s,r})} \right] \quad (A-34)$$

where P_r is the reduced pressure and $P_{s,r}$ is the reduced pressure of the saturated vapor. C and D are constants. A and B are defined by Eqs. (A-26) and (A-27).

$$A = \sum_{i=0}^5 a_i T_r^i \quad (A-35)$$

Table A.5 Coefficients for Generalized COSTALD Correlation

Materials	a	b	c	Avg. Absolute Error in V^*
Paraffins	0.2905331	-0.08057958	0.02276965	1.23%
Olefins & diolefins	0.3070619	-0.2368581	0.2834693	1.43%
Cycloparaffins	0.6564296	-3.391715	7.442388	1.00%
Aromatics	0.2717636	-0.05759377	0.05527757	0.58%
All hydrocarbons	0.2851686	-0.0637911	0.01379173	1.89%
Sulfur compounds	0.3053426	-0.1703247	0.1753972	1.98%
Fluorocarbons	0.5218098	-2.346916	5.407302	0.82%
Cryogenic liquids	0.2960998	-0.05468500	-0.1901563	0.85%
Condensable gases	0.2828447	-0.1183987	0.1050570	3.65%

Table A.6 Parameters for Chang–Zhao Equation for Compressed Liquids

a_0	99.42	b_0	0.38144
a_1	6.502	b_1	−0.30144
a_2	−78.68	b_2	−0.08457
a_3	−75.18	C	2.810
a_4	41.49	D	1.1
a_5	7.259		

$$B = \sum_{j=0}^2 b_j \omega^j \quad (\text{A-36})$$

The ω used for calculating B is the Pitzer acentric factor, which is normally not equal to ω_{SRK} . Chang–Zhao equation needs T_c , P_c , and ω , which are the characteristics for a compound. Parameters a_i , b_j , C , and D are listed in Table A-6. The Chang–Zhao equation can be used up to the critical temperature of a compound. Chang and Zhao had 1126 points of compressed liquid density data for 18 pure compounds, and they reported an average absolute deviation of 0.84%.

Model of Aalto et al. Aalto et al.^{12,13} have proposed a new model for calculating compressed liquid densities using the Hankinson–Thomson¹⁰ correlation for saturated liquids and then using a modified Chang–Zhao equation in the compressed liquid region. This new method can be used to calculate densities of both pure compounds and mixtures with good results, even in the near-critical region. The model was also extended for calculating densities of liquid mixtures. The HBT correlation predictions for compressed liquids in the region $0.95 < T_r < 1.0$ were found to be in error, and there is a zone where calculations are not possible because of an undefined function. The mathematical error preventing calculations was found to come from the logarithmic term in the original Tait equation [see Eq. (A-29)].

Consequently, the method of Hankinson and Thomson could be used in the near-critical region to get saturated densities, and the compressed liquid density values could be computed provided that another pressure correction equation is available. For saturated liquid densities, the correlation of Hankinson and Thomson is used to predict the molar volumes of saturated liquids, V_s . Once the saturated molar volume V_s and the vapor pressure P_s have been calculated at a chosen temperature T , the molar volume V at the actual pressure P of the liquid is calculated. The pressure dependence of the liquid volume is described by the modified Chang–Zhao equation:

$$V = V_s \left[\frac{A + C^{(D-T_r)B}(P_r - P_{s,r})}{A + C(P_r - P_{s,r})} \right] \quad (\text{A-37})$$

Table A.7 Parameters Used in Modified Chang–Zhao Equation

a_0	−170.335	b_0	0.164813
a_1	−28.5784	b_1	−0.0914427
a_2	124.809	C	$\exp(1)$
a_3	−55.5393	D	1.00588
a_4	130.010		

Parameters A and B are defined differently as below. The values for parameters $a_0, \dots, a_4, b_0, b_1, C$, and D are given in Table A-7.

$$A = a_0 + a_1 T_r + a_2 T_r^3 + a_3 T_r^6 + \frac{a_4}{T_r} \quad (\text{A-38})$$

$$B = b_0 + b_1 \omega_{\text{SRK}} \quad (\text{A-39})$$

The parameters of the modified Chang–Zhao equation were fitted using compressed liquid density data for alkanes and alkenes. The objective function (OF) numerically reduced to a minimum was

$$\text{OF} = \sum_i \left(\frac{\rho_{\text{exp},i} - \rho_{\text{calc},i}}{\rho_{\text{exp},i}} \right)^2 \quad (\text{A-40})$$

2.3 Mixing Rules

In order to determine the density of liquid mixtures using the above methods, the critical temperature, critical pressure, and acentric factor of the mixture must be known. Thus, this section presents ways to estimate the critical properties of liquid mixtures in order to determine the values of T_c and P_c for volume calculations.

Mixing Rules for Critical Temperature of Liquid Mixtures The simple way to calculate $T_{c,m}$ is Kay's rule¹

$$T_{c,m} = \sum_i X_i T_{c,i} \quad (\text{A-41})$$

According to Spencer and Danner,⁴ $T_{c,m}$ can be similarly determined by Li's method using volume fractions, ϕ_i , instead of mole fractions, i.e.,

$$T_{c,m} = \sum_i \phi_i T_{c,i} \quad (\text{A-42})$$

where

$$\phi_i = \frac{X_i V_{c,i}}{\sum_j X_j V_{c,j}} \quad (\text{A-43})$$

When these are applied to the HBT model discussed in a later section, V^* should be used instead of V_c in Eq. (A-43). Hankinson and Thomson¹⁰ also tested Eq. (A-44) utilizing ϕ_i from Eq. (A-43) and the pure component parameter V^* .

$$T_{c,m} = \left[\sum_i \phi_i (T_{c,i})^{1/2} \right]^2 \quad (\text{A-44})$$

There are other quadratic mixing rules to obtain the critical temperature of a mixture, $T_{c,m}$. The most typical ones are given by Eqs. (A-45) and (A-46), where these two equations differ in the definition of T_{cij} .

$$T_{c,m} = \sum_i \sum_j X_i X_j T_{cij}; \quad T_{cij} = (1 - k_{ij})(T_{ci} T_{cj})^{1/2} \quad (\text{A-45})$$

$$T_{c,m} = \sum_i \sum_j X_i X_j T_{cij}; \quad T_{cij} = \frac{(1 - k_{ij})(T_{ci} + T_{cj})}{2} \quad (\text{A-46})$$

where the k_{ij} is the binary interaction parameter between i th and j th species. Hankinson and Thomson¹⁰ recommended the following mixing rules for saturated liquids:

$$T_{c,m} = \frac{\sum_i \sum_j X_i X_j V_{ij}^* T_{cij}}{V_m^*}; \quad \text{where } V_{ij}^* T_{cij} = (V_i^* V_j^* T_{ci} T_{cj})^{1/2} \quad (\text{A-47})$$

and the characteristic volume of the mixture, V_m^* , is calculated from Eq. (A-48).

Mixing Rules for Critical Volume $V_{c,m}$ and Characteristic Volume V_m^*
The original HBT mixing rule¹¹ to obtain characteristic volume of a mixture is

$$V_m^* = \frac{1}{4} \left[\sum_i X_i V_i^* + 3 \left(\sum_i X_i V_i^{*2/3} \right) \left(\sum_i X_i V_i^{*1/3} \right) \right] \quad (\text{A-48})$$

The critical volume for mixtures is often calculated from Eq. (A-49)

$$V_{c,m} = \sum_i \sum_j X_i X_j V_{cij} \quad (\text{A-49})$$

where $V_{cij} = \frac{1}{8}(1 - k_{ij})(V_{ci}^{-1/3} + V_{cj}^{-1/3})^3$.

Mixing Rule for Acentric Factor Hankinson and Thomson¹⁰ recommended linear combination for calculating the acentric factor of a mixture.

$$\omega_{\text{SRK},m} = \sum_i X_i \omega_{\text{SRK},i} \quad (\text{A-50})$$

Estimation of the Critical Pressure for a Mixture To calculate compressed liquid densities, the critical pressure is needed. P_c is easily available for pure components, but it has to be estimated for mixtures. Thomson et al.¹¹ recommended Eq. (A-51) for the estimation of critical pressure of a mixture, $P_{c,m}$.

$$P_{c,m} = (0.291 - 0.080\omega_{SRK,m}) \frac{RT_{c,m}}{V_{c,m}} \quad (A-51)$$

Here, the linear function of the acentric factor (the term in the parentheses) is an estimate of the critical compressibility factor. Eq. (A-51) actually comes from the definition of the critical factor, where V_m substitutes V_c^* . The vapor pressure of a mixture $P_{s,m}$ is obtained using Eq. (A-52) and the generalized Riedel vapor pressure equation, Eqs. (A-53) through (A-57).

$$P_{s,m} = P_{c,m} P_{r,m} \quad (A-52)$$

where the reduced pressure of the mixture, $P_{r,m}$, is calculated as

$$\log_{10} P_{r,m} = P_{r,m}^{(0)} + \omega_{SRK,m} P_{r,m}^{(1)} \quad (A-53)$$

The simple fluid pressure $P_{r,m}^{(0)}$ and the reference fluid pressure $P_{r,m}^{(1)}$ are given by Eqs. (A-54) and (A-55), and the function α is defined by Eq. (A-56).

$$P_{r,m}^{(0)} = 5.8031817 \log_{10} T_{r,m} + 0.07608141\alpha \quad (A-54)$$

$$P_{r,m}^{(1)} = 4.86601 \log_{10} T_{r,m} + 0.03721754\alpha \quad (A-55)$$

$$\alpha = (35.0 - 36.0/T_{r,m}) - 96.736 \log_{10} T_{r,m} + T_{r,m}^6 \quad (A-56)$$

The reduced temperature of the mixture is calculated using the mixture critical temperature $T_{c,m}$ obtained from Eq. (A-47).

$$T_{r,m} = \frac{T}{T_{c,m}} \quad (A-57)$$

Thomson et al.¹¹ reported an average absolute deviation of 1.61% for 128 mixtures with 6926 data points.

In general, to perform mixture calculations, four mixing rules are needed (for V_m^* , $T_{c,m}$, $\omega_{SRK,m}$, and $P_{c,m}$) according Aalto et al.^{12,13} The recommend mixing rules are Eq. (A-47) for $T_{c,m}$, Eq. (A-48) for V_m^* , Eq. (A-50) for $\omega_{SRK,m}$, and Eq. (A-51) for $P_{c,m}$. In addition, a method to estimate the vapor pressures of the mixture is needed. The generalized Riedel vapor pressure equation can be used for this purpose in all calculations. The saturated liquid densities are first calculated with the Hankinson–Thomson correlation. A modified Chang–Zhao equation is used for describing the effect of pressure on the liquid to predict the compressed liquid density.

While discussing the accuracy of the models, the significance of experimental errors has to be considered. Errors of 0.1–0.2% are reported for measurement of liquid densities, which could be greater in the near-critical region. Ultimately, experimental error sets the upper limit for accuracy of any model, since a considerable part of the error in a compressed liquid density prediction is caused by the error in the saturated liquid density prediction.

3 GAS SPECIFIC HEAT

3.1 Baseline Method

The following correlations for the evaluation of the specific heats, C_p and C_v , apply to thermally perfect gases whose thermodynamic properties are only a function of temperature. According to Daubert and Danner,¹⁴ the specific heat at constant pressure in units of J/kmol · K can be calculated from

$$C_p = A + B \left[\frac{C/T}{\sinh(C/T)} \right]^2 + D \left[\frac{E/T}{\cosh(E/T)} \right]^2 \quad (\text{A-58})$$

where the coefficients A through E have been fitted from available experimental data. Table A-8 lists the five coefficients for six common gases and the corresponding error for the specified temperature range. The references at the bottom of Table A-8 indicate the source of the raw data either used in regressing the data or found acceptable for analytical purposes but not suited for the determination of the correlation coefficients.

For both calorically perfect gases (gas with constant specific heats) and thermally perfect gases (gas obeying the equation $pV = nR_uT$), the following

Table A.8 Coefficients to Eq. (A-58) for Several Select Gases

Gas	T (K)	Error	A	B	C	D	E	Ref.
Air	50–1500	<5%	2.8958E+04	9.3900E+03	3.0120E+03	7.5800E+03	1.4840E+03	15, 16
N ₂	50–1500	<1%	2.9105E+04	8.6149E+03	1.7016E+03	1.0347E+02	9.0979E+02	17, 18, 19
O ₂	50–1500	<1%	2.9103E+04	1.0040E+04	2.5265E+03	9.3560E+03	1.1538E+03	17, 18, 19, 20
H ₂ ^a	250–1500	<1%	2.7617E+04	9.5600E+03	2.4660E+03	3.7600E+03	5.6760E+02	16, 21, 22
He ^b	100–1500	<1%	2.0786E+04					15, 16, 19
CH ₄	50–1500	<1%	3.3295E+04	8.0295E+04	2.1018E+03	4.2130E+04	9.9510E+02	17, 18, 22

^aCoefficients A through E are for the equilibrium mixture of ortho- and para-hydrogen. At 100 K the value of C_p is 2.8154E+04, and at 200 K the value is 2.7447E+04 J/kmol · K.

^b Helium is a monatomic gas with a constant isobaric specific heat equal to 2.0786E+04 J/kmol · K.

relationship is valid.

$$C_p - C_v = R \quad (\text{A-59})$$

Considering a quantum mechanical approach,²³ the specific heat at constant volume can also be computed from the summation of the specific heat contributions by translational, rotational, and vibrational energy states.

Since a monatomic gas possesses only translational energy at the temperature levels being considered, the constant-volume (isochoric) specific heat does not vary with temperature and is given by

$$C_v = \frac{3}{2}R \quad (\text{A-60})$$

For a diatomic gas, the C_v contribution due to rotational and vibrational energy must be considered:

$$C_v = R \left\{ \frac{5}{2} + \left[\frac{\Theta_v/2T}{\sinh(\Theta_v/2T)} \right]^2 \right\} \quad (\text{A-61})$$

where Θ_v is the characteristic temperature for vibration and is reported for most gases in the literature. The C_v contribution due to electronic energy has been neglected due to its negligible effect on the overall isochoric specific heat at the temperatures under consideration.

Evaluation of Ideal-Gas Heat Capacity at Constant Pressure, J/(mol · K)

The heat capacities of gases at low pressures (ideal gas) are available in the literature (Kobe et al.,²⁴ *TRC Thermodynamic Tables*,²⁰ *Technical Data Book*²⁵). Analytical equations, usually in the form of polynomial or other functional forms, are used in evaluating ideal-gas heat capacity. Some methods are introduced below.

Joback Method¹

$$\begin{aligned} C_p^o(T) &= \left(\sum_j n_j \Delta_a - 37.93 \right) + \left(\sum_j n_j \Delta_b + 0.210 \right) T \\ &\quad + \left(\sum_j n_j \Delta_c - 3.91 \times 10^{-4} \right) T^2 + \left(\sum_j n_j \Delta_d + 2.06 \times 10^{-7} \right) T^3 \end{aligned} \quad (\text{A-62})$$

where n_j is the number of groups of the j th type, and Δ contributions are for the j th atomic or molecular group. The values of these are shown in Table A-9. The temperature, T , is in K. The above equation can be used in the temperature range of 280 to 1100 K.

Table A.9 Joback Group Contributions for Ideal-Gas Properties (adapted from Reid et al.¹)

	Δ Values					
	Δ_H kJ/mol	Δ_G kJ/mol	Δ_a	Δ_b	Δ_c J/mol K	Δ_d
<i>Nonring Increments</i>						
-CH ₃	-76.45	-43.96	1.95E+1	-8.08E-3	1.53E-4	-9.67E-8
>CH ₂	-20.64	8.42	-9.09E-1	9.50E-2	-5.44E-5	1.19E-8
>CH-	29.89	58.36	-2.30E+1	2.04E-1	-2.65E-4	1.20E-7
>C<	82.23	116.02	-6.62E+1	4.27E-1	-6.41E-4	3.01E-7
=CH ₂	-9.63	3.77	2.36E+1	-3.81E-2	1.72E-4	-1.03E-7
=CH-	37.97	48.53	-8.00	1.05E-1	-9.63E-5	3.56E-8
=C <	83.99	92.36	-2.81E+1	2.08E-1	-3.06E-4	1.46E-7
=C =	142.14	136.70	2.74E+1	-5.57E-2	1.01E-4	-5.02E-8
≡CH	79.30	77.71	2.45E+1	-2.71E-2	1.11E-4	-6.78E-8
≡C-	115.51	109.82	7.87	2.01E-2	-8.33E-6	1.39E-9
<i>Ring Increments</i>						
-CH ₂ -	-26.80	-3.68	-6.03	8.54E-2	-8.00E-6	-1.80E-8
>CH-	8.67	40.99	-2.05E+1	1.62E-1	-1.60E-4	6.24E-8
>C<	79.72	87.88	-9.09E+1	5.57E-1	-9.00E-4	4.69E-7
=CH-	2.09	11.30	-2.14	5.74E-2	-1.64E-6	-1.59E-8
=C <	46.43	54.05	-8.25	1.01E-1	-1.42E-4	6.78E-8
<i>Halogen Increments</i>						
-F	-251.92	-247.19	2.65E+1	-9.13E-2	1.91E-4	-1.03E-7
-Cl	-71.55	-64.31	3.33E+1	-9.63E-2	1.87E-4	-9.96E-8
-Br	-29.48	-38.06	2.86E+1	-6.49E-2	1.36E-4	-7.45E-8
-I	21.06	5.74	3.21E+1	-6.41E-2	1.26E-4	-6.87E-8
<i>Oxygen Increments</i>						
-OH (alcohol)	-208.04	-189.20	2.57E+1	-6.91E-2	1.77E-4	-9.88E-8
-OH (phenol)	-221.65	-197.37	-2.81	1.11E-1	-1.16E-4	4.94E-8
-O-	-132.22	-105.00	2.55E+1	-6.32E-2	1.11E-4	-5.48E-8
(nonring)						
-O-(ring)	-138.16	-98.22	1.22E+1	-1.26E-2	6.03E-5	-3.86E-8
>C=O (nonring)	-133.22	-120.50	6.45	6.70E-2	-3.57E-5	2.86E-9
>C=O (ring)	-164.50	-126.27	3.04E+1	-8.29E-2	2.36E-4	-1.31E-7
O=CH-	-162.03	-143.48	3.09E+1	-3.36E-2	1.60E-4	-9.88E-8
(aldehyde)						
-COOH (acid)	-426.72	-387.87	2.41E+1	4.27E-2	8.04E-5	-6.87E-8
-COO-(ester)	-337.92	-301.95	2.45E+1	4.02E-2	4.02E-5	-4.52E-8
=O (except as above)	-247.61	-250.83	6.82	1.96E-2	1.27E-5	-1.78E-8

(continued overleaf)

Table A.9 (continued)

	Δ_H kJ/mol	Δ_G kJ/mol	Δ_a	Δ_b	Δ_c J/mol K	Δ_d
<i>Nitrogen Increments</i>						
-NH ₂	-22.02	14.07	2.69E+1	-4.12E-2	1.64E-4	-9.76E-8
>NH (nonring)	53.47	89.39	-1.21	7.62E-2	-4.86E-5	1.05E-8
>NH (ring)	31.65	75.61	1.18E+1	-2.30E-2	1.07E-4	-6.28E-8
>N-(nonring)	123.34	163.16	-3.11E+1	2.27E-1	-3.20E-4	1.46E-7
-N=(nonring)	23.61	—	—	—	—	—
-N=(ring)	55.52	79.93	8.83	-3.84E-3	4.35E-5	-2.60E-8
=NH	93.70	119.66	5.69	-4.12E-3	1.28E-4	-8.88E-8
-CN	88.43	89.22	3.65E+1	-7.33E-2	1.84E-4	-1.03E-7
-NO ₂	-66.57	-16.83	2.59E+1	-3.74E-3	1.29E-4	-8.88E-8
<i>Sulfur Increments</i>						
-SH	-17.33	-22.99	3.53E+1	-7.58E-2	1.85E-4	-1.03E-7
-S-(nonring)	41.87	33.12	1.96E+1	-5.61E-3	4.02E-5	-2.76E-8
-S-(ring)	39.10	27.76	1.67E+1	4.81E-3	2.77E-5	-2.11E-8

The first step in the procedure for finding C_p^o of a given compound is to determine the number and type of atomic or molecular groups forming the compound. Next, find the corresponding Δ -values (Δ_a , Δ_b , Δ_c , and Δ_d) of the particular groups. Then, use Eq. (A-62) to compute the ideal-gas heat capacity, C_p^o . The tabulated Δ -values of Δ_H and Δ_G can also be used to calculate the standard enthalpy of formation (ΔH_f^o) and the standard Gibbs energy of formation (ΔG_f^o) by the following two equations, recommended by Reid et al.¹

$$\Delta H_f^o(\text{kJ/mol}) = 68.29 + \sum_j n_j \Delta_H \quad (\text{A-63})$$

$$\Delta G_f^o(\text{kJ/mol}) = 53.88 + \sum_j n_j \Delta_G \quad (\text{A-64})$$

*Method of Thinh et al.*²⁶

$$C_p^o(T) = \sum_j n_j \left[A + B_1 \exp\left(\frac{-C_1}{T^{n_1}}\right) - B_2 \exp\left(\frac{-C_2}{T^{n_2}}\right) \right] \quad (\text{A-65})$$

where A , B_1 , C_1 , C_2 , n_1 , and n_2 are tabulated for many hydrocarbon groups in Reid et al.¹ This equation is applicable to the temperature range of 200 to 1500 K.

3.2 High-Pressure Correction

At higher pressures, the heat capacity of real gas deviates from the value calculated for ideal gas at the same conditions. This residual heat capacity is calculated by substituting the experimental pressure-volume-temperature data in the following relationship. The heat capacity of real gases is related to the value in the ideal-gas state, at the same temperature and composition:

$$C_p = C_p^o + \Delta C_p \quad (\text{A-66})$$

$$\Delta C_p = T \int_{\infty}^V \left(\frac{\partial^2 P}{\partial T^2} \right) dV - \frac{T(\partial P/\partial T)_v^2}{(\partial P/\partial V)_T} - R_u \quad (\text{A-67})$$

where ΔC_p is the residual heat capacity.

If P - V - T data are not available for a certain compound or the available data do not cover a given condition, it is imperative to use generalized equations of state to evaluate the residual heat capacity. Various methods to evaluate the residual heat capacity are reported, and a few representative methods are introduced below.

The analytical corrections developed by Lee and Kesler²⁷ are based on the law of corresponding states and cover a range of $T_r = 0.3$ to 4 and $P_r = 0$ to 10 for most gases, specifically hydrocarbons. It is useful to give a brief description of the law of corresponding states before we proceed further with Lee and Kesler's method.

Essentially, the law of corresponding states¹ was proposed by van der Waals in 1873. The law assumes that, in the generalized form, equilibrium properties that depend on intermolecular forces are related to the critical properties of the material in a universal way. Van der Waals showed theoretically that the P - V - T properties of all pure substances could be expressed by a two-constant equation of state such as Eq. (A-2). As shown by Pitzer in 1939, it is similarly valid if the intermolecular potential function requires only two characteristic parameters. As explained by Reid et al.,¹ "Corresponding states holds well for fluids containing simple molecules and upon semi-empirical extension; it also holds for many other substances where molecular orientation is not important, i.e., for molecules that are not strongly polar or hydrogen-bonded."

Physically, the acentric factor, T , represents the acentricity or nonsphericity of a molecule's force field. For monatomic gases, T is essentially zero. For simple gas, the value of T is usually very close to zero. The acentric factor can be regarded as the measure of complexity of molecules with respect to both the geometry and polarity; for higher-molecular-weight hydrocarbons, T is larger. T also rises with the polarity of the molecule. Mathematically, the acentric factor for pure substance can be calculated from

$$\omega = -\log_{10} P_{\text{vpr}} \Big|_{T_r=0.7} - 1.000 \quad (\text{A-68})$$

where P_{vpr} is the reduced vapor pressure at $T_r = 0.7$. To evaluate vapor pressure P_{vp} for a pure substance, one can use the following simple correlation, which is

derived from the Clausius–Clapeyron equation, described in Chapter 1:

$$\log_{10} P_{vp} = A + \frac{B}{T} \quad (\text{A-69})$$

where A and B can be determined from two sets of values [e.g., (T_c, P_c) and $(T_b, P = 1 \text{ atm})$].

The acentric factor can also be calculated from Eq. (A-70), in which the critical pressure, P_c , is expressed in atmospheres, T_b = normal boiling point in Kelvin (at 1 atm), and T_c = critical temperature.

$$\omega = \frac{3}{7} \frac{\theta}{1 - \theta} \log_{10} P_c - 1, \quad \text{where } \theta \equiv T_b/T_c \quad (\text{A-70})$$

The Pitzer equation for the reduced vapor pressure is

$$\ln P_{vpr} = f^{(0)}(T_r) + \omega f^{(1)}(T_r) \quad (\text{A-71})$$

where the functions $f^{(0)}$ and $f^{(1)}$ can be expressed in the analytical form of Lee and Kesler²⁷:

$$\begin{aligned} f^{(0)} &= 5.92714 - \frac{6.09648}{T_r} - 1.28862 \ln T_r + 0.169347 T_r^6 \\ f^{(1)} &= 15.2518 - \frac{15.6875}{T_r} - 13.4721 \ln T_r + 0.43577 T_r^6 \end{aligned} \quad (\text{A-72})$$

The Pitzer acentric factor, T , can be calculated from

$$\omega = \frac{\alpha}{\beta}$$

where

$$\begin{aligned} \alpha &= -\ln P_c - 5.97214 + 6.09648\theta^{-1} + 1.28862\theta - 0.169347\theta^6 \\ \beta &= 15.2518 - 15.6875\theta^{-1} - 13.4721 \ln \theta + 0.43577\theta^6 \end{aligned} \quad (\text{A-73})$$

In two-parameter correlations, the compressibility factor is often expressed as a function of T_r and P_r , i.e., $Z = f(T_r, P_r)$. To obtain a more accurate description of the real-gas effect, three-parameter correlations, using the Pitzer acentric factor,^{28–30} T , in the following linear expression has been adopted.

$$Z = Z^{(0)}(T_r, P_r) + \omega Z^{(1)}(T_r, P_r) \quad (\text{A-74})$$

where the $Z^{(0)}$ function is applicable to spherical molecules and $Z^{(1)}$ represents the deviation function. This linear equation in T is usually adequate for representing Z . At the critical point, the following relationship was used for various

substances: $Z_c = 0.291 - 0.080\omega$. As discussed in Section 1.2 of this appendix, T has been used in various forms of the equation of state. Values of T for various substances can be found in Ref. 1.

From a slightly different point of view, the three-parameter correlation as originally developed for the compressibility factor, Z , takes the form

$$Z = Z^{(o)} + \frac{\omega}{\omega^{(r)}}(Z^{(r)} - Z^{(o)}) \quad (\text{A-75})$$

where ω is the acentric factor and the superscripts (o) and (r) denote the values for a simple fluid and a reference fluid, respectively. This approach is employed to analytically represent other derived thermodynamic functions, such as the departures of isobaric and isochoric specific heats from the ideal gas state. Specifically,

$$\frac{C_p - C_p^o}{R} = \left(\frac{C_p - C_p^o}{R} \right)^{(o)} + \left(\frac{\omega}{\omega^{(r)}} \right) \left[\left(\frac{C_p - C_p^o}{R} \right)^{(r)} - \left(\frac{C_p - C_p^o}{R} \right)^{(o)} \right] \quad (\text{A-76})$$

and

$$\frac{C_v - C_v^o}{R} = \left(\frac{C_v - C_v^o}{R} \right)^{(o)} + \left(\frac{\omega}{\omega^{(r)}} \right) \left[\left(\frac{C_v - C_v^o}{R} \right)^{(r)} - \left(\frac{C_v - C_v^o}{R} \right)^{(o)} \right] \quad (\text{A-77})$$

The relations for the two specific heat departures were derived from the following form of a modified BWR (Benedict, Webb, and Rubin)³¹ equation of state:

$$\begin{aligned} Z^{(o)} &= \left(\frac{P_r V_r^{(o)}}{T_r} \right) = 1 + \frac{B}{V_r^{(o)}} + \frac{C}{(V_r^{(o)})^2} + \frac{D}{(V_r^{(o)})^5} \\ &\quad + \frac{c_4}{T_r^3 (V_r^{(o)})^2} \left[\beta + \frac{\gamma}{(V_r^{(o)})^2} \right] \exp \left[-\frac{\gamma}{(V_r^{(o)})^2} \right] \\ Z^{(r)} &= \left(\frac{P_r V_r^{(r)}}{T_r} \right) = 1 + \frac{B}{V_r^{(r)}} + \frac{C}{(V_r^{(r)})^2} + \frac{D}{(V_r^{(r)})^5} \\ &\quad + \frac{c_4}{T_r^3 (V_r^{(r)})^2} \left[\beta + \frac{\gamma}{(V_r^{(r)})^2} \right] \exp \left[-\frac{\gamma}{(V_r^{(r)})^2} \right] \end{aligned} \quad (\text{A-78})$$

where

$$B = b_1 - \frac{b_2}{T_r} - \frac{b_3}{T_r^2} - \frac{b_4}{T_r^3}, \quad C = c_1 - \frac{c_2}{T_r} + \frac{c_3}{T_r^3}, \quad \text{and} \quad D = d_1 + \frac{d_2}{T_r} \quad (\text{A-79})$$

Experimental data for Ar, Kr, and CH₄ were used to determine the coefficients for the lighter simple fluid. *n*-Octane was selected for the reference fluid since it is the heaviest hydrocarbon for which accurate *P-V-T* data were available over a wide range of conditions. This relation is based on the Pitzer approach¹ to three-parameter corresponding states theory, which assumes that the compressibility

**Table A.10 Coefficients for Eqs. (A-78) and (A-79) (see
Technical Data Book – Petroleum Refining, Vols. I and II,
1977)**

Coefficient	Simple Fluid	Ref. Fluid
b_1	0.1181193	0.2026579
b_2	0.265728	0.331511
b_3	0.15479	0.027655
b_4	0.3030323	0.203488
c_1	0.0236744	0.0313385
c_2	0.0186984	0.0503618
c_3	0	0.016901
c_4	0.042724	0.041577
$d_1 \times 10^4$	0.155488	0.48736
$d_2 \times 10^4$	0.623689	0.0740336
β	0.65392	1.226
γ	0.060167	0.03754

factor Z depends linearly on the Pitzer acentric factor ω . Therefore, there is nothing special about these two reference fluids, and, in fact, any two fluids could be used as reference fluids. The coefficients used are listed in Table A-10.

The relation for the specific heat departures are written as

$$\frac{C_v - C_v^o}{R} = \frac{2(b_3 + 3b_4/T_r)}{T_r^2 V_r} - \frac{3c_3}{T_r^3 V_r^2} - 6E \quad (\text{A-80})$$

and

$$\frac{C_p - C_p^o}{R} = \frac{C_v - C_v^o}{R} + 1 + T_r \frac{(\partial P_r / \partial T_r)_{V_r}^2}{(\partial P_r / \partial V_r)_{T_r}^2} \quad (\text{A-81})$$

where

$$\begin{aligned}
 E &= \frac{c_4}{2T_r^3 \gamma} \left[\beta + 1 - \left(\beta + 1 + \frac{\gamma}{V_r^2} \right) \exp \left(-\frac{\gamma}{V_r^2} \right) \right] \\
 \left(\frac{\partial P_r}{\partial T_r} \right)_{V_r} &= \frac{1}{V_r} \left\{ 1 + \frac{b_1 + b_3/T_r^2 + 2b_4/T_r^3}{V_r} + \frac{c_1 - 2c_3/T_r^3}{V_r^2} + \frac{d_1}{V_r^5} \right. \\
 &\quad \left. - \frac{2c_4}{T_r^3 V_r^2} \left[\left(\beta + \frac{\gamma}{V_r^2} \right) \exp \left(-\frac{\gamma}{V_r^2} \right) \right] \right\} \\
 \left(\frac{\partial P_r}{\partial V_r} \right)_{T_r} &= -\frac{T_r}{V_r^2} \left\{ 1 + \frac{2B}{V_r} + \frac{3C}{V_r^2} + \frac{6D}{V_r^5} \right. \\
 &\quad \left. + \frac{c_4}{T_r^3 V_r^2} \left[3\beta + \left\{ 5 - 2 \left(\beta + \frac{\gamma}{V_r^2} \right) \right\} \frac{\gamma}{V_r^2} \right] \exp \left(-\frac{\gamma}{V_r^2} \right) \right\} \quad (\text{A-82})
 \end{aligned}$$

To calculate the specific heat departures for a given T and P of the fluid of interest, the following procedure should be followed.

1. Determine V_r from the BWR equation of state [Eq. (A-78)] for the simple fluid at T_r and P_r . Use the simple fluid coefficients in Table A-10.
2. Calculate the specific heat departure value for the simple fluid from Eq. (A-80) or (A-81).
3. Repeat step 1 for the same T_r and P_r , but with the reference fluid coefficients of Table A-10.
4. Calculate a specific heat departure value for the reference fluid using Eq. (A-80) or (A-81).
5. Determine the specific heat departure value for the fluid of interest using the three-parameter equation [Eq. (A-76) or (A-77)].

The Pitzer acentric factor of the reference fluid is $\omega(r) = 0.3978$ (for *n*-octane), while the acentric factor of the fluid of interest is calculated from Eq. (A-73), using the normal boiling point and critical properties of the specified fluid.

Comparing the CH_4 data of Jones et al.³² and Yesavage et al.³³ with the computed departure values, an average deviation of 2% was found. In addition, it was observed that the technique was not very accurate near the critical region, where the heat capacity changes rapidly with temperature and pressure.

Reid et al.¹ have recommended a method for adopting P - V - T relations for specific cases. That involves the following steps:

- (a) To characterize small deviations from ideal-gas behavior, use the truncated virial equations.

$$Z = 1 + \frac{BP}{R_u T}$$

where B is the first virial coefficient of Eq. (A-7).

- (b) For nonpolar molecules near saturated conditions, use the Soave or Peng–Robinson equation of state discussed in Section 1.2.
- (c) For expanded ranges of temperature and pressure, use the Lee–Kesler method of Starling's generalized BWR equation of state.¹
- (d) For polar molecules, use the Gmehling equation¹ if the parameters are available.

An alternative method for the calculation of the isobaric specific heat is provided by Sychev et al.³⁴ Their approach was based on an average equation of state using the most reliable experimental data for P , V , and T of the specified gas.

$$Z = 1 + \sum_{i=1}^r \sum_{j=0}^{S_i} b_{ij} \left(\frac{\alpha^i}{\tau^j} \right) \quad (\text{A-83})$$

where $\alpha = \rho/\rho_c$ and $\tau = T/T_c$. The two-dimensional array of b_{ij} coefficients was obtained from a large number of states for a specified gas. The parameter r is the highest index of i , and S_i is the highest index of j for the i th array of b_{ij} . The value of the averaged isobaric specific heat equation is calculated from

$$C_p = C_v^o - R \sum_{i=1}^r \sum_{j=0}^{S_i} \frac{j(j-1)}{i} b_{ij} \left(\frac{\alpha^i}{\tau^j} \right) + \frac{R \left[1 - \sum_{i=1}^r \sum_{j=0}^{S_i} \frac{j-1}{i} b_{ij} \left(\frac{\alpha^i}{\tau^j} \right) \right]^2}{1 + \sum_{i=1}^r \sum_{j=0}^{S_i} \frac{(j+1)}{i} b_{ij} \left(\frac{\alpha^i}{\tau^j} \right)} \quad (\text{A-84})$$

References 34–36 list the coefficients b_{ij} for air, nitrogen, oxygen, and methane. Although the overall accuracy of the correlation is very good, the approach is limited to specific gases and is quite tedious to implement on a computer due to the large number of required coefficients.

3.3 Mixing Rules

For the ideal-gas case, the isobaric and isochoric specific heats for a mixture may be obtained from the mass fraction-weighted method given as

$$C_p = \sum_i Y_i C_{pi} \quad (\text{A-85})$$

where the subscript i represents the i th component and Y_i can be calculated from

$$Y_i = \frac{\rho_i}{\rho} = \frac{X_i M_w i}{\sum_i X_i M_w i} \quad (\text{A-86})$$

Under high pressures, Lee and Kesler²⁷ suggest the following relations to determine P_c , T_c , and V_c of the mixture. Some modification was suggested by Plocke et al.,³⁷ which includes the binary interaction coefficient k'_{jk} , tabulated in Ref. 27.

$$\bar{v}_{ci} = \frac{Z_{ci} R_u T_{ci}}{P_{ci}} \quad (\text{A-87})$$

$$Z_{ci} = 0.2905 - 0.085\omega_i \quad (\text{A-88})$$

$$\bar{v}_{c,m} = \frac{1}{8} \sum_j \sum_k X_j X_k (\bar{v}_{cj}^{1/3} + \bar{v}_{ck}^{1/3})^3 \quad (\text{A-89})$$

$$T_{c,m} = \frac{1}{\bar{v}_{c,m}^{1/4}} \sum_j \sum_k X_j X_k \bar{v}_{cjk}^{1/4} T_{cjk} \quad (\text{A-90})$$

$$\bar{v}_{cjk} = \frac{1}{8}(\bar{v}_{cj}^{1/3} + \bar{v}_{ck}^{1/3})^3 \quad (\text{A-91})$$

$$T_{cjk} = \sqrt{T_{cj} T_{ck}} k'_{jk} \quad (\text{A-92})$$

where k'_{jk} are the binary interaction coefficients and

$$P_{c,m} = \frac{Z_m R_u T_{c,m}}{\bar{v}_{c,m}} = (0.2905 - 0.085\omega_m) \frac{R_u T_{c,m}}{\bar{v}_{c,m}} \quad (\text{A-93})$$

The mixture's acentric factor is based on mole fraction-weighted averaging:

$$\omega_m = \sum_j X_j \omega_j \quad (\text{A-94})$$

where X_j is the mole fraction of the j th component. With the mixture values of P_c and T_c , the reduced pressure and temperature can be calculated and employed in the three-parameter correlating states technique to solve the mixture's specific-heat departures.

4 LIQUID SPECIFIC HEAT

4.1 Baseline Method

Estimation methods applicable for liquid specific heat fall into two general categories: group contribution and corresponding states. They are described below.

Group Contribution Method The assumption is made that each chemical group in a molecule contributes a definite value to the total specific heat, and the sum of contributions from all independent groups gives the total specific heat of the molecule of interest. Both the Chueh-Swanson method³⁸ and the Missenard method³⁹ can be used to estimate the value of C_p . Tables A-11 and A-12 present the group contributions for these two methods.

Example. Estimate the liquid heat capacity of 1,4-pentadiene (C_5H_8) at 293 K by using the Chueh-Swanson group contribution method.

Solution: From Table A-11

$$\begin{aligned} C_{pL}(293 \text{ K}) &= 2(\text{CH}_2=) + 2(-\text{CH}=) + (-\text{CH}_2-) \\ &\quad + \text{corrections noted in Table A-11} \\ &= (2)(21.8) + (2)(21.3) + 30.4 + 10.5 + 18.8 \\ &= 146 \text{ J/(mol} \cdot \text{K)} \end{aligned}$$

Experimental values reported by Tamplin and Zuzic⁴⁰ indicate that $C_{pL} = 147 \text{ J/(mol} \cdot \text{K)}$ at 293 K.

Table A.11 Chueh-Swanson's Group Contributions³⁸ for Molar Heat Capacity of Liquid at 293 K

Group	Value [†]	Group	Value [†]
<i>Alkane</i>		<i>Oxygen</i>	
—CH ₃	36.8	—O—	35
—CH ₂ —	30.4	>C=O	53.0
		H	
—CH—	21.0		
		C=O	53.0
—C—	7.36	O	
		—C—OH	79.9
		O	
		—C—O—	60.7
		—CH ₂ OH	73.2
<i>Olefin</i>			
=CH ₂	21.8		
=C—H	21.3		
=C—	15.9		
<i>Alkyne</i>			
—C≡H	24.7		
—C≡	24.7		
<i>In a Ring</i>			
—CH—	18		
—C= or —C—	12		
—CH=	22	<i>Hydrogen</i>	
—CH ₂ —	26	H—(for formic acid, formates, hydrogen cyanide, etc.)	15.0
<i>Nitrogen</i>			
H		<i>Sulfur</i>	
		—SH	44.8
H—N—	58.6	—S—	33.0
H		<i>Halogen</i>	
		—Cl (first or second on a carbon)	36.0
—N—	43.9	—Cl (third or fourth on a carbon)	25.0
		—Br	38.0
N—	31	—F	17.0
		—I	36.0
N=(in a ring)	19		
C≡N	58.2		

Note: [†]Add 18.8 for any carbon group which fulfills the following criterion: a carbon group which is joined by a single bond to a carbon group connected by a double or triple bond with a third carbon group. In some cases a carbon group fulfills the above criterion in more than one way. In these cases 18.8 should be added each time the group fulfills the criterion. The following are exceptions to the 18.8 addition rule:

1. No 18.8 additions for —CH₃ groups.
2. For a —CH₂—group fulfilling the 18.8 addition criterion, add 10.5 instead of 18.8. However, when the —CH₂—group fulfills the addition criterion in more than one way, the addition should be 10.5 the first time and 18.8 for each subsequent addition.
3. No 18.8 addition for any carbon group in a ring.

Table A.12 Misenard's Group Contributions³⁹ for Molar Heat Capacity of Liquid

Group	Temperature, K					
	248	273	298	323	348	373
-H	12.5	13.4	14.6	15.5	16.7	18.8
-CH ₃	38.5	40.0	41.6	43.5	45.8	48.3
-CH ₂	27.2	27.6	28.2	29.1	29.9	31.0
-CH-	20.9	23.8	24.9	25.7	26.6	28.0
-C—	8.4	8.4	8.4	8.4	8.4	
-C≡C-	46.0	46.0	46.0	46.0		
-O-	28.9	29.3	29.7	30.1	30.5	31.0
-CO-(ketone)	41.8	42.7	43.5	44.4	45.2	46.0
-OH	27.2	33.5	43.9	52.3	61.7	71.1
-COO-(ester)	56.5	57.7	59.0	61.1	63.2	64.9
-COOH	71.1	74.1	78.7	83.7	90.0	94.1
-NH ₂	58.6	58.6	62.8	66.9		
-NH-	51.0	51.0	51.0			
-N—	8.4	8.4	8.4			
-CN	56.1	56.5	56.9			
-NO ₂	64.4	64.9	65.7	66.9	68.2	
-NH-NH-	79.5	79.5	79.5			
C ₆ H ₅ -(phenyl)	108.8	113.0	117.2	123.4	129.7	136.0
C ₁₀ H ₇ -(naphthyl)	179.9	184.1	188.3	196.6	205.0	213.0
-F	24.3	24.3	25.1	25.9	27.0	28.2
-Cl	28.9	29.3	29.7	30.1	30.8	31.4
-Br	35.1	35.6	36.0	36.4	37.2	38.1
-I	39.3	39.7	40.4	41.0		
-S-	37.2	37.7	38.5	39.3		

Example. Estimate the liquid heat capacity of propane at 298 K using the Misénard group contribution method.

Solution: From Table A-12

$$\begin{aligned} C_{pL}(20^\circ\text{C}) &= 2(\text{CH}_3-) + (-\text{CH}_2-) \\ &= (2)(41.6) + 28.2 = 111.4 \text{ J/(mol} \cdot \text{K)} \end{aligned}$$

The reported experimental value of C_p of propane in the literature of liquid propellants is 111 J/(mol · K).

Corresponding States Method This method uses an analytical form of specific heat departure function for calculating liquid specific heat. The specific heat can be estimated by the analytical form of the Lee–Kesler heat capacity departure function ($C_{pL} - C_p^o$). Rowlinson's⁴¹ modified version of Bondi's⁴² liquid hydrocarbon equation has the following form:

$$\frac{C_{pL} - C_p^o}{R_u} = 1.45 + 0.45(1 - T_r)^{-1} + 0.25\omega[17.11 + 25.2(1 - T_r)^{1/3}T_r^{-1} + 1.742(1 - T_r)^{-1}] \quad (\text{A-95})$$

where ω is the Pitzer's acentric factor, and C_p^o is the low-pressure specific heat of ideal gas at constant pressure.

4.2 High-Pressure Correction

Sychev et al.^{34–36} have used the following equation to calculate the specific heat at constant pressure for temperatures of 70 to 1000 K and pressures of 0.1 to 100 MPa.

$$C_p = C_v^o - R \sum_{i=1}^r \sum_{j=0}^{s_i} \frac{j(j-1)}{i} \frac{b_{ij}\alpha^i}{\tau^j} + \frac{R \left[1 - \sum_{i=1}^r \sum_{j=0}^{s_i} (j-1)b_{ij}\alpha^i / \tau^j \right]^2}{1 + \sum_{i=1}^r \sum_{j=0}^{s_i} (i+1)b_{ij}\alpha^i / \tau^j} \quad (\text{A-96})$$

where $\alpha = \rho/\rho_c$ and $\tau = T/T_c$. The values of specific heat for some substances, such as oxygen and nitrogen, are tabulated in Refs. 34–36. The coefficients b_{ij} for liquid oxygen in the above equation are also shown in the same references.

4.3 Mixing Rule for Liquid Mixtures

For liquid mixtures, the specific heat is obtained by the mass fraction–weighted averaging method for all components included in the liquid. Therefore, Equation (A-85) is used in the computation.

5 GAS VISCOSITY

Dynamic viscosity of a fluid is the resistance coefficient between the shear stress and the rate of strain. The resistance is due to cohesion of the molecules and

molecular transfer from one layer to another, setting up a shear stress. In gases, cohesion is weak, but molecular transfer between molecules is significant.¹ Since molecular transfer in gases increases with temperature, gas viscosity increases with temperature. In general, liquid viscosity decreases as temperature increases due to weakened cohesion of the molecules.

5.1 Baseline Method

Dynamic viscosity μ is defined as the ratio of shear stress to the rate of strain with dimensions $N \cdot s/m^2$, $kg/(m \cdot s)$, or centipoise ($\equiv 0.001 N \cdot s/m^2$). Kinematic viscosity ν is defined as the ratio of the dynamic viscosity to the density, i.e., $\nu \equiv \mu/\rho$ with dimensions m^2/s .

A gas can be modeled in a simple manner using kinetic theory. The kinetic model makes use of the following assumptions: (a) all molecules are noninteracting, rigid spheres of diameter σ , (b) each molecule has a mass of m , (c) molecules move randomly with mean velocity v , and (d) the number density of the gas is n molecules per unit volume.

The rate of momentum transfer per unit cross-sectional flow area is proportional to the velocity gradient in the transverse direction. The proportionality constant μ can be expressed as

$$\mu = \frac{vL}{3}mn \quad (A-97)$$

where L is the mean free path; L is proportional to $(n\sigma^2)^{-1}$. The random velocity v is proportional to $(R_u T/M_w)^{1/2}$, where R_u is the universal gas constant, and M_w is the molecular weight of the gas. After substituting these basic kinetic theory relationships, the dynamic viscosity can be expressed as

$$\mu = 26.69 \frac{(M_w T)^{1/2}}{\sigma^2} \quad (A-98)$$

In the above equation, μ is given in μP (micropoise), M_w in g/mol, T in K, and σ , the hard sphere diameter, in Å (ångström $\equiv 10^{-10}$ m).

The rigid, noninteracting sphere model is the simplest gas viscosity model. It shows the general relationship between viscosity, temperature, and molecule size. Typically, correction factors are required to determine the actual viscosity. There are generally two approaches for calculating viscosity: the Chapman–Enskog approach and the method of corresponding states.

Chapman–Enskog Approach The Chapman–Enskog approach^{43,44} uses the collision diameter σ and the collision integral Ω_v , which is a function of dimensionless temperature T^* , where k is the Boltzmann's constant and ε is the characteristic energy.

$$\Omega_v = \Omega_v(T^*) \quad \text{and} \quad T^* \equiv \frac{kT}{\varepsilon} \quad (A-99)$$

The interactions between colliding molecules are described by the intermolecular potential function $\psi(r)$ for gas molecules separated by a distance of r . For example, the Lennard-Jones 12–6 potential is

$$\psi(r) = 4\epsilon \left[\left(\frac{\sigma}{r}\right)^{12} - \left(\frac{\sigma}{r}\right)^6 \right] \quad (\text{A-100})$$

There are many other forms of $\psi(r)$ one can utilize to determine the collision integral Ω_v . In general, Ω_v is not very sensitive to the form of $\psi(r)$. Many scientists¹ have used Eq. (A-100) to obtain Ω_v . Neufeld et al.⁴⁵ suggested the following empirical equation for Ω_v :

$$\Omega_v = [A(T^*)^{-B}] + C[\exp(-DT^*)] + E[\exp(-FT^*)] \quad (\text{A-101})$$

where $A = 1.16145$, $B = 0.14874$, $C = 0.52487$, $D = 0.77320$, $E = 2.16178$, and $F = 2.43787$. It is interesting to note that, for some gases, there are multiple sets of ϵ/k and σ giving the same calculated viscosity.¹ Chung et al.⁴⁶ suggested the use of

$$\frac{\epsilon}{k} = \frac{T_c}{1.2593} \quad \text{and} \quad \sigma = 0.809 V_c^{1/3} \quad (\text{A-102})$$

where T_c is the critical temperature, in K , and V_c is the critical volume, in cm^3/mol .

Reichenberg⁴⁷ found Ω_v to be a power law of T^* , i.e.,

$$\Omega_v = a(T^*)^n \quad (\text{A-103})$$

With the consideration of the interactions between the molecules, Eq. (A-98) is modified as

$$\mu = 26.69 \frac{(\text{Mw}T)^{1/2}}{\sigma^2 \Omega_v} \quad (\text{A-104})$$

Using either Eq. (A-102) or (A-103), the gas viscosity can be calculated from Eq. (A-104). Note that the collision integral Ω_v is equal to 1 if the molecules do not attract each other. To account for molecular shapes and polarities, Chung et al.⁴⁶ suggested the following equation for viscosity calculations:

$$\mu = 40.785 \frac{F_c(\text{Mw}T)^{1/2}}{V_c^{2/3} \Omega_v} \quad (\text{A-105})$$

where the factor F_c is related to ω , the acentric factor, κ , a special correction factor for highly polar substances, and η_r , the dimensionless dipole moment, according to

$$F_c = 1 - 0.2756\omega + 0.059035\eta_r^4 + \kappa \quad (\text{A-106})$$

where the κ values for many hydrocarbons, acids, and water are given in Reid et al.¹

Method of Corresponding States Since gases do not exhibit ideal-gas behavior at high temperature and pressure, deviations from ideal-gas behavior must be considered. The compressibility factor Z can be used with reasonable accuracy to allow the simple modification of the ideal-gas law. Therefore the equation of state¹ becomes

$$Pv = ZRT \quad (\text{A-107})$$

The principle of corresponding states asserts that the Z factor is approximately the same for all gases when the gases have the same reduced pressure and temperature.

Lucas⁴⁸ defines a dimensionless viscosity:

$$\mu_r = \zeta \mu = f(T_r) \quad (\text{A-108})$$

where

$$\zeta = \left[\frac{(R_u T_c)(N_A)^2}{\text{Mw}^3 P_c^4} \right]^{1/6} \quad (\text{A-109})$$

The ζ parameter represents inverse viscosity and therefore has units of $\text{m}^2/(\text{N} \cdot \text{s})$. ζ can be written in a simpler form as

$$\zeta = 0.176 \left[\frac{T_c}{\text{Mw}^3 P_c^4} \right]^{1/6} \quad (\text{A-110})$$

where ζ is in $(\mu\text{Poise})^{-1}$, Mw in g/mol, P_c in bars, and T_c in K. The final form suggested by Lucas is

$$\begin{aligned} \mu\zeta &= [0.807 T_r^{0.618} - 0.357 \exp(-0.449 T_r) + 0.340 \exp(-4.058 T_r) \\ &\quad + 0.018] F_p F_Q \end{aligned} \quad (\text{A-111})$$

where F_p and F_Q are correction factors that account for polarity and quantum effects; therefore, a reduced dipole moment is required. The reduced dipole moment is defined as

$$\eta_r \equiv \frac{52.46 \eta^2 P_c}{T_c} \quad (\text{A-112})$$

where the dipole moment η is in debyes, P_c in bars, and T_c in K. Depending on the value of η_r , F_p can be calculated from

$$\left. \begin{array}{ll} F_p = 1 & 0 < \eta_r \leq 0.022 \\ F_p = 1 + 30.55(0.292 - Z_c)^{1.72} & 0.022 < \eta_r < 0.075 \\ F_p = 1 + 30.55(0.292 - Z_c)^{1.72} \times & 0.075 \leq \eta_r \\ |0.96 + 0.1(T_r - 0.7)| & \end{array} \right\} \quad (\text{A-113})$$

Z_c is the compressibility factor based on critical pressure, temperature, and volume. The quantum correction factor F_Q is used only for quantum gases such as

He, H₂, and D₂. F_Q equals 1 for nonquantum gases. For quantum gases,

$$F_Q = 1.22Q^{0.15}\{1 + 0.00385[(T_r - 12)^2]^{1/M} \cdot \text{sign}(T_r - 12)\} \quad (\text{A-114})$$

$Q = 1.38$ for He, $Q = 0.76$ for H₂, and $Q = 0.52$ for D₂. Note that the sign term indicates that the second term in the braces should be positive if $(T_r - 12) > 0$ and negative if $(T_r - 12) < 0$.

Yoon and Thodos⁴⁹ proposed the following relationship for $T_r \leq 1$:

$$\mu\zeta = (0.606T_r)F_P F_Q \quad (\text{A-115})$$

Based on the comparison between experimental and theoretical values of viscosity,¹ Lucas's method for low-pressure gas viscosity estimation has an average error within 3% accuracy. The calculations of Chung et al.⁴⁶ and Reichenberg⁴⁷ have averages less than 2%; these errors are very low, indicating good accuracy of their predictions.

5.2 High-Pressure Correction

Reichenberg Method The viscosity of a gas can vary significantly with respect to pressure near the critical point and at high pressures with reduced temperatures at about 1 to 2. At high pressures, there is a wide range of temperatures where the viscosity decreases with temperature and the gas exhibits behavior similar to a liquid. At very high reduced temperatures, pressure has little effect on viscosity, but viscosity increases with temperature. In the initiatory study of Enskog,⁴³ the gas viscosity at high pressures normalized by the low-pressure viscosity (μ/μ^o) was expressed as a function of compressibility factor, molar density, and covolume. Following Enskog, many researchers expressed the dense-gas viscosity in terms of μ/μ^o as a function of T_r , P_r , and other reduced volumetric properties. Reichenberg⁴⁷ suggested the following equation:

$$\frac{\mu}{\mu^o} = 1 + Q \frac{A(P_r)^{1.5}}{BP_r + (1 + CP_r^D)^{-1}} \quad (\text{A-116})$$

where the parameters A , B , C , and D are functions of the reduced temperature T_r :

$$A = 0.0019824 \frac{\exp(5.2683T_r^{-0.5767})}{T_r}$$

$$B = A(1.6552T_r - 1.2760)$$

$$C = 0.1319824 \frac{\exp(3.7035T_r^{-79.8678})}{T_r}$$

$$D = 2.9496 \frac{\exp(2.9190T_r^{-16.6169})}{T_r}$$

The parameter Q is equal to

$$Q = 1 - 5.655\eta_r$$

where η_r is given by Eq. (A-112). For nonpolar materials, $Q = 1.0$. Errors are usually a few percent.

Lucas Method Lucas⁴⁸ suggested the following procedure, which accounts for high-pressure correction. For a reduced temperature of interest, the Z_1 parameter can be calculated from

$$Z_1 = [0.807T_r^{0.618} - 0.357 \exp(-0.449T_r) + 0.340 \exp(-4.058T_r) + 0.0181]F_P F_Q \quad (\text{A-117})$$

If $T_r \leq 1.0$ and $P_r < (P_{vp}/P_c)$ where P_{vp} is the vapor pressure, the Z_2 parameter can be determined from

$$Z_2 = 0.600 + 0.760P_r^\alpha + (6.990P_r^\beta - 0.6)(1 - T_r) \quad (\text{A-118})$$

where

$$\alpha = 3.262 + 14.98P_r^{5.508} \quad \text{and} \quad \beta = 1.390 + 5.746P_r$$

If ($1 < T_r < 40$) and ($0 < P_r \leq 100$), then

$$Z_2 = \mu^o \zeta \left[1 + \frac{aP_r^e}{bP_r^f + (1 + cP_r^d)^{-1}} \right] \quad (\text{A-119})$$

where $\mu^o \zeta$ is found from Eq. (A-117) for Z_1 , since the right-hand side of Eq. (A-111) is the same as that of Eq. (A-117). The values for the parameters a , b , c , and d are different from those of Reichenberg.⁴⁷ They are given below:

$$\begin{aligned} a &= 1.245 \times 10^{-3} \frac{\exp(5.1726T_r^{-0.3286})}{T_r} \\ b &= a(1.6553T_r - 1.2723) \\ c &= 0.4489 \frac{\exp(3.0578T_r^{-37.7332})}{T_r} \\ d &= 1.7368 \frac{\exp(2.2310T_r^{-7.6351})}{T_r} \\ e &= 1.3088 \quad \text{and} \quad f = 0.9425 \exp(-0.1853T_r^{0.4489}) \end{aligned}$$

After computing Z_1 and Z_2 , the parameter Y and the correction factors F_P and F_Q can be calculated from

$$Y = \frac{Z_2}{Z_1} \quad (\text{A-120})$$

$$F_P = \frac{1 + (F_P^o - 1)Y^{-3}}{F_P^o} \quad (\text{A-121})$$

$$F_Q = \frac{1 + (F_Q - 1)[Y^{-1} - (0.007)(\ln Y)^4]}{F_Q^o} \quad (\text{A-122})$$

where F_P^o and F_Q^o are the low-pressure polarity and quantum viscosity correction factors. Finally, the dense-gas viscosity can be calculated from

$$\mu = \frac{Z_2 F_P F_Q}{\zeta} \quad (\text{A-123})$$

where ζ can be calculated as in the low-pressure case using Eq. (A-110). Also note that, at low pressures, Y is essentially 1, and therefore, $F_P = 1$, $F_Q = 1$, and $Z_2 = \mu^o \zeta$; therefore, $\mu^o \rightarrow \mu$ as is expected. In most cases, the error of the Lucas method is reported¹ to be less than 5%. The comparison between experimental and calculated dense gas viscosity using various methods can be found in the book by Reid et al.¹ for various gases. In general, very good agreement between the experimental and calculated values has been achieved using the methods described above.

5.3 Mixing Rules

Mixing rules for evaluating the viscosity of gaseous mixtures were studied by Herning and Zipperer,⁵⁰ Wilke,⁵¹ Reichenberg,⁵² and Lucas.⁵³ The corresponding states method of Lucas⁵³ is described below.

The critical temperature of the mixture is calculated from Eq. (A-41), using the mole fractions X_i and $T_{c,i}$ of all species in the mixture. The critical pressure of the mixture is determined from the following equation:

$$P_{cm} = \frac{R_u T_{cm} \sum X_i Z_{ci}}{\sum_i X_i V_{ci}} \quad (\text{A-124})$$

The molecular weight of the mixture is calculated from

$$\text{Mw}_m = \sum X_i \text{Mw}_i \quad (\text{A-125})$$

The polarity correction factor and quantum correction factor for the mixture are calculated from

$$F_{Pm} = \sum_i X_i F_{Pi} \quad (\text{A-126})$$

$$F_{Qm} = A \sum_i X_i F_{Qi} \quad (\text{A-127})$$

The value of the parameter A is determined from the molecular-weight ratio of the species with highest molecular weight (Mw_H) to the species with the lowest molecular weight (Mw_L), according to

$$A = 1 - 0.01 \left(\frac{Mw_H}{Mw_L} \right)^{0.87} \quad \text{for } \left(\frac{Mw_H}{Mw_L} \right) > 9 \quad \text{and} \quad 0.05 < X_H < 0.7 \quad (\text{A-128a})$$

$$A = 1 \quad \text{otherwise} \quad (\text{A-128b})$$

The value of ζ_m is then determined from Eq. (A-109). The reduced dipole moment of the mixture, η_r , is calculated from Eq. (A-112). Then, Eq. (A-113) is used to calculate F_{Pm} , and Eq. (A-114) is used to calculate F_{Qm} . The product of $\mu_m \zeta_m$ is evaluated from Eq. (A-115). Finally, the mixture viscosity is calculated, since the value of ζ_m is known. In general, the estimates of μ_m are very reasonable for most cases.

The mixing rules and high-pressure correction factors can be combined. The reduced pressures and temperatures will be those found based on the critical values obtained using the mixture rules. These are then substituted into the equations for the high-pressure corrections. The corresponding states method of Lucas⁵³ and the other methods previously described can be very useful for determining gas mixture viscosity during supercritical combustion.

6 LIQUID VISCOSITY

While most techniques to estimate gas and gas mixture viscosity are derived from the kinetic theory of gases,^{1,43} there is no comparable theoretical basis for the estimation of liquid viscosity. Several methods were developed to correlate liquid viscosity with temperature. Temperature has a strong effect on liquid viscosity, and pressure has only a moderate effect. In general, gas viscosity increases with temperature, but liquid viscosity decreases with increased temperature. These opposite phenomena are related to gas and liquid molecular behavior.

A noticeable characteristic is that, on a semilog plot of liquid viscosity versus the reciprocal of reduced temperature (T_r), the curve increases monotonically for most liquids. At temperatures below the normal boiling point ($T_r < 0.7$), the plot exhibits an almost linear relationship. Above the normal boiling point, a nonlinear behavior is observed. For the high-temperature, nonlinear region, several corresponding states estimation methods have been suggested. In the low-temperature, linear region, many estimation techniques employ a group contribution approach to emphasize the effects of chemical structure on viscosity.

6.1 Baseline Method

There are three approaches for evaluating liquid viscosity at low temperatures (from the freezing point to near the normal boiling point). These include correlating equations, group contribution approaches, and corresponding states methods.

Correlating Equations Many researchers have proposed correlations to estimate the liquid viscosity of liquids for which experimental data exist. Some representative works are summarized below. The Andrade⁵⁴ equation, first proposed by de Guzman,⁵⁵ has been used to correlate liquid viscosity with temperature.

$$\ln \mu = A + \frac{B}{T} \quad (\text{A-129})$$

Van Velzen et al.⁵⁶ used the above correlation for various liquids, as shown in Table A-13.

Yaws et al.⁵⁷ used the following equation for correlating the temperature effect on liquid viscosity.

$$\ln \mu = A + \frac{B}{T} + CT + DT^2 \quad (\text{A-130})$$

Table A-14 shows the correlation constants for a group of selected liquids.

Goletz and Tassios⁵⁸ used a slightly modified equation based on Eq. (A-129) to correlate the viscosity of many pure liquids. Their equation, called the Vogel equation,⁵⁹ was initially developed in 1921.

$$\ln \mu = A + \frac{B}{T + C} \quad (\text{A-131})$$

Duhne⁶⁰ used both Eq. (A-129) and the following power law expression for correlating the viscosity of various liquids.

$$\mu = AT^B \quad (\text{A-132})$$

Table A.13 Correlation Parameters for the Viscosity of Selected Liquids in Eq. (A-129)⁵⁶

Formula	Name	A	B	Range, °C	μ , cP	at T , °C
CH ₃ NO ₂	Nitromethane	-3.989E + 00	1.042E + 03	0 to 90	0.63	25
C ₂ H ₆ O ₂	Ethylene glycol	-7.811E + 00	3.143E + 03	20 to 110	19.9	20
C ₃ H ₆ O	Acetone	-4.033E + 00	8.456E + 02	-80 to 60	0.32	25
C ₃ H ₈ O ₂	Propylene glycol	-7.577E + 00	3.233E + 03	40 to 180	19.4	40
C ₄ H ₁₀	<i>n</i> -Butane	-3.821E + 00	6.121E + 02	-90 to 0	0.22	-5
C ₅ H ₁₂	<i>n</i> -Pentane	-3.958E + 00	7.222E + 02	-130 to 40	0.225	25
C ₆ H ₁₄	<i>n</i> -Hexane	-4.034E + 00	8.354E + 02	-95 to 70	0.30	25
C ₇ H ₁₆	<i>n</i> -Heptane	-4.325E + 00	1.006E + 03	-90 to 100	0.40	25
C ₈ H ₁₈ O	<i>n</i> -Octanol	-8.166E + 00	3.021E + 03	15 to 100	7.21	25
C ₁₀ H ₂₂	<i>n</i> -Decane	-4.460E + 00	1.286E + 03	-25 to 175	0.86	25
C ₁₁ H ₂₄	<i>n</i> -Undecane	-4.571E + 00	1.394E + 03	-25 to 200	1.09	25
C ₁₂ H ₂₆	<i>n</i> -Dodecane	-4.562E + 00	1.454E + 03	-5 to 220	1.37	25

Table A.14 Correlation Parameters for the Viscosity of Selected Liquids in Eq. (A-130)⁵⁷

Formula	Name	A	B	C	D	Range, °C	μ , cP	at T , °C
Cl ₂	Chlorine	-1.768E + 00	3.486E + 02	-1.857E - 03	7.8 E - 07	-101 to 144	0.34	25
F ₂	Fluorine	-3.629E + 00	1.972E + 02	-9.378E - 04	-6.275E - 06	-219 to -185	0.73	-215
HCl	Hydrogen chloride	-3.488E + 00	4.481E + 02	7.062E - 03	-3.168E - 05	-110 to 50	0.068	25
HF	Hydrogen fluoride	-1.404E + 01	1.879E + 03	2.975E - 02	-3.060E - 05	-80 to 180	0.20	25
H ₂	Hydrogen	-1.118E + 01	5.786E + 01	3.244E - 01	-6.385E - 03	-258 to -240	0.016	-256
H ₂ O	Water	-2.471E + 01	4.209E + 03	4.527E - 02	-3.376E - 05	0 to 370	0.90	25
NH ₃	Ammonia	-1.978E + 01	2.018E + 03	6.173E - 02	-8.317E - 05	-75 to 130	0.13	25
N ₂ H ₄	Hydrazine	-1.848E + 01	2.991E + 03	3.709E - 02	-3.062E - 05	2 to 370	0.90	25
H ₂ O ₂	Hydrogen peroxide	-3.719E + 00	1.160E + 03	8.06E - 04	-2.689E - 06	0 to 400	1.19	25
NO	Nitric oxide	-1.150E + 01	5.487E + 02	8.448E - 02	-3.092E - 04	-160 to -90	0.35	-160
NO ₂	Nitrogen dioxide	-1.941E + 01	2.147E + 03	6.353E - 02	-8.644E - 05	-11 to 150	0.39	25
N ₂	Nitrogen	-2.795E + 01	8.660E + 02	2.763E - 01	-1.084E - 03	-205 to -195	0.18	-200
N ₂ O	Nitrous oxide	1.090E + 00	5.020E + 01	-1.134E - 02	-9.841E - 06	-100 to 30	0.05	25
O ₂	Oxygen	-4.771E + 00	2.146E + 02	1.389E - 02	-6.255E - 05	-218 to -120	0.47	-210
SO ₂	Sulfur dioxide	-6.148E + 00	9.365E + 02	1.414E - 02	-2.887E - 05	-70 to 155	0.26	25
CO	Carbon monoxide	-5.402E + 00	2.422E + 02	1.062E - 02	-4.522E - 05	-200 to -140	0.21	-200
CO ₂	Carbon dioxide	-3.097E + 00	4.886E + 01	2.381E - 02	-7.840E - 05	-56 to 30	0.06	25
CH ₄	Methane	-2.687E + 01	1.150E + 03	1.871E - 01	-5.211E - 04	-180 to -84	0.14	-170
CH ₄ O	Methanol	-3.935E + 01	4.826E + 03	1.091E - 01	-1.127E - 04	-40 to 239	0.55	25
C ₂ H ₄	Ethylene	-1.774E + 01	1.078E + 03	8.577E - 02	-1.758E - 04	-169 to 9	0.031	0
C ₂ H ₆	Ethane	-1.023E + 01	6.680E + 02	4.386E - 02	-9.588E - 05	-183 to 32	0.032	25
C ₂ H ₆ O	Ethanol	-6.210E + 00	1.614E + 03	6.18E - 03	-1.132E - 05	-105 to 243	1.04	25
C ₃ H ₆	Propylene	-1.153E + 01	9.514E + 02	4.078E - 02	-7.120E - 05	-160 to 91	0.081	25
C ₃ H ₈	Propane	-7.764E + 00	7.219E + 02	2.381E - 02	-4.665E - 05	-187 to 96	0.091	25
C ₄ H ₆	1, 3-Butadiene	-6.072E + 00	1.000E + 03	4.46E - 03	-6.694E - 06	-108 to 152	0.14	25
C ₄ H ₈	1-Butene	-1.063E + 01	9.816E + 02	3.525E - 02	-5.593E - 05	-140 to 146	0.17	25

(continued overleaf)

Table A.14 (continued)

Formula	Name	A	B	C	D	Range, °C	μ , cP	at T , °C
C ₄ H ₁₀ O	<i>n</i> -Butanol	-9.722E + 00	2.602E + 03	9.53E - 03	-9.966E - 06	-60 to 289	2.61	25
C ₆ H ₆	Benzene	4.612E + 00	1.489E + 02	-2.544E - 02	2.222E - 05	6 to 288	0.61	25
C ₇ H ₈	Toluene	-5.878E + 00	1.287E + 03	4.575E - 03	-4.499E - 06	-40 to 315	0.55	25

Xiang et al.⁶¹ used the following equation for correlating the viscosity of saturated liquids only.

$$\ln \mu^* = \ln c_0 - \left\{ c_1 \left[\frac{(1 - T_r)^2}{T_r} \right]^{-1/4} + c_2 \left[\frac{(1 - T_r)^2}{T_r} \right] \right\} \ln T_r \quad (\text{A-133})$$

where $\mu^* = \mu$ (saturated liquid viscosity in 10^{-3} cP)/ μ_{ref} . The μ_{ref} is defined as $[(\text{Mw}/N_A)^{1/2} P_c^{2/3}]/(k \cdot T_c)^{1/6}$, where Mw is the molecular weight of the liquid in (kg/mol), k is Boltzmann's constant, and P_c is in (Pa). The correlation parameters used for a number of liquids for Xiang's equation are given in Table A-15.

Low-Temperature Viscosity Estimation Methods In the low-temperature range, liquid viscosity is more sensitive to the structure of the molecule. The following methods are based on the consideration of the molecular structural

Table A.15 Correlation Parameters for the Viscosity of Selected Liquids in Xiang's Equation

Compound	Mw (kg/kmol)	T_c (K)	P_c (MPa)	T_r range (<i>t</i> , tri; <i>c</i> , cri)	μ_{ref} (μ P)	c_0	c_1	c_2	RMS	Max. dev.
Nitrogen	28.013	126.20	3.400	<i>t</i> – <i>c</i>	14.05831	1.426385	2.650477	1.002669	0.98	1.34
Oxygen	31.999	154.58	5.043	0.45– <i>c</i>	18.89206	1.501923	2.387142	0.8311018	0.39	0.59
CO ₂	44.010	304.11	7.372	<i>t</i> – <i>c</i>	25.49400	1.441079	3.188617	2.344998	0.45	0.68
Benzene	78.114	562.20	4.890	<i>t</i> –0.70	23.31842	1.675625	2.780558	2.046971	0.20	0.37
Ethylene	28.054	282.34	5.039	<i>t</i> – <i>c</i>	15.99100	1.711582	2.476574	0.7329897	0.36	1.44
Methane	16.032	190.56	4.598	<i>t</i> – <i>c</i>	12.14260	1.409857	2.403628	1.081937	1.22	2.71
Ethane	30.070	305.32	4.872	<i>t</i> – <i>c</i>	15.97802	1.517536	2.603487	0.5964780	1.14	1.91
Propane	44.094	369.80	4.250	<i>t</i> – <i>c</i>	17.10928	1.508882	2.856378	0.7169267	1.27	3.49
Hexane	86.178	507.60	3.025	0.55–0.77	18.08723	1.763448	2.811273	1.198102	0.38	1.03
Octane	114.232	568.80	2.49	0.49–0.69	17.94640	1.684365	3.095080	1.283836	0.20	0.41
Decane	142.265	617.7	2.11	0.45–0.68	17.68961	1.678560	3.276227	1.460968	0.19	0.36
Dodecane	170.338	658	1.82	0.43–0.64	17.35573	1.999222	3.161546	1.710287	0.35	0.71
Tetradecane	198.392	693	1.57	0.42–0.61	16.82739	2.151911	3.181119	1.843238	0.35	0.58
Ammonia	17.030	405.4	11.333	<i>t</i> – <i>c</i>	20.13217	1.530403	2.526965	1.921239	0.91	1.49
Water	18.015	647.1	22.046	<i>t</i> – <i>c</i>	29.85284	1.534793	1.771178	2.955191	1.10	3.00

effects. The methods are limited for $T_r < 0.75$ and are less reliable than the correlating equations previously described.

*Van Velzen, Cardozo, and Langenkamp's Group Contribution Method*⁶² A slightly modified form of Eq. (A-129) was used by van Velzen et al.

$$\log_{10} \mu = B \left(\frac{1}{T} - \frac{1}{T_0} \right) \quad (\text{A-134})$$

where B and T_0 are related to the molecular structure. These values can be calculated based on the equivalent chain length N^* .

$$N^* = N + \sum \Delta N_i \quad (\text{A-135})$$

where N is the actual number of carbon atoms in the molecule and ΔN_i represents the structural contribution of the i th functional group given in Refs. 62 and 1. The value of T_0 is related to N^* according to the following equation.

$$T_0 = 28.86 + 37.439N^* - 1.3547(N^*)^2 + 0.02076(N^*)^3 \quad N^* < 20 \quad (\text{A-136a})$$

$$T_0 = 8.164N^* + 238.59 \quad N^* \geq 20 \quad (\text{A-136b})$$

The value of B is determined from

$$B = B_A + \sum \Delta B_i \quad (\text{A-137})$$

where ΔB_i for different functional groups can be found in tables of van Velzen et al.⁶² or Reid et al.¹ The parameter B_A in Eq. (A-137) is also related to the chain length N^* by the following equations:

$$B_A = 24.79 + 66.885N^* - 1.3173(N^*)^2 + 0.00377(N^*)^3 \quad N^* < 20 \quad (\text{A-138a})$$

$$B_A = 530.59 + 13.740N^* \quad N^* \geq 20 \quad (\text{A-138b})$$

In a test with 314 liquids with 4500 datum points, large errors were often noted for the many chemical compounds.

*Orrick and Erbar's Group Contribution Method*¹ This method uses an equation very similar that of Eq. (A-129).

$$\ln \left(\frac{\mu}{\rho M_w} \right) = A + \frac{B}{T} \quad (\text{A-139})$$

where μ is given in cP and ρ is the liquid density in g/cm³ evaluated at 20°C. The values of A and B depend on the functional groups of the liquid molecule and are tabulated in Reid et al.¹ In tests of 188 organic liquids, Orrick and Erbar found that errors varied widely from liquid to liquid with an average error of around 15%.

*Przezdziecki and Sridhar's Corresponding States Method*⁶³ Przezdziecki and Sridhar⁶³ suggested the use of the following Hildebrand-modified Batschinski equation⁶⁴ for calculating liquid viscosity.

$$\mu = \frac{v_0}{E(v - v_0)} \quad (\text{A-140})$$

where the liquid viscosity is in cP and the liquid molar volume is in cm³/mol. The parameters E and v_0 are defined below.

$$E = -1.12 + \frac{v_c}{12.94 + 0.10 \text{ Mw} - 0.23 P_c + 0.0424 T_{\text{fr}} - 11.58 (T_{\text{fr}}/T_c)} \quad (\text{A-141})$$

$$v_0 = 0.0085 \omega T_c - 2.02 + \frac{v_m}{0.342 (T_{\text{fr}}/T_c) + 0.894} \quad (\text{A-142})$$

where v_c is the critical molar volume in (cm³/mol) and T_{fr} is the freezing point in K. v_m is the liquid molar volume in cm³/mol evaluated at T_{fr} . To estimate v_m and the liquid molar volume, v , at the temperature of interest, the Gunn-Yamada method⁶⁵ can be utilized. A datum point is required for the liquid viscosity at liquid molar volume v^R evaluated at the temperature T^R . The molar volume at any other temperature T can be calculated from

$$v(T) = \left[\frac{f(T)}{f(T^R)} \right] v^R \quad (\text{A-143})$$

where the temperature function, $f(T)$ is defined as

$$f(T) = H_1(1 - \omega H_2) \quad (\text{A-144})$$

and the parameters H_1 and H_2 can be evaluated from the following polynomial functions of T_r .

$$H_1 = 0.33593 - 0.33953 T_r + 1.51941 T_r^2 - 2.02512 T_r^3 + 1.11422 T_r^4 \quad (\text{A-145})$$

$$H_2 = 0.29607 - 0.09045 T_r - 0.04842 T_r^2 \quad (\text{A-146})$$

In tests of 35 liquids, the technique underestimated the liquid viscosity, and large errors were normally noted at low temperature or for alcohols.¹ Luckas and

Lucas⁶⁶ suggest that the Hildebrand-modified Batschinski equation should not be used below T_r values of about 0.55.

High-Temperature Liquid Viscosity Estimation Methods In the relatively high-temperature range, between $T_r = 0.7$ to the critical point, T_c , many estimation methods are of a corresponding states type, which are similar to those used for evaluating gas viscosities.

*Letsou and Stiel's Method for Saturated Liquids*⁶⁷ For $0.76 < T_r < 0.98$, Letsou and Stiel proposed using the following equation for the saturated liquid:

$$\mu\xi = 10^{-3}[(2.648 - 3.725T_r + 1.309T_r^2) + \omega(7.425 - 13.39T_r + 5.933T_r^2)] \quad (\text{A-147})$$

where the reduced inverse viscosity, ξ in $(\mu\text{P})^{-1}$, is evaluated from Eq. (A-110).

In tests of 14 liquids, mostly simple hydrocarbons, at temperatures up to $T_r \approx 0.92$, an average error of 3% was reported.¹ Larger errors were found as the temperature approached the critical point. In other tests of compounds other than hydrocarbons, errors in the range of 15 to 20% were found.

Brule and Starling's⁶⁸ and Chung et al.'s⁶⁹ Methods These are more general estimation methods that involve the extension of the high-pressure gas viscosity correlation into the high-temperature liquid region. Both of them use the following equations but with slightly different coefficients to compute some of the parameters.

$$\mu = \frac{\mu^* 36.344(\text{Mw}T_c)^{1/2}}{v_c^{2/3}} \quad (\text{A-148})$$

where viscosity is in μP and the liquid critical molar volume is in cm^3/mol .

$$\mu^* = \frac{(T^*)^{1/2} F_C (G^{-1} + E_6 y)}{\Omega_v} + E_7 y^2 G \exp[E_8 + E_9 (T^*)^{-1} + E_{10} (T^*)^{-2}] \quad (\text{A-149})$$

$$T^* = 1.2593 T_r \quad (\text{A-150})$$

$$F_C = 1 - 0.2756\omega + 0.059035 M_d + \kappa \quad (\text{A-151})$$

where M_d is the dimensionless dipole moment and κ is the association factor. The viscosity collision integral, Ω_v , can be calculated from

$$\begin{aligned} \Omega_v = & [1.16145(T^*)^{-0.14874}] + 0.52487[\exp(-0.77320T^*)] \\ & + 2.16178[\exp(-2.43787T^*)] \end{aligned} \quad (\text{A-152})$$

$$G = \frac{E_1[(1 - e^{-E_4 y})/y] + (E_2 e^{E_5 y} + E_3)(1 - 0.5y)/(1 - y)^3}{E_1 E_4 + E_2 + E_3} \quad (\text{A-153})$$

$$y = \frac{\rho v_c}{6} \quad (\text{A-154})$$

Table A.16 Chung et al. Coefficients to Calculate E_i :

$$E_i = a_i + b_i \omega + c_i M_d^4 + d_i \kappa$$

i	a_i	b_i	c_i	d_i
1	6.324	50.412	-51.680	1189.0
2	1.210×10^{-3}	-1.154×10^{-3}	-6.257×10^{-3}	0.03728
3	5.283	254.209	-168.48	3898.0
4	6.623	38.096	-8.464	31.42
5	19.745	7.630	-14.354	31.53
6	-1.900	-12.537	4.985	-18.15
7	24.275	3.450	-11.291	69.35
8	0.7972	1.117	0.01235	-4.117
9	-0.2382	0.06770	-0.8163	4.025
10	0.06863	0.3479	0.5926	-0.727

where ρ is the molar density in mol/cm³ and the values of E_i can be found in Table A-16 based on the work of Chung et al.⁶⁹ The Chung et al. form is preferable for simple molecules. With this method, nonpolar compounds typically result in errors of about 10%. Polar, halogenated, or high-molecular-weight compounds result in higher errors. The Brule and Starling relation gives 10% error for the majority of cases. Neither method is applicable if T_r is less than 0.5.

6.2 High-Pressure Correction

Bridgman⁷⁰ developed an estimation method for liquid viscosity at high pressures. His data, obtained at pressures over several thousand bar, suggest that the logarithm of the viscosity is proportional to pressure and that the structural complexity of the molecule must be considered.

Lucas's Estimation Method⁴⁸ The viscosity of the liquid at a high pressure, P , can be evaluated by using its saturated liquid viscosity, μ_{SL} , at the saturated vapor pressure, P_{vp} .

$$\frac{\mu}{\mu_{SL}} = \frac{1 + D(\Delta P_r / 2.118)^A}{1 + C\omega \Delta P_r} \quad (\text{A-155})$$

where

$$\Delta P_r = \frac{P - P_{vp}}{P_c}$$

$$A = 0.9991 - \frac{4.674 \times 10^{-4}}{1.0523 T_r^{-0.03877} - 1.0513}$$

$$C = -0.07921 + 2.1616 T_r - 13.4040 T_r^2 + 44.1706 T_r^3 - 84.8291 T_r^4 \\ + 96.1209 T_r^5 - 59.8127 T_r^6 + 15.6719 T_r^7$$

$$D = \frac{0.3257}{(1.0039 - T_r^{2.573})^{0.2906}} - 0.2086$$

In a test with 55 liquids, polar and nonpolar, Lucas found errors of less than 10%. Except at high values of T_r , the dimensionless viscosity ratio, μ/μ_{SL} , is approximately proportional to ΔP_r . The effect of pressure is more significant at high temperatures.

6.3 Mixing Rules

The following methods are generally applicable at reduced temperatures of the liquid mixture below or slightly above 0.7. In this temperature range, liquid mixture viscosity is very sensitive to the structure of the constituent molecules. Even mild association effects between different molecular components can often significantly affect the viscosity. It is assumed in all methods that values of the viscosities of the pure components are available. Most methods are based on interpolative techniques with some empirical constants.

Grunberg and Nissan's Method⁷¹

$$\ln \mu_m = \sum_i X_i \ln \mu_i + \sum_i \sum_j X_i X_j G_{ij} \quad (\text{A-156})$$

where $i \neq j$ and G_{ij} is the interaction parameter for components i and j . The G_{ij} value can be calculated from

$$G_{ij} = \sum_i \Delta_i - \sum_j \Delta_j + W \quad (\text{A-157})$$

The value of the parameter, W , is given by

$$W = \frac{(0.3161)(N_i - N_j)^2}{N_i + N_j} - (0.01188)(N_i - N_j) \quad (\text{A-158})$$

where N_i and N_j are the numbers of carbon atoms in the i th and j th components, respectively. If component i or j contains any atoms other than carbon and hydrogen, then $W = 0$.

The values of Δ_i and Δ_j in Eq. (A-157) for different chemical groups at room temperature are tabulated in Reid et al.¹ For binary systems, Eq. (A-156) reduces to

$$\ln \mu_m = X_1 \ln \mu_1 + X_2 \ln \mu_2 + X_1 X_2 G_{12} \quad (\text{A-159})$$

The G_{ij} parameter is a function of both temperature and composition.⁷² Isdale et al.⁷³ introduced the following equation to correct the value of G_{ij} for certain

organic liquid mixtures at temperatures other than room temperature.

$$G_{ij}(T) = 1 - [1 - G_{ij}(298 \text{ K})] \frac{573 - T(\text{K})}{275} \quad (\text{A-160})$$

Isdale⁷² presented the results of very detailed mixture tests with 2000 datum points. For many mixtures containing alcohols, carboxylic acids, and ketones, the regressed experimental data were found to fit satisfactorily, using the interaction parameters as calculated above. The overall root mean square deviation for the mixtures tested was 1.6%. For polar mixtures, errors of 5 to 10% were reported. This method is not recommended for aqueous solutions.

Teja and Rice's Method⁷⁴ This method was proposed based on corresponding states principles, using mixture compressibility factors.⁷⁵ The mixture viscosity can be evaluated from

$$\ln(\mu_m \varepsilon_m) = \ln(\mu \varepsilon)^{(r1)} + \frac{[\ln(\mu \varepsilon)^{(r2)} - \ln(\mu \varepsilon)^{(r1)}](\omega_m - \omega^{(r1)})}{\omega^{(r2)} - \omega^{(r1)}} \quad (\text{A-161})$$

where the superscripts (r1) and (r2) represent two reference liquids. All the viscosities are in cP. The ε parameters given in (cP)⁻¹ are defined as

$$\varepsilon_m = \frac{v_{c,m}^{2/3}}{(T_{c,m} M_w)_m^{1/2}} \quad (\text{A-162a})$$

$$\varepsilon = \frac{v_c^{2/3}}{(T_c M_w)^{1/2}} \quad (\text{A-162b})$$

The $v_{c,m}$ is calculated from Eq. (A-49) and $T_{c,m}$ is evaluated from Eq. (A-163).

$$T_{c,m} = \frac{1}{v_{c,m}} \left(\sum_i \sum_j X_i X_j T_{cij} v_{cij} \right) \quad (\text{A-163})$$

where

$$v_{cij} = (v_{ci}^{1/3} + v_{cj}^{1/3})^3 / 8 \quad (\text{A-164})$$

and

$$T_{cij} v_{cij} = \psi_{ij} (T_{ci} T_{cj} v_{ci} v_{cj})^{1/2} \quad (\text{A-165})$$

In the above equation, the interaction parameter, ψ_{ij} , is determined from experimental data and is of order unity. The molecular weight of the mixture is calculated from Eq. (A-125). The acentric factor of the mixture is determined from Eq. (A-166).

$$\omega_m = \sum_i X_i \omega_i \quad (\text{A-166})$$

In this process, the viscosity values for two reference liquids ($\mu^{(r1)}$, $\mu^{(r2)}$) are to be obtained, not at T , but at temperatures $T \times [(T_c)^{(r1)} / T_{c,m}]$ and $T \times [(T_c)^{(r2)} / T_{c,m}]$ for reference liquids 1 and 2, respectively. This technique is significantly more accurate for polar–polar mixtures and aqueous solutions. For other types of mixtures, this method gives about the same accuracy as that of Grunberg and Nissan's method.

7 GAS THERMAL CONDUCTIVITY

The thermal conductivity of gas and gas mixtures is considered in this section. Based on the kinetic theory of gases, the thermal conductivity of an ideal gas is given by

$$\lambda = \frac{\bar{u} L C_v^{(m)} n^*}{3}$$

where \bar{u} is the average magnitude of the molecular velocity due to random motion, L is the mean free path, $C_v^{(m)}$ is the constant-volume specific heat of a molecule, and n^* is the number density of the molecules. Unfortunately, this theoretical equation does not provide accurate values of the thermal conductivity of many gases. Therefore, correlations for specific circumstances have been developed for many gases. A few representative correlations are presented in the following sections.

7.1 Baseline Method

Available data corresponding to gas thermal conductivity for pure gases at low to moderate pressures are typically correlated as a function of temperature, with coefficients provided for equations of various forms. Equation forms are selected with characteristics that give reasonable extrapolation outside specified temperature ranges. Two widely accepted databases for calculation of vapor thermal conductivity and gas thermal conductivity at atmospheric pressures are those of Daubert and Danner⁷⁶ and Gordon et al.,⁷⁷ respectively.

Daubert and Danner provide coefficients for an equation that correlates vapor thermal conductivity for pressures in the vicinity of 1 atm or below, i.e.,

$$\lambda^0 = \frac{AT^B}{1 + C/T + D/T^2} \quad (\text{A-167})$$

The superscript “0” is to denote low pressure. The coefficients A , C , and D and exponent B were generated to give thermal conductivity in units of $\text{W/m} \cdot \text{K}$ and can be found in Ref. 76 for a wide variety of gases. In this reference, recommended minimum and maximum temperatures for Eq. (A-167) are listed together with calculated values of properties at these limits. Typically, these correlations are valid over temperature ranges from 14 to 1500 K.

Gordon et al.⁷⁷ provide coefficients for an equation applicable for pressures in the vicinity of 1 atm of the form

$$\ln \lambda^0 = A \ln T + \frac{B}{T} + \frac{C}{T^2} + D \quad (\text{A-168})$$

for 154 species. The coefficients in Eq. (A-168) have been generated to give thermal conductivity in units of $\mu\text{W}/\text{cm} \cdot \text{K}$. Depending on the individual chemical species, different sets of coefficients are given for several temperature ranges. For many species, one set of coefficients applies over a temperature range from 300 to 1000 K, and another set applies from 1000 to 5000 K. These are provided in the CEA96 program and documentation by McBride and Gordon.^{78,79} Due to the large size of the data tabulation, the data are not included in this appendix.

7.2 High-Pressure Correction

Stiel and Thodos⁸⁰ obtained a correlation between the residual thermal conductivity ($\lambda - \lambda^0$), the molecular weight, Mw, and the critical properties, P_c , T_c , v_c , and ρ_c , of several nonpolar substances. Application of dimensional analysis led to an equation of the form

$$(\lambda - \lambda^0)\Gamma = \alpha Z_c^m \rho_r^n \quad (\text{A-169})$$

where

$$\Gamma = 210 \left(\frac{T_c \text{Mw}^3}{P_c^4} \right)^{1/6} \quad (\text{A-170})$$

Eq. (A-170) has units of inverse thermal conductivity and serves to nondimensionalize Eq. (A-169). Experimental data available in the literature for 20 nonpolar substances, which included the inert gases, diatomic gases, carbon dioxide, aliphatic hydrocarbons, and aromatics, were used to establish the following correlations.

$$(\lambda - \lambda^0)\Gamma Z_c^5 = 1.22 \times 10^{-2} [\exp(0.535\rho_r) - 1] \quad \rho_r < 0.5 \quad (\text{A-171a})$$

$$(\lambda - \lambda^0)\Gamma Z_c^5 = 1.14 \times 10^{-2} [\exp(0.67\rho_r) - 1.069] \quad 0.5 < \rho_r < 2.0 \quad (\text{A-171b})$$

$$(\lambda - \lambda^0)\Gamma Z_c^5 = 2.60 \times 10^{-3} [\exp(1.155\rho_r) + 2.016] \quad 2.0 < \rho_r < 2.8 \quad (\text{A-171c})$$

where λ^0 is the low-pressure gas thermal conductivity at the same temperature as that in question and can be evaluated using one of the low-pressure techniques previously described. In most cases, this method was found to be in agreement with experimental values to within 10%; however, Reid et al.¹ cites that errors between 10 and 20% are possible. Also, this method should not be used with polar substances, hydrogen, or helium.¹ Note that polar molecules are formed between atoms of different electronegativities and tend to align in an electric field.

7.3 Mixing Rules

The thermal conductivity of a gas mixture cannot usually be determined using a mole fraction average. In addition, several properties of the gas mixture constituents can greatly affect the mixture thermal conductivity, including the polarity, size, and weight of each constituent.¹ Thus, most attempts at developing correlations for the thermal conductivity of mixtures have been empirical and are limited in their range of applicability. Gas thermal conductivity also behaves differently at low and high pressures.

Gas Mixture at Low to Moderate Pressures Most techniques proposed to evaluate thermal conductivity of gas mixtures at low pressure are approximately in the form of the Wassiljewa equation⁸¹ given below.

$$\lambda_m = \frac{\sum_{i=1}^n X_i \lambda_i}{\sum_{j=1}^n X_j A_{ij}} \quad (\text{A-172})$$

where λ_i and λ_j are the thermal conductivity of pure component i and j , respectively. Also note that $A_{ii} = 1.0$. Different expressions of A_{ij} lead to different evaluation methods. Mason and Saxena⁸² suggest that A_{ij} can be expressed as

$$A_{ij} = \frac{\varepsilon [1 + (\lambda_{tri}/\lambda_{trj})^{1/2} (Mw_i/Mw_j)^{1/4}]^2}{[8(1 + Mw_i/Mw_j)]^{1/2}} \quad (\text{A-173})$$

where

$$\frac{\lambda_{tri}}{\lambda_{trj}} = \frac{\Gamma_j [\exp(0.0464 T_{ri}) - \exp(-0.2412 T_{ri})]}{\Gamma_i [\exp(0.0464 T_{rj}) - \exp(-0.2412 T_{rj})]} \quad (\text{A-174})$$

The parameter λ_{tr} is the monatomic value of the thermal conductivity (or the translational conductivity), and ε is the numerical constant near unity and is usually set equal to 1.

Gordon et al.⁷⁷ used this method to obtain the frozen thermal conductivity for 154 gaseous species. In addition, they suggested the Brokow method⁸³ for the contribution of chemical reaction to the thermal conductivity. For nonpolar gas mixtures, λ_m can be estimated satisfactorily using the above method. For nonpolar-polar and polar-polar mixtures, more than 5 ~ 8% errors can be expected, and currently none of the techniques are found to be particularly accurate.¹

Gas Mixture at High Pressures One approach, implemented by Yorizane et al.,⁸⁴ extended the approach of Stiel and Thodos⁸⁰ to high-pressure binary gas mixtures. The basic idea was that the procedure of Stiel and Thodos could be adapted for binary mixtures if mixing and combining rules were available to evaluate Eqs. (A-169), (A-170), and (A-171). In order to obtain these rules,

the single fluid van der Waals model was utilized, resulting in the following equations:

$$T_{c,m} = \frac{\sum_i \sum_j X_i X_j v_{cij} T_{cij}}{v_{c,m}} \quad (\text{A-175})$$

$$v_{c,m} = \sum_i \sum_j X_i X_j v_{cij} \quad (\text{A-176})$$

$$\omega_m = \sum_i X_i \omega_i \quad (\text{A-177})$$

$$Z_{c,m} = 0.291 - 0.08\omega_m \quad (\text{A-178})$$

$$P_{c,m} = \frac{Z_{c,m} R T_{c,m}}{v_{c,m}} \quad (\text{A-179})$$

$$Mw_m = \sum_i X_i Mw_i \quad (\text{A-180})$$

$$T_{cii} = T_{ci} \quad (\text{A-181})$$

$$T_{cij} = (T_{ci} \cdot T_{cj})^{1/2} \quad (\text{A-182})$$

$$v_{cii} = v_{ci} \quad (\text{A-183})$$

$$v_{cij} = \frac{1}{8} \{(v_{ci})^{1/3} + (v_{cj})^{1/3}\}^3 \quad (\text{A-184})$$

Using these rules, thermal conductivity data for N₂-O₂, N₂-Ar, CO-Ar, and CO₂-CH₄ systems correlated quite well at high pressures.

8 LIQUID THERMAL CONDUCTIVITY

The thermal conductivity of most liquid substances decreases with increasing temperature. The exceptions to this rule include ethylene glycol and glycerol, where the inverse relationship holds,⁸⁵ and water, where the conductivity first rises to a maximum value and then falls when temperature is increased. Three main techniques have been historically used to experimentally measure the thermal conductivity of liquids: the plane layer method, the concentric cylinder method, and the hot-wire method. The plane layer method is generally the least-expensive technique, and the hot-wire method is considered one of the better techniques.⁸⁵

8.1 Baseline Method

Miller et al.'s Empirical Correlation⁸⁶ Miller et al. empirically correlated the thermal conductivity of saturated liquids at low to moderate pressures as a function of temperature by the following relation:

$$\lambda = A + BT + CT^2 \quad (\text{A-185})$$

where the coefficients A , B , and C are given by Refs. 86 and 1 for various liquids in their respective valid temperature ranges. For this method, deviations between the experimental data and the calculated empirical correlation results are in most cases less than 2.5%. The usable temperature range covers the saturated liquid phase from the melting point to temperatures above the boiling point and up to 80–90% of the critical temperature. However, the use of the above correlation is not recommended in the immediate vicinity of the critical temperature (90–100% of T_c).

Baroncini et al.'s Method Baroncini et al.⁸⁷ provided a general correlation for estimating organic liquid thermal conductivity.

$$\lambda = A \cdot \frac{(1 - T_r)^{0.38}}{T_r^{1/6}} \quad (\text{A-186})$$

The coefficient A is characteristic of the liquid and is practically temperature independent. The values of A with M_w , T_b , and T_c for a group of selected paraffins are tabulated in Table A-17. Values of A that correspond to important organic liquid families are compiled in Ref. 87. In case the value of A is not available for the liquid of interest, it can be evaluated if experimental values of the thermal conductivity of the liquid are available, preferably at $T_r = 0.55$. With the thermal conductivity data, A can be calculated from Eq. (A-186). Then the thermal conductivity at other temperatures can be determined. The deviations between experimental and the correlated results using Eq. (A-186) were found to be less than 2% by Baroncini et al. However, Eq. (A-186) is only recommended for the reduced temperature range of 0.3 to 0.8.

If both the coefficient A and experimental values for the thermal conductivity are not available, modified forms of Eq. (A-186) can be utilized for estimation purposes. The following equations suggested by Baroncini et al.⁸⁷ are given for specific families of organic liquids:

Paraffins:

$$\lambda = 0.00350 \cdot \frac{T_b^{6/5}}{M_w^{1/2} T_c^{1/6}} \cdot \frac{(1 - T_r)^{0.38}}{T_r^{1/6}} \quad (\text{A-187})$$

Organic Acids:

$$\lambda = 0.00319 \cdot \frac{T_b^{6/5}}{M_w^{1/2} T_c^{1/6}} \cdot \frac{(1 - T_r)^{0.38}}{T_r^{1/6}} \quad (\text{A-188})$$

Alcohols:

$$\lambda = 0.00339 \cdot \frac{T_b^{6/5}}{M_w^{1/2} T_c^{1/6}} \cdot \frac{(1 - T_r)^{0.38}}{T_r^{1/6}} \quad (\text{A-189})$$

Ketones:

$$\lambda = 0.00383 \cdot \frac{T_b^{6/5}}{M_w^{1/2} T_c^{1/6}} \cdot \frac{(1 - T_r)^{0.38}}{T_r^{1/6}} \quad (\text{A-190})$$

Table A.17 Experimental Data and Empirical Constants for Selected Paraffins⁸⁷

Liquid Paraffins	Mw	T_b , K	T_c , K	T_r Range	A, W/mK	% Error	Max. % Error
Methane	16.04	111.7	190.6	0.57–0.92	0.264	0.9	1.4
Propane	44.10	231.1	369.8	0.41–0.63	0.185	2.9	4.6
<i>n</i> -Butane	58.12	272.7	425.2	0.36–0.64	0.168	3.0	5.2
<i>n</i> -Pentane	72.15	309.2	469.8	0.33–0.58	0.149	2.5	4.5
<i>n</i> -Hexane	86.18	342.1	507.4	0.44–0.68	0.152	0.3	0.8
3-Methylpentane	86.18	336.4	504.4	0.60–0.64	0.145	0.3	0.9
2-Methylpentane	86.18	333.4	497.5	0.61–0.65	0.143	0.0	0.0
2,3-Dimethylbutane	86.18	331.2	499.9	0.61–0.65	0.138	0.3	1.0
2,2-Dimethylbutane	86.18	322.9	488.7	0.62–0.65	0.133	0.3	1.0
<i>n</i> -Heptane	100.20	371.6	540.3	0.38–0.70	0.156	1.0	1.9
<i>n</i> -Octane	114.23	398.8	569.2	0.39–0.66	0.149	1.6	3.5
3-Methylheptane	114.23	392.1	563.6	0.52	0.145	0.0	0.0
2,2,4-	114.23	372.4	543.9	0.56–0.67	0.125	0.3	1.2
Trimethylpentane							
<i>n</i> -Nonane	128.26	424.0	594.6	0.38–0.70	0.149	1.1	1.9
<i>n</i> -Decane	142.29	447.3	617.6	0.39–0.70	0.153	1.0	2.8
<i>n</i> -Undecane	156.31	469.1	638.8	0.47–0.71	0.152	0.3	0.9
<i>n</i> -Dodecane	170.34	489.5	658.3	0.46–0.71	0.153	0.6	1.0
<i>n</i> -Tridecane	184.37	508.6	675.8	0.45–0.67	0.151	0.4	0.9
<i>n</i> -Tetradecane	198.39	526.7	694.0	0.42–0.65	0.151	0.1	0.8
<i>n</i> -Pentadecane	212.42	543.8	707.0	0.43–0.67	0.151	0.2	0.8
<i>n</i> -Hexadecane	226.45	560.0	717.0	0.42–0.66	0.153	0.5	1.9
<i>n</i> -Heptadecane	240.47	575.2	733.0	0.43–0.62	0.153	0.0	0.0
<i>n</i> -Octadecane	254.50	589.5	745.0	0.42–0.61	0.151	1.3	2.7
<i>n</i> -Nonadecane	268.53	603.1	756.0	0.41–0.61	0.155	0.1	0.7
<i>n</i> -Eicosane	282.56	617.0	767.0	0.42–0.60	0.150	1.3	2.7
<i>n</i> -Docosane	310.61	641.7	789.0	0.41–0.60	0.153	1.0	1.7
<i>n</i> -Tricosane	324.64	653.3	801.3	0.42–0.57	0.155	0.7	1.4
<i>n</i> -Tetracosane	338.67	664.5	813.7	0.40–0.58	0.155	1.5	2.5

Esters:

$$\lambda = 0.0415 \cdot \frac{T_b^{6/5}}{\text{Mw} T_c^{1/6}} \cdot \frac{(1 - T_r)^{0.38}}{T_r^{1/6}} \quad (\text{A-191})$$

Ethers:

$$\lambda = 0.0385 \cdot \frac{T_b^{6/5}}{\text{Mw} T_c^{1/6}} \cdot \frac{(1 - T_r)^{0.38}}{T_r^{1/6}} \quad (\text{A-192})$$

Aromatics:

$$\lambda = 0.0346 \cdot \frac{T_b^{6/5}}{\text{Mw} T_c^{1/6}} \cdot \frac{(1 - T_r)^{0.38}}{T_r^{1/6}} \quad (\text{A-193})$$

Cycloparaffins:

$$\lambda = 0.0310 \cdot \frac{T_b^{6/5}}{\text{Mw} T_c^{1/6}} \cdot \frac{(1 - T_r)^{0.38}}{T_r^{1/6}} \quad (\text{A-194})$$

Olefins:

$$\lambda = 0.0361 \cdot \frac{T_b^{6/5}}{M_w T_c^{1/6}} \cdot \frac{(1 - T_r)^{0.38}}{T_r^{1/6}} \quad (\text{A-195})$$

Baroncini et al.⁸⁷ determined the mean deviation of the above equations compared with the experimental data of the liquids evaluated to be between 2–5%. Some results have slightly higher than 5% error, around 7 to 10%.

8.2 High-Pressure Correction

Below approximately 3.5 MPa, pressure has little effect on liquid thermal conductivity. At higher pressures, however, liquid thermal conductivity increases with pressure, and corrections are needed. Due to the fact that at high pressures thermal conductivity is a function of both temperature and pressure, it is desirable to develop a general method for the thermal conductivity determination. Tsederberg's experimental results for butanol, tolulene, and pentane indicate that the thermal conductivity of these liquids increases monotonically with increasing pressure.

Missenard⁸⁸ proposed the following equation to correlate the thermal conductivity with the reduced pressure and a coefficient A , which is a function of both reduced pressure and reduced temperature.

$$\frac{\lambda(P_r)}{\lambda_0} = 1 + A \cdot P_r^{0.7} \quad (\text{A-196})$$

where λ_0 is the thermal conductivity of the liquid at room temperature and 1 atm. The value of A is determined by cross-referencing Table A-18.

This correlation is intended for use with organic liquids with viscosity less than 6 millipoise. These liquids must be nonelectrolytic (without the –OH–radical behavior). This method is not recommended for reduced temperatures above 0.9 or absolute pressures above 98 MPa.

8.3 Mixing Rules

The thermal conductivity of liquid mixtures does not usually obey simple mixing rules, and the mixture could have a lower thermal conductivity than a

Table A.18 Coefficient A of Eq. (A-196) as a Function of Reduced Pressure and Temperature⁸⁸

T_r	P_r					
	1	5	10	50	100	200
0.8	0.036	0.038	0.038	0.038	0.038	0.038
0.7	0.018	0.025	0.027	0.031	0.030	0.032
0.6	0.015	0.020	0.022	0.024	0.025	0.025
0.5	0.012	0.0165	0.017	0.019	0.020	0.020

mole-fraction or mass-fraction averaged value.¹ Most methods to determine the thermal conductivity of mixtures require some empirical parameters.

Li⁸⁹ developed a method that generates the thermal conductivity of a mixture based on the properties of the pure components such as volume fractions, thermal conductivities, liquid molar volumes, and mole fractions. The thermal conductivity of a mixture of known composition can be calculated by using the following equations when the conductivities of the pure components are known or estimated via correlations as previously presented.

$$\lambda_m = \sum_i \sum_j \phi_i \phi_j \lambda_{ij} \quad (\text{A-197})$$

where

$$\lambda_{ij} = 2 \left(\frac{1}{\lambda_i} + \frac{1}{\lambda_j} \right)^{-1} \quad (\text{A-198})$$

$$\phi_i = \frac{X_i v_i}{\sum_j X_j v_j} \quad (\text{A-199})$$

$$\sum_i \phi_i = 1 \quad (\text{A-200})$$

The liquid molar volumes v_i and v_j of pure components i and j are given in m^3/kmol . Deviations of calculated values from experimental data are within 3%. This correlation is not recommended for values in the vicinity of the critical point.

9 GAS DIFFUSIVITY

The binary gas diffusion coefficient, \mathcal{D}_{AB} , for a binary mixture of A and B is defined as the proportionality constant between the mass flux and the driving potential, according to Fick's law of diffusion, described in Chapter 3. Some basic relationships between the temperature, pressure, and dimensions of the molecules derived from the principles of kinetic theory of gases are given in Sections 2 and 3 of Chapter 3.

9.1 Baseline Method

The following two baseline methods are applicable to low-to-moderate pressures.

Chapman and Enskog's Method⁴³ By solving the Boltzmann equation, Chapman and Enskog arrived at the following relationship:

$$\mathcal{D}_{AB} = \frac{3}{16} \frac{(4\pi kT/Mw_{AB})^{1/2}}{n^* \pi \sigma_{AB}^2 \Omega_D} f_D \quad (\text{A-201})$$

where Mw_{AB} is the combined molecular weight of species A and B , according to

$$Mw_{AB} = 2.0 \left(\frac{1}{Mw_A} + \frac{1}{Mw_B} \right)^{-1} \quad (\text{A-202})$$

In Eq. (A-201), k is Boltzmann's constant, and σ_{AB} is the interaction characteristic length between A and B , expressed in Å and defined as

$$\sigma_{AB} = \frac{\sigma_A + \sigma_B}{2} \quad (\text{A-203})$$

where σ_A and σ_B are the characteristic Lennard-Jones lengths of species A and B . The dimensionless parameter, Ω_D , represents the collision integral for mass diffusion and is a function of temperature. The value of Ω_D depends on the intermolecular force between the colliding molecules. The f_D parameter in Eq. (A-201) represents a correction term that is on the order of unity. According to Reid et al.,¹ f_D lies between 1.0 and 1.02 if Mw_A and Mw_B are of the same order. If one component has a much lower molecular weight than the other, then f_D could vary between 1.0 and 1.1.

Taking f_D as 1.0 and replacing the number density n^* with the ideal-gas law relationship, Eq. (A-201) becomes

$$\mathcal{D}_{AB} = \frac{0.00266T^{3/2}}{PMw_{AB}^{1/2}\sigma_{AB}^2\Omega_D} \quad (\text{A-204})$$

The \mathcal{D}_{AB} calculated from this equation is in cm^2/s , P is in bars, T in K, and σ_{AB} in Å.

Based on Neufeld et al.,⁴⁵ the dimensionless collision integral Ω_D can be calculated from

$$\Omega_D = \frac{A}{T^{*B}} + \frac{C}{\exp(DT^*)} + \frac{E}{\exp(FT^*)} + \frac{G}{\exp(HT^*)} \quad (\text{A-205})$$

where

$$T^* = \frac{kT}{\varepsilon_{AB}} \quad (\text{A-206})$$

The parameter ε_{AB} depends on the characteristic Lennard-Jones energies of species A and B (ε_A and ε_B), according to the following equation:

$$\varepsilon_{AB} = (\varepsilon_A \varepsilon_B)^{1/2} \quad (\text{A-207})$$

The constants in Eq. (A-205) are defined as follows¹:

$$\begin{aligned} A &= 1.06036 & B &= 0.15610 & C &= 0.19300 & D &= 0.47635 \\ E &= 1.03587 & F &= 1.52996 & G &= 1.76474 & H &= 3.89411 \end{aligned}$$

The procedure for evaluating the binary diffusivity, \mathcal{D}_{AB} , is to first determine σ_{AB} from Eq. (A-203). Next, evaluate ε_A and ε_B using the intermolecular potential function $\Psi(r)$, where r is the distance between the molecules. For example, the Lennard-Jones 12–16 potential given by Eq. (A-100) can be used for this purpose. A simpler way would be to look up the values of ε_A/k and ε_B/k in the tabulated Lennard-Jones potential for various gases in Table A-19, compiled by Svehla.⁹⁰ ε_{AB} and T^* can then be determined from Eqs. (A-207) and (A-206). With this information, Ω_D and \mathcal{D}_{AB} can be calculated from Eqs. (A-205) and (A-204).

Wilke and Lee's Method⁹¹ Chapman and Enskog's method was derived from Boltzmann's equation, based on the kinetic theory of gases and molecular structure. Wilke and Lee's method retains the general form of Chapman and Enskog's formulation with an empirical constant based on experimental data. Generally speaking, Wilke and Lee's method predicts more accurate results than Chapman and Enskog's, since it is based on both theoretical and experimental information.

$$\mathcal{D}_{AB} = \frac{\left[0.00303 - (0.00098/Mw_{AB}^{1/2})\right] T^{3/2}}{PMw_{AB}^{1/2} \sigma_{AB}^2 \Omega_D} \quad (\text{A-208})$$

where all the relationships and units for σ_{AB} , Mw_{AB} , and Ω_D are the same as in Chapman and Enskog's formulation, except that the Lennard-Jones characteristic lengths σ_A and σ_B and energies ε_A and ε_B are directly computed for both species A and B using

$$\sigma = 1.18 v_b^{1/3} \quad (\text{A-209})$$

$$\frac{\varepsilon}{k} = 1.15 T_b \quad (\text{A-210})$$

where v_b represents the liquid molar volume in cm^3/mol and can be found from experimental data or in Le Bas's volume increments of various substances tabulated in Reid et al.¹ T_b is the normal boiling point of the substance at 1 atm, measured in K. Note that although the above calculations concern *gas* diffusivity, v_b represents the *liquid* molar volume.

It is useful to note that both Eqs. (A-204) and (A-208) have an explicit temperature dependency of $T^{3/2}$. Since Ω_D is a temperature-dependent parameter, \mathcal{D}_{AB} is not strictly a function of $T^{3/2}$. Instead, it varies as $T^{3/2}$ to T^2 .

9.2 High-Pressure Correction

As shown by Eqs. (3-25), (A-204), and (A-208), the binary diffusion coefficients are inversely proportional to pressure at low to moderate pressures, up to 10 to 15 atm. At high pressures, the product of $\mathcal{D}_{AB} \cdot P$ is no longer constant but decreases with an increase in pressure. Takahashi⁹² proposed the following

Table A.19 Characteristic Lennard-Jones Lengths and Energies for Selected Substances⁹⁰

Substance		b_0^{\ddagger} cm ³ /g · mol	σ , Å	ε/k , K
Ar	Argon	56.08	3.542	93.3
He	Helium	20.95	2.551 [§]	10.22
Kr	Krypton	61.62	3.655	178.9
Ne	Neon	28.30	2.820	32.8
Xe	Xenon	83.66	4.047	231.0
Air	Air	64.50	3.711	78.6
BCl ₃	Boron chloride	170.1	5.127	337.7
BF ₃	Boron fluoride	93.35	4.198	186.3
B(OCH ₃) ₃	Methyl borate	210.3	5.503	396.7
Br ₂	Bromine	100.1	4.296	507.9
CCl ₄	Carbon tetrachloride	265.5	5.947	322.7
CF ₄	Carbon tetrafluoride	127.9	4.662	134.0
CHCl ₃	Chloroform	197.5	5.389	340.2
CH ₂ Cl ₂	Methylene chloride	148.3	4.898	356.3
CH ₃ Br	Methyl bromide	88.14	4.118	449.2
CH ₃ Cl	Methyl chloride	92.31	4.182	350
CH ₃ OH	Methanol	60.17	3.626	481.8
CH ₄	Methane	66.98	3.758	148.6
CO	Carbon monoxide	63.41	3.690	91.7
COS	Carbonyl sulfide	88.91	4.130	336.0
CO ₂	Carbon dioxide	77.25	3.941	195.2
CS ₂	Carbon disulfide	113.7	4.483	467
C ₂ H ₂	Acetylene	82.79	4.033	231.8
C ₂ H ₄	Ethylene	91.06	4.163	224.7
C ₂ H ₆	Ethane	110.7	4.443	215.7
C ₂ H ₅ Cl	Ethyl chloride	148.3	4.898	300
C ₂ H ₅ OH	Ethanol	117.3	4.530	362.6
C ₂ N ₂	Cyanogen	104.7	4.361	348.6
CH ₃ OCH ₃	Methyl ether	100.9	4.307	395.0
CH ₂ CHCH ₃	Propylene	129.2	4.678	298.9
C ₃ H ₆	Cyclopropane	140.2	4.807	248.9
C ₃ H ₈	Propane	169.2	5.118	237.1
n-C ₃ H ₇ OH	n-Propyl alcohol	118.8	4.549	576.7
CH ₃ COCH ₃	Acetone	122.8	4.600	560.2
CH ₃ COOCH ₃	Methyl acetate	151.8	4.936	469.8
n-C ₄ H ₁₀	n-Butane	130.0	4.687	531.4
iso-C ₄ H ₁₀	Isobutane	185.6	5.278	330.1
C ₂ H ₅ OC ₂ H ₅	Ethyl ether	231.0	5.678	313.8
CH ₃ COOC ₂ H ₅	Ethyl acetate	178.0	5.205	521.3
n-C ₅ H ₁₂	n-Pentane	244.2	5.784	341.1
C(CH ₃) ₄	2,2-Dimethylpropane	340.9	6.464	193.4
C ₆ H ₆	Benzene	193.2	5.349	412.3

(continued overleaf)

Table A.19 (continued)

Substance		$b_0, ^\ddagger$ cm ³ /g · mol	$\sigma, \text{Å}$	$\varepsilon/k, \text{K}$
C ₆ H ₁₂	Cyclohexane	298.2	6.182	297.1
n-C ₆ H ₁₄	n-Hexane	265.7	5.949	399.3
Cl ₂	Chlorine	94.65	4.217	316.0
F ₂	Fluorine	47.75	3357	112.6
HBr	Hydrogen bromide	47.58	3.353	449
HCN	Hydrogen cyanide	60.37	3.630	569.1
HCl	Hydrogen chloride	46.98	3.339	344.7
HF	Hydrogen fluoride	39.37	3.148	330
HI	Hydrogen iodide	94.24	4.211	288.7
H ₂	Hydrogen	28.51	2.827	59.7
H ₂ O	Water	23.25	2.641	809.1
H ₂ O ₂	Hydrogen peroxide	93.24	4.196	289.3
H ₂ S	Hydrogen sulfide	60.02	3.623	301.1
I ₂	Iodine	173.4	5.160	474.2
NH ₃	Ammonia	30.78	2.900	558.3
NO	Nitric oxide	53.74	3.492	116.7
NOCl	Nitrosyl chloride	87.75	4.112	395.3
N ₂	Nitrogen	69.14	3.798	71.4
N ₂ O	Nitrous oxide	70.80	3.828	232.4
O ₂	Oxygen	52.60	3.467	106.7
PH ₃	Phosphine	79.63	3.981	251.5
SF ₆	Sulfur hexafluoride	170.2	5.128	222.1
SO ₂	Sulfur dioxide	87.75	4.112	335.4
SiF ₄	Silicon tetrafluoride	146.7	4.880	171.9
SiH ₄	Silicon hydride	85.97	4.084	207.6

$^\ddagger b_0 = \frac{2}{3} \pi N_A \sigma^3$, where N_A is Avogadro's number.

§ The parameter σ was determined by quantum-mechanical formulas.

equation to correct for this effect.

$$\frac{\mathcal{D}_{AB} P}{(\mathcal{D}_{AB} P)_{lp}} = f(T_r, P_r) \quad (\text{A-211})$$

where the reduced temperature is calculated from the ratio of temperature to the average critical temperature, T_c ($T_r = T/T_c$). For a binary mixture, T_c can be evaluated from

$$T_c = X_A T_{cA} + X_B T_{cB} \quad (\text{A-212})$$

where X_A and X_B are the mole fractions of species A and B , respectively. A similar equation is used for calculating the critical pressure of the binary mixture, i.e.,

$$P_c = X_A P_{cA} + X_B P_{cB} \quad (\text{A-213})$$

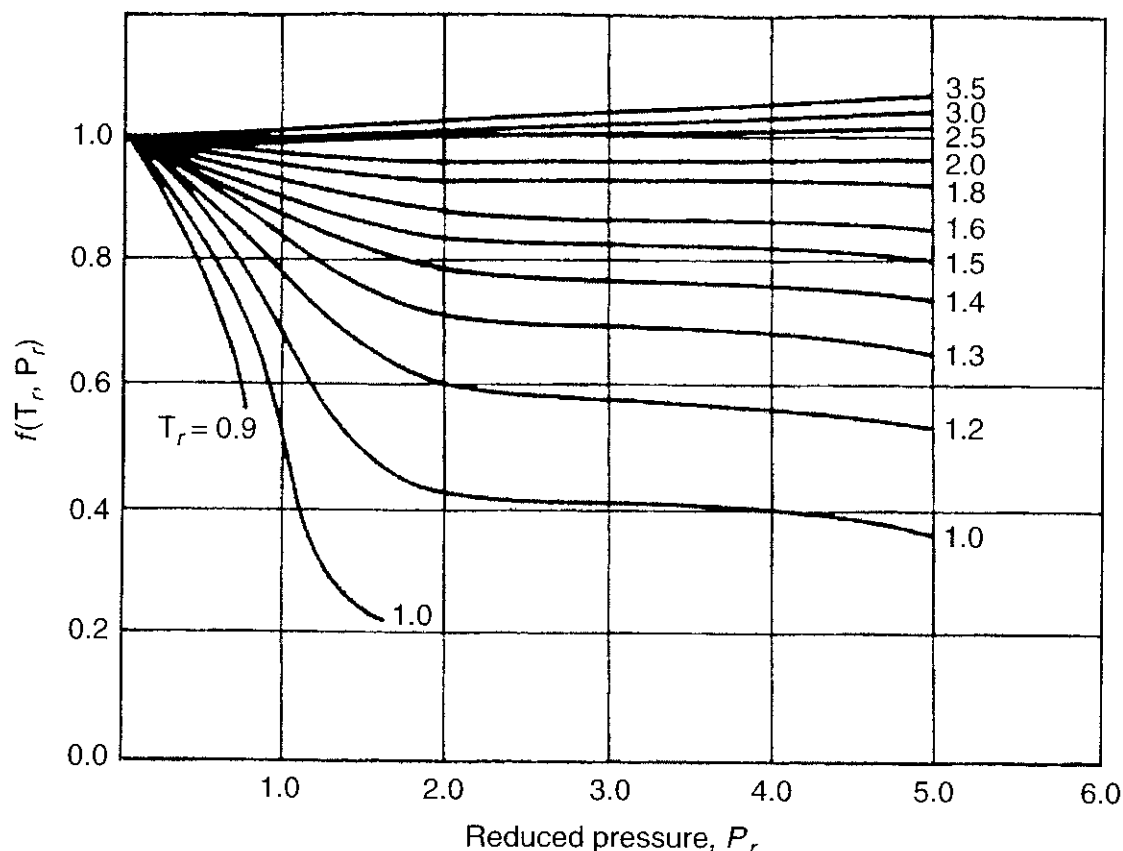


Figure A.1 Takahashi's correction function⁹² for the effect of pressure and temperature on binary diffusion coefficient.

The subscript “lp” in Eq. (A-211) corresponds to the low-pressure value. Usually, the low-pressure values of the product $\mathcal{D}_{AB} \cdot P$ are calculated at 1 atm. The high-pressure correction function $f(T_r, P_r)$ is given by Takahashi in Fig. A-1 in terms of reduced pressure and reduced temperature.

The deviation of binary diffusion coefficients obtained by Takahashi's high-pressure correction relationship from those observed experimentally is about 4% on the average for pressures up to 200 atm. Still, it seems to be a very reliable method at the present time for predicting the binary diffusion coefficients of gases at high-pressure conditions.

9.3 Mixing Rules

A simple formula was proposed by Wilke⁹³ to evaluate the diffusion coefficient in multicomponent gas mixtures. The equation was derived from the Stefan–Maxwell diffusion equation. The diffusion coefficient $\mathcal{D}_{A,m}$ of species A to the remaining mixture, containing B , C , D , and other species, is evaluated from

$$\mathcal{D}_{A,m} = \frac{1 - X_A}{\frac{X_B}{\mathcal{D}_{AB}} + \frac{X_C}{\mathcal{D}_{AC}} + \frac{X_D}{\mathcal{D}_{AD}} + \dots} \quad (\text{A-214})$$

where \mathcal{D}_{AB} , \mathcal{D}_{AC} , \mathcal{D}_{AD} , ... are the binary diffusion coefficients for AB , AC , AD , ..., respectively. Wilke's mixing rule for a mixture is valid for a broad range of pressure conditions. This is simply because each diffusion coefficient \mathcal{D}_{AB} , \mathcal{D}_{AC} , \mathcal{D}_{AD} , ... is corrected individually by using high-pressure correction before computing the effective diffusion coefficient from Wilke's mixing rule.

10 LIQUID DIFFUSIVITY

The diffusion coefficient is a necessary parameter to determine the mass transport due to concentration gradients within a liquid according to Fick's law. The diffusion coefficient for a liquid is typically much smaller than those for gases because the molecules in the liquid are strongly affected by the van der Waals forces of neighboring molecules.

In some cases, the basic relationships for transport properties can be derived from classical physics on a molecular basis or from quantum mechanics. A theoretical estimation of the liquid diffusion coefficient, based on an analysis of large spherical molecules diffusing in a dilute solution, is given by the Stokes–Einstein equation¹:

$$\mathcal{D}_{AB} = \frac{R_u T}{6\pi \mu_B r_A} \quad (\text{A-215})$$

where μ_B is the viscosity of the solvent and r_A is the radius of the spherical solute. This relation is not very accurate; however, its mathematical form can be utilized in developing empirical correlations. For engineering purposes, empirical correlations must be developed. However, experimental methods for determining \mathcal{D}_{AB} are, in general, difficult and often have low accuracy. Only very simplified cases can be determined accurately. These cases involve mainly binary systems with narrow temperature ranges operating at relatively low pressures in very dilute concentrations. Multicomponent mixtures must be limited to a dilute solute diffusing through a homogeneous solution of mixed solvents. Thus, correlations are usually only applicable within the above experimental restrictions. Unless otherwise noted, all correlations are limited to the following conditions: (1) binary mixtures, (2) at temperatures between 273 and 400 K, (3) at atmospheric pressures, (4) with solute concentrations up to 10% by mole, and (5) with negligible convective transport effects.

10.1 Baseline Method

In the following discussions, A is defined as the solute component and B as the solvent component.

Wilke–Chang Correlation⁹⁴ Wilke and Chang⁹⁴ found that solvent molecular weight correlated with most data successfully and suggested the following relationship:

$$\mathcal{D}_{AB} = 7.4 \times 10^{-8} \frac{(\Phi_B M_w B)^{1/2} T}{\mu_B v_A^{0.6}} \quad (\text{A-216})$$

where v_A is the molar volume of the solute, Φ_B is the dimensionless association factor of solvent B , and the product of ($\Phi_B M_B$) is the effective molecular weight of the solvent. After testing many associated solvents, Wilke and Chang determined the following values for the association factor for several commonly used solvents. The Φ_B values for water, methyl alcohol, ethyl alcohol, and nonassociated solvents were found to be 2.6, 1.9, 1.5, and 1.0, respectively.

Equation (A-216) provides acceptable results for many solute–solvent systems, with errors less than 15%. The Wilke–Chang correlation is useful for its generality, relative simplicity, and degree of success. It should not be used when water is the solute.

Tyn and Calus's Method⁹⁵ Tyn and Calus proposed an estimation method for D_{AB} based on the parachors of the solute and the solvent molecules. The parachor of a molecule can be regarded as an empirical constant associated with the surface tension and molecular volume of the molecule and is defined as

$$\mathbf{P} = v \cdot \sigma_s^{1/4} \quad (\text{A-217})$$

where σ_s is the surface tension of the liquid in (10^{-3} N/m²) and v is the molar volume in cm³/mol. Tyn and Calus believe that the parachor is closely related to the diffusion process due to its dependency on the surface tension of a liquid. Tabulations of \mathbf{P} are available for a large number of chemicals, some of which are listed in Ref. 1. The correlation suggested by Tyn and Calus is

$$D_{AB}^o = 8.93 \times 10^{-8} \left(\frac{v_A}{v_B^2} \right)^{1/6} \left(\frac{\mathbf{P}_B}{\mathbf{P}_A} \right)^{0.6} \frac{T}{\mu_B} \quad (\text{A-218})$$

Several additional restrictions apply for this correlation. First, the method should not be used for diffusion in solvents with viscosity greater than 20 cP. Also, if the solute is water, or if the solute is an organic acid and the solvent is not water, methanol, or butanol, the values of v_A and \mathbf{P}_A should be doubled. Finally, for nonpolar solutes diffusing into monohydroxy alcohols, the values of v_B and \mathbf{P}_B should be multiplied by a factor of $8\mu_B$, where μ_B is in cP.

The Tyn–Calus correlation provides an improvement in error over the Wilke–Chang method. The errors produced by this method are normally less than 10%. However, its application is more complex, and tabulations of \mathbf{P} , although extensive, are not complete. Therefore, a simplified version of Eq. (A-218) is useful for more general application. Rewriting Eq. (A-218) as

$$D_{AB}^o = 8.93 \times 10^{-8} \frac{v_B^{0.267}}{v_A^{0.433}} \left(\frac{\sigma_{s,B}}{\sigma_{s,A}} \right)^{0.15} \frac{T}{\mu_B} \quad (\text{A-219})$$

it can be seen that, since many organic liquids have similar values of σ_s and since the exponent on their ratio is very small, the term $(\sigma_{s,B}/\sigma_{s,A})^{0.15}$ can, to

a good approximation, be set to 1. This gives the following useful relation for organic liquids for which parachor data is not available.

$$\mathcal{D}_{AB}^o = 8.93 \times 10^{-8} \frac{v_B^{0.267}}{v_A^{0.433}} \frac{T}{\mu_B} \quad (\text{A-220})$$

Hayduk and Minhas's Method⁹⁶ Hayduk and Minhas performed regression analyses of available data to develop correlations for different solute/solvent systems. Equations for the systems they investigated are presented below. The same restrictions used in the Tyn and Calus correlations apply here.

For normal paraffin solutions:

$$\mathcal{D}_{AB}^o = 13.3 \times 10^{-8} \frac{T^{1.47} \mu_B^{(10.2/v_A)-0.791}}{v_A^{0.71}} \quad (\text{A-221})$$

This equation was developed for C5 to C32 paraffin solutes and C5 to C16 paraffin solvents and provides an average error of 3.4%.

For solutes in aqueous solutions:

$$\mathcal{D}_{AB}^o = 1.25 \times 10^{-8} (v_A^{-0.19} - 0.292) T^{1.52} \mu_w^{(9.58/v_A)-1.12} \quad (\text{A-222})$$

where μ_w is the viscosity of water. This equation provides an average error of about 10%.

For nonaqueous (nonelectrolyte) solutions:

$$\mathcal{D}_{AB}^o = 1.55 \times 10^{-8} \frac{T^{1.29}}{\mu_B^{0.92} v_B^{0.23}} \left(\frac{\mathbf{P}_B^{0.5}}{\mathbf{P}_A^{0.42}} \right) \quad (\text{A-223})$$

This equation provides an average error of about 14%.

The only significant improvement of the Hayduk–Minhas correlations over the Tyn–Calus correlations is the large reduction in error involved in calculations for diffusion in normal paraffins.

Tyn's Method for Higher Temperatures⁹⁷ The previous relations are accurate only over a small range of temperatures. Tyn suggests a correlation that allows the determination of \mathcal{D}_{AB} over the temperature range from 10 K above solvent freezing temperature to 10 K below solvent boiling temperature. This correlation is as follows:

$$\frac{\mathcal{D}_{AB}^o(T_2)}{\mathcal{D}_{AB}^o(T_1)} = \left(\frac{T_c - T_1}{T_c - T_2} \right)^n \quad (\text{A-224})$$

where T_c is the critical temperature of the solvent and n is an exponent depending on the heat of vaporization of the solvent at T_b according to the following table.¹

N	3	4	6	8	10
Heat of vaporization of solvent at T_b , J/mol	7,900 to 30,000	30,000 to 39,700	39,700 to 46,000	46,000 to 50,000	>50,000

This correlation was tested for a number of binary systems, producing an average error of about 9%.

10.2 High-Pressure Correction

Unfortunately, the effect of system pressure on liquid diffusion coefficients has not been studied sufficiently to produce useful correlations. Easteal⁹⁸ studied the pressure dependency of diffusion coefficients based on dilute solutions. The following equation was proposed:

$$\ln \mathcal{D}_j^o = a + b P^{0.75} \quad (\text{A-225})$$

where \mathcal{D}_j^o is the tracer mass diffusivity and a and b are constants for a given solute. Both a and b are functions of temperature. The value of b is negative since diffusivity decreases as pressure increases.

At constant temperature conditions, Eq. (A-215) can be reduced to

$$\mathcal{D}_{AB}^o = \frac{\text{constant}}{\mu_B} \quad (\text{A-226})$$

If the solvent viscosity data at high pressures are available, one could use the above relationship and the low-pressure diffusivity-viscosity data to estimate the diffusivity at elevated pressures.

10.3 Mixing Rules

The diffusion of a solute or multiple solutes in a mixture of solvents is much more complex than the simple binary case. The flux of a component depends on the gradients of all other components in the mixture. No simple correlation methods are available for the general multicomponent case. However, correlations are available for some specific cases.

Perkins and Geankoplis's Method⁹⁹ One important case of multicomponent diffusion is when a dilute solute diffuses through a homogeneous solution of mixed solvents. In this case, no concentration gradients of the solvent species exist, and a single solute diffusivity with respect to the mixture, $\mathcal{D}_{A,m}$, can be

considered. Perkins and Geankoplis proposed the best and most simplistic correlation for this system.

$$\mathcal{D}_{A,m}^o \mu_m^{0.8} = X_B \mathcal{D}_{AB}^o \mu_B^{0.8} + X_C \mathcal{D}_{AC}^o \mu_C^{0.8} \quad (\text{A-227})$$

This was tested on eight ternary systems and provided an average error of less than 10%. Cases involving the CO₂ solute have the worst errors, with the worst system being CO₂ in an ethanol/water mixture providing 22% error. This equation may be extended to larger systems using the following relation, which has not been extensively tested on systems with more than three components.

$$\mathcal{D}_{A,m}^o \mu_m^{0.8} = \sum_{\substack{j=1 \\ j \neq A}}^n X_j \mathcal{D}_{Aj}^o \mu_j^{0.8} \quad (\text{A-228})$$

Perkins and Geankoplis also suggest modifying the Wilke–Chang correlation [Eq. (A-216)] to handle multicomponent systems using the following equation:

$$\mathcal{D}_{A,m} = 7.4 \times 10^{-8} \frac{(\Phi M_w)^{1/2} T}{\mu_m v_A^{0.6}} \quad (\text{A-229})$$

where the product (ΦM) can be evaluated using the following equation:

$$\Phi M_w = \sum_{\substack{j=1 \\ j \neq A}}^n X_j \Phi_j M_w_j \quad (\text{A-230})$$

where j represents the index for solvents in the mixture. So far, more experimental verifications of this method are required.

REFERENCES

1. R. C. Reid, J. M. Prausnitz, and B. E. Poling, *The Properties of Gases and Liquids*, 4th ed., McGraw Hill, 1987.
2. G. J. Van Wylen and R. E. Sonntag, *Fundamentals of Classical Thermodynamics*, 3rd ed., John Wiley, Inc., 1985.
3. R. H. Perry and D. W. Green, *Perry's Chemical Engineers' Handbook*, 6th ed., McGraw Hill Book Co., 1984.
4. C. F. Spencer and R. P. Danner, "Improved Equation for Prediction of Saturated Liquid Density," *J. Chem. Eng. Data* **17**, 236–249 (1972).
5. L. C. Yen and S. S. Woods, "A Generalized Equation for Computer Calculation of Liquid Densities," *A. I. Ch. E. Journal* **12**, 95–99 (1966).
6. R. D. Gunn and T. Yamada, "A Corresponding States Correlation of Saturated Liquid Volumes," *A. I. Ch. E. Journal* **17**, 1341–1345 (1971).

7. H. G. Rackett, "Equation of State for Saturated Liquids," *J. Chem. Eng. Data* **15**, 514–520 (1970).
8. S. W. Campbell and G. Thodos, *J. Chem. Eng. Data* **30**, 102 (1985).
9. C. H. Chang and X. Zhao, *Fluid Phase Equilibria* **58**, 231–238 (1990).
10. R. W. Hankinson and G. H. Thomson, "A New Correlation for Saturated Densities of Liquids and Their Mixtures," *A. I. Ch. E. Journal* **25**, 653–663 (1979).
11. G. H. Thomson, K. R. Brobst, and R. W. Hankinson, "An Improved Correlation for Densities of Compressed Liquids and Liquid Mixtures," *A. I. Ch. E. Journal* **28**, 671–676 (1982).
12. M. Aalto, K. I. Keskinen, J. Aittamaa and S. Liukkonen, "An Improved Correlation for Compressed Liquid Densities of Hydrocarbons Part 1: Pure Compounds," *Fluid Phase Equilibria*, **114**, 1–19 (1996).
13. M. Aalto, K. I. Keskinen, J. Aittamaa and S. Liukkonen, "An Improved Correlation for Compressed Liquid Densities of Hydrocarbons Part 2: Mixtures," *Fluid Phase Equilibria*, **114**, 21–35 (1996).
14. T. E. Daubert and R. P. Danner, *Physical and Thermodynamic Properties of Pure Chemicals*, Hemisphere Publishing Corporation, New York, 1989.
15. T. S. Touloukian and C. Y. Ho, Eds., *Thermophysical Properties of Matter*, (13 Vols.), IFI/Plenum, New York, 1970.
16. Matheson Company, Inc., *Matheson Gas Data Book*, unabridged edition, 4 Vols., East Rutherford, New Jersey, 1974.
17. Thermodynamic Research Center, *TRC Thermodynamic Tables—Hydrocarbons*, Texas A&M University System, College Station, TX, 1985.
18. B. J. McBride, S. Heimel, J. G. Ehlers, and S. Gordon, *Thermodynamic Properties to 6000 K for 210 Substances Involving the First 18 Elements*, Office of Scientific and Technical Services, NASA, Washington, D. C., 1963.
19. JANNAF Thermochemical Tables, 1982 Supplement, *J. Phys. Chem. Ref. Data*, **11**, 3, 695 (1985).
20. Thermodynamics Research Center, *TRC Thermodynamic Tables—Nonhydrocarbons*, Texas A&M University System, College Station, TX, 1985.
21. D. R. Stull, E. F. Westrum, Jr., and G. C. Sinke, *The Chemical Thermodynamics of Organic Compounds*, John Wiley & Sons, New York, 1969.
22. D. D. Wagman, W. H. Evans, V. B. Parker, I. Halow, S. M. Bailey, and R. H. Schumm, *Selected Values of Chemical Thermodynamic Properties*, National Bureau of Standards and Technical Note 270–3, Washington, D. C., 1968.
23. W. G. Vinceti and C. H. Kruger, Jr., *Introduction to Physical Gas Dynamics*, Krieger Publishing Company, Malabar, 1965.
24. K. A. Kobe et al., "Thermochemistry of Petrochemicals," Petroleum Refiner, Gulf Publishing, Houston, reprint, Jan. 1949–July 1958.
25. Technical Data Book, Amer. Pet. Inst., Washington, D. C., 1983.
26. T.-P. Thinh and T. K. Trong, *Can. J. Chem. Eng.*, **54**, 344 (1976).
27. B. I. Lee and M. G. Kesler, "A Generalized Thermodynamic Correlation Based on Three-Parameter Corresponding States," *A. I. Ch. E. Journal*, **21**, No. 3, 510 (1975).
28. K. S. Pitzer, *J. Am. Chem. Soc.*, **77**, 3427 (1955).
29. K. S. Pitzer and R. F. Curl, *J. Am. Chem. Soc.*, **79**, 2369 (1957).

30. K. S. Pitzer, D. Z. Lippman, R. F. Curl, C. M. Huggins, and D. E. Peterson, *J. Am. Chem. Soc.*, **77**, 3433 (1955).
31. M. Benedict, G. B. Webb, and L. C. Rubin, "An Empirical Equation for Thermodynamic Properties of Light Hydrocarbons and Their Mixtures," *J. Chem. Phys.*, **8**, 334 (1940).
32. J. L. Jones, Jr., D. T. Mage, R. C. Faulkner, Jr., and L. D. Katz, "Measurement of the Thermodynamic Properties of Gases at Low Temperature and High Pressure-Methane," *Chem. Eng. Prog. Symp. Er.* **44**, 59, 52 (1963).
33. V. F. Yesavage, D. L. Katz, and J. E. Powers, "Experimental Determination of Some Thermal Properties of Propane: Heat Capacity, Joule-Thomson Coefficient and Latent Heat of Vaporization," *Proc. 4th Symp. on Thermophysical Properties*, ASME, New York, 1968.
34. V. V. Sychev, A. A. Vasserman, A. D. Kozlov, G. A. Spiridonov, and V. A. Tsymarny, "Density, Enthalpy, Entropy and Isobaric Heat Capacity of Liquid and Gaseous Air for Temperatures of 70–1500 K and Pressures of 0.1–100 MPa," *Property Data Update*, **1**, 215–226 (1987).
35. V. V. Sychev, A. A. Vasserman, A. D. Kozlov, G. A. Spiridonov, and V. A. Tsymarny, "Density, Enthalpy, Entropy and Isobaric Heat Capacity of Liquid and Gaseous Air for Temperatures of 70–1500 K and Pressures of 0.1–100 MPa," *Property Data Update*, **1**, 7–20 (1987).
36. V. V. Sychev, A. A. Vasserman, A. D. Kozlov, G. A. Spiridonov, and V. A. Tsymarny, "Density, Enthalpy, Entropy and Isobaric Heat Capacity of Liquid and Gaseous Air for Temperatures of 70–1500 K and Pressures of 0.1–100 MPa," *Property Data Update*, **1**, 527–538 (1987).
37. U. Plocker, H. Knapp, and J. M. Prausnitz, *Ind. Eng. Chem. Process Design Develop.* **17**, 324 (1978).
38. C. F. Chueh and A. C. Swanson, (a) *Chem. Eng. Progr.*, **69**(7), 83 (1973); (b) *Can. J. Chem. Eng.*, **51**, 596 (1973).
39. F. A. Missenard, *C. R.*, **260**, 5521 (1965).
40. W. S. Tamplin and Zuzic, *Hydrocarbon Process. Petrol. Refiner*, **46**(8), 145 (1967).
41. J. S. Rowlinson, *Liquids and Liquid Mixtures*, 2nd ed., Butterworth, London, 1969.
42. A. Bondi, "Estimation of the Heat Capacity of Liquids," *Ind. Eng. Chem. Fundam.*, **5**, 442–469 (1966).
43. S. Chapman and T. G. Cowling, *The Mathematical Theory of Non-uniform Gases*, Cambridge University Press, New York, 1939.
44. J. O. Hirschfelder, C. F. Curtiss, and R. B. Bird, *Molecular Theory of Gases and Liquids*, Wiley, New York, 1954.
45. P. D. Neufeld, A. R. Janzen, and R. A. Aziz, *Journal of Chemical Physics*, **57**, 1100 (1972).
46. T.-H. Chung, L. L. Lee, and K. E. Starling, *Ind. Engr. Chem. Fundam.*, **23**, 8 (1984).
47. D. Reichenberg, (a) DCS report 11, National Physical Laboratory, Teddington, England, August 1971; (b) *A. I. Ch. E. J.*, **19**, 854 (1973); (c) *ibid.*, **21**, 181 (1975).
48. K. Lucas, *Chem. Engr. Tech.*, **53**, 959 (1981).
49. P. Yoon and G. Thodos, *A. I. Ch. E. Journal* **16**, 300 (1970).
50. F. Herning and L. Zipperer, *Gas Wasserfach* **79**, 49 (1936).

51. C. R. Wilke, *Journal Chem. Phys.*, **18**, 517 (1950).
52. D. Reichenberg, "New Simplified Methods for the Estimation of the Viscosities of Gas Mixtures at Moderate Pressures," Natl. Eng. Lab. Report Chem. 53, East Kilbride, Glasgow, Scotland, May 1977.
53. K. Lucas, "Phase Equilibria, and Fluid Properties in the Chemical Industry," *Review of Present Status of Transport Properties Predictions*, Dechema, Frankfurt, 573–587, 1980.
54. E. N. da C. Andrade, *Nature*, **125**, 309 (1930).
55. J. de Guzman, *Anales Soc. Espan. Fia. y Quim.*, **11**, 353 (1913).
56. D. van Velzen, R. L. Cardozo, and H. Langenkamp, "Liquid Viscosity and Chemical Constitution of Organic Compounds: A New Correlation and a Compilation of Literature Data." Euratom, 4735e, Joint Nuclear Research Centre, Ispra Establishment, Italy, 1972.
57. C. L. Yaws, J. W. Miller, P. N. Shah, G. R. Schorr, and P. M. Patel, *Chemical Engineering*, **83**(25), 153 (1976).
58. E. Goletz and D. Tassios: *Ind. Eng. Chem. Process Design Develop.*, **16**, 75 (1977).
59. H. Vogel, *Physik Z.*, **22**, 645 (1921).
60. C. R. Duhne, *Chem. Eng.*, **86**(15), 83 (1979).
61. H. W. Xiang, Y. Y. Duan, and M. S. Zhu, *Fluid Phase Equilibria*, **135**(2), (1997).
62. D. van Velzen, R. L. Cardozo, and H. Langenkamp, *Ind. Eng. Chem. Fundam.*, **11**, 20 (1972).
63. J. W. Przezdziecki and T. Sridhar, *A. I. Ch. E. Journal*, **31**, 333 (1985).
64. J. H. Hildebrand, *Science* **174**, 490 (1971).
65. R. D. Gunn and T. Yamada, *A. I. Ch. E. Journal*, **17**, 1341 (1971).
66. M. Luckas and K. Lucas, *A. I. Ch. E. Journal*, **32**, 139 (1986).
67. A. Letsou and L. I. Stiel, *A. I. Ch. E. Journal*, **19**, 409 (1973).
68. M. R. Brule and K. E. Starling, *Ind. Eng. Chem. Process Design Develop.*, **23**, 833 (1984).
69. T. H. Chung, M. Ajlan, L. L. Lee, and K. E. Starling, *Ind. Eng. Chem. Research*, **27**(4), 671–679 (1988).
70. P. W. Bridgman, *Proc. Am. Acad. Arts Sci.*, **61**, 57 (1926).
71. L. Grunberg and A. H. Nissan, *Nature*, **164**, 799 (1949).
72. J. D. Isdale, Symp. Transp. Prop. Fluids and Fluid Mixtures, Natl. Eng. Lab., East Kilbride, Glasgow, Scotland, 1979.
73. J. D. Isdale, J. C. MacGillivray, and G. Cartwright, "Prediction of Viscosity of Organic Liquid Mixtures by a Group Contribution Method," Natl. Eng. Lab. Rept., East Kilbride, Glasgow, Scotland, 1985.
74. A. S. Teja and P. Rice, *Chem. Eng. Sci.*, **36**, 7 (1981).
75. A. S. Teja, *A. I. Ch. E. Journal*, **26**, 337 (1980).
76. T. E. Daubert and R. P. Danner, *Physical and Thermodynamic Properties of Pure Chemicals: Data Compilation*, Hemisphere Publishing Corp., New York, 1989.
77. S. Gordon, B. J. McBride, and F. J. Zeleznik, "Computer Program for Calculation of Complex Chemical Equilibrium Compositions and Application: Supplement 1—Transportation Properties," NASA TM 86885, 1984.

78. S. Gordon and B. J. McBride, "Computer Program for Calculation of Complex Chemical Equilibrium Compositions and Applications, I. Analysis," NASA Ref. Pub. 1311, Oct. 1994.
79. B. J. McBride and S. Gordon, "Computer Program for Calculation of Complex Chemical Equilibrium Compositions and Applications, II. Users Manual and Program Description," NASA Ref. Pub. 1311, Jun. 1996.
80. L. I. Stiel and G. Thodos, "The Thermal Conductivity of Non-polar Substances in the Dense Gases and Liquids Region," *A. I. Ch. E. Journal*, **10**, 1, 26 (1964).
81. A. Wassiljewa, *Physik, Z.*, **5**, 137 (1904).
82. E. A. Mason and S. C. Saxena, *Phys. Fluids*, **1**: 361 (1958).
83. R. S. Brokaw, "Thermal Conductivity of Gas Mixtures in Chemical Equilibrium," *Journal of Chemical Physics*, **32**, 4, 1005–1006 (1960).
84. M. Yorizane, S. Yoshimura, H. Masuoka, and H. Yoshida, "Thermal Conductivities of Binary Gas Mixtures at High Pressure: N₂-O₂, N₂-Ar, CO₂-Ar and CO₂-CH₄," *Industrial and Engineering Chemistry Fundamentals*, **22**, 4, 458 (1983).
85. N. V. Tsederberg, *Thermal Conductivity of Gases and Liquids*, The M. I. T. Press, Cambridge, Massachusetts, 1965.
86. J. M. Miller, Jr., J. J. McGinley, and C. L. Yaws, "Thermal Conductivities of Liquids," *Chemical Engineering*, **83**, 23, 133 (1976).
87. C. Baroncini, F. Difilippo, G. Latini, and M. Pacetti, "Organic Liquid Thermal Conductivity: A Prediction Method in the Reduced Temperature Range 0.3 to 0.8," *International Journal of Thermophysics* **2**, 1, 21 (1981).
88. A. Missenard, *Review of General Thermodynamics*, **101** 5, 649 (1970).
89. C. C. Li, "Thermal Conductivity of Liquid Mixtures," *A. I. Ch. E. Journal*, **22**, 5, 927 (1976).
90. R. A. Svehla, NASA Technical Report R-132, Lewis Research Center, Cleveland, OH, 1962.
91. C. R. Wilke and C. Y. Lee, "Estimation of Diffusion Coefficients for Gases and Vapors," *Ind. Eng. Chem.*, **47**, 1253–1257 (1955).
92. S. Takahashi, "Preparation of a Generalized Chart for Diffusion Coefficients of Gases at High Pressures," *J. Chem. Eng. Japan*, **7**, 417–420 (1974).
93. C. R. Wilke, "Diffusion Properties of Multicomponent Gases," *Chemical Engineering Progress*, **46** (2), 95–104 (1950).
94. C. R. Wilke and P. Chang, "Correlation of Diffusion Coefficients in Dilute Solutions," *A. I. Ch. E. Journal*, **1**, 264–270 (1955).
95. M. T. Tyn and W. F. Calus, *J. Chem. Eng. Data*, **20**, 106 (1975).
96. W. Hayduk and B. S. Minhas, "Correlations for Prediction of Molecular Diffusivities in Liquids," *The Canadian Journal of Chemical Engineering*, **60**, 295–299 (1982).
97. M. T. Tyn, *Trans. Inst. Chem. Engrs.*, **59**, 2, 112 (1981).
98. A. J. Easteal, *A. I. Ch. E. Journal*, **30**, 641 (1984).
99. L. R. Perkins and C. J. Geankoplis, "Molecular Diffusion in a Ternary Liquid System with the Diffusing Component Dilute," *Chemical Engineering Science*, **24**, 1035–1042 (1969).

APPENDIX **B**

CONSTANTS AND CONVERSION FACTORS OFTEN USED IN COMBUSTION

Universal Gas Constant

$$\begin{aligned} R_u &= 8.3144 \frac{\text{kJ}}{\text{kmole} \cdot \text{K}} = 1545.4 \frac{\text{ft-lb}_f}{\text{lb}_m\text{-mole} \cdot {}^\circ\text{R}} = 1.9872 \frac{\text{Btu}}{\text{lb}_m\text{-mole} \cdot {}^\circ\text{R}} \\ &= 1.9872 \frac{\text{cal}}{\text{g-mole} \cdot \text{K}} = 0.08206 \frac{\text{atm} \cdot \text{liter}}{\text{g-mole} \cdot \text{K}} = 8.3144 \times 10^7 \frac{\text{erg}}{\text{g-mole} \cdot \text{K}} \\ &= 83.144 \frac{\text{bar} \cdot \text{cm}^3}{\text{mole} \cdot \text{K}} = 82.057 \frac{\text{atm} \cdot \text{cm}^3}{\text{g-mole} \cdot \text{K}} = 84,786.85 \frac{\text{g}_f \cdot \text{cm}}{\text{g-mole} \cdot \text{K}} \\ &= 0.729 \frac{\text{atm} \cdot \text{ft}^3}{\text{lb}_m\text{-mole} \cdot {}^\circ\text{R}} = 10.716 \frac{\text{psi} \cdot \text{ft}^3}{\text{lb}_m\text{-mole} \cdot {}^\circ\text{R}} = 8.3144 \frac{\text{J}}{\text{g-mole} \cdot \text{K}} \end{aligned}$$

Dimensional Conversion Factor of Gravity

$$\begin{aligned} g_c &= 32.174 \frac{\text{lb}_m \cdot \text{ft}}{\text{lb}_f \cdot \text{s}^2} = 1 \frac{\text{g} \cdot \text{cm}}{\text{dyne} \cdot \text{s}^2} = 1 \frac{\text{kg}_m \cdot \text{m}}{\text{N} \cdot \text{s}^2} \\ &= 1 \frac{\text{slug} \cdot \text{ft}}{\text{lb}_f \cdot \text{s}^2} = 980.665 \frac{\text{g} \cdot \text{cm}}{\text{g}_f \cdot \text{s}^2} = 9.80665 \frac{\text{kg}_m \cdot \text{m}}{\text{kg}_f \cdot \text{s}^2} \end{aligned}$$

Gravitational Acceleration

$$g = 9.80665 \text{ m/s}^2 = 32.17405 \text{ ft/s}^2$$

Avagadro's Number:

$$N_A = 6.02252 \times 10^{23} \frac{\text{molecules}}{\text{g-mole}}$$

Planck's Constant:

$$h = 6.625 \times 10^{-34} \frac{\text{J} \cdot \text{s}}{\text{molecule}}$$

Stefan-Boltzmann Constant:

$$\begin{aligned}\sigma &= 5.6699 \times 10^{-8} \frac{\text{W}}{\text{m}^2 \cdot \text{K}^4} = 5.6699 \times 10^{-5} \frac{\text{erg}}{\text{cm}^2 \cdot \text{s} \cdot \text{K}^4} \\ &= 0.1714 \times 10^{-8} \frac{\text{Btu}}{\text{ft}^2 \cdot \text{hr} \cdot {}^\circ\text{R}^4} = 1.35514 \times 10^{-12} \frac{\text{cal}}{\text{cm}^2 \cdot \text{s} \cdot \text{K}^4}\end{aligned}$$

Boltzmann's Constant:

$$k = 1.38 \times 10^{-23} \frac{\text{J}}{\text{K} \cdot \text{molecule}}$$

Atomic Mass Unit:

$$m_a = 1.660540 \times 10^{-27} \text{ kg}$$

Proton Mass:

$$m_p = 1.672623 \times 10^{-27} \text{ kg}$$

Electron Mass:

$$m_e = 9.109389 \times 10^{-31} \text{ kg}$$

Electron Charge:

$$e = 1.602177 \times 10^{-19} \text{ coulombs}$$

Speed of Light:

$$c = 2.997925 \times 10^8 \text{ m/s}$$

Work/Energy Conversion Factor:

$$J = 778 \frac{\text{ft-lb}_f}{\text{Btu}} = 42,664.9 \frac{\text{g}_f \cdot \text{cm}}{\text{cal}}$$

Mass Units:

$$1\text{kg} = 2.2046226 \text{ lb}_m$$

$$1 \text{ ton (short)} = 2000 \text{ lb}_m = 907.185 \text{ kg},$$

$$1 \text{ ton (long)} = 2240 \text{ lb}_m = 1.016 \text{ metric ton}$$

$$1 \text{ ton (metric)} = 1000 \text{ kg} = 2204.62 \text{ lb}_m$$

Energy Units:

$$1 \text{ cal} = 4.18400 \text{ J} = 4.184 \times 10^7 \text{ erg} = 0.003968 \text{ Btu}$$

$$1 \text{ J} = 1 \text{ N} \cdot \text{m} = 1 \text{ W} \cdot \text{s} = 10^7 \text{ erg} = 0.737562 \text{ lb}_f \cdot \text{ft}$$

Pressure Units:

$$\begin{aligned} 1 \text{ Pascal (Pa)} &= 1 \text{ N/m}^2 = 1.4504 \times 10^{-4} \text{ psi} = 9.8692 \times 10^{-6} \text{ atm} \\ &= 1.0197 \times 10^{-5} \text{ kg}_f/\text{cm}^2 \end{aligned}$$

$$1 \text{ atm} = 1.01325 \times 10^5 \text{ N/m}^2 = 176 \text{ mmHg} = 760 \text{ Torr}$$

$$1 \text{ bar} = 10^5 \text{ N/m}^2 = 0.1 \text{ MPa}$$

$$1 \text{ psi} = 0.0689476 \text{ bars} = 0.00689476 \text{ MPa}$$

Temperature Units:

$$T(\text{K}) = T(\text{R})/1.8$$

$$T(\text{F}) = T(\text{R}) - 459.67$$

$$T(\text{°C}) = \frac{T(\text{°F}) - 32}{1.8} = T(\text{K}) - 273.15$$

For temperature difference, ΔT , $1 \text{ K} = 1 \text{ °C} = 1.8 \text{ R} = 1.8 \text{ °F}$

Force Units:

$$1 \text{ N} = 1 \text{ kg}_m \cdot \text{m/s}^2 = 100,000 \text{ dynes} = 0.2248089 \text{ lb}_f = 0.10197162 \text{ kg}_f$$

Length Units:

$$1 \text{ m} = 39.370079 \text{ inches (in.)} = 3.2808399 \text{ ft} = 1.0936133 \text{ yard}$$

$$1 \text{ m} = 100 \text{ cm} = 1 \times 10^6 \mu\text{m} = 1 \times 10^{10} \text{ Ångströms}$$

Velocity Units:

$$1 \text{ m/s} = 3.6 \text{ km/hr} = 3.28084 \text{ ft/s} = 2.23694 \text{ miles/hr}$$

Specific Volume Units:

$$1 \text{ m}^3/\text{kg} = 16.01846 \text{ ft}^3/\text{lb}_m$$

$$1 \text{ cm}^3/\text{g} = 1 \text{ L/kg}$$

Density Units:

$$1 \text{ kg/m}^3 = 0.06242797 \text{ lb}_m/\text{ft}^3$$

Thermal Conductivity Units:

$$1 \text{ W/m} \cdot \text{K} = 1 \text{ J/s} \cdot \text{m} \cdot \text{K} = 0.577789 \text{ Btu/hr} \cdot \text{ft} \cdot \text{R}$$

Heat Flux Units:

$$1 \text{ W/m}^2 = 0.316998 \text{ Btu/hr} \cdot \text{ft}^2$$

Heat Capacity or Specific Entropy Units:

$$1 \text{ kJ/kg} \cdot \text{K} = 0.238846 \text{ Btu/lb}_m \cdot \text{R}$$

Heat Transfer Coefficient Units:

$$1 \text{ W/m}^2 \cdot \text{K} = 0.17611 \text{ Btu/hr} \cdot \text{ft}^2 \cdot \text{R}$$

Viscosity Units:

$$1 \text{ centipoise} = 0.001 \text{ N} \cdot \text{s/m}^2$$

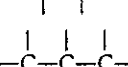
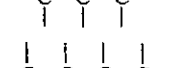
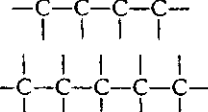
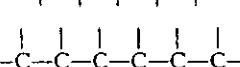
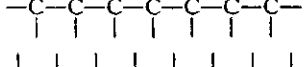
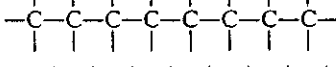
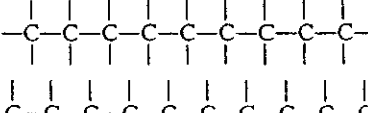
Prefixes:

10^{18}	exa	E
10^{15}	peta	P
10^{12}	tera	T
10^9	giga	G
10^6	mega	M
10^3	kilo	k
10^2	hecto	h
10^1	deka	da
10^{-1}	deci	d
10^{-2}	centi	c
10^{-3}	milli	m
10^{-6}	micro	μ
10^{-9}	nano	n
10^{-12}	pico	p
10^{-15}	femto	f
10^{-18}	atto	a

APPENDIX C

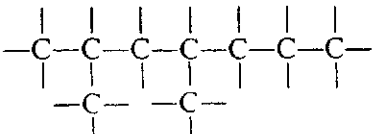
NAMING OF HYDROCARBONS AND PROPERTIES OF HYDROCARBON FUELS

Table C.1 The First 10 Saturated Straight-Chain Hydrocarbons

	methane	from Greek "wood"		
	ethane	from Greek "to burn"		
	propane	from Greek "fat"		
	<i>n</i> -butane	from Latin "butter"		
	<i>n</i> -pentane	penta	five	pentagon
	<i>n</i> -hexane	hexa	six	hexagon
	<i>n</i> -heptane	hepta	seven	
	<i>n</i> -octane	octa	eight	octopus, octave
	<i>n</i> -nonane	nona	nine	
	<i>n</i> -decane	deca	ten	decade

The first 10 saturated straight-chain hydrocarbons

Table C.2 Name of Chain, Group, and Multipliers

Example	Naming Organic Hydrocarbons			
	Number, <i>n</i>	Name of Chain with <i>n</i> Carbon Atoms	Name of Group with <i>n</i> Carbon Atoms	Multiplier*
	1	methane	methyl	mono (rarely used)
	2	ethane	ethyl	di
	3	propane	propyl	tri
	4	<i>n</i> -butane	butyl	tetra
	5	<i>n</i> -pentane	pentyl	penta
	6	<i>n</i> -hexane	hexyl	hexa
	7	<i>n</i> -heptane	heptyl	hepta
	8	<i>n</i> -octane	octyl	octa
	9	<i>n</i> -nonane	nonyl	nona
	10	<i>n</i> -decane	decyl	deca

where

how many

what

main chain

main chain

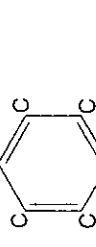
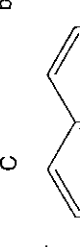
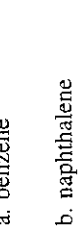
group name

multiplier of group name

position of groups

*Multipliers can be used with any group—not just the one with the same value of *n*. Thus, tetramethyl and dihexyl are valid parts of names.

Table C.3 Families of Organic Compounds and Special Function Groups

	Alkanes	Alkenes	Alkynes	Aromatics	Toluenes	Alcohols	Esters	Amines	Aldehydes	Ketones	Carboxylic Acids
Specific Examples	a. $\text{CH}_3 - \text{CH}_3$ $\text{CH}_2 = \text{CH}_2$	a. $\text{CH}_2 = \text{CH}_3$	a. $\text{HC} = \text{CH}$ $\text{CH}_3\text{CH} = \text{CHCH}_3$	a. 	a. CH_3 	a. CH_3OH	a. $\text{C}_3\text{H}_6\text{O}_2$	a. CH_3NH_2	a. O 	a. O 	a. CH_3COH
IUPAC*	a. ethane	a. ethene	ethyne	a. benzene	a. toluene	a. methanol	a. methyl acetate	a. formaldehyde	a. ethanoic acid	a. acetic acid	a. ethanoic acid
Name	b. propane	b. 2-butene		b. naphthalene	b. trinitro toluene	b. ethanol	b. ethyl acetate	b. ethylamine	b. ethanal	b. acetone	b. benzoic acid
Common Name	a. ethane	a. ethene	acetylene	a. benzene	a. toluene	a. methyl alcohol	a. methyl acetate	a. methylamine	a. formaldehyde	a. acetic acid	a. benzoic acid
	b. propane	b. 2-butene		b. naphthalene	b. TNT	b. ethyl alcohol	b. ethyl acetate	b. ethylamine	b. acetaldehyde		
	c. 1, 3-butadiene										
	c. 1, 2-butadiene										

(continued overleaf)

Table C.3 (continued)

General Formula	Alkanes	Alkenes	Alkynes	Aromatics	Toluenes	Alcohols	Esters	Amines	Aldehydes	Ketones	Carboxylic Acids
C_nH_{2n+2}	C_nH_{2n}	C_nH_{2n-2}	a. C_6H_6 b. $C_{10}H_8$	a. C_7H_8 b. $C_7H_5N_3O_6$	a. CH_3OH b. C_2H_5OH	a. CH_3COH b. CH_3COCH_3	a. CH_3NH_2 b. $C_2H_5NH_2$	a. $HCHO$ b. CH_3CHO	CH_3COOH	a. CH_3COOH b. C_6H_5COOH	
Formula a. $n = 2$ b. $n = 3$											
Using Remaining Species (R) and Functional Groups											
Functional Group	Single C-H bonds & Single C-C bonds										

*IUPAC = International Union of Pure and Applied Chemistry.

Table C.4 Properties of Paraffins, C₁ to C₁₀^a

Compound No.	Compound Name	Formula	Molecular Weight	Boiling Point at 1 atm. °C	Freezing Point at 1 atm. °C	Critical Pressure, MPa	Critical Temperature, °C	Volume, m ³ /kg	Specific Gravity at 15.5°C
1	Methane	CH ₄	16.043	-161.49	-182.48	4.604	-82.57	0.006187	0.3000
2	Ethane	C ₂ H ₆	30.07	-88.60	-183.27	4.880	32.27	0.004919	0.3564
3	Propane	C ₃ H ₈	44.097	-42.04	-187.69	4.249	96.67	0.004601	0.5077
4	n-Butane	C ₄ H ₁₀	58.124	-0.50	-138.36	3.797	152.03	0.004382	0.5844
5	2-Methylpropane (isobutane)	C ₄ H ₁₀	58.124	-11.72	-159.61	3.648	134.99	0.00452	0.5631
6	n-Pentane	C ₅ H ₁₂	72.151	36.07	-129.73	3.369	196.50	0.004214	0.6310
7	2-Methylbutane (isopentane)	C ₅ H ₁₂	72.151	27.84	-159.91	3.381	187.28	0.004239	0.6247
8	2,2-Dimethylpropane (neopentane)	C ₅ H ₁₂	72.151	9.50	-16.57	3.199	160.63	0.004208	0.5967
9	n-Hexane	C ₆ H ₁₄	86.178	68.73	-95.32	3.012	234.28	0.004295	0.6640
10	2-Methylpentane	C ₆ H ₁₄	86.178	60.26	-153.68	3.010	224.35	0.004251	0.6579
11	3-Methylpentane	C ₆ H ₁₄	86.178	63.27	—	3.124	231.28	0.004251	0.6689
12	2,2-Dimethylbutane	C ₆ H ₁₄	86.178	49.73	-99.84	3.081	215.63	0.004164	0.6540
13	2,3-Dimethylbutane	C ₆ H ₁₄	86.178	57.98	-128.54	3.127	226.83	0.004151	0.6664
14	n-Heptane	C ₇ H ₁₆	100.205	98.43	-90.58	2.736	267.11	0.004314	0.6882
15	2-Methylhexane	C ₇ H ₁₆	100.205	90.05	-118.27	2.734	257.22	0.004201	0.6830
16	3-Methylhexane	C ₇ H ₁₆	100.205	91.84	—	2.814	262.10	0.004033	0.6917
17	3-Ethylpentane	C ₇ H ₁₆	100.205	93.47	-118.60	2.891	267.49	0.004151	0.7028
18	2,2-Dimethylpentane	C ₇ H ₁₆	100.205	79.19	-123.81	2.773	247.35	0.004151	0.6782
19	2,3-Dimethylpentane	C ₇ H ₁₆	100.205	89.78	—	2.908	264.20	0.00392	0.6996
20	2,4-Dimethylpentane	C ₇ H ₁₆	100.205	80.49	-28.13	2.736	246.64	0.00417	0.6773
21	3,3-Dimethylpentane	C ₇ H ₁₆	100.205	86.06	-134.45	2.945	263.25	0.004133	0.6976
22	2,2,3-Trimethylbutane	C ₇ H ₁₆	100.205	80.88	-24.90	2.954	258.02	0.00397	0.6946
23	n-Octane	C ₈ H ₁₈	114.232	125.68	-56.77	2.486	295.68	0.0043	0.7068

(continued overleaf)

Table C.4 (continued)

Compound No.	Compound Name	Formula	Molecular Weight	Boiling Point at 1 atm. °C	Freezing Point at 1 atm. °C	Critical Pressure, MPa	Critical Temperature, °C	Critical Volume, m ³ /kg	Specific Gravity at 15.5°C
24	2-Methylheptane	C ₈ H ₁₈	114.232	117.66	-108.99	2.484	286.49	0.004276	0.7021
25	3-Methylheptane	C ₈ H ₁₈	114.232	118.93	-120.54	2.546	290.52	0.004064	0.7101
26	4-Methylheptane	C ₈ H ₁₈	114.232	117.72	-120.96	2.542	288.59	0.004164	0.7090
27	3-Ethylhexane	C ₈ H ₁₈	114.232	118.54	—	2.608	292.34	0.003983	0.7178
28	2,2-Dimethylhexane	C ₈ H ₁₈	114.232	106.84	-121.18	2.529	276.72	0.0042	0.6997
29	2,3-Dimethylhexane	C ₈ H ₁₈	114.232	115.61	—	2.628	290.34	0.004095	0.7165
30	2,4-Dimethylhexane	C ₈ H ₁₈	114.232	109.43	—	2.557	280.37	0.004133	0.7047
31	2,5-Dimethylhexane	C ₈ H ₁₈	114.232	109.11	-91.15	2.486	276.91	0.00422	0.6979
32	3,3-Dimethylhexane	C ₈ H ₁₈	114.232	111.97	-126.10	2.654	288.87	0.003877	0.7143
33	3,4-Dimethylhexane	C ₈ H ₁₈	114.232	117.73	—	2.692	295.70	0.004083	0.7236
34	2-Methyl-3-ethylpentane	C ₈ H ₁₈	114.232	115.66	-114.95	2.700	293.94	0.003877	0.7236
35	3-Methyl-3-ethylpentane	C ₈ H ₁₈	114.232	118.27	-90.84	2.808	303.43	0.003983	0.7315
36	2,2,3-Trimethylpentane	C ₈ H ₁₈	114.232	109.84	-112.26	2.730	290.35	0.003814	0.7202
37	2,2,4-Trimethylpentane	C ₈ H ₁₈	114.232	99.24	-107.37	2.568	270.81	0.004095	0.6962
38	2,3,3-Trimethylpentane	C ₈ H ₁₈	114.232	114.77	-100.93	2.820	300.41	0.003983	0.7303
39	2,3,4-Trimethylpentane	C ₈ H ₁₈	114.232	113.47	-109.20	2.730	293.26	0.004033	0.7233
40	2,2,3,3-Tetramethylbutane	C ₈ H ₁₈	114.232	106.47	100.69	2.868	294.78	0.004033	—
41	n-Nonane	C ₉ H ₂₀	128.259	150.82	-53.49	2.289	321.49	0.00427	0.7217
42	n-Decane	C ₁₀ H ₂₂	142.286	174.16	-29.64	2.096	344.50	0.004239	0.7342

^aExtracted from API Technical Data Book with unit conversion

Table C.5 Properties of Normal Paraffins, C₁₁ to C₃₀^a

Compound No.	Compound Name	Formula	Molecular Weight	Boiling Point at 1 atm. °C	Freezing Point at 1 atm. °C	Critical Pressure, MPa	Critical Temperature, °C	Critical Volume, m ³ /kg	Specific Gravity at 15.5°C
1	<i>n</i> -Undecane	C ₁₁ H ₂₄	156.3	195.89	-25.59	1.965	365.58	0.000386	0.7443
2	<i>n</i> -Dodecane	C ₁₂ H ₂₆	170.33	216.28	-9.59	1.820	385.11	0.000307	0.7526
3	<i>n</i> -Tridecane	C ₁₃ H ₂₈	184.35	235.43	-5.39	1.724	402.61	0.000287	0.7601
4	<i>n</i> -Tetradecane	C ₁₄ H ₃₀	198.38	253.52	5.86	1.620	418.72	0.000274	0.7667
5	<i>n</i> -Pentadecane	C ₁₅ H ₃₂	212.41	270.62	9.93	1.517	433.61	0.000282	0.7721
6	<i>n</i> -Hexadecane	C ₁₆ H ₃₄	226.43	286.79	18.17	1.420	447.39	0.000263	0.7773
7	<i>n</i> -Heptadecane	C ₁₇ H ₃₆	240.46	302.15	21.98	1.317	460.22	0.000265	0.7817
8	<i>n</i> -Octadecane	C ₁₈ H ₃₈	254.48	316.71	28.18	1.213	472.11	0.000263	0.7856
9	<i>n</i> -Nonadecane	C ₁₉ H ₄₀	268.51	330.61	31.90	1.117	482.78	0.000268	0.7892
10	<i>n</i> -Eicosane	C ₂₀ H ₄₂	282.54	343.78	36.44	1.117	493.89	0.000265	0.7924
11	<i>n</i> -Heneicosane	C ₂₁ H ₄₄	296.56	356.50	40.50	—	—	—	0.7954
12	<i>n</i> -Docosane	C ₂₂ H ₄₆	310.59	368.61	44.39	—	>490.00	—	0.7981
13	<i>n</i> -Tricosane	C ₂₃ H ₄₈	324.61	380.22	47.61	—	—	—	0.8006
14	<i>n</i> -Tetracosane	C ₂₄ H ₅₀	338.64	391.28	50.89	—	—	—	0.8027
15	<i>n</i> -Pentacosane	C ₂₅ H ₅₂	352.67	401.89	53.72	—	—	—	0.8048
16	<i>n</i> -Hexacosane	C ₂₆ H ₅₄	366.69	412.22	56.39	—	—	—	0.8069
17	<i>n</i> -Heptacosane	C ₂₇ H ₅₆	380.72	422.11	59.00	—	—	—	0.8086
18	<i>n</i> -Octacosane	C ₂₈ H ₅₈	394.74	431.61	61.39	—	—	—	0.8104
19	<i>n</i> -Nonacosane	C ₂₉ H ₆₀	408.77	440.78	63.72	—	—	—	0.8120
20	<i>n</i> -Triacontane	C ₃₀ H ₆₂	422.80	449.72	65.78	—	—	—	0.8133

^aExtracted from API Technical Data Book with unit conversion

Table C.6 Properties of Alkylcyclopentanes, C₁₁ to C₃₀^a

Compound No.	Compound Name	Formula	Molecular Weight	Boiling Point at 1 atm. °C	Freezing Point at 1 atm. °C	Critical Pressure, MPa	Critical Temperature, °C	Critical Volume, m ³ /kg	Specific Gravity at 15.5°C
1	<i>n</i> -Hexylcyclopentane	C ₁₁ H ₂₂	154.29	202.89	-72.78	2.137	387.00	—	0.8006
2	<i>n</i> -Heptylcyclopentane	C ₁₂ H ₂₄	168.31	223.89	-52.78	1.951	405.78	—	0.8051
3	<i>n</i> -Octylcyclopentane	C ₁₃ H ₂₆	182.34	243.50	-43.89	1.793	421.39	—	0.8088
4	<i>n</i> -Nonylcyclopentane	C ₁₄ H ₂₈	196.36	262.00	-28.89	1.655	437.50	—	0.8121
5	<i>n</i> -Decylcyclopentane	C ₁₅ H ₃₀	210.39	279.38	-22.13	1.524	450.61	—	0.8149
6	<i>n</i> -Undecylcyclopentane	C ₁₆ H ₃₂	224.42	295.78	-10.00	1.407	465.22	—	0.8175
7	<i>n</i> -Dodecylcyclopentane	C ₁₇ H ₃₄	238.44	311.22	-5.00	1.296	476.72	—	0.8197
8	<i>n</i> -Tridecylcyclopentane	C ₁₈ H ₃₆	252.47	325.89	5.00	1.207	488.22	—	0.8217
9	<i>n</i> -Tetradecylcyclopentane	C ₁₉ H ₃₈	266.49	340.00	8.89	1.131	499.22	—	0.8235
10	<i>n</i> -Pentadecylcyclopentane	C ₂₀ H ₄₀	280.52	352.78	17.22	1.027	507.22	—	0.8252
11	<i>n</i> -Hexadecylcyclopentane	C ₂₁ H ₄₂	294.55	366.11	21.11	0.972	517.50	—	0.8267
12	<i>n</i> -Heptadecylcyclopentane	C ₂₂ H ₄₄	308.57	377.22	27.22	0.938	525.00	—	0.8280
13	<i>n</i> -Octadecylcyclopentane	C ₂₃ H ₄₆	322.60	388.89	30.00	0.876	531.11	—	0.8293
14	<i>n</i> -Nonadecylcyclopentane	C ₂₄ H ₄₈	336.62	400.00	35.00	0.855	542.22	—	0.8303
15	<i>n</i> -Eicosylcyclopentane	C ₂₅ H ₅₀	350.65	410.00	37.78	0.793	545.00	—	0.8315
16	<i>n</i> -Heneicosylcyclopentane	C ₂₆ H ₅₂	364.68	420.00	42.22	0.745	552.78	—	0.8324
17	<i>n</i> -Docosylcyclopentane	C ₂₇ H ₅₄	378.7	430.00	45.00	0.710	561.11	—	0.8333
18	<i>n</i> -Tricosylcyclopentane	C ₂₈ H ₅₆	392.73	438.89	48.89	0.607	561.67	—	0.8342
19	<i>n</i> -Tetracosylcyclopentane	C ₂₉ H ₅₈	406.75	447.22	51.11	0.558	567.11	—	0.8350
20	<i>n</i> -Pentacosylcyclopentane	C ₃₀ H ₆₀	420.78	456.11	53.89	0.503	573.89	—	0.8357

^a Extracted from API Technical Data Book with unit conversion

APPENDIX D

MELTING, BOILING, AND CRITICAL TEMPERATURES OF ELEMENTS^a

This table gives the melting point (T_m), normal boiling point (T_b) at a pressure of 101.325 kPa (1 atmosphere), and critical temperature (T_c) for all the elements for which measurements or reliable estimates are available. Values are given in °C on the ITS-90 scale. A “t” after a value indicates a triple point, and “s” indicates sublimation temperature (i.e., vapor pressure of the solid phase reaches 101.325 kPa, or 1 atmosphere).

Name	T_m (°C)	T_b (°C)	T_c (°C)	Name	T_m (°C)	T_b (°C)	T_c (°C)
Actinium		1051	3198	Cadmium		321.07	767
Aluminum	660.32	2519		Calcium	842	1484	
Americium	1176	2011		Californium	900		
Antimony	630.63	1587		Carbon	4492 t	3642 s	
Argon	-189.35	-185.85	-122.28	Cerium	798	3443	
Arsenic	817 t	614 s	1400	Cesium	28.44	671	
Astatine	302			Chlorine	-101.5	-34.04	143.8
Barium	727	1897		Chromium	1907	2671	
Berkelium	1050			Cobalt	1495	2927	
Beryllium	1287	2471		Copper	1084.62	2562	
Bismuth	271.40	1564		Curium	1345		
Boron	2075	4000		Dysprosium	1412	2567	
Bromine	-7.2	58.8	315	Einsteinium	860		

(continued overleaf)

Name	T_m (°C)	T_b (°C)	T_c (°C)	Name	T_m (°C)	T_b (°C)	T_c (°C)
Erbium	1529	2868		Platinum	1768.4	3825	
Europium	822	1596		Plutonium	640	3228	
Fermium	1527			Polonium	254	962	
Fluorine	-219.62	-188.12	-129.02	Potassium	63.38	759	
Francium	27			Praseodymium	931	3520	
Gadolinium	1313	3273		Promethium	1042	3000	
Gallium	29.76	2204		Protactinium	1572		
Germanium	938.25	2833		Radium	700		
Gold	1064.18	2856		Radon	-71	-61.7	104
Hafnium	2233	4603		Rhenium	3186	5596	
Helium		-268.93	-267.96	Rhodium	1964	3695	
Holmium	1474	2700		Rubidium	39.31	688	
Hydrogen	-259.34	-252.87	-240.18	Ruthenium	2334	4150	
Indium	156.60	2072		Samarium	1074	1794	
Iodine	113.7	184.4	546	Scandium	1541	2836	
Iridium	2446	4428		Selenium	221	685	1493
Iron	1538	2861		Silicon	1414	3265	
Krypton	-157.36	-153.22	-63.74	Silver	961.78	2162	
Lanthanum	918	3464		Sodium	97.80	883	
Lawrencium	1627			Strontium	777	1382	
Lead	327.46	1749		Sulfur	115.21	444.60	1041
Lithium	180.5	1342		Tantalum	3017	5458	
Lutetium	1663	3402		Technetium	2157	4265	
Magnesium	650	1090		Tellurium	449.51	988	
Manganese	1246	2061		Terbium	1356	3230	
Mendelevium	827			Thallium	304	1473	
Mercury	-38.83	356.73	1477	Thorium	1750	4788	
Molybdenum	2623	4639		Thulium	1545	1950	
Neodymium	1021	3074		Tin	231.93	2602	
Neon	-248.59	-246.08	-228.7	Titanium	1668	3287	
Neptunium	644			Tungsten	3422	5555	
Nickel	1455	2913		Uranium	1135	4131	
Niobium	2477	4744		Vanadium	1910	3407	
Nitrogen	-210.00	-195.79	-146.94	Xenon	-111.75	-108.04	16.58
Nobelium	827			Ytterbium	819	1196	
Osmium	3033	5012		Yttrium	1522	3345	
Oxygen	-218.79	-182.95	-118.56	Zinc	419.53	907	
Palladium	1554.9	2963		Zirconium	1855	4409	
Phosphorus	44.15	280.5	721				

^a Adapted from the 79th edition of the *CRC Handbook of Chemistry and Physics*, 1998–1999.

APPENDIX E

**PERIODIC TABLE AND
ELECTRONIC
CONFIGURATIONS OF
NEUTRAL ATOMS IN
GROUND STATES**

PERIODIC TABLE OF THE ELEMENTS

708

The new [IUPAC] format numbers the groups from 1 to 18. The previous [IUPAC] numbering system and the system used by Chemical Abstracts Service (CAS) are also shown. For radioactive elements that do not occur in nature, the mass number of the most stable isotope is given in parentheses.

ELECTRON CONFIGURATION OF NEUTRAL ATOMS IN THE GROUND STATE

Atomic No.	Element	K	L	M			N				O				P	Q
		1	2	3			4				5			6	7	
		s	s	p	s	p	d	s	p	d	f	s	p	d	f	s
1	H	1														
2	He	2														
3	Li	2	1													
4	Be	2	2													
5	B	2	2	1												
6	C	2	2	2												
7	N	2	2	3												
8	O	2	2	4												
9	F	2	2	5												
10	Ne	2	2	6												
11	Na	2	2	6	1											
12	Mg	2	2	6	2											
13	Al	2	2	6	2	1										
14	Si	2	2	6	2	2										
15	P	2	2	6	2	3										
16	S	2	2	6	2	4										
17	Cl	2	2	6	2	5										
18	Ar	2	2	6	2	6										
19	K	2	2	6	2	6		1								
20	Ca	2	2	6	2	6		2								
21	Sc	2	2	6	2	6	1	2								
22	Ti	2	2	6	2	6	2	2								
23	V	2	2	6	2	6	3	2								
24	Cr	2	2	6	2	6	5*	1								
25	Mn	2	2	6	2	6	5	2								
26	Fe	2	2	6	2	6	6	2								
27	Co	2	2	6	2	6	7	2								
28	Ni	2	2	6	2	6	8	2								
29	Cu	2	2	6	2	6	10*	1								
30	Zn	2	2	6	2	6	10	2								
31	Ga	2	2	6	2	6	10	2	1							
32	Ge	2	2	6	2	6	10	2	2							
33	As	2	2	6	2	6	10	2	3							
34	Se	2	2	6	2	6	10	2	4							
35	Br	2	2	6	2	6	10	2	5							
36	Kr	2	2	6	2	6	10	2	6							
37	Rb	2	2	6	2	6	10	2	6		1					
38	Sr	2	2	6	2	6	10	2	6		2					
39	Y	2	2	6	2	6	10	2	6	1	2					
40	Zr	2	2	6	2	6	10	2	6	2	2					
41	Nb	2	2	6	2	6	10	2	6	4*	1					
42	Mo	2	2	6	2	6	10	2	6	5	1					
43	Tc	2	2	6	2	6	10	2	6	6	2					
44	Ru	2	2	6	2	6	10	2	6	7	1					

710 PERIODIC TABLE AND ELECTRONIC CONFIGURATIONS OF NEUTRAL ATOMS

Atomic No.	Element	<i>n</i> =	K	L	M			N				O				P	Q		
		1	2		3			4				5				6	7		
		s	s	p	s	p	d	s	p	d	f	s	p	d	f	s	p	d	f
45	Rh	2	2	6	2	6	10	2	6	8		1							
46	Pd	2	2	6	2	6	10	2	6	10*									
47	Ag	2	2	6	2	6	10	2	6	10		1							
48	Cd	2	2	6	2	6	10	2	6	10		2							
49	In	2	2	6	2	6	10	2	6	10		2	1						
50	Sn	2	2	6	2	6	10	2	6	10		2	2						
51	Sb	2	2	6	2	6	10	2	6	10		2	3						
52	Te	2	2	6	2	6	10	2	6	10		2	4						
53	I	2	2	6	2	6	10	2	6	10		2	5						
54	Xe	2	2	6	2	6	10	2	6	10		2	6						
55	Cs	2	2	6	2	6	10	2	6	10		2	6		1				
56	Ba	2	2	6	2	6	10	2	6	10		2	6		2				
57	La	2	2	6	2	6	10	2	6	10		2	6	1		2			
58	Ce	2	2	6	2	6	10	2	6	10	1*	2	6	1		2			
59	Pr	2	2	6	2	6	10	2	6	10	3	2	6		2				
60	Nd	2	2	6	2	6	10	2	6	10	4	2	6		2				
61	Pm	2	2	6	2	6	10	2	6	10	5	2	6		2				
62	Sm	2	2	6	2	6	10	2	6	10	6	2	6		2				
63	Eu	2	2	6	2	6	10	2	6	10	7	2	6		2				
64	Gd	2	2	6	2	6	10	2	6	10	7	2	6	1		2			
65	Tb	2	2	6	2	6	10	2	6	10	9*	2	6		2				
66	Dy	2	2	6	2	6	10	2	6	10	10	2	6		2				
67	Ho	2	2	6	2	6	10	2	6	10	11	2	6		2				
68	Er	2	2	6	2	6	10	2	6	10	12	2	6		2				
69	Tm	2	2	6	2	6	10	2	6	10	13	2	6		2				
70	Yb	2	2	6	2	6	10	2	6	10	14	2	6		2				
71	Lu	2	2	6	2	6	10	2	6	10	14	2	6	1		2			
72	Hf	2	2	6	2	6	10	2	6	10	14	2	6	2		2			
73	Ta	2	2	6	2	6	10	2	6	10	14	2	6	3		2			
74	W	2	2	6	2	6	10	2	6	10	14	2	6	4		2			
75	Re	2	2	6	2	6	10	2	6	10	14	2	6	5		2			
76	Os	2	2	6	2	6	10	2	6	10	14	2	6	6		2			
77	Ir	2	2	6	2	6	10	2	6	10	14	2	6	7		2			
78	Pt	2	2	6	2	6	10	2	6	10	14	2	6	9		1			
79	Au	2	2	6	2	6	10	2	6	10	14	2	6	10		1			
80	Hg	2	2	6	2	6	10	2	6	10	14	2	6	10		2			
81	Tl	2	2	6	2	6	10	2	6	10	14	2	6	10		2	1		
82	Pb	2	2	6	2	6	10	2	6	10	14	2	6	10		2	2		
83	Bi	2	2	6	2	6	10	2	6	10	14	2	6	10		2	3		
84	Po	2	2	6	2	6	10	2	6	10	14	2	6	10		2	4		
85	At	2	2	6	2	6	10	2	6	10	14	2	6	10		2	5		
86	Rn	2	2	6	2	6	10	2	6	10	14	2	6	10		2	6		
87	Fr	2	2	6	2	6	10	2	6	10	14	2	6	10		2	6	1	
88	Ra	2	2	6	2	6	10	2	6	10	14	2	6	10		2	6	2	

Atomic No.	<i>n</i> = Element	K	L	M			N				O				P			Q	
		1	2	3			4				5				6			7	
		s	s	p	s	p	d	s	p	d	f	s	p	d	f	s	p	d	f
89	Ac	2	2	6	2	6	10	2	6	10	14	2	6	10		2	6	1	2
90	Th	2	2	6	2	6	10	2	6	10	14	2	6	10		2	6	2	2
91	Pa	2	2	6	2	6	10	2	6	10	14	2	6	10	2*	2	6	1	2
92	U	2	2	6	2	6	10	2	6	10	14	2	6	10	3	2	6	1	2
93	Np	2	2	6	2	6	10	2	6	10	14	2	6	10	4	2	6	1	2
94	Pu	2	2	6	2	6	10	2	6	10	14	2	6	10	6*	2	6		2
95	Am	2	2	6	2	6	10	2	6	10	14	2	6	10	7	2	6		2
96	Cm	2	2	6	2	6	10	2	6	10	14	2	6	10	7*	2	6	1	2
97	Bk	2	2	6	2	6	10	2	6	10	14	2	6	10	9	2	6		2
98	Cf	2	2	6	2	6	10	2	6	10	14	2	6	10	10	2	6		2
99	Es	2	2	6	2	6	10	2	6	10	14	2	6	10	11	2	6		2
100	Fm	2	2	6	2	6	10	2	6	10	14	2	6	10	12	2	6		2
101	Md	2	2	6	2	6	10	2	6	10	14	2	6	10	13	2	6		2
102	No	2	2	6	2	6	10	2	6	10	14	2	6	10	14	2	6		2
103	Lr	2	2	6	2	6	10	2	6	10	14	2	6	10	14	2	6	1	2
104	Rf	2	2	6	2	6	10	2	6	10	14	2	6	10	14	2	6	2	2

*Note irregularity.

REFERENCE

W. L. Wiese and G. A. Martin, in *A Physicist's Reference*, American Institute of Physics, New York, 1989, p. 94.



AUTHOR INDEX

A

Aalto, M., 626, 637
Abraham, J., 593
Anderson, J. W., 488
Andrews, J. R., 56
Antolik, K., 384
Aris, R., 298
Atkin, 158

B

Babkin, V. S., 415
Bahadori, M. Y., 547
Baronecini, C., 627, 675, 677
Bartenev, A. M., 422
Bartholomé, E., 449, 502
Baulch, D. L., 225, 463
Beer, J. M., 438
Bellan, J., 592, 593, 604
Belles 395, 398, 399
Benedict 596, 626, 647
Benson, S. W., 117, 124
Bechert, K., 449
Berets, D. G., 380
Berlad, A. L., 509
Biblarz, O., 56
Blackshear, P. L., 580
Bondi, A., 654
Boris, J. P., 381
Borisov, A. A., 415, 583, 584
Borman, G. L., 507, 592, 593
Botha, J. P., 447
Bowman, C. T., 235, 259, 261–268
Boys, S. F., 449
Bozzelli, J. W., 270
Brabbs, T. A., 235
Bradley, J. N., 139
Braun, W., 133
Brobst, K. R., 626, 635
Brokaw, R. S. 235, 673

Brule, M. R., 667, 668
Brzustowski, T. A., 592
Buckmaster, J. D., 471
Burke, S. P., 539, 544–547

C

Caldin, E. F., 136
Calus, W. F., 627, 685, 686
Campbell, C., 384, 634
Canada, G. S., 592, 593
Candel, S. M., 471, 476
Chance, B., 137
Chang, W. S., 592, 593, 626, 627, 634,
 636, 637, 684
Chapman, S., 626, 627, 678, 680
Chen, L. W., 612
Chervinsky, A., 592
Chiang, C. H., 612, 613
Chiang, W. T., 592
Chigier, N. A., 438
Christoffel, E. G., 187, 188
Chueh, C. F., 626
Chung, S. H., 475, 547, 626, 656, 658,
 667, 668
Ciccarelli, G., 412
Clarke, J. F., 424
Clavin, P., 523–528
Clingman, W. H., 502, 503
Coffee, T. P., 461, 462, 464–468
Constable, H., 175
Corner, J., 449
Coward, H. F., 395
Curtis, E. W., 592
Curtiss, C. F., 449, 563

D

- Danner, R. P., 626, 627, 633, 634, 638, 641, 671
 Dantzig, G. B., 103
 Daou, J., 592
 Daubert, T. E., 626, 627, 641, 671
 Dean, A. M., 270
 de Boor, C., 466
 de Guzman, J., 661
 Delpanque, J. P., 592
 DeMore, W. B., 133-135
 Deng, Z., 583-585
 de Soete, G., 381
 Denisov, Y. H., 384
 Dibble, R. W., 272, 448
 Dixon-Lewis, G., 225, 483, 492
 Dominicis, D. P., 592
 Döring, W., 381, 382, 403
 Dorofeev, S. B., 424
 Dougherty, E. P., 216-219
 Dove, J. E., 403
 Dowdy, D. R., 477-484
 Dryer, F. L., 223-225, 231, 236, 244
 Dugger, G. L., 459, 460, 501
 Duhne, C. R., 662
 Dupre, G., 406

E

- Easteal, A. J., 627, 687
 Eckbreth, A. C., 448
 Edse, R., 524, 525
 Edwards, D. H., 383, 384, 404, 405
 Egerton, A., 488
 Egolfopoulos, F. N., 490-496
 Eisen, C. L., 375, 376
 Ely, J. F., 594
 Emmett, P. H., 174, 175
 Emmons, H. W., 449
 Evans, M. W., 449, 460

F

- Faeth, G. M., 484-486, 488, 489, 592, 593, 608
 Farrel, P. V., 592
 Fay, J. A., 383, 385, 386, 406
 Fein, R. S., 488
 Fenimore, C. P., 225, 258
 Fishenden, M., 522
 Frank-Kamenetsky, D. A., 424, 449, 451, 459, 460, 520
 Friedman, R., 356, 357
 Freedman, E., 107
 Frenklach, M., 272

- Friauf, J. B., 379, 380
 Fried, L. E., 107
 Fristrom, R. M., 489
 Frolov, S. M., 413
 Fujiwara, T., 386

G

- Gardiner, W. C., 178
 Gavrikov, A. I., 404, 412
 Gaydon, A. G., 438, 440, 449, 550
 Gazley, C., 550, 551
 Geankoplis, C. J., 627, 687, 688
 Gelfand, B. E., 413, 417-419, 422, 428
 Gerstein, M., 460, 461, 497-499
 Getzinger, R. W., 233
 Ghilani, M., 523
 Givler, S. D., 593
 Glarborg, P., 259, 492
 Glassman, I., 216, 233, 438, 439
 Godsake, G. A. E., 577
 Gogos, G., 592
 Goletz, E., 662
 Gordon, S., 45, 57, 98, 101, 171, 376, 378, 379, 405, 627, 671-673
 Goussis, D. A., 247
 Gray, K. L., 488
 Green, D. W., 200
 Greene, E. F., 380
 Grosse, A. V., 466, 467
 Grunberg, L., 627, 669, 671
 Guirao, C. M., 406, 408, 410
 Gunn, R. D., 633

H

- Haar, L., 108
 Haldenwang, P., 592
 Hammes, G. G., 142
 Hampson, R. F., 462
 Hankinson, R. W., 626, 634, 635, 637, 639
 Hanley, H. J. M., 594
 Harstad, K., 592, 593, 604
 Harr, J. A., 449
 Harris, M. E., 488
 Hartmann, E., 496
 Hawthorne, W. R., 550
 Hayduk, W., 627, 686
 Haywood, R. J., 612, 613
 He, L., 523-528
 Heimel, S., 501
 Heimerl, J. M., 461, 462, 464-468
 Herning, F., 660
 Hindmarsh
 Hinze, J. O., 298

Hiroyasu, H., 592, 593
 Hirschfelder, J. O., 449, 563
 Holbrook, K. A., 158
 Howard, W. M., 107
 Hsiao, G. C., 592, 604, 610
 Hsieh, K. C., 592
 Hsieh, W. H., 601
 Hsu, K.-J., 492
 Hwang, J., 205

I

Isdale, J. D., 627, 670
 Ismail, M. A., 484, 486, 488, 489

J

Jacobsen, R. T., 594
 Jahn, G., 458
 Jeng, S. M., 583-585
 Jia, H., 592
 Jiang, T. L., 592
 Johnson, S. M., 103
 Johnston, H. S., 138, 462, 463
 Jones, C. W., 395
 Jones, J. L., 513, 522, 649
 Ju, Y., 471
 Just, Th., 384

K

Kadota, T., 592, 593
 Kanury, A. M., 438, 504, 506, 512
 Kapp, N. M., 551
 Karlovitz, B., 471
 Kasemo, B., 182
 Kailasanath, K., 381
 Kasner, J. H., 133, 135, 136
 Keck, J. C., 500
 Kee, R. J., 164, 468, 492, 563
 Keier, N. P., 174
 Kesler, M. G., 626, 645, 646, 650
 Kistiakowsky, G. B., 139, 380, 383
 Klein, M., 108
 Knystautas, R., 406-409, 426
 Kobe, K. A., 642
 Komiyama, M., 567
 Kordylewski, W., 524
 Kogarko, S. M., 403, 406
 Kozachenko, L. S., 415
 Kramer, M. A., 205, 206
 Kummer, J. T., 174, 175
 Kuo, K. K., 448, 601
 Kurylo, M. J., 133

L

Lafon, P., 592, 604-606

Lagrange, J. L., 105
 Laidler, K. J., 117, 142, 175
 Lam, S. H., 247, 298
 Landau, L. C., 298, 303
 Langmuir, I., 174, 175, 179, 183
 Laplace, P. S., 47, 65, 66
 Larrouturou, B., 523
 Lavoisier, A. L., 47, 65, 66
 Law, C. K., 252-254, 471, 475, 488,
 490-496, 547
 Lawrence, J. R., 524, 525
 Lazar, R. S., 592, 593
 LeChatelier, H. L., 449-451, 458
 Lee, B. I., 626, 627, 645, 646, 650
 Lee, C. Y., 680
 Lee, J. H., 381, 406, 424, 425
 Lee, S. T., 535
 Letsou, A., 627, 667
 Levine, O., 460
 Lewis, B., 145, 220, 221, 379-381, 396,
 445, 449, 500, 505, 509, 512, 513, 522,
 526

Li, C. C., 627, 628
 Li, W. H., 298
 Lifshitz, E. M., 298, 303
 Lin, M. C., 191
 Lindemann, F. A., 156
 Ljungstrom, S., 182
 Lu, T., 252-254, 471
 Lucas, K., 626, 627, 657-661, 667, 668
 Luckas, M., 666
 Luker, J. A., 376

M

Maas, U., 223, 252, 448, 492
 Madsen, B. K., 465
 Mallard, E., 449-451
 Manrique, J. A., 592, 593
 Manson, N., 381, 388, 406, 449
 Markstein, G. H., 471
 Mason, E. A., 627, 673
 Mass, U., 272
 Matalon, M., 471, 475
 McBride, B. J., 13, 45, 57, 98, 101, 171,
 376, 378, 379, 627, 672
 McGill, P. L., 376
 Meng, H., 592
 Metghalchi, M., 500
 Miller, J. A., 239, 240, 259, 261-268
 Miller, J. M., 627, 674
 Missenard, A., 677
 Missenard, F. A., 626, 627, 653
 Mitani, T., 528
 Mitchell, R. E., 564

- Minhas, B. S., 627, 686
 Mitrofanov, V. V., 404
 Moen, I. O., 403-406, 412, 424
 Mooradian, A. J., 405
 Morgan, J. M., 405

N

- Nernst, W. H., 17
 Nettleton, M. A., 413, 419
 Neufeld, P. D., 656, 679
 Nicoli, C., 592
 Nissan, A. H., 627, 669, 671
 Nowak, U., 210-212

O

- Opel, G. L., 386
 Oppenheim, A. K., 381, 388, 391, 393,
 394
 Oran, E. S., 381, 386, 388

P

- Palm-Leis, A., 486, 488, 489
 Parr, T. P., 448
 Pease, R. N., 449, 458-461, 499
 Penner, S. S., 449, 547
 Perkins, L. R., 627, 687, 688
 Peskin, R. L., 592, 593
 Peters, N., 483
 Plocker, U., 650
 Poinsot, T. J., 471, 476
 Poling, B. E., 625
 Polymeropoulos, C. E., 592, 593
 Pope, S. B., 252
 Potter, A. E., 509
 Powell, E. G., 108
 Powling, J., 445
 Prakash, S., 585-590, 610
 Prausnitz, J. M., 625
 Przedziecki, J. W., 627, 666

R

- Rabitz, H., 200, 205, 216-219
 Rackett, H. G., 633
 Ragland, K. W., 507
 Reichenberg, D., 626, 656, 658-660
 Reid, R. C., 625, 634, 643, 644, 649, 656,
 660, 665, 672, 680
 Renksizbulut, M., 612, 613
 Reynolds, T. W., 497, 498
 Reynolds, W. C., 107
 Ribinin, S. S., 415, 416
 Rice, P., 627, 670
 Rideal, E. K., 179
 Roberts, J. K., 175

- Robinson, P. J., 158, 626
 Roginsky, S. Z., 174
 Rosner, D. E., 592, 593
 Rossini, F. D., 35
 Rowlinson, J. S., 626, 654
 Rubin, L. C., 596, 626, 647

S

- Sachsse, H., 502
 Santoro, R. J., 272
 Sastri, M. L. N., 386
 Sato, J., 608
 Saunders, O. A., 533
 Savage, L. D., 485
 Saxena, S. C., 627, 673
 Shchelkin, K. I., 318, 414-416
 Schlichting, H., 304, 553
 Scholte, T. G., 488
 Schott, G. L., 233
 Schumann, T. E. W., 539, 544-547
 Scott, S. K., 524
 Sermange, M., 523
 Semenov, N., 449, 451, 460, 459
 Shames, I. H., 298, 303
 Shapiro, A. H., 384
 Shepherd, J. E., 410-412
 Shimada, Y., 592, 593
 Shuen, J. S., 592, 607-609
 Shvab, V. A., 332
 Simon, D. M., 460, 461
 Sincovec, R. F., 465
 Sirignano, W. A., 585-590, 592, 610
 Slack, M. W., 492
 Smith, M. L., 512
 Smooke, M. D., 269, 561-566
 Soloukhin, R. I., 381, 404
 Sonntag, R. E., 17
 Souers, P. C., 107
 Spalding, D. B., 447, 513, 514, 516, 517,
 521, 522, 553, 555, 558, 569, 572, 580,
 587, 592
 Spencer, C. F., 626, 633, 634, 638
 Sridhar, T., 666
 Starling, K. E., 627, 667, 668
 Stewart, P. H., 165, 168
 Stewart, R. B. J., 594
 Stiel, L. I., 627, 667, 673
 Stinson, K. W., 512
 Strehlow, R. A., 381, 384-386, 485, 486,
 488, 489
 Streng, A. G., 466, 467
 Strong, P., 449
 Summerfield, M., 592
 Svchla, R. A., 98, 101, 680

Swanson, A. C., 626
Sychev, V. V., 596, 626, 649, 654

T

Tada, K., 567
Takagi, T., 566–568
Takahashi, S., 598, 627, 680, 683
Taki, S., 386
Tamplin, W. S., 653
Tanford, C., 449, 458–461, 499
Tassios, D., 662
Taylor, H. S., 174, 200
Taylor, S. C., 488, 489
Teja, A. S., 627, 670
Thinh, T.-P., 626, 644
Thodos, G., 627, 634, 673
Thomson, G. H., 626, 634, 635, 637,
 639, 640
Thorne, A. P., 448
T'ien, J. S., 535
Tilden, J. W., 200
Troe, J., 165, 168
Trong, T. K., 626
Troshin, Y. K., 384, 412
Trowse, F. W., 136
Tsederberg, N. V., 677
Tseng, L.-K., 484, 486–490
Tsiji, H., 488
Turns, S. R., 216
Tyn, M. T., 627, 685, 686

U

Umemura, A., 592, 593
Urtiew, P. A., 388, 391, 393, 394, 412

V

Vaags, P. B., 488
Van Tiggelen, A., 381, 449
van Velzen, D., 627, 662
Van Wylen, G. J., 17
von Elbe, G., 145, 220, 221, 380, 381,
 396, 445, 449, 505, 509, 512, 513, 522,
 526
von Karman, Th., 449
von Neumann, J., 382, 403
Van Tiggelen, A., 449

W

Gg. Wagner, H., 381, 383, 384, 388, 403

Warnatz, J., 182, 186, 202, 210–215,
 223–226, 240, 257, 268, 272, 448, 466,
 467, 471, 483, 492, 496, 523–525

Weast, R. C., 501

Webb, G. B., 596, 626, 647

Weber, J., 175

Weinberg, F. J., 438, 440

Wendlant, R., 403

Westbrook, C. K., 224, 225, 231, 236,
 244, 412

White, D. R., 383, 385, 387, 435

White, W. B., 103

Wilke, C. R., 627, 660, 680, 683,
 684

Williams, D. J., 225

Williams, F. A., 309, 528, 535

Williams, W. R., 191–196

Wilmot, G., 108

Wohl, K., 506, 507, 550, 551

Wolanski, P., 402, 424

Wolfhard, H. G., 438, 440, 449, 550

Wong, E. L., 460

Woodhead, D. W., 384

Woods, S. S., 633

X

Xiang, H. W., 664

Xu, Z., 566–568

Y

Yamada, T., 633

Yamaoka, I., 488

Yang, V., 591–593, 596, 598, 601, 602,
 604, 609–612

Yaws, C. L., 662

Yen, L. C., 633

Yesavage, V. F., 649

Yetter, R. A., 205, 233

Yorizane, M., 627, 673

Yuen, M. C., 612

Z

Zel'dovich, Y. B., 332, 382, 403, 406,
 414–416, 422, 428, 449, 451, 459, 460,
 502, 520

Zelevnik, F. J., 98, 101, 376, 378

Zhao, X., 626, 634, 636, 637

Zipperer, L., 660

Zuzic, M., 653

SUBJECT INDEX

A

Aalto's model, 637
Absorption and emission spectroscopies, 448
Abstraction of H atoms, 242
Acentric factor, 634, 656
mixing rule, 639
Activated complex (energized molecules), 125, 238
Activation energy, 119, 126, 129, 130, 182, 190, 256, 259, 281, 285, 413, 563
Activation energy of the desorption process, 182
Activation reaction, 156
Adiabatic flame temperature, 13, 72, 73, 88, 107, 108, 568
Adiabatic porous catalyst plug, 516
Adsorbate, 175
Adsorption process, 182
Adsorption rate constants, 185
Adsorption theory, 175
Adsorption with dissociation, 177, 178
Affinity (chemical affinity), 11, 32
Alcohols, 675, 699, 700
Aldehydes, 699, 700
Aliphatic hydrocarbon combustion, 210
reaction mechanism, 224, 225
Aliphatic hydrocarbon and oxygen system, 223
Alkanes, 498, 699, 700
Alkanes-air mixture, 410
Alkylcyclopentanes, 704
Alkynes, 699, 700
Amines, 699, 700
Ammonia, 262
Analytically Integrated Magus (AIM), 205
Andrade equation of liquid viscosity, 662
Angular-velocity tensor, 324

Antiknocking compound, 499
Antisymmetric tensor, 234
Apparent stresses, *see* Reynolds stresses
(apparent or turbulent stresses)
Approach velocity, 506, 507
Arbitrary Lagrangian Eulerian (ALE)
numerical algorithm, 583
Aromatics, 676, 699, 700
Arrhenius equation (law), 122–124, 130, 162, 167, 382, 424, 563
Arrhenius factor, 116, 456, 451
Arrhenius rate coefficients, 170
Ash, 272
Atmospheric aerosols, 271
Atmospheric H₂/air flames, 492
Atom-molecule mechanism (or
radical-molecule complex mechanism), 282
Atom and radical combination, *see* Energy
transfer mechanism (atom and radical
combination)
Atom-transfer reaction, *see* Second-order
reaction
Atomic mass unit, 694
Auger Electron Spectroscopy (AES), 187–189
Autoignition temperature, 420
Automobile engines, 270
Average molecular velocity, 120
Avogadro's number, 8, 15, 38, 176, 286,
291, 437, 452, 694

B

Balance of mass-flux at interface, 351
Baroncini et al.'s method for liquid thermal
conductivity, 675
Basis functions of *B*-splines, 466
Beattie–Bridgeman equation of state, 630
Belles model, 395–401

Benedict–Webb–Rubin (BWR) equation of state, 594–596, 630, 649 modified, 647
 Benzene, 244
 Benzene-ring resonance, 50, 51, 65
 Benzoic acid, 63–65
 Bimolecular collision (binary collision), 122, 123, 142, 144
 Binary diffusion coefficient, 623
 Binary diffusivity, 285
 Binary mass diffusivity, 289
 Blasius equation, 418
 Blowout flame, 507
 Body force, 300, 301, 321
 Body force work, 324
 Boiling line, 601
 Boiling point, 701–705
 Boltzmann constant, 122, 176, 183, 286, 291, 694
 Boltzmann factor, 119, 122
 Boltzmann's exponential factor, 183
 Bond energy, 48–52, 63, 399 of OH molecule, 225
 Bond number, 537, 583, 584
 Bondi's liquid hydrocarbon method, 654
 Branched-chain explosion of hydrogen, 395
 Brute force method, 205
 Bulk viscosity, 8, 286, 309, 324, 332
 Bunsen burner, 438–442, 503, 504, 507, 533
 Burner design, 172
 Burning velocity, 482,
 Burning velocity mixtures, 486
 Burning velocity of H₂/O₂ flame, 528
 Burning velocity of H₂/O₂ mixtures at different pressures, 527
 Butadienyl radical, 245
 Buoyancy effect, 557
 Burke–Schumann's theory of laminar diffusion flames, 539–547

C

C₁-Hydrocarbon Oxidation, 226
 Calcium carbonate, 271
 Calcium oxide, 271
 Calorically perfect gases, 641
 Carbon monoxide (CO), 224, 270
 Carboxylic acid, 699, 700
 Cartesian tensor notation, 300
 Catalysis, 174
 Catalyst, 174
 Catalytic combustion, 173
 Catalytic oxidation of H₂ on Pt foil, 192

Catalyst plug postulation, 516
 Catalytic surface reaction, 178
 Cellular flame structure, 444
 Cellular structure, 406
 Centrifugal force, 312
 CH reactions, 226
 CH₂ reactions, 227
 CH₃ oxidation step, 2335
 CH₃ reactions, 227
 CH₄/air flame, 471
 CH₄/air laminar flame, 210
 CH₄ oxidation, 234–236
 CH₄ reactions, 228
 CH₂CHO reactions, 230
 CH₃CHO reactions, 230
 CH₃CO reactions, 229
 CH₂CO (ketene) oxidation, 240
 CH₂CO reactions, 229
 CH₂O reactions, 227, 233, 234
 CH₃O reactions, 228
 CH₂OH reactions, 228
 CH₃OH reactions, 228, 241
 CH₃O₂ reactions, 228
 CH₃O₂H reactions, 229
 CH₄/O₂/Ar mixtures, 503
 CH₄/O₂/He mixtures, 503
 C₂H reactions, 229
 C₂H₂ air mixtures, 409
 C₂H₂ oxidation, 238
 C₂H₂ reactions, 229
 C₂H₃ reactions, 229
 C₂H₄ oxidation, 237
 C₂H₄ reactions, 230
 C₂H₅ reactions, 230
 C₂H₆ reactions, 230
 C₃H₈/air laminar flame, 210
 CH₃CHO (acetaldehyde) reaction, 243
 C₂H₅OH (ethanol) reactions, 242
 Chain-branching reaction, 162–164, 216, 222, 231–234, 245, 261, 421, 523
 Chain-carrying reaction, *see*
 Chain-propagating reaction
 Chain-initiating reactions, 155, 156, 159, 160, 163
 Chain-propagating reactions (chain-carrying reactions), 155, 156, 160–163, 216, 221, 246
 Chain reaction, 154–156, 219, 252
 Chain-terminating reaction (chain-breaking or chain-killing reaction), 155, 156, 160–164, 219, 220, 225, 396, 495, 523
 Chang–Zhao equation, 634, 636, 637 modified, 637, 640

- Chapman–Enskog approach, 655
 Chapman–Enskog's method, 678
 Chapman–Jouguet,
 detonations, 102, 373–381, 413, 415
 theory, 379
 wave velocity, 373, 417, 418
 Chapman–Jouguet point, 355, 360–364,
 366, 368, 372, 406, 410, 412, 416,
 431, 435
 Characteristic reaction zone width, 412
 Charge-coupled-device (CCD), 140
 Chemical affinity, *see* Affinity (chemical affinity)
 Chemical equilibrium, 5, 6, 14, 17, 19, 31,
 33, 34, 36
 Chemical equilibrium application program (NASA-CEA Code), 13, 101–103,
 107, 108, 434
 Chemical nonequilibrium, 15, 18, 22, 23
 Chemical potential, 12, 15, 27, 30, 32, 105,
 106
 Chemical reaction rate expression, 331
 Chemical sensitivity analysis, 199
 Chemisorption process, 174
 CHEMKIN Code, 164–173, 468–471, 523,
 563
 CHO reactions, 226
 Classical models of Belles, 395
 Classical laminar flame theories, 449
 Clausius–Clapeyron vapor-pressure equation, 96–98, 576, 577
 CO emissions, 270, 271
 CO oxidation mechanism, 233
 CO reaction, 226
 with OH radicals, 210
 Coal, 272
 Coal-derived fuels, 262
 Coal matrix, 272
 Coherent and anti-Stokes Raman spectroscopies (CARS), 448
 Collision coefficient, 183
 Collision frequency, 116, 119–122, 176
 Collision frequency factor, 116
 Collision integral, 656
 Collision radius, 116
 Collocation methods, 308
 Combustion of biomass, 270
 Combustion lifetime, 607
 Competitive reactions, 150
 Comprehensive theory, 449
 Compressed liquids, 633, 634, 637
 Compressibility factor, 92, 597, 624, 629,
 647, 657
 Computational singular perturbation methods for stiff equations, 247, 252
 Computational singular perturbation (CSP) theory, 247, 252–255
 Concentration, *see* Mass concentration (concentration)
 Concentration sensitivity, 201
 Concept of molecularity, 180
 Concept of radical-species diffusion, 502
 Conformal mapping, 595
 Consecutive reactions, 148–149, 160
 Conservation equations, 5, 160, 383, 376,
 418
 angular momentum, 6,
 atomic species, 6, 36–38, 73, 94,
 chemical species, 340
 energy, 6, 16, 209, 320–328, 376, 418,
 451–454, 458, 463, 464, 468, 469,
 514, 534, 558
 mass (continuity equation), 6, 18–20,
 293–297, 376, 463, 464, 451, 452,
 458
 molecular species, 6, 451, 514
 momentum (equation of motion), 6,
 297–319, 376, 417
 Conserved property, 41, 559
 Conserved scalar, 40, 41
 Constant pressure combustion, 53–66
 Constant-pressure specific heat, 56
 Constant-volume specific heat, 642, 671
 Constitutive relationship, *see*
 Stress/strain-rate relationship
 (constitutive relationship)
 Contact discontinuity, 381, 392, 394
 Contemporary method for solving
 laminar-flame problems, 461
 Continuity equation, *see* Conservation equations
 Continuum, 6
 Contour of a laminar diffusion flame, 561
 Control emissions of pollutants, 255
 Coriolis force, 312
 Correlating equations, 661
 Corresponding states method, 654, 661
 of Lucas, 661
 Corresponding states liquid density (COSTALD), 626, 634, 636
 Counterflow premixed-flame setup, 492
 Counterflow technique, 491
 Covolume, 628
 Critical Mach number, 398
 Critical mixing line, 601, 604
 Critical mixing point, 601, 602
 Critical pipe diameter consideration, 416

Critical pressure, 591, 701–704
 Critical pressure of gas mixture, 660
 Critical shock Mach number, 397
 for explosion, 397
 Critical shock strengths for explosion, 395
 Critical temperature, 591, 605, 606, 656,
 701–705
 Critical tube diameters, 402, 403, 408
 Critical volume, 656, 701–704
 Cubic equations of state, 629
 Cyclones, 273
 Cycloparaffins, 676
 Cyclopentadienyl radical, 245
 Cylindrical coordinates, 315, 317
 Cylindrical laminar flame, 534

D

d^2 evaporation law, 570, 577, 578, 583
 Dalton's law of partial pressure, 17, 38, 329
 Damköhler number, 538
 Damping parameter, 209
 Deactivation reaction, 156
 Decomposition reaction of CH_3CO radical,
 244
 Decoupled Direct Method (DDM), 205
 Deflagration, 5, 354–428
 Deflagration lean limit, 400
 Deflagration rich limit, 400
 Deflagration-to-detonation transition, 356,
 388–395, 420, 422, 426, 427
 in gaseous mixtures, 388
 Deformation and breakup dynamics, 610
 Degree of reaction, 19
 Dehydration, 182
 Dehydrogenation, 182
 ∇ -operator, 314, 316–318
 Dense gas viscosity, 660
 Desorption and formation rate constants,
 185
 Desorption process, 182, 183
 Detonability criteria, 405
 Detonability limits, 395, 398, 399,
 401–406, 410, 420
 of a hydrogen-oxygen mixture, 395
 of a reactive mixture, 395
 of unconfined mixtures, 402
 Detonation, 5, 225, 232, 239, 354–436
 in stoichiometric hydrogen-oxygen kernel
 size, 427
 mixture, 389
 of methane-air mixtures, 402
 Detonation cell, 404
 size, 405, 407, 412

width, 355, 411, 412
 Detonation lean limit, 400
 Detonation rich limit, 400
 Detonation sensitivity, 411
 Detonation velocity, 376
 Detonation wave speed, 354
 Detonation wave velocity, 379, 380, 434
 Diatomic gas, 503
 Differential diffusion effect, 491
 Differential operations involving the
 ∇ -operator, 316–319
 Diffusion equation, 304, 386
 Diffusion (non-premixed) flames, 5, 269,
 336, 439, 347, 355, 538–547, 551–568
 overventilated flame, 539, 547
 underventilated flame, 539, 547
 Diffusion time, 549
 Dilatation, 474

Dimensionless dipole moment, 656
 Direct detonation initiation, 425
 Dissipation by viscous stress, 324
 Dissociation reactions, 502
 Divergence theorem, 338
 Drag coefficient, 418
 for hard sphere, 613
 Droplet burning in convective stream, 582
 Droplet dynamic deformation, 610
 Droplet heat up time, 622
 Droplet lifetime, 605–607, 622
 Droplet surface temperature, 608
 Droplet relaxation time, 622
 Dufour effect, 6, 320, 321, 324, 327, 330,
 332, 562
 Dynamic viscosity, 624, 655

E

Effect of diluent concentration and initial
 density on detonation wave velocity,
 380
 Effect of temperature on flame speed, 460
 Eigenvalue, 203, 251, 364, 516
 Eigenvector, 251
 analysis, 200, 203
 Electrochemical methods, 142
 Electron charge, 694
 Electron mass, 694
 Electrostatic precipitators (ESPs), 273
 Elementary reaction, 129, 210, 284
 Endothermic decomposition and reactions,
 421
 Endothermic reaction, 44, 61, 126, 127
 Energy equation, 326
 integral form of, 340

- Energy-flux balance, 348
 at the gas-liquid interface, 347
- Energized molecules, 156
- Energy loss spectroscopy (ELS), 189
- Energy transfer mechanism (atom and radical combination), 282
- Enskog theory, modified, 597
- Enthalpy, 11, 43, 44, 52, 285, 320, 325, 348, 349, 354, 568, 603
 change across the interface, 349
 chemical, 348
 sensible, 248
- Entrainment rate, 555
- Entrainment velocity, 555
- Entropy, 12, 16, 24–27, 354
- Entropy distribution, 367
- Equation of continuity for the mixture, 294, 296
- Equation of motion, 311–314
- Equation of state, 5, 6, 9, 17, 29, 103, 359
- Equilibrium composition, 95, 98–107
- Equilibrium constants, 11, 12, 78–90, 151, 177, 197–199, 462
- Equilibrium criteria for closed thermodynamic systems, 36
- Equilibrium, liquid-vapor, 33, 97, 98
- Equivalence ratio, 9, 10, 12, 39, 107, 420, 489, 490, 494, 524
- Esters, 676, 699, 700
- Ethane decomposition reaction, 236
- Ethers, 676
- Ethyl radicals, 236, 237
- Ethylene (C_2H_4), 224
- Ethylene-air flame, 440
- Euler form of the momentum equation, 304
- Eulerian approach, 298, 300, 302
- Eulerian coordinates, 300
- Evaporation coefficient, 570, 577
- Excess and deficit of enthalpy, 568
- Exothermic reaction, 44, 61, 126, 127, 238, 283
- Expanding spherical flames, 477, 478, 480, 481
- Explosion
 branched-chain, 162–164
 branched-chain limit condition, 396
 thermal, 162
- Explosion in an explosion, 389–392
 onset of, 392
- Explosion limits, 216, 220–223, 523
 of H_2/O_2 Systems, 220
- Explosion limit peninsula, 216, 222
- Explosive reactions, 117
- Extended corresponding-state (ECS) principle, 594–597
- Extended X-ray adsorption fine structure (EXFAS), 188
- Extensive property, 15
- F**
- Fabric filters, 273
- Fall-off curves, 158, 159, 165, 167
- Fall-off reaction rate constant methods, 168, 170
- Fall-off region, 237
- Fast subspace, 249
- Femtochemistry techniques, 137, 140–142
- Fenimore mechanism, 255, 259–259, 269
- Fick's law of diffusion, 6, 289–292, 295, 320, 328–334, 345, 563
- Field emission spectroscopy (FES), 189
- Finite element collocation methods, 465
- First law of thermodynamics, 16, 20, 24, 30, 74, 365
- First-order local sensitivity coefficients, 204
- First-order rate law, 152, 158
- First-order reactions, 129, 132, 141, 143, 151–154, 157, 457
- First order sensitivity matrix, 201
- First viscosity, *see* Viscosity, dynamic (first viscosity)
- Flame curvature, 474
 effect of, 477
- Flame front, 392
- Flame height, 548, 561
- Flame length, 560
- Flame quenching, 513
- Flame radius, 560
- Flame speed, 254
- Flame speed at flammability limit, 521
- Flame stability, 506
- Flame stabilization:
 blowoff, 504–507, 510, 535
 boundary velocity ingredient, 437, 504–506, 508
- Flame stretch effect, 478
- Flame stretch factor, 471, 477
- Flame stretch rate, 474
- Flame stretching, 477, 523
- Flame temperature, 437
 of methane/air laminar flame, 212
- Flameholder, 535
- Flamelet concept, 476
- Flammability of laminar flames, 310, 329
- Flammability limits, 420, 447, 471
 heat loss effect, 535

lean, 526, 527
 of pre-mixed gases, 395, 511
 rich, 526, 527
 Flammability studies, 172
 Flammable zone of natural gas-air mixture, 513
 Flash photolysis resonance fluorescence technique, 133, 137, 139, 141, 142
 Flashback, 439–441, 504, 508, 510, 533, 535
 Flashback region, 506
 Flow reactor systems, 136, 142
 Flow work, 324
 Formaldehyde, 233
 Formation of amines or HCN, 258
 Formation of hydrogen cyanide, 262
 Formation mechanism of nitrogen oxides, 255
 Formation of thermal NO, 259
 Formyl radical HCl, 234
 Formyl radical (HCO) deformation reaction, 241
 Fossil fuels, 262
 Fourier's law of heat conduction, 290, 320
 Free radicals (chain carriers and free valences), 154, 155, 161, 220, 222, 264, 266
 Freezing point, 701–704
 FT-IR spectroscopy, 141
 Fuel bound nitrogen route (FN), 255, 262, 269
 Fuel equivalence ratio, 486, 488, 489
 Fuel evaporation rate, 376, 575
 Fuel-injector nozzle, 561
 Fuel mass flux at droplet surface, 573
 Fuel-oxidant ratio, 9, 11, 39, 96, 442, 496, 505, 511
 Fuel-oxidizer mixture, 410
 Fuel-rich flames, 265
 Fugacity, 11, 90–92, 95, 537, 598, 599
 Functional group, 700

G

Galloping detonation, 405
 Gas diffusivity, 678, 680
 Gas-phase kinetics and preprocessors, 169
 Gas-phase reactions, 117, 131–132, 223–245
 Gas-phase relaxation time, 622
 Gas solubility, 592
 Gas-thermal conductivity, 671
 Gas-turbine engines, 551
 Gas viscosity, 656

Gauss's theorem, 298, 303
 Generalized Riedel vapor pressure equation, 640
 Gibbs–Duhem equation, 33
 Gibbs free energy, 11, 15, 27, 30, 32, 35, 73, 75–77, 104–107, 166
 Global activation energy of H₂/O₂ mixtures, 528
 Global gas phase reaction, 129, 352
 Global reaction rates, 203
 Global sensitivity analysis, 200
 Gravitational acceleration, 693
 Green's function coefficient, 207
 Green's function gradients, 200, 206, 207, 547
 Green's function method (GFM), 200, 205, 206
 Group contribution approaches, 661
 Grunberg and Nissan's method, 669

H

H atom abstraction reactions, 238, 243
 H atom generation steps, 216
 H₂/air flame, 471
 H₂-air-CO₂ mixture, 406
 H₂-air-diluents detonations, 410
 H₂-air-stream mixture, 406
 H₂/O₂ reaction mechanism, 217
 HCCO reactions, 229
 HO₂ formation/consumption reaction, 226
 HO₂ hydroperoxyl radical, 219
 H₂O₂ formation/consumption reaction, 226
 H₂O₂ species, 219
 Half-life, 138
 of chemical species, 142
 Halogen containing compounds, 421
 Halogenated hydrocarbons, 421
 Halogenated species, 231
 Hankinson–Brobst–Thomson model, 635
 Hankinson–Thomson correlation, 637, 640
 Harmful effects, 272
 Hayduk and Minhas's method, 686
 Heat capacity of real gases, 645
 Heat of combustion, 62, 63
 Heat conduction equation, 295
 Heat of formation, *see* Standard heat of formation (specific enthalpy of formation)
 Heat of reaction, 12, 43–47, 52, 54, 55, 61, 63, 65, 424, 425, 558
 Heat of vaporization, 12, 69, 602, 603

Heat transfer coefficient to a spherical droplet, 572
Heating value of a fuel, 61
HBT (Hankinson, Brobst, and Thomson) mixing rule for liquid density, 639
Helmholtz free energy, 35, 104
Hess's thermochemical law, 48, 51, 63, 65
Heterogeneous reactions, 117, 174, 283, 351
Heterogeneous chemical kinetics, 165
Hexadecane, 588
Hierarchical structure, 224
High-pressure correction, 626
High-pressure vapor-liquid equilibria, 598
High-temperature liquid viscosity estimation methods, 667
Hill's spherical vortex, 391, 586
Hildebrand-modified Batschinski equation for liquid viscosity, 666
HO₂ formation reaction, 267
Homogeneous differential equation, 336
Homogeneous ignition process, 213
Homogeneous reactions, 5
Hooke's law, 304
Horizontal asymptote, 371
Hugoniot curve, 355, 357–368, 371, 435, 438
 origin of, 361
Hybrid time-integration/Newtonian iteration technique, 492
Hydraulic drag coefficient, 418
Hydrazine decomposition reaction, 345, 533
Hydrocarbon-air laminar flame speed, 496
Hydrocarbon-air mixtures, 408, 410, 501
Hydrocarbon-air reactions, 330, 331, 345, 510
Hydrocarbon-nitrogen prompt-NO channel, 262
Hydrocarbon oxidation kinetics, 224
Hydrocarbon oxidation reaction mechanism, 460
Hydrodynamically smooth walls, 416
Hydrogen/air premixed flames, 484
Hydrogen atom abstraction reaction, 239
Hydrogen cyanide, 262
Hydrogen iodide, 123
Hydrogen-oxygen reactions (H₂-air reactions), 215–223, 225, 390, 391, 395
 on platinum surface, 183
Hydrogen oxidation mechanism, 411
Hydrogen peroxide (H₂O₂) formation and consumption reactions, 231

Hydrogenation, 182
Hydrogenolysis, 182
Hydroperoxyl molecule (HO₂), 222, 230, 231, 242
Hydroxyethyl radical (CH₃CHOH), 243
Hygroscopic substance, 271

I

Ideal gas equation of state, 327, 626
 for a multicomponent system, 331
Ignition, 173, 210
Ignition delay, 424
Ignition delay measurements in shock tube, 232
Importance of HO₂ and H₂O₂ chemistry for ultra lean-burning, 496
Incident shock, 397
Incinerators, 271
Incinerator exhausts, 274
Industrial furnace, 561
Induction period, 382
Induction time, 210, 355, 408
Industry exhaust, 270
Inertia force, 301
Infinitesimal process, 16
Infinitesimal control volume, 293, 298
Infinitesimal particle approach, 297, 298
Infrared spectroscopy (IR), 188
Ignition delay approach, 417
Ignition temperature, 499
Inhibition of flames of normal burning velocity, 421
Inhibitor, 284
Inorganic particles, 271
Integral reaction flow analysis, 212–215
Intensity of turbulence, 549
Intensive property, 15
Intermolecular potential function, 656, 680
Internal circulation of droplet vaporization rate, 585
Internal energy, 12, 21, 23, 166
International System Equation, 103
Ion neutralization spectroscopy (INS), 189
Irreversible process, 14, 17, 25–29, 31
Irreversible thermodynamic processes, 14, 320
ISENTROPIC process, 367, 373
Isobaric specific heat, 650
Isochoric specific heats, 650
Isocomposition contours, 556
Isotopes of elements, 170

Isotropic fluid, 309, 351
 Iterative minimization technique, 136
 IUPAC, 699

J

Jacobian matrix, 201, 208, 209, 251
 normalized, 201
 Jet invariant, 553, 559, 618, 621
 Joback method for constant
 pressure-specific heat, 642, 643

K

Karlovitz number (Ka), 475, 484, 485, 488
 Karman–Pohlhausen integral approach, 586
 Kay's rule, 638
 Kerosene-air reaction, 107
 Ketones, 675, 699, 700
 Ketyl radicals (HCCO), 240
 Kinematic viscosity, 418
 Kinetic energy, 12, 21, 349
 Kinetic spectroscopy technique, 139, 142
 Kinetic theory of gases, 176
 Knocking, 312, 499
 Kronecker delta function, 285, 310

L

Lagrange multiplier, 105, 106
 Lagrangian approach, 298–300, 464
 Lagrangian coordinate, 464
 Laminar burning velocities, 484, 485, 488,
 500
 Laminar diffusion flame jets, 336, 539–547
 Laminar flame (premixed laminar flame),
 173, 210–212, 232, 269, 364, 388,
 422, 439, 471–496
 Laminar flame speed, 373, 423, 437, 444,
 459, 471, 483, 490, 496, 511, 534
 dependence on mixture composition, 497
 effect of additives, 499, 500
 effect of flame temperature, 502
 effect of fuel molecular structure,
 497–499
 effect of initial temperature, 501, 511
 effect of mixture ratio, 496, 497
 effect of pressure, 500, 501
 effect of stretch, 485
 effect of thermal diffusivity and specific
 heat, 502, 503
 flammability limits, 510–528
 various hydrocarbon-air mixtures, 512,
 513

Laminar flame speed measurement:
 constant-volume bomb method, 442, 443
 flat-flame burner method, 445–447
 particle-track method, 445
 soap-bubble (constant-pressure bomb
 method), 443, 444
 Laminar flame stability, 504
 Laminar flame in the stagnation-point flow
 regimes, 491
 Laminar flame theory:
 comprehensive theory, 416, 422,
 451–458
 contemporary method, 461–468
 diffusion theory, 449, 458–461
 thermal theory, 449–451
 Laminar pre-mixed flames, 258, 336
 Landau–Teller formation, 168
 Langmuir adsorption isotherm, 175–177,
 180, 191
 Langmuir's concept of chemisorption, 174
 Langmuir–Hinshelwood mechanism, 179,
 181
 Langmuir–Rideal mechanism, 179–182
 Laplace's law, *see* Lavoisier and Laplace's
 thermochemical law (Laplace's law)
 Laser-based optical techniques, 447
 Laser-beam extinction measurement, 448
 Laser Doppler anemometry (LDA), 448
 Laser Doppler velocimetry, 448
 Laser induced fluorescence (LIF) technique,
 191, 448
 Laser photolysis, 141
 Laser Rayleigh-scattering technique, 448
 Latent heat of vaporization, 591
 Lavoisier and Laplace's thermochemical
 law (Laplace's law), 47, 65, 66
 Law of mass action, 119, 128, 129, 160,
 190, 196, 245, 248
 Lean H₂/O₂/N₂ mixtures, 496
 Lee–Kesler method for C_p calculations, 649
 Lennard-Jones 12–6 potential, 656, 680
 Lennard-Jones energies of species, 679
 Levenburg–Marquardt method, 136
 Lewis number (Lewis–Semenov number),
 6, 290, 334, 336, 337, 491, 547
 Lifetime of a droplet, 570, 577, 586, 587,
 589, 591, 604, 605, 607, 608, 610,
 612–614
 Lift curve, 507
 Lifted flame, 507
 Limiting tube diameter, 406, 409, 410
 Limits of detonability, 397
 Liquid diffusivity, 684–688
 Liquid-phase reactions, 117

Liquid rocket-engine combustor, 561
 Liquid thermal conductivity, 674–678
 Liquid viscosity, 661
 Local reaction flow analysis, 213
 Low-activation energy free radical reactions, 124
 Low-energy electron diffraction (LEED), 189
 Lower Chapman–Jouguet point, 355, 360
 Low-pressure premixed flames, 264
 Low-temperature path, 184
 Low-temperature viscosity estimation methods, 664
 LOX droplet vaporization, 610
 Lucas's Estimation method, 668
 Lucas method for dense gas viscosity, 659
 Lundgren's “fine-grained density” method,
see Turbulent diffusion flame, probabilistic approaches,

M

Mach number, 395, 412, 434
 Magnesium oxide particles, 445
 Mallard and LeChatelier's development, 449
 Markstein length, 478, 482–485, 489, 490
 Markstein numbers, 484, 487
 Mass-average velocity, 285–288, 328
 Mass burning rate, 339
 Mass concentration (concentration), 82, 287
 Mass conservation equation
 for species A, 294
 for *i*th species, 296
 Mass diffusion coefficients, 333
 Mass diffusion velocity, 286, 287, 296, 322
 Mass diffusivity, 6, 289, 290, 292, 349, 460
 Mass flux, 285–290, 294, 343, 345, 346,
 348, 351–353, 478, 479, 514, 526, 573
 Mass flux balance equation, 351
 Mass flux balance of the *i*th species at the gas-solid interface, 346
 Mass fraction, 8, 12, 38, 200, 212, 465,
 514, 573
 Mass-weighted averaging *see* Favre averaging (mass-weighted averages)
 Material derivative, *see* Substantial derivative (total derivative of material derivative)
 Maximum flame speed, 498
 Maximum flame temperature, 216
 Maxwellian distribution of velocity, 139
 Mean free path, 102, 139, 286, 291, 342,
 548, 655, 671

Measurement of gas-phase reaction rates, 131
 Mechanical energy equation, 323, 325
 Mechanical equilibrium, 14
 Mechanism for ethane oxidation, 215
 Mechanism for methane oxidation, 215
 Mechanism of flame anchoring, 503
 Metal combustion, 174
 Metal oxides, 271
 Melting point, 705
 Methane, 83, 92, 93, 177, 210–211, 215,
 234, 235, 244, 261, 262, 402, 484,
 489, 490, 509, 511, 533
 Methane-air flame, 262, 564
 Method of corresponding states, 657
 Methoxy (CH_3O), 242
 Methylene radical, 240
 Missenard group contribution method, 653
 Missenard's equation for liquid thermal conductivity, 677
 Mixing rules, 626, 631, 687, 688
 Mixture compressibility factor, 600
 Mixture fraction, 11, 12, 40–43, 552,
 557–559
 Modification of the GFM (Green's function method), 205
 Modified Yetter kinetic Scheme for atmospheric H_2/air mixtures, 493
 Moist carbon-monoxide flame, 458, 459
 Molar-average velocity, 268, 287
 Molar concentration, 11, 167, 285–290
 Molar diffusion velocity, 286, 287
 Molar flux, 286, 287, 289, 350
 Molar standard free energy of formation, 78, 80
 Mole fraction, 8, 10, 12, 38, 197, 198, 200,
 287, 354, 468, 471
 Molecular beam scattering techniques, 139
 Moment closure methods, *see* Turbulent diffusion flame, direct-closure approach
 Momentum diffusivity, 290
 Momentum equation, 297, 340
 integral form of, 340
 Momentum flux balance at gas-solid interface, 343
 Monatomic gas, 503
 Monolayer adsorption, 175
 Monopropellant decomposition flame, 534
 Monte Carlo solution method, 200
 Multicomponent diffusion equation, 328–330

Multidimensional detonation-wave structure, 384
 Multiheaded detonation, 402, 405, 410
 Multilayer adsorption, 175
 Multiple photo ionization technique (MPI), 137, 140

N

n-decane, 587–589
n-hexane, 588, 589
n-pentane, 606, 608
 NACA Report, 512
 NASA chemical equilibrium code, 165.
See also Chemical equilibrium application code
 Name of chain, 698
 NASA-CEA program, 378, 434
 butadine (C_4H_6), 238
 NASA database, 171
 Name of group, 698
 National Ambient Air Quality Standard for carbon monoxide, 271
 Natural gas-air reaction, 512, 513
 Navier–Stokes equations, 297, 310–319, 612
 Near-critical enhancement, 593
 Neutral preferential-diffusion condition, 487, 490
 Newtonian fluid, 297, 307, 309, 311–315, 317, 319, 351, 562
 Newton's law of momentum transport, 290
 Newton's second law, 303
 Newton–Raphson
 descent method, 88, 95, 106
 iteration methods, 373, 375–379
 iteration procedure, 376
 NH or NH_2 free radical, 266
 Nitric oxide, 173, 255
 Nitrogen diluted flames, 494
 Nitrogen dioxide, 129, 130
 NO production from fuel-bound nitrogen, 262
 $NO \rightarrow HCN \rightarrow N_2$ Mechanism, 264, 265
 $NO \rightarrow NO_2$ conversion, 269
 NO_2 mechanism, 267
 N_2O mechanism, 267–269
 Noble–Abel dense-gas law, 434
 Nonequilibrium thermodynamics, 26–34
 Nonexplosive reactions, 117
 Nonideal detonation, 414
 Nonideal gas effects, *see* Real gas (nonideal) effects

Nonplanar leading shock wave, 385
 Nonpolar compounds, 634
 Nonpolar liquids, 635
 Nonpolar substances, 672
 Non-premixed flames, *see* Diffusion (non-premixed) flames
 Normal boiling point, 624
 Normal paraffins, 686, 703
 Normal unstretched laminar-flame speed, 475
 Normalized velocity deficit, 416
 NO_x emissions, 172
 NO_x formation mechanism, 255, 270
 Nuclear magnetic resonance, 142
 Number density, 679

O

O_2/H_2 system, 601, 602
 O_3 decomposition mechanism, 232
 Olefins, 498, 677
 One-dimensional planar propagating premixed flames, 252
 One-step (single-step) chemical reaction, 118, 141–147
 1–3 butadine (C_4H_6), 238
 Onsager's reciprocal relations, 320
 Onset of retonation in stoichiometric hydrogen-oxygen mixture, 390
 Opposed flow diffusion flames, 173
 Opposing reactions, 150, 151
 Optical spectroscopy, 188
 Order of chemical reaction, 12
 Organic acids, 675
 Organic compounds, 699
 Orrick and Erbar's Group Contribution Method, 665
 Orthogonal curvilinear coordinate system, 472
 Orthonormal relations, 249
 Oscillatory combustion phenomena of H_2/O_2 systems, 216
 Overall continuity equation, 464
 Overall order of the reaction, 128, 162
 Overall rate sensitivity coefficient, 203
 Oxidation of acetaldehyde, 243
 Oxidation of ammonia, 174
 Oxidation of HCN, 262
 Oxidation of ketene, 240
 Oxidation of NH_3 , 265, 266
 Oxyhydrogen reaction mechanism, 224
 Ozone, 133, 232, 419, 420, 434, 461, 464, 467, 468

Ozone/oxygen flame, 461
premixed, 464

P

p-T explosion diagram of H₂/O₂ mixture, 223
Paraffins, 675, 701
Partial equilibrium assumption for O atoms, 257
Partial molar Gibbs function (chemical potential), 32–34
Partial oxidation, 182
Partial pressure of species *i*, 12
Particle image velocimetry (PIV), 448
Particle tracking methods, 448
Particulate matter, 271
Peclet number, 547
Penetration distance, 437, 504
Peng–Robinson equation of state, 649
Perfectly stirred reactors, 252
Periodic table of elements, 708
Perkins and Geankoplis's method for liquid diffusivity, 687, 688
Phase equilibrium, 34, 95–98
Phenyl radical, 245
Photochemical initiation of detonation in mixtures, 425
Photo-stationary methods, 142
Photolysis, 133–142
Pitzer's acentric factor, 595, 624, 646, 654
Pitzer equation for reduced vapor pressure, 646
Planar laser induced fluorescence (PLIF) technique, 448
Planck's constant, 694
Platinum catalyzed surface reaction, 186
Plug flow reactor, 137, 173
Polar molecules, 672
Polyaromatic hydrocarbon (PAH) oxidation, 244
Polycyclic aromatic hydrocarbone (PAH), 272
Porosity, 353
Potential energy, 12, 21
Prakash–Sirignano model of droplet internal circulation, 391, 396, 586
Preexponential factors, 167
Preferential diffusion of heat and species, 568
Prefixes, 696
Premixed ethylene-air flame, 440
Premixed H₂/O₂ gases, 523

Premixed laminar flame, *see* Laminar flame (premixed laminar flame)
Premixed stoichiometric CH₄/air flame, 214
Pressure dependant reactions, 170
Pressure exponent, 500
Pressure oscillation characteristic time, 622
Primary bonds, 52
Primary methods of NO_x control, 270
Production rate of *k*th species, 166
Prompt NO mechanism, 255, 258, 263
Propagation of detonations in rough-walled tubes, 415
Propane/air mixtures, 488, 489
Proton mass, 694
Przezdziecki and Sridhar's Corresponding States Method, 666
Pyrolysis of acetylene, 238
Pyrolysis process of a solid fuel, 353

Q

Quantum correction factor, 657
Quantum gases, 657
Quartz photochemical cell, 135
Quasi-detonation process, 415
Quasi-equilibrium, 251
Quasi-steady assumption, 572
Quasi-steady state assumption, 257
Quasi-steady state assumption (QSSA) and partial Equilibrium assumption, 246
Quenching distance, 437, 440, 504, 507–510
between parallel plates, 509
Quenching of flame-shock complex, 422

R

Radical recombination reaction, 124
Ramjet engine, 538, 551, 590
Random motion molecular velocity, 291
Rankine–Hugoniot relations, 356, 359, 360, 370, 434, 435
Ranz–Marshall correlation, 587, 612
Rapid mixing, 142
Rate-determining (slow) step, 144, 202
Rate of production of chain carriers, 220
Rate of removal of free radicals, 222
Rate limiting reaction steps, 200, 202, 204, 258, 259, 269
Rate of reaction, *see* Reaction rate (rate of reaction)
Rayleigh-line relation, 359, 361, 435
approximate, 375
Reactedness, 558

- Reaction coordinate, 126
 Reaction flow analysis, 211
 Reaction flow diagrams, 212
 Reaction mechanism description, 170
 Reaction mechanism of H₂ oxidation, 225
 Reaction mechanisms of H₂/O₂ systems, 215–223, 524
 Reaction mechanism of hydrogen oxidation on platinum surface, 186
 Reaction path diagram, 263–266
 Reaction product imaging technique, 140
 Reaction progress variable (reactedness), 12, 19
 Reaction rate (rate of reaction), 118, 119, 131, 137, 163, 166, 168, 184, 450, 451, 508
 Reaction rate of adsorption, 177
 Reaction rate of desorption, 177
 Reactivity of C-Si bond, 499
 Reactivity of Si-H bond, 499
 Real (nonideal) gas effects, 90–92
 Real gas equation of state, 626
 Recombination reaction, 282
 Redlich-Kwong (R-K) equation of state, 599, 600, 628, 629
 mixing rules, 631
 Reduced and detailed mechanisms, 254, 255
 Reduced dipole moment, 657
 Reduced mass of molecules, 116, 122
 Reduced mechanism for high temperature H₂/air and CH₄/air oxidation, 252
 Reduced pressure, 597
 Reduced specific molar volume, 595
 Reduced temperature, 597, 623
 Reduction of reaction mechanisms, 245
 Reichenberg Method for dense gas viscosity, 658
 Relationship between X_i and Y_i, 331
 Relative mass-diffusion velocity components, 322
 Relative mass flux, 288,
 Relative molar flux, 288, 291
 Relative rate-constant photolysis technique, 134
 Relative sensitivities, 208, 210
 Relaxation method, 137, 138, 142
 Relation modulus in shear, 344
 Residence time, 549
 Resonance energy, 49–51
 Resonant multiple photo ionization (REMPI) technique, 140
 Retonation wave, 389–391
 Reversible process, 14, 24–26
 Reynolds' transport theorem, 338, 339, 473, 476
 Rossini's approach, 35
 Runge-Kutta integration routine, 157
 Rutherford back-scattering spectroscopy (RBS), 188
- S**
- Saturated liquids, 633
 Saturated straight-chain hydrogen, 697
 Schlieren photographs flash, 388
 streak, 389
 Schmidt number, 6, 390, 337, 549, 556
 Second explosion limit, 222
 Second-order rate law, 158
 Second-order reaction, 122, 132, 143–147, 153, 154, 157, 457, 512
 Secondary bonds, 52
 Secondary droplet-breakup regimes, 584
 Secondary ion mass spectroscopy (SIMS), 188
 Self-ignition induction time, 422
 Self-similarity profiles, 552, 555
 Self-sustained detonation front, 391
 in a 2H₂ + O₂ + 2CO mixture, 387
 region, 405
 Sensitivity analysis, 225, 252, 259
 global methods, 204
 local methods, 204
 theory, 201
 Sensitivity coefficients, 209
 Sensitivity of mass fractions of H atoms and water vapor, 212
 Shchelkin spiral, 405
 Shock front, 392
 Shock-to-detonation transition process, 356
 Shock strength, 395
 Shock tube, 102, 137–139, 142, 232, 233, 237, 240, 242, 244, 381
 Shock waves, 426, 427
 Shock wave amplification by coherent energy release (SWACER), 427
 Shvab-Zel'dovich formulation, 332–336, 453, 538, 540–544, 564, 565, 579
 Shvab-Zel'dovich energy equation, 335
 Shvab-Zel'dovich species equation, 335
 Shvab-Zel'dovich variables, 579
 Simple chemically reacting system (SCRS), 558, 559
 Single fuel droplet burning, 569–581

- Single fuel droplet burning (*continued*)
 double-film model, 569
 effect of internal circulation, 585–590
- Single-headed spin detonation, 402,
 403–405
 onset of, 405
- Single-head detonation wave, 410
- Single-head spinning waves, 409
- Single-step forward reaction, 335, 514
- Singlet electronic excited state of
 methylene, 230
- Slow subspace, 249
- Smoked-foil method, 384–386, 406, 407,
 410
- SO_2 , 271, 272
- Soave–Redlich–Kwong equation of state,
 625, 635, 649
- Sodium-line-reversal method, 448
- Soft X-ray appearance potential
 spectroscopy (SAPS), 189
- Solid-phase reactions, 117
- Sonic velocity, 354
- Soot, 272
- Soot formation and oxidation, 173
- Soret effect, 6, 320, 330, 332, 480, 562
- Spalding transfer number, 580, 581, 587,
 605, 613
- Spalding transfer number at high-pressure,
 605
- Spalding's theory, 513–522
- Spark energies, 485
- Spark plug, 511
- Species continuity equation, 463
- Species diffusion theory, 534
- Species dissociation, 380
- Special function groups, 699
- Species mass-flux balance, 343, 348
 at a gas-solid interface, 345, 352
- Specific enthalpy of formation, 354
- Specific gravity, 701–704
- Specific heat, 623, 641
 at constant pressure, 165
 at constant volume, 166
- Specific impulse, 215
- Specific internal energy, 321
- Specific reaction-rate constant, 116, 119,
 125, 129, 144, 148, 153
- Specific impulse, 3
- Speed of light, 694
- Speed of sound, 423
 behind a detonation wave, 373
- Spherical bomb, 479
- Spherical coordinates, 315, 318
- Spherical deflagration wave, 485
- Spherical detonations, 402
- Spherical flame, 443, 534
- Spherical flameholder, 535
- Spherical flame propagation, 534
- Spin pitch, 406
- Spinning detonation, 384
- SRK and PR equations of state, 595, 628
- Stability diagram for premixed open burner
 flame, 506
- Stable flame region, 506
- Stable preferential-diffusion conditions, 485,
 490
- Stagnation point flow-field, 491
- Standard heat of formation (specific
 enthalpy of formation), 12, 43–47, 66,
- Standard-state enthalpy, 165
- Standard-state entropy, 166
- Static methods, 132
- Stationary 1D C-J detonation, 413
- Steady-state approximation (assumption),
 157, 158, 161, 164, 246, 281, 396
- Steady-state one-dimensional problems,
 205, 208
- Steam reforming, 182
- Stefan–Boltzmann constant, 694
- Steric factor, 116, 123
- Sticking coefficient, 174, 183
 at zero surface coverage, 186
- Stiff ODE solver code (LSODE), 206
- Stiff ordinary differential equations,
 252
- Stiff system of equations, 172, 248
- Stirred reactors, 173
- Stoichiometric coefficients, 12, 76, 78, 116,
 118, 119, 129
- Stoichiometric condition, 9, 10, 107
- Stoichiometric equation, 20, 514
- Stoichiometric H_2/O_2 flame, 471
- Stoichiometric H_2/O_2 mixture, 221, 386,
 391
- Stoichiometric mixture of air and methane,
 533
- Stoichiometric propane/air flame, 211
- Stoichiometric vector, 247, 249
- Stoichiometry, 482, 483
- Stopped flow spectrophotometric technique,
 137, 138
- Stored energy, 11, 15, 16, 20, 321, 347
- Strain-rate tensor, 285, 307, 324, 474
- Stream function, 562, 563
- Stress/strain-rate relationship (constitutive
 relationship), 304–310
- Stress tensor, 301, 304, 305, 307, 311, 314,
 315, 343, 344, 351

- Stretch effects in hydrogen/air mixtures, 477
 Stretch factor, 475, 485
 Stretch rate, 491
 Stretched laminar premix flame, 471
 Stretched vortex ring, 611
 Stretch-free flame speed, 492
 Strong detonation wave, 363
 Structure of self-sustaining detonation waves, 384
 Sublimating surface, 352
 Sublimation temperature, 705
 Substantial derivative (total derivative of material), 300
 Substituted methyl groups, 498, 499
 Sulfur dioxide, 271
 Sulfuric acid, 271
 Supercritical combustion, 591, 661
 Supercritical droplet combustion, 608
 Supercritical burning, 590–614
 Supercritical droplet gasification, 610
 Superdetonation, 389
 Super-equilibrium concentrations of O atoms, 257, 269
 Surface adsorption process, 174
 Surface bond energy for desorption, 183
 Surface catalysis, 174
 Surface chemical composition, 187
 Surface coverage in monolayers, 195
 Surface coverage parameter, 183
 Surface crystallography, 189
 Surface reaction mechanism, 194
 Surface reaction rate, 183, 342
 Surface tension of a liquid, 624
 Surface sites, 177
 Surface stress force, 301
 SWACER, 427
 Symmetric tensor, 324
 System(s)
 closed, 15–19, 22, 24, 26, 27
 isolated, 15, 27
 open, 15, 28
- T**
- Tait equation, 637
 Takahashi's high-pressure correction, 683
 Tangential velocity of flame surface, 475
 Taylor series expansion models, 200
 Teja and Rice's method for liquid viscosity, 670
 Temperature dependence of burning velocity, 525, 526
 Temperature exponent, 500
 Temperature-programmed desorption (TPD), 190
 Temperature-programmed reaction spectra (TPRS), 190
 Temperature reaction paths, 55
 Temperature sensitivities, 203
 Tertiary bonds, 52
 Theory of Zel'dovich, Frank-Kamenetsky, and Semenov, 451
 Thermal conductivity, 624
 Thermal desorption spectroscopy (TDS), 190
 Thermal diffusion coefficient, 286, 330
 Thermal diffusion time, 588
 Thermal diffusivity, 290, 503
 Thermal equilibrium, 14, 16
 Thermal NO mechanism, 255, 256
 Thermal theory, 449
 Thermodynamic coordinates, 14
 Thermodynamic database, 170
 Thermodynamic equilibrium, 14, 150–152
 Thermodynamic property database, 169
 Thickness of unstretched flame, 475
 Thinh's method, 644
 Third body, 151, 160, 167, 170, 223, 225, 233, 265, 282, 396, 411, 493, 462
 chaperon relationship, 233, 462
 efficiencies, 219
 for the trimolecular reaction, 223
 Third explosion limit, 222, 223
 Third law of thermodynamics, 17
 Third-order reactions, 133, 147, 231, 283
 Three-body chain-terminating reactions, 495
 temperature insensitive, 495
 temperature sensitive, 495
 Three-body reaction, 222
 Three-body recombination rate constant, 282
 Threshold Reynolds number, 611
 Time averaging, *see* Reynolds averaging (time averaging)
 Time-dependant one-dimensional problems, 205
 Time-dependant spatial problems, 209
 Time-dependant zero-dimensional problems, 205
 Total derivative, *see* Substantial derivative (total derivative of material)
 Total enthalpy, 285, 325
 Total fixed nitrogen (TFN), 259, 261
 Total number of collisions, 328
 Total oxidation, 182
 Total stored energy, 15
 Total stress tensor, 343

Toluenes, 699, 700
 Transfer number for supercritical vaporization, 613
 Transient flame propagation process, 533
 Transition from a multi-headed detonation to a single-headed spin detonation, 402
 Transport equations, 5, 6
 probability density function, 6
 Transport properties, 101, 557, 558, 560,
 593–598
 Transport property preprocessor, 169
 Trimolecular reaction rate, 216
 Triple bond, 256
 Triple point, 386, 387, 705
 Triplet state of methylene, 230
 Troe-coworker approach, 168
 Truncated virial equations, 649
 Truncation error, 172, 467
 Turbojet engine, 618
 Turbulence dissipation rate, 6
 Turbulence kinetic energy, 6,
 Turbulence (Reynolds) stresses, 6
 Turbulent boundary layer, 420
 Turbulent eddy viscosity, 549
 Turbulent flames, 471, 476, 490
 Two-flux model, 353
 Two-point boundary value problem solver,
 169
 Tyn and Calus's method for liquid diffusivity, 685, 686
 Tyn's method for higher temperatures, 686,
 687

U

Ultraviolet photoemission spectroscopy (UPS), 188
 Ultraviolet radiation, 425
 Unified analyses of thermophysical properties, 593
 Unimolecular reaction, 142, 156, 158
 Unit normal vector, 473
 Universal gas constant, 12, 624, 693
 Unsaturated hydrocarbons, 498
 Unstable preferential diffusion, 485–487,
 490
 Upper Chapman-Jouquet point, 360
 UV-visible absorption spectroscopy, 141

V

Van der Waals equation of state, 628
 Van't Hoff equilibrium box, 32, 74–76
 Van Velzen Group Contribution method, 665

Venting in the early stages of explosion, 421
 Vertical asymptote, 371
 Very lean H₂/air flames, 495
 Vibrational energy transfer process, 170
 Vinyl acetylene, 245
 Vinyl radical (C₂H₃), 237, 245
 Virial coefficients, 629
 Virial equation of state, 629
 Virtual origin of the jet, 621
 Viscoelastic materials, 344
 Viscosity, dynamic (first viscosity), 286,
 309, 351
 Viscous stripping, 611
 Vogel equation of liquid viscosity, 662
 Void fraction, 353
 Volume dilatation, 310, 325
 Von Neumann spike, 383
 Von Neumann state, 413
 Vorticity equation, 563

W

Wall recombination processes, 173
 Wassiljewa equation for gas mixture thermal conductivity, 673
 Weber number, 538, 583
 Wet-bulb temperature, 606
 Wet-bulb state, 604
 Wet scrubbers, 273
 Wilke-Chang Correlation, 684, 685, 688
 Wood-burning stoves, 271

X

Xiang's equation for liquid viscosity, 664
 X-ray adsorption technique, 383
 X-ray photoemission spectroscopy (XPS or ESCA), 188

Z

Zel'dovich, Frank-Kamenetsky, Semenov theory, *see* Laminar flame theory, comprehensive theory
 Zel'dovich mechanism for NO formation, 255–256, 259, 269
 Zero-dimensional ignition delay problem, 210
 Aero-order reaction, 457
 Zeroth law of thermodynamics, 15
 ZND detonation wave structure, 372, 382,
 383, 403, 412, 413
 ZND model, 412
 ZND theory, one dimensional, 413

